Tectonic and sedimentation processes of West Antarctica and the southern Pacific and their relationship to glacial history

Habilitationsschrift

Eingereicht am
Fachbereich Geowissenschaften
der Universität Bremen
von
Dr. Karsten Gohl

Juni 2015

Dr. Karsten Gohl
Alfred-Wegener-Institut
Helmholtz-Zentrum für Polar- und Meeresforschung
Fachbereich Geowissenschaften, Sektion Geophysik
Am Alten Hafen 26
27568 Bremerhaven
Tel.: 0471 4831 1361
E-mail: karsten.gohl@awi.de

Table of contents

Preface

This thesis (*Habilitationsschrift*) highlights the findings of my research activities along the West Antarctic continental margin and the southern Pacific Ocean in the past fifteen years. The studies have focussed on reconstructions of the geodynamic and tectonic evolution, the sedimentary processes from the continental shelves to the deep sea, and the glaciomarine transport and deposition mechanisms. All studies have been directed towards an improved understanding of the paleoenvironmental context of this region, which has gained increasing attention for its role in paleoclimate and ice sheet dynamics. Other research activities (e.g., work on Large Igneous Provinces and non-Antarctic continental margins) and several years spent abroad (Australia) with different research foci interrupted a consecutive continuation of this project. However, my research activity in this region has gained increased momentum, in particular in the last eleven years, due to new opportunities for collecting large essential datasets, which have enabled me and my working group to perform a more thorough synthesis of the geological evolution and processes of this region.

Most of the studies were supported by institutional funding of the Alfred Wegener Institute (AWI) before the Helmholtz Association was founded, and through the AWI Research Programs MARCOPOLI and PACES as part of AWI institutional funding through the Helmholtz Association. Additional funding has been provided by the Deutsche Forschungsgemeinschaft (DFG) through the following projects:

- DFG project GO-724/2-1 and GO-724/2-2 "*Plate-dynamics of the Southeast Pacific* (PLASOPAZ)" (P.I's.: Gohl & Miller) within the DFG "Normalverfahren".
- DFG project GO-724/3-1 "*Reconstruction of the glacial-marine sedimentation in the Amundsen Sea (SEDAMUND)*" (P.I.: Gohl) within the DFG Priority Program 1158 "Antarktisforschung mit vergleichenden Untersuchungen in arktischen Eisgebieten".
- DFG project GO-724/9-1 and GO-724-9-2 "*Sensitivity of Quaternary West Antarctic Ice Sheet advances and retreats in Pine Island Bay* (SEQWAIS-PIB)" (P.I's.: Gohl & Uenzelmann-Neben) within the DFG Priority Program 1158 "Antarktisforschung mit vergleichenden Untersuchungen in arktischen Eisgebieten".
- DFG project GO-724/10-1 "*Circum-Antarctic stratigraphy and paleobathymetry: development of grid-based simulations* (CASP)" (P.I.: Gohl) within the DFG Priority Program 1158 "Antarktisforschung mit vergleichenden Untersuchungen in arktischen Eisgebieten".
- DFG project GO-724/13-1 "*Coupling of lithospheric dynamics, surface processes and ice-sheet evolution – constraints from Marie Byrd Land, West Antarctica*" (P.I's.: Spiegel, Lisker, Gohl) within the DFG Priority Program 1158 "Antarktisforschung mit vergleichenden Untersuchungen in arktischen Eisgebieten".
- DFG project GO-724/14-1 "*Interrelations of tectonic deformation and surface erosion with West Antarctic Ice Sheet dynamics*" (P.I's.: Spiegel, Gohl, Kaul, Lisker) within the DFG Priority Program 1158 "Antarktisforschung mit vergleichenden Untersuchungen in arktischen Eisgebieten".

This thesis is composed of six main chapters after the list of contents, this preface and a summary: In **Chapter 1**, an introduction to the research topic, the region, expeditions and data acquisition is given. **Chapter 2** consists of a summary and synthesis of the 24 papers relevant to this thesis, arranged into four themes. In **Chapter 3**, I discuss the outlook and suggestions for future research. **Chapter 4** acknowledges various persons and organisations I am grateful to. **Chapter 5** includes a list of additional references cited in the previous chapters (incl. other own papers not included as part of this thesis). **Chapter 6** is the appendix and contains all 24 papers, grouped according to the four themes of Chapter 2. Each sub-chapter begins with a statement of the author contributions to the paper. Of all publications included here, 5 papers are first- or single-authored by myself, and to 19 papers (4 of which are two-authored) I made essential contributions as co-author in the form of text passages, figures, datasets, fieldwork or interpretations and discussions. I deselected further 25 first- and co-authored papers from being included in this thesis. These (marked with a *) are listed in the additional references of Chapter 5. Although these papers are relevant to the project, the results in these are either better represented in other papers of this thesis, or my contributions to these are rather minor. All published papers underwent a thorough peer-review process.

Summary / *Zusammenfassung*

West Antarctica is one of the most fascinating and challenging regions for studying the relationship and interplay of geodynamic, tectonic, and sedimentation processes as well as past and present ice-sheet dynamics. Its mostly rift-related tectonic evolution, driven by yet largely enigmatic mantle-dynamic processes, led to a topographic and morphological setting for a dominantly submarine-based ice sheet that is highly sensitive to climate change and ocean warming. Originally an assemblage of various Palaeozoic and Mesozoic crustal blocks and mobile belts, West Antarctica's transformation into the worldwide second largest continental rift system began when subduction at the East Gondwana margin partially stalled and the New Zealand micro-continent separated from Antarctica in the mid-Cretaceous. Crustal extension continued in West Antarctica in various phases creating major rift basins of thin crust, but partial uplift also occurred with the Marie Byrd Land dome event by an intercepting mantle plume. Cretaceous rifting and continental breakup as well as later stages of West Antarctic Rift System activities formed the basement architecture of the major embayments of the Ross Sea, Amundsen Sea and Bellingshausen Sea, which have acted as prominent outlet regions for the West Antarctic Ice Sheet.

The onset of early ice caps and glaciers likely occurred in highly elevated ranges already in the early Cenozoic, but seismic and sediment core records indicate that first glaciers and ice-streams reached the costs and inner shelves not before the Oligocene. A palaeotopographic model of Antarctica, derived from a study on offshore/onshore sedimentary erosion-transport-deposition mass balance, indicates that an early continuous West Antarctic Ice Sheet may have formed on a land-surface higher than today and above sea level in the early Oligocene.

Seismic and sediment records from the continental shelves and rises of the West Antarctic margin demonstrate that most of the terrigenous sedimentary volume deposited has been glacially transported with a minor fraction in a transitional phase between the Oligocene and early Miocene, and the majority in a full glacial phase since the mid-Miocene. Massive glacially driven prograding sequences are responsible for the build-up of shelf extensions towards the deep ocean. Sediment drifts characterize the continental rise and indicate that strong ocean-bottom currents have been active already since the Oligocene. Warm circum-polar deep water, that follows a path along the deeply incised glacial troughs on the shelf, has been identified as the prominent mechanism for melt processes at the glacier's grounding zones and beneath ice-shelves. This seems to be a process in particular characteristically for the Amundsen Sea Embayment where grounded ice retreated relatively fast from is maximum extent on the outer shelf during the last glacial maximum at about 20 thousand years ago to the innermost shelf until the early Holocene. The remarkable present rapid retreat of glaciers in the Amundsen Sea sector, which may lead to a future collapse of the West Antarctic Ice Sheet, is a consequence of recurring warm bottom-water incursions exploiting incised pathways formed mainly by tectonic processes.

This *habilitation* thesis is largely a synthesis of 24 selected publications resulting from many years of focussed research on the geodynamic, tectonic and pre-glacial to glacial sedimentary processes of the Pacific margin of West Antarctica.

Die Westantarktis ist eine der faszinierendsten und herausfordernden Regionen für Studien über die Beziehungen und Wechselwirkungen von geodynamischen, tektonischen und sedimentären Prozessen sowie der Eisschilddynamik der Vergangenheit und Gegenwart. Ihre meist rift-basierende tektonische Entwicklung, getrieben durch weiterhin ungeklärte manteldynamische Prozesse, haben zu einer topografischen und morphologischen Ausprägung geführt, die einen primär unter dem Meeresspiegel aufsitzenden und dadurch auf Klimaänderungen und Ozeanerwärmung empfindlich reagierenden Eisschild ermöglicht. Ausgehend von einer ursprünglichen Collage aus paläozoischen und mesozoischen Krustenblöcken und Orogenen begann die Veränderung der Westantarktis in das weltweit zweitgrößte kontinentale Grabenbruchsystem mit dem Ende der Subduktionstätigkeit entlang des Kontinentalrandes von Ost-Gondwana und dem Aufbruch zwischen dem neuseeländischen Mikrokontinent und der Antarktis in der Kreide. Die Dehnung der westantarktischen Kruste setzte sich in unterschiedlichen Phasen fort und führte zur Ausbildung von diversen Riftbecken über dünner Kruste. Eine teilweise Hebung der Kruste fand unter Marie-Byrd-Land als Folge einer Mantelplume-Aktivität statt. Sowohl die Riftprozesse und der kontinentale Aufbruch in der Kreide als auch spätere Aktivitäten des westantarktischen Riftsystems sind verantwortlich für die Bildung des Grundgebirges der großen Einbuchtungen in den Sektoren des Rossmeeres, des Amundsenmeeres und des Bellingshausenmeeres, die als prominente Ausflussregionen des westantarktischen Eisschildes agieren.

Erste Eiskappen und Gletscher sind in Hochlagen wahrscheinlich schon im frühen Känozoikum aufgetreten, aber seismische Daten und Sedimentkerne belegen, dass Gletscher und Eisströme die Küsten und inneren Kontinentalschelfe nicht vor dem Oligozän erreichten. Ein paläotopografisches Modell der Antarktis, welches über eine Massenbilanz unter Einbindung von Erosions-, Transport- und Ablagerungsprozessen zwischen Festland und Ozean abgeleitet wurde, zeigt auf, dass ein erstes geschlossenes westantarktisches Eisschild im frühen Oligozän auf einer Landoberfläche gebildet wurde, die höher als heute und über dem Meeresspiegel lag.

Analysen von seismischen Daten und Sedimentkernen von den kontinentalen Schelfen und der anliegenden Tiefsee liefern Hinweise, dass der Großteil der terrigenen Ablagerungen von glazialen Prozessen transportiert wurde, wobei der kleinere Anteil aus einer vorglazialen-glazialen Übergangsperiode zwischen dem Oligozän und dem frühen Miozän und der größere Anteil aus der überwiegend glazialen Periode seit dem mittleren Miozän stammt. Mächtige glazial-getriebene progradierende Sequenzen sind verantwortlich für die großräumige Erweiterung der äußeren Schelfe. Driftssedimente charakterisieren den Kontinentalfuß und zeigen, dass starke Ozeanbodenströmungen schon seit dem Oligozän aktiv gewesen sind. Warmes zirkumpolares Tiefenwasser, das seinen Weg über den Schelf durch tief eingeschnittene glaziale Tröge findet, ist als primärer Mechanismus für Schmelzprozesse an den Aufsatzzonen der Gletscher und an der Unterseite der Schelfeise erkannt. Dieser Prozess scheint insbesondere für das Amundsenmeer eine entscheidende Rolle zu spielen, denn aufliegendes Eis hat sich relativ schnell bis zum innersten Schelf bereits nach dem Ende des glazialen Maximums vor ca. 20000 Jahren bis zum frühen Holozän zurückgezogen. Die bemerkenswerten rapiden Rückzüge der Gletscher im Amundsenmeersektor, die möglicherweise zu einem zukünftigen Kollaps des westantarktischen Eisschildes führen können, sind eine Konsequenz aus wiederholten Warmwassereinträgen entlang von bathymetrischen Trögen und Vertiefungen, deren Ausprägung primär durch tektonische Prozesse bestimmt wurden.

Diese Habilitationsschrift besteht größtenteils aus einer Synthese von 24 ausgewählten Publikationen aus vielen Jahren fokussierter Forschung über die geodynamischen, tektonischen und sedimentären Prozesse des pazifischen Kontinentalrandes der Westantarktis.

1 Introduction

1.1 The Pacific realm of West Antarctica

Ranging from the western Antarctic Peninsula to the Ross Sea sector, the southern Pacific realm of West Antarctica (Figure 1) has experienced a diverse tectonic and geological development, which has come under increased attention as it holds the key to understanding one of the most dynamic ice sheets. Due to difficult sea-ice conditions and, therefore, lack of permanent or temporary research stations, the western Bellingshausen Sea and Amundsen Sea region was little explored until the early-1990s, apart from occasional visits by US-American, Russian, Japanese and Norwegian vessels. These visits included early geological sampling from outcrops of coastal areas and nunataks of Marie Byrd Land, Thurston Island, Ellsworth Land and Palmer Land revealing a complex geological history and various phases of past volcanism. Geophysical data and geological samples from the continental shelves, rise and abyssal plain were restricted to a few sites covered with magnetic, single-channel seismics as well as pre-site surveying for the Deep Sea Drilling Project (DSDP) Leg 35 drilling campaign in the Bellingshausen Sea in 1974. This drilling campaign recovered marine sediments from Late Cretaceous and Oligocene times for the first time in this region, although the records remained largely incomplete because of spot coring applied (Hollister & Craddock, 1976).

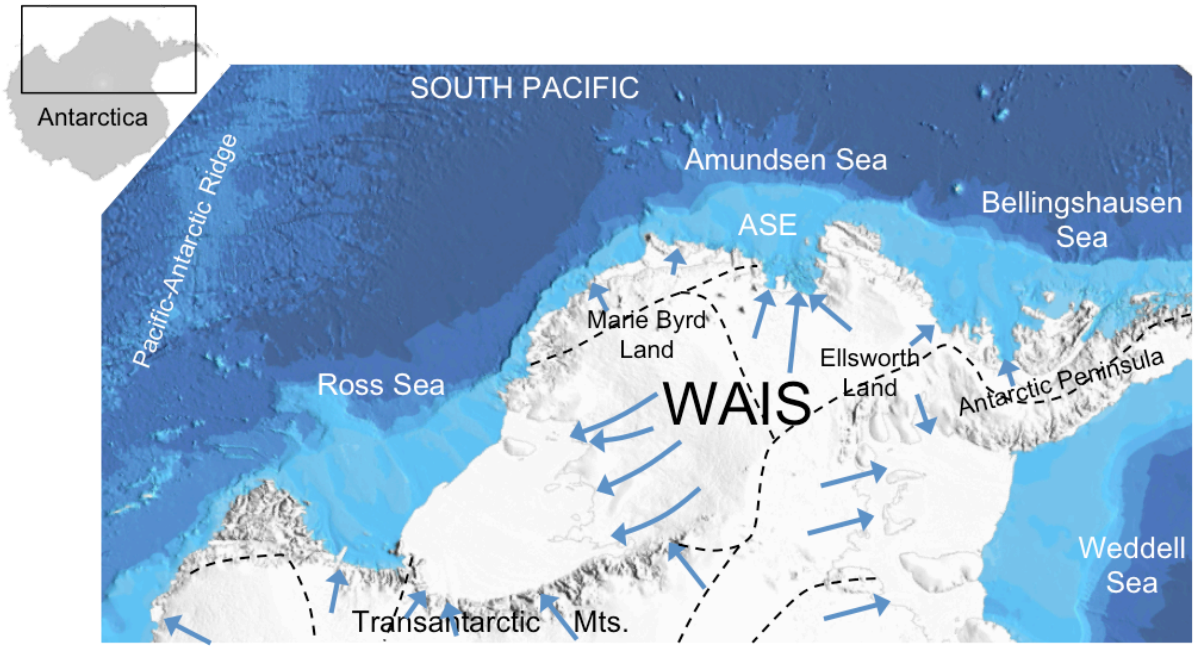

Figure 1. Overview map of West Antarctica and the South Pacific. Bathymetry is from the International Bathymetry Chart of the Southern Ocean (IBCSO) project (Arndt et al., 2013) and topography incl. ice cover is from BEDMAP-2 (Fretwell et al., 2013). Arrows mark main ice flows and hashed lines delineate ice divides. WAIS stands for West Antarctic Ice Sheet and ASE is Amundsen Sea Embayment.

The rising number of marine geoscientific expeditions from the mid-1990s until present have resulted in an advanced knowledge and understanding of the crustal and sedimentary architectures and processes of the West Antarctic margin of the Pacific. Moreover, the sub-ice landscape of sub-marine level beneath central areas

of the West Antarctic Ice Sheet, which seems to be responsible for its dynamic behavior in times of climate change, is recognized as a result of the dominant geodynamic and tectonic processes generating the continent-scale West Antarctic Rift System.

1.2 Geodynamics, tectonics, sedimentation and ice sheet history

Early plate-tectonic reconstructions based on seafloor spreading symmetries and on a few rock type correlations already placed the New Zealand micro-continent opposite West Antarctica as part of the eastern margin of the Gondwana super-continent dominated by the Proto-Pacific subduction. Until the 1980s, the processes and location of the breakup of New Zealand (with its eastern submarine plateaus) from West Antarctica remained enigmatic. It is currently common understanding that the mid-Cretaceous collision of the Hikurangi Plateau with the Chatham Rise of New Zealand ended the subduction at the Proto-Pacific–New Zealand margin and initiated continental rifting, and later breakup, between West Antarctica and the New Zealand micro-continent. However, the question on the exact location, where along the subduction margin the continental rift initiated, has remained unsolved.

Ship-borne and helicopter-borne magnetic measurements along ship-tracks revealed the ages of the oceanic crust in large parts of the southern Pacific. Mapping of isochrones helped identify the transition from a rifted type passive margin of the Amundsen Sea and Marie Byrd Land to a converted convergent-type to non-rifted type passive margin of the Bellingshausen Sea and Antarctic Peninsula. The concept of an independent Bellingshausen Plate verified by geophysical data, indications for an active role of the West Antarctic Rift System and records on magmatic and volcanic processes have resulted in self-consistent models of the tectonic and geodynamic evolution of this region. At the same time, new data from seismic profiling, swath-bathymetric surveying, sub-bottom profiling and sediment coring have revealed sedimentation patterns, geomorphological bedforms and deposition chronologies to constrain dynamic glacial processes from the early glaciation of West Antarctica to the ice retreat since the last glacial period. The current understanding of the region's development shows how tightly linked the dynamics of the largely submarine-based West Antarctic Ice Sheet is with the tectonic history of the continental margin and its hinterland.

A general hypothesis has guided my motivation to focus most of my research activities in this region: *The geodynamic and tectonic evolution of West Antarctica and its margin has controlled the glacial processes from their initiation to the current rapid ice sheet retreat*. My published research work on data analyses and models presented in this thesis lays the basis for testing this hypothesis.

1.3 Expeditions and data acquisition

Most of the research work in this thesis is based on geophysical and geological data collected during five expeditions to the South Pacific and the West Antarctic continental margin with the German research icebreaker *Polarstern* between 1994 and 2010 (Figure 1), in which I participated as head of the geophysics team or as chief-scientist:

During AWI's first visit to the South Pacific on RV *Polarstern* expedition ANT-XI/3 (1994), geophysical reconnaissance surveying and geological probing were conducted along the continental margins of the Bellingshausen Sea and eastern

Amundsen Sea. These data – particularly from extensive seismic profiling – led to a first series of publications on the tectonic and sedimentary architecture of this margin. A three-day immobility of the vessel stuck in heavy sea-ice in the northern Pine Island Bay prevented further work in this relatively unexplored embayment in that season, but ignited my motivation for later expeditions dedicated to this area in particular.

The success of the 1994 expedition prompted a follow-up with expedition ANT-XII/4 (1995) to the central Bellingshausen Sea targeting the suspected Eltanin asteroid impact area, the paleoceanographic conditions of the deep sea and the presumed tectonic lineaments beneath a dominant gravity anomaly system in the western Bellingshausen Sea between the De Gerlache Seamounts and Peter I Island.

Expedition ANT-XVIII/5a (2001) was dedicated to geophysical surveying and sediment sampling in the Bellingshausen Sea and eastern Amundsen Sea in order to obtain sedimentary and paleoceanographic records from the deep sea, to dredge hard-rock samples from the Marie Byrd Seamounts and to target the extent of the Eltanin asteroid impact. Due to failure of the seismic compressor, the seismic program had to be cut short, but managed to record an important linkage profile between the prior existing seismic network of the central Bellingshausen Sea off the Antarctic Peninsula and the few existing seismic lines of the eastern Amundsen Sea. With helicopter-borne magnetic surveying, the mapping of magnetic ocean-spreading anomalies along the continental margin could be extended.

The Amundsen Sea Embayment with its Pine Island Bay was the main destination of expedition ANT-XXIII/4 (2006). Due to ice conditions on the eastern shelf, only the western Amundsen Sea Embayment shelf could be entered first. Later, an opening ice gateway allowed access to the polynyas of the eastern shelf and Pine Island Bay off the Pine Island Glacier, so far a rare opportunity for any research vessel in this area. The ship time on the shelf was used to collect a first set of seismic lines, sediment cores, helicopter-magnetic survey data and to support a rock-sampling and geodetic program on the coastal mainland. Later during the cruise, hard-rock samples were collected from the Marie Byrd Seamounts, sediments were cored and seismic data were recorded from the continental rise of the Amundsen Sea.

Expedition ANT-XXVI/3 (2010) was mainly aimed to collect geoscientific and oceanographic data and samples from the Amundsen Sea Embayment. The cruise schedule with port-calls in Wellington (New Zealand) and Punta Arenas (Chile) opened the first-time opportunity for continuous seismic profiling from the Ross Sea to the eastern Amundsen Sea and, thus, linking both embayments seismo-stratigraphically. Extremely favourable sea-ice conditions allowed extensive seismic surveying, sediment core sampling and oceanographic measurements in the Amundsen Sea Embayment. Helicopter-magnetic surveying complemented and extended the magnetic anomaly grid produced from the 2006 survey. With helicopter support, the land-based rock sample collection for cosmogenic isotope and thermochronological studies and the geodetic measurement program was extended.

Additional data acquired during expeditions with the US research vessel *Nathanial B. Palmer*, the British research ship *James Clark Ross* and the Swedish research icebreaker *Oden* between 1993 and 2010 complemented a number of the published analyses and model interpretation.

2 Synthesis of publications

The results of geodynamic, tectonic, sedimentary and glaciomarine processes and reconstructions are presented in 24 peer-reviewed publications. Arranged into four themes (Chapters 2.1 to 2.4), I summarize and synthesize the main results of these studies. **Citations of own publications, that form the main part of this thesis, are marked with bold letters**. Publications listed in Chapter 5 *Additional References* are cited with normal font letters.

2.1 Geodynamic reconstruction of the South Pacific

The mid-Cretaceous continental margin of East Gondwana, which included present-day West Antarctica and the New Zealand micro-continent, was dominated by the subduction of the proto-Pacific until, at about 100 Ma, the volcanic Hikurangi Plateau collided with the margin north of today's Chatham Rise. In the aftermath of this collisional event, at least three distinct major tectonic activities can be identified to have played a decisive influence on the formation of the West Antarctic margin of the South Pacific (Figure 2).

Subduction lasted until about 97-95 Ma at the Gondwana margin of eastern Marie Byrd Land (Kipf et al., 2012), followed by an early divergence of the Pacific and Antarctic plates which led to rifting and crustal extension between Chatham Rise and the Amundsen Sea Embayment as early as 90 Ma (Larter et al., 2002; **Eagles et al., 2004a**; **Wobbe et al., 2012**). Storey et al. (1999) suggested that a mantle plume may have driven the initial rifting and spreading between West Antarctica and New Zealand. The first phase of crustal extension can be related to capture of part of the Phoenix plate by the Antarctic plate following the collision of the Hikurangi Plateau, and the establishment of a proto-Pacific – Antarctic plate margin in the Bounty Trough and Great South Basin of New Zealand. Rifting possibly continued within the Great South Basin between the Campbell Plateau and the South Island of New Zealand until its abandonment in favour of a new extensional locus to the south, forming the earliest oceanic crust between Campbell Plateau and Marie Byrd Land by 84-83 Ma. Seafloor magnetic anomalies adjacent to Marie Byrd Land near the Pahemo Fracture Zone indicate full-spreading rate during chrons C33–C31 (80–68 Ma) of 60 mm/yr, increasing to 74 mm/yr at C27 (62 Ma), and then dropping to 22 mm/yr by C22 (50 Ma) (**Wobbe et al., 2012**). Spreading rates were lower to the west. This second phase of Pacific–Antarctic extension may have followed the close approach of the Charcot–Pacific ridge to this earlier margin and capture of the Charcot plate by the Antarctic plate (**Eagles et al., 2004a**). The extension, and subsequent separation, of New Zealand and West Antarctica dominate the tectonic signature of the Marie Byrd Land margin and the Amundsen Sea Embayment. West of the Antipodes Fracture Zone, the 145 km wide continent–ocean transition zone (COTZ) of the western Marie Byrd Land sector resembles a typical magma-poor margin (**Gohl, 2008; Wobbe et al., 2012**). Farther east, the COTZ of the eastern Marie Byrd Land sector is even broader and complex with abundant evidence for volcanism (**Gohl, 2008; Wobbe et al., 2012**).

From about 84 Ma, the Bellingshausen Plate (Figure 2) moved independently south of the Pacific and Antarctic Ridge on the southern flank of the Pacific–Antarctic Ridge (**Eagles et al., 2004a,** Eagles et al., 2004b**; Wobbe et al., 2012**). After 80 Ma, the Bellingshausen plate converged with an oceanic part of the Antarctic plate to its east, while its motion simultaneously caused rifting in continental Antarctica to the south.

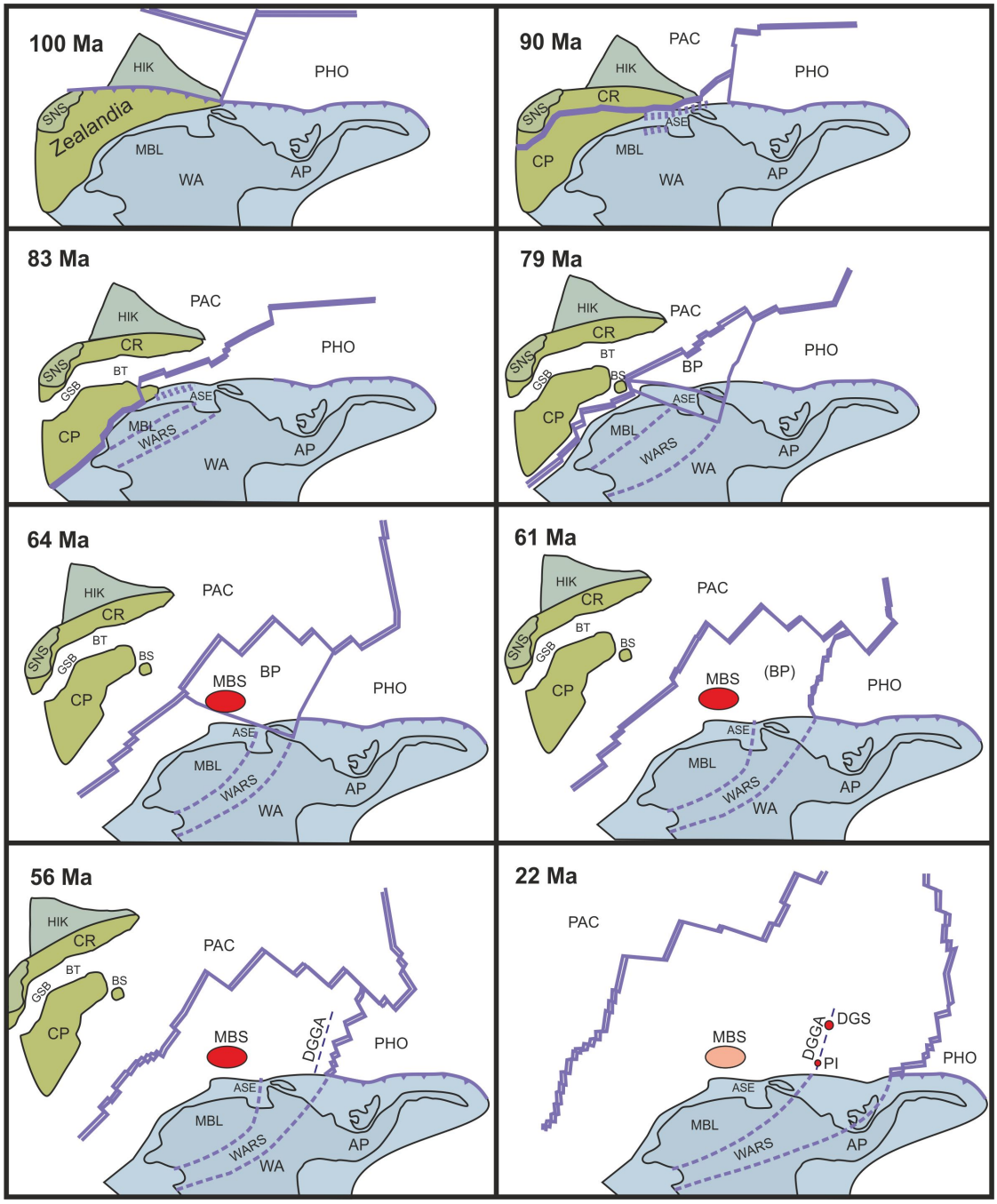

Figure 2. Schematic summary of relevant phases of the reconstructed plate-kinematic development in the South Pacific region off West Antarctica from 100 to 22 Ma, using plate rotation parameters from **Eagles et al. (2004a)**. Illustrated are the collision of Hikurangi Plateau with Chatham Rise of New Zealand at around 100 Ma, the breakup between New Zealand and West Antarctica at 90–80 Ma, the development of the Bellingshausen Plate and the subsequent volcanism (**Kipf et al., 2014**) along the West Antarctic margin. Double lines mark spreading ridge plate boundaries, single solid lines mark other plate boundary types, and dashed lines in West Antarctica illustrate lineaments of the West Antarctic Rift System (**Eagles et al., 2009b; Gohl et al., 2013a**). Abbreviations are: SNS South Island New Zealand, HIK Hikurangi Plateau, CP Campbell Plateau, CR Chatham Rise, GSB Great South Basin, BS Bollons Seamount, BT Bounty Trough, WA West Antarctica, MBL Marie Byrd Land, AP Antarctic Peninsula, ASE Amundsen Sea Embayment, WARS West Antarctic Rift System, PAC Pacific Plate, PHO Phoenix Plate, BP Bellingshausen Plate, MBS Marie Byrd Seamounts (red area marks volcanic activity of the shield phase), DGS De Gerlache Seamounts, PI Peter I Island, DGGA De Gerlache Gravity Anomaly (suture of ridge jump of Phoenix/Bellingshausen plate boundary at about 61 Ma).

Alongside this extensional episode, the eastern margin of the Bellingshausen plate was shortened by up to 200 km of convergence in the north, and by decreasing amounts farther south, along a collision zone that formed by reactivation of a transform fault along the western edge of the part of the Charcot plate that had been inherited by the Antarctic plate. This eastern transpressional boundary of the Bellingshausen Plate lies along the Bellingshausen Gravity Anomaly lineament (Gohl et al., 1997; **Eagles et al., 2004a**). Around 61 Ma, the Bellingshausen plate ceased to have any independent rotation when a major plate reorganisation occurred in the South Pacific (e.g. Larter et al., 2002; **Eagles et al., 2004a;** Eagles et al., 2004b). The Pacific–Antarctic plate system inherited the set of long offset transform faults from the Pacific–Bellingshausen system, and spreading changed direction and decreased in rate soon afterwards. The southern sector of the Pacific–Antarctic ridge saw an increase in the number of transform faults that may be related to the spreading rate decrease. The former Bellingshausen Plate's western boundary passes through the today's region of the Marie Byrd Seamounts, north of the Amundsen Sea Embayment. Although a discrete southern plate boundary has been depicted running from the seamounts onto the shelf and mainland (**Eagles et al., 2004a;** Eagles et al., 2004b), its true nature – possibly a distributed boundary zone – is still poorly identified.

Analyses of volcanic rocks from the Marie Byrd Seamounts yield formation ages of 65 to 56 Ma which is well after the generation of the Pacific-Antarctic Ridge at this location. In **Kipf et al. (2014)** we propose that this HIMU material initially accreted to the base of continental lithosphere during the pre-rifting stage of Marie Byrd Land/New Zealand in order to explain the observed intraplate volcanism in the Amundsen Sea in the absence of a long-lived hotspot. Continental insulation flow may be the most plausible mechanism to transfer the sub-continental accreted plume material into the shallow oceanic mantle. Crustal extension at the southern Bellingshausen Plate boundary may have triggered the adiabatic rise of this material to form the Marie Byrd Seamounts (**Kipf et al., 2014**). Other isolated seamounts in the southernmost Pacific are most likely related to preserved zones of lithospheric weakness as we propose for the De Gerlache Seamounts and Peter I Island (Figure 1) along the De Gerlache Gravity Anomaly (Hagen et al., 1998; Hagedorn et al., 2007; **Kipf et al., 2014**).

The later plate-kinematic development of the South Pacific oceanic crust in this region was dominated by seafloor spreading at the Pacific–Antarctic and Antarctic–Phoenix ridges and the progressive subduction of the Phoenix plate beneath the western Ellsworth Land and Antarctic Peninsula margins east of the Bellingshausen Gravity Anomaly (e.g. Larter et al., 2002; **Gohl, 2008** and refs. therein; **Eagles et al., 2009a**). Segments of spreading centres forming at the trailing edges of the Phoenix plate periodically collided with the subduction zone along the Antarctic Peninsula, resulting in the partial destruction of the Antarctic–Phoenix Ridge, which ceased to operate shortly before its north-easternmost three segments could collide with the Antarctic margin (Figure 2). After these collisions, slab windows should have formed beneath the margin of the Antarctic Peninsula, which may explain the occurrences of alkaline volcanism (**Eagles et al., 2009a**).

2.2 Tectonics of the continental margin of West Antarctica and the West Antarctic Rift System

A consecutive series of convergent and divergent processes dominate the present tectonic signature of the Pacific continental margin of West Antarctica (Figure 2). At

least three main phases of tectonic deformation occurred along the Marie Byrd Land and western Ellsworth Land/Thurston Island margin, consisting of (1) distributed rifting events parallel to the continental breakup front, (2) the influence of the Bellingshausen Plate motion with a southern plate boundary through the Marie Byrd Seamount province and the Amundsen Sea Embayment, and (3) activities of early branches of the eastern West Antarctic Rift System.

The rifted continental margin of West Antarctica exhibits a stunning diversity in crustal characteristics as revealed by our geophysical data. In **Wobbe et al. (2012)**, we can show that its style varies from a narrow rifted, most likely magma-poor (non-volcanic) margin along western and central Marie Byrd Land. The margin nature changes off eastern Marie Byrd Land and off the Amundsen Sea Embayment such that the shelf widens, the continental crust is largely extended and magmatism was abundant. Seismic and gravity data reveal that the crust is up to 29 km thick beneath the inner Amundsen Sea Embayment shelf and thins to 10-14 km at the continental rise. A seismic high-velocity layer at the base of the lower crust of the shelf indicates a margin-wide process of magmatic underplating whose thickness varies up to a maximum of 10 km (**Kalberg and Gohl, 2014**). The present data do not allow being specific about the cause for this underplating, which can be either a result from the initial continental breakup process, or from hot mantle upwelling hypothesized as cause for the Marie Byrd Land uplift (e.g. LeMasurier and Landis, 1996; Sieminski et al., 2003), or from magmatism associated with the Marie Byrd Seamount province (**Kipf et al., 2014**). A superposition of any of these processes seems to be likely.

The location of Pine Island Bay in the Amundsen Sea Embayment (Figure 1) has led several researchers to suggest that it hosts a major crustal boundary between the Marie Byrd Land block to the west and the Thurston Island/Ellsworth Land blocks to the east. These blocks are suggested to have moved with respect to each other during the Late Cretaceous New Zealand – West Antarctic separation and perhaps also in early Mesozoic or Paleozoic times (e.g. Dalziel and Elliot, 1982; Storey, 1991; Grunow et al., 1991). However, direct geophysical or geological evidence of the presence of such a boundary is still missing until today.

Instead, conceptual models inferred that Pine Island Bay and the eastern Amundsen Sea Embayment host faults and basins of the West Antarctic Rift System (Dalziel, 2006). In **Müller et al. (2007)** and **Eagles et al. (2009b)**, we apply plate-kinematic rotations between East and West Antarctica and demonstrate how, at times between 48 and 26 Ma, the West Antarctic Rift System east of its Ross Sea domain operated in either dextral strike-slip or extensional motion through the region to the south and east of the Amundsen Sea Embayment, connecting eventually to a Pacific-Phoenix-East Antarctic triple junction via the Byrd Subglacial Basin and the Bentley Subglacial Trench of Marie Byrd Land (Figure 3). There are indications for an early West Antarctic Rift System extension in western Marie Byrd Land in the mid-Cretaceous (e.g., McFadden et al., 2010), but its eastern continuation is less well understood. Offshore geophysical data (**Gohl et al., 2007, 2013a,b**) reveal that the eastern Amundsen Sea Embayment shelf and its Pine Island Bay host tectonic lineaments and sedimentary basins presumably formed by the West Antarctic Rift System. We infer from potential field and seismic data analyses that an eastern arm of an early manifestation of the rift exists in the north-south striking zone of thinned crust in Pine Island Bay (**Gohl et al., 2013a,b**). Our projected north-south strike direction of a rift branch in Pine Island Bay differs from an east-west directed rift identified for the narrow basin underlying the Pine Island Glacier by Jordan et al. (2010), but it is likely that a distributed system of offsetting faults accommodate the

regional stress regime. The setting of basement troughs and quasi-linear topographic trends, observed from the BEDMAP2 subglacial topographic map of Antarctica (Fretwell et al., 2013), infer such a hypothesis. My concept and model of a distributed rift axis system extending from the Amundsen Sea Embayment to the western margin of the southern Antarctic Peninsula is also consistent with Bingham et al.'s (2012) interpreted association of the Ferrigno Rift, which is inland of Eltanin Bay of the southern Bellingshausen Sea, with the West Antarctic Rift System (Figure 3).

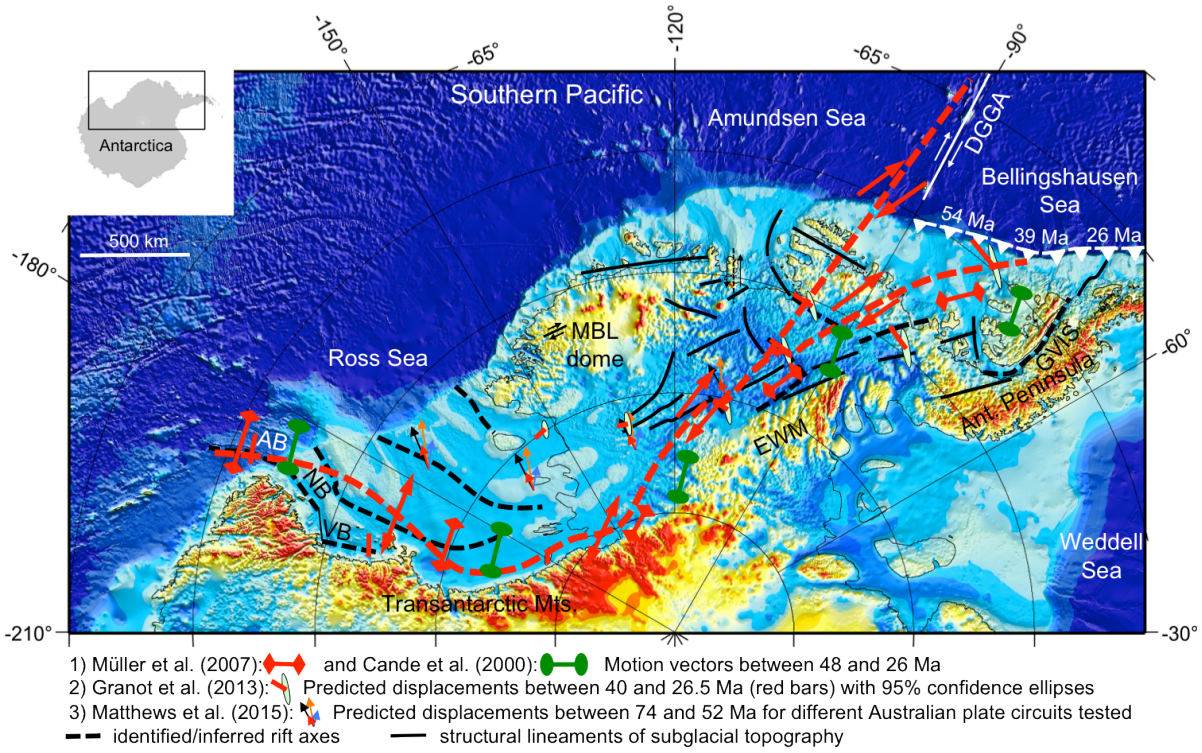

Figure 3. Tectonic outline of the West Antarctica Rift System with identified subglacial rift valleys (black hashed lines), other structural basement lineaments (black solid lines) and predicted plate motion vectors (symbols and references are noted below map) and inferred East-West Antarctic plate boundary (red hashed line). Present subglacial topography is from BEDMAP-2 (Fretwell et al., 2013) and bathymetry is from IBCSO (Arndt et al., 2013). Blue and blue-greenish colors denoting areas below present sea level.

Current ice flow pattern overlain on the recently updated bedrock topography (Fretwell et al., 2013) of West Antarctica and the pattern of deeply incised troughs of the Amundsen Sea and Bellingshausen Sea continental shelves largely linked to tectonic lineaments, demonstrate how glacial flow directions are closely linked to a pre-conditioned system of rift flanks and tectonically controlled subglacial valleys. If the rifts were active in the Neogene, enhanced geothermal heat flux linked to crustal extension and magma leakage along fault zones would probably occur beneath parts of the West Antarctic Ice Sheet. This would lead to excess generation of subglacial meltwater, which in turn would lubricate the bedrock, accelerate ice flow and increase ice sheet thinning in interglacial and particular warm periods.

2.3 Sediment transport and deposition along the Pacific continental margin of West Antarctica

Numerous seismic profiles and other geophysical data were collected by AWI to build seismostratigraphic, glacial-marine sedimentation and paleo-ocean current

models of the continental rise and shelf of the Pacific margin of West Antarctica (e.g., **Scheuer et al., 2006a,b;** Scheuer et al., 2006c; **Uenzelmann-Neben et al., 2007**; **Weigelt et al., 2009**; **Uenzelmann-Neben and Gohl, 2012, 2014**; **Hochmuth and Gohl, 2013**; **Gohl et al., 2013b;** Lindeque et al., submitted). Sediment transport and deposition processes are strongly affected by periods of various glacial activities since the initial onset of Antarctic glaciation. Since ice sheets first advanced onto the continental shelves around West Antarctica, alternations of glacial and interglacial periods have had a major influence on the sediment supply across the shelf and into the deep sea. The patterns of deposition of late Cenozoic sediments along the slope and rise of the West Antarctic continental margin reflect interaction between the effects of ice sheet fluctuations, mass transport processes and bottom currents. However, the West Antarctic margin exhibits strong variations in sedimentation pattern and processes between its South Pacific sectors. For instance, the high sediment deposition rate on the Bellingshausen Sea continental rise implies an increase of sediment supply to the rise due to frequent advances of grounded ice on the shelf in the Pliocene and Quaternary, which is contrary to a decrease of the sediment deposition rate since Pliocene times on other sites of the margin (**Scheuer et al., 2006a**).

The seismic sediment record of the Amundsen Sea continental rise provides insight into the sedimentation processes from pre-glacial to glacial times, with indications for varying ocean-bottom circulation, early ice sheet growth and intensification towards the present icehouse regime. Key seismic shorizons reveal a remarkably continuous sedimentation record from the Ross Sea shelf to the rise and farther along the West Antarctic margin to the Amundsen Sea and Bellingshausen Sea. Seismic units constitute a Cretaceous to Eocene pre-glacial sequence (79-34 Ma), an Eocene to mid-Miocene transitional sequence (34-15.5 Ma), and a mid-Miocene to Quaternary full glacial sequence (15.5-0 Ma). The top pre-glacial boundary horizon correlates with a dominant unconformity of the Ross Sea shelf and is interpreted as the signature of first arrivals of grounded ice on the continental shelves. The top transitional boundary is interpreted as the onset of the full-glacial regime with intensified ice sheet advances onto the outer shelves in the Oligocene and early Miocene. The central-western Amundsen Sea continental rise basin contains up to 4 km thick sediments in its center near the Endeavour Fracture Zone. Seismic facies geometry analysis suggests Paleocene–Eocene bottom-current activity, late Eocene shelf grounding of the West Antarctic Ice Sheet, and no apparent difference in the deep-sea sediment transport processes or temporal shift in deposition between the Amundsen Sea and Ross Sea (Lindeque et al., submitted).

Sediment drifts or contourite features are often associated with an intensification of ocean-bottom current activity (e.g. Uenzelmann-Neben, 2006; Rebesco et al., 2014). Such drift bodies are abundant along the continental rise of West Antarctica. Drifts deposits from Eocene-Oligocene times are observed for the eastern Amundsen Sea rise (Figure 4), indicating early seasonal sea-ice generation even before the early Miocene onset of major Antarctic glaciation with ice grounded across parts of the shelf at this part of the continental margin (**Uenzelmann-Neben & Gohl, 2012, 2014**). In glacial times, deposition centers shifted between different loci on the rise due to changes in major ice-stream directions and ice-flow intensities across the Amundsen Sea Embayment shelf (**Uenzelmann-Neben & Gohl, 2014**).

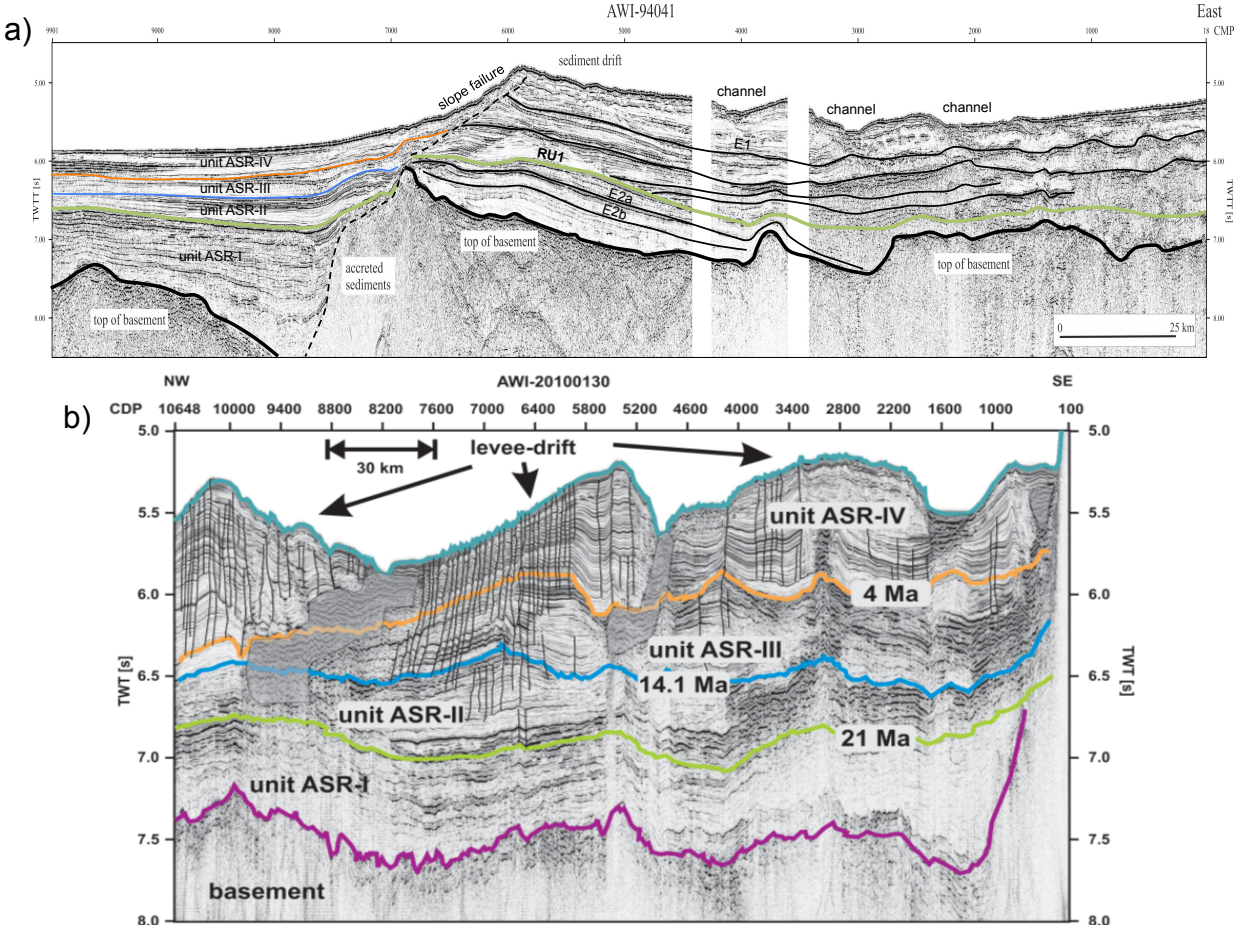

Figure 4. Examples of interpreted seismic records showing distinct reflectivity pattern and unconformities that are related to the intensification of glacially dominated sediment transport and deposition periods in the Miocene and Plio/Pleistocene. A major tectonic suture the western Bellingshausen Sea is the likely cause that a giant sediment drift (a) was formed at this location. Sediments west of it relate to sequences identified from the eastern Amundsen Sea continental rise (b) (Uenzelmann-Neben & Gohl, 2014). East of the suture, the sedimentation pattern changes and horizons can be correlated to the ODP Leg 178 sites off the western Antarctic Peninsula. Unconformity RU1 may be related to the basement uplift of this suture.

Despite the lack of any drill site in the Amundsen Sea, sedimentation processes in the pre-glacial to glacial transition and those by glacial grounded advance and retreat periods seem to have occurred in an almost simultaneous fashion in when comparing seismic records from the Ross Sea and Amundsen Sea embayments, the two major outlet basins of the West Antarctic Ice Sheet (**Gohl et al., 2013b**). However, it remains unclear whether timing is the same, or whether glacial retreat periods vary between the embayments. The few presently remaining narrow ice shelves of the Amundsen Sea Embayment indicate that this sector is prone to longer ice retreat periods than other Antarctic shelves, possibly a persistent effect of ocean and atmospheric circulation patterns in the southern Pacific. This hypothesis, however, needs to be tested by analyses of suitable drill cores.

2.4 Glaciomarine processes on the shelf of the Amundsen Sea Embayment and their relationship to past ice sheet dynamics

The reconstruction of the dynamic history of Antarctic Ice Sheet expansion and retreat since the onset of Southern Hemisphere glaciation improves our understanding of ice sheet growth and melting processes and thus predictions of future ice sheet behavior. Due to the fact that the West Antarctic Ice Sheet (WAIS) has a lower elevation than the East Antarctic Ice Sheet and most of its base is grounded below sea level, the WAIS is likely to have been more sensitive to changes in atmospheric and oceanographic conditions (e.g. Joughin and Alley, 2011). The WAIS volume corresponds to an equivalent of 3-5 m eustatic sea level change (Bamber et al., 2009; Fretwell et al., 2013), and about one third of it is stored in drainage basins that discharge through outlet glaciers onto the Amundsen Sea Embayment. The largest drainage systems are those of the Pine Island and Thwaites glaciers, which are known for their current flow acceleration, fast retreat, rapid thinning and high basal melt rates of floating ice at their termini that exceed those of any other Antarctic outlet glacier outside the Antarctic Peninsula (e.g. Rignot et al., 2011; Pritchard et al., 2012; Joughin et al., 2012). The incursion of warm Circum-Polar Deep-Water (CDW) into the deeply incised glacial troughs of the shelves has been recognized as the major mechanism for subglacial melt (Thoma et al., 2008; Joughin et al., 2012). The important question is how the WAIS has behaved in times when the climatic conditions were close or similar as observed today or in the near future.

Past expansion and retreat of grounded and floating ice across the continental shelf of the Amundsen Sea Embayment must have left signals and traces of glacial sediment accumulation, transport and erosion. Thus, our studies of the sedimentary architecture and characteristics of the Amundsen Sea Embayment margin provides clues of past ice sheet advance-retreat cycles and help improve constraints for paleo-ice dynamic models of the WAIS since early glacial periods (e.g. **Gohl et al., 2013b**). The Amundsen Sea Embayment is our preferred study area for understanding the past West Antarctic Ice Sheet dynamics, because ice sheet discharge into this embayment is entirely sourced from the WAIS and unaffected from the dynamics of other ice sheets.

Observations of sub- and proglacial bedforms in multi-beam swath bathymetry surveys, such as mega-scale lineations and grounding zone wedges, indicate that grounded ice expanded onto the middle to outer shelf during the last glacial maximum (Lowe and Anderson, 2002; Dowdeswell et al., 2006; Evans et al., 2006; **Larter et al., 2009,** 2014; Graham et al., 2009, 2010; Jakobsson et al., 2012; Klages et al., 2013, 2014, 2015). The retreat of the ice sheet from the Amundsen Sea Embayment shelf since the last glacial maximum is documented in both these swath-bathymetric records and sedimentary facies sequences recovered in cores (e.g. Hillenbrand et al., 2010, 2013; Jakobsson et al., 2011; Kirshner et al. 2012; **Nitsche et al., 2007, 2013;** Nitsche et al., 2015a,b**)** and is consistent with results from cosmogenic exposure dating studies (Johnson et al., 2008, 2014; Lindow et al., 2014). According to these studies, most of the grounded ice had retreated to the inner shelf already by the early Holocene.

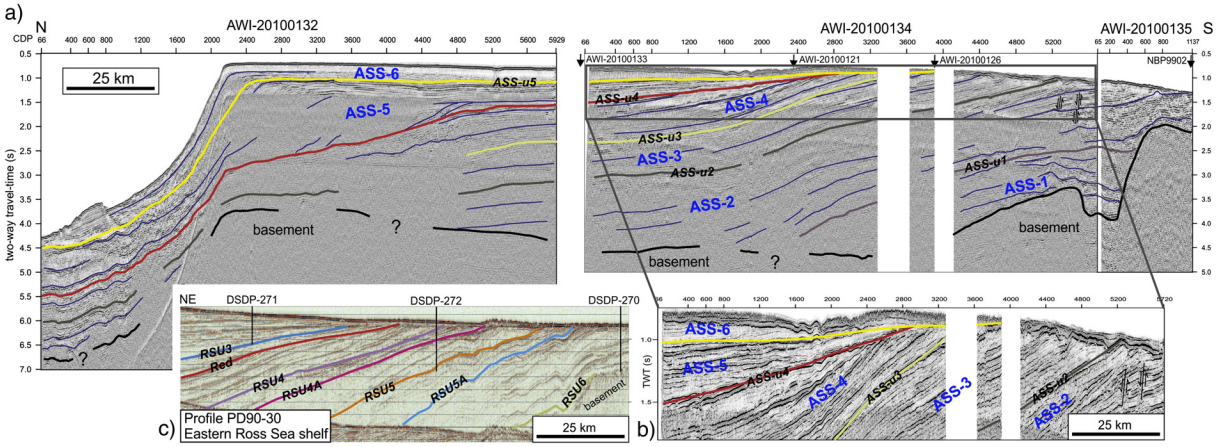

Figure 5. Example of glaciated shelf sequence by seismic imaging. The image (a) is from the eastern Amundsen Sea Embayment shelf and shows glacially dominated stacked layers on top of numerous truncational unconformities generated by advancing grounded ice. (b) illustrates a segment of this seismic record that corresponds surprisingly well in terms of seismic characteristics and unconformities with a seismic record (c) from the eastern Ross Sea shelf where strata was drilled and dated by DSDP Leg 28 (e.g. De Santis et al., 1999). By jump correlation to Ross Sea shelf records, seismic units of the Amundsen Sea shelf are Early Cretaceous (?) for ASS-1, Late Cretaceous to Oligocene (?) for ASS-1, Early/Middle Miocene for ASS-3, Middle Miocene for ASS-4, late Miocene to Early Pliocene for ASS-5, and Plio/Pleistocene for ASS-6. ASS-u1 to ASS-u5 are major unconformities.

The earliest recorded multi-channel seismic reflection data from the Amundsen Sea Embayment show that at 104° W the outer shelf and slope sediments have undergone both progradational and aggradational deposition probably since the Middle Miocene (**Nitsche et al., 2000**). Aggradation dominated the strata geometry in younger stages. The network of seismic profiles reveal oceanward inclined sediment sequences on the middle shelf north of bedrock cropping out on the inner shelf (Figure 5) (Lowe and Anderson, 2002; **Gohl et al., 2013b**). The dipping strata typical for Antarctic shelves are possibly of Cretaceous to Miocene age and buried by aggradational, less consolidated strata of supposedly Pliocene-Pleistocene age (**Gohl et al., 2013b**). Several unconformities separate the dipping strata and represent phases of subglacial erosion. While most of the inner shelf of Pine Island Bay is void of major sedimentary cover, as observed in seismic and acoustic subbottom profiles (Lowe and Anderson, 2002; **Gohl et al., 2013b; Nitsche et al., 2013**) and inferred from magnetic data (**Gohl et al., 2013a**), a few small and shallow basins are observed close to its eastern shore (Uenzelmann-Neben et al., 2007) and close to the front of Pine Island Glacier (**Nitsche et al., 2013**). Oceanward dipping mid-shelf strata north of outcropping basement are observed in seismic data from the Dotson-Getz Trough collected in 1999 and 2006 (Graham et al., 2009; **Weigelt et al., 2009;** Weigelt et al., 2012) and exhibit alternating sequences of low and high reflectivity, which **Weigelt et al. (2009)** interpret as episodes of major glacial advances and retreat in the Miocene.

In **Gohl et al. (2013b)** we showed that at least 4 km of pre-glacial strata have been eroded from the present inner shelf and coastal hinterland by glacial processes. Six major sedimentary units separated by five major erosional unconformities are distinguished from bottom to top on the Amundsen Sea Embayment shelf (Figure 5). At least one unconformity results from a major truncational event by glacial advance to the middle and outer shelf, which was followed by several episodes of glacial advance and retreat as observed from smaller-scale truncational unconformities. Some of the eroded sediments were deposited as a progradional wedge that extends

the outer shelf by 25 to 65 km oceanward of the pre-glacial shelf-break (**Hochmuth and Gohl, 2013; Gohl et al., 2013b**). We compare the observed seismic characteristics with those of other Antarctic shelf sequences and assign stratigraphic ages from Early Cretaceous to Pleistocene/Holocene only by seismic jump correlation due to lacking drill information. Buried grounding zone wedges in the upper sedimentary unit on the outer shelf suggest pronounced warming phases and ice sheet retreats during the early Pliocene, as observed for the Ross Sea shelf and predicted by palaeo-ice sheet models (**Gohl et al., 2013a**), Our data also reveal that on the middle and outer shelf the flow-path of the Pine Island-Thwaites paleo-ice stream system has remained stationary in the central Pine Island Trough since the earliest glacial advances, which is different from the Ross Sea shelf where glacial troughs shifted more dynamically.

3 Outlook and perspectives

Although an enormous progress has been made in the last years in our understanding of the geodynamic, tectonic, sedimentary and glacial development of West Antarctica, many scientific questions and challenges remain. Some of these are summarized in the following:

- Was the initial separation between New Zealand and West Antarctica accompanied by crustal hyper-extension of the Chatham Rise and Amundsen Sea Embayment conjugates?
- Has the West Antarctic Rift System developed as a continuation of the separation between New Zealand and Antarctica? And what has sustained such enduring mantle processes from the Cretaceous to the present?
- What is the extent and intensity of any sub-glacial volcanic activity in West Antarctica?
- What were the environmental and climatic conditions of West Antarctica in the Cretaceous to Eocene greenhouse period?
- Was ice sheet expansion related to crustal uplift in Marie Byrd Land?
- When did the WAIS first expand onto the continental shelves?
- How did the WAIS respond the last times when Earth's atmosphere contained more than 400 ppm CO_2 and when global temperature was similar or higher than today? Did the WAIS completely or partly collapse, and what was its contribution to sea-level change?
- How have the Antarctic Circumpolar Current and Circumpolar Deep Water incursions onto the continental shelf controlled the stability of the marine ice sheet margins?

Some of the scientific questions are currently being addressed in publications of my PhD students that have been submitted and are still in review, or are being prepared for submission. In Wobbe et al. (submitted), we study anomalies in the derived residual bathymetry of the southern Pacific and along the West Antarctic margin with implications for dynamic topography effects by mantle processes. The uplift of Marie Byrd Land is investigated using seismic data and gravity modelling paired with thermochronological constraints from fission-track data (Kalberg et al., in preparation; collaboration with C. Spiegel of Univ. Bremen). Kalberg and Gohl (in preparation) reveal details of the basement tectonics and crustal characteristics of

the Amundsen Sea shelf by integrating gravity, magnetic and seismic data and models. Continuous seismic data between the Ross Sea and Amundsen Sea embayments, acquired during RV *Polarstern* expedition ANT-XXVI/3 in 2010, enable Lindeque et al. (two papers in preparation) to correlate the main pre-glacial, transitional and full glacial sedimentary units over a large area along the West Antarctic margin and between the two main glacial outflow embayments. The result of this is a set of sediment thickness grids and a characterisation of the major glacial deposition centres.

Major questions and challenges will also be addressed in upcoming expeditions and planned future projects:

- An RV *Sonne* cruise (SO-246) to the eastern margin of Chatham Rise (New Zealand) is scheduled for early 2016 to investigate the marginal crust of the Rise, which is conjugate to the Amundsen Sea margin of West Antarctica, using deep crustal seismic, magnetic and gravity surveying. A petrological sampling program is conducted by our collaboration partners K. Hoernle and R. Werner of GEOMAR.

- An RV *Polarstern* expedition is scheduled for February and March 2017 (postponed from early 2015), during which we – in collaboration with MARUM and the British Antarctic Survey – will utilise the *MeBo* seabed drilling system of MARUM to drill cores from up to 70 m long holes along a transect on the Amundsen Sea Embayment shelf and in Pine Island Bay. The objectives are to recover sediments from presumably Late Cretaceous to Quaternary ages that will help constrain the palaeo-environmental and glacial history of this central part of West Antarctica. We also plan to conduct a series of temperature gradient measurements in sediments to derive geothermal heat-flow in collaboration with H. Villinger and N. Kaul of Univ. of Bremen.

- Drilling information is rare along the West Antarctic margin and the Southern Pacific, which is the reason for some of the large uncertainties in stratigraphic ages, paleoenvironmental conditions and paleo-ice sheet dynamics. With IODP proposal 839-Full (by Gohl et al.), we argued for a strong case to conduct deep drilling in the Amundsen Sea Embayment. This proposal has been exceptionally well evaluated with an '*excellent rating*' by the IODP Science Evaluation Panel and external reviewers, and is now forwarded to the Joides Resolution Facility Board for possible scheduling. Likewise, IODP proposal 732-Full2 (by Channel et al. incl. Gohl), aiming to drill into the sediment drifts of the Bellingshausen Sea rise, is also at the JR Facility Board for possible scheduling. In the Ross Sea, the IODP proposal 751-Full2 (McKay et al.) is still being reviewed at this stage, and a possible re-submission of an ANDRILL Coulman High proposal is likely. Drilling targets of all these proposals would generate samples and data from ice-proximal to ice-distal locations that will provide invaluable constraints on reconstructing the West Antarctic Ice Sheet history at varies time scales and resolution.

- Planned future projects include seismic and seismological studies of the West Antarctic Rift System in the western Ross Sea in collaboration with the Korean Polar Research Institute (KOPRI), and new geophysical surveys along the Bellingshausen Sea margin and Eltanin Bay to provide data for tectonic as well as glacio-marine sedimentation analysis in this part of West Antarctica.

4 Acknowledgments

This project and thesis would not have been possible without the opportunities for collecting geophysical data and geological samples from the West Antarctic continental margin and the South Pacific. I want to sincerely thank the masters and crews of RV *Polarstern* expeditions ANT-XI/3, ANT-XII/4, ANT-XVIII/5a, ANT-XXIII/4 and ANT-XXVI/3 as well as the scientific teams who joined me on these expeditions. Gratefully acknowledged are also the masters, crews, chief-scientists and science teams of various other expeditions to the Bellingshausen Sea and Amundsen Sea with RV *Nathaniel B. Palmer* (USA), RRS *James Clark Ross* (UK) and IB *Oden* (Sweden). Some of the data and samples collected during these expeditions were greatly beneficial with analyses having been used in some publications of this thesis.

I highly appreciate the support of my colleagues in the Department of Geosciences at AWI, my Diploma/MSc students, doctoral candidates and postdocs of the last 20 years, and my collaboration partner in various aspects of the project. Of my colleagues in the Geophysics Section at AWI, I want to thank in particular Heinz Miller who initially brought me to the West Antarctic margin and into the fascinating region of Pine Island Bay on my first *Polarstern* cruise in 1994, Wilfried Jokat who supported me in continuing with this project and with always challenging and fruitful discussions, and Gabriele Uenzelmann-Neben whose excellent understanding of seismo-stratigraphy led to various joint expeditions and publications. Rainer Gersonde and Gerhard Kuhn from the Marine Geology Section at AWI are gratefully acknowledged for their support in joint expeditions and projects over many years. Without many of my former and current diploma/MSc and doctoral students, namely Frank Nitsche, Carsten Scheuer, Jan Grobys, Nicole Grobys, Astrid Denk, Katharina Hochmuth, Florian Wobbe, Ansa Lindeque and Thomas Kalberg, as well as my former postdocs Graeme Eagles and Estella Weigelt, many of the publications in this thesis would not have been possible. I thank all of you for the great and productive time! A large number of collaboration partner helped producing many of the results in these papers. I want to name in particular Robert Larter, Claus-Dieter Hillenbrand, Alistair Graham and James Smith from the British Antarctic Survey (UK), Frank Nitsche from Lamont Doherty Earth Observatory (USA), Dietmar Müller from University of Sydney (Australia), Bryan Davy and Rupert Sutherland from GNS Science (New Zealand), and Dmitry Teterin and Gleb Udintsev from Vernadsky Institute of Geochemistry (Russia).

I also would like to thank the Department of Geosciences (FB 5) of the University of Bremen for giving me the opportunity to become engaged in teaching. I have been enjoying this occasional change from the research routine.

Since my early days at AWI, my wife Angelika Barthel has had to put up with me going on long polar and non-polar expeditions, and I want to thank her for her understanding, support and love.

5 Additional references
(incl. other own papers not included as part of this thesis)

The list includes references cited in Chapters 1 to 3 in addition to those included as part of this thesis.

Asterisks * mark 25 cited own papers of which I am first author or co-author and which are relevant to the project but are not included as part of this thesis, because the results in these papers are better presented in those papers that are part of this thesis, or in which my contribution is rather minor (exception is submitted manuscript by Lindeque et al.).

Arndt, J. E., Schenke, H.-W., Jakobsson, M., Nitsche, F.O., Buys, G., Goleby, B., Rebesco, M., Bohoyo, F., Hong, J.K., Black, J., Greku, R., Udintsev, G., Barrios, F., Reynoso-Peralta, W., Taisei, M., Wigley, R. (2013). The International Bathymetric Chart of the Southern Ocean (IBCSO) Version 1.0—A new bathymetric compilation covering circum-Antarctic waters. *Geophysical Research Letters, 40*, 3111–3117, doi:10.1002/grl.50413.

Bamber, J.L., Riva, R.E.M., Vermeersen, B.L.A., LeBrocq, A.M. (2009). Reassessment of the potential sea-level rise from a collapse of the West Antarctic Ice Sheet. *Science*, 324, 901-903, doi:10.1126/science.1169335.

Bingham, R.G., Ferraccioli, F., King, E.C., Larter, R.D., Pritchard, H.D., Smith, A.M., Vaughan, D.G. (2012). Inland thinning of West Antarctic Ice Sheet steered along subglacial rifts. *Nature*, 487, 468-471, doi:10.1038/nature11292.

Cande S.C., Stock, J.M., Müller, R.D., Ishihara T. (2000). Cenozoic motion between East and West Antarctica. *Nature*, 404, 145-150.

*Cunningham, A.P., Larter, R.D., Barker, P.F., **Gohl, K.**, Nitsche, F.O. (2002). Tectonic evolution of the Pacific margin of Antarctica – 2. Structure of Late Cretaceous – early Tertiary plate boundaries in the Bellingshausen Sea from seismic reflection and gravity data. *Journal of Geophysical Res*earch, *107(B12)*, 2346, doi:10.1029/2002JB001897.

Dalziel, I.W.D. (2006). On the extent of the active West Antarctic rift system. In: Siddoway, C.S., Ricci, C.A. (Eds.), *Proceedings of Workshop on Frontiers and Opportunities in Antarctic Geosciences*, *Terra Antartica Reports 12*, Terra Antartica Publications, Siena, Italy, pp. 193–202.

Dalziel, I.W.D., Elliot, D.H. (1982). West Antarctica: problem child of Gondwanaland. *Tectonics*, *1*, 3-19.

De Santis, L., Prato, S., Brancolini, G., Lovo, M., Torelli, L. (1999). The Eastern Ross Sea continental shelf during the Cenozoic: implications for the West Antarctic ice sheet development. *Global and Planetary Change*, 23, 173-196.

Dowdeswell, J.A., Cofaigh, C.Ó., Anderson, J.B. (2006). Morphology and sedimentary processes on the continental slope off Pine Island Bay, Amundsen Sea, West Antarctica. *Geological Society of America Bulletin*, 118, 606–619.

*Eagles, G., **Gohl, K.**, Larter, R.D. (2004b). Life of the Bellingshausen plate. *Geophys. Res. Lett., 31*, L07603, doi:10.1029/2003GL019127.

Evans, J., Dowdeswell, J.A., Cofaigh, C.Ó., Benham, T.J., Anderson, J.B. (2006). Extent and dynamics of the West Antarctic Ice Sheet on the outer continental shelf of Pine Island Bay during the last glaciation. *Marine Geology*, 230, 53–70.

Fretwell, P. & 59 co-authors (2013). Bedmap2: improved ice bed, surface and thickness datasets for Antarctica. *The Cryosphere*, 7, 375-393.

*__Gohl, K.__, Nitsche, F., Miller, H. (1997). Seismic and gravity data reveal Tertiary interplate subduction in the Bellingshausen Sea, southeast Pacific, *Geology, 25*, 371-374.

*__Gohl, K.__, Nitsche, F., Vanneste, K., Miller, H., Fechner, N., Oszko, L., Hübscher, C., Weigelt, E., Lambrecht, A. (1997). Tectonic and sedimentary architecture of the Bellingshausen and Amundsen Sea Basins, SE Pacific, by seismic profiling. In: *The Antarctic Region: Geological Evolution and Processes*, by Ricci, C.A. (ed.), p. 719-723, Terra Antartica Publication, Siena.

*Graham, A.G.C., Larter, R.D., **Gohl, K.**, Hillenbrand, C.-D., Smith, J.A., Kuhn, G. (2009). Bedform signature of a West Antarctic palaeo-ice stream reveals a multi-temporal record of flow and substrate control. *Quaternary Science Reviews*, 28, 2774-2793, doi:10.1016/j.quascirev.2009.07.003.

*Graham, A.G.C., Larter, R.D., **Gohl, K.**, Dowdeswell, J.A., Hillenbrand, C.D., Smith, J.A., Evans, J., Kuhn, G. (2010). Flow and retreat of the Late Quaternary Pine Island-Thwaites palaeo-ice stream, West Antarctica; *Journal of Geophysical Research – Earth Surfaces*, 115, F03025, doi:10.1029/2009JF001482.

Granot, R., Cande, S., Stock, J., Damaske, D. (2013). Revised Eocene-Oligocene kinematics for the West Antarctic rift system. *Geophys. Res. Lett.*, 40, doi:10.1029/2012GL054181.

Grunow, A.M., Kent, D.V., Dalziel, I.W.D. (1991). New paleomagnetic data from Thurston Island: Implications for the tectonics of West Antarctica and Weddell Sea opening. *Journal of Geophysical Research*, 96, doi:10.1029/91JB01507.

Hillenbrand, C.-D., Smith, J.A., Kuhn, G., Esper, O., Gersonde, R., Larter, R.D., Maher, B., Moreton, S.G., Shimmield, T.M., Korte, M. (2010). Age assignment of a diatomaceous ooze deposited in the western Amundsen Sea Embayment after the Last Glacial Maximum. *Journal of Quaternary Science*, 25, 280-295, doi:10.1002/jqs.1308.

*Hillenbrand, C.-D., Kuhn, G., Smith, J.A., **Gohl, K.**, Graham, A.G.C., Larter, R.D., Klages, J. P., Downey, R., Moreton, S.G., Forwick, M., Vaughan, D.G. (2013). Grounding-line retreat of the West Antarctic Ice Sheet from inner Pine Island Bay. *Geology*, 41, 35-38, doi:10.1130/G33469.1.

*Hagedorn, B., Gersonde, R., **Gohl, K.**, Hubberten, H.-W. (2007). Petrology, geochemistry and K/Ar age constraints of the eastern De Gerlache Seamount alkaline basalts (Bellingshausen Sea, southeast Pacific). *Polarforschung,* 76 (3), 87-94.

*Hagen, R.A., **Gohl, K.**, Gersonde, R., Kuhn, G., Völker, D., Kodagali, V.N. (1998). A geophysical survey of the De Gerlache Seamounts: preliminary results, *Geo-Marine Letters, 18*, 19-25.

*Hillenbrand, C.-D., Kuhn, G., Smith, J.A., **Gohl, K.**, Graham, A.G.C., Larter, R.D., Klages, J.P., Downey, R., Moreton, S.G., Forwick, M. & Vaughan, D.G. (2013). Grounding-line retreat of the West Antarctic Ice Sheet from inner Pine Island Bay. *Geology*, 41, 35-38, doi:10.1130/G33469.1.

Jakobsson, M., Anderson, J.B., Nitsche, F.O., Dowdeswell, J.A., Gyllencreutz, R., Kirchner, N., Mohammad, R., O'Regan, M., Alley, R.B., Anandakrishnan, S., Eriksson, B., Kirshner, A., Fernandez, R., Stolldorf, T., Minzoni, R., Majewski, W. (2011). Geological record of ice shelf break-up and grounding line retreat, Pine

Island Bay, West Antarctica. *Geology*, 39, 691-694, doi:10.1130/G32153.1.

Jakobsson, M., Anderson, J.B., Nitsche, F.O., Gyllencreutz, R., Kirshner, A.E., Kirchner, N., O'Regan, M., Mohammad, R., Eriksson, B. (2012). Ice sheet retreat dynamics inferred from glacial morphology of the central Pine Island Bay Trough, West Antarctica. *Quaternary Science Reviews*, 38, 1-10, doi:10.1016/j.quascirev.2011.12.017.

*Johnson, J.S., Bentley, M.J., **Gohl, K.** (2008). First exposure ages from the Amundsen Sea embayment, West Antarctica: the late Quaternary context for recent thinning of Pine Island, Smith and Pope Glaciers; *Geology,* 36, 223-226, doi:10.1130/G24207A.1.

*Johnson, J.S., Bentley, M.J., Smith, J.A., Finkel, R.C., Rood, D.H., **Gohl, K.**, Balco, G., Larter, R.D., Schaefer, J.M. (2014). Rapid thinning of Pine Island Glacier in the early Holocene. *Science*, 343, 999-1001, doi:10.1126/science.1247385.

Jordan, T.A., Ferraccioli, F., Vaughan, D.G., Holt, J.W., Corr, H., Blankenship, D.D., Diehl, T.M. (2010). Aerogravity evidence of a major crustal thinning under the Pine Island Glacier region (West Antarctica). *Bulletin of the Geological Society of America*, 122, 714-726, doi:10.1130/B26417.1.

Joughin, I., Alley, R.B. (2011). Stability of the West Antarctic ice sheet in a warming world. *Nature Geoscience*, 4, 506-513.

Joughin, I., Alley, R.B., Holland, D.M. (2012). Ice-sheet response to oceanic forcing. *Science,* 338, 1172-1176.

*Kipf, A., Mortimer, N., Werner, R., **Gohl, K.**, van den Bogaard, P., Hauff, F., Hoernle, K. (2012). Granitoids and dykes of the Pine Island Bay region, West Antarctica. *Antarctic Science*, 24(5), 473-484, doi:10.1017/S0954102012000259.

Kirshner, A.E., Anderson, J.B., Jakobsson, M., O'Regan, M., Majewski, W., Nitsche, F.O. (2012). Post-LGM deglaciation in Pine Island Bay, West Antarctica. *Quaternary Science Reviews*, 38, 11-26, doi:10.1016/j.quascirev.2012.01.017.

*Klages, J.P., Kuhn, G., Hillenbrand, C.-D., Graham, A.G.C., Smith, J.A., Later, R.D., **Gohl, K.** (2013). First geomorphological record and glacial history of an inter-ice stream ridge on the West Antarctic continental shelf. *Quaternary Science Reviews*, 61, 47-61, doi:10.1016/j.quascirev.2012.11.007.

*Klages, J.P., Kuhn, G., Hillenbrand, C.-D., Graham, A.G., Smith, J.A., Larter, R.D., **Gohl, K.**, Wacker, L. (2014). Retreat of the West Antarctic Ice Sheet from the western Amundsen Sea shelf at a pre- or early LGM stage. *Quaternary Science Reviews*, 91, 1-15, doi:10.1016/j.quascirev.2015.02.017.

*Klages, J.P., Kuhn, G., Graham, A.G.C, Hillenbrand, C.-D., Smith, J.A., Nitsche, F.O., Larter, R.D., **Gohl, K.** (2015). Palaeo-ice stream pathways and retreat style in the easternmost Amundsen Sea Embayment, West Antarctica, revealed by combined multibeam bathymetry and seismic data. *Geomorphology*, doi:10.1016/j.geomorph.2015.05.020.

*Larter, R.D., Cunningham, A.P., Barker, P.F., **Gohl, K.**, Nitsche, F.O. (2002). Tectonic evolution of the Pacific margin of Antarctica – 1. Late Cretaceous tectonic reconstructions; *J. Geoph. Res*., *107(B12)*, 2345, doi:10.1029/2000JB000052.

*Larter, R.D., Anderson, J.B., Graham, A.G.C., **Gohl, K.**, Hillenbrand, C.-D., Jakobsson, M., Johnson, J.S., Kuhn, G., Nitsche, F.O., Smith, J.A., Witus, A., Bentley, M.J., Dowdeswell, J.A., Ehrmann, W., Klages, J.P., Lindow, J., Ó

Cofaigh, C., Spiegel, C. (2014). Reconstruction of changes in the Amundsen Sea and Bellingshausen Sea sector of the West Antarctic Ice Sheet since the Last Glacial Maximum. *Quaternary Science Reviews*, doi:10.1016/j.quascirev.2013.10.016.

LeMasurier, W.E., Landis, C.A. (1996). Mantle-plume activity recorded by low relief erosion surfaces in West Antarctica and New Zealand. *Geological Society of America Bulletin*, 108, 1450-1466.

*Lindeque, A., **Gohl, K.**, Henrys, S., Wobbe, F., Davy, B. (submitted paper). Seismic stratigraphy along the Ross Sea to Amundsen Sea continental rise: A cross-regional record of pre-glacial to glacial processes of the West Antarctic margin, *Palaeogeography, Palaeoclimatology, Palaeoecology*.

*Lindow, J., Castex, M., Wittmann, H., Johnson, J.S., Lisker, F., **Gohl, K.**, Spiegel, C. (2014). Glacial retreat in the Amundsen Sea sector, West Antarctica – first cosmogenic evidence from central Pine Island Bay and the Kohler Range. *Quaternary Science Reviews*, 98, 166-173, doi:10.1016/j.quascirev.2014.05.010.

Lowe, A.L., Anderson, J.B. (2002). Reconstruction of the West Antarctic ice sheet in Pine Island Bay during the Last Glacial Maximum and its subsequent retreat history. *Quaternary Science Reviews*, 21, 1879-1897.

Matthews, K.J., Williams, S.E., Whittaker, J.M., Müller, R.D., Seton, M., Clarke, G.L. (2015). Geologic and kinematic constraints on Late Cretaceous to mid Eocene plate boundaries in the southwest Pacific. *Earth-Science Reviews*, doi:10.1016/j.earscirev.2014.10.008.

McFadden, R.R., Teyssier, C., Siddoway, C.S., Whitney, D.L., Fanning, C.M. (2010). Oblique dilation, melt transfer, and gneiss dome emplacement. *Geology*, 38(4), 375-378, doi:10.1130/G30493.1.

*Nitsche, F.O., **Gohl, K.**, Vanneste, K., Miller, H. (1997). Seismic expression of glacially deposited sequences in the Bellingshausen and Amundsen Seas, West Antarctica, in: *Geology and Seismic Stratigraphy of the Antarctic Margin 2,* by Barker, P.F. and Cooper, A.K. (eds.), Antarctic Research Series, Vol. 71, p. 95-108, American Geophysical Union, Washington, DC.

*Nitsche, F.O., Larter, R.D., **Gohl, K.**, Graham, A.G.C., Kuhn, G. (2015a). Crag and tail features on the Amundsen Sea continental shelf. In: Dowdeswell, J.A., Canals, M., Jakobsson, M., Todd, B.J., Dowdeswell, E.K., Hogan, K.A (Eds.), *Atlas of Submarine Glacial Landforms: Modern, Quaternary and Ancient*, The Geological Society, London.

*Nitsche, F.O., Larter, R.D., **Gohl, K.**, Graham, A.G.C., Kuhn, G. (2015b). Bedrock channels in Pine Island Bay, West Antarctica. In: Dowdeswell, J.A., Canals, M., Jakobsson, M., Todd, B.J., Dowdeswell, E.K., Hogan, K.A (Eds.), *Atlas of Submarine Glacial Landforms: Modern, Quaternary and Ancient*, The Geological Society, London.

Pritchard, H.D., Ligtenberg, S.R.M., Fricker, H.A., Vaughan, D.G., van den Broeke, M.R., Padman, L. (2012). Antarctic ice-sheet loss driven by basal melting of ice shelves. *Nature*, 484, 502-505, doi:10.1038/nature10968.

Rebesco, M., Hernández-Molina, F.H., Van Rooij, D., Wåhlin, A. (2014). Contourites and associated sediments controlled by deep-water circulation processes: State-of-the-art and future considerations. *Marine Geology*, 352, 111-154, doi:10.1016/j.margeo.2014.03.011.

Rignot, E., Mouginot, J., Scheuchl, B. (2011). Ice flow of the Antarctic ice sheet. *Science,* 333, doi:10.1126/science.1208336.

*Scheuer, C., **Gohl, K.**, Udintsev, G. (2006c). Bottom-current control on sedimentation in the western Bellingshausen Sea, West Antarctica. *Geo-Marine Letters,* doi:10.1007/s00367-006-0019-1.

Sieminski, A., Debayle, E., Leveque, J.J. (2003). Seismic evidence for deep low-velocity anomalies in the transition zone beneath West Antarctica. *Earth and Planetary Science Letters*, 216, 645-661.

Storey, B.C. (1991). The crustal blocks of West Antarctica within Gondwana: reconstruction and break-up model. In: Thomson, M.R.A., Crame, J.A., Thomson, J.W. (editors), *Geological Evolution of Antarctica*, pp. 587-592. Cambridge University Press, Cambridge.

Storey, B.C., Leat, P.T., Weaver, S.D., Pankhurst, R.J., Bradshaw, J.D., Kelley, S. (1999). Mantle plumes and Antarctica–New Zealand rifting: evidence from mid-Cretaceous mafic dykes. *J. Geol. Soc. London*, 156(4), 659-671, doi:10.1144/gsjgs.156.4.0659.

Thoma, M., Jenkins, A., Holland, D., Jacobs, S. (2008). Modelling Circumpolar Deep Water intrusions on the Amundsen Sea continental shelf, Antarctica. *Geophysical Research Letters,* 35, L18602, doi:10.1029/2008GL034939.

Uenzelmann-Neben, G. (2006). Depositional patterns at Drift 7, Antarctic Peninsula: along slope versus down-slope sediment transport as indicators for oceanic currents and climatic conditions. *Marine Geology*, 233, 49-62.

*Weigelt, E., Uenzelmann-Neben, G., **Gohl, K.**, Larter, R.D. (2012). Did massive glacial dewatering modify the sedimentary structures on the Amundsen Sea Embayment shelf, West Antarctica? *Global and Planetary Change*, vol. 92-93, p. 8-16, doi:10.1016/j.gloplacha.2012.04.006.

6 Appendix of publications

6.1 Geodynamic reconstruction of the South Pacific

Publication 6.1.1:

Eagles, G., **Gohl, K.**, Larter, R.D. (2004a). High-resolution animated tectonic reconstruction of the South Pacific and West Antarctic margin. *Geochemistry, Geophysics, Geosystems (G^3),* v. 5, no. 7, doi:10.1029/2003GC000657.

Author contributions: This study is result of a postdoc project applied for by Gohl and funded by the Deutsche Forschungsgemeinschaft. Gohl developed the idea of gridded plate-kinematic rotations and contributed with magnetic data from expeditions ANT-XI/3 (1994), ANT-XII/4 (1995) and ANT-XVIII/5a (2001). Eagles (postdoc) compiled the data, developed the model and wrote most of the paper. Gohl and Larter contributed to the model and discussion.

Geochemistry Geophysics Geosystems G3
AN ELECTRONIC JOURNAL OF THE EARTH SCIENCES
Published by AGU and the Geochemical Society

Article
Volume 5, Number 7
10 July 2004
Q07002, doi:10.1029/2003GC000657
ISSN: 1525-2027

High-resolution animated tectonic reconstruction of the South Pacific and West Antarctic Margin

Graeme Eagles and Karsten Gohl
Alfred Wegener Institute for Polar and Marine Research, Postfach 120161, D-27515 Bremerhaven, Germany (geagles@awi-bremerhaven.de)

Robert D. Larter
British Antarctic Survey, High Cross, Madingley Road, Cambridge, CB3 0ET, UK

[1] An animated reconstruction shows South Pacific plate kinematics between 90 and 45 Ma, using the satellite-derived gravity anomaly field, interpolated isochrons and plate rotation parameters from both published and new work on marine geophysical data. The Great South Basin and Bounty Trough, New Zealand, are shown as the earliest Pacific–Antarctic plate boundary that opened before 83 Ma. The earliest true Pacific–Antarctic seafloor formed within the eastern parts of this boundary, but later and farther west, seafloor formed within its Antarctic flank. After 80 Ma, the Bellingshausen plate converged with an oceanic part of the Antarctic plate to its east, while its motion simultaneously caused rifting in continental Antarctica to the south. The Pacific–Bellingshausen spreading center developed a set of long offset transform faults that the Pacific–Antarctic plate boundary inherited around chron C27 when the Bellingshausen plate ceased to move independently as part of a Pacific-wide plate tectonic reorganization event. Southwest of these transforms the Pacific–Antarctic Ridge saw an increase in transform-fault segmentation by ~58 Ma. One of the long offset Pacific–Bellingshausen transforms, referred to as "V," was modified during the C27 reorganization event when a Pacific–Antarctic–Phoenix triple junction initiated on its southern edge. Eastern parts of "V" started to operate in the Pacific–Phoenix spreading system, lengthening it even more, while its western parts operated in the Pacific–Antarctic system. This complicated feature was by-passed and deactivated by ridge axis propagation to its northwest at ~47 Ma. We interpret our animation to highlight possible connections between these events.

Components: 11,268 words, 11 figures, 1 table, 1 animation.

Keywords: plate tectonics; plate reconstructions; Pacific Ocean; Antarctica.

Index Terms: 3040 Marine Geology and Geophysics: Plate tectonics (8150, 8155, 8157, 8158); 8157 Tectonophysics: Plate motions—past (3040); 9310 Information Related to Geographic Region: Antarctica.

Received 30 October 2003; **Revised** 23 March 2004; **Accepted** 5 May 2004; **Published** 10 July 2004.

Eagles, G., K. Gohl, and R. D. Larter (2004), High-resolution animated tectonic reconstruction of the South Pacific and West Antarctic Margin, *Geochem. Geophys. Geosyst.*, *5*, Q07002, doi:10.1029/2003GC000657.

1. Introduction

[2] In this paper, we present an animated reconstruction of gridded, satellite-derived free-air gravity data, and use it as a tool to describe the tectonic history of an important region for global tectonics: the South Pacific and its West Antarctic margin. The animation displays events that are described in the literature, as well as some new interpretations, and

Geochemistry Geophysics Geosystems G3 EAGLES ET AL.: ANIMATED TECTONIC RECONSTRUCTION 10.1029/2003GC000657

it gives a self-consistent view of the region's tectonics.

1.1. Gridded and Animated Reconstructions

[3] Detailed data sets of free-air gravity anomalies, derived from satellite altimetry over the world's oceans [e.g., *McAdoo and Laxon*, 1997; *Sandwell and Smith*, 1997] (Figure 1), illustrate in detail the plate tectonic fabric of the ocean floor, including the fracture zones (FZs) formed at transform faults (TFs), and the traces of triple junction (TJ) migration. Tectonic histories derived from such gridded data are most directly and meaningfully illustrated by reconstruction of the data themselves. Such "state of the art" reconstructions have already been produced for the South Pacific [*Marks and Stock*, 1997; *McAdoo and Laxon*, 1997]. Figure 2 shows that a static reconstruction using gridded gravity data can have the following advantages over a static line drawing (vector) reconstruction: (1) there is a massive increase in the number of reconstructed features, (2) the reconstruction of gridded data is largely free of selection pressure because the choice of "significant" features is confined to the identification of often already well-constrained ancient plate boundaries within which all data are reconstructed, (3) gridded reconstructions explicitly show areas of underlap (compare the Phoenix plate in the two parts of Figure 2; the gray underlap area in the gridded reconstruction clearly shows its destruction at the West Antarctic margin subduction zone, which is not obvious from the vector reconstruction), and (4) reconstructed gridded data are amenable for further quantitative analysis, already in paleocoordinates.

[4] Animated reconstructions are powerful and valuable tools that give viewers a rapid grasp of a tectonic history with which they may be unfamiliar, and a full appreciation of the continuity of plate motion models. They also permit an appreciation of long time series geological data in their paleogeographical context. Like snapshot reconstructions, animated reconstructions can use vector or gridded data.

[5] The PLATES group (http://www.ig.utexas.edu/research/projects/plates/plates.htm#recons), *Reeves and Sahu* [1999] (http://kartoweb.itc.nl/gondwana/), and *Hall* [2002], for example, present animated reconstructions of large volumes of vector data, many digitized from grids, that successfully illustrate global and more detailed regional tectonic models. *Gaina et al.* [1998a, 1998b] (http://www.es.usyd.edu.au/geology/people/staff/dietmar/Movies/tasman.html) present an animated reconstruction of gridded satellite-derived gravity data for the Tasman Sea region. Vector animations have the advantage of lower data volumes, and therefore lower data transfer rates are required to view them, but they suffer some of the same drawbacks as static line drawing reconstructions. In particular, the work associated with digitizing large numbers of features is time consuming and unavoidably involves interpretations and selections that can never fully be documented by the human digitizer. With ongoing increases in computer speed, reconstruction and animation of gridded data becomes both feasible and desirable, and can be achieved with a similar or smaller amount of human effort.

1.2. Tectonic Introduction

[6] The West Antarctic continent (Figure 1) hosts an important example of a continental margin that has changed from an active to a passive setting, and is a crucial yet poorly known link in the Late Cretaceous and Tertiary global plate circuit. The early to mid-Cretaceous proto-Pacific margin of Gondwana was a subduction zone, until Chatham Rise started to separate from it late within the Cretaceous Normal Polarity Superchron (CNS; 118–83 Ma). Subsequently, Campbell Plateau also separated from the Antarctic margin during the reversed part of chron C33 (83–79.1 Ma), leaving a rifted continental margin bordering the Amundsen and westernmost Bellingshausen seas (Figure 1) [*Larter et al.*, 2002]. A spreading center, that was in morphological continuity with the Pacific–Antarctic ridge in the eastern Amundsen Sea, separated a small plate, known as the Bellingshausen plate [*Stock and Molnar*, 1987; *Stock et al.*, 1996], from the Pacific plate until its incorporation into the Antarctic plate around chron C27 (~61 Ma) [*Cande et al.*, 1995]. The "Bellingshausen" parts of the ridge are thought to have been the first to form, before chron C34y (83 Ma), although the Bellingshausen plate probably did not come into existence until shortly afterward [*Eagles et al.*, 2004]. The Bellingshausen plate had slow convergent and divergent margins with Antarctica [*Heinemann et al.*, 1999; *Cunningham et al.*, 2002; *Larter et al.*, 2002]. Further east, the plate facing the West Antarctic

Geochemistry Geophysics Geosystems G3 EAGLES ET AL.: ANIMATED TECTONIC RECONSTRUCTION 10.1029/2003GC000657

margin was the Phoenix (also called Aluk, or Drake) plate. The Phoenix plate's divergent boundaries with the Pacific, Bellingshausen and Antarctic plates have changed over time [*Cande et al.*, 1982, 1995; *McCarron and Larter*, 1998; *Larter and Barker*, 1991], but its southeastern boundary was continuously a subduction zone where it was being overridden by the Antarctic Peninsula. The Phoenix

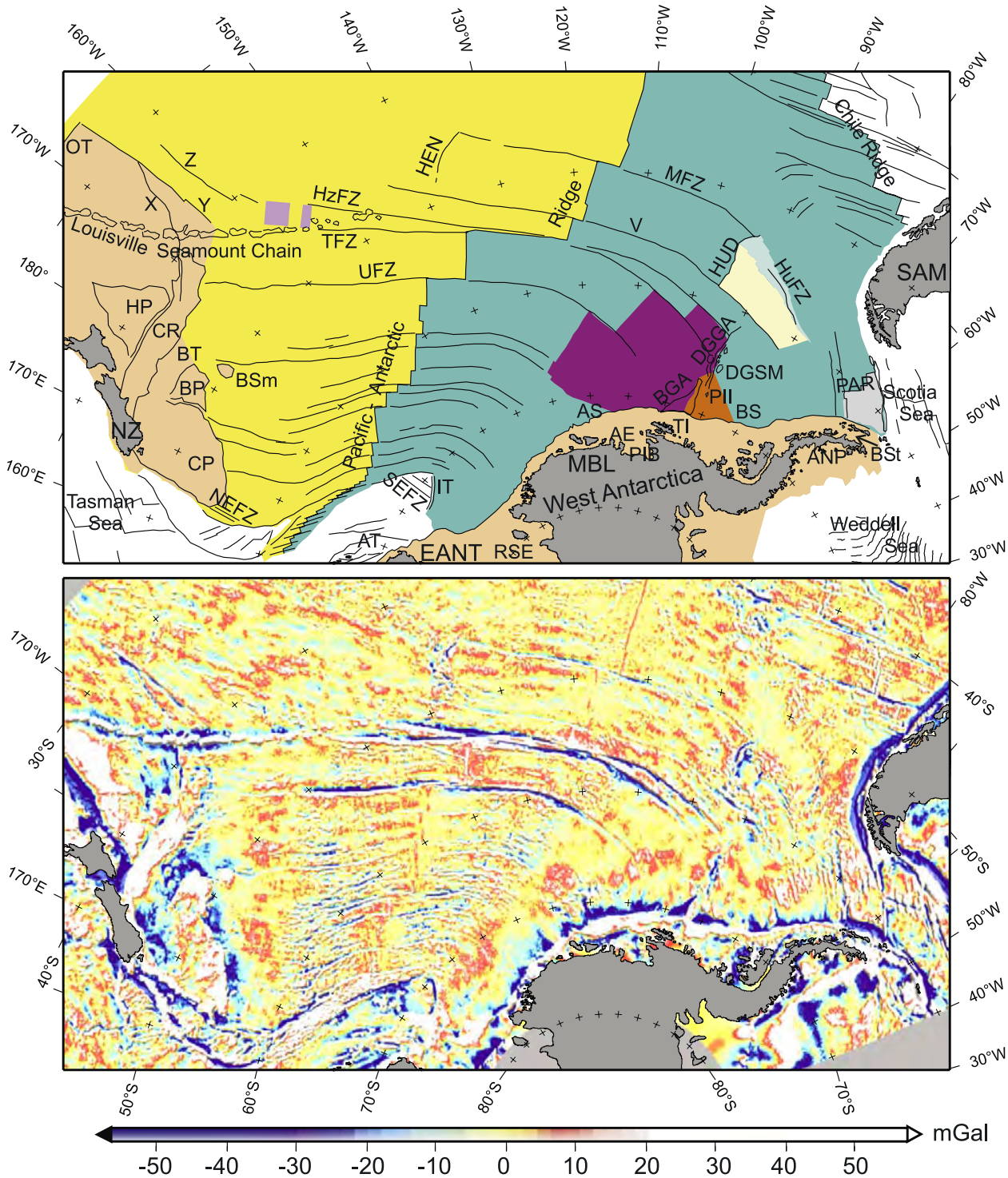

Figure 1

Geochemistry Geophysics Geosystems G3 EAGLES ET AL.: ANIMATED TECTONIC RECONSTRUCTION 10.1029/2003GC000657

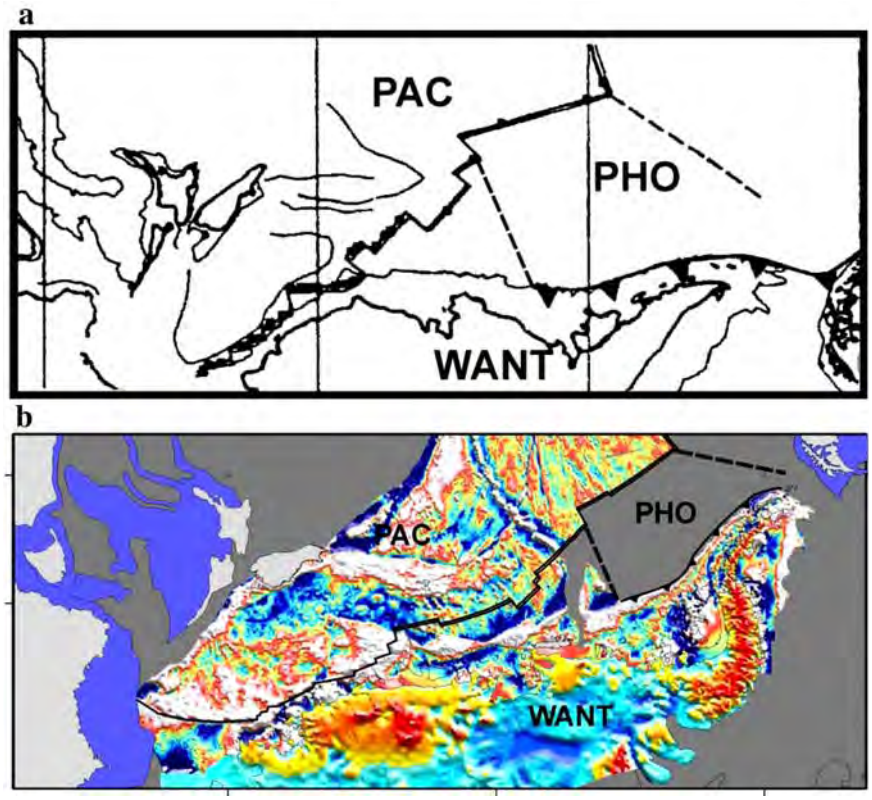

Figure 2. (a) Snapshot line reconstruction of the West Antarctic margin at chron C34y, from *Mayes et al.* [1990]. The label for an Aluk plate has been changed to PHO (Phoenix plate) and that for the Bellingshausen plate has been removed to avoid confusion. (b) Equivalent snapshot gridded free-air gravity reconstruction, with data from the BEDMAP compilation [*Lythe et al.*, 2000] included onshore Antarctica. Graticule interval: 10°. Mercator projection.

plate's later history has seen most of it lost as segments of the Antarctic–Phoenix ridge successively converged with the Antarctic Peninsula from southwest to northeast. This continued until around chron C2A (~3.3 Ma), when the last remnant of the Phoenix plate was incorporated into the Antarctic plate [*Larter and Barker*, 1991; *Livermore et al.*, 2000].

[7] Between the Bellingshausen and Phoenix sectors, a small fragment of the oceanic lithosphere at the margin may have formed on the southern side

Figure 1. (top) Buff, areas already existing at 90 Ma; bright yellow, lithosphere formed on the Pacific plate; bright green, West Antarctic plate; purple, Bellingshausen plate; light yellow, formed on Pacific plate but transferred to Antarctic plate; light green, formed on the Farallon plate and transferred to the Antarctic plate; gray, formed on the Phoenix plate and transferred to the Antarctic plate; light purple, formed on the Bellingshausen plate and transferred to the Pacific plate; orange, formed on the Charcot plate. AE, Amundsen Embayment; ANP, Antarctica Peninsula; AS, Amundsen Sea; AT, Adare Trough; BGA, Bellingshausen Gravity Anomaly; BP, Bounty Platform; BS, Bellingshausen Sea; BSm, Bollons Seamount; BSt, Bransfield Strait; BT, Bounty Trough; CP, Campbell Plateau; CR, Chatham Rise; DGGA, De Gerlache Gravity Anomaly; DGSM, De Gerlache Seamounts; EANT, East Antarctica; HEN, Henry Trough; HUD, Hudson Trough; HP, Hikurangi Plateau; HuFZ, Humboldt FZ; HzFZ, Heezen FZ; IT, Iselin Trough; MBL, Marie Byrd Land; MFZ, Menard FZ; NEFZ, northern parts of Emerald FZs; NZ, New Zealand; OT, Osbourn Trough; PAR, extinct Phoenix–Antarctic ridge; PIB, Pine Island Bay; PII, Peter I Island; RSE, Ross Sea Embayment; SAM, South America; SEFZ, southern parts of Emerald FZs; TI, Thurston Island; TFZ, Tharp FZ; UFZ, Udintsev FZ; V, FZ "V"; and X, Y, Z, gravity lineaments of *Larter et al.* [2002]. Oblique Mercator projection centered on 137.5°W, 65°S and with 74°W, 60°S on the oblique equator. (bottom) Satellite derived free-air gravity anomalies in the study region [*Sandwell and Smith*, 1997; *McAdoo and Laxon*, 1997] (high-pass filtered to remove >1500 km wavelength anomalies and retain those <500 km).

Geochemistry Geophysics Geosystems G3 EAGLES ET AL.: ANIMATED TECTONIC RECONSTRUCTION 10.1029/2003GC000657

of a CNS-age spreading center between the Pacific plate and the Charcot plate, a fragment of the Phoenix plate. The last remnant of the Charcot plate became fused to the West Antarctic plate when its subduction beneath the West Antarctic margin stalled as part of the plate tectonic reorganization that resulted in formation of the rifted margins further west [*Larter et al.*, 2002].

[8] The West Antarctic subcontinent itself has undergone extension in numerous small basins. Many of these basins are parts of the West Antarctic rift system that started to separate West Antarctica from East Antarctica early in the Tertiary [*Behrendt et al.*, 1991]. Examples of such basins are the Adare Trough, that proceeded to seafloor spreading [e.g., *Cande et al.*, 2000], and basins of the Ross Sea Embayment. Others may be related to local complications to regional tectonics, like Bransfield Strait [e.g., *Barker and Austin*, 1998] and the Powell Basin [*Eagles and Livermore*, 2002].

2. Method

2.1. Finite Rotations

[9] All finite rotations for reconstruction of the various plate pairs are shown in Table 1 and all dates are from the magnetic reversal timescale of *Cande and Kent* [1995]. In some cases, it was necessary to extrapolate parameters in order to generate a 90 Ma finite rotation. These finite rotations were then expressed with respect to a fixed West Antarctica, and interpolated for integer numbers of millions of years between 1 and 90.

[10] *Larter et al.*'s [2002] fit of Chatham Rise to the West Antarctic margin at 90 Ma, an age estimated by extrapolation of spreading rates back to the continental margins NE of the Udintsev FZ, implicitly defines the opening of Bounty Trough. New Zealand's South Island, east of the Alpine Fault, is kept fixed to Chatham Rise. From chron C34y (83 Ma) onward, the Pacific plate is taken to include Chatham Rise, Campbell Plateau, and the Bounty Trough, and the Pacific plate finite rotations are taken from *Cande et al.* [1995], an unpublished manuscript by Joann Stock et al. (from which *Larter et al.* [2002] list some rotations), and *Larter et al.* [2002].

[11] A captured fragment of the Pacific plate exists north of FZ "V" (Figure 1) [*Cande et al.*, 1982]. Its growth and movement prior to capture are calculated by reversing an interpolated Pacific–West Antarctic finite rotation for 47.6 Ma (by which the central and southern parts of the Henry and Hudson ridge propagation scars (Figure 1) are reconstructed to one another) and then adding each of the 61–48 Ma Pacific–West Antarctic finite rotations (the oldest part of the captured fragment formed at chron C27). Thus the fragment is described as fixed to the West Antarctic plate since its capture at 47.6 Ma, and moving at earlier times about Pacific–West Antarctic stage rotations in the West Antarctic reference frame. The part of the captured crust that formed at the Pacific-Farallon ridge is treated similarly, except that we use a 46.7 Ma interpolated Pacific–Antarctic finite rotation to reconstruct the northern parts of the Henry and Hudson troughs.

[12] Most of the Bellingshausen–Pacific finite rotations come from the unpublished manuscript by J. Stock et al. reported by *Larter et al.* [2002]. The rotations' origin is in an inversion of seafloor spreading data using *Chang*'s [1987] implementation of the technique of *Hellinger* [1981]. *Eagles et al.* [2004] report two new rotations in the Bellingshausen sector of the South Pacific, made by visual fitting of FZs and anomalies C34y and C33o as seen in new aeromagnetic data, and use them to demonstrate independent movement of the Bellingshausen plate since around C33o. Movements of fragments of the Bellingshausen plate, captured by the Pacific plate by ridge jumps around anomalies C33 and C32 [*Eagles et al.*, 2004], are described by constructing a Bellingshausen–Pacific–West Antarctic circuit with finite rotations generated from reversed interpolated Bellingshausen–Pacific finite rotations at the times of the modeled ridge-jumps, to which are added finite rotations at older times until the ages of the oldest parts of the two captured fragments.

[13] The Bollons Seamount is treated as having moved in the Pacific–West Antarctic system, but to have been transferred from the Antarctic to the Pacific plate just after 79 Ma [*Sutherland*, 1999; *Eagles et al.*, 2004]. We calculated a new finite rotation to reconstruct the Bollons Seamount to a gap within the reconstructed Campbell Plateau–Antarctica boundary, because using an interpolated 79 Ma Pacific–Antarctic rotation instead resulted in some lateral overlap between the seamount and Campbell Plateau.

[14] The finite rotation parameters for the Phoenix plate come from *Eagles* [2003] for periods since 15 Ma and from an unpublished inversion similar to that reported by *Eagles* [2000] for times before

Geochemistry Geophysics Geosystems G3 EAGLES ET AL.: ANIMATED TECTONIC RECONSTRUCTION 10.1029/2003GC000657

Table 1. Finite Rotation Parameters Used for the Animation Process[a]

Latitude	Longitude	Angle	Age	Chron	Source
		Pacific Plate With Respect to Bellingshausen Plate			
71.38	−55.57	44.90	61.28	C27	*Cande et al.* [1995]
70.43	−56.55	46.35	63.80	C28r	Stock et al. (unpublished manuscript)
70.88	−51.01	52.48	67.70	C30r	Stock et al. (unpublished manuscript)
71.40	−42.69	59.57	71.50	C32n.1r	Stock et al. (unpublished manuscript)
70.98	−41.28	62.70	73.60	C33y	Stock et al. (unpublished manuscript)
70.57	−34.34	72.30	79.08	C33o	*Eagles et al.* [2004]
		Pacific Plate With Respect to West Antarctic Plate			
64.25	−79.06	0.68	0.39	C1	*Cande et al.* [1995]
67.03	−73.72	2.42	3.58	C2A	*Cande et al.* [1995]
67.91	−77.93	5.42	6.27	C3A	*Cande et al.* [1995]
69.68	−77.06	7.95	9.64	C4A	*Cande et al.* [1995]
71.75	−73.77	10.92	12.82	C5A	*Cande et al.* [1995]
73.68	−69.85	15.17	16.73	C5C	*Cande et al.* [1995]
74.72	−67.28	19.55	24.12	C6C	*Cande et al.* [1995]
74.55	−67.38	22.95	28.75	C10	*Cande et al.* [1995]
74.38	−64.74	27.34	33.55	C13	*Cande et al.* [1995]
74.90	−51.31	34.54	43.79	C20	*Cande et al.* [1995]
74.52	−50.19	37.64	47.91	C21	*Cande et al.* [1995]
73.62	−52.50	40.03	53.35	C24	*Cande et al.* [1995]
71.38	−55.57	44.90	61.28	C27	*Cande et al.* [1995]
70.55	−55.72	47.00	63.80	C28r	Stock et al. (unpublished manuscript)
68.94	−55.52	49.60	67.74	C30r	Stock et al. (unpublished manuscript)
69.33	−53.44	51.05	68.74	C31	*Cande et al.* [1995]
67.10	−57.40	50.48	71.50	C32n.1r	Stock et al. (unpublished manuscript)
66.72	−55.04	53.74	73.62	C33y	Stock et al. (unpublished manuscript)
		Campbell Plateau With Respect to West Antarctic Plate			
65.58	−52.38	63.07	83.00	C34y	*Larter et al.* [2002]
		Chatham Rise With Respect To West Antarctic Plate			
64.06	−49.94	67.99	90.00	FIT	*Larter et al.* [2002]
		Bollons Seamount With Respect to West Antarctic Plate			
66.28	−54.36	58.52	79.00	FIT	this study
		Pacific Plate With Respect to Hot Spots			
72.000	−80.000	21.000	23.6	Not given	*Yan and Kroenke* [1993]
69.446	−73.652	25.553	30.8	Not given	*Yan and Kroenke* [1993]
67.742	−66.178	33.386	43.0	Not given	*Yan and Kroenke* [1993]
52.375	−79.290	42.427	65.0	Not given	*Yan and Kroenke* [1993]
47.507	−80.108	48.900	74.0	Not given	*Yan and Kroenke* [1993]
		Phoenix Plate With Respect To West Antarctic Plate			
−68.07	−91.96	1.83	5.23	C3	*Eagles* [2003]
−69.21	−97.32	3.07	6.57	C3A	*Eagles* [2003]
−68.98	−90.41	5.85	8.07	C4	*Eagles* [2003]
−69.77	−92.17	7.94	9.31	C4A	*Eagles* [2003]
−69.98	−94.12	11.23	10.95	C5	*Eagles* [2003]
−70.23	−96.68	13.38	12.40	C5A2	*Eagles* [2003]
−70.02	−94.97	18.94	14.61	C5AD	*Eagles* [2003]
−70.03	−79.68	20.75	16.73	C5C	Eagles (unpublished data)
−70.64	−71.93	22.08	20.13	C6	Eagles (unpublished data)
		East Antarctic Plate With Respect to West Antarctic Plate			
−18.15	−17.85	−0.7	33.55	C13	*Cande et al.* [2000]
−18.15	−17.85	−1.7	43.79	C20	*Cande et al.* [2000]
−18.15	−17.85	−1.7	53.3	C24o	*Cande and Stock* [2004]
−18.15	−17.85	−2.2	61.1	C27	*Cande and Stock* [2004]

Table 1. (continued)

Latitude	Longitude	Angle	Age	Chron	Source
		South America Plate With Respect to East Antarctic Plate			
81.80	−33.55	0.63	2.58	C2Ay	*Nankivell* [1997]
81.63	−17.17	2.57	9.74	C5y	*Nankivell* [1997]
79.15	−17.17	5.53	19.05	C6y	*Nankivell* [1997]
75.38	−12.33	7.67	25.82	C8y	*Nankivell* [1997]
74.98	−4.31	10.13	33.06	C13y	*Nankivell* [1997]
76.47	1.81	12.09	38.43	C18y	*Nankivell* [1997]
77.55	10.52	13.66	42.54	C20y	*Nankivell* [1997]
78.14	11.80	14.74	46.26	C21y	*Nankivell* [1997]
79.30	59.56	22.54	65.58	C30y	*Nankivell* [1997]
77.78	53.96	23.92	71.07	C32y	*Nankivell* [1997]
77.73	55.63	25.22	73.62	C33y	*Nankivell* [1997]
77.61	61.48	27.81	79.08	C33Ry	*Nankivell* [1997]
77.36	64.44	29.64	83.00	C34y	*Nankivell* [1997]
		Lord Howe Rise/Challenger Plateau With Respect to Australia			
−14.19	−49.59	0.723	53.3	C24o	*Gaina et al.* [1998a]
−15.93	−46.53	2.112	55.8	C25y	*Gaina et al.* [1998a]
−16.93	−43.77	3.792	57.9	C26o	*Gaina et al.* [1998a]
−4.65	−48.49	4.432	61.2	C27o	*Gaina et al.* [1998a]
−4.71	−47.32	5.168	62.5	C28y	*Gaina et al.* [1998a]
−0.19	−49.63	5.461	64.0	C29y	*Gaina et al.* [1998a]
−3.99	−48.20	6.735	65.6	C30y	*Gaina et al.* [1998a]
−9.04	−45.54	8.83	67.7	C31y	*Gaina et al.* [1998a]
−9.53	−42.8	12.937	73.6	C33y	*Gaina et al.* [1998a]
4.5	−42.26	16.61	90.00	FIT	*Gaina et al.* [1998a]
		East Antarctica With Respect to Australia			
13.45	33.92	20.52	33.6	C13o	*Royer and Rollet* [1997]
14.32	31.75	23.77	40.1	C18o	*Royer and Rollet* [1997]
15.07	31.78	24.55	43.0	C20o	*Tikku and Cande* [2000]
14.00	33.34	24.70	46.0	C21y	*Tikku and Cande* [2000]
10.39	35.59	25.15	53.0	C24o	*Tikku and Cande* [2000]
9.95	36.52	25.55	61.0	C27y	*Tikku and Cande* [2000]
9.48	37.02	26.13	71.0	C32y	*Tikku and Cande* [2000]
5.13	39.80	26.57	79.0	C33o	*Tikku and Cande* [2000]
2.05	40.79	27.12	83.0	FIT	*Tikku and Cande* [2000]
		Eastern South Tasman Rise With Respect to Australia			
−48.23	133.46	0.17	65.6	C30y	*Royer and Rollet* [1997]
−48.23	133.46	2.47	73.6	C33y	*Royer and Rollet* [1997]
−48.23	133.46	5.17	83.0	C34y	*Royer and Rollet* [1997]
−48.23	133.46	8.62	95.0	FIT	*Royer and Rollet* [1997]

[a] Where parameters are quoted from cited references, the precisions used are as given in those references except those from the unpublished Stock et al. manuscript, which are quoted as by *Larter et al.* [2002]. All the rotations are right-handed.

then. We use total reconstruction rotations for the Pacific plate with respect to the hot spots [*Yan and Kroenke*, 1993], in a circuit with *Cande et al.*'s [1995] parameters, to generate parameters for movements between the Louisville hot spot and the West Antarctic plate. We estimated the present-day position of the hot spot, whose trace since ~12 Ma is not obvious [*Wessel and Kroenke*, 1997], by using these parameters to project dated seamounts of the Louisville ridge [*Watts et al.*, 1988] forward in time. The estimated present-day position of the hot spot (134.9°W, 51.5°S) was then rotated by the Hot spots–West Antarctica rotations to give the Louisville hot spot's position for every 1 m.y. interval since 90 Ma.

[15] We use finite rotations for movements between East Antarctica and South America [*Nankivell*, 1997], Australia [*Tikku and Cande*, 2000], the eastern South Tasman Rise [*Royer and Rollet*, 1997] and Challenger Plateau/central Lord Howe Rise [*Gaina et al.*, 1998a] in order to place the gridded animation in its paleogeographical context. These plate movements must be adjusted

in order to take account of what is known of post-90 Ma movements between East and West Antarctica and in New Zealand. However, reconstructions of the Ross Sea region are the subject of controversy, and in view of the lack of consensus on a set of finite rotations there, we have restricted the gridded data reconstruction to those plates linked to West Antarctica via a circuit of long spreading ridge plate boundaries. Outside this circuit, movements are shown simply using outlines defined from free-air gravity data, and present-day coastlines.

[16] For the adjustment of these movements, East–West Antarctica rotations are taken from *Cande et al.* [2000] and *Cande and Stock* [2004], who describe movements in the Adare Trough and basins in the Ross Sea Embayment between chrons C20 and C8, and between chrons C27 and C24. We do not use the finite rotation of *Marks and Stock* [1997] (derived from closure of the Iselin Trough and alignment of the Emerald FZs) because this implies convergence, not divergence, between East and West Antarctica between C27 and C24. This rotation may instead only apply to a microplate that bore the Iselin Bank. The finite rotations we use are based on the closure of reconstruction misfits on short lengths of oceanic plate boundaries, and hence are not tightly constrained. Nonetheless, when combined with *Cande et al.*'s [1995] and *Tikku and Cande*'s [2000] rotations, they do produce a finite rotation for reconstruction of the Emerald basin that is within the estimated uncertainties of a finite rotation [*Sutherland*, 1995] derived from reconstruction of the margins of that basin. Although *Wood et al.* [2000] show that southwestern parts of New Zealand were tectonically quiet between Late Cretaceous rifting in the Tasman Sea and Eocene opening of the Emerald Basin, it is not possible to rule out pre-C27 movements in New Zealand or between East and West Antarctica. For simplicity, prior to C27, we fix East Antarctica and West Antarctica together and leave the boundary within New Zealand free.

[17] Finally, some small basin opening events within West Antarctica (e.g., Bransfield Strait and Powell Basin) are not shown as part of the animation.

2.2. Generating the Animation: Assumptions, Method, and Limitations

[18] Our animation uses many reconstruction parameters derived from inversions of magnetic isochron and FZ data, and so is obliged to illustrate the consequences of the assumptions of the inversions. These inverse techniques may omit information from FZs formed at long offset (>200 km) TFs, either on the assumption that they do not behave passively in changing kinematic settings [e.g., *Shaw and Cande*, 1990] or for reasons of technical unsuitability [*Hellinger*, 1981]. There are observations to support the assumption that some long offset TFs do not behave passively [*Cande et al.*, 1988; *Müller and Roest*, 1992]. An opposing opinion holds that FZs from long offset TFs are the most reliable indicators of plate motion because they exert a strong influence on it. In this view, shorter offset TFs are more likely to behave nonpassively. If, instead, we had chosen to illustrate reconstructions that favor long offset FZ data (e.g., the visual fit-derived reconstructions of *Mayes et al.* [1990]) our animation would have been constrained to illustrate the migratory responses of short-offset TFs to plate motion changes.

[19] To generate the animation, we digitized a set of 471 masks covering whole plates or parts of plates (Figure 3). These masks show the outlines of surviving crust of single plates, at 1 m.y. intervals, between 90 and 1 Ma. The masks parallel the nearest known magnetic anomaly isochrons [*Cande et al.*, 1989] and are offset along FZs interpreted from the gravity data. Where there are no magnetic anomaly data, or their azimuths are poorly-constrained, we generate synthetic age points using interpolated finite rotations to grow synthetic flow lines from seed-points of known age, and assume that isochrons through these points strike normal to the FZs.

[20] It is important to remember that interpolation of isochrons and rotations is sensitive to dating and magnetic timescale errors. Interpolation is also sensitive to some assumptions made implicitly when interpolating rotations and isochrons: firstly that seafloor spreading was continuous, and secondly that it was symmetrical about and, thirdly, perpendicular to, ridge crest segments. The assumption of continuity is reasonable because the reconstruction anomalies used are in quite short time steps, and their rotation parameters define synthetic FZs that are good matches to real ones in gravity data. However, for interpolation of magnetic isochrons, the assumption of symmetrical spreading is often less than reasonable and, if the interpolated stage

Geochemistry Geophysics Geosystems G3 EAGLES ET AL.: ANIMATED TECTONIC RECONSTRUCTION 10.1029/2003GC000657

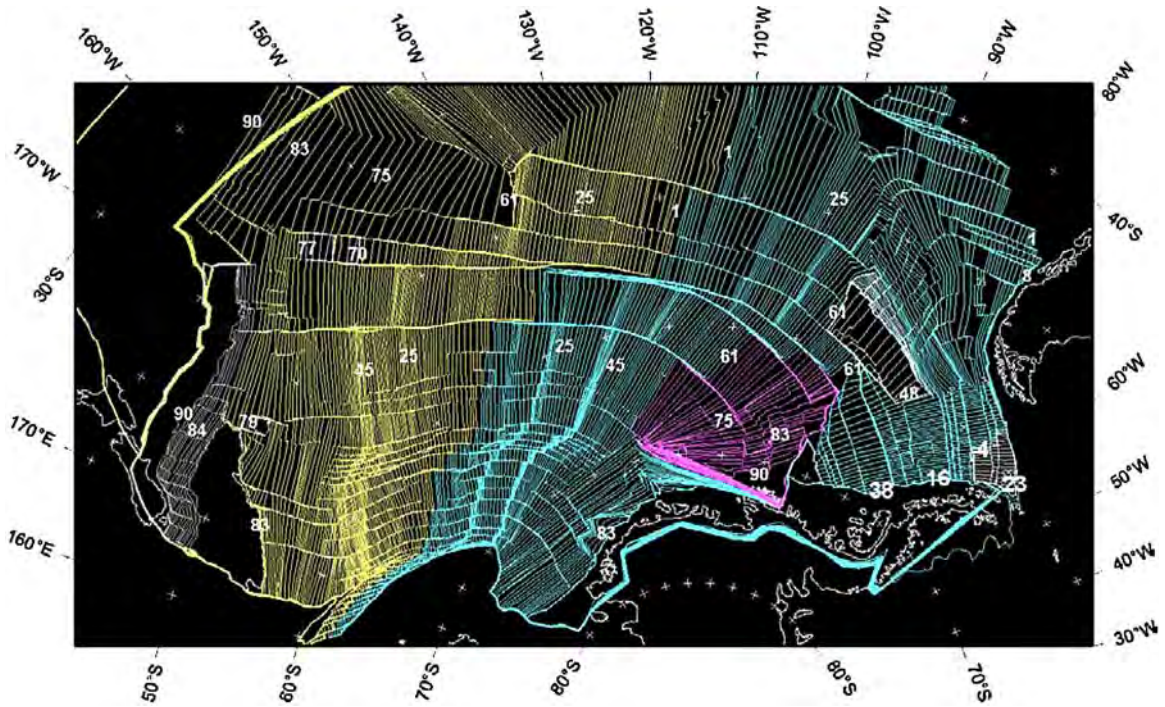

Figure 3. Plate masks on which the animation is based. Yellow, Pacific plate; blue, (West) Antarctic plate; mauve, Bellingshausen plate; light yellow, formed on Pacific plate but transferred to Antarctic plate; light blue, formed on the Farallon plate and transferred to the Antarctic plate; lilac, formed on the Bellingshausen plate and transferred to the Pacific plate; gray, formed on the Phoenix plate and transferred to the Antarctic plate (also Campbell Plateau, Chatham Rise, and Bollons Seamount masks). Numbers indicate the age of the masks (in Ma). Projection as in Figure 1.

is a long one, it could introduce significant inaccuracy into the animation. Oblique spreading is uncommon, and its presence can be tested for, crudely, by comparing the free-air anomaly grid, that often shows an isochron-parallel fabric, to the digitized masks.

[21] The finished masks are the framework for a set of ninety grid files of rotated data that are used to illustrate the steps in the animation. First, each mask is used to extract data from a composite grid file of Bellingshausen Sea and South Pacific free-air gravity anomalies [*Sandwell and Smith*, 1997; *McAdoo and Laxon*, 1997]. The grid file is generated simply, by adding over complementary amplitude ramps in the regions where the two published grids overlap. Any other grid file of suitable extent could, of course, be used. The extracted data are reformatted, rotated, and reregistered to new geographic grids using a combination of GMT [*Wessel and Smith*, 1998] and purpose-written FORTRAN routines and shell scripts.

[22] The reconstructed grid files are used as the bases of color frames for animation. Onshore in West Antarctica, the only significant region of land in the reconstructed region, we substitute the BEDMAP subice topography data set [*Lythe et al.*, 2000]. Selected land areas, mask outlines (to define the reconstructed plate boundaries) and isochron data from *Cande et al.* [1989] are reconstructed with the same set of rotation parameters and overlaid. The isochron data should coincide with the rotated masks at the divergent plate boundaries for reconstruction times that are near to the ages of mapped reversal anomalies. In fact, this is not always the case because our interpretation of divergent boundary segmentation is based on the free-air anomaly expression of FZs, but the compilation of magnetic anomaly isochrons we use [*Cande et al.*, 1989] is often based on sources that predate the widespread use of satellite altimetry data. An updated compilation of magnetic anomaly isochrons for the region that is also compatible with the segmentation evident from FZs in satellite

free-air gravity would improve the usefulness of isochron data overlaid on the grid reconstructions in the individual frames.

3. Results

[23] Animation 1 shows the parts of the animation covering the times discussed in this section (90–45 Ma). Animation 1 shows a "traffic light" symbol in its top-right corner that shows red in frames where finite rotations for the gridded part of the reconstruction are interpolated, amber where they are estimated from fits of continental outlines, and green where they are based on fits of both magnetic isochrons and FZ data. Below, we describe Animation 1 with reference to figures showing still frames from important epochs. The figures are annotated in order to enable readers to refer more easily to the text, whereas the equivalent frames in the animation are not. We present the frames from oldest first to youngest last, but it should be remembered that the two oldest reconstructions (90 and 83 Ma) are more speculative than the younger ones, because they are based on rather less well-constrained rotations based on seafloor fabric and visual fits of the continental margins.

3.1. Earliest Movements: 90-83 Ma

[24] The 90 Ma "complete fit" reconstruction in Figure 4 is based closely on that of *Larter et al.* [2002], and can be compared to that of *Sutherland* [1999]. The Osbourn Trough (OT) lies in the far north of the reconstructions. Although *Billen and Stock* [2000] proposed that OT was a spreading center that ceased activity at ~72 Ma, this was based on magnetic anomaly profiles that were too short to be unequivocal, and is not consistent with the effective elastic thickness of the lithosphere calculated from the loading effect of nearby seamounts of the Louisville chain [*Watts et al.*, 1988]. *Lonsdale* [1997] and *Larter et al.* [2002] suggest instead that OT was part of the Pacific–Phoenix ridge that stopped spreading at ~105 Ma, based on regional palaeomagnetic, geological and plate kinematic considerations. To the south, the Hikurangi Plateau, which is likely to be a thickened oceanic crustal igneous province, is juxtaposed today with Chatham Rise, which may indicate that a collision between them was responsible for extinction of OT [*Mortimer and Parkinson*, 1996]. Such an event would have accreted the Phoenix plate ocean floor south of OT to the Antarctic plate and, subsequently, necessitated a single new Pacific–Antarctic plate boundary to replace the Pacific–Phoenix boundary at OT and the Phoenix–Antarctic subduction zone. This plate boundary could have taken the form of extension of Zealandia, in the manner first suggested by *Luyendyk* [1995], and we show it as the opening of Bounty Trough and the Great South Basin. This depiction is broadly consistent with the subsidence and depositional history of the Great South Basin [*Carter*, 1988; *Cook et al.*, 1999] and with studies of Bounty Trough [*Davy*, 1993; *Cook et al.*, 1999]. Current work in western and central Bounty Trough is investigating whether seafloor spreading occurred there [*Gohl*, 2003].

[25] The animation shows simple southward convergence of the Charcot plate with the Antarctic margin in the period 90–84 Ma [*Larter et al.*, 2002]. Three gravity anomaly lineations, that *Larter et al.* [2002] termed X, Y, and Z and discussed in the context of the Charcot plate, are labeled, although we do not show anomaly X as a ridge-trench TF as those authors did. The Charcot plate's convergence is illustrative only in the absence of reliable indicators of relative movements, but it highlights the possible existence of a long ridge-trench TF along the plate's western edge. This TF, along which gravity anomaly Y may have formed, was later the location of convergence at the BGA [*Larter et al.*, 2002]. The setting of the Charcot plate fragment thus echoes that of the Phoenix plate fragment that is now welded to the Antarctic plate in Drake Passage [*Larter and Barker*, 1991], and present-day convergent motions across the Shackleton FZ [*Thomas et al.*, 2003] make it a useful analogue to the embryonic BGA. If *Lonsdale* [1997] and *Larter et al.* [2002] are correct in their assessment of OT as part of the Pacific–Phoenix ridge, then we can surmise that the Charcot plate must have converged more rapidly with the Antarctic plate than the Phoenix plate did, because of the subsequent development of gravity anomaly Z and its left-handed offset of anomaly C34y.

[26] The 83 Ma (~C34y) frame is shown in Figure 5. This reconstruction is also based on one of *Larter et al.*'s [2002] reconstructions, and can be compared to that of *Mayes et al.* [1990]. *Larter et al.* [2002] suggest that it is possible the timing of breakup was influenced by propagation of the Charcot–Pacific ridge into the gently extending Zealandia region. Hence we show the Pacific–Antarctic ridge as first becoming active in this frame, when extension in the Bounty Trough and Great South Basin ends. Western parts of the

Geochemistry Geophysics Geosystems G3 EAGLES ET AL.: ANIMATED TECTONIC RECONSTRUCTION 10.1029/2003GC000657

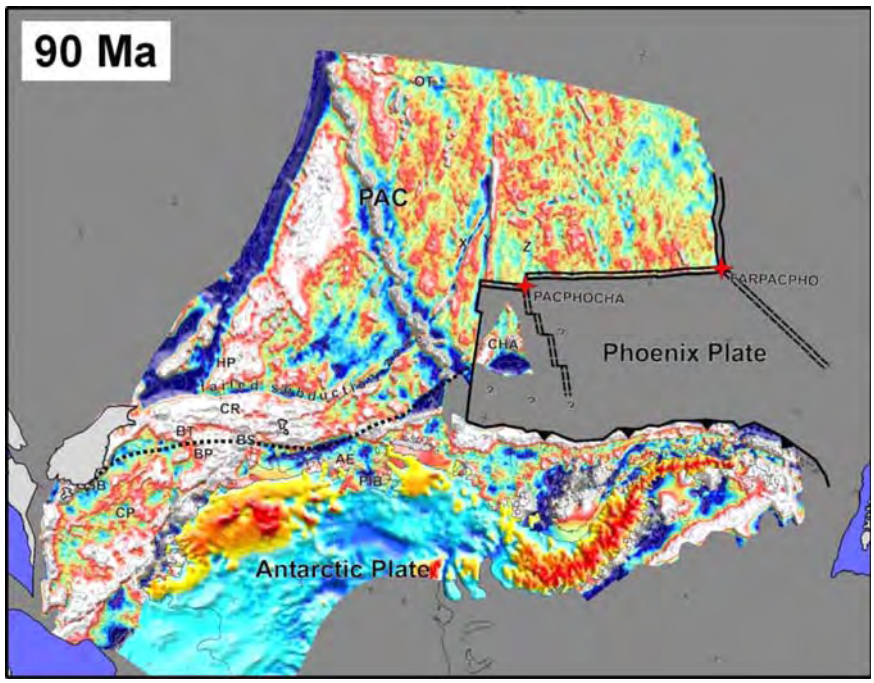

Figure 4. Animation frame for 90 Ma. Red four-point star, TJ; blue fill, continental blocks (defined from satellite-free-air gravity); gray fill, simplified present-day coastlines not in the West Antarctic plate subcircuit (see text). BEDMAP data onshore Antarctica, as in Figure 2; no attempt has been made to define the later plate boundary between West and East Antarctica. Labels as in Figure 1 plus CHA, surviving fragment of Charcot plate; FAR, Farallon; PAC, Pacific plate; PHO, Phoenix. Projection as in Figure 1, graticule interval 10°.

Pacific–Antarctic ridge are only just about to form between the Campbell Plateau and Marie Byrd Land, ~400 km inside the Antarctic flank of the older Bounty Trough/Great South Basin margin. We show the changeover as a simple jump of the entire locus of extension at 83 Ma, but a diachronous changeover could explain the lineament between the Bounty Platform and Campbell Plateau as a short-lived continental transform (dashed line in Figure 5).

[27] In both Figures 4 and 5, Bounty Trough, the Amundsen Embayment's coast, Pine Island Bay and the subglacial beneath Pine Island Glacier can be seen to be colinear features that approximate small circles about a pole nearby to the south. Hence it may be that these features are all lengths of a continental strike-slip zone (a rift zone would follow a great circle trend) that predated extension in the Bounty Trough region. This hypothetical strike-slip zone could be related to strain partitioning in response to oblique subduction or to a much older structure.

3.2. Seafloor Spreading: 83-76 Ma

[28] The 76 Ma (mid-chron C33) frame is shown in Figure 6. *Larter et al.* [2002] suggest the onset of independent movement of the Bellingshausen plate shortly after this time, at about 74 Ma, based on a change in strike of the Udintsev FZ, and two FZs northeast of it. However, *Eagles et al.* [2004] demonstrate Bellingshausen plate movement for times before 74 Ma, and relate these changes in FZ strike to the appearance of the long offset Tharp FZ on the Bellingshausen–Pacific ridge at this time. Hence a Bellingshausen plate is shown with an eastern boundary running through the Bellingshausen Gravity Anomaly (BGA). The plate's southern boundary is more speculatively located, on the bases of its possible identification in seismic reflection data near the Antipodes FZ [*Heinemann et al.*, 1999] and that post-C33y Bellingshausen–Antarctic movements appear to close Peacock Sound tightly [*Larter et al.*, 2002]. The boundary may instead have been confined to the oceanic crust north of Thurston Island (as considered by *Stock et al.* [1996]), or have occurred further into the Antarctic continent [*Larter et al.*, 2002].

[29] The Heezen TF has an offset of ~200 km, which starts to appear in the animation after 80 Ma. Anomaly Z fades out in the region just north of the Heezen and Tharp FZs. *Watts et al.* [1988] and *Larter et al.* [2002] show Z as the trace of a TJ

Geochemistry Geophysics Geosystems G3 EAGLES ET AL.: ANIMATED TECTONIC RECONSTRUCTION 10.1029/2003GC000657

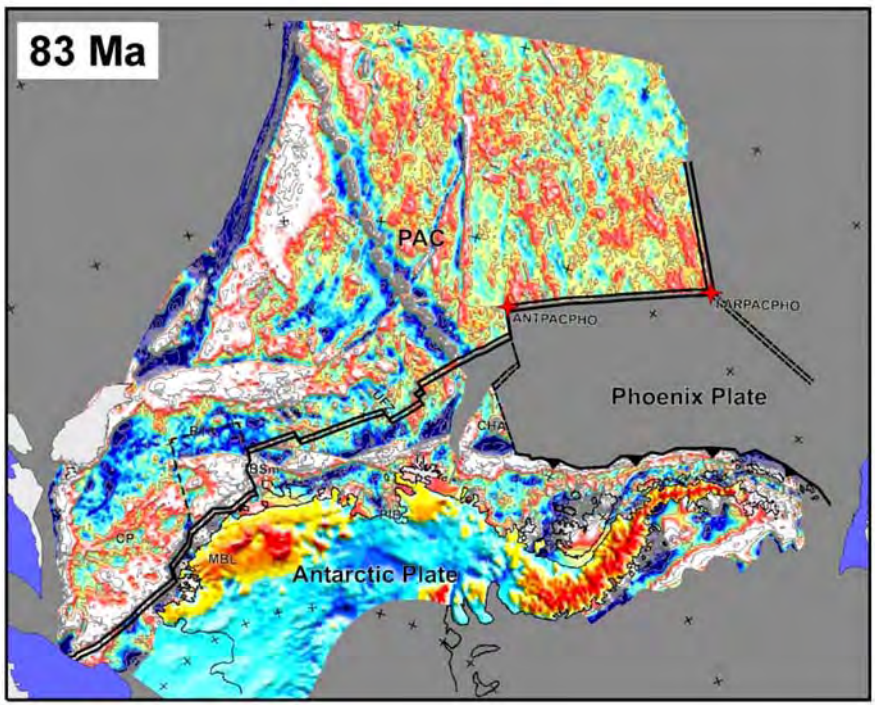

Figure 5. Animation frame for 83 Ma. Projection, graticule, symbols, and labels as for Figures 1 and 4.

between the Pacific, Phoenix and a third plate. *Eagles et al.* [2004] use magnetic anomaly profiles to show how the TJ migrated along a transfrom at Z and into the region now occupied by the Heezen FZ, and how this transform changed its offset sense and started to lengthen at about 80 Ma. They suggest that independent motion of the Bellingshausen plate was related to the appearance of long offset TFs in response to this change. Hence, in this frame (76 Ma), the third plate is the Bellingshausen plate, and the Heezen TF is growing between a northeastern fast spreading Pacific–Phoenix ridge segment and a slower southwestern Pacific–Bellingshausen one.

[30] A Phoenix–Bellingshausen–Antarctic TJ lies not far south of this TJ. The Bellingshausen–Phoenix plate boundary would have been very short at this stage and, by composition of a Bellingshausen–Pacific–Phoenix circuit for the stage C34y–C27o (Figure 7a), is likely to have been divergent [*McCarron and Larter*, 1998] (Figure 7b). The Phoenix–Bellingshausen–Antarctic TJ falls near the north end of a triangular region of underlap between the Bellingshausen plate and the captured Charcot fragment of the Antarctic plate [*Larter et al.*, 2002]. This triangular region represents surface area that no longer exists at the present-day—parts of Bellingshausen plate lithosphere that were compressed and thrust beneath the Antarctic plate. *Gohl et al.* [1997] and *Cunningham et al.* [2002] identified the BGA as a buried inactive compressional zone from seismic reflection data and gravity data modeling: it is the "trench" arm of the TJ. The animation shows ~200 km of horizontal shortening at the northern BGA, decreasing southward to zero southeast of Thurston Island near where the contemporary Bellingshausen–Antarctic stage pole lies, after this frame.

[31] The frame shows a third TJ, the Bellingshausen–Pacific–Antarctic triple junction, in the region of the Marie Byrd seamounts as ridge–ridge–ridge type, although the Bellingshausen–Antarctic arm may not have undergone true seafloor spreading due to its very slow divergence rate. *Heinemann et al.* [1999] identified buried topography in the region that they interpreted as a crossing of the Bellingshausen–Antarctic plate boundary graben, but this could also be interpreted as the TJ trace formed by the presence of a slow spreading arm on a ridge–ridge–ridge triple junction [*Mitchell and Parson*, 1993].

3.3. Seafloor Spreading: 76-68 Ma

[32] The 68 Ma (mid-chron C31) frame is shown in Figure 8. The triangular underlap to the east of the BGA has been greatly reduced by active conver-

Geochemistry Geophysics Geosystems G3 EAGLES ET AL.: ANIMATED TECTONIC RECONSTRUCTION 10.1029/2003GC000657

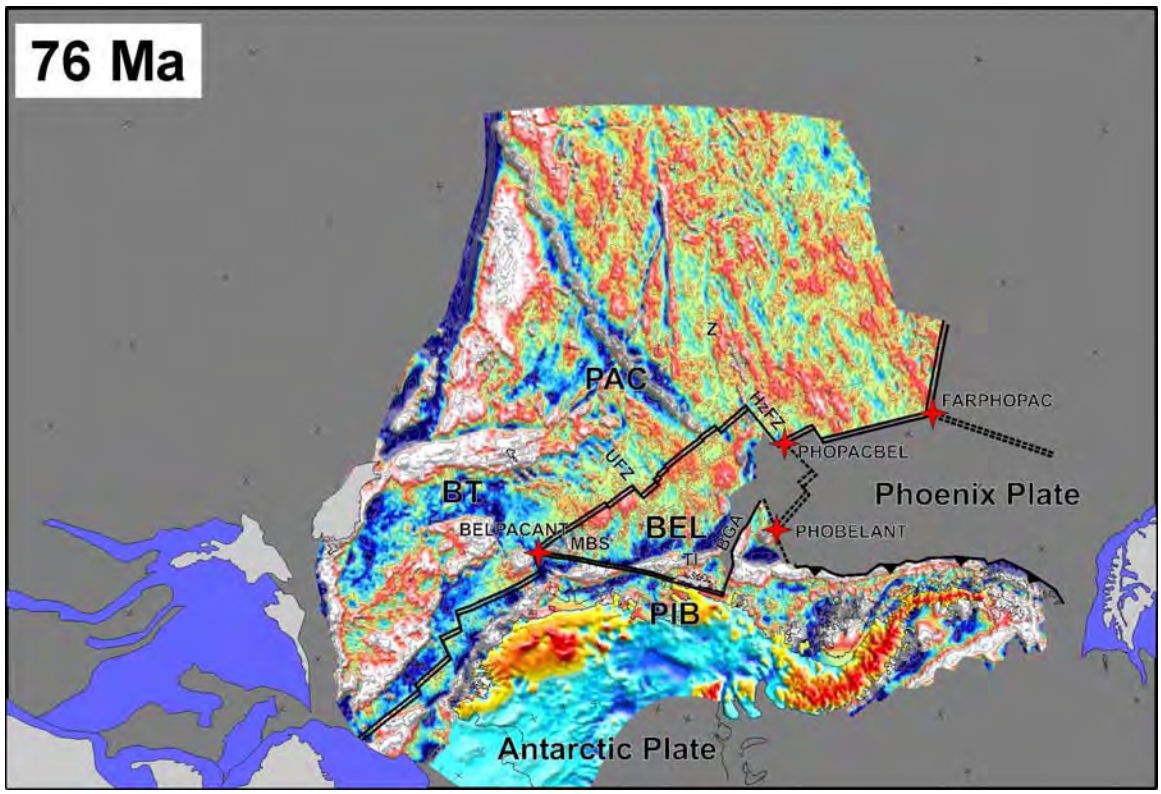

Figure 6. Animation frame for 76 Ma. Projection, graticule, symbols, and labels as for Figures 1 and 4 plus BEL, Bellingshausen plate; MBS, Marie Byrd Seamounts.

gence since the preceding (76 Ma) frame. This convergence occurs as a consequence of rotation of the Bellingshausen plate, relative to the Antarctic plate before chron C31, about stage poles nearby to its SE. The rotation is appropriate, as it corrects the FZ misfits presented by *McAdoo and Laxon*'s [1997] gridded reconstruction as evidence for Bellingshausen plate motion. We show continued rifting at the Bellingshausen–Antarctic boundary in Peacock Sound.

[33] In this frame, the Tharp TF can be seen to have an offset of ~250 km, in contrast to a much shorter offset before. The animation shows this offset to be the result of SE-directed jumps of the Pacific–Bellingshausen ridge at ~74 and ~70 Ma [*Eagles et al.*, 2004]. These events transferred large parts of the Bellingshausen plate to the Pacific plate. The Heezen TF simultaneously shortens due to each of these jumps, but immediately after each it resumes lengthening because it continues to host the Phoenix–Pacific–Bellingshausen TJ. The ridge jumps might have been a response to increasing stress on the lengthening Heezen TF arm of the TJ, which probably had an unstable geometry.

[34] The Udintsev TF is also lengthening in this frame, and does so between 74 Ma and 65 Ma, in response to along-strike variations in spreading asymmetry at the Bellingshausen–Pacific spreading center [*Stock et al.*, 1996; *Larter et al.*, 2002]. This lengthening accompanies that of the Heezen TF that hosted the Phoenix–Pacific–Bellingshausen TJ, and immediately follows the introduction of the Tharp TF into the Bellingshausen–Pacific spreading center by a ridge jump.

[35] There is no known evidence north of the BGA for shortening between the Bellingshausen and Antarctic plates. The Phoenix–Bellingshausen–Antarctic TJ could instead have existed to the southeast in the now-subducted region east of the captured Charcot fragment, perhaps migrating, as shown, along a transform on its NE facing edge and possibly even as far as the subduction zone at the Antarctic margin.

3.4. Seafloor Spreading: 68-61 Ma

[36] Figure 9 shows the reconstruction frame for 61 Ma (near the end of chron C27). The Bellingshausen plate is shown to have ceased independent motion as part of a suite of changes that occurred

Geochemistry Geophysics Geosystems G3 EAGLES ET AL.: ANIMATED TECTONIC RECONSTRUCTION 10.1029/2003GC000657

around Antarctica at about that time that may have included, or was shortly followed by, the onset of movements between East and West Antarctica [*Cande et al.*, 1995; *Müller et al.*, 2000; *Cande and Stock*, 2004]. Hence the underlap on the BGA no longer exists and no Bellingshausen plate boundaries are shown.

[37] The De Gerlache Gravity Anomaly (DGGA) extends north of the BGA as far as FZ "V". *Larter et al.* [1999] show how magnetic anomaly patterns suggest that the DGGA represents a scar from initiation of an Antarctic–Phoenix ridge after extinction of the Bellingshausen plate during the chron C27 tectonic reorganization. We show this new Antarctic–Phoenix ridge, with its crest geometry based on later isochron offsets east of the DGGA. In the previous sections, we noted the presence of the Pacific–Phoenix–Bellingshausen TJ, and its traces, in the region to the north of the BGA, and here we suggest that one of these traces may have formed a suitable target for the initiation of the new plate boundary there. *Gohl et al.* [1997] propose that this line was influential yet again later, as the DGGA formed a sublithospheric channel or upwelling locus for Miocene volcanism at Peter I Island [*Prestvik and Duncan*, 1991] and the De Gerlache Seamounts [*Hagen et al.*, 1998].

[38] The animation shows that the Heezen TF stops lengthening and, north of it, the TF on "V" starts lengthening, at ~64 Ma (young end of chron C29). These observations are subject to the correctness of the picks in *Cande et al.*'s [1989] compilation that come from *Cande et al.* [1982]. These workers interpret the observations to indicate northward movement of the Phoenix–Pacific–Bellingshausen TJ from the Heezen TF to TF "V" at 64 Ma. The Heezen TF thus acted as a simple, long offset, Bellingshausen–Pacific ridge transform after 64 Ma.

[39] Figure 9 shows the backtracked Louisville hot spot, as a red five-pointed star, that first appears in the animation at 73 Ma. The hot spot moves SE with respect to the Pacific plate during the course of the animation, tracking the line of free-air anomalies associated with the Louisville seamount chain. Where a located seamount's age is known, the animation shows it as an orange triangle symbol (as in Figure 9). The animation frames show all the gravity anomalies associated with seamounts on crust older than their age, rather than all those older than the age of the frame. It must be remembered that the "seamount" gravity anomalies SE of the hot spot are most likely not to have existed at the time of the frame being viewed. This failing is one area in which future versions of the animation could be significantly improved.

3.5. Seafloor Spreading: 61-55 Ma

[40] The 55 Ma (chron C24n.3) frame is shown in Figure 10. "V" finds itself in a new setting after the events at around C27. The West Antarctic–Pacific–Phoenix TJ, at the northern tip of the new Antarctic–Phoenix ridge along the DGGA, migrated ESE along "V" from about 91.5°W, 58.8°S. "V" hence underwent a diachronous transition between two settings: east of the TJ it operated in the Phoenix–Pacific system, but west of the TJ it was the site of a new West Antarctic–Pacific plate boundary. "V" was also lengthening all the time due to the spreading rate difference between the Pacific–Antarctic and Pacific–Phoenix ridges at its NW and SE ends, respectively. The nature of the West Antarctic–Pacific boundary on "V" is difficult to predict because it is difficult to define its preexisting trace as a Phoenix–Pacific feature due to complicated free-air anomalies and sparse magnetic anomaly data east of the DGGA. We illustrate a situation in which the Antarctic–Phoenix ridge tip propagates northward to stay in contact with a TJ migrating along a "V" drawn through one of the northernmost free-air anomaly troughs in the area, which retains a strike-slip character. We interpret the SE-trending free-air anomaly troughs to the south of this as FZs formed on the Antarctic–Phoenix ridge. If we had chosen to draw "V" in a more southerly position, then we could interpret the free-air anomaly features as rugged topography formed at, or north of, a reactivated transpressional "V".

[41] Following chron C27, Pacific–West Antarctic spreading gradually rotated into a slightly more WNW azimuth than its previous NW one, and a substantial drop in spreading rate is demonstrable from finite rotations between C27 and C25/C24 [*Mayes et al.*, 1990; *Cande et al.*, 1995]. Our animation shows the Pacific–Antarctic ridge's responses to these changes. In the SW sector of the ridge, the previous set of 4 medium or short offset, mostly left-stepping TFs is replaced by 2–3 times as many short offset, right-stepping TFs, as noted by *Cande et al.* [1995]. In drawing our masks, we have assumed that the process involved was symmetrical and involved simultaneous ridge crest subsegmentation and rotation of the subsegments. If these assumptions are correct, the animation suggests the TF population increase was

Geochemistry Geophysics Geosystems G3 EAGLES ET AL.: ANIMATED TECTONIC RECONSTRUCTION 10.1029/2003GC000657

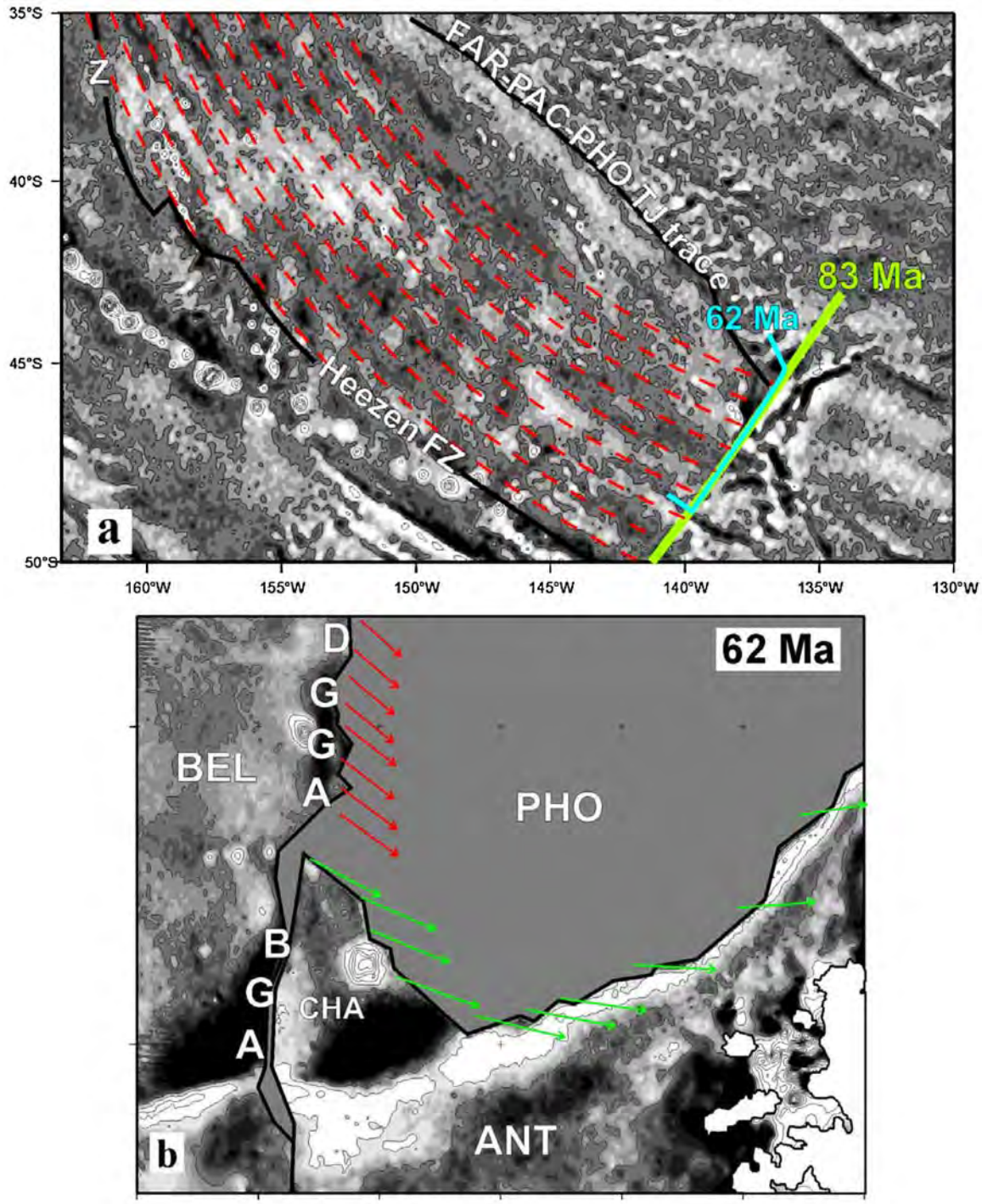

Figure 7. Estimation of relative Bellingshausen–Phoenix and Antarctic–Phoenix plate movements. (a) A Pacific–Phoenix stage pole for C34y–C27, in the Phoenix plate reference frame, is calculated by reconstructing parts of the 83 Ma (∼C34y) and 62 Ma (∼C27) Pacific plate masks (fit shown by green and blue lines, rotation of 30.15° about pole at 126.5°W, 17.2°S). Red dashed lines are segments of small circles about this stage pole, compared to free-air anomaly fabric in the area created by Pacific–Phoenix spreading during that stage. (b) Stage pole from Figure 7a used in the Pacific–Phoenix–Bellingshausen plate circuit to calculate Phoenix–Bellingshausen and Phoenix–Antarctic plate motions, for which ∼1 m.y. long vectors are shown as red and green arrows, respectively. The base map is the 62 Ma reconstruction frame with a 5° graticule interval. Mercator projections.

Geochemistry Geophysics Geosystems G3 EAGLES ET AL.: ANIMATED TECTONIC RECONSTRUCTION 10.1029/2003GC000657

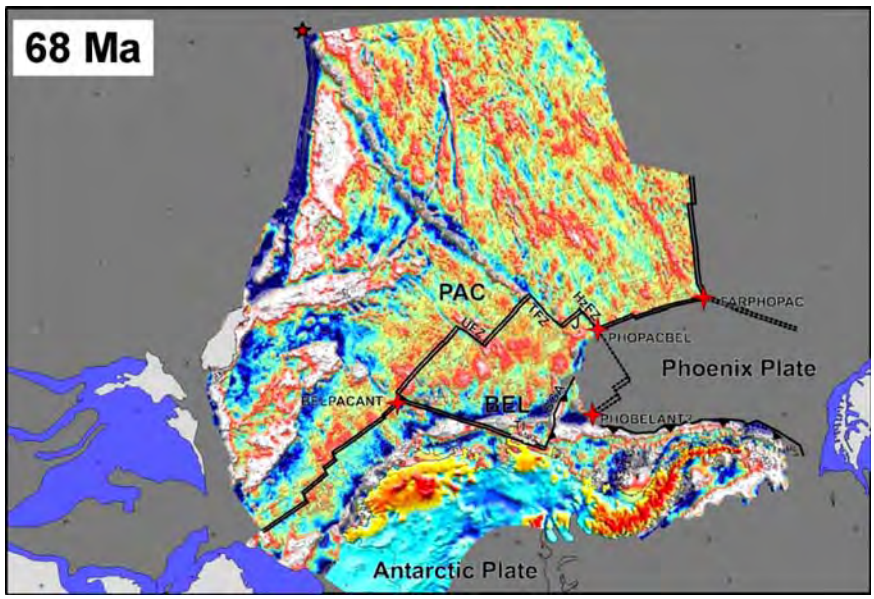

Figure 8. Animation frame for 68 Ma. Projection, graticule, symbols, and labels as for Figures 1 and 4 plus red five-point star, backtracked position of the Louisville Hot spot; J, Segment of PACBEL ridge crest that jumped to the SE at ~70 Ma.

complete by ~58 Ma (chron C26), when the full set of short-offset TFs can be seen for the first time. Similar increases have been documented from the South Atlantic [*Cande et al.*, 1988] between anomalies C30 and C20, and from the Weddell Sea [*Livermore and Hunter*, 1996] near anomaly M4. In both cases, the FZ population increases have been related to spreading rate reductions. A mantle response, involving a change from 2D to 3D mantle upwelling, has been hypothesized as the reason for this connection between decreased spreading rates and increased FZ density [*Phipps*

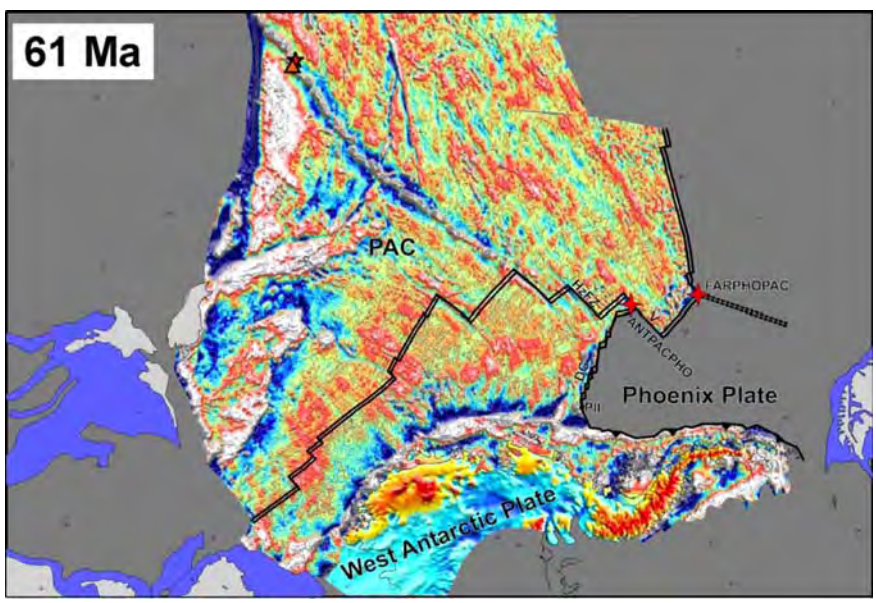

Figure 9. Animation frame for 61 Ma. Projection, graticule, symbols, and labels as for Figures 1 and 4 plus DG, De Gerlache Gravity Anomaly and De Gerlache Seamounts; orange triangle, dated sample from Louisville seamount chain (to the nearest 1 m.y. interval [*Watts et al.*, 1988]).

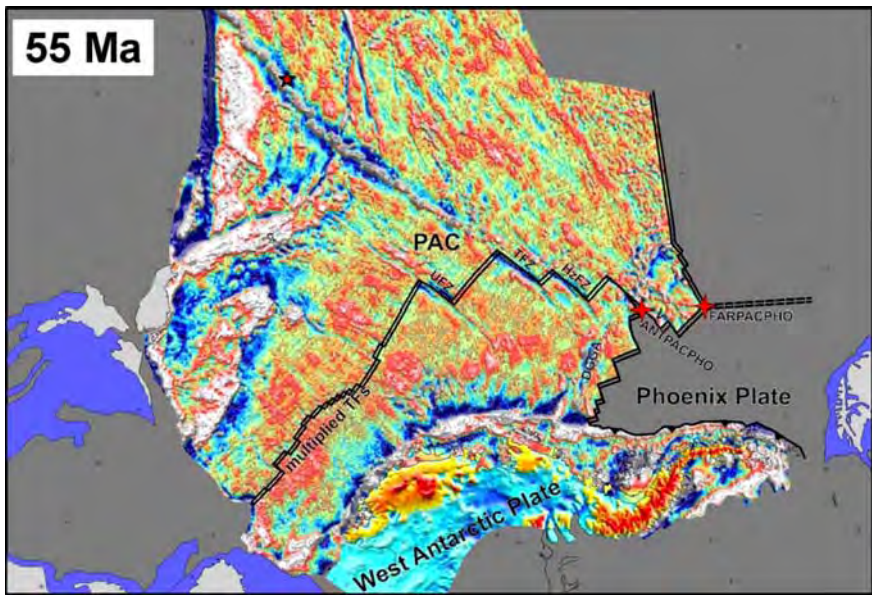

Figure 10. Animation frame for 55 Ma. Projection, graticule, symbols, and labels as for Figures 1 and 4.

Morgan and Parmentier, 1995]. If such a connection is envisaged for the South Pacific, the sudden spreading rate decrease that is visible by between chrons C27 and C25/C24 in predictions from published finite rotations may be more accurately dated to just before chron C26.

[42] The response of the Pacific–Antarctic ridge to the changes around C27 was different further north. In this frame, the amplitudes of the most recently formed parts of linear ridge-trough gravity anomalies marking the Udintsev, Tharp and Heezen TFs are markedly increased. The first appearance of the higher amplitudes along the FZs is also around anomaly C26 and appears to be independent of the different offset lengths of the TFs. Hence we think it is unlikely that the pattern is a result of differential thermal subsidence across the TFs, and suggest instead that it may be the result of transpression across these three long transforms, introduced during the rotation of Pacific–Antarctic relative motion that followed the C27 reorganization event.

3.6. Seafloor Spreading: 55-46 Ma

[43] The 46 Ma (reversed part of chron C20) frame is shown in Figure 11. The long offset Phoenix–Pacific TF on "V" no longer exists, having been bypassed by northward propagation of the Pacific–Antarctic ridge through ~15 m.y. old Pacific plate lithosphere from a starting point over 1000 km northwest of the final position of the West Antarctic–Pacific–Phoenix TJ [*Cande et al.*, 1982; *Mammerickx and Sandwell*, 1986]. This event formed a new Pacific–Antarctic spreading corridor between "V" and the Menard TF, changed the Farallon–Pacific–Phoenix TJ at the southeastern end of the Humboldt FZ to a Farallon–Antarctic–Phoenix one, and created a new Pacific–Antarctic–Farallon TJ at the Menard TF.

[44] The northward propagation of the Pacific–Antarctic ridge that formed the southern and central parts of the Henry and Hudson troughs passed through lithosphere that had formed at the Pacific–Phoenix ridge just prior to C27, and so the path of propagation may have been influenced by features that had developed in response to the C27 event. The reconstructed northern parts of the Henry and Hudson troughs are rotated by some 25°–30°, clockwise, with respect to their more southerly parts, and border anomalies C24–C21 formed between the Farallon and Pacific plates [*Cande et al.*, 1982]. Propagation here is thus likely to have exploited a Farallon–Pacific FZ. Although the active part of "V" was over 1000 km long by the time of propagation, it is tempting to speculate that the build up of stress on it was not alone enough to set off the propagation event, because propagation did not occur until the northern tip of the Antarctic–Phoenix ridge, south of "V", and the southern tip of the Pacific–Phoenix ridge, north of it, coincided, and the Pacific–Phoenix ridge south of "V"

Geochemistry Geophysics Geosystems G3 EAGLES ET AL.: ANIMATED TECTONIC RECONSTRUCTION 10.1029/2003GC000657

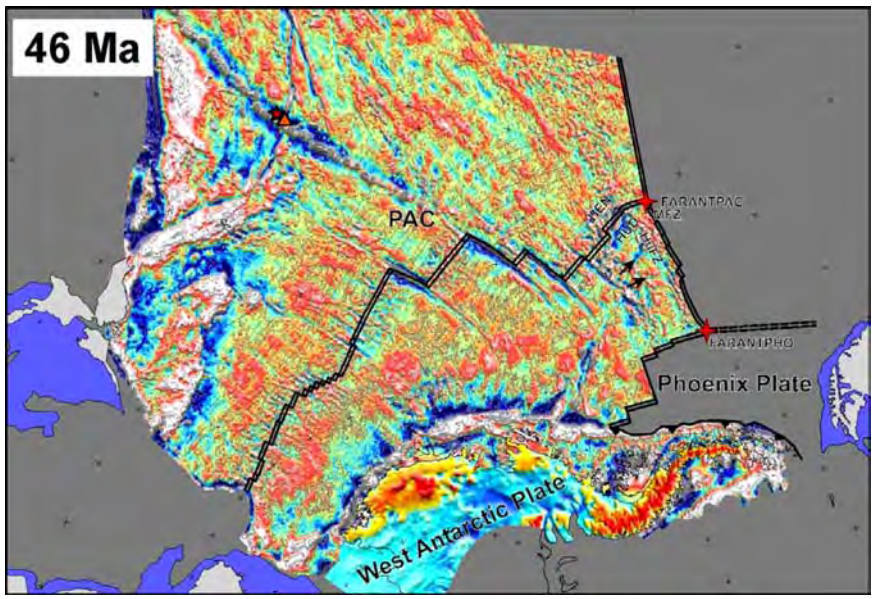

Figure 11. Animation frame for 46 Ma. Projection, graticule, symbols, and labels as for Figures 1 and 4 plus black arrows are isochron-parallel troughs in the captured crust north of "V".

was juxtaposed with Pacific plate lithosphere formed during the C27 reorganization.

[45] Isochron-parallel free-air gravity lows cross, or partially cross, the "V"–Menard corridor east of the Hudson trough, in the region of crust that was captured. *Cande* et al's [1982] profile 11 shows a double peaked magnetic anomaly C26 that coincides with the most westerly of these troughs, suggesting that some limited accretion may have occurred at it. It is possible that these features record failed westward Pacific–Phoenix ridge jumps or failed attempts to initiate a microplate in the "V"–Menard corridor, attempts to maintain "V" as active, by shortening its offset.

4. Discussion: Pre-90 Ma Events North of Chatham Rise

[46] The Hikurangi Plateau has been suggested as a conjugate feature to the ~123 Ma [*Mahoney et al.*, 1993] Manihiki Plateau Large Igneous Province that was separated from it by OT spreading, and OT has been suggested to have been part of the Pacific–Phoenix ridge that was inactivated at ~105 Ma [*Lonsdale*, 1997; *Larter et al.*, 2002]. If this was the case, it would require half spreading rates of ~90km/m.y., which are reasonable when compared to those estimated for the Pacific–Phoenix ridge in the same time period [*Larson et al.*, 2002]. However, a Manihiki-Hikurangi plateau fit would not be possible if the intervening seafloor all appeared as part of the Pacific–Phoenix ridge because it requires overall NNE-oriented relative movements, whereas Pacific–Phoenix movement was N- to NNW-oriented in the same time frame, according to abyssal hill fabric [*Larson et al.*, 2002]. However, if NNE motion had occurred, it gives an opportunity to understand gravity anomaly X other than as a long offset trench-ridge transform, whose long offset is hard to explain in the context of approach of the Charcot plate to the trench when anomaly Y already fills such a role. In fact, anomaly X is crosscut by anomaly Y at ~165.5°W, 31.6°S, and Y seems to have formed after migration of the Pacific–Phoenix ridge away from the extinct OT feature after the Hikurangi Plateau–Chatham Rise collision at ~105 Ma [*Larter et al.*, 2002]. Hence it may be that X initially formed during movements that predate Y, between the Pacific plate and another plate to the south. Specifically, X may be in part a conjugate feature to the transtensional Manihiki Scarp [*Stock et al.*, 1998] that formed after the Pacific–Phoenix ridge jumped to the Manihiki Plateau at ~119 Ma [*Larson et al.*, 2002]. A TJ between the Pacific, Phoenix and this third plate may have passed along the scarp before turning west as the Pacific–Phoenix ridge propagated west to form the ancestor to the OT. The area of seamounts between the southern end of the

Manihiki scarp and the Tonga trench at ~19°S may contain this TJ trace.

5. Summary

[47] Reconstructions made with gridded data are a way of making paleotectonic maps with detailed coverage, and relatively free of interpretation or selection by the paleocartographers, available to the geoscientific community. Animated reconstructions are powerful tools that enable presentation and discussion of paleogeography and plate tectonic histories. Our animation of reconstruction models of plate tectonic motions presents the established tectonic framework of the southern Pacific region in a widely accessible form. The animation, like any reconstruction technique, is confined to be interpreted within the constraints imposed by the starting assumptions of the animation method, and of the procedures used to derive rotation parameters, and by the data. Nonetheless, the animation allows us to illustrate events that are described in existing publications, as well as some new ones, and to connect them all as parts of the evolution of a single large ocean basin.

[48] The mid Cretaceous South Pacific margin of Gondwana was later modified by extension. A first phase of extension before chron C34y can be related to capture of part of the Phoenix plate by the Antarctic plate following collision of the Hikurangi Plateau, and the establishment of a proto Pacific–Antarctic plate margin in the Bounty Trough and Great South Basin. A second phase of Pacific–Antarctic extension, between Campbell Plateau and Marie Byrd Land, may have followed the close approach of the Charcot–Pacific ridge to this earlier margin around chron C34y, and capture of the Charcot plate by the Antarctic plate. The thus-formed mid-ocean ridge was soon afterward seeded with long offset transform faults that formed in relation to the onset and progress of independent movements of the Bellingshausen plate, itself possibly a result of the Pacific–Phoenix ridge having overtaken the Pacific–Antarctic ridge. These movements necessitated yet another extensional episode within Antarctica that may have opened Peacock Sound or other features such as Pine Island Bay between chrons C33o and C27. All of these separate Antarctic extensional plate margins may have reactivated separate lengths of a single preexisting strike-slip plate boundary or structural trend.

[49] Alongside this last extensional episode, the eastern margin of the Bellingshausen plate was shortened by up to ~200 km of convergence in the north, and by decreasing amounts further south, along a collision zone that formed by reactivation of a transform fault along the western edge of the part of the Charcot plate that had been inherited by the Antarctic plate. Around chron C27, the Bellingshausen plate ceased to have any kinematic identity, the Pacific–Antarctic plate system inherited the set of long offset transform faults from the Pacific–Bellingshausen system, and spreading changed direction and decreased in rate soon afterward. The southern sector of the Pacific–Antarctic ridge saw an increase in the number and a reversal in the offset sense of some transforms that may be related to the spreading rate decrease.

[50] The long offset transform at "V" was not simply inherited by the Pacific–Antarctic plate system around C27, because it was intersected by the northern tip of a new Antarctic–Phoenix ridge that appeared SW of it. The thus-formed Phoenix–Pacific–Antarctic triple junction migrated southeastward along the southwestern side of "V". The exact results this would have had are hard to predict because of equivocal data: but overall "V" grew ever longer while its northwestern parts were progressively transferred into the Antarctic–Phoenix system. Eventually, this complicated feature was bypassed by northeastward propagation of the Pacific–Antarctic ridge at its northwestern end. The scene was thus set for the later development of the region that was dominated by seafloor spreading at the Pacific–Antarctic and Antarctic–Phoenix ridges and the progressive subduction of the Phoenix plate beneath the Antarctic Peninsula.

Acknowledgments

[51] This project was funded by the German Research Foundation (DFG) through the grants GO 724/2-1 and GO 724/2-2. We thank Rupert Sutherland and one anonymous reviewer, as well as the numerous people who commented on earlier drafts of the animation during conference, workshop, and other presentations.

References

Barker, D. H. N., and J. A. Austin (1998), Rift propagation, detachment faulting, and associated magmatism in Bransfield Strait, Antarctic Peninsula, *J. Geophys. Res.*, *103*, 24,017–24,043.

Behrendt, J. C., W. E. LeMasurier, A. K. Cooper, F. Tessensohn, A. Trehu, and D. Damaske (1991), Geophysical studies

of the West Antarctic Rift System, *Tectonics*, *15*, 1257–1273.

Billen, M., and J. Stock (2000), Morphology and origin of the Osbourn Trough, *J. Geophys. Res.*, *105*, 13,481–13,489.

Cande, S. C., and D. V. Kent (1995), Revised calibration of the geomagnetic polarity time scale for the late Cretaceous and Cenozoic, *J. Geophys. Res.*, *100*, 6093–6096.

Cande, S. C., and J. M. Stock (2004), Cenozoic reconstructions of the Australia-New Zealand-South Pacific sector of Antarctica, in *Climate Evolution in the Southern Ocean and Australia's Cenozoic Flight North from Antarctica*, edited by N. F. Exon, M. Malone, and J. P. Kennett, AGU, Washington, D. C., in press.

Cande, S. C., E. M. Herron, and B. R. Hall (1982), The early Cenozoic tectonic history of the southeast Pacific, *Earth Planet. Sci. Lett.*, *57*, 63–74.

Cande, S. C., J. L. LaBrecque, and W. F. Haxby (1988), Plate kinematics of the South Atlantic: Chron C34 to present, *J. Geophys. Res.*, *93*, 13,479–13,492.

Cande, S. C., J. L. LaBrecque, R. L. Larson, W. C. Pitman III, X. Golovchenko, and W. F. Haxby (1989), *Magnetic Lineations of the World's Ocean Basins, Map 131*, Am. Assoc. of Pet. Geol., Tulsa, Okla.

Cande, S. C., C. A. Raymond, J. Stock, and W. F. Haxby (1995), Geophysics of the Pitman Fracture Zone and Pacific–Antarctic plate motions during the Cenozoic, *Science*, *270*, 947–953.

Cande, S. C., J. M. Stock, R. D. Müller, and T. Ishihara (2000), Cenozoic motion between East and West Antarctica, *Nature*, *404*, 145–150.

Carter, R. M. (1988), Post-breakup stratigraphy of the Kaikoura System (Cretaceous–Cenozoic), continental margin, southeastern New Zealand, *N. Z. J. Geol. Geophys.*, *31*, 405–429.

Chang, T. (1987), On the statistical properties of estimated rotations, *J. Geophys. Res.*, *92*, 6319–6329.

Cook, R. A., et al. (1999), *Cretaceous-Cenozoic Geology and Petroleum Systems of the Great South Basin, New Zealand*, *Monogr. 20*, 188 pp., Inst. of Geol. Nucl. Sci., Lower Hutt, New Zealand.

Cunningham, A. P., R. D. Larter, P. F. Barker, K. Gohl, and F. O. Nitsche (2002), Tectonic evolution of the Pacific margin of Antarctica: 2. Structure of Late Cretaceous–early Tertiary plate boundaries in the Bellingshausen Sea from seismic reflection and gravity data, *J. Geophys. Res.*, *107*(B12), 2346, doi:10.1029/2002JB001897.

Davy, B. W. (1993), The Bounty Trough—Basement structure influences on sedimentary basin evolution, in *Sedimentary Basins of the World*, vol. 2, *South Pacific Sedimentary Basins*, edited by P. F. Ballance, pp. 69–92, Elsevier Sci., New York.

Eagles, G. (2000), Modelling plate kinematics in the Scotia Sea, Ph.D. thesis, Univ. of Leeds, Leeds, U. K.

Eagles, G. (2003), Tectonic evolution of the Antarctic–Phoenix plate system since 15 Ma, *Earth Planet. Sci. Lett.*, *217*, 97–109.

Eagles, G., and R. A. Livermore (2002), Opening history of Powell Basin, Antarctic Peninsula, *Mar. Geol.*, *185*, 195–205.

Eagles, G., K. Gohl, and R. D. Larter (2004), Life of the Bellingshausen plate, *Geophys. Res. Lett.*, *31*, L07603, doi:10.1029/2003GL019127.

Gaina, C., R. D. Müller, J.-Y. Royer, J. Stock, J. Hardebeck, and P. Symonds (1998a), The tectonic history of the Tasman Sea: A puzzle with 13 pieces, *J. Geophys. Res.*, *103*, 12,413–12,433.

Gaina, C., W. Roest, and P. Symonds (1998b), The opening of the Tasman Sea: A gravity anomaly grid animation, *Earth Inter.*, *2*. (Available at http://EarthInteractions.org)

Gohl, K., F. O. Nitsche, and H. Miller (1997), Seismic and gravity data reveal Tertiary interplate subduction in the Bellingshausen Sea, southeast Pacific, *Geology*, *25*, 371–374.

Gohl, K. (Ed.) (2003), Structure and dynamics of a submarine continent: Tectonic-magmatic evolution of the Campbell Plateau (New Zealand), report of RV *SONNE* cruise SO-169, project CAMP, 17 January to 24 February 2003, *Rep. Polar Mar. Res. 457*, 88 pp., Alfred Wegener Inst., Bremerhaven, Germany.

Hagen, R. A., K. Gohl, R. Gersonde, G. Kuhn, D. Völker, and V. N. Kodagali (1998), A geophysical survey of the De Gerlache Seamounts: Preliminary results, *Geo Mar. Lett.*, *18*, 19–25.

Hall, R. (2002), Cenozoic geological and plate tectonic evolution of SE Asia and the SW Pacific: Computer-based reconstructions and animations, *J. Asian Earth. Sci.*, *20*, 353–434.

Heinemann, J., J. Stock, K. Clayton, S. Hafner, S. Cande, and C. Raymond (1999), Constraints on the proposed Marie-Byrd Land–Bellingshausen plate boundary from seismic reflection data, *J. Geophys. Res.*, *104*, 25,321–25,330.

Hellinger, S. J. (1981), The uncertainties of finite rotations in plate tectonics, *J. Geophys. Res.*, *86*, 9312–9318.

Larson, R. L., R. A. Pockalny, R. F. Viso, E. Erba, L. J. Abrams, B. P. Luyendyk, J. M. Stock, and R. W. Clayton (2002), Mid-Cretaceous tectonic evolution of the Tongareva triple junction in the southwestern Pacific Basin, *Geology*, *30*, 67–70.

Larter, R. D., and P. F. Barker (1991), Effects of ridge-crest–trench interaction on Antarctic-Phoenix spreading: Forces on a young subducting plate, *J. Geophys. Res.*, *96*, 19,583–19,607.

Larter, R. D., A. P. Cunningham, P. F. Barker, K. Gohl, and F. O. Nitsche (1999), Structure and tectonic evolution of the West Antarctic continental margin and Bellingshausen Sea, *Korean J. Polar Res.*, *10*, 125–133.

Larter, R. D., A. P. Cunningham, P. F. Barker, K. Gohl, and F. O. Nitsche (2002), Tectonic evolution of the Pacific margin of Antarctica: 1. Late Cretaceous tectonic reconstructions, *J. Geophys. Res.*, *107*(B12), 2345, doi:10.1029/2000JB000052.

Livermore, R. A., and R. J. Hunter (1996), Mesozoic seafloor spreading in the southern Weddell Sea, in *Weddell Sea Tec-*

tonics and Gondwana Break-up, edited by B. C. Storey, E. C. King, and R. A. Livermore, *Geol. Soc. Spec. Publ.*, *108*, 227–241.

Livermore, R. A., et al. (2000), Autopsy on a dead spreading center: The Phoenix Ridge, Drake Passage, Antarctica, *Geology*, *28*, 607–610.

Lonsdale, P. (1997), An incomplete geologic history of the southwest Pacific basin, *Geol. Soc. Am. Abstr. Programs*, *29*, 4574.

Luyendyk, B. P. (1995), Hypothesis for Cretaceous rifting of east Gondwana caused by subducted slab capture, *Geology*, *23*, 373–376.

Lythe, M. B., D. G. Vaughan, and the BEDMAP Consortium (2000), BEDMAP—Bed topography of the Antarctic, scale 1:10,000,000, Br. Antarct. Surv., Cambridge, U. K.

Mahoney, J. J., M. Storey, R. A. Duncan, K. J. Spencer, and M. Pringle (1993), Geochemistry and age of the Ontong Java Plateau, in *The Mesozoic Pacific: Geology, Tectonics and Volcanism*, *Geophys. Monogr. Ser.*, vol. 77, edited by M. S. Pringle et al., pp. 233–261, AGU, Washington, D. C.

Mammerickx, J., and D. Sandwell (1986), Rifting of old oceanic lithosphere, *J. Geophys. Res.*, *91*, 1975–1988.

Marks, K. M., and J. M. Stock (1997), Early Tertiary gravity field reconstructions of the Southwest Pacific, *Earth Planet. Sci. Lett.*, *152*, 267–274.

Mayes, C. L., L. A. Lawver, and D. T. Sandwell (1990), Tectonic history and new isochron chart of the South Pacific, *J. Geophys. Res.*, *95*, 8543–8567.

McAdoo, D. C., and S. Laxon (1997), Antarctic tectonics: Constraints from an ERS-1 satellite marine gravity field, *Science*, *276*, 556–560.

McCarron, J. J., and R. D. Larter (1998), Late Cretaceous to early Tertiary subduction history of the Antarctic Peninsula, *J. Geol. Soc. London*, *155*, 255–268.

Mitchell, N. C., and L. M. Parson (1993), The tectonic evolution of the Indian Ocean Triple Junction, anomaly 6 to present, *J. Geophys. Res.*, *98*, 1793–1812.

Mortimer, N., and D. Parkinson (1996), Hikurangi Plateau: A Cretaceous large igneous province in the southwest Pacific, *J. Geophys. Res.*, *101*, 687–696.

Müller, R. D., and W. R. Roest (1992), FZs in the North Atlantic from combined Geosat and Seasat data, *J. Geophys. Res.*, *97*, 3337–3350.

Müller, R. D., C. Gaina, A. Tikku, D. Mihut, S. C. Cande, and J. M. Stock (2000), Mesozoic/Cenozoic tectonic events around Australia, in *The History and Dynamics of Global Plate Motions*, *Geophys. Monogr. Ser.*, vol. 121, pp. 161–188, AGU, Washington, D. C.

Nankivell, A. P. (1997), Tectonic history of the Southern Ocean since 83 Ma, Ph.D. thesis, Oxford Univ., Oxford, U. K.

Phipps Morgan, J., and E. M. Parmentier (1995), Crenulated seafloor: Evidence for spreading-rate dependent structure of mantle upwelling and melting beneath a mid-oceanic spreading centre, *Earth Planet. Sci. Lett.*, *129*, 73–84.

Prestvik, T., and R. A. Duncan (1991), The geology and age of Peter I Øy, Antarctica, *Polar Res.*, *9*, 89–98.

Reeves, C., and B. K. Sahu (1999), Computer animation of Gondwana dispersal and the history of igneous extrusion in the Indian Ocean, paper presented at IUGG99, Int. Union of Geod. and Geophys., Birmingham, U. K.

Royer, J.-Y., and N. Rollet (1997), Plate-tectonic setting of the Tasmanian region, in *West Tasmanian Margin and Offshore Plateaus: Geology, Tectonic and Climatic History, and Resource Potential*, edited by N. F. Exon, and A. J. Crawford, *Aust. J. Earth Sci.*, *44*, 543–560.

Sandwell, D. T., and W. H. F. Smith (1997), Marine gravity anomaly from Geosat and ERS 1 satellite altimetry, *J. Geophys. Res.*, *102*, 10,039–10,054.

Shaw, P. R., and S. C. Cande (1990), High resolution inversion for South Atlantic plate kinematics using joint altimeter and magnetic anomaly data, *J. Geophys. Res.*, *95*, 2625–2644.

Stock, J. M., and P. Molnar (1987), Revised early Tertiary history of plate motions in the southwest Pacific, *Nature*, *325*, 495–499.

Stock, J. M., S. C. Cande, and C. A. Raymond (1996), Updated history of the Bellingshausen Plate, *Eos Trans. AGU*, *77*, Fall Meet. Suppl., F647.

Stock, J. M., B. P. Luyendyk, R. W. Clayton, and Shipboard Scientific Party (1998), Tectonics and structure of the Manihiki Plateau, western Pacific Ocean, *Eos Trans. AGU*, *79*, Fall Meet. Suppl., F870.

Sutherland, R. (1995), The Australia-Pacific boundary and Cenozoic plate motions in the SW Pacific: Some constraints from Geosat data, *Tectonics*, *14*, 819–831.

Sutherland, R. (1999), Basement geology and tectonic development of the greater New Zealand region: An interpretation from regional magnetic data, *Tectonophysics*, *308*, 341–362.

Thomas, T., R. A. Livermore, and F. Pollitz (2003), Motion of the Scotia Sea plates, *Geophys. J. Int.*, *155*, 789–804.

Tikku, A., and S. C. Cande (2000), On the fit of Broken Ridge and Kerguelen plateau, *Earth Planet. Sci. Lett.*, *180*, 117–132.

Watts, A. B., J. K. Weissel, R. A. Duncan, and R. L. Larson (1988), Origin of the Louisville Ridge and its relationship to the Eltanin Fracture Zone System, *J. Geophys. Res.*, *93*, 3051–3077.

Wessel, P., and L. Kroenke (1997), A geometric technique for relocating hotspots and refining absolute plate motions, *Nature*, *387*, 365–369.

Wessel, P., and W. H. F. Smith (1998), New, improved version of Generic Mapping Tools released, *Eos Trans. AGU*, *79*, 579.

Wood, R., R. Herzer, R. Sutherland, and A. Melhuish (2000), Cretaceous-Tertiary tectonic history of the Fiordland margin, New Zealand, *N. Z. J. Geol. Geophys.*, *43*, 289–302.

Yan, C.-Y., and L. W. Kroenke (1993), A plate tectonic reconstruction of the southwest Pacific, 0–100 Ma, *Proc. Ocean Drill. Program Sci. Results*, *130*, 697–709.

Publication 6.1.2:

Eagles, G., **Gohl, K.**, Larter, R.D. (2009a). Animated tectonic reconstruction of the southern Pacific and alkaline volcanism at its convergent margins since Eocene times. *Tectonophysics*, v. 464, pp. 21-29, doi:10.1016/j.tecto.2007.10.005.

Author contributions: This study is an ‘add-on’ to the earlier postdoc project of Eagles which was originally applied for by Gohl and funded by the Deutsche Forschungsgemeinschaft (see 6.1.4 and 6.1.5). The paper was written by Eagles with contributions in additional data and text parts by Gohl and Larter.

Available online at www.sciencedirect.com
ScienceDirect
Tectonophysics 464 (2009) 21–29
TECTONOPHYSICS
www.elsevier.com/locate/tecto

Animated tectonic reconstruction of the Southern Pacific and alkaline volcanism at its convergent margins since Eocene times

Graeme Eagles [a,*], Karsten Gohl [b], Robert D. Larter [c]

[a] Geology Department, Royal Holloway University of London, Egham, TW20 0EX, UK
[b] Alfred Wegener Institute for Polar and Marine Research, Postfach 120161, Bremerhaven D-27515, Germany
[c] British Antarctic Survey, High Cross, Madingley Road, Cambridge, CB3 0ET, UK

Received 8 May 2007; received in revised form 11 October 2007; accepted 31 October 2007
Available online 6 November 2007

Abstract

An animated reconstruction shows South Pacific plate kinematics, in the reference frame of West Antarctica, between 55 Ma and the present-day. The ocean floor in the region formed due to seafloor spreading between the Antarctic, Pacific, Phoenix and Nazca plates (a plate formed by fragmentation of the Farallon plate early in Oligocene times). The Pacific–Antarctic Ridge remained fairly stable throughout this time, migrating relatively northwestwards, by various mechanisms, behind the rapidly-moving Pacific plate. The Nazca and Phoenix plates also moved quickly, but relatively towards the east or southeast, and were subducted in these directions beneath the South American and Antarctic plates. Segments of spreading centres forming at the trailing edges of the Nazca and Phoenix plates periodically collided with these subduction zones, resulting in the total destruction of the Nazca–Phoenix spreading centre and the partial destruction of the Nazca–Antarctica spreading centre (the Chile Ridge) and Antarctic–Phoenix Ridge, which ceased to operate shortly before its northeasternmost three segments could collide with the Antarctic margin. Following collision of segments of the Chile Ridge, parts of the Antarctic plate underwent subduction at the Chile Trench. After these collisions, slab windows should have formed beneath both the South American and Antarctic convergent margins, and the animation shows occurrences of alkaline volcanism that have been, or can newly be, related to them. Further occurrences of alkali basalts, at the margins of the Powell Basin and, more speculatively, James Ross Island, can be related to the formation of a slab window beneath them following the collision of segments of the South America–Antarctica spreading centre in the northwest Weddell Sea.

Keywords: Plate kinematics; Subduction; Slab windows; Alkaline volcanism; Antarctica; South America

1. Introduction

The Late Cretaceous and early Tertiary plate kinematic history of the Southwest Pacific was complicated and involved independent movements of a small oceanic plate (Stock and Molnar, 1987; Stock et al., 1996; Eagles et al., 2004a), subduction and the consequences of its cessation (Larter et al., 2002), and a major plate-tectonic reorganization around chron C27 (~61 Ma) (Cande et al., 1995).

Further north and east (Fig. 1), and during later times, the situation was somewhat simpler. The Phoenix plate underwent subduction beneath the Antarctic Peninsula at its southeastern boundary, with which segments of the Antarctic–Phoenix ridge periodically collided leading to near-total destruction of the Phoenix plate (Larter and Barker, 1991). During much of Paleogene times, Antarctica underwent extension as the West Antarctic rift system slowly moved East Antarctica apart from West Antarctica, which we assume here included the Antarctic Peninsula (Behrendt et al., 1991; Cande et al., 2000). In addition to this, a complex of oceanic basins developed in the Scotia Sea at the region's eastern extremity, where west-directed subduction of the South American plate resulted in slow eastwards motion of an arc plate, as seen from Antarctica (Eagles et al., 2005). In the northeast of the study area, the Farallon plate moved rapidly eastwards towards a subduction zone at the western margin of South America (Cande and Leslie, 1986). At its southern and western edges, new seafloor material accreted

* Corresponding author. Tel.: +44 1784 443890; fax: +44 1784 471780.
E-mail address: g.eagles@gl.rhul.ac.uk (G. Eagles).

0040-1951/$ - see front matter © 2007 Elsevier B.V. All rights reserved.
doi:10.1016/j.tecto.2007.10.005

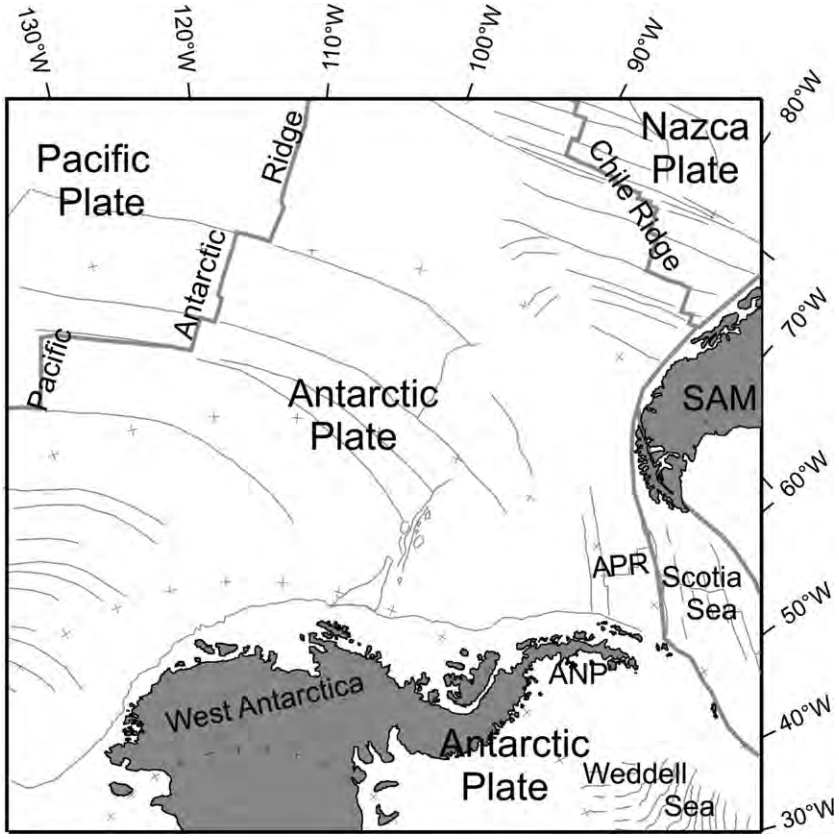

Fig. 1. Prominent lineaments interpreted from gravity anomalies of the southern Pacific, illustrating places referred to in the introduction. ANP: Antarctic Peninsula, APR: Antarctic–Phoenix Ridge, SAM: South America. Present-day plate boundaries are shown as bold grey lines.

to the Farallon plate at its margins with the Pacific, Antarctic and Phoenix plates (Cande et al., 1982). At about 23 Ma, the Farallon plate broke up into two smaller plates (Meschede and Barckhausen, 2000) the southern of which, Nazca, continued to subduct at the southern Chile Trench.

From time to time, ridge crests and/or transform faults collided with the subduction zones at the east of the region, changing the identity of the overriding plate and, with it, the rate and azimuth of relative plate motion. As a result, subduction either ceased, or changed in such a way that the subducted slabs momentarily or permanently disappeared from the depths they had previously occupied below the overriding plates, forming so-called slab windows. Worldwide, the formation of slab windows has been related to the presence of alkaline volcanism on the overriding plates in those locations lacking features that are usually taken as independent evidence for extension or mantle plumes, to which such volcanism is otherwise usually attributed (Thorkelson and Taylor, 1989). Because these rocks contain little or no trace of contamination by subduction-related processes, it is thought that they originate when mantle material that had previously been trapped beneath the slab rapidly ascends into the volume vacated by the slab, and undergoes decompression melting.

Here we review together the plate tectonic history of the southern Pacific Ocean and the alkaline volcanism at its convergent margins, using a high resolution animation of plate kinematics illustrated by its oceanic free-air gravity anomalies (McAdoo and Laxon, 1997; Sandwell and Smith, 1997).

2. Method

Eagles et al (2004b) describe the creation of a set of grid files showing reconstructed gravity anomalies and the BEDMAP sub-ice topography data set (Lythe et al., 2000) that are used as the bases of colour frames for an animation concentrating on the period 90–45 Ma. In addition to these, for this new animation we have included gridded data showing the onshore topography of South America (Smith and Sandwell, 1996), and gravity data showing the formation of the Powell Basin and motion of the Nazca plate east of the Chile Ridge. To do this we used rotation parameters for Antarctica–Nazca and Powell Basin relative motions taken from Tebbens and Cande (1997) and Eagles and Livermore (2002). Small motions of the Hudson microplate (Eakins, 2002), and the Selkirk, Friday, and other microplates at the margins of the Nazca plate (Tebbens and Cande, 1997; Tebbens et al., 1997) are not depicted as there are no rotations published to describe them, although the incorporated microplates are shown after their extinctions.

As in the earlier study, we show reconstructed plate boundaries and isochron data from Cande et al. (1989) as vector data overlaid on the individual frames. All magnetic anomalies are dated based on the magnetic reversal timescale of

Cande and Kent (1995). To these vector data, here, we add data showing the occurrence of alkali basalts that have been, or can be, related to the formation and presence of slab windows. In South America, these are shown as either violet-filled point locations or outcrop patterns, and each location persists in the animation for all times between the oldest and youngest published radiometric ages for the occurrence. In Antarctica, where outcrop is limited or alkaline volcanism is known from dredged seafloor samples, we only show point data. The published ages are of varying vintage and reliability, with both K–Ar (particularly in Antarctica) and Ar–Ar dating methods having been used. Where no published dates exist, we have assigned outcrops ages that are the same as the nearest dated occurrences. Where the locations of rocks with published dates are not precisely given, we have assigned the ages to the nearest mapped occurrence of alkaline volcanic rocks that we found in the literature.

3. Results

A *QuickTime* movie shows the parts of the animation covering the period 55 Ma to the present day. The first 10 million years of the animation also appear in Eagles et al's (2004b) contribution. The animation shows a 'traffic light' symbol in its top-right corner that shows red in frames where finite rotations for the gridded part of the reconstruction are interpolated and green where they are based on fits of both magnetic isochrons and fracture zone data. Below, we describe the animation with reference to still frames from important epochs. The figures are annotated in order to enable readers to

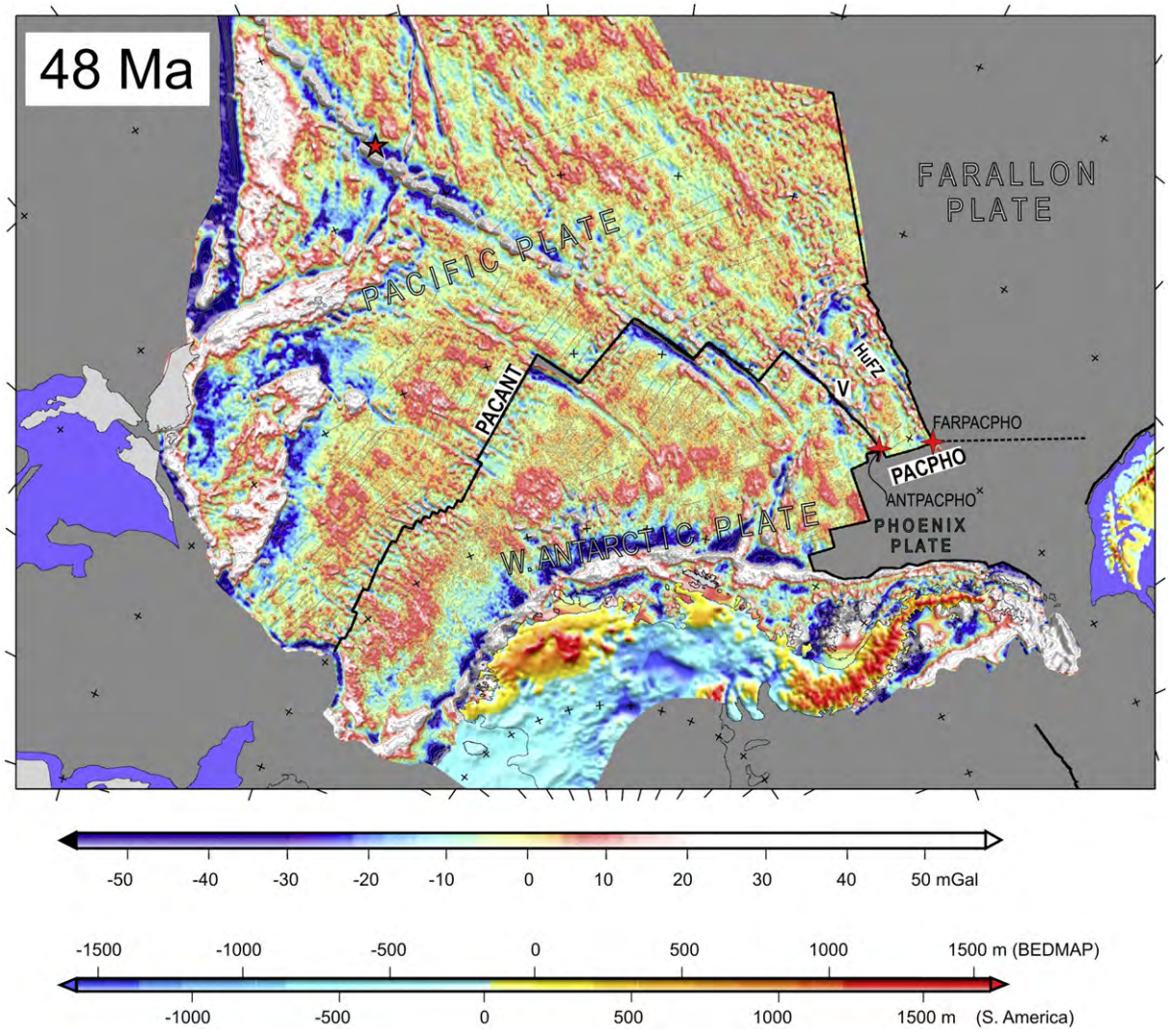

Fig. 2. Reconstruction animation frame for 48 Ma, made with respect to a fixed West Antarctica. Red four-point star symbol: triple junctions, in this and following figures labelled with identities of bordering plates: ANT: Antarctica, FAR: Farallon, NAZ: Nazca, PAC: Pacific, PHO: Phoenix. Blue fill: continental shelves (edges defined using satellite-free-air gravity), pale gray fill: simplified present day coastlines. BEDMAP sub-ice topography (Lythe et al., 2000) and surface topography (Smith and Sandwell, 1997) are shown onshore West Antarctica and South America. No attempt has been made to define the plate boundary between West Antarctica and East Antarctica. Oblique Mercator projection centred on 137.5°W, 65°S and with 74°W, 60°S on the oblique equator. Graticule interval 10°. HuFZ: Humboldt Fracture Zone, PACANT: Pacific–Antarctic Ridge, PACPHO: Pacific–Phoenix Ridge, V: Fracture Zone "V".

refer more easily to the text, whereas the equivalent frames in the animation are not.

3.1. Aftermath of a tectonic reorganisation: 55–46 Ma

The 48 Ma (chron C20r) reconstruction is shown in Fig. 2. A very long offset transform fault, now visible as the fracture zone "V", has reached its greatest length. The animation shows how this feature grows longer between segments of the Pacific–Antarctic Ridge, at its northwestern tip, and the Phoenix–Pacific Ridge, at its southeastern tip. Subsequently, at 47–46 Ma, the transform is deactivated when the Pacific–Antarctic ridge propagates through ~15 m.y. old Pacific plate lithosphere at its western end (Cande et al., 1982; Mammerickx and Sandwell, 1986). This event formed a new Pacific–Antarctic spreading corridor between "V" and the Menard transform fault, changed the Farallon–Pacific–Phoenix triple junction at the southeastern end of the Humboldt Fracture Zone to a Farallon–Antarctic–Phoenix one, and created a new Pacific–Antarctic–Farallon triple junction at the Menard transform fault. Further south on the Pacific–Antarctic Ridge, a corrugated seafloor pattern can be seen to have just come into existence, which has been related to a decrease in spreading rates occurring during a plate tectonic reorganization at 61 Ma (Eagles et al., 2004b). This event is the latest in a series of events whose consequences are northeastwards lengthening of the Pacific–Antarctic plate boundary.

3.2. Slab window south of the Tula Fracture Zone: 40 Ma

In the period after 46 Ma, lengthening of the Pacific–Antarctic plate boundary continues by migration of a stable ridge–ridge–ridge triple junction between the Pacific, Antarctic and Farallon plates (Fig. 3). The Antarctic–Farallon–Phoenix triple junction, further south, migrates NE. In the period 35–25 Ma, a large change in relative motions occurs between the Farallon and Antarctica plates. This can be seen in the orientation of fracture zones formed on the Farallon–Antarctic plate boundary, which changes from N–S to almost E–W. This event expresses changes that occurred in the relative motions of the Pacific and Farallon plates in the run-up to the disintegration of the Farallon plate into the Cocos and Nazca plates by the initiation of spreading on the Galapagos Ridge at about 23 Ma (Meschede and Barckhausen, 2000). The Nazca–Antarctic and Pacific–Antarctic plate boundaries propagate rapidly northwards at about 21 Ma, in the process capturing an area of the seafloor that is thought to have formed at a ridge crest microplate south of the Valdivia fracture zone (Tebbens and Cande, 1997).

In the northeast, seafloor of the Farallon (and later Nazca) plate subducts beneath South America. As this seafloor no longer exists, it cannot be represented in the animation and appears there as unfilled grey space. Here, we refer to space like this as 'underlap'. Further south, the earliest collisions between segments of the Antarctic–Phoenix Ridge and the subduction

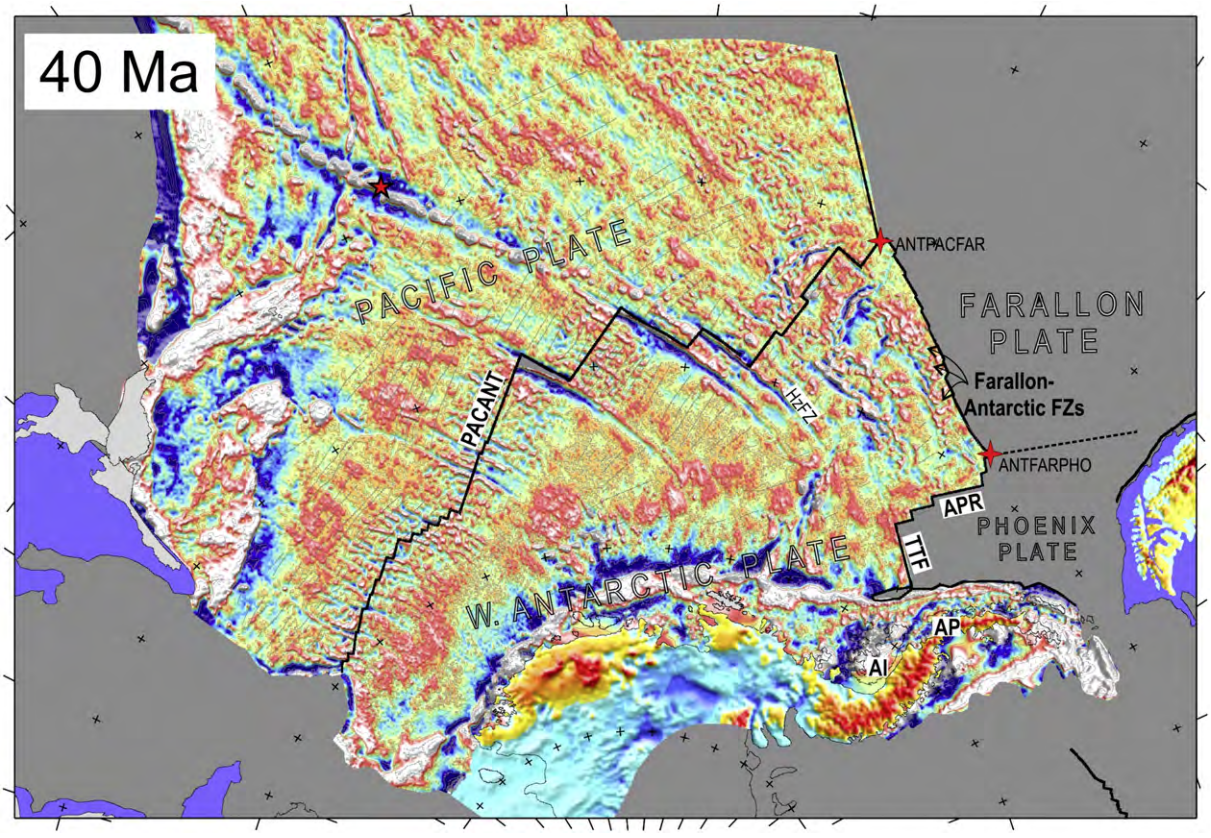

Fig. 3. Animation frame for 40 Ma. Projection, graticule, symbols and labels as for Figs. 1 and 2, plus AI: Alexander Island, AP: Antarctic Peninsula, HzFZ: Heezen Fracture Zone, TTF: transform fault forming the Tula Fracture Zone. Dotted lines: approximate limits of selected slab windows (see text for details).

zone at the West Antarctic margin occur starting at around 44 Ma, to the south of the transform fault whose action formed the Tula Fracture Zone (McCarron & Larter, 1998). In this setting, the Antarctic plate was both the trailing plate and the overriding plate, meaning that subduction ought to have stopped after each collision. Consistent with this scenario, calc–alkaline flows and intrusions over and into accretionary prism rocks of the LeMay Group on Alexander Island, all of which can be related to the subduction, cease at about the same time as the ridge crest–trench collisions (Hole, 1988). By halting subduction, each collision should also have contributed to the growth of a slab window beneath the southern parts of the Antarctic Peninsula and Alexander Island. We show the approximate shape of this slab window, assuming subduction at an angle of 45° and no deformation of the downgoing slab, with a dotted line in Fig. 3 and later figures. The animation, however, shows that alkaline volcanism is not known from above this window until 25 m.y. later, in the form of Miocene-aged lamprophyre dykes on Alexander Island (Smellie et al., 1988).

3.3. Slab window beneath Powell Basin: 35–20 Ma

Powell Basin, at the northern tip of the Antarctic Peninsula, opened as a result of the slow eastward movement of the upper, arc, plate to the ancestral South Sandwich–Discovery Trench with respect to Antarctica, as shown by differences in spreading rates between the West Scotia and South American–Antarctic ridges (Eagles et al., 2005; Fig. 4). Barker et al (1982) show that this subduction zone, whose present-day successor is to be found at the South Sandwich Trench, reached at least as far south as the southern edge of the South Orkney Microcontinent, a continental crustal fragment that bears the South Orkney Islands on the basin's eastern flank. A bathymetric ridge about 100 km southeast of the microcontinent, with highs named Jane Bank and Discovery Bank, is interpreted as the extinct Discovery arc that formed above the subduction zone. Subduction ceased as segments of the South-American–Antarctic Ridge in the northern Weddell Sea collided with, or ceased operating just outboard of, the Discovery arc, starting as early as chron C6 (20 Ma) in the SW and most recently at chron C3 (6 Ma) in the northeast (Barker et al., 1982, 1984). The animation shows the active parts of the spreading centre as a black line in the northern Weddell Sea. The cessation of subduction east of the Powell Basin resulted in the basin's extinction by around 20 Ma (Eagles and Livermore, 2002).

These ridge crest–trench collisions would have resulted in the development of a slab window beneath the South Orkney Microcontinent because, as was the case on the western side of the Antarctic Peninsula, the overriding and trailing plates in the subduction system were, by these times, identical: the Antarctic plate. Consistent with the development of such a slab window, dredge samples from the western margin of the South Orkney Microcontinent yielded young (0–4.5 Ma) alkali basalts that

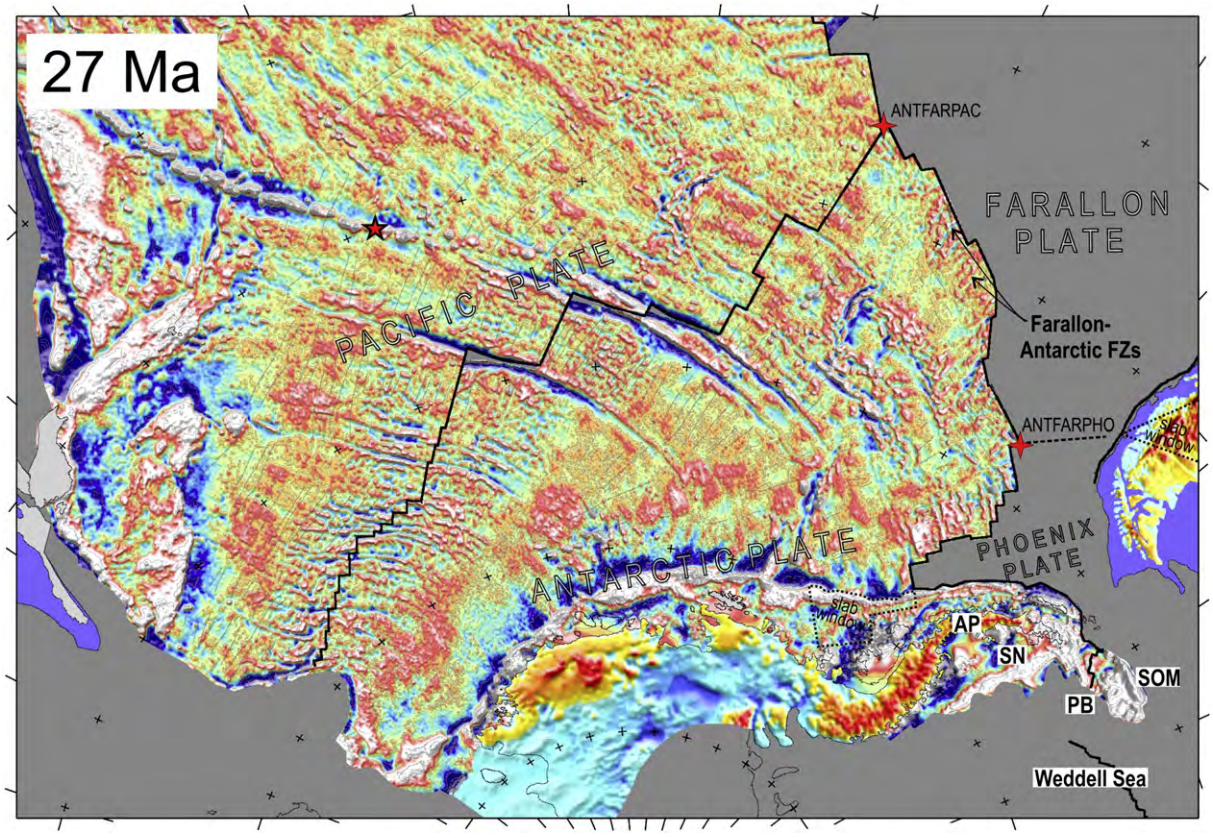

Fig. 4. Animation frame for 27 Ma. Projection, graticule, symbols and labels as for Figs. 2 and 3, plus PB: Powell Basin, SN: Seal Nunataks, SOM: South Orkney Microcontinent.

Barber et al (1991) found to be geochemically closely comparable to those reported from further south on the Antarctic Peninsula (Smellie et al., 1988). The timing of the start of slab window development here is rather difficult to assess, because the slow spreading rates in the northern Weddell Sea make it difficult to model magnetic profiles running up to the extinct subduction zone with any confidence. If the ages given above are reliable, the time lag between the start of slab window development in the southeast and the eruption of the dredged alkali basalts in Powell Basin is about 15 m.y.

3.4. Slab windows beneath Cape Horn and north of the Tula Fracture Zone: 20–4 Ma

Following 20 Ma, and the northward propagation of the Pacific–Antarctic and Nazca–Antarctic ridges, the Valdivia transform fault lengthens rapidly by several hundred kilometres between the two northern ridge tips. This process ends at about 13 Ma, when the Nazca–Antarctic ridge propagates northwards to the Chile transform fault (beyond the northern edge of the figures and animation), in the process trapping the core of a further ridge-crest microplate, the Friday microplate (Tebbens and Cande, 1997). During the same period, the animation shows how the northeastern tip of the Antarctic–Phoenix ridge very obliquely approaches, and eventually collides with, the southernmost part of the Chile Trench. Before collision, this tip would have been the site of a Nazca–Phoenix–Antarctica triple junction, to the east of which a Nazca–Phoenix spreading centre would have existed and may have been undergoing subduction beneath southernmost South America (e.g. Larter and Barker, 1991). This process should have formed a slab window between the subducting slabs attached to the diverging Nazca and Phoenix plates, to which it is possible to relate the 18.8–18.2 Ma alkali basalts of Packsaddle Island and the Hardy Peninsula, near Cape Horn (Puig et al., 1984). If this is appropriate, the same publication's reported occurrence of ~21 m.y. old calc–alkaline volcanic rocks also on Hardy Peninsula leads us to conclude that the ridge crest would have been subducted some time between 21 and 19 Ma. Fig. 5, the reconstruction for 20 Ma, accordingly shows the Nazca–Phoenix spreading centre immediately south of the Chile Trench. With the possible exception of the area lying today immediately west of Elephant Island, all of the seafloor added to the Phoenix plate at this spreading centre seems to have been subducted, meaning there is little chance of being able to independently confirm or refute the proposed presence and action of the slab window caused by its collision.

All this time, and afterwards, accretion continued at the Antarctic–Phoenix Ridge, and the Phoenix plate continued to be subducted beneath the Antarctic Peninsula (Larter and Barker, 1991;Livermore et al., 2000; Eagles, 2003). This situation inevitably led to further ridge crest–trench collisions

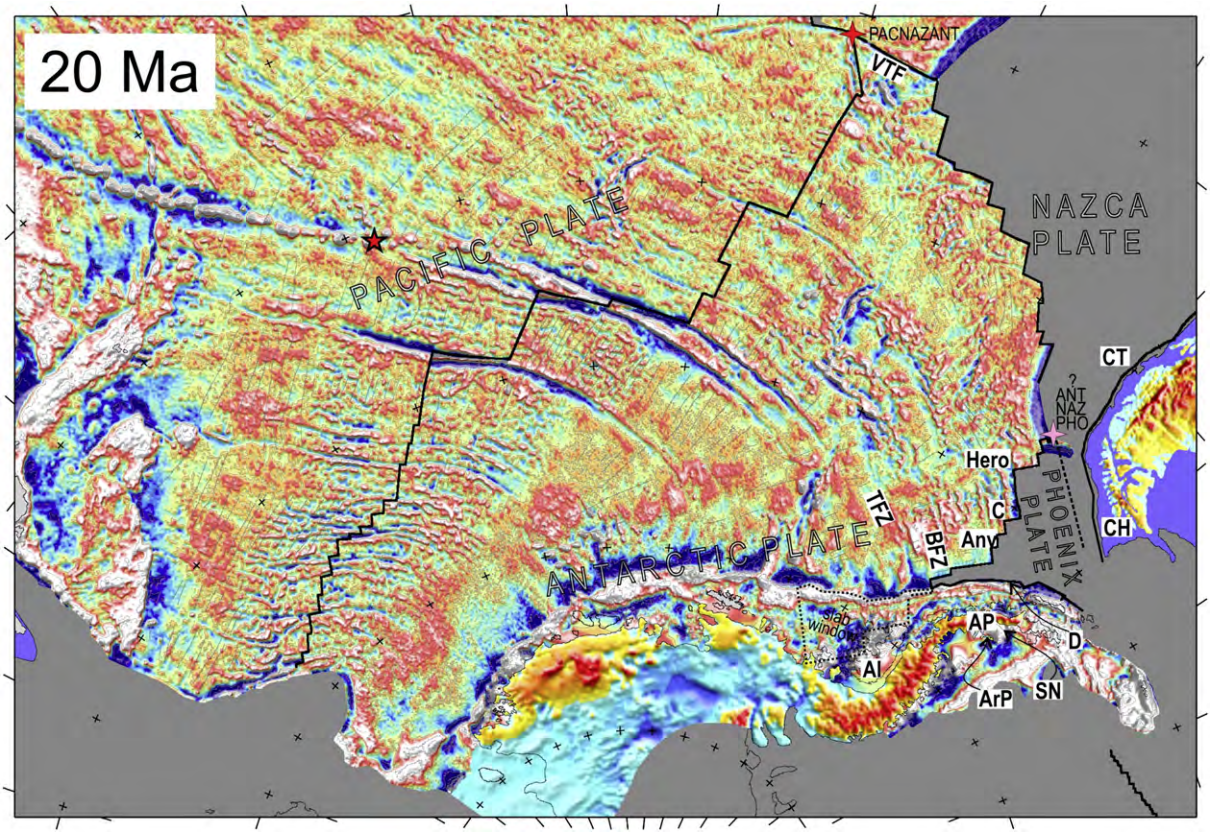

Fig. 5. Animation frame for 20 Ma. Projection, graticule, symbols and labels as for Figs. 2–4 plus Anv: Anvers transform fault and fracture zone, ArP: Argo Point, BFZ: Biscoe Fracture Zone, C: Fracture Zone 'C', CH: Cape Horn, CT: Chile Trench, D: Dredge 138, Hero: Hero Fracture Zone, TFZ: Tula Fracture Zone, VTF: transform fault forming the Valdivia Fracture Zone.

like those described southwest of the Tula Fracture Zone, but because of the long-offset on the Tula transform fault the first of these later collisions dates from around 20 Ma (Fig. 5). The animation shows the shortening of this offset as the ridge crest northeast of the Tula Fracture Zone migrates towards the subduction zone in the period 40–20 Ma, the ensuing collisions, and the related occurrences of alkali basalts at 'Dredge 138' (recent) Argo Point (1.0 Ma) and Seal Nunataks (4.0 Ma—recent). Like the Alexander Island occurrences further south, these rocks postdate the opposing ridge crest–trench collisions, in these cases between the Biscoe, Anvers, C, and Hero fracture zones and by 15 m.y., 5.9–5.5 m.y., and 2.4–0 m.y. (Hole and Larter, 1993; Larter et al., 1997).

3.5. Collisions at the Chile Trench: 15 Ma—present

The animation illustrates how seafloor of the Farallon/Nazca plates was consumed at the Chile Trench, in the form of the narrowing of the underlap between the oldest surviving Nazca seafloor and the collisional margin of South America. Following collisions of segments of the Nazca–Antarctic plate boundary (the Chile Ridge) with the trench, which started in mid Miocene times in the south and are ongoing at the Chile Triple Junction today, the Antarctic plate followed the Nazca plate into subduction. Because of this subduction of Antarctic seafloor, we can only show the southern segments of the Chile Ridge as a dotted line crossing the underlap in the animation during the period 20–1 Ma (Fig. 6). The animation shows how segments of this ridge crest collided periodically with the Chile Trench and entered the subduction zone, starting in the south before 15 Ma.

Following these collisions, a slab window formed beneath Patagonia due to the differential rates of subduction; the Antarctica plate converges with South America more slowly than the Nazca plate does, and presumably sinks more slowly into the asthenosphere too. That a slab window did form is consistent with the widespread Miocene alkaline volcanic rocks (Ramos and Kay, 1992; D'Orazio et al., 2000; 2001; 2004; Gorring et al., 1997). The slab window is mapped approximately in Fig. 6, using the same assumptions as for the slab window beneath the Antarctic Peninsula. The animation shows that, unlike most occurrences on the Antarctic Peninsula, the Patagonian alkaline volcanic rocks are much more closely related in time with the presence of the slab window. The differences in delay times might most simply be related to the erosion of older alkali basalt occurrences by ice sheets on the Antarctic Peninsula and/or their burial beneath ice and younger flows in long lived complexes. One observation consistent with these possibilities is that where ridge-crest–trench collisions have occurred more recently off the northern Antarctic Peninsula, the oldest known alkaline volcanism tends to occur after a smaller time lag. Alternatively, Hole et al (1995) suggested the time lags observed for the Antarctic Peninsula alkaline volcanism may be meaningful in terms of the geometry

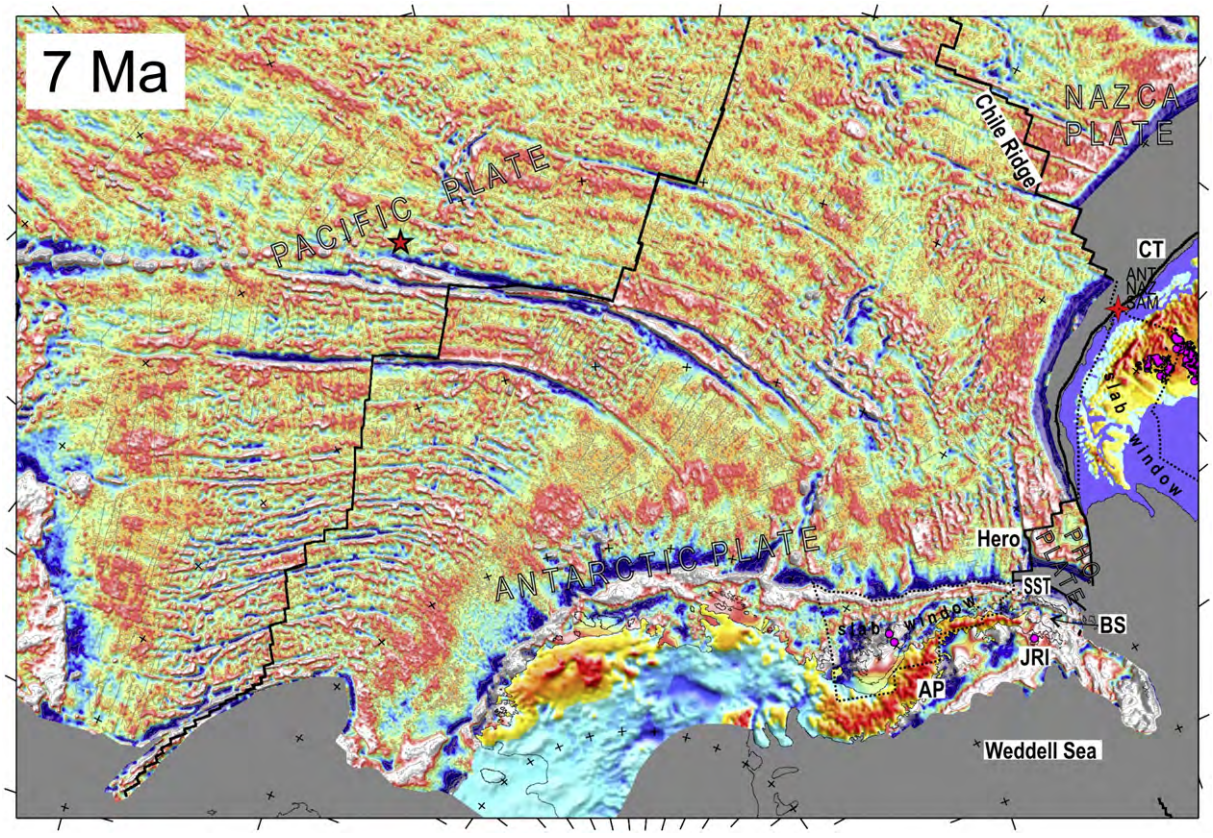

Fig. 6. Animation frame for 7 Ma. Projection, graticule, symbols and labels as for Figs. 2–5 plus BS: Bransfield Strait, JRI: James Ross Island, SST: South Shetland Trench. Violet disks and shapes: alkaline volcanism localities.

of the slab window, with more delayed occurrences occurring over the 'subducted transform' edges of the window. Similar relationships have not, however, been reported in Patagonia.

The animation shows occurrences of Miocene alkaline volcanic rocks in southern Patagonia that pre-date the collisions that initiated slab-window opening, or that occur north of the Chile Triple Junction. Because they could not have formed by upwelling through the post-15 Ma Nazca–Antarctica slab window, these occurrences have been related to supra-slab processes (as summarised by D'Orazio et al., 2004). Further alkali basalt complexes, dating back through Oligocene and Eocene times, are widespread north of the present-day Chile Triple Junction as far as 43°S, and have been related to a slab window formed between the Farallon and Phoenix slabs as the spreading centre between these plates was subducted off Chile (Ramos and Kay, 1992). This collision is poorly known but, by assuming the spreading centre had no large offsets, Cande and Leslie (1986) suggested it migrated rapidly southwards during Eocene times from 43°S to Tierra del Fuego, leaving subduction of the Farallon Plate in its wake. Earlier, we showed that a Nazca–Phoenix ridge-crest–trench collision probably occurred off Cape Horn at around 18 Ma, suggesting the Farallon/Nazca–Phoenix slab window may have developed more widely and lingered beneath Patagonia longer than previously thought, perhaps making it possible to relate some of the proposed 'supra-slab' volcanics to a slab window after all.

4. Discussion: James Ross Island volcanism and slab windows

At James Ross Island, alkaline volcanism dating from 7.1 Ma to recent times cannot be related to a ridge crest–trench collision at the western margin of the Antarctic Peninsula, as the Antarctic–Phoenix Ridge northeast of the Hero Fracture Zone never reached the South Shetland Trench (Hole et al., 1995). Because of this, those authors suggested that the James Ross Island Volcanic Group is not slab-window related, but instead the result of decompression melting that occurred when slab rollback induced asthenospheric flow into the region below a pre-existing rift basin. Flow may instead have occurred around the edges of the very narrow late-stage Phoenix slab, as Barker and Austin (1998) suggested played a role in the initiation of trench rollback and back-arc extension in Bransfield Strait.

Alternatively, we suggest that the James Ross Island Volcanic Group could be related to the slab window that formed below Powell Basin after ridge-crest–trench collisions in the northern Weddell Sea. This possibility is hard to assess with any rigour due to the sparsity of geophysical data in the northwestern corner of the Weddell Sea, which makes it difficult to pinpoint the western limit of the extinct subduction zone there, and the lack of information relating to the relative positions of the South American and Phoenix slabs in the asthenosphere below the northeastern Antarctic Peninsula (Robertson Maurice et al., 2003). Nonetheless, evidence for a Maastrichtian–Paleogene calc–alkaline volcanic source nearby to the east of James Ross Island (Lomas and Dingle, 1999) supports the idea that west-directed subduction may indeed have introduced a slab into the asthenosphere very close by, making the later opening of a slab window a possibility that should be taken into account for the James Ross Island Volcanic Group.

5. Summary

An animated reconstruction shows the post-Eocene plate tectonic development of the southern Pacific Ocean.

- The animation depicts known ridge crest trench collision events at the margins of South America and the Antarctic Peninsula along with known occurrences of alkali volcanism, and is consistent with published studies that connect these observations with the concept of decompression melting in slab windows.
- The occurrence of 18 m.y. old alkali volcanism near Cape Horn prompts us to suggest that a slab window formed there following collision of part of a Nazca–Phoenix spreading centre with the southernmost Chile Trench, although no seafloor record of this event remains.
- The animation prompts us to relate the formation of a slab window beneath the northeastern Antarctic Peninsula, as suggested by seafloor data, to alkali volcanism in the Powell and, more speculatively, James Ross basins.

Acknowledgements

This project was funded by the German Research Foundation (DFG) through the grants GO 724/2-1 and GO 724/2-2. The figures and animation were produced making much use of the Generic Mapping Tools (Wessell and Smith, 1998).

Appendix A. Supplementary data

Supplementary data associated with this article can be found, in the online version, at doi:10.1016/j.tecto.2007.10.005.

References

Barber, P.L., Barker, P.F., Pankhurst, R.J., 1991. Dredged rocks from Powell Basin and the South Orkney Microcontinent. In: Thomson, M.R.A., Crame, J.A., Thomson, J.W. (Eds.), Geological Evolution of Antarctica. Proceedings V International Conference, Antarctic Earth Sciences. Cambridge University Press, Cambridge, UK, pp. 361–367.

Barker, P.F., Hill, I.A., Weaver, S.D., Pankhurst, R.J., 1982. The origin of the eastern South Scotia Ridge as an intraoceanic island arc. In: Craddock, C. (Ed.), Antarctic Geoscience. U. Wisconsin Press, Madison, pp. 203–211.

Barker, P.F., Barber, P.L., King, E.C., 1984. An early Miocene ridge crest–trench collision on the South Scotia Ridge near 36°W. Tectonophysics 102, 315–332.

Barker, D.H.N., Austin, J.A., 1998. Rift propagation, detachment faulting, and associated magmatism in Bransfield Strait, Antarctic Peninsula. J. Geophys. Res. 103, 24017–24043.

Behrendt, J.C., LeMasurier, W.E., Cooper, A.K., Tessensohn, F., Trehu, A., Damaske, D., 1991. Geophysical studies of the West Antarctic Rift System. Tectonics 15, 1257–1273.

Cande, S.C., Herron, E.M., Hall, B.R., 1982. The early Cenozoic tectonic history of the southeast Pacific. Earth Planet. Sci. Lett. 57, 63–74.

Cande, S.C., Leslie, R.B., 1986. Late Cenozoic tectonics of the southern Chile Trench. J. Geophys. Res. 91, 471–496.

Cande, S.C., LaBrecque, J.L., Larson, R.L., Pitman III, W.C., Golovchenko, X., Haxby, W.F., 1989. Magnetic lineations of the worlds ocean basins (map no. 131). Am. Assoc. Pet. Geol. Tulsa, OK, USA.

Cande, S.C., Stock, J.M., Müller, R.D., Ishihara, T., 2000. Cenozoic motion between East and West Antarctica. Nature 404, 145–150.

Cande, S.C., Kent, D.V., 1995. Revised calibration of the geomagnetic polarity time scale for the late Cretaceous and Cenozoic. J. Geophys. Res. 100, 6093–6096.

Cande, S.C., Raymond, C.A., Stock, J., Haxby, W.F., 1995. Geophysics of the Pitman Fracture Zone and Pacific–Antarctic plate motions during the Cenozoic. Science 270, 947–953.

D'Orazio, M., Agostini, S., Mazzarini, F., Innocenti, F., Manetti, P., Haller, M.J., Lahsen, A., 2000. The Pali Aike volcanic field, Patagonia: slab-window magmatism near the southern tip of South America. Tectonophysics 321, 407–427.

D'Orazio, M., Agostini, S., Innocenti, F., Haller, M.J., Manetti, P., Mazzarini, F., 2001. Slab window-related magmatism from southernmost South America: the late Miocene mafic volcanics from the Estancia Glencross area (~52°S, Argentina–Chile). Lithos 57, 67–89.

D'Orazio, M., Innocenti, F., Manetti, P., Haller, M.J., 2004. Cenozoic back-arc magmatism of the southern extra-Andean Patagonia (44° 30'S- 52°S): A review of geochemical data and geodynamic interpretations. Revista de la Asociación Geológica Argentina 59, 525–538.

Eagles, G., 2003. Tectonic evolution of the Antarctic–Phoenix plate system since 15 Ma. Earth Planet. Sci. Lett. 217, 97–109.

Eagles, G., Livermore, R.A., 2002. Opening history of Powell Basin, Antarctic Peninsula. Marine Geology 185, 195–205.

Eagles, G., Gohl, K., Larter, R.D., 2004a. Life of the Bellingshausen plate. Geophys. Res. Lett. 31, L07603. doi:10.1029/2003GL019127.

Eagles, G., Gohl, K., Larter, R.D., 2004b. High resolution animated tectonic reconstruction of the South Pacific and West Antarctic margin. Geochem., Geophys., Geosystems 5, Q07002. doi:10.1029/2003GC000657.

Eagles, G., Livermore, R.A., Fairhead, J.D., Morris, P., 2005. Tectonic evolution of the west Scotia Sea. J. Geophys. Res. 110, B02401. doi:10.1029/JB2004003154.

Eakins, B.W., Structure and Development of Oceanic Rifted Margins, PhD Thesis, University of California San Diego, 2002.

Gorring, M.L., Kay, S.M., Zeitler, P.K., Ramos, V.A., Rubiolo, D., Fernandez, M.I., Panza, J.L., 1997. Neogene Patagonian plateau lavas: continental magmas associated with ridge collision at the Chile Triple Junction. Tectonics 16, 1–17.

Hole, M., 1988. Post subduction alkaline volcanism along the Antarctic Peninsula. J. Geol. Soc. Lond. 145, 985–998.

Hole, M., Larter, R.D., 1993. Trench-proximal volcanism following ridge-crest–trench collision along the Antarctic Peninsula. Tectonics 12, 897–910.

Hole, M.J., Saunders, A.D., Rogers, G., Sykes, M.A., 1995. The relationship between alkaline magmatism, lithospheric extension and slab window formation along continental destructive plate boundaries. In: Smellie, J.L. (Ed.), Volcanism Associated with Extension at Consuming Plate Margins. Geol. Soc. Lond. Spec. Pub., 81, pp. 265–285.

Larter, R.D., Barker, P.F., 1991. Effects of ridge-crest–trench interaction on Antarctic–Phoenix spreading: forces on a young subducting plate. J. Geophys. Res. 96, 19583–19607.

Larter, R.D., Cunningham, A.P., Barker, P.F., Gohl, K., Nitsche, F.O., 2002. Tectonic evolution of the Pacific margin of Antarctica 1. Late Cretaceous tectonic reconstructions. J. Geophys. Res. 107 (B12), 2345. doi:10.1029/2000JB000052.

Larter, R.D., Rebesco, M., Vanneste, L.E., Gambôa, L.A.P., Barker, P.F., 1997. Cenozoic tectonic, sedimentary and glacial history of the continental shelf west of Graham Land, Antarctic Peninsula. In: Barker, P.F., Cooper, A.K. (Eds.), Geology and Seismic Stratigraphy of the Antarctic Margin, 2. AGU Antarct. Res. Ser., vol. 71, pp. 1–27.

Livermore, R.A., Balanyá, J.C., Maldonado, A., Martínez, J.M., Rodríguez-Fernández, J., Sanz de Galdeano, C., Galindo-Zaldívar, J., Jabaloy, A., Barnolas, A., Somoza, L., Hernández-Molina, J., Suriñach, E., Viseras, C., 2000. Autopsy on a dead spreading center: the Phoenix Ridge, Drake Passage, Antarctica. Geology 28, 607–610.

Lomas, S.A., Dingle, R.V., 1999. Possible evidence for Late Cretaceous off-axis volcanism in the outer James Ross Basin. Antarct. Sci. 11, 332–337.

Lythe, M.B., Vaughan, D.G., and the BEDMAP Consortium, 2000. BEDMAP-bed topography of the Antarctic. 1:10,000,000 scale map. BAS, 2000. (Misc) 9. Cambridge, British Antarctic Survey,.

Mammerickx, J., Sandwell, D., 1986. Rifting of old oceanic lithosphere. J. Geophys. Res. 91, 1975–1988.

McAdoo, D.C., Laxon, S., 1997. Antarctic tectonics: constraints from an ERS-1 satellite marine gravity field. Science 276, 556–560.

McCarron, J.J., Larter, R.D., 1998. Late Cretaceous to early Tertiary subduction history of the Antarctic Peninsula. J. Geol. Soc. London 155, 255–268.

Meschede, M., Barckhausen, U., 2000. In: Silver, E.A., Kimura, G., Shipley, T.H. (Eds.), Plate tectonic evolution of the Cocos–Nazca spreading center. Proc. ODP, Sci. Results, 170. Ocean Drilling Program, College Station, TX. [Online]. Available from World Wide Web:http://www-odp.tamu.edu/publications/170_SR/chap_07/chap_07.htm.

Puig, A., Herve, M., Suarez, M., Saunders, A.D., 1984. Calc–alkaline and alkaline Miocene and calc–alkaline Recent volcanism in the southernmost Patagonian cordillera, Chile. J. Volcanol. Geotherm. Res. 21, 149–163.

Ramos, V.A., Kay, S.M., 1992. Southern Patagonian plateau basalts and deformation: backarc testimony of ridge collisions. Tectonophysics 205, 261–282.

Robertson Maurice, S.D., Wiens, D.A., Shore, P.J., Vera, E., Dorman, L.M., 2003. Seismicity and tectonics of the South Shetland Islands and Bransfield Strait from a regional broadband seismograph deployment. J. Geophys. Res. 108 (B10), 2461. doi:10.1029/2003JB002416.

Sandwell, D.T., Smith, W.H.F., 1997. Marine gravity anomaly from Geosat and ERS 1 satellite altimetry. J. Geophys. Res. 102, 10039–10054.

Smellie, J.L., Pankhurst, R.J., Hole, M.J., Thomson, J.W., 1988. Age, distribution and eruptive conditions of Late Cenozoic alkaline volcanism in the Antarctic Peninsula and Ellsworth Land: review. Br. Antarct. Surv. Bull. 80.

Smith, W.H.F., Sandwell, D.T., 1997. Global seafloor topography from satellite altimetry and ship depth soundings. Science 277, 1956–1962.

Stock, J.M., Molnar, P., 1987. Revised early Tertiary history of plate motions in the Southwest Pacific. Nature 325, 495–499.

Stock, J.M., Cande, S.C., Raymond, C.A., 1996. Updated history of the Bellingshausen Plate, Eos Trans. AGU, 77, Fall Meet. Suppl., F647.

Tebbens, S.F., Cande, S.C., 1997. Southeast Pacific tectonic evolution from early Oligocene to Present. J. Geophys. Res. 102, 12061–12084.

Tebbens, S.F., Cande, S.C., Kovacs, L., Parra, J.C., LaBrecque, J.L., Vergara, H., 1997. The Chile Ridge: a tectonic framework. J. Geophys. Res. 102, 12035–12059.

Thorkelson, D.J., Taylor, R.P., 1989. Cordilleran slab windows. Geology 17, 833–836.

Wessel, P., Smith, W.H.F., 1998. New, improved version of Generic Mapping Tools released. EOS 79, 579.

Publication 6.1.3:

Gohl, K. (2008). Antarctica's continent-ocean transitions: consequences for tectonic reconstructions. In: Cooper, A.K., Barrett, P.J., Stagg, H., Storey, B., Stump, E., Wise, W. (eds.), *Antarctica: A Keystone in a Changing World*. Proceedings of the 10th International Symposium on Antarctic Earth Sciences; Washington, DC; The National Academies Press, pp. 29-38, doi:10.3133/of2007-1047.kp04.

Author contribution: This peer-reviewed paper was entirely written by Gohl on invitation to present a keynote talk at the conference.

Cooper, A. K., P. J. Barrett, H. Stagg, B. Storey, E. Stump, W. Wise, and the 10th ISAES editorial team, eds. (2008). *Antarctica: A Keystone in a Changing World.* Proceedings of the 10th International Symposium on Antarctic Earth Sciences. Washington, DC: The National Academies Press. doi:10.3133/of2007-1047.kp04

Antarctica's Continent-Ocean Transitions: Consequences for Tectonic Reconstructions

K. Gohl[1]

ABSTRACT

Antarctica was the centerpiece of the Gondwana supercontinent. About 13,900 km of Antarctica's 15,900-km-long continental margins (87 percent) are of rifted divergent type, 1600 km (10 percent) were converted from a subduction type to a passive margin after ridge-trench collision along the Pacific side of the Antarctic Peninsula, and 400 km (3 percent) are of active convergent type. In recent years the volume of geophysical data along the continental margin of Antarctica has increased substantially, which allows differentiation of the crustal characteristics of its continent-ocean boundaries and transitions (COB/COT). These data and geodynamic modeling indicate that the cause, style, and process of breakup and separation were quite different along the Antarctic margins. A circum-Antarctic map shows the crustal styles of the margins and the location and geophysical characteristics of the COT. The data indicate that only a quarter of the rifted margins are of volcanic type. About 70 percent of the rifted passive margins contain extended continental crust stretching between 50 and 300 km oceanward of the shelf edge. Definitions of the COT and an understanding of its process of formation has consequences for plate-kinematic reconstructions and geodynamic syntheses.

INTRODUCTION

About 13,900 km of the 15,900-km-long continental margins of the Antarctic plate are of rifted divergent type, 1600 km were converted from a subduction-type to a passive margin after ridge-trench collision along the Pacific side of the Antarctic Peninsula, and 400 km are of active convergent type. The structure and composition of continental margins, in particular those of rifted margins, can be used to elucidate the geodynamic processes of continental dispersion and accretion. The margins of Antarctica have mostly been subject to regional studies mainly in areas near research stations in the Ross Sea, Prydz Bay, Weddell Sea, and along the Antarctic Peninsula near national research facilities. In recent years—mainly motivated by the United Nations Convention on the Law of the Sea—large volumes of new offshore geophysical data have been collected, primarily along the East Antarctic margin. For the first time this provides the opportunity to make a comprehensive analysis of the development of these continental margins over large tracts of extended continental crust that were previously unknown. The coverage of circum-Antarctic multichannel seismic lines from the Antarctic Seismic Data Library System for Cooperative Research (SDLS) of the Scientific Committee on Antarctic Research (SCAR) (Wardell et al., 2007) (Figure 1) is, with the exception of some areas in the central Weddell Sea, off western Marie Byrd Land and off the Ross Sea shelf, dense enough for quantifying basement types and volcanic and nonvolcanic characteristics of the margins. The track map (Figure 1) shows that deep crustal seismic data, necessary for a complete and accurate characterization of the marginal crust to upper mantle level, are still absent over most margins.

In this paper I first present a compilation of the structural types of the circum-Antarctic continental margins based on a review of relevant published data of diverse types together with new data. Then I contemplate implications of the knowledge of margin crustal types and properties for plate-kinematic and paleobathymetric reconstructions and for isostatic response models.

[1]Alfred Wegener Institute for Polar and Marine Research, Postbox 120161, 27515 Bremerhaven, Germany (karsten.gohl@awi.de).

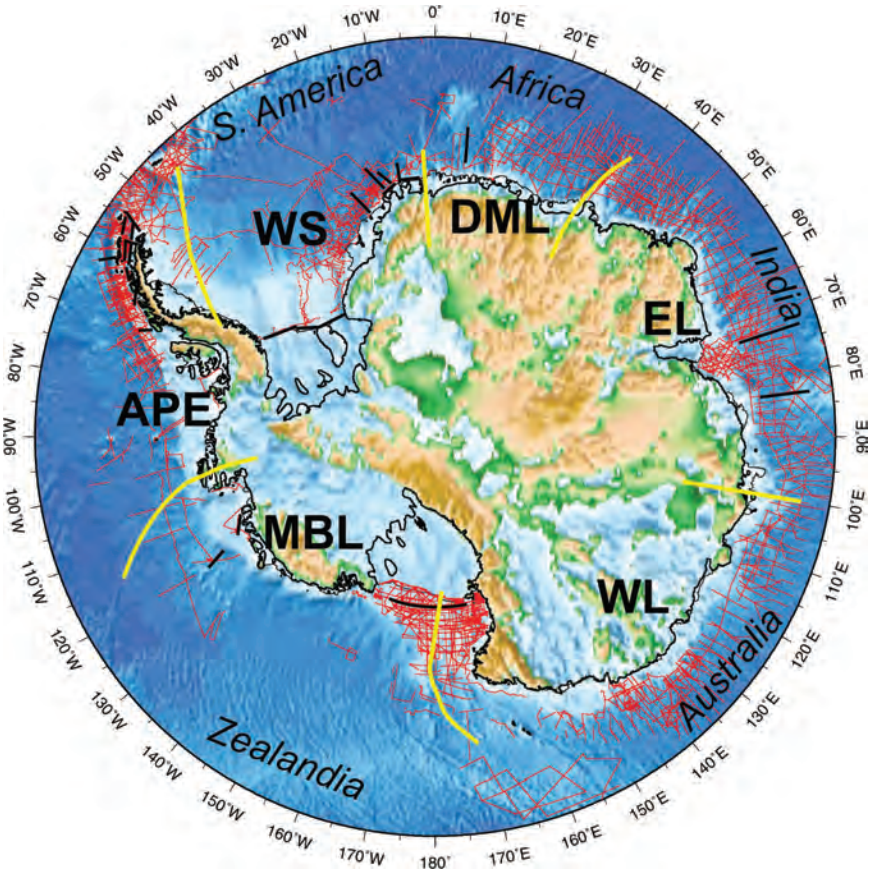

FIGURE 1 Overview map of Antarctica and surrounding ocean floor using a combined BEDMAP (bedrock topography with ice sheet removed) (Lythe et al., 2001) and satellite-derived bathymetry grid (McAdoo and Laxon, 1997). White areas on the continent are below sea level if the ice sheet is removed (without isostatic compensation). Yellow lines mark boundaries between the six crustal breakup sectors of respective conjugate continents in this paper. Red lines show the tracks of offshore multichannel seismic profiles of the SCAR Seismic Data Library System (SDLS) (compiled by M. Breitzke, AWI). Black lines mark the locations of offshore deep crustal seismic refraction profiles. WS = Weddell Sea sector; DML = Dronning Maud Land sector; EL = Ellsworth-Lambert Rift sector; WL = Wilkes Land sector; MBL = Marie Byrd Land sector; APE = Antarctic Peninsula-Ellsworth Land sector.

STRETCHING AND BREAKING: PASSIVE MARGIN TYPES

Weddell Sea (WS) Sector Conjugate to South America

The complex tectonic development of the Weddell Sea sector (Figure 2) has more recently been reconstructed by Hübscher et al. (1996a), Jokat et al. (1996, 1997, 2003, 2004), Leitchenkov et al. (1996), Ghidella and LaBrecque (1997), Golynsky and Aleshkova (2000), Ghidella et al. (2002), Rogenhagen and Jokat (2002), and König and Jokat (2006). Deciphering of the crustal types in the central Weddell Sea is still hampered by the lack of deep crustal seismic data. In the southern Weddell Sea seismic refraction data reveal a thinned continental crust of about 20 km thickness beneath the northern edge of the Filchner-Ronne ice shelf (Hübscher et al., 1996a). It can be assumed that this thinned crust extends northward to a boundary marked by the northern limit of a large positive gravity anomaly (Figure 2). König and Jokat (2006) associate an east-west rifting of this crust (stretching factor of 2.5) with the motion of the Antarctic Peninsula from East Antarctica as the earliest event in the Weddell Sea plate circuit at about 167 Ma prior to the early Weddell Sea opening in a north-south direction at about 147 Ma. It is not clear, however, whether some of the crustal extension is also associated with this early Weddell Sea opening. The crust between the northern end of the large positive gravity anomaly and the magnetic Orion Anomaly and Andenes Anomaly (Figure 2) is interpreted as a COT with the Orion Anomaly suggested to represent an extensive zone of volcanics that erupted during the final breakup between South America and Antarctica (König and Jokat, 2006). Deep crustal seismic refraction data across the Orion and Andenes anomalies and the assumed COT south of it are needed in order to constrain their crustal composition and type. Although the Orion Anomaly may provide a hint toward a volcanic-type margin, the few seismic data do not allow a complete characterization of the COT in the southern Weddell Sea. Identified magnetic spreading anomalies (oldest is M17) show evidence that oceanic crust exists north of the Orion and Andenes anomalies with the prominent T-Anomaly marking supposedly the changeover from slow to ultraslow spreading-type crust (König and Jokat, 2006).

The Weddell Sea margin along the east coast of the Antarctic Peninsula is still rather enigmatic due to missing data. König and Jokat (2006) show that it rifted from the western Patagonian margin as part of the earliest plate motion in the Weddell Sea region at about 167 Ma. They follow Ghidella

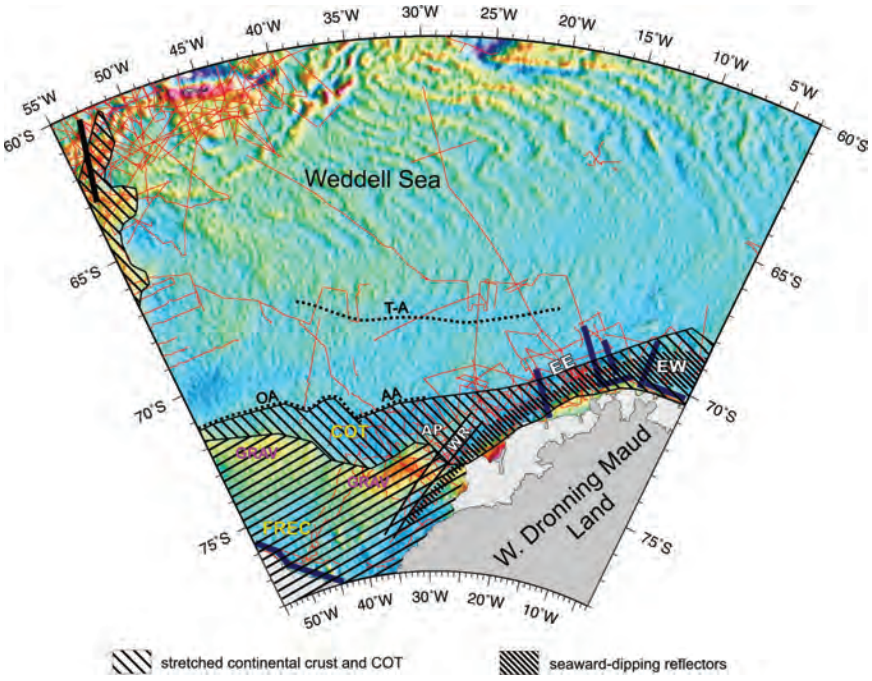

FIGURE 2 Weddell Sea sector with satellite-derived gravity field (McAdoo and Laxon, 1997) and continental margin features. Red lines show the tracks of offshore multichannel seismic profiles of SDLS. Dark blue lines mark the locations of offshore deep crustal seismic refraction profiles. COT = continent-ocean boundary; GRAV = positive gravity anomaly marking northern limit of thinned continental crust; FREC = Filchner-Ronne extended crust; EE = Explora Escarpment; EW = Explora Wedge; AP = Andenes Plateau; WR = Weddell Sea Rift; T-A = T-Anomaly; OA = Orion Anomaly; AA = Andenes Anomaly.

and LaBrecque's (1997) argument for a nonvolcanic margin based on low-amplitude magnetic anomalies and a characteristic bathymetry.

The margin of the eastern Weddell Sea along the western Dronning Maud Land coast is more clearly characterized by the prominent bathymetric expression of the Explora Escarpment and the massive volcanic flows along the Explora Wedge (Figure 2), identified by the abundance of seaward dipping reflectors (SDRs) in the seismic reflection data. A number of deep crustal seismic refraction profiles cross the Explora Wedge and the Explora Escarpment and allow models showing a 70-km to 90-km-wide transitional crust thinning from about 20 km thickness to 10 km thickness toward the north (e.g., Jokat et al., 2004). Relatively high P-wave velocities in the lower crust and in the upper crustal section of the SDRs (Jokat et al., 2004) are evidence for a volcanic-type continental margin.

Dronning Maud Land (DML) Sector Conjugate to Africa

Data and syntheses of the central and eastern Dronning Maud Land (DML) margin stem from work by Hinz and Krause (1982), Hübscher et al. (1996b), Roeser et al. (1996), Jokat et al. (2003, 2004), Hinz et al. (2004), and König and Jokat (2006). The recent plate-kinematic reconstructions by Jokat et al. (2003) and König and Jokat (2006) show that southeast Africa was conjugate to the DML margin (Figure 3) from just east of the Explora Escarpment to the Gunnerus Ridge. However, this DML margin has two distinct parts, separated by the Astrid Ridge. The eastern Lazarev Sea margin is characterized by a COT consisting of a broad stretched continental crust and up to 6-km-thick volcanic wedges clearly identified by SDR sequences. Deep crustal seismic data show that the crust thins in two steps from 23 km to about 10 km thickness over a distance of 180 km (König and Jokat, 2006). Their velocity-depth model reveals high seismic P-wave velocities in the lower crust of this COT, suggesting voluminous underplating and intrusion of magmatic material. A coast-parallel strong positive and negative magnetic anomaly pair marks the northern limit of the COT and is interpreted as the onset of the first oceanic crust generated by spreading processes at chron M12 (136 Ma). The volcanic characteristics of the eastern Lazarev Sea segment is very likely to be related to the same magmatic events leading to the Early Cretaceous crustal accretion of a Large Igneous Province (LIP) consisting of the separated oceanic plateaus Maud Rise, Agulhas Plateau, and Northeast Georgia Rise (Gohl and Uenzelmann-Neben, 2001) and to which also parts of the Mozambique Ridge may have belonged.

At the Riiser-Larsen Sea margin east of the Astrid Ridge, the outer limit of the COB is constrained by densely spaced aeromagnetic data revealing spreading anomalies up to M24 (155 Ma) (Jokat et al., 2003). This is so far the oldest magnetic seafloor spreading anomaly observed along any of the circum-Antarctic margins. Seismic reflection data (Hinz et al., 2004) indicate a COT of stretched continental crust that is with 50 km width much narrower compared with the COT of the Lazarev Sea margin. However, the data do not seem to indicate a strong magmatic influence of the COT as major

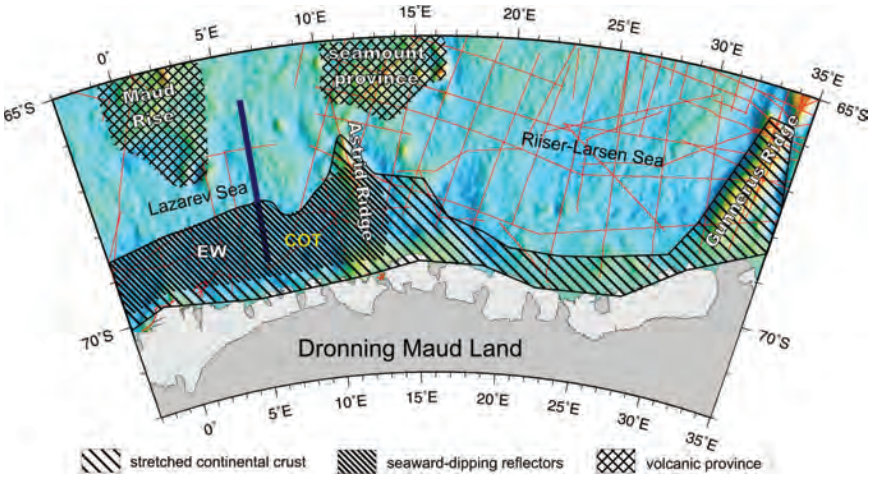

FIGURE 3 Dronning Maud Land sector with satellite-derived gravity field (McAdoo and Laxon, 1997) and continental margin features. Red lines show the tracks of offshore multichannel seismic profiles of SDLS. The dark blue line marks the location of an offshore deep crustal seismic refraction profile. COT = continent-ocean boundary; EW = Explora Wedge.

SDRs are missing (Hinz et al., 2004). Deep crustal seismic refraction data do not exist to better characterize this part of the DML margin and its COT or COB.

Enderby Land to Lambert Rift (EL) Sector Conjugate to India

Most of the crustal and sedimentary structures of the continental margins off Enderby Land (east of Gunnerus Ridge), between Prydz Bay and the Kerguelen Plateau, off Wilhelm II Land and Queen Mary Land (Figure 4) have been revealed by large seismic datasets acquired by Russian and Australian surveys (e.g., Stagg et al., 2004, 2005; Guseva et al., 2007; Leitchenkov et al., 2007a; Solli et al., 2007). Gaina et al. (2007) developed a breakup model between India and this East Antarctic sector based on compiled magnetic data of the southernmost Indian Ocean and the structures of the continental margin interpreted from the seismic data. Despite the large amount of high-quality seismic reflection data, the definition of the COB or COT is equivocal due to the lack of deep crustal seismic refraction data with the exception of nonreversed sonobuoy data. Stagg et al. (2004, 2005) defined the COB as the boundary to a zone by which the first purely oceanic crust was accreted and which shows a changeover from faulted basement geometry of stretched continental crust to a relatively smoother basement of ocean crust. This boundary is often accompanied by a basement ridge or trough.

The Enderby margin can be divided into two zones of distinct character. West of about 58°W the ocean fractures zone terminates in an oblique sense at the margin, thus giving it a mixed rift-transform setting (Stagg et al., 2004). Their defined COB lies between 100 km and 170 km oceanward of the shelf edge. Gaina et al. (2007) identified spreading anomalies from M0 to M9 east of Gunnerus Ridge from relatively sparse shipborne magnetic data. Most of both magnetic and seismic profiles do not parallel the spreading flow lines and may be biased by the structure and signal of crossing fracture zones. The eastern Enderby margin zone has more of a normal rifted margin setting with a COB up to 300 km north of the shelf edge (Stagg et al., 2004). The prominent magnetic Mac Robertson Coastal Anomaly (MCA) correlates with the northern limit of the COT in this eastern zone. Ocean-bottom seismograph data along two seismic refraction profiles were recently acquired in the eastern Enderby Basin and across the Princess Elizabeth Trough (PET) between the Kerguelen Plateau and Princess Elizabeth Land as part of a German-Russian cooperation project (Gohl et al., 2007a) (Figure 4). The western profile confirms an extremely stretched crystalline continental crust, which thins to 7 km thickness (plus 4 km sediments on top), from the shelf edge to the location of the MCA. It is interesting to note that apart from a few scattered observations close to the marked COBs, major SDR sequences do not seem to exist on the Enderby Land margin (Stagg et al., 2004, 2005), suggesting the lack of a mantle plume at the time of breakup at about 130 Ma (Gaina et al., 2007).

The characteristics of the margin off central and eastern Prydz Bay is affected by both the inherited structure of the Paleozoic-Mesozoic Lambert Rift system as well as by magmatic events of the Kerguelen Plateau LIP, probably postdating the initial India-Antarctica breakup by about 10 million to 15 million years (Gaina et al., 2007). Guseva et al. (2007) proposed a direct connection between the volcanic Southern Kerguelen Plateau crust and stretched continental crust of Wilhelm II Land. The recent deep crustal seismic refraction data and a helicopter-magnetic survey, however, provides constraints that the central part of the PET consists of oceanic crust, possibly affected by the LIP event (Gohl et al., 2007a). This result is used to draw a narrow zone of stretched continental crust that widens eastward along the margin of the Davis Sea (Figure 4), where it reaches the width of the COT in the area of Bruce Rise as suggested by Guseva et

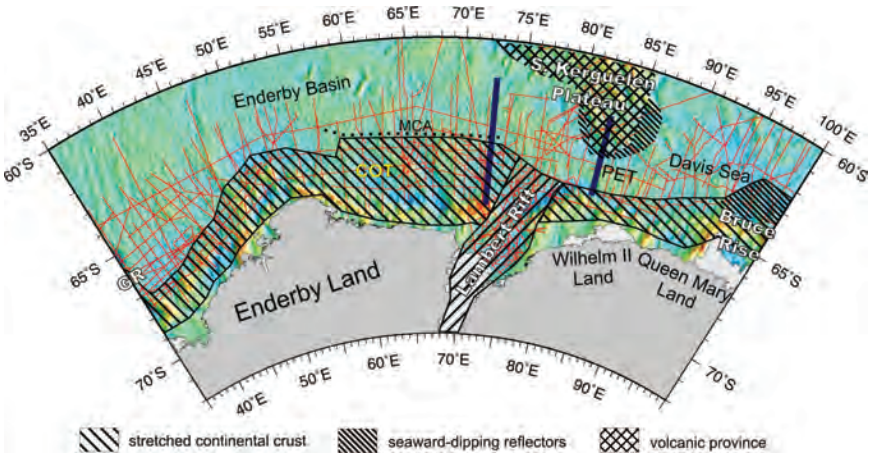

FIGURE 4 Enderby Land-Lambert Rift sector with satellite-derived gravity field (McAdoo and Laxon, 1997) and continental margin features. Red lines show the tracks of offshore multichannel seismic profiles of SDLS. Dark blue lines mark the locations of offshore deep crustal seismic refraction profiles. COT = continent-ocean boundary; PET = Princess Elizabeth Trough; GR = Gunnerus Ridge; MCA = Mac Robertson Coastal Anomaly.

al. (2007). Similar to observations along the Enderby Land margin, major SDR sequences are not observed on the Antarctic margin of the Davis Sea but only around the margins of the Southern Kerguelen Plateau. However, SDRs appear as strongly reflecting sequences at Bruce Rise (Guseva et al., 2007).

Wilkes Land (WL) Sector Conjugate to Australia

A vast amount of seismic reflection, gravity, and magnetic data as well as nonreversed sonobuoy refraction data collected by Australian and Russian scientists in the last few years allows a characterization of the Wilkes Land and Terre Adélie Coast margin east of Bruce Rise (Figure 5) (Stagg et al., 2005; Colwell et al., 2006; Leitchenkov et al., 2007b). Along most of this margin the shelf slope is underlain by a marginal rift zone of stretched and faulted basement. From the northern limit of this marginal rift zone to 90-180 km farther oceanward, Eittreim et al. (1985), Eittreim and Smith (1987), Colwell et al. (2006), and Leitchenkov et al. (2007b) identified a COT consisting primarily of strongly stretched and faulted continental crust with embedded magmatic segments following linear trends parallel to the margin. The interpretation of the COB along parts of the margin is debatable, as mainly basement characteristics were used for the differentiation of crustal types. It cannot be completely excluded that the magnetic anomalies interpreted as magmatic components are actually true seafloor spreading anomalies C33y and C34y, which would move the COB farther south. However, this seems unlikely based on the results of Colwell et al. (2006), Direen et al. (2007), and Sayers et al. (2001) in a comparison of the conjugate magnetic anomalies as well as new theoretical and analogue examples published in Sibuet et al. (2007). Reversed deep crustal refraction data would provide better constraints on the composition of the crustal units but are missing anywhere along this margin. However, in the absence of better data I adopted the interpretation by Colwell et al. (2006) and Leitchenkov et al. (2007b) of an up-to-300-km-wide zone of stretched continental crust (Figure 5).

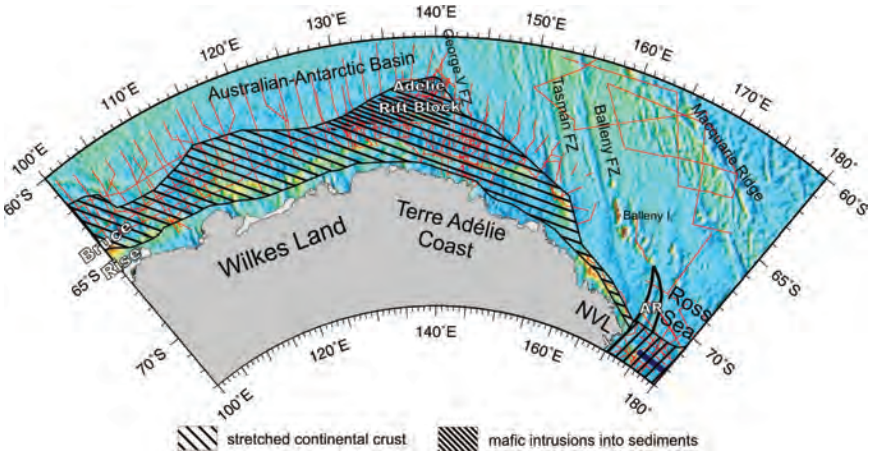

FIGURE 5 Wilkes Land sector with satellite-derived gravity field (McAdoo and Laxon, 1997) and continental margin features. Red lines show the tracks of offshore multichannel seismic profiles of SDLS. The dark blue line marks the location of an offshore deep crustal seismic refraction profile. NVR = Northern Victoria Land; AR = Adare Rift.

Off the Terre Adélie Coast margin the Adélie Rift Block, which is interpreted as a continental crustal block, is part of the stretched marginal crust. Major sequences of SDRs are not observed along the margin of the Wilkes Land sector, although Eittreim et al. (1985), Eittreim and Smith (1987), and Colwell et al. (2006) describe significant volumes of mafic intrusions within the sedimentary sequences of the landward edge of the Adélie Rift Block. The margin east of about 155°E toward the Ross Sea is characterized by prominent oblique fracture zones (e.g., Balleny FZ) reaching close to the shelf edge. This is similar to the rift-transform setting as observed in the western Enderby Basin but in an opposite directional sense. Stock and Cande (2002) and Damaske et al. (2007) suggest that a broad zone of distributed deformation was active at the margin, affecting the continental crustal blocks of Northern Victoria Land even after the initiation of ocean spreading.

The continental margin in the western Ross Sea underwent a rather complex development that makes a clear delineation of the COB difficult. A major proportion of the Ross Sea crustal extension is associated with a 180 km plate separation between East and West Antarctica when the Adare Trough was formed in Eocene and Oligocene time (Cande et al., 2000; Stock and Cande, 2002). The southward extension of this rift dissects the continental shelf region of the western Ross Sea (Davey et al., 2006).

Marie Byrd Land (MBL) Sector Conjugate to Zealandia

The eastern Ross Sea margin (Figure 6) is conjugate to the southwesternmost margin of the Campbell Plateau of New Zealand. Unlike the western Ross Sea margin, this margin can be considered a typical rifted continental margin with the oldest identified shelf-edge parallel spreading anomaly being C33y just east of the Iselin Rift (Stock and Cande, 2002). Seismic refraction data from a profile across the Ross Sea shelf by Cooper et al. (1997) and Trey et al. (1997) show a crust of 17-km to 24-km thickness with the thinnest parts beneath two troughs in the eastern and western region. It can be assumed that this type of stretched continental crust extends to the shelf edge at least. Whether crustal thinning is a result of the New Zealand-Antarctic breakup or extensional processes of the West Antarctic Rift System or both cannot be answered due to insufficient data in this area. It is also not known whether magmatic events affected the structure of the marginal crust.

Structural models of the continental margin of western Marie Byrd Land also suffer from the lack of seismic and other geophysical data. The only assumption for a sharp breakup structure and a very narrow transitional crust is derived from the close fit of the steep southeastern Campbell Plateau margin to the western MBL margin and coastal gravity anomaly (e.g., Mayes et al., 1990; Sutherland, 1999; Larter et al., 2002; Eagles et al., 2004). The same approach was applied for the closest fit between Chatham Rise and eastern MBL. However, new deep crustal seismic data from the Amundsen Sea indicate that the inner to middle shelf of the Amundsen Sea Embayment consists of crust thinned to about 21- to 23-km thickness with a pre- or syn-breakup failed rift structure (Gohl et al., 2007b). Here the continental margin structure is rather complex due to the propagating and rotating rifting processes between the breakup of Chatham Rise from the western Thurston Island block at about 90 Ma (Eagles et al., 2004), the opening of the Bounty Trough between Chatham Rise and Campbell Plateau (Eagles et al., 2004; Grobys et al., 2007), and the initiation of the breakup of Campbell Plateau from MBL at about 84-83 Ma (e.g., Larter et al., 2002; Eagles et al., 2004). The analysis of a crustal seismic refraction profile (Gohl et al., 2007b) and a seismic reflection dataset (Gohl et al., 1997b) between the

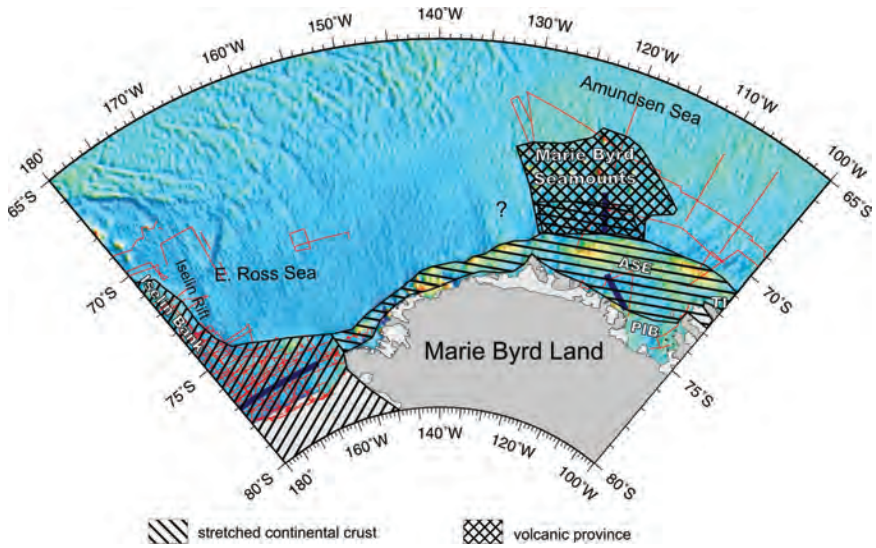

FIGURE 6 Marie Byrd Land sector with satellite-derived gravity field (McAdoo and Laxon, 1997) and continental margin features. Red lines show the tracks of offshore multichannel seismic profiles of SDLS. Dark blue lines mark the locations of offshore deep crustal seismic refraction profiles. ASE = Amundsen Sea Embayment; PIB = Pine Island Bay; TI = Thurston Island.

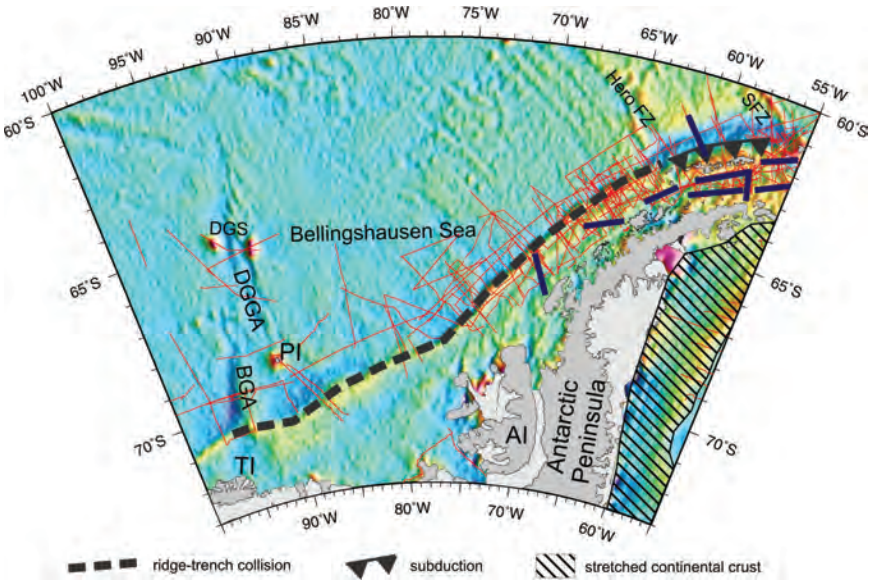

FIGURE 7 Antarctic Peninsula-Ellsworth Land sector with satellite-derived gravity field (McAdoo and Laxon, 1997) and continental margin features. Red lines show the tracks of offshore multichannel seismic profiles of SDLS. Dark blue lines mark the locations of offshore deep crustal seismic refraction profiles. AI = Alexander Island; TI = Thurston Island; PI = Peter Island; DGS = De Gerlache Seamounts; DGGA = De Gerlache Gravity Anomaly; BGA = Bellingshausen Gravity Anomaly; SFZ = Shackleton Fracture Zone.

shelf edge and the Marie Byrd Seamount province reveals that the crust in this corridor is 12-18 km thick, highly fractured, and volcanically overprinted. Lower crustal velocities suggest a continental affinity, which implies highly stretched continental crust or continental fragments, possibly even into the area of the seamount province. SDRs are not observed in the few existing seismic reflection profiles crossing the shelf and margin (Gohl et al., 1997a,b, 2007b; Nitsche et al., 2000; Cunningham et al., 2002; Uenzelmann-Neben et al., 2007).

SUBDUCTION TO RIDGE COLLISIONS: THE CONVERTED ACTIVE-TO-PASSIVE MARGIN

Antarctic Peninsula to Ellsworth Land (APE) Sector—Proto-Pacific Margin

Subduction of the Phoenix plate and subsequent collision of the Phoenix-Pacific spreading ridge resulted in a converted active to passive nonrifted margin along the Ellsworth Land and western Antarctic Peninsula margin between Thurston Island and the Hero Fracture Zone (e.g., Barker, 1982; Larter and Barker, 1991) (see Figure 7). The age for the oldest ridge-trench collision in the western Bellingshausen Sea can be roughly estimated to be about 50 Ma, using a few identified spreading anomalies (Eagles et al., 2004; Scheuer et al., 2006). Oceanic crustal age along the margin becomes progressively younger toward the northeast (Larter and Barker, 1991). Ultraslow subduction is still active in the segment of the remaining Phoenix plate between the Hero FZ and the Shackleton FZ along the South Shetland Trench. The only deep crustal seismic data along this converted margin south of the Hero FZ are from two profiles by Grad et al. (2002), showing that the crust thins oceanward from about 37 km thickness beneath the Antarctic Peninsula to a thickness of 25 to 30 km beneath the middle and outer continental shelf. The remains of the collided ridge segments cannot be resolved by the models. Data are also not sufficient to estimate any possible crustal extension of the western Antarctic Peninsula due to stress release after subduction ceded.

GEODYNAMIC AND PLATE-TECTONIC IMPLICATIONS AND COMPLICATIONS

The compilation of circum-Antarctic margin characteristics indicates that only a quarter (3400 km) of the rifted margins is of volcanic type, although uncertainties on volcanic and nonvolcanic affinity exist for about 4900 km (35 percent) of the rifted margins due to the lack of data in the Weddell Sea and along the MBL and Ross Sea margins. Only the eastern WL and western DML sectors as well as some isolated areas such as Bruce Rise of the EL sector and the Adélie Rift Block in the WL sector show well-observed magmatic characteristics that are explained by syn-rift mantle plumes or other smaller-scale magmatic events. Most other margins seem to have been formed by processes similar to those proposed for other nonvolcanic margins, such as the Iberian-Newfoundland conjugate margins (e.g., Sibuet et al., 2007) and the Nova Scotia margin (e.g., Funck et al., 2003), which exhibit widely extended, thinned, and block-faulted continental crust. Whether any updoming of lower continental crust is a possible process, as Gaina et al. (2007) suggest for the Enderby Land margin, is difficult to assess because of a lack of drill information.

Approximately 70 percent of the rifted passive margins contain continental crust stretched over more than 50 km oceanward of the shelf edge. In about two-thirds of these extended margins the COT has a width of more than 100 km, in many cases up to 300 km. The total area of extended con-

tinental crust on the continental shelf and beyond the shelf edge, including COTs with substantial syn-rift magmatic-volcanic accretion, is estimated to be about 2.9×10^6 km^2. Crustal stretching factors still remain uncertain for a good proportion of the extended margins due to a lack of crustal thickness measurements in most sectors. However, assuming stretching factors between 1.5 close to the shelf edge and in marginal rifts and increasing to 2 or 3 outboards in the deep sea, the continental crust, which has to be added to the original continent of normal crustal thickness, makes up about 1.5×10^6 km^2. The quantification of extended marginal crust has implications for plate-kinematic reconstructions, paleobathymetric models, and possibly for isostatic balancing of the Antarctic continent in glacial-interglacial cycles.

In almost all large-scale plate-kinematic reconstructions in which Antarctica is a key component, plate motions are calculated by applying rotation parameters derived from spreading anomalies and fracture zone directions, and continent-ocean boundaries are fixed single-order discontinuities, in most cases identified by the shelf edge or the associated margin-parallel gravity anomaly gradient (e.g., Lawver and Gahagan, 2003; Cande and Stock, 2004). This has caused misfits in terms of substantial overlaps or gaps when plates are reconstructed to close fit. For instance, a large misfit occurs when fitting the southeastern Australian margin to the eastern Wilkes Land margin in the area between 142°E and 160°E where extended continental crust reaches up to 300 km off the Terre Adélie Coast (Stock and Cande, 2002; Cande and Stock, 2004). In their reconstruction of the breakup processes of the Weddell Sea region, König and Jokat (2006) accounted for extended continental crust in the southern Weddell Sea and derived a reasonable fit of the conjugate margins of South America, Antarctica, and Africa. An appropriate approach for reconstructing best fits of continents and continental fragments is to apply a crustal balancing technique by restoring crustal thickness in rift zones and plate margins (Grobys et al., 2008). This, however, requires detailed knowledge of pre- and postrift crustal thickness, crustal composition, and magmatic accretion.

Detailed delineations of the COT and COB are important ingredients for paleobathymetric reconstructions. In the reconstruction of the circum-Antarctic ocean gateways (e.g., Lawver and Gahagan, 2003; Brown et al., 2006; Eagles et al., 2006), but also of the bathymetric features along nongateway continental margins, the differentiation between continental crust that was stretched and faulted and possibly intruded by magmatic material on one side and oceanic crust generated from spreading processes on the other side may make a significant difference in estimating the widths and depths along and across pathways for paleo-ocean currents.

Parameters of crustal and lithospheric extensions, depths, and viscoelastic properties are key boundary conditions for accurate calculation of the isostatic response from a varying ice sheet in glacial-interglacial cycles. Ice-sheet modelers still use relatively rudimentary crustal and lithospheric models of the Antarctic continent. Although the tomographic inversion of seismological data has improved the knowledge of the lithospheric structure beneath Antarctica and surrounding ocean basins (e.g., Morelli and Danesi, 2004), its spatial resolution of the upper 60-70 km of the relevant elastic lithosphere (Ivins and James, 2005), and in particular of the boundary between continental and oceanic lithosphere, is still extremely crude. Considering that ice sheets advanced to the shelf breaks of most Antarctic continental margins during glacial maxima, the isostatic response must be directly related to the width and depths of any extended continental crust and lithosphere oceanward of the shelf, which would probably have an effect on estimates of sea-level change. To quantify this effect, good-quality deep crustal and lithospheric data are needed to derive the geometries and rheologies of the extended crust and lithospheric mantle.

CONCLUSIONS

In a comprehensive compilation of circum-Antarctic continental margin types, about 70 percent of the rifted passive margins contain extended continental crust stretching more than 50 km oceanward of the shelf edge. Most of these extended margins have a continent-ocean transition with a width of more than 100 km—in many cases up to 300 km. Only a quarter of the rifted margins seem to be of volcanic type. The total area of extended continental crust on the shelf and oceanward of the shelf edge, including COTs with substantial syn-rift magmatic-volcanic accretion, is estimated to be about 2.9×10^6 km^2. This has implications for improved plate-kinematic and paleobathymetric reconstructions and provides new constraints for accurate calculations of isostatic responses along the Antarctic margin.

ACKNOWLEDGMENTS

I gratefully acknowledge the masters, crews, and scientists of the many marine expeditions during which the geophysical data used in this paper were acquired. Many thanks go to Nick Direen and an anonymous reviewer whose review comments substantially helped improve the paper. I also thank the co-editor Howard Stagg for useful comments and the editorial work.

REFERENCES

Barker, P. F. 1982. The Cenozoic subduction history of the Pacific margin of the Antarctic Peninsula: Ridge crest-trench interactions. *Journal of the Geological Society of London* 139:787-801.

Brown, B., C. Gaina, and R. D. Müller. 2006. Circum-Antarctic palaeobathymetry: Illustrated examples from Cenozoic to recent times. *Palaeogeography, Palaeoclimatology, Palaeoecology* 231:158-168.

Cande, S. C., and J. M. Stock. 2004. Cenozoic reconstructions of the Australia-New Zealand-South Pacific Sector of Antarctica. In *The Cenozoic Southern Ocean: Tectonics, Sedimentation and Climate Change Between Australia and Antarctica*, eds. N. Exon, J. K. Kennett, and M. Malone. Geophysical Monograph 151:5-17. Washington, D.C.: American Geophysical Union.

Cande, S. C., J. M. Stock, D. Müller, and T. Ishihara. 2000. Cenozoic motion between East and West Antarctica. *Nature* 404:145-150.

Colwell, J. B., H. M. J. Stagg, N. G. Direen, G. Bernardel, and I. Borissova. 2006. The structure of the continental margin off Wilkes Land and Terre Adélie Coast, East Antarctica. In *Antarctica: Contributions to Global Earth Sciences*, eds. D. K. Fütterer, D. Damaske, G. Kleinschmidt, H. Miller, and F. Tessensohn, pp. 327-340. New York: Springer-Verlag.

Cooper, A. K., H. Trey, G. Pellis, G. Cochrane, F. Egloff, M. Busetti, and ACRUP Working Group. 1997. Crustal structure of the southern Central Trough, western Ross Sea. In *The Antarctic Region: Geological Evolution and Processes*, ed. C. A. Ricci, pp. 637-642. Siena: *Terra Antartica* Publication.

Cunningham, A. P., R. D. Larter, P. F. Barker, K. Gohl, and F. O. Nitsche. 2002. Tectonic evolution of the Pacific margin of Antarctica. 2. Structure of Late Cretaceous-early Tertiary plate boundaries in the Bellingshausen Sea from seismic reflection and gravity data. *Journal of Geophysical Research* 107(B12):2346, doi:10.1029/2002JB001897.

Damaske, D., A. L. Läufer, F. Goldmann, H.-D. Möller, and F. Lisker. 2007. Magnetic anomalies northeast of Cape Adare, northern Victoria Land (Antarctica), and their relation to onshore structures. In *Antarctica: A Keystone in a Changing World—Online Proceedings for the Tenth International Symposium on Antarctic Earth Sciences,* eds. Cooper, A. K., C. R. Raymond et al., USGS Open-File Report 2007-1047, Short Research Paper 016, doi:10.3133/of2007-1047.srp016.

Davey, F. J., S. C. Cande, and J. M. Stock. 2006. Extension in the western Ross Sea region—links between Adare Basin and Victoria Basin. *Geophysical Research Letters* 33, L20315, doi:10.1029/2006GL027383.

Direen, N. G., J. Borissova, H. M. J. Stagg, J. B. Colwell, and P. A. Symonds. 2007. Nature of the continent-ocean transition zone along the southern Australian continental margin: A comparison of the Naturaliste Plateau, south-western Australia, and the central Great Australian Bight sectors. In *Imaging, Mapping and Modelling Continental Lithosphere Extension and Breakup,* eds. G. Karner, G. Manatschal, and L. M. Pinheiro. *Geological Society Special Publication* 282:239-263.

Eagles, G., K. Gohl, and R. B. Larter. 2004. High resolution animated tectonic reconstruction of the South Pacific and West Antarctic margin. *Geochemistry, Geophysics, Geosystems (G^3)* 5, doi:10.1029/2003GC000657.

Eagles, G., R. Livermore, and P. Morris. 2006. Small basins in the Scotia Sea: The Eocene Drake Passage gateway. *Earth and Planetary Science Letters* 242:343-353.

Eittreim, S. L., and G. L. Smith. 1987. Seismic sequences and their distribution on the Wilkes Land margin. In *The Antarctic Continental Margin: Geology and Geophysics of Offshore Wilkes Land*, eds. S. L. Eittreim and M. A. Hampton. *Earth Sciences Series* 5A:15-43. Tulsa, OK: Circum-Pacific Council for Energy and Mineral Resources.

Eittreim, S. L., M. A. Hampton, and J. R. Childs. 1985. Seismic-reflection signature of Cretaceous continental breakup on the Wilkes Land margin, Antarctica. *Science* 229:1082-1084.

Funck, T., J. R. Hopper, H. C. Larsen, K. E. Louden, B. E. Tucholke, and W. S. Holbrook. 2003. Crustal structure of the ocean-continent transition at Flemish Cap: Seismic refraction results. *Journal of Geophysical Research* 108(B11), 2531, doi:10.1029/2003JB002434.

Gaina, C., R. D. Müller, B. Brown, T. Ishihara, and S. Ivanov. 2007. Breakup and early seafloor spreading between India and Antarctica. *Geophysical Journal International* 170:151-169, doi:10.1111/j.1365-246X.2007.03450.

Ghidella, M. E., and J. L. LaBrecque. 1997. The Jurassic conjugate margins of the Weddell Sea: Considerations based on magnetic, gravity and paleobathymetric data. In *The Antarctic Region: Geological Evolution and Processes*, ed. C. A. Ricci, pp. 441-451. Siena: *Terra Antartica* Publication.

Ghidella, M. E., G. Yáñez, and J. L. LaBrecque. 2002. Revised tectonic implications for the magnetic anomalies of the western Weddell Sea. *Tectonophysics* 347:65-86.

Gohl, K., and G. Uenzelmann-Neben. 2001. The crustal role of the Agulhas Plateau, southwest Indian Ocean: Evidence from seismic profiling. *Geophysical Journal International* 144:632-646.

Gohl, K., F. Nitsche, and H. Miller. 1997a. Seismic and gravity data reveal Tertiary interplate subduction in the Bellingshausen Sea, southeast Pacific. *Geology* 25:371-374.

Gohl, K., F. O. Nitsche, K. Vanneste, H. Miller, N. Fechner, L. Oszko, C. Hübscher, E. Weigelt, and A. Lambrecht. 1997b. Tectonic and sedimentary architecture of the Bellingshausen and Amundsen Sea Basins, SE Pacific, by seismic profiling. In *The Antarctic Region: Geological Evolution and Processes*, ed. C. A. Ricci, pp. 719-723. Siena: *Terra Antartica* Publication.

Gohl, K., G. L. Leitchenkov, N. Parsiegla, B.-M. Ehlers, C. Kopsch, D. Damaske, Y. B. Guseva, and V. V. Gandyukhin. 2007a. Crustal types and continent-ocean boundaries between the Kerguelen Plateau and Prydz Bay, East Antarctica. In *Antarctica: A Keystone in a Changing World—Online Proceedings for the Tenth International Symposium on Antarctic Earth Sciences,* eds. Cooper, A. K., C. R. Raymond et al., USGS Open-File Report 2007-1047, Extended Abstract 038, http://pubs.usgs.gov/of/2007/1047/.

Gohl, K., D. Teterin, G. Eagles, G. Netzeband, J. W. G. Grobys, N. Parsiegla, P. Schlüter, V. Leinweber, R. D. Larter, G. Uenzelmann-Neben, and G. B. Udintsev. 2007b. Geophysical survey reveals tectonic structures in the Amundsen Sea embayment, West Antarctica. In *Antarctica: A Keystone in a Changing World—Online Proceedings for the Tenth International Symposium on Antarctic Earth Sciences,* eds. Cooper, A. K., C. R. Raymond et al., USGS Open-File Report 2007-1047, Short Research Paper 047, doi:10.3133/Of2007-1047.srp047.

Golynsky, A. V., and N. D. Aleshkova. 2000. New aspects of crustal structure in the Weddell Sea region from aeromagnetic studies. *Polarforschung* 67:133-141.

Grad, M., A. Guterch, T. Janik, and P. Sroda. 2002. Seismic characteristics of the crust in the transition zone from the Pacific Ocean to the northern Antarctic Peninsula, West Antarctica. In *Antarctica at the Close of a Millennium*, eds. J. A. Gamble, D. N. B. Skinner, and S. Henrys. *Royal Society of New Zealand Bulletin* 35:493-498.

Grobys, J. W. G., K. Gohl, B. Davy, G. Uenzelmann-Neben, T. Deen, and D. Barker. 2007. Is the Bounty Trough, off eastern New Zealand, an aborted rift? *Journal of Geophysical Research* 112, B03103, doi:10.1029/2005JB004229.

Grobys, J. W. G., K. Gohl, and G. Eagles. 2008. Quantitative tectonic reconstructions of Zealandia based on crustal thickness estimates. *Geochemistry, Geophysics, Geosystems (G^3)* 9:Q01005, doi:10.1029/2007GC001691.

Guseva, Y. B., G. L. Leitchenkov, and V. V. Gandyukhin. 2007. Basement and crustal structure of the Davis Sea region (East Antarctica): Implications for tectonic setting and COB definition. In *Antarctica: A Keystone in a Changing World—Online Proceedings for the Tenth International Symposium on Antarctic Earth Sciences,* eds. Cooper, A. K., C. R. Raymond et al., USGS Open-File Report 2007-1047, Short Research Paper 025, doi:10.3133/of2007-1047.srp025.

Hinz, K., and W. Krause. 1982. The continental margin of Queen Maud Land/Antarctica: Seismic sequences, structural elements and geological development. *Geologisches Jahrbuch E* 23:17-41.

Hinz, K., S. Neben, Y. B. Gouseva, and G. A. Kudryavtsev. 2004. A compilation of geophysical data from the Lazarev Sea and the Rijser-Larsen Sea, Antarctica. *Marine Geophysical Researches* 25:233-245, doi:10.1007/s11001-005-1319-y.

Hübscher, C., W. Jokat, and H. Miller. 1996a. Structure and origin of southern Weddell Sea crust: Results and implications. In *Weddell Sea Tectonics and Gondwana Break-up*, eds. B. C. Storey, E. C. King, and R. A. Livermore. *Geological Society Special Publication* 108:201-211.

Hübscher, C., W. Jokat, and H. Miller. 1996b. Crustal structure of the Antarctic continental margin in the eastern Weddell Sea. In *Weddell Sea Tectonics and Gondwana Break-up*, eds. B. C. Storey, E. C. King, and R. A. Livermore. *Geological Society Special Publication* 108:165-174.

Ivins, E. R., and T. S. James. 2005. Antarctic glacial isostatic adjustment: A new assessment. *Antarctic Science* 17:537-549, doi:10.1017/S0954102004.

Jokat, W., C. Hübscher, U. Meyer, L. Oszko, T. Schöne, W. Versteeg, and H. Miller. 1996. The continental margin off East Antarctica between 10°W and 30°W. In *Weddell Sea Tectonics and Gondwana Break-up,* eds. B. C. Storey, E. C. King, and R. A. Livermore. *Geological Society Special Publication* 108:129-141.

Jokat, W., N. Fechner, and M. Studinger. 1997. Geodynamic models of the Weddell Sea Embayment in view of new geophysical data. In *The Antarctic Region: Geological Evolution and Processes*, ed. C. A. Ricci, pp. 453-459. Siena: *Terra Antartica* Publication.

Jokat, W., T. Boebel, M. König, and U. Meyer. 2003. Timing and geometry of early Gondwana breakup. *Journal of Geophysical Research* 108(B9), doi:10.1029/2002JB001802.

Jokat, W., O. Ritzmann, C. Reichert, and K. Hinz. 2004. Deep crustal structure of the continental margin off the Explora Escarpment and in the Lazarev Sea, East Antarctica. *Marine Geophysical Researches* 25:283-304, doi:10.1007/s11001-005-1337-9.

König, M., and W. Jokat. 2006. The Mesozoic breakup of the Weddell Sea. *Journal of Geophysical Research* 111, B12102, doi:10.1029/2005JB004035.

Larter, R. D., and P. F. Barker. 1991. Effects of ridge crest-trench interaction on Phoenix-Antarctic spreading: Forces on a young subducting plate. *Journal of Geophysical Research* 96(B12):19586-19607.

Larter, R. D., A. P. Cunningham, P. F. Barker, K. Gohl, and F. O. Nitsche. 2002. Tectonic evolution of the Pacific margin of Antarctica. 1. Late Cretaceous tectonic reconstructions. *Journal of Geophysical Research* 107, B12:2345, doi:10.1029/2000JB000052.

Lawver, L. A., and L. M. Gahagan. 2003. Evolution of Cenozoic seaways in the circum-Antarctic region. *Palaeogeography, Palaeoclimatology, Palaeoecology* 3115:1-27.

Leitchenkov, G. L., H. Miller, and E. N. Zatzepin. 1996. Structure and Mesozoic evolution of the eastern Weddell Sea, Antarctica: History of early Gondwana break-up. In *Weddell Sea Tectonics and Gondwana Break-up*, eds. B. C. Storey, E. C. King, and R. A. Livermore. *Geological Society Special Publication* 108:175-190.

Leitchenkov, G. L., Y. B. Guseva, and V. V. Gandyukhin. 2007a. Cenozoic environmental changes along the East Antarctic continental margin inferred from regional seismic stratigraphy. In *Antarctica: A Keystone in a Changing World—Online Proceedings for the Tenth International Symposium on Antarctic Earth Sciences,* eds. Cooper, A. K., C. R. Raymond et al., USGS Open-File Report 2007-1047, Short Research Paper 005, doi:10.3133/of2007-1047.srp005.

Leitchenkov, G. L., V. V. Gandyukhin, Y. B. Guseva, and A. Y. Kazankov. 2007b. Crustal structure and evolution of the Mawson Sea, western Wilkes Land margin, East Antarctica. In *Antarctica: A Keystone in a Changing World—Online Proceedings for the Tenth International Symposium on Antarctic Earth Sciences,* eds. Cooper, A. K., C. R. Raymond et al., USGS Open-File Report 2007-1047, Short Research Paper 028, doi:10.3133/of2007-1047.srp028.

Lythe, M. B., D. G. Vaughan, and the BEDMAP Consortium. 2001. BEDMAP: A new ice thickness and subglacial topographic model of Antarctica. *Journal of Geophysical Research* 106(B6):11335-11351.

Mayes, C. L., L. A. Lawver, and D. T. Sandwell. 1990. Tectonic history and new isochron chart of the South Pacific. *Journal of Geophysical Research* 95(B6):8543-8567.

McAdoo, D. C., and S. Laxon. 1997. Antarctic tectonics: Constraints from an ERS-1 satellite marine gravity field. *Science* 276:556-560.

Morelli, A., and S. Danesi. 2004. Seismological imaging of the Antarctic continental lithosphere: A review. *Global Planetary Change* 42:155-165.

Nitsche, F. O., A. P. Cunningham, R. D. Larter, and K. Gohl. 2000. Geometry and development of glacial continental margin depositional systems in the Bellingshausen Sea. *Marine Geology* 162:277-302.

Roeser, H. A., J. Fritsch, and K. Hinz. 1996. The development of the crust off Donning Maud Land, East Antarctica. In *Weddell Sea Tectonics and Gondwana Break-up*, eds. B. C. Storey, E. C. King, and R. A. Livermore. *Geological Society Special Publication* 108:243-264.

Rogenhagen, J., and W. Jokat. 2002. Origin of the gravity ridges and Anomaly-T in the southern Weddell Sea. In *Antarctica at the Close of a Millennium*, eds. J. A. Gamble, D. N. B. Skinner, and S. Henrys. *Royal Society of New Zealand Bulletin* 35:227-231.

Sayers, J., P. A. Symonds, N. G. Direen, and G. Bernardel. 2001. Nature of the continent-ocean transition on the non-volcanic rifted margin of the central Great Australian Bight. In *Non-volcanic Rifting of Continental Margins: A Comparison of Evidence from Land and Sea*, eds. R. C. L. Wilson, R. B. Whitmarsh, B. Taylor, and N. Froitzheim. *Geological Society Special Publication* 187:51-76.

Scheuer, C., K. Gohl, R. D. Larter, M. Rebesco, and G. Udintsev. 2006. Variability in Cenozoic sedimentation along the continental rise of the Bellingshausen Sea, West Antarctica. *Marine Geology* 277:279-298.

Sibuet, J.-C., S. Srivastava, and G. Manatschal. 2007. Exhumed mantle-forming transitional crust in the Newfoundland-Iberia rift and associated magnetic anomalies. *Journal of Geophysical Research* 112, B06105, doi:10.1029/2005JB003856.

Solli, K., B. Kuvaas, Y. Kristoffersen, G. Leitchenkov, J. Guseva, and V. Gandyukhin. 2007. The Cosmonaut Sea Wedge. In *Antarctica: A Keystone in a Changing World—Online Proceedings for the Tenth International Symposium on Antarctic Earth Sciences,* eds. Cooper, A. K., C. R. Raymond et al., USGS Open-File Report 2007-1047, Short Research Paper 009, doi:10.3133/of2007-1047.srp009.

Stagg, H. M. J., J. B. Colwell, N. G. Direen, P. E. O'Brien, G. Bernardel, I. Borissova, B. J. Brown, and T. Ishihara. 2004. Geology of the continental margin of Enderby and Mac Robertson Lands, East Antarctica: Insights from a regional data set. *Marine Geophysical Researches* 25:183-218.

Stagg, H. M. J., J. B. Colwell, N. G. Direen, P. E. O'Brien, B. J. Brown, G. Bernadel, I. Borissova, L. Carson, and D. B. Close. 2005. Geological framework of the continental margin in the region of the Australian Antarctic Territory. *Geoscience Australia Record* 2004/25.

Stock, J. M., and S. C. Cande. 2002. Tectonic history of Antarctic seafloor in the Australia-New Zealand-South Pacific sector: Implications for Antarctic continental tectonics. In *Antarctica at the Close of a Millennium*, eds. J. A. Gamble, D. N. B. Skinner, and S. Henrys. *Royal Society of New Zealand Bulletin* 35:251-259.

Sutherland, R. 1999. Basement geology and tectonic development of the greater New Zealand region: An interpretation from regional magnetic data. *Tectonophysics* 308:341-362.

Trey, H., J. Makris, G. Brancolini, A. K. Cooper, G. Cochrane, B. Della Vedova, and ACRUP Working Group. 1997. The Eastern Basin crustal model from wide-angle reflection data, Ross Sea, Antarctica. In *The Antarctic Region: Geological Evolution and Processes*, ed. C. A. Ricci, pp. 637-642. Siena: *Terra Antartica* Publication.

Uenzelmann-Neben, G., K. Gohl, R. D. Larter, and P. Schlüter. 2007. Differences in ice retreat across Pine Island Bay, West Antarctica, since the Last Glacial Maximum: Indications from multichannel seismic reflection data. USGS Open-File Report 2007-1047, Short Research Paper 001, doi:10.3133/of2007-1047.srp084.

Wardell, N., J. R. Childs, and A. K. Cooper. 2007. Advances through collaboration: Sharing seismic reflection data via the Antarctic Seismic Data Library System for Cooperative Research (SDLS). In *Antarctica: A Keystone in a Changing World—Online Proceedings for the Tenth International Symposium on Antarctic Earth Sciences,* eds. Cooper, A. K., C. R. Raymond et al., USGS Open-File Report 2007-1047, Short Research Paper 001, doi:10.3133/of2007-1047.srp001.

Publication 6.1.4:

Wobbe, F., **Gohl, K.**, Chambord, A., Sutherland, R. (2012). Structure and breakup history of the rifted margin of West Antarctica in relation to Cretaceous separation from Zealandia and Bellingshausen plate motion. *Geochemistry, Geophysics, Geosystems (G^3),* v. 13, no. 4, Q04W12, doi:10.1029/2011GC003742.

Author contributions: The paper was mainly written by Wobbe as part of his PhD project under the supervision of Gohl. Gohl was involved in providing the conceptual idea and significantly contributing to the discussion of the results. Chambord and Sutherland provided some of the magnetic data and helped discuss the reconstruction model.

Geochemistry Geophysics Geosystems G3
Article
Volume 13, Number 4
1 May 2012
Q04W12, doi:10.1029/2011GC003742
ISSN: 1525-2027
Published by AGU and the Geochemical Society

Structure and breakup history of the rifted margin of West Antarctica in relation to Cretaceous separation from Zealandia and Bellingshausen plate motion

F. Wobbe and K. Gohl
Alfred Wegener Institute for Polar and Marine Research, PO Box 120161, D-27515 Bremerhaven, Germany (fwobbe@awi.de)

A. Chambord and R. Sutherland
GNS Science, 1 Fairview Drive, Lower Hutt 5040, New Zealand

[1] Geophysical data acquired using R/V Polarstern constrain the structure and age of the rifted oceanic margin of West Antarctica. West of the Antipodes Fracture Zone, the 145 km wide continent–ocean transition zone (COTZ) of the Marie Byrd Land sector resembles a typical magma-poor margin. New gravity and seismic reflection data indicates initial continental crust of thickness 24 km, that was stretched 90 km. Farther east, the Bellingshausen sector is broad and complex with abundant evidence for volcanism, the COTZ is ~670 km wide, and the nature of crust within the COTZ is uncertain. Margin extension is estimated to be 106–304 km in this sector. Seafloor magnetic anomalies adjacent to Marie Byrd Land near the Pahemo Fracture Zone indicate full-spreading rate during c33–c31 (80–68 Myr) of 60 mm yr^{-1}, increasing to 74 mm yr^{-1} at c27 (62 Myr), and then dropping to 22 mm yr^{-1} by c22 (50 Myr). Spreading rates were lower to the west. Extrapolation towards the continental margin indicates initial oceanic crust formation at around c34y (84 Myr). Subsequent motion of the Bellingshausen plate relative to Antarctica (84–62 Myr) took place east of the Antipodes Fracture Zone at rates <40 mm yr^{-1}, typically 5–20 mm yr^{-1}. The high extension rate of 30–60 mm yr^{-1} during initial margin formation is consistent with steep and symmetrical margin morphology, but subsequent motion of the Bellingshausen plate was slow and complex, and modified rift morphology through migrating deformation and volcanic centers to create a broad and complex COTZ.

Components: 11,300 words, 9 figures, 1 table.

Keywords: continent–ocean transition zone; crustal thickness; magnetic spreading anomaly; plate reconstruction.

Index Terms: 1517 Geomagnetism and Paleomagnetism: Magnetic anomalies: modeling and interpretation; 8105 Tectonophysics: Continental margins: divergent (1212, 8124); 8157 Tectonophysics: Plate motions: past (3040).

Received 6 June 2011; **Revised** 9 March 2012; **Accepted** 9 March 2012; **Published** 1 May 2012.

Wobbe, F., K. Gohl, A. Chambord, and R. Sutherland (2012), Structure and breakup history of the rifted margin of West Antarctica in relation to Cretaceous separation from Zealandia and Bellingshausen plate motion, *Geochem. Geophys. Geosyst.*, *13*, Q04W12, doi:10.1029/2011GC003742.

Theme: Plate Reconstructions, Mantle Convection, and Tomography Models: A Complementary Vision of Earth's Interior

Geochemistry Geophysics Geosystems G3 WOBBE ET AL.: BREAKUP HISTORY OF ZEALANDIA–MARIE BYRD LAND 10.1029/2011GC003742

1. Introduction

[2] The formation of continental passive margins by rifting is affected by the rate of rifting, the initial configuration of continental lithosphere, and the temperature and composition of the asthenosphere [*White et al.*, 1992; *van Wijk and Cloetingh*, 2002]. The final breakup of Gondwana occurred during Late Cretaceous time as rifted continental crust of New Zealand separated from Antarctica at an intermediate-rate spreading ridge to produce typical oceanic crust [*Molnar et al.*, 1975; *Cande et al.*, 1995; *Eagles et al.*, 2004a; *Sutherland et al.*, 2010]. Hence, the region presents an ideal opportunity to study classical conjugate rifted margins, but this outcome has been frustrated by extreme logistic difficulties associated with collecting data adjacent to Antarctica. We present a substantial new marine geophysical dataset collected using R/V Polarstern, which has general relevance for the study of continental margins, has substantial regional implications, and adds to the body of knowledge required to construct reliable global plate kinematic estimates. Of particular regional interest is the complication of a small and short-lived oceanic plate, the Bellingshausen plate, which was active after break-up adjacent to the Antarctic margin.

[3] Geological samples, gravity data and receiver-function analysis of teleseismic earthquakes suggest that both West Antarctica [*Llubes et al.*, 2003; *Luyendyk et al.*, 2003; *Winberry and Anandakrishnan*, 2004; *Block et al.*, 2009] and the submarine plateaus surrounding New Zealand [*Grobys et al.*, 2009, and references therein] consist of extended continental crust. Widespread continental extension is thought to have been largely complete before the continental margins were formed and Zealandia drifted from Antarctica. Breakup reconstructions of Zealandia from Antarctica consider a narrow continent–ocean transition zone [*Larter et al.*, 2002; *Eagles et al.*, 2004a].

[4] In this study, we present new crustal thickness and density models of the Marie Byrd Land continental margin of Antarctica, and new magnetic anomaly interpretations from adjacent oceanic crust. The crustal thickness models provide a foundation for reconstructing the continent–ocean transition zone (COTZ), and hence better reconstructing the past positions of the conjugate continental fragments. Magnetic anomalies provide new constraints on the timing and rate of rifting during continental margin formation, and on subsequent plate motions.

2. Data Acquisition and Processing

[5] During the Polarstern cruises in 2006 (ANT-23/4) and 2010 (ANT-26/3), ship- and airborne magnetic and shipborne gravity data have been acquired. These data were combined with seismic reflection and refraction/wide-angle reflection surveys from the same cruises to constrain the COTZ of Marie Byrd Land. Regions where measured ship-data are unavailable were filled with public domain satellite-derived free-air gravity data [*Andersen and Knudsen*, 2009], global seafloor topography data (version 13.1, 2010) [*Smith and Sandwell*, 1997], and ship-magnetic data from the GEODAS marine trackline geophysics database [*National Geophysical Data Center*, 2007]. Data acquisition and subsequent processing for each of the acquired datasets are described in the following sections.

2.1. Helicopter Magnetics

[6] In 2010, five thousand kilometers of aeromagnetic data were recorded at a sampling rate of 10 Hz during the North–South transit from New Zealand to the Amundsen Sea south of 69°S (Figures 1–5). A helicopter towed the optically pumped cesium vapor magnetometer 30 m below its airframe to avoid magnetic disturbances. Flight lines were arranged perpendicular to the expected magnetic lineation of the seafloor at an average line spacing of 10–20 km, covering a profile distance of about 450 km at a flight elevation of 100 m above sea level. Geographic position, speed and altitude of the aircraft as well as time were recorded at a rate of 5 Hz [*Gohl*, 2010].

[7] The cesium vapor magnetometer recorded data with a general heading error below 5 nT so that no calibration was necessary. Processing included removal of electromagnetic noise, resampling at 100 m intervals, and correction for the International Geomagnetic Reference Field using the IGRF-11 coefficients [*Finlay et al.*, 2010].

[8] Measured magnetic anomaly amplitudes of 50–400 nT were greater than the daily variation of 20–30 nT, observed at the Eyrewell Geomagnetic Observatory in New Zealand. Local daily variations were therefore considered negligible.

2.2. Shipborne Magnetics

[9] Two three-component fluxgate vector magnetometers mounted on the crow's nest of R/V

Geochemistry Geophysics Geosystems G3 WOBBE ET AL.: BREAKUP HISTORY OF ZEALANDIA–MARIE BYRD LAND 10.1029/2011GC003742

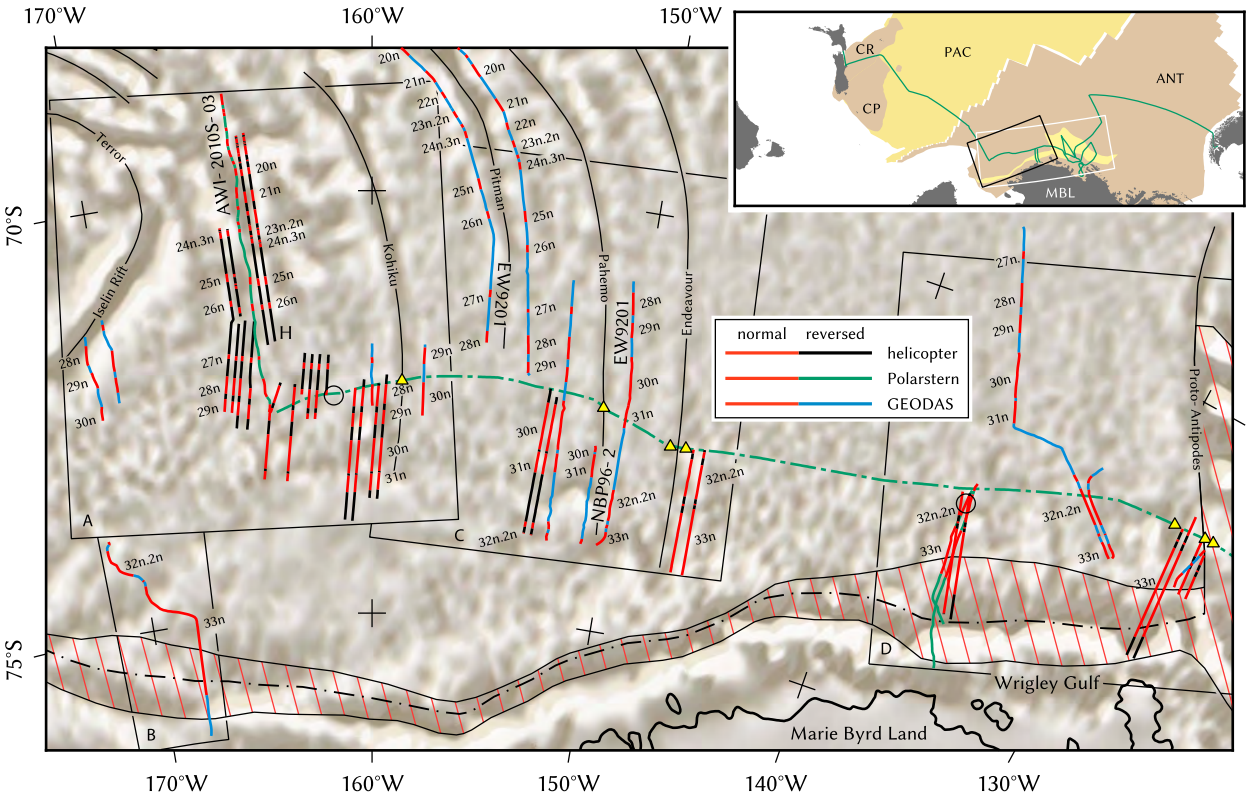

Figure 1. Identified magnetic spreading anomalies along helicopter- and ship-magnetic lines (R/V Polarstern lines AWI-2010S-00–AWI-2010S-03; GEODAS lines EW9201, NBP94-2, NBP96-2, NBP9702). Magnetic model of helicopter-magnetic line AWI-2010H-08-15-17 (H) and ship-magnetic line AWI-2010S-03 in Figure A.IX in Text S1 in the auxiliary material. Magnetic compensation loops during ANT-26/3 (circles); fracture zones (thin black lines); fracture zones evident in seismic lines AWI-20100110 and AWI-20100117 (yellow triangles); COTZ (striated area); and reconstructed pre-rift suture (dashed line). Black frames indicate locations of Figures 2–4. All features superimposed on DNSC08 satellite gravity map [*Andersen and Knudsen*, 2009]. Lambert conformal conic projection with central meridian 160°W and standard parallels 75°S and 69°S. Inset map shows ship track of R/V Polarstern expedition ANT-26/3 (green line); location of maps in Figure 1 and in Figure 6 (black and white frames); CP – Campbell Plateau; CR – Chatham Rise; ANT – West Antarctic plate; MBL – Marie Byrd Land; PAC – belonging to Pacific plate. Magnetic model of lines EW9201 and NBP96-2 in Figure A.VIII in Text S1 in the auxiliary material.

Polarstern measured shipborne magnetic data. The total magnetic field as well as the heading, roll, pitch, velocity, and position of the ship were logged at 1 Hz.

[10] Calibration loops provide coefficients relating the ship orientation (heading, roll, pitch) and speed to the variations in magnetometer measurements. To compensate for perturbations due to ship-induced magnetic fields, we measured a total of 13 calibration loops, five of which are located in our study area (Figure 6). During a calibration loop, the ship follows an eight-shaped course of two consecutive turns of opposite veer with a radius of about 1.8 km (1 NM) and a velocity of 5–7 kn.

[11] In the small area of a calibration loop, variations of the magnetic field due to crustal magnetization are considered negligible. In the larger area around the calibration loop, the shipborne magnetic measurements were corrected with the motion coefficients according to *König* [2006]. The calibrated data have a maximum residual error of 20–30 nT under normal conditions at sea. Since the interference of the ship on the magnetic fields is larger than the daily magnetic variation, the daily variations were neglected in the determination of seafloor spreading anomalies.

[12] The induced magnetic field of the ship is not static, but instead depends on the strength, inclination, and declination of the ambient magnetic field. Since the inclination and declination show a high local variance in the higher latitudes, calibration coefficients are only adequate to fully correct their influence when the vessel operates inside a radius of 500–1500 km around the location of the calibration loop.

Geochemistry Geophysics Geosystems G3 WOBBE ET AL.: BREAKUP HISTORY OF ZEALANDIA–MARIE BYRD LAND 10.1029/2011GC003742

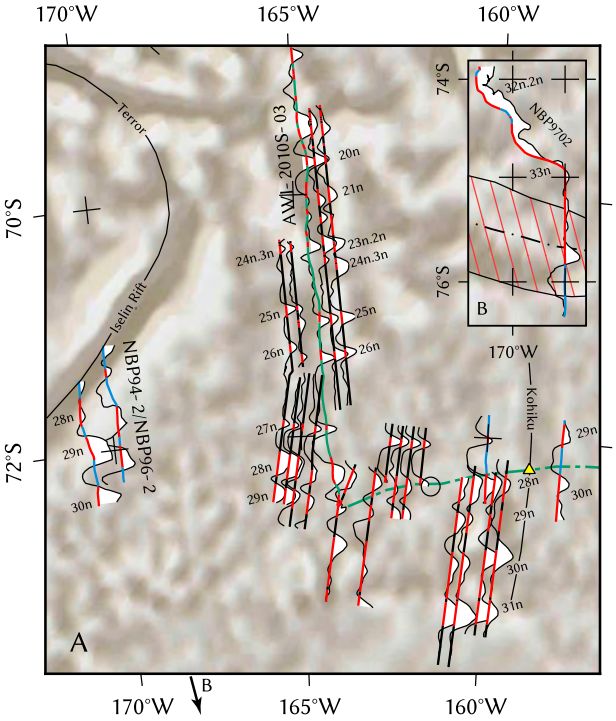

Figure 2. Magnifications of regions A and B in Figure 1. Magnetic identifications on top of measured anomalies along tracks; positive anomalies in white. Lambert conformal conic projection with central meridian 163°W and standard parallels 75°S and 69°S.

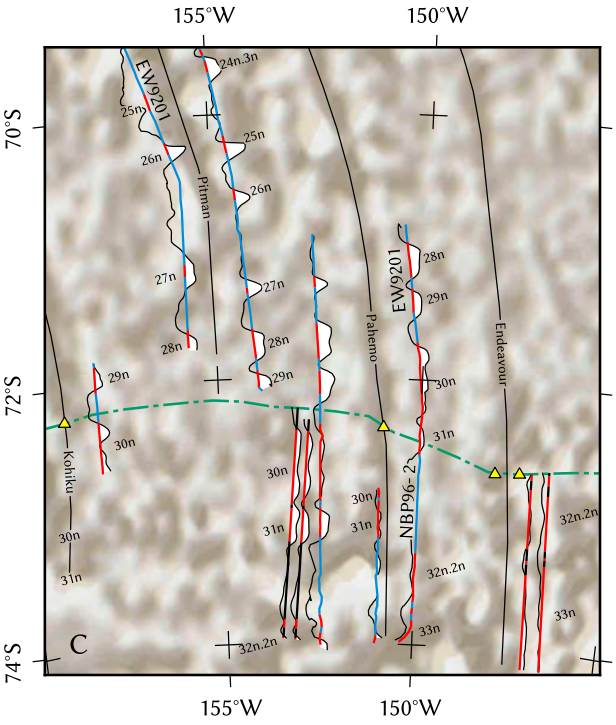

Figure 3. Magnification of region C in Figure 1. Lambert conformal conic projection with central meridian 152.5°W and standard parallels 75°S and 69°S.

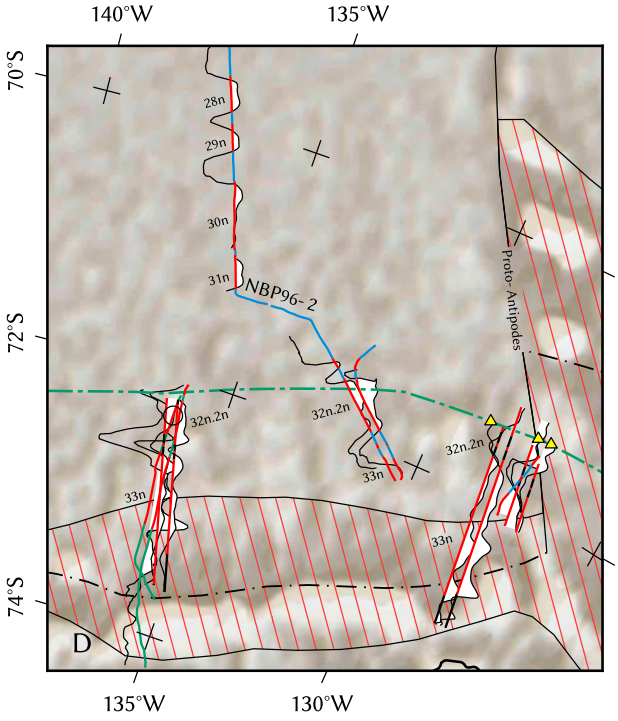

Figure 4. Magnification of region D in Figure 1. Lambert conformal conic projection with central meridian 155°W and standard parallels 75°S and 69°S.

[13] The necessity for carrying out a new calibration loop was determined by comparing the calibrated data from the two separate magnetometer sensors. Once the difference between both increased steadily, the set of calibration coefficients was insufficient to compensate the magnetic readings [*Gohl*, 2010].

[14] Some magnetic profiles retained long wavelength residual anomalies after processing, possibly due to the high regional variation in the geomagnetic field and the large operating area. The long wavelength anomalies were removed by leveling the magnetic data of the ship to that measured by the airborne magnetics. In areas without aeromagnetic profiles, a 500 km wide high-pass filter was applied.

2.3. Shipborne Gravity and Seismic Data

[15] A gravity meter installed on-board measured the ambient gravitational field at 1 Hz during the ANT-23/4 and ANT-26/3 expeditions. The gravity readings were drift corrected via onshore reference measurements at the beginning of the cruise ANT-26/3 in Wellington Harbor, New Zealand, and at the end of the cruise in Punta Arenas, Chile [*Gohl*, 2010]. *Gohl* [2007] processed the gravity data of the cruise ANT-23/4 in the same manner. A median filter with a 5 km window size was applied to remove heave variability.

Geochemistry Geophysics Geosystems G3 WOBBE ET AL.: BREAKUP HISTORY OF ZEALANDIA–MARIE BYRD LAND 10.1029/2011GC003742

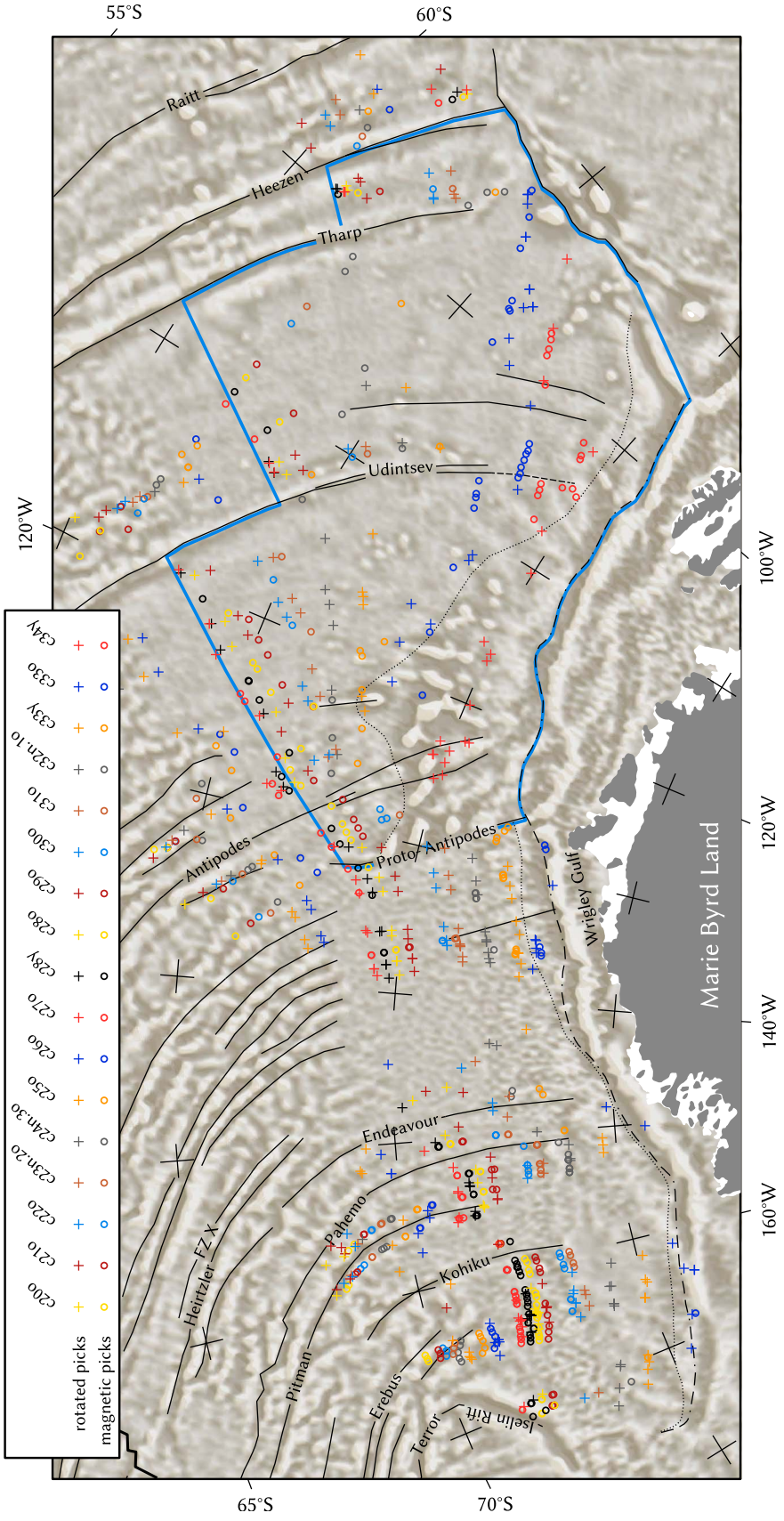

Figure 5

Geochemistry Geophysics Geosystems G3 WOBBE ET AL.: BREAKUP HISTORY OF ZEALANDIA–MARIE BYRD LAND 10.1029/2011GC003742

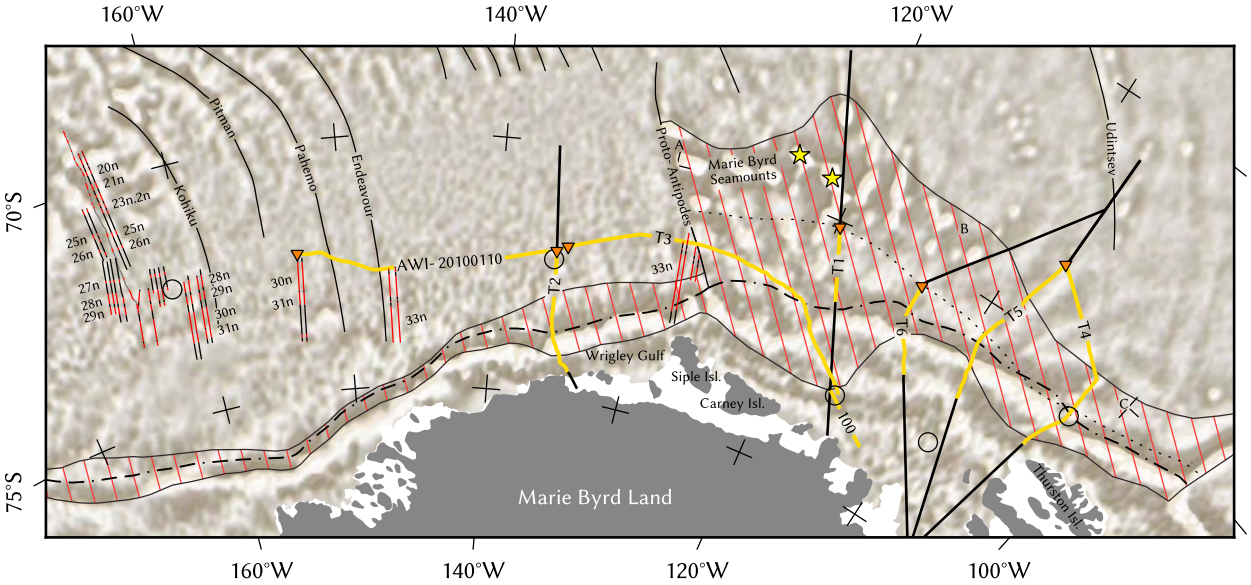

Figure 6. COTZ (striated) with reconstructed pre-rift suture (dashed line); calculated pre-rift suture, disregarding crustal addition (dotted line); seismic transects (thick yellow lines; 100 – AWI-20060100; T1 – AWI-20060200; T2 – AWI-20100111, AWI-20100112, AWI-20100113; T3 – AWI-20100117, AWI-20100118, AWI-20100119; T4 – AWI-20100126, AWI-20100129, AWI-20100130; T5 – AWI-20100131, AWI-20100132; T6 – AWI-20100139, AWI-20100140), and extensions (thick black lines); inverted triangles mark origin of each transect in Figure 7; identified magnetic spreading anomalies along ship profile ANT-2010S-03, and helicopter-magnetic lines (red – normal polarity, black – reversed); fracture zones (thin black lines); magnetic compensation loops (circles); A, B, C – see Figure A.VII in Text S1 in the auxiliary material; stars — locations of Haxby and Hubert Miller Seamount (from west to east). Base map: DNSC08 satellite gravity [*Andersen and Knudsen*, 2009], Lambert conformal conic projection with central meridian 145°W and standard parallels 74°S and 66°S.

[16] Deep crustal seismic refraction profiles, AWI-20060100 [*Gohl et al.*, 2007] and AWI-20060200 [*Gohl*, 2007; *Lindeque and Gohl*, 2010], acquired during the ANT-23/4 cruise in 2006, and a series of multichannel seismic reflection profiles, obtained during the ANT-26/3 cruise in 2010, lie within our study area (yellow lines in Figure 6). These seismic reflection profiles are currently being processed in-house (T. Kalberg, A. Lindeque, G. Uenzelmann-Neben, and E. Weigelt, personal communication, 2011). The most relevant parameters for this study, basement depth, seafloor and total sediment thickness, were picked in two-way-travel time (TWT) from the preliminary single channel seismic data. The TWT values were converted to depth (in km) using the sediment layer interval velocities from the finer AWI-20060200 P-wave refraction model [*Lindeque and Gohl*, 2010], and velocities for the deeper crust were obtained from both the AWI-20060100 and AWI-20060200 models. The converted basement depths and total sediment thicknesses were incorporated in the gravity model.

3. Models

3.1. Magnetic Modeling

[17] The first step in our modeling was to identify the marine magnetic spreading anomalies along our profiles. This was done based on the methods and techniques of *Vine and Matthews* [1963]. The synthetic spreading models were calculated using the open-source program MODMAG [*Mendel et al.*, 2005], applying the geomagnetic polarity timescale of *Gradstein et al.* [2004]. Two magnetic GEODAS profiles (Figure 1), EW9201 (R/V Maurice Ewing, 1992) and NBP96-2 (R/V Nathaniel B. Palmer, 1996), served as reference to tie the newly acquired aeromagnetic data to existing Pacific–Antarctic spreading models [*Cande et al.*, 1995; *Croon et al.*, 2008].

Figure 5. Compilation of magnetic picks on the West Antarctic and Bellingshausen plate, and rotated picks from the Pacific plate used for plate-tectonic reconstruction. Fracture zones (black lines); pre-rift suture (dashed line); COB (dotted line); and Bellingshausen plate (blue outline). Base map: DNSC08 satellite gravity [*Andersen and Knudsen*, 2009], Lambert conformal conic projection with central meridian 145°W and standard parallels 72°S and 60°S.

[18] Helicopter- and ship-magnetic lines, obtained during the Polarstern cruise ANT-26/3, and GEODAS lines NBP94-2 and NBP9702, included in the existing model, increased the density of the magnetic spreading anomaly picks in the eastern Ross Sea and western Amundsen Sea. Figures 1–5 show the identified magnetic spreading anomalies from all available datasets (see auxiliary material for additional data).[1]

3.2. Gravimetric Modeling

[19] Since refraction models in the area are sparsely distributed, gravity modeling was used to further estimate the crustal thickness, location of the continent–ocean boundary (COB) and width of the COTZ. We chose six transects from the continental shelf break to the abyssal plane, all approximately perpendicular to the continental shelf, so as to cross the potential COB and COTZ optimally (Figure 6). Lines reaching beyond the continental shelf were extended with satellite-derived gravity data [*Andersen and Knudsen*, 2009], bathymetry data [*Andersen and Knudsen*, 2009] and sediment thickness values [*Scheuer et al.*, 2006]. The seafloor and basement depth, as well as total sediment thickness from the 2010 seismic reflection data, were imported in the gravity model as fixed layers. Where available, on-board gravity and echosound bathymetry data were used to supplement the seafloor picked in the single channel seismic data. The gravity response was then calculated by forward modeling using the method of *Watts* [1988] and *Watts and Fairhead* [1999]. We estimated densities of sedimentary rocks from P-wave velocities according to *Gardner et al.* [1974] and assumed uniform densities for the upper crust, the lower crust and the mantle on all transects to obtain crustal models. Then we created a start model that is similar to the deep crustal profile (T1) and tried to fit the measured gravity by altering the structure of the crust as little as possible. When the thickness of the sediments overlying the basement is known from seismics we did not change them. Fortunately, the geometry of the sediments and water column have the biggest influence on the gravity signal, so there is less freedom for fitting the underlying crust in the model.

[20] The resulting gravity models (examples T1 and T2 in Figure 7) constrained the pre- and post-rift crustal thickness well, allowing us to assess the amount of continental deformation involved during the initial rifting process and subsequent Zealandia–Antarctica breakup.

3.3. Continental Deformation Model

[21] Our model considers deformation that is located in the COTZ (stippled area in Figure 8), an area, where the origin of the crust cannot be classified unequivocally as either continental or oceanic. In this zone, oceanic crust can be interleaved with segments of transitional crust, but the crustal thickness generally increases from its outer edge to the inner bound. Contrary, the amount of generated melt increases towards the outer edge, where the thickness of the oceanic crust equals the melt thickness.

[22] In order to reconstruct the pre-rift shape of the Marie Byrd Land margin, we determined the width of the COTZ, l_e, and the crustal thickness prior to its extension, t_0, within each of the six seismic transects T1 to T6. We assumed volume constancy of the continental crust during deformation, and—reduced to a 2D profile—a continuous cross section area, A_c.

[23] The aforementioned parameters permitted the calculation of the pre-rift width of the COTZ, l_0, the mean thickness of the extended crust, t_r, and the stretching factor, β, according to the equations in Figure 8. Both, t_r and β, are independent from the obliquity of the 2D section with respect to the COTZ, when a three-dimensional continuation of the geological units to either side of the 2D section is presumed. The areal extent of the COTZ, depicted in Figures 1 and 6, was estimated by interpolation between the seismic transects.

3.4. Plate-Tectonic Reconstruction

[24] Visual fitting of picks of the magnetic spreading anomalies from *Cande et al.* [1995], *Eagles et al.* [2004b], and this study as well as fracture zone traces using GPlates [*Boyden et al.*, 2011] yielded new finite rotations (Figure 5; see also Figure A.IV and Table B.I in Text S1 in the auxiliary material).

[25] Occasionally, ambiguities in the magnetic identifications allowed for multiple rotation solutions. In these cases, we regarded the position of flow lines and fracture zones to be more trustworthy than the location of modeled magnetic isochrons and preferred a better fit of flow lines over that of magnetic isochrons. Fracture zones were digitized from seismic lines and satellite gravity data. Lateral shifts of magnetic identifications in adjacent

[1] Auxiliary materials are available in the HTML. doi:10.1029/2011GC003742.

Geochemistry Geophysics Geosystems G3 WOBBE ET AL.: BREAKUP HISTORY OF ZEALANDIA–MARIE BYRD LAND 10.1029/2011GC003742

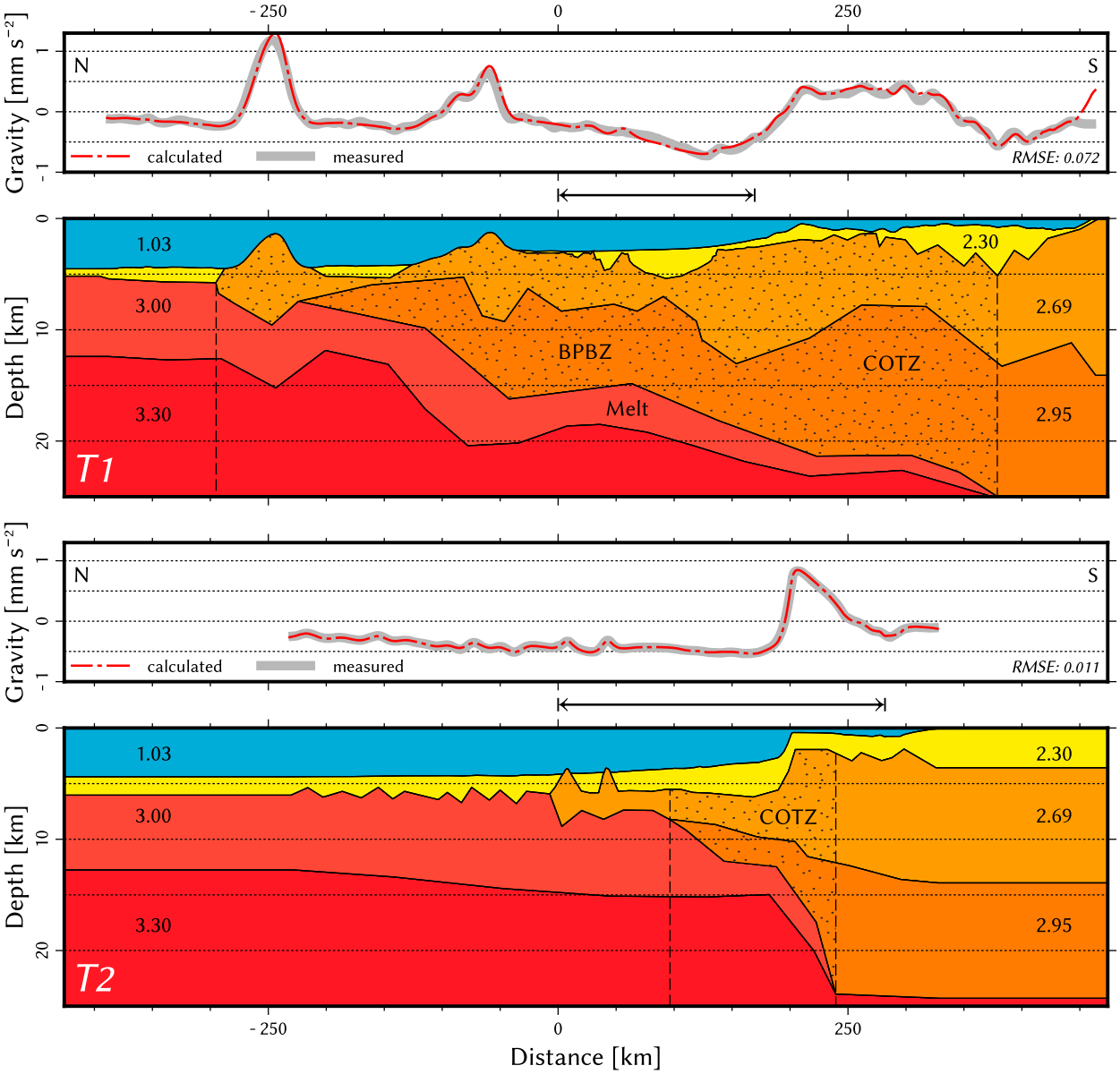

Figure 7. Crustal models along seismic transects T1 and T2 (locations on map in Figure 6). Numbers in the cross-section represent density (g cm^{-3}); stippled area indicates extended transitional crust/Bellingshausen Plate Boundary Zone (COTZ/BPBZ). Arrows indicate area covered by seismic transect. Transects T3 to T6 in auxiliary material.

profiles further constrained fracture zone traces that are not apparent as flow lines in the gravity data.

[26] Whenever magnetic data were unavailable due to the Cretaceous Normal Superchron (84–125 Myr) or tectonic/magmatic overprinting, we attempted to determine the finite rotation pole by extrapolating spreading rates from the oldest distinguishable chron back to the margin. For this we assumed that spreading rates were constant during the Cretaceous Normal Superchron and resembled the rate that was determined at c34y (84 Myr). In some cases, it was possible to estimate the spreading rate directly from existing spreading anomalies on the conjugate margin assuming identical half-spreading rates. The pre-rift reconstruction of Marie Byrd Land, Chatham Rise, and Campbell Plateau originated from the fit of the pre-rift sutures of the continental margins at 90 Myr.

4. Data Analysis and Discussion

4.1. Crustal Model

[27] The crustal models (Figure 7), obtained from gravity inversion along seismic transects T1 to T6

Geochemistry Geophysics Geosystems G3 WOBBE ET AL.: BREAKUP HISTORY OF ZEALANDIA–MARIE BYRD LAND 10.1029/2011GC003742

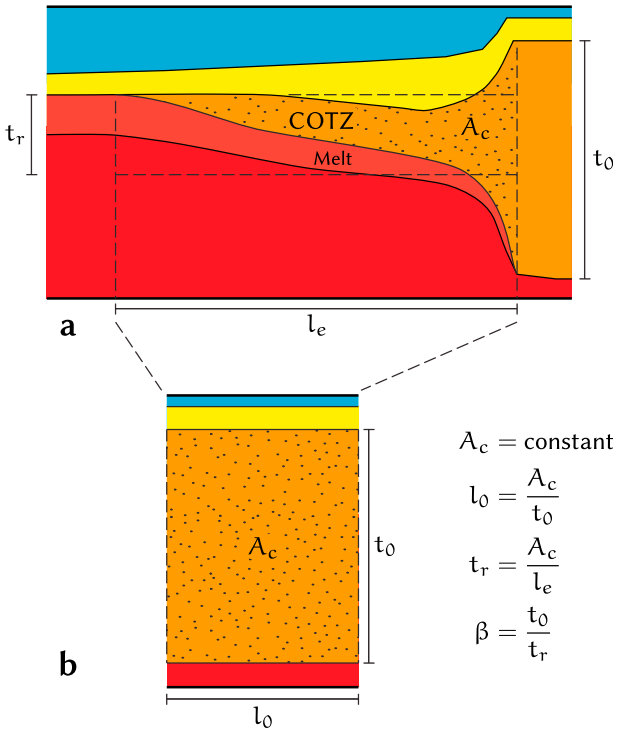

Figure 8. Determination of the COTZ width prior to rifting. (a) Extended transitional crust (stippled area) on passive continental margin from gravity inversion model (Figure 7). (b) Reconstruction of the stippled area in Figure 8a before rifting. β — stretching factor; A_c/l_e — COTZ area/width; l_0 — pre-rift width of COTZ; t_0/t_r — initial/extended crustal thickness.

(Figure 6), image an uneven basement, covered by sediments up to 2.8 km thick. If we compare the top-of-basement of *Grobys et al.* [2009] with our crustal models, we observe a 1 km elevation difference between Zealandia and Marie Byrd Land, consistent with the findings of *Sutherland et al.* [2010]. The Moho depth varies around 24 km, and the lower crust is generally 10 km thick.

[28] Two representative crustal models along the seismic transects T1 and T2 are displayed in Figure 7. The models consist of five layers—sedimentary cover (2.3 g cm^{-3}), upper crust (2.69 g cm^{-3}), lower crust (2.95 g cm^{-3}), melt addition/oceanic crust (3.0 g cm^{-3}), and mantle (3.3 g cm^{-3})—whose densities and thicknesses were obtained from the velocity–depth model.

[29] Apart from slight deviations, the gravity-derived crustal model of transect T1 reflects the observations from the velocity–depth model: Crust with a low density, but anomalously large thickness extends seaward of the continental slope. The Moho and the boundary between upper and lower crust rise gradually towards the shelf, and the gravity anomaly describes the rugged topography of the upper crust and the Marie Byrd Seamounts. The upper part of the submarine volcanoes consists of material with approximately equal density as the upper crust. Subsidence of the transitional crust and subsequent formation of small sediment basins increase the distance of the denser material to the surface and generate negative gravity anomalies.

[30] By contrast, transect T2, which lies west of the Marie Byrd Seamounts, displays an elongated positive free-air gravity anomaly aligned with the Moho step. This anomaly is caused by gravimetric superposition of the Moho step with the bathymetric step of the steep continental slope and some minor sedimentary effect. The gravity high is followed by a less pronounced landward low close to the shelf that trends subparallel to shelf edge. Comparable elongate gravity anomalies are considered commonly associated with Atlantic-type passive continental margins [*Watts*, 1988; *Watts and Fairhead*, 1999]. Unlike T1, the transition from thick continental crust to thin oceanic crust is abrupt with the Moho raising about 8 km. The sedimentary cover reaches thicknesses of up to 4 km.

[31] Transects T3 to T6 (see auxiliary material) are more similar to transect T1 than to T2. The former transects feature an equally thick low-density crust extending far from the slope. The free-air anomaly, also similar to that in the transect T1, indicates the same rugged crust topography and sedimentary cover. Compared to the cross sections further west, transects T4 and T5 are characterized by increased amounts of sediments (3–4 km) on the slope. We observed a small but distinct increase of the upper crust thickness, where transect T3 crosses the Proto-Antipodes Fracture Zone.

[32] Except for the central part of transect T1, which is covered by the velocity–depth model, the gravity models are based only on reflection seismic data. This leads to lower confidence on sediment thickness estimates due to poorly constrained interval velocity, as well as a lack of information about basement properties. However, variations of sediment and basement properties within commonly-accepted bounds would not be enough to explain the gravity field differences between the transects. Hence, we expect the effects of these uncertainties on the determination of the crustal thickness, COTZ, and β-factors to be small.

[33] We can distinguish between the Marie Byrd Land sector with a sharp transition in the free-air

Geochemistry Geophysics Geosystems G3 WOBBE ET AL.: BREAKUP HISTORY OF ZEALANDIA–MARIE BYRD LAND 10.1029/2011GC003742

Table 1. COTZ Properties of the Marie Byrd Seamount Province Along Seismic Transects (Figure 6)

Number	β-Factor	COTZ Width	Cont. Stretching
T1	1.83	670 km	304 km
T2	2.62	145 km	90 km
T3	—	—	—
T4	1.89	225 km	106 km
T5	3.55	220 km	158 km
T6	3.12	345 km	234 km

anomaly and a narrow COTZ, and the extremely wide Bellingshausen Plate Boundary Zone (BPBZ).

[34] The Marie Byrd Land margin best compares to magma-poor passive continental margins in the central South Atlantic, e.g., the Brazilian Espírito Santo margin and conjugate North Angolan margin [*Blaich et al.*, 2011; *Huismans and Beaumont*, 2011]. Despite the uncertainties in the crustal models, several features support this classification: There are no indications of syn-rift magmatism like oceanic seaward dipping reflectors or anomalously high P-wave velocities within the transitional crust. Instead, seismic velocities of the lower crust [*Gohl et al.*, 2007; *Gohl*, 2007; *Lindeque and Gohl*, 2010] are consistent with magmatic underplating. Throughout the entire Marie Byrd Land margin, we observed a wide region of thinned transitional crust of low density. Sedimentation patterns in the seismic image of line AWI-20100110 reveal sedimentation patterns of a type similar to those observed off the southeastern Brazil–Angola margin (A. Lindeque, personal communication, 2011). Unlike the Marie Byrd Land sector, the Bellingshausen sector is unique in that it was subject to ongoing deformation and volcanism after breakup. This is further discussed in section 4.5.3.

[35] Close to the Antarctic shelf—where thick sediment layers attenuate the gravity signal of the basement—flow lines, indicating fracture zones, cannot be traced anymore. On the seismic image of line AWI-20100110, the basement reflectors are discontinuous and show a vertical offset of 0.2–0.3 s TWT. These features are interpreted as spatially coincident fracture zones, which are also evident in the bathymetry (A. Lindeque, personal communication, 2011), and correspond to the magnetic anomaly signatures in our study (Figure 6). The seismic transect and observed shifts in the magnetic pattern between parallel magnetic profiles along the Kohiku Fracture Zone support the proposed position and extend the fracture zone interpretation further south. We further constrained the locations of Pahemo and Endeavour Fracture Zones at their southern tips from seismics and magnetic spreading anomalies (Figure 1).

4.2. Continental Extension of Marie Byrd Land

[36] We identified domains of transitional crust, illustrated as stippled areas in the cross-sections in Figure 7, along each of the six crustal models T1 to T6. Consequently, the area representing the present-day COTZ was determined by interpolation between the transects (striped area in Figure 6). We derived the parameters A_c, t_o, t_r and l_e from the cross-sections and calculated the (along-profile) pre-rift width of the COTZ, the pre-rift suture as well as the amount of continental stretching and the associated stretching factors (β) according to the scheme in Figure 8. The results, summarized in Table 1 and Figure 6, indicate a strong regional variation of the COTZ width. The width of the COTZ steps from 50–130 km west of the Proto-Antipodes Fracture Zone to more than 650 km east of that fracture zone. By contrast, the stretching factors remain low to moderate (1.8–3.5) on the entire Marie Byrd Land margin.

[37] We determined the amount of generated melt along the transects to obtain unbiased β-factors by fitting the gravity anomalies with an extra underplate layer. This layer gradually increases in thickness from its inner (continental) bound to the outer (oceanic) side, where it eventually transforms into oceanic crust. There is not much room for big melt thickness and initial crustal volume variability in fitting transect T2 so that we can assume a constant volume of the deformed crust. The estimation of added material due to volcanism in the Marie Byrd Seamount province remains speculative with the available data. Therefore, fitting Chatham Rise to Marie Byrd Land can only be attempted via the plate circuit West Antarctica–Campbell Plateau–Chatham Rise–Bellingshausen plate.

[38] The initial crustal thickness of 20–24 km for Marie Byrd Land is equivalent to the thickness of the submarine plateaus of Zealandia [*Grobys et al.*, 2009, and references therein]. Further, the crustal thickness model of *Grobys et al.* [2008] suggests a mean COTZ width of 100 km for the Campbell Plateau and Chatham Rise. Although these widths are similar to those on the western Marie Byrd Land margin, they differ much from those of the eastern part of Marie Byrd Land, which raises the question

whether extensive continental stretching was associated with rifting only (see section 4.5.3).

4.3. Age and Spreading Model

[39] We identified magnetic spreading anomalies along 44 helicopter- and ship-magnetic profiles in the eastern Ross Sea (Figures 1–5). Both data sources show clearly identifiable seafloor spreading anomalies with similar amplitudes (Figure A.IX in Text S1 in the auxiliary material), even though the shipborne data are preprocessed more aggressively.

[40] The oldest identified magnetic spreading anomaly, c33n (73.6–79.5 Myr), occurs in several locations in the Ross Sea, the Wrigley Gulf and to the west of the Marie Byrd Seamounts/Proto-Antipodes Fracture Zone (Figure 1). A reversed magnetic anomaly occurs south of c33n. Based on its proximity and location within the COTZ, it is more likely to be of continental origin than a c33r magnetic seafloor spreading anomaly.

[41] The spreading model in Figure A.VIII in Text S1 in the auxiliary material suggests a half-spreading rate of about 30 mm yr^{-1} along the Pahemo Fracture Zone during c32n.2n (72 Myr). Later, the spreading rate increased up to 37 mm yr^{-1}, where it peaked around chron c27n, and steadily decreased to 11 mm yr^{-1} between chrons c26n and c22n. Further west, the spreading rate was slower by about 10 mm yr^{-1} (Figure A.IX in Text S1 in the auxiliary material).

4.4. Fitting Fracture Zones

[42] Fracture zones and flow lines in the South Pacific (Figure 5; see also Figure A.IV in Text S1 in the auxiliary material) are essential constraints for the lateral alignment of conjugate plates in the plate-tectonic reconstruction (Figure 9; see also Figure A.V in Text S1 in the auxiliary material). Although fracture zones prior to 43 Myr are explained well by synthetic flow lines derived from the models of *Cande et al.* [1995], *Larter et al.* [2002], and *Eagles et al.* [2004a], the fit of older fracture zones of conjugate plates is not ideal. There are particularly large model differences during the initial rifting phase between Zealandia and Marie Byrd Land. We suspect this to be due to fitting unreliable or not well constrained magnetic isochrons using the *Hellinger* [1981] criteria [*Cande et al.*, 1995; *Larter et al.*, 2002]. In this study, we improved the plate-tectonic reconstruction by visually fitting magnetic picks and fracture zones while ensuring that the model would be geologically sound (Figure 5; see also Figure A.V in Text S1 in the auxiliary material).

[43] Fracture zones, as observed in satellite gravity, are generally 10 km wide and have clearly defined boundaries in the gravity signal. We assume that we can achieve an accuracy of about 2 km if we take care to digitize the same boundary or the centerline on both conjugate plates. As there are many parallel fracture zones along the margin, these errors average out in the end. We determined the offsets between conjugate fracture zone segments in the Ross Sea sector using the rotation poles of *Eagles et al.* [2004a], and compared these results to the offsets in our model. We obtained a general misfit of considerably less than 5 km, whereas offsets as large as 60 km occur in the former model.

4.5. Plate-Tectonic Reconstruction

[44] In Figure 9, we present the key frames of the improved plate-tectonic reconstruction of the conjugate Marie Byrd Land and Zealandia margins. *Croon et al.* [2008] refined the Pacific–Antarctic plate rotations of previous studies by *Cande et al.* [1995], *Cande and Stock* [2004], and *Eagles et al.* [2004a], however, their model does not include rotations prior to c20o (43 Myr). Here, we focus on the evolution of Marie Byrd Land and Zealandia beyond that point. An animation included in Text S1 in the auxiliary material shows the deduced plate movements, which could be divided into the following major phases of plate reorganizations:

[45] *90–84 Myr (c34n)* Onset of continental extension; Chatham Rise separated from Marie Byrd Land as a fragment of Zealandia with a velocity of 30–40 mm yr^{-1}. Rifting started in the Amundsen Sea, where the oldest seafloor spreading anomalies (c34y) are observed, and then propagated west.

[46] *84–80 Myr (c33r)* Zealandia and Marie Byrd Land initially rotated about a pole located in Wilkes Land; spreading propagates into the Ross Sea.

[47] *84–62 Myr (c33r–c27r)* The Bellingshausen plate moved as an independent plate for about 22 Myr. During this time, the southern plate boundary was subject to extensive transtension located in an up to 670 km wide deformation zone.

[48] *80–74 Myr (c33n)* The Campbell Plateau and Chatham Rise rotated against each other and the Bounty Trough was opened. The Bollons Seamount was transferred to the southeastern plate

Geochemistry Geophysics Geosystems G3 WOBBE ET AL.: BREAKUP HISTORY OF ZEALANDIA–MARIE BYRD LAND 10.1029/2011GC003742

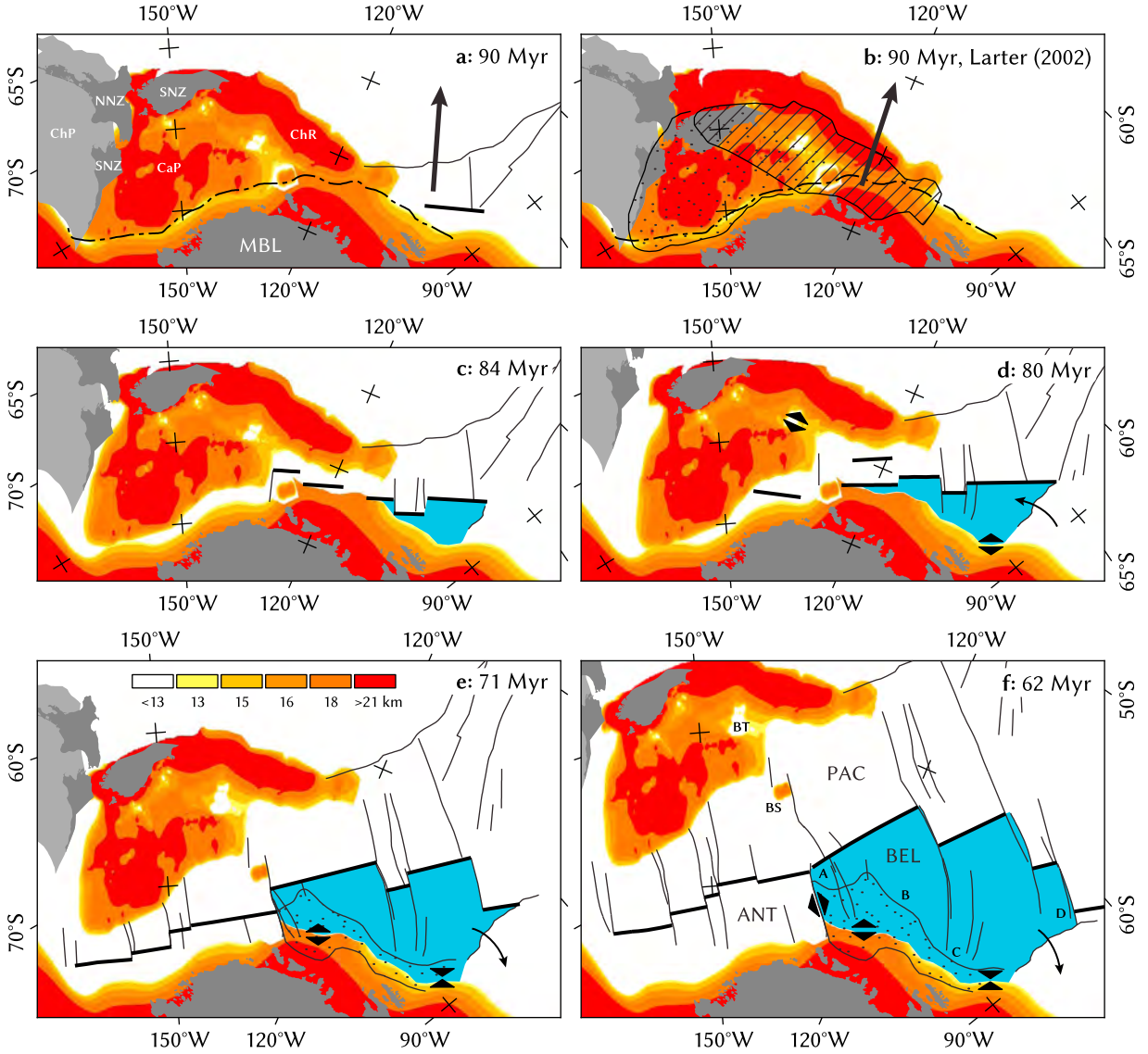

Figure 9. Pre-rift reconstruction models of Marie Byrd Land, Chatham Rise, and Campbell Plateau (a and c–f) using finite rotations of this study and from *Grobys et al.* [2008], and (b) using rotation parameters from *Larter et al.* [2002] and *Eagles et al.* [2004a]. Chatham Rise (striated), Campbell Plateau (stippled), and Marie Byrd Land overlap the pre-rift suture (dashed line) from this study. Arrows indicate initial plate motion direction of Pacific plate/Chatham Rise. Plate-tectonic reconstruction models of Zealandia, Marie Byrd Land, and Bellingshausen plate (Figures 9c–9f) at magnetic chrons c34y (84 Myr), c33o (80 Myr), c32n.1o (71 Myr), and c27o (62 Myr). The Bellingshausen plate (blue) moved independently from the Antarctic plate between c34y and c27o (small arrows). Oceanic crust formed along the southern Bellingshausen plate margin (Figures 9c and 9d) was later deformed (BPBZ, stippled area, Figures 9e and 9f). The tectonic regime in the BPBZ and Bounty Trough is illustrated by arrowheads pointing towards (convergent) and away (divergent) from each other. The Bollons Seamount was transferred from the West Antarctic to the Pacific plate around c33o. The rotation between Chatham Rise and Campbell Plateau occurred during chron c33n. Parallel spreading centers at 120°W (Figure 9d) represent ridge jumps. Thin black lines — fracture zones, thick black lines — mid-ocean ridge segments; ANT — West Antarctic plate, BEL — Bellingshausen plate, BS — Bollons Seamount, BT — Bounty Trough, CaP — Campbell Plateau, ChP — Challenger Plateau, ChR — Chatham Rise, MBL — Marie Byrd Land, NNZ — North Island of New Zealand, PAC — Pacific plate, SNZ — South Island; A, B, C, D — see Figure A.VII in Text S1 in the auxiliary material. Base map: crustal thickness of Zealandia [*Grobys et al.*, 2008] and Antarctica, Lambert conformal conic projection with central meridian 145°W and standard parallels 72°S and 60°S.

boundary of the Campbell Plateau. The lateral displacement between Marie Byrd Land, Campbell Plateau and Chatham Rise was shifted from the Bollons transform fault west of Bollons Seamount to the Proto-Antipodes Fracture Zone. Plate motion velocities between Marie Byrd Land and Zealandia ranged from 50 (west of the Proto-Antipodes Fracture Zone) to 80 mm yr^{-1} (east of the Proto-Antipodes Fracture Zone). The tectonic regime in the Ross Sea changed from transtension to extension, and first fracture zones were formed.

[49] *74–62 Myr (c32r.2r–c27r)* The rotation between Campbell Plateau and Chatham Rise ceased, and the Pacific–Antarctic separation velocity decreased to 55–70 mm yr^{-1}. The rotation of the Bellingshausen plate shifted from counterclockwise to clockwise (Figure A.VII in Text S1 in the auxiliary material), causing a characteristic curve in the trace of the Udintsev Fracture Zone and the Eltanin Fault System. Eventually, the independent motion of the Bellingshausen plate stopped around 62 Myr, and the plate became fixed to the West Antarctic plate.

[50] *71–69 Myr (c31r)* The traces of the Pahemo, Endeavour, and Kohiku Fracture Zones begin to bend left in direction from the Ross Sea towards the spreading center, indicating a slight shift of the Pacific plate motion direction. The Bollons Seamount passed the northern tip of the Proto-Antipodes Fracture Zone during the same time, and the overall spreading velocity decreased by about 10 mm yr^{-1}.

[51] *62–45 Myr (c26r–c21n)* Following the end of the independent Bellingshausen plate movement, full-spreading rates constantly decreased from 60–70 mm yr^{-1} to 30–40 mm yr^{-1}.

[52] *45–42 Myr (c20r–c20n)* For a short period, the rotation pole between the West Antarctic and Pacific plates moved into the Ross Sea (163°49.8′W, 71°17.4′S) and initiated a 3.5° counterclockwise rotation of the Pacific plate relative to West Antarctica in only 3.8 Myr.

4.5.1. Estimation of Breakup Time

[53] The time of onset of the COTZ formation is not constrained by our observations, but we interpret the margin west of the Proto-Antipodes Fracture Zone as forming during c33r and the end of c33n (79.5 Myr). Supporting our interpretation, *Siddoway et al.* [2004] relate a rapid cooling event during 80–71 Myr—recorded by apatite fission-track ages of samples from the Cape Colbeck region in the Eastern Ross Sea—to denudation associated with the breakup of Campbell Plateau from Marie Byrd Land.

[54] Breakup time estimates in the range of 105–81 Myr in earlier works [e.g., *Molnar et al.*, 1975; *Cande et al.*, 1995; *Luyendyk*, 1995; *Larter et al.*, 2002; *Stock and Cande*, 2002; *Cande and Stock*, 2004; *Eagles et al.*, 2004a] are based on paleomagnetic data or extrapolation of spreading rates back into the Cretaceous Normal Superchron (c34n). Without the benefit of dated samples from the margin or magnetic anomalies of the appropriate age, the onset of COTZ formation and the initial rate of COTZ deformation are basically unknown, but likely fall within a certain range of possibilities.

[55] The new magnetic data we collected in vicinity of the Proto-Antipodes Fracture Zone indicates that Chatham Rise and Campbell Plateau separated from Marie Byrd Land with a velocity of 30–40 mm yr^{-1} during chron c33r (79.5–84 Myr). These velocities also match spreading rates based upon extrapolation beyond the oldest chrons detected along the margin west of the Proto-Antipodes Fracture Zone.

[56] Taking into account the continental deformation (∼90 km extension along the margin of Campbell Plateau and Marie Byrd Land) during breakup and assuming a constant spreading rate during chrons c33r and c34n, a close fit of the modeled pre-rift suture between Zealandia and West Antarctica is reached at about 89 Myr. Subduction of the Hikurangi Plateau beneath the Chatham Rise stopped around 96 Myr [*Davy et al.*, 2008]. Aside from maybe back-arc extension before that time, we consider this to be the earliest possible onset of the Zealandia–Antarctic rifting with an implied minimal plate motion velocity of 14 mm yr^{-1} during the rifting phase.

[57] Numeric lithosphere extension models suggest that the rifting time—before continental breakup occurs—is a function of extension velocity [*van Wijk and Cloetingh*, 2002]. For rapid breakup times (in this case 5–12 Myr with an initial extension between 96 and 89 Myr), their models predict extension rates of more than 30 mm yr^{-1}.

[58] Although the crustal thickness of the modeled crust is greater than that of the Marie Byrd Land margin and the rheology of the latter is unknown, which could alter the relationship between rifting time and extension velocity, we nevertheless attempted to estimate the breakup time based on the data of *van Wijk and Cloetingh* [2002]. In our

Geochemistry Geophysics Geosystems G3 WOBBE ET AL.: BREAKUP HISTORY OF ZEALANDIA–MARIE BYRD LAND 10.1029/2011GC003742

reconstruction, a late extension (starting at 90 Myr and with a separation velocity of >30 mm yr^{-1}) as opposed to an earlier extension (at 96 Myr with a slower velocity of about 14 mm yr^{-1}) fits the *van Wijk and Cloetingh* [2002] model better.

4.5.2. Early Breakup and Opening of Bounty Trough

[59] New evaluation of continental extension on the Marie Byrd Land margin in this study and the crustal thickness model of *Grobys et al.* [2008] have enabled numerous improvements to the reconstruction of the early Zealandia–Marie Byrd Land breakup history. Also they provided answers to open questions and voids of previous studies that originated from a lack of constraints regarding the dynamics of the plate margins.

[60] Unresolved issues remaining in previous reconstructions include:

[61] 1. The rotation of Chatham Rise with respect to Campbell Plateau by *Larter et al.* [2002] causes a 350 km wide overlap because the extend of the COTZ on both margins was underestimated. This close fit reconstruction of Marie Byrd Land and Chatham Rise introduces an overlap of the latter with the continental shelf of Marie Byrd Land as far as Siple and Camey Islands (Figure 9b). Further, the Bollons Seamount is traversed by Chatham Rise, and the southwest margin of Campbell Plateau overlaps the continental shelf of the West Antarctic Plate by about 100 km. A compression of this dimension cannot be explained by our continental deformation model, since the transitional crust of the continental shelf of Marie Byrd Land, the crust of the Bounty Trough, and its adjacent plateaus [*Grobys et al.*, 2008] is relatively thick (low β-factors).

[62] 2. *Davy et al.* [2008] interpreted the cessation of subduction of the Hikurangi Plateau beneath the Chatham Rise at about 96 Myr, followed by a switch in the tectonic regime in New Zealand from northeast to northwest directed extension, which *Davy et al.* [2008] construed to be parallel to the breakup orientation. The southern branches of Udintsev and adjacent Fracture Zones further east (Figure 5; see also Figure A.IV in Text S1 in the auxiliary material) strike northwest–southeast, thus confirming a northwest directed separation of Chatham Rise from Marie Byrd Land. *Larter et al.* [2002] and *Eagles et al.* [2004a] suggest a north by west directed initial movement of Chatham Rise (90–84 Myr, arrow in Figure A.VI and supporting animation in Text S1 in the auxiliary material) which is oblique to the fracture zones and contradicts the interpretation of *Davy et al.* [2008].

[63] Our updated plate reconstruction, based on the location of the pre-rift suture between Marie Byrd Land, Chatham Rise, and Campbell Plateau, ensures that there are no or only minor overlaps between Marie Byrd Land and Zealandia as well as Chatham Rise and Campbell Plateau. Further drawbacks of previous reconstructions were circumvented in this study by first rotating Zealandia with respect to Marie Byrd Land and then rotating Chatham Rise with respect to Campbell Plateau in a separate step, after the Bollons Seamount was transferred to the margin of the Campbell Plateau at about 80 Myr. This allowed a fit of the conjugate ends of the Udintsev Fracture Zone as well as adjacent fracture zones further east and guaranteed a northwest directed extension in New Zealand.

[64] The plate-tectonic reconstruction of Zealandia [*Grobys et al.*, 2008] does not constrain the time and duration of the rotation between Chatham Rise and Campbell Plateau. However, a rotation is not possible prior to chron c33n without introducing a cycle of rapid extension followed by compression along the southern boundary of the Bellingshausen plate (see animations in Text S1 in the auxiliary material). Furthermore, the reliability of the c34y identifications in the Bounty Trough area is questionable [*Davy*, 2006]. Rifting on the northern Campbell Plateau was complete by 84 Myr [*Cook et al.*, 1999], but the age of cessation of rifting is unconstrained for the Bounty Platform or southern Campbell Plateau. *Sutherland* [1999] suggests that a ridge may have existed during c33n in the outer part of the Bounty Trough and then jumped southward. By initiating the rotation between Chatham Rise and Campbell Plateau during chron c33n (as opposed to c34n [*Larter et al.*, 2002]), we can fit c33o south of Bollons Seamount while minimizing the Bellingshausen plate motion relative to Marie Byrd Land at the same time. This implies that until c33y, when the Chatham Rise vs. Campbell Plateau rotation ceased, the Proto-Antipodes Fracture Zone separated two independent spreading centers (Antarctic–Pacific and Antarctic–Campbell Plateau).

4.5.3. Transitional Crust of the Bellingshausen Plate

[65] In section 4.2, we concluded that pre-rift crustal thicknesses of Marie Byrd Land, Campbell Plateau, and Chatham Rise were alike. Moreover,

the width of the COTZ of west Marie Byrd Land, Campbell Plateau, and Chatham Rise were uniform, whereas the BPBZ is three to five times wider (Figures 6 and 7 and Table 1). Because the opening of the Amundsen Sea and Ross Sea propagated from east to west, leading to lower spreading velocities in the west and increasing the potential of basin propagation [*van Wijk and Cloetingh*, 2002], we should expect a widening of the COTZ towards the Ross Sea. By contrast, we observed a narrow COTZ west of the Bellingshausen sector.

[66] There are several indicators implying that the extensive continental stretching between Chatham Rise and east Marie Byrd Land was not associated with the initial rifting alone, but instead developed partly after their separation:

[67] 1. Alkali basalt samples, dredged from Haxby Seamount and Hubert Miller Seamount (Figure 6) yield $^{40}Ar/^{39}Ar$ ages ranging from 64.73 ± 0.84 to 55.72 ± 0.63 Myr [*Kipf et al.*, 2008; A. Kipf et al., Seamounts off the West Antarctic margin of the Pacific: A case of non–hotspot intraplate volcanism, manuscript in preparation, 2012]. This dating clearly marks the end of the independent Bellingshausen plate movement and is too young to be associated with the rifting between Zealandia and Marie Byrd Land.

[68] 2. We determined an extension velocity of >30 mm yr^{-1} (section 4.5.1) associated with a short rifting time. Continental deformation along the Campbell Plateau and western Marie Byrd Land margin ceased in less than 10 Myr, and lithosphere extension models [*van Wijk and Cloetingh*, 2002] suggest that deformation should have stopped in eastern Marie Byrd Land as well.

[69] 3. Magnetic spreading anomalies c34n, c33r, and partly c33n cannot be detected on the central Marie Byrd Land margin (Figure 5), although they exist on the conjugate margin (Chatham Rise). It is likely that oceanic crust formed on the Marie Byrd Land side as well and transformed later on.

[70] We propose that the complete Marie Byrd Land margin developed similar to the conjugate margin of Zealandia during the initial separation. Rifting between Chatham Rise and Marie Byrd Land stopped before c34y (84 Myr), and, consequently, oceanic crust formed in the Amundsen Sea. Most of this oceanic crust, generated on the Bellingshausen plate margin until the end of chron c33r, was either magmatically altered or tectonically interleaved with transitional crust at a 1:1 ratio.

[71] The Bellingshausen plate moved independently of the West Antarctic plate for about 22 Myr since c34y. Its plate motion trajectories indicate an overall plate drift to the northeast with respect to Marie Byrd Land and a velocity varying from 3 to 36 mm yr^{-1} with a peak around 9 mm yr^{-1} (Figure A.VII in Text S1 in the auxiliary material). The southern and western border of the Bellingshausen plate were subject to a 8–14 mm yr^{-1} dextral motion relative to Marie Byrd Land and subparallel to its plate boundary.

[72] First counterclockwise, then clockwise rotation of the Bellingshausen plate caused a tectonic regime of alternating convergence and extension west of the balance point B (Figure 9; see also Figure A.VII in Text S1 in the auxiliary material) and vice versa east of it. This is supported by previous studies by *Larter et al.* [2002], *Cunningham et al.* [2002], and *Eagles et al.* [2004b], who interpreted the Bellingshausen Gravity Anomaly (southeast of point C) and the continental margin off Thurston Island as zone of accommodated convergent motion between the Bellingshausen and West Antarctic plates. Seamounts occur en echelon along the southern plate boundary of the Bellingshausen plate near point A. Their strike is approximately northeast–southwest directed and perpendicular to the motion path of A during the second half of the existence of the autonomous Bellingshausen plate. The clockwise rotation, the strike of the seamount chains and the dated sample from Hubert Miller Seamount are indicators that the seamounts formed during the end of the independent Bellingshausen plate movement (65–55 Myr).

[73] Traditionally, the chemistry signal [*Kipf et al.*, 2008, also manuscript in preparation, 2012], increased crustal thickness (Figure 7), local highs in the gravity field, and disrupted magnetic signature were used as indicators to suggest intraplate volcanism as a simple solution to account for the transitional crust in the Bellingshausen plate [e.g., *Storey et al.*, 1999]. Our data, the geochemical signature, and the age of the Marie Byrd Seamounts [*Kipf et al.*, 2008, also manuscript in preparation, 2012] indicate that the Bellingshausen plate motion preceded intraplate volcanism. The tectonic setting at the time the seamounts formed indicates an enriched mantle source [*Halliday et al.*, 1995; *Pilet et al.*, 2008], which released melts through fissures created by lithospheric extension on the southern Bellingshausen plate margin. Fertilization of the mantle could either be explained by Mesozoic

subduction beneath the Gondwana convergent margin or by metasomatism of the lithospheric mantle through fractures in the weakened Bellingshausen plate.

[74] Especially during chron c33r (79.5–84 Myr) and at the end of the existence of the plate, there was very little movement relative to Marie Byrd Land. Lithosphere extension models show that rifting velocities lower than 8 mm yr^{-1} do not lead to seafloor spreading because the lithosphere in the formed basin cools and becomes stronger than in the surrounding regions [*van Wijk and Cloetingh*, 2002]. Consequently, the deformation zone migrates and the process repeats itself, forming a wide COTZ. We assume, a similar process, combined with oscillating transpression and transtension along the Bellingshausen plate margin, lead to the formation of an up to 670 km wide zone of transitional crust interleaved with segments of oceanic crust (BPBZ, in Figure 7). The deformation was intense enough to annihilate signs of oceanic crust such as magnetic seafloor spreading anomalies.

5. Summary

[75] We present and analyze an extensive new dataset of air- and shipborne geophysical measurements acquired during R/V Polarstern cruises in 2006 (ANT-23/4) and 2010 (ANT-26/3) at the rifted oceanic margin of Antarctica in the eastern Ross Sea and Bellingshausen Sea. We construct models of seafloor magnetic anomalies to interpret oceanic age, and models of the continental margin crust that are constrained by active-source seismic reflection and refraction data as well as gravity data. We subdivide the continental margin into two sectors divided by the Proto-Antipodes Fracture Zone (Figure 6).

[76] The western sector of the continental margin, the Marie Byrd Land sector, has a relatively narrow steep slope and resembles a typical magma-poor margin. The width of the COTZ on our modeled transect is 145 km, which we interpret—based on our crustal model—to represent an initial continental crust of thickness 24 km and width 55 km. It was stretched 90 km and intruded at its base by melt, eventually transitioning to normal-thickness oceanic crust (~7 km) [*White et al.*, 1992] at its seaward limit.

[77] The eastern sector of the continental margin, the Bellingshausen sector, is broad and complex with abundant morphologic evidence for later volcanism, confirmed by dredging [*Kipf et al.*, 2008]. The widths of the COTZ/BPBZ on our modeled transects are up to 670 km, and substantial uncertainty remains as to the nature of the crust within the COTZ/BPBZ because we have little control on crustal thickness or density. Our preferred interpretation is that some stretched continental crust is present throughout this zone, but that it has been substantially added to by basaltic igneous rocks (density 3.0 ± 0.1 g cm^{-3}). The extension estimates fall in the range of 106–304 km for the COTZ/BPBZ (Table 1).

[78] We identify seafloor magnetic anomalies c33n (79.5 Myr) to c20n (42 Myr) on a number of transects adjacent to the Marie Byrd Land sector (Figures 1–5). The Bellingshausen sector is too complex and sparsely sampled for us to reliably interpret magnetic anomalies as isochrons. At the longitude of the Pahemo Fracture Zone, in the central part of the Marie Byrd Land sector, the full-spreading rate during chrons 33–31 (80–68 Myr) was 60 mm yr^{-1}, increasing to a maximum of 74 mm yr^{-1} at chron 27, and then dropping to 22 mm yr^{-1} by chron 22. Spreading rates generally decrease westward. Based upon extrapolation towards the continental margin, we estimate that initial oceanic crust formation in the Bellingshausen sector was at approximately chron 34y (84 Myr) and that it formed rapidly. West of the Proto-Antipodes Fracture Zone, seafloor spreading initiated at chron 33n (79.5 Myr). At rates of 30–60 mm yr^{-1}, the 90 km of inferred extension could be achieved in 1.5 to 3.0 Myr.

[79] We construct an improved set of plate reconstructions utilizing our updated analysis of the Antarctic continental margin to place our local interpretations of Antarctica in context. From these we make inferences regarding the general sequence of events during inception of seafloor spreading, and calculate the subsequent motion history of the Bellingshausen plate, which is the oceanic plate adjacent to the Bellingshausen sector of the continental margin (see auxiliary material). Our preferred interpretation is that the tipline of the spreading ridge and hence initial seafloor formation propagated westward between ~89 and 84 Myr. Subsequent motion of the Bellingshausen plate relative to Antarctica was at rates <40 mm yr^{-1} and was most commonly 5–20 mm yr^{-1}. Although we have not attempted a quantitative uncertainty analysis, our predictions that motion direction and rate varied spatially and temporally and involved both

local compression and extension are supported by local geology and geophysics [e.g., *Cunningham et al.*, 2002; *Larter et al.*, 2002; *Gohl*, 2012; *Gohl et al.*, 2011].

[80] Our new data and interpretations are generally consistent with previous analyses that indicate Gondwana breakup along this part of the margin was at ~84 Myr, and there was subsequent formation of the Bellingshausen plate east of the Proto-Antipodes Fracture Zone [*Molnar et al.*, 1975; *Stock and Molnar*, 1987; *Cande et al.*, 1995; *Larter et al.*, 2002; *Stock and Cande*, 2002; *Cande and Stock*, 2004; *Eagles et al.*, 2004a, 2004b]. The relatively high rifting rate of 30–60 mm yr^{-1} during initial margin formation is consistent with the relatively sharp and symmetrical morphology of the margin, and confirms predictions from numerical models [*van Wijk and Cloetingh*, 2002]. By contrast, subsequent motion of the Bellingshausen plate relative to Antarctica has been slow and complex, and has modified the initial rift morphology to create a broad deformed BPBZ that was strongly affected by migrating patterns of deformation and volcanism.

Acknowledgments

[81] This project is funded by the Earth System Sciences Research School (ESSReS), an initiative of the Helmholtz Association of German research centers (HGF) at the Alfred Wegener Institute for Polar and Marine Research (AWI). We thank the master, crew and scientists of R/V Polarstern and especially the pilots and technicians of HeliService international for their support and assistance. We are grateful to Graeme Eagles for his constructive review, and two other reviewers, who chose to remain anonymous, as well as the numerous people who commented on earlier drafts of the manuscript. Figures 1–7 and 9 as well as Figures A.I–A.VII in Text S1 in the auxiliary material were created using Generic Mapping Tools (GMT) [*Wessel and Smith*, 1991]. We especially thank Paul Wessel for coding extra features into GMT5 overnight.

References

Andersen, O. B., and P. Knudsen (2009), DNSC08 mean sea surface and mean dynamic topography models, *J. Geophys. Res.*, *114*, C11001, doi:10.1029/2008JC005179.

Blaich, O. A., J. I. Faleide, and F. Tsikalas (2011), Crustal breakup and continent-ocean transition at South Atlantic conjugate margins, *J. Geophys. Res.*, *116*, B01402, doi:10.1029/2010JB007686.

Block, A. E., R. E. Bell, and M. Studinger (2009), Antarctic crustal thickness from satellite gravity: Implications for the Transantarctic and Gamburtsev Subglacial Mountains, *Earth Planet. Sci. Lett.*, *288*(1–2), 194–203, doi:10.1016/j.epsl.2009.09.022.

Boyden, J., R. Müller, M. Gurnis, T. Torsvik, J. Clark, M. Turner, H. Ivey-Law, R. Watson, and J. Cannon (2011), Next-generation plate-tectonic reconstructions using GPlates, in *Geoinformatics: Cyberinfrastructure for the Solid Earth Sciences*, edited by G. Keller and C. Baru, pp. 95–114, Cambridge Univ. Press, Cambridge, U. K.

Cande, S. C., and J. M. Stock (2004), Cenozoic reconstructions of the Australia-New Zealand-South Pacific sector of Antarctica, in *The Cenozoic Southern Ocean: Tectonics, Sedimentation and Climate Change Between Australia and Antarctica*, *Geophys. Monogr. Ser.*, vol. 151, edited by N. F. Exon, J. P. Kennett, and M. J. Malone, pp. 5–18, AGU, Washington, D. C.

Cande, S. C., C. A. Raymond, J. Stock, and W. F. Haxby (1995), Geophysics of the Pitman Fracture Zone and Pacific-Antarctic plate motions during the Cenozoic, *Science*, *270*(5238), 947–953, doi:10.1126/science.270.5238.947.

Cook, R., R. Sutherland, and H. Zhu (1999), *Cretaceous-Cenozoic Geology and Petroleum Systems of the Great South Basin, New Zealand*, *Inst. of Geol. and Nucl. Sci. Monogr.*, vol. 20, 188 pp., Inst. of Geol. and Nucl. Sci., Lower Hutt, New Zealand.

Croon, M. B., S. C. Cande, and J. M. Stock (2008), Revised Pacific-Antarctic plate motions and geophysics of the Menard Fracture Zone, *Geochem. Geophys. Geosyst.*, *9*, Q07001, doi:10.1029/2008GC002019.

Cunningham, A. P., R. D. Larter, P. F. Barker, K. Gohl, and F. O. Nitsche (2002), Tectonic evolution of the Pacific margin of Antarctica: 2. Structure of Late Cretaceous–early Tertiary plate boundaries in the Bellingshausen Sea from seismic reflection and gravity data, *J. Geophys. Res.*, *107*(B12), 2346, doi:10.1029/2002JB001897.

Davy, B. (2006), Bollons Seamount and early New Zealand–Antarctic seafloor spreading, *Geochem. Geophys. Geosyst.*, *7*, Q06021, doi:10.1029/2005GC001191.

Davy, B., K. Hoernle, and R. Werner (2008), Hikurangi Plateau: Crustal structure, rifted formation, and Gondwana subduction history, *Geochem. Geophys. Geosyst.*, *9*, Q07004, doi:10.1029/2007GC001855.

Eagles, G., K. Gohl, and R. Larter (2004a), High-resolution animated tectonic reconstruction of the South Pacific and West Antarctic margin, *Geochem. Geophys. Geosyst.*, *5*, Q07002, doi:10.1029/2003GC000657.

Eagles, G., K. Gohl, and R. D. Larter (2004b), Life of the Bellingshausen plate, *Geophys. Res. Lett.*, *31*, L07603, doi:10.1029/2003GL019127.

Finlay, C. C., et al. (2010), International Geomagnetic Reference Field: The eleventh generation, *Geophys. J. Int.*, *183*(3), 1216–1230, doi:10.1111/j.1365-246X.2010.04804.x.

Gardner, G. H. F., L. W. Gardner, and A. R. Gregory (1974), Formation velocity and density—The diagnostic basics for stratigraphic traps, *Geophysics*, *39*(6), 770–780, doi:10.1190/1.1440465.

Gohl, K. (Ed.) (2007), The expedition ANTARKTIS-XXIII/4 of the Research Vessel *Polarstern* in 2006, *Rep. Polar Mar. Res.*, *557*, Alfred Wegener Inst. for Polar and Mar. Res., Bremerhaven, Germany, doi:10013/epic.27102.d001.

Gohl, K. (Ed.) (2010), The expedition of the Research Vessel *Polarstern* to the Amundsen Sea, Antarctica, in 2010 (ANT-XXVI/3), *Rep. Polar Mar. Res.*, *617*, Alfred Wegener Inst. for Polar and Mar. Res., Bremerhaven, Germany, doi:10013/epic.35668.d001.

Gohl, K. (2012), Basement control on past ice sheet dynamics in the Amundsen Sea Embayment, West Antarctica, *Palaeogeogr. Palaeoclimatol. Palaeoecol.*, doi:10.1016/j.palaeo.2011.02.022, in press.

Gohl, K., et al. (2007), Geophysical survey reveals tectonic structures in the Amundsen Sea Embayment, West Antarctica [online], in *Antarctica: A Keystone in a Changing World—Online Proceedings of the 10th ISAES*, edited by A. K. Cooper, C. R. Raymond, and the 10th ISAES Editorial Team, *U.S. Geol. Soc. Open File Rep.*, *2007-1047*, paper 047, doi:10.3133/of2007-1047.srp047.

Gohl, K., G. Uenzelmann-Neben, E. Weigelt, A. Lindeque, T. Kalberg, G. Kuhn, C. D. Hillenbrand, and R. D. Larter (2011), Sedimentary and glacial processes of the Amundsen Sea Embayment, West Antarctica, paper presented at General Assembly, Eur. Geosci. Union, Vienna, 3–8 April.

Gradstein, F., J. Ogg, A. Smith, W. Bleeker, and L. Lourens (2004), A new geologic time scale with special reference to Precambrian and Neogene, *Episodes*, *27*(2), 83–100.

Grobys, J. W. G., K. Gohl, and G. Eagles (2008), Quantitative tectonic reconstructions of Zealandia based on crustal thickness estimates, *Geochem. Geophys. Geosyst.*, *9*, Q01005, doi:10.1029/2007GC001691.

Grobys, J., K. Gohl, G. Uenzelmann-Neben, B. Davy, and D. Barker (2009), Extensional and magmatic nature of the Campbell Plateau and Great South Basin from deep crustal studies, *Tectonophysics*, *472*(1–4), 213–225, doi:10.1016/j.tecto.2008.05.003.

Halliday, A. N., D.-C. Lee, S. Tommasini, G. R. Davies, C. R. Paslick, J. G. Fitton, and D. E. James (1995), Incompatible trace elements in OIB and MORB and source enrichment in the sub-oceanic mantle, *Earth Planet. Sci. Lett.*, *133*(3–4), 379–395, doi:10.1016/0012-821X(95)00097-V.

Hellinger, S. J. (1981), The uncertainties of finite rotations in plate tectonics, *J. Geophys. Res.*, *86*(B10), 9312–9318, doi:10.1029/JB086iB10p09312.

Huismans, R., and C. Beaumont (2011), Depth-dependent extension, two-stage breakup and cratonic underplating at rifted margins, *Nature*, *473*(7345), 74–78, doi:10.1038/nature09988.

Kipf, A., R. Werner, K. Gohl, F. Hauff, P. van den Bogaard, and K. Hoernle (2008), Age and origin of magmatism at the Marie Byrd Seamounts (Amundsen Sea), paper presented at General Assembly, Eur. Geosci. Union, Vienna, 13–18 Apr.

König, M. (2006), Processing of shipborne magnetometer data and revision of the timing and geometry of the Mesozoic break-up of Gondwana, PhD thesis, Univ. of Bremen, Bremen, Germany.

Larter, R. D., A. P. Cunningham, P. F. Barker, K. Gohl, and F. O. Nitsche (2002), Tectonic evolution of the Pacific margin of Antarctica: 1. Late Cretaceous tectonic reconstructions, *J. Geophys. Res.*, *107*(B12), 2345, doi:10.1029/2000JB000052.

Lindeque, A., and K. Gohl (2010), Western Antarctic palaeostratigraphy: Implications for palaeobathymetry and palaeoclimate modelling, paper presented at IPY Oslo Science Conference, World Meteorol. Organ., Oslo, 8–12 June.

Llubes, M., N. Florsch, B. Legresy, J.-M. Lemoine, S. Loyer, D. Crossley, and F. Remy (2003), Crustal thickness in Antarctica from CHAMP gravimetry, *Earth Planet. Sci. Lett.*, *212*(1–2), 103–117, doi:10.1016/S0012-821X(03)00245-0.

Luyendyk, B. P. (1995), Hypothesis for Cretaceous rifting of east Gondwana caused by subducted slab capture, *Geology*, *23*(4), 373–376, doi:10.1130/0091-7613(1995)023<0373:HFCROE>2.3.CO;2.

Luyendyk, B. P., D. S. Wilson, and C. S. Siddoway (2003), Eastern margin of the Ross Sea Rift in western Marie Byrd Land, Antarctica: Crustal structure and tectonic development, *Geochem. Geophys. Geosyst.*, *4*(10), 1090, doi:10.1029/2002GC000462.

Mendel, V., M. Munschy, and D. Sauter (2005), MODMAG, a MATLAB program to model marine magnetic anomalies, *Comput. Geosci.*, *31*(5), 589–597, doi:10.1016/j.cageo.2004.11.007.

Molnar, P., T. Atwater, J. Mammerickx, and S. M. Smith (1975), Magnetic anomalies, bathymetry and the tectonic evolution of the South Pacific since the Late Cretaceous, *J. R. Astron. Soc.*, *40*(3), 383–420, doi:10.1111/j.1365-246X.1975.tb04139.x.

National Geophysical Data Center (2007), Marine trackline geophysics data (GEODAS), *Data Announce., 2003-MGG-02*, NOAA, Boulder, Colo.

Pilet, S., M. B. Baker, and E. M. Stolper (2008), Metasomatized lithosphere and the origin of alkaline lavas, *Science*, *320*(5878), 916–919, doi:10.1126/science.1156563.

Scheuer, C., K. Gohl, and G. Eagles (2006), Gridded isopach maps from the South Pacific and their use in interpreting the sedimentation history of the West Antarctic continental margin, *Geochem. Geophys. Geosyst.*, *7*, Q11015, doi:10.1029/2006GC001315.

Siddoway, C. S., S. L. Baldwin, P. G. Fitzgerald, C. M. Fanning, and B. P. Luyendyk (2004), Ross Sea mylonites and the timing of intracontinental extension within the West Antarctic rift system, *Geology*, *32*(1), 57–60, doi:10.1130/G20005.1.

Smith, W. H. F., and D. T. Sandwell (1997), Global sea floor topography from satellite altimetry and ship depth soundings, *Science*, *277*(5334), 1956–1962, doi:10.1126/science.277.5334.1956.

Stock, J., and P. Molnar (1987), Revised history of early Tertiary plate motion in the south-west Pacific, *Nature*, *325*(6104), 495–499, doi:10.1038/325495a0.

Stock, J. M., and S. C. Cande (2002), Tectonic history of Antarctic seafloor in the Australia–New Zealand–South Pacific sector: Implications for Antarctic continental tectonics, in *Antarctica at the Close of a Millennium*, edited by J. A. Gamble, D. N. B. Skinner, and S. Henrys, *Bull. R. Soc. N. Z.*, *35*, 251–259.

Storey, B. C., P. T. Leat, S. D. Weaver, R. J. Pankhurst, J. D. Bradshaw, and S. Kelley (1999), Mantle plumes and Antarctica-New Zealand rifting: Evidence from mid-Cretaceous mafic dykes, *J. Geol. Soc. London*, *156*(4), 659–671, doi:10.1144/gsjgs.156.4.0659.

Sutherland, R. (1999), Basement geology and tectonic development of the greater New Zealand region: An interpretation from regional magnetic data, *Tectonophysics*, *308*(3), 341–362, doi:10.1016/S0040-1951(99)00108-0.

Sutherland, R., S. Spasojevic, and M. Gurnis (2010), Mantle upwelling after Gondwana subduction death explains anomalous topography and subsidence histories of eastern New Zealand and West Antarctica, *Geology*, *38*(2), 155–158, doi:10.1130/G30613.1.

van Wijk, J., and S. Cloetingh (2002), Basin migration caused by slow lithospheric extension, *Earth Planet. Sci. Lett.*, *198*(3–4), 275–288, doi:10.1016/S0012-821X(02)00560-5.

Vine, F. J., and D. H. Matthews (1963), Magnetic anomalies over oceanic ridges, *Nature*, *199*(4897), 947–949, doi:10.1038/199947a0.

Watts, A. (1988), Gravity anomalies, crustal structure and flexure of the lithosphere at the Baltimore Canyon Trough, *Earth Planet. Sci. Lett.*, *89*(2), 221–238, doi:10.1016/0012-821X(88)90174-4.

Watts, A. B., and J. D. Fairhead (1999), A process-oriented approach to modeling the gravity signature of continental margins, *Leading Edge*, *18*(2), 258–263, doi:10.1190/1.1438270.

Wessel, P., and W. H. F. Smith (1991), Free software helps map and display data, *Eos Trans. AGU*, *72*(41), 441, doi:10.1029/90EO00319.

White, R. S., D. McKenzie, and R. K. O'Nions (1992), Oceanic crustal thickness from seismic measurements and rare Earth element inversions, *J. Geophys. Res.*, *97*(B13), 19,683–19,715, doi:10.1029/92JB01749.

Winberry, J. P., and S. Anandakrishnan (2004), Crustal structure of the West Antarctic rift system and Marie Byrd Land hotspot, *Geology*, *32*(11), 977–980, doi:10.1130/G20768.1.

Publication 6.1.5:

Kipf, A., Hauff, F., Werner, R., **Gohl, K.**, van den Bogaard, P., Hoernle, K., Maicher, D., Klügel, A. (2014). Seamounts off the West Antarctic margin: A case for non-hotspot driven intraplate volcanism. *Gondwana Research*, 25, 1660-1679, doi:10.1016/j.gr.2013.06.013.

Author contributions: This study, based on petrological and geochemical data from samples collected during Polarstern expedition ANT-XXVI/3, was mainly conducted by Kipf as part of her PhD project under the supervision of Hoernle, Werner and Hauff at GEOMAR. Gohl's contribution consisted of the discussion and input on the geodynamic process model for the South Pacific and West Antarctic margin to help explain the geochemical observations. The other co-authors contributed with specific sample analyses and discussions to the text.

Gondwana Research 25 (2014) 1660–1679

Contents lists available at ScienceDirect

Gondwana Research

journal homepage: www.elsevier.com/locate/gr

Seamounts off the West Antarctic margin: A case for non-hotspot driven intraplate volcanism

A. Kipf [a,*], F. Hauff [a], R. Werner [a], K. Gohl [b], P. van den Bogaard [a], K. Hoernle [a], D. Maicher [a], A. Klügel [c]

[a] GEOMAR Helmholtz Centre for Ocean Research Kiel, Wischhofstr. 1-3, D-24148 Kiel, Germany
[b] Alfred-Wegener-Institute for Polar and Marine Research, Postfach 120161, D-27515 Bremerhaven, Germany
[c] University of Bremen, Postfach 330440, D-28334 Bremen, Germany

ARTICLE INFO

Article history:
Received 21 December 2012
Received in revised form 28 May 2013
Accepted 11 June 2013
Available online 16 July 2013

Handling Editor: I. Safonova

Keywords:
Antarctica
Marie Byrd Seamounts
Intraplate volcanism
$^{40}Ar/^{39}Ar$ age dates
Major and trace element and Sr–Nd–Pb–Hf Isotope geochemistry

ABSTRACT

New radiometric age and geochemical data of volcanic rocks from the guyot-type Marie Byrd Seamounts (MBS) and the De Gerlache Seamounts and Peter I Island (Amundsen Sea) are presented. $^{40}Ar/^{39}Ar$ ages of the shield phase of three MBS are Early Cenozoic (65 to 56 Ma) and indicate formation well after creation of the Pacific–Antarctic Ridge. A Pliocene age (3.0 Ma) documents a younger phase of volcanism at one MBS and a Pleistocene age (1.8 Ma) for the submarine base of Peter I Island. Together with published data, the new age data imply that Cenozoic intraplate magmatism occurred at distinct time intervals in spatially confined areas of the Amundsen Sea, excluding an origin through a fixed mantle plume. Peter I Island appears strongly influenced by an EMII type mantle component that may reflect shallow mantle recycling of a continental raft during the final breakup of Gondwana. By contrast the Sr–Nd–Pb–Hf isotopic compositions of the MBS display a strong affinity to a HIMU-type mantle source. On a regional scale the isotopic signatures overlap with those from volcanics related to the West Antarctic Rift System, and Cretaceous intraplate volcanics in and off New Zealand. We propose reactivation of the HIMU material, initially accreted to the base of continental lithosphere during the pre-rifting stage of Marie Byrd Land/Zealandia to explain intraplate volcanism in the Amundsen Sea in the absence of a long-lived hotspot. We propose continental insulation flow as the most plausible mechanism to transfer the sub-continental accreted plume material into the shallow oceanic mantle. Crustal extension at the southern boundary of the Bellingshausen Plate from about 74 to 62 Ma may have triggered adiabatic rise of the HIMU material from the base of Marie Byrd Land to form the MBS. The De Gerlache Seamounts are most likely related to a preserved zone of lithospheric weakness underneath the De Gerlache Gravity Anomaly.

1. Introduction

Seamounts are common bathymetric features on the seafloor and most are of volcanic origin. Although only a fraction of them have been mapped by ship-based echo-sounding, satellite altimetry has identified more than 13,000 seamounts taller than 1.5 km and predicts more than 100,000 seamounts higher than 1 km (e.g., Smith and Sandwell, 1997; Wessel et al., 2010). Seamounts are important probes of the composition and dynamics of the oceanic mantle and, if they form parts of hotspot tracks, they can also be important recorders of past plate motions (Hofmann, 2003; Tarduno et al., 2003; Koppers et al., 2012). They also form oases for marine life and biodiversity (e.g., Shank, 2010 for a recent review) and are significant components of hydrogeological systems focusing the exchange of heat and fluids between the oceanic lithosphere and the oceans (e.g., Fisher et al., 2003; Harris et al., 2004; Hutnak et al., 2008; Klügel et al., 2011). The latter processes can lead to the formation of economically important mineral deposits (e.g., Hein et al., 2010), which are, for example, commercially mined in some accreted seamount complexes (e.g., Safonova, 2009). Seamounts are also sites of geological hazards such as tsunamis through sector collapse during their growth stage (e.g., McMurtry et al., 2004). Upon subduction of the ocean floor, seamounts can also serve as prominent asperities generating earthquakes (e.g., Watts et al., 2010 for a recent review). As the subduction process can lead to crustal accretion of seamounts, they can be preserved in the accessible geological record, providing important insights from the evolution of hotspot tracks and continental margins to biological exchange between continents (e.g., Hoernle et al., 2002; Geldmacher et al., 2008; Portnyagin et al., 2008; Buchs et al., 2011; Safonova and Santosh, 2012). Despite the manifold contributions of seamounts to the dynamics of diverse earth systems, their process of formation is still debated. Most commonly the occurrence of isolated volcanoes distant from plate boundaries is attributed to the upwelling of mantle plumes (e.g., Wilson, 1963; Morgan, 1971; Courtillot et al., 2003). The absence of linear volcanic chains and lack of spatially age progressive magmatism in many areas has stimulated a vigorous debate on the origin of intraplate volcanism (e.g., Anderson, 2000; Foulger and Natland, 2003; see also "Great

* Corresponding author. Tel.: +49 431 600 2645.
E-mail address: akipf@geomar.de (A. Kipf).

1342-937X/$ – see front matter
http://dx.doi.org/10.1016/j.gr.2013.06.013

Plume debate", www.mantleplumes.org). Other important mechanisms of seamount formation include off-axis volcanism in the vicinity of spreading ridges by lateral expansion of the ridge melting regime (e.g., Batiza et al., 1990; Brandl et al., 2012 and references therein), recycling of delaminated continental lithosphere (Hoernle et al., 2011) and plate fracturing (e.g., Winterer and Sandwell, 1987; Natland and Winterer, 2005). In this paper, we report for the first time an integrated bathymetric, geochronological and geochemical data set from three seamount provinces off West Antarctica and show that these intraplate volcanoes are not directly linked to the activity of a mantle plume but rather reflect remobilization and transfer of fertile mantle from beneath West Antarctica.

The Marie Byrd Seamounts (MBS), located in the western Amundsen Sea north of the continental shelf of Marie Byrd Land, West Antarctica (Fig. 1), are a good example of enigmatic intraplate volcanism. They are located on oceanic crust possibly older than 72 Ma (Heinemann et al., 1999; Eagles et al., 2004a,b) and form an elongated cluster of volcanic edifices, that extends for more than 800 km between ~114° and ~131°W, and ~68° and ~71°S. Based on rock fragments found in corers and dredges carried out at a single MBS (Hubert Miller Seamount), Udintsev et al. (2007) assumed that this structure represents a relict fragment of continental crust which was destructed and altered by a mantle plume. The authors, however, admit that the material recovered cannot unambiguously be interpreted as in situ rocks. Although the MBS form a vast seamount province covering over 200,000 km^2, their remote location made sampling difficult, inhibiting elucidation of their age, magma sources and volcanic evolution. Moreover, the relationship of the MBS to the magmatism associated with the final break-up of Gondwana and/or to the widespread but low volume intraplate volcanism in the SW Pacific region (e.g., Weaver et al., 1994; Storey et al., 1999; Rocchi et al., 2002a; Finn et al., 2005; Hoernle et al., 2006, 2010; Timm et al., 2010) was poorly constrained.

In 2006, the R/V Polarstern cruise ANT-XXIII/4 conducted a bathymetric mapping and dredge sampling survey of five MBS and associated structures. Samples from two other volcanic complexes in the Amundsen Sea, namely the previously studied ocean island volcano Peter I Island (e.g., Prestvik et al., 1990; Prestvik and Duncan, 1991; Hart et al., 1995) and the Belgica Seamount (De Gerlache Seamounts, Hagedorn et al., 2007) (Fig. 1), are included in our study to more fully characterize the sources and spatial evolution of intraplate magmatism in this region. Both Peter I Island and the De Gerlache Seamounts have been related to hotspot activity by most previous authors.

Here, we present results of the bathymetric surveys together with $^{40}Ar/^{39}Ar$ ages and geochemical data (major and trace element and radiogenic Sr–Nd–Pb–Hf isotope ratios) of the recovered rocks. We show that magmatism in the Amundsen Sea occurred at distinct time intervals in spatially confined areas ruling out an origin through a single stationary hotspot. Notably this volcanism appears predominantly influenced by HIMU (high time-integrated $^{238}U/^{204}Pb$) type mantle, requiring emplacement and upwelling of such material in the depleted upper oceanic mantle well after the breakup of Zealandia from Antarctica. After briefly summarizing the tectonic and magmatic evolution affecting this part of the SW Pacific over the past 100 Ma, we discuss our results and evaluate processes, which may cause non-hotspot related HIMU-type intraplate volcanism in the Amundsen Sea.

2. Tectonic and magmatic evolution of the SW-Pacific over the past 100 Ma

Plate-kinematic reconstructions (Fig. 2) demonstrate that Marie Byrd Land was attached to the southeastern margin of Zealandia prior to the final breakup of Gondwana (Fig. 2a; e.g., Eagles et al., 2004a). After the collision of the Hikurangi Plateau with the Gondwana margin (e.g., Davy et al., 2008; Hoernle et al., 2010) and cessation of subduction along the northern margin of Zealandia at c. 100 Ma (e.g., Weaver et al., 1994), extensional processes set in, causing Zealandia to rift from Marie Byrd Land (e.g., Larter et al., 2002; Eagles et al., 2004a; Boger, 2011 for a recent review). The continental breakup initiated with the Chatham Rise separating from the Amundsen Sea Embayment sector during the Cretaceous Normal Polarity Superchron (CNS) at about 90 Ma (Fig. 2b). Thereafter the southwestward rift propagation jumped farther south and separated the Campbell Plateau from Marie Byrd Land just before chron C33 (83–79 Ma), leaving a rifted West Antarctic continental

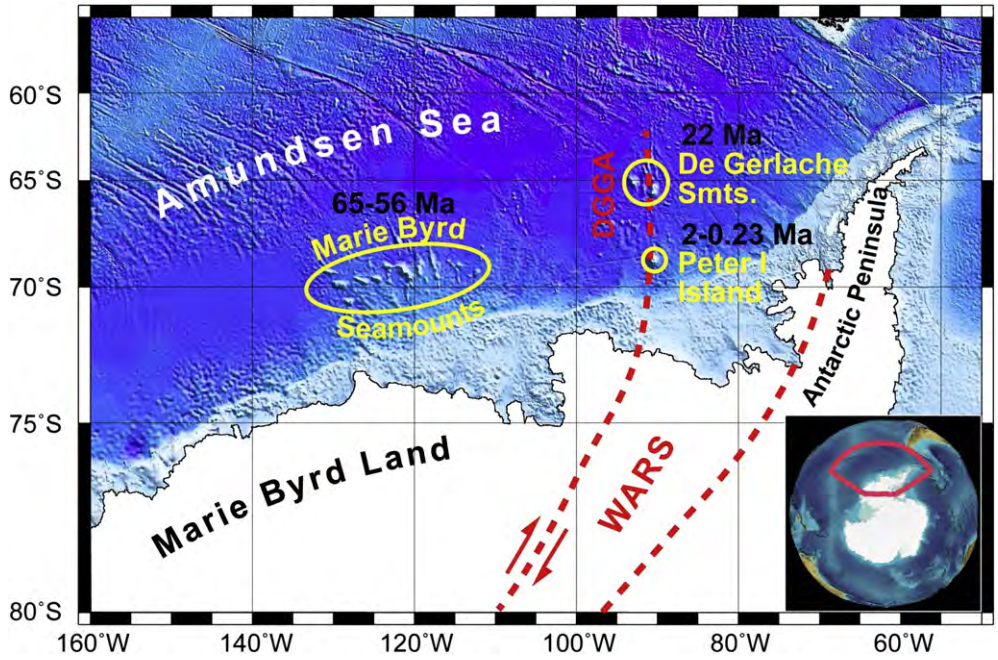

Fig. 1. Overview map of West Antarctica and the Amundsen Sea. The three seamount/ocean island volcanic provinces of the Amundsen Sea are marked by yellow circles. Dashed red lines indicate major tectonic lineaments (WARS — West Antarctic Rift System from Müller et al. (2007); DGGA — De Gerlache Gravity Anomaly). The map is based on the GEBCO_08 Grid (version 20091120, http://www.gebco.net).

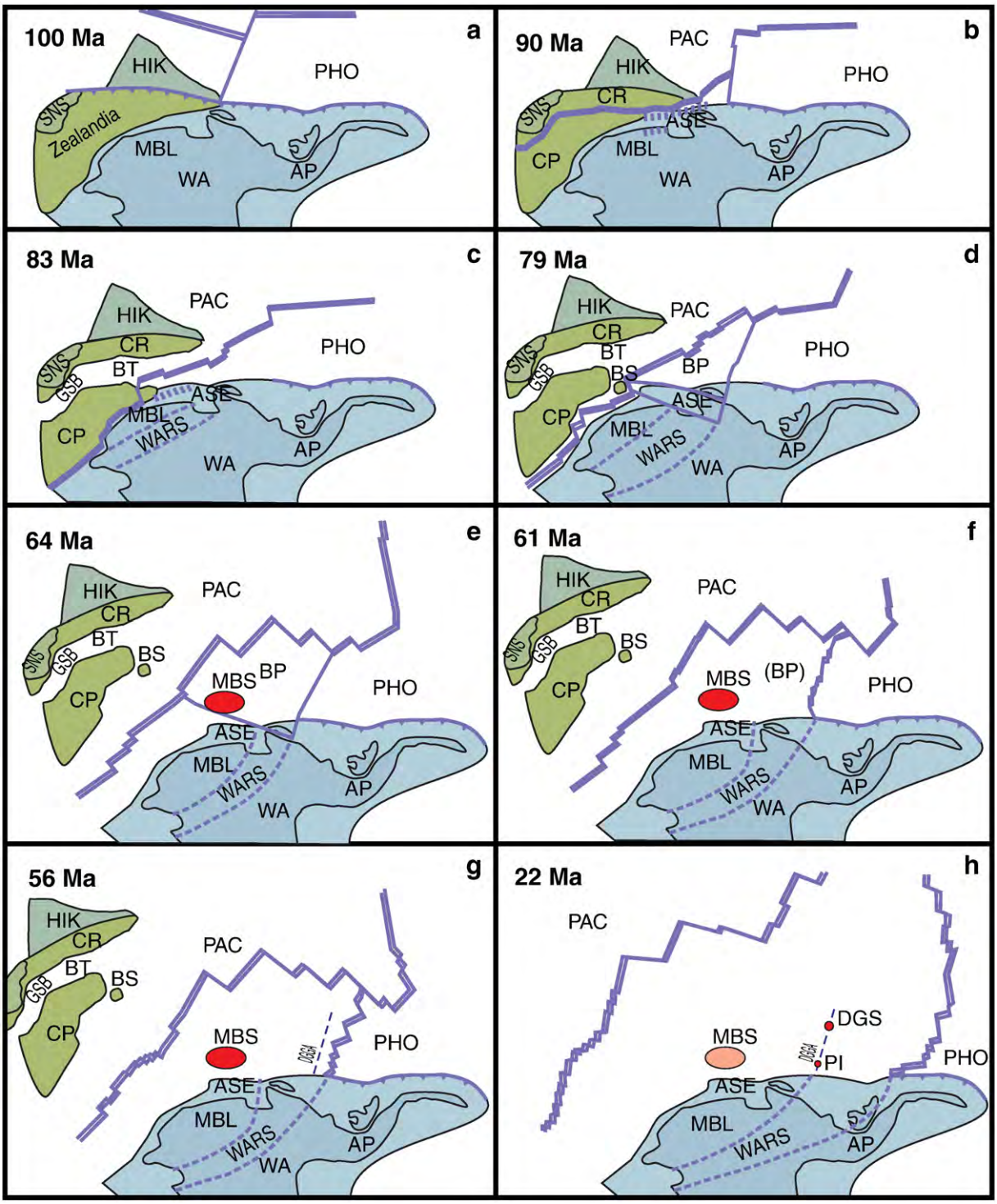

Fig. 2. Plate-tectonic reconstruction from 100 Ma to 22 Ma, using rotation parameters by Eagles et al. (2004a). Illustrated are the collision of Hikurangi Plateau with Zealandia at around 100 Ma, the breakup between Zealandia and West Antarctica at 90–80 Ma, the development of the Bellingshausen Plate and the subsequent volcanism along the West Antarctic margin. Double lines mark spreading ridge plate boundaries, single solid lines mark other plate boundary types, and dashed lines in West Antarctica illustrate lineaments of the West Antarctic Rift System (Eagles et al., 2009; Gohl et al., 2013). Abbreviations are: SNS South Island New Zealand, HIK Hikurangi Plateau, CP Campbell Plateau, CR Chatham Rise, GSB Great South Basin, BS Bollons Seamount, BT Bounty Trough, WA West Antarctica, MBL Marie Byrd Land, AP Antarctic Peninsula, ASE Amundsen Sea Embayment, WARS West Antarctic Rift System, PAC Pacific Plate, PHO Phoenix Plate, BP Bellingshausen Plate, MBS Marie Byrd Seamounts (red area marks volcanic activity of the shield phase), DGS De Gerlache Seamounts, PI Peter I Island, DGGA De Gerlache Gravity Anomaly (suture of former PHO-BP ridge jump).

margin bordering the Amundsen Sea (Fig. 2c, d; Larter et al., 2002; Eagles et al., 2004a).

During the late Cretaceous/Early Tertiary the southern Pacific region was sectioned into a minimum of three major tectonic plates (Bradshaw, 1989; Larter et al., 2002; Eagles et al., 2004a; Wobbe et al., 2012), the Pacific Plate, the Bellingshausen Plate, and the Phoenix or Aluk Plate adjacent to the Antarctic Plate (Fig. 2e). While the Phoenix Plate subducted beneath the eastern portion of the Antarctic Plate, the other plate boundaries were divergent or transform margins. During C27 (61 Ma) the Bellingshausen Plate ceased from being a separate

plate and became incorporated into the Antarctic Plate (Fig. 2f; Eagles et al., 2004a,b; Wobbe et al., 2012). Heinemann et al. (1999) and Stock (1997) suggest that the MBS province formed in the vicinity of the Antarctic–Pacific–Bellingshausen triple junction. Between C27 and C25/C24 (57–54 Ma), a substantial drop in spreading rate occurred at the Pacific–Antarctic Ridge, and together with a gradual rotation of the spreading direction (Müller et al., 2000), an increase in fracture zone density is notable (Eagles et al., 2004a). At the same time, the West Antarctic Rift System (WARS) continued its crustal extension in Marie Byrd Land and possibly into the Amundsen Sea Embayment just south of the MBS (Gohl et al., 2013). The De Gerlache Seamounts and Peter I Island are aligned along the so-called De Gerlache Gravity Anomaly (DGGA) (Gohl et al., 1997a; McAdoo and Laxon, 1997; Hagedorn et al., 2007) (Fig. 2g + h) which was initially interpreted as a fracture zone of the earlier Phoenix–Antarctic Ridge (Hart et al., 1995). However, magnetic seafloor spreading data imply that this is a tectonic scar caused by a westward jump of the Pacific–Phoenix ridge at chron C27 (Larter et al., 2002; Eagles et al., 2004a). Müller et al. (2007) suggested that this zone of possible lithospheric weakness was reactivated by a northward extension of a later WARS branch (Figs. 1 and 2h).

The Late Cretaceous tectonic events were accompanied by intense volcanism in East Gondwana and Marie Byrd Land at c. 95–110 Ma (e.g., Hart et al., 1997; Storey et al., 1999). This magmatism has been related to large-scale mantle upwelling in conjunction with extension-induced rifting (Finn et al., 2005). Others assume an active mantle plume in the area of the Bellingshausen–Amundsen Sea or beneath East Gondwana (Hole and LeMasurier, 1994; Weaver et al., 1994; Rocholl et al., 1995; Hart et al., 1995, 1997; Panter et al., 2000; Hoernle et al., 2010; Sutherland et al., 2010), which may have caused the final break-up of Zealandia from Antarctica (e.g., Weaver et al., 1994; Storey et al., 1999; Hoernle et al., 2010). As the region underwent further plate reorganization, a second phase of volcanism occurred (Rocchi et al., 2002a,b; Nardini et al., 2009 and references therein, LeMasurier et al., 1990). This younger magmatism (30–25 Ma until recent) is mainly of alkaline nature and has been related to rifting and crustal extension associated with the WARS. Based on a HIMU (high time-integrated U/Pb) component found in many WARS volcanics, many authors suggest reactivation of old plume material embedded at the base of the continental lithosphere (e.g., Weaver et al., 1994) others favor a metasomatic origin (e.g., Nardini et al., 2009).

3. Bathymetry and morphology of Marie Byrd Seamounts and Peter I Island

During cruise ANT-XXIII/4, the onboard Atlas Hydrosweep DS-2 multi-beam echo-sounding system of the R/V Polarstern was used to generate maps of five MBS (summarized in Table 1; Fig. 3a) and of the submarine base of Peter I Island (Gohl, 2007). Combined with bathymetric data of previous cruises (RV Nathaniel B. Palmer in 1996, RV Polarstern ANT-XI/3 in 1994, and ANT-XVIII/5a in 2001; e.g., Miller and Grobe, 1996; Feldberg, 1997), these data reveal that the MBS are characterized by steep sides with relatively flat tops and additional small cones on the upper flanks and/or on the platforms. The guyot-like morphology of the main edifices is attributed to seamount growth above sea level to form ocean island volcanoes, which subsequently eroded to sea level and then subsided to their present position. The small cones must have formed after subsidence of the erosional platforms below wave base and therefore represent a late stage or post-erosional phase of volcanism.

The westernmost studied seamount, Seamount 6 (informal name), has an elongate WNW–ESE striking base (Fig. 3b). The steep-sided edifice is topped by a flat plateau, on which several well-preserved small volcanic cones are scattered, rising up to 200 m above the plateau. Seamount 9 (informal name) is located about 45 km east of Seamount 6. One track was surveyed across Seamount 9 (not shown in Fig. 3), which revealed an oval shaped guyot and a c. 10 km long WNW–ESE-trending ridge emanating from its western base. This ridge is composed of several aligned small volcanic cones and interpreted as volcanic rift zone. Haxby Seamount (named by the ANT-XIII/4 cruise participants) (Fig. 3c), which has been mapped previously on RV Nathaniel B. Palmer Cruise in 1996 (Feldberg, 1997), has a slightly curvilinear volcanic rift system with numerous cones on its top emanating from the eastern flank of the guyot and extending >30 km to the east. Two less pronounced, c. 12–15 km long chains of cones and ridges emanating from the western flank may be the western continuation of the volcanic rift. Hubert Miller Seamount (Fig. 3d) is located ~75 km ESE of Haxby Seamount. This seamount is the largest MBS with frequent small cones and ridges scattered along its flanks but infrequent on the plateau. Several up to 8 km long volcanic rift zones extend from the base of Hubert Miller Seamount. The easternmost mapped seamount, Seamount C (informal name; Fig. 3e), is the smallest of the studied volcanoes. Its guyot-shaped edifice has a crudely circular base and a plateau of ~7 km diameter. Volcanic rifts extend from the base in northern and southern directions and NNE–SSW trending, curvilinear graben and ridge structures are adjacent to its eastern flank. The existence of further, most likely sediment covered, volcanic cones and ridge-like basement structures between the main MBS cluster and Marie Byrd Land are predicted from satellite gravity data (Smith and Sandwell, 1997) and observed in seismic data (Gohl et al., 1997b; Uenzelmann-Neben and Gohl, 2012). The original volume of MBS magmatism, however, remains unclear because of incomplete data and the largely unknown initial volume of the eroded islands. Based on the available bathymetric data (multi-beam and satellite gravity), the total volume of all present MBS can roughly be estimated to more than 20,000 km^3. The aerial extent of the former Marie Byrd Islands were similar in size to Canary Islands, such as La Palma (compared to Hubert Miller Seamount) or El Hierro (compared to

Table 1
Morphological features of the Marie Byrd Seamounts.

	Seamount 6	Seamount 9	Haxby Seamount	Hubert Miller Seamount	Seamount C
Coordinates (center)	69°47′S, 126°17′W	69°40′S, 124°45′W	69°07′S, 123°35′W	69°17′S, 121°20′W	69°12′S, 117°30′W
Shape	Oval shaped guyot	Oval shaped guyot	Oval shaped guyot	Oval shaped guyot	Crudely circular guyot
Secondary features	Small cones on flanks and plateau	Small cones on flanks and plateau; WNW–ESE trending rift zone	Small cones on flanks and plateau; WNW–ESE trending major rift zone, minor W–E and WSW–ENE rifts	Small cones on flanks and plateau; several rift zones, most of them ~SW–NE	Small cones on flanks and plateau; rift zones mainly trending from SSW–NNE to SSE–NNW
Base level (mbsl)	3000–2800	3600–3400	4000	4000–3600	3500
Diameter at base (km)	80 × 20	Long axis 25	30	75 × 50	17
Water depth of plateau (mbsl)	1600–1350	1600–1400	1800–1600	1600–1200	2400–2200
Edifice height (m)	~1650	~2200	~2400	~2800	~1300
Volume estimate (km^3)	~2000	–	~1600	~8000	~200
Dredge samples[a]	–	–	PS69/317-1	PS69/321-1 PS69/324-1 PS69/325-1	PS69/327-1

[a] A detailed description of dredge operations and recovered material is provided in Gohl (2007).

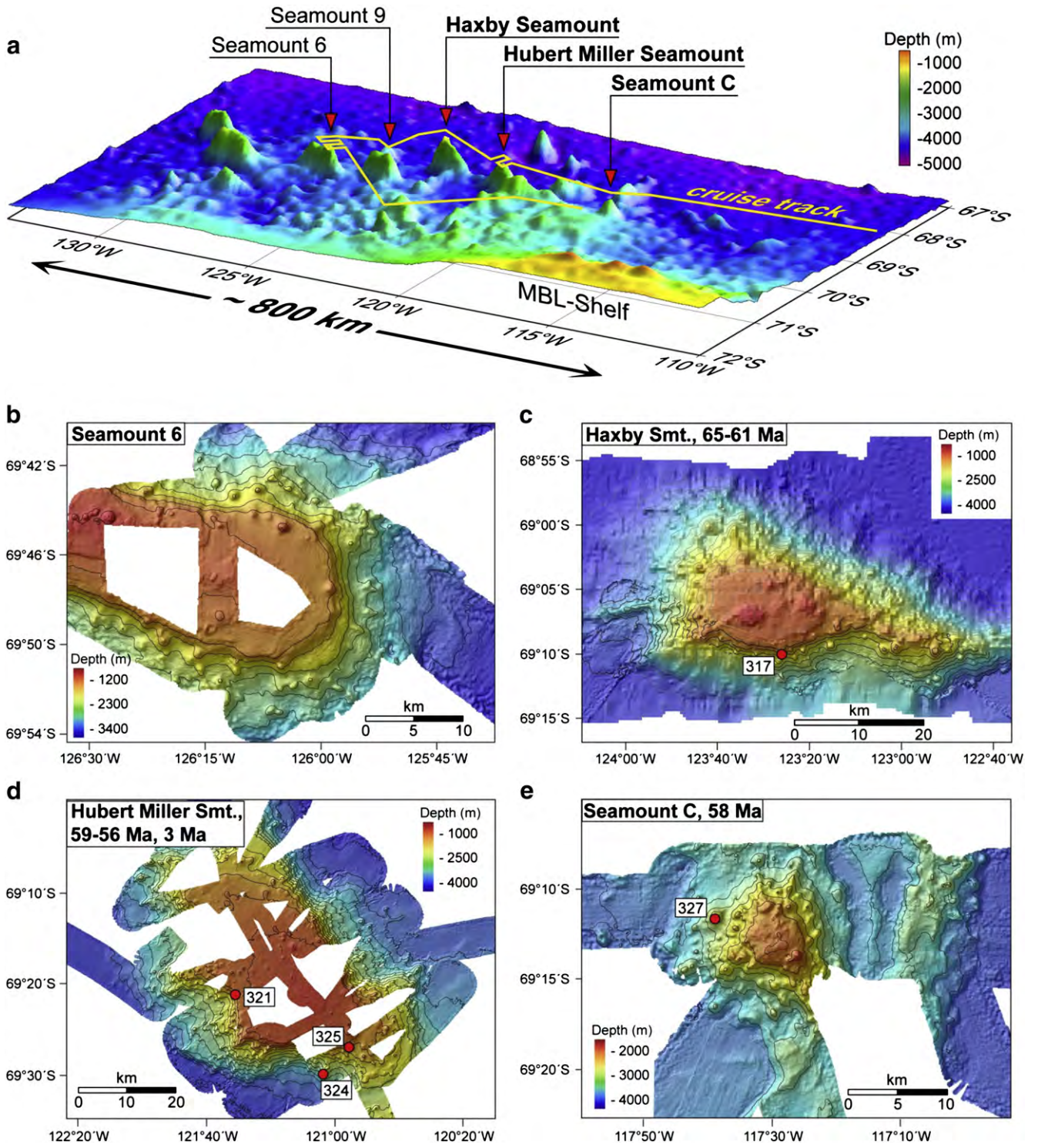

Fig. 3. (a) Overview of the Marie Byrd Seamount Province. Red arrows mark the MBS surveyed during R/V Polarstern cruise ANT-XXIII/4 in 2006, letters in bold signify those which have been successfully dredged. Predicted bathymetry is after Smith and Sandwell (1997). (b) Multi-beam bathymetry of the eastern part of Seamount 6. This is the westernmost studied during ANT-XXIII/4 and has not been mapped before. It appears to be one of the largest MBS. (c) Haxby Seamount (named by the ANT-XIII/4 cruise participants) has completely been mapped on the R/V N.B. Palmer cruise in 1996 and morphologically studied in detail by Feldberg (1997). (d) Combined ANT-XVIII/5a (2001) and ANT-XXIII/4 multi-beam bathymetry of Hubert Miller Seamount. This Seamount is located ~40 nm ESE of Haxby and appears to be the largest of the MBS. (e) Combined ANT-XVI/3 (Miller and Grobe, 1996) and ANT-XXIII/4 multi-beam bathymetry of Seamount C. This seamount does not appear in the bathymetric maps derived from satellite gravity data. Note that Seamount C differs in size, high, and morphology from the other surveyed MBS guyots. The red dots with numbers mark dredge station of cruise ANT-XXIII/4 which yielded in situ volcanic rocks.

Seamount 6), which are believed to be the product of a mantle plume (e.g., Montelli et al., 2006).

The submarine base of Peter I Island was only partially surveyed prior to ANT-XXIII/4 and, except for dredge hauls directly off the coast of the island (Broch, 1927), un-sampled (Fig. 4). The island is elongated in N–S direction and represents the top of a large volcano, which measures ~65 km in diameter at its base and rises from the abyssal plain at ~3500–4000 m to an elevation of 1640 m above sea

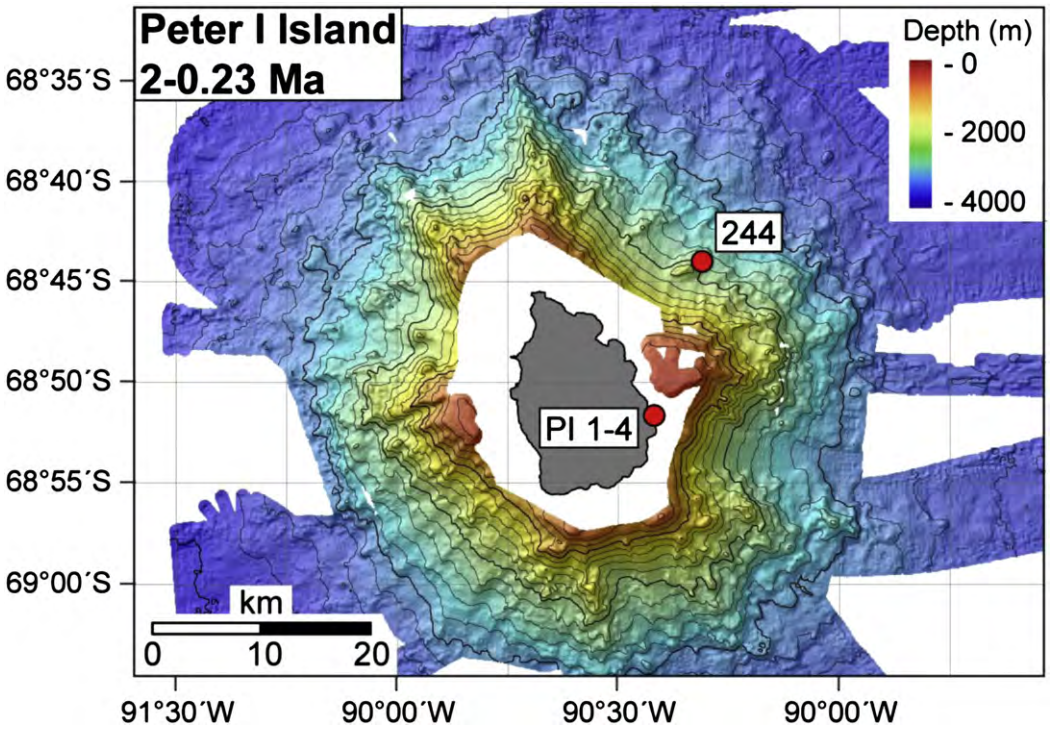

Fig. 4. Multi-beam bathymetry of the base of Peter I Island. The map reveals several small cone- and ridge-like structures on its flanks and a steep canyon at its eastern side which most likely has been formed by slope failure or sector collapse. The red dots indicate locations sampled during cruise during R/V Polarstern cruise ANT-XXIII/4 in 2006 (244 — dredge station at the eastern base of Peter I Island; PI 1–4 — subaerial samples taken on Michajlovodden Peninsula).

level. Volcanic rifts emanate from the submarine flank of the island mainly in northern and southern directions. A striking feature of Peter I Island is a c. 9 km wide depression in the eastern flank of its base, which most likely has been formed by a major slope failure or sector collapse.

4. Sample background

Volcanic rocks were recovered at five dredge stations of the main MBS edifices and associated small cones (Fig. 3b–e). In addition a single dredge haul along the northeastern submarine flank of Peter I Island has been carried out (Fig. 4). At all dredge sites discussed here, the angular shape of the rocks, freshly broken surfaces and homogeneity of rock types within a single dredge were taken as evidence for an in-situ origin (and non-ice rafted) of the rocks. Our samples represent the first in-situ volcanic rocks recovered from the MBS. A detailed description of dredge operations and recovered material is provided in chapter 7 of Gohl (2007).

At Haxby Seamount, dredge haul PS69-317-1 from the upper southern slope beneath the plateau edge contained freshly broken carbonate cemented breccias, which consist of aphyric basaltic clasts up to 8 cm in size (Fig. 5a). At Hubert Miller Seamount, three dredges yielded mainly lava fragments; dredge PS69-321-1 along a steep slope below the SE plateau edge gave olivine (ol)–clinopyroxene (cpx)–phyric lava Fig. 5b, dredge PS69-324-1 at the lower SE slope beneath a cone like structure provided dense feldspar (fsp)–cpx–phyric basalt lava and (carbonate) cemented Mn-encrusted volcanic breccia, and dredge PS69-325-1 obtained vesicular fsp–phyric lava from the upper southern flank. At Seamount C, vesicular ol–fsp–phyric and dense fsp–phyric pillow fragments (Fig. 5c) were dredged from a cone on the lower western flank.

At Peter I Island, a 150 m high ridge located in ~1800 m water depth on the NE slope of the volcano was dredged (PS69-244-1). The rocks are predominantly vesicular pillow and sheet flow lava fragments (Fig. 5d). Both are feldspar (fsp)–phyric and have up to 1 cm thick, fresh, glassy rims. Vesicles are generally unfilled and only a few glassy surfaces show early stages of palagonitization. The subaerial samples from Peter I Island were taken at the Michajlovodden Peninsula (Fig. 4). They comprise vesicular lava (up to 15% vesicles; sample PI-1), aphyric agglutinates of a >1.5 m thick, partially red oxidized layer outcropping in the northern part of the peninsula (sample PI-3), and part of a reddish volcanic bomb with 10–20% vesicles (sample PI-4).

Belgica Seamount is the easternmost edifice of the De Gerlache Seamount group. It is guyot-shaped and has a N–S elongated base diameter of c. 60 × 90 km with a flat-topped summit at c. 400–500 m below sea level. Belgica was dredge-sampled during Polarstern cruise ANTXII-4 in 800 to 600 water depths (Hagedorn et al., 2007). Hagedorn et al. (2007) initially determined K–Ar ages and major and trace element geochemistry on the recovered samples. Here we complement the existing data with Sr–Nd–Pb isotope data on a subset of newly prepared sample material.

5. Petrography and rock classification

The petrography of the MBS volcanics is quite uniform being slightly phyric with a few large phenocrysts of altered olivine and zoned plagioclase in a fine-grained groundmass of olivine, plagioclase and clinopyroxene. Occasionally, ilmenite and magnetite occur as accessory phases. Olivine is commonly altered to iddingsite and the latter is sometimes replaced by calcite. The groundmass is variably altered by low temperature processes ranging from hydrated glass at Haxby Seamount to replacement by secondary minerals such as zeolite and dolomite at Hubert Miller Seamount and Seamount C. The altered state of the MBS volcanic rocks is also manifested in elevated H_2O contents of up to 2 wt.% in most samples, except that samples from Dredge 324 at Hubert Miller Seamount have <1 wt.% H_2O and those from Seamount C have 3 wt.% H_2O (Table 2). CO_2 contents are generally low (<0.3 wt.%) and only two samples show slightly elevated CO_2 > 0.5 wt.%, due to secondary carbonate. Unusually high phosphorous contents were detected in 5 samples (marked with [a] in Table 2) and are interpreted to reflect the presence of secondary phosphate that is, however, not detected in thin section. Only samples

Fig. 5. Basaltic rocks dredged at the MBS and the submarine base of Peter I Island. (a) Typical monomict breccia from Haxby Seamount composed of dense, aphyric irregular-shaped and angular coarse lapilli set in a carbonaceous matrix (PS69/317-1). (b) Dense ol–cpx–phyric basaltic lava fragment from Hubert Miller Seamount, note angularity and freshly broken surfaces of the sample (PS69/321-1). (c) Dense fsp–phyric pillow fragment of Seamount C (PS69/327-1). (d) Sheet lava flow fragment with fresh, 1 cm thick glassy rim from the submarine base of Peter I Island (PS69/244-1).

with $P_2O_5 \leq 1$ wt.% are considered meaningful when treating the major element chemistry further below.

The submarine samples of Peter I Island are slightly porphyric with zoned plagioclase laths and small, homogeneously distributed clinopyroxene phenocrysts, set in a microcrystalline groundmass of clinopyroxene and plagioclase. Magnetite occurs as an accessory mineral and fresh glass is common. The subaerial volcanics of Peter I Island are more aphyric than those from the submarine flanks. The fine-grained crystalline groundmass of these samples contains pyroxene, plagioclase and possibly glass, and accessory minerals of magnetite, ilmenite and hematite. All samples from Peter I Island are generally very fresh as manifested by low H_2O (0.3–0.9 wt.%) and CO_2 (<0.06 wt.%) contents (Table 2).

The silica content of the entire sample suite ranges from 53.1 to 45.7 wt.% SiO_2. On a total alkali vs. silica diagram (TAS; Fig. 6), the majority of the samples plots above the alkalic–sub-alkalic division line and are classified as basalts, trachybasalts and basaltic trachyandesites. All but one of MBS samples lie along an alkali basaltic differentiation trend. The samples from the submarine flank of Peter I Island are tholeiitic basalts (SiO_2 ~ 49 wt.%; $Na_2O + K_2O$ 4.1–4.3 wt.%), whereas the subaerial samples are slightly more alkaline transitional tholeiites (SiO_2 ~ 47 wt.%; $Na_2O + K_2O$ 4.3–4.5 wt.%).

6. Analytical results

6.1. $^{40}Ar/^{39}Ar$ age dating

The $^{40}Ar/^{39}Ar$ age dating results are summarized in Table 3. Age and alteration index spectra (based on the measured $^{36}Ar/^{37}Ar$ ratios after Baksi, 2007) are shown in Fig. 7. A detailed description of the methods and the full analytical data are provided in Appendix 1.

Glasses from two hyaloclastite breccia samples at Haxby Seamount yield plateau ages of 64.2 ± 0.9 Ma (317-1-1gls) and of 62.3 ± 0.4 (317-1-2gls) and 61.2 ± 0.5 Ma (317-1-2gl2), slightly outside of the two sigma analytical errors. Alteration indices are relatively high even in the plateau sections (0.001 to 0.01), reflecting partial hydration of the basalt glass and uptake of atmospheric ^{36}Ar.

Three samples of porphyric lava from Hubert Miller Seamount yield plagioclase step-heating plateau ages of 56.7 ± 1.9 Ma (321-1-2), 56.5 ± 0.6 Ma (325-1-2B) and 57.0 ± 0.9 Ma (321-1-5). Alteration indices are high in the low-temperature heating steps indicating partial alteration of the feldspars, but systematically low in the plateau steps (<0.0002) indicating degassing from little or un-altered sites. Matrix step-heating analyses from the same rock samples yield plateau age results within error of the feldspar step-heating results (321-1-2: 58.9 ± 0.6 Ma; 321-1-5: 55.7 ± 0.5 Ma), but are considered inferior with respect to scatter and alteration effects.

The matrix step-heating analysis of aphyric basalt lava sample 324-1-3, in contrast, yields a plateau age of 3.0 ± 0.5 Ma. Alteration indices are high in the plateau section (0.003 to 0.01), possibly indicating a partial loss of radiogenic ^{40}Ar. Nevertheless, the analysis shows that Hubert Miller Seamount comprises both Paleocene and Pliocene lavas.

The least-altered aphyric lava sample from Seamount "C" (327-1-2) yields a low-probability plateau age of 58.7 ± 0.8 Ma, with intermediate plateau-step alteration indices (0.002 to 0.008). Fresh basaltic glass from Peter I Seamount yields plateau steps alteration indices of <0.0009 (244-1-1) and <0.0001 (244-1-3), and plateau ages of 1.9 ± 0.3 Ma, 1.7 ± 0.3 Ma respectively.

6.2. Major and trace elements

A total of 19 samples from the MBS and Peter I Island were analyzed for major and trace elements compositions and the results are

Table 2
Results of major and trace element analyses.

	PS69/317-1-1 Haxby Smt	PS69/317-1-1 Replicate ICP-MS	PS69/317-1-2 Haxby Smt	PS69/321-1-2 Hubert Miller Smt	PS69/321-1-4 Hubert Miller Smt	PS69/321-1-5 Hubert Miller Smt	PS69/321-1-12a Hubert Miller Smt	PS69/324-1-3 Hubert Miller Smt	PS69/324-1-4 Hubert Miller Smt	PS69/324-1-6 Hubert Miller Smt
SiO_2	46.13		42.03	50.22	46.23	45.95	50.19	45.80	52.85	46.74
TiO_2	3.39		3.57	1.89	3.59	3.44	2.09	2.60	0.85	3.26
Al_2O_3	16.33		18.2	17.15	17.59	16.62	18.46	15.02	17.18	14.86
Fe_2O_3	14.81		15.91	11.49	14.19	13.95	11.09	13.05	8.63	14.73
MnO	0.21		0.21	0.22	0.19	0.22	0.17	0.19	0.18	0.20
MgO	3.46		3.41	2.58	2.85	3.96	2.07	8.13	5.52	4.87
CaO	7.72		9.02	6.39	8.84	8.44	6.76	10.65	8.68	10.31
Na_2O	3.82		3.51	4.57	3.54	3.53	4.53	3.29	3.99	3.65
K_2O	1.54		0.74	2.61	2.09	2.05	2.15	1.04	1.45	1.24
P_2O_5	0.91		1.44[a]	0.73	0.92	0.79	0.87	0.48	0.21	0.54
H_2O	1.91		2.38	2.23	1.80	1.86	2.10	0.74	0.98	0.82
CO_2	0.06		0.17	0.30	0.08	0.07	0.07	0.13	0.07	0.08
Total	100.29		100.59	100.38	101.91	100.88	100.55	101.12	100.59	101.30
Rb	28.1	28.1	6.66	53.4	37.3	50.4	23.9	24.1	35.8	28.0
Ba	330	330	264	725	462	493	784	311	455	320
Th	4.79	4.72	4.60	6.89	4.57	4.43	7.31	2.99	4.72	3.91
U	1.52	1.52	0.427	1.75	0.816	0.695	0.296	0.743	0.819	0.982
Nb	70.3	70.6	68.1	123	78.5	77.2	119	46.0	78.5	56.6
Ta	4.21	4.18	4.27	6.60	4.59	4.45	6.97	2.78	4.60	3.39
La	49.6	48.9	64.4	76.8	52.4	51.4	65.9	32.1	53.1	38.3
Ce	106	106	114	154	106	103	146	66.2	107	78.4
Pb	2.75	2.35	2.41	3.81	2.44	2.65	3.37	2.47	2.30	1.89
Pr	13.1	13.1	14.4	17.0	12.2	11.6	16.1	7.74	12.3	8.98
Nd	55.6	55.2	57.6	63.2	46.0	44.3	61.6	30.1	46.5	35.5
Sr	760	756	1219	825	969	925	891	626	967	568
Sm	12.1	12.1	13.3	12.6	9.86	9.49	12.5	6.69	9.97	8.08
Hf	8.06	8.02	8.35	8.83	6.36	5.94	9.36	4.30	6.35	5.55
Zr	404	402	413	475	323	317	446	205	321	261
Eu	3.79	3.75	4.14	3.92	3.09	2.91	4.12	2.19	3.04	2.49
Gd	10.8	10.7	11.4	10.2	8.00	7.45	9.66	5.89	8.10	7.17
Tb	1.45	1.47	1.56	1.40	1.05	0.979	1.29	0.814	1.02	1.02
Dy	7.98	7.89	8.36	7.50	5.40	5.04	6.58	4.38	5.49	5.74
Ho	1.43	1.46	1.54	1.33	0.97	0.92	1.14	0.787	0.971	1.02
Y	42.3	42.0	51.6	43.6	32.5	31.5	35.5	25.2	31.6	31.8
Er	3.59	3.72	3.84	3.47	2.49	2.31	2.79	2.07	2.50	2.66
Tm	0.457	0.479	0.475	0.455	0.310	0.291	0.345	0.261	0.325	0.350
Yb	3.13	3.14	3.84	3.54	2.57	2.45	2.76	2.08	2.49	2.65
Lu	0.450	0.447	0.554	0.496	0.359	0.332	0.366	0.278	0.350	0.364

[a] Results with unusual high values not shown in Fig. 6.

	PS69/325-1-2a Hubert Miller Smt	PS69/325-1-2b Hubert Miller Smt	PS69/327-1-1 Seamount C	PS69/327-1-2 Seamount C	PS69/244-1-1 Peter I submarine	PS69/244-1-3 Peter I submarine	PS69/244-1-5 Peter I submarine	PS69/PI-1 Peter I subaerial	PS69/PI-3 Peter I subaerial	PS69/PI-4 Peter I subaerial
SiO_2	47.72	47.72	41.98	46.00	49.48	49.09	49.26	47.79	47.26	48.15
TiO_2	2.52	2.49	2.26	2.70	2.79	2.74	2.75	3.53	3.48	3.46
Al_2O_3	16.78	17.24	18.15	20.31	13.68	13.26	13.61	12.79	12.52	12.73
Fe_2O_3	11.58	12.02	8.92	11.30	12.58	12.55	12.85	13.48	13.36	13.03
MnO	0.14	0.14	0.08	0.15	0.14	0.15	0.14	0.15	0.15	0.14
MgO	2.54	1.34	0.97	1.24	8.18	9.2	8.55	9.64	9.86	9.42
CaO	7.93	7.40	12.84	8.73	9.00	8.68	8.91	9.03	8.83	8.67
Na_2O	3.88	4.19	3.55	3.44	3.17	3.03	3.00	3.07	3.03	3.17
K_2O	2.74	3.24	1.74	1.38	1.16	1.08	1.15	1.37	1.42	1.47
P_2O_5	1.69[a]	2.12[a]	5.02[a]	1.62[a]	0.50	0.51	0.48	0.64	0.69	0.78
H_2O	2.12	2.13	2.92	3.03	0.86	0.87	0.94	0.28	0.45	0.38
CO_2	0.59	0.18	0.56	0.24	0.05	0.05	0.06	0.04	0.04	0.04
Total	100.23	100.21	98.99	100.14	101.59	101.21	101.70	101.81	101.09	101.44
Rb	90.1	57.3	27.2	21.5	20.3	19.8	19.2	23.9	26.5	26.3
Ba	469	480	404	427	240	228	226	308	315	332
Th	6.93	7.02	5.21	5.06	2.85	2.68	2.57	3.53	3.74	3.78
U	1.34	1.33	1.78	1.43	0.887	0.725	0.704	0.920	0.984	1.02
Nb	95.6	96.8	55.6	58.7	30.2	29.4	28.9	48.5	48.7	50.6
Ta	5.38	5.44	3.48	3.58	1.88	1.83	1.76	2.82	2.89	2.90
La	73.5	73.8	66.2	44.6	27.2	26.7	26.1	38.0	40.3	43.1
Ce	141	144	80.4	84.5	58.5	57.1	55.6	80.9	85.2	92.4
Pb	3.38	3.21	3.07	2.24	2.30	2.26	2.22	2.26	2.46	2.31
Pr	16.3	16.3	10.4	9.36	7.49	7.20	6.95	10.2	10.4	11.4
Nd	62.4	62.3	39.0	35.6	32.7	30.8	29.2	43.1	43.6	48.5
Sr	674	717	811	843	624	622	632	797	804	871
Sm	12.9	13.3	8.09	7.89	7.57	7.54	7.48	9.80	10.2	11.0
Hf	7.99	8.02	4.99	5.37	5.22	5.19	5.03	7.03	7.42	7.59
Zr	412	417	250	258	233	230	227	315	326	344
Eu	3.59	3.56	2.45	2.49	2.43	2.48	2.39	3.14	3.21	3.52
Gd	10.9	10.9	7.78	6.87	6.78	6.55	6.38	8.50	8.63	9.61
Tb	1.48	1.41	1.07	0.957	0.874	0.882	0.854	1.14	1.13	1.19
Dy	7.39	7.51	6.32	5.30	4.69	4.54	4.40	5.70	5.52	5.85
Ho	1.35	1.36	1.33	0.979	0.792	0.737	0.706	0.924	0.894	0.963
Y	48.7	46.1	66.5	32.0	22.5	21.6	21.6	24.9	24.9	25.7
Er	3.50	3.52	3.71	2.70	1.83	1.72	1.73	2.14	2.05	2.14
Tm	0.458	0.449	0.509	0.349	0.226	0.207	0.204	0.255	0.246	0.256
Yb	3.63	3.54	4.21	2.72	1.53	1.50	1.49	1.58	1.54	1.56
Lu	0.515	0.506	0.674	0.377	0.192	0.193	0.186	0.206	0.209	0.203

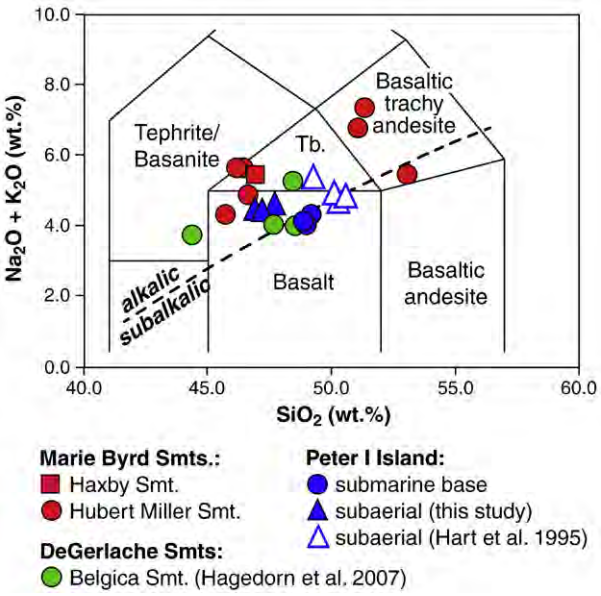

Fig. 6. Total alkali versus SiO_2 diagram illustrating the alkali basaltic to basaltic trachyandesitic composition of most samples from MBS, Peter I Island, and Belgica Seamount. Subdivision between alkalic and sub-alkaline rock suites is after Irvine and Baragar (1971). All data are normalized to a 100% volatile free basis. Samples displaying unusual high phosphor contents are not shown in this diagram (cf. Table 2). Tb — Trachybasalt.

shown in Table 2. Descriptions of methods and uncertainties are given in Appendix 1. A full table with sample locations, radiometric ages and geochemical data is provided in Table A4 of the Appendix. The majority of MBS samples are fairly evolved (8 to 2 wt.% MgO), whereas samples from Peter I Island are more primitive and cluster between 10 and 8 wt.% MgO. Al_2O_3 shows a good negative correlation with decreasing MgO, suggesting fractionation of pyroxene and olivine. In the most evolved MBS lavas (<3 wt.% MgO), FeOt and TiO_2 significantly decrease which may reflect fractionation of ilmenite in late stage melts. Subaerial and submarine samples of Peter I Island exhibit small compositional differences. The submarine samples have higher SiO_2 and Al_2O_3 and slightly lower MgO, FeOt and TiO_2 contents than the subaerial samples.

Trace elements patterns of the MBS are typical for ocean islands basalts (OIB; Fig. 8a) with characteristic troughs for Pb and K and strong enrichments for Nb and Ta relative to primitive mantle. The Nb and Ta enrichments are most pronounced in samples from Hubert Miller Seamount while Haxby Seamount and Seamount C are less enriched in the most incompatible elements (Rb, Ba and Th). All MBS samples show strong enrichment of the light REE (LREE) relative to the heavy REE (HREE) (see Fig. 8c), suggesting small degrees of partial melting while differentiation of the HREE indicates melting within the garnet stability field (>70–80 km).

The new trace element data from Peter I Island also display trace element patterns similar to OIB (Fig. 8b) that compares well with the data of Prestvik et al. (1990) and Hart et al. (1995). Overall the subaerial samples are slightly more enriched in incompatible elements than the submarine sample but show similar HREE abundances (Fig. 8d), which is consistent with lower degrees of melting for the subaerial lavas. In contrast to the MBS, Peter I Island samples are slightly less enriched in LREE and the most incompatible elements (Rb through Ta) and show lower La/Sm ratios (Fig. 9a), indicating higher degrees of partial melting than observed for the MBS. Notably the LREE are more strongly enriched relative to the HREE through a more pronounced HREE depletion. The higher (Sm/Yb)n ratios of the Peter I Island melts suggest that their source had a higher garnet content (Fig. 9b).

6.3. Sr–Nd–Pb–Hf isotopes

Sr–Nd–Pb–Hf isotopic ratios of representative samples from the MBS, Belgica Seamount, and Peter I Island are shown in Table 4. Descriptions of analytical methods and accuracy along with initial isotopic ratios are given in Appendix 1 and Table A4. Figs. 10 and 11 compare the new MBS, Peter I Island and Belgica Seamount isotope data with data of West Antarctic volcanic rocks, related to the WARS (for data sources see figure captions) and the Hikurangi Seamounts (Hoernle et al., 2010). Excluding two samples with anomalously high $^{87}Sr/^{86}Sr$ isotope ratios that may have been affected by seawater alteration, the MBS samples form a crude negative array on the Sr–Nd isotope diagram (Fig. 10). The samples from Seamount C have the most radiogenic Nd and least radiogenic Sr isotope ratios and fall between Pacific MORB and the high $^{238}U/^{204}Pb$ (HIMU) mantle endmember. Samples from Hubert Miller Seamount have the least radiogenic Nd isotope ratios and trend vaguely towards an enriched mantle (EM) type component (Fig. 10). The Belgica samples plot within the Pacific MORB field and the Peter I Island samples lie within the published field for this island (Prestvik et al., 1990; Hart et al., 1995) and are displaced to slightly more radiogenic Sr and less radiogenic Nd isotope ratios i.e. to faintly more EM flavored compositions than the majority of Hubert Miller Seamount samples. In Pb–Pb isotope space (Fig. 11a), the MBS volcanic rocks do not form a simple two component mixing array as the majority of samples extends from a HIMU-type component with radiogenic Pb towards enriched mantle one (EMI) while two samples having significantly lower $^{207}Pb/^{204}Pb$ which displaces them towards the extension of the Pacific MORB field. Sample 324-1-4 from Hubert Miller Seamount has the least radiogenic Pb composition of all MBS and plots above the Pacific MORB field away from the main MBS array while samples from Haxby Seamount possess the most radiogenic Pb composition. The Belgica Seamount samples plot near the unradiogenic end of the main MBS field in Pb–Pb isotope space (Fig. 11a) but possess more radiogenic $^{143}Nd/^{144}Nd$ compositions than the MBS (Fig. 11b). The majority of MBS samples and all Belgica

Table 3
$^{40}Ar/^{39}Ar$ step heating analyses results.

Seamount	Sample ID PS69-	Analysis ID	Dated material	Plateau ± 2 sigma age (Ma)	^{39}Ar fraction	MSWD	Probability
Haxby	317-1-1	gls	Glass	64.7 ± 0.8	63.1	0.95	0.46
	317-1-2	gls	Glass	62.3 ± 0.4	56.8	0.99	0.44
	317-1-2	gl2	Glass	61.2 ± 0.5	72.9	1.19	0.27
Hubert Miller	321-1-2	fss	Plag	56.7 ± 1.9	73.9	0.61	0.72
	321-1-2	mx2	Matrix	58.9 ± 0.6	95.6	1.10	0.34
	321-1-5	fss	Plag	57.0 ± 0.9	58.4	1.30	0.23
	321-1-5	mx2	Matrix	55.7 ± 0.5	63.5	0.78	0.45
	325-1-2B	fss	Plag	56.5 ± 0.6	61.1	1.20	0.30
	324-1-3	mxs	Matrix	3.0 ± 0.5	84.6	1.30	0.21
"C"	327-1-2	mx2	Matrix	58.7 ± 0.8	55.7	1.90	0.04
Peter I[a]	244-1-1	gls	Glass	1.9 ± 0.3	83.8	1.03	0.41
	244-1-3	gl2	Glass	1.7 ± 0.3	96.4	0.58	0.87

[a] Dated samples from Peter I Island are dredge samples from its submarine base.

Table 4
Sr-Nd-Pb-Hf-Isotope analyses.

	$^{87}Sr/^{86}Sr$	2 sigma	$^{143}Nd/^{144}Nd$	2 sigma	$^{206}Pb/^{204}Pb$	2 sigma	$^{207}Pb/^{204}Pb$	2 sigma	$^{208}Pb/^{204}Pb$	2 sigma	$^{176}Hf/^{177}Hf$	2 sigma
Marie Byrd Smts.												
PS69/317-1-1	0.703093	0.000003	0.512885	0.000003	20.7725	0.0015	15.7739	0.0016	40.1472	0.0056	0.282871	0.000005
PS69/317-1-2	0.704186	0.000003	0.512881	0.000003	20.4116	0.0020	15.7561	0.0022	39.9679	0.0075	0.282875	0.000004
PS69/321-1-2	0.703384	0.000003	0.512798	0.000003	20.2467	0.0016	15.7229	0.0017	40.0393	0.0057	0.282879	0.000003
PS69/321-1-4	0.703277	0.000002	0.512806	0.000002	20.1075	0.0006	15.7153	0.0006	39.9521	0.0018	0.282880	0.000004
PS69/321-1-5	0.703335	0.000002	0.512816	0.000003	20.1005	0.0008	15.7160	0.0008	39.9815	0.0028		
PS69/321-1-12a	0.703230	0.000003	0.512811	0.000003	19.9595	0.0008	15.7082	0.0009	39.9274	0.0028	0.282875	0.000004
PS69/324-1-3	0.703094	0.000003	0.512906	0.000003	19.6713	0.0011	15.6140	0.0013	39.5216	0.0044	0.282787	0.000007
PS69/324-1-4	0.704027	0.000003	0.512881	0.000003	18.7063	0.0006	15.6189	0.0007	38.4900	0.0020	0.282877	0.000004
PS69/324-1-4[d]	0.704043	0.000003	0.512870	0.000003	18.7110	0.0006	15.6184	0.0007	38.4973	0.0019		
PS69/324-1-6	0.703108	0.000003	0.512899	0.000003	19.8645	0.0009	15.6339	0.0009	39.7163	0.0027	0.283003	0.000004
PS69/324-1-6[d]					19.8661	0.0013	15.6331	0.0014	39.7173	0.0048		
PS69/325-1-2a	0.703502	0.000003	0.512809	0.000003	20.1218	0.0008	15.7193	0.0006	39.9100	0.0016	0.282862	0.000004
PS69/325-1-2b	0.703417	0.000002	0.512817	0.000003	20.0871	0.0008	15.7180	0.0006	39.8863	0.0017		
PS69/327-1-1	0.702888	0.000003	0.512913	0.000006	19.8152	0.0010	15.6835	0.0010	39.2970	0.0031	0.282927	0.000004
PS69/327-1-2	0.702805	0.000003	0.512918	0.000009	19.8530	0.0008	15.6903	0.0008	39.3447	0.0024		
PS69/327-1-2[d]	0.702831	0.000003	0.512927	0.000004								
De Gerlache Smts.												
PS-2693-1_(1)[e]	0.703015	0.000005	0.512967	0.000002	19.8515	0.0021	15.6878	0.0018	39.5057	0.0049		
PS-2693-1_(2)[e]	0.703023	0.000005	0.512966	0.000003	19.8376	0.0025	15.6795	0.0021	39.4705	0.0056		
PS-2693-1_(3)[e]	0.703029	0.000005	0.512966	0.000003	19.8278	0.0032	15.6804	0.0027	39.4777	0.0063		
PS-2693-1_(4)[e]	0.703029	0.000004	0.512957	0.000003	19.9238	0.0037	15.6834	0.0030	39.4845	0.0081		
PS-2693-1_(5)[e]	0.702998	0.000005	0.512983	0.000004	19.7441	0.0025	15.6641	0.0024	39.3550	0.0069		
PS-2693-1_(6)[e]	0.702994	0.000005	0.512975	0.000003	19.7447	0.0016	15.6601	0.0012	39.3438	0.0032		
Peter I Island												
PS69/244-1-1	0.703748	0.000003	0.512759	0.000002	19.2360	0.0015	15.7437	0.0017	39.3779	0.0056	0.282798	0.000003
PS69/244-1-3	0.703752	0.000003	0.512750	0.000003	19.2517	0.0006	15.7520	0.0006	39.4162	0.0019		
PS69/PI-1[f]	0.703759	0.000005	0.512805	0.000002	19.3013	0.0012	15.7216	0.0010	39.3230	0.0026		
PS69/PI-3	0.703837	0.000002	0.512782	0.000002	19.3015	0.0007	15.7409	0.0006	39.3865	0.0015		
PS69/PI-4	0.703871	0.000002	0.512775	0.000003	19.3244	0.0007	15.7456	0.0006	39.4265	0.0014		

[d] Replicate analyses.
[e] $^{87}Sr/^{86}Sr$ determined on MAT262 TIMS.
[f] Pb isotope ratios without Pb DS.

Seamount samples largely overlap with the fields of the West Antarctic volcanics and the Hikurangi Seamounts (Fig. 11). The Peter I Island samples overlap the published data from this island and have Pb isotope compositions near the enriched mantle two (EMII) component.

The above mixing relations are also seen in co-variations of $^{206}Pb/^{204}Pb$ versus $^{143}Nd/^{144}Nd$ (Fig. 11b) and εNd versus εHf (Fig. 12). On the Pb vs Nd isotope diagram, it is clear that at least three distinct components are required in the source of the MBS seamounts. Haxby Seamount has radiogenic Pb and intermediate Nd isotope ratios, similar to the HIMU mantle endmember. Seamount C and two Hubert Miller Seamount samples have less radiogenic Pb and intermediate Nd, trending toward Pacific MORB (or depleted mantle = DM). The remaining Hubert Miller seamount samples except sample 324-1-4 have radiogenic Pb but the least radiogenic Nd, so that they are somewhat displaced toward EM like compositions. On the Nd–Hf isotope diagram, the MBS seamounts show a relatively restricted range in Nd but a large range in Hf isotope ratios that fall between Pacific MORB (DM) and the HIMU and EM mantle endmembers. The Belgica Seamount samples have the most MORB-like compositions in Nd, but their $^{206}Pb/^{204}Pb$ isotopic compositions are more radiogenic than commonly found in MORB. The Peter I Island samples have a clear EMII-type isotope signal with respect to Pb while Sr, Nd and Hf isotopes are just EM indicative.

7. Discussion

7.1. Spatial distribution of Cenozoic volcanism in the Amundsen Sea and Bellingshausen Sea

$^{40}Ar/^{39}Ar$ dating of six samples from the MBS yielded Early Cenozoic ages ranging from 64 to 57 Ma. A clear spatial age progression between the three dated MBS is not observed. The oldest ages are from Haxby Seamount in the west (64–61 Ma) and clearly younger ages are from Hubert Miller Seamount to the east (57 Ma, three feldspar ages). Seamount C, the easternmost seamount, yielded an intermediate age (59 Ma), but this matrix age with a very low probability should be treated with caution. The Pliocene age of 3.0 ± 0.5 Ma determined for sample 324-1-3 was collected right beneath a small volcanic cone along the upper slope of Hubert Miller Seamount (Fig. 3d) and most likely represents the age of this cone. Similar cones are scattered on the plateau and slopes of all mapped MBS (cf. Fig. 3), indicating widespread and possibly long-lasting low volume post-erosional volcanism, as has been observed at other seamount provinces worldwide (e.g., Hoernle et al., 2004; Geldmacher et al., 2005; Hoernle et al., 2010).

Assuming that the $^{40}Ar/^{39}Ar$ ages obtained at the three MBS are close (within a few million years) to the time when these islands were eroded and submerged below sea-level, a minimum subsidence rate can be calculated for each seamount taking the age and present water depth of the plateau of the seamount into account. Seamount C, the smallest and deepest edifice, displays the highest subsidence rate of ~41 m/Ma if it is actually a guyot. In contrast, the larger Haxby and Hubert Miller Seamounts both yield minimum subsidence rates of ~28 m/Ma despite their apparent age difference of ~5 Ma. We note that the plateau edges of the westernmost Seamounts 6 and 9 lie at roughly similar water depth (1600–1350 m, Table 1) as observed for Haxby and Hubert Miller Seamounts (1800–1200 m), which in turn may indicate a comparable subsidence history provided similarities in lithospheric age and structure west of Haxby Seamount as well as analogous formation ages of 60 ± 5 Ma.

The new ages (1.9 ± 0.3 Ma to 1.7 ± 0.3 Ma) for samples from the eastern submarine flank of Peter I Island are significantly older

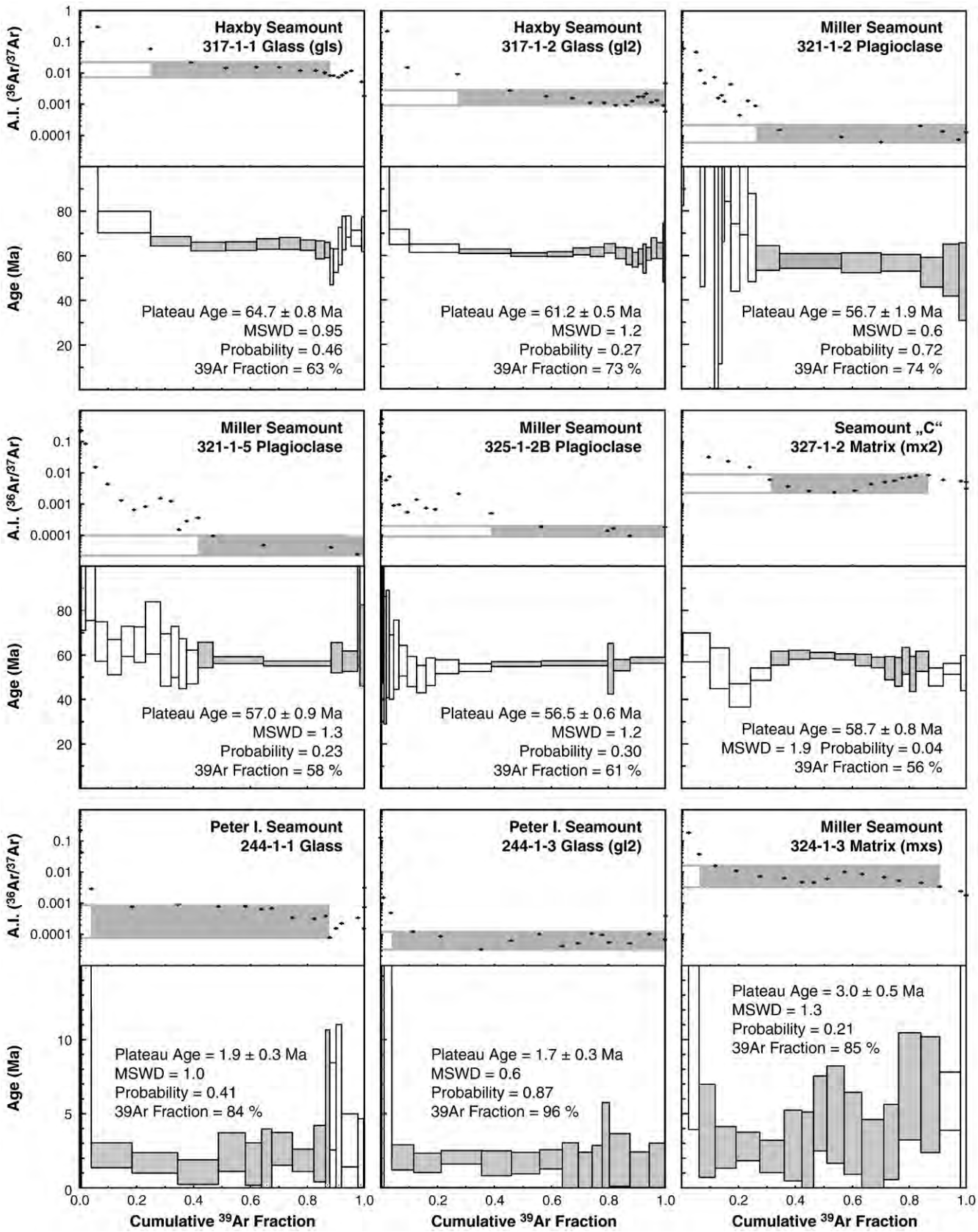

Fig. 7. Age spectra and alteration indices (A.I.) from $^{40}Ar/^{39}Ar$ laser step-heating experiments. Plateau steps and corresponding range of alteration index values are accentuated by gray shading. Stated errors are $\pm 2\sigma$.

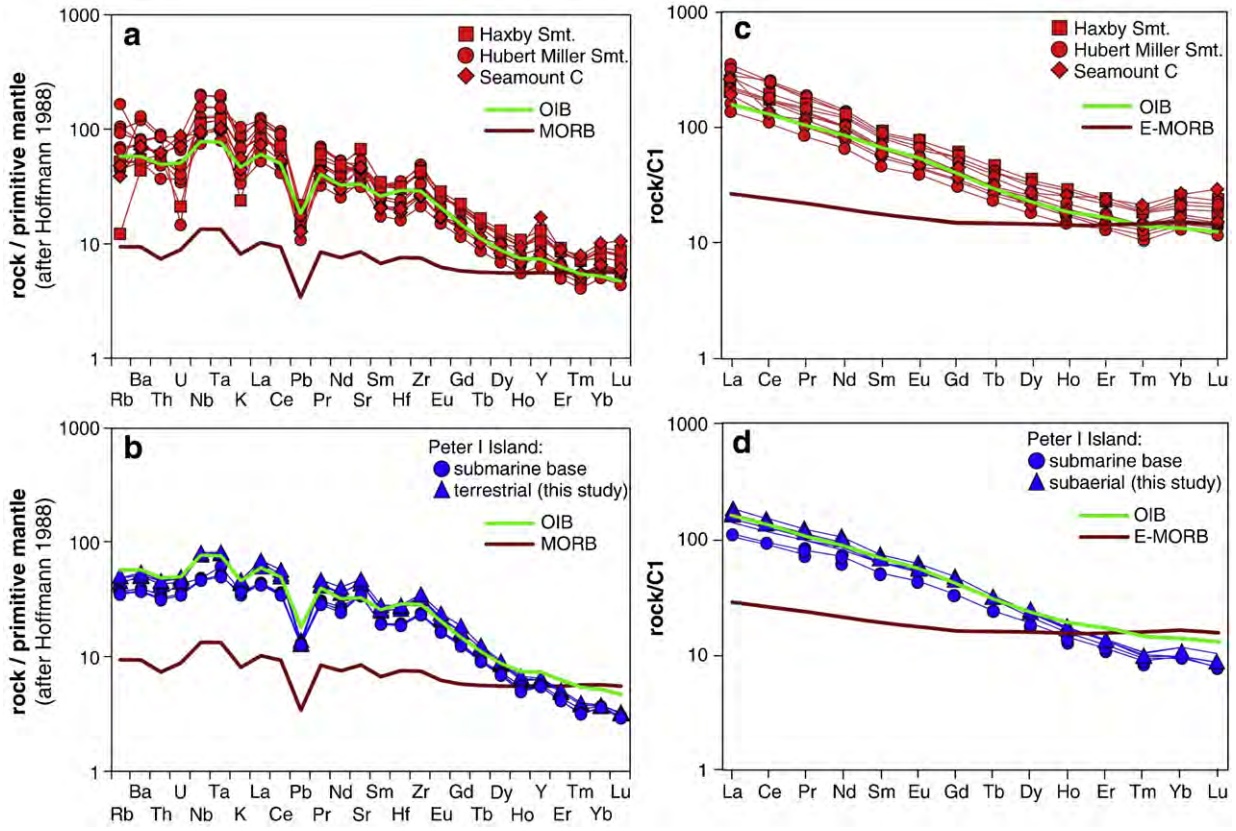

Fig. 8. Multi-element diagram normalized to primitive mantle after Hofmann (1988) for (a) MBS and (b) Peter I Island samples. The trace elements patterns of all the samples are similar to those of ocean islands basalts (OIB). OIB and E-MORB patterns are after Sun and McDonough (1989). REE diagrams normalized to C1 are after McDonough and Sun (1995) for (c) MBS and (d) Peter I Island samples.

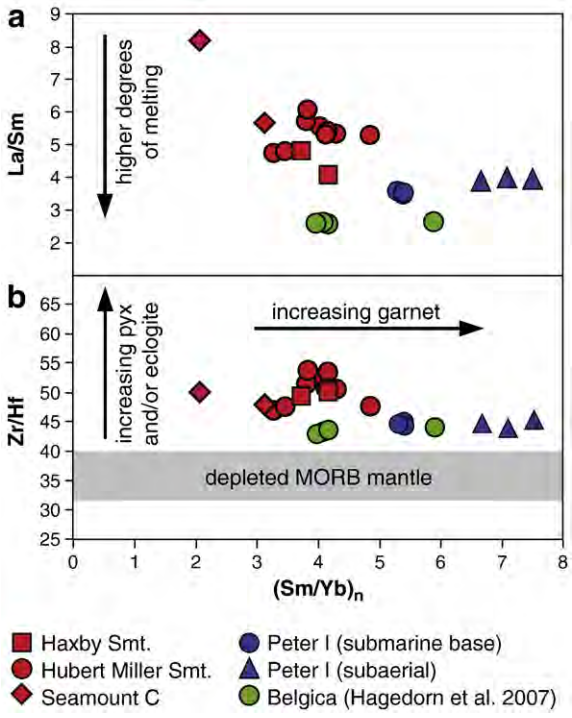

Fig. 9. (Sm/Yb)n (n = normalized to primitive mantle after Hofmann, 1988) versus (a) La/Sm and (b) Zr/Hf ratios. Lower La/Sm ratios indicate slightly higher degrees of partial melting for Peter I Island and Belgica Seamount than for MBS. Residual garnet and pyroxene and/or eclogite in the magma source is indicated by high $(Sm/Yb)_n$ ratios of 2 to 8 and relatively high Zr/Hf ratios (>40), respectively. Zr/Hf ratios for depleted MORB mantle (32–40) are after Salters and Stracke (2004) and Workman and Hart (2005).

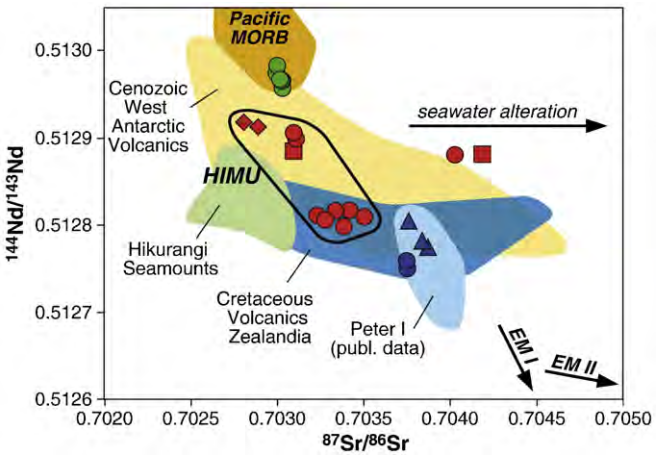

Fig. 10. $^{87}Sr/^{86}Sr$ versus $^{143}Nd/^{144}Nd$ isotope correlation diagram for MBS, Peter I Island, and Belgica Seamount samples. Symbols are as in Fig. 9. The field for West Antarctic volcanics is defined by data of the WARS (Rocholl et al., 1995; Rocchi et al., 2002a), the Jones Mountains in Ellsworth Land (Hart et al., 1995), and the Marie Byrd Land Volcanic Province (Hart et al., 1997; Panter et al., 1997, 2000), which extends along the Pacific margin of Marie Byrd Land. Most authors consider the volcanism at the Marie Byrd Land Volcanic Province and Jones Mountains as related to the WARS (e.g., Hart et al., 1995, 1997; Panter et al., 2000). The field for the Hikurangi Seamounts is based on data by Hoernle et al. (2010), published data for Peter I Island comprise analyses of subaerial basaltic lavas from Prestvik et al. (1990) and Hart et al. (1995). The field for Cretaceous volcanics of New Zealand is based on Tappenden (2003); Panter et al. (2006) and McCoy-West et al. (2010). HIMU, EM I, and EM II are after Zindler and Hart (1986) and Hart et al. (1992). Fields for Pacific MORB are from PetDB (http://www.earthchem.org/petdb) based on analyses of fresh glass.

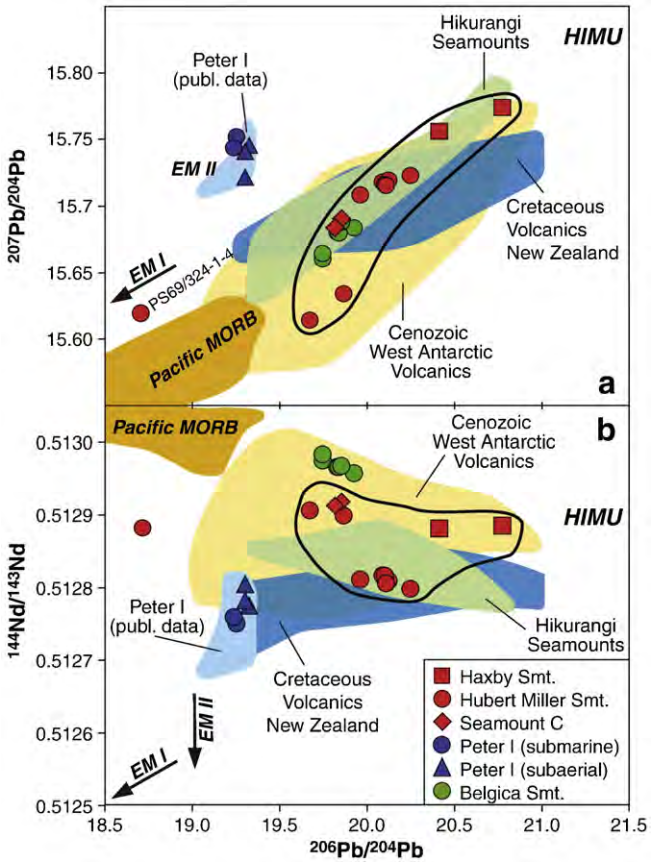

Fig. 11. (a) $^{206}Pb/^{204}Pb$ versus $^{207}Pb/^{204}Pb$, and (b) $^{143}Nd/^{144}Nd$ isotope correlation diagrams for MBS, Peter I Island, and Belgica Seamount samples. Symbols and data sources are as in Fig. 10.

than earlier published K–Ar ages (327 ± 88 ka to 111 ± 36 ka [1 sigma errors], Prestvik and Duncan, 1991) obtained on subaerial samples, which suggests that the fresh pillow glasses belong to an earlier submarine phase of this volcano.

Together with published Upper Miocene K–Ar ages for the Belgica Seamount (20–23 Ma, Hagedorn et al., 2007), the three seamount/ocean island volcanic provinces of the Amundsen and Bellingshausen Sea appear to have formed at distinct age intervals of 64–57 Ma for the MBS, at ~22 Ma for the De Gerlache Seamounts and at least

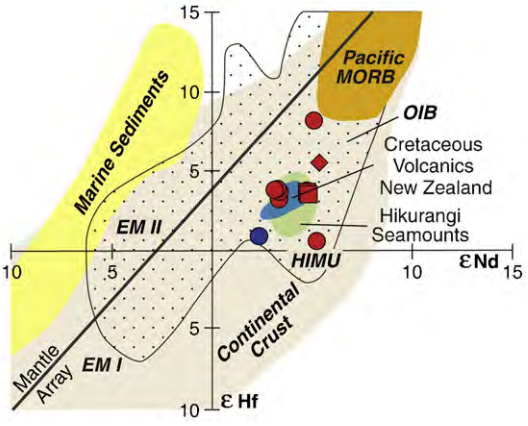

Fig. 12. εNd versus εHf isotope correlation diagram for MBS and Peter I Island samples. Figure modified after Geldmacher et al. (2003), symbols and data sources for Hikurangi Seamounts and Pacific MORB are as in Fig. 10. The New Zealand Cretaceous field includes Nd values by Tappenden (2003) and Hf values analyzed by Timm et al. (2010) for the Mandamus Complex, as well as data from McCoy-West et al. (2010) for Lookout Volcanics.

since ~2 Ma at Peter I Island. The three seamount/ocean island groups are spatially arranged in a highly elongated triangle with the MBS lying at its western tip and the De Gerlache Seamounts and Peter I Island forming the eastern limit (Fig. 1). The age distribution neither shows a correlation with spatial distribution nor a correlation with the age of the underlying ocean crust (e.g., Eagles et al., 2004a). A relationship between ages and plate motion cannot be observed, because neither the relative motion between the Bellingshausen Plate and the Antarctic Plate nor the absolute plate motion of the Antarctic Plate was significant for this time period (Eagles et al., 2004a,b; Wobbe et al., 2012; Doubrovine et al., 2012).

Therefore, the irregular spatial distribution of seamount ages in the Amundsen Sea and Bellingshausen Sea indicates that this magmatism occurred at distinct time intervals in spatially confined areas. This observation excludes an origin through a single stationary hotspot sensu Morgan (1971). Instead this regional age pattern of intraplate volcanism favors the presence of three melting anomalies independent in space and time. Before we explore possibilities of non-plume related intraplate volcanism, we will first briefly reiterate geochemical constraints on the origin of the magma sources.

7.2. Geochemical constraints on the origin of seamount magmatism

Lavas of all three seamount provinces (MBS, De Gerlache and Peter I Island) display a strong enrichment of the LREE relative to the HREE (Fig. 8c + d), clearly indicating partial melting in the presence of garnet. Likewise $(Sm/Yb)_N$, $(Gd/Yb)_N$ and $(Dy/Yb)_N$ are all >1 which, is consistent with residual garnet in the source (cf. Fig. 9b). Furthermore, the slight enrichment of Zr relative to Hf on the mantle-normalized plot (Fig. 8a + b) is also consistent with residual garnet (Hauri et al., 1994). Consequently, melt segregation in all three areas must have occurred in the garnet stability field >60–80 km or 40–50 km if garnet pyroxenite was in the source (Hirschmann and Stolper, 1996). High Zr/Hf (43–54, Fig. 9b), Nb/Ta (16–19) and low Zr/Sm (31–38) provide additional support for partial melting of eclogite/garnet pyroxenite (i.e. recycled ocean crust), rather than garnet peridotite, consistent with a HIMU component in the mantle source.

The isotopic signatures of MBS volcanic rocks are consistent with the presence of a HIMU-type mantle component in the source of these rocks (Figs. 10–12). The extremely radiogenic $^{206}Pb/^{204}Pb$ of the HIMU-endmember requires a high $^{238}U/^{204}Pb$ in the source; a component unlikely to develop in significant amounts within the convecting upper oceanic mantle without crustal recycling (see Stracke, 2012 for a recent review). HIMU is classically thought to reflect deep mantle recycling of oceanic crust by mantle plumes, ascending from deep in the mantle (Hofmann and White, 1982; White, 2010), however, from the lack of clear indications for the long-term existence of a classical mantle plume in the Amundsen Sea it is clear that alternative mechanisms are required to explain the occurrence of HIMU-type intraplate volcanism in this area, as has also been proposed for HIMU-type volcanic rocks in New Zealand (Hoernle et al., 2006).

Subaerial and submarine samples of Peter I Island exhibit small compositional differences with the submarine samples having higher SiO_2 and Al_2O_3 and slightly lower MgO, FeOt and TiO_2 contents than the subaerial samples. The slight differences in MgO, FeOt, Al_2O_3 and TiO_2 between submarine and subaerial lavas could be related through fractionation of olivine, pyroxene and possibly ilmenite from a subaerial melt composition, but this scenario cannot explain the higher incompatible element abundances in the subaerial lavas. Along with the slightly more alkaline character of the subaerial lavas in our sample set, the data indicates that the subaerial lavas could reflect slightly lower degrees of mantle melting, which would also explain their higher incompatible element abundances. Variations in the extent of partial melting are common during the life cycle of ocean island volcanoes with more alkaline compositions of lavas during the subaerial stage compared to less alkaline (tholeiitic) compositions during the

submarine shield stage (e.g., Frey et al., 1990). Even during the submarine stage, short-term variations in the degree of partial melting have been observed at Loihi Seamount in the Hawaiian Islands (Garcia et al., 1993).

The Pb isotopic composition of lavas from Peter I Island carries a clear EM II source signal (Fig. 11a) that is commonly thought to reflect contributions from pelagic sediments or upper continental crust (e.g., Zindler and Hart, 1986; Willbold and Stracke, 2010). The mafic composition of Peter I Island lavas, negative Pb anomalies and high Ce/Pb (~25 in submarine samples, 34–40 in subaerial samples) argue against shallow AFC processes such as sediment assimilation or preferred leaching of sedimentary Pb. This conclusion is similar to that of Hart et al. (1995), who explain the high $^{207}Pb/^{204}Pb$ signature of Peter I Island melts as evidence for the involvement of a mantle plume with EM II characteristics. We also note that the majority of global pelagic sediments have lower $^{206}Pb/^{204}Pb$ and $^{207}Pb/^{204}Pb$ ratios than observed in the Peter I Island lavas and thus involvement of modern pelagic sediment seems less likely. This is consistent with the Hf–Nd isotope ratios, which show that marine sediments did not influence the submarine sample of Peter I Island (Fig. 12). Ce/Pb lying within (or slightly above) the canonical array of 25 ± 5 for global OIB and MORB (after Hofmann et al., 1986) provides additional evidence for derivation from oceanic mantle rather than involvement of continental crust, which has Ce/Pb of 3–5. The solitary location of Peter I Island suggests that magmatism is related to a localized upwelling of EMII-like mantle but it is unclear whether this is connected to a blob rising from a thermal boundary such as the SW Pacific superswell or melting of a continental raft that drifted into the oceanic upper mantle during the final Gondwana breakup.

In summary, Cenozoic intraplate volcanism in the Amundsen Sea and Bellingshausen Sea requires involvement of depleted MORB mantle in the source with significant contributions of enriched components of HIMU and EM affinity. Due to the lack of clear evidence for the existence of a mantle plume in this region, a model is needed to explain the evidence for enriched (plume like) components in the source of Amundsen Sea intraplate volcanism and a non-plume related process to accomplish adiabatic mantle melting in an intraplate environment.

7.3. Origin of the HIMU component in non-hotspot related Southwest-Pacific and Antarctic volcanic provinces

Alkalic volcanism with HIMU-like incompatible-element and isotopic signatures, similar to the samples from MBS, is reported from numerous locations throughout the SW Pacific and West Antarctica. These include the Chatham Rise, Hikurangi Seamounts, intraplate volcanic fields in New Zealand, sub-Antarctic islands and West Antarctica (e.g., Weaver and Pankhurst, 1991; Baker et al., 1994; Weaver et al., 1994; Rocholl et al., 1995; Hart et al., 1997; Panter et al., 2000; Tappenden, 2003; Panter et al., 2006; Nardini et al., 2009; Hoernle et al., 2010). In all these localities, volcanic centers are diffusely distributed and do not show any age progression relative to plate motion. Most commonly, models suggest localized extension/upwelling of asthenosphere that induces melting of metasomatized lithosphere in thin spots to produce the diffuse alkaline magmatism.

Finn et al. (2005) postulate a "diffuse alkaline magmatic province (DAMP)", which formed without any rifting or plume upwelling. They temporally extend the DAMP into the Cenozoic and explain this magmatism by detachment of subducted slabs from the base of Gondwana lithosphere in the late Cretaceous. The sinking of material into the mantle is thought to have introduced Rayleigh Taylor instabilities

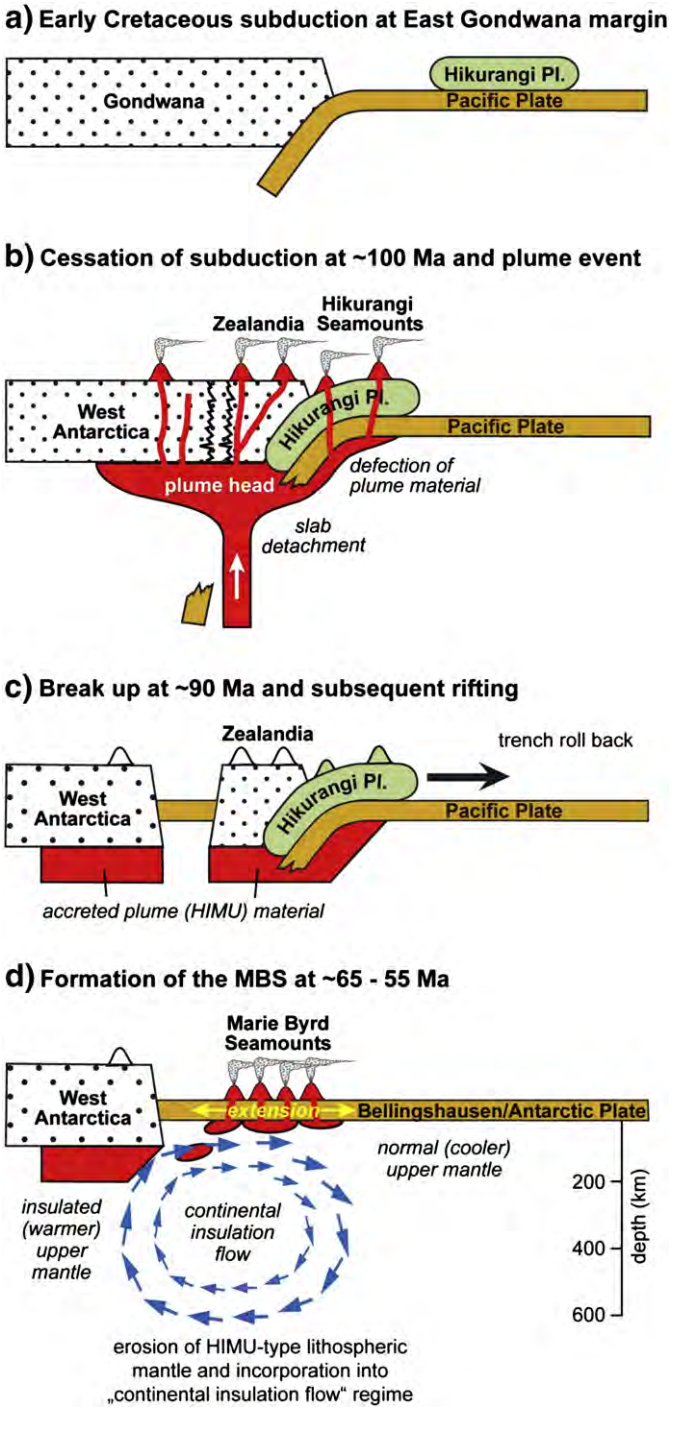

Fig. 13. Schematic sketch placing the origin of the MBS in a regional geodynamic context. (a) During the final stage of subduction of the Pacific Plate beneath the Zealandia/West Antarctic Gondwana margin, the Hikurangi Plateau approaches the subduction zone. (b) Forces acting upon the plate margin as, for example, the collision of the Hikurangi Plateau with Zealandia (e.g., Bradshaw, 1989; Davy et al., 2008) cause cessation of subduction and slab detachment. The impact of a plume head at that time was accompanied by large scale underplating of HIMU material beneath East Gondwana (e.g., Weaver et al., 1994; Hart et al., 1997) and the Hikurangi Plateau (possibly by deflection of the plume material by the subducting plate; Hoernle et al., 2010), triggering volcanism on West Antarctica and Zealandia and the formation of the Hikurangi Seamounts. (c) After subduction ended, extensional processes set in, causing the break-up of Zealandia from Marie Byrd Land at ~90 Ma and subsequent rifting, forming the oceanic crust of the Amundsen Sea (Eagles et al., 2004a). (d) Lateral temperature differences between warm mantle beneath the continental lithosphere and normal upper mantle drove continental-insulation flow (model modified after King and Anderson, 1995), allowing sub-continental mantle material to rise into the upper mantle beneath the adjacent oceanic lithosphere. At the Cretaceous/Tertiary boundary lithospheric extension at the southern margin of the Bellingshausen Plate (e.g., Wobbe et al., 2012) formed deep reaching faults that allowed rise of plume type melts and formation of the MBS from a magma source similar to that of the Hikurangi Seamounts and the West-Antarctic/Zealandia volcanoes. For further details and references see text.

along the Gondwana margin and activated lateral and vertical flow of warm Pacific mantle. After Finn et al. (2005) the interaction of the warm mantle with metasomatized lithosphere generated the HIMU geochemical characteristics of the DAMP. A shortcoming of this model is, however, that Finn et al. (2005) had to focus their study on old, continental fragments of East Gondwana, and could not include oceanic occurrences like the MBS, the De Gerlache Seamounts or the Hikurangi Seamounts which are situated on top of Hikurangi Plateau off New Zealand. An important difference between the seamounts and the continental alkaline provinces is that the majority of seamount provinces formed on relatively young oceanic crust. While HIMU signatures can be found in old continental terranes, HIMU-type volcanism in the oceans either requires rise of HIMU material from depth or some sort of refertilization of the upper mantle, especially when required shortly after ocean crust formation. No doubt, small-scale heterogeneities exist in the upper mantle away from mantle plumes as is evident from small off-axis seamounts that often have more enriched element and isotopic signatures than associated MORB (e.g., Brandl et al., 2012 and references therein). It seems, however, unlikely that such small-scale heterogeneities are present shortly after formation of the ocean crust to an extent that can explain the c. 1000–8000 km^3 of enriched melt required to form individual MBS (see Table 1 for volume estimates). In other words, even if Raleigh Taylor instabilities affected the Gondwana margin it seems unlikely that upwelling of regular Pacific upper mantle that underwent high degrees of melting shortly before can serve as the source of the HIMU-type compositions without refertilization.

Alternatively, the superplume beneath the SW-Pacific could have supplied a dense swarm of widely distributed and contemporaneously active secondary plumes causing diffuse alkaline volcanism (Suetsugu et al., 2009). Since it is in principle possible that secondary plumelets or blobs are continuously rising from the SW Pacific superswell (presumed to have stalled at the 660 km transition zone; Courtillot et al., 2003) they may also serve as the cause of volcanism forming the MBS and De Gerlache Seamounts. The age–distance relationship between MBS and the much farther north located Pacific Superswell is, however, unclear. Alternatively, Timm et al. (2010 and references therein) identify a low velocity anomaly extending from Chatham Rise off New Zealand to western Antarctica in at 600–1500 km depth and suggest that this could be the HIMU source polluting the upper mantle in this area since Cretaceous. Still it appears accidental that only the Marie Byrd Land margin was hit by a short-lived swarm of plumelets and no other oceanic region above this low velocity zone. Therefore we explore an alternative scenario for the oceanic seamount provinces off Marie Byrd Land based on reactivation of (HIMU) material, added to the base of continental lithosphere by plume activity during the pre-rifting stage of Marie Byrd Land/Zealandia.

On a regional scale, the MBS and Belgica Seamount data overlap with the data field of the Hikurangi Seamounts (Hoernle et al., 2010) in most isotope correlation diagrams (Figs. 10–12). A similar HIMU signature of Cretaceous rocks is also found at the Mandamus complex, the Lookout Volcanics in southern New Zealand, and the Chatham Islands (Weaver and Pankhurst, 1991; Tappenden, 2003; Panter et al., 2006; McCoy-West et al., 2010). During the Cretaceous these localities were assembled adjacent to Marie Byrd Land. It has been proposed that a HIMU-type plume or plume head may have caused breakup of the Gondwana margin in this region (e.g., Weaver et al., 1994; Hart et al., 1997; Storey et al., 1999; Hoernle et al., 2010). This plume event may have also influenced the source characteristics of the Hikurangi Seamounts (Hoernle et al., 2010) and may have been accompanied by large scale underplating of the Zealandia continental lithosphere by HIMU material (e.g. Weaver et al., 1994; Hart et al., 1997; Panter et al., 2000) (Fig. 13). During the mid Cretaceous the plume head expanded and thus forced rifting and the breakup of Gondwana as it impacted at the base of the continental lithosphere (Weaver et al., 1994). We note, however, that in contrast to other continental breakup related mantle plumes such as the Tristan-Gough in the South-Atlantic (and related Paraná and Entendeka continental flood basalts), a flood basalt event is absent on Zealandia and West Antarctica, possibly reflecting the convergent margin setting and associated thick continental lithosphere along the Gondwana margin. Together with the observation that the Cretaceous HIMU volcanism occurred only locally and was of relatively low volume, it seems likely that unmelted HIMU-mantle got attached at the base the Gondwana lithosphere, which underwent extension and rifting during that period. The proposed large-scale underplating of HIMU material beneath East Gondwana is consistent with the HIMU signature of many Cenozoic continental volcanics from West Antarctica (e.g., Hobbs Coast, Marie Byrd Land Volcanic Province, and WARS; cf. Figs. 10 and 11). Accordingly, many authors relate the Cenozoic HIMU similarities in West Antarctica to the reactivation of HIMU material, added to the base of the continental lithosphere during the earliest pre-rifting stage of the Marie Byrd Land through plume activity (e.g., Weaver et al., 1994; Rocholl et al., 1995; Hart et al., 1997; Panter et al., 2000). Alternatively Nardini et al. (2009 and references therein) call upon a late Cretaceous metasomatic event that caused variable elevation of U/Pb ratios in the sub-lithospheric mantle to an extend that explains the high $^{206}Pb/^{204}Pb$ of <20 Ma WARS volcanics and generation of their HIMU isotopic source signatures through radiogenic ingrowth over extremely short time scales. The regional context, however, requires the presence of a HIMU component that is already present in the Cretaceous, so that the metasomatic model of Nardini et al. (2009) for the formation of HIMU appears less likely.

Notably, the field for continental volcanic rocks of West Antarctica overlaps the data of the oceanic seamount provinces (Hikurangi Seamounts, MBS, De Gerlache) (Figs. 10 and 11), which have been formed close to the East Gondwana and West Antarctic margin, respectively. The samples also fall within the range of Cretaceous volcanic rocks of southern New Zealand, suggesting that all the above-mentioned volcanic suites originate from a similar HIMU source. This material may therefore also represent reactivation of fossil Cretaceous plume material that was originally attached to the base of the continental lithosphere during Marie Byrd Land/Zealandia break up. In contrast to the above mentioned onshore occurrences of Cenozoic HIMU volcanism, an additional transport mechanism and mode of reactivation is required to explain the marine equivalents of HIMU volcanism, because this material needs first of all be transferred into the oceanic mantle beneath the newly formed ocean basins of the Amundsen/Bellingshausen Sea followed by decompression melting (see Section 7.4 for details).

Admittedly, the arguments for an initial upwelling of plume-like material and storage at the base of the Gondwana lithosphere are solely based on geochemistry, which points to a HIMU like mantle. Such a source is unlikely to develop in situ in a mantle region affected by long-term subduction zone volcanism and small scale convection cells operating within the mantle wedge both leading to continuous depletion and replenishment of the arc mantle. On the other hand, upwelling of refertilized sub-continental lithospheric mantle (SCLM), isolated from mantle circulation for several billion years, can lead to the formation of EM type melts (e.g., Rudnick, 1995; Griffin et al., 2009; Hoernle et al., 2011; Soager et al., 2013). Ancient SCLM, however, features low $^{206}Pb/^{204}Pb$ and $^{143}Nd/^{144}Nd$ along with high $^{207}Pb/^{204}Pb$ and $^{87}Sr/^{86}Sr$ ratios, reflecting an ancient source that evolved with low U/Pb, Sm/Nd but high Rb/Sr (see Tang et al., 2013 for a recent review). Mantle regions that underwent such a fractionation and/or metasomatic event early in the earth's history are commonly thought to be involved in the formation of the early continental crust, having resided thereafter in the roots of stable Achaean cratons. In conclusion, SCLM seems to be a very unlikely candidate as source of the Cretaceous HIMU-type intraplate volcanism due the conflicting isotopic composition of SCLM (EM-like) and the long-term subduction zone setting of this area. Therefore, our preferred model for the origin of the HIMU component in the MBS and De Gerlache lavas is reactivation of fossil Cretaceous plume material, which was attached and stored at the base of the West Antarctic continental lithosphere during East Gondwana breakup.

7.4. Model for the formation of the Marie Byrd Seamounts

In the case of the West Antarctic volcanoes, underplated HIMU material may have been reactivated and caused to upwell during the WARS extension (e.g., Hart et al., 1997). For the formation of the c. 99 to 67 Ma Hikurangi Seamounts, Hoernle et al. (2010) propose the rise of HIMU-type material directly beneath the Hikurangi Plateau — a ~118 Ma oceanic LIP (Hoernle et al., 2010) that formed in connection with the Manihiki (Timm et al., 2011) and possibly the Ontong Java Plateaus (Taylor, 2006), through deflection of rising plume material beneath Zealandia by the subducting plate towards the Hikurangi Plateau, which was about to collide with the Zealandia margin at that time (Fig. 13a + b). For the MBS and De Gerlache Seamounts, however, a mechanism is required that enables lateral transport of the earlier emplaced HIMU material under Marie Byrd Land beneath the newly formed bordering oceanic lithosphere.

When the new oceanic crust of the Amundsen Sea formed, Zealandia (including the Hikurangi Plateau) rifted away from Marie Byrd Land in a northward direction (Fig. 13c), whereas the West Antarctic continental margin remained more or less fixed and developed as a relatively stable passive margin thereafter (e.g., Eagles et al., 2004a; Wobbe et al., 2012). Mutter et al. (1988) proposed a transition zone directly at the edge of thicker to thinner lithosphere where small convective flow is focused. In case of the MBS and De Gerlache Seamounts, the transition zone lies at the edge of the Antarctic continental lithosphere and the beginning of the adjacent oceanic crust. Several mechanisms such as edge-driven convection (EDC), small-scale convection (SSC) or shear-driven upwelling (SDU) have been suggested to explain edge-driven buoyant flow between young, thin and old, thicker lithosphere (e.g., King and Anderson, 1995, 1998; King and Ritsema, 2000; Huang et al., 2003; Dumoulin et al., 2008; Conrad and Behn, 2010 and references therein). For example, (super-) continents may effectively insulate the upper mantle, leading to a buildup of heat (Anderson, 1994; Lowman and Jarvis, 1995, 1996; Gurnis et al., 1998). These lateral temperature differences between the warm mantle beneath the continental lithosphere and normal upper mantle can drive an upper mantle convective flow pattern that leads to upwelling beneath the continent–ocean transition zone (Fig. 13d), the so-called "continental-insulation flow" (e.g., King and Anderson, 1995, 1998). From numerical modeling, King and Anderson (1998) suggest that lateral variations in temperature of at least 30 °C are required for continental insulation flow to significantly modify or even shut off the normal, downwelling EDC flow. Higher temperature anomalies (150–200 °C) would drive major upper mantle convection cells. In case of the Cretaceous East Gondwana lithosphere, the impact of the hot plume head may have caused additional heating of the mantle beneath the continental lithosphere and therefore reinforced the lateral variations in mantle temperature and consequently mantle convection. Notably, the pattern of flow resulting from continental insulation is opposite to that of normal EDC flow (King and Anderson, 1995, 1998). At the initial stages of rifting of a continent, upwelling should occur as warm mantle from beneath the continent that occupies the space created by spreading between the continental masses. At the Late Cretaceous Marie Byrd Land margin, this process would transfer mantle material directly from beneath the continent into the upper mantle under the adjacent oceanic lithosphere on which the MBS started to form at that time (Fig. 13d). Therefore we consider continental insulation flow as the most plausible mechanism to bring the HIMU plume-like material previously attached beneath Marie Byrd Land upwards beneath the adjacent oceanic lithosphere of the Bellingshausen/Antarctic Plate.

As the HIMU material was transported upwards beneath the newly formed oceanic lithosphere from beneath the thick Antarctica continental crust, the material will melt by decompression. The volcanism forming the De Gerlache Seamounts at ~22 Ma and the Pleistocene activity of Peter I Island, on the other hand, was most likely related to the De Gerlache Gravity Anomaly (Figs. 1 and 2), which represents a zone of lithospheric weakness resulting from a presumed WARS activity in this region (Müller et al., 2007), where pre-existing N–S striking faults allowed rise (and decompression melting) of HIMU-type material brought up beneath the oceanic lithosphere by mantle convection. The formation of the MBS may therefore have been triggered by a complex sequence of plate reorganization events that affected the West Antarctic margin and the Bellingshausen Plate in Late Cretaceous and Early Cenozoic (e.g., Eagles et al., 2004a; Wobbe et al., 2012). Shortly before the Bellingshausen Plate became incorporated into the Antarctic Plate at 61 Ma (Eagles et al., 2004a,b; Wobbe et al., 2012), a change in rotation of the Bellingshausen Plate from counterclockwise to clockwise was accompanied by lithospheric extension on its southern margin between 74 and 62 Ma (Wobbe et al., 2012). Contemporaneously the MBS started to form in that area (Fig. 2) (Fig. 13d), suggesting that lithospheric extension lead to upwelling of sub-lithospherically attached HIMU material and deep reaching faults that allowed rise of the HIMU-type melts and formation of large volcanic islands (Fig. 13d).

8. Conclusions

Our new morphological, geochronological, and geochemical data for the MBS combined with additional data for the De Gerlache and Peter I Island volcanic complexes (complementing previously published data) permit for the first time a comprehensive reconstruction of the origin and evolution of Cenozoic intraplate volcanism in the Amundsen Sea. The most important results are:

(1) Intraplate volcanism occurred during the entire Cenozoic at distinct time intervals in spatially confined areas in the Amundsen Sea, excluding an origin of this volcanism by a single stationary hotspot.
(2) The MBS and De Gerlache Seamount lavas show OIB signatures and posses a distinct HIMU component in their magma source similar to Late Cretaceous–Cenozoic volcanics of the Hikurangi Seamounts off New Zealand, intraplate volcanic fields in New Zealand, sub-Antarctic islands and the WARS, suggesting a common mantle source for these volcanic provinces.
(3) Peter I Island displays a strong EM affinity probably caused by shallow mantle recycling of a continental fragment.

Consequently, the formation of the MBS and De Gerlache Seamounts intraplate volcanism requires an alternative, non-hotspot scenario, which takes distinct melting anomalies independent in space and time and a non-hotspot related HIMU source into account.

Placing the morphological, geochronological, and geochemical data in a regional plate tectonic context, we conclude that the most plausible explanation for the HIMU-type intraplate volcanism in the Amundsen Sea is reactivation of HIMU-material, added to the base of the Antarctic lithosphere by a Late Cretaceous plume event. Major tectonic events, namely the separation of Zealandia from Antarctica during the final stage of the Gondwana break-up and subsequent formation of ocean crust give way for transport of the sub-lithospheric HIMU material beneath the Amundsen Sea oceanic crust by continental insulation flow. Extension caused by plate tectonic reorganization (MBS) and/or lithospheric weakening underneath the De Gerlache Gravity Anomaly (De Gerlache, Peter I Island) allow rise and adiabatic melting of the HIMU material resulting in the formation of these volcanic edifices. Reactivation of the MBS magmatism resulting in Pliocene low volume volcanism and the Pleistocene formation of Peter I Island documents ongoing magmatism in the Amundsen Sea.

The new model for the Amundsen Sea volcanism presented here adds to case examples for non-hotspot intraplate volcanism and provides additional evidence that HIMU-type intraplate volcanism is not necessarily a direct consequence of an actively upwelling, stationary mantle plume or hotspot.

Supplementary data to this article can be found online at http://dx.doi.org/10.1016/j.gr.2013.06.013.

Acknowledgments

We are grateful to Captain Pahl, the crew, and shipboard scientific party for their excellent support during RV Polarstern cruise ANT-XXIII/4. R. Gersonde (AWI) kindly provided the dredge samples from Belgica Seamount. D. Rau, S. Hauff, J. Sticklus (GEOMAR) and H. Anders (Uni-Bremen) are thanked for technical assistance during lab work and S. Gauger for help with processing of the bathymetric data. Discussions with Maxim Portnyagin, Jan Grobys, Graeme Eagles, and Christian Timm significantly helped to develop this paper. Furthermore, we are grateful for the constructive reviews of John Gamble and Tsuyoshi Komiya that helped to improve an earlier version of the manuscript. We thank Inna Yu Safonova for editorial handling and useful comments that helped to emphasize the importance of seamount formation. The German Research Foundation (DFG; Grants HO1833/15-1 to -3 to KH and FH) funded this research.

References

Anderson, D.L., 1994. Superplumes or supercontinents? Geology 22, 39–42. http://dx.doi.org/10.1130/0091-7613(1994)022<0039:SOS>2.3.CO;2.
Anderson, D.L., 2000. The thermal state of the upper mantle; no role for mantle plumes. Geophysical Research Letters 27 (22), 3623–3626. http://dx.doi.org/10.1029/2000GL011533.
Baker, I.A., Gamble, J.A., Graham, I.J., 1994. The age, geology, and geochemistry of the Tapuaenuku Igneous Complex, Marlborough, New Zealand. New Zealand Journal of Geology and Geophysics 37, 249–268. http://dx.doi.org/10.1080/00288306.1994.9514620.
Baksi, A.K., 2007. A quantitative tool for detecting alteration in undisturbed rocks and minerals — I: water, chemical weathering, and atmospheric argon. Special Paper of the Geological Society of America 430 (1197), 285–303. http://dx.doi.org/10.1130/2007.2430(16).
Batiza, R., Niu, Y., Zayac, W.C., 1990. Chemistry of seamounts near the East Pacific Rise: implications for the geometry of subaxial mantle flow. Geology 18, 1122–1125 (doi:1122-112510.1130/0091-7613(1990)018 < 1122:COSNTE > 2.3.CO;2).
Boger, S.D., 2011. Antarctica — before and after Gondwana. Gondwana Research 19 (2), 335–371. http://dx.doi.org/10.1016/j.gr.2010.09.003.
Bradshaw, J.D., 1989. Cretaceous geotectonic patterns in the New Zealand region. Tectonics 8, 803–820. http://dx.doi.org/10.1029/TC008i004p00803.
Brandl, P.A., Beier, C., Regelous, M., Abouchami, W., Haase, K.M., Garbe-Schönberg, D., Galer, S.J.G., 2012. Volcanism on the flanks of the East Pacific Rise: quantitative constraints on mantle heterogeneity and melting processes. Chemical Geology 298–299, 41–56. http://dx.doi.org/10.1016/j.chemgeo.2011.12.015.
Broch, O.A., 1927. Gesteine von der Peter I.-Insel, West Antarktis. Avhandlinger/Det Norske Videnskaps-Akademi, I, Matematisk-Naturvidenskapelig Oslo KL 9, 1–41.
Buchs, D.M., Arculus, R.J., Baumgartner, P.O., Ulianov, A., 2011. Oceanic intraplate volcanoes exposed: example from seamounts accreted in Panama. Geology 39, 335–338. http://dx.doi.org/10.1130/G31703.1.
Conrad, C.P., Behn, M.D., 2010. Constraints on lithosphere net rotation and asthenospheric viscosity from global mantle flow models and seismic anisotropy. Geochemistry, Geophysics, Geosystems 11, Q05W05. http://dx.doi.org/10.1029/2009GC002970.
Courtillot, V., Davaille, A., Besse, J., Stock, J., 2003. Three distinct types of hotspots in the Earth's mantle. Earth and Planetary Science Letters 205, 295–308. http://dx.doi.org/10.1016/S0012-821X(02)01048-8.
Davy, B.W., Hoernle, K., Werner, R., 2008. Hikurangi Plateau: crustal structure, rifted formation, and Gondwana subduction history. Geochemistry, Geophysics, Geosystems 9, Q07004. http://dx.doi.org/10.1029/2007GC001855.
Doubrovine, P.V., Steinberger, B., Torsvik, T.H., 2012. Absolute plate motions in a reference frame defined by moving hot spots in the Pacific, Atlantic, and Indian oceans. Journal of Geophysical Research 117, B09101. http://dx.doi.org/10.1029/2011JB009072.
Dumoulin, C., Choblet, G., Doin, M.P., 2008. Convective interactions between oceanic lithosphere and asthenosphere: influence of a transform fault. Earth and Planetary Science Letters 274, 301–309. http://dx.doi.org/10.1016/j.epsl.2008.07.017.
Eagles, G., Gohl, K., Larter, R., 2004a. High-resolution animated tectonic reconstruction of the South Pacific and West Antarctic Margin. Geochemistry, Geophysics, Geosystems 5, Q07002. http://dx.doi.org/10.1029/2003GC000657.
Eagles, G., Gohl, K., Larter, R., 2004b. Life of the Bellingshausen Plate. Geophysical Research Letters 31, L07603. http://dx.doi.org/10.1029/2003GL019127.
Eagles, G., Larter, R., Gohl, K., Vaughan, A.P.M., 2009. West Antarctic Rift System in the Antarctic Peninsula. Geophysical Research Letters 36, L21305. http://dx.doi.org/10.1029/2009GL040721.
Feldberg, M.J., 1997. A Geophysical Study of Seamount E, Bellingshausen Sea, Antarctica. Diploma Degree of Bachelor of Arts Wesleyan University, USA.
Finn, C.A., Müller, R.D., Panter, K.S., 2005. A Cenozoic diffuse alkaline magmatic province in the SW Pacific without rift or plume origin. Geochemistry, Geophysics, Geosystems 6, Q02005. http://dx.doi.org/10.1029/2004GC000723.
Fisher, A.T., Davis, E.E., Hutnak, M., Spiess, V., Zühlsdorff, L., Cherkaoui, A., Christiansen, L., Edwards, K., Macdonald, R., Villinger, H., Mottl, M.J., Wheat, C.G., Becker, K., 2003. Hydrothermal recharge and discharge across 50 km guided by seamounts on a young ridge flank. Nature 421, 618–621. http://dx.doi.org/10.1038/nature01352.
Foulger, G.R., Natland, J.H., 2003. Is "hotspot" volcanism a consequence of plate tectonics? Science 300, 921–922. http://dx.doi.org/10.1126/science.1083376.
Frey, F.A., Wise, W.S., Garcia, M.O., West, H., Kwon, S.-T., Kennedy, A., 1990. Evolution of Mauna Kea Volcano, Hawaii: petrologic and geochemical constraints on postshield volcanism. Journal of Geophysical Research 95 (B2), 1271–1300. http://dx.doi.org/10.1029/JB095iB02p01271.
Garcia, M.O., Jorgenson, B.A., Mahoney, J.J., Ito, E., Irving, A.J., 1993. An evaluation of temporal geochemical evolution of Loihi Summit Lavas: results from Alvin submersible dives. Journal of Geophysical Research 98 (B1), 537–550. http://dx.doi.org/10.1029/92JB01707.
Geldmacher, J., Hanan, B.B., Blichert-Toft, J., Harpp, K., Hoernle, K., Hauff, F., Werner, R., und Kerr, A., 2003. Hf isotopic variations in volcanic rocks from the Caribbean Large Igneous Province and Galápagos hotspot tracks. Geochemistry, Geophysics, Geosystems 422 (7). http://dx.doi.org/10.1029/2002GC000477.
Geldmacher, J., Hoernle, K., van den Bogaard, P., Duggen, S., Werner, R., 2005. New $^{40}Ar/^{39}Ar$ age and geochemical data from seamounts in the Canary and Madeira volcanic provinces: support for the mantle plume hypothesis. Earth and Planetary Science Letters 237, 85–101. http://dx.doi.org/10.1016/j.epsl.2005.04.037.
Geldmacher, J., Hoernle, K., van den Bogaard, P., Hauff, F., Klügel, A., 2008. Age and geochemistry of the Central American forearc basement (DSDP Leg 67 and 84): insights into Mesozoic arc volcanism and seamount accretion on the fringe of the Caribbean LIP. Journal of Petrology 49, 1781–1815. http://dx.doi.org/10.1093/petrology/egn046.
Gohl, K., 2007. The expedition ANTARKTIS-XXIII/4 of the research vessel Polarstern in 2006. Berichte zur Polar- und Meeresforschung (Reports on Polar and Marine Research), no. 557. Alfred Wegener Institute for Polar and Marine Research, Bremerhaven (166 pp. http://epic.awi.de/26756/).
Gohl, K., Nitsche, F.O., Miller, H., 1997a. Seismic and gravity data reveal Tertiary interplate subduction in the Bellingshausen Sea, Southeast Pacific. Geology 25, 371–374. http://dx.doi.org/10.1130/0091-7613(1997)025<0371:SAGDRT>2.3.CO;2.
Gohl, K., Nitsche, F., Vanneste, K., Miller, H., Fechner, N., Oszko, L., Hübscher, C., Weigelt, E., Lambrecht, A., 1997b. Tectonic and sedimentary architecture of the Bellingshausen and Amundsen Sea Basins, SE Pacific, by seismic profiling. In: Ricci, C.A. (Ed.), The Antarctic Region: Geological Evolution and Processes. Terra Antartica Publication, Siena, pp. 719–723.
Gohl, K., Denk, A., Wobbe, F., Eagles, G., 2013. Deciphering tectonic phases of the Amundsen Sea Embayment shelf, West Antarctica, from a magnetic anomaly grid. Tectonophysics 585, 113–123. http://dx.doi.org/10.1016/j.tecto.2012.06.036.
Griffin, W.L., O'Reilly, S.Y., Afonso, J.C., Begg, G.C., 2009. The composition and evolution of lithospheric mantle: a re-evaluation and its tectonic implications. Journal of Petrology 50, 1185–1204. http://dx.doi.org/10.1093/petrology/egn033.
Gurnis, M., Mueller, R.D., Moresi, L., 1998. Dynamics of Cretaceous vertical motion of Australia and the Australian–Antarctic discordance. Science 279, 1499–1504. http://dx.doi.org/10.1126/science.279.5356.1499.
Hagedorn, B., Gersonde, R., Gohl, K., Hubberten, H.-W., 2007. Petrology, geochemistry and K–Ar age constraints of the eastern De Gerlache Seamount alkaline basalts (Bellingshausen Sea, Southeast Pacific). Polarforschung 76 (3), 87–94 (http://epic.28876.d001).
Harris, R.N., Fisher, A.T., Chapman, D.S., 2004. Fluid flow through seamounts and implications for global mass fluxes. Geology 32, 725–728. http://dx.doi.org/10.1130/G20387.1.
Hart, S.R., Hauri, E.H., Oschmann, L.A., Whitehead, J.A., 1992. Mantle plumes and entrainment: isotopic evidence. Science 256, 517–520. http://dx.doi.org/10.1126/science.256.5056.517.
Hart, S.R., Blusztajn, J., Craddock, C., 1995. Cenozoic volcanism in Antarctica: Jones Mountains and Peter I Island. Geochimica et Cosmochimica Acta 59, 3379–3388. http://dx.doi.org/10.1016/0016-7037(95)00212-I.
Hart, S.R., Blusztajn, J., LeMasurier, W.E., Rex, D.C., 1997. Hobbs Coast Cenozoic volcanism, implications for the West Antarctic Rift System. Chemical Geology 139, 223–248. http://dx.doi.org/10.1016/S0009-2541(97)00037-5.
Hauri, E.H., Whitehead, J.A., Hart, S.A., 1994. Fluid dynamic and geochemical aspects of entrainment in mantle plumes. Journal of Geophysical Research 99 (B12), 24275–24300. http://dx.doi.org/10.1029/94JB01257.
Hein, J.R., Conrad, T.A., Staudigel, H., 2010. Seamount mineral deposits: a source of rare metals for high-technology industries. Oceanography 23, 184–189. http://dx.doi.org/10.5670/oceanog.2010.70.
Heinemann, J., Stock, J., Clayton, R., Hafner, K., Cande, S., Raymond, C., 1999. Constraints on the proposed Marie Byrd Land–Bellingshausen Plate boundary from seismic reflection data. Journal of Geophysical Research 104 (B11), 25321–25330. http://dx.doi.org/10.1029/1998JB900079.
Hirschmann, M.M., Stolper, E.M., 1996. A possible role for garnet pyroxenite in the origin of the "garnet signature" in MORB. Contributions to Mineralogy and Petrology 124, 185–208. http://dx.doi.org/10.1007/s004100050184.
Hoernle, K., van den Bogaard, P., Werner, R., Lissina, B., Hauff, F., Alvarado, G., Garbe-Schönberg, D., 2002. Missing history (16–71 Ma) of the Galápagos hotspot: implications for the tectonic and biological evolution of the Americas. Geology 30, 795–798. http://dx.doi.org/10.1130/0091-7613(2002)030<0795:mhmotg>2.0.co;2.
Hoernle, K., Hauff, F., Werner, R., Mortimer, N., 2004. New insights into the origin and evolution of the Hikurangi Oceanic Plateau (Southwest Pacific) from multi-beam mapping and sampling. Eos, Transactions of the American Geophysical Union 85 (41), 401–408. http://dx.doi.org/10.1029/2004EO410001.
Hoernle, K., White, J.D.L., van den Bogaard, P., Hauff, F., Coombs, D.S., Werner, R., Timm, C., Garbe-Schoenberg, D., Reay, A., Cooper, A.F., 2006. Cenozoic intraplate volcanism on

New Zealand: upwelling induced by lithospheric removal. Earth and Planetary Science Letters 248, 350–367. http://dx.doi.org/10.1016/j.epsl.2006.06.001.
Hoernle, K., Hauff, F., van den Bogaard, P., Werner, R., Mortimer, N., Geldmacher, J., Garbe-Schoenberg, D., Davy, B., 2010. Age and geochemistry of volcanic rocks from the Hikurangi and Manihiki Oceanic Plateaus. Geochimica et Cosmochimica Acta 74 (24), 7196–7219. http://dx.doi.org/10.1016/j.gca.2010.09.030.
Hoernle, K., Hauff, F., Werner, R., van den Bogaard, P., Gibbons, A.D., Conrad, S., Müller, R.D., 2011. Origin of Indian Ocean Seamount Province by shallow recycling of continental lithosphere. Nature Geoscience 4, 883–887. http://dx.doi.org/10.1038/ngeo1331.
Hofmann, A.W., 1988. Chemical differentiation of the Earth: the relationship between mantle, continental and oceanic crust. Earth and Planetary Science Letters 90, 297–314. http://dx.doi.org/10.1016/0012-821X(88)90132-X.
Hofmann, A.W., 2003. Sampling mantle heterogeneity through oceanic basalts: isotopes and trace elements. In: Carlson, R.W. (Ed.), The Mantle and Core. Elsevier, Amsterdam, pp. 61–101. http://dx.doi.org/10.1016/B0-08-043751-6/02123-X.
Hofmann, A.W., White, W.M., 1982. Mantle plumes from ancient oceanic crust. Earth and Planetary Science Letters 57, 421–436. http://dx.doi.org/10.1016/0012-821X(82)90161-3.
Hofmann, A.W., Jochum, K.-P., Seufert, M., White, W.M., 1986. Nb and Pb in oceanic basalts: new constraints on mantle evolution. Earth and Planetary Science Letters 79, 33–45. http://dx.doi.org/10.1016/0012-821X(86)90038-5.
Hole, M.J., LeMasurier, W.E., 1994. Tectonic controls on the geochemical composition of Cenozoic, mafic alkaline volcanic rocks from West Antarctica. Contributions to Mineralogy and Petrology 117, 187–202. http://dx.doi.org/10.1007/BF00286842.
Huang, J., Zhong, S., van Hunen, J., 2003. Controls on sub-lithospheric small-scale convection. Journal of Geophysical Research 108 (B8), 2405. http://dx.doi.org/10.1029/2003JB002456.
Hutnak, M., Fisher, A.T., Harris, R., Stein, C., Wang, K., Spinelli, G., Schindler, M., Villinger, H., Silver, E., 2008. Large heat and fluid fluxes driven through mid-plate outcrops on ocean crust. Nature Geoscience 1, 611–614. http://dx.doi.org/10.1038/ngeo264.
Irvine, T.N., Baragar, W.R.A., 1971. A guide to the chemical classification of the common volcanic rocks. Canadian Journal of Earth Sciences 8, 523–548. http://dx.doi.org/10.1139/e71-055.
King, S.D., Anderson, D.L., 1995. An alternative mechanism to flood basalt formation. Earth and Planetary Science Letters 136, 269–279. http://dx.doi.org/10.1016/0012-821X(95)00205-Q.
King, S.D., Anderson, D.L., 1998. Edge-driven convection. Earth and Planetary Science Letters 160, 289–296. http://dx.doi.org/10.1016/S0012-821X(98)00089-2.
King, S.D., Ritsema, J., 2000. African hotspot volcanism: small-scale convection in the upper mantle beneath cratons. Science 290, 1137–1140. http://dx.doi.org/10.1126/science.290.5494.1137.
Klügel, A., Hansteen, T.H., van den Bogaard, P., Strauss, H., Hauff, F., 2011. Holocene fluid venting at an extinct Cretaceous seamount, Canary Archipelago. Geology 39, 855–858. http://dx.doi.org/10.1130/G32006.1.
Koppers, A.A.P., Yamazaki, T., Geldmacher, J., Gee, J.S., Pressling, N., IODP Expedition 330 Scientific Party, 2012. Limited latitudinal mantle plume motion for the Louisville hotspot. Nature Geoscience 5, 911–917. http://dx.doi.org/10.1038/ngeo1638.
Larter, R.D., Cunningham, A.P., Barker, P.F., Gohl, K., Nitsche, F.O., 2002. Tectonic evolution of the Pacific margin of Antarctica — 1. Late Cretaceous tectonic reconstructions. Journal of Geophysical Research 107 (B12), 2345. http://dx.doi.org/10.1029/2000JB000052.
LeMasurier, W.E., Thomson, J.W., Baker, P., Kyle, P., Rowley, P., Smellie, J., Verwoerd, W. (Eds.), 1990. Volcanoes of the Antarctic Plate and Southern Oceans. Antarctic Research Series, 48. AGU, Washington, D.C., p. 487. http://dx.doi.org/10.1029/AR048.
Lowman, J.P., Jarvis, G.T., 1995. Mantle convection models of continental collision and breakup incorporating finite thickness plates. Physics of the Earth and Planetary Interiors 88, 53–68. http://dx.doi.org/10.1016/0031-9201(94)05076-A.
Lowman, J.P., Jarvis, G.T., 1996. Continental collisions in wide aspect ratio and high Rayleigh number two-dimensional mantle convection models. Journal of Geophysical Research 101 (B11), 25485–25497. http://dx.doi.org/10.1029/96JB02568.
McAdoo, D.C., Laxon, S., 1997. Antarctic tectonics: constraints from an ERS-1 satellite marine gravity field. Science 276, 556–560. http://dx.doi.org/10.1126/science.276.5312.556.
McCoy-West, A.J., Baker, J.A., Faure, K., Wysoczanski, R., 2010. Petrogenesis and origins of mid-Cretaceous continental intraplate volcanism in Marlborough, New Zealand: implications for the long-lived HIMU magmatic mega-province of the SW Pacific. Journal of Petrology 51, 2003–2045. http://dx.doi.org/10.1093/petrology/egq046.
McDonough, W.F., Sun, S.-S., 1995. The composition of the earth. Chemical Geology 120, 223–253. http://dx.doi.org/10.1016/0009-2541(94)00140-4.
McMurtry, G.M., Fryer, G.J., Tappin, D.R., Wilkinson, I.P., Williams, M., Fietzke, J., Garbe-Schönberg, D., Watts, P., 2004. Megatsunami deposits on Kohala Volcano, Hawaii, from flank collapse of Mauna Loa. Geology 32, 741–744. http://dx.doi.org/10.1130/G20642.1.
Miller, H., Grobe, H., 1996. The expedition ANTARKTIS-XI/3 of RV 'Polarstern' in 1994. Berichte zur Polarforschung, no. 188 (http://epic.10189.d001).
Montelli, R., Nolet, G., Dahlen, F.A., Masters, G., 2006. A catalogue of deep mantle plumes: new results from finite-frequency tomography. Geochemistry, Geophysics, Geosystems 7, Q11007. http://dx.doi.org/10.1029/2006GC001248.
Morgan, W.J., 1971. Convection plumes in the lower mantle. Nature 230, 42–43. http://dx.doi.org/10.1038/230042a0.
Müller, R.D., Gaina, C., Tikku, A., Mihut, D., Cande, S.C., Stock, J.M., 2000. Mesozoic/Cenozoic tectonic events around Australia. Geophysical Monograph 121, 161–188. http://dx.doi.org/10.1029/GM121p0161.
Müller, R.D., Gohl, K., Cande, S.C., Goncharov, A., Golynsky, A.V., 2007. Eocene to Miocene geometry of the West Antarctic Rift System. Australian Journal of Earth Sciences 54, 1033–1045. http://dx.doi.org/10.1080/08120090701615691.
Mutter, J.C., Buck, W.R., Zehnder, C.M., 1988. Convective partial melting 1. A model for the formation of thick basaltic sequences during the initiation of spreading. Journal of Geophysical Research 93 (B2), 1031–1048. http://dx.doi.org/10.1029/JB093iB02p01031.
Nardini, I., Armienti, P., Rocchi, S., Dallai, L., Harrison, D., 2009. Sr–Nd–Pb–He–O isotope and geochemical constraints on the genesis of Cenozoic magmas from the West Antarctic Rift. Journal of Petrology 50 (7), 1359–1375. http://dx.doi.org/10.1093/petrology/egn082.
Natland, J.H., Winterer, E.L., 2005. Fissure control on volcanic action in the Pacific. In: Foulger, G.R., Natland, J.H., Presnall, D.C., Anderson, D.L. (Eds.), Plumes, Plates and Paradigms. Geological Society of America, Boulder CO, pp. 687–710. http://dx.doi.org/10.1130/0-8137-2388-4.687.
Panter, K.S., Kyle, P.R., Smellie, J.L., 1997. Petrogenesis of a phonolite–trachyte succession at Mount Sidley, Marie Byrd Land, Antarctica. Journal of Petrology 38 (9), 1225–1253. http://dx.doi.org/10.1093/petroj/38.9.1225.
Panter, K.S., Hart, S.R., Kyle, P., Blusztanjn, J., Wilch, T., 2000. Geochemistry of Late Cenozoic basalts from the Crary Mountains: characterization of mantle sources in Marie Byrd Land, Antarctica. Chemical Geology 165, 215–241. http://dx.doi.org/10.1016/S0009-2541(99)00171-0.
Panter, K.S., Blusztanjn, J., Hart, S.R., Kyle, P.R., Esser, R., McIntash, W.C., 2006. The origin of HIMU in the SW Pacific: evidence from intraplate volcanism in southern New Zealand and Subantarctic islands. Journal of Petrology 47, 1673–1704. http://dx.doi.org/10.1093/petrology/egl024.
Portnyagin, M., Savelyev, D., Hoernle, K., Hauff, F., Garbe-Schönberg, D., 2008. Mid-Cretaceous Hawaiian tholeiites preserved in Kamchatka. Geology 36, 903–906. http://dx.doi.org/10.1130/g25171a.1.
Prestvik, T., Duncan, R.A., 1991. The geology and age of Peter I Øy, Antarctica. Polar Research 9, 89–98. http://dx.doi.org/10.1111/j.1751-8369.1991.tb00404.x.
Prestvik, T., Barnes, C.G., Sundvoll, B., Duncan, R.A., 1990. Petrology of Peter I Øy (Peter I Island), West Antarctica. Journal of Volcanology and Geothermal Research 44, 315–338. http://dx.doi.org/10.1016/0377-0273(90)90025-B.
Rocchi, S., Armienti, P., D'Orazio, M., Tonarini, S., Wijbrans, J., Di Vincenzo, G., 2002a. Cenozoic magmatism in the western Ross Embayment: role of mantle plume versus plate dynamics in the development of the West Antarctic Rift System. Journal of Geophysical Research 107 (B9), 2195. http://dx.doi.org/10.1029/2001JB000515.
Rocchi, S., LeMasurier, W.E., Di Vincenzo, G., 2002b. Uplift and erosion history in Marie Byrd Land as a key to possible mid-Cenozoic plate motion between East and West Antarctica. Geological Society of America Abstracts with Programs 34 (6), 238.
Rocholl, A., Stein, M., Molzahn, M., Hart, S.R., Wörner, G., 1995. Geochemical evolution of rift magmas by progressive tapping of a stratified mantle source beneath the Ross Sea Rift, Northern Victoria Land, Antarctica. Earth and Planetary Science Letters 131, 207–224. http://dx.doi.org/10.1016/0012-821X(95)00024-7.
Rudnick, R.L., 1995. Making continental crust. Nature 378, 571–578. http://dx.doi.org/10.1038/378571a0.
Safonova, I.Y., 2009. Intraplate magmatism and oceanic plate stratigraphy of the Paleo-Asian and Paleo-Pacific Oceans from 600 to 140 Ma. Ore Geology Reviews 35, 137–154. http://dx.doi.org/10.1016/j.oregeorev.2008.09.002.
Safonova, I.Y., Santosh, M., 2012. Accretionary complexes in the Asia–Pacific region: tracing archives of ocean plate stratigraphy and tracking mantle plumes. Gondwana Research 25, 126–158.
Salters, V.J.M., Stracke, A., 2004. Composition of the depleted mantle. Geochemistry, Geophysics, Geosystems 5, Q05B07. http://dx.doi.org/10.1029/2003GC000597.
Shank, T.M., 2010. Seamounts: deep-ocean laboratories of faunal connectivity, evolution, and endemism. Oceanography 23, 108–122. http://dx.doi.org/10.5670/oceanog.2010.65.
Smith, W.H.F., Sandwell, D.T., 1997. Global sea floor topography from satellite altimetry and ship depth soundings. Science 277, 1956–1962. http://dx.doi.org/10.1126/science.277.5334.1956.
Soager, N., Holm, P.M., Llambias, E.J., 2013. Payenia volcanic province, southern Mendoza, Argentina: OIB mantle upwelling in a backarc environment. Chemical Geology 349–350, 36–53. http://dx.doi.org/10.1016/j.chemgeo.2013.04.007.
Stock, J.M., 1997. Geophysical secrets beneath Antarctic waters. Engineering Sciences 60 (3), 18–27.
Storey, B.C., Leat, P.T., Weaver, S.D., Pankhurst, R.J., Bradshaw, J.D., Kelley, S., 1999. Mantle plumes and Antarctica–New Zealand rifting; evidence from Mid-Cretaceous mafic dykes. Journal of the Geological Society 156, 659–671. http://dx.doi.org/10.1144/gsjgs.156.4.0659.
Stracke, A., 2012. Earth's heterogeneous mantle: a product of convection-driven interaction between crust and mantle. Chemical Geology 330–331, 274–299. http://dx.doi.org/10.1016/j.chemgeo.2012.08.007.
Suetsugu, D., Isse, T., Tanaka, S., Obayashi, M., Shiobara, H., Sugioka, H., Kanazawa, T., Fukao, Y., Barruol, G., Reymond, D., 2009. South Pacific mantle plumes imaged by seismic observation on islands and seafloor. Geochemistry, Geophysics, Geosystems 10, Q11014. http://dx.doi.org/10.1029/2009GC002533.
Sun, S.S., McDonough, W.F., 1989. Chemical and isotopic systematics of oceanic basalts: implications for mantle composition and processes. In: Saunders, A.D., Norry, M.J. (Eds.), Magmatism in the Ocean Basins. Geological Society Special Publications, 42, pp. 313–345. http://dx.doi.org/10.1144/GSL.SP.1989.042.01.19.
Sutherland, R., Spasojevic, S., Gurnis, M., 2010. Mantle upwelling after Gondwana subduction death explains anomalous topography and subsidence history of eastern New Zealand and West Antarctic. Geology 38, 155–158. http://dx.doi.org/10.1130/G30613.1.
Tang, Y.-J., Zhang, H.-F., Ying, J.-F., Su, B.-X., 2013. Widespread refertilization of cratonic and circum-cratonic lithospheric mantle. Earth-Science Reviews 118, 45–68. http://dx.doi.org/10.1016/j.earscirev.2013.01.004.
Tappenden, V.E., 2003. Magmatic Response to the Evolving New Zealand Margin of Gondwana During the Mid–Late Cretaceous. (PhD thesis) University of Canterbury, Christchurch, New Zealand.
Tarduno, J.A., Duncan, R.A., Scholl, D.W., Cottrell, R.D., Steinberger, B., Thordason, T., Kerr, B.C., Neal, C.R., Frey, F.A., Torii, M., Carvallo, C., 2003. The Emperor Seamounts:

southward motion of the Hawaiian hotspot plume in earth's mantle. Science 301, 1064–1069. http://dx.doi.org/10.1126/science.1086442.

Taylor, B., 2006. The single largest oceanic plateau: Ontong Java–Manihiki–Hikurangi. Earth and Planetary Science Letters 241, 372–380. http://dx.doi.org/10.1016/j.epsl.2005.11.049.

Timm, C., Hoernle, K., Werner, R., Hauff, F., van den Bogaard, P., White, J., Mortimer, N., Garbe-Schoenberg, D., 2010. Temporal and geochemical evolution of the Cenozoic intraplate volcanism of Zealandia. Earth-Science Reviews 98, 38–64. http://dx.doi.org/10.1016/j.earscirev.2009.10.002.

Timm, C., Hoernle, K., Werner, R., Hauff, F., van den Bogaard, P., Michael, P., Coffin, M., Koppers, A., 2011. Age and geochemistry of the oceanic Manihiki Plateau, SW Pacific: new evidence for a plume origin. Earth and Planetary Science Letters 304 (1–2), 135–146. http://dx.doi.org/10.1016/j.epsl.2011.01.025.

Udintsev, G.B., Kurentsova, N.A., Teterin, D.E., Roshchina, I.A., 2007. Petrology of the Hubert Miller Seamount, Marie Byrd Seamounts Province, West Antarctic, Southern Ocean. Doklady Earth Sciences 415A (6), 895–900. http://dx.doi.org/10.1134/S1028334X07060141.

Uenzelmann-Neben, G., Gohl, K., 2012. Amundsen Sea sediment drifts: archives of modifications in oceanographic and climatic conditions. Marine Geology 299–302, 51–62. http://dx.doi.org/10.1016/j.margeo.2011.12.007.

Watts, A.B., Koppers, A.A.P., Robinson, D.P., 2010. Seamount subduction and earthquakes. Oceanography 23 (1), 166–173. http://dx.doi.org/10.5670/oceanog.2010.68#sthash.6fn0xSSg.dpuf.

Weaver, S.D., Pankhurst, R.J., 1991. A precise Rb–Sr age for the Mandamus Igneous Complex, North Canterbury, and regional tectonic implications. New Zealand Journal of Geology and Geophysics 34, 341–345. http://dx.doi.org/10.1080/00288306.1991.9514472.

Weaver, S.D., Storey, B.C., Pankhurst, R.J., Mukasa, S.B., DiVenere, V.J., Bradshaw, J.D., 1994. Antarctica–New Zealand rifting and Marie Byrd Land lithospheric magmatism linked to ridge subduction and mantle plume activity. Geology 22, 811–814. http://dx.doi.org/10.1130/0091-7613(1994)022<0811:ANZRAM>2.3.CO;2.

Wessel, P., Sandwell, D.T., Kim, S.-S., 2010. The global seamount census. Oceanography 23, 24–33. http://dx.doi.org/10.5670/oceanog.2010.60.

White, W.M., 2010. Oceanic island basalts and mantle plumes: the geochemical perspective. Annual Review of Earth and Planetary Sciences 38, 133–160. http://dx.doi.org/10.1146/annurev-earth-040809-152450.

Willbold, M., Stracke, A., 2010. Formation of enriched mantle components by recycling of upper and lower continental crust. Chemical Geology 276, 188–197. http://dx.doi.org/10.1016/j.chemgeo.2010.06.005.

Wilson, J.T., 1963. Evidence from islands on the spreading of the ocean floor. Nature 197, 536–538. http://dx.doi.org/10.1038/197536a0.

Winterer, E.L., Sandwell, D.T., 1987. Evidence from en-echelon cross-grain ridges for tensional cracks in the Pacific Plate. Nature 329, 534–537. http://dx.doi.org/10.1038/329534a0.

Wobbe, F., Gohl, K., Chambord, A., Sutherland, R., 2012. Structure and breakup history of the rifted margin of West Antarctica in relation to Cretaceous separation from Zealandia and Bellingshausen Plate motion. Geochemistry, Geophysics, Geosystems 13, Q04W12. http://dx.doi.org/10.1029/2011GC003742.

Workman, R.K., Hart, S.R., 2005. Major and trace element composition of the depleted MORB mantle (DMM). Earth and Planetary Science Letters 231, 53–72. http://dx.doi.org/10.1016/j.epsl.2004.12.005.

Zindler, A., Hart, S.R., 1986. Chemical geodynamics. Annual Review of Earth and Planetary Sciences 14, 493–571. http://dx.doi.org/10.1146/annurev.ea.14.050186.002425.

Publication 6.1.6:

Wobbe, F., Lindeque, A., **Gohl, K.** (2014). Anomalous South Pacific lithosphere dynamics derived from new total sediment thickness estimates off the West Antarctic margin. *Global and Planetary Change*, 123, 139-149, doi:10.1016/j.gloplacha.2014.09.006.

Author contributions: The paper was mainly written by Wobbe as part of his PhD project under the supervision of Gohl. Gohl was involved in providing the conceptual idea and significantly contributing to the discussion of the results. Lindeque (PhD student also under Gohl's supervision) contributed with seismostratigraphic analysis and sediment thickness estimates.

Global and Planetary Change 123 (2014) 139–149

Contents lists available at ScienceDirect

Global and Planetary Change

journal homepage: www.elsevier.com/locate/gloplacha

Anomalous South Pacific lithosphere dynamics derived from new total sediment thickness estimates off the West Antarctic margin

Florian Wobbe [a,*], Ansa Lindeque [b], Karsten Gohl [a]

[a] Alfred Wegener Institute for Polar and Marine Research, Am Alten Hafen 26, 27568 Bremerhaven, Germany
[b] TGS Geophysical Company (UK) Limited, 1 The Crescent, Surbiton, Surrey, KT6 4BN, United Kingdom

ARTICLE INFO

Article history:
Received 18 January 2014
Received in revised form 22 September 2014
Accepted 25 September 2014
Available online 28 October 2014

Keywords:
Sediment isopach map
Sediment thickness grid
Sediment volume
Residual basement depth
Dynamic topography
Paleotopography

ABSTRACT

Paleotopographic models of the West Antarctic margin, which are essential for robust simulations of paleoclimate scenarios, lack information on sediment thickness and geodynamic conditions, resulting in large uncertainties. A new total sediment thickness grid spanning the Ross Sea–Amundsen Sea–Bellingshausen Sea basins is presented and is based on all the available seismic reflection, borehole, and gravity modeling data offshore West Antarctica. This grid was combined with NGDC's global 5 arc minute grid of ocean sediment thickness (Whittaker et al., 2013) and extends the NGDC grid further to the south. Sediment thickness along the West Antarctic margin tends to be 3–4 km larger than previously assumed. The sediment volume in the Bellingshausen, Amundsen, and Ross Sea basins amounts to 3.61, 3.58, and 2.78 million km^3, respectively. The residual basement topography of the South Pacific has been revised and the new data show an asymmetric trend over the Pacific–Antarctic Ridge. Values are anomalously high south of the spreading ridge and in the Ross Sea area, where the topography seems to be affected by persistent mantle processes. In contrast, the basement topography offshore Marie Byrd Land cannot be attributed to dynamic topography, but rather to crustal thickening due to intraplate volcanism. Present-day dynamic topography models disagree with the presented revised basement topography of the South Pacific, rendering paleotopographic reconstructions with such a limited dataset still fairly uncertain.

1. Introduction

The accurate reconstruction of paleotopography is the main prerequisite for robust simulations of paleoclimate scenarios. Current paleotopographic models contain large uncertainties due to absent or sparse sediment thickness data and constraints on geodynamic conditions. Since the Southern Ocean plays an important role in global climate processes, we assess the sedimentary and geodynamic conditions of the Southern Pacific to ascertain these essential factors for modern paleotopographic reconstructions.

We present an improved sediment thickness grid for the West Antarctic margin, which is now based on all the available seismic reflection, borehole, and gravity modeling data. This new grid spans the Antarctic Peninsula, Bellingshausen Sea, Amundsen Sea, and Ross Sea and links to Whittaker et al.'s (2013) data off Victoria Land. In the first part of this publication, we compare our results to previous work and discuss possible implications for paleotopography and paleoclimate reconstructions of Antarctica.

In the second part, we analyze and re-evaluate the Late Cretaceous to present lithosphere dynamics of the South Pacific after the final breakup of Gondwana. The rifted continental margins of New Zealand and West Antarctica experienced different tectonic histories: As New Zealand drifted away from Antarctica it was subjected to excess tectonic subsidence of 500–900 m, with a maximum during the interval 70–40 Myr (Spasojevic et al., 2010; Sutherland et al., 2010). The conjugate Marie Byrd Land margin, by contrast, was deformed by movement of the Bellingshausen plate relative to Antarctica (Wobbe et al., 2012), affected by intraplate volcanism (Kipf et al., 2013), and covered by large amounts of glacial sediments (e.g., Rebesco et al., 1997; Scheuer et al., 2006a). The West Antarctic margin and its adjacent seafloor is currently more than 1000 m shallower than the conjugate New Zealand margin. It has been suggested that mantle upwelling following the Gondwana subduction cessation could have caused this anomalously high topography (e.g., Storey et al., 1999; Sieminski et al., 2003; Winberry and Anandakrishnan, 2004; Finn et al., 2005; Spasojevic et al., 2010; Sutherland et al., 2010). In order to test this hypothesis with new data, we determined the sediment-corrected basement topography for the South Pacific and compared it to (i) an empirical sediment-corrected depth model from the North Pacific (Crosby et al., 2006), (ii) various dynamic topography models (e.g., Ricard et al., 1993; Steinberger, 2007; Conrad and Husson, 2009; Spasojevic and Gurnis, 2012; Flament et al., 2013), and (iii) a current mantle shear wave velocity model (Schaeffer and Lebedev, 2013). The differences

* Corresponding author.
E-mail address: fwobbe@awi.de (F. Wobbe).

http://dx.doi.org/10.1016/j.gloplacha.2014.09.006

between the dynamic topography models are discussed and the implications for reconstructing the South Pacific paleobathymetry and paleotopography are highlighted.

2. Sediment thickness grids of the West Antarctic margin

We derived new 5 km and 5 arc minute resolution sediment thickness grids from seismic reflection and refraction data, from gravity models, and from data of selected drill sites on the West Antarctic margin of the Pacific (Ross Sea–Amundsen Sea–Bellingshausen Sea–Antarctic Peninsula).

2.1. Sediment thickness calculation

Total sediment thickness estimates of the continental margin and the deep ocean floor are largely based on multichannel seismic reflection surveys (Fig. 1). We used the two-way travel times (TWT) between the seafloor and the acoustic basement reflections along seismic reflection transects available from the Antarctic Seismic Data Library System (SDLS, Wardell et al., 2007, Table A.1 in the supplement) and along recently acquired and processed seismic profiles (e.g., ANT-18/5a, ANT-23/4, and ANT-26/3: Scheuer et al., 2006a,b; Lindeque and Gohl, 2010; Uenzelmann-Neben and Gohl, 2012; Wobbe et al., 2012; Gohl et al., 2013b; Kalberg and Gohl, 2014).

The TWT values, $2T$ in s, were converted to depth, Z in km, using Carlson et al.'s (1986) empirical relation $Z = 3.03\ln(1 - 0.52T)$. This method has been applied to seismic data acquired along the Antarctic Peninsula in past work (Rebesco et al., 1997; Scheuer et al., 2006a,b). Carlson et al.'s (1986) TWT–depth relationship is calibrated for sediments up to 1.4 km thick (~1.4 s TWT) only and the sediment thickness is considerably overestimated for TWTs larger than 2.8 s. This affects <5% of the data points, mainly located on the continental rise–slope transition. Due to the lack of area-wide seismic velocity models or downhole velocity measurements at drilling sites, we have to assume the acoustic velocity of sediments thicker than 2.8 s TWT.

P-wave velocities of 5–6 km thick sediments on the continental rise in polar regions typically range from 1800 to 4000 m s^{-1} (e.g., West Greenland, Chian et al., 1995; Suckro et al., 2012) or even 4200 m s^{-1} (e.g., East Greenland, Voss and Jokat, 2007). On the Amundsen Sea continental rise, sediment layer interval velocities from a P-wave refraction model (Lindeque and Gohl, 2010; Kalberg and Gohl, 2014) and from stacking velocities (Gohl et al., 2007; Uenzelmann-Neben and Gohl, 2012; Gohl et al., 2013b) range from 1600 to 4200 m s^{-1}. We determined the best fitting average acoustic velocity of sediments thicker than 2.8 s TWT to be 2818 m s^{-1} and converted all TWT values greater than 2.8 s to depth using this velocity.

The seismic data coverage of the Amundsen Sea Embayment shelf (Gohl et al., 2013b) is better than what the profiles used for this publication imply (Fig. 1). However, only few seismic lines reveal the top of basement, and those which do not were excluded. The limit of the sedimentary cover approaching the inner shelf is well documented (e.g., Gohl et al., 2013a,b, dotted line in Fig. 1).

2.2. Data merging and gridding

In order to extend data coverage of the mapped basement horizons from multichannel seismic data (Fig. 1) to the Ross Sea region, we incorporated total sediment thickness above the acoustic basement from Cooper et al. (1991). Wilson and Luyendyk (2009), whose data we included as well, estimated sediment thickness under the Ross Ice Shelf by extrapolating thickness trends in the Ross Sea from gravity anomalies. Four Deep Sea Drilling Project (DSDP) boreholes in the area of interest reach the basement. Their borehole depth measurements complement the sediment thickness data from the Ross Sea (sites 270 and 274, Hayes et al., 1975) and fill in the gaps of the most distal areas along the Antarctic Peninsula (sites 322 and 323, Hollister et al.,

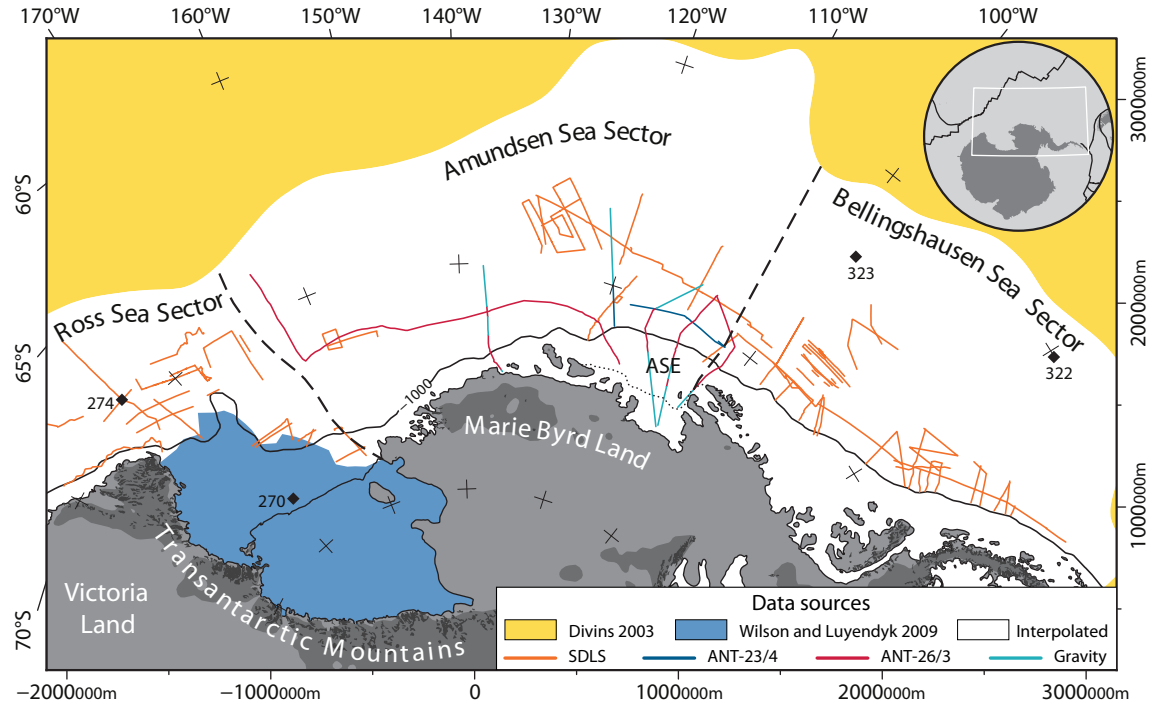

Fig. 1. Data sources used for compiling total sediment thickness and estimating sediment volumes. Areas based on gridded external data sources filled with solid colors (Divins, 2003; Wilson and Luyendyk, 2009). Data collected on transects are mostly multichannel seismic-reflection data available from the Antarctic Seismic Data Library System (SDLS, Wardell et al., 2007) and recent publications (ANT-23/4 and ANT-26/3: Scheuer et al., 2006a; Lindeque and Gohl, 2010; Uenzelmann-Neben and Gohl, 2012; Wobbe et al., 2012; Gohl et al., 2013b; Kalberg and Gohl, 2014). Some sediment thickness estimates in the Amundsen Sea sector are based on 2D gravity models (Wobbe et al., 2012). Dotted line outlines limit of sedimentary cover on inner Amundsen Sea Embayment (ASE) shelf (Gohl et al., 2013b). Polar stereographic projection with central meridian of 138°W and latitude of true scale at 71°S referenced to WGS84.

1976). Data from other DSDP, Ocean Drilling Project (ODP), and Antarctic Drilling (ANDRILL) drill sites along the West Antarctic margin were discarded because these boreholes do not yield the basement. Some sediment thickness estimates in the Amundsen Sea sector are based on a P-wave refraction model (Lindeque and Gohl, 2010; Kalberg and Gohl, 2014) and two-dimensional gravity models from Wobbe et al. (2012). The latter provide sediment thickness estimates along the axial extensions of adjacent seismic lines (light blue lines in Fig. 1). The limit of the sedimentary cover on the Amundsen Sea Embayment shelf was extrapolated east onto the Bellingshausen Sea shelf guided by gravity anomalies. We allocated values from the original ocean sediment thickness grid of the National Geophysical Data Center (NGDC, Divins, 2003) to areas further north and distant from the constrained data sources. These areas are roughly defined by the 100 m sediment isopach in the NGDC sediment thickness grid.

The compiled total sediment thickness point-based data (cf. Fig. A.1 in the supplement) were pruned by calculating 10 by 10 km block medians to remove short wavelengths and to avoid spatial aliasing during gridding. To fill the gaps between the points (white area in Fig. 1), the dataset was gridded using Smith and Wessel's (1990) continuous curvature splines algorithm with a tension factor of 0.2 to suppress local maxima and minima. Although data along the coastline were tapered to zero, we had to introduce about 150 further estimates of total sediment thickness to maintain a sensible appearance of the grid in areas remote from constrained sediment thickness. This is mostly the case, where the acoustic basement could not be identified on seismic profiles crossing the continental shelf. Our estimates are either plausible assumptions based on local geomorphology or inferred from the nearest constrained value.

Short range variations from the sediment thickness grid were removed by a second-order Butterworth low-pass filter with a cutoff wavelength of 100 km. We chose the Butterworth filter because it has no ripple in the passband at the expense of a relatively wide roll-off (Oppenheim and Schafer, 2009). The final grid was further resampled by bicubic interpolation to 5 km resolution. This new total sediment thickness grid is available in Antarctic Polar Stereographic Projection with a latitude of true scale at 71°S, referenced to WGS84 (Fig. 2).

The new regional Southern Pacific total sediment thickness grid was combined with the recently updated global sediment thickness grid of NGDC (Divins, 2003; Whittaker et al., 2013) to create an updated 5 by 5 minute global grid of ocean sediment thickness. The blending of the datasets was done by interpolating a 40 km buffer between the global and our smaller, regional grid, using continuous curvature splines with a tension factor of 0.2. The new total sediment thickness grids are available from PANGAEA (Wobbe et al., 2014).

2.3. Comparison to previous work and uncertainties

The presented total sediment thickness grid (Fig. 2) covers an area of more than 8 million km^2 and reveals major differences when compared to the sediment thickness compilation of Divins (2003). Divins' (2003) original NGDC global sediment thickness grid has recently been updated for the Australian–Antarctic region (Whittaker et al., 2013), as it became apparent that sediment thickness along the continental margins has been underestimated by more than 2000 m. The current NGDC grid, which excludes areas south of 70°S, largely underestimates sediment thickness off the Antarctic Peninsula and off Marie Byrd Land while slightly overestimating total sediment thickness around the De Gerlache Seamounts and the Marie Byrd Seamounts (cf. Figs. A.2 and A.3 in the supplement). Sediments in West Antarctic waters are approximately 4–4.8 km thick around the continental slope (approximately −1000 m contour in Fig. 2), which is about 3 km thicker than what Divins' (2003) NGDC compilation indicates. Sediments reach a maximum thickness of 6–8 km in glacial troughs on the Ross Sea shelf but taper off to less than 2 km further north. Total sediment thickness is estimated as larger than 4 km off the Antarctic Peninsula but less than 2–2.5 km off the coast of Marie Byrd Land and Victoria Land (west of DSDP site 274), and is maintained farther west (cf. Whittaker et al., 2013). Data from several proprietary seismic profiles (R/V Tangaroa, TAN0207 survey for the New Zealand UNCLOS program) off Chatham Rise indicate that Divins'

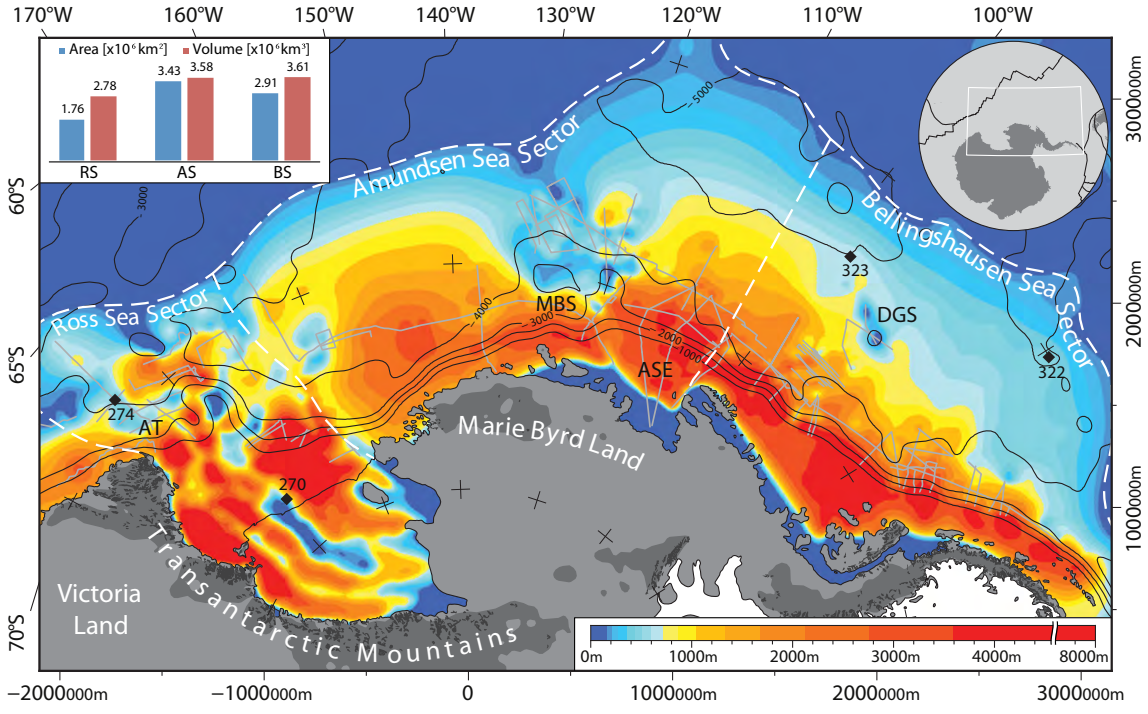

Fig. 2. The new total sediment thickness map of the Pacific margin of West Antarctica. Isopachs are color coded, contour lines indicate water depth in meter. White dashed lines delineate sediment catchment areas for the Ross Sea (RS), Amundsen Sea (AS) and Bellingshausen Sea (BS) basins. Compacted sediment volume estimates for these regions are illustrated in the top left corner. Black diamonds indicate locations of DSDP sites taken into account. Darker gray shading inland shows topography above 500 m. Rock outcrops from SCAR Antarctic Digital Database. AT — Adare Trough, DGS — De Gerlache Seamounts, MBS — Marie Byrd Seamounts. Polar stereographic projection with central meridian 138°W and true scale at 71°S.

(2003) sediment thickness estimates of West Antarctica's conjugate margin are accurate and do not compromise our residual basement depth calculation south of New Zealand in Section 3.

The mean West Antarctic sediment thickness (volume per deposition area ratio) varies slightly. It is largest in the Ross Sea and Bellingshausen Sea sectors (1.6 and 1.2 km), consistent with the very large flux associated with glacial sediment transport, and decreases to about 1.0 km in the Amundsen Sea sector. The total sediment volume amounts to 10 million cubic kilometers of which approximately 70% is equally distributed between the Amundsen and Bellingshausen Sea sectors (3.58 resp. 3.61×10^6 km^3), and the remaining 30% is spread across the Ross Sea sector (2.78×10^6 km^3).

Neglecting any margin parallel sediment transport, our calculations indicate that most of the terrigenous sediment influx from the West Antarctic originates from the smallest source area—the Antarctic Peninsula (15% of all area draining into the South Pacific). To illustrate this we determined the hypothetical minimum height of a sediment pile that would cover West Antarctica if all sediments were returned to their source areas by applying Wilson et al.'s (2012) estimates for in situ sediment density (1.95–2.1 g cm^3) and source rock density (2.6 g cm^3). DSDP and ODP boreholes around Antarctica yield a maximum pelagic fraction of 15%, which is not restored to the continent in this calculation. The terrigenous sediment source areas, draining into our three West Antarctic sectors, were determined from Zwally et al. (2012) present-day drainage system divides within the grounding line and west of the Transantarctic Mountains. Assuming these drainage system divides and their areas did not change with time, our calculations predict that sediments from the Ross Sea sector would pile up to a thickness of 2.9 km (or 640 m if source areas of East Antarctica are considered as well). Sediments from the Amundsen Sea sector would accumulate to a thickness of 3.8 km, and those from the Bellingshausen Sea sector would reach a height of 11 km. The very large value for the Bellingshausen drainage area can be explained by West Antarctica's high paleotopography (Wilson et al., 2012) which led to more erosion during the glacial. Earlier, subduction tectonics adjacent to the Antarctic Peninsula (e.g., Larter et al., 2002) may also have fostered an increased sediment influx into the basin.

Wilson and Luyendyk (2009) estimated a sediment volume of 2.0×10^6 km^3 above the oldest Ross Sea unconformity (RSU6, Oligocene and younger, e.g., Cooper et al., 1991). Our calculation takes into account a c. 30% larger Ross Sea deposition area and additional sediment thickness estimates along SDLS seismic reflection transects. Even though, the new sediment volume estimates above RSU6, 2.08×10^6 km^3, are not significantly larger, because the added distal deposition areas contain much less sediment than the ones in the central and western Ross Sea.

Although Scheuer et al.'s (2006a) sediment thickness grid of the Bellingshausen Sea and eastern Amundsen Sea shows east–west directed low frequency oscillation artifacts and occasionally large local minima and maxima, it compares reasonably well to our results in that the total sediment volume deviates by about 0.35×10^6 km^3 (cf. Figs. A.2 and A.3 in the supplement). This similarity can be attributed to the common database constraining the sediment thickness along seismic profiles, whereas the deviation is likely caused by a varied degree of data pruning and low-pass filtering.

The accuracy of the presented total sediment thickness grid varies proportionally to the distribution and abundance of seismic data offshore West Antarctica (Fig. 1). To a lesser degree, the sediment thickness data is affected by the TWT to depth conversion uncertainties rooted in the lack of seismic velocity models and drilling sites with key constraining downhole velocity data. The Ross Sea area is exceptionally well surveyed with a densely distributed seismic profile network and two basement yielding DSDP sites provide good calibration. The continental rise and slope within all sectors, except the westernmost and deeper Amundsen Sea are well mapped. In other places, where total sediment thickness is less constrained due to the absence of seismic reflection and borehole data, the thickness was interpolated over several hundred to thousand kilometers. Fortunately, most of these less constrained areas fall into the abyssal plains north of 70°S in the western Amundsen Sea sector, and north of 65°S in the eastern Amundsen Sea and Bellingshausen Sea sectors, where DSDP sites 322 and 323 hardly reported any sediment cover. Sediment thickness on the shelves of the Bellingshausen Sea and western Amundsen Sea could not be constrained by data but were based on observations from the central and eastern Amundsen Sea shelves. The largest uncertainties in the total sediment thickness grid are the limit of sedimentary cover and the sediment thickness on the inner Bellingshausen Sea.

3. Age of the oceanic lithosphere and basement depth

In Figs. 3 to 5 we present the derived set of digital grids that represent the South Pacific ocean floor ages, sediment-corrected basement depth, and oceanic residual basement depth. Collectively these provide an opportunity to study lithosphere dynamics of the West Antarctic margin. The residual basement depth (Fig. 5) is the difference between the sediment-unloaded basement depth (Fig. 4) and the predicted basement depth. The latter was derived from converting the crustal age (Fig. 3, Wobbe et al., 2012) to basement depth by using Crosby et al.'s (2006) North Pacific depth–age relationship, $d = -2821 - 315\sqrt{t}$.

We decided to apply Crosby et al.'s (2006) model for converting age to depth because it is based on sediment-corrected basement depths from the Pacific, and because it is unbiased by igneous crustal thickening. Therefore, it is considered suitable for detecting anomalies in the basement depth caused by, e.g., hotspot swells, plateaus, and seamounts. It should be noted however, that the differences between this chosen model and models proposed by other authors such as Stein and Stein (1992) GDH1 depth–age relationship are marginal (cf. profile 6 in Fig. 7), and in the context of the scale of this study considered negligible for studying large-scale basement depth anomalies (see Müller et al., 2008). In brief, the differences between GDH1 and Crosby et al.'s (2006) depth–age relationship range from −32 to 360 m for ages less than or equal to 90 Myr. The mean difference is 87 m and the median difference equals 55 m during this time interval. Both models are remarkably similar for ages younger than 80 Myr, which encompasses more than 96% of the area of interest (Fig. 3). Subsequently, GDH1 follows a shallower trend than Crosby et al.'s (2006) depth–age relationship.

Sediment loading was estimated from our total sediment thickness grid (Fig. 2), using the relationship between sediment thickness and isostatic correction from Sykes (1996). We calculated the sediment-unloaded basement depth by subtracting the isostatic effect using the water depths of the International Bathymetric Chart of the Southern Ocean (IBCSO, Arndt et al., 2013).

3.1. Residual basement depth anomalies

The residual basement depth of the South Pacific (Fig. 5) is largely positive, with a few exceptions along the Udintsev, Hazen and Tharp fracture zones (labeled in Fig. 3), southeast of the Campbell Plateau, and northwest of the Antarctic Peninsula. A positive residual basement depth anomaly indicates that the sediment-unloaded basement is shallower than expected based on Crosby et al.'s (2006) half-space cooling model. The magnitude of the residual basement depth anomaly and its irregular surface tend to correlate with hotspot trails, and with the size and abundance of seamounts. The sediment-unloaded basement is generally shallower in proximity to Antarctica. This is reflected in the values of the mean residual basement depth of the Antarctic and Pacific plate, being 485 and 204 m, respectively. The depth variation is best expressed by the root mean square, 699 and 394 m, respectively.

Fig. 6 illustrates the sediment-unloaded basement depth and the predicted basement depth on selected profiles that are parallel to flow lines crossing the Pacific–Antarctic Ridge. The profiles, which were selected carefully to avoid undulations near fracture zones, confirm that

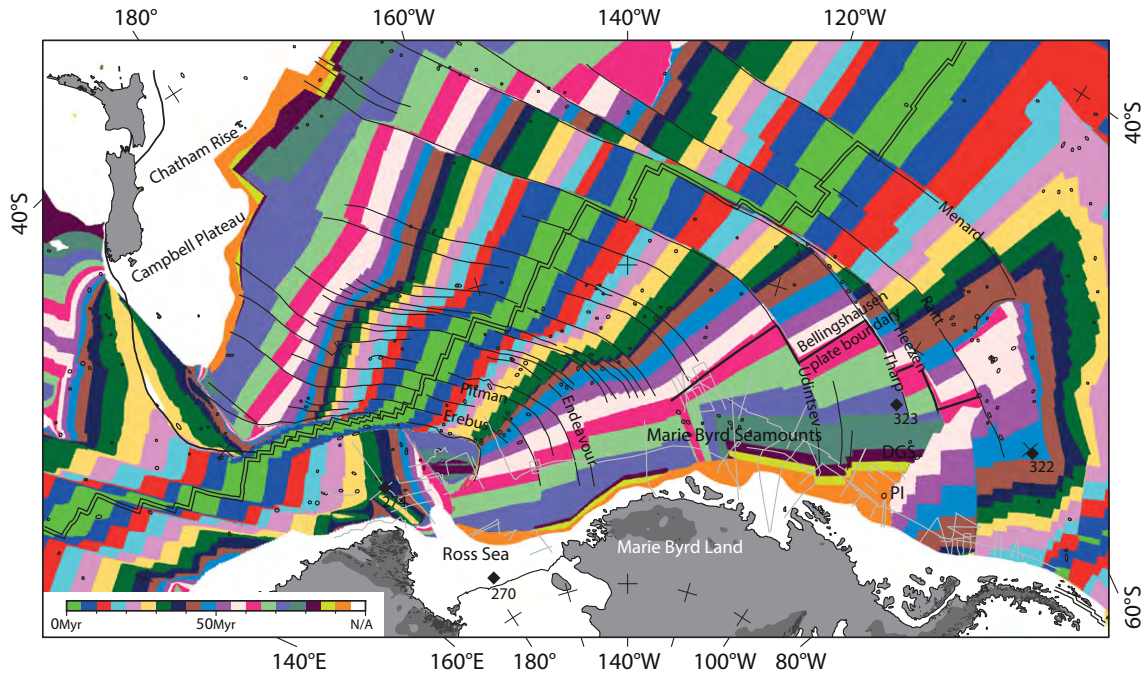

Fig. 3. Age of the oceanic lithosphere (Wobbe et al., 2012) overlain with locations of seamounts (black circles, Global Seamount Database, Kim and Wessel, 2011), fracture zones (black lines), and seismic and gravity profiles (light gray lines). Abbreviations same as Fig. 2 and PI — Peter I Island. Lambert conformal conic projection with central meridian 160°W and standard parallels 75°S and 69°S referenced to WGS84.

the sediment-corrected basement depth of the Antarctic plate is considerably higher than that of the Pacific plate. Due to the excessive sediment cover offshore West Antarctica, seafloor topography is more than 1000 m shallower compared to the conjugate New Zealand margin (Fig. 6). This is reflected by the isostatic correction for sediment thickness, which varies from 100 to 500 m south of the Campbell Plateau and Chatham Rise but then reaches 800–1500 m and, occasionally, more than 2000 m in the Ross Sea and Amundsen Sea. Despite the large difference in seafloor topography between the two conjugate margins, the sediment-unloaded basement depth, and hence the residual basement depth off Marie Byrd Land, usually differs by less than 250 m (Figs. 7 and A.4 in the supplement). Confined areas in the western Ross Sea, Marie Byrd Seamount area, and the Balleny Islands hotspot area south of the Pacific–Antarctic Ridge show residual basement depths exceeding 2000 m. Fig. 7 demonstrates that the residual basement depth usually oscillates between 0 and 500 m, and that a local

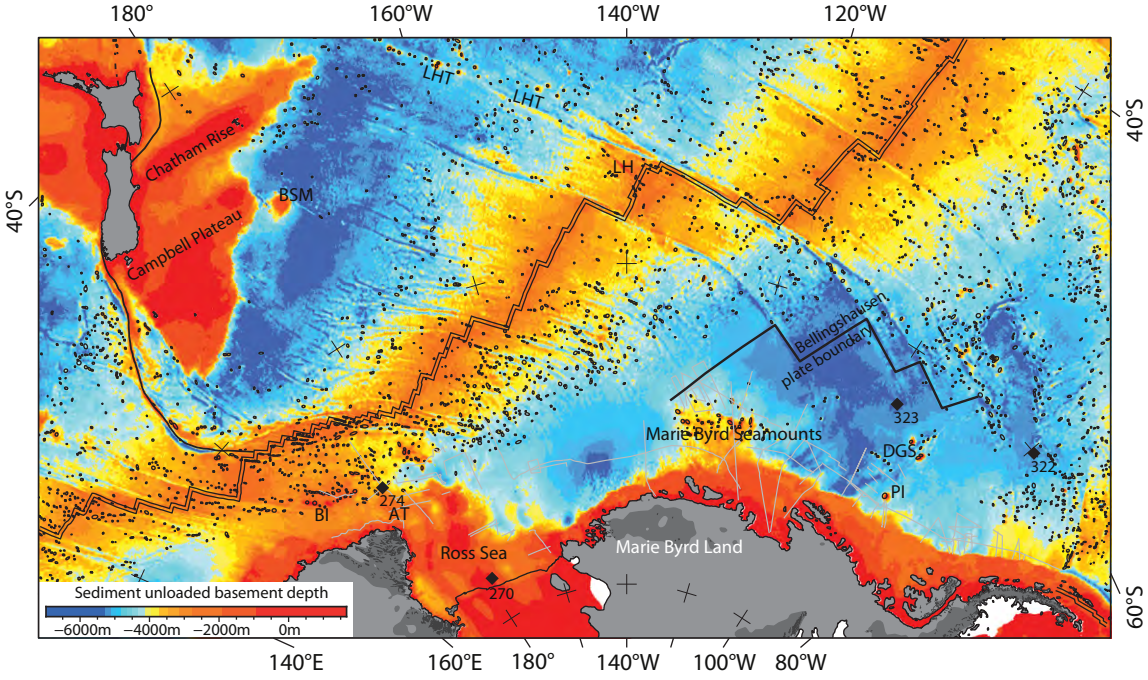

Fig. 4. Sediment-unloaded basement depth determined by applying the correction from Sykes (1996) using the sediment thickness from Fig. 2. Overlain with locations of seamounts (black circles, Global Seamount Database, Kim and Wessel, 2011). Abbreviations same as in previous figures and BI — Balleny Islands hotspot/Charcot Ridge, BSM — Bollons Seamount, LH — Louisville hotspot, LHT — Louisville hotspot trail. Lambert conformal conic projection with central meridian 160°W and standard parallels 75°S and 69°S.

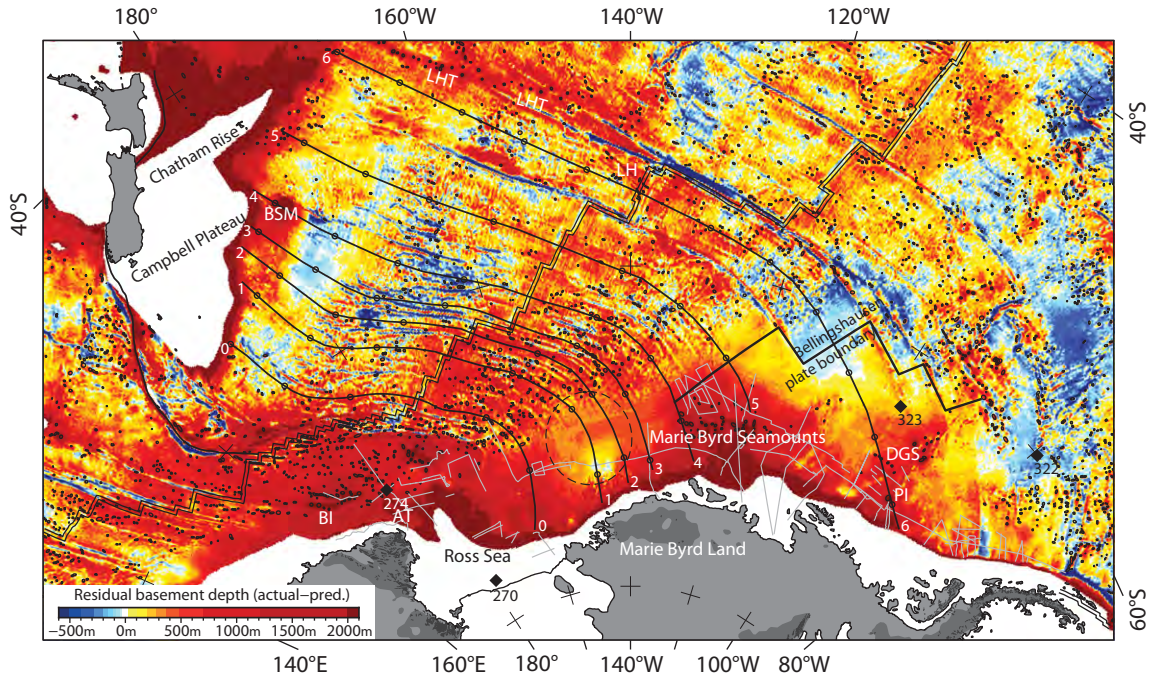

Fig. 5. Residual basement depth of the oceanic crust determined by calculating the difference between sediment-unloaded basement depth (Fig. 4) and predicted basement depth from applying Crosby et al.'s (2006) North Pacific depth–age relationship to the age distribution from Fig. 3. Profiles 0–6 along flow lines shown in Figs. 6, 7, and 10. Small circles along profiles placed 500 km apart. Dashed circle delineates Endeavour Anomaly. Abbreviations same as in previous figures. Lambert conformal conic projection with central meridian 160°W and standard parallels 75°S and 69°S.

maximum is located 200–700 km southeast from the Pacific–Antarctic Ridge in an area with a significantly higher seamount density (Global Seamount Database, Kim and Wessel, 2011 Fig. 5). Another distinctive feature within a circular area north of Marie Byrd Land is defined by an anomalously deep sediment-unloaded basement depth with values 500 m below the surrounding region. We name this the Endeavour Anomaly. The acoustic basement topography and sediment thickness at the Endeavour Anomaly are only constrained along a single west–east directed seismic profile across the Endeavour Fracture Zone (cf. Figs. 1 and 2). Further seismic data are not available in this region. The circular shape of the Endeavour anomaly is attributable to the interpolation algorithm used to grid the sediment thickness data, and its north–south expansion cannot be resolved.

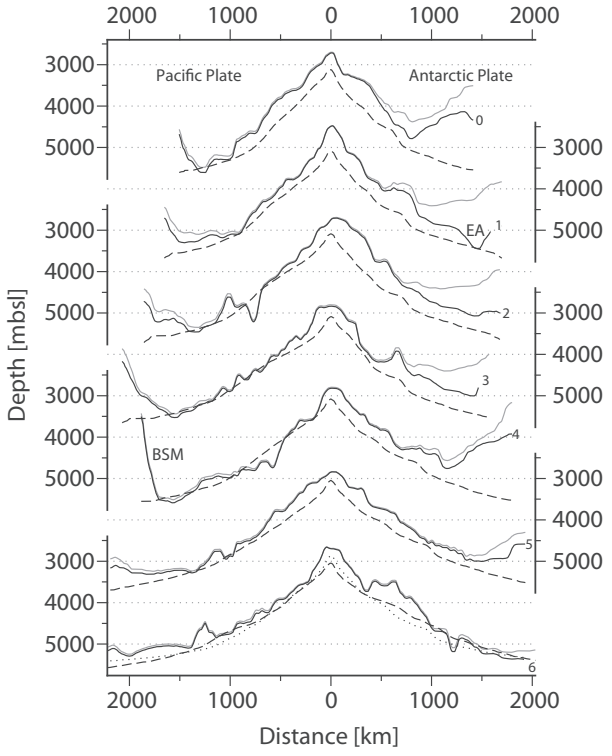

Fig. 6. IBCSO/GEBCO_08 bathymetry (gray line), sediment-unloaded basement depth from Fig. 4 (solid line), and predicted basement depth (dashed, Crosby et al., 2006) along profiles 0–6 across the Pacific–Antarctic Ridge (Fig. 5). Predicted basement depth from Stein and Stein's (1992) depth–age relationship (dotted line, profile 6, cf. Section 3). Abbreviations same as in previous figures and EA — Endeavour Anomaly.

3.2. Residual basement depth vs. seafloor roughness

Models explaining the morphology of mid-ocean ridge systems suggest that basement roughness depends on seafloor spreading rate and that an abrupt roughness intensification develops below a full spreading rate threshold of 60–70 mm Myr^{-1} (Small and Sandwell, 1989; Malinverno, 1991). This effect is readily visible in the roughness map in Fig. 8, where morphologically flat basement close to New Zealand and its conjugate margin off West Antarctica, formed along an initially fast spreading Pacific–Antarctic Ridge (>60 mm Myr^{-1}, Wobbe et al., 2012). Other parts of the ocean floor with large slope variability were formed less than 55 Myr ago when full-spreading velocities dropped below 60 mm Myr^{-1} (e.g., Larter et al., 2002; Eagles et al., 2004; Wobbe et al., 2012).

In the South Pacific, increased roughness is additionally caused by confined geological features including oceanic troughs, ridges, fracture zones, and seamounts. Cenozoic magmatism has been attributed to increased heat flow from the mantle (e.g., LeMasurier, 1990; Rocchi et al., 2002; Finn et al., 2005; Kipf et al., 2013). While seamounts such as the Balleny Islands, Marie Byrd Seamounts, De Gerlache Seamounts, and Peter I Island are limited morphological surface expressions of these magmatic centers, oceanic crust may respond to the underlying heat source with thermal uplift. Consequently, residual basement depth and seafloor roughness of the Antarctic plate often correlate (Figs. 5 and 8). However, the area with increased roughness between

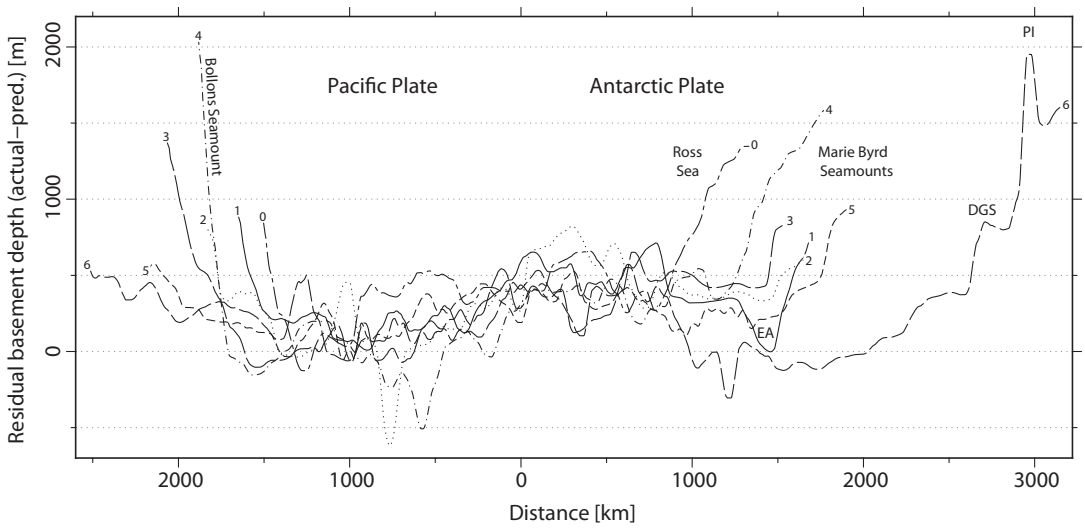

Fig. 7. Residual basement depth vs. distance from Pacific–Antarctic Ridge along profiles from Fig. 5. Abbreviations same as in previous figures.

Campbell Plateau and Pacific–Antarctic Ridge, for example, shows an opposing trend. Hence, seafloor roughness alone cannot be used to explain the residual basement depth distribution.

3.3. Residual basement depth vs. shear wave velocity

Schaeffer and Lebedev (2013) recently published a global tomographic shear wave velocity model of the upper mantle, which extends to a depth of 660 km. Fig. 9 displays the shear wave velocity anomaly of the uppermost mantle in four slices at different depths.

As expected, low shear wave velocities, which indicate increased heat flow in the mantle, coincide well with magmatic centers of Marie Byrd Land, Balleny Islands, and the Ross Sea area. In contrast, the Marie Byrd Seamounts, the De Gerlache Seamounts, and Peter I Island are underlain by mantle with anomalously high shear wave velocities that by implication may mean lower heat flow in the mantle. In these magmatic provinces off West Antarctica, the heat does not stem from the mantle directly below, as is the case in underplating, but may be provided by an upper mantle convective flow from warm mantle beneath the continental lithosphere of Marie Byrd Land (continental-insulation flow, Kipf et al., 2013, and references therein).

The distribution of seamounts that did not evolve from continental-insulation flow (e.g., Balleny Islands) matches the low shear wave velocity anomaly remarkably well. Similarly, the residual basement depth (Fig. 5) matches the shear wave velocity anomaly too. Noticeably, the shear wave velocity anomaly minimum below the mid-ocean ridges shifts asymmetrically in all depth slices. Particularly south of 60°S, the shear wave velocity anomaly is located 500 km south of the Pacific–Antarctic Ridge, where it also coincides with a local maximum of the residual basement depth (Figs. 7 and 10).

We chose Schaeffer and Lebedev's (2013) shear wave tomography as the most recently updated global mantle tomography model with

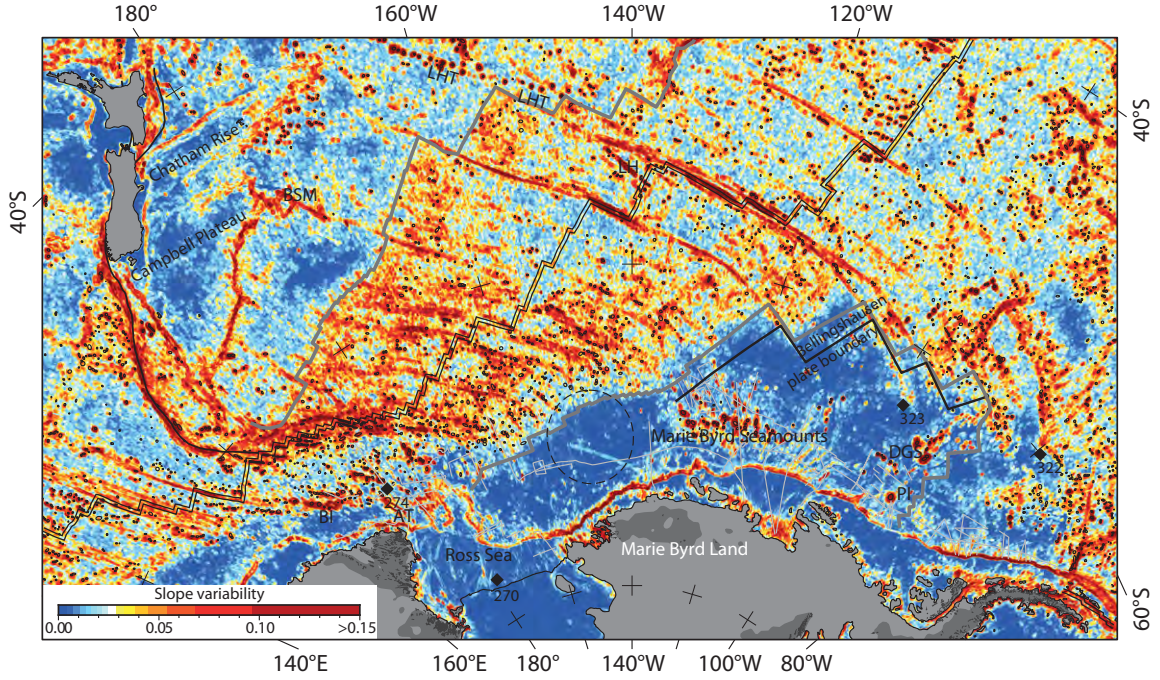

Fig. 8. Seafloor roughness computed by calculating the slope variability, $S_v = S_{max} - S_{min}$, over a 10′ × 10′ roving window from IBCSO/GEBCO_08 bathymetry. Thick gray lines are 55 Myr isochrons.

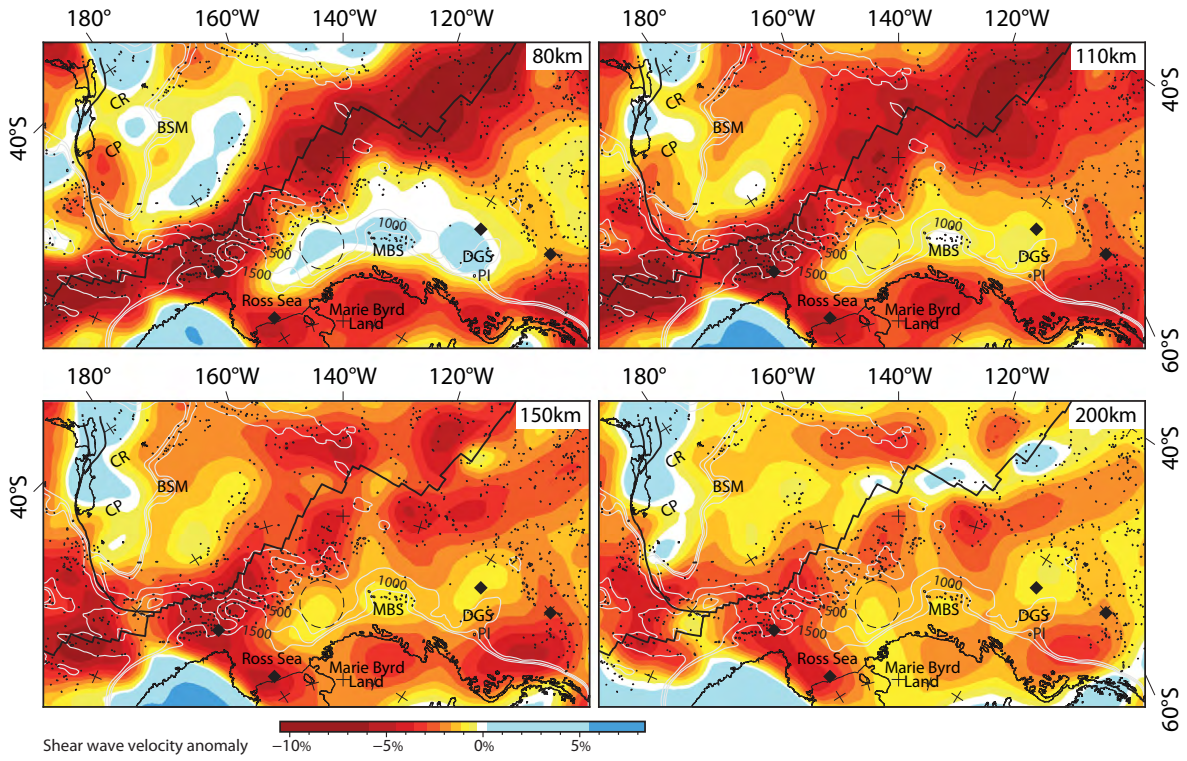

Fig. 9. Shear wave velocity anomalies (SL2013sv model, Schaeffer and Lebedev, 2013) of the upper mantle at 80, 110, 150, and 200 km depth with reference velocities of 4.38, 4.38, 4.39, and 4.45 km/s. Residual basement depth contours (500, 1000 and 1500 m) in gray.

major improvements on the resolution in oceanic regions and the Southern Hemisphere. However, the amplitude of the shear wave velocity anomaly in the study area decreases with depth and deviates less than 1% from zero at depths greater than 400 km. Distinct trends over the region or local extrema are absent. Well resolved shear wave velocity anomalies in this depth with an amplitude of less than 1% would require seismic velocity uncertainties better than 50 m s^{-1}.

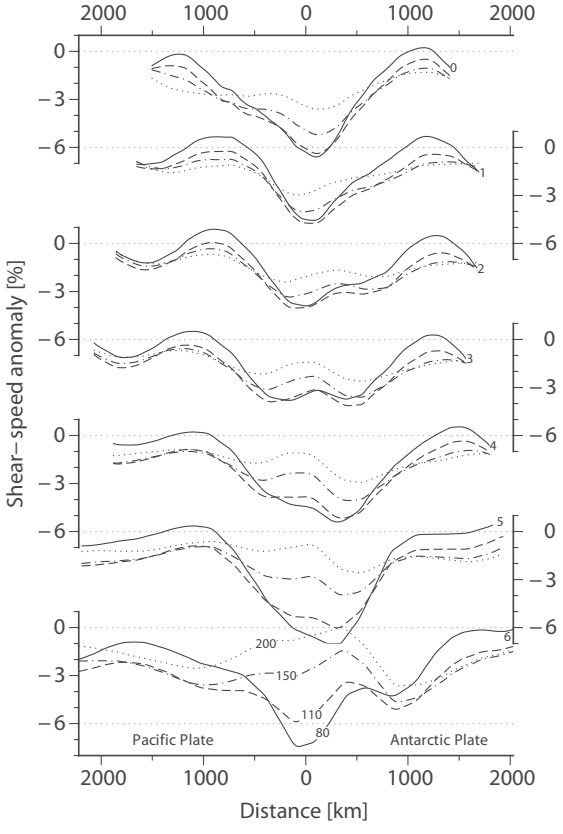

Fig. 10. Shear wave velocity anomalies of the upper mantle at 80, 110, 150, and 200 km depth vs. distance from Pacific–Antarctic Ridge along profiles 0–6 from Fig. 5.

4. Discussion

Improved paleoclimate and paleo-ice sheet models are subject to known limitations of current sediment volume approximations. With more robust sediment estimates, future reconstructions of paleotopography will improve our understanding of Antarctica's glaciation history. For instance, Wilson et al. (2013) estimated, based on the denudation history, that the total Antarctic ice volume since the Eocene–Oligocene transition was more than 1.4 times greater than previously assumed. This study and a recent work from Whittaker et al. (2013) both indicate that sediment thickness along the Antarctic margin has largely been underestimated. The landmass reduction of Antarctica due to erosion, therefore, has probably been larger than predicted (Wilson et al., 2012), and even larger ice sheet volumes may have covered Antarctica in the early times of glaciation. Of course, additional identifications of the volume and distribution of the pre-glacial to glacial components in the offshore sedimentary records are required in order to reconstruct the past topography for periods associated with large changes in climate proxies, such as the Eocene–Oligocene transition. However, the construction of pre-glacial to glacial sediment thickness grids is beyond the scope of this publication.

The previous section shows that there is a connection between residual basement depth and shear wave velocity on the one hand and magmatic processes on the other. Residual basement depth should also resemble the present-day dynamic topography. As opposed to isostatic topography resulting from density and thickness contrasts in the lithosphere, dynamic topography refers to the earth surface elevation effect due to mantle density inhomogeneities (e.g. Flament et al., 2013, and references therein). It develops over tens of millions of years and can exhibit several hundreds of meters in surface elevation

difference at long wavelengths. Dynamic topography models are derived from the present-day density structure of the mantle, subduction history, and plate-tectonic reconstructions. Uncertainties lie, for example, in the varying resolution of regional mantle convection models derived from global seismic tomography. As published dynamic topography models over the Southern Pacific suffer from large uncertainties, we compared our results with five different models (Ricard et al., 1993; Steinberger, 2007; Conrad and Husson, 2009; Spasojevic and Gurnis, 2012; Flament et al., 2013, Fig. A.5 in the supplement). These global studies of dynamic topography are limited to a lateral resolution of about 3000–5000 km. There are regional mismatches at scales below 10 000 km and even inverse correlations, especially in the Pacific realm (Flament et al., 2013). None of the five above mentioned dynamic topography models resolve local residual basement anomalies in the South Pacific. Although absolute amplitudes vary as much as 1500 m, all models propose a topographic high beneath the Pacific Plate, north of 60°S/150°W, which is in contrast with the residual basement depth (Fig. 5) and the shear wave anomaly (Fig. 9). Depending on the chosen model, dynamic topography beneath the Antarctic Plate and West Antarctica varies between −500 and 1000 m, and the magnitude beneath New Zealand is usually consistent with that beneath Marie Byrd Land.

Mantle upwelling following the Gondwana subduction cessation around 100 Myr (e.g. Laird and Bradshaw, 2004) has been suggested, but its extension beneath the West Antarctic margin remains unclear (e.g., Storey et al., 1999; Sieminski et al., 2003; Winberry and Anandakrishnan, 2004; Finn et al., 2005). However, basement depth, mantle shear wave velocity anomaly (Schaeffer and Lebedev, 2013), and Kipf et al.'s (2013) continental-insulation flow model show that upper mantle convective flow is solely confined to an area located beneath Marie Byrd Land and the Ross Sea. Spasojevic et al. (2010) and Sutherland et al. (2010) constructed models of Late Cretaceous to Cenozoic mantle flow, attributed to low density material above the Gondwana slab graveyard beneath Antarctica, to predict dynamic topography. Their models, which are based on present-day bathymetry, explain the high topography of the Ross Sea and Marie Byrd Land region as well as anomalous postrift Campbell Plateau subsidence. Our findings complement Sutherland et al.'s (2010) dynamic topography model, and our total sediment thickness estimates confine areas of anomalous basement elevation more precisely. For example, Sutherland et al. (2010) attributed excess topography (0.5–2.0 km) offshore Marie Byrd Land and in the Ross Sea region to dynamic topography. Our results confirm this for the Ross Sea as well as the Balleny Islands hotspot area. However, the residual basement depth off Marie Byrd Land does not exceed that south of Campbell Plateau by more than 250 m (Figs. 7 and A.4 in the supplement). East of the Ross Sea area, anomalously high basement topography is associated with magmatic processes driven by continental-insulation flow only (Marie Byrd Seamounts, De Gerlache Seamounts, Peter I Island, e.g., Kipf et al., 2013). Oceanic crust elsewhere in that region seems unaffected by mantle processes (e.g., Endeavour Anomaly). Sutherland et al.'s (2010) present day dynamic topography model coincides with our positive residual basement depth anomaly in the Ross Sea, but their proposed topography high beneath the Pacific Plate north of the Pacific–Antarctic Ridge lacks an equal counterpart anomaly in the residual basement depth.

A peculiar feature of the residual basement anomaly is its asymmetry over the Pacific–Antarctic Ridge, with a local maximum south of the spreading center, exactly where Campbell Plateau passed through—according to recent South Pacific plate motion models (e.g., Larter et al., 2002; Eagles et al., 2004; Wobbe et al., 2012)—during 70–40 Myr (cf. Fig. A.6 in the supplement). This time interval also marks the peak subsidence of the Campbell Plateau as it moved away from Antarctica to its present-day position (Sutherland et al., 2010). Although residual basement depth represents only a snapshot of dynamic topography, which occurs over tens of millions of years (Flament et al., 2013), the anomalous basement elevation south of the Pacific–Antarctic Ridge seems to be caused by processes persisting since the Cretaceous separation of New Zealand from Antarctica. It should be kept in mind, though, that until more robust dynamic topography models become available, predictions of the South Pacific paleotopography remain highly speculative.

5. Conclusions

Seismic data, recently acquired along the West Antarctic margin, suggests that Divins' (2003) minimum sediment thickness estimates along the West Antarctic margin are much too low. We present a new total sediment thickness grid spanning the Ross Sea–Amundsen Sea–Bellingshausen Sea basins based on available seismic reflection, borehole, and gravity modeling data in West Antarctica (Fig. 2). Our sediment thickness and volume estimates are consistent with previous analyses that indicate larger sediment amounts on Antarctica's margin than previously assumed (e.g., Rebesco et al., 1997; Scheuer et al., 2006a; Whittaker et al., 2013). We therefore extended Divins' (2003) original NGDC grid further south by merging our new data with data from Scheuer et al. (2006a), Wilson and Luyendyk (2009), and Whittaker et al. (2013) into an updated 5 by 5 minute global grid of total ocean sediment thickness. The sediment thickness estimation involved interpolation over areas without data constraints, but fortunately most of the less constrained areas fall into the abyssal plains where sediment cover is usually sparse. Due to a wider, better constrained dataset, the presented sediment volume estimates off West Antarctica are considered to be fairly accurate. The sediment volume is the largest in the Bellingshausen Sea basin, with 3.61 million km^3, although its sediment source area is the smallest (15% of all area draining into the South Pacific). Contrary, the Ross Sea basin, into which sediments are supplied from a much larger area (43%), contains just 2.78 million km^3 of sediment. The Amundsen Sea basin, into which 42% of the present-day West Antarctic landmass on the Pacific side drain, is estimated to contain 3.58 million km^3 of sediment.

We determined the sediment-corrected basement topography for the South Pacific from our total sediment thickness model (Fig. 4). In addition, we obtained the residual basement depth of the oceanic crust (Fig. 5) by subtracting the sediment-corrected basement depth from the theoretical basement depth, using a current South Pacific crustal age model (Wobbe et al., 2012) and Crosby et al.'s (2006) North Pacific depth–age relationship. The mean residual basement depths of the Antarctic and Pacific plate differ by about 300 m. The Antarctic Plate has a residual basement depth of nearly 500 m, but the excessive sediment cover offshore West Antarctica leads to seafloor depths in excess of 1000 m shallower than those of the conjugate New Zealand margin. No direct relationship between seafloor roughness (Fig. 8) and residual basement depth or overlying sediment accumulation has been observed. Ocean floor with large slope variability rather formed from 55 Myr ago until present, when full-spreading velocities dropped below 60 mm Myr^{-1}.

Dynamic topography models (e.g., Ricard et al., 1993; Steinberger, 2007; Conrad and Husson, 2009; Spasojevic and Gurnis, 2012; Flament et al., 2013) of the South Pacific are inconsistent with our local residual basement anomalies or even reversely correlate, and it remains unclear why. The pattern of residual basement depth, however, matches the distribution of seamounts and the shear wave velocity anomaly of the upper mantle (Fig. 9). Collectively these observations suggest that mantle dynamics play a role and that the resolution of dynamic topography models still lack the precision to pinpoint present-day small-scale residual basement anomalies. Our findings support Sutherland et al.'s (2010) model of Late Cretaceous to Cenozoic persistent mantle flow beneath West Antarctica following the Gondwana subduction cessation, but show that basement elevation, estimated from seafloor topography only, has been overestimated off Marie Byrd Land. We demonstrate through our analysis that the Marie Byrd Land margin is only affected by magmatic processes in the context of

continental-insulation flow (Kipf et al., 2013, e.g., Marie Byrd Seamounts, De Gerlache Seamounts, Peter I Island). This seems to be supported by the observation that oceanic crust farther away from these magmatic centers is elevated less than 250 m higher than oceanic crust from the conjugate New Zealand margin. The Ross Sea as well as the Balleny Islands hotspot area, and a region south of the Pacific–Antarctic Ridge, however, have been subject to mantle processes that lead to anomalously high basement elevations more than 1500 m higher as expected. A persistent basement high south of the ridge would explain the rapid subsidence of the Campbell Plateau during 70–40 Myr en route to its present day position. Until more accurate dynamic topography models, that can explain the present-day anomalous basement depth both at the Pacific–Antarctic Ridge and along the continental margins, become available, predictions of the South Pacific paleotopography remain speculative.

Acknowledgments

This project has been funded by the Earth System Sciences Research School (ESSReS), a graduate school of the Helmholtz Association of German Research Centres (HGF) at the Alfred Wegener Institute (AWI), and through the Priority Program 1158 'Antarctic Research' of the Deutsche Forschungsgemeinschaft under project number GO 724/10-1. We thank Doug Wilson and Carsten Scheuer, with whom we had helpful discussions, for sharing their results, and Nicolas Flament for the data exchange. Special thanks go to the New Zealand UNCLOS project for granting insight into seismic data off Chatham Rise. All of the figures in this publication were created using GMT (Generic Mapping Tools, Version 5, by Wessel et al., 2013). We thank Carmen Gaina and Joanne Whittaker for their constructive reviews.

Appendix A. Supplementary data

Supplementary data associated with this article can be found in the online version, at http://dx.doi.org/10.1016/j.gloplacha.2014.09.006. Gridded data sets are available from PANGAEA at http://dx.doi.org/10.1594/PANGAEA.835589.

References

Arndt, J.E., Schenke, H.W., Jakobsson, M., Nitsche, F.O., Buys, G., Goleby, B., Rebesco, M., Bohoyo, F., Hong, J., Black, J., Greku, R., Udintsev, G., Barrios, F., Reynoso-Peralta, W., Taisei, M., Wigley, R., 2013. The International Bathymetric Chart of the Southern Ocean (IBCSO) version 1.0 — a new bathymetric compilation covering circum-Antarctic waters. Geophys. Res. Lett. http://dx.doi.org/10.1002/grl.50413.

Carlson, R.L., Gangi, A.F., Snow, K.R., 1986. Empirical reflection travel time versus depth and velocity versus depth functions for the deep-sea sediment column. J. Geophys. Res. 91 (B8), 8249–8266. http://dx.doi.org/10.1029/JB091iB08p08249.

Chian, D., Louden, K.E., Reid, I., 1995. Crustal structure of the Labrador Sea conjugate margin and implications for the formation of nonvolcanic continental margins. J. Geophys. Res. Solid Earth 100 (B12), 24239–24253. http://dx.doi.org/10.1029/95JB02162.

Conrad, C.P., Husson, L., 2009. Influence of dynamic topography on sea level and its rate of change. Lithosphere 1 (2), 110–120. http://dx.doi.org/10.1130/L32.1.

Cooper, A.K., Davey, F.J., Hinz, K., 1991. Crustal extension and origin of sedimentary basins beneath the Ross Sea and Ross Ice Shelf. In: Thomson, M.R.A., Crame, J.A., Thomson, J.W. (Eds.), Geological Evolution of AntarcticaCambridge World and Regional Geology. Cambridge University Press, Cambridge. ISBN: 978-0521372664, pp. 285–291.

Crosby, A.G., McKenzie, D., Sclater, J.G., 2006. The relationship between depth, age and gravity in the oceans. Geophys. J. Int. 166 (2), 553–573. http://dx.doi.org/10.1111/j.1365-246X.2006.03015.x.

Divins, D.L., 2003. Total Sediment Thickness of the World's Oceans & Marginal Seas. NOAA National Geophysical Data Center, Boulder, CO Available from: http://www.ngdc.noaa.gov/mgg/sedthick/.

Eagles, G., Gohl, K., Larter, R., 2004. High-resolution animated tectonic reconstruction of the South Pacific and West Antarctic margin. Geochem. Geophys. Geosyst. 5, Q07002. http://dx.doi.org/10.1029/2003GC000657.

Finn, C.A., Müller, R.D., Panter, K.S., 2005. A Cenozoic diffuse alkaline magmatic province (DAMP) in the southwest Pacific without rift or plume origin. Geochem. Geophys. Geosyst. 6 (2). http://dx.doi.org/10.1029/2004GC000723.

Flament, N., Gurnis, M., Müller, R.D., 2013. A review of observations and models of dynamic topography. Lithosphere 5 (2), 189–210. http://dx.doi.org/10.1130/L245.1.

Gohl, K., Teterin, D., Eagles, G.G., Netzeband, G., Grobys, J.W.G., Parsiegla, N., Schlüter, P., Leinweber, V., Larter, R.D., Uenzelmann-Neben, G., Udintsev, G.B., 2007. Geophysical survey reveals tectonic structures in the Amundsen Sea Embayment, West Antarctica. In: Cooper, A.K., Raymond, C.R., the 10th ISAES Editorial Team (Eds.), Antarctica: A Keystone in a Changing World — Online Proceedings of the 10th International Symposium on Antarctic Earth SciencesUSGS Open-File Report 2007-1047, Short Research Paper 047. USGS. http://dx.doi.org/10.3133/of2007-1047.srp047.

Gohl, K., Denk, A., Eagles, G., Wobbe, F., 2013a. Deciphering tectonic phases of the Amundsen Sea Embayment shelf, West Antarctica, from a magnetic anomaly grid. Tectonophysics 585, 113–123. http://dx.doi.org/10.1016/j.tecto.2012.06.036.

Gohl, K., Uenzelmann-Neben, G., Larter, R.D., Hillenbrand, C.-D., Hochmuth, K., Kalberg, T., Weigelt, E., Davy, B., Kuhn, G., Nitsche, F.O., 2013b. Seismic stratigraphic record of the Amundsen Sea Embayment shelf from pre-glacial to recent times: evidence for a dynamic West Antarctic ice sheet. Mar. Geol. 344, 115–131. http://dx.doi.org/10.1016/j.margeo.2013.06.011.

Hayes, D.E., Frakes, L.A., Barrett, P.J., Burns, D.A., Chen, P.-H., Ford, A.B., Kaneps, A.G., Kemp, E.M., McCollum, D.W., Piper, D.J.W., Wall, R.E., Webb, P.N. (Eds.), 1975. Initial Reports of the Deep Sea Drilling Project vol. 28. U.S. Government Printing Office, Washington, D.C. http://dx.doi.org/10.2973/dsdp.proc.28.1975.

Hollister, C.D., Craddock, C., Bogdanov, Y.A., Edgar, N.T., Gieskes, J.M., Haq, B.U., Lawrence, J.R., Roegl, F., Schrader, H.-J., Tucholke, B.E., Vennum, W.R., Weaver, F.M., Zhivago, V.N., Worstell, P. (Eds.), 1976. Initial Reports of the Deep Sea Drilling Project vol. 35. U.S. Government Printing Office, Washington, D.C.. http://dx.doi.org/10.2973/dsdp.proc.35.1976.

Kalberg, T., Gohl, K., 2014. The crustal structure and tectonic development of the continental margin of the Amundsen Sea Embayment, West Antarctica: implications from geophysical data. Geophys. J. Int. 198 (1), 327–341. http://dx.doi.org/10.1093/gji/ggu118.

Kim, S.-S., Wessel, P., 2011. New global seamount census from altimetry-derived gravity data. Geophys. J. Int. 186 (2), 615–631. http://dx.doi.org/10.1111/j.1365-246X.2011.05076.x.

Kipf, A., Hauff, F., Werner, R., Gohl, K., van den Bogaard, P., Hoernle, K.A., Maicher, D., Klügel, A., 2013. Seamounts off the West Antarctic margin of the Pacific: a case of non-hotspot intraplate volcanism. Gondwana Res. http://dx.doi.org/10.1016/j.gr.2013.06.013.

Laird, M.G., Bradshaw, J.D., 2004. The break-up of a long-term relationship: the Cretaceous separation of New Zealand from Gondwana. Gondwana Res. 7 (1), 273–286. http://dx.doi.org/10.1016/S1342-937X(05)70325-7.

Larter, R.D., Cunningham, A.P., Barker, P.F., Gohl, K., Nitsche, F.O., 2002. Tectonic evolution of the Pacific margin of Antarctica 1. Late Cretaceous tectonic reconstructions. J. Geophys. Res. 107 (B12), 2345. http://dx.doi.org/10.1029/2000JB000052.

LeMasurier, W.E., 1990. Late Cenozoic volcanism on the Antarctic Plate: an overview. In: LeMasurier, W.E., Thomson, J.W., Baker, P., Kyle, P., Rowley, P., Smellie, J., Verwoerd, W. (Eds.), Volcanoes of the Antarctic Plate and Southern OceansAntarct. Res. Ser vol. 48. AGU, Washington, D.C.. ISBN: 978-0-87590-172-5, pp. 1–17. http://dx.doi.org/10.1029/AR048p0001.

Lindeque, A., Gohl, K., 2010. Western Antarctic palaeostratigraphy: implications for palaeobathymetry and palaeoclimate modelling. Poster presentation at IPY Oslo Science Conference, Oslo, 8–12 June 2010 Available from: http://elsevier.conference-services.net/resources/247/1976/pdf/Oslo2010_0377.pdf.

Malinverno, A., 1991. Inverse square-root dependence of mid-ocean-ridge flank roughness on spreading rate. Nature 352 (6330), 58–60. http://dx.doi.org/10.1038/352058a0.

Müller, R.D., Sdrolias, M., Gaina, C., Roest, W.R., 2008. Age, spreading rates, and spreading asymmetry of the world's ocean crust. Geochem. Geophys. Geosyst. 9, Q04006. http://dx.doi.org/10.1029/2007GC001743.

Oppenheim, A.V., Schafer, R.W., 2009. Discrete-time signal processing, Prentice Hall Signal Processing3 ed. Prentice Hall 978-0-13-198842-2.

Rebesco, M., Larter, R.D., Barker, P.F., Camerlenghi, A., Vanneste, L.E., 1997. The history of sedimentation on the continental rise west of the Antarctic Peninsula. In: Barker, P.F., Cooper, A.K. (Eds.), Geology and Seismic Stratigraphy of the Antarctic Margin, 2Antarct. Res. Ser vol. 71. AGU, Washington, D.C., pp. 29–49. http://dx.doi.org/10.1029/AR071p0029.

Ricard, Y., Richards, M., Lithgow-Bertelloni, C., Le Stunff, Y., 1993. A geodynamic model of mantle density heterogeneity. J. Geophys. Res. Solid Earth 98 (B12), 21895–21909. http://dx.doi.org/10.1029/93JB02216.

Rocchi, S., Armienti, P., D'Orazio, M., Tonarini, S., Wijbrans, J.R., Di Vincenzo, G., 2002. Cenozoic magmatism in the western Ross Embayment: role of mantle plume versus plate dynamics in the development of the West Antarctic Rift System. J. Geophys. Res. Solid Earth 107 (B9). http://dx.doi.org/10.1029/2001JB000515.

Schaeffer, A.J., Lebedev, S., 2013. Global shear-speed structure of the upper mantle and transition zone. Geophys. J. Int. http://dx.doi.org/10.1093/gji/ggt095.

Scheuer, C., Gohl, K., Eagles, G., 2006a. Gridded isopach maps from the South Pacific and their use in interpreting the sedimentation history of the West Antarctic continental margin. Geochem. Geophys. Geosyst. 7 (11), Q11015. http://dx.doi.org/10.1029/2006GC001315.

Scheuer, C., Gohl, K., Larter, R.D., Rebesco, M., Udintsev, G., 2006b. Variability in Cenozoic sedimentation along the continental rise of the Bellingshausen Sea, West Antarctica. Mar. Geol. 227 (3–4), 279–298. http://dx.doi.org/10.1016/j.margeo.2005.12.007.

Sieminski, A., Debayle, E., Lévêque, J.-J., 2003. Seismic evidence for deep low-velocity anomalies in the transition zone beneath West Antarctica. Earth Planet. Sci. Lett. 216 (4), 645–661. http://dx.doi.org/10.1016/S0012-821X(03)00518-1.

Small, C., Sandwell, D.T., 1989. An abrupt change in ridge axis gravity with spreading rate. J. Geophys. Res. Solid Earth 94 (B12), 17383–17392. http://dx.doi.org/10.1029/JB094iB12p17383.

Smith, W.H.F., Wessel, P., 1990. Gridding with continuous curvature splines in tension. Geophysics 55, 293–305.

Spasojevic, S., Gurnis, M., 2012. Sea level and vertical motion of continents from dynamic earth models since the Late Cretaceous. AAPG Bull. 96 (11), 2037–2064. http://dx.doi.org/10.1306/03261211121.

Spasojevic, S., Gurnis, M., Sutherland, R., 2010. Inferring mantle properties with an evolving dynamic model of the Antarctica–New Zealand region from the Late Cretaceous. J. Geophys. Res. Solid Earth 115 (B5). http://dx.doi.org/10.1029/2009JB006612.

Stein, C.A., Stein, S., 1992. A model for the global variation in oceanic depth and heat flow with lithospheric age. Nature 359 (6391), 123–129. http://dx.doi.org/10.1038/359123a0.

Steinberger, B., 2007. Effects of latent heat release at phase boundaries on flow in the Earth's mantle, phase boundary topography and dynamic topography at the Earth's surface. Phys. Earth Planet. Inter. 164 (1–2), 2–20. http://dx.doi.org/10.1016/j.pepi.2007.04.021.

Storey, B.C., Leat, P.T., Weaver, S.D., Pankhurst, R.J., Bradshaw, J.D., Kelley, S., 1999. Mantle plumes and Antarctica–New Zealand rifting: evidence from mid-Cretaceous mafic dykes. J. Geol. Soc. London 156 (4), 659–671. http://dx.doi.org/10.1144/gsjgs.156.4.0659.

Suckro, S.K., Gohl, K., Funck, T., Heyde, I., Ehrhardt, A., Schreckenberger, B., Gerlings, J., Damm, V., Jokat, W., 2012. The crustal structure of southern Baffin Bay: implications from a seismic refraction experiment. Geophys. J. Int. 190 (1), 37–58. http://dx.doi.org/10.1111/j.1365-246X.2012.05477.x.

Sutherland, R., Spasojevic, S., Gurnis, M., 2010. Mantle upwelling after Gondwana subduction death explains anomalous topography and subsidence histories of eastern New Zealand and West Antarctica. Geology 38 (2), 155–158. http://dx.doi.org/10.1130/G30613.1.

Sykes, T.J.S., 1996. A correction for sediment load upon the ocean floor: Uniform versus varying sediment density estimations—implications for isostatic correction. Mar. Geol. 133 (1–2), 35–49. http://dx.doi.org/10.1016/0025-3227(96)00016-3.

Uenzelmann-Neben, G., Gohl, K., 2012. Amundsen Sea sediment drifts: archives of modifications in oceanographic and climatic conditions. Mar. Geol. 299–302, 51–62. http://dx.doi.org/10.1016/j.margeo.2011.12.007.

Voss, M., Jokat, W., 2007. Continent–ocean transition and voluminous magmatic underplating derived from P-wave velocity modelling of the East Greenland continental margin. Geophys. J. Int. 170 (2), 580–604. http://dx.doi.org/10.1111/j.1365-246X.2007.03438.x.

Wardell, N., Childs, J.R., Cooper, A.K., 2007. Advances through collaboration: sharing seismic reflection data via the Antarctic Seismic Data Library System for Cooperative Research (SDLS). In: Cooper, A.K., Raymond, C.R., the 10th ISAES Editorial Team (Eds.), Antarctica: A Keystone in a Changing World — Online Proceedings of the 10th International Symposium on Antarctic Earth SciencesUSGS Open-File Report 2007-1047, Short Research Paper 001. USGS. http://dx.doi.org/10.3133/of2007-1047.srp001.

Wessel, P., Smith, W.H.F., Scharroo, R., Luis, J., Wobbe, F., 2013. Generic mapping tools: improved version released. EOS Trans. Am. Geophys. Union 94 (45), 409–410. http://dx.doi.org/10.1002/2013EO450001.

Whittaker, J., Goncharov, A., Williams, S., Müller, R.D., Leitchenkov, G., 2013. Global sediment thickness dataset updated for the Australian–Antarctic Southern Ocean. Geochem. Geophys. Geosyst. http://dx.doi.org/10.1002/ggge.20181.

Wilson, D.S., Luyendyk, B.P., 2009. West Antarctic paleotopography estimated at the Eocene–Oligocene climate transition. Geophys. Res. Lett. 36 (16), L16302. http://dx.doi.org/10.1029/2009GL039297.

Wilson, D.S., Jamieson, S.S.R., Barrett, P.J., Leitchenkov, G., Gohl, K., Larter, R.D., 2012. Antarctic topography at the Eocene–Oligocene boundary. Palaeogeogr. Palaeoclimatol. Palaeoecol. 24–34. http://dx.doi.org/10.1016/j.palaeo.2011.05.028 (Cenozoic Evolution of Antarctic Climates, Oceans and Ice Sheets).

Wilson, D.S., Pollard, D., DeConto, R.M., Jamieson, S.S., Luyendyk, B.P., 2013. Initiation of the West Antarctic ice sheet and estimates of total Antarctic ice volume in the earliest Oligocene. Geophys. Res. Lett. 40 (16), 4305–4309. http://dx.doi.org/10.1002/grl.50797.

Winberry, J.P., Anandakrishnan, S., 2004. Crustal structure of the West Antarctic rift system and Marie Byrd Land hotspot. Geology 32 (11), 977–980. http://dx.doi.org/10.1130/G20768.1.

Wobbe, F., Gohl, K., Chambord, A., Sutherland, R., 2012. Structure and breakup history of the rifted margin of West Antarctica in relation to Cretaceous separation from Zealandia and Bellingshausen plate motion. Geochem. Geophys. Geosyst. 13 (4), Q04W12. http://dx.doi.org/10.1029/2011GC003742.

Wobbe, F., Lindeque, A., Gohl, K., 2014. Total Sediment Thickness Grid of the Southern Pacific Ocean off West Antarctica, Data Repository. PANGAEA. http://dx.doi.org/10.1594/PANGAEA.835589.

Zwally, H.J., Giovinetto, M.B., Beckley, M.A., Saba, J.L., 2012. Antarctic and Greenland Drainage Systems, GSFC Cryospheric Sciences Laboratory, [online], Available from: http://icesat4.gsfc.nasa.gov/cryo_data/ant_grn_drainage_systems.php.

6.2 Tectonics of the continental margin of West Antarctica and the West Antarctic Rift System

Publication 6.2.1:

Müller, R.D., **Gohl, K.**, Cande, S.C., Goncharov, A., Golynsky, A.V. (2007). Eocene to Miocene geometry of the West Antarctic rift system. *Australian Journal of Earth Sciences,* v. 54, pp. 1033-1045, doi:10.1080/08120090701615691.

Author contributions: This paper is the result of data interpretations and discussions during a sabbatical visit of Gohl to Univ. of Sydney. Müller (60%) and Gohl (40%) wrote the text and produced the figures. Cande contributed with ideas on rotations, while Goncharov and Golynsky made a previously unpublished crustal thickness model available.

Australian Journal of Earth Sciences (2007) **54**, (1033 – 1045)

Eocene to Miocene geometry of the West Antarctic Rift System

R. D. MÜLLER[1]*, K. GOHL[2], S. C. CANDE[3], A. GONCHAROV[4] AND A. V. GOLYNSKY[5]

[1]*School of Geosciences, University of Sydney, NSW 2006, Australia.*
[2]*Alfred Wegener Institute for Polar and Marine Research, PO Box 120161, D-27515 Bremerhaven, Germany.*
[3]*Scripps Institution of Oceanography, 9500 Gilman Drive, La Jolla, CA 92093, USA.*
[4]*Geoscience Australia, GPO Box 378, Canberra ACT 2601, Australia.*
[5]*All-Russian Research Institute for Geology and Mineral Resources of the World Ocean (VNIIOkeangeologia), 1 Angliysky Avenue, St Petersburg 190121, Russia.*

Tectonic models for the Late Cretaceous/Tertiary evolution of the West Antarctic Rift System range from hundreds of kilometres of extension to negligible strike-slip displacement and are based on a variety of observations, as well as kinematic and geodynamic models. Most data constraining these models originate from the Ross Sea/Adare Trough area and the Transantarctic Mountains. We use a new Antarctic continental crustal-thinning grid, combined with a revised plate-kinematic model based on East Antarctic – Australia – Pacific – West Antarctic plate circuit closure, to trace the geometry and extensional style of the Eocene – Oligocene West Antarctic Rift from the Ross Sea to the South Shetland Trench. The combined data suggest that from chron 21 (48 Ma) to chron 8 (26 Ma), the West Antarctic Rift System was characterised by extension in the west to dextral strike-slip in the east, where it was connected to the Pacific – Phoenix – East Antarctic triple junction via the Byrd Subglacial Basin and the Bentley Subglacial Trench, interpreted as pullapart basins. Seismic-reflection profiles crossing the De Gerlache Gravity Anomaly, a tectonic scar from a former spreading ridge jump in the Bellingshausen Sea, suggest Late Tertiary reactivation in a dextral strike-slip mode. This is supported by seismic-reflection profiles crossing the De Gerlache Gravity Anomaly in the Bellingshausen Sea, which show incised narrow sediment troughs and vertical faults indicating strike-slip movement along a north – south direction. Using pre-48 Ma plate circuit closure, we test the hypothesis that the Lord Howe Rise was attached to the Pacific Plate during the opening of the Tasman Sea. We show that this plate geometry may be plausible at least between 74 and 48 Ma, but further work especially on Australian – Antarctic relative plate motions is required to test this hypothesis.

KEY WORDS: Antarctica, crustal stretching, crustal thickness, plate kinematics, rift system.

INTRODUCTION

Understanding the Cenozoic tectonic history of Antarctica is crucial for global plate circuit closure during this time. In turn, the closure of the plate circuit between the Pacific Plate and the plates surrounding the Atlantic and Indian Oceans is required to construct correct global relative and absolute plate motion models. Based on a mantle convection model constrained by a plate-kinematic model, Steinberger *et al.* (2004) recently proposed that the bend in the Hawaiian – Emperor chain can be modelled best if the Pacific Plate is fixed to the Lord Howe Rise before about 43 Ma and back to 83 Ma. This model is intriguing in the context that arc magmatism is unknown in the period after the cessation of subduction along the eastern Gondwanaland margin at around 100 Ma [111 – 108 Ma in Fiordland, New Zealand (Scott & Copper 2006)] and before 50 Ma (Finn *et al.* 2005). This suggests an absence of subduction during this time period, but the kinematics of the area north of New Zealand have alternatively been modelled as characterised by ongoing subduction before 50 Ma (Sdrolias *et al.* 2003; Schellart *et al.* 2006), mainly based on plate circuit closure arguments. In Steinberger *et al.*'s (2004) scenario, the Tasman Sea would have opened simply reflecting Pacific – Australian plate divergence during that time, without any plate boundary between the Lord Howe Rise and the Pacific Plate. However, the rotations used by Steinberger *et al.* (2004) imply substantial displacement (namely compression) between East and West Antarctica for the time period between 83 and 52 Ma, while the Tasman Sea was opening, putting this model into question. Here we investigate the viability of this model via plate circuit closure, testing alternative rotations for Australia – Antarctica separation during the Late Cretaceous/Early Tertiary.

*Corresponding author: dietmar@geosci.usyd.edu.au

ISSN 0812-0099 print/ISSN 1440-0952 online © 2007 Geological Society of Australia
DOI: 10.1080/08120090701615691

The primary evidence for Tertiary extension between East and West Antarctica is found in the Adare Trough, located 100 km northeast of Cape Adare. It represents the extinct third arm of a Tertiary spreading ridge system near a triple junction that separated East and West Antarctica between 43 Ma and 28–26 Ma (Cande *et al.* 2000). Recently, Cande & Stock (2005) extended this period of extension back to 61 Ma (Chron 27), based on additional magnetic and bathymetric data from the area northeast of the Adare Trough, resulting in a total of about 200 km separation between East and West Antarctica in the northern Ross Sea region in the Cenozoic. This model is generally supported by the stratigraphy and fault orientations of drillcores from the western Ross Sea suggesting Oligocene to mid-Miocene extension in the Ross Sea (Cape Roberts Science Team 1998, 1999, 2000). However, the idea of any substantial Cenozoic extension between East and West Antarctica is not universally accepted. Siddoway *et al.* (2004) and Walcott (1998) argued that the lack of geological evidence for large Cenozoic faults does not support large-magnitude, regional extension in much of the region. According to Rocchi *et al.* (2003) and Wilson (1995), the Transantarctic Mountains front, as well as offshore faults and fractures, identify a stress regime compatible with regional Late Cenozoic, but not Early Cenozoic, dextral transtension. There is no published geological or geophysical evidence that deformation between East and West Antarctica may have occurred before 61 Ma, other than the model implications of Steinberger *et al.* (2004).

Our objective is to test these competing models first by using a new crustal thickness and a published sediment-thickness grid for Antarctica to compute rough estimates of crustal stretching factors and to outline the most likely geometry and rift axis of the West Antarctic Rift System from the Ross Sea to the Bellingshausen Sea to the De Gerlache Gravity Anomaly (Figures 1a, 2). We use published plate-kinematic models (Cande *et al.* 1995, 2000; Royer & Rollet 1997; Gaina *et al.* 1998; Larter *et al.* 2002; Keller 2004; Cande & Stock 2005) to compute the predicted relative motion along the axis of the East–West Antarctic plate boundary back to chron 34 (83 Ma), testing the hypothesis that the Pacific Plate was fixed to the Lord Howe Rise before 43 Ma (Steinberger *et al.* 2004) and taking into account two alternative (Royer & Rollet 1997; Tikku & Cande 1999) rotation models for the pre-chron 24 separation between Australia and Antarctica. We utilise seismic-reflection profiles across the inferred East–West Antarctic plate boundary location in the Bellingshausen Sea to test the implications of competing kinematic models for this area.

ANTARCTIC CRUSTAL AND SEDIMENT THICKNESS

Early estimates of crustal thickness in Antarctica were obtained from surface-wave-dispersion studies (Evison *et al.* 1959; Kovach & Press 1961), as well as an analysis that combined the dispersion data with West Antarctic gravity data (Bentley & Ostenso 1962). Regional crustal thickness variations have also been obtained by deep seismic-refraction profiles (Kogan 1972; Ito & Ikami 1986; Trey *et al.* 1999; Leitchenkov & Kudryavtzev 2000; Bannister *et al.* 2003). Segawa *et al.* (1986) analysed the gradients of the power spectrum of Bouguer gravity anomalies that were determined from mean free-air anomaly estimates, whereas Groushinsky & Sazhina (1982) used a linear relation between Moho depths and mean Bouguer gravity anomalies. Von Frese *et al.* (1999) investigated the use of enhanced spectral correlation theory for modelling the crustal features of the Antarctic from regional observations of gravity and terrain, whereas Ritzwoller *et al.* (2001) produced a new model of the crust and upper mantle beneath Antarctica by using a large, new dataset of fundamental mode surface-wave dispersion measurements.

For this study, we compute the Antarctic continental crustal thickness by using an empirical dependence between crustal thickness and topography of solid cover (Demenitskaya 1975):

$$H = 33 \times th\ (0.38 \times Dh - 0.18) + 38$$

where Dh is surface elevation in kilometres (positive on land, negative offshore), and th is hyperbolic tangent.

To estimate bedrock topography for our purposes, we used the BEDMAP grids (at 5 km intervals) (<http://www.nerc-bas.ac.uk/public/aedc/bedmap/>) with information about the bedrock topography and ice thickness (Lythe *et al.* 2000). Total errors of about 1–5% (radar data) and 3% (seismic data) on the related ice thickness determinations suggest that the results in Figure 1 may involve uncertainties of roughly 0.04 km for typical thickness values to possibly as much as 0.12–0.15 km for the thickest ice estimates. The result of this application provides a unique view of the Antarctic crust that is consistent with our current understanding of the region's terrain and that can be tested against the results of other crustal investigations.

We utilise the calculation of 'effective topography' to account for the effect of ice cover in Antarctica. One-third of the ice thickness (the density of ice is $\sim 1/3$ of standard upper continental crust density of 2.67 g/cm^3) is added to bedrock topography resulting in an estimate of 'effective topography'. That value is then used as Dh in the formula of Demenitskaya (1975) at each calculation point to derive a new crustal thickness grid (Figure 1b). Comparison of these results with post-1975 seismic estimates of crustal thickness in Antarctica shows that the accuracy of crustal thickness estimates derived by this method is within ± 5 km. We are aware of Zoback & Mooney's (2003) global analysis of topography and crustal thickness, suggesting that a wide range of crustal thicknesses between 25 and 55 km can be associated with topography at or close to sea-level. Our simple approach for estimating crustal thickness is therefore mainly useful for delineating rifted continental crust < 25 km thick, representing our main objective. A comparison of our crustal thickness estimates for Marie Byrd Land with those by Winberry & Anandakrishnan (2004) demonstrates that our model results compare well with crustal thickness estimates from broadband seismic experiments in West Antarctica.

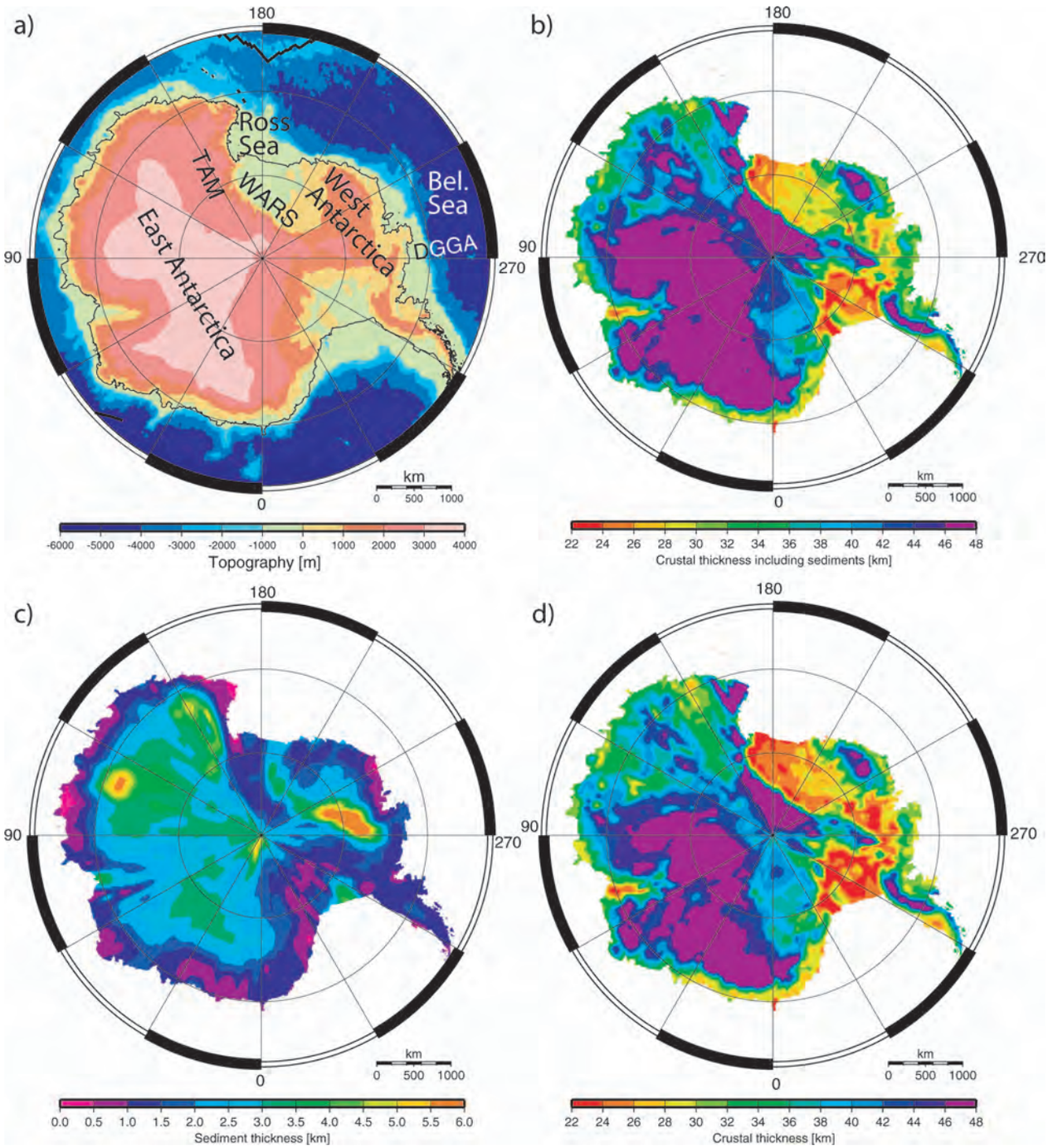

Figure 1 (a) Circum Antarctic bathymetry/topography (WARS, West Antarctic Rift System; DGGA, De Gerlache Gravity Anomaly; TAM, Transantarctic Mountains). (b) Crustal thickness, including sediment thickness. (c) Sediment thickness from CRUST5.2 model. (d) Crustal thickness without sediments derived by subtracting grid (c) from grid (b).

In order to outline the geometry of the West Antarctic Rift System, an estimate of crustal stretching is useful. For this purpose, we need to remove the sediment thickness from the grid shown in Figure 1b. The best available Antarctic sediment-thickness grid is that as part of the CRUST5.2 dataset (Figure 1c), superseding CRUST5.1 (Mooney *et al.* 1998). Figure 1c illustrates that this dataset includes some artefacts such as a questionable general thinning of the sedimentary cover from Antarctica's interior towards its coast. However, despite its shortcomings, we prefer to use this dataset to compute crustal thickness without sediments in order to obtain a crustal stretching factor estimate, as the only alternative would be to use crustal thickness including all sediments (Figure 1b) for this purpose. The latter method would without doubt result in a substantially more inaccurate estimate for crustal stretching.

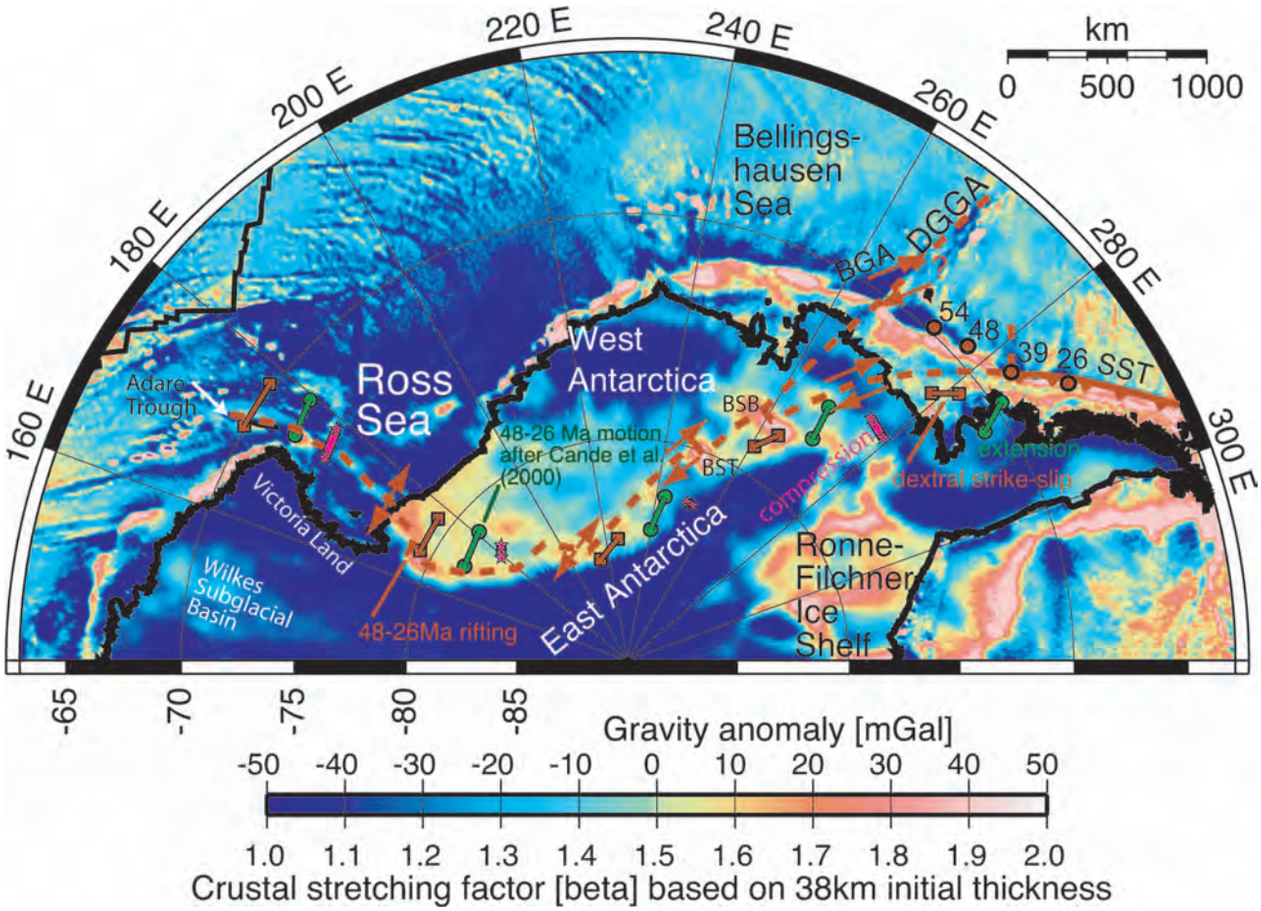

Figure 2 Crustal stretching factor (beta) of Antarctic continental crust assuming initial crustal thickness of 38 km (global average crustal thickness for unthinned plateau-type crust) landward of coastline, based on crustal thickness grid from Figure 1d, combined with marine free-air gravity from satellite altimetry seaward of coastline (McAdoo & Laxon 1997). The combined grid highlights the continuity of tectonic features from onshore Antarctica to offshore areas. Red dashed line corresponds to interpreted West Antarctic Rift System axis, based on locations of crustal stretching maxima and our plate-kinematic model. Predicted relative plate-motion vectors between East and West Antarctica between chron 21 (48 Ma) and chron 8 (26 Ma) are shown based on rotations in Table 1: red lines with diamonds correspond to the model suggested in this paper (pole at 71.1°S, 22.8°W), whereas green lines with circles correspond to stage pole by Cande *et al.* (2000) and magenta lines with stars correspond to stage pole by Davey *et al.* (2006) (see Table 1). BGA, Bellingshausen Gravity Anomaly; BSB, Byrd Subglacial Basin; BST, Bentley Subglacial Trench; DGGA, De Gerlache Gravity Anomaly; SST, South Shetland Trench; TU, Thurston Island. Note that all three models predict extension in the Ross Sea area, but the model from Cande *et al.* (2000) (green) predicts extension for the entire rift system, whereas Davey *et al.*'s (2006) model (magenta) predicts compression southeast of the DGGA, and our model (red) predicts right lateral strike-slip along the eastern branch of the rift system. Plate-motion arrows with arrowheads are symbolic for illustrating direction of motion based on our preferred rotation model (red). The red circles with black outlines and associated numbers indicate the times (in Ma) and locations of a triple junction between Phoenix Plate, Pacific Plate and West Antarctica which migrated from west to east as a result of the ridge–trench collision along the Bellingshausen Sea margin of the Antarctic Peninsula (Eagles *et al.* 2004).

We subtract the CRUST5.2 sediment-thickness grid (Figure 1c) from the crustal-thickness grid shown in Figure 1b to derive a crustal-thickness grid without sediments (Figure 1d). This grid clearly outlines the thinned crust associated with the West Antarctic Rift System, as well as crustal-thickness lows associated with several known subglacial basins (Figures 2, 3). Assuming an initial crustal thickness of 38 km, corresponding to the global average crustal thickness for unthinned plateau-type crust from Mooney *et al.* (1998), we compute a grid for the Antarctic crustal stretching factor (beta), combined with marine free-air gravity from satellite altimetry seaward of coastline to highlight the continuity of tectonic features from onshore Antarctica to offshore areas (Figure 2). The assumption of an initial thickness of 38 km introduces another uncertainty into the computed beta stretching factors, as the initial crustal thickness of the West Antarctic Rift System is unknown. It may well have been <38 km. For this reason, as well as other uncertainties in deriving the crustal thickness grid described above, we do not consider our beta factor grid to be of sufficient fidelity to test different kinematic models quantitatively in terms of their predictions for the amount of stretching along the West Antarctic Rift System.

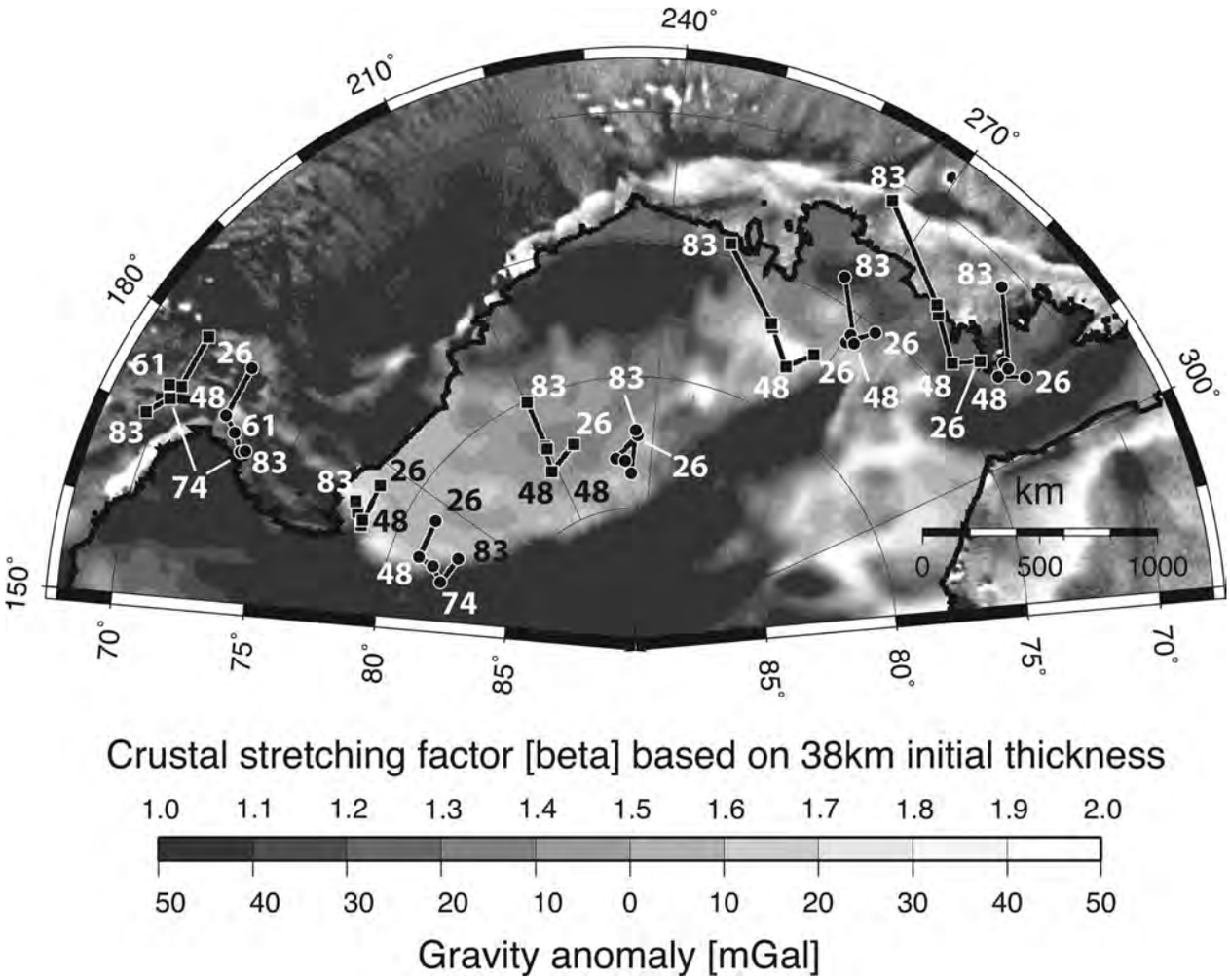

Figure 3 Predicted relative plate motions of West Antarctica relative to East Antarctica within the West Antarctic Rift System from 83 to 26 Ma, based on keeping the Pacific Plate fixed to the Lord Howe Rise between 83 and 52 Ma, as suggested by Steinberger *et al.* (2004), and using two alternative models for relative motion between Australia and Antarctica. Squares and circles for plate motion paths are always plotted for times 83, 74, 51, 48 and 26 Ma. Model 1 (squares) is based on rotations from Cande *et al.* (1995, 2000), Gaina *et al.* (1998), Tikku & Cande (2000), Larter *et al.* (2002), and Keller (2004) (see Table 1), whereas model 2 (circles) is based on the same rotations as model 1 with the exception of the rotations between Australia and Antarctica from chron 27 (61.1 Ma) to chron 34 (83.5 Ma) which are taken from Royer & Rollet (1997). Plate-motion vectors are overlain over combined crustal stretching and gravity anomaly grid as in Figure 2. See text for discussion.

We locate the axis of the West Antarctic Rift System by following crustal stretching maxima, starting with the known location of extension in the Adare Trough at the well-mapped northwestern extension of the rift system (Figure 2). To the southeast, the rift axis follows the edge of the Transantarctic Mountains (Figure 2) until it is offset by a transform fault connecting it to the Bentley Subglacial Trough (Figure 2), which we interpret as part of the rift centre. A second transform fault connects the extinct rift system to the Byrd Subglacial Basin (Figure 2). In this model, both the Bentley Subglacial Trough and the Byrd Subglacial Basin are predicted to have formed as pullapart basins at right-lateral offsets of the plate boundary, which continues east towards the Antarctic Peninsula where it connects with the South Shetland Trench (Figure 2).

MODELLED KINEMATICS BETWEEN EAST AND WEST ANTARCTICA

After outlining the likely location and geometry of the West Antarctic Rift System, we compute the predicted relative motion through time between East and West Antarctica, based on keeping the Pacific Plate fixed to the Lord Howe Rise between 83 and 52 Ma, as suggested by Steinberger *et al.* (2004), and using two alternative models for relative motion between Australia and Antarctica (2005) (Figure 3). Pacific–West Antarctic rotations are well established based on Cande *et al.* (1995) and Larter *et al.* (2002), as well as Lord Howe Rise–Australia rotations (Gaina *et al.* 1998). Recently, Keller (2004) computed Australia–Pacific rotations for the time period between chrons 21 and 8 (*ca* 48–26 Ma). Here we use a plate circuit closure approach, including

Keller's (2004) rotations, to estimate a revised rotation between East and West Antarctica for *ca* 48–26 Ma (Table 1). This preliminary rotation (71.1°S, 22.80°W, rotation angle 3.43°) slightly overestimates the amount of extension in the Adare Trough area, as compared with the magnetic lineations mapped by Cande *et al.* (2000), but results in a more geologically reasonable tectonic regime for the West Antarctic Rift System, indicating strike-slip instead of extension along the eastern portion of the rift system, where little crustal thinning is suggested by our crustal extension map (Figure 2).

The main uncertainty in closing this plate circuit, besides uncertainties in relative motion between the Pacific Plate and the Lord Howe Rise, and in East–West Antarctic motion, is the relative motion history between Australia and Antarctica before 52 Ma. Tikku & Cande (1999) raised and discussed the question whether or not the oldest magnetic anomalies between the two plates actually represent isochrons, and the early opening history between this plate pair is substantially different comparing the rotations from Tikku & Cande (1999) with those of Royer & Rollet (1997). Following Steinberger *et al.*'s (2004) hypothesis, in terms of fixing the Pacific Plate to the Lord Howe Rise between 83 and 52 Ma, we compute the resulting relative motion between East and West Antarctica based on Tikku & Cande's (1999) and alternatively on Royer & Rollet's (1997) rotations. Uncertainties of all combined rotations are currently impossible to compute, because the magnetic anomalies in the ocean basins involved have not been identified based on the same chrons, prohibiting the quantitative addition of coeval rotations for plate circuit closure.

Nevertheless, both models result in a plausible relative motion history dominated by extension/transtension in the Ross Sea, but model 1, based on Tikku & Cande's (1999) model, results in severe compression between East and West Antarctica before 48 Ma along the Transantarctic Mountains, increasing eastwards, for which there is no geological evidence (Figure 3). In contrast, model 2, using Royer & Rollet's (1997) rotations, results in negligible relative motion between 74 and 48 Ma along the eastern portion of the rift system. Reconstructions between 74 and 83 Ma are ill-constrained for nearly all plates involved in plate circuit closure, resulting in unreasonable compression for all plate pairs, but model 2 minimises relative motion in this area. Both models also result in compression increasing eastwards to 300–400 km between 83 and 74 Ma in the Antarctic peninsula, for which there is clearly no evidence. Model 1 (squares) gives smaller 74–48 Ma relative motion along the Transantarctic Mountains, whereas model 2 predicts extension from 74 to 48 Ma along the Transantarctic Mountains (Figure 3).

An alternative rotation between East and West Antarctica for the time period between about 45 and 26 Ma has recently been proposed by Davey *et al.* (2006), based on using the constraint of the amount of extension in the Victoria Land Basin in addition to marine magnetic anomalies and fracture zones. The combined constraints result in a best-fit rotation pole at 84.85°S, 139.37°W and a rotation angle of 4.82° (Table 1). This pole is located close to the geographic south pole, within the large 95% error ellipse of the earlier rotation computed by Cande *et al.* (2000). Even though this rotation satisfies the constraints of the Adare Trough magnetic lineations and the assumed Victoria Land extension [modelled to be 95 km based on gravity modelling (Davey & De Santis 2005), although the exact age and amount of this extension are subject to some uncertainty], it results in compression within a substantial portion of Antarctica east of this rotation pole, irrespective of exactly where the plate boundary would have been located. Evidence for such compression does not exist, but depending on the uncertainties assigned to the Victoria Land Basin extension, a 95% error ellipse for this rotation can be obtained that allows for a pole location close to the southernmost South Atlantic, potentially removing the need for compression within Antarctica during this time period in the model of Davey *et al.* (2006). However, the further this rotation pole is moved into the South Atlantic, the larger the amount of extension required for the Victoria Land Basin (as the colatitude between the rotation pole and the basin increases).

EVIDENCE FOR TECTONIC ACTIVITY ACROSS THE DE GERLACHE GRAVITY ANOMALY

As the geometries of the eastern West Antarctic Rift System seem to be aligned with prominent gravity anomalies in the Bellingshausen Sea (Figure 2), we search for structural connections between West Antarctic Rift System and the tectonics of this area. This system of gravity anomaly lineations is aligned in direct northward prolongation of the eastern West Antarctic Rift System axis through the Bentley Subglacial Trough and the Byrd Subglacial Basin (Figure 2). Geophysical data and detailed plate-kinematic reconstructions have shown that these lineations are primarily associated with the eastern boundary of the former Bellingshausen Plate and tectonic events resulting from a plate reorganisation in the South Pacific around chron C27o (61 Ma) (Larter *et al.* 2002; Eagles 2004). The Bellingshausen Plate existed from about 80 to 61 Ma with a strike-slip and transpressional eastern plate boundary at the location of the Bellingshausen Gravity Anomaly (Figures 2, 4). Gravity and seismic data show that the Bellingshausen Gravity Anomaly extends across the continental slope and shelf northeast of Thurston Island. Analyses of these data also provide evidence for crustal convergence across this boundary (Gohl *et al.* 1997; Cunningham *et al.* 2002), and plate-kinematic modelling suggests up to 200 km of crustal shortening between 80 and 61 Ma (Eagles 2004).

The De Gerlache Gravity Anomaly system stretches from Peter I Island northward across the De Gerlache Seamounts (Figure 4) and fades away north of 62°S. A possible low-amplitude continuation may be correlated along longitude 270°E from 55° to 59°S. Seismic data have shown that the De Gerlache Gravity Anomaly south of 62°S is caused by a north–south-trending system of single and subparallel basement ridges (Hagen *et al.* 1998; Cunningham *et al.* 2002) (Figure 5). A clear crustal

Table 1 Finite rotations used to compute Marie Byrd Land—East Antarctica stage rotation (bold) from plate circuit closure based on references 1–8. Published alternative stage rotations for Marie Byrd Land relative to East Antarctica (italics) from references 4 and 9.

Moving plate	Fixed plate	Age (Ma)	Chron	Latitude (°)	Longitude (°)	Angle (°)	Reference
AUS	ANT	26.55	8o	13.80	33.56	−15.92	1
AUS	ANT	47.9	21o	14.00	33.34	−24.70	1
AUS	ANT	61.1	27o	9.95	36.52	−25.55	1
AUS	ANT	73.6	33y	8.10	37.90	−26.25	Interpolated from 1
AUS	ANT	83.5	34	2.05	40.79	−27.12	1
AUS	ANT	61.1	27o	12.10	32.90	−25.75	Interpolated from 5
AUS	ANT	73.6	33y	11.27	33.08	−26.59	5
AUS	ANT	83.5	34	10.67	33.22	−27.22	5
MBL	PAC	26.0	20o	74.60	−67.30	−21.11	2
MBL	PAC	43.8	20o	74.90	−51.31	−34.54	2
MBL	PAC	47.9	21o	74.52	−50.19	−37.64	2
MBL	PAC	61.1	27o	71.38	−55.57	−44.90	2
MBL	PAC	73.6	33y	66.72	−55.04	−53.74	6
MBL	PAC	83.5	34	65.58	−52.38	−63.07	6
LHR	AUS	61.1	27o	−4.70	131.50	4.43	7
LHR	AUS	73.6	33y	−9.50	137.20	12.94	7
LHR	AUS	83.5	34	−2.70	136.40	14.60	8
PAC	LHR	26.0	8o	55.05	3.13	29.23	3
PAC	LHR	Unknown (see text)	20o–24o	−49.66	177.95	−47.86	3
MBL	ANT	61.1	27o	45.40	144.40	3.28	LHR-PAC fixed and based on rotations from 1 for Australia and Antarctica
MBL	ANT	73.6	33y	50.40	133.20	4.29	LHR-PAC fixed and based on rotations from 1 for Australia and Antarctica
MBL	ANT	83.5	34	77.60	84.50	9.48	LHR-PAC fixed and based on rotations from 1 for Australia and Antarctica
MBL	ANT	61.1	27o	57.00	145.60	3.18	LHR-PAC fixed and based on rotations from 5 for Australia and Antarctica
MBL	ANT	73.6	33y	68.00	127.80	4.65	LHR-PAC fixed and based on rotations from 5 for Australia and Antarctica
MBL	ANT	83.5	34	83.70	27.10	13.13	LHR-PAC fixed and based on rotations from 5 for Australia and Antarctica
MBL	**ANT**	**26.55–47.9**	**21o**	**−71.10**	**−22.80**	**3.43**	Stage rotation based on rotations from 1, 2, 3 (this paper)
MBL	*ANT*	*26.0–47.9*	*21o*	*−18.15*	*−17.85*	*1.70*	Stage rotation from 4
MBL	*ANT*	*26.0–47.9*	*21o*	*−84.85*	*−139.37*	*4.82*	Stage rotation from 9

1, Tikku and Cande (2000); 2, Cande *et al.* (1995); 3, Keller (2004); 4, Cande *et al.* (2000); 5, Royer and Rollet (1997); 6, Larter *et al.* (2002); 7, Gaina *et al.* (1998); 8, this paper; 9, Davey *et al.* (2006). ANT, East Antarctica; AUS, Australian Plate; LHR, Lord Howe Rise; MBL, Marie Byrd Land (West Antarctica); PAC, Pacific Plate. Positive rotation angles indicate counterclockwise motion.

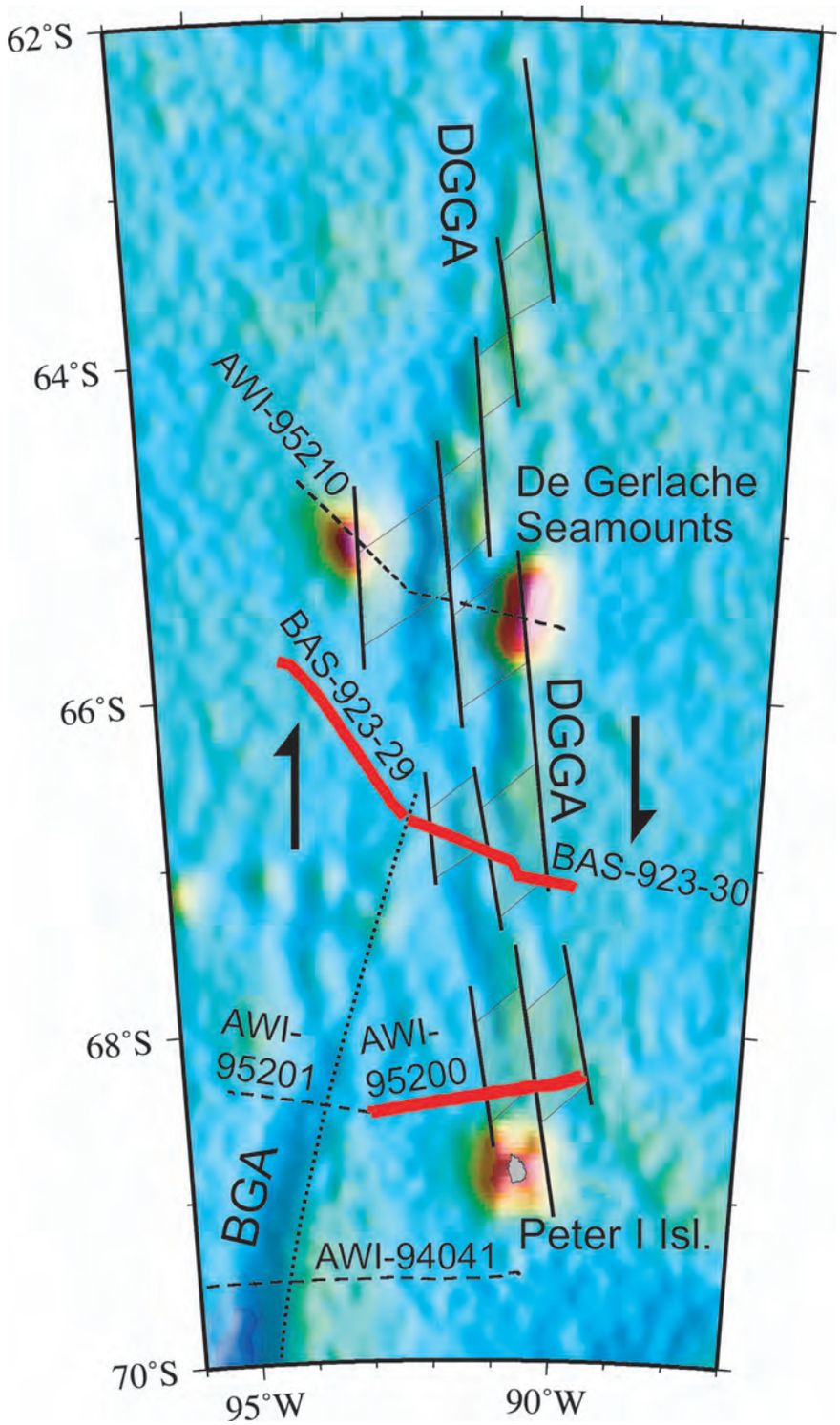

Figure 4 Satellite-derived gravity anomaly map (McAdoo & Laxon 1997) of the Bellingshausen Gravity Anomaly (BGA) and De Gerlache Gravity Anomaly (DGGA) systems of the western Bellingshausen Sea with tracks of seismic profiles (bold solid lines) used in this study and related profiles published in Gohl *et al.* (1997) and Hagen *et al.* (1998) (dashed lines). Thin solid lines and hatched areas illustrate our schematic setting of a Tertiary regime of strike-slip plate motion with near-vertical faults connected with pullapart basins along the DGGA. The dotted line marks an older lineament along the BGA from the time when this acted as the eastern oblique-convergent boundary of the Bellingshausen Plate (Eagles *et al.* 2004).

age difference across the De Gerlache Gravity Anomaly is observed from seafloor-spreading magnetic anomalies C32–34 west of it and C26–24 east of it, indicating that the gravity lineation represents the scar of a ridge jump of the Phoenix–Pacific Ridge at chron C27 (61 Ma) (Larter *et al.* 2002; Eagles 2004). Sampled volcanics along the De Gerlache Gravity Anomaly are of much younger age than the structure of the ridge jump scar. Extrusions of alkaline volcanics of the 23–20 Ma De Gerlache Seamounts (Hagen *et al.* 1998) and the 13–0.1 Ma Peter I Island (Prestvik *et al.* 1990) suggest that the De Gerlache Gravity Anomaly has acted as a preserved zone of lithospheric weakness after the West Antarctic Rift system became extinct. Miocene to present-day mantle plume activities of the West Antarctic Rift System may have acted as the magmatic source for the volcanics.

We investigate tectonic activity along the De Gerlache Gravity Anomaly using multi-channel seismic

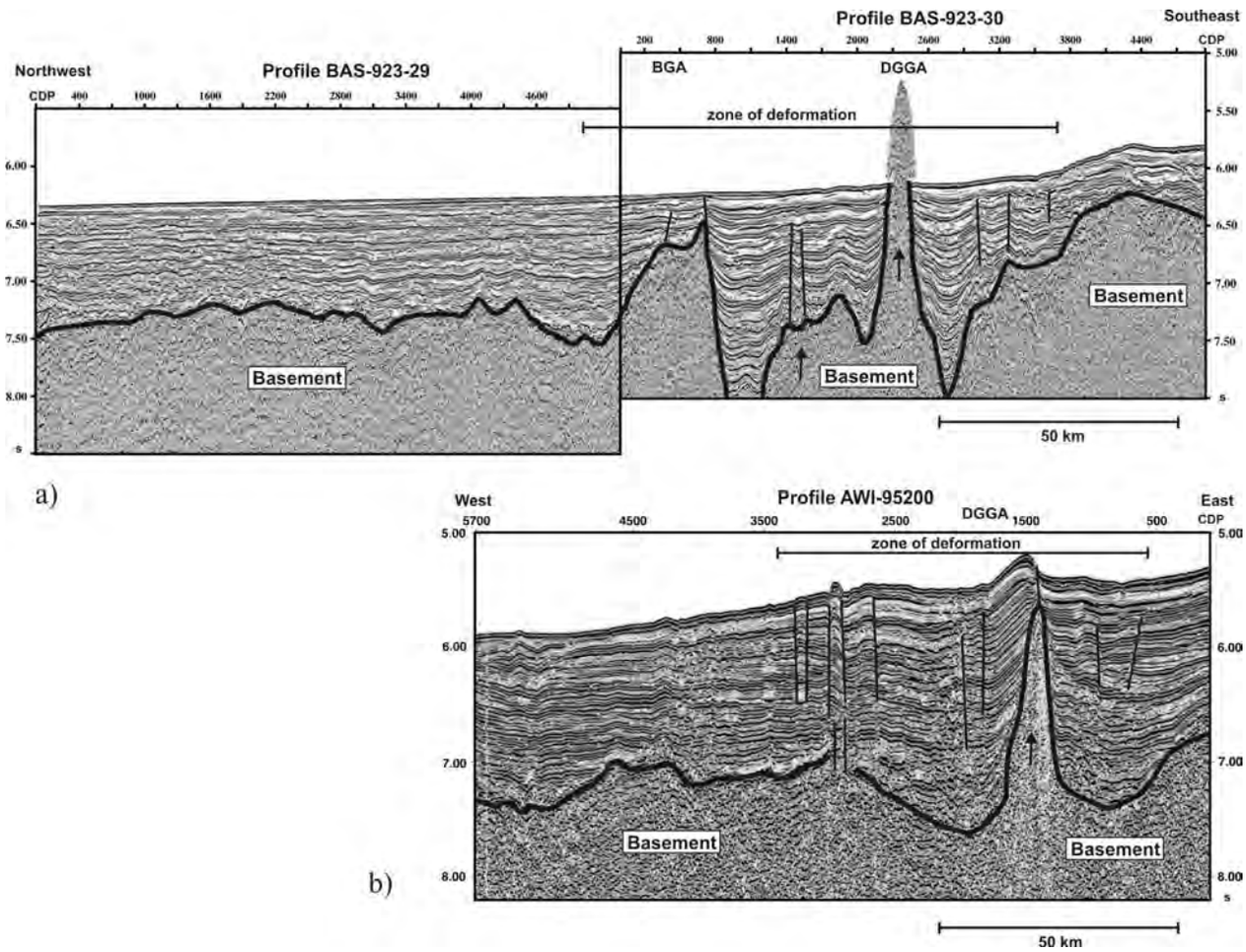

Figure 5 (a) Seismic profile BAS-923-29/30 across the tectonic lineaments under the De Gerlache Gravity Anomaly (DGGA) and the northern part of the Bellinghausen Gravity Anomaly. (b) Seismic profile AWI-95200 crosses the DGGA north of Peter I Island. Top of basement is marked with bold solid lines. Both profiles reveal a zone in which sediments are deformed by basement tectonics and the rise of volcanic cones. Vertical faults (thin solid lines) and overdeepened sediment troughs indicate transtensional deformation. See Figure 4 for locations.

profiles that cross the De Gerlache Gravity Anomaly at two locations between Peter I Island and the De Gerlache Seamounts. Profiles BAS-923-29/30 and AWI-95200 (Figure 5a, b) reveal a zone in which a strongly undulating basement is characterised by intrusions of volcanic cones or ridges under the Bellingshausen Gravity Anomaly (BAS-923-30) and De Gerlache Gravity Anomaly (both profiles). Such a north–south-oriented ridge has been imaged with multibeam data (Figure 6) and seismic profile BAS-923-30 north of Peter I Island. Although we do not have direct evidence for its origin, we can infer its volcanic origin from the observation that it is the only edifice rising above the sediments between volcanic Peter I Island and the De Gerlache Seamounts, which both display north–south-trending flanks. The multibeam image shows that the north-trending axis of this ridge has a lateral offset close to its peak. Any later lateral tectonic deformation of an elongated ridge would result in fracturing which is not observed in this case. We therefore suggest that this ridge is a result of volcanic eruption along a pre-existing orthogonal fault system in the basement.

Some of the basement peaks within the De Gerlache Gravity Anomaly correlate with near-vertical faults situated above them. These faults continue to the upper level of the widely folded sediments observed in this area. Deep narrow troughs with total sediment thicknesses of 2–3 km (~2 s TWT) are situated next to the flanks of the major basement uplifts and intrusions on profile BAS-923-29/30. The troughs observed on this profile reach about 1 km deeper than the undisturbed basement surface farther west, while the sediment troughs on profile AWI-95200 are less deep but wider. On the northern profile (Figure 5a), the sediment trough adjacent to the east of the main basement ridge is deeper than that directly adjacent to the western flank. Along the southern profile, the opposite basement geometry is observed. Almost all sedimentary sequences are dragged up along the flanks of the basement highs, except on the wide basement high at the eastern end of profile BAS-923-29/30. Here, only the deepest sediments of the trough appear to be dragged up along the basement flank, while the mid-level and shallower sequences onlap the basement. Three

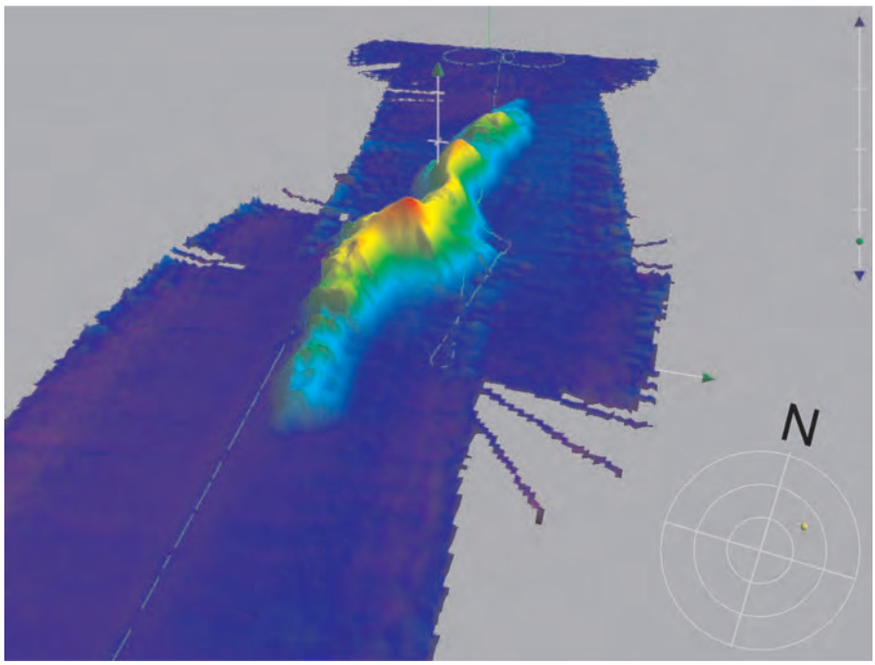

Figure 6 Multibeam bathymetric map of an exposed volcanic ridge at the De Gerlache Gravity Anomaly which was crossed by seismic profile BAS-923-30 (Figure 5a). Data were collected during RV *Polarstern* expedition ANT-XXIII/4 in early 2006.

tectonic events can be discriminated from the observed structures.

(1) A basement block uplift or a major magmatic intrusion occurred to the east as indicated by the onlapping sediments. We correlate this event with the suggested jump of the Phoenix–Pacific spreading ridge to the location of the De Gerlache Gravity Anomaly at 61 Ma (Larter *et al.* 2002; Eagles 2004). At the initial stage of such a ridge jump, a fair amount of magmatic material presumably intruded into the pre-existing crust.

(2) The incised narrow sediment troughs and the vertical faults, offsetting the reflectors by only a small amount, indicate strike-slip movement along a north–south strike direction. We interpret the troughs as small, but overdeepened, pullapart basins (Figures 4, 5), which are commonly associated with the development of transtensional fault zones (Aydin & Nur 1982). The beginning of strike-slip movement cannot be older than the formation of the uplifted or intruded basement block to the east, as the onlapping sediments indicate, therefore post-dating 61 Ma. The youngest possible age of the deformation is vaguely constrained by the upper limit of the majority of the vertical faults. Most upper limits can be observed to about 150–300 m (0.2–0.3 s TWT) below seafloor. The sediments at this depth are up to 2–8 million years old assuming a regional deposition rate of 4–8 cm/10^3 y since onset of glaciation, as estimated from the nearest Deep Sea Drilling Project Leg 35, Site 324 (Hollister & Craddock 1976).

(3) Both tectonic events are overprinted by magmatic intrusions of relatively young or even recent age as indicated by the pulled-up and faulted sediments along the flanks and on top of the intrusions. The intrusive bodies can be associated with the same magmatic events that formed the De Gerlache Seamounts and Peter I Island between 23 and 0.1 Ma along the De Gerlache Gravity Anomaly. The satellite-derived gravity anomaly map of the De Gerlache Gravity Anomaly shows north–south-trending basement ridge segments (Figures 4, 5). We suggest that the intruding magmatic material followed pre-existing north–south-striking fault zones. The right-stepping axis offset of an imaged volcanic ridge (Figure 6) indicates that basement underwent strike-slip motion with sideward displacement of the fault zone prior to the extrusive event. It is possible that early intrusions occurred already during the formation of strike-slip faults at the time of the proposed relative motion between the East and West Antarctic Plates in the Bellingshausen Sea.

These observations tentatively suggest that transtensional tectonic reactivation may have occurred along the De Gerlache Gravity Anomaly in the Early/mid-Tertiary as part of the eastern tectonic activity of the West Antarctic Rift System. Evidence for this consists of: (i) the alignment of the De Gerlache Gravity Anomaly with the directional trend of the extension in the West Antarctic Rift System and its transform fault to the Byrd Subglacial Basin; (ii) the observation of a strike-slip motion along the De Gerlache Gravity Anomaly between mid-Tertiary and the Late Miocene or even Pliocene; and (iii) the estimated timing of the development of the strike-slip deformation. Such a transtensional system may have acted as an accommodation zone as a response to the northeastward migration of this triple junction to which the plate boundary was connected. Alternatively, it is also possible that the De Gerlache Gravity Anomaly was reactivated only after the main extension phase of the West Antarctic Rift System was completed at about 26 Ma, given that the evidence for pre-26 Ma tectonic reactivation along the De Gerlache Gravity Anomaly is circumstantial.

PLATE-KINEMATIC IMPLICATIONS

Plate circuit closure, together with a complete mapping of the axis of the West Antarctic Rift System from the Adare Trough to the Bellingshausen Sea, allows us to evaluate the implications of the hypothesis that the Pacific Plate was attached to the Lord Howe Rise between about 83 and 52 Ma (Steinberger *et al.* 2004), during the opening of the Tasman Sea. Given that the errors in published Pacific–Antarctic, Pacific–Bellingshausen, and Australian–Lord Howe Rise reconstructions are relatively small, we focus on the implication of two alternative Australian–Antarctic reconstructions. The Australian–Antarctic end-member reconstructions considered here represent a set of reconstructions in which the pre-chron 27 (61 Ma) Australian–Antarctic magnetic anomalies are considered as isochrons or some conjugate magnetic anomaly misfits are permitted to avoid unreasonable overlaps between continental margins during the early opening of the Great Australian Bight.

An isochron fit of the pre-chron 27 Australian–Antarctic magnetic anomaly data results in a tight fit between Tasmania and Antarctica with finite rotation poles relatively close to the Kerguelen Plateau, and in negligible motion between the Kerguelen Plateau and the Broken Ridge before chron 20 (43 Ma) (Tikku & Cande 1999, 2000; Cande & Stock 2005), whereas reconstructions which allow for some misfit between pre-chron 27 magnetic anomalies in the Great Australian Bight and offshore Antarctica result in a looser fit between Tasmania and Antarctica (Royer & Rollet 1997). Between 83 and 74 Ma, both models result in substantial compression in the eastern portion of the West Antarctic rift system, if combined with published rotations for the closure of the Tasman Sea and the Southwest Pacific (Table 1; Figure 3). There is no evidence that such an episode of crustal shortening has occurred along the West Antarctic Rift System. From 74 to 48 Ma, model 2 predicts little relative motion at the eastern branch of the rift system, compared with model 1. This implies that, using Royer & Rollet's rotations (1997), a fixed Pacific–Lord Howe Rise is conceivable during the time of Tasman Sea opening, at least after 74 Ma, without requiring an active West Antarctic Rift System.

CONCLUSIONS

Combined mapping of crustal continental extension in Antarctica and a revised plate-kinematic model allow us to estimate the geometry of the Oligocene to Miocene West Antarctic Rift System. However, the exact kinematic history of this extension is still subject to large uncertainties, as indicated by the different pole locations for the main extension period (*ca* 48–26 Ma) suggested here, by Cande *et al.* (2000) and by Davey *et al.* (2006). The model presented here results in strike-slip for the eastern extension of the plate boundary within Marie Byrd Land, instead of extension as implied by Cande *et al.*'s (2000) rotation pole. In our scenario, the eastern strike-slip portion of the West Antarctic Rift System would have connected to the South Shetland Trench via a triple junction between the Pacific, Phoenix and East Antarctic Plates. In contrast, Davey *et al.*'s (2006) best-fit rotation pole implies compression for the eastern portion of the rift system between 48 and 26 Ma, a scenario we regard as unlikely. Seismic-reflection data suggest that the older tectonic lineaments in the Bellingshausen Sea under the De Gerlache Gravity Anomaly, and possibly the Bellingshausen Gravity Anomaly, may have been reactivated during this time in a right-lateral strike-slip sense. Using Australia–Antarctica rotations from Royer & Rollet (1997), and rotations for the remaining plate circuit as listed in Table 1, we show that it is plausible that no subduction (or other relative motion) existed between the Lord Howe Rise and the Pacific Plate at least between 74 and 48 Ma. Such a model is consistent with the complete lack of arc-volcanics from this time period in the area of the Lord Howe Rise and associated backarc basins, even though a fairly extensive sample base exists for this area (Mortimer *et al.* 1998).

Published relative plate-motion parameters are not consistent with the notion that the Pacific Plate was fixed to the Lord Howe Rise before 74 Ma. The implied episode of shortening between East and West Antarctica is unlikely, meaning either that a plate boundary still existed at that time between the Pacific Plate and the Lord Howe Rise, or that one or several of the published rotations involved for Chron 34 are associated with large errors. This may indicate problems with Tikku & Cande's (1999) Australian–Antarctic fit for chrons 31–34, or it may indicate that a plate boundary still existed before 74 Ma between the Pacific Plate and the Lord Howe Rise, continuing through New Zealand, where some deformation during this time period is suggested by geological data (Sutherland 1999). A more robust method for computing a better-constrained Australia–Antarctic fit for this time would be triple-junction closure, simultaneously fitting data for chrons 31, 33 and 34 between Australia, Antarctic and India. Tikku & Cande's (1999) rotations for this time period, if combined with published rotations for India–Antarctica, result in flow-lines for the Wharton Basin west of Australia which deviate from the fracture zone azimuths in this area, which are well mapped from the marine gravity field derived from satellite altimetry (Sandwell & Smith 1997). Therefore, revised Indian Ocean reconstructions using triple-junction closure, and including uncertainties, will be an essential next step to further test whether a self-consistent plate circuit closure before chron 31 (74 Ma) is possible while fixing the Pacific Plate to the Lord Howe Rise.

ACKNOWLEDGEMENTS

We thank Rob Larter of the British Antarctic Survey for providing two of the seismic profiles used in this paper, and Joanne Whittaker and Nadege Rollet for careful internal reviews prior to submission. We also thank Bernhard Steinberger and Neville Exon for careful reviews, which improved the paper significantly. The digital crustal thickness and crustal stretching maps presented in this paper can be downloaded at <http://www.earthbyte.org>.

REFERENCES

AYDIN A. & NUR A. 1982. Evolution of pull-apart basins and their scale dependence. *Tectonics* **1**, 91–105.

BANNISTER S., YU J., LEITNER B. & KENNETT B. L. N. 2003. Variations in crustal structure across the transition from West to East Antarctica, Southern Victoria land. *Geophysical Journal International* **155**, 870–884.

BENTLEY C. R. & OSTENSO N. A. 1962. Thickness of the Earth's crust in Antarctica and the surrounding oceans. *Geophysical Journal* **6**, 292–297.

CANDE S. C., RAYMOND C. A., STOCK J. & HAXBY W. F. 1995. Geophysics of the Pitman Fracture Zone and Pacific–Antarctic plate motions during the Cenozoic. *Science* **270**, 947–953.

CANDE S. C. & STOCK J. M. 2005. Cenozoic reconstructions of the Australia–New Zealand–South Pacific sector of Antarctica. *In*: Exon N. F., Kennett J. P. & Malone M. J. eds. *The Cenozoic Southern Ocean: Tectonics, Sedimentation and Climate Change between Australia and Antarctica*, pp. 5–18. American Geophysical Union Geophysical Monograph **151**.

CANDE S. C., STOCK J. M., MÜLLER R. D. & ISHIHARA T. 2000. Cenozoic motion between East and West Antarctica. *Nature* **404**, 145–150.

CAPE ROBERTS SCIENCE TEAM 1998. Studies from the Cape Roberts Project, Ross Sea, Antarctica: Initial Report on CRP-1. *Terra Antartica* **5**(1), 1–187.

CAPE ROBERTS SCIENCE TEAM 1999. Studies from the Cape Roberts Project, Ross Sea, Antarctica: Initial Report on CRP-2/2A. *Terra Antartica* **6**(1/2), 1–173.

CAPE ROBERTS SCIENCE TEAM 2000. Studies from the Cape Roberts Project, Ross Sea, Antarctica: Initial Report on CRP-3. *Terra Antartica* **7**(1/2), 1–209.

CUNNINGHAM A. P., LARTER R. D., BARKER P. F., GOHL K. & NITSCHE F. O. 2002. Tectonic evolution of the Pacific margin of Antarctica. 2. Structure of Late Cretaceous–early Tertiary plate boundaries in the Bellingshausen Sea from seismic reflection and gravity data. *Journal of Geophysical Research* **107**(B12), 2346–2346.

DAVEY F. J., CANDE S. C. & STOCK J. M. 2006. Extension in the western Ross Sea region—links between Adare Basin and Victoria Land basin. *Geophysical Research Letters* **33**, no. L20315, doi:10.1029/2006GL027383.

DAVEY F. J. & DE SANTIS L. 2005. A multi-phase rifting model for the Victoria Land basin, Western Ross Sea. *In*: Fütterer D. K., Damaske D., Kleinschmidt G., Miller H. & Tessensohn F. eds. *Antarctica, Contributions to Global Earth Sciences*, pp. 301–306. Springer, New York.

DEMENITSKAYA R. M. 1975. *Crust and Mantle of the Earth.* Nedra, Moscow.

EAGLES G. 2004. Tectonic evolution of the Antarctic–Phoenix plate system since 15 Ma. *Earth and Planetary Science Letters* **217**, 97–109.

EAGLES G., GOHL K. & LARTER R. D. 2004. High-resolution animated tectonic reconstruction of the South Pacific and West Antarctic margin. *Geochemistry Geophysics Geosystems* **5**, Q07002, doi:10.1029/2003GC000657, 2004.

EVISON F. F., INGHAM C. E. & ORR R. H. 1959. Thickness of the Earth's crust in Antarctica. *Nature* **183**, 306–308.

FINN C. A., MÜLLER R. D. & PANTER K. S. 2005. A Cenozoic diffuse alkaline magmatic province (DAMP) in the southwest Pacific without rift or plume origin. *Geochemistry, Geophysics, Geosystems* **6**, Q02005, doi:10.1029/2004GC000723, 2005.

GAINA C., MÜLLER D. R., ROYER J-Y., STOCK J., HARDEBECK J. L. & SYMONDS P. 1998. The tectonic history of the Tasman Sea: a puzzle with 13 pieces. *Journal of Geophysical Research* **103B**, 12413–12433.

GOHL K., NITSCHE F. & MILLER H. 1997. Seismic and gravity data reveal Tertiary interplate subduction in the Bellingshausen Sea, Southeast Pacific. *Geology* **25**, 371–374.

GROUSHINSKY N. P. & SAZHINA N. B. 1982. Some features of Antarctic crustal structure. *In*: Craddock C. ed. *Antarctic Geosciences*, pp. 907–911. University of Wisconsin Press, Madison.

HAGEN R. A., GOHL K., GERSONDE R., KUHN G., VOELKER D. & KODAGALI V. N. 1998. A geophysical survey of the De Gerlache Seamounts: preliminary results. *Geo-Marine Letters* **18**, 19–25.

HOLLISTER C. D. & CRADDOCK C. 1976. Introduction, principal results—Leg 35, Deep Sea Drilling Project. *Initial Reports of the Deep Sea Drilling Project* **35**, 5–14.

ITO K. & IKAMI A. 1986. Crustal structure of the Mizuho Plateau, East Antarctica, from geophysical data. *Journal of Geodynamics* **6**, 285–296.

KELLER W. R. 2004. Cenozoic plate tectonic reconstructions and plate boundary processes in the Southwest Pacific. PhD thesis, California Institute of Technology, Pasadena (unpubl.).

KOGAN A. L. 1972. Results of deep seismic soundings of the earth's crust in East Antarctica. *In*: Adie R. J. ed. *Antarctic Geology and Geophysics*, pp. 485–489. Universitetsforlaget, Oslo.

KOVACH R. L. & PRESS F. 1961. Surface wave dispersion and crustal structure in Antarctica and the surrounding oceans. *Annali di Geofisica* **14**, 211–224.

LARTER R. D., CUNNINGHAM A. P., BARKER P. F., GOHL K. & NITSCHE F. O. 2002. Tectonic evolution of the Pacific margin of Antarctica. 1. Late Cretaceous tectonic reconstructions. *Journal of Geophysical Research* **107**(B12), 2345–2345.

LEITCHENKOV G. L. & KUDRYAVTZEV G. A. 2000. Structure and origin of the Earth's crust in the Weddell Sea Embayment (beneath the front of the Filchner and Ronne Ice Shelves from the Deep Seismic Soundings data. *Polarforschung* **67**, 143–154.

LYTHE M. B., VAUGHAN D. G. & THE BEDMAP CONSORTIUM 2000. *BEDMAP—Bed Topography of the Antarctic* (scale 1:10 000 000). BAS (Misc) **9**. British Antarctic Survey, Cambridge.

MCADOO D. & LAXON S. 1997. Antarctic tectonics: constraints from an ERS-1 satellite marine gravity field. *Science* **276**, 556–560.

MOONEY W. D., LASKE G. & MASTERS T. G. 1998. CRUST 5.1: a global crustal model at 5 degrees × 5 degrees. *Journal of Geophysical Research* **103**, 727–747.

MORTIMER N., HERZER R. H., GANS P. B., PARKINSON D. L. & SEWARD D. 1998. Basement geology from Three Kings Ridge to West Norfolk Ridge, southwest Pacific Ocean: evidence from petrology, geochemistry and isotopic dating of dredge samples. *Marine Geology* **148**, 135–162.

PRESTVIK T., BARNES C. G., SUNDVOLL B. & DUNCAN R. A. 1990. Petrology of Peter I Øy (Peter I Island), West Antarctica. *Journal of Volcanological and Geothermal Research* **44**, 315–338.

RITZWOLLER M. H., SHAPIRO N. M., LEVSHIN A. L. & LEAHY G. M. 2001. Crustal and upper mantle structure beneath Antarctica and surrounding oceans. *Journal of Geophysical Research* **106**, 30645–30670.

ROCCHI S., STORTI F., DI VINCENZO G. & ROSSETTI F. 2003. Intraplate strike-slip tectonics as an alternative to mantle plume activity for the Cenozoic rift magmatism in the Ross Sea region, Antarctica. *In*: Storti F., Holdsworth R. E. & Salvini F. eds. *Intraplate Strike-Slip Deformation Belts*, pp. 145–158. Geological Society of London Special Publication **210**.

ROYER J-Y. & ROLLET N. 1997. Plate-tectonic setting of the Tasmanian region. *Australian Journal of Earth Sciences* **44**, 543–560.

SANDWELL D. T. & SMITH W. H. F. 1997. Marine gravity anomaly from Geosat and ERS 1 satellite altimetry. *Journal of Geophysical Research* **102B**, 10039–10054.

SCHELLART W. P., LISTER G. S. & TOY V. G. 2006. A Late Cretaceous and Cenozoic reconstruction of the southwest Pacific Region: tectonics controlled by subduction and slab rollback processes. *Earth-Science Reviews* **76**, 191–223.

SCOTT J. M. & COPPER A. F. 2006. Early Cretaceous extensional exhumation of the lower crust of a magmatic arc: evidence from the Mount Irene Shear Zone, Fiordland, New Zealand. *Tectonics* **25**, no. TC3018, doi:10.1029/2005TC001890, pp. 1–15.

SDROLIAS M., MÜLLER R. D. & GAINA C. 2003. Tectonic evolution of the southwest Pacific using constraints from backarc basins. *In*: Hillis R. R. & Müller R. D. eds. *Evolution and Dynamics of the Australian Plate*, pp. 343–359. Geological Society of Australia Special Publication **22** and Geological Society of America Special Paper **372**.

SEGAWA J., MATSUMOTO T. & KAMINUMA K. 1986. Gravity anomaly in and around Antarctica and its tectonic implication. *Journal of Geodynamics* **6**, 309–326.

SIDDOWAY C. S., BALDWIN S. L., FITZGERALD P. G., FANNING C. M. & LUYENDYK B. P. 2004. Ross Sea mylonites and the timing of intracontinental extension within the West Antarctic rift system. *Geology* **32**, 57–60.

STEINBERGER B., SUTHERLAND R. & O'CONNELL R. J. 2004. Prediction of Emperor-Hawaii seamount locations from a revised model of global plate motion and mantle flow. *Nature* **430**, 167–173.

SUTHERLAND R. 1999. Basement geology and tectonic development of the greater New Zealand region: an interpretation from regional magnetic data. *Tectonophysics* **308**, 341–362.

TIKKU A. A. & CANDE S. C. 1999. The oldest magnetic anomalies in the Australian–Antarctic Basin: are they isochrons? *Journal of Geophysical Research* **104B**, 661–677.

TIKKU A. A. & CANDE S. C. 2000. On the fit of Broken Ridge and Kerguelen plateau. *Earth and Planetary Science Letters* **180**, 117–132.

TREY H., COOPER A. K., PELLIS G., DELLA VEDOVA B., COCHRANE G., BRANCOLINI G. & MAKRIS J. 1999. Transect across the West Antarctic rift system in the Ross Sea, Antarctica. *Tectonophysics* **301**, 61–74.

VON FRESE R. R. B. 1999. Polar magnetic anomaly maps; problems & progress. *Istituto Nazionale di Geofisica Pubblicazione* **601**, 91.

WALCOTT R. I. 1998. Modes of oblique compression: late Cenozoic tectonics of the South Island of New Zealand. *Reviews of Geophysics* **36**, 1–26.

WILSON T. J. 1995. Cenozoic transtension along the Transantarctic Mountains–West Antarctic Rift boundary, southern Victoria Land, Antarctica. *Tectonics* **14**, 531–545.

WINBERRY J. P. & ANANDAKRISHNAN S. 2004. Crustal structure of the West Antarctic rift system and Marie Byrd Land hotspot. *Geology* **32**, 977–980.

ZOBACK M. L. & MOONEY W. D. 2003. Lithospheric buoyancy and continental intraplate stress. *International Geology Review* **45**, 95–118.

Received 27 October 2006; accepted 20 June 2007

Publication 6.2.2:

Eagles, G., Larter, R.D., **Gohl, K.**, Vaughan, A.P.M. (2009b). West Antarctic Rift System in the Antarctic Peninsula. *Geophysical Research Letters*, v. 36, L21305, doi:10.1029/2009GL040721.

Author contributions: Eagles wrote most of this paper with contributions in data interpretation and discussions by Larter, Gohl and Vaughan. The modelled extent of the West Antarctic Rift System from Müller et al. (2007) (publication 6.2.1) provided the basic idea for this paper.

GEOPHYSICAL RESEARCH LETTERS, VOL. 36, L21305, doi:10.1029/2009GL040721, 2009

West Antarctic Rift System in the Antarctic Peninsula

Graeme Eagles,[1] Robert D. Larter,[2] Karsten Gohl,[3] and Alan P. M. Vaughan[2]

Received 27 August 2009; revised 21 September 2009; accepted 21 September 2009; published 7 November 2009.

[1] Decades after the recognition of the West Antarctic Rift System, and in spite of its global importance, the location and nature of the plate boundary it formed at are unknown east of the Byrd Subglacial Basin. Alternative constructions of the circuit of South Pacific plate boundaries suggest the presence of either a transcurrent plate boundary or a continuation of the extensional rift system. We identify George VI Sound, a curved depression separating Alexander Island from Palmer Land, as the easternmost basin of a rift system that terminated at a triple junction with the Antarctic Peninsula subduction zone. The history of the triple junction's third, transform, arm suggests extension started around 33.5–30 Ma. A more speculatively identified basin further west may have formed earlier during the same episode of rifting, starting around 43 Ma. Proposals of earlier Cenozoic relative motion between East and West Antarctica cannot be verified from this region.
Citation: Eagles, G., R. D. Larter, K. Gohl, and A. P. M. Vaughan (2009), West Antarctic Rift System in the Antarctic Peninsula, *Geophys. Res. Lett.*, *36*, L21305, doi:10.1029/2009GL040721.

1. Introduction

[2] The West Antarctic Rift System formed at a plate boundary that separated East and West Antarctica (Figure 1). Observation-based quantifications of the mobility of thermal plumes in the mantle depend on accurate knowledge of this boundary's development, and disagree prior to mid Eocene times [*Steinberger et al.*, 2004; *Tarduno et al.*, 2009]. The base of the West Antarctic Ice Sheet lies well below sea level in the rift system's basins, and its consequent instability makes it a key factor in past and future sea level change [*Vaughan*, 2008; *Bamber et al.*, 2009]. Understanding the rift system's development through time is therefore important, and plate kinematic models are crucial to this understanding.

[3] Direct knowledge of the rift system comes from geological and geophysical surveying and drilling in the Ross Sea region. Late Cretaceous rifting of southern New Zealand from Marie Byrd Land is recorded in rocks exposed at the margins of the Eastern Basin [e.g., *Luyendyk et al.*, 2001]. On the other side of the Ross Sea, fission track analyses betray later unroofing of the Transantarctic Mountains in Victoria Land starting at 55–45 Ma [*Fitzgerald and Baldwin*, 1997], and magnetic anomalies in the Adare Trough record seafloor spreading in the period 43–26 Ma [*Cande et al.*, 2000]. Strata seen on seismic data from the Central, Northern, and Victoria Land basins are interpreted as dating from this period [*Cande and Stock*, 2004a, 2006], and coring to the base of the Victoria Land Basin returned sediments with a maximum age of 34 Ma [*Wilson et al.*, 1998; *Hannah et al.*, 2001]. Sub-ice topography maps show that the rift system continues eastwards between the Transantarctic Mountains and Marie Byrd Land as far as the Byrd Subglacial Basin [*Lythe et al.*, 2001]. Beyond this, although the Transantarctic Mountains continue to the northeast, it is not clear from surveying within Antarctica where the plate boundary lies and what form it takes.

2. Plate Kinematic Models for the West Antarctic Rift System

[4] Despite being very short, the spreading anomalies in the Adare Trough are confidently dated because they form parts of prominent magnetic bights in seafloor around the triple junction of the Australian, East and West Antarctic plates [*Cande and Stock*, 2006]. *Cande et al.* [2000] used data from the bights to close the circuit of those plates, giving Euler parameters that describe the orientation and separation of the Adare Trough anomalies. *Müller et al.* [2007] used a longer circuit involving the Australia–Pacific plate boundary in the Macquarie and Emerald basins south of New Zealand [*Keller*, 2004], and also reproduced the Adare Trough record. Although the resulting stage pole falls within the 95% confidence ellipse of *Cande et al.*'s [2000] stage pole (Figure 1), the two are separated by over 5000 km, and yield very different models of the eastern end of the East-West Antarctic plate boundary. *Müller et al.*'s [2007] stage pole predicts a transcurrent boundary, whereas *Cande et al.*'s [2000] predicts further extensional basins.

[5] Unlike the southern offshore reaches of the East African Rift, where it hosts its own instantaneous motion pole [*Chu and Gordon*, 1999], both stage poles require the eastern parts of the East-West Antarctic plate boundary to have accommodated significant relative motion (Figure 1). Because of this, it is most likely to have terminated at a triple junction with another active plate boundary. The nearest of these was at the western margin of the Antarctic Peninsula where the oceanic Phoenix plate was subducting [*Larter and Barker*, 1991]. Various Cenozoic basins are known from this margin. In the following, we show how the formation of one of them, George VI Sound (GVIS), might be related to extension in the West Antarctic Rift System.

3. Extension and Transtension in George VI Sound

[6] The 800 m deep north-striking arm of GVIS separates the largely sedimentary Fossil Bluff Group of Alexander Island from the intruded metamorphic basement of Palmer Land and probably originated as a terrane boundary in Cretaceous times [*Ferraccioli et al.*, 2006; *Vaughan and Storey*,

[1]Department of Earth Sciences, Royal Holloway University of London, Egham, UK.
[2]British Antarctic Survey, High Cross, Cambridge, UK.
[3]Alfred Wegener Institute for Polar and Marine Research, Bremerhaven, Germany.

0094-8276/09/2009GL040721$05.00

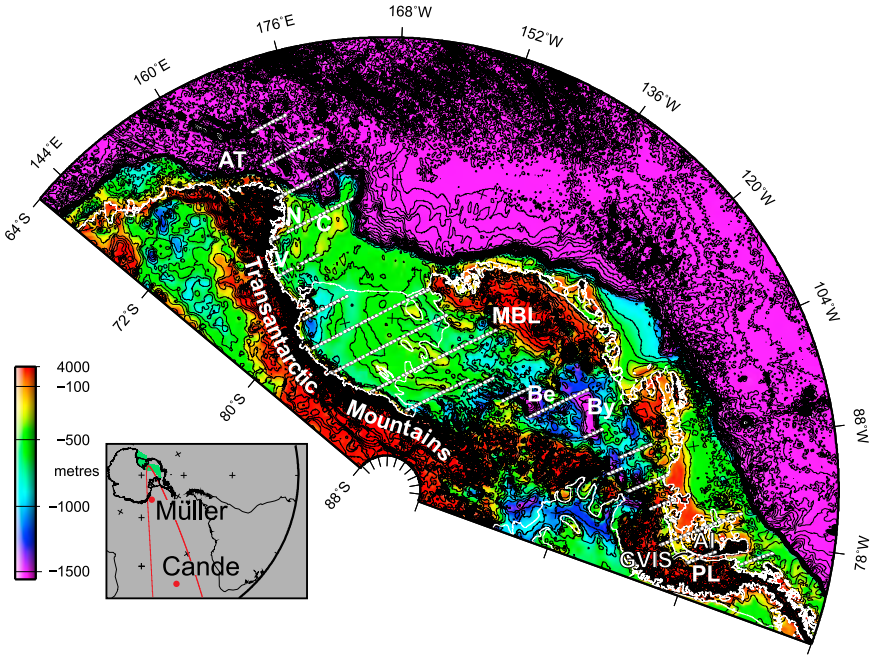

Figure 1. Sub ice topography [*Lythe et al.*, 2001] of the West Antarctic Rift System. AI: Alexander Island, AT: Adare Trough, Be: Bentley Subglacial Trench, By: Byrd Subglacial Basin, C: Central Basin, GVIS: George VI Sound, MBL: Marie Byrd Land, N: Northern Basin, PL: Palmer Land, V: Victoria Land Basin. White lines: segments of small circles about *Cande et al.*'s [2000] rotation pole. Inset: red dots: two alternative stage poles for East–West Antarctic relative motion during 48–26 Ma from *Cande et al.* [2000] (with red line part of its 95% confidence ellipse) and *Müller et al.* [2007].

2000]. Structural studies show that this boundary ultimately evolved into a basin that opened in dextral transtension [*Storey and Nell*, 1988], which may have started around 40–35 Ma as interpreted from fission track data from Alexander Island [*Storey et al.*, 1996]. Gravity modeling implies a stretching factor of ~1.3 [*Maslanyj*, 1988]. A free-air (Figure 2) and Bouguer gravity low suggests the basin continues north across the shelf north of Alexander Island where it is named George VI trough [*Johnson*, 1997; *McAdoo and Laxon*, 1997]. The trough merges opposite the Tula Fracture Zone, via a discrete step in Bouguer gravity, with a margin-parallel sedimentary basin on the continental shelf [*Larter et al.*, 1997; *Johnson*, 1997]. The east-striking southern arm is wider and deeper; here a simple gravity model implies a stretching factor of ~1.5, consistent with formation by lower-obliquity extension than in the northern arm [*Maslanyj*, 1987, 1988]. Volcanic activity resulting from this much stretching may explain the large positive magnetic anomalies observed along the southern arm [*Golynsky et al.*, 2001].

[7] Given the timing of these processes and their position between the Byrd Subglacial Basin and formerly active Antarctic Peninsula margin (Figure 1), it is conceivable that GVIS formed a segment of the West Antarctic Rift System. If so, the distinctive transtensional and extensional tectonics should obey the constraints of a rotation pole for relative motions between East and West Antarctica. This is indeed the case with *Cande et al.*'s [2000] pole, which prescribes a NNW translation of Alexander Island away from Palmer Land (Figure 2). With the margins of the stretched region taken to be beneath ice covered scarps in Palmer Land, and along the LeMay Range Fault in Alexander Island [*Crabtree et al.*, 1985], stretching factors like those *Maslanyj* [1988] modeled require a rotation of ~0.7° about this pole. Assuming stretching occurred on the extensional arm of a ridge-trench-fault triple junction, its onset can be dated to a ridge-crest–trench collision SW of the Tula Fracture Zone at 30.1 ± 3 Ma [*Larter et al.*, 1997]. *Cande et al.*'s [2000] West

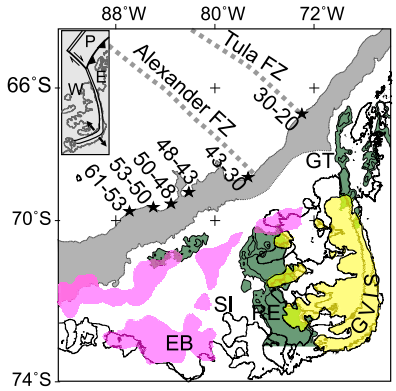

Figure 2. Reconstruction of a closed GVIS. EB: Eltanin Bay; GT: George VI trough; RE: Ronne Entrance; SI: Smyley Island. Light gray: positive free-air gravity anomaly related to modern continental shelf edge, green: negative anomalies (<−20 mgal) on the continental shelf [*McAdoo and Laxon*, 1997]. Stars: positions of possible past triple junctions at the West Antarctic margin, age ranges (in Ma) of their residence [*Larter et al.*, 1997]. Yellow: Alexander Island rotated by 0.7° about *Cande et al.*'s [2000] stage pole. Magenta: positive magnetic anomalies >100 nT [*Golynsky et al.*, 2001]. Inset: triple junction near Alexander Island at ~27 Ma. E: East Antarctic Plate, P: Phoenix Plate, W: West Antarctic plate.

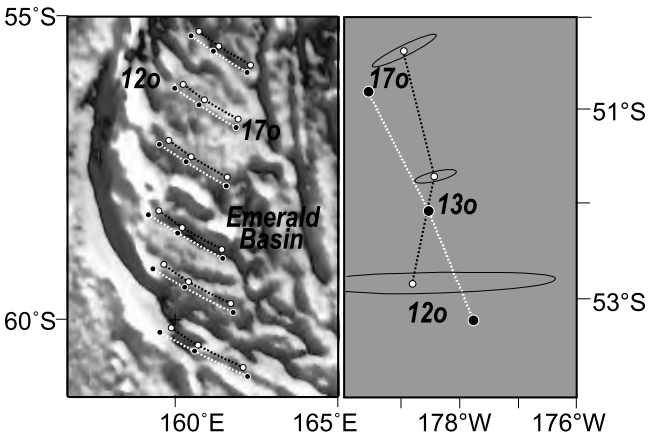

Figure 3. Results of interrogating the South Pacific circuit for Pacific–Australia motions. (left) New synthetic flowlines (white lines with black age points) compared to those of *Keller* [2004] (black lines with white age points); both sets of lines originate from the same seed points, and are overlain on satellite gravity showing fracture zones. (right) Finite rotation poles from circuit (black dots) compared to those of *Keller* [2004] (white dots), with 95% confidence ellipses. Comparisons not possible before chron 17o and after chron 12o as no suitable rotations are available.

Antarctica–East Antarctica rotation for chron C13 (33.5 Ma) also uses an angle of 0.7°, and so we adopt 33.5–30 Ma as a reasonable estimated time range for the onset of GVIS extension.

[8] In contrast, *Müller et al.* [2007] interpret a dominantly transcurrent East Antarctica–West Antarctica boundary in and offshore of the Antarctic Peninsula. The interpretation is based on a grid of crustal stretching factors calculated using sub ice topography and sediment thickness data [*Lythe et al.*, 2001; *Laske and Masters*, 1997]. Examination of the sub ice topography data set reveals that depths in GVIS are erroneously depicted some 600–800 m shallower than have been measured seismically [*Maslanyj*, 1987; *Bell and King*, 1998]. Using more appropriate depths of 800–1000 m, *Müller et al.*'s [2007] method of calculating crustal stretching factors returns values of 1.50–1.64, similar to the results of gravity modelling, consistent with an extensional eastern West Antarctic Rift System.

4. Accuracy in the South Pacific Plate Circuit

[9] This interpretation of GVIS is persuasive in its simplicity. Accepting it, however, draws attention back to the fact that the South Pacific plate circuit yields very different East Antarctica–West Antarctica rotations when constructed with the Pacific–Australia rotations of *Keller* [2004]. Figure 3 illustrates that the differences are artifacts of those rotations by using *Cande et al.*'s [2000] East Antarctica–West Antarctica rotation along with Australia–East Antarctica and Pacific–West Antarctica rotations [*Cande and Stock*, 2004b; *Croon et al.*, 2008] to predict Pacific–Australia motion independently of *Keller*'s [2004] data. The resulting rotations cannot be compared quantitatively to *Keller*'s [2004] as *Cande et al.* [2000] did not provide formal error estimates that would enable us to calculate a set of confidence ellipses. Nonetheless, the circuit-derived finite poles produce synthetic flowline orientations that are qualitatively almost identical both to *Keller*'s [2004] and to fracture zone traces in free-air gravity data.

[10] The artifacts arise from the magnification of small inaccuracies in the Pacific–Australia parameters through their large rotation angles. Despite being small, these inaccuracies are evidently larger than might be expected from *Keller*'s [2004] error analysis (Figure 3), and so must be attributed to factors he did not consider for it. Amongst these factors, we note that some of *Keller*'s [2004] data occupy a broad zone of post-Pliocene deformation attributed to incipient subduction south of New Zealand [*Cande and Stock*, 2004b; *Hayes et al.*, 2009]. These data are not likely to describe relative motions between the Pacific and Australian plates as completely as they would have done if they had not experienced this deformation.

5. Cenozoic Motion Between East and West Antarctica

[11] Sixty percent of *Cande et al.*'s [2000] modeled post-43 Ma West Antarctica–East Antarctica motion would have been expressed prior to and away from the extension in GVIS. By analogy, one can hypothesise a rift basin connecting the precursor to the 'Tula' triple junction, which existed since 43 Ma at the SE end of the Alexander Fracture Zone (Figure 2) [*Larter et al.*, 1997; *Scheuer et al.*, 2006]. Although the fission track evidence from Alexander Island [*Storey et al.*, 1996] is consistent with this timing, evidence for the presence of the basin itself is not overwhelmingly strong. Satellite altimetry data show a broad free-air gravity anomaly crossing the shelf towards the fracture zone. Despite a smooth sedimented seafloor, reverberations in seismic data mask any indication of how deep beneath the anomaly the sediments continue, except near the east coast of Smyley Island [*Nitsche*, 1998]. A positive magnetic anomaly at ~79°W might be interpreted in terms of an uplifted rift flank (Figure 2). High smectite concentrations in sediments from the Ronne Entrance suggest the presence of volcanic or volcaniclastic rocks, perhaps related to rifting, at the seabed [*Hillenbrand et al.*, 2009].

[12] Before 43 Ma, reconstruction misfits between Lord Howe Rise and Campbell Plateau suggest even earlier motion between East and West Antarctica [*Cande and Stock*, 2004a; *Steinberger et al.*, 2004]. Although it has been suggested that this motion created some of the basins of the Ross Sea, there is no firmly-established record of it there in the form of cored or sampled Paleocene or older Eocene sediments. Added to this, there is no evidence for basins connecting to pre-43 Ma triple junctions off Eltanin Bay, where they might be expected (Figure 2). While this absence of evidence is no basis on which to dismiss the idea of Paleocene relative motions between West and East Antarctic plates, it should be taken as a reminder that that idea, while intuitively attractive, remains only indirectly proved and should be applied with caution.

6. Conclusion

[13] The geology of the GVIS region can be interpreted in terms of the eastern reaches of an extensional West Antarctic Rift System. The interpretation reinforces the already strong

evidence for intra-Antarctic extension since 34–30 Ma, and to a lesser degree since 43 Ma, but there is as yet no evidence here for earlier extension. This interpretation further implies that the Antarctic Peninsula has been part of a stable East Antarctic plate since mid Eocene times, and that additional rift basins exist in Ellsworth Land, linking GVIS and the Byrd Subglacial Basin, where elevated heat flow is likely to have influenced ice sheet development and stability.

[14] **Acknowledgments.** This study is a contribution to the British Antarctic Survey Polar Science for Planet Earth Programme. It was funded by Royal Holloway University of London, the Natural Environment Research Council, and the Alfred Wegener Institute for Polar and Marine Research. Figures were created with the Generic Mapping Tools. We thank the organisers of the ANTscape workshop at the University of Leeds in 2009, where we first started together generating the ideas expressed here.

References

Bamber, J. L., R. E. M. Riva, B. L. A. Vermeersen, and A. M. LeBrocq (2009), Reassessment of the potential sea-level rise from a collapse of the West Antarctic Ice Sheet, *Science*, *324*, 901–903, doi:10.1126/science.1169335.

Bell, A. C., and E. C. King (1998), New seismic data support Cenozoic rifting in George VI Sound, Antarctic Peninsula, *Geophys. J. Int.*, *134*, 889–902, doi:10.1046/j.1365-246x.1998.00605.x.

Cande, S. C., and J. M. Stock (2004a), Cenozoic reconstructions of the Australia-New Zealand-South Pacific sector of Antarctica, in *The Cenozoic Southern Ocean: Tectonics, Sedimentation and Climate Change Between Australia and Antarctica*, *Geophys. Monogr. Ser.*, vol. 151, edited by N. Exon, J. Kennett, and M. Malone, pp. 5–18, AGU, Washington, D. C.

Cande, S. C., and J. M. Stock (2004b), Pacific-Antarctic-Australia motion and the formation of the Macquarie Plate, *Geophys. J. Int.*, *157*, 399–414, doi:10.1111/j.1365-246X.2004.02224.x.

Cande, S. C., and J. M. Stock (2006), Constraints on the timing of extension in the Northern Basin, Ross Sea, in *Antarctic Contributions to Global Earth Science*, edited by D. K. Fütterer et al., pp. 317–324, Springer, Berlin.

Cande, S. C., J. Stock, R. D. Müller, and T. Ishihara (2000), Cenozoic motion between East and West Antarctica, *Nature*, *404*, 145–150, doi:10.1038/35004501.

Chu, D., and R. G. Gordon (1999), Evidence for motion between Nubia and Somalia along the southwest Indian ridge, *Nature*, *398*, 64–66, doi:10.1038/18014.

Crabtree, R. D., B. C. Storey, and C. S. M. Doake (1985), The structural evolution of George VI sound, Antarctic Peninsula, *Tectonophysics*, *114*, 431–442, doi:10.1016/0040-1951(85)90025-3.

Croon, M. B., S. C. Cande, and J. M. Stock (2008), Revised Pacific-Antarctic plate motions and geophysics of the Menard Fracture Zone, *Geochem. Geophys. Geosyst.*, *9*, Q07001, doi:10.1029/2008GC002019.

Ferraccioli, F., P. C. Jones, A. P. M. Vaughan, and P. T. Leat (2006), New aerogeophysical view of the Antarctic Peninsula: More pieces, less puzzle, *Geophys. Res. Lett.*, *33*, L05310, doi:10.1029/2005GL024636.

Fitzgerald, P. G., and S. L. Baldwin (1997), Detachment fault model for the evolution of the Ross Embayment, in *The Antarctic Region: Geological Evolution and Processes*, edited by C. A. Ricci, pp. 555–564, Terra Antarct., Siena, Italy.

Golynsky, A., et al. (2001), ADMAP—Magnetic anomaly map of the Antarctic, scale 1:10,000,000, *BAS Misc. 10*, Br. Antarct. Surv., Cambridge, U. K.

Hannah, M. J., et al. (2001), Chronostratigraphy of the CRP-3 drillhole, Victoria Land Basin, Antarctica, *Terra Antarct.*, *8*, 615–620.

Hayes, G. P., K. P. Furlong, and C. J. Ammon (2009), Intraplate deformation adjacent to the Macquarie Ridge south of New Zealand—The tectonic evolution of a complex plate boundary, *Tectonophysics*, *463*, 1–14, doi:10.1016/j.tecto.2008.09.024.

Hillenbrand, C.-D., W. Ehrmann, R. D. Larter, S. Benetti, J. A. Dowdeswell, C. Ó. Cofaigh, A. G. C. Graham, and H. Grobe (2009), Clay mineral provenance of sediments in the southern Bellingshausen sea reveals drainage changes of the West Antarctic ice sheet during the late quaternary, *Mar. Geol.*, *265*, 1–18.

Johnson, A. C. (1997), Cenozoic tectonic evolution of the Marguerite Bay area, Antarctic Peninsula, interpreted from geophysical data, *Antarct. Sci.*, *9*, 268–280.

Keller, W. R. (2004), Cenozoic plate tectonic reconstructions and plate boundary processes in the southwest Pacific, Ph.D. thesis, Calif. Inst. of Technol., Pasadena.

Larter, R. D., and P. F. Barker (1991), Effects of ridge-crest trench interaction on Antarctic-Phoenix spreading: Forces on a young subducting plate, *J. Geophys. Res.*, *96*, 19,583–19,607, doi:10.1029/91JB02053.

Larter, R. D., M. Rebesco, L. E. Vanneste, L. A. P. Gambôa, and P. F. Barker (1997), Cenozoic tectonic, sedimentary and glacial history of the continental shelf west of Graham Land, Antarctic Peninsula, in *Geology and Seismic Stratigraphy of the Antarctic Margin, 2*, *Antarct. Res. Ser.*, vol. 71, edited by P. F. Barker and A. K. Cooper, pp. 1–27, AGU, Washington, D. C.

Laske, G., and G. Masters (1997), A global digital map of sediment thickness, *Eos Trans. AGU*, *78*, F483.

Luyendyk, B. P., C. C. Sorlien, D. Wilson, L. Bartek, and C. S. Siddoway (2001), Structural and tectonic evolution of the Ross Sea rift in the Cape Colbeck region, eastern Ross Sea, Antarctica, *Tectonics*, *20*, 933–958, doi:10.1029/2000TC001260.

Lythe, M. B., et al. (2001), BEDMAP: A new ice thickness and subglacial topographic model of Antarctica, *J. Geophys. Res.*, *106*, 11,335–11,351, doi:10.1029/2000JB900449.

Maslanyj, M. P. (1987), Seismic bedrock depth measurements and the origin of George VI Sound, Antarctic Peninsula, *Br. Antarct. Surv. Bull.*, *75*, 51–65.

Maslanyj, M. P. (1988), Gravity and aeromagnetic evidence for the crustal structure of George VI Sound, Antarctic Peninsula, *Br. Antarct. Surv. Bull.*, *79*, 1–16.

McAdoo, D., and S. Laxon (1997), Antarctic tectonics: Constraints from a new ERS-1 satellite marine gravity field, *Science*, *276*, 556–561, doi:10.1126/science.276.5312.556.

Müller, R. D., K. Gohl, S. C. Cande, A. Goncharov, and A. Golynsky (2007), Eocene to Miocene geometry of the West Antarctic Rift System, *Aust. J. Earth Sci.*, *54*, 1033–1045, doi:10.1080/08120090701615691.

Nitsche, F.-O. (1998), Bellingshausen- und Amundsenmeer: Entwicklung eines Sedimentationsmodells, *Ber. Polarforsch. 258*, 144 pp., Alfred Wegener Inst. fuer Polar- und Meeresforsch., Bremerhaven, Germany.

Scheuer, C., K. Gohl, R. D. Larter, M. Rebesco, and G. B. Udintsev (2006), Variability in Cenozoic sedimentation along the continental rise of the Bellingshausen Sea, West Antarctica, *Mar. Geol.*, *227*, 279–298, doi:10.1016/j.margeo.2005.12.007.

Steinberger, B., R. Sutherland, and R. J. O'Connell (2004), Prediction of Emperor-Hawaii seamount locations from a revised model of plate motion and mantle flow, *Nature*, *430*, 167–173, doi:10.1038/nature02660.

Storey, B. C., and P. A. R. Nell (1988), Role of strike-slip faulting in the tectonic evolution of the Antarctic Peninsula, *J. Geol. Soc.*, *145*, 333–337, doi:10.1144/gsjgs.145.2.0333.

Storey, B. C., R. W. Brown, A. Carter, P. A. Doubleday, A. J. Hurford, D. I. M. MacDonald, and P. A. R. Nell (1996), Fission-track evidence for the thermotectonic evolution of a Mesozoic-Cenozoic fore-arc, Antarctica, *J. Geol. Soc.*, *153*, 65–82, doi:10.1144/gsjgs.153.1.0065.

Tarduno, J., H.-P. Bunge, N. Sleep, and U. Hansen (2009), The bent Hawaiian-Emperor hotspot track: Inheriting the mantle wind, *Science*, *324*, 50–53, doi:10.1126/science.1161256.

Vaughan, D. (2008), West Antarctic ice-sheet collapse—The fall and rise of a paradigm, *Clim. Change*, *91*, 65–79, doi:10.1007/s10584-008-9448-3.

Vaughan, A. P. M., and B. C. Storey (2000), The eastern Palmer Land shear zone: A new terrane accretion model for the Mesozoic development of the Antarctic Peninsula, *J. Geol. Soc.*, *157*, 1243–1256.

Wilson, G. S., A. P. Roberts, K. L. Verosub, F. Florindo, and L. Sagnotti (1998), Magnetobiostratigraphic chronology of the Eocene-Oligocene transition in the CIROS-1 core, Victoria Land margin, Antarctica; implications for Antarctic glacial history, *Geol. Soc. Am. Bull.*, *110*, 35–47, doi:10.1130/0016-7606[1998]110<0035:MCOTEO>2.3.CO;2.

G. Eagles, Department of Earth Sciences, Royal Holloway University of London, Egham TW20 0EX, UK. (g.eagles@es.rhul.ac.uk)

K. Gohl, Alfred Wegener Institute for Polar and Marine Research, Am Alten Hafen 6, Bremerhaven D-27620, Germany.

R. D. Larter and A. P. M. Vaughan, British Antarctic Survey, High Cross, Madingley Road, Cambridge CB3 0ET, UK.

Publication 6.2.3:

Gohl, K., Teterin, D., Eagles, G., Netzeband, G., Grobys, J., Parsiegla, N., Schlüter, P., Leinweber, V., Larter, R.D., Uenzelmann-Neben, G., Udintsev, G.B. (2007). Geophysical survey reveals tectonic structures in the Amundsen Sea embayment, West Antarctica; Proceedings of the 10th Int. Symposium of Antarctic Earth Sciences, edited by A.K. Cooper and C.R. Raymond et al., *USGS Open-File Report 2007-1047*, doi:10.3133/of2007-1047.srp047.

Author contributions: This peer-reviewed proceedings paper was mostly written by Gohl. Gravity data inversions by Teterin were used to derive a Moho depth grid. Eagles, Netzeband, Grobys, Parsiegla, Schlüter and Leinweber helped acquire and model seismic and magnetic data during Polarstern expedition ANT-XXIII/4 (2006) under supervision of Gohl (chief-scientist). Larter, Uenzelmann-Neben and Udintsev contributed to the discussion.

U.S. Geological Survey and The National Academies; USGS OF-2007-1047, Short Research Paper 047; doi:10.3133/of2007-1047.srp047

Geophysical survey reveals tectonic structures in the Amundsen Sea embayment, West Antarctica

K. Gohl,[1] D. Teterin,[2] G. Eagles,[1] G. Netzeband,[3] J. W. G. Grobys,[1] N. Parsiegla,[1] P. Schlüter,[1] V. Leinweber,[1] R. D. Larter,[1] G. Uenzelmann-Neben,[1] and G. B. Udintsev[2]

[1]Alfred Wegener Institute for Polar and Marine Research, Postbox 120161, 27515 Bremerhaven, Germany (karsten.gohl@awi.de)
[2]Vernadsky Institute of Geochemistry and Analytical Chemistry, Laboratory of Geomorphology and Tectonics of the Ocean Floor, 19 Kosygin St., 117975 Moscow, Russia (d_e_teterin@mail.ru)
[3]Institute for Geophysics, University of Hamburg, Bundesstr. 55, 20146 Hamburg, Germany (now at: gnetzeband@ifm-geomar.de)
[5]British Antarctic Survey, High Cross, Madingley Road, Cambridge, CB3 0ET, UK (r.larter@bas.ac.uk)

Abstract The Amundsen Sea embayment of West Antarctica is in a prominent location for a series of tectonic and magmatic events from Paleozoic to Cenozoic times. Seismic, magnetic and gravity data from the embayment and Pine Island Bay (PIB) reveal the crustal thickness and some tectonic features. The Moho is 24-22 km deep on the shelf. NE-SW trending magnetic and gravity anomalies and the thin crust indicate a former rift zone that was active during or in the run-up to breakup between Chatham Rise and West Antarctica before or at 90 Ma. NW-SE trending gravity and magnetic anomalies, following a prolongation of Peacock Sound, indicate the extensional southern boundary to the Bellingshausen Plate which was active between 79 and 61 Ma.

Citation: Gohl, K., D. Teterin, G. Eagles, G. Netzeband, J. W. G. Grobys, N. Parsiegla, P. Schlüter, V. Leinweber, R. D. Larter, G. Uenzelmann-Neben, and G. B. Udintsev (2007), Geophysical survey reveals tectonic structures in the Amundsen Sea embayment, West Antarctica, in Antarctica: A Keystone in a Changing World – Online Proceedings of the 10th ISAES, edited by A. K. Cooper and C. R. Raymond et al., USGS Open-File Report 2007-1047, Short Research Paper 047, 4 p.; doi:10.3133/of2007-1047.srp047

Introduction

The Amundsen Sea embayment with its eastern sector, Pine Island Bay (PIB) (Figure 1), is in a tectonically prominent position suggested to be the location of a crustal boundary between the Marie Byrd Land block to the west and the Thurston Island/Ellsworth Land blocks to the east which was active during the Mesozoic break-up of Gondwana or even before (e.g. Dalziel and Elliot, 1982; Storey, 1991; Grunow et al., 1991). Eagles et al. (2004) illustrate that early Pacific-Antarctic separation evolved first as rifting and crustal extension along the present-day Bounty Trough between Chatham Rise and Campbell Plateau (Grobys et al., 2007). It possibly continued along the present Great South Basin between the Campbell Plateau and the South Island of New Zealand at 90 Ma until the rift was abandoned in favour of a new extensional locus to the south, forming the earliest oceanic crust between Campbell Plateau and Marie Byrd Land at 84-83 Ma. The boundary between Chatham Rise and Campbell Plateau – with Bounty Trough closed before 90 Ma – is situated off the western Amundsen Sea Embayment at about 120°-125° W.

The Bellingshausen Plate (Stock and Molnar, 1987) moved independently on the southern flank of the mid-Pacific spreading ridge from Late Cretaceous times until about 61 Ma when a major plate reorganisation occurred in the South Pacific (e.g. Larter et al., 2002; Eagles et al., 2004). The small plate's western boundary was situated in the area of the Marie Byrd Seamounts (Heinemann et al., 1999), its eastern transpressional boundary along a gravity anomaly lineament in the western Bellingshausen Sea. The southern boundary may have been active along the WNW-ESE striking Peacock Gravity Anomaly (PGA) across the outer continental shelf of the Amundsen Sea embayment (Larter et al., 2002; Eagles et al., 2004).

The newest geophysical data from the Amundsen Sea Embayment and PIB (Figure 1) reveal crustal thickness and tectonic features and lineations. These early results are discussed in context with plate-kinematic reconstructions of the early stages of continental breakup and southern Pacific seafloor spreading.

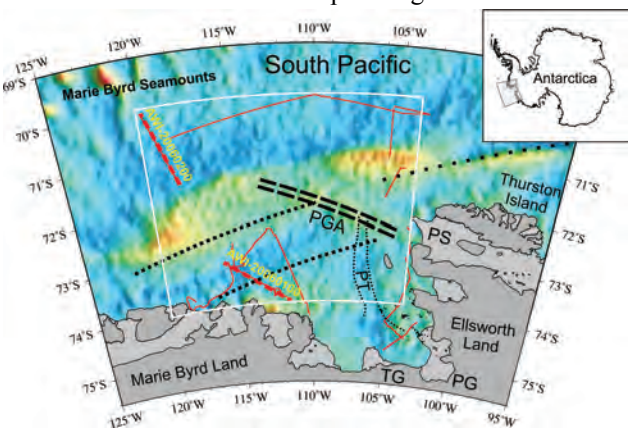

Figure 1. Overview map of the Amundsen Sea embayment and Pine Island Bay showing the satellite-derived gravity anomaly grid of McAdoo and Laxon (1997) and the locations of two deep crustal seismic (dashed red lines) and multi-channel seismic profiles (red lines) collected during RV *Polarstern* expedition ANT-XXIII/4. The dotted bold black lines mark the approximate location of the interpreted incipient narrow rift basin. Its trend is aligned with a gravity anomaly north of Thurston Island. The dashed black lines illustrate the presumed location of the southern Bellingshausen Plate boundary. The box marks the area of the Moho depth map of Figure 4. PT Pine Island Through, PGA Peacock Gravity Anomaly, PS Peacock Sound, PG Pine Island Glacier, TG Thwaites Glacier.

Geophysical data acquisition in the Amundsen Sea Embayment

The Alfred Wegener Institute and British Antarctic Survey cooperated closely during early 2006 with RV *Polarstern*'s expedition ANT-XXIII/4 and RRS *James C. Ross*' cruise JR141. Extensive geophysical datasets were collected as part of a research program dedicated to the study of tectonic, sedimentary and glacial advance/retreat processes in the Amundsen Sea Embayment and PIB (Larter et al., 2007). For this paper, we primarily use the resulting deep crustal seismic profiles, shipborne gravity and magnetic data collected from the *Polarstern*, and an extensive aeromagnetic survey of 20,000 km flown by the *Polarstern* helicopters (Figures 1 and 2). Due to an area of inaccessibility, the magnetic data mainly cover two separate areas: the western Amundsen Sea embayment and the southern and eastern PIB region. The analysis of these data was complemented by the few previously-existing seismic and potential field data from the shelf break to the oceanic parts of the Amundsen Sea (Gohl et al., 1997; Nitsche et al., 2000) and by the satellite-derived gravity anomaly field of McAdoo & Laxon (1997).

We acquired deep crustal seismic wide-angle reflection and refraction data with one profile across the inner to middle continental shelf of the western embayment (AWI-20060100) and another running from the foot of the slope towards the Marie Byrd Seamount cluster of the continental rise (AWI-20060200) (Figure 1). Shots from an airgun cluster, consisting of 8 G.Guns™ with a total volume of 68 liters (4160 in^3), fired with 190 bar at a 1-minute interval (150 m nominal spacing), resulted in good quality data with identified phases from the upper to lower crust and the uppermost mantle on both profiles. Restricted by massive pack-ice to the north, west and east and by drifting sea-ice patches, only nine ocean-bottom hydrophone (OBH) systems could be deployed at 18-19 km spacing on the shelf, in order to minimize the risk of instrument loss. Seven OBH systems with the same nominal spacing were deployed along the deep-sea profile. About 2200 km of multi-channel seismic (MCS) profiles were acquired in the Amundsen Sea Embayment and in PIB using a 600-m long analogue streamer. We also recorded low-fold normal-incidence reflection data from the airgun shots along both OBH profiles with the same streamer. 530 km of single-channel seismic data were recorded in the embayment during the JR141 cruise (Larter et al., 2007). For this study, we use parts of the MCS dataset to identify the depth of the acoustic basement to constrain thickness and geometries of the sediment cover in the seismic refraction and gravity modelling process. Details of the seismic reflection data with regard to glacial-marine sedimentation processes will be given elsewhere (e.g. Uenzelmann-Neben et al., this volume).

Magnetic grid, seismic and gravity models

The combined helicopter and shipboard magnetic grid reveals a NE-SW trending system of near-parallel positive magnetic anomaly lineations as the dominant feature in the western embayment (Figure 2). The lineations run parallel to the trend of the satellite-derived gravity anomalies across the middle shelf and that of sharp positive linear gravity anomaly north of Thurston Island. The magnetic grid over the eastern PIB reveals scattered patches of positive and negative anomalies with no significant lineations, except for a the short WNW trend of positive anomalies west of the Peacock Sound. This anomaly lies on top of, and has the same orientation as, the PGA, but it does not follow the PGA farther northwest. However, gravity modeling indicates an elongated body of high-density, possibly magmatic material along the PGA. Some of the scattered magnetic anomalies in the south may be attributed to the numerous igneous and meta-igneous bodies observed in outcrops on islands in PIB and along its eastern mainland shore as observed by the SPRITE Group (1992) and on our *Polarstern* cruise.

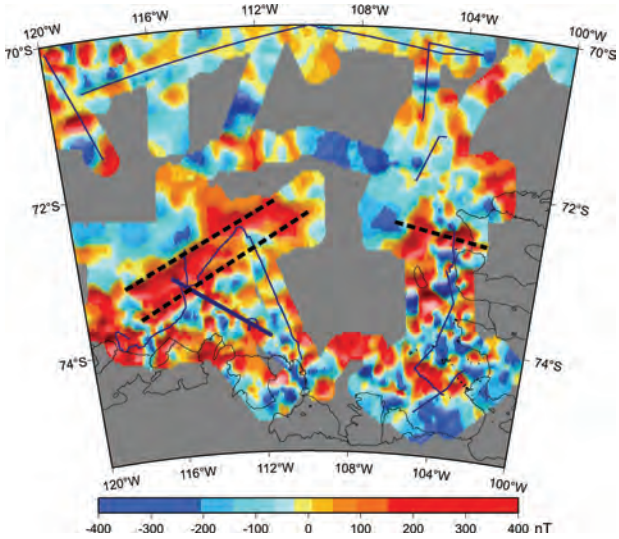

Figure 2. Map of gridded magnetic anomalies in the Amundsen Sea embayment from helicopter-magnetic surveying and ship-board magnetic data of ANT-XXIII/4. Dashed black lines indicate linear anomaly trends. Thin dark blue lines denote seismic reflection profiles of ANT-XXIII/4. Thick dark blue lines mark the locations of deep crustal seismic profiles (the southern profile AWI-20060100 corresponds to model in Figure 3).

The P-wave phases recorded by eight OBH systems of shelf profile AWI-20060100 were modeled for a crustal velocity-depth structure using a raytracing and travel-time inversion method. The final velocity-depth model (Figure 3) shows a 22-23 km thick crust with velocities of 2.0-3.5 km/s for the sediments above the acoustic basement, 5.0-6.2 km/s for the upper crust below the acoustic basement, and 6.4-6.9 km/s for the lower crust. Pn phases indicate an upper mantle velocity of 7.9-

8.0 km/s. The relatively thin crust, the regular vertical velocity distribution, and the average crustal velocity of about 6.4 km/s, all suggest that the inner continental shelf of the Amundsen Sea embayment rests on stretched continental crust, but is largely unaffected by magmatic intrusions. Unfortunately, the coverage at the northwestern end of the profile does not reach into the area of the linear SW-NE trending magnetic anomalies.

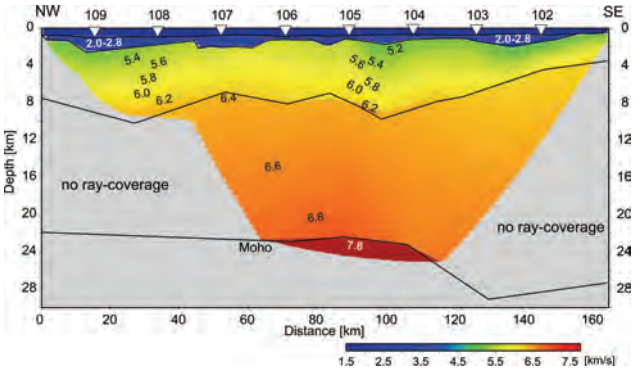

Figure 3. Velocity-depth model of OBH profile AWI-20060100 across the inner and middle continental shelf of the western Amundsen Sea embayment. OBH stations are marked by triangles. Layers outside the coloured grid are not constrained by travel-time information but constrained by gravity modelling.

A series of 2-D gravity models were calculated along the seismic and other quasi-linear profiles across the Amundsen Sea embayment primarily using shipboard data complemented by satellite-derived gravity data (McAdoo and Laxon, 1997) in gaps and to extend the profiles. We constrained the models with observations of sediment thickness using seismic reflection data and the crustal structure and thickness from the two OBH profiles. Next, we integrated the 2-D models into a 3-D gravity anomaly model of the embayment. The resulting map of Moho depth (Figure 4) shows the crust thinning above a Moho at about 24 km depth beneath the eastern embayment and about 22 km in the western embayment. Beneath the oceanic crust, the Moho depth increases from 14-15 km in the east to 15-17 km in the west between the Marie Byrd Seamounts and the foot of the shelf slope.

Tectonic implications

The potential field data indicate two dominant and crossing trends of linear anomalies in the Amundsen Sea embayment. The linear gravity and magnetic anomalies of the western Amundsen Sea embayment, running sub-parallel to each other, can be interpreted as indicating an intrusive crustal origin. Their NE-SW trend parallels the initial spreading center's azimuth between Chatham Rise and West Antarctica and can thus be related to processes occurring during breakup or just beforehand. The anomalously thin crust beneath the inner shelf - in particular of the western embayment - suggests a crustal thinning process. These three observations lead to a model of a failed initial rift or distributed extension in the Amundsen Sea embayment crust. This rift must have been active before 90 Ma or it accompanied the rifting in Bounty Trough and its northward translation of Chatham Rise at this time.

We interpret the WNW trending PGA and its underlying high-density body as a magmatic zone which overprinted the NE-SW trending rift structure. This seems to confirm the suggestion by Eagles et al. (2004) that this zone acted as the southern boundary of the Bellingshausen Plate between 79 and 61 Ma. Plate-kinematics demonstrates that this plate boundary was active as a zone of relatively minor extensional and translational movements. Our new data show that magmatic intrusions were emplaced in some places along this boundary.

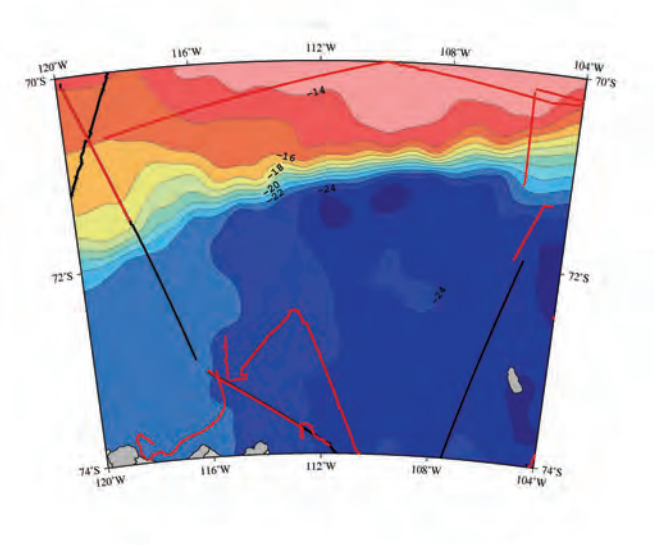

Figure 4. Moho depth map of the Amundsen Sea embayment derived from 2D (along profiles annotated with black lines) and 3D gravity anomaly modeling constrained by satellite-derived gravity data (McAdoo and Laxon, 1997) and seismic data (red lines).

The presumed Paleozoic crustal boundary between the Thurston Island/Ellsworth Land block and the Marie Byrd Land block in PIB is not obvious from the potential field data. If present, the difficulty in interpreting its presence may be traced back to overprinting by Mesozoic and Cenozoic magmatic intrusions and volcanism (e.g. LeMasurier, 1990). What is more, the deeply incised inner and middle shelf of PIB with glacial troughs and channels reaching 1000-1500 m depth (Lowe and Anderson, 2002; Larter et al., 2007) may obscure interpretations of the magnetic anomaly field. We agree with an earlier suggestion by the SPRITE Group (1992) that the main deep glacial erosional trough, here named Pine Island Trough (Figure 1), stretching from the mouth of the Pine Island Glacier to the middle shelf in NW and

NNW orientation may have exploited such a former crustal block boundary.

Conclusions

Seismic, magnetic and gravity surveying of the Amundsen Sea embayment and PIB reveal important phases of the tectonic evolution in this area. The main results are:

(1) The Moho depth of the inner and middle shelf is between 24 and 22 km and thins from east to west.

(2) Dominant NE-SW trending magnetic and gravity anomalies and the thin crust indicate a former rift zone proposed to be active during or prior to the breakup between Chatham Rise and West Antarctica before or at 90 Ma.

(3) NW-SE trending gravity and short magnetic anomalies in the prolongation of the Peacock Sound are consistent with the proposed tectonic activity and location of the southern Bellingshausen Plate boundary between 79 and 61 Ma.

(4) A presumed crustal block boundary between Thurston Island/Ellsworth Land block and the Marie Byrd Land block cannot be clearly observed in PIB. It is possible, however, that the glacial Pine Island Trough exploited such a former crustal block boundary or inherited structure.

Acknowledgments. We gratefully acknowledge the excellent support of Captain Uwe Pahl and his officers and crew of RV *Polarstern* during expedition ANT-XXIII/4. We thank Ernst Flüh of IfM-GEOMAR for lending us four OBH systems. Many thanks go to Ian Dalziel and Michael Studinger for very helpful reviews and to the co-editor Bryan Storey for the editorial work.

References

Dalziel, I.W.D., and D. H. Elliot (1982), West Antarctica: problem child of Gondwanaland, Tectonics, 1, 3-19.

Eagles, G., K. Gohl, and R. B. Larter (2004), High resolution animated tectonic reconstruction of the South Pacific and West Antarctic margin; Geochemistry, Geophysics, Geosystems (G^3), 5, doi:10.1029/2003GC000657.

Gohl, K., F. Nitsche, K. Vanneste, H. Miller, N. Fechner, L. Oszko, C. Hübscher, E. Weigelt, and A. Lambrecht (1997), Tectonic and sedimentary architecture of the Bellingshausen and Amundsen Sea Basins, SE Pacific, by seismic profiling, in The Antarctic Region: Geological Evolution and Processes, edited by C. A. Ricci, pp. 719-723, Terra Antartica Publication, Siena.

Grobys, J. W. G., K. Gohl, B. Davy, G. Uenzelmann-Neben, T. Deen, and D. Barker (2007), Is the Bounty Trough, off eastern New Zealand, an aborted rift?, J. Geophys. Res., 112, B03103, doi:10.1029/2005JB004229.

Grunow, A. M., D. V. Kent, and I. W. D. Dalziel (1991), New paleomagnetic data from Thurston Island: Implications for the tectonics of West Antarctica and Weddell Sea opening, J. Geophys. Res, 96, B11, 17935-17954.

Heinemann, J., J. Stock, K. Clayton, S. Hafner, S. Cande, and C. Raymond (1999), Constraints on the proposed Marie Byrd Land–Bellingshausen plate boundary from seismic reflection data, J. Geophys. Res., 104, 25321–25330.

Larter, R. D., A. P. Cunningham, P. F. Barker, K. Gohl, and F. O. Nitsche (2002), Tectonic evolution of the Pacific margin of Antarctica – 1. Late Cretaceous tectonic reconstructions, J. Geoph. Res., 107(B12), 2345, doi:10.1029/2000JB000052.

Larter, R.D., K. Gohl, C. D. Hillenbrand, G. Kuhn, T. J. Deen, R. Dietrich, G. Eagles, J. S. Johnson, R. A. Livermore, F. O. Nitsche, C. J. Pudsey, H.-W. Schenke, J. A. Smith, G. Udintsev, and G. Uenzelmann-Neben (2007), West Antarctic Ice Sheet change since the last glacial period, EOS Trans., Am. Geophys. Union, 88, 189-196.

LeMasurier, W. E. (1990), Late Cenozoic volcanism on the Antarctic plate: an overview, in Volcanoes of the Antarctic Plate and Southern Oceans, edited by W. E. LeMasurier and J. W. Thomson, Am. Geophys. Union Antarct. Res. Ser., 48, pp. 1-19.

Lowe, A. L., and J. B. Anderson (2000), Reconstruction of the West Antarctic ice sheet in Pine Island Bay during the Last Glacial Maximum and its subsequent retreat history, Quat. Sci. Reviews, 21, 1879-1897.

McAdoo, D.C., and S. Laxon (1997), Antarctic tectonics: Constraints from an ERS-1 satellite marine gravity field, Science, 276, 556-560.

Nitsche, F. O., A. P. Cunningham, R. D. Larter, and K. Gohl (2000), Geometry and development of glacial continental margin depositional systems in the Bellingshausen Sea, Marine Geology, 162, 277-302.

SPRITE Group (1992), The southern rim of the Pacific Ocean: Preliminary geologic report of the Amundsen Sea - Bellingshausen Sea cruise of the *Polar Sea*, 12 February – 21 March 1992, Ant. J. of the U.S., 27, 11-14.

Stock, J., and P. M. Molnar (1987), Revised history of early Tertiary plate motion in the south-west Pacific, Nature, 325, 495-499.

Storey, B. C. (1991), The crustal blocks of West Antarctica within Gondwana: reconstruction and break-up model, in Geological Evolution of Antarctica, edited by M. R. A. Thomson, J. A. Crane, and J. W. Thomson, Cambridge Univ. Press, Cambridge.

Uenzelmann-Neben, G., K. Gohl, R. D. Larter, and P. Schlüter (this volume), Differences in ice retreat across Pine Island Bay, West Antarctica, since the Last Glacial Maximum: indications from multichannel seismic reflection data, in Antarctica: A Keystone in a Changing World – Online Proceedings of the 10th ISAES, edited by A. K. Cooper and C. R. Raymond et al., USGS Open-File Report.

Publication 6.2.4:

Gohl, K., Denk, A., Wobbe, F., Eagles, G. (2013a). Deciphering tectonic phases of the Amundsen Sea Embayment shelf, West Antarctica, from a magnetic anomaly grid. *Tectonophysics*, v. 585, pp. 113-123, doi:10.1016/j.tecto.2012.06.036.

Author contributions: This paper, which presents the first compiled and interpreted magnetic anomaly grid of the Amundsen Sea Embayment, was to its largest extent written by Gohl (70%) and includes processing methods and some results from a Diplom-thesis of Denk (30%) supervised by Gohl. Wobbe and Eagles helped acquire and process the magnetic data from Polarstern expeditions ANT-XXIII/4 (2006) and ANT-XXVI/3 (2010) (under supervision of chief-scientist Gohl).

Tectonophysics 585 (2013) 113–123

Contents lists available at SciVerse ScienceDirect

Tectonophysics

journal homepage: www.elsevier.com/locate/tecto

Deciphering tectonic phases of the Amundsen Sea Embayment shelf, West Antarctica, from a magnetic anomaly grid

Karsten Gohl [a,*], Astrid Denk [a,b,1], Graeme Eagles [c], Florian Wobbe [a]

[a] Alfred Wegener Institute for Polar and Marine Research, Am Alten Hafen 26, Bremerhaven 27568, Germany
[b] Institute of Geophysics and Meteorology, University of Cologne, Zülpicher Straße 49a, Köln 50674, Germany
[c] Dept. of Earth Sciences, Royal Holloway University of London, Egham TW20 0EX, UK

ARTICLE INFO

Article history:
Received 7 September 2011
Received in revised form 15 May 2012
Accepted 20 June 2012
Available online 2 July 2012

Keywords:
Aeromagnetics
Data processing
Pine Island Bay
Gondwana breakup
Bellingshausen Plate
West Antarctic Rift System

ABSTRACT

The Amundsen Sea Embayment (ASE), with Pine Island Bay (PIB) in the eastern embayment, is a key location to understanding tectonic processes of the Pacific margin of West Antarctica. PIB has for a long time been suggested to contain the crustal boundary between the Thurston Island block and the Marie Byrd Land block. Plate tectonic reconstructions have shown that the initial rifting and breakup of New Zealand from West Antarctica occurred between Chatham Rise and the eastern Marie Byrd Land at the ASE. Recent concepts have discussed the possibility of PIB being the site of one of the eastern branches of the West Antarctic Rift System (WARS). About 30,000 km of aeromagnetic data – collected opportunistically by ship-based helicopter flights – and tracks of ship-borne magnetics were recorded over the ASE shelf during two RV *Polarstern* expeditions in 2006 and 2010. Grid processing, Euler deconvolution and 2D modelling were applied for the analysis of magnetic anomaly patterns, identification of structural lineaments and characterisation of magnetic source bodies. The grid clearly outlines the boundary zone between the inner shelf with outcropping basement rocks and the sedimentary basins of the middle to outer shelf. Distinct zones of anomaly patterns and lineaments can be associated with at least three tectonic phases from (1) magmatic emplacement zones of Cretaceous rifting and breakup (100–85 Ma), to (2) a southern distributed plate boundary zone of the Bellingshausen Plate (80–61 Ma) and (3) activities of the WARS indicated by NNE–SSW trending lineaments (55–30 Ma?). The analysis and interpretation are also used for constraining the directions of some of the flow paths of past grounded ice streams across the shelf.

1. Introduction

The Amundsen Sea Embayment contains one of the largest continental shelves of the Pacific margin of West Antarctica. Pine Island Bay, in the eastern part of the embayment, has for a long time been suggested to contain the crustal boundary between the Thurston Island block and the Marie Byrd Land block (e.g. Dalziel and Elliot, 1982; Grunow et al., 1991; Storey, 1991). Plate tectonic reconstructions suggest that this region was a key area for the initiation of continental breakup, that it was the location of a possible plate boundary, and that it may have been, or still is, an active branch of the West Antarctic Rift System (Dalziel, 2006; Eagles et al., 2004a; Gohl et al., 2007; Jordan et al., 2010; Larter et al., 2002; Wobbe et al., 2012). In spite of all this, little is known about the tectonic evolution and architecture of the embayment from direct study there.

Tectonically induced displacements of the crust are the underlying processes controlling the development of landscapes upon which climate processes play out. This context is of particular importance for reconstructing continental ice sheet evolution. In the Amundsen Sea Embayment, the Pine Island, Thwaites, Smith and Kohler glacier systems are thinning at rapid rates, and some of them have also started to flow at dramatically increased rates (e.g. Rignot et al., 2008; Pritchard et al., 2009). If these glaciers were to drain their catchment area, the volume of ice lost to the ocean could potentially lead to 1.5 m of sea-level rise (Vaughan et al., 2006). Modelling results (Pollard and DeConto, 2009) suggest that the ice sheet in the Amundsen Sea Embayment may have retreated with similar dynamics several times since the Pliocene. Identifying tectonic lineaments and understanding the tectonic architecture of the shelf of the Amundsen Sea Embayment may thus not only help explaining the geodynamic and kinematic processes of continental rifting in this West Antarctic realm, but also provide valuable constraints on flow paths and subglacial substrate of basement for palaeo-ice sheet modellers.

* Corresponding author at: Dept. of Geosciences, Alfred Wegener Institute for Polar and Marine Research, Am Alten Hafen 26, Bremerhaven 27568, Germany. Tel.: +49 471 48311361; fax: +49 471 48311271.
E-mail addresses: karsten.gohl@awi.de (K. Gohl), astrid.denk@ifg.uni-tuebingen.de (A. Denk), g.eagles@gl.rhul.ac.uk (G. Eagles), florian.wobbe@awi.de (F. Wobbe).
[1] Present address: Dept. of Geosciences, University of Tübingen, Hölderlinstr. 12, Tübingen 72074, Germany.

0040-1951/$ – see front matter © 2012 Elsevier B.V. All rights reserved.
doi:10.1016/j.tecto.2012.06.036

An extensive ship-borne and helicopter-borne magnetic dataset was collected for the first time in the Amundsen Sea Embayment and Pine Island Bay by the Alfred Wegener Institute during RV *Polarstern* expeditions ANT-XXIII/4 in 2006 and ANT-XXVI/3 in 2010. The distribution and spacing of the survey tracks are suitable to allow spatial gridding and 3D field analysis for delineating crustal and basement features. In this paper, we describe the workflow from magnetic data acquisition to processing and modelling and put forward a model for the tectonic architecture of the offshore Amundsen Sea Embayment.

2. Geological and geophysical background

Fig. 2 summarizes the main stages in the tectonic development of the Pacific margin of West Antarctica. At least three distinct phases since Late Cretaceous have been discussed in recent literature.

The extension, and subsequent separation, of New Zealand and West Antarctica dominate the tectonic signature of the Amundsen Sea Embayment. This early divergence of the Pacific and Antarctic plates led first to rifting and crustal extension between Chatham Rise and the Amundsen Sea Embayment off easternmost Marie Byrd Land as early as 90 Ma (Eagles et al., 2004a; Larter et al., 2002; Wobbe et al., 2012). Rifting possibly continued within the Great South Basin between the Campbell Plateau and the South Island of New Zealand until its abandonment in favour of a new extensional locus to the south, forming the earliest oceanic crust between Campbell Plateau and Marie Byrd Land by 84–83 Ma.

From about 79 Ma, the Bellingshausen Plate moved independently of the Pacific and Antarctic Ridge on the southern flank of the Pacific–Antarctic Ridge until about 61 Ma, when a major plate reorganisation occurred in the South Pacific (e.g. Eagles et al., 2004a,b; Larter et al., 2002). This small plate's western boundary passed through the region of the Marie Byrd Seamounts, north of the Amundsen Sea Embayment. Its eastern transpressional boundary lies along the Bellingshausen Gravity Anomaly lineament in the western Bellingshausen Sea (Eagles et al., 2004a; Gohl et al., 1997). Although a discrete southern plate boundary has been depicted running from the seamounts onto the shelf and mainland, its true nature is poorly known (Eagles et al., 2004a,b) and it may be a more distributed feature.

The location of Pine Island Bay has led several researchers to suggest that it hosts a major crustal boundary between the Marie Byrd Land block to the west and the Thurston Island/Ellsworth Land blocks to the east. These blocks are suggested to have moved with respect to each other during the Late Cretaceous New Zealand–Antarctic separation and perhaps also in early Mesozoic or Palaeozoic times (e.g. Dalziel and Elliot, 1982; Grunow et al., 1991; Storey, 1991). However, direct evidence of the presence of such a boundary is still missing. Conceptual models also suggest that Pine Island Bay and the eastern Amundsen Sea Embayment hosted basins of the West Antarctic Rift System. Jordan et al. (2010) invert airborne gravity data to reveal an extremely thin crust and low lithospheric rigidity beneath the onshore Pine Island Rift. Müller et al. (2007) and Eagles et al. (2009) considered how, at times between chrons 21 and 8 (48–26 Ma), the West Antarctic Rift System east of the Ross Sea operated in either dextral strike-slip or extensional motion through the region to the south and east of the Amundsen Sea Embayment connecting eventually to a Pacific–Phoenix–East Antarctic triple junction via the Byrd Subglacial Basin and the Bentley Subglacial Trench. There are indications for an early West Antarctic Rift System extension in western Marie Byrd Land in the mid-Cretaceous (e.g. McFadden et al., 2010), but its eastern continuation is less well understood. It is possible that in the north–south striking zone of thinned crust in Pine Island Bay was an eastern arm of this early manifestation of the West Antarctic Rift System (Dalziel, 2006; Ferraccioli et al., 2007; Gohl et al., 2007; Jordan et al., 2010).

3. Magnetic surveys and data processing

The Amundsen Sea was the target area for geoscientific, oceanographic and biological studies during the RV *Polarstern* expeditions ANT-XXIII/4 in 2006 and ANT-XXVI/3 in 2010. Ship-borne magnetic data were continuously recorded with two 3-component fluxgate magnetometer sensors, which are permanently installed on the crow's nest. One of the two BO-105 helicopters on board was equipped with a caesium-vapour magnetometer sensor towed by a

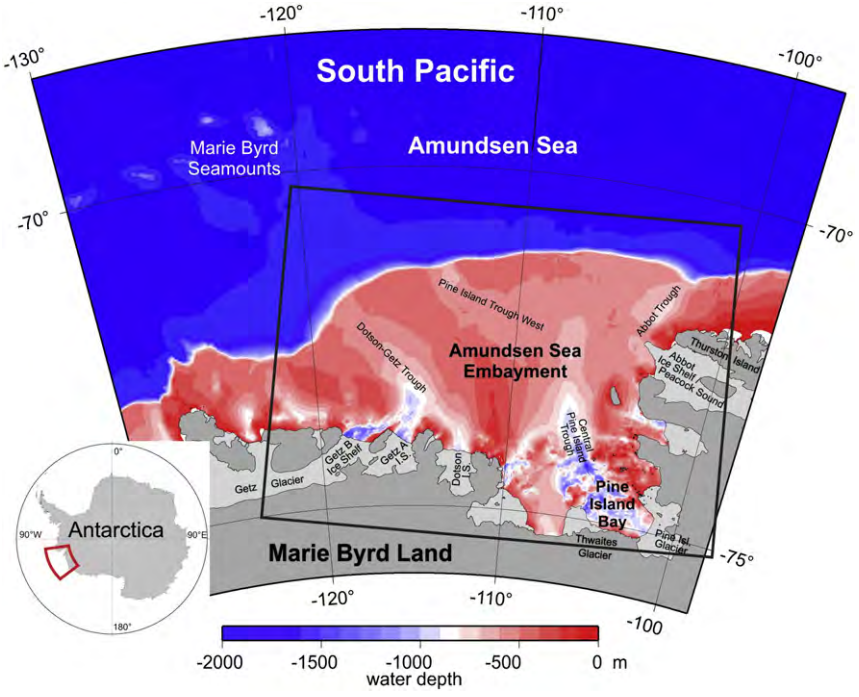

Fig. 1. Overview map of the Pacific margin of West Antarctica with the Amundsen Sea Embayment and Pine Island Bay. The bathymetry was compiled by Nitsche et al. (2007) and illustrates the glacially eroded deep troughs on the continental shelf. Middle grey areas are land regions with grounded ice, and light grey areas mark ice shelves. The black box marks the area of the magnetic survey shown and discussed in this paper.

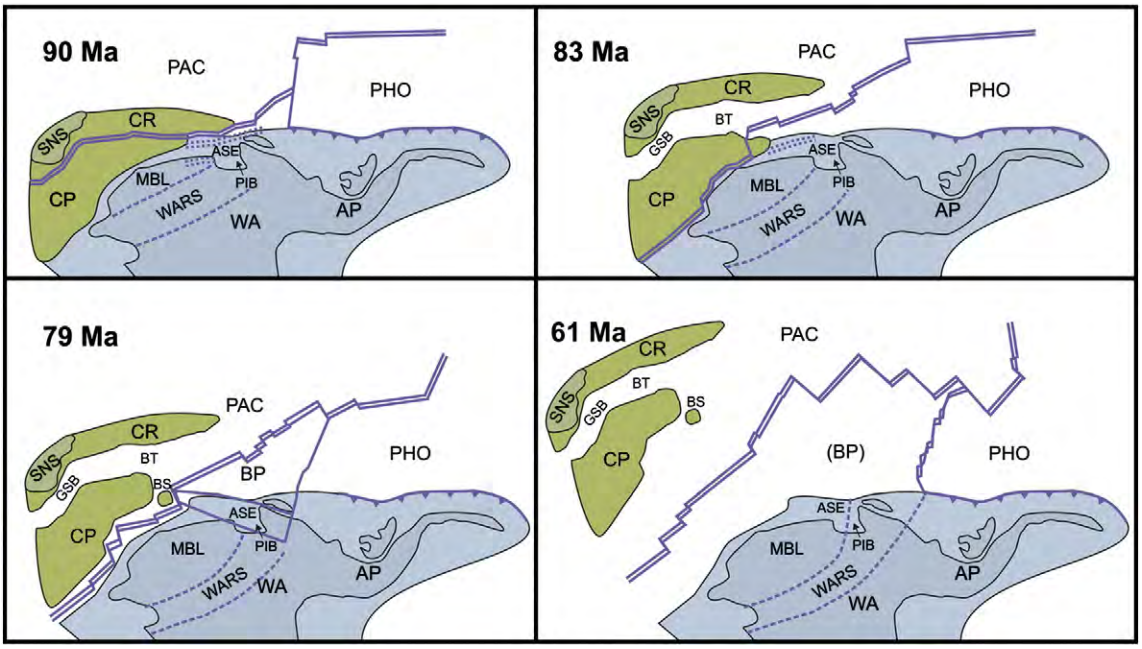

Fig. 2. Plate tectonic reconstruction of the tectonic development in the Amundsen Sea area from 90 to 61 Ma. The plates are rotated according to rotation parameters compiled and derived by Eagles et al. (2004a). The outline of the West Antarctic Rift System (WARS) faults or boundaries is an approximate estimation, because an accurate geometry of the rift system has not been identified yet. Abbreviations are: AP Antarctic Peninsula, ASE Amundsen Sea Embayment, BP Bellingshausen Plate, BT Bounty Trough, BS Bollons Seamount, CP Campbell Plateau, CR Chatham Rise, GSB Great South Basin, MBL Marie Byrd Land, PAC Pacific plate, PHO Phoenix Plate, PIB Pine Island Bay, SNS South Island New Zealand, and WA West Antarctica.
Modified from Gohl (2011).

30 m long cable. Helicopter-borne magnetic data were collected opportunistically along track lines as far as possible within a predetermined survey pattern, but subject to the constraints of the vessel's primary marine geoscientific and oceanographic tasks. Each survey flight covered 350–450 km in 2 to 2.5 h at a nominal 100 m flight height with a sampling interval of 3–5 m. Up to 3 or 4 flights were conducted on days with good flight conditions and no other transport tasks. With this survey approach, the Amundsen Sea Embayment shelf was effectively covered with patches of survey lines that total about 30,000 km of data (Fig. 3). The survey line spacing

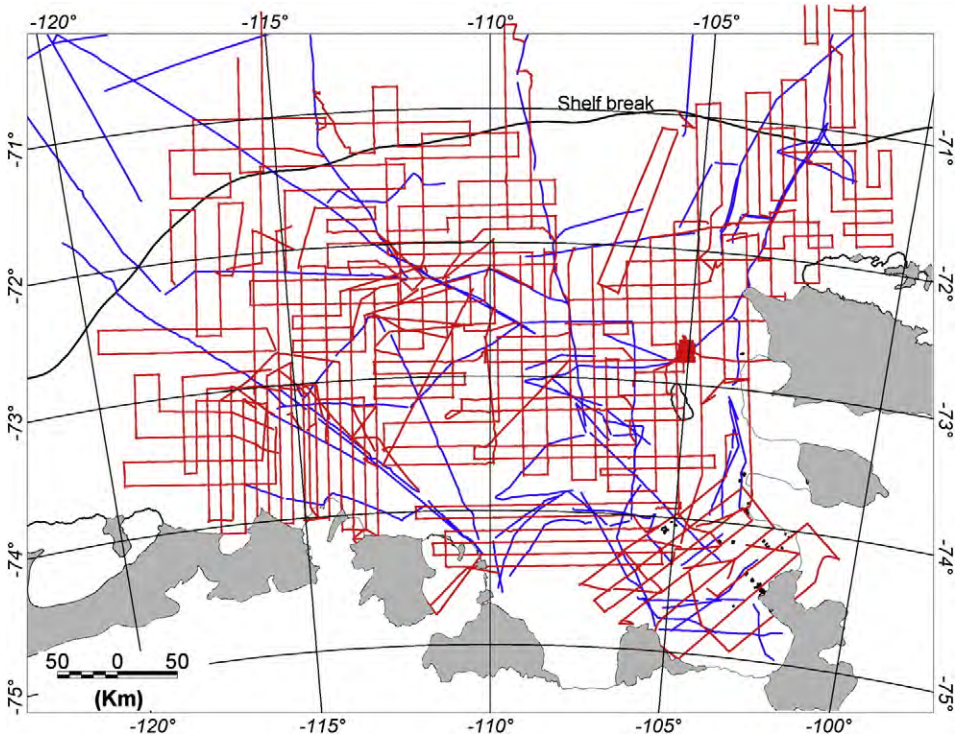

Fig. 3. Map with combined helicopter-borne (red lines) and ship-borne (blue lines) magnetic tracks of both RV *Polarstern* expeditions in 2006 and 2010, which are included in the preparation of the magnetic anomaly grids. The irregular line geometry is due to opportunistic surveying.

Table 1
Magnetic data processing and analysis flow.

Removal of IGRF
↓
Editing and filtering
↓
Upward field continuation of ship-borne data to 150 m
↓
Cross-point analysis and levelling
↓
Gridding and micro-levelling
↓
Derivatives, field continuations, high-pass filtering, analytical signal
↓
Power spectra, Euler deconvolution
↓
2-D forward modelling

varies between 5 and 25 km and – although a regular flight grid could not be maintained – allows spatial gridding and 3-D field analysis for delineating regional crustal and basement features.

Before merging into the processing stream with the helicopter-magnetic data, the 3-component ship-borne magnetic data had to be pre-processed to compensate for interactions between the ship's ferrous body and the variable geomagnetic field. To facilitate this, a number of figure-eight shaped magnetic compensation loops were completed during the cruises from which compensation coefficients for all headings were calculated. Corrections were applied using these coefficients according to the methods and descriptions of König (2006) and Wobbe et al. (2012). The main contribution to an erroneous shift of the measured magnetic data comes from the ship's heading (Nogi and Kaminuma, 1999). For instance, a one degree change of the ship's heading causes about 300 nT of variation in the horizontal components. The vertical component is less affected by the ship's heading but shows noise due to roll and pitch. In order to avoid noise in the total intensity field, the data acquired during and immediately after substantial heading changes were excluded from further processing.

The total magnetic field data of helicopter-borne caesium-vapour sensor turned out to be rather unaffected by the helicopter's heading, except for major turns at flight line change. Such data were also removed from further processing. In general, the helicopter-magnetic records appeared to be less noisy than the ship-borne data.

After this initial pre-processing, both ship-borne and helicopter-borne data went through the same principal processing steps (Table 1) using *Geosoft Oasis montaj™* software for most applications:

Removal of International Geomagnetic Reference Field (*IGRF*): We removed the IGRFs of 2005 and 2010 from the data of 2006 and 2010, respectively. We used the mean date for each survey.

Editing and filtering: Visual editing of obvious erroneous data improved the overall data quality of the datasets of both expeditions. For instance, data affected by tilts in loops of the helicopter's flight tracks were removed. Large numbers of data were removed in particular from the ship-borne records, owing to noise induced during ship manoeuvres, heading changes and crane movements. A band-pass filter removed spikes and other short-wavelength noise from all datasets. As it was not possible to set up a magnetic base station in the coastal area of the Amundsen Sea Embayment for the duration of both cruises, the data may still be affected by diurnal variations of the geomagnetic field.

Levelling: This process is required to the data in order to minimise the differences at cross-points before any gridding is applied. The plane tolerance of crossing survey line points was chosen to be 0.0005° (~50 m). As the helicopter data have shown to provide more reliable results than the ship-borne data, the two datasets were treated separately. The differences at cross-points within the dataset were minimised using an iterative approach to their mean values. We divided the intersection points of the helicopter lines into reliable intersection points (differences vary less then ± 10 nT) and less reliable intersections points (all other intersection points). In the first step, these lines were levelled separately: Lines with reliable intersection points were levelled using an 'iterative levelling' algorithm. Lines with less reliable intersections were levelled using 'full levelling' algorithm. 'Iterative levelling' calculates a least-squares trend line through the error data to derive a linear trend error curve, which is then added to the data to be levelled. These steps are repeated for crossing lines until a convergence is reached. 'Full levelling' adjusts the values of an input channel by adding a correction defined in an error channel. In a second step, an iterative levelling algorithm was again applied, this time simultaneously to all profiles from both platforms. In

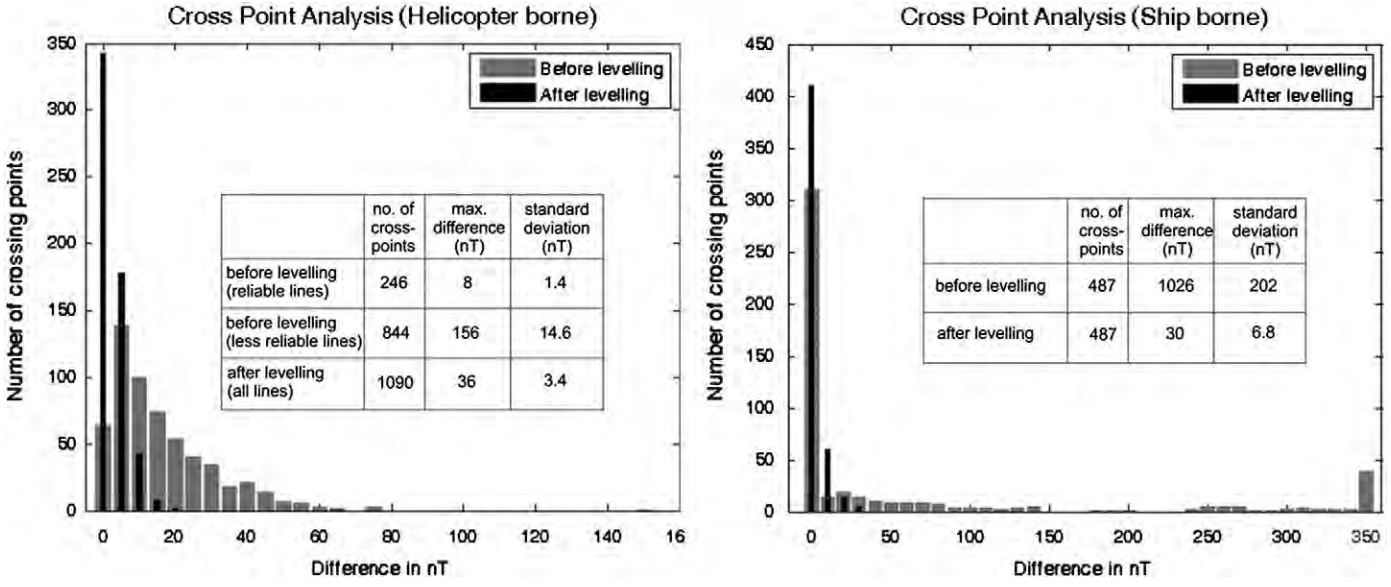

Fig. 4. Results of the cross-point analysis for the helicopter-borne and ship-borne survey lines before and after levelling.

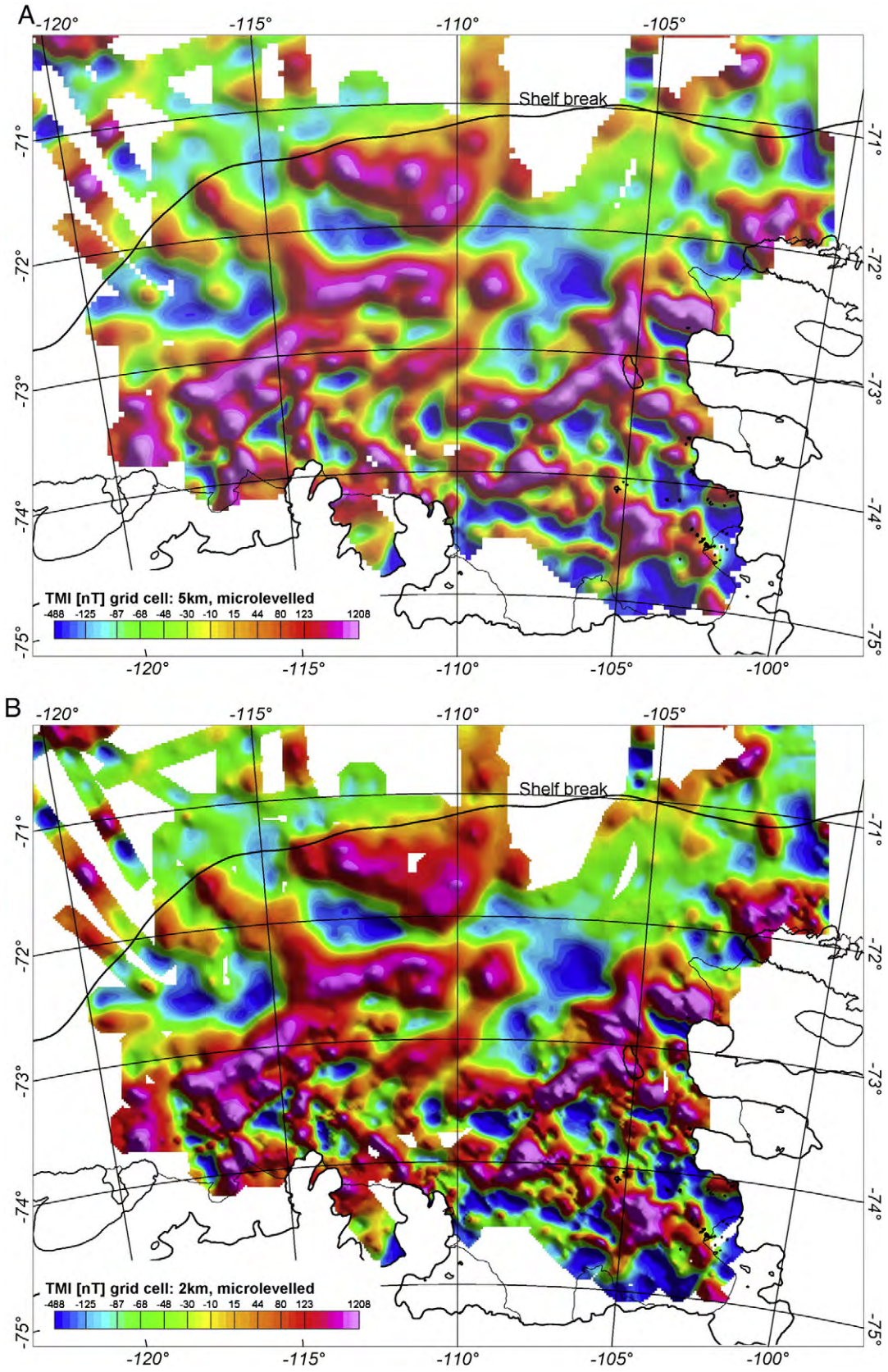

Fig. 5. Processed magnetic anomaly grids with grid cell sizes of (A) 5 km, (B) 2 km, and (C) 2 km with a 30-km cut-off high-pass filter. Fig. 5c also shows the boundary (white line) between the outcropping basement of the inner shelf in the south and the sediment basin in the north, and an estimated 3-km-depth marker (hashed black line) to which the top of basement dips northward from this boundary.

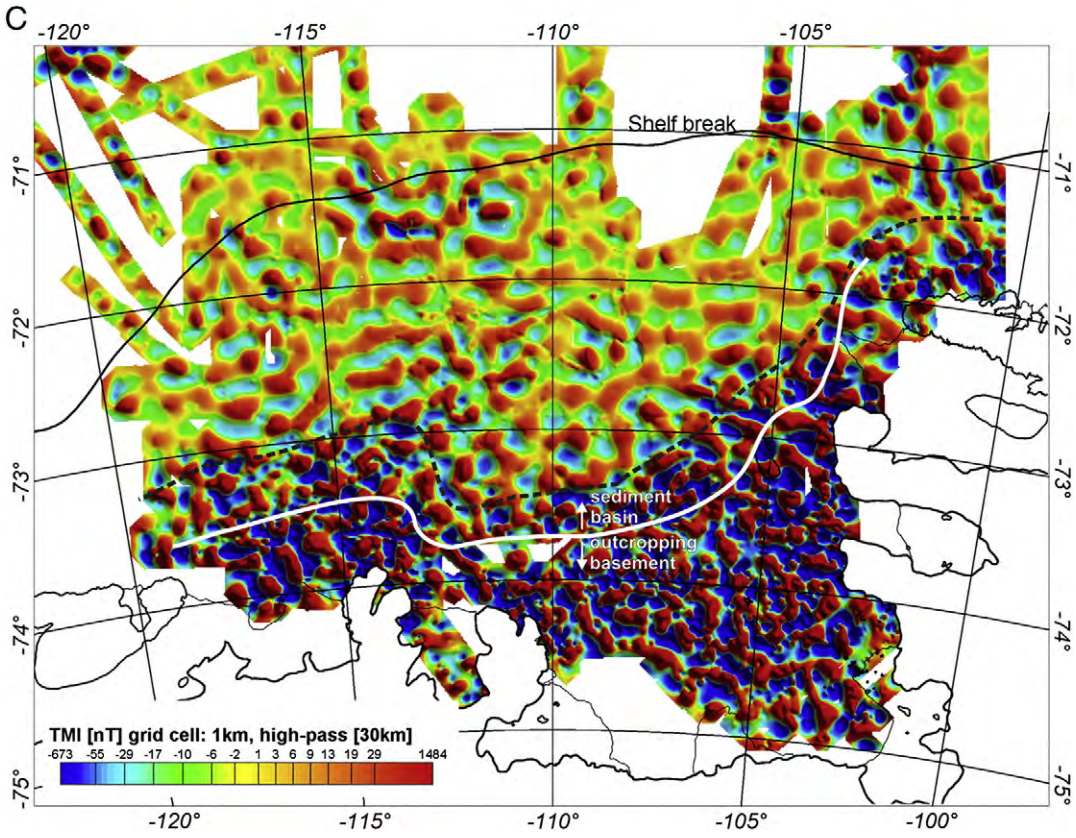

Fig. 5 (*continued*).

this step, we levelled the ship-borne data into the levelled framework of helicopter data after splitting the ship-borne data into straight segments and generating an intersection table with points of ship-borne data crossing helicopter survey lines. Intersection points within the ship-borne dataset were ignored. The cross-point histograms and tables (Fig. 4) show the large reduction in intersection misfits brought about by the levelling. It is noteworthy that the levelling process removes the large errors (~350 nT) at ship-line cross-points in south-eastern Pine Island Bay, which are a long distance from the nearest compensation loop.

Gridding and micro-levelling: Particular care was taken in gridding the data because of the irregular line spacing and orientation. We applied a minimum curvature approach between less sampled areas and those areas with good coverage. Initially, a coarse grid with a large grid cell size is used. Nodes represent either the real data, which is found within a specific radius, or an average of all data points of the grid. Iteratively, the grid is adjusted to the real data nearest to the grid nodes. If an acceptable misfit between real data and coarse grid node is achieved, the cell size is divided by two and the procedure starts again. The gridded data still show some noise resulting from residual levelling and gridding errors. Although these errors are small in comparison to the measured anomalies, they account considerably for noise in further processing. Removing these errors by the application of a low-pass filter to smooth derivative grids is a process known as micro-levelling (Ferraccioli et al., 1998; Green, 1983). As the screening of the line data indicated, the shelf is partitioned into two magnetic anomaly domains characterised by different wavelengths. We found that micro-levelled grids of 5 and 2 km cell size best represent both domains with a minimum of artefacts (Fig. 5A,B). A further decrease of the cell size to 1 km in combination with a 30-km high-pass filter (Fig. 5C) shows clearly the wave-field distinction between the inner shelf domain and the middle to outer shelf but also creates numerous artificial anomalies.

Further analytical field analysis: We applied a wide spectrum of standard wave-field processing methods to the grid in order to constrain directional trends and the shapes and edges of magnetic anomaly units. These methods included the calculation and application of (1) horizontal, vertical and tilt derivatives, (2) upward field continuations, (3) high-pass filters, (4) pseudo gravity and (5) analytical signal. At moderate wavelengths, these methods serve to highlight the magnetic bodies and tectonic lineation trends that can be coarsely interpreted from the regular anomaly grids. High-pass filtering, in particular, much more readily delineates the boundary zone between outcropping basement of the inner shelf and the sedimentary cover of the middle and outer shelf (Fig. 5C).

4. Depth estimates

In addition to standard power spectra analyses for estimating the depths of magnetic anomaly sources, we applied the Euler deconvolution method to the grid in an attempt to better delineate the spatial distribution and extent of the tops and edges of source bodies. We used the approach of Thomson (1982) and Reid et al. (1990) in which the depth solution is related to a chosen structural index *SI* (0 for a planar contact, 1 for a dike or sill, 2 for a vertical pipe, 3 for a sphere). A square window is defined within the grid, which contains at least 3×3 grid cells. For each grid cell, the deconvolution is calculated. Hence, a 3×3 cell window results in 9 equations, which are solved via a least-squares inversion. The

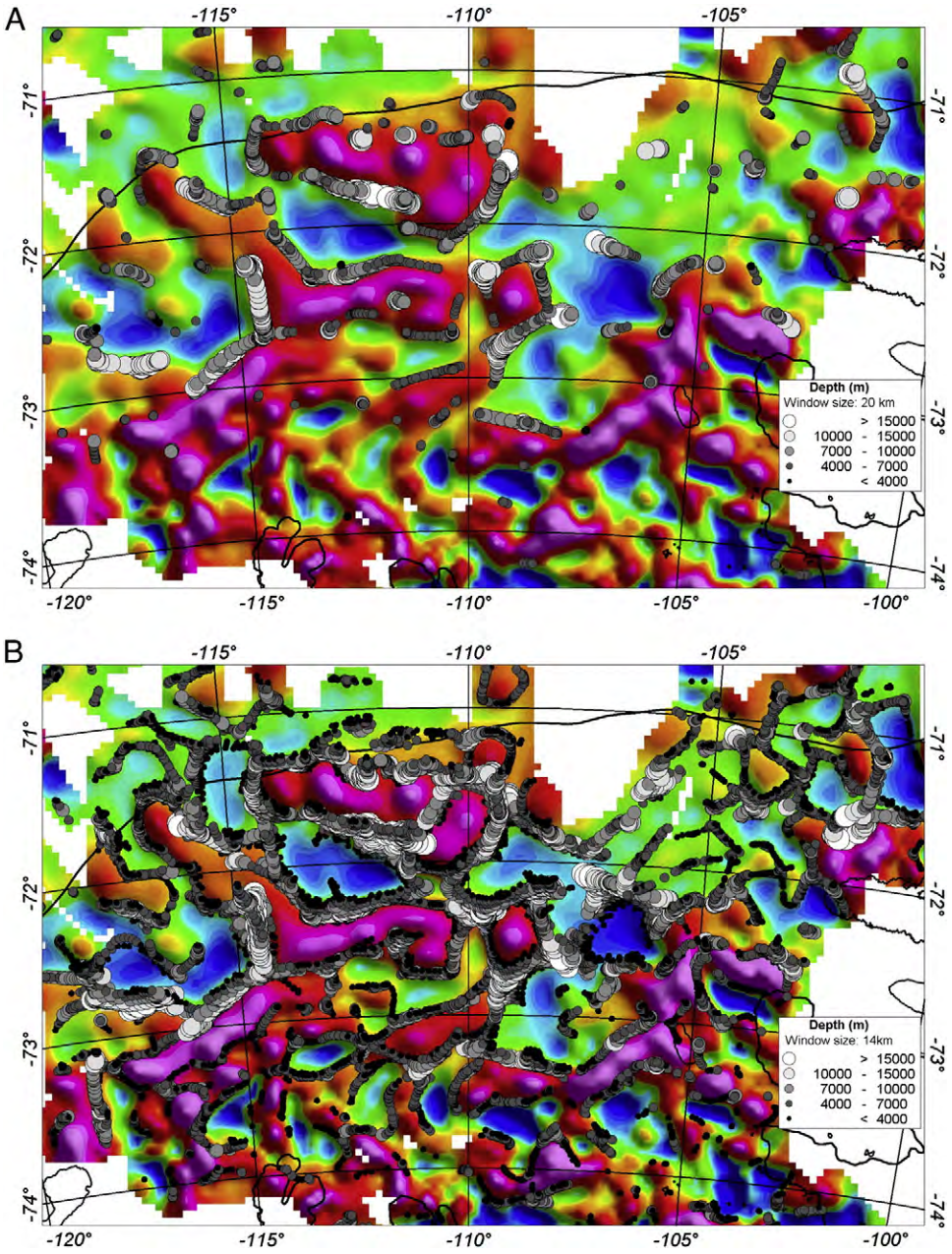

Fig. 6. Anomaly grids (grid cell size of 2 km, micro-levelled) of the central embayment with top of magnetic source depth estimates from Euler deconvolution using the same structural index of $SI = 0$, but different window sizes of (A) 20 km and (B) 14 km.

window is then shifted across the grid and the same procedure is applied. It is obvious that the solution is dependent on the chosen window size. If the window size is so large that neighbouring anomalies intrude into it, the inversion can fail and its solutions are rejected. This is the case for distinct anomalies on the inner shelf in the south (Fig. 6A). On the other hand, if a window size is too small, then anomalies from deep-seated sources may not be adequately represented in the inversion, interfering with the solutions for shallower sources and resulting in artificially shallow source solutions. Fig. 6B shows that smaller window sizes generate more solutions and that long-wavelength anomalies yield shallower depth solutions than when a larger window is used.

Our two examples of Euler deconvolution solutions use different window sizes of 14 and 20 km but the same structural index (Fig. 6). The solutions provide estimates of a dense distribution of source tops at depths below 7 km over the middle to outer shelf, while further south, below the inner shelf, source tops are typically located at depths shallower than 7 km.

5. Tectonic lineaments and 2D modelling

One of the most striking observations in the magnetic anomaly grid is the domination of the inner shelf by relatively short-wavelength anomalies and the middle and outer shelf by middle to long wavelength anomalies (Fig. 5A,B). The boundary between the two domains is abrupt and clearly shown in the high-pass filtered wavefield (Fig. 5C). This boundary is the northern limit of a coastal and inner shelf domain in which basement crops out or exists in shallow subcrop, as suggested by the rugged topography (Fig. 1). It can be assumed that most of this basement is composed of crystalline rocks similar in type to the granitoids and porphyritic dykes observed from coastal and island outcrops of the embayment (e.g. Kipf et al., 2012; Pankhurst et al., 1993). Conversely, the longer wavelength signals over the middle and outer shelf are consistent with the presence of a thick drape of sediments overlying the basement (Lowe and Anderson, 2002; Weigelt et al., 2009). Depth estimates from Euler deconvolution help identify a boundary zone

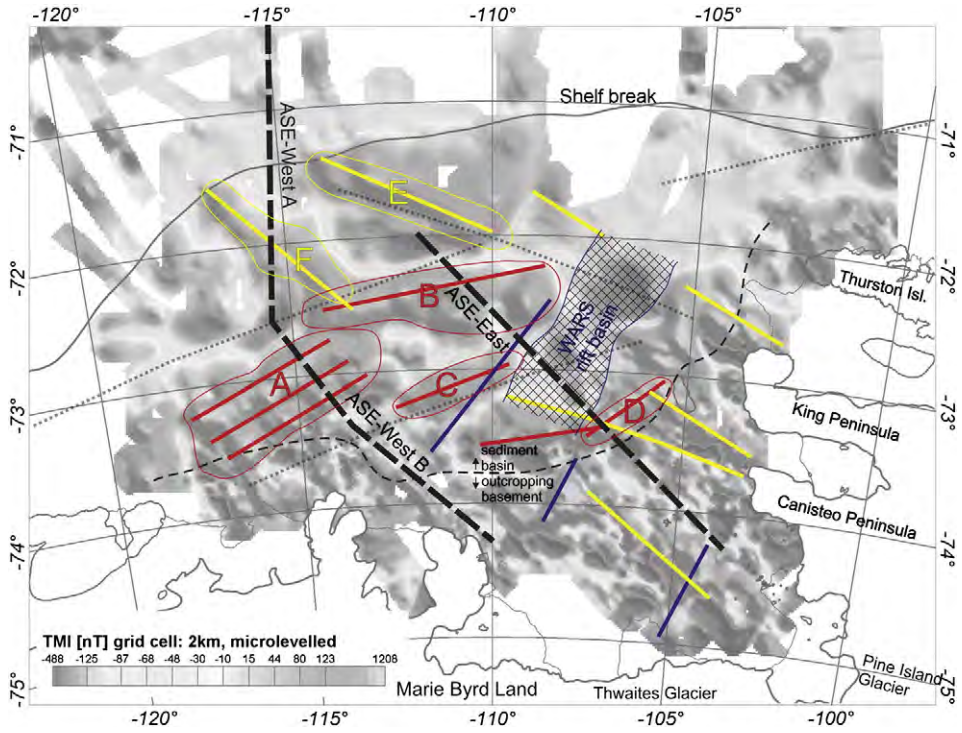

Fig. 7. Map with major directional anomaly trends and tectonic features identified in the magnetic anomaly grid. The grid is shown slightly subdued and in grey scale with superposed trends of major satellite-derived gravity anomalies (thin dotted grey lines; from Gohl et al., 2007). The outcropping basement–sediment boundary is marked with a thin, hashed black line. NW–SE trending anomalies are marked in yellow lines and fields; ENE–WSW trends are in red; NNE–SSW trends are in blue. The largest anomalies or anomaly groups with directional trends are encircled with a thin line in the respective colour and annotated from A to F. Thick, hashed black lines show the modelled profiles of Fig. 8. The WARS rift basin is interpreted as a branch of the West Antarctic Rift System.

across which the basement drops downwards to the north to about 3 km depth (Fig. 5C), which is consistent with observations from seismic data across this boundary (Graham et al., 2009; Lowe and Anderson, 2002; Uenzelmann-Neben et al., 2007; Weigelt et al., 2009).

One of the objectives of the magnetic surveys was to identify crustal features for delineating tectonic events in the history of the crustal formation in the Amundsen Sea Embayment (Fig. 7). The middle and outer shelf show fundamentally different preferential anomaly strikes. While a major set of long-wavelength anomalies strike WSW–ENE along the middle shelf, the outer shelf west of 107° W exhibits mainly NW–SE striking anomalies which may continue on the inner shelf of the eastern embayment. A third directional trend is observed for positive anomalies on the inner and middle shelf striking NNE–SSW. These are less pronounced but seem to border a broad magnetic zone of low amplitude negative anomalies on the middle shelf at 106–109° W.

We selected two 2D modelling transects crossing the Amundsen Sea Embayment shelf from north to south and NW to SE across the major observed magnetic anomaly lineaments and proposed source bodies (Fig. 7). The data along the transects were taken from the magnetic anomaly grid at 5 km cell size. *Encom ModelVision*™ was used as modelling software. The depth estimates from Euler deconvolution solutions provided some constraints for the parameterisation of these magnetic susceptibility models. Other constraints on crustal properties, such as crustal thickness, sediment thickness and the approximate locations of mafic (high density, high susceptibility) bodies, were implemented from seismic reflection data (Weigelt et al., 2009), a deep crustal seismic refraction model and a gravity anomaly inversion of the Amundsen Sea shelf region with crustal thicknesses of 20–25 km (Gohl et al., 2007). Water depths were taken from the bathymetry compilation of Nitsche et al. (2007).

We chose a modelling procedure in which we parameterized the model starting with thick layers and large bodies from the lower crust for long-wavelength signals and moving on to small-size layers and bodies of the upper crust to generate short-wavelength signals. The responses were iteratively calculated for a range of susceptibilities and body sizes such that the root-mean-square (rms) misfit between observed and calculated total intensities could be minimised. Due to the different wave-field characteristics of transects ASE-West A, ASE-West B and ASE-East, each model was treated independently of the others. Although various studies show that the ranges of susceptibilities of individual rock types can span several orders of magnitude, it is possible to distinguish domains of sedimentary, felsic and mafic composition on the basis of susceptibilities. Most published susceptibilities of intrusive felsic rocks range from 0.0001 to 0.02 SI unit (average 0.0012 SI), while those of intrusive rocks of mafic composition have values of 0.0001 to 0.13 SI (average 0.012 SI) (e.g. Sanger and Glen, 2003). We applied a constant susceptibility of 0.000005 SI for sediments and of 0.001 SI for the bulk of the continental crust in all models and started modelling with the average values of intrusive bodies by Sanger and Glen (2003). By adjusting the susceptibilities of these bodies, we stayed within the above given ranges.

The model transect ASE-West A (Fig. 8A) covers the continental slope and the outer shelf and includes two high-susceptibility bodies embedded into the upper crust of the continental rise. Much of the upper surface of the large high-susceptibility body 3 beneath the

Fig. 8. Results of magnetic 2-D forward modelling along profiles (A) ASE-West A, (B) ASE-West B and (C) ASE-East. Black lines mark the measured anomaly data, and red lines represent the calculated model response, respectively. Model bodies are annotated with their respective magnetic susceptibility values in SI units. Profile locations are marked in the map of Fig. 7.

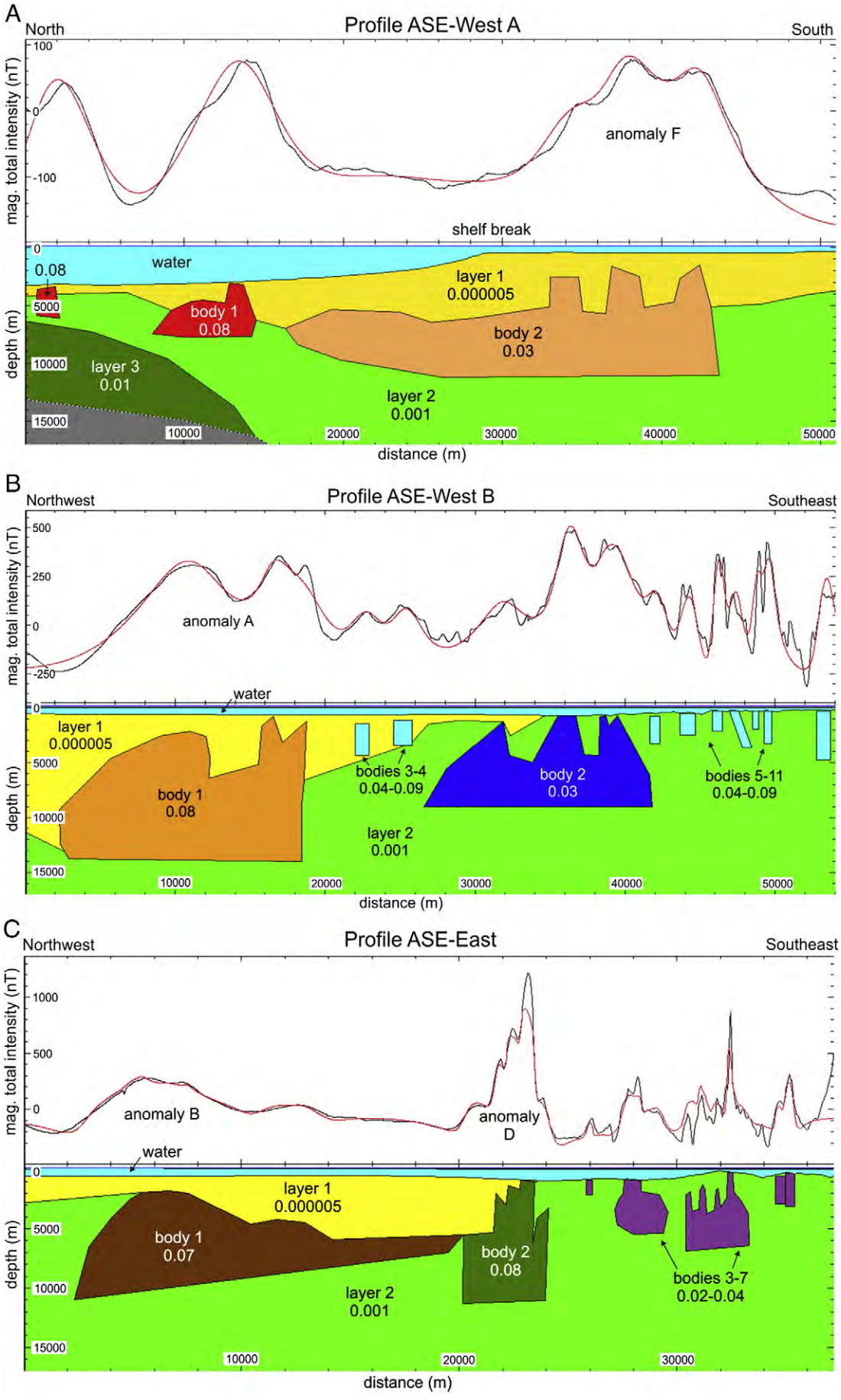
A
Profile ASE-West A
North
South
mag. total intensity (nT)
anomaly F
shelf break
water
0.08
layer 1
0.000005
body 1
0.08
body 2
0.03
layer 3
0.01
layer 2
0.001
depth (m)
distance (m)
B
Profile ASE-West B
Northwest
Southeast
anomaly A
water
layer 1
0.000005
bodies 3-4
0.04-0.09
body 2
0.03
bodies 5-11
0.04-0.09
body 1
0.08
layer 2
0.001
C
Profile ASE-East
Northwest
Southeast
anomaly B
anomaly
D
water
layer 1
0.000005
body 1
0.07
body 2
0.08
bodies 3-7
0.02-0.04
layer 2
0.001

slope and outer shelf is located beneath 5 km depth, with shallower peaks at 2–3 km depth, producing the long-wavelength high with superposed short-wavelength fluctuations seen in the data. Similar high-susceptibility bodies were required to fit the anomalies of the middle and inner shelf model transects ASE-West B (Fig. 8B) and ASE-East (Fig. 8C). In both models, we inserted shallow, small-sized bodies of high susceptibilities to fit the shortest wavelength anomalies. On the inner shelf, where basement crops out, we topped most of the source bodies at the seafloor.

6. Superposed tectonic events

The modelled properties of the dominant ENE–WSW trending magnetic anomalies A, B, C and D (Fig. 7) indicate that they are caused by major elongated and deep-seated features of predominantly mafic composition. They parallel the initial spreading centre's azimuth between Chatham Rise and West Antarctica and can thus be related to rift processes occurring before breakup as early as 100 Ma and during breakup between 90 and 85 Ma (Eagles et al., 2004a; Larter et al., 2002; Wobbe et al., 2012). With their seaward-dipping outer edges, bodies of anomalies A and B might be interpreted as thick wedges of basaltic lava and mafic intrusions of the kind known from volcanic extended continental margins such as the Vøring margin or Afar Rift (Planke and Eldholm, 1994; Wolfenden et al., 2005). The body modelled for anomaly A reaches near the seafloor at its southern limit which correlates with the steep northern flank of the inner Dotson–Getz Trough (Graham et al., 2009; Larter et al., 2009). The trough coming from the Getz B Ice Shelf strikes nearly in east–west direction on the inner shelf before merging with the outflow troughs originating from the Getz A and Dotson Ice Shelves and turning northwards on the middle shelf and to the northwest on the outer shelf (Fig. 1). We suggest that this intrusive body is more resistant to pre-glacial and glacial erosion and caused an east to northeastward deviation of grounded ice streams from the eastern Getz Glacier.

The NW–SE trending set of magnetic anomalies (including E and F of Fig. 7) is parallel to the so-called Peacock Gravity Anomaly northwest of Peacock Sound (Eagles et al., 2004a; Larter et al., 2002) which has been modelled with an underlying high-density body (Gohl et al., 2007). It is interpreted as a magmatic zone, which interferes with the ENE–WSW trending rift structure (causing anomalies A to D). Modelling along transect ASE-West A indicates that the magnetic anomalies in this zone are caused by elongated bodies of similar depth, dimension and susceptibility as those causing the ENE–WSW trending anomalies. Consistent with the plate tectonic process described for the Bellingshausen Plate (Eagles et al., 2004a,b; Wobbe et al., 2012) we infer that these features represent mafic intrusions emplaced when the southern Bellingshausen Plate boundary was active between 80 and 61 Ma, giving rise to a distributed pattern of compressional, extensional and translateral movements at various stages of the activity of this boundary. The location of these magmatic units over a long time period in a very wide continent–ocean transition zone (Wobbe et al., 2012) suggests the Amundsen Sea Embayment may be the product of a long-lived zone of distributed crustal deformation, and that it may host multiple failed rifts and rift accommodation zones.

The third set of magnetic anomaly lineaments runs NNE–SSW, is rather subtle in amplitude, and more spatially limited than the other anomaly sets (Fig. 7). The broad magnetic anomaly low indicates the presence of a sedimentary sub-basin within the middle shelf. The margins of this low are asymmetrical; its southeastern margin is characterised by greater amplitudes and shorter wavelength anomalies than its northwestern margin. The basin, therefore, might be interpreted as having a half-graben geometry, with a bounding basement-involved normal fault zone on its southeastern edge, and a downthrown floor characterised by broad flexure northwestward away from the fault zone. The Palaeogene plate tectonic model of Müller et al. (2007) predicts that a crustal boundary with this orientation would have responded to West Antarctica–East Antarctica relative motion along the WARS in right-lateral strike-slip motion. They suggest that this boundary extended from the Bentley Subglacial Trough and Byrd Subglacial Basin across western Ellsworth Land and the Thurston Island block, where it continues into the area of the dominant north-trending gravity anomaly lineaments of the Bellingshausen Sea. More consistent with the interpretation of a NNE-trending basin, however, the alternative plate tectonic model of Cande et al. (2000) predicts a strongly oblique right-lateral extension. In any case, the orientation of the identified sub-basin on the eastern ASE shelf (annotated as 'WARS rift basin' in Fig. 7) infers that it may be related to eastern WARS motion, possibly active as early as 55 Ma and lasting until at least 30 Ma before the zone of translateral deformation migrated or jumped eastward to join the triple junction at the spreading ridge colliding with the convergent margin of the southern Antarctic Peninsula as postulated by Müller et al. (2007). Somewhat more speculative, but not unrealistic, is a correlation of the sub-basin with the dextral transtensional strain in western Marie Byrd Land observed by Siddoway (2008), who interprets this strain as an expression of an early WARS activity in the Late Cretaceous.

The shallow, small-sized bodies of very high susceptibilities between 0.02 and 0.09 SI unit on the inner shelf (Fig. 8b,c), are interpreted to be caused by a mafic dyke field related to the Cenozoic volcanic province of eastern Marie Byrd Land and western Ellsworth Land (e.g. LeMasurier, 1990; Paulsen and Wilson, 2010). Due to the presence of the nearby volcanic Hudson Mountains, one might expect volcanic, ~5 km radius cone-like features on the shelf as well, but the line spacing of the survey does not allow for the unequivocal identification or clear resolution of such features.

7. Conclusions

Newly acquired magnetic datasets from helicopter-borne and ship-borne surveys in 2006 and 2010 were used to generate levelled anomaly grids from the shelf of the Amundsen Sea Embayment. We applied grid processing, Euler deconvolution and 2D modelling for the analysis of magnetic anomaly patterns, identification of structural lineaments, and characterisation of magnetic source bodies.

The magnetic anomaly grid clearly outlines the boundary zone between the inner shelf where basement rocks crop out and a more thickly-sedimented middle to outer shelf. This sedimentation can be related to a long history of distributed extension inferred from the regional plate tectonic setting and from the presence of distinct zones of anomaly patterns and lineaments that can be associated with at least three tectonic phases in that history.

The first of these phases was the establishment of magmatic emplacement zones during Cretaceous New Zealand–Antarctic rifting and breakup (100–85 Ma). The second phase involved further magmatism in a distributed plate boundary zone between the Bellingshausen and Antarctic plates (80–61 Ma). Finally, the West Antarctic Rift System may have caused further extension in the region at later times (55–30 Ma?), focussed within a possible half-graben basin system bounded by NNE–SSW trending tectonic lineaments. Mafic dykes cross the inner shelf of the embayment and Pine Island Bay and may be associated with Cenozoic volcanism observed on land. They possibly relate to activities of one of the eastern branches of the West Antarctic Rift System.

Our magnetic data and the analysis show for the first time an identification of at least three sets of superposed tectonic lineaments in the Amundsen Sea Embayment shelf. The correlation of this observation to plate tectonic motion and associated magmatic emplacement in the West Antarctic realm suggests that the wide shelf of the Amundsen Sea Embayment may be the product of a long-lived zone

of distributed crustal deformation, and that it may host multiple failed rifts and rift accommodation zones.

By an example of a modelled intrusive body, this study also shows that such emplacement of resistive material acted as an obstacle for past ice flows across the inner shelf.

Acknowledgements

Many thanks to the ship crews, the helicopter pilots of Heli-Service GmbH and the geophysical teams for their support of acquiring the magnetic data during RV *Polarstern* expeditions ANT-XXIII/4 (2006) and ANT-XXVI/3 (2010). We, in particular, thank Volker Leinweber, Sonja Suckro and Christina Mayr for their engagement in the helicopter-magnetic team of 2006. The collaboration with Prof. B. Tezkan of the University of Cologne in co-supervising A. Denk's Diploma/MSc thesis, of which parts contributed to this paper, is gratefully acknowledged. This project is entirely supported by institutional funds of the Alfred Wegener Institute.

References

Cande, S.C., Stock, J.M., Müller, R.D., Ishihara, T., 2000. Cenozoic motion between East and West Antarctica. Nature 404, 145–150.

Dalziel, I.W.D., 2006. On the extent of the active West Antarctic rift system. In: Siddoway, C.S., Ricci, C.A. (Eds.), Proceedings of Workshop on Frontiers and Opportunities in Antarctic Geosciences. : Terra Antarctica Reports, 12. Terra Antarctica Publications, Siena, Italy, pp. 193–202.

Dalziel, I.W.D., Elliot, D.H., 1982. West Antarctica: problem child of Gondwanaland. Tectonics 1, 3–19.

Eagles, G., Gohl, K., Larter, R.D., 2004a. High-resolution animated tectonic reconstruction of the South Pacific and West Antarctic margin. Geochemistry, Geophysics, Geosystems 5. http://dx.doi.org/10.1029/2003GC000657.

Eagles, G., Gohl, K., Larter, R.D., 2004b. Life of the Bellingshausen plate. Geophysical Research Letters 31, L07603. http://dx.doi.org/10.1029/2003GL019127.

Eagles, G., Larter, R.D., Gohl, K., Vaughan, A.P.M., 2009. Antarctic Rift System in the Antarctic Peninsula. Geophysical Research Letters 36, L21305. http://dx.doi.org/10.1029/2009GL040721.

Ferraccioli, F., Gambetta, M., Bozzo, E., 1998. Microlevelling procedures applied to regional aeromagnetic data: an example from the Transantarctic Mountains Antarctica. Geophysical Prospecting 46, 177.

Ferraccioli, F., Jordan, T.A., Vaughan, D.G., Holt, J., James, M., Corr, H., Blankenship, D.D., Fairhead, J.D., Diehl, T.M., 2007. New aerogeophysical survey targets the extent of the West Antarctic Rift System over Ellsworth Land. In: Cooper, A.K., Raymond, C.R. (Eds.), Proceedings of the 10th Int. Symposium of Antarctic Earth Sciences: USGS Open-File Report 2007–1047, 113. Extended Abstract.

Gohl, K., 2011. Basement tectonics and ice sheet dynamics in the Amundsen Sea Embayment, West Antarctica. Palaeogeography, Palaeoclimatology, Palaeoecology. http://dx.doi.org/10.1016/j.palaeo.2011.02.022.

Gohl, K., Nitsche, F., Miller, H., 1997. Seismic and gravity data reveal Tertiary interplate subduction in the Bellingshausen Sea, southeast Pacific. Geology 25, 371–374.

Gohl, K., Teterin, D., Eagles, G., Netzeband, G., Grobys, J., Parsiegla, N., Schlüter, P., Leinweber, V., Larter, R.D., Uenzelmann-Neben, G., Udintsev, G.B., 2007. Geophysical survey reveals tectonic structures in the Amundsen Sea Embayment, West Antarctica. In: Cooper, A.K., Raymond, C.R., et al. (Eds.), Proceedings of the 10th Int. Symposium of Antarctic Earth Sciences: USGS Open-File Report 2007–1047. http://dx.doi.org/10.3133/of2007-1047.srp047.

Graham, A.G.C., Larter, R.D., Gohl, K., Hillenbrand, C.-D., Smith, J.A., Kuhn, G., 2009. Bedform signature of a West Antarctic palaeo-ice stream reveals a multi-temporal record of flow and substrate control. Quaternary Science Reviews 28, 2774–2793. http://dx.doi.org/10.1016/j.quascirev.2009.07.003.

Green, A., 1983. A comparison of adjustment procedures for leveling aeromagnetic survey data. Geophysics 48, 745–753.

Grunow, A.M., Kent, D.V., Dalziel, I.W.D., 1991. New paleomagnetic data from Thurston Island: implications for the tectonics of West Antarctica and Weddell Sea opening. Journal of Geophysical Research 96 (B11), 17935–17954.

Jordan, T.A., Ferraccioli, F., Vaughan, D.G., Holt, J.W., Corr, H., Blankenship, D.D., Diehl, T.M., 2010. Aerogravity evidence for major crustal thinning under the Pine Island Glacier region (West Antarctica). Geological Society of America Bulletin 122, 714–726. http://dx.doi.org/10.1130/B26417.1.

Kipf, A., Mortimer, N., Werner, R., Gohl, K., van den Bogaard, P., Hauff, F., Hoernle, K., 2012. Granitoids and dykes of the Pine Island Bay region, West Antarctica. Antarctic Science. http://dx.doi.org/10.1017/S0954102012000259.

König, M., 2006. Processing of shipborne magnetometer data and revision of the timing and geometry of the Mesozoic break-up of Gondwana. PhD thesis, University of Bremen, Reports on Polar and Marine Research, no. 525, 137 pp.

Larter, R.D., Cunningham, A.P., Barker, P.F., Gohl, K., Nitsche, F.O., 2002. Tectonic evolution of the Pacific margin of Antarctica — 1. Late Cretaceous tectonic reconstructions. Journal of Geophysical Research 107 (B12), 2345. http://dx.doi.org/10.1029/2000JB000052.

Larter, R.D., Graham, A.G.C., Gohl, K., Kuhn, G., Hillenbrand, C.-D., Smith, J.A., Deen, T.J., Livermore, R., Schenke, H.-W., 2009. Subglacial bedforms reveal complex basal regime in a zone of paleo-ice stream convergence, Amundsen Sea Embayment, West Antarctica. Geology 37, 411–414. http://dx.doi.org/10.1130/G25505A.

LeMasurier, W.E., 1990. Late Cenozoic volcanism on the Antarctic plate: an overview. In: LeMasurier, W.E., Thomson, J.W. (Eds.), Volcanoes of the Antarctic Plate and Southern Oceans: American Geophysical Union Antarctic Research Series, 48, pp. 1–17.

Lowe, A.L., Anderson, J.B., 2002. Reconstruction of the West Antarctic ice sheet in Pine Island Bay during the Last Glacial Maximum and its subsequent retreat history. Quaternary Science Reviews 21, 1879–1897.

McFadden, R.R., Teyssier, C., Siddoway, C.S., Whitney, D.L., Fanning, C.M., 2010. Oblique dilation, melt transfer, and gneiss dome emplacement oblique dilation, melt transfer, and gneiss dome emplacement. Geology 38, 375–378. http://dx.doi.org/10.1130/G30493.1.

Müller, R.D., Gohl, K., Cande, S.C., Goncharov, A., Golynsky, A.V., 2007. Eocene to Miocene geometry of the West Antarctic rift system. Australian Journal of Earth Sciences 54, 1033–1045. http://dx.doi.org/10.1080/08120090701615691.

Nitsche, F.O., Jacobs, S., Larter, R.D., Gohl, K., 2007. Bathymetry of the Amundsen Sea continental shelf: implications for geology, oceanography, and glaciology. Geochemistry, Geophysics, Geosystems 8, Q10009. http://dx.doi.org/10.1029/2007GC001694.

Nogi, Y., Kaminuma, K., 1999. Measurements of vector magnetic anomalies on board the icebreaker Shirase and the magnetization of the ship. Annali di Geofisica 42, 161–170.

Pankhurst, R.J., Millar, I.L., Grunow, A.M., Storey, B.C., 1993. The pre-Cenozoic magmatic history of the Thurston Island crustal block, West Antarctica. Journal of Geophysical Research 98 (B7), 11835–11849. http://dx.doi.org/10.1029/93JB01157.

Paulsen, T.S., Wilson, T.J., 2010. Evolution of Neogene volcanism and stress patterns in the glaciated West Antarctic Rift, Marie Byrd Land, Antarctica. Journal of the Geological Society 167, 401–416. http://dx.doi.org/10.1144/0016-76492009-044.

Planke, S., Eldholm, O., 1994. Seismic response and construction of seaward dipping wedges of flood basalts: Vøring volcanic margin. Journal of Geophysical Research 99, 9263–9278.

Pollard, D., DeConto, R.M., 2009. Modelling West Antarctic ice sheet growth and collapse through the past five million years. Nature 458, 329–333. http://dx.doi.org/10.1038/nature07809.

Pritchard, H.D., Arthern, R.J., Vaughan, D.G., Edwards, L.A., 2009. Extensive dynamic thinning on the margins of the Greenland and Antarctic ice sheets. Nature 461, 971–975. http://dx.doi.org/10.1038/nature08471.

Reid, A., Allsop, J., Granser, H., Millett, A., Somerton, I., 1990. Magnetic interpretation in three dimensions using Euler deconvolution. Geophysics 55, 80–91.

Rignot, E.J., Bamber, J.L., van den Broeke, M.R., Davis, C., Li, Y., van de Berg, W., van Meijgaard, E., 2008. Recent Antarctic ice mass loss from radar interferometry and regional climate modelling. Nature Geoscience 1, 106–110. http://dx.doi.org/10.1038/ngeo102.

Sanger, E.A., Glen, J.M.G., 2003. Density and magnetic susceptibility values for rocks in the Talkeetna Mountains and adjacent region, South-Central Alaska. U.S. Geological Survey Open-File Report 03–268.

Siddoway, C.S., 2008. Tectonics of the West Antarctic Rift System: new light on the history and dynamics of distributed intracontinental extension. In: Cooper, A.K., Barrett, P.J., Stagg, H., Storey, B., Stump, E., Wise, W. (Eds.), Antarctica: A Keystone in a Changing World. : Proceedings of the 10th International Symposium on Antarctic Earth Sciences. The National Academies Press, Washington, DC, pp. 91–114. http://dx.doi.org/10.3133/of2007-1047.kp09.

Storey, B.C., 1991. The crustal blocks of West Antarctica within Gondwana: reconstruction and break-up model. In: Thomson, M.R.A., Crane, J.A., Thomson, J.W. (Eds.), Geological Evolution of Antarctica. Cambridge University Press, Cambridge.

Thomson, D.T., 1982. EULDPH: a new technique for making computer-assisted depth estimates from magnetic data. Geophysics 47, 31–37.

Uenzelmann-Neben, G., Gohl, K., Larter, R.D., Schlüter, P., 2007. Differences in ice retreat across Pine Island Bay, West Antarctica, since the Last Glacial Maximum: indications from multichannel seismic reflection data. In: Cooper, A.K., Raymond, C.R., et al. (Eds.), Proceedings of the 10th ISAES: USGS Open-File Report 2007–1047. http://dx.doi.org/10.3133/of2007-1047.srp084.

Vaughan, D.G., Corr, H.F.J., Ferraccioli, F., Frearson, N., O'Hare, A., Mach, D., Holt, J.W., Blankenship, D.D., Morse, D., Young, D.A., 2006. New boundary conditions for the West Antarctic ice sheet: subglacial topography beneath Pine Island Glacier. Geophysical Research Letters 33, L09501.

Weigelt, E., Gohl, K., Uenzelmann-Neben, G., Larter, R.D., 2009. Late Cenozoic ice sheet cyclicity in the western Amundsen Sea Embayment — evidence from seismic records. Global and Planetary Change 69, 162–169. http://dx.doi.org/10.1016/j.gloplacha.2009.07.004.

Wobbe, F., Gohl, K., Chambord, A., Sutherland, R., 2012. Structure and breakup history of the rifted margin of West Antarctica in relation to Cretaceous separation from Zealandia and Bellingshausen plate motion. Geochemistry, Geophysics, Geosystems 13, Q04W12. http://dx.doi.org/10.1029/2011GC003742.

Wolfenden, E., Ebinger, C., Yirgu, G., Renne, P.R., Kelley, S.P., 2005. Evolution of a volcanic rifted margin: Southern Red Sea, Ethiopia. Geological Society of America Bulletin 117, 846–864. http://dx.doi.org/10.1130/B25516.1.

Publication 6.2.5:

Kalberg, T., **Gohl, K.** (2014). The crustal structure and tectonic development of the continental margin of the Amundsen Sea Embayment, West Antarctica: implications from geophysical data. *Geophysical Journal International*, 198, 327-341, doi:10.1093/gji/ggu118.

Author contributions: This paper presents an analysis of deep crustal seismic refraction data and gravity models across the continental margin of the Amundsen Sea Embayment. Gohl was the initiator and principle investigator of this project, funded by the Deutsche Forschungsgemeinschaft, on lithospheric processes processes of this margin and Marie Byrd Land. Kalberg processed and modelled the data and wrote most of this paper as part of his PhD project, supervised by Gohl. The seismic data were collected during Polarstern expedition ANT-XXIII/4 (2006) with Gohl as chief-scientist.

Geophys. J. Int. (2014) **198,** 327–341
Advance Access publication 2014 May 20
GJI Geodynamics and tectonics
doi: 10.1093/gji/ggu118

The crustal structure and tectonic development of the continental margin of the Amundsen Sea Embayment, West Antarctica: implications from geophysical data

Thomas Kalberg and Karsten Gohl

Alfred Wegener Institute Helmholtz-Centre for Polar and Marine Research, Am Alten Hafen 26, D-27568 *Bremerhaven, Germany.*
E-mail: thomas.kalberg@awi.de

Accepted 2014 March 26. Received 2014 March 25; in original form 2013 June 19

SUMMARY

The Amundsen Sea Embayment of West Antarctica represents a key component in the tectonic history of Antarctic–New Zealand continental breakup. The region played a major role in the plate-kinematic development of the southern Pacific from the inferred collision of the Hikurangi Plateau with the Gondwana subduction margin at approximately 110–100 Ma to the evolution of the West Antarctic Rift System. However, little is known about the crustal architecture and the tectonic processes creating the embayment. During two 'RV Polarstern' expeditions in 2006 and 2010 a large geophysical data set was collected consisting of seismic-refraction and reflection data, ship-borne gravity and helicopter-borne magnetic measurements. Two *P*-wave velocity–depth models based on forward traveltime modelling of nine ocean bottom hydrophone recordings provide an insight into the lithospheric structure beneath the Amundsen Sea Embayment. Seismic-reflection data image the sedimentary architecture and the top-of-basement. The seismic data provide constraints for 2-D gravity modelling, which supports and complements *P*-wave modelling. Our final model shows 10–14-km-thick stretched continental crust at the continental rise that thickens to as much as 28 km beneath the inner shelf. The homogenous crustal architecture of the continental rise, including horst and graben structures are interpreted as indicating that wide-mode rifting affected the entire region. We observe a high-velocity layer of variable thickness beneath the margin and related it, contrary to other 'normal volcanic type margins', to a proposed magma flow along the base of the crust from beneath eastern Marie Byrd Land—West Antarctica to the Marie Byrd Seamount province. Furthermore, we discuss the possibility of upper mantle serpentinization by seawater penetration at the Marie Byrd Seamount province. Hints of seaward-dipping reflectors indicate some degree of volcanism in the area after break-up. A set of gravity anomaly data indicate several phases of fully developed and failed rift systems, including a possible branch of the West Antarctic Rift System in the Amundsen Sea Embayment.

Key words: Submarine tectonics and volcanism; Tectonics and landscape evolution; Dynamics of lithosphere and mantle; Dynamics: gravity and tectonics; Antarctica.

1 INTRODUCTION

Studying the lithospheric architecture of the Amundsen Sea Embayment (ASE) of West Antarctica (Fig. 1) provides constraints on tectono-magmatic reconstructions of the West Antarctic continental margin and the embayment itself from Palaeozoic to Cenozoic times. Improved knowledge of the structure and development of the lithosphere is the key to unravelling the evolution of the West Antarctic continental margin and the corresponding landscapes. The area experienced a number of key events during the tectonic history of the southern Pacific, including the inferred collision of the Hikurangi Plateau with the Gondwana at approximately 110–100 Ma subduction margin (Davy & Wood 1994; Mortimer *et al.* 2006) to the evolution of the West Antarctic Rift System. A number of plate-kinematic reconstructions are centred on the region, most recently by Eagles *et al.* (2004a) and Wobbe *et al.* (2012), but suffer from a lack of information about the deep crustal structure of the West Antarctic continental margin. The ASE also experienced a number of magmatic events from mid-Mesozoic to Late Cenozoic times (Wobbe *et al.* 2012). Analysis and modelling of magnetic data provides a first insight into the basement structure of the ASE shelf and implies that the present-day basement morphology of the ASE shelf may control the dynamic behaviour of grounded parts of the West Antarctic Ice Sheet (WAIS; Gohl 2012; Gohl *et al.* 2013a).

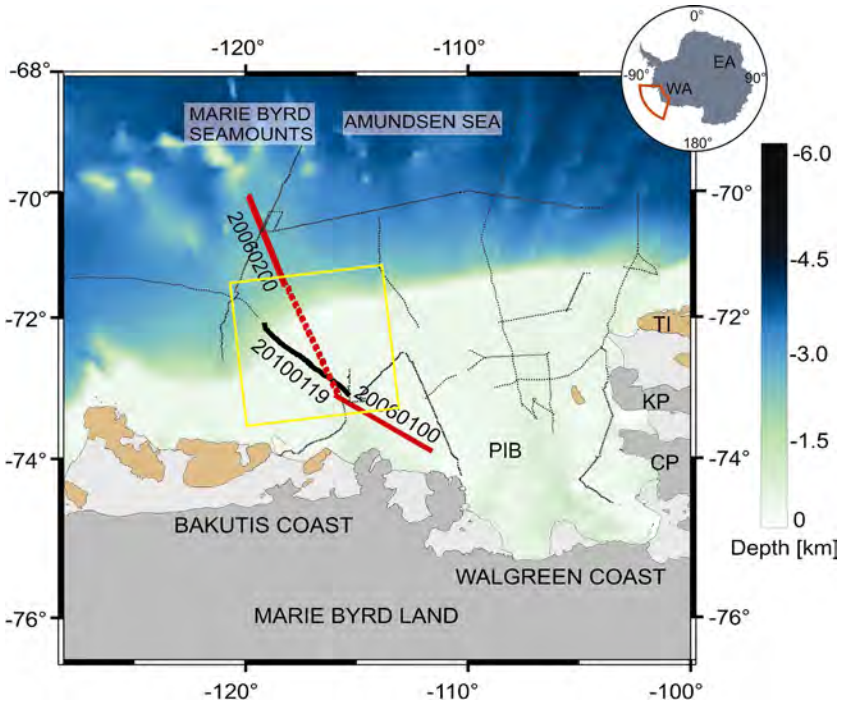

Figure 1. Bathymetric map of the Amundsen Sea Embayment after Nitsche *et al.* (2007) showing the locations of two OBH profiles and corresponding multichannel seismic reflection profiles (thick black lines). The red dashed line marks the interpolated profile AWI-100/200, connecting the profiles AWI-20060100 and AWI-20060200. Thin dotted black lines mark other seismic reflection profiles. The thin yellow frame shows the window which was used for the spectral analysis. TI, Thurston Island; PIB, Pine Island Bay; KP, King Peninsula; CP, Canisteo Peninsula.

An improved understanding of the tectono-magmatic processes and of the formation of basement ridges and sedimentary basins provides further constraints on palaeo and modern ice sheet dynamics as demonstrated in Bingham *et al.* (2012) or Smith *et al.* (2013).

This study presents a combination of geophysical data from the ASE, which were collected to study the lithospheric architecture and tectono-magmatic evolution of the West Antarctic continental margin. At first, we present and highlight the results of each individual data set. A continental rise-to-shelf seismic reflection transect provides constraints on the top- of-basement morphology and sedimentary architecture of the margin. Two deep crustal seismic refraction and wide-angle reflection profiles are used to derive velocity–depth profiles. Supported by a spectral analysis of gravity data, two different continuous 2-D forward gravity models place constraints on the crustal architecture and formation of the continental margin and shelf of the ASE. Following this, we propose a new integrated model of the tectonic evolution of the margin of the ASE. With this model we attempt to reconstruct the tectono-magmatic development of this margin from its breakup from New Zealand as early as 90 Ma (Wobbe *et al.* 2012) to the PRESENT which further supports boundary conditions for ice-sheet modelling attempts in this part of West Antarctica.

2 TECTONIC AND GEOLOGICAL BACKGROUND

The tectonic development of the Pacific margin of West Antarctica since Late Cretaceous times consisted of several distinct phases (Fig. 2). The southwestward propagation of rifting and breakup began with the separation of Chatham Rise from the Amundsen Sea margin of eastern Marie Byrd Land as early as 90 Ma and continued around 83 Ma with the breakup of Campbell Plateau from central Marie Byrd Land (e.g. Mayes *et al.* 1990; Bradshaw 1991; Larter *et al.* 2002; Eagles *et al.* 2004a; Wobbe *et al.* 2012).

From about 80 Ma, the Bellingshausen Plate started acting as an independently rotating plate, and continued to do so until about 61 Ma (e.g. Larter *et al.* 2002; Eagles *et al.* 2004a,b). Its incorporation into the Antarctic Plate occurred as part of a major plate reorganization in the South Pacific (Cande *et al.* 2000). Kipf *et al.* (2012) postulated that at around 65–56 Ma, the Marie Byrd Seamounts were formed from magmatic material that was transported from beneath the West Antarctic continental crust by a so-called continental insulation flow.

The eastern shelf, which contains Pine Island Bay, has been suggested by Dalziel & Elliot (1982), Storey (1991) and Grunow *et al.* (1991) as the site of a Palaeozoic–Mesozoic crustal boundary zone between the Marie Byrd Land block in the west and the Thurston Island crustal block in the east, whose apparent palaeomagnetic polar wander paths differ.

Recent analysis of magnetic and seismic data from the ASE shelf show that tectonic lineaments and sedimentary subbasins cross the shelf of which some may be related to a branch of the eastern West Antarctic Rift System (Gohl *et al.* 2013a,b). Apatite-He age trends, derived from rock samples of the eastern Pine Island Bay, infer rift-related block faulting indicating that the present glacially formed Pine Island Trough may have originated from tectonic activity as part of the West Antarctic Rift System (Lindow *et al.* 2011). Different thermal signatures of the Mt Murphy area and its neighbouring areas indicate a major fault system which was active during or after Oligocene (Lindow *et al.* 2011).

Latest geological studies in Marie Byrd Land show Cretaceous multistage rifting phases and strike slip faulting superimposed by transtension (Siddoway 2008). Gravity data, receiver-function analysis of teleseismic earthquakes and geological analysis suggest that the submarine plateaus of New Zealand and conjugate Marie Byrd

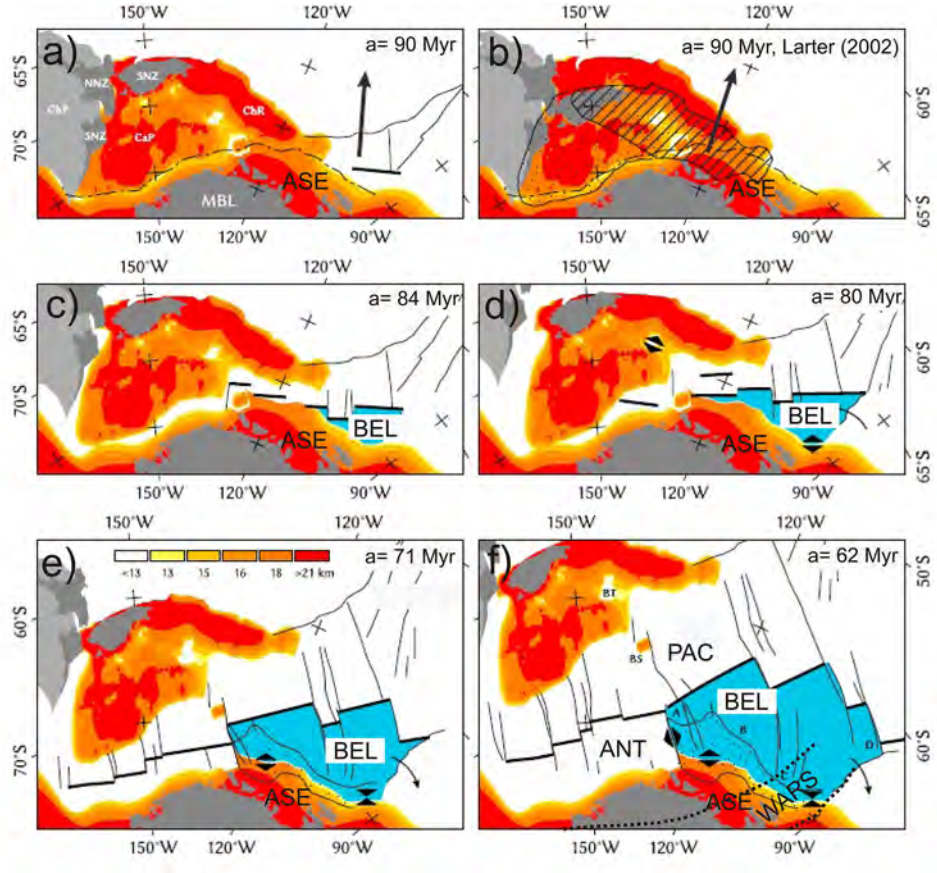

Figure 2. Pre-rift reconstruction model of distinct tectonic phases from the late Cretaceous to early Palaeocene of the Amundsen Sea Embayment including Chatham Rise (striated) and Campbell Plateau (stippled) modified after Wobbe *et al.* (2012) (Figs 2a, c–f) using the rotation parameters of Wobbe *et al.* (2012) and Grobys *et al.* (2008). Fig. 2(b) shows configuration using the rotation parameters from Larter *et al.* (2002). The black arrows in Figs 2(a) and (b) show the direction of movement of the Bellingshausen Plate. Thin black lines show fracture zones, thick black lines show mid ocean ridge segments. Thin black dashed line show suspected rift arm of the West Antarctic Rift System. Stippled area in Figs 2(e) and (f) shows oceanic crust which was formed along the Bellingshausen Plate margin. The colour scale in Fig. 2(e) shows the crustal thickness after modelling results of Wobbe *et al.* (2012). ANT, West Antarctic Plate; BEL, Bellingshausen Plate; BS, Bollons Seamount; BT, Bounty Trough; CaP, Campbell Plateau; ChP, Challenger Plateau; ChR, Chatham Rise; MBL, Marie Byrd Land; NNZ, North Island of New Zealand; PAC, Pacific Plate; SNZ, South Island; ASE, Amundsen Sea Embayment; WARS, West Antarctic Rift System.

Land consist both of thinned continental crust of only 25–28 km thickness (Llubes *et al.* 2003; Luyendyk *et al.* 2003; Winberry & Anandakrishnan 2004; Grobys *et al.* 2009). In the ASE, gravity modelling showed the crust of the inner to middle shelf to be of 24–28 km thickness. Moreover, it seems that the ASE was affected by magmatic intrusions interpreted from distinct zones of anomaly patterns and lineaments which can be associated with three major tectonic phases (Gohl *et al.* 2007, 2013a,b).

Jordan *et al.* (2010) calculated a Moho depth of about 19 km under the Byrd Subglacial Basin and the newly identified Pine Island Rift based on gravity inversion. Additionally, Bingham *et al.* (2012) also inferred crustal thinning leading to 25–21-km-thick crust beneath the Ferrigno rift and the adjacent Siple Trough region.

3 SEISMIC EXPERIMENT

The seismic data set presented in this study consist of two deep-crustal seismic refraction profiles and a suite of multichannel seismic reflection profiles (Fig. 1), that were acquired during RV Polarstern expeditions ANT-XXIII/4 in 2006 and ANTXXVI/3 in 2010. The seismic source used for both refraction and reflection recordings of the profiles AWI-20060100 and AWI-20060200 consisted of 8 G-Guns (68.2 l in total) and a Bolt air gun (32 l). The shot interval of 60 s corresponded to an average shot spacing of 150 m. Additionally, seismic reflection profile AWI-20100119 was acquired with three GI-Guns, fired every 10 s (Gohl *et al.* 2013b). The multi-beam bathymetry was measured with the Hydrosweep DS-III system.

3.1 Seismic reflection data

We mapped the top-of-basement along the refraction profiles AWI-20060100 and AWI-20060200, in coincident seismic reflection data (Fig. 1). These were acquired by using a 600-m-long analogue streamer with 96 channels. The data were recorded with a sampling interval of 4 ms. The data gap between the seismic reflection profiles AWI-20060100 and AWI-20060200 (Fig. 1) was bridged with the nearest seismic reflection profile

AWI-20100119 (Fig. 1) in order to generate an almost continuous transect. Data processing comprised CDP sorting with binning of 100 m, owing to the long shot interval for the profiles AWI-20060100 and AWI-20060200 and 25 m for the profile AWI-20100119, bandpass filtering of 10–200 Hz and a detailed velocity analysis followed by stacking and post-stack migration.

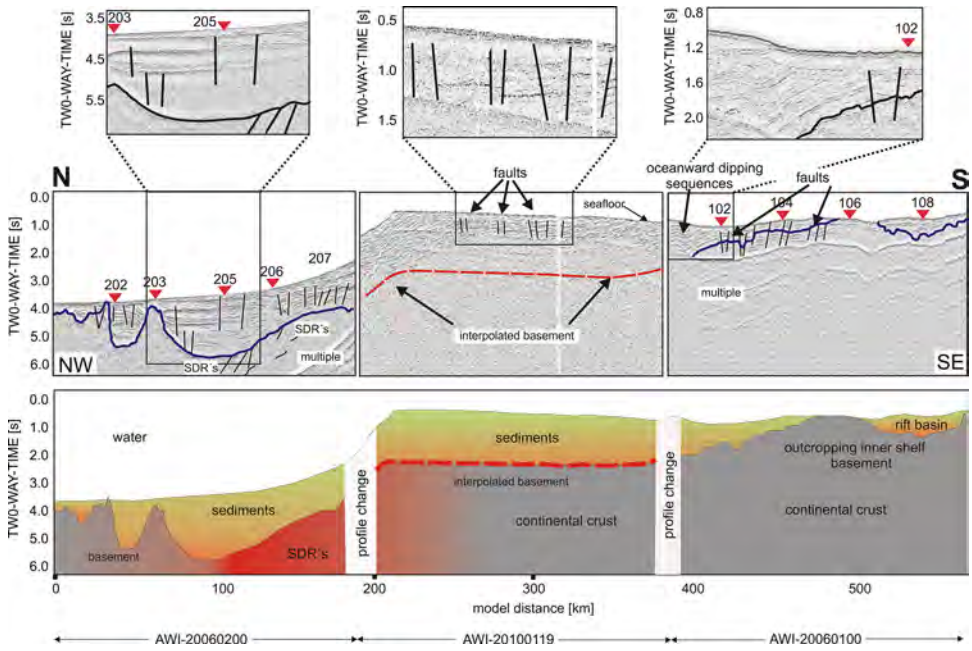

Figure 3. Compilation, line drawing and interpretation of seismic-reflection profiles AWI-20060100, AWI-20060200 and AWI-20100119 across the continental margin of the Amundsen Sea Embayment. The thick blue line indicates the interpreted top-of-basement. The dashed red line shows the interpolated top-of-basement based on a spectral analysis of free-air gravity data. The thin black lines within the sedimentary layer indicate unconformities, horst and graben and rift structures. Numbers including red triangles show the position of the OBH stations along the transect. The red lines indicate SDR, seaward dipping reflectors.

Attempts to suppress the shallow-water multiples on the shelf (Fig. 3) using techniques such as FK-filtering, Radon-transformation and predictive deconvolution produced minimal improvements due to the limited streamer length. Multiple suppression yielded, however, better results with the data of profile AWI-20100119 (Gohl *et al.* 2013b). We composed the three seismic reflection profiles into a single projected seismic transect (Fig. 3).

On the continental rise, the reflection data show stratified sediments to a two-way time of 2.5 s (∼3 km depth) in the deepest basins. Below the sediments, the rise is dominated by seamounts of the Marie Byrd Seamount province. We observe indications of normal faults and horst and graben structures within the continental rise sediments. At the foot of the slope, some reflections beneath the top of the acoustic basement are reminiscent of the seaward-dipping reflectors (SDR) known for many passive continental margins of volcanic type. The top basement reflector disappears south of profile distance 160 km (AWI-20060200; Fig. 3) and beyond which strong seafloor multiples on the shelf and the slope mask deeper signals.

The seismic shelf records show that the basement is exposed on the inner shelf of the ASE Fig. 3). Sediment sequences beneath the middle shelf dip seawards at 0.5°, and at 1.5° beneath the inner shelf. The outer shelf is dominated by large progradational sedimentary wedges (Gohl *et al.* 2013b).

3.2 Seismic refraction data and traveltime modelling

Due to sea ice coverage, and in order to minimize the risk of instrument loss, only nine ocean bottom hydrophone (OBH) systems were deployed along the 165 km long profile AWI-20060100, with a regular interval of 18–19 km (Fig. 3). Four of the systems (OBH 102, 104, 106 and 108) recorded usable data. Along the 171-km-long profile AWI-20060200 (Fig. 1), seven OBH systems were deployed with the same spacing between the Marie Byrd Seamount province and the foot of the continental slope (Fig. 3). Only five of these recorded usable data (OBH 202, 203, 205, 206 and 207). The raw OBH data were merged with the navigation data and then converted to SEG-Y format. The exact position of the OBH stations on the seafloor along the tracks were relocated by using direct *P*-wave arrivals. A bandpass filter of 4–20 Hz was applied to the seismic traces for reducing high and low frequent noise from the seismic signal.

We identify coherent *P*-wave phases of up to 120 km source-to-receiver offset at some stations (Fig. 4). All records show good-quality refracted *P*-wave phases from the crust (Pc1 and Pc2 phases; Fig. 5), some recordings contain high-amplitude wide-angle Moho reflections (PmP-phase) and intracrustal reflections (PcP-phase) as well as low-amplitude refracted phases from the upper mantle (Pn-phase). The Moho was identified as velocity contrast between the crustal layer and the upper mantle at velocities higher than 8.0 km s^{-1}.

We assigned a picking uncertainty of 150 ms to all *P*-wave arrivals. The traveltime inversion software *RAYINVR* (Zelt & Smith 1992) was then used for ray tracing to forward model the traveltime branches, by applying a layer-stripping procedure from top to bottom. This was followed by a traveltime inversion for fine-tuning the model parameters.

For the lower crust a resolution between 0.5 and 0.6 is reasonable at the shelf edge and continental rise, where 0 means no ray coverage and 1.0 represent maximum ray coverage (Fig. 7). Hence, the resolution of our *P*-wave models is the better in the upper and lower crust and the ray coverage is the densest at the middle section of both OBH profiles. Limited offsets lead to a lack of Pn- and PmP phases recordings at the ends of the profiles. The velocity distribution is laterally homogenous within the entire crust.

The velocity–depth model of profile AWI-20060200 (Fig. 6a) consists also of a sedimentary layer, upper and lower crustal

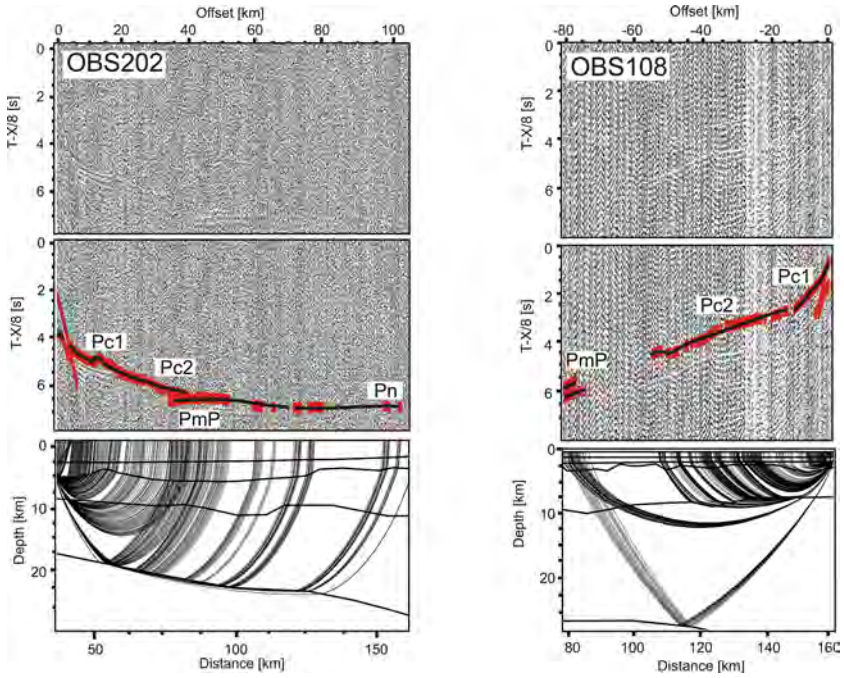

Figure 4. Top panel: part of seismic section from OBS 202 and 108, both plotted with a reduction velocity of 8 km s^{-1} and a bandpass filter of 4–20 Hz. Middle panel: Same section with modelled phases (black lines) and picked signals (red bars with bar length representing the pick uncertainty). Bottom panel: ray tracing results with ray coverage in the *P*-wave velocity model.

layers underlain by an upper mantle layer. Sediment velocities range from 1.7 to 2.5 km s^{-1} in the upper part to 3.5 km s^{-1} in the deepest basin. The depth to basement increases slightly towards the shelf. Two basement highs separate the area into three distinct areas (Figs 6a and b). In satellite-altimetry data (McAdoo & Laxon 1997), these highs correspond to circular features south of the Marie Byrd Seamount province. They probably therefore represent buried seamounts of the province. The northernmost area is around 30 km wide and 1.0–1.5 km thick. A second area in the middle part of the profile is 25 km wide and filled with sedimentary rocks of around 1.8 km thickness. At the southern flank of the profile the largest basin is 120 km wide and the sediments are up to 2.1 km thick. The upper crust thickens slightly from 3 km in the north to 6 km at the southern profile end. *P*-wave velocities in the upper crust range from 5 to 6 km s^{-1}. The lower crust also thickens slightly southward, from 7 km in the northern ASE to around 13 km towards the shelf. The crust-mantle boundary (seismic Moho) can be identified at a depth of 14 km in the north, which increases to 23 km near the foot of the continental slope.

Lower crustal velocities range from 6 km s^{-1} at the top of the layer to 7 km s^{-1} at its base in the north and 7.7 km s^{-1} in the south. The seismic Moho can be recognized at the base of the lower crustal high velocity layer by upper mantle velocities larger than 8 km s^{-1}.

The data of OBH profile AWI-20060100 (Fig. 6b) were inverted to yield a 2-D velocity–depth model that comprises a sedimentary layer, and upper and lower crustal layers underlain by the uppermost mantle. We identify five distinct sedimentary basins with variable (0.7–1.5 km) fill thickness and velocities ranging between 1.7 and 3 km s^{-1}. The upper crust is between 4.1 and 6.3 km thick with *P*-wave velocities ranging from 5 to 6.2 km s^{-1}. The lower crustal thickness increases southward from 14 km in the north to 24 km beneath the inner shelf. Velocities in this layer range between 6.2 and 7.1 km s^{-1} in northern part and between 7 and 7.6 km s^{-1} in the southern part. The seismic Moho was identified at depths between 25 and 30 km. Similar ss on profile AWI-20060200, the seismic Moho is identified at the base of the lower crustal high velocity layer.

4 GRAVITY ANOMALIES AND MODELLING

The interpretation and modelling of potential field data is carried out to investigate regional geological issues and to highlight deep and shallow crustal anomalies as well as basin structures. A joint interpretation of profile-based seismic data with free-air gravity anomaly (FAA; Fig. 8a) and Bouguer anomaly (BA; Fig. 8b) grids sets the seismic data into a regional geological context.

We calculated the BA of the area between 75°S–71°S and 100°E–120°E by using the satellite derived FAA of McAdoo & Laxon (1997), the latest bathymetry grid of Nitsche *et al.* (2007) (Fig. 1) and a Bouguer reduction density of 2.67 g cm^{-3}.

Additionally, we used the spectrum of the gravity data to fill the data gap between the seismic refraction profiles AWI-20060100 and AWI-20060200, which exhibits a prominent gravity anomaly high. This high is similar to those observed close to various shelf breaks worldwide, which can be related to various density contrasts including those resulting from crustal thinning, thick accumulations of sediments, and magmatic underplating (Watts & Fairhead 1999).

However, in order to calculate the depths of significant density interfaces in our data gap, we applied the power spectral analysis based on the method of Spector & Grant (1970) to the FAA of McAdoo & Laxon (1997). The method was developed for magnetic data and adapted for gravity data by Karner & Watts (1983). The method is based on the assumption of geological interfaces that are essentially horizontal with some small relief. With this assumption, the power spectrum of a group of prismatic sources distributed over the subsurface topography reveals a quasi-linear relationship between the power spectral density (PSD) and the wavenumber k_r. In

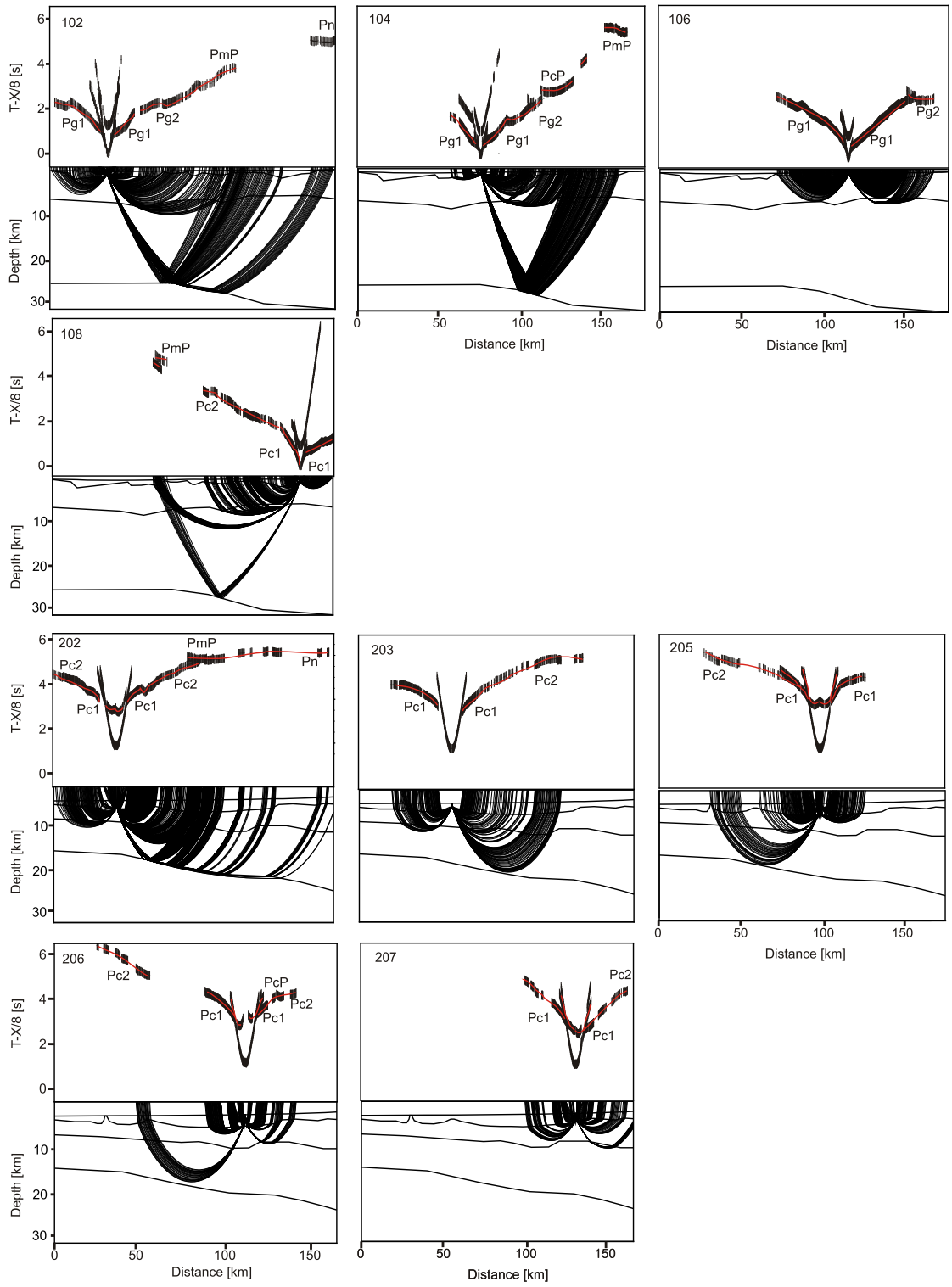

Figure 5. Comparison of picked and computed traveltime branches from the *P*-wave velocity models for each OBH station combined with the corresponding ray path. Depth is annotated in kilometres, the sections are plotted with a reduction-velocity T-X/8 in (s). The error bars indicate observed picking times and the size of the bars corresponds to the picking uncertainty. Solid red lines show the calculated traveltimes. Near-offset phases (P_{sed}, direct waves) are not annotated. Position of each OBH along the profiles is shown in Fig. 3.

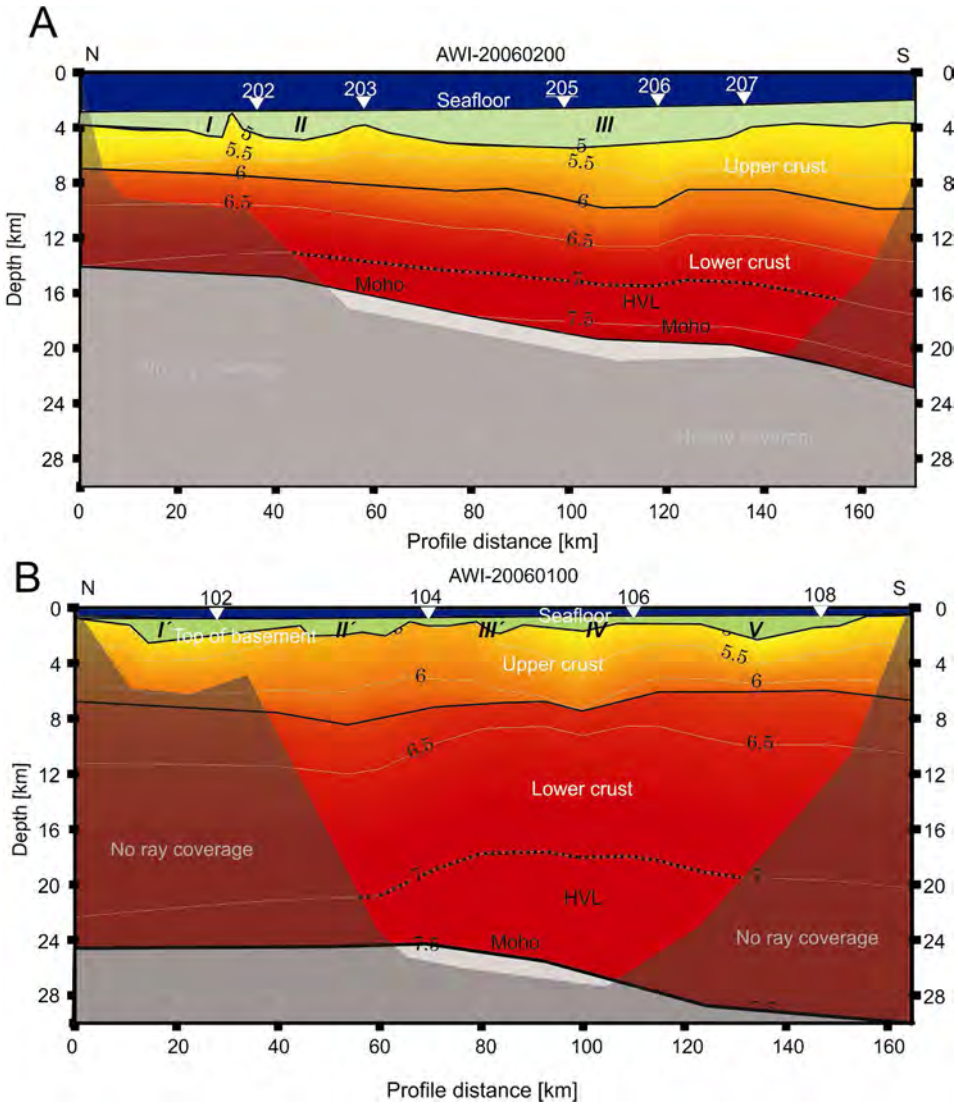

Figure 6. Final *P*-wave velocity models of the seismic refraction profiles. (b) AWI-20060100 (bottom) and (a) AWI-20060200 (top). The models are overlain by a semitransparent mask showing areas without ray coverage. Numbers and triangles show the OBH stations along the profiles. I, II, III and I′, II′, III′, IV and V label sedimentary basins along the profiles.

a plot of the natural logarithm of the FAA's power spectrum against k_r, a set of distinct linear segments is related to the mean anomalies of the mass anomaly. The slope of a linear segment multiplied by –0.5 yields the mean depth to its source. The window used for the spectral analysis covers an area of 200 km^2 and is a compromise between uniform size and area (Fig. 1). The chosen area should contain provinces of uniform geology, but on the other hand should be large enough to resolve longer wavelengths and therefore greater depths.

4.1 Satellite-derived free-air gravity anomalies

The FAA of the outer shelf is dominated by two highs of up to 80 mGal which correspond to the bathymetrically elevated Western and Eastern Outer Banks (Gohl *et al.* 2013b). Over the middle shelf area, we identify a major WSW–ENE trending negative anomaly with a minimum of –70 mGal and name it the Amundsen Sea Embayment Low (ASEL). This anomaly is interrupted by the so-called Peacock Gravity Anomaly (PGA) that is northwest–southeast orientated (Eagles *et al.* 2004a) and which continues to Thurston Island (TI) as the Thurston Island Low (TIL). Pine Island Bay (PIB) is divided by the north-striking glacial Pine Island Trough (PIT) with a gravity low of –50 mGal (Fig. 8).

4.2 Satellite derived BAs

The gravity effect of topography and bathymetry is removed from the FAA to generate the BA such that only information on rock density variations is retained. At long wavelengths, the transition from oceanic to continental crust can be clearly identified from a pronounced southward decrease of the BA from 140 to 40 mGal (Fig. 8b). The inner shelf is characterized by shorter wavelength anomalies of between 0 and 70 mGal whereas the outer shelf shows predominantly long wavelength anomalies of between –20 and 70 mGal, that correlate with bodies identified in a recent magnetic analysis of the ASE (Gohl *et al.* 2013a). We also identify a significant BA high larger as 60 mGal in the PIB region. As in the FAA, the ASEL and TIL appear as a WSW–ENE trending low dominating the middle shelf (Fig. 8b) which is interrupted by a positive WNW trending anomaly of up to 70 mGal corresponding to the PGA.

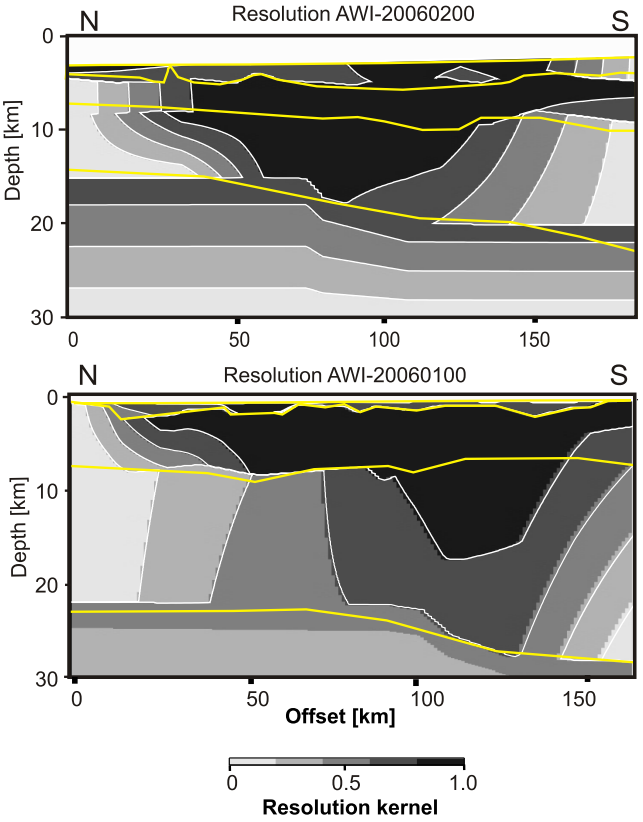

Figure 7. Resolution values of the two seismic traveltime inversion models for the *P*-wave velocity–depth models (B) AWI-20060100 (bottom) and (A) AWI-20060200 (bottom). The grey shading corresponds to the resolution value. Resolution values of greater than 0.5 indicate a moderate to good resolution. The yellow lines show the layer boundaries from the corresponding velocity–depth model. Contour lines are plotted at an interval of 0.2.

The outer shelf area is dominated by a major gravity low which we name the Outer Low. The boundary between the outcropping basement in the south and the sedimentary basin on the shelf corresponds to a change in the BA from 0 to 50 mGal. At least a prominent BA high up to 60 mGal over the PIB can be identified.

4.3 Spectral analysis results

Spectral analysis for the gap between the two seismic refraction profiles (Fig. 1) reveals two distinct linear segments for which linear regressions suggest a deeper and a shallower interface (Fig. 9). The choices of endpoints for the linear regression were made by visual inspection. The slope of the low-frequency (deeper) segment **A** corresponds to a mass anomaly depth of 22 ± 2 km whereas the slope of high-frequency (lower) segment **B** corresponds to an anomaly depth of about 4 ± 2 km. The uncertainty of the depths of the interfaces is controlled by the sampling interval of the spectral analysis and can be estimated to be around 2 km for crustal depths (Ciancara & Marcak 1976).

5 SHIP-BORNE GRAVITY DATA AND 2-D MODELLING

5.1 Data processing and description

Shipborne gravity data were collected continuously along all profiles with a KSS-31 sea gravimeter at a sampling interval of 1 s. The raw data were corrected for instrument drift during the cruise by using reference measurements in Punta Arenas, Chile. We reduced the data to FAA with respect to the GRS80 gravity model using a standard processing procedure (Torge 1989), including an Eötvös correction calculated with the ships navigation. The ∼200-km-wide data gap between profiles AWI-20060100 and AWI-20060200 was filled using the free air gravity data of McAdoo & Laxon (1997).

The gravity anomaly decreases linearly from model distance 0–150 km from –10 to –70 mGal (Fig. 10). Two short wavelength undulations of a few mGal in the north correlate with the buried seamounts in the seismic data (Fig. 3). Across the shelf edge, the FAA increases up to 50 mGal at profile distance 250 km. This gravity high is similar to other observations at various shelf breaks, named the 'sedimentation anomaly' according to Watts & Fairhead (1999). If a 2-D model profile is oriented perpendicular to the shelf break the density contrast between the sediments and the water is sufficient to model the anomaly. As our profile runs more or less perpendicular to the shelf edge (Fig. 1), it is likely that a 3-D effect of the shelf break contributes to the upward anomaly. Over the middle shelf, the FAA reaches a local minimum of –50 mGal at 400 km profile distance and increases up to 20 mGal towards the inner shelf.

5.2 2-D Density–depth modelling

We used the software *IGMAS* (Götze & Lahmeyer 1988) to model a composite FAA transect. To calculate the 2-D gravity effect of a mass anomaly, the IGMAS algorithm uses triangulated polyhedra built from a set of polygons defined in parallel vertical cross sections. The triangulation between these vertical planes is done automatically during the modelling procedure. We defined polygons using ship-borne bathymetry data, seismic refraction and seismic-reflection data along profiles AWI-20060100, AWI-20060200 and AWI-20100119, and the results of the spectral analysis in order to setup a starting model. The model geometries at the ends of the profiles were edited to account for the regional gravity field. To simplify the model, we combined all observed sedimentary units into one layer and calculated an average density of 2050 kg m^{-3} using the velocity–density relationship of Nafe & Drake (1963). As the observed *P*-wave velocities of the crust indicate continental affinity along the modelled profile (Christensen & Mooney 1995) we used the velocity–density relationship of Barton (1986) to define upper-crust density of 2650 kg m^{-3} and a lower-crust density of 2800 kg m^{-3}. Finally, we modelled the observed high-velocity layer with a density of 3150 kg m^{-3}, also after Barton (1986). The uppermost mantle was modelled with a density 3300 kg m^{-3}. During the modelling procedure, we compared the density with results of the *P*-wave velocity–depth models and adjusted every layer boundary to obtain a best fit between the measured and modelled anomaly by varying the crustal geometry as little as possible.

Owing to the inherently non-unique testimony of gravity signals, we present two models that each explain the observed anomaly (Fig. 10). The standard deviation between the measured and modelled FAA in model A is 1.53 mGal along profile AWI-20060100 and 1.32 mGal along profile AWI-20060200 including the interpolated part. With model B, these values are 1.53 and 2.01 mGal. In general, the correspondence between the velocity–depth and density–depth models is acceptable.

In its central part (Fig. 10) the model suffers from the absence of seismic-reflection data and a velocity–depth model. We constrained the range of models applicable to this part using the results of the power-spectral analysis of its FAA field. As noted above, this part of

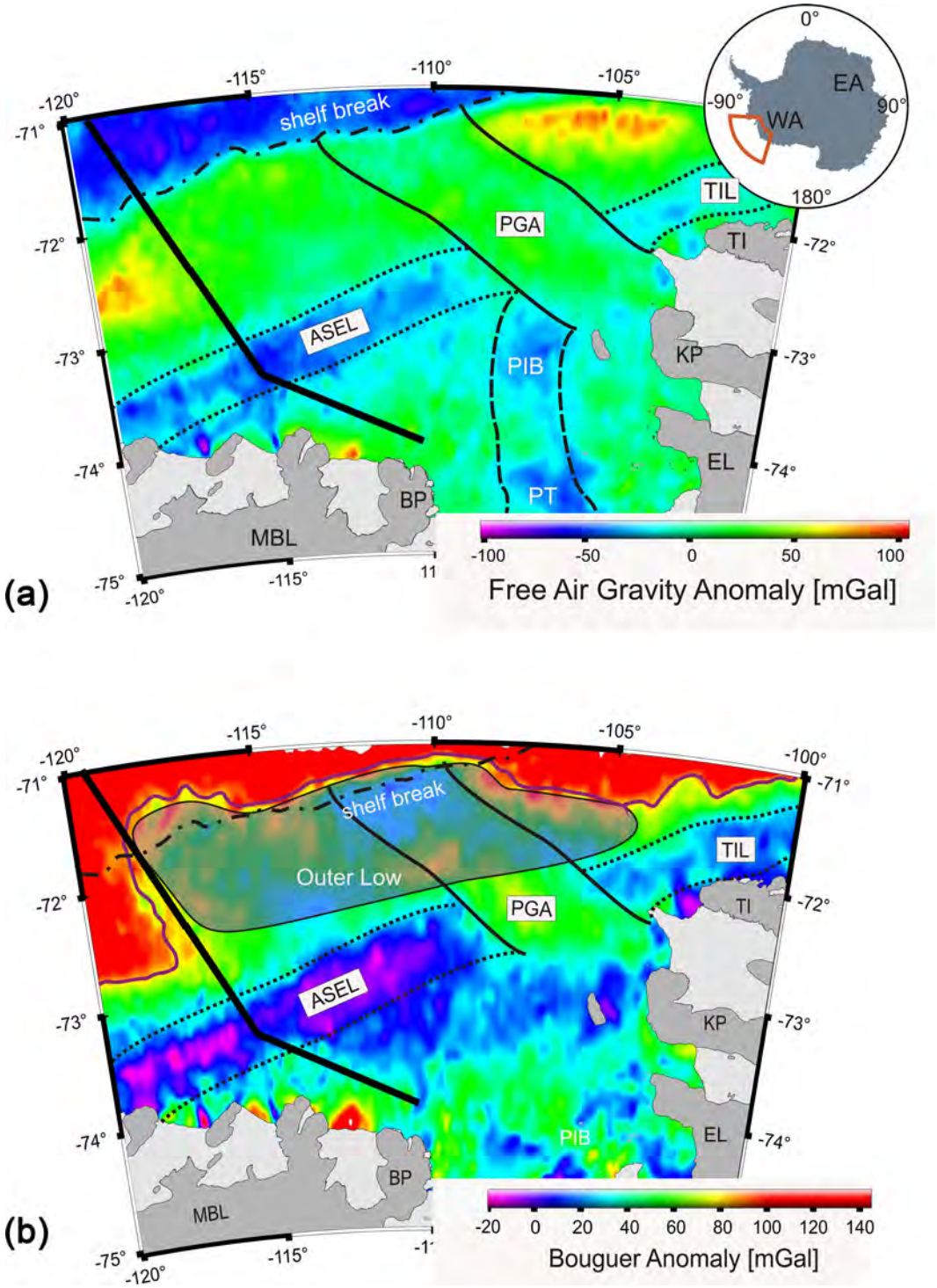

Figure 8. Compilation of gravity data. (a) Maps the satellite-derived free-air gravity anomaly of the Amundsen Sea Embayment (McAdoo & Laxon 1997). The thin black dotted and continues lines mark prominent gravity anomalies along the middle and outer shelf of the Amundsen Sea Embayment. (b) Images the calculated Bouguer Anomaly. The framed semi-transparent area beneath shelf break shows a prominent low (Outer Low). The thick black dotted line marks the 2-D gravity rise-to-shelf model transect (Fig. 10). ASEL, Amundsen Sea Embayment Low; TIL, Thurston Island Low; PGA, Peacock Gravity Anomaly; PT, Pine Island Trough; BP, Bear Peninsula; MBL, Marie Byrd Land; EL, Ellsworth Land; TI, Thurston Island; KP, King Peninsula.

the profile crosses the gravity high of the Western Outer Bank (Gohl *et al.* 2013a). In model A, the sedimentary layer is up to 3 km thick, consistent with the power spectral analysis. The top-of-basement interface is rough south of the gravity high at profile distance of 300–370 km. The Moho steps down from a depth of about 22–27 km between profile distance 170–200 km, again consistent with the power spectral analysis, and remains at this depth until after profile distance 400 km, where it is constrained once again by refraction results on profile AWI-20060100. With these layers, it becomes necessary to model the gravity high as the signal from a 10 km high

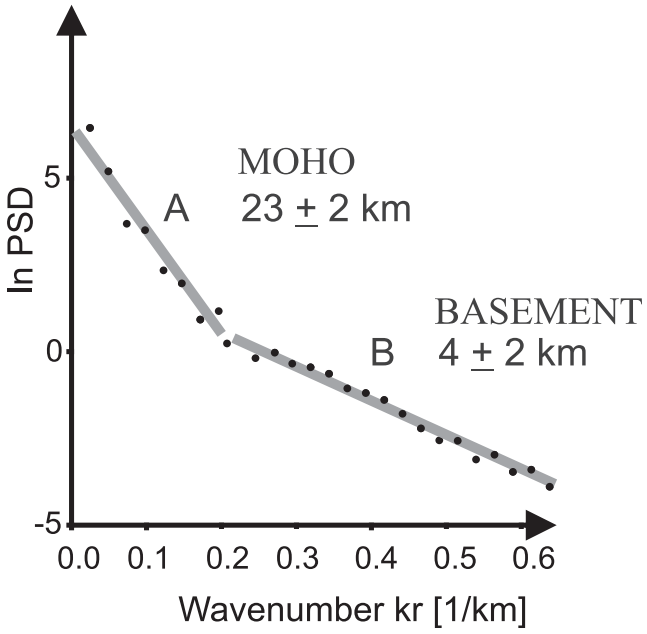

Figure 9. Spectral analysis of the satellite-derived free air gravity anomaly of McAdoo & Laxon (1997). The natural logarithm of the energy spectra (PSD) in $mGal^2km$ is plotted against the wavenumber in km^{-1}. The black dots show the values of the energy spectra and the grey line is the result of a linear regression for the depth estimation. The slope of the regression line corresponds to the anomaly mass depth. Anomaly mass depth is presented in km. Line A show the low frequency area (wavenumber lower than 0.1 km^{-1}) and line B the high frequency area.

bulge in the high-density/high-velocity layer of the lowermost crust between profile distance 210–370 km. In model B, the high can be explained by thinning of the sedimentary layer between profile distance 170–250 km, and its absence between profile distance 250–370 km, although this latter depiction is not consistent with the power spectral analysis. The high-density layer is 4–7 km thick with no significant bulge.

6 DISCUSSION

6.1 Crustal structure

The FAA predominantly reflects the seafloor topography (Fig. 8a), whereas the BA portrays density and thickness variations of the lithosphere, including the gradual negative gradient that indicates the transition from continental to oceanic crust (Fig. 8b). However, our transect lies mostly within the interpreted continental crust. The Outer Low of the ASE shelf correlates with an elevated basement identified in seismic-reflection data from the ASE, named the Western Outer Bank (Gohl *et al.* 2013b). Contrary to the FAA, the corresponding BA signal reaches into the continental rise indicating that its source is not topographic (Fig. 8). The corresponding BA signal is probably the gravimetric signal of a thicker continental sliver generated during the Cretaceous extension that led to the separation of West Antarctica and Zealandia.

We subdivide the crust of the ASE into an upper crust, a lower crust and a high velocity lowermost crustal layer. The average upper crustal *P*-wave velocity of around 5.5 km/s along the entire transect is typical of uppermost continental crust (Christensen & Mooney 1995; Fig. 10). The absence of any *P*-wave velocity or density variations below the two Marie Byrd seamounts indicates that these basement highs consist of similar material as the surrounding crust. The northern end of profile AWI-20060200 is less certain due to the lack of ray coverage and reversed records.

In general, the lower crustal *P*-wave velocities and densities are greater than expected for normal continental crust indicating a more mafic crustal composition (Christensen & Mooney 1995). Between model distances 180–380 km, our models are not constrained by deep seismic data. However, based on the gravity spectral analysis and an adjacent seismic-reflection profile, we argue that the sedimentary layer and the upper and lower crust have architectures similar to those beneath the continental slope and the inner shelf. The modelled rougher basement explains the high-frequency variations of the FAA. In Model A the estimated depth to top basement fits better to the flanking seismically constrained profiles than Model B, suggesting that its geometry is more appropriate to describe the ASE.

6.2 High-velocity layer

Traveltime modelling reveals *P*-wave velocities of 7.0–7.6 km s^{-1} in the lower crust along both seismic refraction profiles corresponding to densities between 3140 and 3160 kg m^{-3} in the gravity models (Barton 1986). These densities differ significantly from those expected for normal upper mantle density (3300 kg m^{-3}) or for normal lower continental crust (Anderson 1989). The maximum 10 km thickness of this layer is comparable to the thickness of high-velocity bodies known from other extended and volcanic type continental margins like the East Greenland continental margin (Voss & Jokat 2007) or its conjugate Vøring margin offshore mid-Norway (Mjelde *et al.* 2002). In these settings, the high-velocity bodies are interpreted as underplating of gabbro by accumulation of magma at the Moho during extension. By analogy, therefore we propose that the high-velocity layer beneath the ASE may represent widespread magmatic underplating (Fig. 10) indicating that the margin is of volcanic-type rather than of magma-poor type (Mutter *et al.* 1984). Hints of SDRs farther north reinforce the notion that the breakup process between greater New Zealand and West Antarctica was accompanied by magmatism. Grobys *et al.* (2009) interpret the observed high-velocity body of the conjugate southern Bounty Trough off eastern New Zealand as a mafic body intruded into the lower and upper crust and its high-velocity zone, as possible underplating at the base of the crust. However, the continental margins of eastern Zealandia, the Chatham Rise and the Campbell Plateau are not characterized well enough to match the categories of volcanic or non-volcanic type margins due to the lack of deep crustal data.

If the SDRs found along line AWI-20060200 (Fig. 3) of the Amundsen Sea do not find a counterpart on the New Zealand margin, the Amundsen Sea SDRs may be sequences of post-breakup volcanic phases. A study of the Southeast Greenland margin of Hopper *et al.* (2003) reports volcanic seaward dipping reflectors on oceanic crust, 180 km seaward of the continent-ocean-boundary which suggests that SDRs are not necessarily related to initial break-up.

Kipf *et al.* (2012) propose the generation of magma from partial melting of upper mantle rocks convecting as part of a so-called continental insulation flow on the basis of HIMU-type magmatic rocks (high time-integrated $^{238}U/^{204}Pb$) from beneath the Marie Byrd Land to the present-day Marie Byrd Seamount province between Late Cretaceous and Palaeocene. They suggested the upwelling arm of the convection cell exists beneath Marie Byrd Land at the present-day. This hypothesis suggests an alternative source

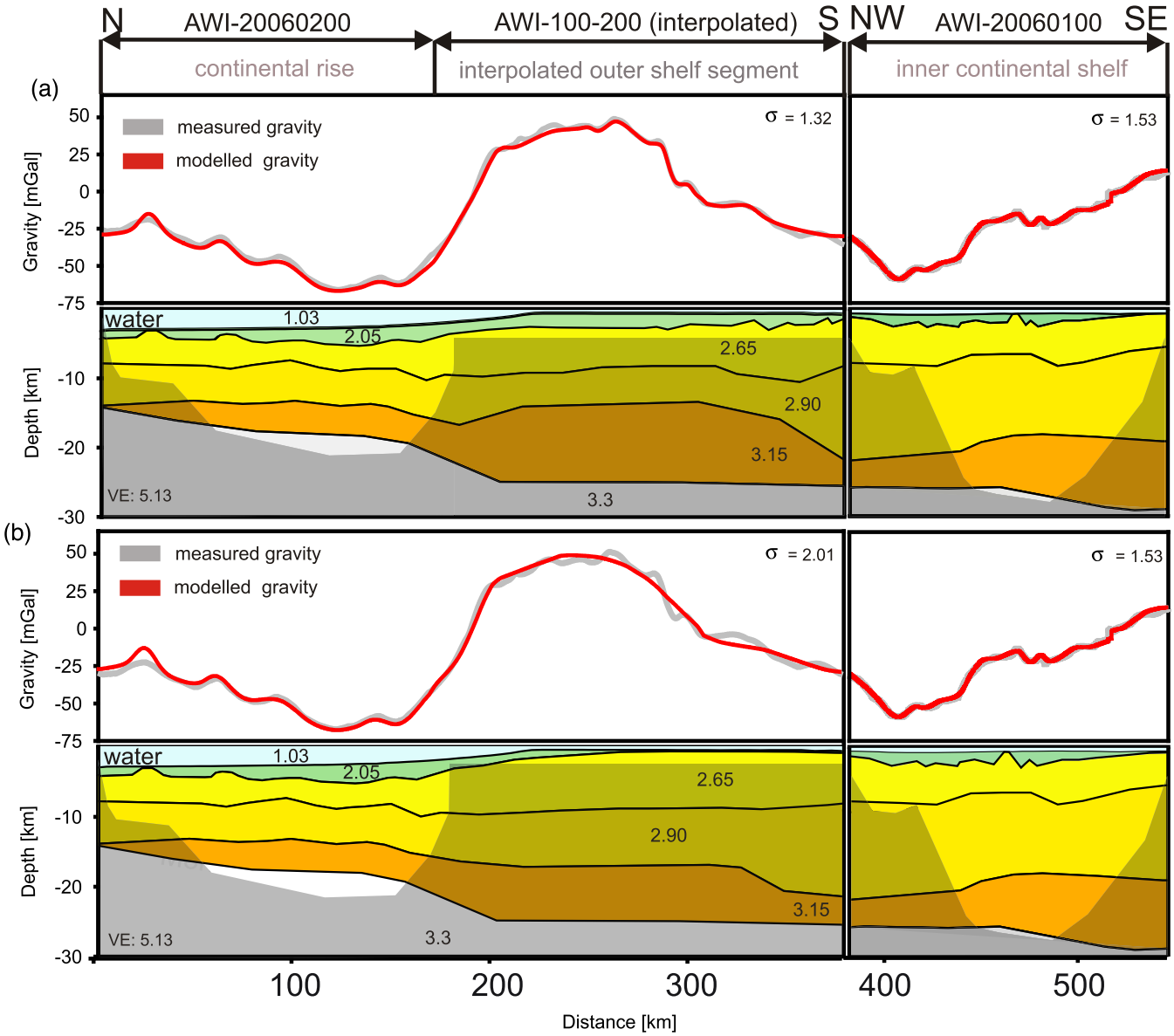

Figure 10. Two different 2-D forward gravity models of the seismic refraction profiles AWI-20060100 and AWI-20060200. The data gap between the two seismic refraction profiles was bridged with satellite-derived gravity data from McAdoo & Laxon (1997) and modelled using constraints from spectral analysis of the satellite-derived gravity data of McAdoo & Laxon (1997) and the adjacent seismic reflection profile AWI-20100119 (Fig. 2). Bathymetric surface is after Nitsche *et al.* (2007). Density values are given in 10^3 kg m^{-3}.

of gabbroic lower crust on the ASE shelf, in direct proximity to the Marie Byrd Land Seamount province.

However, if the bulge would be constituted by gabbroic melt, the expected density would be around 2800 kg m^{-3}, which is significant lower than the observed 3150 kg m^{-3}.

In the end the density of the HVL is too high for magma of Phanerozoic origin. On the other hand, the occurrence of cumulated layers could significantly rise the density of the material.

6.3 Serpentinization

An alternative explanation for the HVL is serpentinization of mantle material (e.g. Carlson & Miller 2003). Serpentinized peridotite can have velocities and densities similar to those of lower continental crust (Boillot *et al.* 1992). Serpentinite was observed along many non-volcanic passive margins such as the West Iberian margin (Boillot & Winterer 1988; Whitmarsh *et al.* 1996) or the Newfoundland margin (Reid 1994). Boillot *et al.* (1992) suggested that the formation and accretion of serpentinite beneath the crust may play a role in areas of rifted continental margins.

However, in these settings serpentinization requires the penetration of seawater downward via faults, and low-angle detachment surfaces. Another possibility is via deep hydrothermal circulation. Hydrothermal activity was observed at intraplate volcanoes such as the Lo'ihi volcano (Malahoff *et al.* 2006). The Marie Byrd Seamount province is identified as a system of intraplate volcanoes (Kipf *et al.* 2012). Hence, the crust of this area has a potential for seawater penetration.

Serpentinization is a gradual process creating no clear boundary between unaltered peridotite and serpentinized mantle material. Magma-poor margins are often characterized by an increasing *P*-wave velocity from the crystalline basement to the mantle without

a clear Moho response due to serpentinized mantle material (Minshull 2009). At the West Iberian margin, the absence of clear Moho reflections were interpreted as the result of partial serpentinized mantle peridotite (Chian *et al.* 1999).

Mjelde *et al.* (2002) discussed the possible occurrence of serpentinized mantle in combination with magmatic underplating along the Vøring volcanic passive margin offshore mid-Norway. The observation of clear Moho reflections was the key argument for favouring the underplating hypothesis (Mjelde *et al.* 2002). We modelled the observed HVL with a density of 3300 kg m^{-3} and hence, of significant higher density than the average density of serpentinite at this depth (Christensen 1996). We therefore imply a continental margin that is likely more influenced by magmatism than undercrusted by serpentinite.

6.4 Tectono-magmatic evolution

The seismic reflection data of the ASE reveal dipping lowermost strata on the inner ASE shelf, which may represent the earliest sedimentary rocks in the Amundsen Sea (see also Gohl *et al.* 2013b). We interpret the different northward dipping sedimentary reflectors as probable results of different extensional phases during the formation of the area. Normal faults indicate crustal extension affected the area. The present-day crustal architecture beneath the shelf infers wide-mode rifting such as observed in the Basin and Range Province of western North America (Hamilton 1987) rather than narrow-mode rifting such as the east African Rift System (e.g. Ebinger *et al.* 1989; Buck 1991; Rosenbaum *et al.* 2002) but the existence cannot be excluded from our data. Horst and graben structures are a further indication that the region evolved by wide-mode rifting (Buck 1991). Fault-like structures on the shelf may represent block-faulting during early stage and aborted rifting. The BA of the ASE shelf (Fig. 8b) shows several pronounced local highs and lows suggesting a pattern of rift basins and intervening highs. It is possible to speculate that the basins in the ASE (Fig. 3) are related to the pre-breakup dextral transtensional strain known from western MBL (Siddoway 2008) which is a hint for activity of the WARS affecting the entire ASE. A southward decrease of the BA with a gradient of about 1.5 mGal km^{-1} may also indicate that the crust was affected by rifting. The WSW-ENE trending ASEL and TIL strike parallel to the Pacific Antarctic Ridge in the north and the Bentley Subglacial Trough in the south and where our model crosses the ASEL it shows a thinned, 20-km-thick continental crust.

We interpret these observations as a record of a multistage initial Cretaceous wide-mode rifting event and thermal subsidence that followed the eventual successful breakup Zealandia from Antarctica. Our data show evidence for crustal extension connected to activities of the WARS since Cretaceous that resulted in the abandonment or evolution of a young-stage wide rift zone in favour of a fully developed extended continental margin and mature oceanic crust. It is possible that this rifting is connected to the well documented distributed Cenozoic extension superposed by narrow mode extensional events within the eastern Ross Sea sector of the WARS and the onshore parts of the ASE (Luyendyk *et al.* 2003; Davey & De Santis 2006; Jordan *et al.* 2010). However, the absence of implications for narrow-mode rifting in the offshore part of the ASE is not in conflict with this interpretation.

The orientation of lineaments in potential field data infer that these rifting events continued to affect the ASE after breakup from Zealandia, becoming a site for Bellingshausen-West Antarctic and East Antarctic–West Antarctic Plate divergence in Palaeocene and Oligocene times (Eagles *et al.* 2004a; Gohl *et al.* 2013a).

Fig. 11 presents a schematic tectono-magmatic reconstruction of the continental margin segment sampled by our model from late Cretaceous breakup of New Zealand and West Antarctica until Oligocene times (Figs 11e to b) and the present-day configuration (Fig. 11a). Fig. 11(e) shows the possible lithospheric configuration during or short before breakup between New Zealand and West Antarctica at around 100 Ma.

The crustal architecture was homogenous along the entire profile. At this time, extension may starts between Zealandia and West Antarctica. Mukasa & Dalziel (2000) inferred subduction-related I-type magmatism occurred at least until 94 ± 3 Ma (U-Pb zircon date) from the Walgreen Coast–eastern MBL (Fig. 1) to western Pine Island.

Fig. 11(d) shows the possible configuration during onset of wide-mode rifting between 60 and 80 Ma. We infer the onset of magmatism at this time based on magmatic flow estimations as discussed above. Fig. 11(c) images ongoing magma flow, the occurrence of the Marie Byrd Seamount province which was accompanied by thermal subsidence of the palaeo shelf of the ASE. The time slice shown in Fig. 11(b) illustrates the lithospheric configuration during 30 Ma. Ongoing magma accumulation was accompanied by tectonic rifting. At least Fig. 11(a) illustrates the present-day configuration. The reconstruction is based on the crustal architecture of our gravity and seismic model (Fig. 10b). The basin development we illustrate at the top surface of our transect is based on a schematic back-strippe reconstruction applied for the ASE shelf by Gohl *et al.* (2013b).

Due to the absence of evidence for a volcanic extended margin south of Zealandia, we prefer to explain the magmatic underplating as a product of partial melting during convective mantle flow set up by long-lived continental insulation. There are no robust constraints about the timing of this flow but Kipf *et al.* (2013) propose the formation of the Marie Byrd Seamounts to be in Early Cenozoic (~56 Ma). With respect to the present-day distance of around 800–1000 km between the central Marie Byrd Seamount province and coast of eastern Marie Byrd Land (Fig. 1) and an average convective velocity of around 1–5 cm a^{-1} (Schubert *et al.* 2001), the onset of magma flow may have occurred around 10 Myr earlier at about 65 Ma. This is consistent with a suspected major plate reorganization in the South Pacific in Palaeocene (Cande *et al.* 2000).

Further, the assumed increasing magmatic activity beneath the ASE shelf shown in Fig. 11(b) at about 30 Ma correlates with the emplacement age of the Dorrel Rock intrusive complex in Marie Byrd Land (Rocchi *et al.* 2006) implying that a major or several single magmatic events related to multistage tectonic activity affected the Amundsen Sea margin. Additionally, the observation of different thermal signatures in the Mt Murphy area of western Marie Byrd Land, which indicate a major fault system and which was active during or after the Oligocene (Lindow *et al.* 2011) is an implication for tectonic activity in this region. We interpret this as a further indication that tectonic and magmatism were coupled processes during the Oligocene and are related to the active branch of the WARS in the ASE (Gohl *et al.* 2013a,b).

Following the recent hypothesis of Kipf *et al.* (2013) we infer that the magmatic bulge at the Moho discontinuity was the result of a long-distance magma flow which reached the Moho, grew continuously and then spilled over (Fig. 11). This magma bulge is likely to be responsible for the Outer Low in the BA and the corresponding elevated top-of-basement which is identified in seismic data (Gohl *et al.* 2013b). It seems reasonable, that the accumulation of magmatic material at the Moho cause uplift of the overlying structures (Burov & Guillou-Frottier 2005).

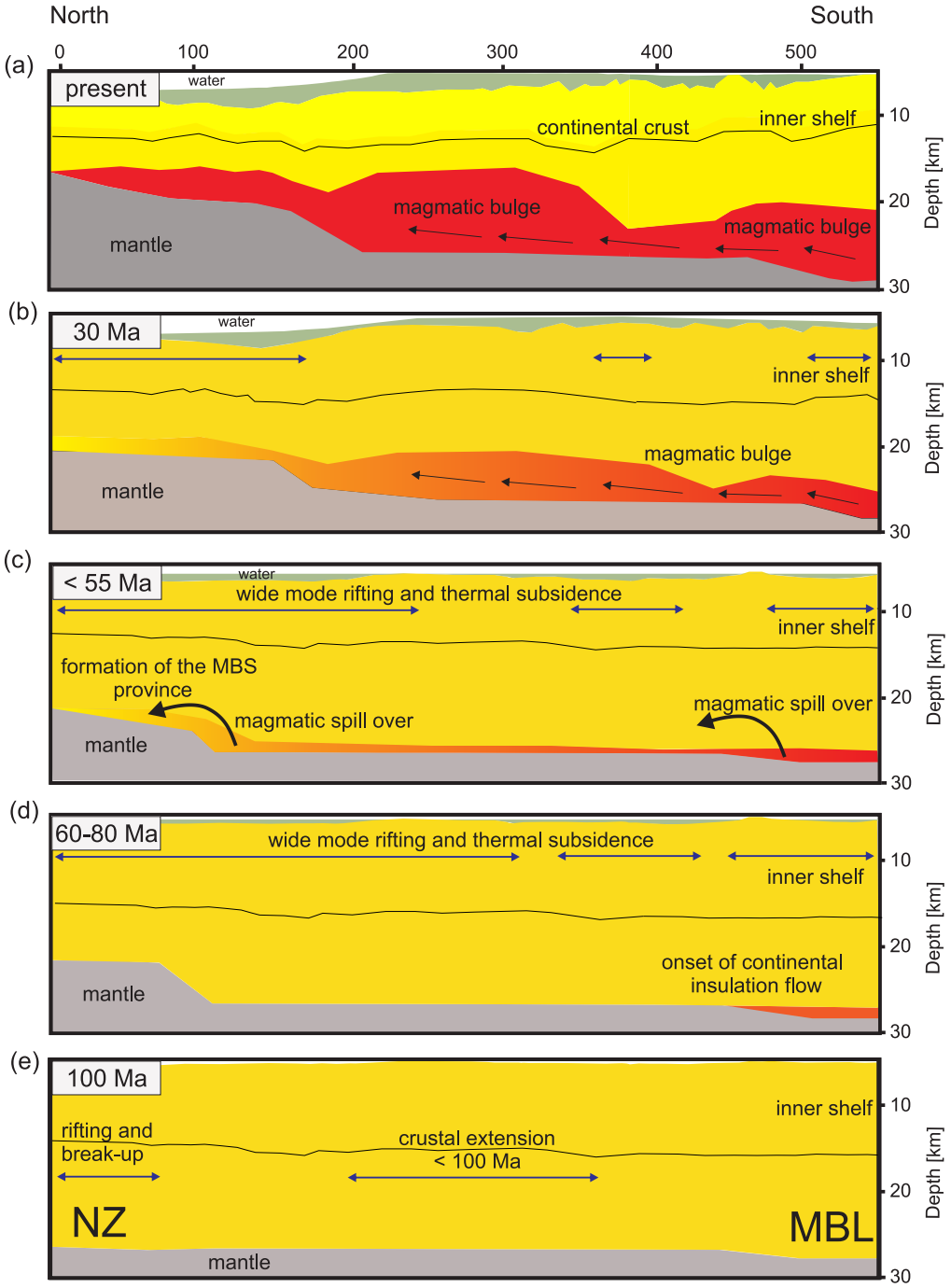

Figure 11. (a) interpreted 2-D gravity model based on the seismic refraction profiles AWI-20060100 and AWI-20060200. The top-of-basement was mapped by using the seismic reflection profiles AWI-20060100, AWI-20060200 and AWI-20100119. The black arrows show the flow direction of the inferred continental insulation flow (Kipf *et al.* 2013) from beneath Marie Byrd Land to the Marie Byrd Seamount Province. The blue arrows represent extensional rifting. The slides (b) to (e) show schematically the tectono-magmatic development of the margin from breakup of New Zealand and West Antarctica to Oligocene. MBL, Marie Byrd Land; NZ, New Zealand.

7 CONCLUSION

Geophysical data from the ASE provide new insights into the lithospheric architecture and tectono-magmatic development of this continental margin. Two deep crustal seismic profiles image the crustal and upper mantle structure of parts of the continental rise, slope and shelf. A continuous rise-to-shelf 2-D gravity model supports and expands on the velocity–depth models and enables the interpretation of a tectono-magmatic history for the ASE margin from its breakup with Zealandia to the present and indicating a margin-wide process of magmatic underplating. The main findings are summarized as follows:

1. The geophysical data image the upper and lower crust and reveal a high-velocity layer at the base of the lower crust beneath the shelf. The crust is 10–14 km thick at the continental rise and up

to 29 km thick beneath the inner shelf. Seismic refraction data reveal *P*-wave velocities between 7.1 and 7.6 km s^{-1} in the high-velocity layer indicating a margin-wide process of magmatic underplating whose thickness varies up to a maximum 10 km.

2. 2-D gravity modelling supports the hypothesis of a magmatic layer beneath the shelf and is consistent with the velocity–depth model. Indications of seaward-dipping reflectors in the seismic data suggest that breakup between greater New Zealand and West Antarctica may have been accompanied by magmatism not necessarily related to initial break-up.

3. Following the interpretation of Kipf *et al.* (2013), the high-velocity layer can be related to the Marie Byrd Seamount Province as product of a continental insulation flow which transported mantle material from beneath West Antarctica to the present-day Marie Byrd Seamount Province. The onset of the magma flow in the Palaeocene, which is maybe mantle originated, correlates with a major plate reorganization in the South Pacific (Cande *et al.* 2000). Magma accumulation at the base of the crust seems to be responsible for the elevated basement beneath the outer shelf of the Amundsen Sea Embayment. The absence of a gradational transition between the velocity body, normal upper crustal seismic velocities and a significant higher density of the observed HVL suggest that serpentinized mantle not is present beneath the ASE.

4. The crustal architecture, sedimentary setting and potential field data from the ASE indicate its formation during crustal extension. The constant crustal thickness and horst and graben structures suggest that this process was an expression of wide-mode rifting. Geophysical data show early stage, fully developed and failed initial rifting structures within the ASE suggesting a late active branch or integrated feature of the West Antarctic Rift System.

ACKNOWLEDGEMENTS

We are grateful to the master, crews and scientific teams of the *RV Polarstern* expeditions ANT-XXIII/4 (2006) und ANT-XXVI/3 (2010) for their support in collecting new geophysical data from the ASE. This project was funded by the Deutsche Forschungsgemeinschaft (DFG) under project number GO 724/13–1 and is affiliated with Work Package 3.2 of the AWI research program PACES.

REFERENCES

Anderson Don, L., 1989. *Theory of the Earth,* Blackwell Scientific Publications, http://resolver.caltech.edu/CaltechBOOK:1989.001.

Barton, P., 1986. The relationship between seismic velocity and density of continental crust – a useful constraint? *Geophys. J. R. astr. Soc*., **87,** 195–208.

Bingham, R.G., Ferraccioli, F., King, E.C., Larter, R.D., Pritchard, H.D., Smith, A.M. & Vaughan, D.G., 2012. Inland thinning of West Antarctic Ice Sheet steered along subglacial rifts, *Nature,* **487,** 468–471.

Boillot, G. & Winterer, E.L., 1988. Drilling on the Galicia Margin: retrospect and prospect, in *Proceedings of the Ocean Drilling Program, Scientific Results,* Vol. 103, pp. 809–828, eds Boillot, G. & Winterer, E.L. Ocean Drilling Program, College Station.

Boillot, G., Beslier, M-O. & Comas, M., 1992. Seismic image of undercrusted serpentinite beneath a rifted margin, *Terra Nova,* **4,** 25–33.

Bradshaw, J.D., 1991. Cretaceous dispersion of Gondwana: continental and oceanic spreading in the south-west Pacific-Antarctic sector, in *Geological Evolution of Antarctica,* pp. 581–585, eds Thompson, M.R.A., Crame, J.A. & Thompson, J.W., Cambridge Univ. Press.

Buck, W.R., 1991. Modes of continental lithospheric extension, *J. geophys. Res.,* **96,** 20 161–20 178.

Burov, E. & Guillou-Frottier, L. 2005. The plume head-continental lithosphere interaction using a tectonically realistic formulation for the lithosphere, *Geophys. J. Int.* **161,** 469–490.

Cande, S.C., Stock, J.M., Müller, R.D. & Ishihara, T., 2000. Cenozoic motion between East and West Antarctica, *Nature,* **404,** 145–150.

Carlson, R.L. & Miller, D.J., 2003. Mantle wedge water contents estimated from seismic velocities in partially serpentinized peridotites, *Geophys. Res. Lett.,* **30**(5), doi:10.1029/2002GL016600.

Chian, D., Louden, K.E., Minshull, T.A. & Whitmarsh, R.B., 1999. Deep structure of the ocean-continent transition in the southern Iberia Abyssal Plain from seismic refraction profiles: ocean Drilling Program (Legs 149 and 173) transect, *J. geophys. Res.,* **104,** 7443–7462.

Christensen, N.I. & Mooney, W.D., 1995. Seismic velocity structure and composition of the continental crust. A global view, *J. geophys. Res.,* **100,** 9761–9788.

Christensen, N.I., 1996. Poisson's ratio and crustal seismology, *J. geophys. Res.,* **101,** 3139–3156.

Cianciara, B. & Marcak, H., 1976. Interpretation of gravity anomalies by means of local power spectra, *Geophys. Prosp.,* **24,** 273–286.

Dalziel, I.W.D. & Elliot, D.H., 1982. West Antarctica: problem child of Gondwanaland, *Tectonics,* **1,** 3–19.

Davey, F.J. & De Santis, L., 2006. A multi-phase rifting model for the Victoria Land Basin, Western Ross Sea, *Antarctica,* 303–308.

Davy, B. & Wood, R.A., 1994. Gravity and magnetic modelling of the Hikurangi Plateau, *Mar. Geol.,* **118,** 139–151.

Eagles, G., Gohl, K. & Larter, R.D., 2004a. High-resolution animated tectonic reconstruction of the South Pacific and West Antarctic margin, *Geochem., Geophys., Geosyst.,* **5,** doi:10.1029/2003GC000657.

Eagles, G., Gohl, K. & Larter, R., 2004b. Life of the Bellingshausen plate, *Geophys. Res. Lett.,* **31,** doi:10.1029/2003GL019127.

Ebinger, C., Deino, J.A., Drake, R.E., Tesha, A.L., Kronenberg, A. & Tullis, F., 1989. Chronology of volcanism and rift basin propagation: Rungwe volcanic province, East Africa, *J. geophys. Res.,* **94,** 15 785–15 803.

Gohl, K., 2012. Basement control on past ice sheet dynamics in the Amundsen Sea Embayment, West Antarctica, *Palaeogeog. Palaeclimat. Palaeoecol.,* **335–336,** 35–41.

Gohl, K. *et al.*, 2007. Geophysical survey reveals tectonic structures in the Amundsen Sea embayment, West Antarctica, in *Proceedings of the 10th Int. Symposium of Antarctic Earth Sciences,* eds Cooper, A.K. & Raymond, C.R., USGS Open-File Report 2007–1047, doi:10.3133/of2007–1047.srp047.

Gohl, K., Denk, A., Eagles, G. & Wobbe, F., 2013a. Deciphering tectonic phases of the Amundsen Sea Embayment shelf, West Antarctica from a magnetic anomaly grid, *Tectonophysics,* **585,** 113–123.

Gohl, K. *et al.*, 2013b. Seismic stratigraphic record of the Amundsen Sea Embayment shelf from pre-glacial to recent times: evidence for a dynamic West Antarctic ice sheet, *Mar. Geol.,* **344,** 115–131.

Götze, H.J. & Lahmeyer, B., 1988. Application of three-dimensional interactive modelling In gravity and magnetics, *Geophysics* **53**(8), 1096–1108.

Grobys, J.W.G., Gohl, K. & Eagles, G. 2008. Quantitative tectonic reconstructions of Zealandia based on crustal thickness estimates, *Geochem., Geophys., Geosyst.,* **9**(1), Q01005, doi:10.1029/2007GC001691.

Grobys, J.W.G., Gohl, K., Uenzelmann-Neben, G. & Barker, 2009. Extensional and Magmatic nature of the Campbell Plateau and Great South Basin from deep crustal studies, *Tectonophysics,* **472,** 213–225.

Grunow, A.M., Kent, D.V. & Dalziel, I.W.D., 1991. New paleomagnetic data from Thurston Island: implications for the tectonics of West Antarctica and Weddell Sea opening, *J. geophys. Res.,* **96**(B11) 17 935–17 954.

Hopper, J., Dahl-Jensen, T., Holbrook, W., Larsen, H., Lizarralde, D., Korenaga, J., Kent, G. & Kelemen, P., 2003. Structure of the SE Greenland margin from seismic reflection and refraction data: implications for nascent spreading center subsidence and asymmetric crustal accretion during North Atlantic opening, *J. geophys. Res.,* **108,** B5, doi:10.1029/2002JB001996.

Hamilton, W., 1987. Crustal extension in the Basin and Range Province, south-western United States, in *Continental Extensional Tectonics,* Vol. 28, pp. 155–176, eds Coward, M.P., Dewey, J.F. & Hancock, P.L., Geological Society Special Publications.

Jordan, T.A., Ferraccioli, F., Vaughan, D.G., Holt, J.W., Corr, H., Blankenship, D.D. & Diehl, T.M., 2010. Aerogravity evidence for major crustal thinning under the Pine Island Glacier region (West Antarctica), *Bull. geol. Soc. Am.,* **122,** 714–726.

Karner, G.D. & Watts, A.B., 1983. Gravity anomalies and flexure of the lithosphere at mountain ranges, *J. geophys. Res.,* **88,** 10 449—10 477.

Kipf, A., Mortimer, N., Werner, R., Gohl, K., van den Bogaard, P., Hauff, F. & Hoernle, K. (2012). Granitoids and dykes of the Pine Island Bay region, West Antarctica, *Antarctic Sci.,* **24**(5), 473–484.

Kipf, A., Hauff, F., Werner, R., Gohl, K., van den Bogaard, P., Hoernle, K., Maicher, D. & Klügel, A., 2013. Seamounts off the West Antarctic margin: a case of non-hotspot intraplate volcanism, *Gondwana Res.,* doi:10.1016/j.gr.2013.06.013.

Larter, R.D., Cunningham, A.P., Barker, P.F., Gohl, K. & Nitsche, F.O., 2002. Tectonic evolution of the Pacific margin of Antarctica—1. Late Cretaceous tectonic reconstructions, *J. geophys. Res.,* **107**(B12), 2345, doi:10.1029/2000JB000052.

Lindow, J., Spiegel, C., Johnson, J., Lisker, F. & Gohl, K., 2011. Constraining the latest stage exhumation of Marie Byrd and Ellsworth Land, West Antarctica, in *Proceedings of the 11th International Symposium on Antarctic Earth Science,* Edinburgh, Scotland.

Llubes, M., Florsch, N., Legresy, B., Lemoine, J., Loyer, S., Crossly, D. & Remy, F. 2003. Crustal thickness in Antarctica from CHAMP gravimetry, *Earth planet. Sci. Lett.,* **212,** 103–117.

Luyendyk, B., Wilson, D.S. & Siddoway, C.S., 2003. Eastern margin of the Ross Sea Rift in western Marie Byrd Land, Antarctic: crustal structure and tectonic development, *Geochem., Geophys., Geosyst.* **4,** doi:10.1029/2002GC000462.

Malahoff, A., Kolotyrkina, I.Y., Midson, B.P. & Massoth, G.I., 2006. A decade of exploring a submarine intraplate volcano: hydrothermal manganese and iron at Lo'ihi volcano, *Geochem., Geophys., Geosyst.,* **7,** 1525–2027.

Mayes, C.L., Lawver, L.A. & Sandwell, D.T., 1990. Tectonic history and new isochron chart of the South Pacific, *J. geophys. Res.,* **95,** 8543–8567.

McAdoo, D.C. & Laxon, D., 1997. Antarctic tectonics: constraints from an ERS-1 satellite marine gravity field, *Science,* **276,** 556–560.

Minshull, T., 2009. Geophysical characterisation of ocean-continent transition at magma-poor rifted margins, *C. R. Geosci.,* **341,** 382–393.

Mjelde, R., Kasahara, J., Shimamura, H., Kamimura, A., Kanazawa, T., Kodaira, S. & Shiobara, T., 2002. Lower crustal seismic velocity-anomalies; magmatic underplating or serpentinized peridotite? Evidence from the Voring Margin, NE Atlantic, *Mar. geophys. Res.,* **23,** 169–183

Mortimer, N., Hoernle, K., Hauff, F., Palin, J.M., Dunlap, W.J., Werner, R. & Faure, K., 2006. New constraints on the age and evolution of the Wishbone Ridge, southwest Pacific Cretaceousmicroplates, and Zealandia–West Antarctica breakup, *Geology* **34,** 185–188.

Mukasa, S.B. & Dalziel, I.W.D., 2000. Marie Byrd Land, West Antarctica: evolution of the Gondwana's Pacific margin constrained by zircon U-Pb geochronology and feldspar common-Pb isotopic compositions. *Bull. geol. Soc. Am.,* **112,** 611–627.

Mutter, J.C., Talwani, M. & Stoffa, P.L., 1984. Evidence for a thick oceanic crust off Norway, *J. geophys. Res.,* **89,** 483–502.

Nafe, J.E. & Drake, C.L., 1963. Physical properties of marine sediments, in *The Sea,* Vol. **3,** pp. 794–815, ed. Hill, M.N., Interscience.

Nitsche, F.O., Jacobs, S., Larter, R.D. & Gohl, K., 2007. Bathymetry of the Amundsen Sea Continental Shelf: implications for geology, oceanography, and glaciology, *Geochem., Geophys., Geosyst.,* **8,** Q10009, doi:10.1029/2007GC001694.

Reid, I., 1994. Crustal structure of a non-volcanic rifted margin east of Newfoundland, *J. geophys. Res.,* **99,** 161–180.

Rocchi, S., LeMasurier, W.E. & Di Vincenzo, G., 2006. Oligocene to Holocene erosion and glacial history in MBL, West Antarctica, inferred from exhumation of the Dorrel Rock intrusive complex and from volcano morphologies, *Geol. Soc. Am. Bull*. **118,** 991–1005.

Rosenbaum, G., Lister, G.S. & Duboz, C., 2002. Relative motions of Africa, Iberia and Europe during Alpine orogeny, *Tectonophysics,* **359,** 117–129.

Schubert, G., Trucotte, D.L. & Olsen, P., 2001. *Mantle Convection in the Earth and Planets,* 1st edn, Cambridge Univ. Press.

Siddoway, C., 2008. Tectonics of the West Antarctic rift system: new light on the history and dynamics of distributed intracontinental extension. Antarctica: a keystone in a Changing World, in *Proceedings of the 10th International Symposium on Antarctic Earth Sciences,* The National Academies Press, Washington, DC, pp. 91–114.

Smith, A.M., Jordan, T.A., Ferraccioli, F. & Bingham, R.G., 2013. Influence of subglacial conditions on ice stream dynamics: seismic and potential field data from Pine Island Glacier, West Antarctica, *J. geophys. Res.,* **118**(4), 1471–1482.

Spector, A. & Grant, F.S., 1970. Statistical models for interpreting aeromagnetic data, *Geophysics,* **35,** 293–302.

Storey, B.C., 1991. The crustal blocks of West Antarctica within Gondwana: Reconstruction and breakup model, in *Geological Evolution of Antarctica,* pp. 587–592, eds. Thompson, M.R.A., Crame, J.A. & Thompson, J.W., Cambridge University Press.

Torge, W., 1989. *Gravimetry*, *Walter de Gruyter,* pp. 465.

Voss, M. & Jokat, W., 2007. Continent-ocean transition and voluminous magmatic underplating derived from *P*-wave velocity modelling of the Greenland continental margin, *Geophys. J. Int.,* **170**. 580–604.

Watts, A.B. & Fairhead, J.D., 1999. A process-oriented approach to modelling the gravity signature of continental margins, *Leading Edge,* **18**(2), 258–263.

Whitmarsh, R.B., White, R.S., Horsefield, S.J., Sibuet, J., Recq, M. & Louvel, V., 1996. The ocean-continent boundary off the western continental margin of Iberia: crustal's structure west of Galician Bank, *J. geophys. Res.,* **101,** 291–314.

Winberry, J.P. & Anandakrishnan, S., 2004. Crustal structure of the West Antarctic rift system and Marie Byrd Land hotspot, *Geology,* **32**(11), 977–980.

Wobbe, F., Gohl, K., Chambord, A. & Sutherland, R., 2012. Structure and break-up history of the rifted margin of West Antarctica in relation to Cretaceous separation from Zealandia and Bellingshausen plate motion, *Geochem., Geophys., Geosyst.,* **13,** Q04W12, doi:10.1029/2011GC003742.

Zelt, C.A. & Smith, R.B., 1992. Seismic traveltime inversion for 2-D crustal velocity structure, *Geophys. J. Int.,* **108**(1), 16–34.

6.3 Sediment transport and deposition along the Pacific continental margin of West Antarctica

Publication 6.3.1:

Nitsche, F.O., Cunningham, A.P., Larter, R.D., **Gohl, K.** (2000). Geometry and development of glacial continental margin depositional systems in the Bellingshausen Sea. *Marine Geology,* v. 162, pp. 277-302.

Author contributions: As part of his PhD project supervised by Gohl, Nitsche wrote most this paper. Cunningham, Larter and Gohl discussed various aspects of the data interpretation and results. Most of the data were collected during Polarstern expedition ANT-XI/3 (1994) under project leadership of Gohl and during a James Clark Ross expedition JR04 (1993) under project leadership of Larter.

ELSEVIER

Marine Geology 162 (2000) 277–302

MARINE GEOLOGY
INTERNATIONAL JOURNAL OF MARINE GEOLOGY, GEOCHEMISTRY AND GEOPHYSICS

www.elsevier.nl/locate/margeo

Geometry and development of glacial continental margin depositional systems in the Bellingshausen Sea

Frank O. Nitsche [a,*], Alex P. Cunningham [b], Rob D. Larter [b], Karsten Gohl [a,1]

[a] *Alfred Wegener Institute for Polar and Marine Research, Columbusstrasse, Bremerhaven D-27568, Germany*
[b] *British Antarctic Survey, High Cross, Madingley Road, Cambridge CB3 0ET, UK*

Received 1 December 1998; accepted 4 June 1999

Abstract

We present multi-channel seismic (MCS) reflection profiles and bathymetry data acquired across a remote and poorly surveyed part of the Antarctic continental margin in the Bellingshausen and Amundsen Seas. This new information has been combined with published data and used to interpret the style of sedimentation on the continental shelf, slope and rise, and to describe sedimentation processes which have been active in this region. Most seismic reflection profiles crossing the continental margin show prograded sequences beneath the outer shelf and upper slope, and we infer that the stratal characteristics of these sequences indicate that grounded ice sheets reached the shelf edge during previous glacial times. Although there are general similarities in stratal geometry on these profiles, in detail, they reveal significant longitudinal variations in sediment input from the shelf to the upper slope. On several profiles, we found evidence of mass wasting of the continental slope in the form of slump and debris flow deposits. At greater depth, turbidity flows, bottom currents and Coriolis force have controlled the further transportation and deposition of sediment, which has resulted in the development of mounds, channels and sediment wave fields. The distribution, and variations in the size and geometry of the mounds reflect sediment input and the relative contribution of these other factors which control sedimentation on the continental rise.

Keywords: Bellingshausen Sea; Amundsen Sea; reflection seismic survey; glacial marine sedimentation; sediment drifts

1. Introduction

To understand the climatic history of Antarctica and relate it to proxy records of global sea level and ice volume, we need to know the glacial record preserved in sediment derived from Antarctica (e.g., Miller et al., 1987; Cooper and Webb, 1992). Studies on the Antarctic continental shelves (e.g., Antarctic Peninsula: Bart and Anderson, 1995; Larter et al., 1997; Ross Sea: De Santis et al., 1995) show that the sediments there are unlikely to contain a complete record. Sediments deposited during earlier glacial advances might have been partially or completely eroded by later glacial advances. Also, ice might not have covered all parts of the continental shelf during some glacial periods, so that the proximal glacial sediment record may be incomplete. As a conse-

* Corresponding author. Institute of Geophysics, ETH Zürich, ETH Hönggerberg, Zürich CH-8093, Switzerland. Fax: +41-1-633-1065; E-mail: frankn@aug.ig.erdw.ethz.ch

[1] Present address: Macquarie University, Department of Earth and Planetary Sciences, Sydney NSW 2109, Australia.

0025-3227/00/$ - see front matter
PII: S0025-3227(99)00074-2

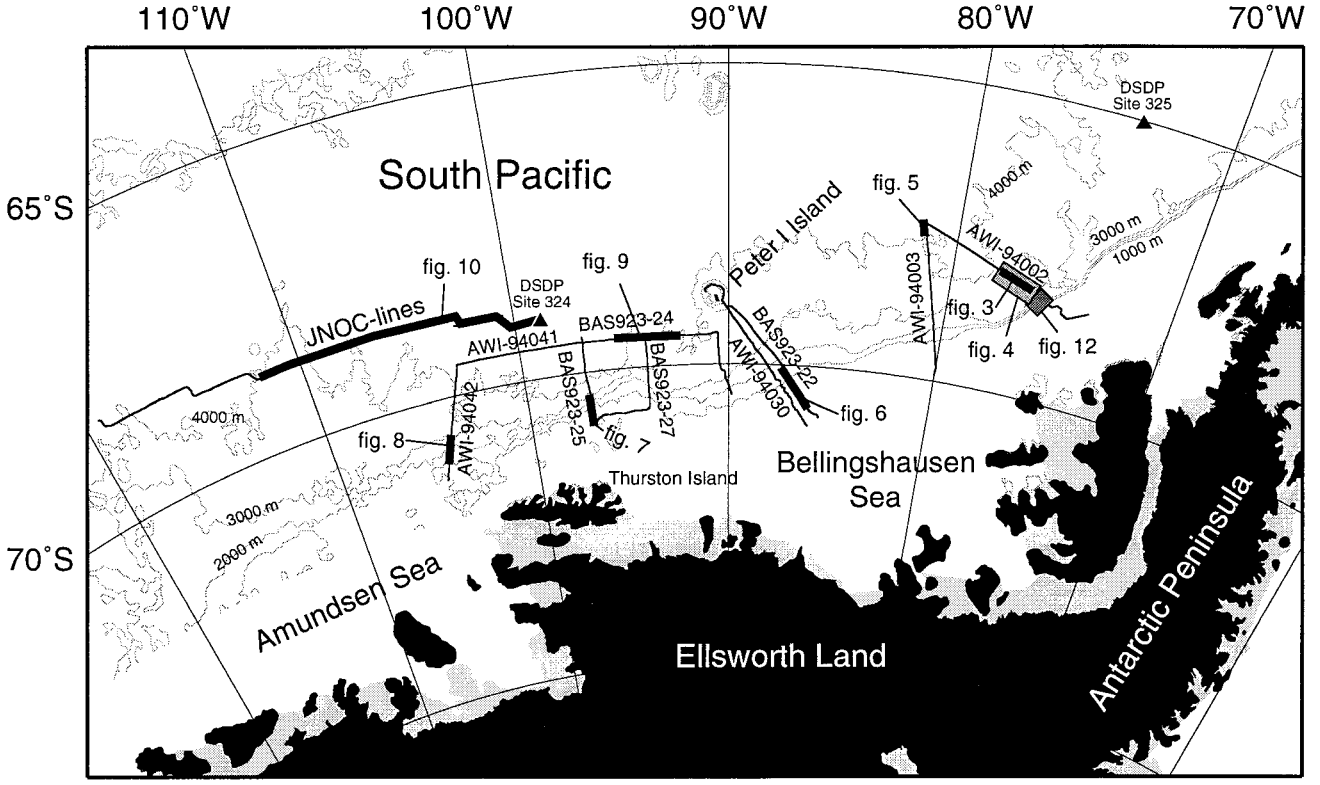

Fig. 1. Location map showing the area investigated in this study. Bathymetry (Smith and Sandwell, 1997) is contoured at 1000-m intervals. MCS profiles are shown as thin black lines; thick lines locate seismic sections reproduced in this paper; grey boxes show swath bathymetry images. Grey areas near the coast are floating ice shelves.

quence, diverse types of sediment accumulations reported on the continental rise (e.g., drifts along the Antarctic Peninsula: McGinnis and Hayes, 1995; Rebesco et al., 1996; drifts and turbidites off Prydz Bay: Kuvaas and Leitchenkov, 1992; Crary fan in the Weddell Sea: Moons et al., 1992) are becoming increasingly important because they can contain a more complete and more easily recoverable palaeoenvironmental record. However, a full understanding of continental rise sedimentation requires some knowledge of shelf and slope depositional processes; e.g., information about the volume and type of sediment supplied to the upper slope, and the variation of these parameters with time. To understand the sedimentary record of the rise, the whole sediment transport path from shelf to slope to rise must be understood.

Owing to its remoteness, the Antarctic continental margin in the Bellingshausen and the Amundsen Seas has been poorly surveyed, and consequently, the glacial history of the neighbouring Ross Sea and Antarctic Peninsula regions is better understood (Fig. 1). Studies of the eastern Ross Sea suggest that large ice sheets first extended onto the continental shelf in the early Miocene (De Santis et al., 1995), whereas studies of the shelf west of the Antarctic Peninsula suggest that grounded ice did not extend onto the outer continental shelf there until late Miocene (Larter et al., 1997). It seems unlikely that extensive ice sheets would have developed on the Bellingshausen Sea shelf earlier than in the Ross Sea, and it is possible that they did not develop before ice sheets on the Antarctic Peninsula shelf.

Sediment distribution in the Bellingshausen Sea has also been affected by the tectonic evolution of the region, as discussed by Tucholke and Houtz (1976). Plate tectonic reconstructions (Mayes et al., 1990; McCarron and Larter, 1998) indicate that this section of the West Antarctic margin can be divided into two parts. The western part is a rifted margin conjugate to Chatham Rise, which separated from West Antarctica between 90 and 85 Ma ago. The eastern part was an active margin and subduction continued until the Antarctic–Phoenix spreading ridge segments migrated into the trench during the Tertiary. This sequence of ridge–trench collisions took place along the Antarctic Peninsula margin from the Middle Eocene or earlier until Pliocene times (Larter and Barker, 1991a; McCarron and Larter, 1998). The boundary between the rifted margin and the part of the margin where the ridge–trench collision took place lies somewhere between 85° and 105°W (McCarron and Larter, 1998). Hence, ocean floor age varies considerably within the study area, and this provides a constraint on the maximum age of overlying rise sediments. It is likely also, that the Antarctic–Phoenix ridge acted as a barrier to the northwestward transport of terrigenous sediment until it migrated into the trench, so the earliest sediments on the Bellingshausen Sea continental rise are likely to be a condensed sequence.

In this paper, we use reconnaissance multi-channel seismic reflection (MCS) and swath bathymetry data to describe the distribution and pattern of accumulation of glacigenic sediments from the outer shelf to the rise in the Bellingshausen and Amundsen Seas. We also consider how the observed pattern of accumulation is influenced by factors such as the length of the glacial drainage pathway, the lateral variability of ice input to the shelf, and the distal position of the rise in this area from presumed sources of bottom water. Previous studies of sedimentary features in this region were based on sparse, analogue single-channel seismic profiles (Tucholke, 1977), or were restricted mainly to the area west of 104°W (Yamaguchi et al., 1988). More recently, Cunningham et al. (1994) and Nitsche et al. (1997) reported the existence of prograding sequences on MCS lines crossing the Bellingshausen and Amundsen Seas continental margins, and observed that there are striking similarities in the general stratal patterns.

2. Data

2.1. Bathymetry and sub-bottom profile data

Compilations of marine geophysical data (e.g., National Geophysical Data Center, 1996) show a paucity of ship tracks in the Bellingshausen and Amundsen Seas. As a consequence, bathymetry maps derived solely from these sparse shipboard measurements (e.g., GEBCO: Mammerickx and Cande, 1982) do not describe sea-floor topography of the region in great detail. In this study, we combine new track and

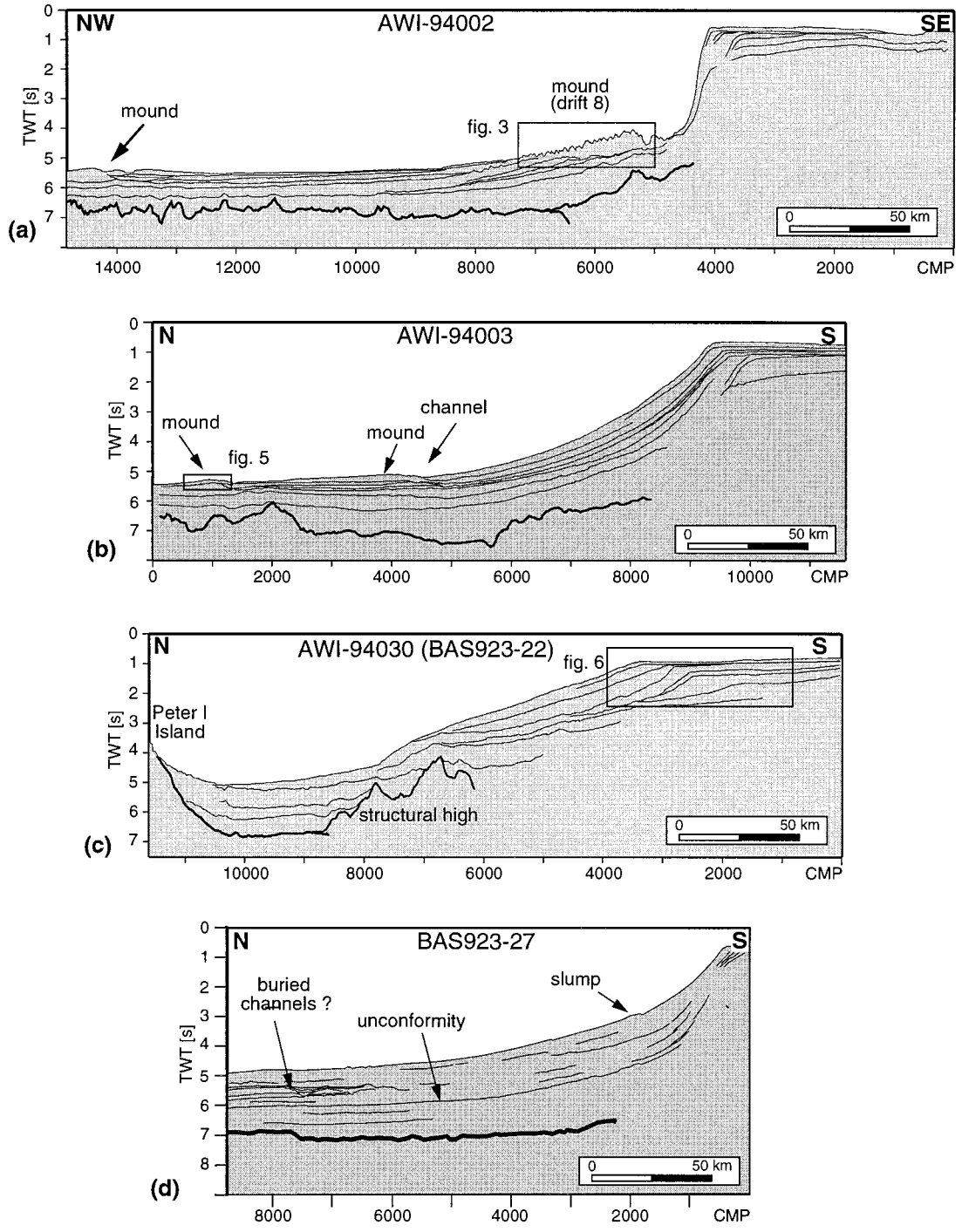

Fig. 2. Interpreted line drawings of MCS profiles (located in Fig. 1). (a) to (f) show a series of MCS transects which extends across the Antarctic continental margin progressively from east to west. (g) shows a profile on the continental rise which runs parallel to the margin. All profiles are drawn with the same scale and vertical exaggeration (ca. 16:1 at the sea floor). Bold lines represent reflections that correspond to the top of the acoustic basement.

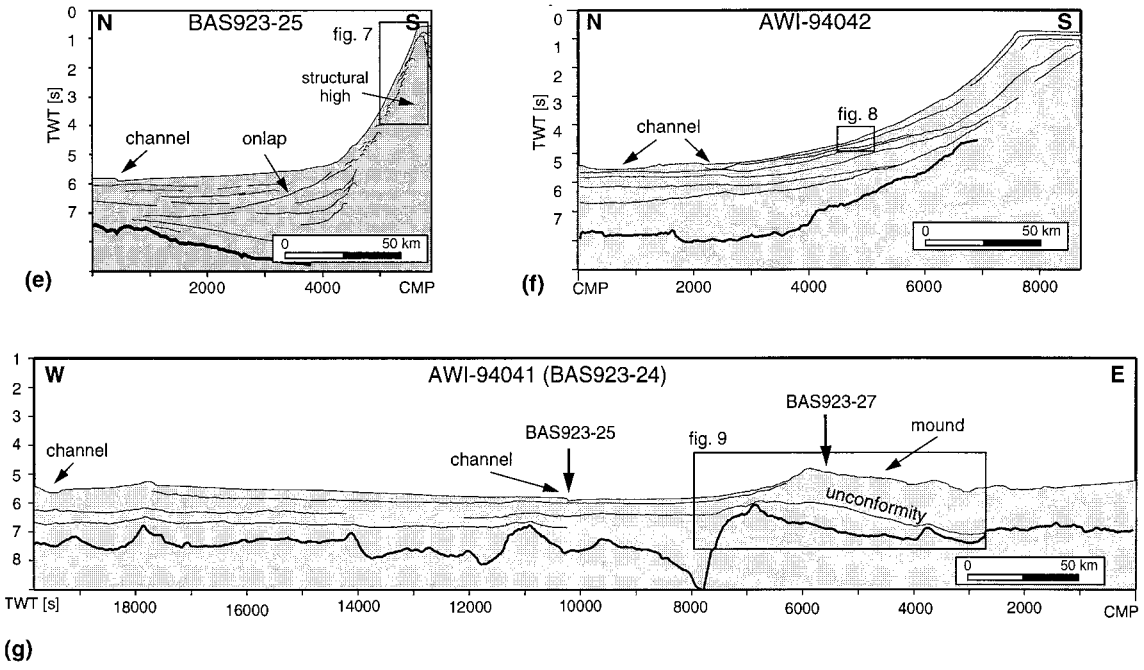

Fig. 2 (continued).

swath bathymetry data acquired by the British Antarctic Survey (BAS) and the Alfred Wegener Institute for Polar and Marine Research (AWI) across the Antarctic continental shelf, slope and rise. These data have been used to determine the orientation and extent of sea-floor features apparent in seismic reflection profiles, and to describe sea-floor morphology in areas beyond the MCS surveys. In addition, interpretations of BAS and AWI data have been conducted with reference to the predicted sea-floor topography of Smith and Sandwell (1997), generated by combining satellite altimetry data with existing bathymetric soundings. Comparison of the predicted topography with our new data suggests that the predicted surface describes the position and shape of sea-floor features (at 15–160 km wavelength, to 72°S) quite well, where shipboard soundings are absent. However, the predicted topography of the Antarctic continental shelf should be interpreted with care, because few soundings have been incorporated in the data near its southern limit, and therefore, the satellite-derived component is poorly constrained in this area.

BAS and AWI have also collected 3.5 kHz and 'Parasound' sub-bottom profiles. These high-resolution profile data were used to map channel paths and sediment waves, and to help distinguish areas of modern deposition and non-deposition.

2.2. Seismic reflection data

BAS and AWI have acquired MCS profiles across the Antarctic continental margin in the Bellingshausen and Amundsen Seas during three scientific cruises: BAS cruise JR04 (1992/1993, Cunningham et al., 1994) conducted on RRS *James Clark Ross*, and AWI cruises ANT 11/3 (1994) and ANT 12/4 (1995) conducted on RV *Polarstern* (Miller and Grobe, 1996). During these cruises, ca. 1500 line km of MCS data were acquired by BAS and ca. 3400 line km of MCS data were acquired by AWI. In this study, we present a subset of these data totalling ca. 2700 line km, which extends across the Antarctic continental margin between 76°W and 105°W. BAS MCS profiles were acquired using an airgun source with a combined chamber capacity of ca. 55.9 l, and

a streamer with an active length of 2400 m. AWI MCS profiles were acquired using an airgun source with a combined chamber capacity of ca. 24 l, and a streamer with active lengths of either 2400 or 600 m.

As part of this study, we also describe MCS profiles acquired by the Japan National Oil (JNOC), published through the SCAR-database (Yamaguchi et al., 1988; SCAR, 1992). Most MCS profiles extend across the outer continental shelf, slope and rise (Fig. 1). However, we also include BAS and AWI profiles AWI-94041/BAS923-24, and JNOC profiles TH-86002 and TH-86003 which lie nearly parallel to the continental margin. Fig. 2a–g show interpreted line drawings of these data.

BAS and AWI MCS profiles presented in this study have been processed using standard seismic processing procedures including trace editing, deconvolution, velocity analysis, normal moveout correction, bandpass frequency filtering, stack and migration. All lines have a CMP spacing of 25 m.

3. Interpretation of seismic reflection profiles and bathymetry data

3.1. AWI-94002

MCS profile AWI-94002 is the easternmost line described in this study (Figs. 1 and 2a). AWI-94002 crosses the Antarctic continental margin near 76°W, and shows a steep continental slope, with a gradient (ca. 13°) comparable to that observed on many lines crossing the Pacific margin of the Antarctic Peninsula to the northeast (Larter and Barker, 1991b; Larter and Cunningham, 1993). On the outer continental shelf, three different acoustic–stratigraphic units can be distinguished on the basis of their geometry and internal reflection configuration (Units 1–3 of Nitsche et al., 1997). The lowermost unit is composed of comparatively gently dipping strata, which formed a mainly aggradational shelf. In contrast, the upper two units show steeper slopes and a more progradational geometry, which has resulted in a seaward migration of the continental shelf break of ca. 15 km. The middle unit (Unit 2 of Nitsche et al., 1997) clearly shows erosional truncation of foreset reflections beneath a series of sub-horizontal unconformities. These reflection geometries resemble those of units S1, S2 and S3 reported by Larter and Barker (1989) along the continental margin of the Antarctic Peninsula (although numbered in the opposite sense). We note, however, that equivalent units in the two provinces are not necessarily coeval.

Farther north, profile AWI-94002 extends across the Antarctic continental slope and rise. Here, the irregular top of oceanic acoustic basement is clearly imaged between 5 and 7 s two-way time (STWT). We confidently trace this surface southward from the end of line to ca. CMP 4500 (beneath the lower continental slope, Fig. 2a). At shallower depth, we identify two separate mounds developed within the overlying sedimentary succession. Between CMPs 5250 and 8000, the largest mound extends northward from the base of the continental slope (Figs. 3 and 4). This structure has been identified by Rebesco et al. (1996) as a sediment drift (their drift '8', imaged on MCS profile IT92-109). Profile AWI-94002 (Fig. 2a and Fig. 3) and accompanying swath bathymetry data (Fig. 4) show that most of the drifts are separated from the continental margin by a large channel (between CMPs 5100 and 5250, Fig. 3). Also, Figs. 3 and 4 show that this part of the drift has been dissected by several small erosional gullies, which suggests that erosion has progressed more quickly than recent deposition at this locality. Farther north (between CMPs 7500 and 8500, Fig. 2a), younger sediments cover and in-fill the erosional gullies. Part of this mound is shown in cross-section by Rebesco et al. (1996) in their seismic line IT92-109. This profile shows an acoustic–stratigraphic boundary within the mound, overlain by sediments which we interpret as correlating with the gully fill sediments seen on line AWI-94002. This interpretation is supported by swath bathymetry data (reproduced in perspective view, Fig. 4) which show a gradual northward suppression of gullied topography towards the intersection of profiles AWI-94002 and IT92-109. The origin of these gullies is uncertain; it is possible that they formed by small-scale slumping of the unstable northern slope of the mound into the adjacent channel.

On the lower rise, at a distance of 200–250 km from the Antarctic continental slope (between CMPs 13500 and 14900, Fig. 2a), a separate, smaller sediment mound is seen. This smaller mound does not show any clear signs of gullying or slope failure.

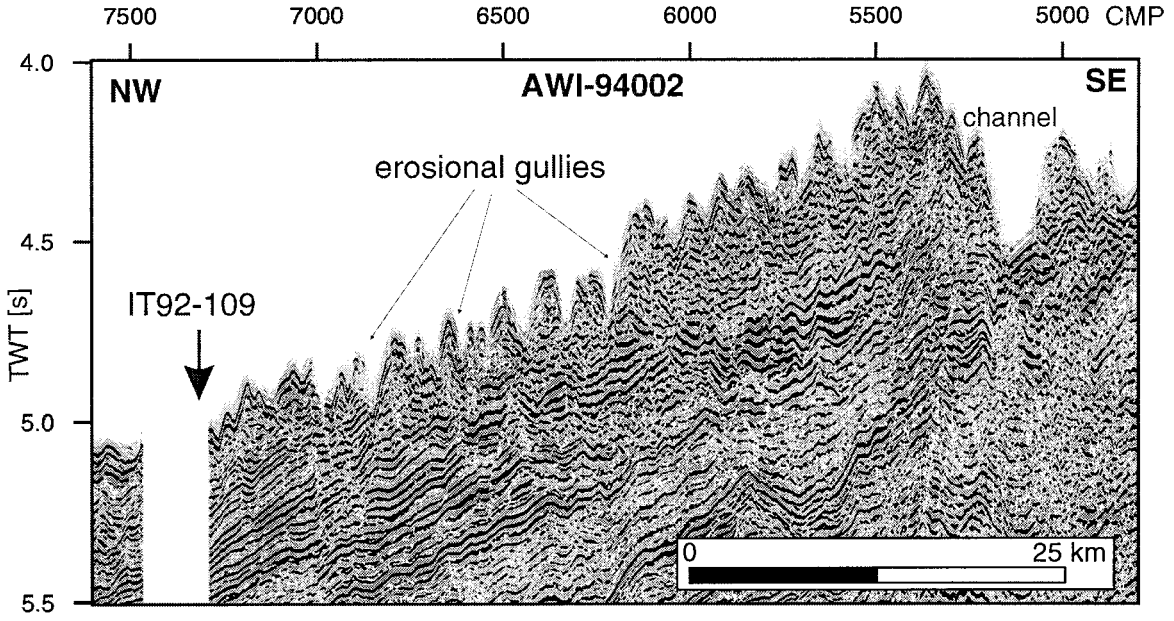

Fig. 3. Part of MCS profile AWI-94002 (located in Fig. 1) showing a cross-section of the large mound on the upper continental rise (vertical exaggeration ca. 30:1 at the sea floor). The profile lies close to the crest of the mound (compare Fig. 4).

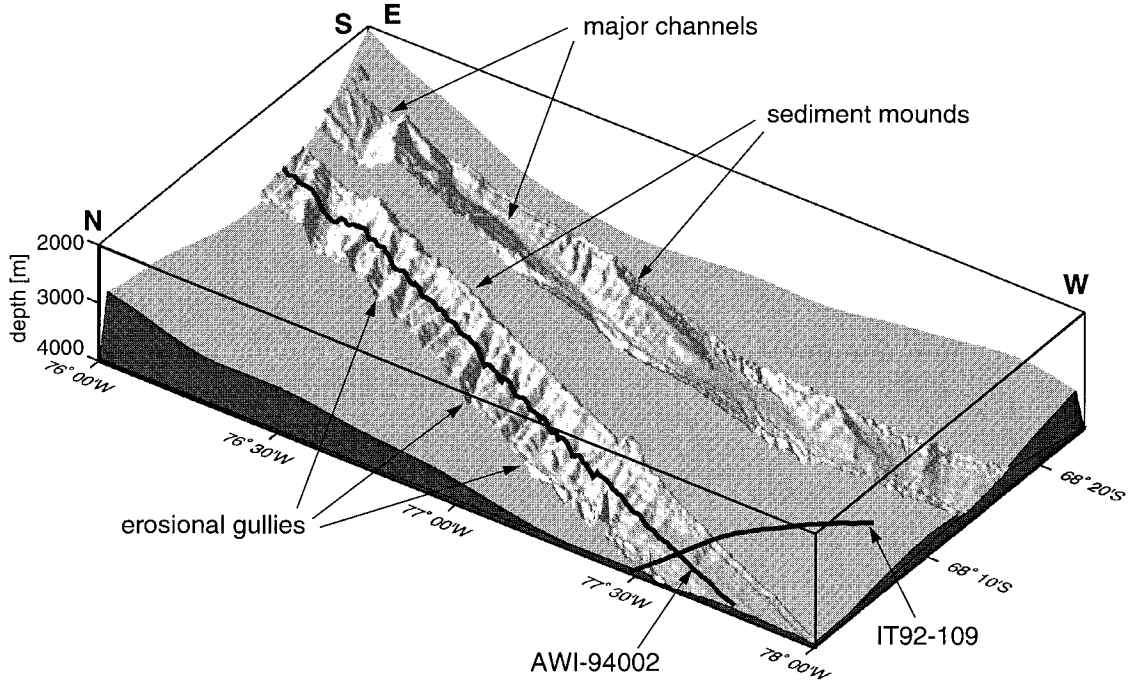

Fig. 4. Perspective view of two Hydrosweep swath bathymetry stripes from the continental rise north of Alexander Island (located in Fig. 1). These data are illuminated from NE. The northern stripe was obtained along MCS profile AWI-94002 (located with a thick black line, and shown in Fig. 3). The line extending nearly perpendicular to the strip locates MCS profile IT92-109 of Rebesco et al. (1996; 1997). The data show small gullies which have been progressively filled toward the NW.

Instead, sub-bottom profile data suggest that it is a site of modern deposition, and show well-formed migrating sediment waves at its surface (imaged also along nearby profile AWI-94003, Fig. 5). Accompanying swath bathymetry data show that the crests of the waves are orientated in a NE–SW direction.

MCS profile AWI-94002 shows that neither mound is built directly upon oceanic acoustic basement; the base of both mounds is separated from the basement by an intervening sedimentary layer with a time-thickness of 0.5–1.0 STWT. The reflection configuration of this layer differs from that of the mounds; underlying strata typically show more uniform, parallel to sub-parallel, lower-amplitude reflections. An equivalent older or 'pre-drift stage' of sedimentation has been reported by McGinnis and Hayes (1995) and Rebesco et al. (1996) for the mounds they identified on the continental rise to the northeast.

3.2. AWI-94003

Profile AWI-94003 extends SSE from the end of line AWI-94002, across the continental rise and slope, and crosses the shelf break near 80°W (Figs. 1 and 2b). On AWI-94003, the acoustic architecture of the outer shelf resembles that observed farther east (on profile AWI-94002, Fig. 2a), and shows a change from a mainly aggradational to a progradational geometry (Nitsche et al., 1997). Here, foreset progradation has resulted in a seaward migration of the continental shelf break of 20 km (between CMPs 9300 and 10100, Fig. 2b). In contrast to AWI-94002, the continental slope on AWI-94003 has a comparatively gentle dip of ca. 3°. Here also, the prograded wedge clearly extends beneath the continental slope (Fig. 2b and Fig. 5 of Nitsche et al., 1997), and farther north (near CMP 4500, Fig. 2b), the toe of the prograded wedge thins against a low relief sediment mound developed on the upper continental rise (between CMPs 2500 and 4500, Fig. 2b). On the continental slope, several packages of chaotic and discontinuous reflections can be seen at shallow depth, which resemble those shown in Fig. 8. These acoustically chaotic packages are thought to represent debris flow deposits. At the northern end of the line, AWI-94003 shows a second, separate sediment mound (between CMPs 1 and 1350, Fig. 2b). This more northerly mound is also seen at the northern end of line AWI-94002. On profile AWI-94003, the mound shows fine acoustic lamination; older mound sediments show uniform, parallel to sub-parallel reflections, whereas younger mound units show a migrating-wave acoustic facies (e.g., Fig. 6 of Nitsche et al., 1997) which extends to the surface of the mound. High-resolution sub-bottom data (Fig. 5) show these bedforms in more detail, and suggest that the sediment waves are probably active. Swath

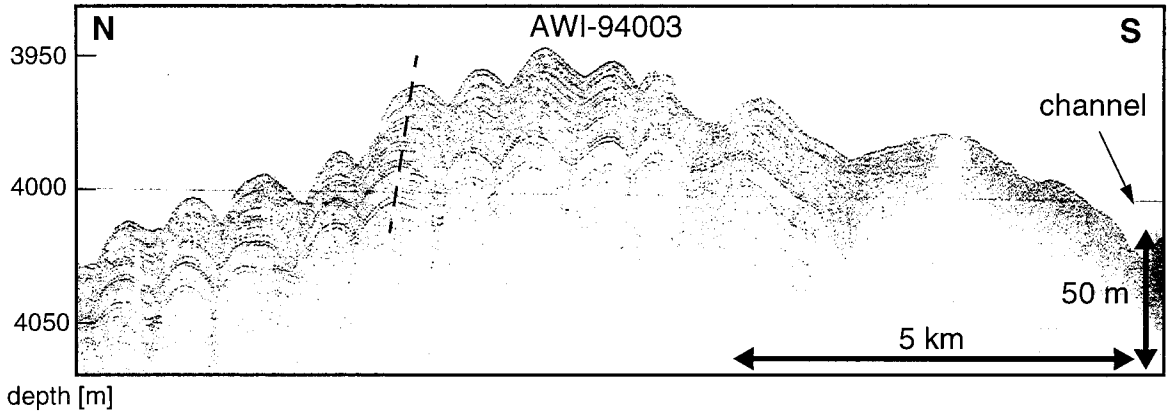

Fig. 5. Parasound high-resolution sub-bottom profile of the sediment mound at the northern end of MCS line AWI-94003 (located in Fig. 1). The mound is also seen at the northwestern end of MCS profile AWI-94002. Sub-bottom penetration is ca. 50 m. This profile shows sediment waves (wavelengths of 850–900 m) with a south component of migration towards an adjacent channel. Coincident swath bathymetry data suggest that waves trend obliquely to the profile, and have a true migration direction towards the southeast.

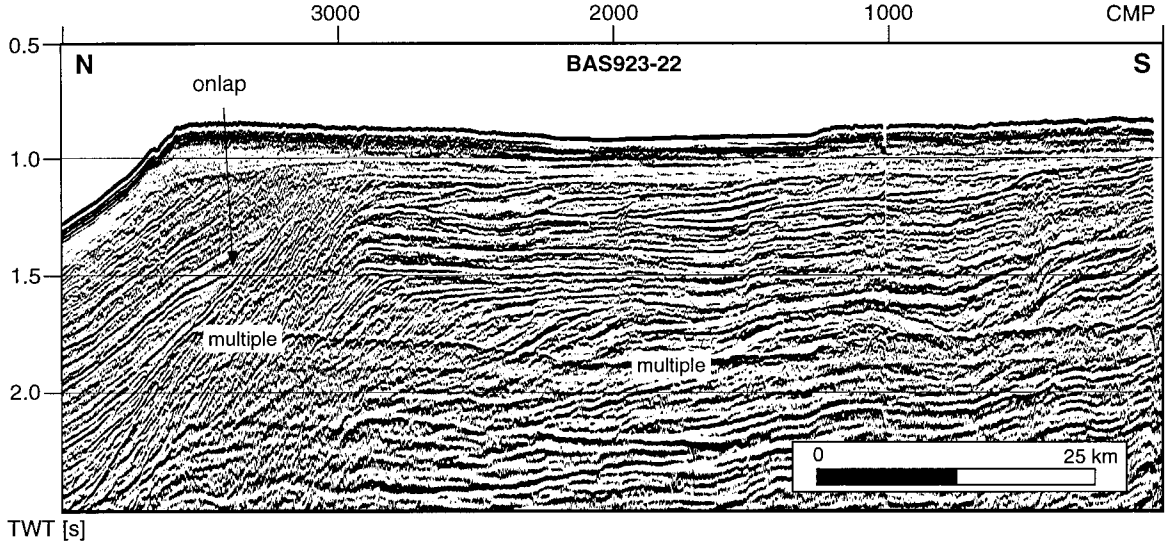

Fig. 6. Section from MCS profile BAS923-22 (located in Fig. 1) showing the outer continental shelf near 87°30′W. Vertical exaggeration is ca. 24:1 at the sea floor.

bathymetry data combined with seismic lines AWI-94002 and AWI-94003 show that the sediment waves have migrated southeastward, toward an adjacent channel (near CMP 1350, Fig. 2b). On profile AWI-94003, channels lie along the southern edge of both sediment mounds, and accompanying swath bathymetry data show that these channels obliquely cross the seismic line. As observed on nearby profile AWI-94002, AWI-94003 shows that the sediment mounds are separated from basement by an older sediment sequence with a thickness of 0.5–1.7 STWT.

3.3. BAS923-22 and AWI-94030

Farther west, MCS profiles BAS923-22 and AWI-94030 trend NW–SE and cross the continental shelf break near 87°30′W (Figs. 1 and 2c). These profiles lie less than 25 km apart (Fig. 1), and show similar successions of depositional sequences. Here, we calculated a depth of the shelf break between 630 m (on profile BAS923-22) and 680 m (on profile AWI-94030) below sea level from the seismic sections using a water velocity of 1500 m s^{-1}. Across the outermost 20–30 km of the continental shelf, both MCS profiles show that the sea floor deepens gradually landward. Farther inshore, however, the sea floor shallows towards the southern end of both MCS profiles. The acoustic architecture of the outer shelf on these lines (shown in detail, Fig. 6) is more complex than that described elsewhere in this study; while we identify a general trend from an aggradational to a progradational geometry, the transition is not as clear as on other lines (Nitsche et al., 1997). Profile BAS923-22 shows aggradational units overlain by a first set of prograded foresets (e.g., between 1.7 and 1.5 STWT, CMPs 2200–2900, Fig. 6). These older prograded forests are overlain by a mainly aggradational sub-unit represented by vertically stacked palaeo-shelf breaks near CMP 2900 (between 1.5 and 1.2 STWT, Fig. 6), which is overlain in turn by a second series of prograded foresets (e.g., above 1.2 STWT at CMP 2900, Fig. 6). These sub-units are all incorporated within units ‘1’ and ‘2’ of Nitsche et al. (1997).

At 1.2 STWT (e.g., at CMP 2800, Fig. 6), profile BAS923-22 shows an unusual unconformity which set back the offlap break more than 60 km landwards. Downlapping onto this unconformity, prograded foresets record the readvance of the offlap break towards its previous position at CMP 2900. The reason for this remarkable landward movement of the offlap break is unclear, although we propose different scenarios which might result in the devel-

opment of such a structure. This geometry may have been caused by a long interruption in glacial sediment supply to this part of the margin during which time the shelf subsided. Alternatively, it may reflect a short period of rapid local subsidence during the deposition of glacial margin sequences. It is possible also that this geometry could reflect a local change in glacial regime, leading to thinner grounded ice sheets, perhaps resulting from a change in glacial catchment area, or other factors controlling glacial flow. On profiles BAS923-22 and AWI-94030, the sequence of stratal geometry transitions (aggradation–progradation–aggradation–retrogradation– progradation) reflects the balance between sediment supply and the generation of accommodation space, and shows that, for a period of time, accommodation outstripped sediment supply to this part of the margin. However, it is not possible to unravel the relative effects of sediment supply, subsidence and ice grounding depth without additional information.

Profiles BAS923-22 and AWI-94030 also show a distinct change in the geometry and acoustic facies of sediments preserved below the outermost shelf and slope. North of CMP 3000 (Fig. 6), high-amplitude, high-frequency, fairly continuous reflections onlap more steeply dipping strata deposited during the second phase of progradation described above. The reflection characteristics of these younger sediments contrast with those of the underlying foresets, which show more irregular, less continuous reflections. At shallower depth (e.g., at 1.1 STWT near CMP 3480, Fig. 6), younger reflections in this onlapping sequence are erosionally truncated at their upper limit. The origin of this onlapping and partly truncated sequence north of CMP 3000 remains uncertain, although we suspect that it mostly consists of mud and silt deposited by ambient bottom currents flowing along the continental slope. A potential source of sediment is a large sediment ridge or mound east of these lines indicated in the bathymetry data (Figs. 1 and 11). It is noteworthy also, that palaeo-slope angles in this unit are 1°–2°, considerably less than those of the underlying foresets, and that these sediments underlie the most gently dipping part of the continental slope in this region.

Farther north, profiles BAS923-22 and AWI-94030 show two separate structural highs located beneath the lowermost continental slope and the continental rise (Fig. 2c). The northernmost structural high represents the buried southern flank of Peter I Island (between CMP 10500 and the northern end of profile AWI-94030, Fig. 2c). Here, sediments deposited on the adjacent ocean floor onlap the volcanic base of the island. A separate structural high is seen beneath the base of the continental slope (between CMPs 6000 and 8500, Fig. 2c). On profile BAS923-22, this structure shows a chaotic internal reflection configuration, with few coherent, laterally persistent reflections. On nearby profile AWI-94030, this structural high also has a chaotic reflection configuration, although acoustically stratified layers are seen at shallow depths within it. Gravity profiles along the seismic tracks show a negative free-air anomaly over this feature, suggesting that it is composed of deformed sediment rather than oceanic basement. In contrast to MCS lines farther east, profiles BAS923-22 and AWI-94030 show no sediment mounds or channels on the continental rise.

3.4. BAS923-27

MCS profile BAS923-27 lies nearly N–S and extends across the outer continental shelf, slope and rise near 94°W (Figs. 1 and 2d). At its southern limit, BAS923-27 crosses only the outermost 6 km of the continental shelf, and consequently, it is not possible to infer much about the stratal geometry of the shelf in this area. Nonetheless, these data do show prograded foresets and a sub-horizontal erosional unconformity at shallow depth, resembling those on the other lines. On profile BAS923-27, the continental slope has a dip of 6°–7°. Sediments deposited on the slope show high-amplitude reflections that are fairly continuous in the dip direction, and we believe that the slope is primarily constructed of debris flow deposits. On the mid-lower slope (e.g near CMP 2000, Fig. 2d), there is some indication of small-scale slumping.

Farther north, profile BAS923-27 crosses the continental rise close to the crest of a large sediment mound (represented by a northward loop in the 4000 m isobath, Fig. 1). Here, smooth oceanic basement is overlain by a seismic stratigraphic sequence with a time-thickness of 1.0–1.2 STWT. This lower sequence is characterised by parallel-to-sub-parallel continuous reflections, and shows no indication of

migrating sediment waves or buried channel systems. The top boundary of this sequence is marked by a continuous, high-amplitude reflection which can be traced from the northern end of the line (at ca. 6 STWT, Fig. 2d) southward beneath the rise and lower continental slope (to about CMP 1200, Fig. 2d). The sequence boundary appears to be conformably overlain by younger rise sediments on this line. However, E–W-trending MCS profiles AWI-94041/BAS923-24 (described below, and shown in Fig. 9), which intersect line BAS923-27 near its northern end, show the unconformable nature of this sequence boundary more clearly. This unconformity is overlain by a sequence with a time-thickness of 1.0–1.2 STWT, which extends to the sea floor, and shows less continuous reflections. Between CMPs 6000 and 8000 (Fig. 2d), BAS923-27 shows local truncation of horizontally layered strata in this upper sequence. This pattern resembles a channel 'cut-and-fill' reflection configuration, and may indeed describe a buried channel system. Alternatively, these structures may represent listric fault planes which have been crossed at a low angle by the seismic profile. Listric faults are clearly seen in the intersecting E–W lines AWI-94041/BAS923-24 (described below, and shown in Fig. 9), and these profiles confirm that BAS923-27 runs close to the crest of a large mound or sediment drift (profile intersection marked, Fig. 9). Profile BAS923-27 also shows irregularities at or near the sea floor. The low resolution of the MCS profile prevents confident identification of these surficial features; they could represent sediment waves, channels, gullies or slump scars.

3.5. BAS923-25

MCS profile BAS923-25 trends N–S and crosses the Antarctic continental shelf, slope and rise near 97°W (Figs. 1 and 2e). The acoustic architecture of the outer shelf and slope on this profile differs markedly from that observed elsewhere within the area of survey. Here, prograded foresets are absent, and the outer continental shelf is underlain by a structural high which appears acoustically chaotic, with no coherent internal structure (centered on CMP 5750, Fig. 7). This structure rises to 0.2 STWT below the sea floor. On unmigrated profiles, the structural high beneath the shelf and the steep continental slope (gradient = 7°–9°) show numerous strong diffractions. Beneath the slope, diffractions are generated by discontinuities associated with slope failure (slumps, and perhaps debris flows), and at greater depth, by deformed and contorted structure. In contrast to MCS profiles acquired nearby, profile BAS923-25 does not show prograded foresets beneath the outer continental shelf. Instead, shelf strata onlap the southern flank of the marginal high (e.g., at 0.8 STWT south of CMP 5750, Fig. 7).

Farther north, profile BAS923-25 crosses the continental rise. Here, the oceanic basement dips towards the continental margin, and is overlain by a sedimentary sequence of uniform thickness (0.5–0.7 STWT), characterised by parallel reflections which follow the dip of basement (e.g., below 7.9 STWT near CMP 3000, Fig. 2e). This lower sequence is overlain by a middle sequence that thickens appreciably towards the margin and shows strongly divergent reflections (e.g., between 6.6 and 7.9 STWT at CMP 3000, Fig. 2e), which suggests syn-tectonic deposition. The middle sequence is overlain, in turn, by an upper acoustic sequence, characterised by sub-parallel, fairly continuous reflections (e.g., between 6.6 STWT and the sea floor at CMP 3000, Fig. 2e). The upper sequence shows basal onlap (labelled in Fig. 2e) against a prominent unconformity which extends northward beneath the rise from the base of the continental slope. On profile BAS923-25, the stratal geometry and thickness of the individual sequences suggest that the lower sequence was deposited before the basement was tilted to the south, and that deposition of the middle sequence accompanied basement tectonism. At present, we do not know when, or by what means, this section of oceanic crust became tilted, although this process was probably related to nearby basement tectonism described by Gohl et al. (1997).

Profile BAS923-25 shows no indication of sediment drifts or migrating sediment waves on this part of the continental rise, although a small channel is seen near the northern end of the line (near CMP 450, Fig. 2e).

3.6. AWI-94042

MCS profile AWI-94042 trends NNE–SSW and crosses the Antarctic continental shelf, slope and rise

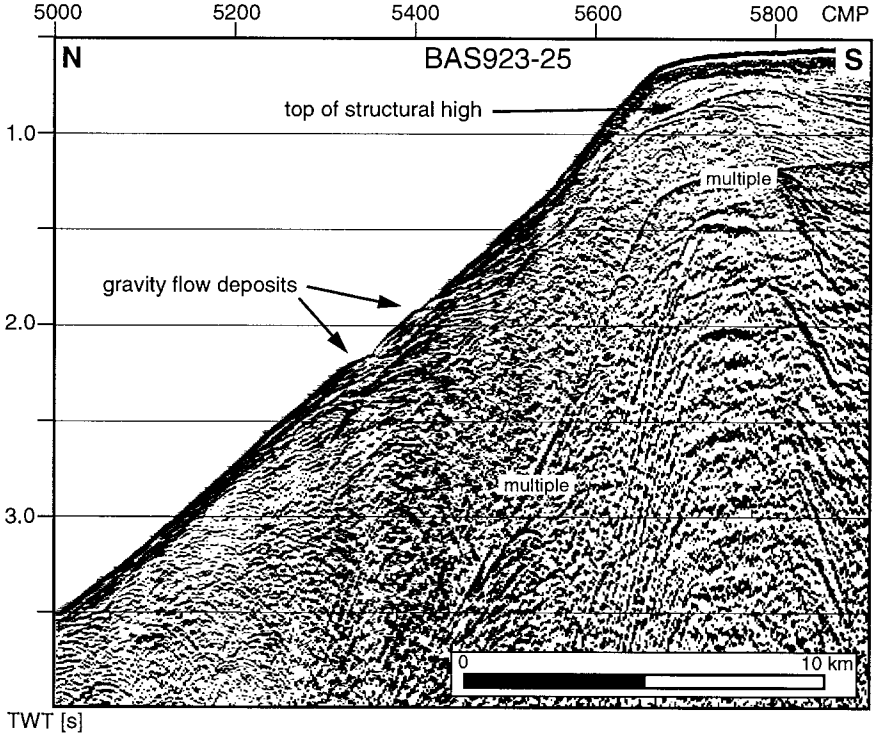

Fig. 7. Section from MCS profile BAS923-25 (located in Fig. 1) showing the outer continental shelf and slope near 97°W. Vertical exaggeration is ca. 7:1 at the sea floor.

near 105°W (Figs. 1 and 2f). Profile AWI-94042 is the westernmost transect described in this study, and lies in the eastern part of the Amundsen Sea. Here, the continental shelf break lies 540 m below sea level, and the continental slope has a gradient of 3°–4°. Unfavourable ice conditions during the MCS survey hampered data acquisition across the continental shelf, and AWI-94042 extended only 25 km landward of the shelf break. As a consequence, we are unable to properly distinguish separate acoustic units beneath the outer shelf on this profile. Nonetheless, AWI-94042 shows prograded foresets, which have been truncated by a series of sub-horizontal erosional unconformities (Fig. 2f, and shown in detail in Fig. 8 of Nitsche et al., 1997).

Farther north, MCS profile AWI-94042 and coincident sub-bottom Parasound data show several discrete, acoustically chaotic-transparent packages which are separated by bright, coherent reflections (Fig. 8). We interpret these packages as debris flow deposits resulting from mass wasting of the upper slope. On the nearby continental rise, AWI-94042 shows mainly horizontally layered strata, although sediment mounds and channels are seen at depths of < 0.5 STWT below sea floor. Swath bathymetry data show that the unburied channels form part of a single-channel system which meanders across the line as it runs northwards. A cross-section of this channel system is also seen at the western end of E–W profile AWI-94041 (Fig. 2g). We note that profile AWI-94042 and possibly profile BAS923-25 (Fig. 2e) cross the part of the Antarctic continental margin that separated from Chatham Rise ca. 80–90 Ma ago. This region forms the oldest oceanic province within the survey area, and therefore, the sediment record on this part of the rise may be expected to span a greater time interval than that seen on the more easterly profiles.

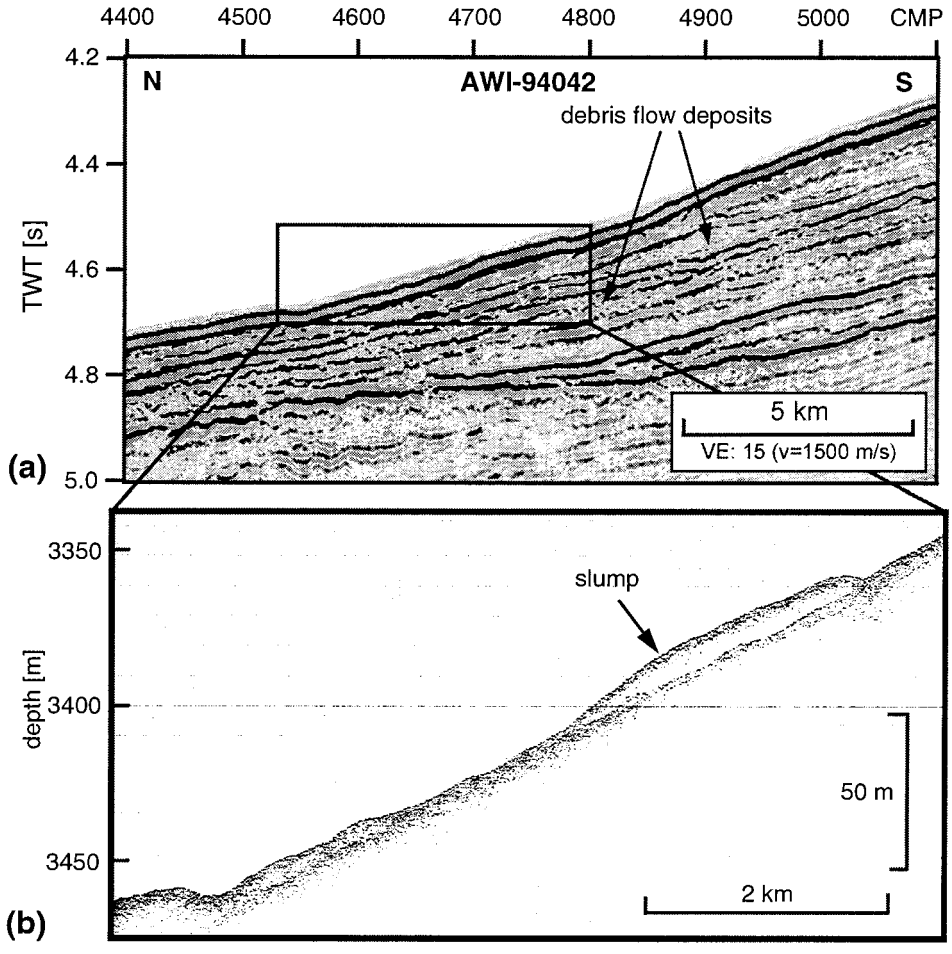

Fig. 8. (a) Section of MCS profile AWI-94042 (located in Fig. 1) showing debris flow deposits beneath the continental slope near 105°W. Similar reflection patterns are seen on all slope transects crossing the area of investigation. (b) Part of the coincident Parasound high-resolution sub-bottom profile.

Some of the transects described above are connected by lines running parallel to the continental margin (Fig. 1).

3.7. AWI-94041 / BAS923-24

MCS profiles AWI-94041 and BAS923-24 are nearly coincident, and trend E–W along 69°30′S, parallel to the margin (Figs. 1 and 2g). These data show a large sediment mound or drift developed on the continental rise. The interpreted line drawing of profile AWI-94041 (Fig. 2g) shows the mound in relation to surrounding ocean floor, and a separate MCS data panel from profile BAS923-24 (Fig. 9) shows the internal acoustic architecture of the mound in detail.

Profile AWI-94041 shows that the sediment mound is built close to a large buried basement trough (centered on CMP 7800, Fig. 2g), where the oceanic crust to the east may have overridden crust to the west (Gohl et al., 1997). In particular, the mound developed above elevated crust to the east of the trough, and we suggest that uplift of this area may have contributed to the later formation of the mound. Here, profiles AWI-94041 and BAS923-24 show that early basement tectonism (described by Gohl et al., 1997) led to uplift of the ocean floor east of the trough, and the development of an erosional

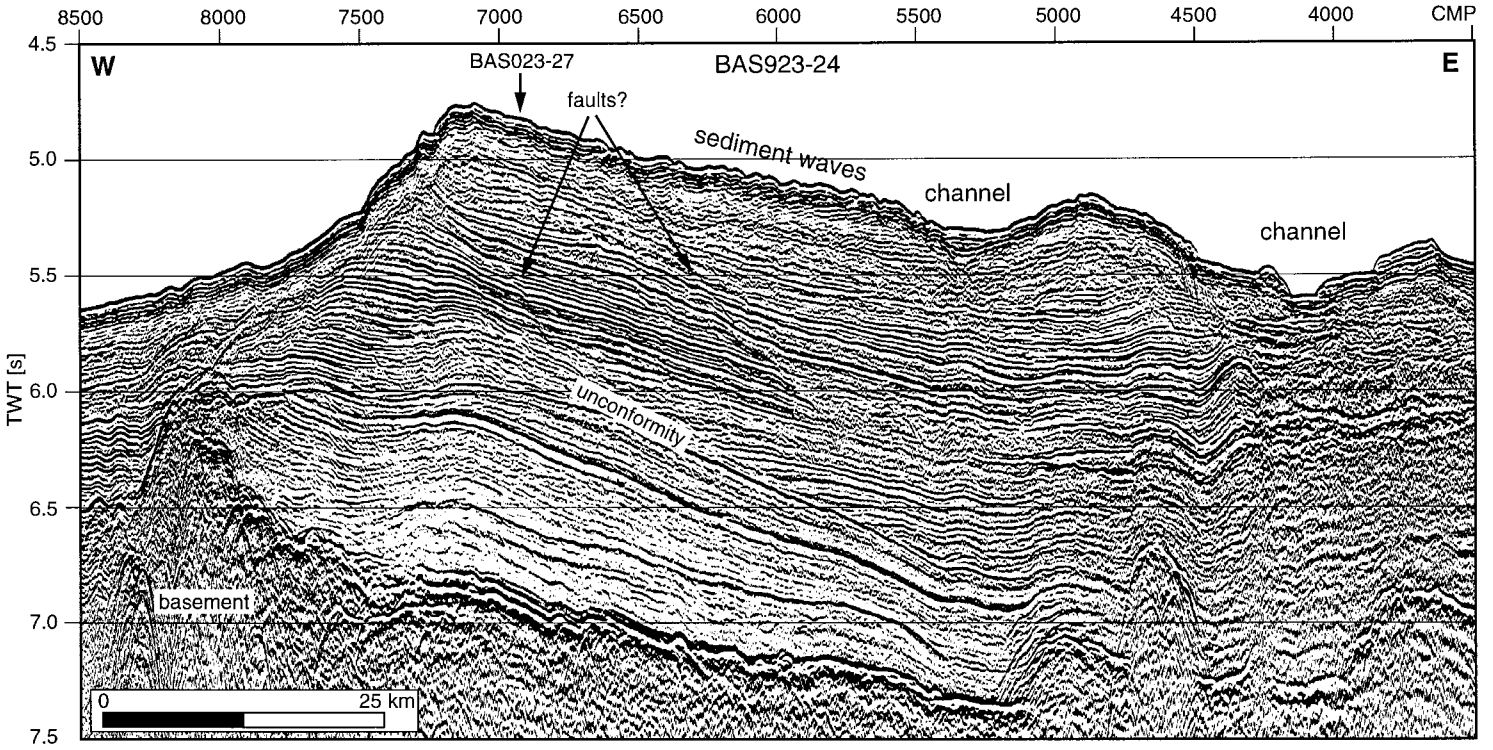

Fig. 9. Section of MCS profile BAS923-24 (located in Fig. 1) showing a large sediment mound on the continental rise near 94°W. Vertical exaggeration is ca. 27:1 at the sea floor.

unconformity (labelled at 6.1 STWT near CMP 6500, Fig. 9). This unconformity is seen also on N–S profile BAS923-27 (at ca. 6 STWT near the northern end of line, Fig. 2d). Onlap of post-tectonic sediments against this surface (e.g., at 6.7 STWT near CMP 5500, Fig. 9) indicates that a palaeo-high between ca. CMPs 7000 and 8200 existed during accumulation of these sediments. Profile BAS923-24 shows that the sediment mound has a width of ca. 100 km (extending between CMPs 4000 and 8000, Fig. 9), and that its crest rises ca. 700 m above the surrounding ocean floor (at CMP 7100, Fig. 9). BAS923-24 also shows that the mound is asymmetric in cross-section, with a gentle eastern flank (east of CMP 7100) and a steeper western flank (west of CMP 7100). Two channels are developed on the eastern flank of the mound (centered on CMPs 4100 and 5300, Fig. 9), and sediment waves are clearly developed at its surface (between CMPs 5500 and 6200, Fig. 9).

An area of higher reflection amplitude beneath the easternmost channel (CMP 4000–4300, at about 5.7 STWT, Fig. 9) probably represents channel lag deposits, indicating that the position of the channel has

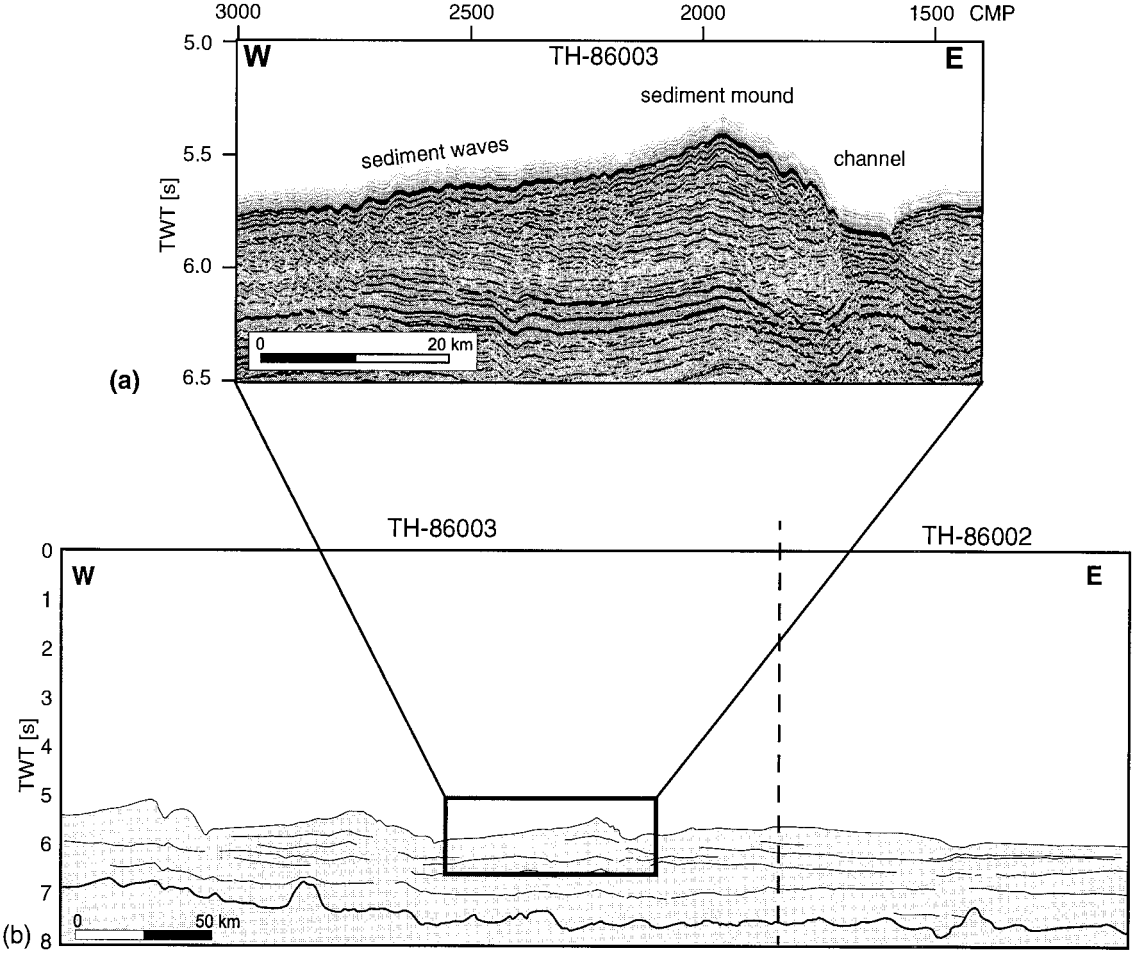

Fig. 10. MCS profiles TH-86002 and TH-86003 (located in Fig. 1) of JNOC. (a) Part of MCS profile TH-86003 showing one of the sediment mounds in detail. Vertical exaggeration is ca. 30:1 at the sea floor. (b) Interpreted line drawing of MCS profiles TH-86002 and TH-86003 showing (a) in relation to the surrounding sea floor. The thicker line indicates the top of the acoustic basement. Vertical exaggeration is ca. 24:1 at the sea floor.

moved slightly to the west over time. This westward channel migration conflicts with observations of Tucholke and Houtz (1976), although their data extend across different parts of the Bellingshausen Sea, mostly farther offshore. MCS profiles AWI-94041 and BAS923-24 also show that the channels were probably generated later than a prominent reflection at about 6.2 STWT (CMP 4000, Fig. 9). Between this reflection and the underlying major unconformity, there is a sequence of reflections (maximum time-thickness of 0.5 STWT) which onlaps the unconformity. This suggests that the development of the channels and probably that of the mound took place quite some time after the tectonism that caused the unconformity.

West of the mound, MCS profiles AWI-94041 and BAS923-24 show a flat-lying seafloor, and near-surface sediments appear horizontally layered. Here, the uppermost sequences are intersected by a small channel at CMP 10100 and a larger channel at CMP 19500 (Fig. 2g). Unfortunately, reflections cannot be traced with confidence from one side of the mound to the other.

3.8. Japan National Oil profiles

Two additional MCS profiles, TH-86002 and TH-86003, collected by the JNOC have been included in this study. These lines have been published through the SCAR-database (Yamaguchi et al., 1988; SCAR, 1992). They trend parallel to the margin, across the lower continental rise in the Amundsen Sea (Figs. 1 and 10), and show a series of channels and sediment mounds (Fig. 10b). Fig. 10a (expanded part of profile TH-86003, Fig. 10b) is representative of these data and shows one of the sediment mounds in detail. Here, profile TH-86003 shows a mound which rises ca. 350 m above the surrounding seafloor, and has an apparent width of ca. 60 km. This mound is smaller than the one seen to the east (e.g., on profiles AWI-94041 and BAS923-24, Fig. 9), although we note that this cross-section is farther away from the margin. This mound also differs from others described in this study because its eastern slope (which dips towards an adjacent channel) is more steeply dipping than its western slope. The gentle western slope has clearly defined sediment waves in its upper part. The mound is built above a strong reflection seen at ca. 6.2 STWT (Fig. 10a). Between CMPs 1600 and 1800, high-amplitude reflections indicate that the palaeo-position of the nearby channel has not migrated during the development of the mound.

4. Discussion

We have used the data described above, published echo sounding data (National Geophysical Data Center, 1996), and published data covering the eastern part of the area (McGinnis et al., 1997; Rebesco et al., 1997) to compile a map showing the distribution of channels, sediment mounds and seamounts in the Bellingshausen Sea region (Fig. 11). On this map, long thick arrows represent channels that have been interpolated between two or more bathymetry and/or seismic lines, assuming a straight or curvilinear path between ship tracks. Small thin arrows represent channels that have been identified on single lines only, or channels that cannot be traced confidently from line to line. In this case, the channel direction is assumed to trend directly down-slope (as defined by regional bathymetry data), although we recognise that some channels will trend obliquely across the continental rise. Hence, small arrows describe channel distribution rather than true channel paths.

The continental shelf break has been mapped from identifications on seismic or echo sounding profiles where such data exist. Elsewhere, the position of the shelf break has been inferred from the predicted topography of Smith and Sandwell (1997), although a lack of satellite data south of 72°S means that the position of the shelf edge remains uncertain in the Amundsen Sea. Seamounts and other outcropping basement structures are also marked where they have been identified on seismic lines. In the following discussion, we use these data to describe sedimentation processes operating on the continental shelf, slope and rise in the Bellingshausen and Amundsen Seas.

4.1. Sedimentation processes on the continental shelf, slope and rise

4.1.1. The outer continental shelf

As observed elsewhere on the Antarctic margin (Anderson et al., 1983; Larter and Barker, 1989;

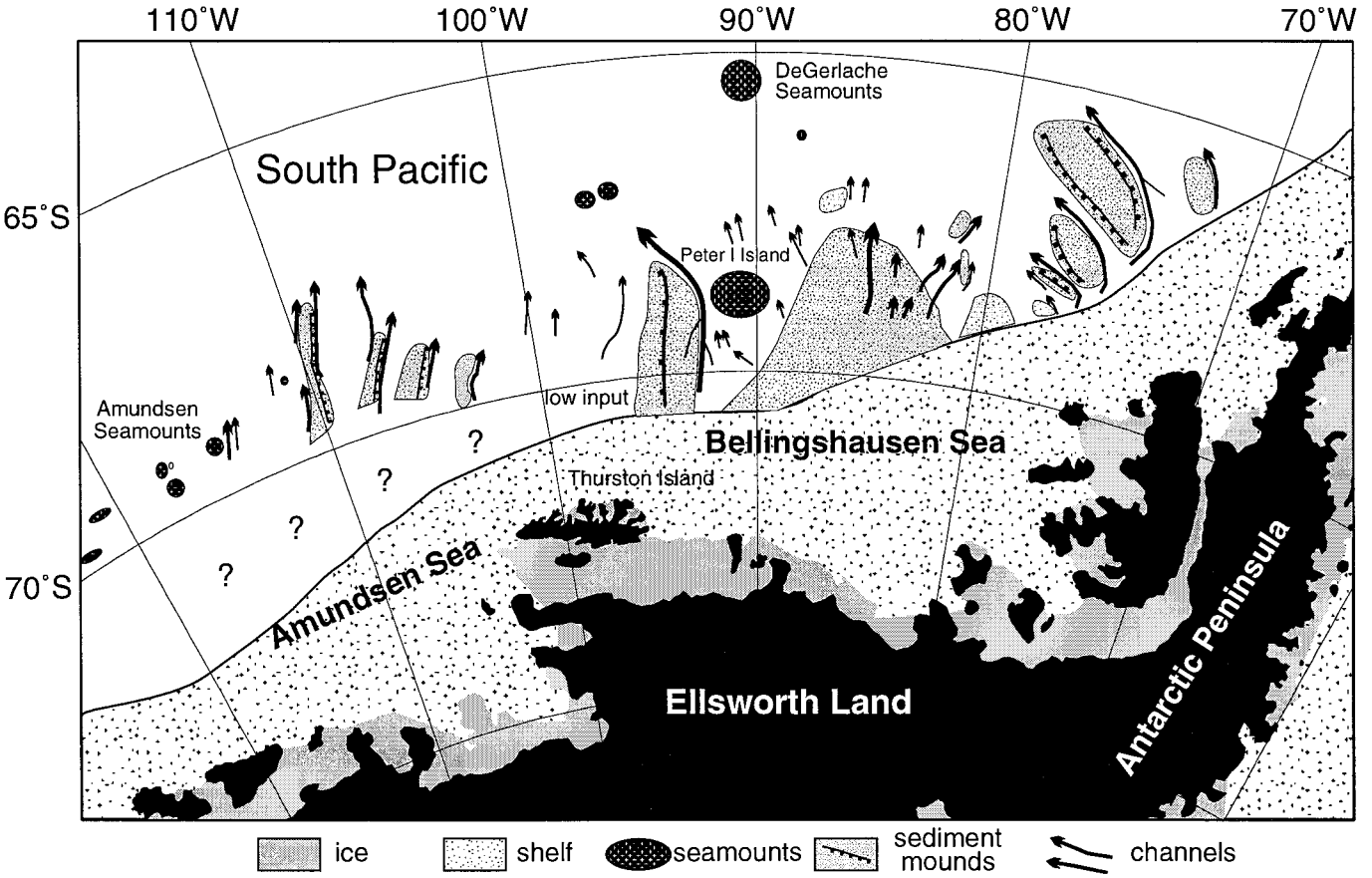

Fig. 11. Map showing the distribution of main sedimentary and bathymetric features mapped in the area of investigation including channels, sediment mounds and seamounts. The crests of major mounds are marked with a black line, and ticks mark the steeper flank of the mounds. The continental shelf break position has been derived from seismic profiles and bathymetry soundings, and interpolated from predicted bathymetry data (Smith and Sandwell, 1997).

F.O. Nitsche et al. / Marine Geology 162 (2000) 277–302

Cooper et al., 1991), the continental shelf in the Bellingshausen and Amundsen Seas is generally deeper (400–600 m below sea level) than that seen at lower latitudes. It is notable also, that profiles AWI-94002, AWI-94003, BAS923-22, AWI-94030 and AWI-94042 (Fig. 2a–c,f) show a gradual increase in water depth across the outermost continental shelf, landward of the shelf break. Most MCS profiles crossing the outer shelf show steep, prograded foresets which have been erosionally truncated by sub-horizontal unconformities. Similar characteristics have been reported on other parts of the Antarctic continental margin (e.g., Larter and Barker, 1989; Cooper et al., 1991), and have been interpreted as an indication of deposition by ice sheets grounded to the shelf edge during times of glacial maximum. These similarities lead us to conclude that grounded ice has reached the continental shelf edge many times on most parts of the Bellingshausen Sea margin. On several MCS profiles, the stratal geometry of sequences preserved beneath the outer shelf consists of three distinct units. The lower unit '1' (Nitsche et al., 1997) is characterised by gently dipping aggradational strata, and has a similar acoustic structure to the 'Type IIA' sequences of Cooper et al. (1991). These sequences were probably deposited in an environment where the West Antarctic ice sheet had not reached the present outer shelf; while glaciers or the ice sheet margin may have reached the sea, sediments were mainly transported across the continental shelf by marine and glacial marine processes. We attribute the change in geometry from unit 1 to overlying units '2' and '3' (Nitsche et al., 1997) to a fundamental change in the mechanism of sediment transport across the continental shelf. These upper units are characterised by more steeply dipping foreset reflections, which are usually less continuous than those of unit 1, and are truncated by sub-horizontal unconformities at their upper limit. Units 2 and 3 have similar characteristics to the 'Type IA' sequences of Cooper et al. (1991). These sediments were probably transported at the base of an ice sheet and deposited where the ice lost contact with the sea floor, i.e., along the grounding line (Larter and Barker, 1989; Cooper et al., 1991; Powell and Alley, 1997). When the grounding line lay at or near the shelf edge, glacial sediments were deposited directly onto the upper slope, leading to the generation of foresets and shelf-edge progradation observed in the MCS profiles.

The stratal geometry of the outer shelf and the amount of progradation apparent within it may be considered a function of sediment supply and the rate of increase in accommodation space (the sum of shelf subsidence and sea level change) during the development of the prograded wedge. MCS profile BAS923-25 (Fig. 2e) also suggests local tectonic control on the development of the wedge. However, existing data do not allow us to properly separate these effects. On the basis of the regional tectonic framework (e.g., Mayes et al., 1990; McCarron and Larter, 1998), we expect the rate of thermal subsidence of the margin to increase gradually from west to east, in relation to the length of time since the last major thermo-tectonic event (rifting or ridge–trench collision). If we assume that the initial formation of the prograded wedge occurred after the start of the Miocene (by analogy with neighbouring areas: Larter and Barker, 1991b; De Santis et al., 1995), subsidence resulting from thermal effects should already have been relatively slow by that time along the entire Amundsen–Bellingshausen Seas margin. Therefore, there does not appear to be any reason why the rate of accommodation should have varied appreciably along the margin during its subsequent development. Hence, we surmise that variations in the total amount of progradation identified in the MCS data over distances of a few hundred kilometers are principally a function of sediment supply. Sediment supply to the margin would have been affected, in turn, by a variety of factors controlling the volume and dynamics of the ice sheet. An important factor would have been the focusing of sediment transport by ice streams, but data acquired on the continental shelf are still too sparse to identify source areas and transport patterns in this region.

The rate of sediment supply to the outer shelf would have fluctuated with variations in the distance between the ice grounding line and the continental shelf edge. When the grounding line advanced to the shelf edge, the ice sheet could have transported large volumes of poorly sorted material directly to the upper slope. However, when the grounding line lay significantly inshore, some finer-grained sediment might have been transported to the outer shelf and slope by tidal motion and shelf currents, but most

glacial sediments were probably trapped within the deeper inner shelf area.

MCS profiles presented in this study show along-margin variation in the acoustic architecture of the outer shelf, and the amount of shelf-edge progradation. Spatial variations in the size of the prograded wedge are also suggested by predicted bathymetry data (Smith and Sandwell, 1997) which show 'lobes' similar to those shown to have been produced by progradation along the Antarctic Peninsula (Larter et al., 1997). The lobate form of the margin appears to be confirmed by the few bathymetry tracks available in the area. On MCS profile BAS923-25 (Fig. 2e and Fig. 7), prograded sequences appear to be absent, which may suggest low sediment supply to the shelf edge. Here, nearby Thurston Island (Fig. 1) might have acted as a barrier to ice streams supplying sediment from the West Antarctic continent. It is possible also, that the local structural high observed beneath the outer shelf (near CMP 5750, Fig. 7) restricted sediment transport to this part of the upper slope. At its southern end, profile BAS923-25 is connected to BAS923-27 by E–W MCS profile BAS923-26, extending along the continental shelf (unpublished BAS data). BAS923-26 extends obliquely across prograded sequences just a few kilometers east of line BAS923-25. Hence, we infer that the absence of prograded foresets on profile BAS923-25 is of local extent, although additional data are required to confirm this.

4.1.2. The continental slope

Seismic transects presented in this study (Fig. 2) show a marked difference in continental slope gradient between profile AWI-94002 and the other lines. Easternmost profile AWI-94002 shows a much steeper gradient ($>12°$, Fig. 2a) than the more westerly transects (2°–5°, Fig. 2b–d,f). This steep slope gradient is typical of many published profiles from the Pacific margin of the Antarctic Peninsula (Larter and Barker, 1989, 1991b). We consider two possible factors that may have contributed to this difference. Firstly, the present variation in slope angle may partly reflect along-slope variations that pre-date deposition from grounded ice and are the result of older tectonic processes. Antarctic–Phoenix ridge segments migrated into the trench west of 80°W before 40 Ma, but did not reach the part of the margin east of 80°W until after 30 Ma (Larter et al., 1997; McCarron and Larter, 1998). As a consequence of changes in subduction convergence rate and direction, changes in spreading rate, and possible microplate tectonics during the early Tertiary, the last stages of subduction might have had different effects on these different sectors of the margin. Slope gradient may also have been affected by the textural composition of the glacial sediment supplied to the margin. Larter and Barker (1989) suggested that the immaturity (poor sorting and particle roughness) of glacial sediment might be a factor in the apparent stability of the steep Antarctic Peninsula slope. We note that the glacial transport path from Ellsworth Land to the Bellingshausen Sea margin is considerably longer than equivalent paths in the Antarctic Peninsula region. Prolonged shearing in a deforming basal till may break up some of the coarser fraction of the till and therefore increase the degree of sorting. Hence, if sorting occurs by this means, and if sediment texture is indeed a factor in slope stability on glacial margins, then the longer transport path in the Bellingshausen Sea would result in a lower slope angle. It is interesting to note that the Antarctic continental slope has a relatively low gradient (1°–3°) in other places where long glacial transport paths reached the margin at times of glacial maximum, e.g., eastern Ross Sea, Crary Fan and Prydz Channel Fan (Haugland et al., 1985; Cooper et al., 1991).

Variations in sediment composition may also be related to variations in sea-floor reflection strength observed on BAS and AWI MCS profiles. A comparison of MCS profiles crossing the continental shelf in the Bellingshausen Sea and Antarctic Peninsula regions suggests that sea-floor multiple reflections are weaker in the Bellingshausen Sea, which implies a lower sea-floor reflection coefficient in this region. This is consistent with estimates of interval velocities for shallow shelf sediments derived from semblance analyses during processing, which are typically >2000 m s^{-1} in the Antarctic Peninsula region (Larter and Barker, 1989), but only 1800–1900 m s^{-1} in the Bellingshausen Sea. If sediments deposited on the outer shelf in the Bellingshausen Sea are, on average, finer-grained, they would tend to retain more water, and this would explain the slightly lower seismic velocities, resulting in a lower reflection coefficient at the sea floor. Alternatively,

the lower seismic velocities for shallow shelf sediments in the Bellingshausen Sea could indicate that they have been subject to less glacial loading and compaction.

Published studies (Rebesco et al., 1997) have shown that sediment drifts on the continental rise near the Antarctic Peninsula are separated from the continental margin by non-depositional bathymetric troughs which extend along the foot of the continental slope. In contrast, the larger sediment mounds in the Bellingshausen Sea form topographic ridges which extend to the continental margin (Fig. 11, and shown by MCS profile BAS923-27, Fig. 2d). The absence of a non-depositional trough at the base of slope may be related to the difference in continental slope gradient described above. Very high energy gravity flows generated on the steep slope of the Antarctic Peninsula margin may have eroded drift sediments near the base of the slope. However, in the Bellingshausen Sea, the continental slope is shallower, and down-slope gravity flows may be less energetic, leading to sediment preservation at the base of slope. Rebesco et al. (1997) also described drift sediments which onlap the lower slope adjacent to their lobe '2', and suggested that this part of the Antarctic Peninsula margin had been less active during recent glaciations. Hence, we suggest that preservation of sediments on the lower continental slope may be controlled, in part, by the energy of down-slope gravity flows generated during times of glacial maximum.

MCS profiles BAS923-22 and AWI-94030 show acoustically laminated units which onlap the upper continental palaeo-slope (Fig. 6). This geometry could reflect hemipelagic deposition in the presence of a contour current on the slope. Predicted bathymetry data (Smith and Sandwell, 1997) suggest that here, the upper slope forms part of a broad sediment ridge, with its crest lying farther to the east (between 85°W and 87°W, Fig. 1). The unusual landward movement of the palaeo-shelf edge in profile BAS923-22 shows that the rate of increase in accommodation space outstripped sediment supply to this part of the margin at least once during the growth of the prograded wedge. Hence, there have been times when the sediment input from the inner shelf to this flank of the sediment ridge near 87°30′W appears to have been comparatively low. This has led to the preservation of slope facies which were probably sourced along-slope to the east.

Farther west, the depositional pattern of sediments beneath the outer shelf remains poorly defined. However, the acoustic architecture of MCS profile AWI-94042 suggests that grounded ice has, at some time, reached the continental shelf edge and transported sediment to the upper slope in the eastern Amundsen Sea.

Along most parts of the continental margin investigated in this study, MCS and high-resolution sub-bottom profiles show evidence of small-scale slope failure and debris flow deposits (e.g., profile AWI-94042, Fig. 8). However, we find no evidence of sub-marine canyons along the continental shelf edge and slope on the existing margin crossings. This observation conflicts with results of a previous study based on older and more poorly located bathymetric soundings (Vanney and Johnson, 1976) that showed canyons for which we have found no supporting evidence.

The channels seen in BAS and AWI profile data appear to extend northward from the foot of the continental slope (Fig. 11). This is shown in swath bathymetry data acquired north of Alexander Island (Figs. 1 and 12). On the upper continental slope, these data show numerous small gullies and scarps, whereas central parts of the slope have a comparatively smooth sea floor. At greater depth, elongated mounds are seen near the base of slope. Between the mounds, small channels merge together to form larger channels on the upper continental rise. Similar features have been seen in GLORIA sonographs of the Antarctic Peninsula margin (Tomlinson et al., 1992).

4.1.3. The continental rise

On the continental rise, we have identified a series of sediment mounds and intervening channels (Fig. 11). The mounds are usually located along the western side of the channels, consistent with observations of Tucholke and Houtz (1976). In places where channels lie along both sides of a mound, the mound is thought to have been built up from sediment supplied through the more easterly channel.

Turbidites in sediment cores from the abyssal plains (Hollister et al., 1976; Wright et al., 1983) suggest that the rise channels formed pathways for turbidity currents, and it is likely that the intervening

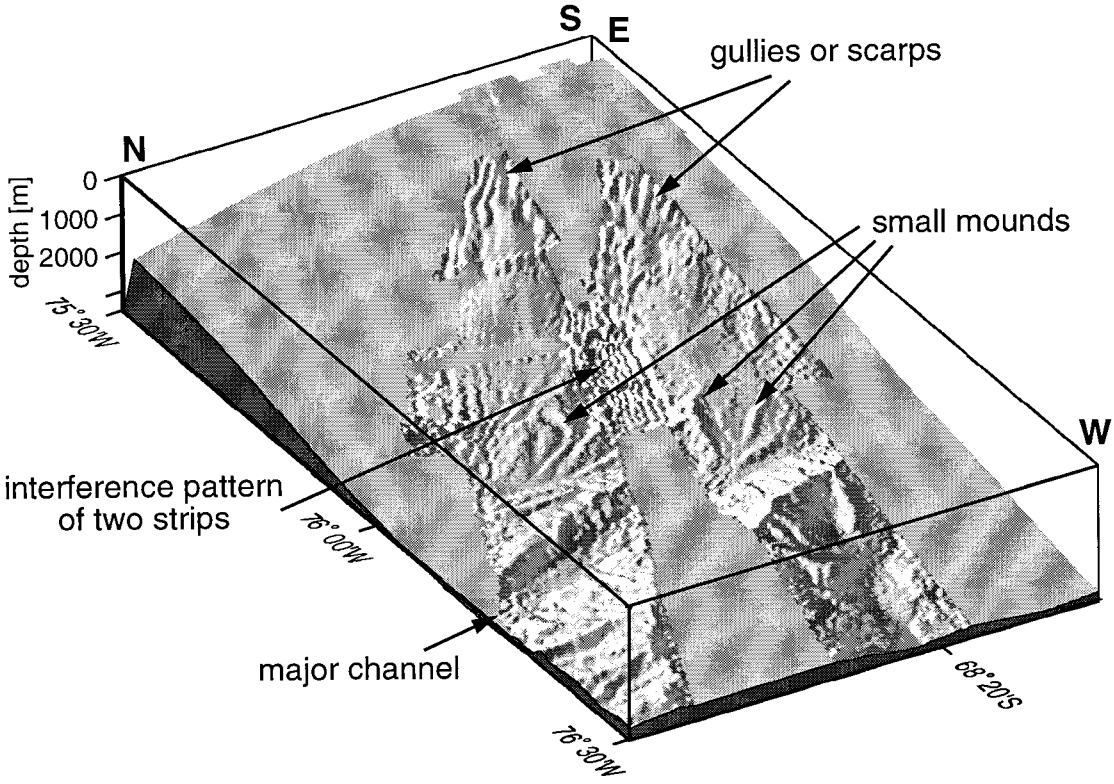

Fig. 12. Perspective view of two Hydrosweep swath bathymetry stripes from the continental slope north of Alexander Island (located in Fig. 1, and illuminated from NE). These data show small channels on the lower continental slope merging to form the major channel which separates the large mound in the foreground from the continental slope.

sediment mounds are composed primarily of fine-grained components from these turbidity currents which were entrained in ambient bottom currents. The fact, that mounds or levees are usually seen on the western sides of the channels, can be explained by deposition in the presence of a westward-flowing bottom current and Coriolis force (e.g., Tucholke, 1977; Rebesco et al., 1996). Variations in the shape and size of the mounds along the margin could reflect differences in the influence of the bottom current and sediment supply: while the mound on profiles BAS923-24/AWI-94030 (Fig. 9) has a similar acoustic architecture to sediment drifts on the rise to the northeast (e.g., Rebesco et al., 1996), the geometry of the mounds on profile TH-86003 (Fig. 10) more closely resembles that of a classical channel levee (as described by Stow, 1994). Direct oceanographic measurements (e.g., Hellmer et al., 1998) are sparse in this region, and do not describe bottom current flow in the vicinity of the sediment mounds; as a consequence, the bottom current regime in the southern Bellingshausen and Amundsen Seas remains poorly understood. Nonetheless, westward-flowing ambient bottom currents have been inferred previously on the basis of seabed photographs (Hollister and Heezen, 1967) and nepheloid measurements (Tucholke, 1977). The nearest published direct current measurements at the South Shetland trench (Nowlin and Zenk, 1988) and on the rise north of the Antarctic Peninsula (Camerlenghi et al., 1997) describe westward bottom current flow, with speeds decreasing southwestward from 10–20 cm s^{-1} at the South Shetland trench to ca. 6 cm s^{-1} near 77°W. In addition to a westward-flowing boundary current, the action of Coriolis force on turbidity currents would also promote deposition along the western side of the channels. However, the vertical relief of some mounds described in this study is larger than that of

any channel levees reported in areas lacking significant bottom current activity. It is possible also, that bottom circulation varied appreciably during past glacial cycles. In particular, Pudsey (1992) proposed weaker bottom currents during glacial periods in the Weddell Sea, which is presumed to be the source area for bottom water flowing westward along the Antarctic Peninsula margin and Bellingshausen Sea continental rise.

Farther north, sedimentation processes are thought to be dominated by the Antarctic Circumpolar Current (ACC, e.g., Nowlin and Klinck, 1986), which is wind-forced at the sea surface, and affects the entire water column. ACC flow probably began after the opening of Drake Passage ca. 23 Ma ago (Barker and Burrell, 1977). In the eastern Bellingshausen Sea, Read et al. (1995) showed that the modern ACC extends as far south as 67°S.

Seismic reflection and high-resolution sub-bottom profiles presented here and elsewhere (e.g., Tucholke, 1977) show well-formed migrating sediment waves on the rise in the Bellingshausen Sea. Sediment waves have been associated with ambient thermohaline current flow across sediment drifts (Flood et al., 1993) and turbidity current flow across deep-sea channel levees (e.g., Damuth, 1979; Normark et al., 1980; Carter et al., 1990). Comparison of BAS and AWI profile data suggests that sediment waves are more common on the continental rise in the Bellingshausen and Amundsen Seas than on the rise adjacent to the Antarctic Peninsula. This may be due, in part, to the existing distribution of data; sediment waves described in this study are located farther away from the margin (100–200 km) than most MCS profiles obtained in the Antarctic Peninsula region. Hence, it is possible that sediment waves have not been widely reported in the Antarctic Peninsula region due to the lack of data over distal parts of the rise. Alternatively, it is possible that the characteristics of the sediment (e.g., grain size or cohesion) or the bottom currents (e.g., speed or directional stability) favour sediment wave formation in the Bellingshausen Sea.

4.2. Glacial margin sedimentation model

The sedimentation processes described above can be incorporated into a preliminary sedimentation model for the glacial margin depositional systems in the Bellingshausen Sea (shown in perspective view, Fig. 13). Before a large ice sheet developed on West Antarctica, the main sedimentation processes were probably similar to those found on lower latitude margins. When ice sheets first reached the open sea, marine and glacial marine processes were probably still the main means of sediment transport across the continental shelf. During subsequent glacial–interglacial cycles, the advance and retreat of grounded

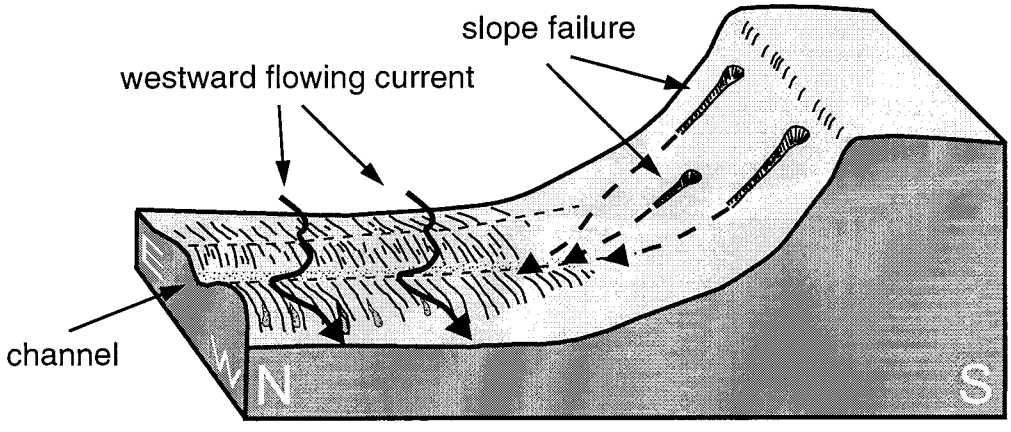

Fig. 13. Simple model describing sedimentation processes in the Bellingshausen Sea.

ice sheets across the continental shelf would have resulted in a fundamental change in the shelf–slope–rise sediment transport system. At glacial maximum, grounded ice probably reached the shelf edge in many parts of the Bellingshausen and Amundsen Seas, which would have caused an increase in the supply of terrigenous material to the upper slope. Sediment supply would have been especially high in the vicinity of ice stream termini. This was probably accompanied by increased sediment transport down the continental slope by means of small-scale slumps and debris flows. While the coarsest fraction settled on the lower slope, other components were probably incorporated in turbidity currents which flowed along the channels on the continental rise toward the abyssal plain. Sediment preservation on the uppermost rise may have been controlled, in part, by the energy of subsequent down-slope flows. MCS and sub-bottom profiles suggest that slumps and debris flows have been generated on a broad part of the slope, and that remobilised material has been transported in tributary channels which meet near the base of slope to form major channels on the rise. Here, fine-grained components from turbidity currents have settled mainly on the western bank of the channels, having been entrained in westward-flowing bottom currents and deflected by Coriolis force. We note that mounds are closely associated with channels (Fig. 11), and that appreciable volumes of terrigenous sediment have been deposited in the vicinity of channels. Similar mounds have been found to the northeast, on the Antarctic Peninsula rise (McGinnis and Hayes, 1995; Rebesco et al., 1996, 1997; McGinnis et al., 1997). Rebesco et al. (1996) interpret these mounds as sediment drifts, constructed mainly from the fine-grained components of turbidity currents originating on the continental slope, entrained in a nepheloid layer within the ambient southwesterly bottom currents, and deposited downcurrent. In contrast, McGinnis and Hayes (1995) and McGinnis et al. (1997) suggest that the mounds were generated mainly by down-slope depositional processes with less influence of bottom currents. From our data, we surmise that long-distance nepheloid layer transport at the base of the westward-flowing boundary current has played a comparatively minor role on the rise in the Bellingshausen and Amundsen Seas, although in some places, bottom currents have had a major influence on the pattern of deposition of fine-grained terrigenous sediment, and hence, on construction of mounds. Our model seeks to account for the wide range of depositional styles observed on the continental shelf, slope and rise in this region through variations in sediment supply, and the strength and stability of bottom currents.

The BAS and AWI MCS profiles in the Bellingshausen and Amundsen Seas do not extend through drill sites, and consequently, we have no reliable constraints on the age of the prograded sequences described in this study. Existing studies suggest that grounded ice reached the continental shelf edge in the eastern Ross Sea by the early Miocene (De Santis et al., 1995), and reached the shelf edge in the Antarctic Peninsula region in the latest Miocene (Larter et al., 1997). In the absence of reliable age control, the timing of the onset of glacial progradation in the Bellingshausen and Amundsen Seas remains uncertain, although we suspect that it falls within the Miocene. While uncertainties remain concerning the regional significance of stratal geometry transitions within the depositional sequences observed beneath the outer continental shelf, thick drift accumulations identified on the adjacent continental rise may still yield a palaeo-environmental record which is representative of the region as a whole. Existing studies suggest that the acoustic stratigraphy of rise drifts may be jump-correlated over large distances (i.e., 400 km, Rebesco et al., 1997), and that these sediment bodies provide a more continuous sedimentary record.

Owing to a paucity of data, the morphology and depositional architecture of the shelf and slope in the central Amundsen Sea remains poorly understood. Predicted bathymetry data (Smith and Sandwell, 1997) and one available bathymetry profile suggest that canyons may be present in the upper slope between 108°W and 112°W. JNOC MCS profiles (Fig. 10) show channels, mounds and sediment waves on the continental rise similar to those in the Bellingshausen Sea, which suggests that similar sedimentation processes have been active in both areas. Differences in the geometry of the mounds observed on the JNOC profiles from those in the Bellingshausen Sea suggest a lesser influence of westward-flowing bottom currents. This could result from a westward

decrease in bottom current velocity, or a decrease in bottom current velocity with increasing distance from the margin. Additional data are required to resolve this uncertainty.

5. Conclusions

In this study, we present new MCS profiles, high-resolution sub-bottom profiles and bathymetry data acquired across a remote and poorly surveyed part of the Antarctic margin in the Bellingshausen and Amundsen Seas. These data show regional variations in the depositional style of the Antarctic continental margin. Some specific findings are listed below.

(1) Although there are some general similarities in the stratal geometry of shelf sequences, MCS data also show longitudinal variations in the development of depositional systems on the Antarctic continental shelf, slope and rise in the Bellingshausen and Amundsen Seas. Comparison between data acquired in the Bellingshausen Sea and Antarctic Peninsula regions also shows similar overall patterns of shelf sequences, as well as demonstrating differences in detail between the development history of the margin in these areas. These differences result from a variety of factors which affect southern-hemisphere glacial margin sedimentation including: variations in source lithology, the rate of sediment supply to the outer shelf, the length of the glacial transport path, local tectonic controls, and the influence of bottom currents on sedimentation.

(2) On most MCS profiles crossing the outer continental shelf, we identify a broad transition from gently dipping aggradational sequences, to sequences with more steeply dipping prograded foresets, which are truncated at their upper limit by sub-horizontal unconformities. By analogy with previous studies, we suggest that the lower aggradational sequences were deposited in a glacial marine environment where the West Antarctic ice sheet had not reached the present outer shelf, and that the upper progradational sequences were deposited at or near the shelf edge by grounded ice during times of glacial maximum. MCS profiles also show large variations in the amount of shelf edge progradation over distances of a few hundred kilometers. We suspect that this principally reflects variations in sediment supply to the outer shelf, which would have been affected, in turn, by the geology of the glacial catchment area and other factors controlling the dynamics of the West Antarctic ice sheet.

(3) Near 87°30′W, MCS profiles crossing the Antarctic continental margin show a thick, current-influenced slope sequence on the upper continental slope. Here also, an abrupt landward shift of the offlap break is observed within progradational/aggradational sequences beneath the adjacent outer shelf. We infer from these observations that there have been times when sediment input from the inner shelf was comparatively low along this part of the margin. Elsewhere in the Bellingshausen Sea and Antarctic Peninsula regions, equivalent slope-front facies are thought to have been overwhelmed by sediments transported along the shelf–slope–rise sediment transport path.

(4) We identify sediment mounds developed on the upper continental rise. We interpret these mounds as being principally composed of fine-grained material which has been transported to the rise by turbidity currents. Coriolis force will have influenced turbidity currents throughout the region, but the size and shape of one mound in the western Bellingshausen Sea implies that entrainment of fine-grained sediments in westward-flowing ambient bottom currents was important in this area. Similar bottom current influence on mound construction to the northeast on the Antarctic Peninsula continental rise has been proposed by McGinnis and Hayes (1995), Rebesco et al. (1996; 1997), and McGinnis et al. (1997), although their models differ with regard to the relative influence of these currents. We consider that the distribution, structure and external form of the mounds in the Amundsen and Bellingshausen Seas reflect the relative influence of the bottom currents, and the nature and volume of sediment supplied from the adjacent continental margin.

This study shows that sedimentation processes on the Antarctic continental shelf, slope and rise are affected by many physical and environmental factors. In order to distinguish these effects, the whole sediment transport path from shelf to slope to rise must be understood. Additional insights may be gained from comparisons with northern-hemisphere glacial margin systems.

Acknowledgements

We thank the captains, crews and scientists of the cruises of the RRS *James Clark Ross* and RV *Polarstern* on which the data used in this paper were collected. We also thank Peter Barker and the reviewers, G. Leitchenkov and A. Maldonado, for thoughtful comments. This is AWI contribution No. 1512.

References

Anderson, J.B., Brake, C., Domack, E.W., Myers, N., Singer, J., 1983. Sedimentary dynamics of the Antarctic continental shelf. In: Oliver, R.L., James, P.R., Jago, J.B. (Eds.), Antarctic Earth Science. Australian Academy of Science, Canberra, pp. 387–389.

Barker, P.F., Burrell, J., 1977. The opening of the Drake Passage. Marine Geology 25, 15–34.

Bart, P.J., Anderson, J.B., 1995. Seismic record of glacial events affecting the Pacific margin of the northwestern Antarctic Peninsula. In: Cooper, A.K., Barker, P.F., Brancolini, G. (Eds.), Geology and Seismic Stratigraphy of the Antarctic Margin. Antarctic Research Series, Vol. 68. American Geophysical Union, Washington, DC, pp. 75–95.

Camerlenghi, A., Crise, A., Pudsey, C.J., Accerboni, E., Laterza, R., Rebesco, M., 1997. Ten-month observation of the bottom current regime across a sediment drift of the Pacific margin of the Antarctic Peninsula. Antarctic Science 9, 426–433.

Carter, L., Carter, R.M., Nelson, C.S., Fulthorpe, C.S., Neil, H.L., 1990. Evolution of Pliocene to recent abyssal sediment waves on Bounty Channel levees, New Zealand. Marine Geology 95, 97–109.

Cooper, A.K., Webb, P.N., 1992. International offshore studies on Antarctic Cenozoic history, glaciation, and sea-level change: the ANTOSTRAT project. In: Yoshida, Y., Kaminuma, K., Shiraishi, K. (Eds.), Recent Progress in Antarctic Earth Science. Terra Scientific Publishing, Tokyo, pp. 655–659.

Cooper, A.K., Barrett, P., Hinz, K., Traube, V., Leitchenkov, G., Stagg, H., 1991. Cenozoic prograding sequences of the Antarctic continental margin: a record of glacio-eustatic and tectonic events. Marine Geology 102, 175–213.

Cunningham, A.P., Larter, R.D., Barker, P.F., 1994. Glacially prograded sequences on the Bellingshausen Sea continental margin near 90°W. Terra Antartica 1, 267–268.

Damuth, J.E., 1979. Migrating sediment waves created by turbidity currents in the northern South China Basin. Geology 7, 520–523.

De Santis, L., Anderson, J.B., Brancolini, G., Zayatz, I., 1995. Seismic record of late Oligocene through Miocene glaciation on the central and eastern continental shelf of the Ross Sea. In: Cooper, A.K., Barker, P.F., Brancolini, G. (Eds.), Geology and Seismic Stratigraphy of the Antarctic Margin. Antarctic Research Series, Vol. 71. American Geophysical Union, Washington, DC, pp. 235–260.

Flood, R.D., Shor, A.N., Manley, P.D., 1993. Morphology of abyssal mudwaves at Project Mudwaves sites in the Argentine Basin. Deep-Sea Research II 40, 859–888.

Gohl, K., Nitsche, F.O., Miller, H., 1997. Seismic and gravity data reveal Tertiary interplate subduction in the Bellingshausen Sea, Southeast Pacific. Geology 25, 371–374.

Haugland, K., Kristoffersen, Y., Velde, A., 1985. Seismic investigations in the Weddell Sea embayment. Tectonophysics 114, 293–313.

Hellmer, H.H., Jacobs, S.S., Jenkins, A., 1998. Oceanic erosion of a floating Antarctic glacier in the Amundsen Sea. In: Jacobs, S., Weiss, R. (Eds.), Ocean, Ice, and Atmosphere: Interactions at the Antarctic Continental Margin. Antarctic Research Series, Vol. 75. American Geophysical Union, Washington, DC, pp. 83–99.

Hollister, C.D., Heezen, B.C., 1967. The sea floor of the Bellingshausen Sea. In: Hersey, J.B. (Ed.), Deep-Sea Photography. Johns Hopkins Univ. Press, Baltimore, MD, pp. 177–189.

Hollister, C.D., Craddock, C., et al., 1976. Initial Reports of the Deep-Sea Drilling Project, Vol. 35. US Government Printing Office, Washington, DC, 929 pp.

Kuvaas, B., Leitchenkov, G., 1992. Glaciomarine turbidite and current controlled deposits in Prydz Bay, Antarctica. Marine Geology 108, 365–381.

Larter, R.D., Barker, P.F., 1989. Seismic stratigraphy of the Antarctic Peninsula Pacific margin: a record of Pliocene–Pleistocene ice volume and palaeoclimate. Geology 17, 731–734.

Larter, R.D., Barker, P.F., 1991a. Effects of ridge crest–trench interaction on Antarctic–Phoenix spreading: forces on a young subducting plate. J. Geophys. Res. 96B, 19583–19607.

Larter, R.D., Barker, P.F., 1991. Neogene interaction of tectonic and glacial processes at the Pacific margin of the Antarctic Peninsula. In: Macdonald, D.I.M. (Ed.), Sedimentation, Tectonics and Eustasy, Vol. 12. Int. Assoc. Sedimentol. Spec. Publ., pp. 165–186.

Larter, R.D., Cunningham, A.P., 1993. The depositional pattern and distribution of glacial–interglacial sequences on the Antarctic Peninsula Pacific margin. Marine Geology 109, 203–219.

Larter, R.D., Rebesco, M., Vanneste, L.E., Gambôa, L.A.P., Barker, P.F., 1997. Cenozoic tectonic, sedimentary and glacial history of the continental shelf west of Graham Land, Antarctic Peninsula. In: Barker, P.F., Cooper, A.K. (Eds.), Geology and Seismic Stratigraphy of the Antarctic margin: 2. Antarctic Research Series, Vol. 71. American Geophysical Union, Washington, DC, pp. 1–27.

Mammerickx, J., Cande, S., 1982. General Bathymetric Charts of the Oceans (GEBCO), Vol. 515. Canadian Hydrographic Survey, Ottawa.

Mayes, C.L., Lawver, L.A., Sandwell, D.T., 1990. Tectonic history and new isochron chart of the South Pacific. J. Geophys. Res. 95B, 8543–8567.

McCarron, J.J., Larter, R.D., 1998. Late Cretaceous to early Tertiary subduction history of the Antarctic Peninsula. Journal of the Geological Society 155, 255–258.

McGinnis, J.P., Hayes, D.E., 1995. The role of downslope and

along-slope depositional processes: southern Antarctic Peninsula continental rise. In: Cooper, A.K., Barker, P.F., Brancolini, G. (Eds.), Geology and Seismic Stratigraphy of the Antarctic Margin. Antarctic Research Series, Vol. 68. American Geophysical Union, Washington, DC, pp. 141–156.

McGinnis, J.P., Hayes, D.E., Driscoll, N.W., 1997. Sedimentary processes across the continental rise of the southern Antarctic Peninsula. Marine Geology 141, 91–109.

Miller, H., Grobe, H., 1996. The expedition ANTARKTIS-XI/3 of RV 'Polarstern' 1994. Berichte zur Polarforschung, Vol. 188, 115 pp.

Miller, K.G., Fairbanks, R.G., Mountain, G.S., 1987. Tertiary oxygen isotope synthesis, sea-level history, and continental margin erosion. Palaeoceanography 2, 1–19.

Moons, A., DeBatist, M., Henriet, J.P., Miller, H., 1992. Sequence stratigraphy of the Crary Fan, Southeastern Weddell Sea. In: Yoshida, Y., Kaminuma, K., Shiraishi, K. (Eds.), Recent Progress in Antarctic Earth Science, Tokyo. Terra Scientific Publishing, Tokyo, pp. 613–618.

National Geophysical Data Center, 1996. Marine Geophysical trackline data (GEODAS/TRACKDAS). Data Announcement 96-MGG-01, Natl. Oceanic Atmos. Admin. US Dept. Commer., Boulder, CO.

Nitsche, F.O., Gohl, K., Vanneste, K., Miller, H., 1997. Seismic expression of glacially deposited sequences in the Bellingshausen and Amundsen Seas, West Antarctica. In: Barker, P.F., Cooper, A.K. (Eds.), Geology and Seismic Stratigraphy of the Antarctic Margin: 2. Antarctic Research Series, Vol. 71. American Geophysical Union, Washington, DC, pp. 95–108.

Normark, W.R., Hess, G.R., Stow, D.A.V., Bowen, A.J., 1980. Sediment waves on the Monterey Fan levee: a preliminary physical interpretation. Marine Geology 37, 1–18.

Nowlin, W.D., Klinck, J.M., 1986. The physics of the Antarctic Circumpolar Current. Reviews of Geophysics 24, 469–491.

Nowlin, W.D., Zenk, W., 1988. Westward bottom currents along the margin of the South Shetland Island Arc. Deep-Sea Research 35, 269–301.

Powell, R.D., Alley, R.B., 1997. Grounding-line systems: processes, glaciological inferences and the stratigraphic record. In: Barker, P.F., Cooper, A.K. (Eds.), Geology and Seismic Stratigraphy of the Antarctic Margin: 2. Antarctic Research Series, Vol. 71. American Geophysical Union, Washington, DC, pp. 169–142.

Pudsey, C.J., 1992. Late Quaternary changes in Antarctic bottom water velocity inferred from sediment grain size in the northern Weddell Sea. Marine Geology 107, 9–33.

Read, J.F., Pollard, R.T., Morrison, A.I., Symon, C., 1995. On the southerly extent of the Antarctic Circumpolar Current in the southeast Pacific. Deep-Sea Research II 42, 933–954.

Rebesco, M., Larter, R.D., Camerlenghi, A., Barker, P.F., 1996. Giant sediment drifts on the continental rise west of Antarctic Peninsula. Geo-Marine Letters 16, 65–75.

Rebesco, M., Larter, R.D., Barker, P.F., Camerlenghi, A., Vanneste, L.E., 1997. The history of sedimentation on the continental rise west of Antarctic Peninsula. In: Barker, P.F., Cooper, A.K. (Eds.), Geology and Seismic Stratigraphy of the Antarctic Margin: 2. Antarctic Research Series, Vol. 71. American Geophysical Union, Washington, DC, pp. 29–49.

SCAR, 1992. A SCAR seismic data library system for cooperative research: summary of the international workshop on Antarctic seismic data. SCAR Report No. 9, Scott Polar Research Institute, Cambridge, 15 pp.

Smith, W.H.F., Sandwell, D.T., 1997. Global seafloor topography from satellite altimetry and ship depth soundings. Science 277, 1956–1962.

Stow, D.A.V., 1994. Deep-sea processes of sediment transport and deposition. In: Pye, K. (Ed.), Sediment Transport and Depositional Processes. Blackwell, Oxford, pp. 257–291.

Tomlinson, J.S., Pudsey, C.J., Livermore, R.A., Larter, R.D., Barker, P.F., 1992. Long-range sidescan sonar (GLORIA) survey of the Antarctic Peninsula pacific margin. In: Yoshida, Y., Kaminuma, K., Shiraishi, K. (Eds.), Recent Progress in Antarctic Earth Science. Terra Scientific Publishing, Tokyo, pp. 423–429.

Tucholke, B.E., 1977. Sedimentation processes and acoustic stratigraphy in the Bellingshausen Basin. Marine Geology 25, 209–230.

Tucholke, B.E., Houtz, R.E., 1976. Sedimentary framework of the Bellingshausen Basin from seismic profiler data. In: Hollister, C.D., et al. (Eds.), Initial Reports of the Deep Sea Drilling Project, Vol. 35. US Government Printing Office, Washington, DC, pp. 197–227.

Vanney, J.R., Johnson, G.L., 1976. The Bellingshausen–Amundsen basins (southeastern Pacific): major sea-floor units and problems. Marine Geology 22, 71–101.

Wright, R., Anderson, J.B., Fisco, P.P., 1983. Distribution and association of sediment gravity flow deposits and glacial/glacial marine sediments around the continental margin of Antarctica. In: Molina, B.F. (Ed.), Glacial Marine Sedimentation. Plenum, New York, pp. 265–300.

Yamaguchi, K., Tamura, Y., Mizukosho, I., Tsuru, I., 1988. Preliminary report of geophysical and geological surveys in the Amundsen Sea, West Antarctica. Proc. NIPR Symp. Antarctic Geosci. 2, 55–67.

Publication 6.3.2:

Scheuer, C., **Gohl, K.**, Larter, R.D., Rebesco, M., Udintsev, G. (2006a). Variability in Cenozoic sedimentation along the continental rise of the Bellingshausen Sea, West Antarctica. *Marine Geology,* v. 277, pp. 279-298.

Author contributions: Gohl was the initiator and principle investigator of this project, funded by the Deutsche Forschungsgemeinschaft, on sedimentation processes of the continental rise along the Bellingshausen and Amundsen Sea margin. Scheuer wrote most of this paper as part of his PhD project supervised by Gohl. Larter, Rebesco and Udintsev added to the discussion of the results. Most of the seismic data were collected during Polarstern expedition ANT-XXVIII/5a (2001) with Gohl as project leader. Rebesco provided additional data.

ELSEVIER

Marine Geology 227 (2006) 279 – 298

MARINE GEOLOGY
INTERNATIONAL JOURNAL OF MARINE GEOLOGY, GEOCHEMISTRY AND GEOPHYSICS

www.elsevier.com/locate/margeo

Variability in Cenozoic sedimentation along the continental rise of the Bellingshausen Sea, West Antarctica

Carsten Scheuer [a,*], Karsten Gohl [a], Robert D. Larter [b], Michele Rebesco [c], Gleb Udintsev [d]

[a] *Alfred Wegener Institute for Polar and Marine Research (AWI), Postfach 120161, D-27515, Bremerhaven, Germany*
[b] *British Antarctic Survey (BAS), High Cross, Madingley Road, Cambridge CB3 OET, UK*
[c] *Istituto Nazionale di Oceanografia e di Geofisica Sperimentale (OGS), Borgo Grotta Gigante 42/C, 34010 Sconico (TS), Italy*
[d] *Vernadsky Institute of Geochemistry and Analytical Chemistry, Russian Academy of Sciences, 19, Kosygin Str, 117975 Moscow, Russia*

Received 29 September 2004; received in revised form 16 December 2005; accepted 21 December 2005

Abstract

Seismic reflection profiles, bathymetric and magnetic data collected along and across the continental margin of the Bellingshausen Sea provide new constraints and interpretations of the oceanic basement structure and Cenozoic glacial history of West Antarctica. Evidence for tectonic boundaries that lie perpendicular to the margin has been identified on the basis of one previously unpublished along-slope multichannel seismic reflection profile. By combining several magnetic data sets, we determined basement ages and verified the positions of possible fracture zones, enabling us to improve previous tectonic and stratigraphic models. We establish three main sediment units on the basis of one seismic along-slope profile and by correlation to the continental shelf via one cross-slope profile. We interpret a lowermost unit, Be3 (older then 9.6 Ma), as representing a long period of slow accumulation of mainly turbiditic sediments. Unit Be2 (from about 9.6 to 5.3 Ma) may represent a period of short-lived ice advances on the continental shelf. The uppermost unit, Be1 (from about 5.3 Ma to present), apparently consists of rapidly deposited terrigenous sediment that we interpret as having been transported to the shelf edge by frequent advances of grounded ice. Listric faults are observed in Be1 and indicate sediment instability due to interactions between different depositional processes. Correlation of the sediment classification scheme with the continental rise of the western Antarctic Peninsula shows obvious differences in sediment depositional patterns. We estimate a very high sedimentation rate for Unit Be1 (up to 295 m/my) which points to an increase in glacial sediment supply due to major glacial outlets that flowed to nearby parts of the shelf edge in Pliocene and Quaternary times. This is in contrast to the situation at the adjacent Antarctic Peninsular margin and many other parts of the continental rise around Antarctica.

Keywords: West Antarctica; Bellingshausen Sea; continental margin; continental rise; sedimentation; Miocene; seismic reflection; sediment drifts

1. Introduction

Since ice sheets first advanced onto the continental shelves around West Antarctica, alternations of glacial and interglacial periods have had a major influence on the sediment supply across the shelf and into the deep

* Corresponding author. Tel.: +49 471 4831 1948; fax: +49 471 4831 1271.
E-mail addresses: cscheuer@awi-bremerhaven.de (C. Scheuer), rdla@bas.ac.uk (R.D. Larter), rebesco@ogs.trieste.it (M. Rebesco).

0025-3227/$ - see front matter © 2006 Elsevier B.V. All rights reserved.
doi:10.1016/j.margeo.2005.12.007

sea. The patterns of deposition of late Cenozoic sediments along the slope and rise of the West Antarctic continental margin reflect interaction between the effects of ice sheet fluctuations, mass transport processes and bottom currents (Larter and Cunningham, 1993; Rebesco et al., 1996, 1997, 2002; Nitsche et al., 2000). Thus, both the sediment stratigraphy and the physiography of the sea floor reflect the history of the West Antarctic glaciation as well as the processes that eroded, transported and deposited sediments on the outer shelf, slope and rise of the continental margin.

The first multi-channel seismic profiles in the Bellingshausen Sea were collected in 1993 (Cunningham et al., 1994). In this paper we present a new profile, AWI-20010001, which connects a grid of previously recorded profiles west of the Antarctic Peninsula with a set of profiles in the western Bellingshausen Sea and eastern Amundsen Sea (Fig. 1). Together with slope-parallel seismic lines in the east and west, it forms a transect that is over 2000 km long and enables a correlation of deposition and transport processes along the entire West Antarctic continental rise of the south-eastern Pacific.

Previous investigations at different sites on the Antarctic continental margins show glacial related sediment supply to the continental rise since the Late Miocene and a decrease in sedimentation rates since the Pliocene (results from ODP Legs 178 and 188, see e.g. De Santis et al., 1995; Barker and Camerlenghi, 2002; Iwai et al., 2002). The continuation of this survey effort into the largely unexplored Bellingshausen Sea is one of the goals of this study. In particular, this paper will discuss the influence of grounding ice development on sedimentation processes since the Late Miocene.

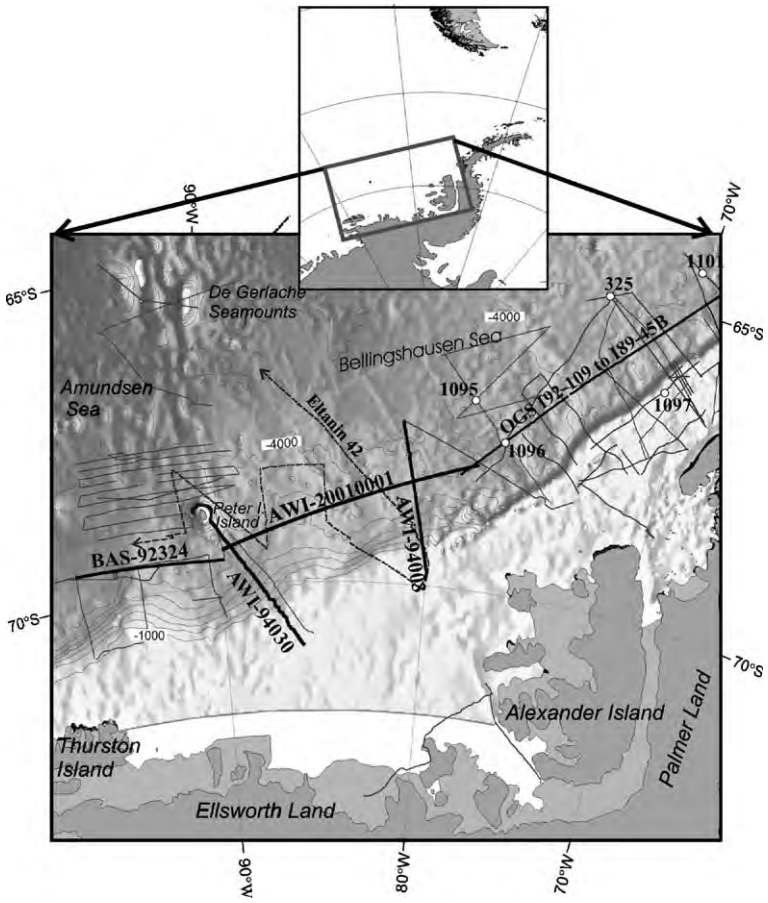

Fig. 1. Satellite-derived predicted bathymetric map (Smith and Sandwell, 1997) of the Bellingshausen and eastern Amundsen Sea and the West Antarctic continental margin with tracks of seismic lines. The multichannel seismic (MCS) profiles AWI-94003, AWI-94030 and AWI-20010001 were recorded in 1994 and 2001, respectively, with *RV Polarstern*. The British Antarctic Survey collected MCS profile BAS-92324 during a *RRS James Clark Ross* cruise in 1993. The dashed line shows the track of single channel seismic data, acquired during a *USNS Eltanin* cruise in 1970 (e.g. Tucholke and Houtz, 1976). The thin lines show additional seismic profiles which are not used in this paper. Drill sites of DSDP Leg 35 and ODP Leg 178 are marked with white dots.

2. Tectonic–sedimentary background

This section briefly summarises previous knowledge of the tectonic and sedimentary history of the West Antarctic continental margin. An understanding of the evolution of the oceanic basement and its tectonic structures is important for the estimation of sediment ages. Furthermore, an understanding of the glacial sediment transport processes should help clarify the relationship between advances of grounded ice on the continental shelf during glacial times and the associated development and structure of sediment deposits on the continental slope and rise.

2.1. Basement evolution

The active continental margin of the Bellingshausen Sea and the western Antarctic Peninsula was converted to a passive margin via a series of ridge–trench collisions of the Antarctic–Phoenix ridge that progressively migrated towards the northeast. Such ridge–trench interactions began at about 50 Ma east of Peter I Island and continued until about 3 Ma at the northern end of the Antarctic Peninsula at about 62.5°S (e.g. Barker, 1982; Larter and Barker, 1991; Larter et al., 1997, 1999; Eagles et al., 2004b). The spreading corridors that formed by the action of these ridge segments are separated from one another by fracture zones that are oriented approximately perpendicular to the trench.

The boundary with the Amundsen Sea just to the west can be defined along a set of north–south trending tectonic lineations of which the western branch is named the Bellingshausen Gravity Anomaly (BGA). The BGA corresponds to a buried basement trough where Cretaceous oceanic basement dips beneath more elevated basement to the east (Gohl et al., 1997; Cunningham et al., 2002). Convergent motion at this tectonic boundary occurred in the late Cretaceous from 79 to 61 Ma (Larter et al., 2002; Cunningham et al., 2002; Eagles et al., 2004a,b). The oceanic crust in between the BGA and Peter I Island has recently been interpreted as having formed as part of the erstwhile Charcot Plate (Larter et al., 2002; Eagles et al., 2004b).

2.2. Glacial history and sediment transport

Geophysical and geological data constraining the glacial history of the Antarctic Peninsula and the Bellingshausen Sea come from both on- and offshore, predominantly from the Antarctic Peninsula margin. The earliest evidence of ice-rafted debris in the region has been found in sediments exposed on the King George Island in the South Shetland Islands. These sediments were dated as early Eocene by Birkenmajer (1991), but have been reinterpreted as Oligocene sediments by Dingle and Lavelle (1998) and Troedson and Smellie (2002). The earliest ice-rafted debris at DSDP Site 325 was identified in a Middle Miocene core (Hollister et al., 1976). A number of authors interpret compilations of benthic foraminiferal oxygen isotope data (e.g. Miller et al., 1987; Zachos et al., 2001) in terms of major ice-sheet expansions at the Eocene–Oligocene boundary and in the Middle Miocene. The Eocene–Oligocene shift in oxygen isotope ratios is now widely thought to be related to development of the East Antarctic ice sheet. However, the timing of the first development of large ice sheets on West Antarctic continental shelves remains a subject of debate. Data from the Pacific margin between the Antarctic Peninsula and the Ross Sea are sparse, but geophysical and ODP data acquired from the continental shelf and rise (Location shown in Fig. 1) give evidence that glacially transported sediments were supplied to the continental margin in the middle to Late Miocene (e.g. Bart and Anderson, 1995; Rebesco et al., 1997; Larter et al., 1997; Nitsche et al., 1997; Barker and Camerlenghi, 2002). A major change in sequence geometry on the outer shelf (start of progradation) was dated as Late Miocene at ODP Site 1097 and interpreted as the start of regular advances of grounded ice to the shelf edge (Barker and Camerlenghi, 2002). A widely held conceptual model of glacial sediment transport processes on this margin may be summarized as follows:

Deformation of subglacial till beneath ice streams is thought to be the main mechanism transporting sediment to the shelf edge, at least during the Late Miocene, Pliocene and Quaternary (Larter and Cunningham, 1993; Dowdeswell et al., 2004a). The ice grounding line advanced and retreated, controlled by climatic forcing and ice-sheet dynamics. During glacial maxima, grounded ice extended to the continental shelf edge, resulting in the transport of sediment by ice streams and deposition onto the slope (Fig. 2). Thus, prograding sequences and large oblique wedges developed often on the outer shelf and slope (e.g. Larter et al., 1997). Mass transport processes (slumps, slides, debris flows and turbidity currents) transported large volumes of sediment material from the continental slope to the deep basin. Numerous, large turbidity current channels, which cut on the lower slope and rise, are identified on many parts of the continental margin (e.g. Tomlinson et al., 1992; McGinnes et al., 1997; Anderson et al., 2001, Rebesco et al., 2002; Dowdeswell et al., 2004b).

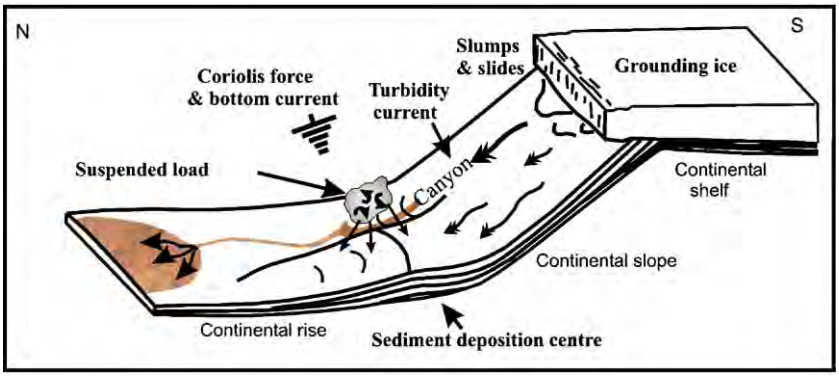

Fig. 2. Transport processes of eroded sediment material across the slope and depositional processes on the continental rise along the West Antarctic margin during glacial maxima (modified after Rebesco et al., 1997).

2.3. Physiographic expression

Published data on the physiographic expression of the Bellingshausen Sea is very sparse, coming from satellite derived bathymetry data (Smith and Sandwell, 1997) and a few seismic profiles (Fig. 1). The satellite bathymetry suggests a relatively even continental shelf and shelf widths varying from about 390 km east of Thurston Island to about 480 km west of Alexander Island. Three lobes on the continental shelf break that may have been produced by oceanward migration can be observed. Sediment supply from the vicinity of these lobes seems to have fed large sediment depocentres on the continental rise. The continental slope in the Bellingshausen Sea is gently inclined with a gradient between 1° and 4° and thus shallower than the slope observed northeast of 77°W along the western Antarctic Peninsula (gradient between 13° and 17°) (e.g. Cunningham et al., 1994; Nitsche et al., 1997).

3. Magnetic database

We interpreted helicopter magnetic data that were acquired during the *RV Polarstern* cruise ANT18-5a in 2001 in the eastern Bellingshausen Sea in order to investigate basement tectonic structures. Acquisition was with a Scintrex™ caesium-vapour magnetometer. The sensor tow-length was 30 m. Altitude ranged between 150 and 300 m, and the average helicopter speed was about 80 kn. Values of total magnetic intensity (measured in nT) were sampled at 100-ms intervals. All total magnetic intensity data were subsequently processed to eliminate high-frequency noise and spikes, and the global magnetic reference field (IGRF) was then subtracted from the data.

4. Seismic database and observations

Two cross-slope MCS profiles, AWI-94003 and AWI-94030, permit correlations between the outer continental shelf and the along-slope MCS profiles AWI-20010001 and BAS-92324 on the continental rise and, thus, enable a determination and interpretation of the sedimentary architecture on the continental margin of the Bellingshausen Sea. The recording methods for, and processing of the two cross-slope profiles are described by Nitsche et al. (1997). The acquisition and processing of Profile BAS-92324 were described by Cunningham et al. (1994). Profile AWI-20010001 was recorded using a 96 channel, 600 m hydrophone streamer and an array consisting of eight airguns with a total chamber capacity of 24 l. The shot interval was 12 s and the sampling interval was 2 ms. The seismic data were processed with standard procedures. After demultiplexing and applying a spherical divergence correction, the data were sorted and binned into 12.5 m spaced CDP's. A bandpass filter between 10 and 90 Hz was applied prior to normal move-out correction and stacking. We used a deconvolution filter to minimize the bubble effect and sharpen the reflection arrivals. Due to the short streamer and thus short move-out, the quality of the velocity model was not good enough for an appropriate estimate of interval velocities. Hence, all depth values in the following section are only roughly estimated by assuming an average interval velocity in sediment of 2000 m/s.

4.1. Basement structure

The along-slope seismic reflection profile AWI-20010001 (Figs. 3, and 4a, b and c) shows a distinct sediment-basement boundary, characterised by a downwards change from weak to very strong reflectivity. The

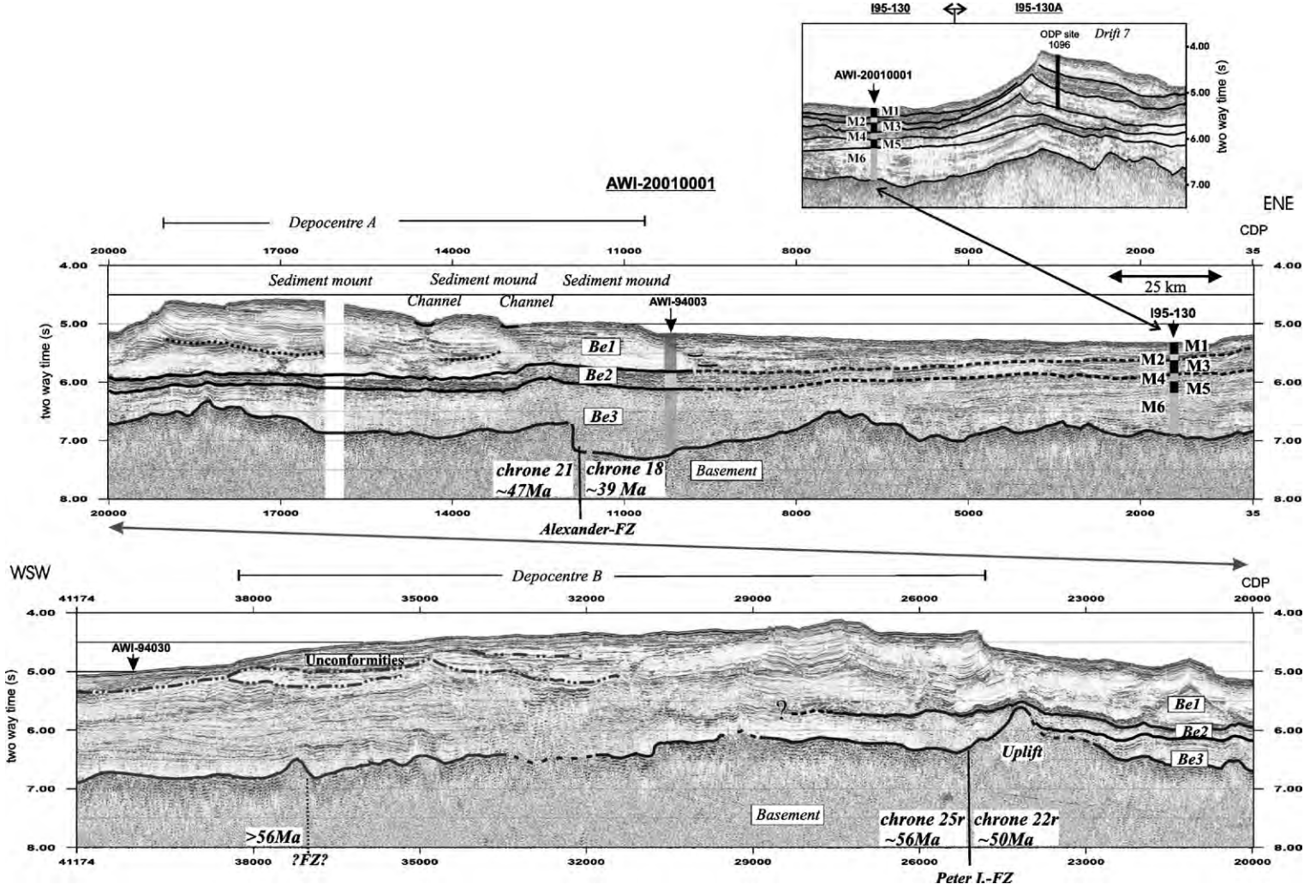

Fig. 3. Seismic reflection profile AWI-20010001, showing the inferred fracture zones and sediment units Be1–Be3. The eastward correlating profile I95-130 (shown above AWI-20010001) clarifies the age-correlation between both sediment classification schemes.

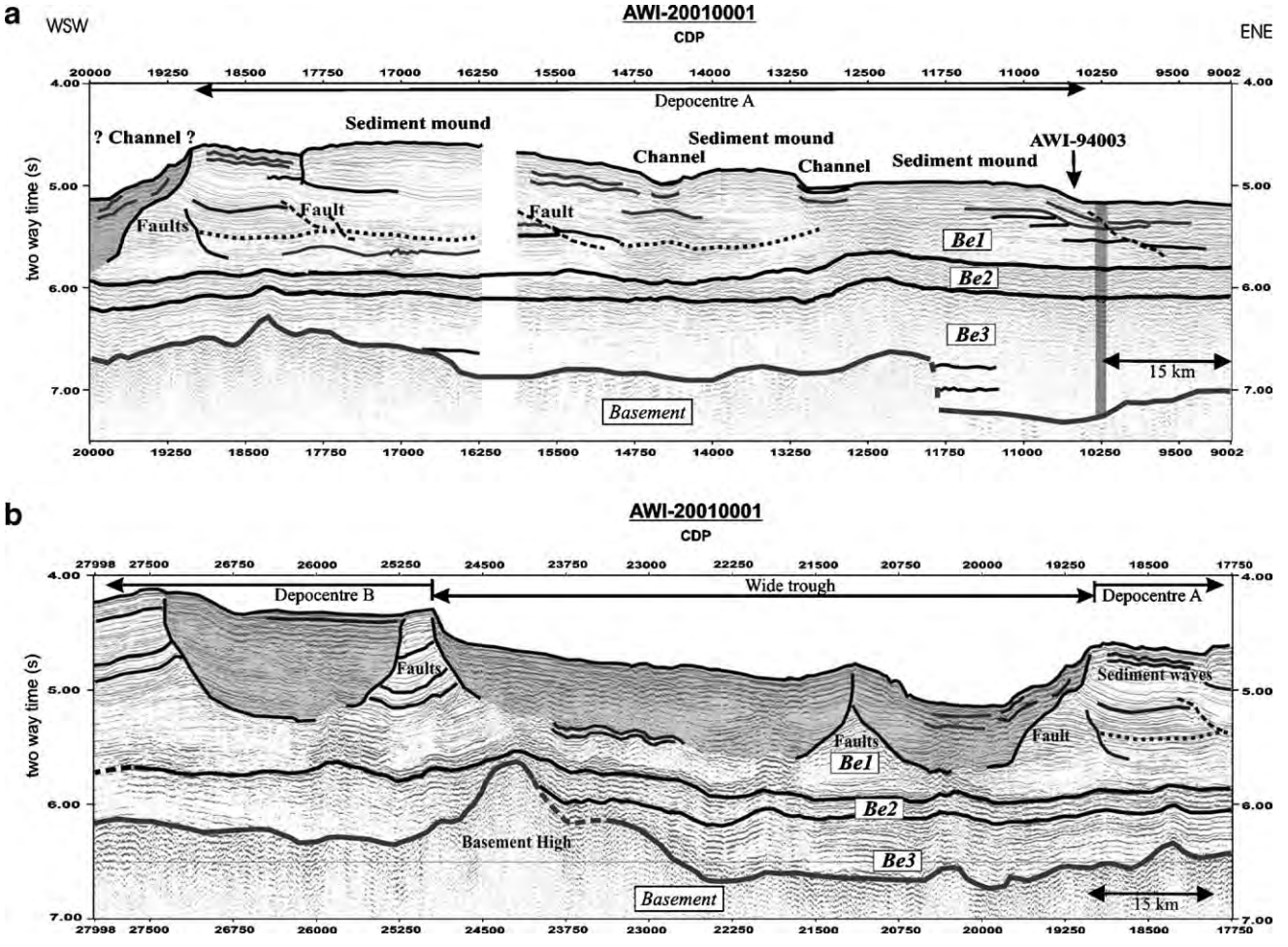

Fig. 4. Profile AWI-20010001 between (a) CDP 9000 and 20000, (b) CDP 17750 and 28000 and (c) CDP 24000 and 40000 with detailed sediment units. Arrows mark intersections with profiles AWI-94003 and AWI-94030.

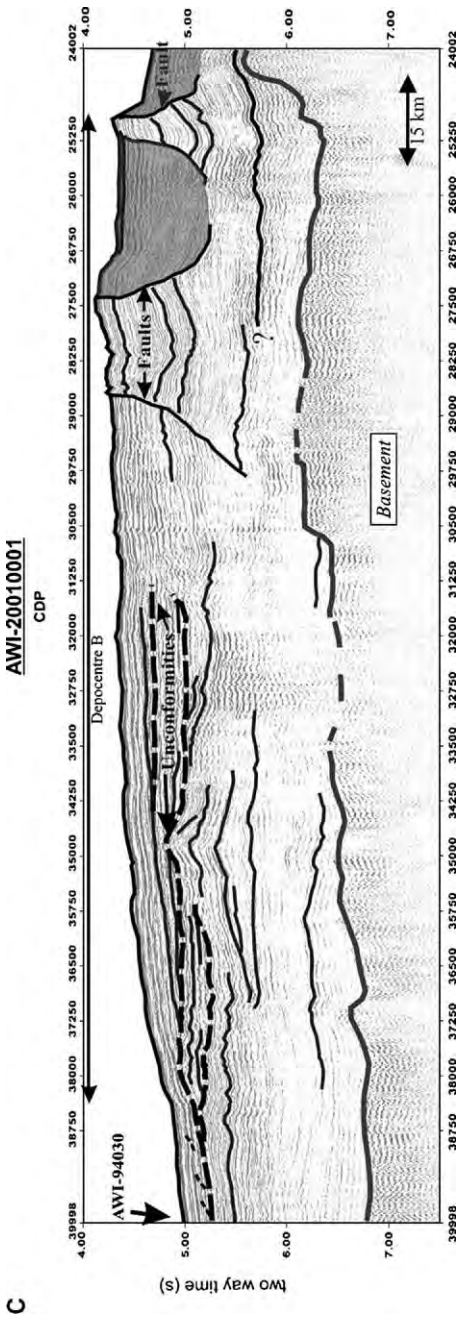

Fig. 4 (*continued*).

basement surface shows considerable relief, with basement highs, depressions and vertical offsets. Most conspicuous of these are a basement depression between CDPs 8000 and 11750 (up to 7.5 s TWT, about 2250 m b.s.f.), a steep basement step, of about 0.5 s TWT, to the west, and a wide basement high between CDPs 22500 and 25000. This basement high rises to approximately 5.8 s TWT (about 1000 m b.s.f.) with a relief of about 0.75 s TWT on the eastern side. The basement surface west of this basement high descends slightly to 6.75 s TWT at the end of the profile.

Continuing farther west, on profile BAS 92324 (Fig. 5), the basement surface descends smoothly westward between CDPs 1 and 1900. The rough and elevated basement between CDPs 1900 and 4000 descends to the west at a similar angle but it is characterized by several basement steps. West of CDP 5100, the basement rises up to 6 s TWT (400 m b.s.f.) towards a wide basement high at CDP 8200 on the eastern side of the BGA. The steep westerly dipping flank of the basement high dips to more than 8.5 s TWT (>2700 m b.s.f.), indicating the tectonic boundary at the BGA.

4.2. Sediment units

The cross-slope profiles AWI-94003 and AWI-94030 stretch from the outer shelf to the continental rise and cross profile AWI-20010001 near its eastern and western ends (at CDPs 10500 and 40000), respectively (Figs. 1 and 3). Profile AWI-94003 (Fig. 6) shows three units, Unit 1–Unit 3, previously defined beneath the outer shelf by Nitsche et al. (1997), and allows a regional continuation of their boundaries up to profile AWI-20010001 on the continental rise. This profile shows three sedimentary units, named as units Be1-3, whose boundaries present the distal paraconformities of the unit boundaries beneath the outer shelf. Be1–Be3 show different seismic reflections characteristics between CDPs 10000 and 28000 (eastern section, Figs. 3, and 4a, b and c). The lower unit, Be3, is characterized by low-amplitude and sub-parallel to parallel reflections, which are overlain by a set of strong reflections, unit Be2. The upper unit, Be1, is characterized by distinct parallel but weaker and faulted reflections and gentle mounds separated by channels.

In order to estimate sediment ages, we correlated the boundaries of units Be1–Be3 with previously established seismic units on the western Antarctic Peninsula continental rise (Rebesco et al., 1997) and continued the boundaries along assumed isochron reflections of profile AWI-20010001. The classification into three units cannot be adopted on profile AWI-20010001 west of about CDP 28000, where the sedimentary reflectors are characterised by undulations and unconformities (middle section). Accordingly, we describe the western part of the profile separately. Farther west, within the domain of the BGA, the sediments are strongly affected by basement tectonics as seen on profile BAS-92324 (western section, Fig. 5). This profile was previously described by Nitsche et al. (1997) and Cunningham et al. (2002) and here we give only a short overview of the main seismic features that are important for the later discussion.

4.2.1. Eastern section (profiles AWI-94003, AWI-20010001)

4.2.1.1. Outer continental shelf units (Unit 1, Unit 2, Unit 3). On the cross-slope profile AWI-94003, the lowermost outer shelf unit, Unit 1, consists of parallel and gently seaward dipping reflections, which are truncated seaward along the Unit 1/Unit 2 boundary (Fig. 6). Unit 1 closely resembles the Type IIA sequence as defined by Cooper et al. (1991) at various locations along the Antarctic continental margin. Unit 2 shows upward increasing seaward inclination of the reflections and truncation of reflections on top of the shelf deposits. On the basis of identification of foreset reflections and defining Unit 2 as containing few oblique foreset truncations beneath the outer shelf, we place the Unit 1/Unit 2 boundary approximately 0.8 s deeper than Nitsche et al. (1997) did. The uppermost unit, Unit 3, shows a mainly prograding character on the outer shelf, building a sediment wedge on the slope, whereas the uppermost 0.3 s TWT near the shelf edge is characterised by a smooth decrease in progradation. In contrast to Nitsche et al. (1997), we consider the Unit 2/Unit 3 boundary to lie about 0.2 s TWT deeper, because we interpret the boundary as the deepest erosional truncation to cross the entire outer shelf and truncate the top of Unit 2 on profile AWI-94003. Unit 3 and Unit 2 are characterized as having a Type IA geometry, after Cooper et al. (1991).

4.2.1.2. Lowermost continental rise unit (Be3). The lowermost sedimentary unit, Be3, that we define on Profile AWI 20010001 is a succession of weak but mostly horizontal and parallel-bedded reflections with variable amplitudes (Figs. 3, 4a and b). The maximum thickness of Be3 is 0.9 s TWT in the eastern part of the profile (at about CDP 10 500). Due to its low reflectivity, no distinct faults, hiatuses, or buried channels can be identified within Be3. The basal sediments fill basement

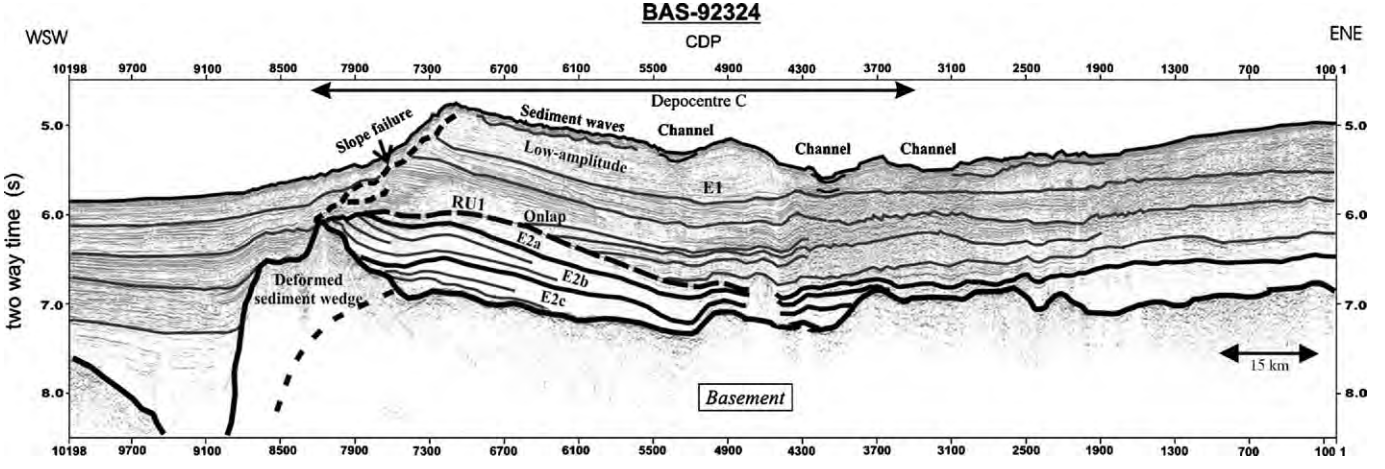

Fig. 5. Profile BAS-92324 between CDP 1 and 10200 with sediment units, modified after Cunningham et al. (2002) and Nitsche et al. (1997).

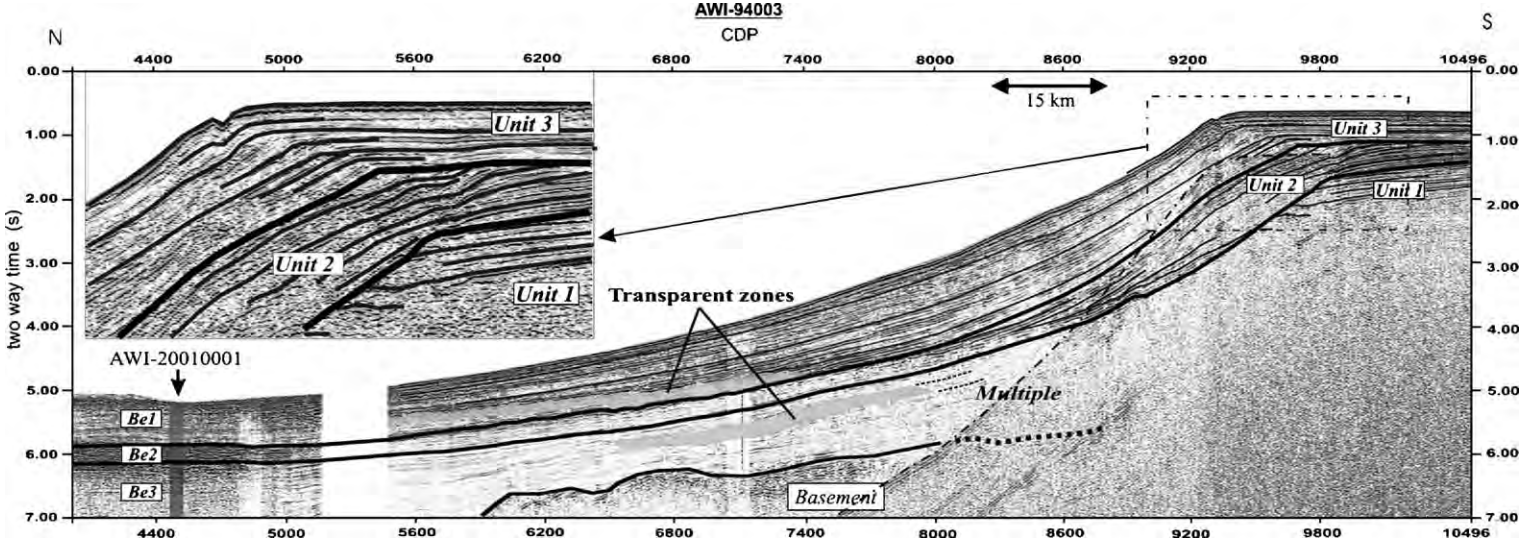

Fig. 6. Profile AWI-94003 with sediment units, Units 1–3, modified after Cunningham et al. (2002) and Nitsche et al. (1997).

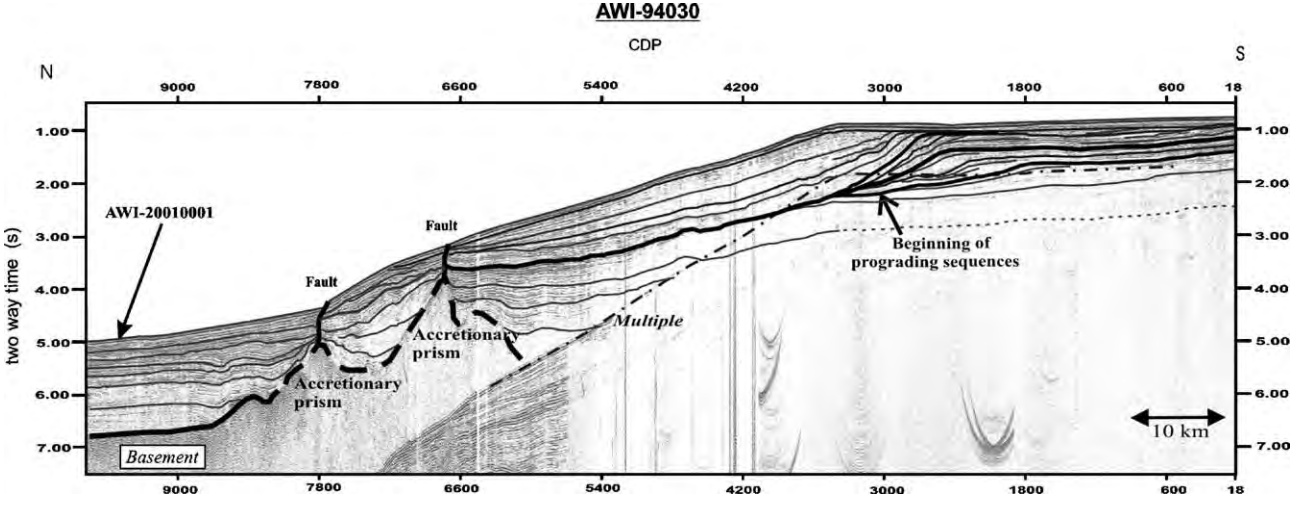

Fig. 7. Profile AWI-94030 with seismic stratigraphic sections, modified after Cunningham et al. (2002) and Nitsche et al. (1997).

C. Scheuer et al. / Marine Geology 227 (2006) 279–298

troughs and onlap the basement steps and most other basement highs, indicating pre-sedimentary tectonic activity (e.g. CDP 2500, 11900). The low reflectivity of this unit changes to stronger parallel reflections between CDP 18250 and the basement high at about CDP 24000. The sediments that cover the crest of the basement high are uplifted, which indicate post-sedimentary tectonic activity.

4.2.1.3. Intermediate continental rise unit (Be2). The low-amplitude reflections of unit Be3 are covered by a set of continuous and high amplitude reflections, unit Be2 (Figs. 3, 4a and b). The transition between these two units is gradual. The thickness of Be2 varies between approximately 0.4 s TWT (e.g. CDP 14250) and 0.5 s TWT (CDP 17750). Approaching the eastern side of the basement high (at about CDP 24000), the boundary becomes less clear due to the high-amplitude character of reflectors in both Be2 and Be3.

4.2.1.4. Uppermost continental rise unit (Be1). A change from the strong reflections of unit Be2 to the weaker reflections of unit Be1 above indicates a distinct change in depositional conditions (Figs. 3, 4a and b). Along profile AWI-20010001, Be1 can be seen to occur in two broad sediment depocentres, which we named Depocentre A (CDPs 10000–20000, east–west extent of approx. 125 km) and Depocentre B (CDPs 24500–38750, extent of approx. 180 km). Two channels divide Depocentre A into three sediment mounds (Figs. 3 and 4a). The lowermost part of Unit Be1 within Depocentre A shows low-amplitude reflections (Fig. 4a). This character changes upward to long, continuous, parallel, higher-amplitude, and smoothly undulating reflections.

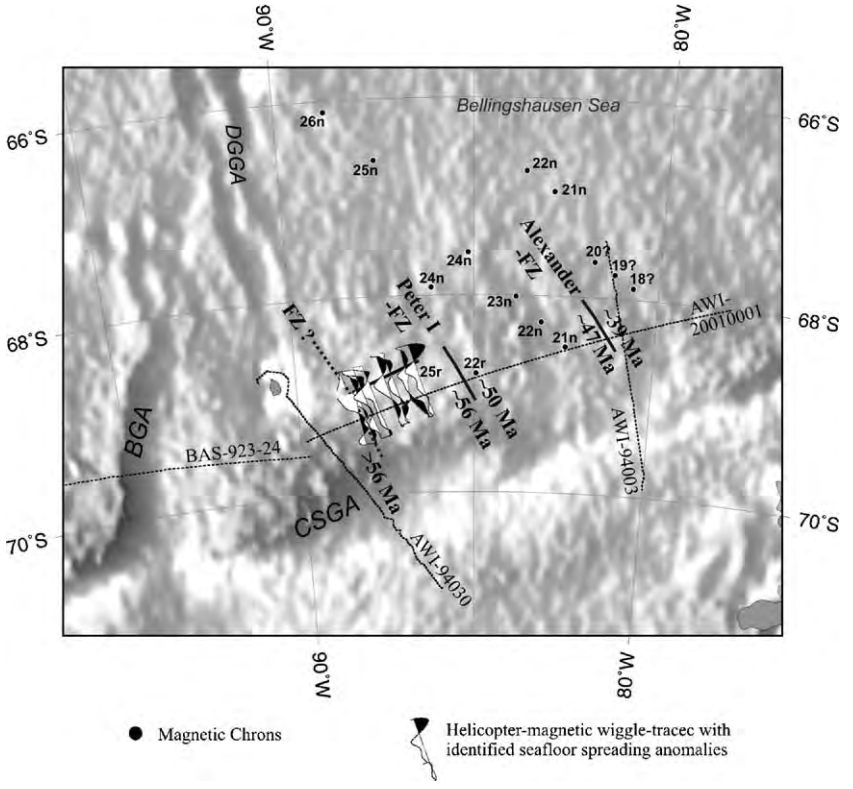

Fig. 8. Illuminated satellite-derived gravity anomaly map (McAdoo and Laxon, 1997) of the Bellingshausen Sea margin with isochrons identified from several cruises' ship-magnetic data and helicopter-magnetic data: The anomaly identifications 22n and 21n in the northwest are from a profile collected by *R/V Nathaniel B Palmer 9308* (2003), which we obtained from the National Geophysical Data Center GEODAS database (available online at http://www.ngdc.noaa.gov/mgg/gdas/gd_sys.html). The anomaly identifications to the southeast marked with question marks (20n–18n) are from a *R/V Hakurei-Maru* (1981) profile first published by Kimura (1982). Our interpretation of this profile is different from that published by Kimura. We interpret the anomaly he labelled as 20 as 18n. The two lines of anomaly identifications from 26n to 21n and from 24n and 22r were acquired by *USNS Eltanin 42* in 1970. A synthetic magnetic anomaly profile justifying the interpretation of the anomalies on the first of these two lines is included in McCarron and Larter (1998). The helicopter-magnetic wiggle plots in the eastern Bellingshausen Sea were produced from tracks flown during a *R/V Polarstern* cruise in 2001.

The uppermost 0.2 s TWT of Be1 show high-amplitude reflections and locally irregular sediment waves (e.g. CDPs 17000–19000). The ocean floor is rough, and two recent channels (CDPs 13000 and 14500) can be seen. Patches of chaotic and irregular reflections occur in a wide trough west of sediment Depocentre A (between CDP's 19250 and 24750), dissected by rounded, listric faults (Fig. 4b). Unit Be1 shows a similar succession of reflections in Depocentre B (CDP's 24750 to 28000), but they appear even more irregular, disturbed and wavy (e.g. CDP 28750) (Fig. 4b and c).

4.2.2. Middle section (profiles AWI-94030, AWI-20010001)

The characteristics of the sedimentary reflections change within Depocentre B, west of approximately CDP 28000. The lowermost 0.7–1.0 s TWT show weak and smooth reflectivity, so that there is no clear basis for differentiation of units Be3 and Be2. The uppermost 1–1.5 s TWT appear more laterally variable in reflection amplitude, showing sediment bulges (CDP 34750) and buried sediment waves (between CDPs 37250 and 38750). Inside this uppermost rough section we can identify unconformities (dashed lines, Fig. 4c), shown by onlapping and downlapping reflectors.

The cross-slope Profile AWI-94030 serves as another seismic connection between the continental rise and shelf (Fig. 7). This profile reveals two acoustic basement highs on the continental slope (CDP 5700 to 8800), interpreted as the top of an accretionary wedge, and probably composed of deformed and consolidated sediments (Cunningham et al., 2002). These features are probably the source of the negative "Continental Slope Gravity Anomaly" (CSGA) between 87°W and 92°W (Fig. 8). We identify several sedimentary sequences on the outer shelf where the prograding character increases upwards, following Nitsche et al. (1997). The boundaries of these sequences seem to merge farther down the slope (bold line), but reflectors cannot be reliably correlated with sediment deposits on the shelf due to the acoustic basement highs and faults within the sediment sequences.

4.2.3. Western section (profile 92324)

The sediments in the western section of the Bellingshausen Sea, within the domain of the BGA, are strongly affected by the underlying basement tectonics as seen on profile BAS-92324 (Fig. 5). An obvious sedimentary feature is a prominent unconformity, RU1, on the western side of the basement high (bold dashed line). Cunningham et al. (2002) divided the underlying sediments into three sediment units, E2a, E2b and E2c. Unit E2c consists of mostly basement-parallel reflectors and onlaps the crest of the basement high. All three units thin out to the east whereas Units E2b and E2a are truncated by RU1 to the west. This gently eastward dipping unconformity is characterised by onlap of the overlying reflectors, but it does not continue east of CDP 5000.

5. Discussion

5.1. Tectonic implications

Studies of magnetic seafloor spreading anomalies on the continental margin of the Bellingshausen Sea define basement ages ranging from 30 Ma northwest of Alexander Island (Larter and Barker, 1991) to 45 Ma in the Bellingshausen Sea at about 87°W (McCarron and Larter, 1998) (Fig. 8). The basement step at CDP 11900 on Profile AWI-20010001 seems to coincide with a change in basement age from about 39 Ma (chron 18) in the east to about 47 Ma (chron 21) in the west (Figs. 3 and 8), if chron 18 is accurately extrapolated from observed anomalies further northeast along the paleo-subduction zone. We interpret this basement step as a fracture zone (FZ), here named the Alexander FZ, although a clear identification in the satellite-derived gravity anomaly field is not possible. Another basement offset occurs at CDP 25000, with its eastern side elevated by about 0.5 s TWT. We suggest that this step may also have formed at a FZ, here named Peter I FZ (in reference to Kimura, 1982), because at the margin it separates anomaly 22r (50 Ma) in the east from anomaly 25r (56 Ma) in the west. The Alexander and Peter I FZs were previously interpreted as extensions of the Heezen and Tharp FZs, respectively (Barker, 1982). However, the Heezen and Tharp FZs were formed at the Pacific–Antarctic ridge and its precursor, the Pacific–Bellingshausen ridge, whereas the Alexander and Peter I FZs were formed in the Antarctic–Phoenix spreading system (e.g. Larter et al., 2002). Other basement offsets occur at CDPs 16250 and 37000, but magnetic data are too sparse to be able to say if they are related to FZs as well.

Basement ages west of the Peter I FZ, within the suggested Charcot plate fragment, remain uncertain due to a lack of reliable magnetic data. However, the lowermost sediments on the eastern part of profile BAS-92324 (CDP's 2100 and 4000) onlap uplifted basement segments, indicating tectonic movements prior to sedimentation (Fig. 5). The unconformity RU1 on the eastern side of the BGA, and the lowermost, slightly elevated, sediments above the unconformity indicate post-sedimentary movements on this eastern side of

the BGA, which represented a zone of convergence between 79 and 61 Ma (e.g. Eagles et al., 2004a,b; Larter et al., 2002; Gohl et al., 1997). If we assume that the unconformity formed at the end of uplift along the BGA at around 61 Ma (e.g. Cunningham et al., 2002), the sediments beneath this unconformity must be older than 61 Ma. It is possible that the westward thickening of the minor sedimentary units E2a, E2b and E2c (Cunningham et al., 2002) indicate a slightly westward dipping orientation of the basement before the uplift. The occurrence of three different minor units may indicate several phases of tectonic movements along the BGA (e.g. Eagles et al., 2004b). Alternatively, it cannot be excluded that bottom currents and climate changes might have been responsible for the differing reflection characteristics and deposition rates of these minor units.

5.2. Sedimentation processes

5.2.1. Geometric expression

Based on satellite-derived predicted bathymetry (Smith and Sandwell, 1997, Fig. 1) and seismic profiles (Figs. 3 and 5) we identified three sediment depocentres on the continental margin of the Bellingshausen Sea, lying in front of three shelf edge lobes. We refer to these as Depocentres A, B and C, from east to west (Fig. 9). Channels dissect Depocentre A into three minor sediment mounds that do not show the typical characteristics of sediment drifts as those observed along the

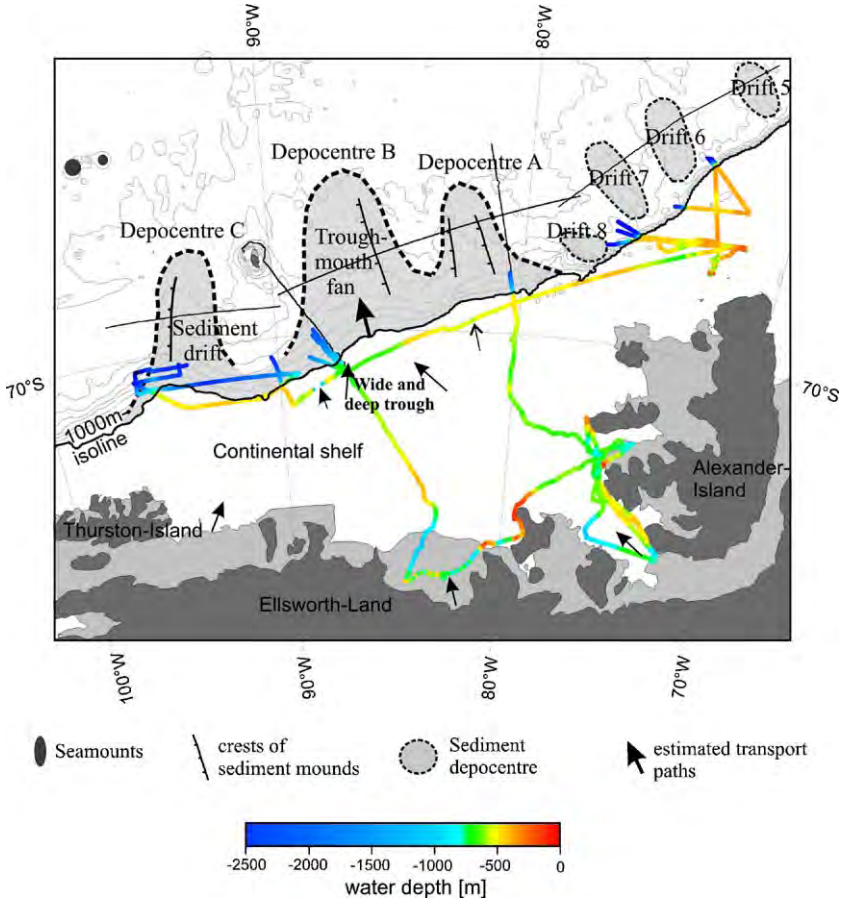

Fig. 9. Schematic model of sediment transport processes along the continental margin of the Bellingshausen Sea. Sparse bathymetric ship track data over the wide continental shelf between Alexander Island and Thurston Island, acquired on *RV Polarstern* cruises in 1994 and 2001, reveal depressions that may be parts of major cross-shelf glacial transport pathways. They show a broad trough in front of sediment Depocentre B, with water depths of up to 680 m in the centre and about 450 m at the rim. The existence of this trough is confirmed by additional bathymetric data recently collected on *RRS James Clark Ross* (Ó Cofaigh et al., 2005) and is consistent with our interpretation of Depocentre B being a wide deep-sea trough-mouth fan. A further, but shallower, outer shelf depression was observed farther northeast along the shelf-edge in front of sediment Depocentre A and may indicate the presence of a further, smaller glacial trough. The locations of the sediment drifts along the Antarctic Peninsula are schematically adopted from Rebesco et al. (2002).

western Antarctic Peninsula. Depocentre B is the broadest and lies in front of a seafloor depression on the continental shelf indicated by bathymetric ship track data (Fig. 9) and verified by multibeam echo soundings surveys on the outer shelf (Ó Cofaigh et al., 2005; Larter et al., 2004). Depocentre C lies over uplifted basement along the BGA lineation and constitutes a large asymmetric sediment mound with an east–west extent of about 100 km. This mound has been interpreted as a sediment drift, characterized by a steep western and a gentle eastern side, and two recent channels are observed on its gentle side (e.g. Nitsche et al., 1997). This entire depositional geometry on the continental rise of the Bellingshausen Sea is different to that on the adjacent Antarctic Peninsula margin where continental rise deposits developed as several discrete sediment mounds and drifts that are clearly separated by erosional channels (e.g. Rebesco et al., 1997, 2002).

5.2.2. Nature of sedimentary units

The correlation between continental rise- and shelf deposits via profile AWI-94003 and different seismic reflection characteristics of units Be1, Be2 and Be3 shows different sediment accumulation patterns, suggesting changes of sediment supply processes. We assume a mainly turbiditic origin for the lowermost continental rise unit Be3, following the interpretation, of "Pre-drift" and "Drift-growth" stages along the western Antarctic Peninsula by Rebesco et al. (1997). On the continental rise, the sediments infill low lying areas first and onlap onto basement topography, which is typical for turbidites. Furthermore, Early Miocene sediments, recovered in the deepest cores at DSDP Site 235, are primarily mostly terrigenous (Hollister et al., 1976).

The seismic characteristics of the outer shelf units, Unit 2 and Unit 3 (Fig. 6), appear similar to the sediment sequence groups S3–S2 and S1, respectively, which were established on the continental shelf of the western Antarctic Peninsula (e.g. Larter and Cunningham, 1993; Larter et al., 1997; Barker et al., 1999). Results from site 1097 of ODP Leg 178 show glacial influences as ice rafted till in S1, S2 and the upper part of S3 (e.g. Barker and Camerlenghi, 2002). The similarities of seismic reflection characteristics between S2 and Unit 2, and S1 and Unit 3, suggest glacial sediment transport during deposition of Unit 2 and Unit 3 and their correlating units Be2 and Be1 on the continental rise. Furthermore, Unit 2 and Unit 1 resemble the Type IA sequence, as defined by Cooper et al. (1991), which was interpreted to have been influenced by glacial erosion and transport processes. However, erosional truncations of prograding foresets are rarely seen within Unit 2, which may indicate ice expansion without a strong erosional effect on the outer continental shelf. One possible origin of the strong acoustic impedance contrasts in Be2 is the presence of extensive slide/debris flow deposits interbedded with fine grained hemipelagic sediments. The question of whether or not the base of Be2 represents the time of the first advance of grounded ice to the shelf edge remains open.

We think that the truncating unconformity beneath the outer shelf, between Unit 2 and Unit 3 (Fig. 6), most likely represents a strong erosional advance of grounded ice to the shelf edge, but we cannot define this as the first advance or advances of grounded ice to the shelf edge, because it could have removed evidence of previous ice advances. The onset of grounded ice events on the West-Antarctic continental shelf is still the subject of controversy and cannot be clarified in this study. However, we think that the change to strongly prograding units as shown by the Unit 2/Unit 3 boundary probably represents an important change in glacial dynamics that led to more strongly erosional ice advances. The boundary between units Be2 and Be1 coincides with a distinct buried acoustic reflector identified over a wide area on the Bellingshausen Sea continental rise by Tucholke and Houtz (1976) on *Eltanin-42* single channel data (track shown in Fig. 1), which demonstrates the regional extend of this boundary. Tucholke and Houtz named this reflector Horizon S. Comparison with data from other parts of the Antarctic continental slope and rise shows similar variations of seismic reflection characteristics from stratified units in the deeper part of a section to faulted reflections, channel levee complexes and other products of gravity driven processes in the upper part, as seen between Be2 and Be1. This change of seismic pattern is related to glacial erosion due to glaciation on the continental shelf (e.g. Hampton et al., 1987; Miller et al., 1990; Larter and Cunningham, 1993; Anderson, 1999).

The slightly decreasing progradation in the uppermost 0.3 s TWT of the outer shelf unit, Unit 3 (Fig. 6), is observed in the uppermost prograded sediments in many lines across the Antarctic Peninsula margin and elsewhere around Antarctica (e.g. Cooper et al., 1991; Bart and Anderson, 1995; Larter et al., 1997). Besides changes in climate and ice regime, a further influence on this change of progradation may be the fact that the most easily eroded sediment material is removed from the shelf by the first glaciations, leaving each subsequent glaciation with a deeper middle shelf and a more consolidated substrate. In this way, it is to be expected that erosion rates, and therefore sediment production rates, will decline with time given a sequence of glacial

advances of similar magnitude. A statement on the frequency of ice advances over the continental margin of the Bellingshausen Sea is not possible with available data because the nearest age control comes from drilling at ODP Leg 178 on the western Antarctic Peninsula margin (Fig. 1).

5.2.3. Age of sediment units

Direct correlation of the continental rise units Be1–Be3 with those of seismic profile I95-130 (of the Italian Programma Nazionale di Ricerche in Antartide, PNRA), recorded along the western Antarctic Peninsula, shows distinct differences in seismic stratigraphic pattern (Figs. 1 and 3) from which it is possible to infer differences in sediment supply and deposition on the Bellingshausen Sea and western Antarctic Peninsula margin. The units on the continental rise of the western Antarctic Peninsula were dated and classified by Rebesco et al. (1997, 2002) by correlation with ODP-sites from Leg 178 and one DSDP-site from Leg 35. The authors defined six stratigraphic units, numbered M1 to M6 from the seafloor down (Fig. 3). Units M6 (36–25 Ma) and M5 (25–15 Ma) were defined as a "Pre-drift Stage" and constitute turbiditic hemipelagic/pelagic, non-glacial sediments. Units M4 (15–9.6 Ma) and M3 (9.6–5.3 Ma), whose development was influenced by bottom currents, were ascribed to a "Drift growth Stage". The Units M2 (5.3–3.0) and M1 (3.0 Ma to the present) were interpreted as a "Drift maintenance Stage", showing mixed influence of bottom currents and glacial sediment transport. The westward continuation of sediment units M1–M6 on profile AWI-20010001 is not advisable due to the differences of the two sediment classification schemes. However, we can estimate the ages of units Be1–Be3 by correlating them with the units M1–M6. The correlation shows that the base of unit Be2 lies about 0.1 s TWT deeper than the base of Unit M3 (Fig. 3), interpreted as the base of mainly glacially derived sediment (Rebesco et al., 1997), and dated at 9.6 Ma using magnetostratigraphic data from ODP site 1095 (Iwai et al., 2002). Thus, discontinuous glacial sediment transport to the continental rise, which we infer to have produced Be2, started prior to 9.6 Ma. This conclusion is consistent with the result from ODP site 1095, where the base of glacially transported sediments was not reached and the oldest recovered material is dated at 9.6 Ma (Barker and Camerlenghi, 2002). The boundary between Be1 and Be2 coincides with the base of Unit M2, dated at 5.3 Ma (Iwai et al., 2002). With respect to our interpretation of the corresponding Unit 2/Unit 3 boundary on the outer continental shelf, we infer that the unit Be1/Be2 boundary indicates an increased sediment supply to the slope and rise due to grounded ice advances in the early Pliocene.

The change of seismic reflection characteristics west of approximately CDP 28 000 of profile AWI-20010001 can be explained by changing down-slope sedimentation processes. The acoustic basement highs along the continental slope acted as a barrier to the downslope sediment supply, as seen on Profile AWI-94030 (Fig. 7) and led to discontinuous sedimentation between the continental shelf and rise. This results in different sediment accumulation patterns, compared to the eastern section of the Bellingshausen Sea continental rise. The unconformities in the upper western part of profile AWI-20010001 (dashed lines, Figs. 3 and 4c) may be caused by changing patterns of downslope sediment deposition, for example in response to changes in sediment input, slope instability or bottom currents. Due to the discontinuity of reflectors across CDP 28 000, it is difficult to estimate the ages of sediment units identified on profile BAS-92324 (Fig. 5). Only the prominent unconformity, which may record the end of an uplift phase at the BGA at about 61 Ma (e.g. Cunningham et al., 2002), constitutes a datable reflector. The sediments above the unconformity must therefore constitute the entire sediment deposition of the last 61 m.y. but a reason for the lower sedimentation rate is not obvious from available data.

5.2.4. Sediment deposition rates

Estimates of sediment deposition rates in the depocentres provide the opportunity to evaluate their respective glacial-derived sediment supplies and compare these to other sediment depocentres on the Antarctic continental rise. In order to roughly estimate the sediment deposition rates of units Be1, Be2 and Be3, we calculated sediment thicknesses at two locations on profile AWI-20010001 using the empirical travel-time versus depth relation of Carlson et al. (1986). We chose positions at CDPs 16500 and CDP 27400, at the crests of sediment Depocentres A and B because of their great sediment thicknesses (Fig. 3). The results are very high sedimentation rates for Be1, with values of 247 m/m.y. (CDP 16500) and 295 m/m.y. (CDP 27500), in contrast to sedimentation rates in Be2 (106 m/m.y.) and Be3 (21 and 13 m/m.y.) (Table 1). In comparison, the highest known sedimentation rate on the western Antarctic Peninsula rise is about 180 m/m.y. in the early Pliocene (mainly Unit M2), calculated on the basis of magneto-biochronologic data from ODP site 1096 (Iwai et al., 2002). The low sedimentation rates of Be2 and Be3 are less then those of their equivalent units (M3, M4, M5, M6) farther north-east on the western Antarctic

Table 1
Variability in sedimentation of the Bellingshausen Sea

CDP	Unit	TWT [s]	Compacted thickness [s]	Sub-bott. depth [m]	Compacted thickness [m]	Age [Ma]	Sediment deposition rate [m/my]
16500	Be1	1.35	1.35	1310	1310	5.3	247
	Be2	1.70	0.35	1770	460	9.6	106
	Be3	2.20	0.50	2550	780	47	21
27400	Be1	1.55	1.55	1560	1560	5.3	295
	Be2 and 3	2.00	0.45	2220	660	56	13

Sediment depths, thicknesses and accumulation rates as estimated from the empirical travel-time versus depth relations for deep-sea sediments from Carlson et al. (1986). Depth (in km) is calculated as $Z=-(3.03\pm0.24)\ln[1-(0.52\pm0.04)T]$ where T is two-way travel-time in s.

Peninsula margin (Rebesco et al., 1997). The difference could be explained by a low rate of erosion prior to Pliocene times in the source area onshore. The BEDMAP compilation of subglacial topography (Lythe et al., 2000) shows that a large part of the subglacial rock surface in Ellsworth Land is below sea level. If the situation in the early Tertiary was similar, this area is unlikely to have been a significant source of eroded sediment material supplied to the continental margin. In contrast, the axis of the Antarctic Peninsula is a plateau, with peaks higher then 2000 m, and thus a more likely site for ice sheet nucleation during the Miocene and a more plentiful source of eroded sediment material.

High sedimentation rates within unit Be1 may be associated with development of very large ice drainage basins, high erosion rates on- and offshore, and high ice flow velocities during the Pliocene and Quaternary. Furthermore, the great width of the continental shelf (up to 480 km west of Alexander Island) may have led to increased glacial basal erosion and entrainment of sedimentary material due to the long transport distance. Sparse physiographic information about the Bellingshausen Sea continental shelf make estimates about transport paths during advances of grounded ice difficult. However, we assume that the western shelf trough indicated by swath bathymetry and sub-bottom profiler data in front of sediment Depocentre B (Fig. 9) acted as a major transport path for glacial sediment transport to the shelf edge. The cross-slope profile AWI-94030 shows that Depocentre B is not separated from the margin, but is in fact the lower part of a very uniform, low-angle, prograded slope (Fig. 7). These are typical characteristics of a trough mouth fan. Our estimation of a very high sediment deposition rate of unit Be1 and the structure and enormous width of Depocentre B support the interpretation of a trough mouth fan which seems to have been active in Pliocene and Quaternary times.

Although our calculations are crude approximations to sedimentation rates, the results nonetheless indicate a trend of increasing sediment accumulation rates since the early Pliocene. Conversely, ODP drilling on the continental margin of the western Antarctic Peninsula (Leg 178) indicate increasing deposition rates in the Late Miocene (base of unit M3) and a decrease in the Pliocene (base of unit M2, after Rebesco et al., 1997) (e.g. Iwai et al., 2002). This shows a remarkable difference in time of onset of high sediment deposition rates, which implies differences in the timing of the first erosional advance of grounded ice and, thus, variations of the glacial regime between the western Antarctic Peninsula and the Bellingshausen Sea continental margin. Further evaluations which could explain these differences in glacial development are not possible with existing data, but a complex history of multiple glacial advances and retreats in the Bellingshausen Sea can be inferred based on the presence of several thick prograding and aggrading sequence groups beneath the outer shelf as shown on Profile AWI-94030 (Fig. 7).

5.2.5. Faults in Unit Be1

Various processes may account for the structures in unit Be1 that resemble faults and listric shear planes, mainly observed between sediment Depocentres A and B (between CDPs 19000 and 28000) on profile AWI-20010001 (Fig. 4b). We suppose that these features are the product of complex interactions between depositional processes and slope instability. The high sedimentation rate could have led to a high pore-water content, which was expelled during diagenesis. A further important diagenetic process may have been the transformation of opal-A to opal-CT, as observed at sites 1095 and 1096 of ODP-Leg 178 (Volpi et al., 2003). Local differential compression and compaction affected the sediment pile's stability. This process may have resulted in stress-discharge of sediments to the sides of the sediment depocentres and in the development of faults. The fault between CDPs 19000 and 21000 may have developed along the migrating locus

of a facies boundary between the parallel layered sediments that accumulated on Depocentre A and a more chaotic regime on its steep western flank. At about CDP 24500, we can see the influence of basement structure on the stability of the upper sediments. Here, the crest of a basement high seems to act as a vertical wedge that amplifies the instability of the overlying sediments due to differential strain. Similar patterns have been observed in inter-drift areas along other Antarctic continental margins, such as along the western Antarctic Peninsula (e.g. Rebesco et al., 1997; Volpi et al., 2003) and in the Weddell Sea (e.g. Michels et al., 2002). Additional parallel seismic and bathymetric data are required to verify our suppositions concerning the occurrence of these faults.

6. Conclusions

This paper provides new constraints on the tectonic and large scale sedimentary architecture of the largely unexplored continental rise of the Bellingshausen Sea, mainly based on multi-channel seismic data. This study provides the following conclusions:

1) The basement structure on the continental rise permits the identification of tectonic fracture zones. At least two fracture zones (Alexander and Peter I FZs) and the ages of four spreading corridors can be estimated from seismic and magnetic data.

2) The sediment deposits in the middle part of the continental rise in the study area show distinct vertical variations in reflectivity characteristics. We divided the deposits into three sedimentary units, Be1–Be3, based on a correlation between the continental rise and the outer shelf via on cross-slope profile. On the continental rise, these three units can be correlated with stratigraphic Units M1–M6, identified on along-slope profiles on the western Antarctic Peninsula margin. Based on these correlations we infer:

The lowermost sedimentary unit, Be3, is older than 9.6 Ma. It probably consists of predominantly turbiditic sediments and the estimated sediment accumulation rate was low (up to 21 m/m.y.).

The intermediate sedimentary unit, Be2, was developed between about 9.6 and 5.3 Ma and can be correlated with an intermediate prograding sedimentary unit on the shelf edge. We assume that unit Be2 mainly consists of sediments transported by ice advances on the continental shelf, but without strong erosion of the shelf surface. The sediment accumulation rate is estimated to be up to 106 m/m.y.

The age of the uppermost sedimentary unit, Be1, ranges from about 5.3 Ma up to present. We interpret this unit as consisting predominantly of terrigenous sediment transported across the shelf edge by strongly eroding grounded ice on the shelf, as shown by strong truncations of underlain foresets and strong progradation. An approximate sediment accumulation rate of around 295 m/m.y. is the highest known on the west Antarctic margin.

3) The high sediment deposition rate of unit Be3 implies an increase of sediment supply to the continental rise due to frequent advances of grounded ice on the continental shelf in the Pliocene and Quaternary, which is contrary to a decrease of the sediment deposition rate since Pliocene times on other sites of the Antarctic continental margin. The reason for this discrepancy remains unclear.

4) Two wide and previously unsurveyed sediment depocentres are identified on the continental margin of the Bellingshausen Sea. We name them Depocentre A in the east and Depocentre B in the west, and we show that they have developed in Pliocene and Quaternary times. Depocentre B is interpreted as a trough mouth fan and may constitute the main discharge area for glacially derived sediment material.

5) We interpret faults and listric shear planes inside unit Be1, mainly observed between the two sediment Depocentres A and B, as the products of complex interactions between depositional processes and slope instability, reflecting the variability of sediment stability along the continental rise.

6) In the western Bellingshausen Sea, the characteristics of seismic reflections change entirely. Two along-slope orientated acoustic basement highs acted as barriers to sediment material supplied from the shelf, leading to a change in the conditions of sediment transport and deposition. The only clue to estimation of sediment ages west of 87°W is a prominent unconformity, identified on the elevated eastern side of a basement trough along the BGA. The unconformity is assumed to have developed at the end of tectonic uplift that occurred there around 61 Ma. The orientation of three westward thickening sedimentary minor units beneath the prominent unconformity may indicate a slightly westward dipping orientation of the basement before the uplift along the BGA.

Finally, we must emphasise that our interpretations in this paper about tectonic features and sediment deposits are mainly based on only one along-slope and one cross-slope seismic profile. To verify our conclusions and to improve knowledge about the tectonic and sedimentation history in the Bellingshausen Sea additional geophysical and geological investigations are required.

Acknowledgments

We are grateful to the masters, officers and crews of *RV Polarstern* and *RRS James Clark Ross*. This study is partly funded through grant no. GO 724/3-1 of the Deutsche Forschungsgemeinschaft (DFG). Italian contribution is supported by SEDANO and MAGICO projects of the Italian Programma Nazionale di Ricerche in Antartide (PNRA).

References

Anderson, J.B., 1999. Antarctic Marine Geology. Cambridge Univ. Press. 289 pp.

Anderson, J.B., Wellner, J.S., Lowe, A.L., Mosola, A.B., Shipp, S.S., 2001. The footprint of the expanded West Antarctic ice sheet: ice stream history and behaviour. GSA Today 11, 4–9.

Barker, P.F., 1982. The Cenozoic subduction history of the Pacific margin of the Antarctic Peninsula: ridge crest interactions. J. Geol. Sci. 139, 787–801.

Barker, P.F., Camerlenghi, A., 2002. In: Barker, P.F., Camerlenghi, A., Acton, G.D., Ramsay, A.T.S. (Eds.), Glacial history of the Antarctic Peninsula from Pacific margin sedimentsProc. ODP, Sci. Results, vol. 178. [online]. Available from World Wide Web: <http://wwwodp.tamu.edu/publications/178_SR/synth/synth.htm>.

Barker, P.F., Camerlenghi, A., Acton, G.D., et al., 1999. Proc. ODP, Init. Repts., 178 (CD-ROM). Available from: Ocean Drilling Program. Texas A&M University, Collage Station, TX 77845-9547, USA.

Bart, P.J., Anderson, J.B., 1995. Seismic record of glacial events affecting the Pacific margin of the northwestern Antarctic Peninsula. In: Cooper, A.K., Barker, P.F., Brancolini, G. (Eds.), Geology and Seismic Stratigraphy of the Antarctic Margin. Antarctic Research Series, vol. 68. American Geophysical Union, Washington, DC, pp. 75–95.

Birkenmajer, K., 1991. Tertiary glaciation in the South Shetland Islands, West Antarctica: evaluation of data. In: Thomson, M. R.A., Crame, J.A., Thomson, J.W. (Eds.), Geological Evolution of Antarctica. Cambridge University Press, Cambridge, pp. 629–632.

Carlson, R.L., Gangi, A.F., Snow, K.R., 1986. Empirical reflection travel time versus depth and velocity versus depth functions for the deep sea sediment column. J. Geophys. Res. 91, 8249–8266.

Cooper, A.K., Barrett, P., Hinz, K., Traubea, V., Leitchenkov, G., Stagg, H., 1991. Cenozoic prograding sequences of the Antarctic continental margin: a record of glacioeustatic and tectonic events. Mar. Geol. 102, 175–213.

Cunningham, A.P., Larter, R.D., Barker, P.F., 1994. Glacially prograded sequences on the Bellingshausen Sea continental margin near 90°W. Terra Antarctica 1, 267–268.

Cunningham, A.P., Larter, R.D., Barker, P.F., Gohl, K., Nitsche, F.-O., 2002. Tectonic evolution of the pacific margin of Antarctica: 2. Structure of late Cretaceous–early Tertiary plate boundaries in the Bellingshausen Sea from seismic reflection and gravity data. J. Geophy. Res. 107 (B12), 2346. doi:10.1029/2002JB001897.

De Santis, L., Anderson, J.B., Brancolini, G., Zayatz, I., 1995. Seismic record of late Oligocene through Miocene glaciation on the central and eastern continental shelf of the Ross Sea. Antarct. Res. Ser. 68, 235–260.

Dingle, R.V., Lavelle, M., 1998. Antarctic peninsular cryosphere: early Oligocene (c. 30 Ma) initiation and revised glacial chronology. J. Geol. Soc. 155 (3), 433–437.

Dowdeswell, J.A., Ó Cofaigh, C., Pudsey, C.J., 2004a. Thickness and extent of the subglacial till layer beneath an Antarctic paleo-ice stream. Geology 32, 13–16.

Dowdeswell, J.A., Ó Cofaigh, C., Pudsey, C.J., 2004b. Continental slope morphology and sedimentary processes at the mouth of an Antarctic palaeo-ice stream. Mar. Geol. 204, 203–214.

Eagles, G., Gohl, K., Larter, R.D., 2004a. Life of the Bellingshausen plate. Geophys. Res. Lett. 31, L07603.

Eagles, G., Gohl, K., Larter, R.D., 2004b. High resolution animated tectonic reconstruction of the South Pacific and West Antarctic margin. Geochem. Geophys. Geosyst. 5 (7), 1–21.

Gohl, K., Nitsche, F.O., Miller, H., 1997. Seismic and gravity data reveal Tertiary intraplate subduction in the Bellingshausen Sea, southeast Pacific. Geology 25, 371–374.

Hampton, M.A., Eittreim, S.L., Richmond, B.M., 1987. Post-breakup sedimentation on the Wilkes Land Margin, Antarctica. In: Eittreim, S.L., Hampton, M.A. (Eds.), The Antarctic Continental Margin, Geology and Geophysics of Offshore Wilkes LandCircum-Pacific Council for Energy and Mineral Recourses, Earth Science Series, vol. 5A, pp. 75–89.

Hollister, C.D., Craddock, C., et al., 1976. Initial Reports of Deep Sea Drilling Project, vol. 35. U.S. Government Printing Office, Washington D.C. 929 pp.

Iwai, M., Acton, G.D., Lazarus, D., Osterman, L.E., Williams, T., 2002. Magnetobiochronologic synthesis of ODP Leg 178 rise sediments from the Pacific sector of the Southern Ocean: Sites 1095, 1096 and 1101. In: Barker, P.F., Camerlenghi, A., Acton, G.D., Ramsay, A.T.S., (Eds.), Proc. ODP, Sci. Results, vol. 178, pp. 1–40. CD-Rom.

Kimura, K., 1982. Geological and geophysical survey in the Bellingshausen Basin, off Antarctica. Antarct. Rec. 75, 12–24.

Larter, R.D., Barker, P.F., 1991. Effects of ridge crest–trench interaction on Antarctic–Phoenix spreading: forces on a young subducting plate. J. Geophys. Res. 96, 19583–19608. doi:10.1029/2000JB000052 (2345).

Larter, R.D., Cunningham, A.P., 1993. The depositional pattern and distribution of glacial–interglacial sequences on the Antarctic Peninsula Pacific margin. Mar. Geol. 109, 203–219.

Larter, R.D., Rebesco, M., Vanneste, L.E., Gambôa, L.A.P., Barker, P. F., 1997. Cenozoic tectonic, sedimentary and glacial history of the continental shelf west of Graham Land, Antarctic Peninsula. In: Cooper, A.K., Barker, P.F. (Eds.), Geology and Seismic Stratigraphy on the Antarctic Margin: Part 2. American Geophysical Union, Antarctic Research Series, vol. 71. American Geophysical Union, Washington, DC, pp. 1–27.

Larter, R.D., Cunningham, A.P., Barker, P.F., Gohl, K., Nitsche, F.-O., 1999. Structure and tectonic evolution of the West Antarctic continental margin and Bellingshausen Sea. Korean J. Polar Res. 10, 125–133.

Larter, R.D., Cunningham, A.P., Barker, P.F., Gohl, K., Nitsche, F.-O., 2002. Tectonic evolution of the pacific margin of Antarctica: 1. Late Cretaceous tectonic reconstructions. J. Geophys. Res. 107 (B12).

Larter, R.D., Dowdeswell, J.A., Pudsey, C.J., Evans, J., Hillenbrand, C.-D., Morris, P., Ó Cofaigh, C., 2004. Investigations of a major palaeo-outlet of the West Antarctic ice sheet in the southern Bellingshausen Sea: preliminary results from *RRS James Clark Ross* Cruise JR104, Terra Nostra, Schriften der Alfred-Wegener_ Stiftung 2004/4, SCAR Open Science Conference Abstract

Volume, 252. http://www.scar28.org/SCAR/SCARmeeting/Wednesday/PDF/S_11_oral.pdf.

Lythe, M.B., Vaughan, D. G., BEDMAP Consortium, 2000. BEDMAP —Bed topography of the Antarctic, scale 1:10,000,000. Brit. Antarct. Surv., Cambridge, U.K. Available from World Wide Web: <http://www.antarctica.ac.uk/aedc/bedmap/database/>.

McAdoo, D.C., Laxon, S., 1997. Antarctic tectonics: constraints from an ERS-1 satellite marine gravity field. Science 276, 556–560.

McCarron, J.J., Larter, R.D., 1998. Late Cretaceous to early Tertiary subduction history of the Antarctic Peninsula. J. Geol. Soc. (Lond.) 155, 255–268.

McGinnes, J.P., Hayes, D.E., Driscoll, N.W., 1997. Sedimentary processes across the continental rise of the southern Antarctic Peninsula. Mar. Geol. 141, 91–109.

Miller, K.G., Fairbanks, R.G., Mountain, G.S., 1987. Tertiary oxygen isotope synthesis, sea-level history and continental margin erosion. Paleoceanography 2, 1–19.

Miller, H., Henriet, J.P., Kaul, N., Moons, A., 1990. A fine scale seismic stratigraphy of the eastern margin of the Weddell Sea. In: Bleil, U., Thiede, J. (Eds.), Geological History of the Polar Oceans: Arctic versus Antarctic. Kluwer Academ. Publ., Boston, pp. 131–161.

Michels, K.H., Kuhn, G., Hillenbrand, C.-D., Diekmann, B., Fütterer, D.K., Grobe, H., Uenzelmann-Neben, G., 2002. The southern Weddell Sea: combined contourite–turbidite sedimentation at the southeastern margin of the Weddell Gyre. In: Stow, D.A.V., Pudsey, C.J., Howe, J., Faugeres, J.-C., Viana, A. (Eds.), Deep-Water Contourite Systems: Modern Drifts and Ancient Series, Seismic and Sedimentary CharacteristicsSpec. Publ. Geol. Soc. London. Memoirs, vol. 22, pp. 305–323.

Nitsche, F.O., Gohl, K., Vanneste, K., Miller, H., 1997. Seismic expression of glacially deposited sequences in the Bellingshausen and Amundsen Seas, West Antarctica. In: Barker, P.F., Cooper, A. K. (Eds.), Geology and Seismic Stratigraphy of the Antarctic Margin: 2. Antarctic Research Series, vol. 71. American Geophysical Union, Washington, DC, pp. 95–108.

Nitsche, F.O., Cunningham, A.P., Larter, R.D., Gohl, K., 2000. Geometry and development of glacial continental margin depositional systems in the Bellingshausen Sea. Mar. Geol. 162, 277–302.

Ó Cofaigh, C., Larter, R.D., Dowdeswell, J.A., Hillenbrand, C-D., Pudsey, C.J., Evans, J., Morris, P., 2005. Flow of the West Antarctic ice sheet on the continental margin of the Bellingshausen Sea at the Last Glacial Maximum. J. Geophys. Res., 110, doi: 10.1029. 2005JB003619.

Rebesco, M., Larter, R.D., Camerlenghi, A., Barker, P.F., 1996. Giant sediment drifts on the continental rise west of the Antarctic Peninsula. Geo Mar. Lett. 16, 65–75.

Rebesco, M., Larter, R.D., Barker, P.F., Camerlenghi, A., Vanneste, L. E., 1997. History of sedimentation on the continental rise west of the Antarctic Peninsula. In: Cooper, A.K., Barker, P.F. (Eds.), Geology and Seismic Stratigraphy on the Antarctic Margin: 2. Antarctic Research Series, vol. 71. American Geophysical Union, Washington, DC, pp. 29–49.

Rebesco, M., Pudsey, C.J., Canals, M., Camerlenghi, A., Barker, P.F., Estrada, F., Giorgetti, A., 2002. Case study 27: sediment drifts and deep-sea channel systems, Antarctic Peninsula Pacific margin, mid-Miocene to present. In: Stow, D.A.V., Pudsey, C.J., Howe, J., Faugeres, J.-C., Viana, A. (Eds.), Deep-Water Contourite Systems: Modern Drifts and Ancient Series, Seismic and Sedimentary Characteristics. Spec. Publ. Geol. Soc. London. Memoirs, vol. 22, pp. 353–371.

Smith, W.H.F., Sandwell, D.T., 1997. Global seafloor topography from satellite altimetry and ship depth soundings. Science 277, 1956–1961.

Tomlinson, J.S., Pudsey, C.J., Livermore, R.A., Larter, R.D., Barker, P. F., 1992. Long-range sidescan sonar (GLORIA) survey of the Antarctic Peninsula pacific margin. In: Yoshida, Y., Kaminuma, K., Shiraishi, K. (Eds.), Recent Progress in Antarctic Earth Science. Terra Scientific Publishing Company, Tokyo, pp. 423–429.

Troedson, A.L., Smellie, J.L., 2002. The Polonez Cove Formation of King George Island, West Antarctica: stratigraphy, facies and palaeoenvironmental implications. Sedimentology 49, 277–301.

Tucholke, B.E., Houtz, R.E., 1976. Sedimentary framework of the Bellingshausen Basin from seismic profile data. In: Hollister, C.D., Craddock, C.D., et al. (Eds.), Initial Reports of the Deep Sea Drilling Project, vol. 35. U.S. Government Printing Office, Washington, DC, pp. 197–227.

Volpi, V., Camerlenghi, A., Hillenbrand, C.-D., Rebesco, M., Ivaldi, R., 2003. Effects of biogenic silica on sediment compaction and slope stability on the Pacific margin of the Antarctic Peninsula. Basin Res. 15, 339–363.

Zachos, J., Pagani, M., Sloan, L., Thomas, E., Billups, K., 2001. Trends, rhythms, and aberrations in global climate 65 Ma to present. Science 292, 686–693.

Publication 6.3.3:

Scheuer, C., **Gohl, K.**, Eagles, G. (2006b). Gridded isopach maps from the South Pacific and their use in interpreting the sedimentation history of the West Antarctic continental margin. *Geochemistry, Geophysics, Geosystems (G^3),* v. 7, doi:10.1029/2006GC001315.

Author contributions: Scheuer wrote most of this paper as part of his PhD project, supervised by Gohl, as extended synthesis with results of the previous two papers (6.3.3 and 6.3.4) and additional analyses. Gohl was the initiator and principle investigator of this project, funded by the Deutsche Forschungsgemeinschaft, on sedimentation processes of the continental rise along the Bellingshausen and Amundsen Sea margin. Gohl and Eagles added to the discussion of the results. A large part of the seismic data was collected during Polarstern expedition ANT-XXVIII/5a (2001) with Gohl as project leader.

Geochemistry Geophysics Geosystems G3
AN ELECTRONIC JOURNAL OF THE EARTH SCIENCES
Published by AGU and the Geochemical Society

Article
Volume 7, Number 11
21 November 2006
Q11015, doi:10.1029/2006GC001315
ISSN: 1525-2027

Gridded isopach maps from the South Pacific and their use in interpreting the sedimentation history of the West Antarctic continental margin

Carsten Scheuer, Karsten Gohl, and Graeme Eagles

Alfred Wegener Institute for Polar and Marine Research, Postfach 120161, D-27515 Bremerhaven, Germany (cscheuer@awi-bremerhaven.de)

[1] We model sediment isopach grids for the southern Pacific margin of West Antarctica on the basis of a compilation of more than 10,000 km of single-channel and multichannel seismic reflection data and correlations with ocean drilling sites. Following recent seismic stratigraphic models, we differentiate two main sequences, the upper of which alone is defined by seismostratigraphic indications for frequent grounded ice advances to the shelf edge off West Antarctica. The subsequent modeling of sediment thickness grids allows us to compare the pre-glacially dominated and glacially dominated sedimentary development of the study area. On the basis of available age constraints from drilling sites, we assume the onset of accumulation of sediments on the continental rise that were supplied by frequent advances of grounding ice on the continental shelf to have occurred at about 10 Ma. The thickest glacial sediment accumulations occur in front of major glacial drainage outlets, i.e., Marguerite Trough on the western Antarctic Peninsula margin, Belgica Trough in the Bellingshausen Sea, and a depression on the inner and middle shelves off Pine Island Bay in the Amundsen Sea. Glacially dominated sedimentation rates of between 140 and 170 m/m.y. are calculated for these sites.

Components: 10,227 words, 8 figures, 3 tables.

Keywords: Southern Pacific; West Antarctica; isopach grid; continental margin; sedimentation; sediment thickness; glaciation.

Index Terms: 3022 Marine Geology and Geophysics: Marine sediments: processes and transport; 3025 Marine Geology and Geophysics: Marine seismics (0935, 7294); 3045 Marine Geology and Geophysics: Seafloor morphology, geology, and geophysics.

Received 22 March 2006; **Revised** 31 July 2006; **Accepted** 11 August 2006; **Published** 21 November 2006.

Scheuer, C., K. Gohl, and G. Eagles (2006), Gridded isopach maps from the South Pacific and their use in interpreting the sedimentation history of the West Antarctic continental margin, *Geochem. Geophys. Geosyst.*, *7*, Q11015, doi:10.1029/2006GC001315.

1. Introduction

[2] The separation of Antarctica from the Australian and South American continents in Cenozoic times initiated the development of Southern Ocean currents, which were important for climate change [e.g., *Kennett*, 1977]. The opening of the Tasmanian and Drake Passage gateways were essential prerequisites for the development of the ring-shaped Antarctic Circumpolar Current (ACC), an important component of the modern oceans. This process may also have led to the gradual climatic

isolation of Antarctica [*Kennett*, 1977] and thus has been the focus of various climate model experiments investigating the glacial development of Antarctica [e.g., *Sijp and England*, 2004]. However, the opening of gateways is only one of the factors that influenced the development of circum-Antarctic currents. Several studies have shown that the ACC and Antarctic Bottom Water (AABW) are strongly guided by seafloor topography [e.g., *Lazarus and Caulet*, 1993; *Rack*, 1993]. Recent palaeobathymetric models were based on the kinematics and thermal subsidence rates of oceanic crust [e.g., *Sykes et al.*, 1998; *Brown et al.*, 2006], but lack any consideration of the effects of sediment distribution. For greater accuracy, sediment accumulations should also be taken into account in the next generation of paleobathymetric reconstructions. To do so will require gridded maps of sediment thickness.

[3] In this study, we present gridded sediment isopachs for the Pacific margin of West Antarctica. Large-scale maps of sediment thicknesses are essential prerequisites for the next generation of high-resolution paleobathymetric reconstructions. In addition, maps of sediment thicknesses on continental margins are useful for studies of terrigenous sediment supply and sediment distribution on the ocean floor. Thick sediments, deposited during glacial periods when grounded ice streams eroded the continental shelf, characterize high-latitude continental margins. These deposits provide an indirect record of glacial climate [e.g., *Cooper et al.*, 1991; *Tomlinson et al.*, 1992; *Larter et al.*, 1997; *McGinnes et al.*, 1997; *Anderson et al.*, 2001, *Rebesco et al.*, 1996]. It is possible to identify features in seismic data that are consistent with such an amplification of terrigenous sediment supply, and which can be related to the advance of grounded ice over the continental shelf to the shelf edge.

[4] In this study, we use features observed in seismic profiles to identify and map sedimentary units that formed (1) prior to advances of grounded ice on the continental shelf and (2) during later times when sediment supply was amplified due to advances of grounded ice to the shelf edge. The adoption of a date for the first development of grounded ice allows us to approximate sedimentation rates and thus make first, tentative, comparisons of local glacial sedimentation histories on the West Antarctic continental margin. Finally, comparisons of sedimentary structures on the Antarctic Peninsula and Amundsen Sea continental rises enable some speculations on the role of bottom currents in the Amundsen Sea.

2. Data and Knowledge Base

[5] Our calculation of sediment thicknesses is based on single-channel and multichannel reflection seismic profiles acquired between 1989 and 2001. Most of the seismic data are publicly available in the digital database of the SCAR Seismic Data Library System (SDLS, available from Instituto Nazionale di Oceanografia e Geophysica Sperimentale(OGS), Trieste, Italy). Seismic data that are not yet available in digital form are not included in this study. In addition, we have taken account of drilling data from Deep Sea Drilling Project (DSDP) Leg 35 and Ocean Drilling Program (ODP) Leg 178. All the seismic profiles and the ocean drilling sites are shown in Figure. 1.

2.1. Geological Setting

[6] The highest-resolution records of Cenozoic glaciation of West Antarctica are found in the thick sediments of trough mouth fans, such as the Crary Fan in the southern Weddell Sea [e.g., *Kuvaas and Kristoffersen*, 1991] or the recently mapped Belgica fan in the Bellingshausen Sea [*Ó Cofaigh et al.*, 2005; *Scheuer et al.*, 2006a]. Thick sediments have also accumulated on the sediment mounds, channel levees, and contourite drifts that developed due to interactions between turbidity currents and along slope bottom currents [e.g., *Rebesco et al.*, 1996, 1997, 2002; *Faugères et al.*, 1999; *Nitsche et al.*, 2000].

[7] Many authors have related features observed in seismic profiles to glacial influences on terrigenous sediment input. Studies show that these features include extensive prograding sequences on the outer continental shelf, thick sediment wedges on the slope, unconformities overlain by sediment mounds or drifts on the rise, and erosional channels caused by turbidity currents [e.g., *Hampton et al.*, 1987; *Cooper et al.*, 1991, 1995; *Rebesco et al.*, 1997, 2002; *Nitsche et al.*, 2000; *Cunningham et al.*, 2002; *DeSantis et al.*, 2003]. Around much of Antarctica, where the oceanic basement is old enough, the seismic stratigraphy shows a transition to these features from earlier patterns that resemble those on nonglaciated continental margins and are therefore presumably not influenced, or far less heavily influenced, by glacial processes.

[8] In the following, we give a brief overview of the topographic setting and recent knowledge of the sedimentation processes of the area offshore of

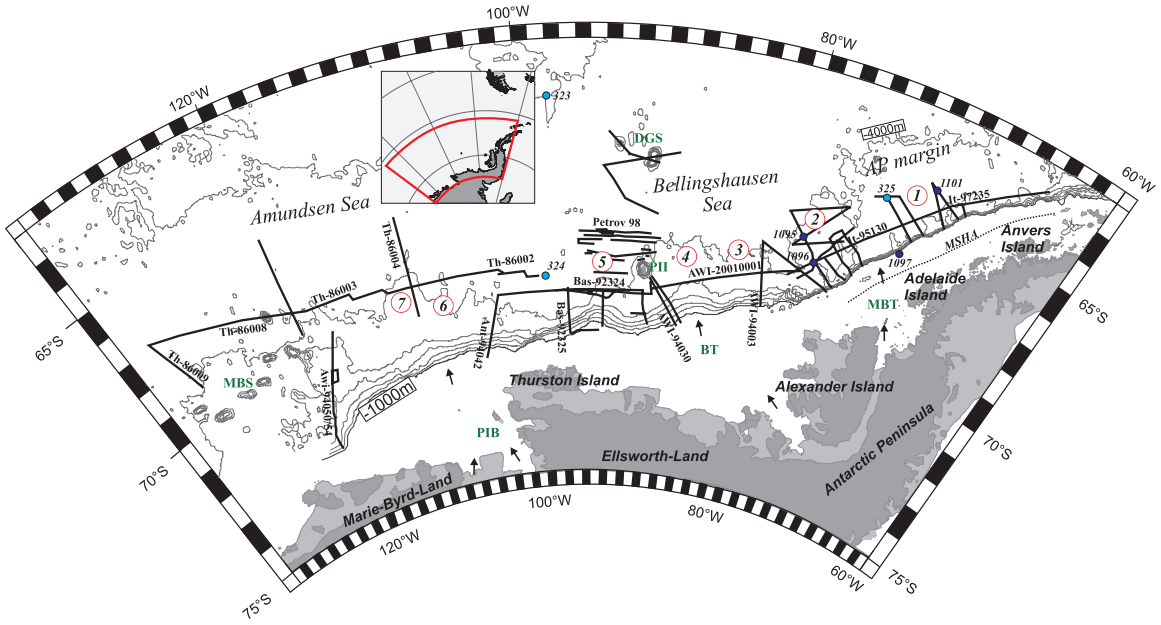

Figure 1. Overview of the South Pacific continental margin of West Antarctica, showing a network of digital available multichannel (MC) and single-channel (SC) seismic profiles (black lines) and contours of the satellite-derived predicted bathymetry from *Smith and Sandwell* [1997] (faint lines). Drill sites of DSDP Leg 35 and ODP Leg 178 are marked with black circles. Dark gray areas indicate landmasses, and medium gray indicates ice shelves. Important topographic locations are annotated. MBS, Marie Byrd Seamounts; PII, Peter I Island; DGS, DeGerlache Seamounts; PIB, Pine Island Bay; BT, Belgica Trough; MB, Marguerite Bay; MSHA, middle shelf high axis [after *Larter et al.*, 1997]. The numbers in red circles indicate the positions of some of the main sediment accumulation areas, also indicated by bathymetric contour lines. 1, drifts 3 and 4; 2, drifts 6 and 7; 3, depocenter A; 4, depocenter B; 5, depocenter C; 6, mounds Am3 and 3; 7, mound Am4.

the Antarctic Peninsula, the Bellingshausen Sea, and the Amundsen Sea.

2.1.1. Western Antarctic Peninsula Continental Margin

[9] A large number of seismic and bathymetric data [e.g., *Larter and Cunningham*, 1993; *Bart and Anderson*, 1995; *Rebesco et al.*, 1996, 1997, 2002; *McGinnes et al.*, 1997; *Dowdeswell et al.*, 2004; *Hernández-Molina et al.*, 2004, 2006] and the results of DSDP Leg 35, site 325 [e.g., *Hollister et al.*, 1976] and ODP Leg 178 [e.g., *Barker and Camerlenghi*, 2002] gave insights into the sedimentation history of the western Antarctic Peninsula margin (Figure 1). The interaction of a westward flowing bottom current with downslope turbidity currents led to the development of eight contourite drifts and three sediment mounds on the sides of downslope turbidity channels [e.g., *Larter and Cunningham*, 1993; *Camerlenghi et al.*, 1997; *Rebesco et al.*, 1997]. *Rebesco et al.* [1996, 1997] identified six sedimentary units, numbered M1 to M6, and related the M3/M4 boundary, where they observed amplified development of sediment drifts and the onset of erosional channels on the continental rise, to the onset of grounded ice advances on the shelf (e.g., drifts 6 and 7; Figure 2a). Ocean drilling at ODP site 1095 of Leg 178 recovered glacially transported sediment from just above the M3/M4 boundary, and dated it to 9.6 Ma, but did not reach the lower boundary of glacially influenced sediment units.

2.1.2. Bellingshausen Sea

[10] Seismic data from the Bellingshausen Sea are sparse, but allow the identification of three wide sediment depocenters on the continental slope (Figure 1). The largest, depocenter B, is interpreted as a trough mouth fan [*Ó Cofaigh et al.*, 2005; *Scheuer et al.*, 2006a]. Correlation of aggrading and prograding sequences, named units 1–3 and identified on the continental shelf/upper slope by *Nitsche et al.* [1997], with sediments on the continental rise near the easternmost depocenter, A, allowed the definition of three continental rise units, named Be1 to Be3 (e.g., Figures 2b and 2c) [*Scheuer et al.*, 2006a]. Correlation with the outer shelf units, the stratigraphy of the Antarctic Peninsula margin [*Rebesco et al.*, 1997], and ODP Leg 178 drilling results indicated that Be1 and Be2 consist predom-

Geochemistry Geophysics Geosystems G3 SCHEUER ET AL.: GRIDDED ISOPACH MAPS 10.1029/2006GC001315

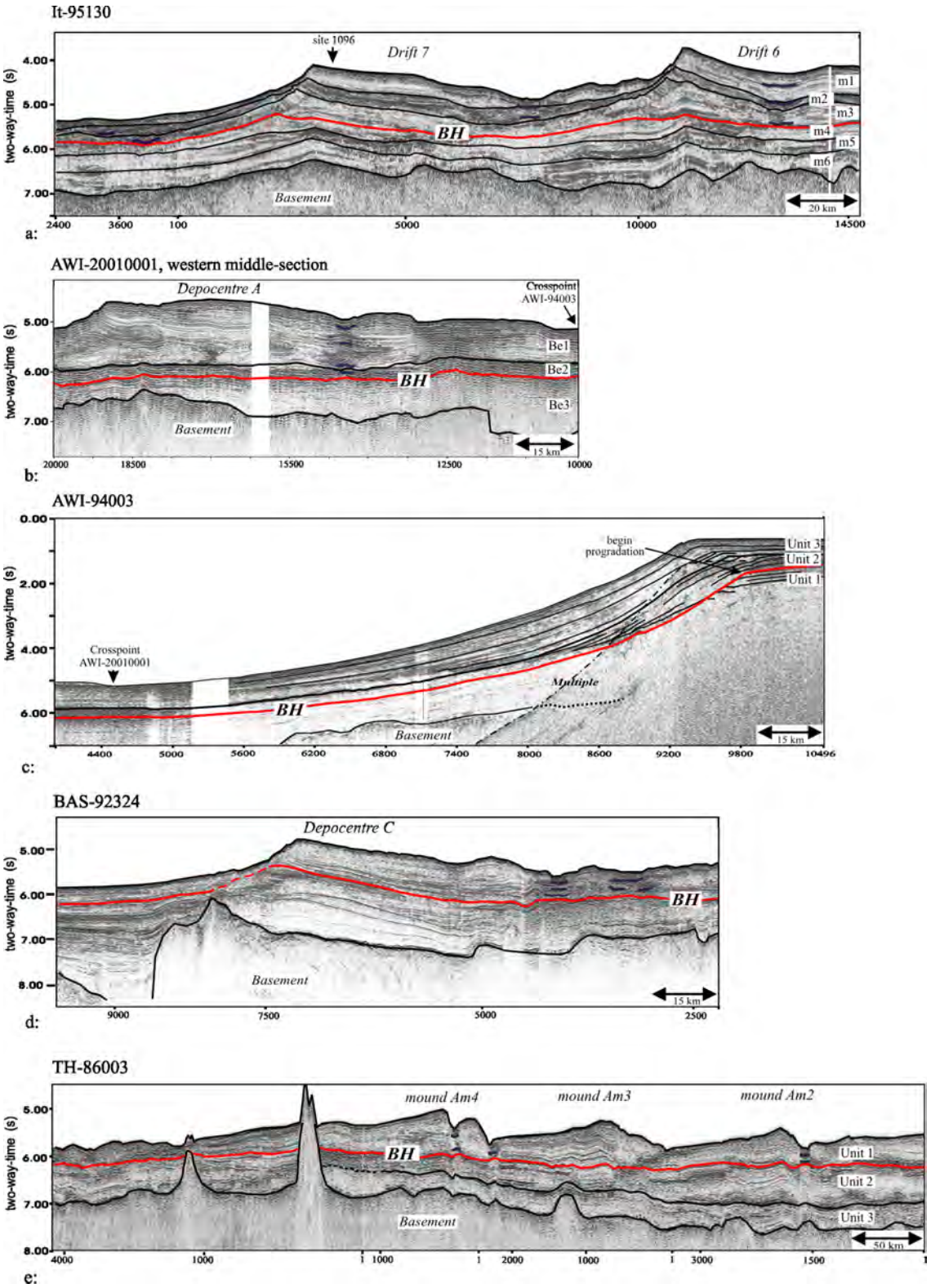

Figure 2. Interpreted line drawings of five MCS profiles on the South Pacific continental margin of West Antarctica. Interpretation of (2a) profile IT-95130 refers to *Rebesco et al.* [1997], (b and c) AWI-20010001 and AWI-94003 refers to *Scheuer et al.* [2006a], (d) BAS-92324 refers to *Cunningham et al.* [2002] and *Scheuer et al.* [2006a], and (e) TH-86003 refers to *Yamaguchi et al.* [1988]. In consideration of these interpretations we defined a boundary horizon (BH) between pre-glacially dominated and glacially dominated sediments derived from frequent grounding ice advances to the shelf edge.

inantly of glacially derived sediments, whereas the lowermost unit, Be3, developed prior to the onset of grounded ice on the shelf. No such correlation was possible for the western Bellingshausen Sea and Amundsen Sea, due to along-strike changes in the seismic stratigraphic characteristics [*Scheuer et al.*, 2006a]. Depocenter C is situated above a basement uplift at a north-south trending late Cretaceous tectonic lineation [e.g., *Gohl et al.*, 1997; *Larter et al.*, 2002] (Figure 1). On the upper continental rise, depocenter C resembles a sediment drift, but distally it has the features of a simple channel levee [*Nitsche et al.*, 1997; *Cunningham et al.*, 2002; *Scheuer et al.*, 2006a]. According to *Larter and Cunningham* [1993] and *Scheuer et al.* [2006b], the base of the drifts and channel levees indicate enhanced sediment supply to the continental rise due to advances of grounded ice to the continental shelf edge (Figure 2d).

2.1.3. Amundsen Sea

[11] The relief of the continental shelf is influenced by a large drainage outlet of the West Antarctic Ice Sheet in Pine Island Bay, which is fed by the Pine Island and Thwaites glaciers [e.g., *Vaughan et al.*, 2001; *Lowe and Anderson*, 2003; *Dowdeswell et al.*, 2006; *Evans et al.*, 2006]. Data on the continental slope and rise are scant. One seismic profile shows a prograding shelf edge [*Nitsche et al.*, 2000]. The Japan National Oil Company published seismic profiles that show several sediment mounds separated by channels in the east, and shallow basement and decreasing sediment thickness to the west, near the Marie Byrd Seamounts [*Yamaguchi et al.*, 1988] (Figures 1 and 2e). *Kimura* [1982] identified three sediment units, A, B and C, and interpreted the uppermost two, A and B, as consisting of post middle Miocene terrigenous turbidites, ice-rafted detritus and pelagic sediments. Site 323 of DSDP-Leg 35, drilled on the abyssal plain, revealed ice rafted debris in Middle Miocene sediments at a depth of approximately 300 m bsf [*Hollister et al.*, 1976].

2.2. Previous Models of Total Sediment Thicknesses

[12] The first sediment isopach maps of the South Pacific region were compiled by *Houtz et al.* [1973] and *Rodrigues et al.* [1986], based on sparse and mainly analogue seismic data acquired during early RV *Eltanin* cruises [e.g., *Tucholke and Houtz*, 1976], and on surveys related to DSDP Leg 35 [e.g., *Hollister et al.*, 1976]. *Hayes and LaBrecque* [1991] published a revised version of this sediment isopach map by adding data from more recent seismic reflection profiles and DSDP/ODP drilling. Recently, the Hayes and LaBrecque data set was incorporated into the world isopach maps of *Laske and Masters* [1997] and *Divins* [2006]. Since publication of this second compilation, ODP Leg 178 was completed on the western Antarctic Peninsula margin [e.g., *Barker and Camerlenghi*, 2002] and new digital seismic data were acquired along the West Antarctic continental margin.

[13] *Eagles* [2006] modeled a thermally subsided South Pacific oceanic lithosphere using *Stein and Stein*'s [1992] subsidence relationship, and subtracted it from predicted bathymetry [*Smith and Sandwell*, 1997] to produce residual bathymetric anomalies. Under the assumption that most of this anomaly can be attributed to the presence of sediments on the seafloor, he used a polynomial for isostatic correction [*Sykes*, 1996] to predict total sediment thickness in the South Pacific.

3. Methods

3.1. Definition of Horizons

[14] In order to calculate sediment thicknesses and to differentiate between an upper sequence of sediments whose supply was glacially dominated and a lower sequence where glacial influence is less evident, we picked points along correlatable seismic reflections that define the seafloor, acoustic basement, and an intervening boundary horizon (BH). Reflections from the acoustic basement surface were in most cases clearly identifiable, with the exception of some of the single-channel R/V *Boris Petrov* 1998 profiles where reflection amplitudes were too low, or beneath the continental slope where seafloor multiples obscure them (Figure 1). As described in section 2.1, we used the presence or absence of certain seismic stratigraphic features as the criteria for defining the BH. For example, in the Amundsen Sea, we defined the BH at the bases of sediment mounds where we observe the initial occurrence of channels, following the interpretations of similar features on the Antarctic Peninsula margin. We interpolated the horizons through regions where low data quality, inconclusive seismic stratigraphy, or tectonic boundaries prevented correlations. After picking the horizons, we extracted their two way traveltimes (TWT [s]) at a spacing of 50 CDPs or traces.

3.2. TWT [s] to Depth [m] Conversion

[15] Sound velocities in the sediments of the Antarctic margin are sparsely known. Downhole meas-

Table 1. Comparison of Subbottom Depths, TWT, and Sound Velocities

	Subbottom Depth TWT, ms	Subbottom Depth, m	Sound Velocity, m/s
	ODP Site 1095		
BH (M3/M4-boundary)	580	505	~1740
Basement	1380[a]	1430[a]	~2070[a]
	ODP Site 1096		
BH (M3/M4-boundary)	1100[a]	950[a]	~1730[a]
Basement	2180[a]	2155[a]	~1980[a]
	Seismic Data at CDP 1276 on Profile It-95135a[b]		
BH (M3/M4-boundary)	550	480	~1735
Basement	1305	1286	~1970
	Seismic Data at CDP 4276 on Profile It-95130a[b]		
BH (M3/M4-boundary)	1116	1060	1900
Basement	2148	2477	2306

[a] Extrapolated.
[b] These values were calculated with the empirical formula of *Carlson et al.* [1986] using average seismic interval velocities from profiles IT-95135a (CDP 1276) and IT-95130a (CDP 4276). The comparative depth and velocities come from in situ velocity check shots on site 1095 and 1096 of ODP Leg 178 (Figure 1).

urements of velocity at ocean drilling sites are very sparse and the use of short streamers during acquisition (due to ice conditions) often precludes the generation of a reliable velocity model. The study of *Volpi et al.* [2001], for example, shows seismic interval velocities from stacking velocities that are very different to downhole velocities measured during ODP Leg 178. Because of this, we used an empirical relation [*Carlson et al.*, 1986] for the transformation of TWT [s] into depth [m], which is based on 233 correlated depths from Deep Sea Drilling Project (DSDP) data, ranging up to a depth of 1.4 s (TWT). Estimated subbottom depths (in km) are calculated using $Z = -(3.03 \pm 0.24) \ln [1 - (0.52 \pm 0.04) T]$ where T is two-way traveltime in [s]; the RMS error in these estimates is 26 m in depth. The method successfully reproduces the generally decreasing seismic velocity with decreasing depth and has previously been applied to seismic data acquired on the western Antarctic Peninsula and Bellingshausen Sea continental rises [*Rebesco et al.*, 1997; *Scheuer et al.*, 2006a]. A comparison of the downhole velocities in sediments above the BH at sites 1095 and 1096 of ODP Leg 178 [*Volpi et al.*, 2001] to calculated velocities shows a good agreement, and thus allows confidence in the calculated depth of the BH. The comparison also shows increasing differences with depth, as shown by the estimated and true depth of the acoustic basement (Table 1).

[16] A small number of sound velocities were determined with sonobuoys deployed along the seismic profiles TH-86002-009 in the Amundsen Sea [*Yamaguchi et al.*, 1988]. Table 2 shows comparisons of the sonobuoy data with the values calculated after *Carlson et al.* [1986]. Unfortunately, details of the sonobuoy deployments, processing method and exact parameters are not published, making it impossible to evaluate the reliability of the sonobuoy sound velocities. Furthermore, sonobuoy measurements mainly measure the horizontal velocity component, which often leads to an overestimation of velocity values, as the comparison indicates. Hence we decided to retain the sediment thicknesses calculated after *Carlson et al.* [1986] in the Amundsen Sea.

[17] The formula from *Carlson et al.* [1986] has some limitations. TWT-to-depth conversions for values higher then 1.4 s TWT are extrapolated and thus not associated with an RMS error. Furthermore, the formula becomes insolvable for values higher than 3.8 s TWT. Therefore we converted all TWT values greater than 3.0 s to depth by assuming an average velocity of 3200 m/s. This assumption affects only ~9% of the data points of the acoustic basement horizon (Table 2), mainly observed on the continental slope/rise transition, and none of the BH picks.

3.3. Additional Input Information

[18] Because of strong seafloor multiple reflections, we were not able to define acoustic basement on most profiles crossing the continental shelf. Here, we used estimates of total sediment thickness from gravity models made along seismic profiles BAS-92325 and AWI-94003 instead [*Cunningham*

Table 2. Comparison of Depth, Sediment Thicknesses, and Sound Velocities Coming From Sonobuoy Data and Seismic Profiles, Which Were Acquired on the Continental Rise of the Amundsen Sea During the TH-86 Cruise of the RV *Hakurei-Maru*[a]

		Data From Sonobuoy				Data From Seismic Profiles			
Location	Profile/ Trace	Seafloor, m	Depth to Basement, s TWT	Sediment Thickness, m	Velocity, m/s	Seafloor, m	Depth to Basement, s TWT	Sediment Thickness, m	Velocity, m/s
SB 1	86002a/300	4280	1.57	1800	2300	4455	1.70	1792	2108
SB 2	86003a/2300	4180	2.28	3420	3000	4215	2.04	2290	2245
SB 4	86004c/2650	4560	2.01	2410	2400	4451	1.94	2124	2194
SB 7	86006/1550	4160	0.99	940	1900	4109	0.81	714	1770

[a] Sonobuoy data were read off a figure published by *Yamaguchi et al.* [1988]. The comparative data were calculated on the basis of the digital seismic profiles TH-86002-009 at the approximate sonobuoy locations, using the formula of *Carlson et al.* [1986].

et al., 2002; Alfred Wegener Institute, unpublished gravimetric data, 2001]. We exclude estimates of sediment thicknesses on the middle and inner shelf due to the lack of reliable data.

[19] In addition to this, in order to maintain a realistically smooth appearance of the grids in areas remote from seismic data control, it was necessary to include about 50 further estimates of total sediment thickness. On the continental slope and rise, our estimates were either reasonable guesses based on the physiographic context, or by comparison to the nearest seismic profile. We also referred to regional trends, but not absolute values, in the predicted sediment thickness grid of *Eagles* [2006]. As the abyssal plain is largely uncovered by newer seismic profiles, we included estimates of total sediment thicknesses from the NGDC data set, originally produced by *Hayes and LaBrecque* [1991], in the area north of 63°S and west of 80°W, sampled at 1° spacing. To us, this section of the data set appears reliable as it is based on analogue seismic profiles and results from site 323 of DSDP Leg 35 (Figures 3a and 3b).

[20] Because of discontinuous seismic reflections beneath the continental slope, we were forced to interpolate the BH along many of the cross-slope profiles. To do so, we added control points where necessary along the 1000 m bathymetric contour based on the average thickness (1800 m) of sediments above the BH where it is seen in profile crossings of this contour. On the central part of the abyssal plain, we assumed that the onset of ice rafted material, drilled in a depth of approximately 300 m at DSDP site 323, represents the distal complementary boundary to the BH horizon. We made no attempt to identify the BH beneath the Bellingshausen Sea and western Amundsen Sea abyssal plains, where drilling data are absent.

3.4. Gridding of Sediment Thicknesses

[21] We produced isopach grids of total sediment thicknesses and of thicknesses of sediments above and below the BH in the region between 60°W and 133°W and 62°S and 72°S, with a grid spacing of 2 × 2 min, using a continuous curvature gridding algorithm [*Wessel and Smith*, 2004]. We used a low tension factor in view of the large areas to be interpolated between data profiles. Before gridding, we applied a high cut cosine filter (Figure 4) to the profile data along slope in the Amundsen Sea in order to prevent short wavelength anomalies related to seamounts having an effect on the finished grid. Elsewhere, low relief of the bounding surfaces, especially the BH, means that no filtering was required.

4. Results

4.1. Total Sediment Thicknesses

[22] Figures 3a and 3b allow a comparison between the isopach grid of *Hayes and LaBrecque* [1991] and our grid of total sediment thicknesses. The Hayes and LaBrecque isopachs do not show the general trends of thick sediment accumulations on the shelf and slope, and decreasing thicknesses to the deep sea that recent cross-slope seismic profiles lend to our grid. Numerous sediment mounds, drifts and channels on the continental rise only appear in our grid. In contrast, thicknesses on the abyssal plain correspond well, as our compilation is largely based on Hayes and LaBrecque's there. Our TWT-to-depth conversion is more appropriate than that applied by Hayes and LaBrec-

Geochemistry Geophysics Geosystems G3 SCHEUER ET AL.: GRIDDED ISOPACH MAPS 10.1029/2006GC001315

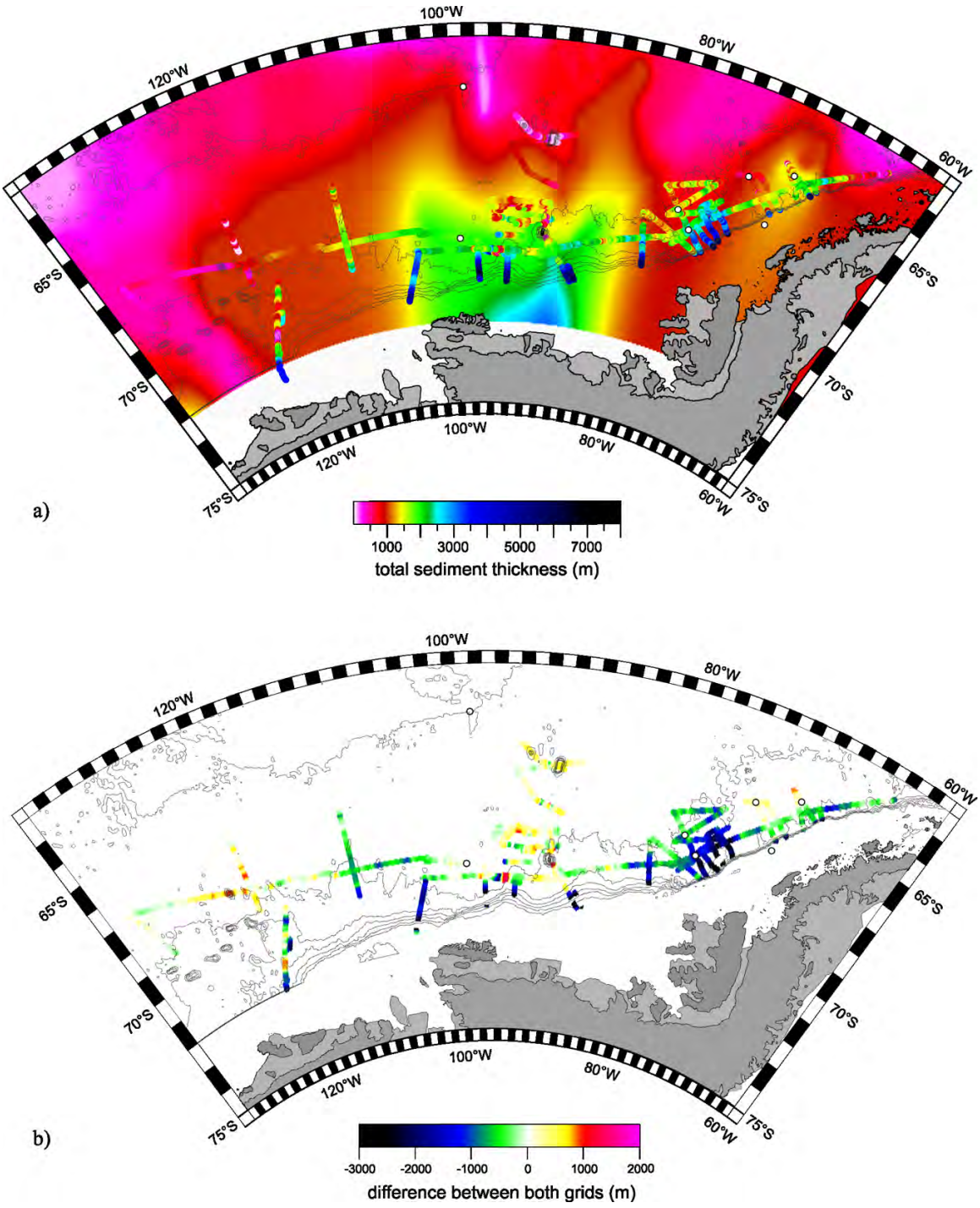

Figure 3. (a) Comparison between total sediment thicknesses, based on the latest seismic data (displayed along the seismic tracks), and the isopach grid from *Divins* [2006], previously published by *Hayes and LaBrecque* [1991] (color image in the background). (b) Differences between both grids imaged along the seismic tracks.

que, who assumed an average sound velocity of 2 km/s in sediments, unless other sound velocities had been published in the original reports.

[23] Figure 5 shows some of the new observations that are possible with our grid of total sediment thickness. Peak thicknesses, exceeding 4000 m, occur along the continental shelf and slope of the entire SE Pacific continental margin, with a general decrease toward the deep sea (e.g., to 700 m at site 323, DSDP Leg 35). Sediment thicknesses on the

Geochemistry Geophysics Geosystems G3 SCHEUER ET AL.: GRIDDED ISOPACH MAPS 10.1029/2006GC001315

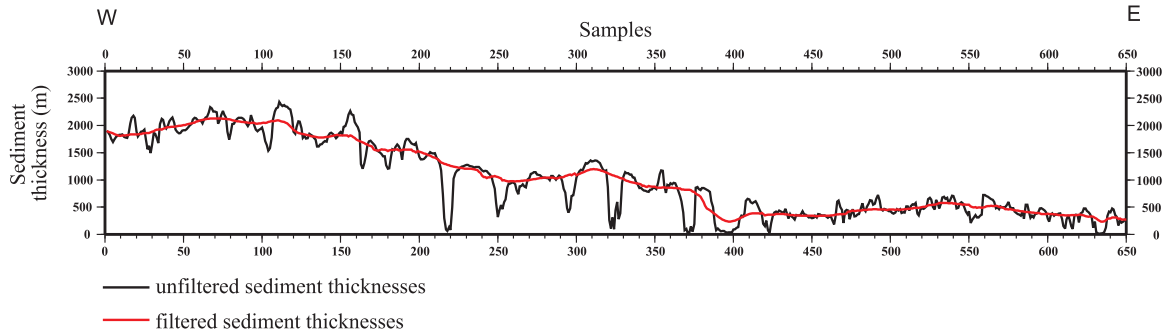

Figure 4. Filtered and unfiltered sediment thicknesses of the profiles Th-86-002/3/8/9, along-slope orientated in the Amundsen Sea. Gaussian filter with a filter width of 50 traces is used.

continental rise and abyssal plain increase from east to west. Discrete sediment mounds, drifts and wide depocenters are visible on the continental rise. Drift 3, north of Adelaide Island (thickness up to 2700 m on profile It-97235) and drifts 6 and Drift 7 (Figures 5 and 2a), north of Alexander Island (maxima of 3200 m at Drift 6 on profile It-95130) are observed on the western Antarctic Peninsula margin. Depocenters A, B and C in the Bellingshausen Sea can also be clearly identified, with thicknesses of up to 2500 m (depocenter A, Figures 5 and 2b) and 2600 m (depocenter B) on profile AWI-20010001. Depocenter C shows a north striking step in sediment thickness, downward to the west from 4500 to 450 m, which is related to the underlying basement step (profile BAS-92324, Figures 5 and 2d). Extending northward from Peter I Island, low sediment thicknesses coincide with the basement ridge that produces the De Gerlache Gravity anomaly [*Gohl et al.*, 1997]. Profiles TH-86002 and 003 show widespread thick sediment cover in the eastern Amundsen Sea (Figures 5 and 2d). Maximum thicknesses of 2200 m are observed on profile TH-86003, and thick sediments are recorded along the northern part of profile TH-86004. To the west of this profile, sediment thicknesses show a marked decrease to less then 250 m.

[24] A comparison between our grid of total sediment thickness and that of predicted sediment thicknesses [*Eagles*, 2006] is shown on Figure 6.

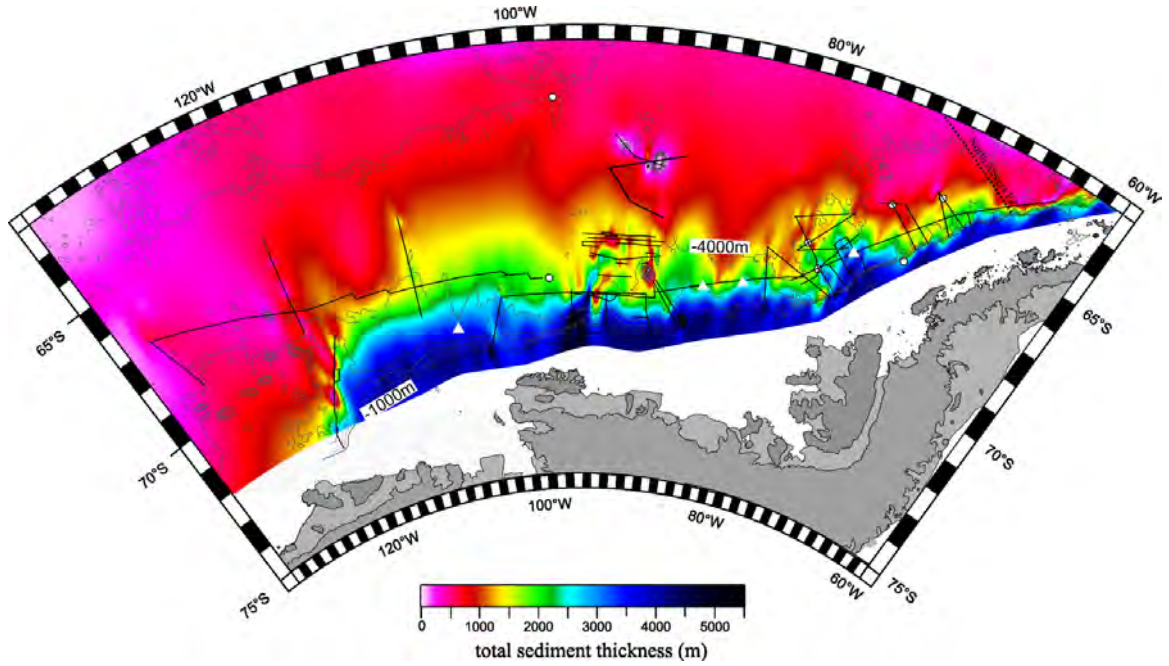

Figure 5. Isopach grid of total sediment thickness, calculated on the basis of MCS and SCS data. The faint contours indicate the satellite-derived predicted bathymetry from *Smith and Sandwell* [1997].

Geochemistry Geophysics Geosystems G3 SCHEUER ET AL.: GRIDDED ISOPACH MAPS 10.1029/2006GC001315

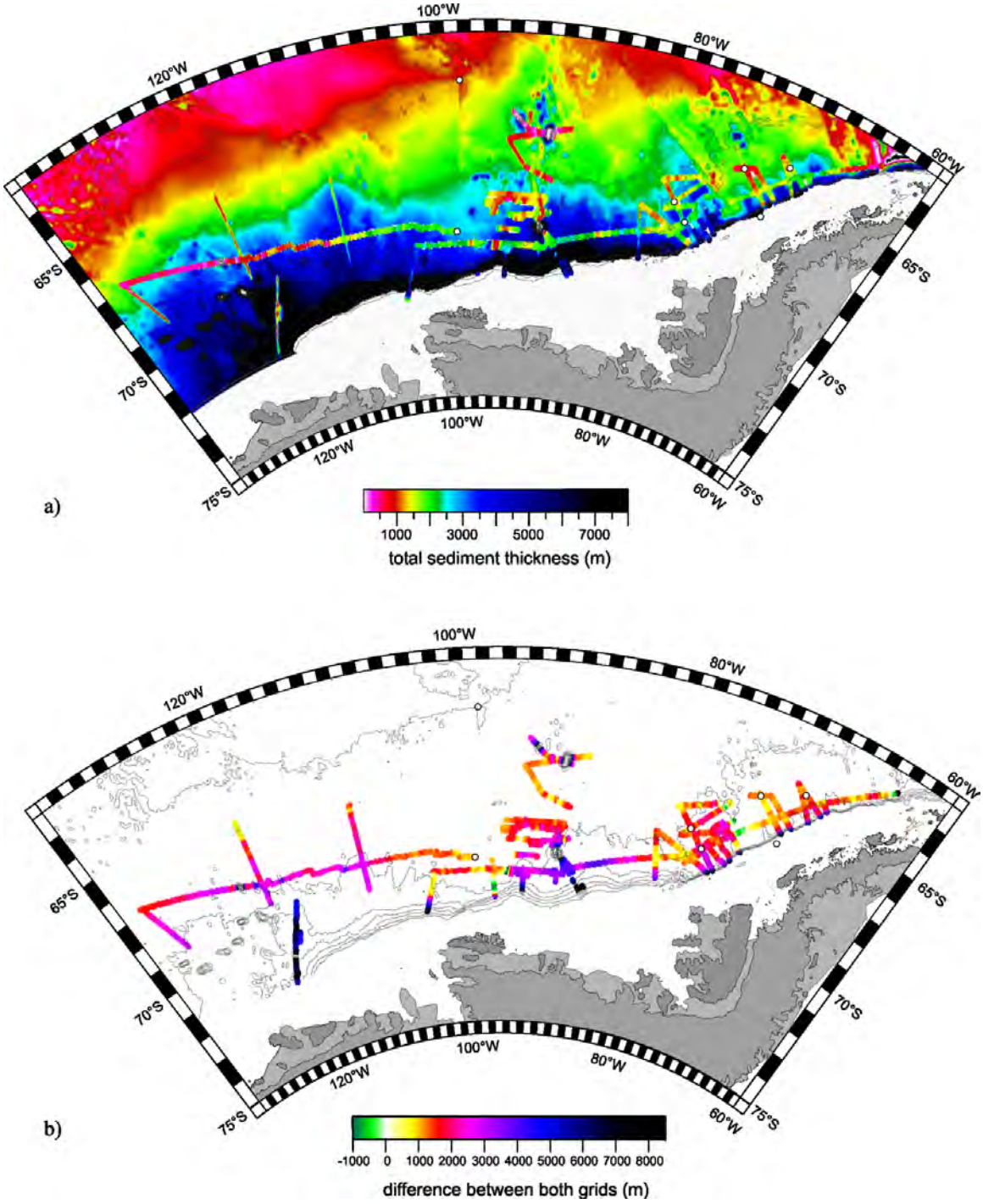

Figure 6. (a) Comparison between the total sediment thicknesses, based on the latest seismic data (displayed along the seismic tracks), and predicted sediment thicknesses derived from the grid of isostatically corrected residual bathymetry from *Eagles* [2006] (color image in the background). (b) Differences between both grids derived by subtracting the thicknesses based on seismic data from predicted sediment thicknesses, imaged along the seismic tracks.

The sediment thicknesses calculated from residual bathymetric anomalies are generally much higher than those measured in our seismic profiles. Peak differences of about 7 km occur on the upper continental slope and on the continental rise of the western Amundsen Sea. In general, the greatest differences on the continental rise, of around 2000 m, are shown in areas of high sediment

Geochemistry Geophysics Geosystems G3 SCHEUER ET AL.: GRIDDED ISOPACH MAPS 10.1029/2006GC001315

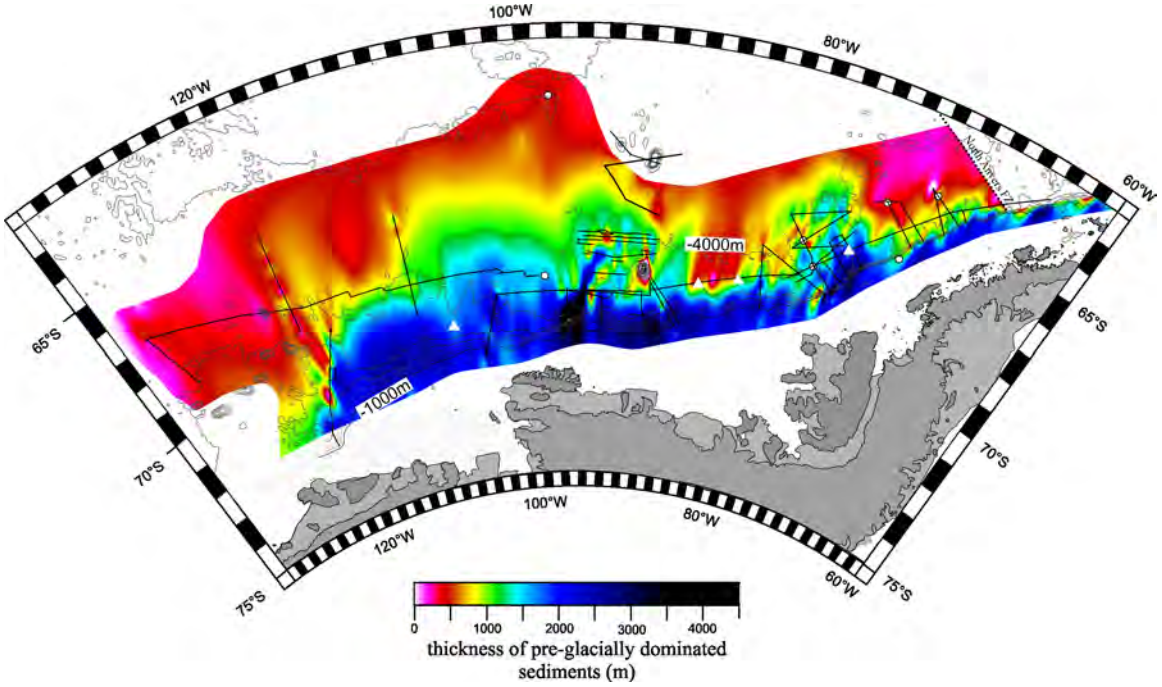

Figure 7. Isopach grid of pre-glacially dominated sediments, related to the period prior to frequent advances of grounded ice to the shelf edge. Thicknesses are calculated on the basis of MCS and SCS data. The faint contours indicate the satellite-derived predicted bathymetry from *Smith and Sandwell* [1997].

thicknesses such as at Drift 6/Drift 7. In the western Bellingshausen Sea and near Peter I Island, predicted sediment thicknesses are up to 4 km greater than seen in seismic profiles. Elsewhere, the predicted thicknesses are consistently 1–3 km greater than seismic data show.

4.2. Pre-glacially Dominated and Glacially Dominated Sediments

[25] On the continental rise, we observe an overall trend of westward increasing thicknesses in sediments above the BH (Figure 7), similar to that in the grid of total sediment thicknesses. Thicknesses of more than 1500 m occur at drifts 6 and 7, depocenters B and C, and in the eastern Amundsen Sea. Prominent basement highs, probably related to magmatic intrusions or seamounts around Peter I Island, or depressions such as that coinciding with the Bellingshausen Gravity Anomaly (sediment thicknesses exceeding 3500 m) can be clearly seen. The low thicknesses of sediments below the BH in the central Bellingshausen Sea (100–500 m), and in the western Amundsen Sea near the Marie Byrd Seamounts are conspicuous. The BH and sediments below it are not seen off the northernmost Antarctic Peninsula, where the oceanic basement is younger than 10 Ma [e.g., *Larter and Barker*, 1991; *Larter et al.*, 2002].

[26] The variability in the thickness of sediments above the BH (Figure 8) resembles that for total sediment thickness. The greatest thickness, of about 2000 m, is observed on the outer continental shelf (e.g., profile AWI-94003), and overall thicknesses decrease toward the deep sea. The thickest sediments on the continental rise are observed at the sediment depocenters, mounds and drifts (Figure 8; e.g., 1200 m at Drift 3 and 1400 m at drifts 6 and 7 on profiles IT-97235 and IT-95130). Sediment thicknesses west of Drift 7 decrease to 250 m in a wide seafloor trough. Very high thicknesses of glacial sediments are seen on depocenters A and B (up to 1500 m and 1700 m on profile AWI-20010001). Values north of profile AWI-20010001 can only be guessed at, as there are no other reliable data. We suppose these depocenters extend further out to sea than drifts 6 and 7, because of the thicker sediments above the BH and the gentler continental slope inclination. Sediment thicknesses above the BH decrease west of Peter I Island, as shown on profile BAS-92324 crossing sediment depocenter C near the continental slope (maximum thickness of 750 m). The Petrov 98 profiles indicate a strong northward decrease of sediment thicknesses above the BH to less then 200 m. However, the northernmost of these profiles, in the vicinity of the De Gerlache

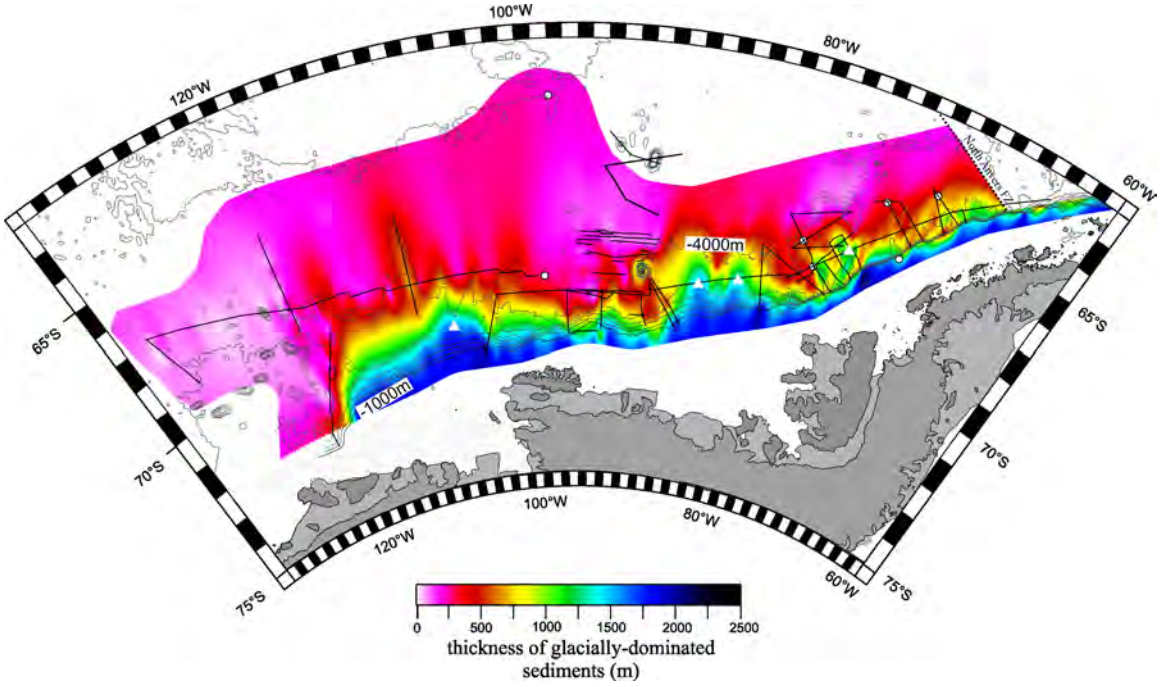

Figure 8. Isopach grid of glacially dominated sediments, which we relate to amplified downslope sediment supply due to grounded ice advances on the continental shelf to the shelf edge. Thicknesses are calculated on the basis of MCS and SCS data. The faint contours indicate the satellite-derived predicted bathymetry from *Smith and Sandwell* [1997].

Seamounts, show no features that enable us to define the BH.

[27] The seismic profiles in the Amundsen Sea show sediment mounds and drifts separated by channels above the BH, similar to those on the Antarctic Peninsula margin (Figures 2a and 2e). Sediment thicknesses along profile TH-86002 and the eastern section of TH-86003 indicate four sediment mounds, which we refer to as Am1–Am4, from east to west. Profile TH-86003 shows a westward increasing trend of sediment thicknesses west of Am4. The north-south trending profile TH-86004 indicates maximum thicknesses of about 700 m and a wide northward extent of mound Am4. From here, sediment thicknesses decrease to the west.

5. Discussion

5.1. Terrigenous Sediment Supply

[28] The main reason for the overall east to west trend of increasing total and pre-glacially dominated sediment thicknesses on the continental rise and abyssal plain is the variation in the age of underlying oceanic crust, which is mostly due to diachronous cessation of oblique subduction at the continental margin. Oceanic basement ages vary from about 3 Ma on the northern Antarctic Peninsula margin to about 90–83 Ma in the Amundsen Sea. [e.g., *Barker*, 1982; *Larter and Barker*, 1991; *McCarron and Larter*, 1998; *Cunningham et al.*, 2002; *Eagles et al.*, 2004].

[29] The western shelf of the Antarctic Peninsula is divided into four major paleoice drainage basins, which during glacial times fed sediment to turbidity channels offshore and, ultimately, sediment mounds and drifts on the continental rise [e.g., *Larter et al.*, 1997; *Rebesco et al.*, 2002]. The greatest sediment thicknesses are found off these main glacial drainage areas (Figures 5 and 7), indicating that the supply of sediment by grounded ice streams during glacial periods is the primary factor for the sediment distribution on the West Antarctic continental margin. The greatest sediment thickness is observed at drifts 6 and 7, SW of Marguerite Trough, the deepest depression on the western Antarctic Peninsula continental shelf, excavated by fluctuations of paleoice streams between Alexander and Adelaide islands [e.g., *Ó Cofaigh et al.*, 2002].

[30] The topography and the development of sediment accumulations on the Bellingshausen Sea

continental margin east of Peter I Island shows some distinct differences from the western Antarctic Peninsula continental margin. Instead of several smaller turbidity channel-related sediment mounds and drifts, large depocenters have developed. Bathymetric investigations of the Bellingshausen Sea outer continental shelf revealed a wide trough named Belgica Trough, which is interpreted as the path of a major paleoice stream between Alexander and Thurston islands [*Ó Cofaigh et al.*, 2005; *Scheuer et al.*, 2006a]. Depocenter B developed seaward of this trough and thus was interpreted as a trough mouth fan by Scheuer et al., which we will refer to as the Belgica Fan. The thickness of sediments above the BH on depocenter C is low compared to those on depocenters A and B, which may indicate a lesser supply of downslope sediments on the continental margin east of Thurston Island during times of frequent grounded ice advances. Many authors interpret depocenter C as a contourite drift consisting of glacially dominated sediments built up by a westward flowing bottom current, deposited on the elevated eastern side of a basement step [e.g., *Cunningham et al.*, 1994; *Nitsche et al.*, 2000; *Scheuer et al.*, 2006b].

[31] The Amundsen Sea continental shelf is fed by two very active and fast flowing ice streams, the Pine Island and Thwaites glaciers, which account for approximately 4% of the outflow from the entire Antarctic Ice Sheet [*Vaughan et al.*, 2001]. Advances of these streams across the continental shelf during glacial maxima led to the development of glacial drainage troughs on the inner to middle shelf, of which the Pine Island Bay trough is one of the deepest (>1000 m [*Kellogg and Kellogg*, 1987; *Lowe and Anderson*, 2003]). The cross-slope profile ANT-94042 shows prograding foresets truncated by erosional unconformities [*Nitsche et al.*, 2000], through which we infer a significant supply of glacially transported sediment to the continental slope and rise. As the Pine Island Bay trough reaches the central part of the shelf in front of mound Am4 [*Lowe and Anderson*, 2003], and along-slope profiles show the highest thicknesses of sediments above the BH at mounds Am3 and Am4, we infer this area to be the main accumulation zone of glacially transported sediments.

[32] The reason for the relatively great thickness of sediments we interpreted as occurring above the BH at site 323 (about 300 m), in comparison to the northernmost RV *Petrov 98* profiles (about 200 m), may be a higher biogenic sedimentation rate. This location lies beyond the Southern ACC Front and thus in a zone of higher organic production. However, it should be remembered that the ice rafted debris recovered near 300 m bsf at DSDP site 323 cannot be unequivocally related to the begin of grounded ice advances on the continental shelves.

5.2. Sediment Accumulation Rates

[33] The dating of the onset of grounded ice reaching the shelf edge and the accompanying amplification of large sediment accumulations such as drifts or trough mouth fans remains the subject of debate. The deepest samples of sediment drilled at site 1095, which were magnetostratigraphically dated to about 9.6 Ma [*Iwai et al.*, 2002], were deposited under glacially dominated conditions [e.g., *Barker and Camerlenghi*, 2002]. The base of glacially transported sediments was not drilled, meaning it was not possible to date the onset of grounded ice on the continental shelf reaching the shelf edge.

[34] However, drilling at ODP site 1095 just reached the boundary between *Rebesco et al.*'s [1997] seismic units M3 and M4, or our BH. This boundary indicates an important change in sediment drift development due to enhanced downslope supply of sediments, in the form of turbidity currents, which can be related to grounded ice advances on the continental shelf. Hence it may be appropriate to apply a minimum age of about 10 Ma to the BH throughout the eastern and central Bellingshausen Sea in those areas where we can correlate the M3/M4 boundary. In the western Bellingshausen Sea and Amundsen Sea, dating of the BH to 10 Ma is more speculative, as no tie to site 1095 was possible and recent studies indicate differences in the dynamic development of grounded ice reaching the shelf edge since late Miocene times [*Scheuer et al.*, 2006a].

[35] Our assumption that the BH dates everywhere to ~10 Ma is most likely an oversimplification, but it is useful because it allows us to make a coarse comparison of sedimentation histories along the West Antarctic margin. To do so, we calculated deposition rates, assuming uncompacted sediments, at locations in the four highest sediment thicknesses areas (Figures 5, 7, and 8). Of these, mound Am3 is sampled more distally, by seismic profile TH-86003, than the others. In order to calculate comparable sediment deposition rates we therefore chose a more proximal point sampled from our grid, halfway between the seismic profile and the shelf edge (Table 3).

Table 3. Average Sediment Thicknesses and Sediment Deposition Rates Calculated in the Major Accumulation Areas[a]

Location	Sediment	Deposition Period, m.y.	Sediment Thickness, m	Sediment Deposition Rate, m/m.y.
Drift 6	glacially dominated sediments	10	1400	140
Drift 6	pre-glacially dominated sediments	29	1600	55
Drift 6	total sediments	39	3000	76
Depocenter A	glacially dominated sediments	10	1550	155
Depocenter A	pre-glacially dominated sediments	37	950	26
Depocenter A	total sediments	47	2500	53
Depocenter B (eastern part)	glacially dominated sediments	10	1700	170
Depocenter B (eastern part)	pre-glacially dominated sediments	46	850	18
Depocenter B (eastern part)	total sediments	56	2550	46
Mound Am3	glacially dominated sediments	10	1600[b]	160[b]
Mound Am3	pre-glacially dominated sediments	74	1500[b]	20[b]
Mound Am3	total sediments	~85	3100[b]	36[b]

[a] We chose locations with approximately the same distance to the shelf edge in order to enable comparisons. Locations are marked by white triangles on Figures 5, 7, and 8.
[b] Sampled values from the grid.

[36] Despite the overall increase of sediment thicknesses from east to west (Figures 5, 7, and 8), we observe a decrease of the total and pre-BH sediment accumulation rates. The high rate of sedimentation below the BH off the western Antarctic Peninsula suggests a high sediment supply prior to late Miocene times. This is consistent with *Rebesco et al.*'s [1997] interpretation of seismic unit M4 (Figure 2a) as an initial drift growth stage, with an estimated onset at 15 Ma. Those authors mentioned that M4 may already have been deposited under glacial influence and in interaction with a bottom current. One explanation for this could be the mountainous nature of the Antarctic Peninsula [*Lythe et al.*, 2000]. Today, it acts as a major barrier to tropospheric circulation, resulting in high snowfall and accumulation onshore [e.g., *Reynolds*, 1981]. If this region was similarly sensitive in Miocene times, then it is possible to envisage it having responded to Miocene climate changes with earlier development of eroding ice streams than the adjacent, more flat-lying regions. Consistent with this, *Scheuer et al.* [2006a] estimated a relatively low sediment accumulation rate in the neighboring Bellingshausen Sea prior to 5.3 Ma (106 m/m.y. at depocenter A), which they attributed to the region facing a wide continental shelf with a hinterland below sea level [*Lythe et al.*, 2000]. Similar conditions apply for the Amundsen Sea, and can be invoked to explain the low accumulation rate there too.

[37] The highest accumulation rate of sediments above the BH, averaging 170 m/m.y., was estimated at depocenter B, which correlates with a peak deposition rate (295 m/m.y.) in Pliocene-Pleistocene times (since 5.3 Ma) calculated by *Scheuer et al.* [2006a]. Those authors relate the high sedimentation rate to the development of a very large ice drainage basin (Belgica Trough), high erosion rates onshore and offshore, high ice flow velocities and the great width of the continental shelf (up to 480 km west of Alexander Island). Accumulation rates on the western Antarctic Peninsula, at depocenter A and mound Am3 are very similar, varying between 140 and 160 m/m.y. Even though sparse data in the Amundsen Sea make estimates of sediment thicknesses and accumulation rates speculative, an estimated accumulation of 160 m/m.y. on the upper continental rise seems reasonable, with respect to the similar widths of the Amundsen Sea and Bellingshausen Sea continental shelves, and the fact that Pine Island Bay is a large glacial drainage outlet.

5.3. Influence of Ocean Bottom Currents

[38] Temperature measurements [*Gordon*, 1966], seabed photography [*Hollister and Heezen*, 1967], and current meter readings [*Nowlin and Zenk*, 1988; *Camerlenghi et al.*, 1997] suggest that a westward flowing bottom contour current follows the western margin of the Antarctic Peninsula. The influence of bottom currents on the distribution of sediments and structures of sediment deposits along the West Antarctic continental margin is well documented by several studies of contourite drifts at the Antarctic Peninsula margin [e.g., *Rebesco et al.*, 1997] (Figure 2a). In addition to these, *Scheuer et al.* [2006b] identified a channel related sediment drift at depocenter C in the western Bellingshausen Sea (Figure 2d). The development of such features seems to be related to the availability of contouritic

detritus scavenged from continental slopes by frequently occurring turbidity currents.

[39] The sediment accumulations on the Antarctic Peninsula margin and in the Amundsen Sea show similarities, consisting as they do of sediment mounds with one steep and one gentle flank separated by erosional channels (Figures 2a and 2e). Although this may be taken as indicating a contour current influence in the Amundsen Sea, it should be remembered that the asymmetries of the contourite drifts on the Antarctic Peninsula margin are not always consistent with a westward current flow [*Rebesco et al.*, 2002], and so the orientations of the Amundsen Sea mounds, with their steep easterly edges, cannot be considered a strong indicator of the proposed current's direction. The higher elevation of the western channel levees may be related to the influence of the Coriolis force on turbidity currents.

5.4. Implications for Geodynamics

[40] *Eagles* [2006] noted that values in his grid of predicted sediment thicknesses (Figure 6a) were consistently greater than those in the Hayes and LaBrecque data set, and attributed this to either or both of two causes. The first cause was underestimation of sediment thicknesses by Hayes and LaBrecque due to nonimaging of seismic basement in many of their data. Although our grid confirms that the Hayes and LaBrecque data set underestimates thicknesses, the underestimation is far smaller than the difference to Eagles' predicted thicknesses. The second cause was long wavelength residual bathymetry anomalies formed due to crustal thickness variations and uplift due to flow occurring in the mantle, known as dynamic topography. *Eagles* [2006] noted that dynamic uplift of 1 km would contribute to overestimates of 3.8–6.9 km in his predicted sediment thicknesses. The regional systematic overestimate of 1–3 km in relation to our grid, shown in Figure 6b, thus suggests dynamic uplift in the range of 140–790 m affects the region.

[41] Consistent with this uplift, *Shapiro and Ritzwoller* [2004] show evidence of a peak in heat flow beneath Marie Byrd Land, which *Morelli and Danesi*'s [2004] tomographic images show is connected to a widespread low-velocity anomaly beneath the Bellingshausen and Amundsen Seas that can be interpreted in terms of warm upwelling mantle material. Dynamic topography is also often correlated with other surface manifestations of mantle convection, notably excess volcanism, for instance around Iceland [e.g., *Louden et al.*, 2004]. Studies of volcanic rocks from Marie Byrd Land provide ample evidence for late Cenozoic volcanic activity [e.g., *Hole and LeMasurier*, 1994; *Behrendt*, 1999; *Rocchi et al.*, 2002]. Offshore, in the Amundsen Sea, there is further evidence for excess volcanism at the Marie Byrd Seamounts, although seismic data and subsidence calculations on guyots suggest this occurred in Paleogene times. Peter I Island, further east, is an active volcano that may also be attributed, along with the nearby De Gerlache seamounts, to the same cause as the regional uplift. The peak sediment thickness overestimates in *Eagles'* [2006] grid coincide with these centers and thus may be related to increased dynamic topography around them, or to crustal thickening associated with the volcanic activity.

5.5. Outlook

[42] The interpolated sediment isopach grids can be used to adjust existing paleobathymetric models for the effects of sedimentation. Such grids should be a central element of paleoceanographic models that set out to investigate the origins and effects of topographically steered currents like the ACC or AABW. To do this for the various times that might be of interest in the region will require the classification of the entire sediment package into discrete dated sediment units. As yet, the sparse data acquired in the study area do not allow the establishment of such a classification. The lack of data coming from deep penetrating ocean boreholes in the Amundsen Sea makes a dating of sediment units there especially difficult. Our coarse classification into pre-glacially dominated and glacially dominated sediments along seismic profiles and its northward extrapolation is the first classification of the sediments ranging across the South Pacific. Our assumption that these sequences are separated by an isochronous surface, BH, is an oversimplification, but it enables a first tentative comparison of sedimentation histories along the West Antarctic margin which can be used to guide future data acquisition efforts.

6. Summary and Conclusions

[43] A large set of seismic reflection data acquired in the Southern Pacific off West Antarctica is used to model isopach grids that provide insights into the tectonic structure and sedimentary architecture of the study area. In the future, grids like these can be used to improve existing paleobathymetric models by considering the effects of sedimentation, in order to provide more precise boundary conditions for models of paleoceanographic develop-

ment. The approximation of an age of about 10 Ma for the boundary between predominantly nonglacial related sediments and those supplied due to the advances of grounded ice on the continental shelf allows approximations of sedimentation rates on the continental rise and thus a comparison of local sedimentation histories.

[44] In comparison to the Bellingshausen and Amundsen Seas, high sedimentation rates on the western margin of the Antarctic Peninsula prior to 10 Ma can be related to the elevated topography of the Antarctic Peninsula hundreds of meters above sea level. This topography presented a source of terrigenous sediments that was missing from most other parts of West Antarctica, and may have promoted weather patterns that gave rise to the earlier development of ice streams that transported sediment to the continental rise. In contrast, preglacial sediment accumulation rates in the Bellingshausen Sea and Amundsen Sea are about half as much as on the Antarctic Peninsula, which can be related to low relief of the sediment source area, most of which lies below sea level.

[45] The distribution of glacially dominated sediments on the continental rise is, in general, consistent with the arrangement of recent drainage outlets on the shelf, as the thickest deposits were identified at the mouths of the Marguerite Trough (Antarctic Peninsula), Belgica Trough (Bellingshausen Sea) and in the central Amundsen Sea. Maximum sedimentation of glacially dominated sediments is estimated in the western Bellingshausen Sea and central Amundsen Sea.

[46] However, differences in sediment accumulation rates suggest significant local variability in the timing of glaciations and ice advances over the West Antarctic continental margin. So, we reiterate the tentative nature of our classification, which is due to sparse coverage of seismic profiles and very limited or absent drill hole information.

Acknowledgments

[47] This study is partly funded through grant GO 724/3-1 of the Deutsche Forschungsgemeinschaft (DFG). We are grateful to all scientists and institutions contributing data to the SCAR Seismic Data Library System (SDLS).

References

Anderson, J. B., J. S. Wellner, A. L. Lowe, A. B. Mosola, and S. S. Shipp (2001), The footprint of the expanded West Antarctic Ice Sheet: Ice stream history and behavior, *GSA Today*, *11*, 4–9.

Barker, P. F. (1982), The Cenozoic subduction history of the Pacific margin of the Antarctic Peninsula: Ridge crest interactions, *J. Geol. Soc. London*, *139*, 787–801.

Barker, P. F., and A. Camerlenghi (2002), Glacial history of the Antarctic Peninsula from Pacific margin sediments [online], *Proc. Ocean Drill. Program Sci. Results*, *178*, 40 pp. (Available at http://www-odp.tamu.edu/publications/178_SR/synth/synth.htm)

Bart, P. J., and J. B. Anderson (1995), Seismic record of glacial events affecting the Pacific margin of the northwestern Antarctic Peninsula, in *Geology and Seismic Stratigraphy of the Antarctic Margin*, *Antarct. Res. Ser.*, vol. 68, edited by A. K. Cooper, P. F. Barker, and G. Brancolini, pp. 75–95, AGU, Washington, D. C.

Behrendt, J. C. (1999), Crustal and lithospheric structure of the West Antarctic Rift System from geophysical investigations—A review, *Global Planet. Change*, *23*, 25–44.

Brown, B., C. Gaina, and R. D. Müller (2006), Circum-Antarctic palaeobathymetry: Illustrated examples from Cenozoic to recent times, *Palaeogeogr. Palaeoclimatol. Palaeoecol.*, *231*, 158–168, doi:10.1016/j.palaeo.2005.07.033.

Camerlenghi, A., A. Crise, C. J. Pudsey, E. Accerboni, R. Laterza, and M. Rebesco (1997), Ten-month observation of the bottom current regime across a sediment drift of the Pacific margin of the Antarctic Peninsula, *Antarct. Sci.*, *9*, 426–433.

Carlson, R. L., A. F. Gangi, and K. R. Snow (1986), Empirical reflection travel time versus depth and velocity versus depth functions for the deep sea sediment column, *J. Geophys. Res.*, *91*, 8249–8266.

Cooper, A. K., P. Barrett, K. Hinz, V. Traubea, G. Leitchenkov, and H. Stagg (1991), Cenozoic prograding sequences of the Antarctic continental margin: A record of glacioeustatic and tectonic events, *Mar. Geol.*, *102*, 175–213.

Cooper, A. K., P. F. Barker, and G. Brancolini (1995), *Geology and Seismic Stratigraphy of the Antarctic Margin*, *Antarct. Res. Ser.*, vol. 68, 301 pp., AGU, Washington, D. C.

Cunningham, A. P., R. D. Larter, and P. F. Barker (1994), Glacially prograded sequences on the Bellingshausen Sea continental margin near 90°W, *Terra Antart.*, *1*, 267–268.

Cunningham, A. P., R. D. Larter, P. F. Barker, K. Gohl, and F.-O. Nitsche (2002), Tectonic evolution of the pacific margin of Antarctica: 2. Structure of Late Cretaceous–early Tertiary plate boundaries in the Bellingshausen Sea from seismic reflection and gravity data, *J. Geophys. Res.*, *107*(B12), 2346, doi:10.1029/2002JB001897.

DeSantis, L., G. Brancolini, and F. Donda (2003), Seismostratigraphic analysis of the Wilkes Land continental margin (East Antarctica): Influence of glacially driven processes on the Cenocoic deposition, *Deep Sea Res., Part II*, *50*, 1563–1594.

Divins, D. L. (2006), NGDC Total Sediment Thickness of the World's Oceans & Marginal Seas, Total Sediment Thickness of the World's Oceans and Marginal Seas, http://www.ngdc.noaa.gov/mgg/sedthick/sedthick.html, Natl. Geophys. Data Cent., Boulder, Colo.

Dowdeswell, J. A., C. Ó. Cofaigh, and C. J. Pudsey (2004), Continental slope morphology and sedimentary processes at the mouth of an Antarctic palaeo-ice stream, *Mar. Geol.*, *204*, 203–214.

Dowdeswell, J. A., J. Evans, C. Ó. Cofaigh, and J. B. Anderson (2006), Morphology of the continental slope off Pine Island Bay, Amundsen Sea, West Antarctica, *Bull. Geol. Soc. Am.*, *118*(5), 606–619.

Eagles, G. (2006), Deviations from an ideal thermal subsidence surface in the southern Pacific Ocean, in *Frontiers*

in Antarctic Earth Sciences, *Terra Antart. Rep. 12*, pp. 109–118, Terra Antart. Publ., Siena, Italy.

Eagles, G., K. Gohl, and R. D. Larter (2004), High-resolution animated tectonic reconstruction of the South Pacific and West Antarctic margin, *Geochem. Geophys. Geosyst.*, *5*, Q07002, doi:10.1029/2003GC000657.

Evans, J., J. A. Dowdeswell, C. Ó. Cofaigh, J. B. Anderson, and T. J. Benham (2006), Extent and dynamics and processes of the West Antarctic ice sheet on the outer continental shelf of Pine Island Bay during the last glaciation, *Mar. Geol.*, *230*, *1–2*, 53–72.

Faugères, J. C., D. A. D. Stow, P. Imbert, and A. Viana (1999), Seismic features diagnostic of contourite drifts, *Mar. Geol.*, *162*, 1–38.

Gohl, K., F. Nitsche, and H. Miller (1997), Seismic and gravity data reveal Tertiary interplate subduction in the Bellingshausen Sea, southeast Pacific, *Geology*, *25*, 371–374.

Gordon, A. L. (1966), Potential temperature, oxygen and circulation of bottom water in the Southern Ocean, *Deep Sea Res.*, *13*, 1125–1138.

Hampton, M. A., S. L. Eittreim, and B. M. Richmond (1987), Post-breakup sedimentation on the Wilkes Land Margin, Antarctica, in *The Antarctic Continental margin, Geology and Geophysics of Offshore Wilkes Land*, *Earth Sci. Ser.*, vol. 5A, edited by S. L. Eittreim and M. A. Hampton, pp. 75–89, Circum-Pac. Counc. for Energy and Miner. Recour., Reston, Va.

Hayes, D. E., and J. L. LaBrecque (1991), Sediment isopachs: Circum-Antarctic to 30°S, in *Marine Geological and Geophysical Atlas of the Circum-Antarctic to 30°S*, *Antarct. Res. Ser.*, vol. 54, edited by D. E. Hayes, pp. 29–33, AGU, Washington, D. C.

Hernández-Molina, F. J., R. D. Larter, M. Rebesco, and A. Maldonado (2004), Miocene changes in bottom current regime recorded in continental rise sediments on the continental margin of the Antarctic Peninsula, *Geophys. Res. Lett.*, *31*, L22606, doi:10.1029/2004GL020298.

Hernández-Molina, F. J., R. D. Larter, M. Rebesco, and A. Maldonado (2006), Miocene reversal of bottom water flow along the Pacific Margin of the Antarctic Peninsula: Stratigraphic evidence from a contourite sedimentary tail, *Mar. Geol.*, *228*, 93–116, doi:10.1016/j.margeo.2005.12.010.

Hole, M. J., and W. E. LeMasurier (1994), Tectonic controls on the geochemical composition of Cenozoic alkali basalts from West Antarctica, *Contrib. Mineral. Petrol.*, *117*, 187–202.

Hollister, C. D., and B. C. Heezen (1967), The floor of the Bellingshausen Sea, in *Deep-Sea Photography*, *Johns Hopkins Oceanogr. Stud.*, vol. 3, edited by J. B. Hersey, pp. 177–189, Johns Hopkins Press, Baltimore, Md.

Hollister, C. D., et al. (1976), *Initial Reports of Deep Sea Drilling Project*, vol. 35, 929 pp., U.S. Gov. Print. Off., Washington, D. C.

Houtz, R. E., M. Ewing, D. E. Hayes, and B. Naini (1973), Sediments isopachs in the Indian and Pacific sector (105°E to 70°W), *Antarct. Map Folio Ser.*, *Folio 17*, Plate 5.

Iwai, M., G. D. Acton, D. Lazarus, L. E. Osterman, and T. Williams (2002), Magnetobiochronologic synthesis of ODP Leg 178 rise sediments from the Pacific sector of the Southern Ocean: Sites 1095, 1096 and 1101, *Proc. Ocean Drill. ProgramSci. Results* [CD-ROM], *178*, 1–40.

Kellogg, T. B., and D. E. Kellogg (1987), Recent glacial history and rapid ice stream retreat in the Amundsen Sea, *J. Geophys. Res.*, *92*, 8859–8864.

Kennett, J. P. (1977), Cenozoic evolution of Antarctic glaciation, the circum-Antarctic Ocean, and their impact on global paleoceanography, *J. Geophys. Res.*, *82*, 3843–3860.

Kimura, K. (1982), Geological and geophysical survey in the Bellingshausen Basin, off Antarctica, *Antarct. Rec.*, *75*, 12–24.

Kuvaas, B., and Y. Kristoffersen (1991), The Crary Fan: A trough-mouth fan on the Weddell Sea continental margin, Antarctica, *Mar. Geol.*, *97*, 345–362.

Larter, R. D., and P. F. Barker (1991), Effects of ridge crest-trench interaction on Antarctic-Phoenix spreading forces on a young subducting plate, *J. Geophys. Res.*, *96*, 19,583–19,608.

Larter, R. D., and A. P. Cunningham (1993), The depositional pattern and distribution of glacial-interglacial sequences on the Antarctic Peninsula Pacific margin, *Mar. Geol.*, *109*, 203–219.

Larter, R. D., M. Rebesco, L. E. Vanneste, L. A. P. Gamboa, and P. F. Barker (1997), Cenozoic tectonic, sedimentary and glacial history of the continental shelf west of Graham Land, Antarctic Peninsula, in *Geology and Seismic Stratigraphy on the Antarctic Margin*, part 2, *Antarct. Res. Ser.*, vol. 71, edited by A. K. Cooper and P. F. Barker, pp. 1–27, AGU, Washington, D. C.

Larter, R. D., A. P. Cunningham, P. F. Barker, K. Gohl, and F.-O. Nitsche (2002), Tectonic evolution of the Pacific margin of Antarctica: 1 Late Cretaceous tectonic reconstructions, *J. Geophys. Res.*, *107*(B12), 2345, doi:10.1029/2000JB000052.

Laske, G., and G. Masters (1997), A global digital map of sediment thickness, *Eos Trans. AGU*, *78*(46), Fall Meet. Suppl., F483.

Lazarus, D., and J.-P. Caulet (1993), Cenozoic Southern Ocean reconstruction from sedimentologic, radiolarian, and other microfossil data, in *The Antarctic Paleoenvironment: A Perspective on Global Change*, *Antarct. Res. Ser.*, vol. 56, edited by L.-P. Kennet and D. A. Warnke, pp. 145–174, AGU, Washington, D. C.

Louden, K. E., B. E. Tucholke, and G. N. Oakey (2004), Regional anomalies of sediment thickness, basement depth and isostatic crustal thickness in the North Atlantic Ocean, *Earth Planet. Sci. Lett.*, *224*, 193–211.

Lowe, A. L., and J. B. Anderson (2003), Evidence for abundant subglacial meltwater beneath the paleo-ice sheet in Pine Island Bay, Antarctica, *J. Glaciol.*, *49*(164), 125–138.

Lythe, M. B., D. G. Vaughan, and the BEDMAP Consortium (2000), BEDMAP–Bed topography of the Antarctic, scale 1:10,000,000, Br. Antarct. Surv., Cambridge, U.K.

McCarron, J. J., and R. D. Larter (1998), Late Cretaceous to early Tertiary subduction history of the Antarctic Peninsula, *J. Geol. Soc. London*, *155*, 255–268.

McGinnes, J. P., D. E. Hayes, and N. W. Driscoll (1997), Sedimentary processes across the continental rise of the southern Antarctic Peninsula, *Mar. Geol.*, *141*, 91–109.

Morelli, A., and S. Danesi (2004), Seismological imaging of the Antarctic continental lithosphere: A review, *Global Planet. Change*, *42*, 155–165.

Nitsche, F. O., K. Gohl, K. Vanneste, and H. Miller (1997), Seismic expression of glacially deposited sequences in the Bellingshausen and Amundsen Seas, West Antarctica, in *Geology and Seismic Stratigraphy of the Antarctic Margin*, part 2, *Antarct. Res. Ser.*, vol. 71, edited by P. F. Barker and A. K. Cooper, pp. 95–108, AGU, Washington, D. C.

Nitsche, F. O., A. P. Cunningham, R. D. Larter, and K. Gohl (2000), Geometry and development of glacial continental margin depositional systems in the Bellingshausen Sea, *Mar. Geol.*, *162*, 277–302.

Nowlin, W. D.Jr., and W. Zenk (1988), Currents along the margin of the South Shetland Island Arc, *Deep Sea Res.*, *35*, 805–833.

Ó Cofaigh, C., C. J. Pudsey, J. A. Dowdeswell, and P. Morris (2002), Evolution of subglacial bedforms along a paleo-ice stream, Antarctic Peninsula continental shelf, *Geophys. Res. Lett.*, *29*(8), 1199, doi:10.1029/2001GL014488.

Ó Cofaigh, C., R. D. Larter, J. A. Dowdeswell, C.-D. Hillenbrand, C. J. Pudsey, J. Evans, and P. Morris (2005), Flow of the West Antarctic ice sheet on the continental margin of the Bellingshausen Sea at the Last Glacial Maximum, *J. Geophys. Res.*, *110*, B11103, doi:10.1029/2005JB003619.

Rack, F. R. (1993), A geologic perspective on the Miocene evolution of the Antarctic Circumpolar Current system, *Tectonophysics*, *222*, 397–415.

Rebesco, M., R. D. Larter, A. Camerlenghi, and P. F. Barker (1996), Giant sediment drifts on the continental rise west of the Antarctic Peninsula, *Geo Mar. Lett.*, *16*, 65–75.

Rebesco, M., R. D. Larter, P. F. Barker, A. Camerlenghi, and L. E. Vanneste (1997), History of sedimentation on the continental rise west of the Antarctic Peninsula, in *Geology and Seismic Stratigraphy on the Antarctic Margin*, part 2, *Antarct. Res. Ser.*, vol. 71, edited by A. K. Cooper and P. F. Barker, pp. 29–49, AGU, Washington, D. C.

Rebesco, M., C. J. Pudsey, M. Canals, A. Camerlenghi, P. F. Barker, F. Estrada, and A. Giorgetti (2002), Case study 27: Sediment drifts and deep-sea channel systems, Antarctic Peninsula Pacific margin, mid-Miocene to present, in *Deep-Water Contourite Systems: Modern Drifts and Ancient Series, Seismic and Sedimentary Characteristics*, edited by D. A. V. Stow et al., *Mem. Geol. Soc. London*, *22*, 353–371.

Reynolds, J. M. (1981), The distribution of mean annual temperatures in the Antarctic Peninsula, *Br. Antarct. Surv. Bull.*, *54*, 123–133.

Rocchi, S., P. Armienti, M. D'Orazio, S. Tonarini, J. R. Wijbrans, and G. Di Vincenzo (2002), Cenozoic magmatism in the western Ross Embayment: Role of mantle plume versus plate dynamics in the development of the West Antarctic Rift System, *J. Geophys. Res.*, *107*(B9), 2195, doi:10.1029/2001JB000515.

Rodrigues, E. A., R. E. Houtz, J. L. LaBrecque, and D. A. Drewry (1986), Total sediment thickness, south; total sediment thickness, northwest; total sediment thickness, northeast, in *South Atlantic Ocean and Adjacent Antarctic Continental Margin*, *Reg. Atlas. Ser.*, vol. 13, p. 6, Mar. Sci. Int., Woods Hole, Mass.

Scheuer, C., K. Gohl, R. D. Larter, M. Rebesco, and G. Udintsev (2006a), Variability in Cenozoic sedimentation along the continental rise of the Bellingshausen Sea, West Antarctica, *Mar. Geol.*, *227*, 279–298.

Scheuer, C., K. Gohl, and G. Udintsev (2006b), Bottom-current control on sedimentation in the western Bellingshausen Sea, West Antarctica, *Geo Mar. Lett.*, *26*, 90–101, doi:10.1007/S00367-006-0019-1.

Shapiro, N. M., and M. H. Ritzwoller (2004), Inferring surface heat flux distributions guided by a global seismic model: Particular application to Antarctica, *Earth Planet. Sci. Lett.*, *223*, *1–2*, 213–224.

Sijp, W., and M. H. England (2004), Effect of the Drake Passage throughflow on global climate, *J. Phys. Oceanogr.*, *34*, 1254–1266.

Smith, W. H. F., and D. T. Sandwell (1997), Global seafloor topography from satellite altimetry and ship depth soundings, *Science*, *277*, 1956–1961.

Stein, C., and S. Stein (1992), A model for the global variation in oceanic depth and heat flow with lithospheric age, *Nature*, *359*, 123–128.

Sykes, T. J. S. (1996), A correction for sediment load upon the ocean floor: Uniform versus varying sediment density estimations-implications for isostatic correction, *Mar. Geol.*, *133*, 35–49.

Sykes, T. J. S., J.-Y. Royer, A. T. S. Ramsay, and R. B. Kidd (1998), Southern Hemisphere palaeobathymetry, in *Geological Evolution of Ocean Basins: Results From the Ocean Drilling Program*, edited by A. Cramp et al., *Geol. Soc. Spec. Publ.*, *131*, 3–42.

Tomlinson, J. S., C. J. Pudsey, R. A. Livermore, R. D. Larter, and P. F. Barker (1992), Long-range sidescan sonar (GLORIA) survey of the Antarctic Peninsula Pacific margin, in *Recent Progress in Antarctic Earth Science*, edited by Y. Yoshida, K. Kaminuma, and K. Shiraishi, pp. 423–429, Terra Sci., Tokyo.

Tucholke, B. E., and R. E. Houtz (1976), Sedimentary framework of the Bellingshausen Basin from seismic profile data, *Initial Rep. Deep Sea Drill. Proj.*, *35*, 197–227.

Vaughan, D. G., A. M. Smith, H. F. J. Corr, A. Jenkins, C. R. Bentley, M. D. Stenoien, S. S. Jacobs, T. B. Kellog, E. Rignot, and B. K. Lucchitta (2001), A review of Pine Island Glacier, West Antarctica: Hypotheses of instability vs. observations of change, in *The West Antarctic Ice Sheet: Behavior and Environment*, *Antarct. Res. Ser.*, vol. 77, edited by R. B. Alley and R. A. Bindschadler, pp. 237–256, AGU, Washington, D. C.

Volpi, V., A. Camerlenghi, T. Moerz, P. Corubolo, M. Rebesco, and U. Tinivella (2001), Data report: Physical properties relevant to seismic stratigraphic studies, continental rise sites 1095, 1096, and 1101, ODP Leg 178, Antarctic Peninsula, in *Proc. Ocean Drill. Program Sci. Results* [CD-ROM], *178*, 1–40.

Wessel, P., and W. H. F. Smith (2004), The Generic Mapping Tool (GMT), version 3.4.5, technical reference and cookbook, report, NOAA, Silver Spring, Md.

Yamaguchi, K., Y. Tamura, I. Mizukoshi, and T. Tsuru (1988), Preliminary report of geophysical and geological surveys in the Amundsen Sea, West Antarctica, *Proc. NIPR Symp. Antarct. Geosci.*, *2*, 55–67.

Publication 6.3.4:

Uenzelmann-Neben, G., **Gohl, K.**, 2012. Amundsen Sea sediment drifts: Archives of modifications in oceanographic and climatic conditions. *Marine Geology*, v. 299-302, pp. 51-62, doi:10.1016/j.margeo.2011.12.007.

Author contributions: Uenzelmann-Neben developed the seismostratigraphy and the age model and wrote most of this paper. Gohl collected most of the data and contributed with parts of the interpretation and the discussion. A large part of the seismic data was collected during Polarstern expedition ANT-XXIII/4 (2006) with Gohl as chief-scientist.

Marine Geology 299–302 (2012) 51–62

Contents lists available at SciVerse ScienceDirect

Marine Geology

journal homepage: www.elsevier.com/locate/margeo

Amundsen Sea sediment drifts: Archives of modifications in oceanographic and climatic conditions

Gabriele Uenzelmann-Neben *, Karsten Gohl

Alfred-Wegener-Institut für Polar- und Meeresforschung, Am Alten Hafen 26, 27568 Bremerhaven, Germany

ARTICLE INFO

Article history:
Received 9 February 2011
Received in revised form 15 December 2011
Accepted 20 December 2011
Available online 9 January 2012

Communicated by D.J.W. Piper

Keywords:
Amundsen Sea
Antarctica
Sediment drifts
Seismic reflection data
Bottom water

ABSTRACT

Drift deposits document stages of particular dynamic bottom-currents and associated sedimentary transport activities. The analysis of seismic reflection data from the Amundsen Sea, southern Pacific Ocean, reveals sediment drift formation already in Eocene/Oligocene times. This observation indicates bottom current activity and hence a cold climate for the late Palaeogene in an area, which today lies under the influence of Antarctic Bottom Water (AABW) originating in the Ross Sea. The generation of sediment drifts is accompanied by the occurrence of mass transport deposits leading to the identification of a phase of strong ice sheet expansion (15–4 Ma), which due to a change in ice regime from wet- to dry-based was followed by less material input during the last ~4 Ma.

1. Introduction

During the last years the West Antarctic Ice Sheet (WAIS) has been reported to undergo significant changes, especially in the area of Pine Island Bay, Amundsen Sea Embayment, where large glaciers draining the ice sheet have shown rapid flow acceleration, increased thinning, and grounding line retreat (Rignot and Jacobs, 2002; Shepherd et al., 2004; Thomas et al., 2004). In order to better understand the dynamics of the WAIS and be able to provide reliable constraints for numerical simulations of a possible future behaviour of the ice sheet, information on the development of the WAIS is needed. This, especially for the early phase, is still under debate and not known in much detail both chronologically and regionally. While good progress has been made over the last years in reconstructing the development of the ice sheet since the late Miocene for the western Antarctic Peninsula and Bellingshausen Sea, the Pliocene for the Ross Sea area and the late Quaternary for Pine Island Bay, little is known from the greater Amundsen Sea, which lies between the Ross and Bellingshausen Seas under the east setting Antarctic Circumpolar Current (ACC) (Orsi et al., 1995; Carter et al., 2009).

The Amundsen Sea is located along the southern Pacific margin of West Antarctica (Fig. 1). This part of the southern Pacific was created by rift and breakup processes and the formation of the earliest oceanic crust between Campbell Plateau/Chatham Rise and Marie Byrd Land/Thurston Island Block at 90–80 Ma (Eagles et al., 2004; Gohl et al., 2007, and references therein). The emplacement of the Marie Byrd Seamounts (MBS) was a result of magmatic activity at 65–55 Ma or older (Kipf et al., 2008, submitted for publication). Up to 4 km of sediment have been deposited on top of basement. These sediment deposits have been subject to extensive reworking by oceanic currents and, on the shelf, advance-retreat cycles of the ice sheet.

Presently, the Amundsen Sea lies under the flow of Antarctic Bottom Water (AABW), which here is formed mainly in the western Ross Sea (Gordon et al., 2009; Orsi and Wiederwohl, 2009) and participates in the cyclonic circulation of the Subpolar gyres once it has reached the oceanic domain (Orsi et al., 1999). Circumpolar Deep Water (CDW) is observed to flow onto the shelf areas of the Amundsen Sea via bathymetric troughs (Jacobs et al., 1996; Thoma et al., 2008). In the Bellingshausen Sea, a southwest setting flow of bottom water has been observed close to the continental slope as far west as 83°W (see Hillenbrand et al. (2008) for a detailed presentation). Based on the study of sediment drifts, Scheuer et al. (2006b) and Hillenbrand et al. (2003) inferred that this bottom water flow extends even farther west to 93°W.

The work presented here will provide insight on the palaeoceanographic evolution of the greater Amundsen Sea, which represents one of the outflow regions of the Ross Sea gyre into the deep Pacific–Antarctic Basin (Orsi, 2010) and into which the glaciers of the Pine Island Bay area drain, by analysing sedimentary features observed in seismic reflection data.

* Corresponding author. Tel.: +49 471 4831 1208; fax: +49 471 4831 1149.
E-mail address: Gabriele.Uenzelmann-Neben@awi.de (G. Uenzelmann-Neben).

0025-3227/$ – see front matter © 2012 Elsevier B.V. All rights reserved.
doi:10.1016/j.margeo.2011.12.007

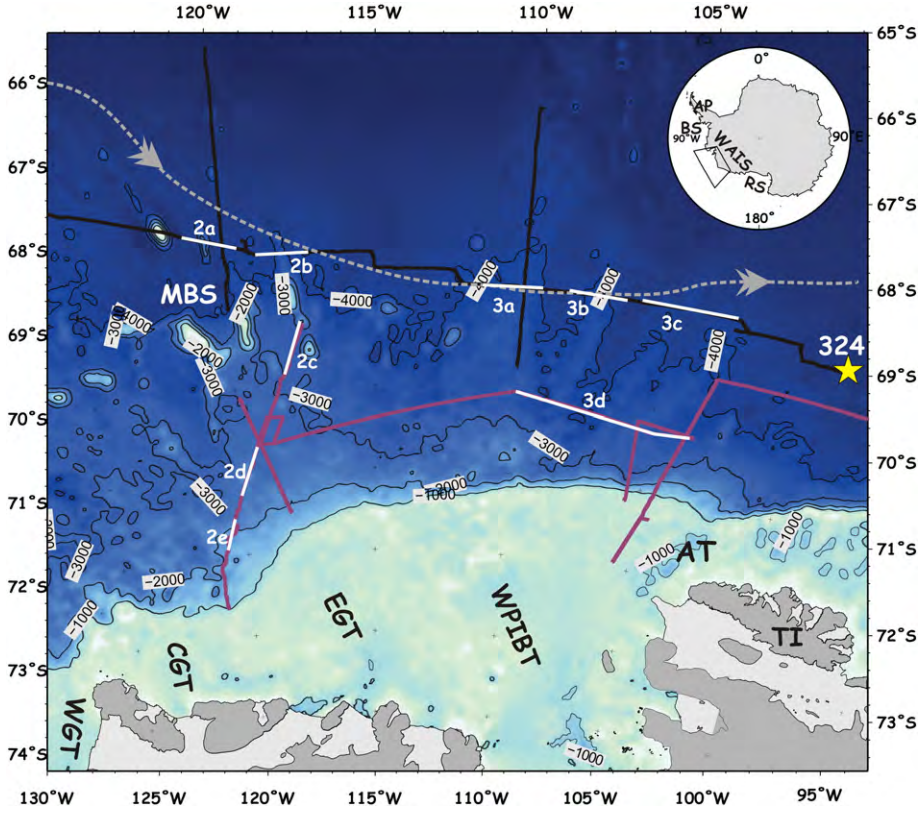

Fig. 1. Bathymetric map of the Amundsen Sea (Nitsche et al., 2007). The seismic line locations are shown in purple (AWI) and black (JNOC), the yellow star refers to the location of DSDP Leg 35 Site 324 (Shipboard Scientific Party, 1976). The white lines and numbers show the parts of the seismic lines presented as figures. The grey dashed line shows the approximate path of AABW (Orsi et al., 1999). AT = Abbot Trough, CGT = central Getz Trough, EGT = eastern Getz Trough, WGT = western Getz Trough, MBS = Marie Byrd Seamounts, TI = Thurston Island, WPIBT = Western Pine Island Bay Trough. Insert map shows the area presented. AP = Antarctic Peninsula, BS = Bellingshausen Sea, RS = Ross Sea, WAIS = West Antarctic Ice Sheet.

2. Geological setting

No direct evidence for an ice sheet extending onto the West Antarctic continental shelves could be detected for the early Cenozoic (Anderson, 1999). A cooling of the surface waters has been reported for the Eocene by Anderson (1999), which may be due to an already existing proto-Ross Gyre as proposed by Huber et al. (2004). A direct relationship between tectonic movements and the onset of massive glaciations can be ruled out because both the opening of the Drake Passage commencing in the middle Eocene and the Tasman Gateway (~35.5 Ma) preceded the largest $\delta^{18}O$ increase (Oi1) of the past 50 Ma at 33.55 Ma indicating major glaciation (Huber et al., 2004; Francis et al., 2008; Miller et al., 2008).

Observations for early Oligocene times are contradictory. While Anderson (1999) interpreted mountain glaciers and ice caps appearing in West Antarctica and ice streams spreading into the western Ross Sea by mid-Oligocene, Miller et al. (2008) reported that the ice advanced from elevated land areas to sea level in the WAIS region already in the earliest Oligocene. According to Ivany et al. (2006) the Antarctic Peninsula was covered by a regionally extensive ice sheet during the Oligocene. The shelf was mainly aggrading during the Oligocene, the slope was characterised by high-relief canyons and the rise by channel–levees (Cooper et al., 2009).

Across the Oligocene–Miocene boundary the ice volume experienced a short-lived (200 ka) increase from 40% to 125% of the present volume (Mi1 incursion) (Wilson et al., 2009). Further growth of the WAIS was observed at 14 Ma (Haywood et al., 2009). Bart (2003) reported at least two WAIS expansions to the shelf edge in the Ross Sea during this period. Uniform progradation with erosion of topset strata characterise the Miocene shelf, while the slope and rise showed fan growth and the construction of large sediment drift bodies and channel–levees (Cooper et al., 2009). Glacial-interglacial volumes decreased on the rise but increased on the slope. They have shifted further landwards since the late Miocene.

The Miocene–Pliocene boundary is characterised by a prominent regional unconformity (Cooper et al., 2009). During the Pliocene several warm intervals occurred leading to a strong increase in sea surface temperatures SST (Escutia et al., 2009; Haywood et al., 2009). Rebesco and Camerlenghi (2008) observe changes in depositional style on the shelf and slope at ~3 Ma and speculate on a climate change having led to the transition from polythermal to polar cold, dry-based ice sheets. Drill information from the Ross Sea gives evidence for rapid oscillations of the WAIS and volume changes between open water and grounded ice at 2.6 Ma (Naish et al., 2009a, 2009b). A numerical simulation of WAIS variations by Pollard and DeConto (2009) for the past 5 Ma ranges from full glacial extents to intermediate states and brief stages of strong retreat leaving only small isolated ice caps.

WAIS retreat dynamics have become best known for the period since the Last Glacial Maximum (LGM) (Domack et al., 1999; Wellner et al., 2001; Anderson et al., 2002; Lowe and Anderson, 2002, 2003; Ó Cofaigh et al., 2005; Dowdeswell et al., 2006; Evans et al., 2006; Hillenbrand et

Fig. 2. a. JNOC profile TH-86008 from the Marie Byrd Seamount area. Note the sediment drifts near the fracture zone. b. JNOC profile TH-86003 F from the western Amundsen Sea. Note the sediment drifts in units I, II and III. The thin black lines are small scale faults. c: Northern part of profile AWI-94050 from the area of the Marie Byrd Seamounts. Note the sediment drift developing directly on top of the basement, initially as a confined drift (unit I), then as an elongate drift (unit II) and lastly as an attached drift (unit III). The dark grey dashed line shows the migration of the drift apex towards the north. The thin black lines are small scale faults. d: Northern part of profile AWI-94054 from the western Amundsen Sea. Note the interpreted debris flow (mtd— mass transport deposit) in unit II, the patched drift (pd) in units III and IV and the sediment waves (sw) in unit IV. e: Southern part of profile AWI-94054 from the western Amundsen Sea. Note the channel–levee system (C— channel, L— levee) in unit I and the mass transport deposits such as mass transport deposits (mtd) and the patched drift (pd) in unit IV.

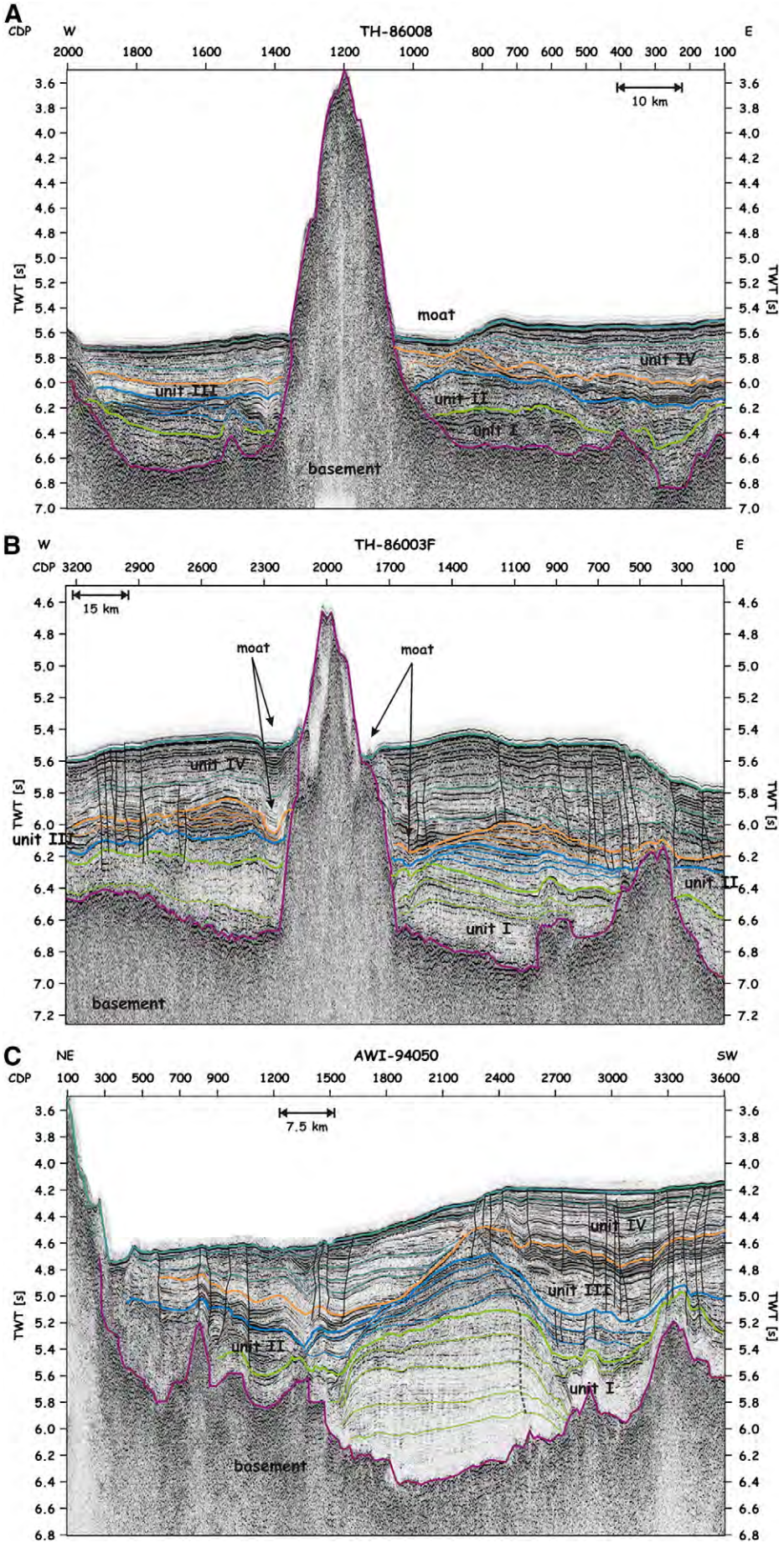
A
CDP
W
TH-86008
E
2000 1800 1600 1400 1200 1000 800 700 600 500 400 300 200 100
10 km
TWT [s]
moat
unit IV
unit III
unit II
unit I
basement
B
W
TH-86003F
E
CDP 3200 2900 2600 2300 2000 1700 1400 1100 900 700 500 300 100
15 km
moat
moat
unit IV
unit III
unit II
unit I
basement
C
NE
AWI-94050
SW
CDP 100 300 500 700 900 1200 1500 1800 2100 2400 2700 3000 3300 3600
7.5 km
unit IV
unit III
unit II
unit I
basement

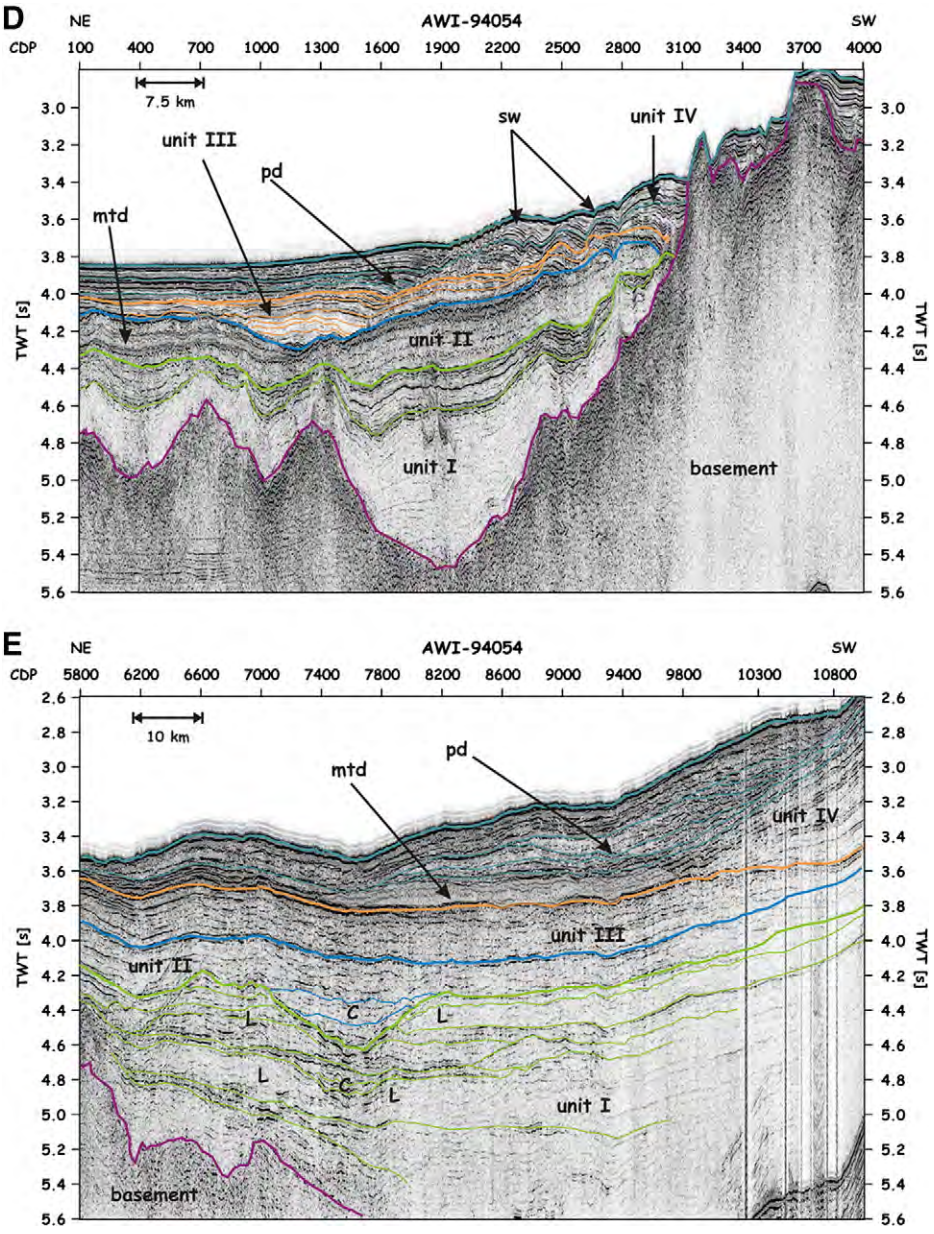

Fig. 2 (*continued*).

al., 2009a, 2009b). These studies have mainly concentrated on Pine Island Bay and the Ross Sea. The relationship between ice sheet dynamics and changes in oceanographic conditions have been dealt with for the western Antarctic Peninsula and the Bellingshausen Sea (e.g. Nitsche et al., 2000; Rebesco et al., 2002; Hernandez-Molina et al., 2004, 2006; Scheuer et al., 2006b; Rebesco and Camerlenghi, 2008). For the Bellingshausen Sea, which lies east of the Amundsen Sea along the Antarctic Peninsula margin, studies have shown bottom current activities since ~9.6 Ma (Rebesco et al., 2002; Hernandez-Molina et al., 2004; Hillenbrand and Ehrmann, 2005; Scheuer et al., 2006b; Uenzelmann-Neben, 2006). A close interaction of along-slope and down-slope sediment transport was identified west of the Antarctic Peninsula with indications for a major advance of the local ice sheet shortly after 15 Ma (Uenzelmann-Neben, 2006).

According to Haywood et al. (2009) WAIS reached its maximum extent in the Ross Sea by late Miocene and in the Bellingshausen and Amundsen Seas by early Pliocene. Due to only few published seismic data and no drilling information this hypothesis is little constrained for the deep sea part of the greater Amundsen Sea.

3. Database

Multichannel seismic reflection data gathered by the Alfred-Wegener-Institut (AWI) in 1994 and 2006 form the base of this study (Fig. 1). Details of field parameters and processing of the seismic data can be found in Gohl et al. (1997), Nitsche et al. (2000) and Uenzelmann-Neben et al. (2007). No gain was applied to the data, neither during processing nor for display. Differences in reflection amplitude discussed in the following thus are real. Additional seismic data (Yamaguchi et al., 1988) were available via the digital database of the SCAR Antarctic Seismic Data Library System (SDLS).

A detailed stratigraphic model with age-depth control does not exist yet. Although profile TH-86002A (Yamaguchi et al., 1988) crosses the location of DSDP Leg 35 Site 324 (Fig. 1), this only provides information on the uppermost 200 m of the sedimentary column (Shipboard Scientific Party, 1976; Tucholke et al., 1976a). Core recovery was relatively poor (51%) producing a lithology of sand, silty clay and diatomaceous clay of Pliocene to Pleistocene age (Shipboard

Scientific Party, 1976). For the rest of the sedimentary column, general changes in sediment structure occurrence and reflection characteristics are interpreted to represent modifications in the depositional regime, e.g. the local circulation system and ice sheet dynamics. Those are then compared to observations from the Bellingshausen Sea (Tucholke and Houtz, 1976; Tucholke et al., 1976b; Rebesco et al., 1996; Nitsche et al., 1997, 2000; Rebesco et al., 2002; Scheuer et al., 2006a, 2006b) and the Ross Sea (De Santis et al., 1995, 1999; Böhm et al., 2009) to derive estimates for an age model.

We are aware of the fact that (a) a direct tie to both Bellingshausen Sea and Ross Sea is not possible and the sedimentary packages there will reflect local modifications in the depositional environment, and (b) most seismic data from the Ross Sea are from the shelf as the data from the rise are very limited and not yet published. Still, the major events observed in those areas provide general information on the nature of discontinuities and processes shaping the sedimentary column such as modifications in climate resulting in waxing/waning of the ice sheet leading to erosion on the shelf and increased material input on the slope and rise.

4. Sedimentary features observed

Before describing the sedimentary units observed in our data in detail we define the three sedimentary features primarily observed.

4.1. Sediment drifts

On most seismic lines we observe asymmetric mounded, elongated sediment bodies, which show a steep and a less inclined flank (e.g. Fig. 2c, CDP 1500–2700, 4.6–6.0 TWT). These mounds show discontinuities at their bases and, in places, internal discontinuities. The internal reflectors are subparallel with mostly moderate amplitudes. They show onlap and downlap onto the discontinuities. In general, the different seismic units forming these mounds are lenticular and upward convex. The vertical stacking of the seismic units shows a lateral migration. Following the classifications of Faugères et al. (1999), Rebesco and Stow (2001), Stow et al. (2002), and Shanmugam (2006) we interpret these features as sediment drifts, which have been shaped by bottom currents. Bottom currents are driven by thermohaline circulation. They persist for long periods of time and can develop equilibrium conditions (Zenk and Camerlenghi, 2008). Periodic modifications in flow pattern linked to changes in plate tectonics (e.g. opening/closure of gate ways, formation of barriers such as fracture zones or volcanic plateaus) and/or climatic conditions lead to the formation of the basal and internal discontinuities observed in sediment drifts (Faugères et al., 1993; Stow et al., 2002).

Based on their overall morphology and setting, sediment drifts can be grouped into different classes (Stow et al., 2002): (i) contourite sheet drifts with a low relief as a basin fill or plastered against the continental slope. Contourite sheet drifts show a relatively constant thickness and cover large areas. (ii) Elongate mounded drifts are distinctly mounded and elongate in shape. They can be 1000 km long and up to 2 km thick. They are generally elongated parallel to the margin and can be both detached and separated from the margin. Elongate drifts typically show lenticular, convex-upward depositional units overlying a major erosional discontinuity (Stow et al., 2002). (iii) Channel-related drifts are related to deep channels or gateways, where the velocity of the bottom circulation is markedly increased. Patch drifts and contourite fans fall into this category. (iv) Modified drift–turbidite systems are the result of interacting down-slope and along-slope processes (Faugères et al., 1999; Michels et al., 2001; Stow et al., 2002). Variations in climate, sea-level and bottom circulation lead to an alternation in the dominating sediment transport process. Levee–drifts are the result showing a marked asymmetry in the size of their levees and an extended tail in the direction of the dominant bottom current flow (Faugères et al., 1999; Michels et al., 2001).

4.2. Channel–levee system deposits

On parts of our seismic lines we observe pairs of slightly asymmetrical mounds facing each other, i.e. the steeper flanks are located on the inner side separated by a channel (e.g. Fig. 2e, CDPs 6300–8800, 4.2–4.5 and 4.6–4.8 s TWT). The western mound of the pair usually is built-up higher than the eastern one. These mounds also show highly reflective units separated by discontinuities. These channel systems flanked by two clear levees are characteristics common for turbidite systems (Emery and Myers, 1996; Reading, 1996; Faugères et al., 1999; Michels et al., 2001). They are the result of episodic turbidity currents. In contrast to the quasi steady, often along-slope flow of bottom currents, turbidity currents are event-controlled and act perpendicular to the continental slope (Zenk and Camerlenghi, 2008). The stronger build-up of the western mound is the result of the interaction of the down-slope turbidity current with the Coriolis force, which acts to the left on the Southern Hemisphere.

4.3. Mass transport deposits

A number of chaotic units can be identified on our lines. These are both laterally and vertically defined with sharp contacts (e.g. Fig. 2e, CDPs 7800–9800, 3.6–3.8 s TWT). These seismic characteristics point towards mass transport deposits (Emery and Myers, 1996). According to Laberg and Vorren (1995; 2000) glacigenic sediments are temporarily stored on the upper slope when the ice sheet reaches the shelf break. Due to the high sedimentation rates the sediments become unstable and mass movement such as mass transport deposits or slumps are generated (Laberg and Vorren, 1995; Reading, 1996; Laberg and Vorren, 2000). Mass transport deposits can appears transparent, opaque as well as chaotic with discontinuous reflections on seismic lines (Laberg and Vorren, 1995; Laberg and Vorren, 2000; Nitsche et al., 2000; Dahlgren et al., 2002; Ó Cofaigh et al., 2003, 2004). They form mounded packages separated by bright coherent reflections (Nitsche et al., 2000). Mass transport deposits are found at slopes with gradients <1° (Ó Cofaigh et al., 2003).

5. Observations

Our seismic data show an up to 3400 ms TWT (~4.2 km using a conversion velocity of $v_p = 2.5$ km/s) thick pile of sediments on top of oceanic basement. We can distinguish up to four sedimentary units (units I–IV) based on seismic reflection characteristics and sedimentary features observed.

The oldest sedimentary unit I shows a thickness of 100–1600 ms TWT (~0.1–2 km) depending of the underlying basement topography. Unit I mainly fills depressions between basement highs and thus levels out the basement topography (e.g. Fig. 2d, CDPs 100–2500). Unit I is generally characterised by weak internal reflections and often appears transparent, which indicates a uniform lithology (Emery and Myers, 1996). We observe stronger, more continuous reflectors only in the upper part of unit I. In the area of the Marie Byrd Seamounts, sediment drifts can be identified within unit I resting directly on basement (e.g. Fig. 2c, CDPs 1600–2700). Moats separate the sediment drifts from the seamounts and other basement highs (e.g. Fig. 2b, CDPs 1600–1800 and 2200–2400).

Sedimentary unit II shows a thickness ranging from 100 ms TWT to 600 ms TWT (~0.1–0.8 km). The reflection characteristics of this unit are variable, often showing continuous internal reflections of moderate to high amplitude either in the lower or upper part of the unit (Fig. 3c). Downlap onto the base can be observed (Fig. 3c, CDPs 2000–2200, 2800, 3100). The sediment drifts with the associated moats observed in unit I in the area of the Marie Byrd Seamounts also extend into unit II. Additional sediment drifts are observed in unit II north of Thurston Island (Fig. 4b). The steeper flanks of the sediment drifts face towards the east, while the gentler flanks face the west (Fig. 3c, west of CDP 1800). We observe channels adjacent to the steep flanks of these sediment drifts, which later have been filled (Fig. 3c, CDPs 1500–1800).

Reflections of the channel fill dip away from the apex of the channel axis, which is characteristic for channel–levee systems according to Emery and Myers (1996). The sediment drifts show a number of small scale faults. In a few locations mass transport deposits can be identified in the upper part of unit II.

Sedimentary unit III shows a thickness of 100–800 ms TWT (~0.1–1 km). We observe a distinct increase in the number of internal reflections (e.g. Fig. 3b). Within unit III we can identify a large number of high amplitude chaotic bodies, which we interpret as mass transport deposits such as debris flows. They occur primarily in the central and eastern Amundsen Sea (Fig. 4c). Those mass transport deposits partly extend upwards from mass transport deposits in sedimentary unit II (Fig. 3b, CDPs 100–700). Several sediment drifts of the eastern Amundsen Sea have their steep flanks facing east. In contrast, the sediment drifts in the area of the Marie Byrd Seamounts show a steep flank facing the basement highs separated by a moat from the high (Fig. 2b, CDPs 500–1800 and 2150–2700). The sediment drifts in the eastern Amundsen Sea are separated from each other by channels (Fig. 3d, CDPs 100–8700). Small scale faults cut through the thicker sediment drifts. Close to the continental slope two channel–levee systems are observed (Fig. 4c).

Sedimentary unit IV shows a thickness of 200–1300 ms TWT (~0.2–1.5 km). We observe weak to moderate, well-layered reflections separated by several unconformities (Fig. 3d, CDP 100–8700). In the eastern Amundsen Sea and in the area of the Marie Byrd Seamounts sediment drifts are observed. Again the steep flank of the eastern Amundsen Sea sediment drifts face eastward, while the steep flanks of the Marie

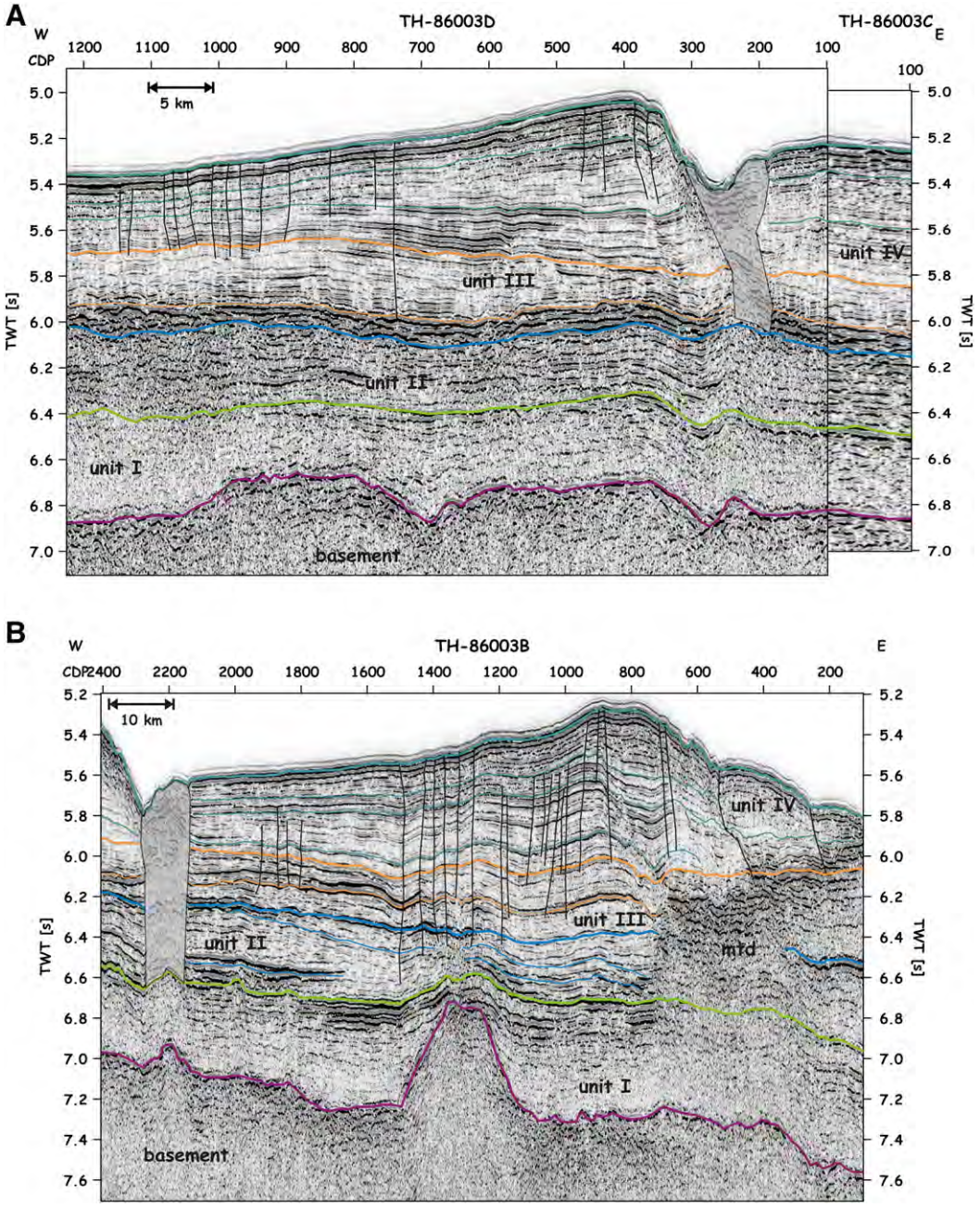

Fig. 3. a: JNOC profile TH-86003D from the eastern Amundsen Sea. Note the levee drift. The grey shaded areas show filled channels, the thin black lines are small scale faults. b: JNOC profile TH-86003B from the eastern Amundsen Sea. Note the levee drift. The grey shaded areas show filled channels, the thin black lines are small scale faults, the arrows show downlapping reflections. mtd = mass transport deposit. c: JNOC profile TH-86003A from the eastern Amundsen Sea. Note the levee drift west of CDP 1700. The grey shaded areas show filled channels, the thin black lines are small scale faults, the arrows (black and white) show downlapping reflections. mtd = mass transport deposit. d: Eastern part of profile AWI-20060023 from the eastern Amundsen Sea. Note the different levee drifts. The grey shaded areas show filled channels, the thin black lines are small scale faults. mtd = mass transport deposit.

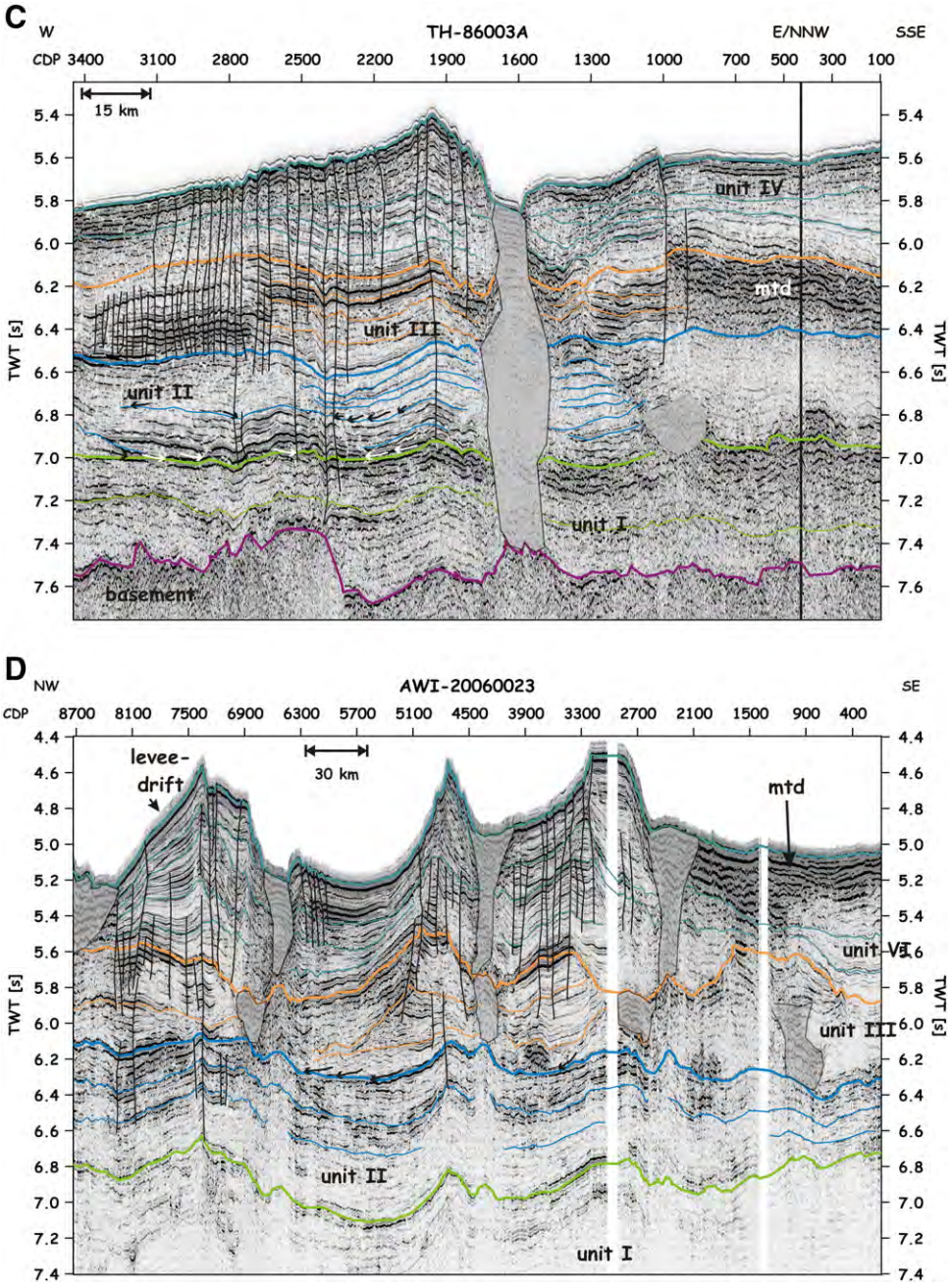

Fig. 3 (*continued*).

Byrd Seamount drifts face the basement highs (Figs. 2b, CDPs 2100–2900 and 3b, CDPs 100–8900, 10, CDPs 500–1100,). Especially the sediment drifts in the eastern Amundsen Sea are dissected by small scale faults (Fig. 3d, CDPs 100–8700). Channels separate the sediment drifts in the eastern Amundsen Sea. They are partly filled.

In the central Amundsen Sea unit IV is characterised by channel–levee systems. Those are particularly prominent close to the continental slope (Fig. 4d). Mass transport deposits occur mainly in the central Amundsen Sea also close to the continental slope.

6. Discussion

The sedimentary structures observed in the seismic data show a distinct distribution for the different sedimentary units and migration from one unit to the other. We are aware of the fact that only few seismic lines cover this huge area and the sedimentary structures may have been imaged obliquely. This limits the validity of the inferred sediment transport directions. We still analyse the geometry of the sediment drifts and channel–levee systems to derive a working hypothesis for the oceanographic development. We will discuss the distribution and possible implications for both down-slope (turbiditic) and along-slope (contouritic) sediment transport in the following. From this discussion we will infer modifications in the oceanographic and climatic conditions.

Within sedimentary unit I we observe sediment drifts only in the area of the Marie Byrd Seamounts (Fig. 4a). They show a steep flank towards the seamounts, and a moat separates the drifts from the seamounts (Fig. 2a, CDPs 600–1200, and b, CDPs 1500–1800). These sediment drifts rest directly on basement. Basalts dredged from the Marie Byrd Seamounts have been dated as young as 65–55 Ma (Kipf et al., 2008, submitted for publication). However, the basement of the Marie Byrd Seamount area is likely to be older than the seamounts and may even contain fragments of thinned continental crust (Gohl, 2008). We can infer an Eocene or older age for the oldest sediments deposited. Since sediment drifts are created and shaped by bottom currents

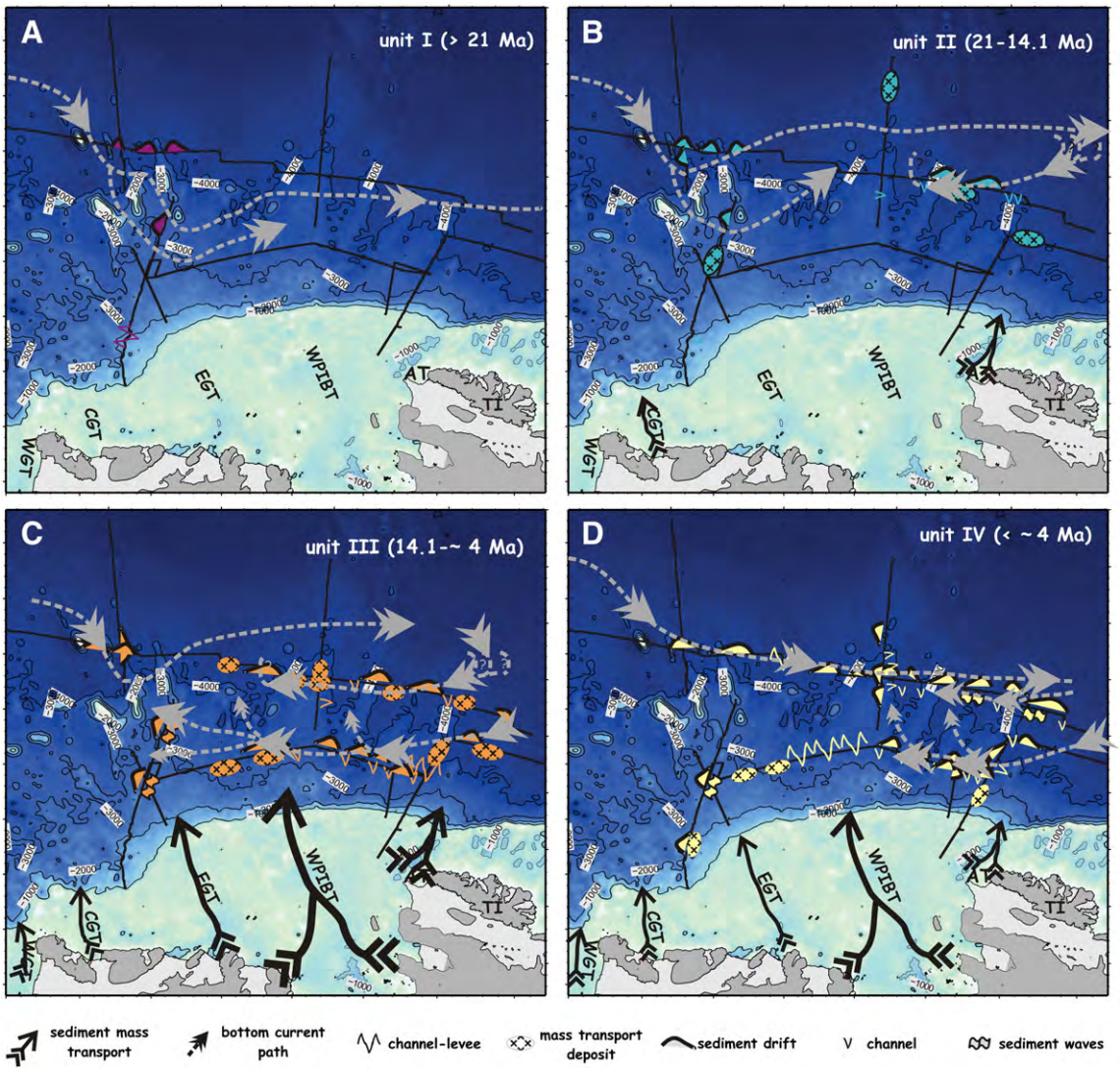

Fig. 4. Depositional and oceanographic model showing the observed sedimentary structures, and the inferred sediment input and bottom current paths for the four distinguished sedimentary units. AT = Abbot Trough, CGT = central Getz Trough, EGT = eastern Getz Trough, WGT = western Getz Trough, WPIBT = Western Pine Island Bay Trough.

(Stow et al., 2002; Shanmugam, 2006; Shanmugam and Camerlenghi, 2008) this implies a certain bottom current activity already in Paleogene times. Bottom water is formed by sea surface heat loss leading to an increase in sea surface density (Van Aken, 2007). The formation of sea ice and the increase of the sea surface salinity as a result of the heat loss both additionally increase the surface density generating an unstable upper water column. This then leads to the onset of a convective mixing (Van Aken, 2007). Today, a deep geostrophic outflow of bottom water from the Ross Sea into the deep Pacific–Antarctic Basin can be observed near 140°W (Van Aken, 2007; Orsi and Wiederwohl, 2009).

The indication of bottom water activity in the western Amundsen Sea already in Paleogene times derived from the observation of sediment drifts points towards a cool climate, as suggested by Miller et al. (2005) and Tripati et al. (2005), with at least a substantial sea ice cover allowing bottom water formation. The onset of the ACC following the opening of Drake Passage (after the middle Eocene) and the Tasman gateway (35.5 Ma) with its incorporated Circumpolar Deep Water (CDW) may be discussed as another origin for the formation of sediment drifts in the Amundsen Sea during the Paleogene. CDW is formed by the supply of saline North Atlantic Deep Water (NADW) exported from the Atlantic, this creates Lower CDW (LCDW), and the return of slightly less dense, low-oxygen water from the Indian and Pacific Basins creating Upper CDW (UCDW) (Rintoul et al., 2001). Without NADW, whose existence has only been reported for the last 14 My (Frank et al., 2002), CDW is not produced. So, CDW as the primary water mass shaping sediment drifts in Eocene/Oligocene times is unlikely. Additionally, Anderson (1999) reported a cooling of the surface waters for the Eocene, which fits an already existing Proto-Ross gyre as proposed by Huber et al. (2004).

It can be assumed that the Marie Byrd Seamount province was thermally raised during its formation. Only after cessation of magmatism a subsidence process could start. This raised position of the seamount province led to the deflection of the proto-AABW and made it an ideal target for reworking of sedimentary deposits into sediment drifts. No observations exist yet for the depositional environment during the Eocene in this part of Antarctica. De Santis et al. (1995), however, reported on the earliest traces of glacial processes in the eastern Ross Sea in late Oligocene times, while De Santis et al. (1999) refined this interpretation to indications of valley glaciers during the period late Oligocene (~30 Ma) to early Miocene (~21 Ma). This indicates a cooler climate for the Ross Sea region, which may have led to the formation of sea ice and hence production of bottom water. This provides a minimum age frame (Oligocene/early Miocene) following De Santis et al. (1999). So, we propose the east-setting flow of a proto-AABW, which originated in the Ross Sea and was deviated by the topography of the Marie Byrd Seamounts, there formed sediment drifts and flowed onwards to the east in the Eocene to early Miocene (Fig. 4a).

Sedimentary unit II shows sediment drifts in the Marie Byrd Seamount area with a steep flank towards the basement highs and a

Table 1
Oceanographic/climatological model proposed here in relation to published geological events. 1 (Anderson, 1999), 2 (Bart, 2003), 3 (Böhm et al., 2009), 4 (De Santis et al., 1999), 5 (Escutia et al., 2005), 6 (Francis et al., 2009), 7 (Haywood et al., 2009), 8 (Hernandez-Molina et al., 2004), 9 (Hillenbrand and Ehrmann, 2005), 10 (Huber et al., 2004), 11 (Miller et al., 2008), 12 (Naish et al., 2009a), 13 (Naish et al., 2009b), 14 (Pollard and DeConto, 2009), 15 (Rebesco et al., 2006), 16 (Rebesco et al., 2002), 17 (Scheuer et al., 2006b), 18 (Uenzelmann-Neben, 2006).

	Geological setting	Model proposed here				
		Sedimentary unit	Proposed age	Sedimentary features	Main area of occurrence	Oceanographic/climatological interpretation
Early Cenozoic	No evidence for ice sheet on continental shelf[1]	I	60–21 Ma	Elongate sediment drifts	Marie Byrd Seamounts	Eastward flow of bottom water (proto-AABW?)
Eocene	Cooling of surface waters[1], Existing proto-Ross gyre[10]					
Middle Eocene	Beginning of opening of Drake Passage[6]					
35.5 Ma	Opening of Tasman gateway[10]					
Earliest Oligocene	Advance of ice from elevated areas to sea level in WAIS region[11]					
Middle Oligocene	Mountain glaciers and ice caps[1]					
30–21 Ma	Valley glaciers in Ross Sea[4]					
21–14.1 Ma	Transitional stage with expansions of ice caps onto Ross Sea shelf[4]	II	21–15	Elongate drifts levee–drifts	Marie Byrd Seamounts eastern Amundsen Sea	Intensified bottom water activity cyclonic eddies shed from bottom water?
14 Ma	Growth of WAIS[7], two reported WAIS expansions to the shelf edge in Ross Sea[2]	III	15–4	Elongate drifts levee–drifts	Marie Byrd Seamounts eastern Amundsen Sea	Intensified bottom water activity cyclonic eddies shed from bottom water
14.1–4 Ma	Large and thick ice sheet in Ross Sea, Indications for major glacial sediment transport[4]			mass transport deposits	central/eastern Amundsen Sea	advancing ice sheet
9.6 Ma	Bottom current activity in Bellingshausen Sea[8, 9, 16, 17, 18]					
Pliocene	Several warm intervals leading to strong increase in surface temperatures[5], ice retreat in Ross Sea after 4 Ma[4]	IV	4–0	Levee–drifts mass transport deposits	eastern Amundsen Sea near continental rise	Bottom water activity has shifted southwards, less intense change in ice regime from wet- to dry-based
3 Ma	Change from wet- to dry based ice sheets[15]					
2.6 Ma	Rapid oscillations of WAIS and volume changes between open water and grounded ice[12, 13, 14]					

moat separating the drifts from the highs (Fig. 2a, CDPs 600–1200, and c, CDPs 1600–2700) but we also identify a few sediment drifts in the eastern Amundsen Sea (Figs.3c, CDPs 1700–3400, and 4b). These eastern Amundsen Sea drifts have a steep flank facing eastwards and are separated by filled channels. These sediment drifts represent the levee–drift type. Levee–drifts comprise a mixed system, where a bottom current controls or modifies the morphology of sediment accumulations sourced by different processes such as turbidity currents (e.g. Michels et al., 2001; Rebesco and Stow, 2001; Michels et al., 2002; Stow et al., 2002). Levee–drifts often are characterised by a marked asymmetry with one very well developed and one small levee (Fig. 3a, CDPs 100–1200, and d, CDPs 2200–8700). The occurrence of levee–drifts already indicates an increased material input from the continent with the entrainment of the suspended load of down-slope turbidity currents within the ambient, in this case, southwest (on the Southern Hemisphere the Coriolis force deflects to the left, hence a better developed western levee points to a west-setting current) directed bottom currents and their deposition down-current.

The increased material input may well be the result of repeated erosion due to growing mountain glaciers or a local or regional ice sheet. The occurrence of mass transport deposits mainly in the eastern and central Amundsen Sea (Fig. 4b) also supports this interpretation (Laberg and Vorren, 1995; King, 1997; Laberg and Vorren, 2000; Ó Cofaigh et al., 2003, 2004). Analysing the distribution of levee–drifts and mass transport deposits we suggest that the sedimentary material was supplied via the glacial Abbot Trough on the shelf northwest of Thurston Island, as well as from the central and western Getz Glacier troughs (Fig. 4b) in the westernmost Amundsen Sea Embayment. The glaciers originate at the mountain ranges of coastal Marie Byrd land, which has been uplifted since about 29–25 Ma due to a mantle plume (LeMasurier, 2008). There, the shelf is relatively narrow and the material can be transported across the shelf at short distances.

The southernmost sediment drift observed in the Marie Byrd Seamount area is now built-up into an elongate drift with the steep flank facing south (Fig. 2c, CDPs 1600–2700). Here, the bottom current flows along the sediment drift. We can see that the apex of the drift slightly migrates towards the north indicating a northward relocation of the shaping bottom current. De Santis et al. (1999) reported on a transitional stage with expansions of ice caps onto the continental shelf of the eastern Ross Sea for the period 21–14.1 Ma. Bart (2003) identified at least two WAIS grounding events on the Ross Sea outer shelf at 17.3–15.7 Ma and 15.7–14.4 Ma. This suggests a larger scale cooling and ice expansion leading to a northward shift of the proto-AABW formed in the Ross Sea. This northward shifted proto-AABW is inferred to have shaped the sediment drifts in the Marie Byrd Seamount area as documented in the migration of the apex of the elongated drift (Fig. 2c, CDP 1600–2700). We thus correlate the deposition of our sedimentary unit II with the period of De Santis' et al. (1999) transitional stage and assign an age of 21–14.1 Ma.

The geometry of the levee–drifts (steeper flank facing the east) in the eastern Amundsen Sea points towards a southwest-setting bottom current shaping them. Two possible explanations exist for this bottom current: a) small cyclonic eddies shed by the east-setting proto-AABW, or b) a westward continued flow of modified Weddell Sea Deep Water (WSDW) or Lower Circumpolar Deep Water (LCDW), which has already been reported to shape sediment drifts in the Bellingshausen Sea and on the continental margin of the western Antarctic Peninsula (Camerlenghi et al., 1997; Smith et al., 1999; Nitsche et al., 2000; Giorgetti et al., 2003; Scheuer et al., 2006b; Uenzelmann-Neben, 2006; Hillenbrand et al., 2008). Unfortunately, no oceanographic information has been published yet to clarify the origin of this possible southwest-setting bottom current.

Sedimentary unit III still shows sediment drift formation in the area of the Marie Byrd Seamounts. In the southern Marie Byrd Seamount area we now observe the formation of an attached drift instead of an elongate drift (Fig. 2c, CDPs 1800–3300). The steep flank of this drift faces northwards compared to a south facing flank of unit II elongate drift. This points towards a relocation of the bottom current to the north.

Levee–drift formation significantly increased in the central and eastern Amundsen Sea (Fig. 4c). Additionally, more mass transport deposits have been formed (Fig. 4c). We interpret these observations to represent a steep increase in material input from the continent. Especially the rise in debris flow formation is an indication for glacial grounding zone advances (Laberg and Vorren, 1995, 2000; Ó Cofaigh et al., 2003, 2004). This corresponds well to the change in reflection characteristics to now recurrently appearing moderate to strong internal reflections (Fig. 3b), which is an indication for episodic material input e.g. as the result of a growing ice sheet. Rebesco et al. (2002) identify a similar change in reflection characteristics in seismic unit M4 at Drift 7 west of the Antarctic Peninsula. This unit has also been interpreted to be the result of increased material input due to a growing local ice sheet with a slight decrease of this process during deposition of unit M3 (Uenzelmann-Neben, 2006). Using information from ODP Leg 178 Site 1095, ages of 15–9.5 Ma and 9.5–5.3 Ma were assigned to units M4 and M3, respectively (Acton et al., 2002; Iwai et al., 2002; Uenzelmann-Neben, 2006). Haywood et al. (2009) found evidence for a significant growth of WAIS following 14 Ma. In the Ross Sea, a large and thick ice sheet, deeply shaping the continental shelf up to the shelf edge, was interpreted for the late Miocene–Pliocene (14.1–4 Ma) (De Santis et al., 1999). Analogue to this we suggest an age of 14.1–~4 Ma for our sedimentary unit III.

Within the lower part of the Miocene/Pliocene unit III (14.1–10 Ma) De Santis et al. (1999) observed mounded sediment bodies, which they interpret as a document of major glacial sediment transport. Glacial–interglacial volumes were found to increase on the continental slope (Cooper et al., 2009). We also have identified indications for an advance of the grounding line in the area of the Amundsen Sea via the increase in mass transport deposits. Material is interpreted to have increasingly been supplied via the Western Pine Island Bay Trough (WPIBT) as well as Getz Trough (WBT, CGT, and EGT) and the Abbot Trough (AT) northwest of Thurston Island. Dowdeswell et al. (2006) and Evans et al. (2006) reported on a similar major cross-shelf trough at ~114°W through which fast-flowing ice drained the WAIS under fully-glaciated conditions. Increased input of sediment leads to down-slope transport via turbidity currents and mass transport deposits with the formation of channels. The material is picked up by a bottom current and deposited as levee–drifts. This bottom current could have its origin in a) local cyclonic eddies shed from the east-setting proto-AABW, or b) a westward continued flow of WSDW or LCDW. The east-setting proto-AABW has shifted further north with a modification in sediment drift type in the southern Marie Byrd Seamount area (Fig. 4c).

For sedimentary unit IV, we observe reduction in sediment drift formation in the Marie Byrd Seamount area (Fig. 4d). The central and eastern Amundsen Sea also show less sediment drifts and mass transport deposits but more channel–levee systems. This points towards a general reduction in material input, which could be a result of a waning local ice sheet or a modification in ice regime. A retreat of the ice sheet was observed for the Bellingshausen Sea for the period since 5.3 Ma (units M2 and M1) (Uenzelmann-Neben, 2006). Rebesco and Camerlenghi (2008) observed a modification in seismic stratigraphy from deep erosion of the continental shelf and slope to prominent growth of steep wedges at ~3 Ma. They suggested this to reflect a change in texture and water content of sediment delivered by the Antarctic ice sheet following the transition from wet- to dry-based ice regimes. Information from DSDP Leg 35 Site 324 (Shipboard Scientific Party, 1976; Tucholke et al., 1976a) allows an assignment of ~4 Ma (Pliocene) — present to sedimentary unit I, which is in accordance with the observations in the Bellingshausen Sea. The influence of the bottom current appears to be reduced. In the central Amundsen Sea the material is solely transported by turbidity currents and deposited in channel–levee systems. The eastern Amundsen Sea still shows the effect of the bottom current.

In the Ross Sea, Böhm et al. (2009) also observed a change from wet-based to dry-based ice dynamics of WAIS expansion in the late Pliocene and considered this to have been a regional modification. Instead of overcompaction, the sediments on the shelf now appear to be

normally compacted (Böhm et al., 2009). De Santis et al. (1999) interpreted a maximum extension of the WAIS for the period 10–4 Ma. After 4 Ma, they see long periods of ice sheets retreating from the Ross Sea. This further supports our observations.

We suggest the reduction in material input into the Amundsen Sea since ~4 Ma to be the result of a modification in ice regime from wet- to dry-based. Episodic down-slope movement primarily via the Western Pine Island Bay Trough (WPIBT) resulted in the formation of channel–levee systems, while in the eastern Amundsen Sea along-slope transport appears to have prevailed. (Fig. 4d).

The model for the oceanographic and climatic development put forward unfortunately suffers from a quite imprecise age-depth model. The only available tie to a drill site (DSDP Leg 38 Site 324) just provides information on the upper 200 m of the sedimentary column. Information from a deeper drill site is thus desperately needed to better constrain the interpretation of seismic data and obtain input parameters for numerical simulations of climatic and oceanographic variations.

7. Conclusions

Analysing seismic reflection data with respect to sedimentary structures on the continental rise of the southern Amundsen Sea, we observe sediment drifts, mass transport deposits such as debris flows, and channel–levee systems as predominant features showing a distinct regional and chronological development. We can identify four major stages in sediment deposition related to modification in the oceanographic and climatic system (Table 1).

Sediment drifts have already been formed in the oldest sedimentary sequences deposited in the Marie Byrd Seamount area. A correlation with erosional events resulting from glacial activity from the Ross Sea (De Santis et al., 1999) provides a minimum age frame of roughly 60–21 Ma for the oldest sedimentary unit identified. This indicates bottom current activity and hence a significant sea ice cover already in Eocene/Oligocene times. The bottom water shaping the sediment drifts is supposed to originate in the Ross Sea and flow eastwards with a southward deflection in the area of the Marie Byrd Seamounts. We thus interpret this bottom water to constitute a kind of proto-AABW.

Bottom currents then appear to have intensified with the formation of drifts in the eastern Amundsen Sea during the period 21–15 Ma. The proto-AABW is inferred to have moved slightly north allowing for the shaping of levee–drifts by a southwest-setting bottom current closer to the continental slope. This we interpret to be the result of either cyclonic eddies shed from the proto-AABW or a westward extension of modified WSDW or LCDW (Hillenbrand et al., 2008).

During the third stage the sediment input has significantly increased documented by a large number of mass transport deposits such as debris flows. This can be interpreted as the result of an advancing ice sheet, and we suggest that this stage represents the major onset of glaciations. Proto-AABW is shifted further to the north and the southwest-setting bottom current has also intensified.

A reduction in sediment input since 4 Ma points towards a change in ice regime from wet- to dry-based. The central Amundsen Sea appears to have been affected primarily by down-slope sediment transport whereas in the eastern Amundsen Sea along-slope sediment transport appears to have remained the dominant process. The flow of proto-AABW accordingly shifted southward and the intensity of the southwest-flowing bottom current shaping levee–drifts also decreased.

Due to the limited data base, research in the greater Amundsen Sea is still in its infancy. More seismic as well as deep reaching geological data are needed to add to the reliability of the presented model.

Acknowledgements

We are grateful to the captains, crews and scientists for their support during the RV Polarstern cruises ANT-XI/3 (1994) and ANT-XXIII/4 (2006) during which the data used in this paper were collected. We further thank the helpful comments of three reviewers and Dr. D. Piper. This is AWI publication No. 25584.

References

Acton, G.D., Guyodo, Y., Brachfeld, S.A., 2002. Magnetostratigraphy of sediment drifts on the continental rise of West Antarctica (ODP Leg 178, Sites 1095, 1096, and 1101). In: Barker, P.F., Camerlenghi, A., Acton, G.D., Ramsay, A.T.S. (Eds.), Proceedings of the Ocean Drilling Program. Scientific Results, Volume 178. Ocean Drilling Program, College Station.
Anderson, J.B., 1999. Antarctic Marine Geology. Cambridge University Press, Cambridge.
Anderson, J.B., Shipp, S.S., Lowe, A.L., Wellner, J.S., Mosola, A.B., 2002. The Antarctic ice sheet during the Last Glacial Maximum and its subsequent retreat history: a review. Quaternary Science Reviews 21, 49–70.
Bart, P.J., 2003. Were West Antarctic Ice Sheet grounding events in the Ross Sea a consequence of East Antarctic Ice Sheet expansion during the middle Miocene? Earth and Planetary Science Letters 216 (1–2), 93–107.
Böhm, G., Ocakoglu, N., Picotti, S., De Santis, L., 2009. West Antarctic Ice Sheet evolution: new insights from a seismic tomographic 3D depth model in the Eastern Ross Sea (Antarctica). Marine Geology 266 (1–4), 109–128.
Camerlenghi, A., et al., 1997. Ten-month observation of the bottom current regime across a sediment drift of the Pacific margin of the Antarctic Peninsula. Antarctic Science 9.
Carter, L., McCave, I.N., Williams, M.J.M., Florindo, F., Siegert, M., 2009. Chapter 4 Circulation and Water Masses of the Southern Ocean: A Review, Developments in Earth and Environmental Sciences. Elsevier, pp. 85–114.
Cooper, A.K., et al., 2009. Cenozoic climate history from seismic reflection and drilling studies on the Antarctic Continental Margin. In: Florindo, F., Siegert, M. (Eds.), Antarctic Climate Evolution. Developments in Earth and Environmental Sciences. Elsevier, pp. 115–228.
Dahlgren, K.I.T., Vorren, T.O., Laberg, J.S., 2002. The role of grounding-line sediment supply in ice-sheet advances and growth on continental shelves: an example from the mid-Norwegian sector of the Fennoscandian ice sheet during the Saalian and Weichselian. Quaternary International 95–96, 25–33.
De Santis, L., Anderson, J.B., Brancolini, G., Zayatz, I., 1995. Seismic record of late Oligocene through Miocene glaciation on the central and eastern continental shelf of the Ross Sea. In: Cooper, A.F., Barker, P.F., Brancolini, G. (Eds.), Geology and seismic Stratigraphy of the Antarctic Margin. American Geophysical Union, Washington, pp. 235–260.
De Santis, L., Prato, S., Brancolini, G., Lovo, M., Torelli, L., 1999. The Eastern Ross Sea continental shelf during the Cenozoic: implications for the West Antarctic ice sheet development. Global and Planetary Change 23 (1–4), 173–196.
Domack, E.W., Jacobson, E.A., Shipp, S., Anderson, J.B., 1999. Late Pleistocene/Holocene retreat of the West Antarctic Ice-Sheet system in the Ross Sea: Part 2 — Sedimentologic and stratigraphic signature. Geological Society of America Bulletin 111 (10), 1517–1536.
Dowdeswell, J.A., Evans, J., O Cofaigh, C., Anderson, J.B., 2006. Morphology and sedimentary processes on the continental slope off Pine Island Bay, Amundsen Sea, West Antarctica. Geological Society of America Bulletin 118, 606–619.
Eagles, G., Gohl, K., Larter, R.D., 2004. High-resolution animated tectonic reconstruction of the South Pacific and West Antarctic Margin. Geochemistry, Geophysics, Geosystems 5.
Emery, D., Myers, K., 1996. Sequence Stratigraphy. Blackwell Science Ltd. 297 pp.
Escutia, C., et al., 2005. Cenozoic ice sheet history from East Antarctic Wilkes Land continental margin sediments. Global and Planetary Change 45, 51–81.
Escutia, C., et al., 2009. Circum-Antarctic warming events between 4 and 3.5 Ma recorded in marine sediments from the Prydz Bay (ODP Leg 188) and the Antarctic Peninsula (ODP Leg 178) margins. Global and Planetary Change 69 (3), 170–184.
Evans, J., Dowdeswell, J.A., O Cofaigh, C., Benham, T.J., Anderson, J.B., 2006. Extent and dynamics of the West Antarctic Ice Sheet on the outer continental shelf of Pine Island Bay during the last glaciation. Marine Geology 230, 53–72.
Faugères, J.C., Mezerais, M.L., Stow, D.A.V., 1993. Bottom-controlled sedimentation: a synthesis of the contourite problem. Sedimentary Geology 82, 287–297.
Faugères, J.C., Stow, D.A.V., Imbert, P., Viana, A.R., 1999. Seismic features diagnostic of contourite drifts. Marine Geology 162, 1–38.
Francis, J.E., et al., 2008. From Greenhouse to Icehouse — the Eocene/Oligocene in Antarctica. In: Florindo, F., Siegert, M. (Eds.), Antarctic Climate Evolution. Developments in Earth and Environmental Sciences. Elsevier, pp. 309–368.
Francis, J.E., et al., 2009. From Greenhouse to Icehouse — the Eocene/Oligocene in Antarctica. In: Florindo, F., Siegert, M. (Eds.), Antarctic Climate Evolution. Developments in Earth and Environmental Sciences. Elsevier, pp. 309–368.
Frank, M., Whiteley, N., Kasten, S., Hein, J.R., O'Nions, R.K., 2002. North Atlantic Deep Water export to the Southern Ocean over the past 14 Myr: evidence from Nd and Pb isotopes in ferromanganese crusts. Paleoceanography 17.
Giorgetti, A., et al., 2003. Water masses and bottom boundary layer dynamics above a sediment drift of the Antarctic Peninsula Pacific Margin. Antarctic Science 15.
Gohl, K., 2008. Antarctica's continent–ocean transitions: consequences for tectonic reconstructions. In: Cooper, A.K., et al. (Ed.), Antarctica: A Keystone in a Changing World. Proceedings of the 10th International Symposium on Antarctic Earth Sciences. The National Academies Press, Washington, DC, pp. 29–38.
Gohl, K., et al., 1997. Tectonic and sedimentary architecture of the Bellingshausen and Amundsen Sea Basins, SE Pacific, by seismic profiling. In: Ricci, C.A. (Ed.), The Antarctic Region: Geological Evolution and Processes. Terra Antartica Publication, Siena, pp. 719–723.
Gohl, K., et al., 2007. Geophysical survey reveals tectonic structures in the Amundsen Sea embayment, West Antarctica. In: Cooper, A.K., Raymond, C.R., et al. (Eds.), Antarctica: A Keystone in a Changing World. USGS Open-File Report 2007–1047, Sta Barbara, USA.
Gordon, A.L., et al., 2009. Western Ross Sea continental slope gravity currents. Deep Sea Research Part II: Topical Studies in Oceanography 56 (13–14), 796–817.
Haywood, A.M., et al., 2009. Middle Miocene to Pliocene History of Antarctica and the Southern Ocean. In: Florindo, F., Siegert, M. (Eds.), Antarctic Climate Evolution. Developments in Earth and Environmental Sciences. Elsevier, pp. 401–463.

Hernandez-Molina, F.J., Larter, R.D., Rebesco, M., Maldonado, A., 2004. Miocene changes in bottom current regime recorded in continental rise sediments on the Pacific margin of the Antarctic Peninsula. Geophysical Research Letters 31.
Hernandez-Molina, F.J., Larter, R.D., Rebesco, M., Maldonado, A., 2006. Miocene reversal of bottom water flow along the Pacific Margin of the Antarctic Peninsula: Stratigraphic evidence from a contourite sedimentary tail. Marine Geology 228, 93–116.
Hillenbrand, C.-D., Ehrmann, W., 2005. Late Neogene to Quaternary environmental changes in the Antarctic Peninsula region: evidence from drift sediments. Global and Planetary Change 45, 165–191.
Hillenbrand, C.-D., Grobe, H., Diekmann, B., Kuhn, G., Fütterer, D.K., 2003. Distribution of clay minerals and proxies for productivity in surface sediments of the Bellingshausen and Amundsen seas (West Antarctica) — relation to modern environmental conditions. Marine Geology 193 (3–4), 253–271.
Hillenbrand, C.-D., et al., 2008. The present and past bottom-current flow regime around the sediment drifts on the continental rise west of the Antarctic Peninsula. Marine Geology 255.
Hillenbrand, C.-D., et al., 2009a. Age assignment of a diatomaceous ooze deposited in the western Amundsen Sea Embayment after the Last Glacial Maximum. Journal of Quaternay Science 25 (3), 280–295.
Hillenbrand, C.D., Kuhn, G., Frederichs, T., 2009b. Record of a Mid-Pleistocene depositional anomaly in West Antarctic continental margin sediments: an indicator for ice-sheet collapse? Quaternary Science Reviews 28 (13–14), 1147–1159.
Huber, M., et al., 2004. Eocene circulation of the Southern Ocean: was Antarctica kept warm by subtropical waters? Paleoceanography 19.
Ivany, L.C., Van Simaeys, S., Domack, E.W., Samson, S.D., 2006. Evidence for an earliest Oligocene ice sheet on the Antarctic Peninsula. Geology 34 (5), 377–380.
Iwai, M., Acton, G., Lazarus, D., Osterman, L.E., Williams, T., 2002. Magnetobiochronologic Synthesis of ODP Leg 178 Rise Sediments from the Pacific Sector of the Southern Ocean: Sites 1095, 1096, and 1101. In: Barker, P.F., Camerlenghi, A., Acton, G.D., Ramsay, A.T.S. (Eds.), Proceedings of the Ocean Drilling Program, Scientific Results, Volume 178. Ocean Drilling Program, College Station.
Jacobs, S.S., Hellmer, H.H., Jenkins, A., 1996. Antarctic Ice Sheet melting in the southeast Pacific. Geophysical Research Letters 23 (9), 957–960.
King, E.L., 1997. Debris flows on a glacial trough mouth fan, Norwegian Channel and North Sea fan. In: Davies, T.A., et al. (Ed.), Glaciated continental margins — an atlas of acoustic images. Chapman & Hall, London, pp. 124–125.
Kipf, A., et al., 2008. Age and Origin of Magmatism at the Marie Byrd Seamounts (Amundsen Sea). EGU General Assembly, Vienna, Austria.
Kipf, A. et al., submitted for publication. Seamounts off the West Antarctic margin of the Pacific: A case of non-hotspot intraplate volcanism.
Laberg, J.S., Vorren, T.O., 1995. Late Weichselian submarine debris flow deposits on the Bear Island Trough Mouth Fan. Marine Geology 127 (1–4), 45–72.
Laberg, J.S., Vorren, T.O., 2000. Flow behaviour of the submarine glacigenic debris flows on the Bear Island Trough Mouth Fan, western Barents Sea. Sedimentology 47 (6), 1105–1117.
LeMasurier, W.E., 2008. Neogene extension and basin deepening in the West Antarctic rift inferred from comparisons with the East African rift and other analogues. Geology 36, 247–250.
Lowe, A.J., Anderson, J.B., 2002. Reconstruction of the West Antarctic ice sheet in Pine Island Bay during the Last Glacial Maximum and its subsequent retreat history. Quaternary Science Reviews 21, 1879–1897.
Lowe, A.J., Anderson, J.B., 2003. Evidence for abundant subglacial meltwater beneath the paleo-ice sheet in Pine Island Bay, Antarctica. Journal of Glaciology 49, 125–138.
Michels, K.H., Rogenhagen, J., Kuhn, G., 2001. Recognition of contour-current influence in mixed contourite–turbidite sequences of the western Weddell Sea, Antarctica. Marine Geophysical Researches 22, 465–485.
Michels, K.H., et al., 2002. The southern Weddell Sea: combined contourite–turbidite sedimentation at the southeastern margin of the Weddell Gyre. In: Stow, D.A.V., Pudsey, C.J., Howe, J.A., Faugeres, J.-C., Viana, A.R. (Eds.), Deep-water contourite systems: Modern drifts and ancient series, seismic and sedimentary characteristics. Geological Society London, pp. 305–323.
Miller, K.G., Wright, J.D., Browning, J.V., 2005. Visions of ice sheets in a greenhouse world. Marine Geology 217 (3–4), 215–231.
Miller, K.G., et al., 2008. A view of Antarctic ice sheet evolution from sea-level and deep-sea isotope changes during the Late Cretaceous–Cenozoic. In: Cooper, A.F., et al. (Ed.), Antarctica: A keystone in a changing world. National Academic Press, Washington, D.C., pp. 55–70.
Naish, T., et al., 2009a. Chapter 11 Late Pliocene–Pleistocene Antarctic Climate Variability at Orbital and Suborbital Scale: Ice Sheet, Ocean and Atmospheric Interactions, Developments in Earth and Environmental Sciences. Elsevier, pp. 465–529.
Naish, T., et al., 2009b. Obliquity-paced Pliocene West Antarctic ice sheet oscillations. Nature 458 (7236), 322–328.
Nitsche, F.O., Gohl, K., Vanneste, K., Miller, H., 1997. Seismic expression of glacially deposited sequences in the Bellingshausen and Amundsen Sea, West Antarctica. In: Barker, P.F., Cooper, A.F. (Eds.), Geology and Seismic Stratigraphy of the Antarctic Margin, 2. American Geophysical Union, Washington, pp. 95–108.
Nitsche, F.O., Cunningham, A.P., Larter, R.D., Gohl, K., 2000. Geometry and development of glacial continental margin depositional systems in the Bellingshausen Sea. Marine Geology 162 (2–4), 277–302.
Nitsche, F.O., Jacobs, S.S., Larter, R.D., Gohl, K., 2007. Bathymetry of the Amundsen Sea continental shelf: Implications for geology, oceanography, and glaciology. Geochemistry, Geophysics, Geosystems 8.
Ó Cofaigh, C., Taylor, J., Dowdeswell, J.A., Pudsey, C.J., 2003. Palaeo-ice streams, trough mouth fans and high-latitude continental slope sedimentation. Boreas 32 (1), 37–55.
Ó Cofaigh, C., et al., 2004. Timing and significance of glacially influenced mass-wasting in the submarine channels of the Greenland Basin. Marine Geology 207 (1–4), 39–54.
Ó Cofaigh, C., et al., 2005. Flow of the West Antarctic Ice Sheet on the continental margin of the Bellingshausen Sea at the Last Glacial Maximum. Journal of Geophysical Research 110.
Orsi, A.H., 2010. Oceanography: recycling bottom waters. Nature Geoscience 3 (5), 307–309.
Orsi, A.H., Wiederwohl, C.L., 2009. A recount of Ross Sea waters. Deep Sea Research Part II: Topical Studies in Oceanography 56 (13–14), 778–795.
Orsi, A.H., Whitworth, T., Nowlin, W.D., 1995. On the meridional extent and fronts of the Antarctic Circumpolar Current. Deep Sea Research Part I: Oceanographic Research Papers 42 (5), 641–673.
Orsi, A.H., Johnson, G.C., Bullister, J.L., 1999. Circulation, mixing, and production of Antarctic Bottom Water. Progress in Oceanography 43, 55–109.
Pollard, D., DeConto, R.M., 2009. Modelling West Antarctic ice sheet growth and collapse through the past five million years. Nature 458 (7236), 329–332.
Reading, H.G., 1996. Sedimentary Environments: Processes, Facies and Stratigraphy. Blackwell Science, Oxford. 688 pp.
Rebesco, M., Camerlenghi, A., 2008. Late Pliocene margin development and mega-debris flow deposits on the Antarctic continental margins: evidence of the onset of the modern Antarctic ice-sheet? Palaeogeography, Palaeoclimatology, Palaeoecocolgy 260, 149–167.
Rebesco, M., Stow, D.A.V., 2001. Seismic expression of contourites and related deposits: a preface. Marine Geophysical Research 22, 303–308.
Rebesco, M., Larter, R.D., Camerlenghi, A., Barker, P.F., 1996. Giant sediment drifts on the continental rise west of the Antarctic Peninsula. Geo-Marine Letters 16 (2), 65–75.
Rebesco, M., et al., 2002. Sediment drifts and deep-sea channel systems, Antarctic Peninsula Pacific Margin. In: Stow, D.A.V., Pudsey, C.J., Howe, J.A., Faugeres, J.-C., Viana, A.R. (Eds.), Deep-water contourite systems: Modern drifts and ancient series, seismic and sedimentary characteristics. Geological Society London, pp. 353–372.
Rebesco, M., Camerlenghi, A., Geletti, R., Canals, M., 2006. Margin architecture reveals the transition to the modern Antarctic ice sheet ca. 3 Ma. Geology 34, 301–304.
Rignot, E., Jacobs, S.S., 2002. Rapid bottom melting widespread near Antarctic Ice Sheet grounding lines. Science 296, 2020–2023.
Rintoul, S.R., Hughes, C.W., Olbers, D., 2001. The Antarctic circumpolar current system. In: Siedler, G., Church, J.A., Gould, J. (Eds.), Ocean Circulation and Climate. Academic Press, San Diego, pp. 271–302.
Scheuer, C., Gohl, K., Larter, R.D., Rebesco, M., Udintsev, G., 2006a. Variability in Cenozoic sedimentation along the continental rise of the Bellingshausen Sea, West Antarctica. Marine Geology 227 (3–4), 279–298.
Scheuer, C., Gohl, K., Udintsev, G., 2006b. Bottom-current control on sedimentation in the western Bellingshausen Sea, West Antarctica. Geo-Marine Letters 26 (2), 90–101.
Shanmugam, G., 2006. Deep-water processes and facies models. Handbook of petroleum exploration and production, 5. Elsevier, Amsterdam. 476 pp.
Shanmugam, G., Camerlenghi, M.R.a.A., 2008. Chapter 5 deep-water bottom currents and their deposits. Developments in Sedimentology. Elsevier, pp. 59–81.
Shepherd, A., Wingham, D., Rignot, E., 2004. Warm ocean is eroding West Antarctic Ice Sheet. Geophysical Research Letters 31.
Shipboard Scientific Party, 1976. Site 324. In: Hollister, C.D., Craddock, C. (Eds.), Initial Reports. Deep Sea Drilling Project, Washington, D.C., pp. 127–156.
Smith, D.A., Hofmann, E.E., Klinck, J.M., Lascara, C.M., 1999. Hydrography and circulation of the West Antarctic Peninsula continental shelf. Deep-Sea Research I 46, 925–949.
Stow, D.A.V., Faugères, J.-C., Howe, J.A., Pudsey, C.J., Viana, A.R., 2002. Bottom currents, contourites and deep-sea sediment drifts: current state-of-the-art. In: Stow, D.A.V., Pudsey, C.J., Howe, J.A., Faugeres, J.-C., Viana, A.R. (Eds.), Deep-water contourite systems: Modern drifts and ancient series. Memoir. Geological Society of London, London, pp. 7–20.
Thoma, M., Jenkins, A., Holland, D.M., Jacobs, S., 2008. Modelling circumpolar deep water intrusions on the Amundsen Sea continental shelf, Antarctica. Geophysical Research Letters 35 (18), L18602.
Thomas, R., et al., 2004. Accelerated sea-level rise from West Antarctica. Science 306, 255–258.
Tripati, A., Backman, J., Elderfield, H., Ferretti, P., 2005. Eocene bipolar glaciation associated with global carbon cycle changes. Nature 436 (7049), 341–346.
Tucholke, B.E., Houtz, R.E., 1976. Sedimentary framework of the Bellinghausen Basin from seismic profiler data. In: Hollister, C.D., Craddock, C. (Eds.), Initial Reports. Deep Sea Drilling Project, Washington, D.C., pp. 197–227.
Tucholke, B.E., Edgar, N.T., Boyce, R.E., 1976a. Physical properties of sediments and correlations with acoustic stratigraphy: Leg 35, Deep Sea Drilling Project. In: Hollister, C.D., Craddock, C. (Eds.), Initial Reports. Deep Sea Drilling Project, Washington, D.C., pp. 229–249.
Tucholke, B.E., Hollister, C.D., Weaver, F.M., Vennum, W.R., 1976b. Continental rise and abyssal plain sedimentation in the southeast Pacific Basin: Leg 35 Deep Sea Drilling Project. In: Hollister, C.D., Craddock, C. (Eds.), Initial Reports. Deep Sea Drilling Project, Washington, D.C., pp. 359–400.
Uenzelmann-Neben, G., 2006. Depositional patterns at Drift 7, Antarctic Peninsula: along-slope versus down-slope sediment transport as indicators for oceanic currents and climatic conditions. Marine Geology 233, 49–62.
Uenzelmann-Neben, G., Gohl, K., Larter, R.D., Schlüter, P., 2007. Differences in ice retreat across Pine Island Bay, West Antarctica, since the Last Glacial Maximum: indications from multichannel seismic reflection data. In: Cooper, A.K., Raymond, C.R.e.a. (Eds.), Antarctica — A keystone in a changing world. USGS Open File Report.
Van Aken, H.M., 2007. The oceanic thermohaline circulation. Atmospheric and Oceanographic Sciences Library, 39. Springer, New York.
Wellner, J.S., Lowe, A.J., Shipp, S.S., Anderson, J.B., 2001. Distribution of glacial geomorphic features on the Antarctic continental shelf and correlation with substrate: implications for ice behavior. Journal of Glaciology 47, 391–411.
Wilson, G.S., Pekar, S.F., Naish, T.R., Passchier, S., DeConto, R., 2009. Chapter 9 The Oligocene–Miocene Boundary — Antarctic climate response to orbital forcing. In: Florindo, F., Siegert, M. (Eds.), Developments in Earth and Environmental Sciences. Elsevier, pp. 369–400.
Yamaguchi, K., Tamura, Y., Mizukosho, I., Tsuru, I., 1988. Preliminary report of geophysical and geological surveys in the Amundsen Sea, West Antarctica. Proceedings NIPR Symposium Antarctic Geoscience 2, 55–67.
Zenk, W. and Camerlenghi, M.R.a.A., 2008. Chapter 4 Abyssal and Contour Currents, Developments in Sedimentology. Elsevier, pp. 35, 37–57.

Publication 6.3.5:

Wilson, D.S., Jamieson, S.S., Barrett, P.J., Leitchenkov, G., **Gohl, K.**, Larter, R.D. (2012). Antarctic topography at the Eocene-Oligocene boundary. *Palaeogeography, Palaeoclimatology, Palaeoecology*, v. 335-336, pp. 24-34, doi:10.1016/j.palaeo.2011.05.028.

Author contributions: Wilson developed the method for reconstructing Antarctic topography, implemented the parameters into the model and, together with Jamieson, wrote most of the paper. Gohl, Leitchenkov and Larter contributed with marine sediment data and their implementation into the model. All co-authors added to the model interpretation and discussion.

Palaeogeography, Palaeoclimatology, Palaeoecology 335-336 (2012) 24–34

Contents lists available at ScienceDirect

Palaeogeography, Palaeoclimatology, Palaeoecology

journal homepage: www.elsevier.com/locate/palaeo

Antarctic topography at the Eocene–Oligocene boundary

Douglas S. Wilson [a,*], Stewart S.R. Jamieson [b], Peter J. Barrett [c], German Leitchenkov [d], Karsten Gohl [e], Robert D. Larter [f]

[a] Marine Sciences Institute, University of California, Santa Barbara, CA 93106, United States
[b] Department of Geography, Durham University, South Road, Durham, DH1 3LE, UK
[c] Antarctic Research Centre, Victoria University of Wellington, P.O. Box 600, Wellington, New Zealand,
[d] Institute for Geology and Mineral Resources of the World Ocean, 1, Angliysky Ave. 190121, St.-Petersburg, Russia
[e] Alfred Wegener Institute for Polar and Marine Research, Postfach 120161, D-27515 Bremerhaven, Germany
[f] British Antarctic Survey, Madingley Road, High Cross, Cambridge, Cambridgeshire CB3 0ET, UK

ARTICLE INFO

Article history:
Received 1 November 2010
Received in revised form 12 May 2011
Accepted 16 May 2011
Available online 24 May 2011

Keywords:
Topography
Tectonics
Glacial erosion
Reconstruction
Antarctica

ABSTRACT

We present a reconstruction of the Antarctic topography at the Eocene–Oligocene (ca. 34 Ma) climate transition. This provides a realistic key boundary condition for modeling the first big Antarctic ice sheets at this time instead of using the present day bedrock topography, which has changed significantly from millions of years of tectonism and erosion. We reconstruct topography using a set of tools including ice sheet-erosion models, models of thermal subsidence and plate movement. Erosion estimates are constrained with offshore sediment volumes estimated from seismic stratigraphy. Maximum and minimum topographic reconstructions are presented as indicators of the range of uncertainty. Our results point to a significant upland area in the Ross Sea/Marie Byrd Land and Weddell Sea sectors. In addition, East Antarctic coastal troughs are much shallower than today due to the restoration of material that has been selectively eroded by the evolving ice sheets. Parts of East Antarctica have not changed since the E–O boundary because they were protected under non-erosive cold-based ice. The reconstructions provide a better-defined boundary condition for modeling that seeks to understand interaction between the Antarctic ice sheet and climate, along with more robust estimates of past ice volumes under a range of orbital settings and greenhouse gas concentrations.

1. Introduction

The aim is to reconstruct the Antarctic landscape at the Eocene–Oligocene (E–O) climate transition (ca. 34 Ma). This is important because experiments to test the sensitivity of ice sheet growth at this time have thus far relied upon the present day subglacial bedrock topography, rebounded for removal of ice load, as a boundary condition (DeConto and Pollard, 2003; DeConto et al., 2007, 2008). These simulations assumed that tectonism and erosion had made no significant changes to the Antarctic landscape over the past 34 million years. However a recent reconstruction of West Antarctica by Wilson and Luyendyk (2009) suggested this region used to lie largely above sea level, with tectonism and erosion shrinking it considerably, reducing the continental area of the whole continent of Antarctica by 10–20% since the Eocene. Land area is a key factor in limiting both present and past continental ice sheet growth and topography determines where ice grows, flows and erodes. Hence the robustness of the results of modeling past ice sheets using different orbital parameters and greenhouse gas concentrations depends crucially on using a realistic landscape.

This study follows the general method of Wilson and Luyendyk (2009) in separately reversing processes that have changed Antarctic topography: loading of the modern ice sheet; sedimentary deposition, at least for selected continental shelf areas; erosion; thermal subsidence of extended terranes; and horizontal plate motion. We extend the previous work in two important ways: (1) expanding the restoration for erosion to the entire continent, with constraints from estimates of circum-Antarctic sediment volume; and (2) expressing the many significant uncertainties in the reconstruction process by offering separate reconstructions of maximum and minimum topography. We do not claim to present accurate topographic models, but rather two plausible end-members that are more suitable than the modern topography for predicting climate and ice sheet behaviour. We hope that differences in climate or ice sheet predictions between our maximum and minimum reconstructions will inspire further data collection including geophysical mapping and drilling to constrain the gaps in our current knowledge. Because of the limited resolution that is currently feasible for long-term climate and ice models, we generally do not address features smaller than about 40 km. We do not systematically address the evolution of deep-water bathymetry (below ~1000 m). That issue will be addressed by the ongoing work of

* Corresponding author. Tel.: +1 805 893 8033; fax: +1 805 293 2314.
E-mail addresses: dwilson@geol.ucsb.edu (D.S. Wilson), Stewart.Jamieson@dur.ac.uk (S.S.R. Jamieson).

0031-0182/$ – see front matter © 2011 Elsevier B.V. All rights reserved.
doi:10.1016/j.palaeo.2011.05.028

the Circum-Antarctic Stratigraphy and Paleobathymetry (CASP) project of a working group under the Scientific Committee for Antarctic Research (SCAR) Antarctic Climate Evolution program.

The techniques employed in our reconstruction are simple, with detailed explanations only for our method for flexural isostatic compensation with partial flooding of the continent, and our model for glacial erosion of the East Antarctic craton (Section 3 below).

2. Geologic background

2.1. Regional tectonics

The Antarctic continent is generally recognized as having a long-stable, East Antarctic sector (Fig. 1), with little Mesozoic or Cenozoic tectonic activity other than passive-margin formation with the rifting of Gondwana (e.g., Lawver and Gahagan, 1994). The West Antarctic sector has been more active with considerable Cretaceous and Cenozoic activity including subduction, gradually decreasing from most of the margin in the Early Cretaceous to hardly any in the late Cenozoic (e.g., Larter et al., 2002), extensional rifting in the West Antarctic Rift System (Behrendt et al., 1991), and volcanism. The Transantarctic Mountains, a major range with many peaks above 4000 m, form the boundary between East and West Antarctica. Several lines of evidence indicate that the modern relief in these mountains was largely established ~55–35 Ma, with subsequent glacial erosion strongly affecting only limited areas (e.g., Sugden and Denton, 2004; Miller et al., 2010).

The history of tectonic extension in the WARS is only broadly understood, as most of the extended area is hidden beneath the Ross Ice Shelf. Extension in western Marie Byrd Land and the eastern Ross Sea has been dated at 90–100 Ma (Fitzgerald and Baldwin, 1997; Luyendyk et al., 2003; Siddoway et al., 2004). The youngest phase of extension is better understood, having been interpreted from the seafloor spreading record of motion between East Antarctica and West Antarctica in the northwestern Ross Sea (Cande et al., 2000).

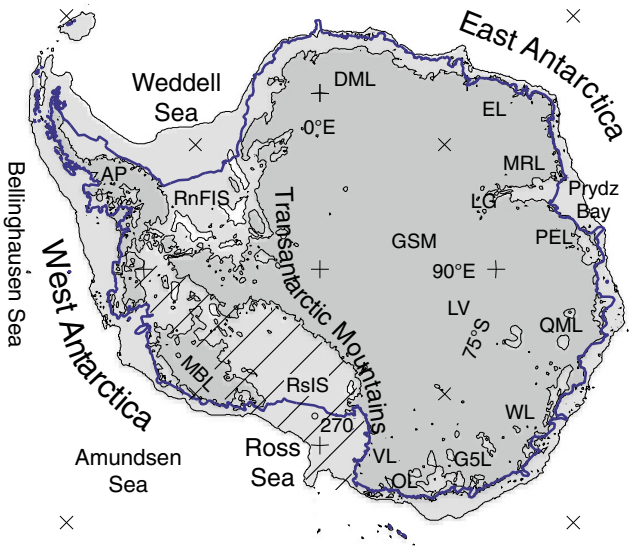

Fig. 1. Location map. Bold line shows recent Antarctic coastline, including ice shelves. Darker gray shading shows bed elevation above modern sea level, after applying a rebound correction for ice load (Fig. 2b); lighter shading shows bed shallower than −1000 m. Hachures show West Antarctic Rift System, active in Late Cretaceous and Cenozoic (Behrendt et al., 1991). Abbreviations: DML, Dronning Maud Land; EL, Enderby Land; MRL, MacRoberston Land; PEL, Princess Elizabeth Land; QML, Queen Maud Land; WL, Wilkes Land; G5L, George V Land; OL, Oates Land; VL, Victoria Land; MBL, Marie Byrd Land; AP, Antarctic Peninsula; LG, Lambert graben; GSM, Gamburtsev Subglacial Mountains; RsIS, Ross Ice Shelf; RnFIS, Ronne-Filchner Ice Shelf; 270, DSDP Site 270.

Spreading there since 45 Ma is ~170 km, and since 34 Ma is ~70 km. Total extension of the WARS can only be inferred from indirect arguments; estimates range about 300–600 km (Behrendt et al., 1991; Cande et al., 2000; Wilson and Luyendyk, 2009).

2.2. Sediment volume

The strongest constraint on the extent of continental erosion is the volume of sediment deposited around the continent. For Oligocene and younger, sediment distributions are fairly well mapped in the shallow Ross Sea, most of the East Antarctic margin, and the eastern Weddell Sea. In contrast, the western Weddell Sea and areas under the Ross, Ronne, and Filchner Ice Shelves are almost totally unmapped. For the purpose of estimating minimum and maximum palaeo-topographic surfaces, we separately estimate minimum and maximum sediment volumes, as well as densities and the biogenic fraction needed to calculate the original volume of the source material.

For the Indian Ocean sector, our observed volumes are based on the work of Kuvaas et al. (2004) and Leitchenkov et al. (2007, 2008) (Table 1). The sediment is almost entirely in deep water. We estimate volume uncertainty at ±10% except for the eastern subdivision which increases to ±20% due to limited mapping.

In the Ross Sea, our estimates are based on the volume of sedimentary units RSS-2 and younger from ANTOSTRAT (1995). Units are well mapped on the continental shelf, poorly mapped in deep water, and unmapped under the Ross Ice Shelf. Significant uncertainty also arises because there is only a minimum age for the base of RSS-2 at ~26 Ma (McDougall, 1977; ANTOSTRAT, 1995); we account for the possibility that a significant volume of sediment below RSS-2 is younger than 34 Ma. In parts of the Ross Sea, considerable thicknesses of sediments judged to be older than 34 Ma are not restored.

For the Amundsen Sea and western Bellinghausen Sea sector, our estimates are derived from the isopach grids of Scheuer et al. (2006a) and additional thickness estimates from more recently acquired seismic data in the southern Amundsen Sea (K. Gohl, unpublished). The seismic horizons which are interpreted as the onset of glacially deposited sediments (e.g., Nitsche et al., 2000) are correlated from the drilled and dated continental rise records of the Antarctic Peninsula, through the Bellingshausen Sea (Scheuer et al., 2006b), and farther to the Amundsen Sea. With no drill records in this latter sector, any age estimate for the major onset of deposition of glacially transported sediments on the shelf and continental rise remains speculative. Whilst glacially-derived sediments were accumulating on the Antarctic Peninsula continental rise since at least 9.5 Ma, the timing of onset of glacial sedimentation in the southern Bellingshausen and Amundsen seas is presently unconstrained by drilling and may have occurred either earlier or later than along the Antarctic Peninsula. Uncertainties are large due to incomplete mapping and limited age control.

Sediment volumes along the Antarctic Peninsula are based on seismic data from Tucholke and Houtz (1976), Larter and Barker (1991), Nitsche et al. (1997, 2000), and Cooper et al. (2009), with age control from DSDP Sites 322 and 325 (Hollister and Craddock, 1976). We set a significant upper bound for volume based on the possibility of substantial sediment subduction beneath the northern Peninsula.

Sediment volume for the Weddell Sea is primarily derived and extrapolated from the seismic stratigraphy mapped by Rogenhagen et al. (2004) in the eastern Weddell Sea, with age control from ODP Site 693 (Barker et al., 1988; Miller et al., 1990). Extrapolation was guided by the very few existing seismic records (Hübscher et al., 1996; Rogenhagen and Jokat, 2000). Uncertainty is large and can only be estimated subjectively, due to lack of data under nearly permanent sea ice. We assume the transition between net deposition and net erosion since 34 Ma occurs north of the Ronne-Filchner Ice Shelf.

Table 1
Observed sediment volume and source estimates.

Region		Observed Volume 10^6 km^3		In situ density (g/cm^3)		Biogenic fraction		Source density (g/cm^3)		Target source volume 10^6 km^3	
Name	Longitude	A—Min	B—Max	A	B	A	B	A	B	A—Min	B—Max
DML	0°–30°E	0.54	0.66	1.95	2.15	0.15	0.05	2.6	2.5	0.34	0.54
EL	30°–60°E	0.63	0.77	1.95	2.15	0.15	0.05	2.6	2.5	0.40	0.63
MRL-PEL	60°–94°E	1.17	1.43	1.95	2.15	0.15	0.05	2.6	2.5	0.75	1.17
QML-WL	94°–124°E	0.54	0.66	1.95	2.15	0.15	0.05	2.6	2.5	0.34	0.54
G5L-OL	124°–165°E	0.48	0.72	1.95	2.15	0.15	0.05	2.6	2.5	0.31	0.59
Ross	165°E–150°W	1.50	3.00	2.10	2.30	0.15	0.05	2.6	2.4	1.03	2.73
Bell-Amun	150°–80°W	1.60	2.60	1.95	2.15	0.15	0.05	2.6	2.4	1.02	2.21
W Penins	80°–~50°W	1.00	2.00	1.95	2.15	0.15	0.05	2.6	2.4	0.64	1.70
Weddell	~50°W–0°	2.40	4.40	2.10	2.30	0.15	0.05	2.5	2.3	1.71	4.18
Totals		9.86	16.24							6.54	14.29

Target volume = Obs Vol. × (1.0 − BioFrac.) × IDens/SDens. Region abbreviations from Fig. 1.

The factors relevant for converting sediment volume to source volume are not well known. We assume a biogenic fraction, which we do not restore to the continent, of 5–15%, guided by DSDP and ODP results around Antarctica. We assume a minimum in-situ density of 1950 kg/m^3 for thinner, deep-water sediments and a maximum of 2300 kg/m^3 for thicker, shelf sediments. Density of the original source is assumed in the range of 2500–2600 kg/m^3 for the East Antarctic craton, but possibly as low as 2300 kg/m3 for a largely sedimentary source for the Weddell Sea. There is a clear division of Nd-isotope populations of young sediments into East- and West Antarctic sources (Roy et al., 2007), suggesting that the sediments are largely derived from the adjacent part of the continent.

2.3. Climate history

To understand the glacial regime under which the Antarctic landscape evolved, the stepwise glacial history of Antarctica is pieced together (Table 2). As will become clear, our approach relies on modeling glacial extents in East Antarctica. Following the growth of an initial continental-scale ice sheet at 34 Ma (Barrett, 1989; Hambrey et al., 1991; Zachos et al., 1992; Zachos and Kump, 2005) ice sheets did not permanently stabilise at the coast. Isotopic records show that the initial ice sheet had reduced in size by 33.6 Ma (Zachos and Kump, 2005) and the preservation of *Nothofagus* pollen assemblages in the CIROS-1 and CRP-3 cores suggest that the climate was at times similar to present day southern Patagonia (Mildenhall, 1989; Raine and Askin, 2001). After 33.6 Ma the ice sheet margin oscillated in pace with orbital cycles until at least 17 Ma as recorded by sedimentary cycles in the Cape Roberts cores (Cape Roberts Science Team, 1999, 2000; Fielding et al., 2000; Naish et al., 2001; Barrett, 2007) and isotopic records suggest this cyclicity probably continued until the mid-Miocene (Pekar and DeConto, 2006). Ice sheet modeling forced by orbital cycles under a reduced atmospheric CO_2 indicate these fluctuations may have been on a similar scale to those of northern hemisphere Pleistocene ice sheets (DeConto and Pollard, 2003; Jamieson and Sugden, 2008) and probably represented Antarctic ice volumes ranging between ca. 10 and ca. 21 million km^3, or 24 to 50 m of sea level equivalent (Bertler and Barrett, 2010).

A 6–7 °C reduction in Pacific surface water temperature records mid-Miocene cooling at around 14.2–12.7 Ma (Shevenell et al., 2004; Holbourn et al., 2005) and was experienced onshore as a transition from warm- to cold-based localised glaciation in the Transantarctic mountains (Lewis et al., 2007) and by an expansion of continental ice under a hyperarid polar climate. By ca. 14 Ma the ice sheet achieved its maximum extent, reaching the continental shelf edge in most areas (Sugden and Denton, 2004). However, by 13.6 Ma the ice sheet had retreated and in East Antarctica had dimensions similar to present day, fluctuating in response to sea level and ocean temperature changes for the majority of the period until present and occasionally expanding to the continental shelf edge (Denton and Hughes, 1986; Anderson, 1999; Sugden and Denton, 2004; Mackintosh et al., 2007; Cooper et al., 2009; Mackintosh et al., 2011).

The glacial history of West Antarctica is more dynamic and less certain. Stratigraphic evidence from the Ross Sea has been used to suggest that during the Pliocene it advanced onto the continental shelf in the Ross Sea multiple times (Bart, 2001) and collapsed

Table 2
Stepwise climate variability.

Time (Ma)	Ice configuration	Evidence
34.0–33.6	Continental ice sheet initiation.	Initial continental-scale ice recorded in oxygen isotope and sedimentary records (Barrett, 1989; Hambrey et al., 1991; Zachos et al., 1992; Zachos and Kump, 2005).
33.6–14.0	Fluctuations between near modern and near fully deglaciated states.	Ice reduced in scale by 33.4 Ma (Zachos and Kump, 2005) and *Nothofagus* pollen in CIROS-1 and CRP-3 indicates conditions similar to present-day Patagonia (Mildenhall, 1989; Raine and Askin, 2001). Sedimentary cycles in Cape Roberts (Cape Roberts Science Team, 1999; 2000, Barrett, 2007; Fielding et al. (2000); Naish et al. (2001). Model comparison with geomorphology suggests ice volume range of 10–25 million km^3 (DeConto and Pollard, 2003; Jamieson et al., 2010).
14.0–13.6	Maximum polar ice sheet.	Step cooling in ocean waters (Shevenell et al., 2004; Holbourn et al., 2005). Switch from warm- to cold-based glaciers in Victoria Land (Lewis et al., 2007). East Antarctic ice sheet stabilises. Ice reaches continental shelf edge (Anderson, 1999).
13.6–0.0	Similar to present day and fluctuating in response to sea level.	Ice retreats from shelf edge by ca. 13.6 Ma (Anderson, 1999; Sugden and Denton, 2004). Hyper-arid polar conditions prevail (Denton et al., 1993). West Antarctic ice sheet collapses and reforms in the warmer climate that prevailed until 3–2 Ma ((Naish et al., 2009; Pollard and DeConto, 2009) after which both ice sheets fluctuate in a reduced way in response to sea level changes from growth and collapse of N Hemisphere ice sheets (Denton and Hughes, 1986; Mackintosh et al., 2007).

periodically (Naish et al., 2009). Modeling suggests collapse (up to +7 m sea level equivalent) could be driven by obliquity-paced ocean-induced melting under globally higher temperature and CO_2 conditions (ca. 3 °C above present and 400 p.p.m.v.; Pollard and DeConto, 2009). Collapses may not have been limited to the Pliocene and the presence of late Pleistocene diatoms beneath the Whillans ice stream suggests that there was a more recent collapse of the West Antarctic Ice Sheet (Scherer et al., 1998). Conversely, the lack of erosional features on volcanoes in Marie Byrd Land has led to suggestions that a stable cold climate has existed since the mid-Miocene (Rocchi et al., 2006).

3. Modeled processes

Our approach is to integrate simulations of ice sheet behaviour, glacial erosion, tectonics, plate movement and lithospheric dynamics to reconstruct the palaeotopography of Antarctica at the E–O transition. The reconstruction is constrained using local-, regional- and continental-scale evidence for the pattern of landscape evolution as well as an understanding of landscape evolution gained from the beds of former northern hemisphere ice sheets.

3.1. Flexural isostasy

Many steps of our reconstructions incorporate flexural isostatic response to changes in surface loads. We use the standard model of a thin elastic plate overlying an inviscid fluid, implemented using Fourier transforms following Banks et al. (1977). The effective elastic thickness of the plate is a free parameter of the model; for simplicity we use a uniform value of 35 km for the entire continent, which is neither absurdly low for the East Antarctic craton nor absurdly high for recently active West Antarctica. It is common for the flexure model to predict partial flooding or emergence of continental areas. This flooding or emergence changes the load imposed by water on the top of the plate, indicating that a simple, single-step calculation does not accurately reflect the flexural response. We therefore iterate toward an internally consistent model by using the flexed topography to calculate a new water load, and repeat the process several times until the magnitude of flexure is less than a few meters. The reconstructed pre-glacial water load also includes the effect of adding the modern Antarctic ice to the ocean, which we approximate as a simple 60-m sea level rise, ignoring spherical-earth effects.

3.2. Glacial erosion model

Erosion of sediment by ice is the most widely distributed physical process that we aim to account for in this reconstruction. We use the GLIMMER-CISM 3-dimensional ice sheet model (Rutt et al., 2009) with a coupled erosion model (Jamieson et al., 2008) to understand patterns of long-term glacial landscape evolution. The ice sheet model uses the shallow ice approximation and therefore assumes that ice surface and bed slopes are shallow and thus that longitudinal stress has a negligible effect upon ice behaviour (Hutter, 1983). Given that we model ice configurations at a 20 km resolution this assumption is robust. The model is thermomechanically coupled and therefore enables the pattern of basal melting and basal ice velocity to be simulated.

Glacial erosion occurs where there is water at the base of the ice to provide lubrication between the ice and its bed to enable sliding (Boulton, 1972). Therefore, modeled erosion patterns are determined by the distribution of basal melt-rates (as a proxy for water pressure) at the ice sheet base, basal sliding velocity and lithological susceptibility to erosion. The latter term is treated initially as a constant due to the inaccessibility of the Antarctic bed as is geothermal heat flux which is important for predicting melting (Näslund et al., 2005; Jamieson et al., 2008), but for which no long-term reconstruction exists. Basal sliding velocity is controlled by basal shear stress and a 'slipperiness' parameter describing the tractive conditions at the ice/bed interface. This 'slipperiness' term is modeled as a function of basal melt-rate such that as pressure melting point is reached and melting begins and increases, the most rapid increase in slip (and therefore basal sliding velocity and erosion) is felt at low melt-rates (Jamieson et al., 2008). By tuning the relationship between basal melt-rate and slip it is possible to alter the sensitivity of glacial erosion to basal velocity. This can ensure that constrained incision depths (e.g. the depth of a coastal trough) are achieved whilst also balancing a basin-wide sediment budget against offshore volume constraints. Where there is no basal melting in the model, the ice sheet is frozen to its bed and therefore protects the landscape from erosion. Such a model is well suited to understanding landscape evolution in regions like East Antarctica where the ice sheet is terrestrial and topographically confined (Jamieson and Sugden, 2008; Jamieson et al., 2010).

4. Reconstruction steps

We describe our reconstruction steps in the order they are performed. The amplitude of the isostatic response to each step can depend on the sequence because of the sensitivity of water load to the intermediate steps. We perform the erosion restoration after horizontal plate motion, as this sequence simplifies generating sensible models in the area of faults modeled as active in the Oligocene but not since, with abrupt changes across the speculatively-located faults present in the thickness of the erosion restoration but not the modern topography. Revisions from the Wilson and Luyendyk (2009) model are extensive for restoring erosion. However, for other processes we follow the Wilson and Luyendyk (2009) approach closely, but incorporate estimates of uncertainty in the scale of the modifications as we construct the minimum and maximum models.

4.1. Initial topography

Our starting point for topography is the BEDMAP dataset of Lythe et al. (2001), downsampled to 10-km grid spacing (Fig. 2a). In the Marie Byrd Land area of West Antarctica, several recent studies have reported significant improvements to the topographic database (Luyendyk et al., 2003; Behrendt et al., 2004; Holt et al., 2006; Vaughan et al., 2006; Wilson and Luyendyk, 2006), and we incorporate these updates in our grid (Fig. S1). Additionally, we remove several volcanic edifices younger than 34 Ma in Marie Byrd Land and Victoria Land (e.g. LeMasurier and Rex, 1989). For simplicity, and because the edifices may be associated with significant intrusive bodies, we do not account for isostatic compensation of the edifices.

4.2. Ice load

Our restoration for load of the modern ice closely follows Wilson and Luyendyk (2009). We start with a small restoration for the ongoing rebound for ice removed since the Last Glacial Maximum. This effect is poorly known (e.g. James and Ivins, 1998) so we use the model for present vertical motion of Denton et al. (1991) multiplied by 3000 years. The maximum change is a ca. 50 m increase in the elevation of the southern Antarctic Peninsula. Next we apply the weight of the current grounded ice from BEDMAP as an upward load and calculate flexural rebound as previously described. The resulting topography is shown in Fig. 2b.

4.3. Thermal subsidence

Our restoration for thermal subsidence in the WARS also closely follows Wilson and Luyendyk (2009). The tectonic extension history is approximated as a series of adjacent, non-overlapping regions each

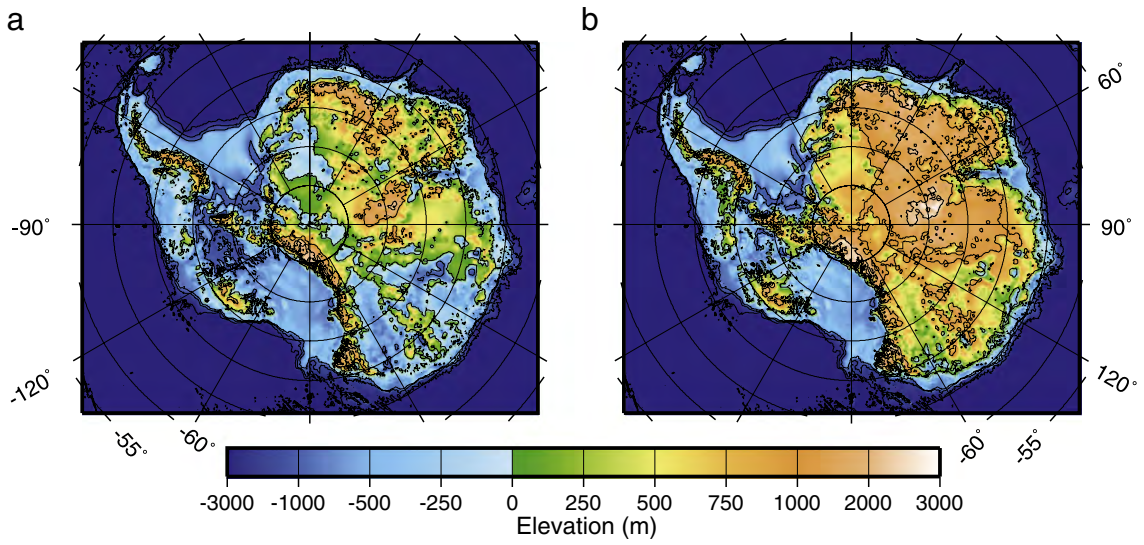

Fig. 2. (a) Present-day Antarctic bed topography, slightly updated from BEDMAP (Lythe et al., 2001). (b) Topography after isostatic rebound from removal of the present-day ice load.

with a uniform stretching factor and an instantaneous extension age. This simplification allows application of McKenzie's (1978) 1-D model for subsidence in response to increase of the thermal gradient during extension. We calculate predicted subsidence within each region in the absence of a water load and smooth the resulting grid on a scale of 40 km to approximate horizontal heat conduction. We then iteratively calculate the flexural isostatic response to flooding the subsided area with water. For our maximum reconstruction, we use a slight modification of the thermal subsidence model as Wilson and Luyendyk (2009, Fig. S2), but for the minimum reconstruction we reduce the thermal subsidence by a factor of 0.9 and recalculate the isostatic response to flooding as a simple model of potential overestimation of subsidence.

4.4. Shelf sedimentation

In the Ross Sea, we remove stratigraphic units RSS-2 and younger, as mapped by ANTOSTRAT (1995). Under the Ross Ice Shelf, our minimum surface uses the same sediment thickness as Wilson and Luyendyk (2009), following the assumption that most of area has incurred net sedimentation. In contrast, our maximum surface follows the assumption that most of the area has incurred net erosion. In the Weddell Sea, we remove sediment to the W4 reflector of Rogenhagen et al. (2004), extrapolated to the western Weddell Sea (Fig. S3). We apply flexural compensation of the sediment load based on a density of 2300 kg/m^3.

4.5. Horizontal plate motion

The amount of relative motion between East and West Antarctica since 34 Ma in the Ross Sea is well constrained at about 70 km by the anomaly C13 reconstruction of Cande et al. (2000). We use the same finite rotation as Wilson and Luyendyk (2009) (71.5°S, 35.8°W, 1.14°) to extrapolate this motion across the WARS. This alternative, within the Cande et al. (2000) confidence interval, tapers the relative motion to about one-third of the Ross Sea value where we connect the plate boundary to the triple junction with the Phoenix plate at the subduction zone adjacent to the Antarctic Peninsula. We include small motion to undo back-arc spreading at Bransfield Strait (68.5°S, 79°W, −3.2°). We also include motion of the South Orkney microplate (68.2°S, 34.4°W, 12.60°) following Eagles and Livermore (2002). Because the motions since 34 Ma are relatively small, we simply remove grid cells in the extended area and translate West Antarctic elevations based on the finite rotations (Fig. S4).

4.6. East Antarctic erosion restoration

We underpin our erosion restoration model with a set of assumptions. The beds of former northern hemisphere ice sheets show that an array of glacial features would be expected to evolve as an ice sheet waxes and wanes (Kleman et al., 2008). These range from small-scale alpine glacial features on localised highlands, to large-scale radial troughs incised at the coast under continental-scale ice conditions. Glacial erosion has lowered the interior of Scandinavia by on the order of 10's of meters during the Quaternary. We assume that similar landscapes evolved at comparable rates in Antarctica where ice sheets have fluctuated between local, regional and continental scales since 34 Ma. We also assume that the large-scale coastal troughs that drain East Antarctica already existed at the E–O boundary and have since been enhanced by selective glacial erosion (Jamieson and Sugden, 2008; Jamieson et al., 2010). For glacial troughs to evolve and selective erosion to occur, an existing topographic feature must have existed, probably in a lower amplitude form, before the growth of an ice mass. Evidence for the pre-existence of valley systems includes the Palaeozoic-Mesozoic age Penck-Jutul Trough in Dronning Maud Land, and the Mesozoic Lambert graben (Mishra et al., 1999; Näslund, 2001). On shorter timescales, geomorphic evidence indicates that parts of the Transantarctic Mountains retain signals of pre-glacial fluvial incision and passive-margin development (Baroni et al., 2005; Jamieson and Sugden, 2008) and that much of East Antarctica may retain its large-scale fluvial drainage spacing (Jamieson et al., 2005).

We simulate a set of 13 successively larger 'steady-state' ice masses over Antarctica following and extending the approach of Jamieson et al. (2010). Their extents are not prescribed, but instead reflect the simplicity with which the modeled climate is stepped from a 'Patagonian' regime towards a 'Polar' regime in order to generate equilibrium glacial configurations. Given the stepwise history of key climate changes for Antarctica since the Oligocene (Table 2), each of the configurations are assigned to a time period so that we can calculate the overall lifespan of each scale of ice sheet. By calculating erosion potential for each ice mass scenario and scaling it by the length of time over which it may have existed, we calculate total erosion potential. Sensitivity tests reflect the uncertainty in our understanding of ice sheet history between 33.6 and 14 Ma and therefore the potential variation in the scales and erosive capacity of

ice sheets during that time. Additional uncertainty is inherent in the model due to the difficulty of predicting the onset zone for basal melting in the interior of East Antarctica because of potential sensitivity to changes in geothermal heat flux (Pollard et al., 2005; Jamieson et al., 2008). However, because this onset zone tends to be found on flatter areas of the bed where the ice surface gradient is shallow and where streaming does not occur at the present day, modeled sliding velocities are never high. Therefore the error in erosion potential resulting from uncertainties in geothermal heat flux, which is kept constant at 42 mW/m^2, is likely to be small. The final erosion potential calculation reflects an intermediate-scaled set of modeled ice sheet scenarios (Fig. 3).

To obtain a final maximum and minimum erosion estimate for East Antarctica, erosion potential is adjusted so that: 1) incision does not exceed present day trough depths; 2) incision is limited to zero where cold-based ice is predicted to have protected the landscape; 3) inland erosion is within reasonable bounds as defined by extrapolating Quaternary erosion patterns in the Scandinavian ice sheet (Stroeven et al., 2002; Kleman et al., 2008); 4) total erosion reflects either the maximum or the minimum offshore sediment volumes after adjustment for biogenic fraction and compaction. The latter step requires individual scaling of drainage basin 'erodibility', which was initially assumed to be uniform across the continent, so that the correct sediment volumes are produced by each basin (Table 3). Scaling factors for each basin reflect the upper and lower error bounds for offshore sediment volumes.

Our initial attempts to restore glacial erosion tended to fill the coastal valleys whilst only replacing a fraction of the total source volume deduced from offshore sediment volume. We therefore infer that the model underpredicts the amount of material eroded from zones where ice slides at low-to-medium velocities. Accordingly, we scale the erosion calculation using power-law of less than 1 so that the contribution of intermediate basal ice velocities to erosion rates is enhanced relative to minimum and maximum rates. This adjustment is the equivalent of making an adjustment in the relationship between basal melt-rate and basal slip so that efficient erosion can be achieved with less water at the bed than initially assumed. We find that if the power is too small, erosion is over-balanced towards the interior of East Antarctica. If it is too large the coastal troughs are overfilled. A continent-wide exponent of 0.4 satisfies constraints provided by offshore sediment volume and coastal trough depth, and compares well with expected rates of erosion inferred from interior zones of ice sheets in the Northern hemisphere (Kleman et al., 2008). The modeled pattern of erosion is shown in Fig. 4.

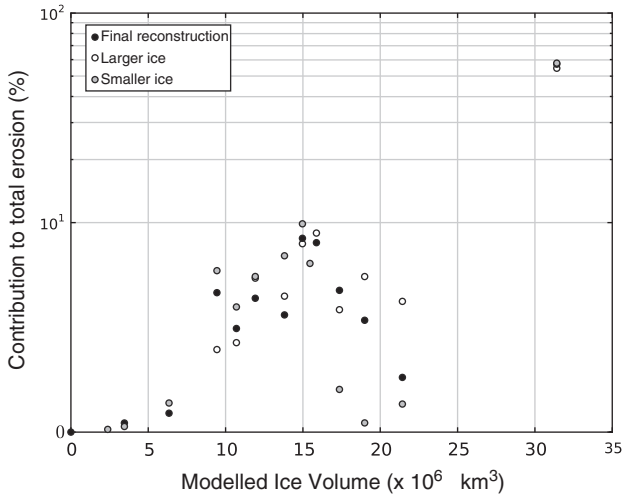

Fig. 3. Ice sheet scales and their contributions to modeled sediment restoration. The most significant contribution of sediment (between 50 and 60%) comes from the continental-scale ice sheet. The distinction between scales of ice sheet follows a similar approach to Jamieson et al. (2010) and reflects the size of steps in climate forcing used to generate successively larger steady-state ice masses. Sensitivity tests using larger or smaller ice sheets in the periods between 33.6 and 14.2 Ma show that variation in ice-sheet scale does not significantly change the overall pattern of eroded sediment. However, in analysing the difference between the small and large ice scenarios, the model is shown to be sensitive to uncertainty in the longevity of ice volumes of over 16 million km^3 volume. Therefore an intermediate longevity for such ice volumes is assumed in the final reconstruction.

4.7. West Antarctic erosion restoration

Existing ice sheet and glacial erosion models are not suited to marine-based systems like West Antarctica which are underlain by soft sediment, the deformation of which means that the links between mechanical erosion and ice velocity decouple. Thus, for the large amounts of erosion needed to restore the non-cratonal areas of West Antarctica we employ a constrained system of surface fitting. Following Wilson and Luyendyk (2009), we fit a smooth surface to a series of trial points above the topography, determine the load removed by subtracting the topography from the trial surface (assuming a uniform rock density of 2500 kg/m^3 as a simple average for both sediment and basement), and calculate isostatic compensation of the restored surface. We iteratively adjust the trial surface to fit constraints including the source volume inferred from sediment volume (Table 1) and the assumption that modern glacial drainage approximately follows the pre-34-Ma drainage. We join the separate models for East and West Antarctic erosion by allowing the predictions to overlap and simply taking the maximum.

For the area of the Ronne-Filchner Ice Shelves, draining to the Weddell Sea, our maximum model follows the assumption that the area in the Eocene was a mature sedimentary basin, filled to approximately Eocene sea level. In contrast, our minimum model assumes sediment supply was not adequate to fill the basin. Alternatives for restored regional average elevation ranging from near sea level to near −500 m are permitted by the poorly known offshore sediment volume. For the Ross and Amundsen Sea drainages, relations between sediment volume, source area, and present topography require that most of the drainages reconstruct above sea level. In the latter areas, large differences in erosion thickness produce only moderate changes in predicted topography because isostatic compensation preserves only ca. 20% of the change in thickness as change in surface elevation.

4.8. Special cases

The Lambert graben is an early Mesozoic rift extending well into the continental interior (Mishra et al., 1999). Current water depth does not permit grounding of ice, even for ice sheets moderately thicker than at present (Taylor et al., 2004). Because of the age of the graben, we assume it had filled with sediments to sea level by the Eocene. We use iterative surface fitting as used for most of West Antarctica to model the post-Eocene erosion of the graben fill.

LeMasurier and Landis (1996) argue that the present highlands of Marie Byrd Land have been uplifted from near sea level since Eocene by mantle plume activity. While this suggestion remains controversial, we allow for the possibility by adjusting our minimum model by subtracting an elliptical dome surface, dimensions 1000×500 km, with maximum amplitude of 1 km (Fig. S5). Our maximum model does not include this adjustment.

5. Results and discussion

In general, our model-eroded volumes (Table 3) are within reasonable bounds of the target volumes derived from observed sediment volumes (Table 1). Exceptions include the Dronning Maud Land and Enderby Land sectors (0–60°E), where we limit the restored eroded volume to avoid overfilling coastal troughs. Our model-eroded

Table 3
Modeled eroded volume restored.

Region		Minimum model				Maximum model			
Name	Longitude	Target volume (10^6 km^3)	Model volume (10^6 km^3)	Area 10^6 km^2	Average thickness (km)	Target volume 10^6 km^3	Model volume 10^6 km^3	Area 10^6 km^2	Average thickness (km)
DML	0°–30°E	0.34	0.30	0.57	0.52	0.54	0.30	0.57	0.52
EL	30°–60°E	0.40	0.37	0.69	0.55	0.63	0.37	0.69	0.55
MRL-PEL	60°–94°E	0.75	0.83	1.96	0.42	1.17	1.16	1.96	0.59
QML-WL	94°–124°E	0.34	0.37	1.78	0.21	0.54	0.53	1.78	0.30
G5L-OL	124°–165°E	0.31	0.34	1.34	0.25	0.59	0.51	1.34	0.38
Ross	165°E–150°W	1.03	1.24	2.17	0.57	2.73	2.35	2.34	1.00
Bell-Amun	150°–80°W	1.02	1.13	1.03	1.10	2.21	1.75	1.03	1.70
W Penins	80°–~50°W	0.64	0.29	0.50	0.58	1.70	0.38	0.51	0.75
Weddell	~50°W–0°	1.71	2.38	3.81	0.63	4.18	3.70	3.82	0.97
Totals:		6.54	7.25	13.85	0.52	14.29	11.05	14.04	0.79

volumes here, the same for our maximum and minimum models, are slightly below the minimum target values. In western Dronning Maud Land, Jacobs and Lisker (1999) infer that a large volume of Jurassic lava was eroded from the present highlands by 100 Ma. We speculate that at 34 Ma, much of the resulting sediment was on the shallow continental shelf, and was later eroded and redeposited in deep water. We have not attempted to tune the model for such an erosion pattern that departs from predictions based on the assumption of ice acting on a uniform substrate. A more serious mismatch occurs for the Antarctic Peninsula, where fitting the minimum and maximum target volumes would require average eroded thicknesses of 1.3 and 3.4 km, respectively. We probably have underestimated the erosion of the southern Peninsula, the only place with enough room to provide the source volume. For the Ross, Amundsen, and Weddell sectors, where the uncertainty in the volume of observed sediment is large and subjective, and the effort to revise the model erosion volume is significant, we have not forced the model volumes to the full range of the targets estimated from sediment volume. We allow a moderate buffer so that the models are not likely to be rendered obsolete by modest improvements in our knowledge of the offshore sediment volume.

In West Antarctica, our reconstructions (Fig. 5) contain a substantial upland feature as a result of the infilling of the Ross Sea and Amundsen Sea sectors. The large volumes of sediment offshore of these sectors require a minimum average reconstructed elevation slightly above present sea level and permit an average elevation many hundreds of meters higher. Our reconstruction is certainly artificially smooth, as horst-and-graben fabric visible in ice-penetrating radar (Luyendyk et al., 2003; Behrendt et al., 2004) would be expected to have already been present prior to glacial erosion.

In East Antarctica, the changes to the topography are more subtle because the volume of sediment restored is smaller (Table 3), but the area over which it is distributed is larger. Key features include the partial filling of coastal troughs including the Lambert graben which is filled to near present day sea level (Taylor et al., 2004) but remains a significant feature (Mishra et al., 1999). Our erosion model predicts that highland areas now buried under cold-based zones of the East Antarctic ice sheet existed on a similar scale to present in the Oligocene. For example on the Gamburtsev subglacial mountains our topographies retain the alpine glacial landscape which was recently mapped by Bo et al. (2009) thus adding to evidence suggesting it was sculpted before the E–O boundary and continental-scale glaciation. In Dronning Maud Land we change the upland areas very little. This is consistent with evidence that although focussed glacial erosion by wet-based ice and local alpine glaciers in the Jutulsessen area excavated a ca. 1200 m deep valley system at between 34 and 14 Ma, an early Permian palaeo-plateau is otherwise preserved (Näslund, 1997, 2001).

On the flanks of the Gamburtsev subglacial mountains, the depression which now contains subglacial Lake Vostok is intact but is shallower at the E–O boundary according to our reconstructions. Other subglacial overdeepenings of varying scales including the

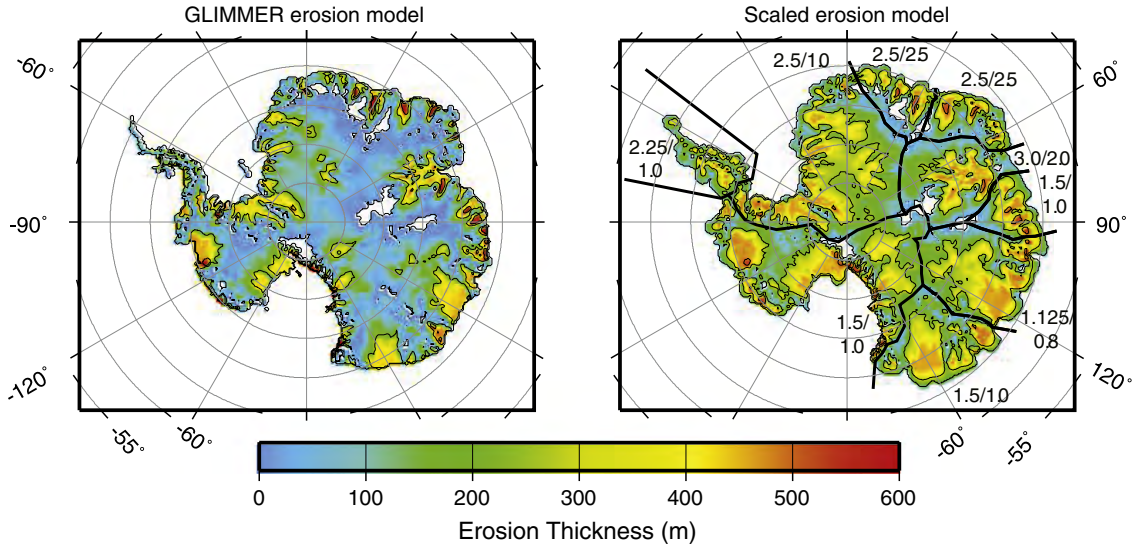

Fig. 4. Modeled erosion pattern before (left) and after (right) power-law scaling. Maximum and minimum scaling factors for each drainage system are noted outboard of each system. The scaling factors tune the erosion volumes to match the targets based on sediment volumes with the caveat that drainage valleys should not be overfilled.

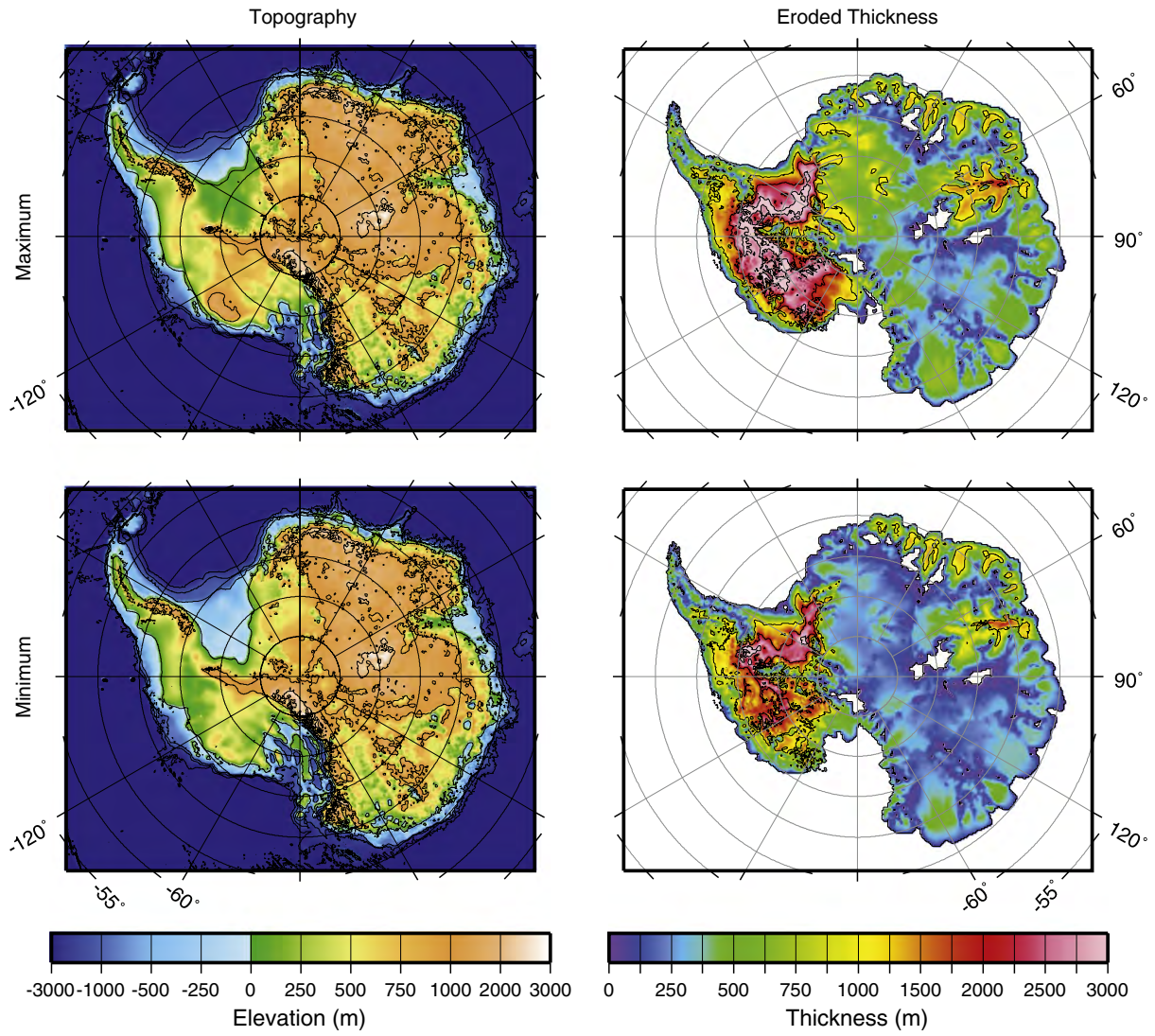

Fig. 5. Maximum and minimum reconstructed topography and eroded thickness maps, 1000-m contour interval. Land area above present sea level is 13.0×10^6 km^2 for the maximum and 12.4×10^6 km^2 for the minimum, compared with 10.5×10^6 km^2 for the ice-rebounded modern topography of Fig. 2b. The maximum and minimum reconstructed topographies are available to download in the supplementary information or via www.antscape.org.

Aurora and Wilkes basins are not significantly different to the present day. Indeed, across much of the interior of East Antarctica, our model suggests that the landscape has been lowered by less than 300 m since the E–O boundary. This is in line with the depths expected if rates from the shorter-lived northern hemisphere glacial landscapes such as Scandinavia are extrapolated over longer periods (Kleman et al., 2008).

Important constraints for several aspects of our reconstruction come from the geologic record at DSDP Site 270 in the Ross Sea, which shows an Oligocene marine transgression over terrestrial regolith (palaeosol) on basement gneiss now at ~1000 m below sea level (Ford and Barrett, 1975; Hayes et al., 1975). DeSantis et al. (1999) tested simple models for sediment loading and thermal subsidence of this area and found few models consistent with this rather large subsidence for an area often considered tectonically stable through the Cenozoic. They found that either the effective elastic lithosphere must be very thick (70 km) for the load of thick sediment in the adjacent basin to drive the subsidence, or the time of tectonic extension must be younger than the commonly assumed 90–100 Ma for thermal contraction to drive the subsidence. Our results are generally similar, with the Site 270 basement most easily restoring above sea level at 34 Ma if extension in the central Ross Sea is younger

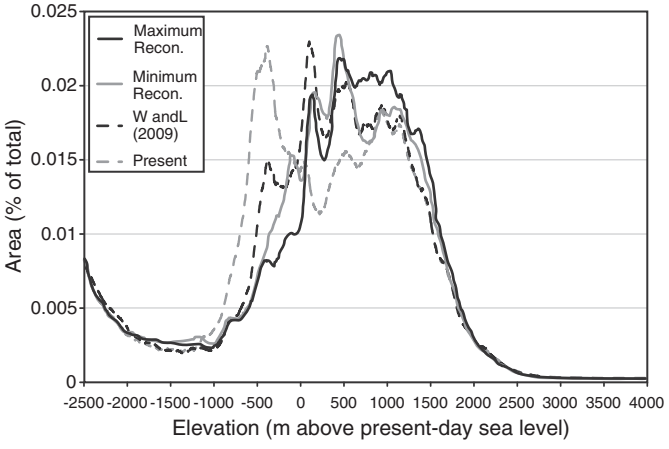

Fig. 6. Hypsometry of Antarctic topographies comparing fraction of land surface area against elevation. This illustrates the shift between land below sea level at present day to land above sea level in the reconstructions. Solid black line: Maximum reconstruction; Solid grey line: Minimum reconstruction; Dashed black line: Reconstruction presented in Wilson and Luyendyk (2009); Dashed grey line: Present day topography rebounded for ice load removal as used as our boundary condition for the reconstructions.

than 70 Ma with a stretching factor at least 2.0. Our maximum model restores the site to 120 m above modern sea level, while our minimum, with slightly reduced thermal subsidence, restores to 30 m. Larger reductions in modeled thermal subsidence would not satisfy the observational constraint here. We found that for models with thin elastic lithosphere (20 km or less), isostatic compensation was essentially local and extreme models of recent extension or high stretching factor would be required for basement to have subsided 1000 m since after 34 Ma. These experiments guided our choice of the simplifying assumption of a uniform elastic thickness of 35 km.

We compare the hypsometry of our reconstructions against a previous reconstruction of West Antarctica (Wilson and Luyendyk, 2009) and the present day bed dataset used as the basemap for our reconstruction (Fig. 6). Hypsometric analysis of the reconstructions elucidates the changes in distribution of land area over elevation. Key differences include a significant increase in area above sea level caused by the filling of the Ross and Weddell Seas and the Lambert Trough and the associated decreases in the area at between 0 and 700 m depth. The filling of the Ross and Weddell Seas are strongest in the Maximum reconstruction and the majority of the material restored is added to a source area below 1000 m elevation. Above this height the present hypsometry is very close to that of Wilson and Luyendyk (2009). Thus at elevations above ca. 1000 m, the difference in topographic distribution between the present bed and the reconstructions are the result of sediment restoration in the central uplands of East Antarctica where relatively small amounts of material are distributed over a wide area.

The implications of the differences in topography between present day and our reconstructions are that the feedbacks between topography and climate would support increased ice volume at the E–O boundary. Much of this would result from the changes in West Antarctica with the increased elevations in East Antarctica making a small but nonetheless important contribution. Compared with an area above modern sea level of 10.5×10^6 km^2 for the ice-rebounded modern topography of Fig. 2b, our minimum reconstruction has an area of 12.4×10^6 km^2 above modern sea level, and our maximum, 13.0×10^6 km^2. We suggest that volume may be on the order of magnitude that is currently lost in the gap between ice volume records and modeled ice sheets (e.g. DeConto et al., 2008; Miller et al., 2008). Any Early Oligocene ice sheet in West Antarctica would not have been marine-based in nature as hitherto assumed in models of E–O ice. Rather, we suggest that Early Oligocene West Antarctic Ice Sheet was dynamically different due to its terrestrial nature as it would have been grounded to a lesser extent below sea level. Therefore it is likely to have been less responsive to changes in sea level and ocean temperature. This indicates that the dynamics of the ice streams which dominate the drainage of the present day West Antarctic system may have changed significantly over time. For example perhaps such fast-flowing regimes underlain by deformable sediment did not exist on such a scale in the early evolution of the ice sheet. The implication is that as the bed was lowered it may have evolved into a more dynamic marine-based ice sheet, with significant volumes of eroded material being deposited offshore in the West Antarctic Rift System.

The work described herein forms part of the wider ANTscape project to reconstruct palaeotopographies at a range of key transitions over the last ~100 Ma. We anticipate that the E–O boundary reconstructions will be refined in response to a number of future dataset releases. These are likely to include an improved present day dataset along the lines of ALBMAP (Le Brocq et al., 2010) that will provide a more accurate present day topography upon which to base our reconstructions. New high-resolution bed data of the present Antarctic bed, including that introduced by Bell et al. (2011) will strengthen our knowledge of subglacial topography and basal processes in East Antarctica. Improvements in the accuracy of offshore sediment data used to constrain our erosion models are anticipated as a result of the CASP project to develop an age controlled circum-Antarctic dataset of sediment thicknesses. Ongoing work will also help separate the signals of ice sheet and climate fluctuations recorded in deep sea sediment cores. This will enable higher temporal resolution ice sheet and erosion modeling to be carried out and may clarify the importance of various ice sheet scales in contributing sediment to the shelf. Therefore we anticipate a more accurate picture of onshore glacial erosion dynamics will be made possible.

Supplementary materials related to this article can be found online at doi:10.1016/j.palaeo.2011.05.028.

Acknowledgments

We are grateful to the Scientific Committee for Antarctic Research and to the Antarctic Climate Evolution program for funding and to the ANTscape working group (www.antscape.org) for the discussions from which this paper was developed. We thank Graeme Eagles and an anonymous reviewer for their constructive criticism and encouraging comments. Stewart Jamieson was funded by the Natural Environmental Research Council UK. This material is based upon work supported by the National Science Foundation under Cooperative Agreement No. 0342484 through subawards administered and issued by the ANDRILL Science Management Office at the University of Nebraska-Lincoln, as part of the ANDRILL U.S. Science Support Program.

References

Anderson, J.B., 1999. Antarctic Marine Geology. Cambridge University Press, Cambridge.
ANTOSTRAT, 1995. Seismic stratigraphic atlas of the Ross Sea. In: Cooper, A.K., Brancolini, G. (Eds.), Geology and Seismic Stratigraphy of the Antarctic Margin. American Geophysical Union, Washington D.C.
Banks, R.J., Parker, R.L., Huestis, S.P., 1977. Isostatic compensation on a continental scale: local versus regional mechanisms. Geophysical Journal of the Royal Astronomical Society 51, 431–452.
Barker, P.F., Kennett, J.P., Party, S.S., 1988. Proceedings of the Ocean Drilling Program, Initial Reports, Weddell Sea, Antarctica, College Station, Texas.
Baroni, C., Noti, V., Ciccacci, S., Righini, G., Salvatore, M.C., 2005. Fluvial origin of the valley system in northern Victoria Land (Antarctica) from quantitative geomorphic analysis. Bulletin of the Geological Society of America 117, 212.
Barrett, P.J., 1989. Antarctic Cenozoic history from the CIROS-1 drill-hole, McMurdo Sound, Antarctica. NZDSIR Bulletin. 245 pp.
Barrett, P.J., 2007. Cenozoic climate and sea level history from glacimarine strata off the Victoria Land coast, Cape Roberts Project, Antarctica. In: Hambrey, M.J., Christoffersen, P., Glasser, N.F., Hubbard, B. (Eds.), Glacial processes and products: International Association of Sedimentologists Special Publication, pp. 259–287.
Bart, P.J., 2001. Did the Antarctic ice sheets expand during the early Pliocene? Geology 29, 67–70.
Behrendt, J.C., LeMasurier, W.E., Cooper, A.K., Tessensohn, F., Trehu, A., Damaske, D., 1991. Geophysical studies of the West Antarctic Rift System. Tectonics 10, 1257–1273.
Behrendt, J.C., Blankenship, D.D., Morse, D.L., Bell, R.E., 2004. Shallow-source aeromagnetic anomalies observed over the West Antarctic Ice Sheet compared with coincident bed topography from radar ice sounding—new evidence for glacial "removal" of subglacially erupted late Cenozoic rift-related volcanic edifices. Global and Planetary Change 42 (1–4), 177–193.
Bell, R.E., Ferraccioli, F., Creyts, T.T., Braaten, D., Corr, H., Das, I., Damaske, D., Frearson, N., Jordan, T., Rose, K., Studinger, M., Wolovick, M., 2011. Widespread persistent thickening of the East Antarctic Ice Sheet by freezing from the base. Science 331 (6024), 1592–1595.
Bertler, N.A.N., Barrett, P.J., 2010. Vanishing polar ice sheets. In: Dodson, J. (Ed.), Changing climates, earth systems and society. : International Year of Planet Earth. Springer, N.Y., pp. 49–82. doi:10.1007/978-90-481-8716-4_4.
Bo, S., Siegert, M.J., Mudd, S., S\ugden, D., Fujita, S., Xiangbin, C., Yunyun, J., Xueyuan, T., Yuansheng, L., 2009. The Gamburtsev mountains and the origin and early evolution of the Antarctic Ice Sheet. Nature 459, 690–693.
Boulton, G.S., 1972. The role of thermal regime in glacial sedimentation. In: Price, R.J., Sugden, D.E. (Eds.), Polar geomorphology: Special Publication of the Institute of British Geographers, 4, pp. 1–19.
Cande, S.C., Stock, J.M., Müller, D., Ishihara, T., 2000. Cenozoic motion between East and West Antarctica. Nature 404, 145–150.
Cape Roberts Science Team, 1999. Studies from the Cape Roberts Project, Ross Sea, Antarctica. Initial report on CRP-2/2A. Terra Antarctica 6, 1–173.
Cape Roberts Science Team, 2000. Studies from the Cape Roberts Project, Ross Sea, Antarctica. Initial report on CRP-3. Terra Antarctica 7, 1–209.
Cooper, A.K., Brancolini, G., Escutia, C., Kristoffersen, Y., Larter, R., Leitchenkov, G., O'Brien, P., Jokat, W., 2009. Cenozoic climate history from seismic reflection and

drilling studies on the Antarctic continental margin. In: Florindo, F., Siegert, M. (Eds.), Antarctic Climate Evolution. Elsevier.
DeConto, R.M., Pollard, D., 2003. Rapid Cenozoic glaciation of Antarctica induced by declining atmospheric CO_2. Nature 421, 245–249.
DeConto, R.M., Pollard, D., Harwood, D., 2007. Sea ice feedback and Cenozoic evolution of Antarctic climate and ice sheets. Paleoceanography 22, PA3214. doi:10.1029/2006PA001350.
DeConto, R.M., Pollard, D., Wilson, P.A., Palike, H., Lear, C.H., Pagani, M., 2008. Thresholds for Cenozoic bipolar glaciation. Nature 455, 652–656.
Denton, G.H., Hughes, T.J., 1986. Global ice-sheet system interlocked by sea-level. Quaternary Research 26, 3–26.
Denton, G.H., Prentice, M.L., Burckle, L.H., 1991. Cainozoic history of the Antarctic Ice Sheet. In: Tingey, R.J. (Ed.), The Geology of Antarctica. Clarendon Press, Oxford, pp. 365–433.
Denton, G.H., Wilch, T.I., Sugden, D.E., Marchant, D.R., Hall, B.L., 1993. East Antarctic ice sheet sensitivity to Pliocene climatic change from a dry valleys perspective. Geografiska Annaler Series A 75, A (4), 155–204.
DeSantis, L., Prato, S., Brancolini, G., Lovo, M., Torelli, L., 1999. The Eastern Ross Sea continental shelf during the Cenozoic: implications for West Antarctic ice sheet development. Global and Planetary Change 23, 173–196.
Eagles, G., Livermore, R.A., 2002. Opening history of Powell Basin, Antarctic Peninsula. Marine Geology 185, 195–202.
Fielding, C.R., Naish, T.R., Woolfe, K.J., Lavelle, M.A., 2000. Facies analysis and sequence stratigraphy of CRP-2/2A, Victoria Land Basin, Antarctica. Terra Antartica 7, 323–338.
Fitzgerald, P.G., Baldwin, S.L., 1997. Detachment fault model for the evolution of the Ross Embayment. In: Ricci, C.A. (Ed.), The Antarctic Region: Geological Evolution and Processes. Terra Antarctica Publication, Siena, pp. 555–564.
Ford, A.B., Barrett, P.J., 1975. Basement rocks of the South-Central Ross Sea, Site 270, DSDP Leg 28. Initial Reports of the Deep Sea Drilling Project, 28, pp. 861–868.
Hambrey, M.J., Ehrmann, W.U., Larsen, B., 1991. Cenozoic glacial record of the Prydz Bay Continental Shelf, East Antarctica. Proceedings of the Ocean Drilling Program Scientific Results. Texas A&M, College Station, pp. 77–132.
Hayes, D.E., Frakes, L.A., Shipboard Scientific Party, 1975. Sites 270,271,272. In: Hayes, D.E., Frakes, L.A. (Eds.), Initial Reports of the Deep Sea Drilling Project, pp. 211–334.
Holbourn, A., Kuhnt, W., Schulz, M., Erlenkeuser, H., 2005. Impacts of orbital forcing and atmospheric carbon dioxide on Miocene ice-sheet expansion. Nature 438, 483–487.
Hollister, C.D., Craddock, C., 1976. Introduction, principal results—Leg 35 Deep Sea Drilling Project. In: Hollister, C.D., Craddock, C. (Eds.), Initial Reports of the Deep Sea Drilling Project, 35, pp. 5–14. U.S. Government Printing Office, Washington D.C.
Holt, J.W., Blankenship, D.D., Morse, D.L., Young, D.A., Peters, M.E., Kempf, S.D., Richter, T.G., Vaughan, D.G., Corr, H.F.J., 2006. New boundary conditions for the West Antarctic Ice Sheet: subglacial topography of the Thwaites and Smith glacier catchments. Geophysical Research Letters 33, L09502.
Hübscher, C., Jokat, W., Miller, H., 1996. Structure and origin of southern Weddell Sea crust: results and implications. In: Storey, B.C., King, E.C., Livermore, R.A. (Eds.), Weddell Sea Tectonics and Gondwana Break-up: Geological Society Special Publication, pp. 201–211.
Hutter, K., 1983. Theoretical Glaciology. Mathematical Approaches to Geophysics. D. Reidel Publishing Company, Boston, Lancaster.
Jacobs, J., Lisker, F., 1999. Post-Permian tectono-thermal evolution of western Dronning Maud Land, East Antarctica: an apatite fission-track approach. Antarctic Science 11, 451–460.
James, T.S., Ivins, E.R., 1998. Predictions of Antarctic crustal motions driven by present-day ice sheet evolution and by isostatic memory of the Last Glacial Maximum. Journal of Geophysical Research B: Solid Earth and Planets 103, 4933–5017.
Jamieson, S.S.R., Sugden, D.E., 2008. Landscape evolution of Antarctica. In: Cooper, A.K., Barrett, P.J., Stagg, H., Storey, B., Stump, E., Wise, W., 10th ISAES editorial team (Eds.), Antarctica: a keystone in a changing world. : Proceedings of the 10th International Symposium on Antarctic Earth Sciences. The National Academies Press, Washington D.C, pp. 39–54.
Jamieson, S.S.R., Hulton, N.R.J., Sugden, D.E., Payne, A.J., Taylor, J., 2005. Cenozoic landscape evolution of the Lambert basin, East Antarctica: the relative role of rivers and ice sheets. Global and Planetary Change 45, 35–49.
Jamieson, S.S.R., Hulton, N.R.J., Hagdorn, M., 2008. Modelling landscape evolution under ice sheets. Geomorphology 97, 91–108.
Jamieson, S.S.R., Sugden, D.E., Hulton, N.R.J., 2010. The evolution of the subglacial landscape of Antarctica. Earth and Planetary Science Letters 293, 1–27.
Kleman, J., Stroeven, A.P., Lundqvist, J., 2008. Patterns of Quaternary ice sheet erosion and deposition in Fennoscandia and a theoretical framework for explanation. Geomorphology 97, 73–90.
Kuvaas, B., Kristoffersen, Y., Guseva, J., Leitchenkov, G., Gandjukhin, V., Kudryavtsev, G., 2004. Input of glaciomarine sediments along the East Antarctic continental margin; depositional processes on the Cosmonaut Sea continental slope and rise and a regional acoustic stratigraphic correlation from 40 W to 80E. Marine Geophysical Researches 25, 247–263.
Larter, R.D., Barker, P., 1991. Effects of ridge crest–trench interaction on Antarctic-Phoenix spreading: forces on a young subducting plate. Journal of Geophysical Research 96, 19,583–19,607.
Larter, R.D., Cunningham, A.P., Barker, P.F., Gohl, K., Nitsche, F.O., 2002. Tectonic evolution of the Pacific margin of Antarctica 1. Late Cretaceous tectonic reconstructions. Journal of Geophysical Research 107, 2345.
Lawver, L.A., Gahagan, L.M., 1994. Constraints on timing of extension in the Ross Sea region. Terra Antarctica 1, 545–552.
Le Brocq, A.M., Payne, A.J., Vieli, A., 2010. An improved Antarctic dataset for high resolution numerical ice sheet models (ALBMAP v1). Earth System Science Data 2, 247–260.
Leitchenkov, G.L., Guseva, Y.B., Gandyukhin, V.V., 2007. Cenozoic environmental changes along the East Antarctic continental margin inferred from regional seismic stratigraphy. In: Cooper, A.K., Raymond, C.R. (Eds.), Antarctica: A Keystone in a Changing World. USGS.
Leitchenkov, G., Guseva, J., Gandjukhin, V., Grikurov, G., Kristoffersen, Y., Sand, M., Golynsky, A., Aleshkova, N., 2008. Crustal structure and tectonic provinces of the Riiser-Larsen Sea area (East Antarctica): results of geophysical studies. Marine Geophysical Researches 29, 135–158.
LeMasurier, W.E., Landis, C.A., 1996. Mantle plume activity recorded by low relief erosion surfaces in West Antarctica and New Zealand. Geological Society of America Bulletin 108, 1450–1466.
LeMasurier, W.E., Rex, D.C., 1989. Evolution of linear volcanic ranges in Marie Byrd Land, West Antarctica. Journal of Geophysical Research 94, 7223–7236.
Lewis, A.R., Marchant, D.R., Ashworth, A.C., Hemming, S.R., Machlus, M.L., 2007. Major middle Miocene global climate change: evidence from East Antarctica and the Transantarctic Mountains. Geological Society of America Bulletin 119, 1449–1461.
Luyendyk, B.P., Wilson, D.S., Siddoway, C.S., 2003. Eastern Margin of the Ross Sea Rift in western Marie Byrd Land, Antarctica: crustal structure and tectonic development. Geochemistry Geophysics Geosystems 4, 1090.
Lythe, M.B., Vaughan, D.G., the BEDMAP Consortium, 2001. BEDMAP: a new ice thickness and subglacial topographic model of Antarctica. Journal of Geophysical Research 106 (B6), 11335–11351.
Mackintosh, A., White, D., Fink, D., Gore, D.B., Pickard, J., Fanning, P.C., 2007. Exposure ages from mountain dipsticks in Mac. Robertson Land, East Antarctica, indicate little change in ice-sheet thickness since the Last Glacial Maximum. Geology 35, 551–554.
Mackintosh, A., Golledge, N., Domack, E., Dunbar, R., Leventer, A., White, D., Pollard, D., DeConto, R., Fink, D., Zwartz, D., Gore, D., Lavoie, C., 2011. Retreat of the East Antarctic ice sheet during the last glacial termination. Nature Geoscience 4, 195–202.
McDougall, I., 1977. Potassium–argon dating of glauconite from a greensand drilled at Site 270 in the Ross Sea, DSDP Leg 28. In: Hayes, D.E., Frakes, L.A. (Eds.), Initial Reports of the Deep Sea Drilling Project, Washington D.C, pp. 1071–1072.
McKenzie, D., 1978. Some remarks on the development of sedimentary basins. Earth and Planetary Science Letters 40, 25–32.
Mildenhall, D.C., 1989. Terrestrial palynology. In: Barrett, P.J. (Ed.), Antarctic Cenozoic history from the CIROS-1 Drillhole, McMurdo Sound: DSIR Bulletin, 245, pp. 119–127.
Miller, H., Henriet, J.P., Kaul, N., Moons, A., 1990. A fine-scale stratigraphy of the eastern margin of the Weddell Sea. In: Bleil, U., Thiede, J. (Eds.), Geological History of the Polar Oceans: Arctic Versus Antarctic. Kluwer Academic Publishers, pp. 131–161.
Miller, K.G., Wright, J.D., Katz, M.E., Browning, J.V., Cramer, B.S., Wade, B.S., Mizintseva, S.F., 2008. A view of Antarctic ice-sheet evolution from sea-level and deep-sea isotope changes during the Late Cretaceous–Cenozoic. In: Cooper, A.K., et al. (Ed.), Antarctica: A Keystone in a Changing World: Proceedings of the 10th International Symposium on Antarctic Earth Sciences, pp. 55–70.
Miller, S.R., Fitzgerald, P.G., Baldwin, S.L., 2010. Cenozoic range-front faulting and development of the Transantarctic Mountains near Cape Surprise, Antarctica: thermochronologic and geomorphologic constraints. Tectonics 29, TC1003.
Mishra, D.C., Sekhar, D.V.C., Raju, D.C.V., Kumar, V.V., 1999. Crustal structure based on gravity-magnetic modelling constrained from seismic studies under Lambert Rift, Antarctica and Godavari and Mahanadi rifts, India and their interrelationship. Earth and Planetary Science Letters 172, 287–300.
Naish, T.R., Woolfe, K.J., Barrett, P.J., Wilson, G.S., Atkins, C., Bohaty, S.M., Bucker, C.J., Claps, M., Davey, F.J., Dunbar, G.B., Dunn, A.G., Fielding, C.R., Florindo, F., Hannah, M.J., Harwood, D.M., Henrys, S.A., Krissek, L.A., Lavelle, M., van der Meer, J., McIntosh, W.C., Niessen, F., Passchier, S., Powell, R.D., Roberts, A.P., Sagnotti, L., Scherer, R.P., Strong, C.P., Talarico, F., Verosub, K.L., Villa, G., Watkins, D.K., Webb, P.N., Wonik, T., 2001. Orbitally induced oscillations in the East Antarctic ice sheet at the Oligocene/Miocene boundary. Nature 413, 719–723.
Naish, T., Powell, R., Levy, R., Wilson, G., et al., 2009. Obliquity-paced Pliocene West Antarctic ice sheet oscillations. Nature 458, 322–328.
Näslund, J.O., 1997. Subglacial preservation of valley morphology at Amundsenisen, Western Dronning Maud Land, Antarctica. Earth Surface Processes & Landforms 22, 441–455.
Näslund, J.O., 2001. Landscape development in western and central Dronning Maud Land, East Antarctica. Antarctic Science 13, 302–311.
Näslund, J.O., Jansson, P., Fastook, J., Johnson, J., Andersson, L., 2005. Detailed spatially distributed geothermal heat-flow data for modeling of basal temperatures and meltwater production beneath the Fennoscandian ice sheet. Annals of Glaciology 40, 95–101.
Nitsche, F.O., Gohl, K., Vanneste, K., Miller, H., 1997. Seismic expression of glacially deposited sequences in the Bellinghausen and Amundsen Seas, West Antarctica. In: Barker, P.F., Cooper, A.K. (Eds.), Geology and Seismic Stratigraphy of the Antarctic Margin 2: American Geophysical Union, Antarctic Research Series, 71, pp. 95–108.
Nitsche, F.O., Cunningham, A.P., Larter, R.D., Gohl, K., 2000. Geometry and development of glacial continental margin depositional systems in the Bellingshausen Sea. Marine Geology 162, 277–302.
Pekar, S.F., DeConto, R.M., 2006. High-resolution ice-volume estimates for the early Miocene: evidence for a dynamic ice sheet in Antarctica. Palaeogeography Palaeoclimatology Palaeoecology 231, 101–109.
Pollard, D., DeConto, R.M., 2009. Modeling West Antarctic ice sheet growth and collapse through the last 5 million years. Nature 458, 329–332.
Pollard, D., DeConto, R.M., Nyblade, A.A., 2005. Sensitivity of Cenozoic Antarctic ice sheet variations to geothermal heat flux. Global and Planetary Change 49, 63–74.
Raine, J.I., Askin, R.A., 2001. Terrestrial palynology of Cape Roberts drillhole CRP-3, Victoria Land Basin, Antarctica. Terra Antarctica 8.

Rocchi, S., LeMasurier, W.E., Vincenzo, G., 2006. Oligocene to Holocene erosion and glacial history in Marie Byrd Land, West Antarctica, inferred from exhumation of the Dorrel Rock intrusive complex and volcano morphologies. Geological Society of America Bulletin 118, 991–1005.

Rogenhagen, J., Jokat, W., 2000. The sedimentary structure in the western Weddell Sea. Marine Geology 168, 45–60.

Rogenhagen, J., Jokat, W., Hinz, K., Kristoffersen, Y., 2004. Improved seismic stratigraphy of the Mesozoic Weddell Sea. Marine Geophysical Researches 25, 265–282.

Roy, M., van de Flierdt, T., Hemming, S.R., Goldstein, S.L., 2007. $^{40}Ar/^{39}Ar$ ages of hornblende grains and bulk Sm/Nd isotopes of circum-Antarctic glacio-marine sediments: implications for sediment provenance in the southern ocean. Chemical Geology 244 (3–4), 507–519.

Rutt, I.C., Hagdorn, M., Hulton, N.R.J., Payne, A.J., 2009. The 'GLIMMER' community ice sheet model. Journal of Geophysical Research 114, F02004.

Scherer, R.P., Aldahan, A., Tulaczyk, S., Possnert, G., Engelhardt, H., Kamb, B., 1998. Pleistocene collapse of the West Antarctic Ice Sheet. Science 281, 82–85.

Scheuer, C., Gohl, K., Eagles, G., 2006a. Gridded isopach maps from the South Pacific and their use in interpreting the sedimentation history of the West Antarctic continental margin. Geochemistry, Geophysics, Geosystems 7, Q11015.

Scheuer, C., Gohl, K., Larter, R.D., Rebesco, M., Udintsev, G., 2006b. Variability in Cenozoic sedimentation along the continental rise of the Bellingshausen Sea, West Antarctica. Marine Geology 277, 279–298.

Shevenell, A.E., Kennett, J.P., Lea, D.W., 2004. Middle Miocene Southern Ocean cooling and Antarctic cryosphere expansion. Science 305, 1766–1770.

Siddoway, C.S., Baldwin, S.L., Fitzgerald, P.G., Fanning, C.M., Luyendyk, B.P., 2004. Ross Sea mylonites and the timing of continental extension between East and West Antarctica. Geology 32, 57–60.

Stroeven, A.P., Fabel, D., Harbor, J., Hattestrand, C., Kleman, J., 2002. Quantifying the erosional impact of the Fennoscandian ice sheet in the Tornetrask–Narvik corridor, northern Sweden, based on cosmogenic radionuclide data. Geografiska Annaler 84A (3–4), 275–287.

Sugden, D., Denton, G., 2004. Cenozoic landscape evolution of the Convoy Range to Mackay Glacier area, Transantarctic Mountains: onshore to offshore synthesis. Bulletin of the Geological Society of America 116, 840–857.

Taylor, J., O'Brien, P.E., Cooper, A.K., Leitchenkov, G., Siegert, M.J., Payne, A.J., Hambrey, M.J., 2004. Topographic controls on post-Oligocene changes in ice-sheet dynamics, Prydz Bay region, East Antarctica. Geology 32, 197–200.

Tucholke, B.E., Houtz, R.E., 1976. Sedimentary framework of the Bellinghausen basin from seismic profiler data. In: Hollister, C.D., Craddock, C. (Eds.), Initial Reports of the Deep Sea Drilling Project, 35, pp. 197–227. U.S. Government Printing Office, Washington D.C.

Vaughan, D.G., Corr, H.F.J., Ferraccioli, F., Frearson, N., O'Hare, A., Mach, D., Holt, J.W., Blankenship, D.D., Morse, D.L., Young, D.A., 2006. New boundary conditions for the West Antarctic ice sheet: subglacial topography beneath Pine Island Glacier. Geophysical Research Letters 33, L09501.

Wilson, D.S., Luyendyk, B.P., 2006. Bedrock platforms within the Ross Embayment, West Antarctica: hypotheses for ice sheet history, wave erosion, Cenozoic extension, and thermal subsidence. Geochemistry, Geophysics, Geosystems 7, Q12011.

Wilson, D.S., Luyendyk, B.P., 2009. West Antarctic paleotopography estimated at the Eocene–Oligocene climate transition. Geophysical Research Letters 36, L16302.

Zachos, J.C., Kump, L.R., 2005. Carbon cycle feedbacks and the initiation of Antarctic glaciation in the earliest Oligocene. Global and Planetary Change 47, 51–66.

Zachos, J.C., Breza, J.R., Wise, S.W., 1992. Early Oligocene ice sheet expansion on Antarctica—stable isotope and sedimentological evidence from Kerguelen Plateau, Southern Indian Ocean. Geology 20 (6), 569–573.

Publication 6.3.6:

Uenzelmann-Neben, G., **Gohl, K.** (2014). Early glaciation already during the Early Miocene in the Amundsen Sea, Southern Pacific: Indications from the distribution of sedimentary sequences. *Global and Planetary Change,* 120, 92-104, doi:10.1016/j.gloplacha.2014.06.004.

Author contributions: Uenzelmann-Neben processed and analysed the data, developed the sedimentation grids and wrote most of this paper. Gohl collected the data and contributed with to the interpretation and discussion, in particular in comparing with glacial sedimentation processes on the adjacent shelf. Most of the seismic data used in this paper were collected during Polarstern expedition ANT-XXVI/3 (2010) with Gohl as chief-scientist.

Global and Planetary Change 120 (2014) 92–104

Contents lists available at ScienceDirect

Global and Planetary Change

journal homepage: www.elsevier.com/locate/gloplacha

Early glaciation already during the Early Miocene in the Amundsen Sea, Southern Pacific: Indications from the distribution of sedimentary sequences

Gabriele Uenzelmann-Neben *, Karsten Gohl

Alfred-Wegener-Institut Helmholtz-Zentrum für Polar- und Meeresforschung, Am Alten Hafen 26, 27568 Bremerhaven, Germany

ARTICLE INFO

Article history:
Received 14 October 2013
Received in revised form 12 June 2014
Accepted 24 June 2014
Available online 1 July 2014

Keywords:
West Antarctic Ice Sheet
sedimentary sequences
sediment drifts
bottom water circulation
variations in material input
glacial development

ABSTRACT

The distribution and internal architecture of seismostratigraphic sequences observed on the Antarctic continental slope and rise are results of sediment transport and deposition by bottom currents and ice sheets. Analysis of seismic reflection data allows to reconstruct sediment input and sediment transport patterns and to infer past changes in climate and oceanography. We observe four seismostratigraphic units which show distinct differences in location and shape of their depocentres and which accumulated at variable sedimentation rates. We used an age–depth model based on DSDP Leg 35 Site 324 for the Plio/Pleistocene and a correlation with seismic reflection characteristics from the Ross and Bellingshausen Seas, which unfortunately has large uncertainties. For the period before 21 Ma, we interpret low energy input of detritus via a palaeo-delta originating in an area of the Amundsen Sea shelf, where a palaeo-ice stream trough (Pine Island Trough East, PITE) is located today, and deposition of this material on the continental rise under sea ice coverage. For the period 21–14.1 Ma we postulate glacial erosion for the hinterland of this part of West Antarctica, which resulted in a larger depocentre and an increase in mass transport deposits. Warming during the Mid Miocene Climatic Optimum resulted in a polythermal ice sheet and led to a higher sediment supply along a broad front but with a focus via two palaeo-ice stream troughs, PITE and Abbot Trough (AT). Most of the glaciogenic debris was transported onto the eastern Amundsen Sea rise where it was shaped into levee-drifts by a re-circulating bottom current. A reduced sediment accumulation in the deep-sea subsequent to the onset of climatic cooling after 14 Ma indicates a reduced sediment supply probably in response to a colder and drier ice sheet. A dynamic ice sheet since 4 Ma delivered material offshore mainly via AT and Pine Island Trough West (PITW). Interaction of this glaciogenic detritus with a west-setting bottom current resulted in the continued formation of levee-drifts in the eastern and central Amundsen Sea.

1. Introduction

Because of modern global warming and their possible contribution to sea level rise and flooding of low lying coastal areas (e.g. Bamber et al., 2009; Gomez et al., 2010; Hu et al., 2011) both Antarctic and Greenland ice sheets have moved into the focus of public and scientific interest. Research has concentrated on short-term dynamics of the ice sheets in order to understand their vulnerability to a changing climate by collecting multi-disciplinary data (e.g. Wellner et al., 2001; Lowe and Anderson, 2002; ÓCofaigh et al., 2005; Naish et al., 2007; Nitsche et al., 2007; Bentley et al., 2010; Gomez et al., 2010; Jakobsson et al., 2010; Bart et al., 2011; Bradley et al., 2012; Konfirst et al., 2012; Hillenbrand et al., 2013) as well as carrying out numerical simulations (e.g. Thoma et al., 2008; Pollard and DeConto, 2009; DeConto et al., 2012; Assmann et al., 2013; Jacobs et al., 2013).

Little has been known about the long-term development especially of the West Antarctic Ice Sheet (WAIS), which as a marine based ice sheet generally reacts more sensitively to both atmospheric and oceanic warming than the largely terrestrial East Antarctic Ice Sheet (EAIS). Information on the early phase of WAIS formation and the Cainozoic glacial history in the greater Amundsen Sea is scarce. Drilling in Wilkes Land, an area influenced by the EAIS, has shown that mid Eocene cooling there was initiated by early flow of the cold Antarctic Counter Current across the Tasmanian Gateway (Expedition 318 Scientists, 2011; Pross et al., 2012; Bijl et al., 2013). This cold Antarctic Counter Current has also bathed the Amundsen Sea implying a cold climate for that area during the Paleogene. Uenzelmann-Neben and Gohl (2012) presented indications for a pre-Miocene sea-ice cover in the Amundsen Sea based on the study of sedimentary features imaged by seismic reflection data. We here add to the discussion of the transition from pre-glacial to glacial deposition in the Cainozoic by analysing depositional patterns and the distribution of the sedimentary sequences.

Antarctic Bottom Water (AABW) originating in the Ross Sea (Gordon et al., 2009; Orsi and Wiederwohl, 2009) flows through the Amundsen

* Corresponding author.
E-mail address: Gabriele.Uenzelmann-Neben@awi.de (G. Uenzelmann-Neben).

http://dx.doi.org/10.1016/j.gloplacha.2014.06.004
0921-8181/

Sea within the cyclonic Antarctic Circumpolar Current (ACC) (Orsi et al., 1999). The shelf of the Amundsen Sea is influenced by CDW reaching the fringes of the WAIS via bathymetric troughs (Jacobs et al., 1996; Thoma et al., 2008; Jacobs et al., 2011; Arneborg et al., 2012). A southwest setting flow of bottom water has been observed close to the continental slope of the Bellingshausen Sea (see Hillenbrand et al., 2008, for a detailed presentation).

Our analysis of the depositional pattern and distribution of sedimentary strata in the Amundsen Sea rise allows the reconstruction of material input from the West Antarctic continent and sediment transport processes. These in turn are strongly influenced by, and hence help us to decipher, modifications in climatic and oceanographic conditions in the Amundsen Sea, which is affected by the outflow of the Ross gyre (Orsi, 2010) and WAIS drainage.

2. Palaeoenvironmental setting

The Amundsen Sea along the southern Pacific margin of West Antarctica (Fig. 1) originates from rift and breakup processes and the formation of oceanic crust between Campbell Plateau/Chatham Rise and the Marie Byrd Land/Thurston Island Block at 90–80 Ma (Eagles et al., 2004; Gohl et al., 2007; and references therein). Intraplate volcanism at 65–56 Ma led to the formation of the Marie Byrd Seamounts (Kipf et al., 2013). The crystalline basement is covered by up to 4 km of sedimentary strata, which have been extensively reworked by oceanic currents in the deep sea (Yamaguchi et al., 1988; Nitsche et al., 2000; Uenzelmann-Neben and Gohl, 2012) and by advance–retreat cycles of the ice sheet on the shelf (Lowe and Anderson, 2002; Dowdeswell et al., 2006; Nitsche et al., 2007; Uenzelmann-Neben et al., 2007; Graham et al., 2009; Weigelt et al., 2009; Weigelt et al., 2012; Gohl et al., 2013; Hochmuth and Gohl, 2013).

The existence and size of an early Cainozoic ice sheet in West Antarctica is still under debate as no clear evidence has been found, yet. A proto-Ross gyre (Huber et al., 2004) may have led to a cooling of surface water (Anderson, 1999). Indirect evidence points towards a significant sea ice cover in the Ross Sea in the Oligocene (Uenzelmann-Neben and Gohl, 2012). Both the opening of the Drake Passage commencing in middle Eocene times and the Tasmanian Gateway (36–30 Ma) predate the largest $\delta^{18}O$ increase (Oi1) of the past 50 Ma, which is interpreted to represent the onset of major glaciation in Antarctica (Huber et al., 2004; Miller et al., 2008; Francis et al., 2009).

It has been suggested that mountain glaciers and ice caps existed in West Antarctica during the Oligocene, with ice streams spreading into the western Ross Sea (Anderson, 1999) and advancing to sea level in other regions (Miller et al., 2008). Ivany et al. (2006) reported a regionally extensive ice sheet for the Antarctic Peninsula during the Oligocene, while Cooper et al. (2009) observed aggradation on the West Antarctic shelf, high-relief canyons on the continental slope and channel-levees on the rise during that time.

The Mi1 excursion (Oligocene–Miocene boundary) represents a short-lived (200 ka) increase in ice volume from 40% to 125% of the present volume (Wilson et al., 2009). Haywood et al. (2009) report further growth of the WAIS at 14 Ma with Bart (2003) observing at least two WAIS expansions to the Ross Sea shelf edge. The West Antarctic shelf during the Miocene is characterised by uniform progradation with erosion of topset strata (Cooper et al., 2009). The slope and rise showed fan growth and the construction of large sediment drift bodies and channel-levees (Cooper et al., 2009; Uenzelmann-Neben and Gohl,

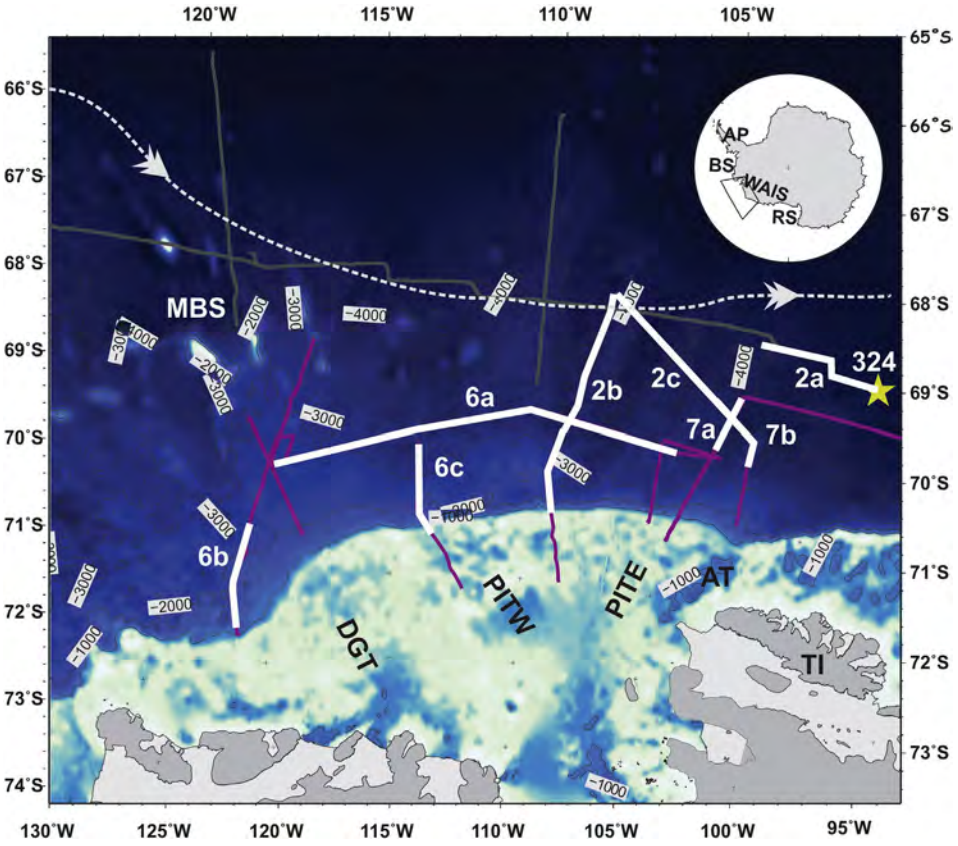

Fig. 1. Bathymetric map of the Amundsen Sea (Nitsche et al., 2007). The seismic line locations are shown in purple (AWI) and grey (JNOC), the yellow star refers to the location of DSDP Leg 35 Site 324 (Shipboard Scientific Party, 1976). The white lines and numbers show the parts of the seismic lines presented as Figs. 2, 6 and 7. The light grey dashed line shows the approximate path of AABW (Orsi et al., 1999). AT = Abbot Trough, DGT = Dotson Getz Trough, MBS = Marie Byrd seamount area, PITE = Pine Island Trough East, PITW = Pine Island Trough West, TI = Thurston Island. Insert map shows the area presented. AP = Antarctic Peninsula, BS = Bellingshausen Sea, RS = Ross Sea, WAIS = West Antarctic Ice Sheet.

2012). Starting in late Miocene glacial–interglacial volumes were deposited further landward.

A regional unconformity characterises the Miocene–Pliocene boundary at the West Antarctic continental margin (Cooper et al., 2009). A strong increase in sea surface temperatures occurred during several warm intervals in the Pliocene (Escutia et al., 2009; Haywood et al., 2009). A change from polythermal to polar cold, dry-based ice sheets at ca. 3 Ma has been suggested by Rebesco and Camerlenghi (2008). Rapid oscillations and volume changes of the WAIS in the Ross Sea region during the middle Pliocene were reconstructed from sedimentary sequences deposited in open water and at the base of grounded ice, respectively (Naish et al., 2009a; Naish et al., 2009b). Numerical simulations of WAIS variations for the past 5 million years supported by drilling results from the Ross Sea indicate phases with intermediate to full glacial extent and brief intervals of ice-sheet collapse leaving only small isolated ice caps (Pollard and DeConto, 2009).

Most information on WAIS dynamics is available for the period since the last glacial maximum and is based on geomorphological, sedimentological and chronological data sets collected predominantly from the shelves in the Amundsen and Ross seas (e.g. Domack et al., 1999; Lowe and Anderson, 2002; Smellie et al., 2009; Anderson et al., 2011; Jakobsson et al., 2012; Kirshner et al., 2012; Livingstone et al., 2012; Klages et al., 2013). On the outer continental shelf of the eastern Amundsen Sea Embayment the glacial trough eroded by the Pine Island–Thwaites palaeo-ice stream had two outlets: The eastern Pine Island Trough (PITE) with a mouth at ~106°W (Graham et al., 2010) and the western Pine Island Trough (PITW) with a mouth at ~114°W (Evans et al., 2006). During the last few glacial periods palaeo-ice stream flow may either have switched between these two outlets or ice streamed in the whole area between PITW and PITE (Lowe and Anderson, 2002; Evans et al., 2006; Graham et al., 2010; Jakobsson et al., 2012).

A few studies investigated the relationship between ice sheet dynamics and changes in oceanographic conditions for the Amundsen and Bellingshausen Seas. On the basis of seismic reflection profiles from the western Antarctic Peninsula margin that were correlated with drill cores, Rebesco et al. (2002) and Uenzelmann-Neben (2006) identified a close interaction of contouritic and turbiditic sediment transport with indications for a major advance of the local ice sheet shortly after 15 Ma. There is widespread evidence for bottom current activity since ~9.6 Ma in this area and in the Bellingshausen Sea further to the west (e.g. Nitsche et al., 2000; Rebesco et al., 2002; Hernandez-Molina et al., 2004; Hillenbrand and Ehrmann, 2005; Scheuer et al., 2006b; Uenzelmann-Neben, 2006). Uenzelmann-Neben and Gohl (2012) inferred bottom current activity as early as the Paleogene and the onset of major glaciations in West Antarctica at 14.1 Ma from seismic reflection profiles on the continental rise in the Amundsen Sea, but chronological control was poor.

The study presented here builds on the analysis of sedimentary structures by Uenzelmann-Neben and Gohl (2012). Adding new seismic profiles and analysing the distribution of the seismic units we will contribute to a better understanding of material input from the West Antarctic continent and sediment transport processes.

3. Methods

3.1. Database

This study is based on multichannel seismic reflection data gathered by the Alfred-Wegener-Institut (AWI) in 1994, 2006 and 2010 (Fig. 1). Details of field parameters and processing of the seismic data gathered in 1994 and 2006 can be found in Gohl et al. (1997), Nitsche et al. (2000) and Uenzelmann-Neben et al. (2007). During the cruise in 2010 four GI-guns©, with a volume of about 2.4 l each, were used as a seismic source. Each of the GI-guns© consisted of a generator chamber (0.72 l volume) producing the seismic signal, and an injector chamber (1.68 l volume), which was triggered with a 33 ms delay to suppress the bubble. The GI-guns© were fired every 10 s (corresponding to a shot-spacing of approximately 25 m), producing signals with frequencies of up to 300 Hz. Data were received using a digital seismic data acquisition system (SERCEL SEAL©), consisting of both onboard and in-sea equipment. The total active streamer length was 3000 m, consisting of 240 channels.

Processing of the seismic reflection data comprised geometry definition using the ship's navigation data, and CDP-sorting with a CDP spacing of 25 m. No deconvolution was carried out, since the short signal and absence of seafloor multiples in our data did not require this. A precise velocity analysis (every 50 CDP) was carried out and used for normal move-out correction. Stacking velocities are accurate within 10% and were converted to interval velocities using Dix's formula (Yilmaz, 2001). Residual static corrections and coherency filters were applied to further improve the data quality. After stacking, an Omega-X time migration was carried out, to correctly image strongly inclined surfaces (Yilmaz, 2001). No gain was applied to the data, neither during processing nor for display. Thus, differences in reflection amplitude discussed in the following are real. Additional seismic data (Yamaguchi et al., 1988) were available via the digital database of the SCAR Antarctic Seismic Data Library System (SDLS).

DSDP Leg 35 Site 324 (Fig. 1), the only drill site in the study area, was crossed by profile TH-86002a (Yamaguchi et al., 1988) but unfortunately this site only provided information on the uppermost 200 m of the sedimentary column (Shipboard Scientific Party, 1976; Tucholke et al., 1976a). Core 324 retrieved sediments consisting of sand, silty clay and diatomaceous clay of Pliocene to Pleistocene age, but recovery was relatively poor (51%) (Shipboard Scientific Party, 1976). Other direct information concerning the time frame from drill sites is either too far away or from different environments or both (DSDP Leg 35 Site 323–380 nm, deep sea (Tucholke et al., 1976b); ODP Leg 178 Sites 1095 and 1096–540 nm, continental rise (Iwai et al., 2002); DSDP Leg 28 Site 271–1500 nm, Ross Sea shelf (Shipboard Scientific Party, 1975b); DSDP Leg 28 Site 274–2000 nm, continental rise (Shipboard Scientific Party, 1975a)).

3.2. Seismostratigraphic model

Uenzelmann-Neben and Gohl (2012) put forward a seismostratigraphic model for the wider Amundsen Sea. They used the age–depth model provided by DSDP Leg 35 Site 324 (Shipboard Scientific Party, 1976) for the upper 200 m of the sedimentary column comprising Pliocene/Pleistocene units and correlated this with observations on general changes in reflections characteristics. Variations in reflection characteristics for the deeper lying sequences were interpreted to represent modifications in the depositional regime and compared to observations from the Bellingshausen Sea (; Tucholke and Houtz, 1976; Tucholke et al., 1976b; Rebesco et al., 1996; Nitsche et al., 1997; Nitsche et al., 2000; Rebesco et al., 2002; Scheuer et al., 2006a; Scheuer et al., 2006b), which were tied to DSDP Leg 35 and ODP Leg 178 results, and the Ross Sea (De Santis et al., 1995; De Santis et al., 1999; Böhm et al., 2009), there correlated with results from DSDP Leg 28, to derive an age model. We make use of this stratigraphic model being aware of its poor chronological control but modify the names of the sedimentary units to distinguish them from the Ross Sea and Amundsen Sea shelf by adding the acronym ASR (Amundsen Sea rise).

Uenzelmann-Neben and Gohl (2012) identified four sedimentary units on top of basement (Fig. 2, Table 1). The oldest unit ASR-I is characterised by weak internal reflections and is partly transparent. This unit fills the basement topography (Fig. 2a) and is assumed to represent the period from ~60 to 21 Ma. Unit ASR-I shows elongate sedimentary drifts in the Marie Byrd Seamount area as a result of an eastward flow of bottom water. Sedimentary unit ASR-II was deposited between 21 Ma and 14.1 Ma and shows variable, continuous internal reflections of moderate to high amplitude (Fig. 2a, b and e, Table 1).

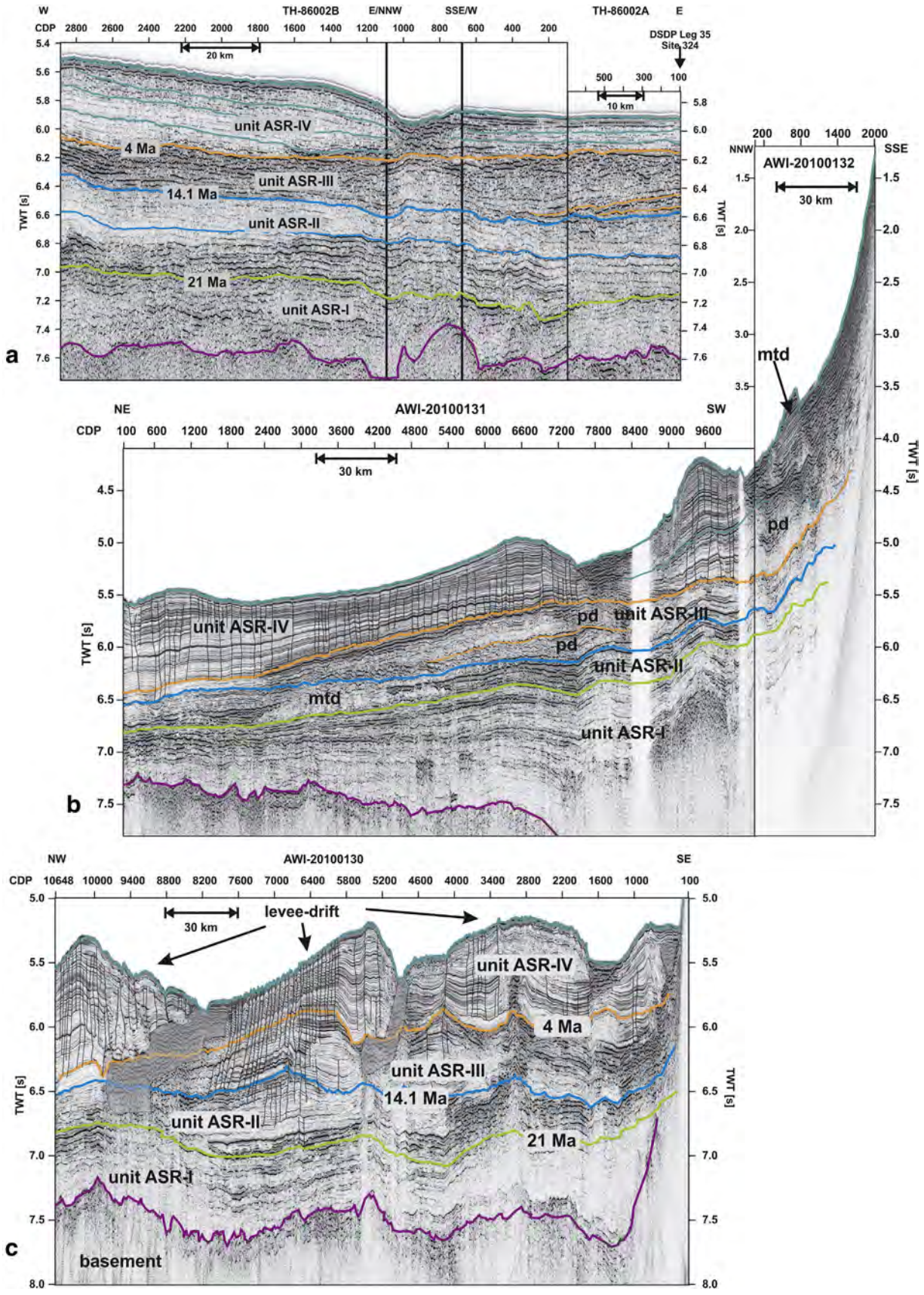

Fig. 2. a) JNOC profile TH-86002 from the eastern Amundsen Sea. In the east the profile crosses DSDP Leg 35 Site 324. b) Profile AWI-20100131/20100132 from the central Amundsen Sea. mtd = mass transport deposit, pd = patched drift. c) Profile AWI-20100130. d) Uninterpreted blow-up of sediment drift on profile AWI-20100131. e) Uninterpreted blow-up of sediment drift on profile AWI-20100130. Note the onset of levee-drift formation in unit ASR-II. The thin black lines represent small-scale faults and the shaded areas filled channels. For location see Fig. 1.

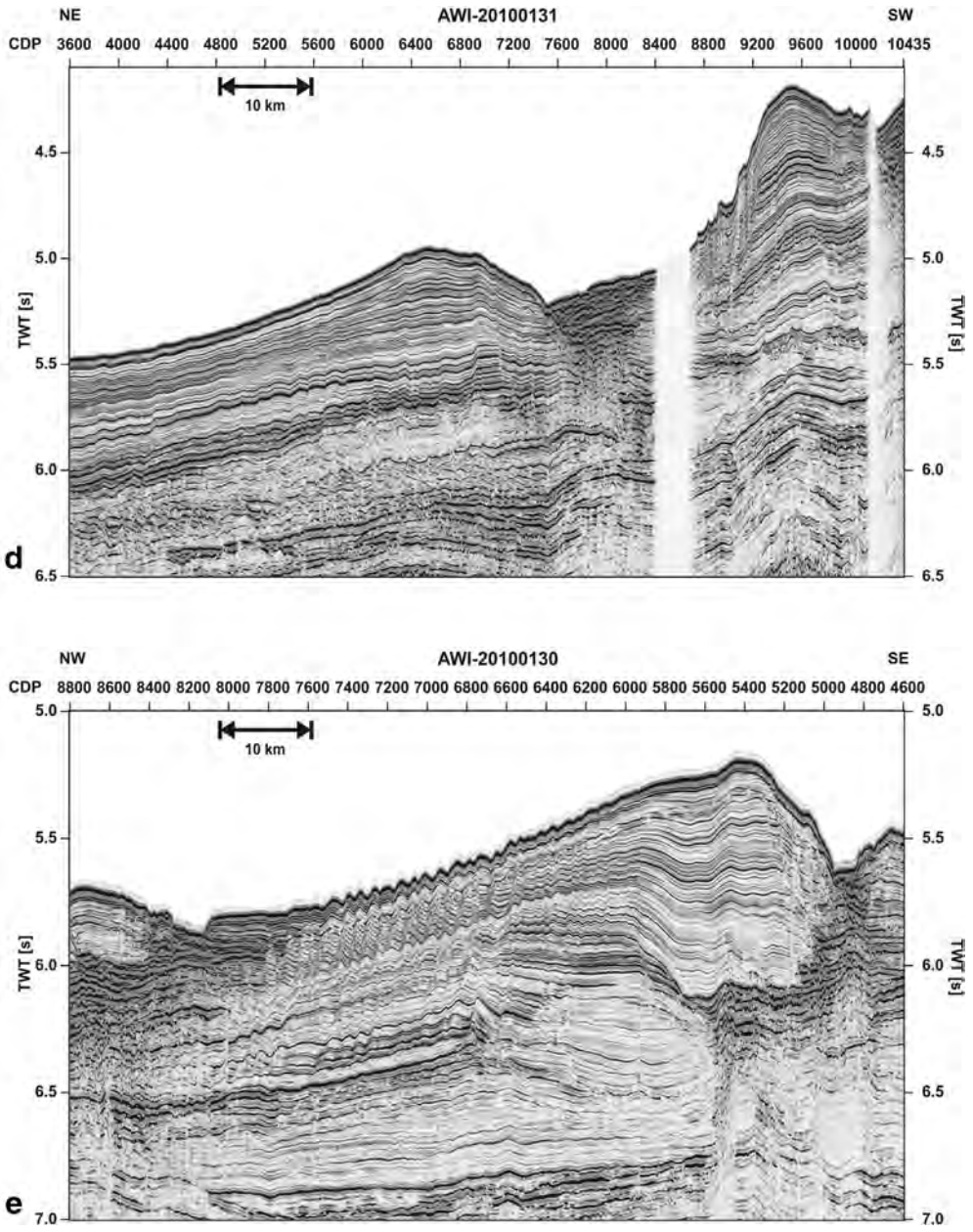

Fig. 2 (*continued*).

Elongate drifts can be observed within this unit in the Marie Byrd Seamount area while levee-drifts characterise the unit in the eastern Amundsen Sea (Fig. 2c and e). Both drift types are interpreted to relate to intensified bottom water activity.

In sedimentary unit ASR-III (14.1–4 Ma) an increase in internal reflections and mass transport deposits additionally to elongate and levee-drifts were observed (Fig. 2, Table 1). This was interpreted to represent a further intensification of bottom water activity and an advancing ice sheet. The youngest sedimentary unit ASR-IV (4–0 Ma) shows moderate, well layered reflections separated by several unconformities (Fig. 2, Table 1). Levee-drifts and mass transport deposits observed in this unit were interpreted as results of a southward shift of the bottom water and a change in basal ice-sheet conditions to polythermal.

The basal reflectors of units ASR-I to ASR-IV, and the seafloor reflection of all existing seismic profiles of the Amundsen Sea slope and rise were tracked, thicknesses of the different units computed, and maps of reflector depths and unit thicknesses compiled with the aim to better define and describe the sedimentary environments. We converted the reflector depths and unit thicknesses into depth using interval velocities derived from stacking velocities using Dix's Formula.

Palaeo-seafloor highs and depocentres will be presented and discussed. Although these terms usually are used as the highest locations and thickest part, respectively, we specifically defined them as the root mean square (rms) value of the reflector depth and unit thickness, respectively, in order to be explicit and avoid equivocality. Within the depocentres we observed additional foci of deposition, which we pointed out. Shape and location of a depocentre relative to the continental slope and older depocentres reveal the loci of major sediment accumulation and allow conclusions about transport pathways and processes. A depocentre oriented parallel to the slope is interpreted to document dominance of along-slope sediment transport, whereas a depocentre perpendicular to the slope is interpreted to indicate dominance of down-slope sediment transport. We also computed accumulation rates for the depocentres (Table 2). These observations are combined with the occurrence of sedimentary features in the study area, such as sediment drifts and

Table 1
Seismostratigraphic model of Uenzelmann-Neben and Gohl (2012).

Sedimentary unit	Proposed age	Thickness (min, max) in ms TWT (in m)	Reflection characteristics	Sedimentary features	Main area of occurrence	Oceanographic/climatological interpretation
ASR-I	60 (?)–21 Ma	100–1600 (250–4000)	Weak internal reflections, partly transparent, infill of basement topography	Elongate sediment drifts	Marie Byrd Seamounts	Eastward flow of bottom water (proto-AABW?)
ASR-II	21–14.1	100–600 (175–1050)	Variable, continuous internal reflections of moderate to high amplitude in either the lower or upper part, downlap onto base	Elongate drifts levee-drifts	Marie Byrd Seamounts eastern Amundsen Sea	Intensified bottom water activity cyclonic eddies shed from bottom water?
ASR-III	14.1–4	100–800 (150–1200)	Increase in number of internal reflections	Elongate drifts levee-drifts mass transport deposits	Marie Byrd Seamounts eastern Amundsen Sea central/eastern Amundsen Sea	Intensified bottom water activity cyclonic eddies shed from bottom water advancing ice sheet
ASR-IV	4–0	200–1300 (200–1300)	Moderate, well-layered reflections separated by several unconformities	Levee-drifts mass transport deposits	Eastern Amundsen Sea near continental rise	Bottom water activity has shifted southwards, less intense change in ice regime from wet- to dry-based

mass transport deposits (mass transport deposits), that have been previously reported.

We are aware of the fact that the number of seismic lines is small and they are far apart. This results in a certain ambiguity of our findings. Still, we consider it important to report and discuss our observations to provoke further research in this area. We thus limit the discussion to changes and trends.

4. Results

The top of the basement shows a high in the area of the Marie Byrd Seamounts (MBS) (Fig. 3a, shaded area). This high extends slightly NE-wards. The deepest basement is observed between PITW and AT. Unit ASR-I shows a broad depocentre (shaded area in Fig. 4a) parallel to the continental slope, which does not extend far into the ocean. The thickest parts of the depocentre (>2500 m, bold outline) can be observed a) continent-wards of the MBS in front of the Dotson-Getz Trough (DGT), b) between Pine Island Trough West (PITW) and PITE, and c) in front of Abbott Trough (AT) (Fig. 4a, black outlined areas).

The base of unit ASR-II also shows a high in the MBS area (shaded in Fig. 3b). This high is smaller than the one observed for the basement. We observe an extension towards the SE (to the slope offshore from PITW) rather than towards the NE. The deepest part of the horizon is located in the NE of the area of investigation with two smaller troughs seaward of PITW. Unit ASR-II again shows a broad depocentre (shaded in Fig. 4b) parallel to the continental slope, which extends further into the ocean than unit ASR-I's depocentre (Fig. 4a and b). The thickest parts of the depocentre as outlined by the black lines in Fig. 4b (>750 m) can be observed a) in the NE offshore from PITE, b) in three locations in front of PITW and further to the W, and c) in front of AT. Two of the three thick depocentres have been deposited in up to 250 m deep troughs (Fig. 3b) but the westernmost depocentre directly indicates an increased sediment input. The foci of the depocentres have shifted relative to those of unit ASR-I except the one in front of AT.

The MBS area appears still elevated at the base of unit ASR-III but is less pronounced (Fig. 3c). The shallowest part is found closer towards the continental slope. Similar to the base of ASR-II that of ASR-III lies relatively deep in the NE. For unit ASR-III we observe no longer a single, but two depocentres that coincide with locations where ASR-II had been thickest: a) in front and slightly west of PITW, and b) in front and slightly west of AT (Fig. 4c). Depocentre a) is still parallel to the shelf break and the continental slope, whereas depocentre b) is oriented perpendicular to shelf break and continental slope.

For the base of unit ASR-IV we observe a broad high, which extends eastwards from the MBS and is oriented parallel to the shelf break (Fig. 3d). The NE is characterised by a deep lying base of ASR-IV, which is less pronounced and deepens towards the deep sea. Unit ASR-IV shows depocentres only in the eastern part of the study area, where they cover about the same areas as the depocentres in unit ASR-III (Fig. 4c and d, Table 2). Three depocentres are located between AT and PITW and are oriented perpendicular to the continental slope. The thickest parts (>800 ms TWT) are found on the continental slope.

5. Discussion

The sedimentary units show distinct depocentres and some of those have shifted through time. The distance between the seismic lines covering the study area is large in parts (Fig. 1) and thus the

Table 2
Characteristics for the sedimentary units and the associated depocentres.

Unit, age	Base reflector	Depocentre					
		Form (rms value of unit thickness)	A (km^2) with v_P (m/s)	Thickness (m)	Volume (10^{13} m^3)	Sedimentation rate (m/my)	Accumulation rate (m^3/my)
ASR-I, (60?)–21 Ma	High in MBS area, low in the east	Broad front of shelf, does not extend far into ocean; thickest part between AT and PITW	29,511 (5000)	1778	5.247	45	$1.3 * 10^{12}$
ASR-II 21–14.1 Ma	MBS high smaller, closer to continental slope, low in the NE	Broad, extending farther into ocean, thickest part in NE and in front of AT and PITE	53,255 (3500)	599	3.189	86.7	$4.6 * 10^{12}$
ASR-III 14.1–4 Ma	MBS high less pronounced	2 main depocentres: a) in front and west of AT, ⊥ shelf break, b) in front and west of PITW, || shelf break	32,918 (3000)	594	1.955	58.96	$1.9 * 10^{12}$
ASR-IV 4–0 Ma	MBS high || to shelf break, still highest in the W	Between AT and PITW, ⊥ shelf break	30,412 (2000)	578	1.758	144.5	$4.4 * 10^{12}$

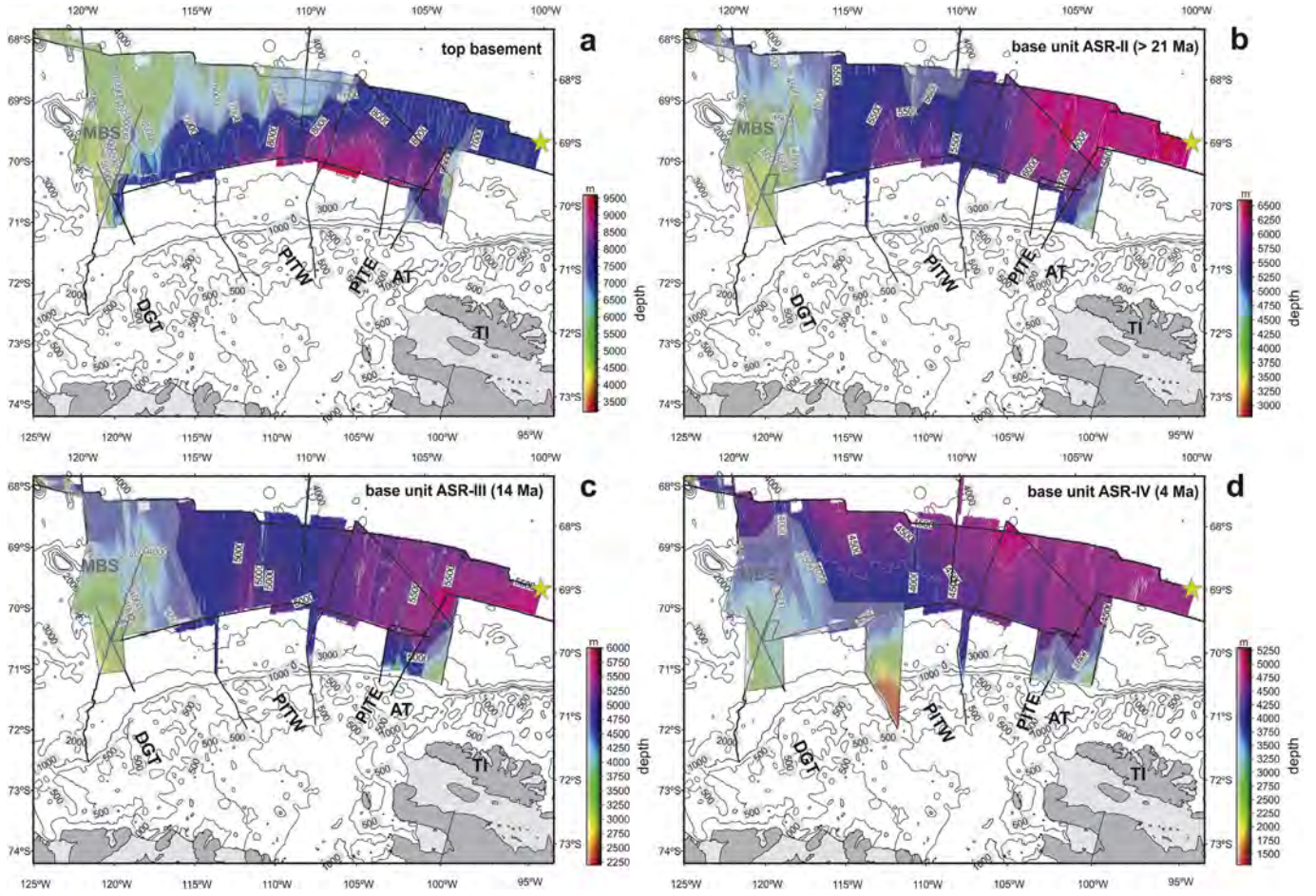

Fig. 3. Depth to horizon maps for the horizons a) top basement, b) base unit ASR-II, c) base unit ASR-III, and d) base unit ASR-IV. Note the different depth scales for the different maps. The shaded areas show the high stands of the horizons. There, the horizons rise above the rms-value of the horizon depth. AT = Abbot Trough, DGT = Dotson Getz Trough, MBS = Marie Byrd seamount area, PITE = Pine Island Bay Trough East, PITW = Pine Island Trough West, TI = Thurston Island.

interpolation of the picked horizons and sedimentary units into the uncovered parts is affected by uncertainties. Nevertheless, the general trend observed in both horizon depth and unit thickness is probably correct and will be interpreted with respect to sediment material input (dimension and favoured path) and transport process (downslope versus along-slope). This discussion will then lead to inferences on modifications in climatic and oceanographic conditions. The bottom current paths are inferred from the occurrence and distribution of sedimentary features, e.g. sediment drifts and mass transport deposits (for details see (Uenzelmann-Neben and Gohl, 2012)).

Sedimentary unit ASR-I appears to be dominated by the basement high in the area of the MBS (Figs. 3a and 4a). This area obviously had been elevated since the MBS magmatism, which is at least 56 Ma old (Kipf et al., 2013). This high appears to have prevented material transport from the slope to the northwest, which is documented by the depocentre observed between the MBS and the continental shelf (Fig. 4a). The thickest part of the unit ASR-I depocentre is found in the eastern part of the study area, where sediments filled a depression in the basement (Figs. 3a and 4 a). This depocentre lies between AT and PITW.

The sedimentation rate with an rms value of 45 m/my lies well within the range for a deep sea environment (Table 2). We observe sediment input along the whole continental margin with a focus between AT and PITW (Fig. 5a). Unit ASR-I appears to level out the basement topography. Uenzelmann-Neben and Gohl (2012) reported sediment drift formation within sedimentary unit ASR-I north of and within the MBS area. They concluded that a bottom current shaping those drifts was deflected by the MBS around them, but did not influence the upper continental rise. The sedimentation east of the MBS therefore was not influenced by the bottom current and thus the basement topography there could be levelled out by sediment infill (Fig. 5a).

As the area of the MBS was elevated (~2000 m at 56 Ma, (Kipf et al., 2013)), the water mass shaping the sediment into sediment drifts (see Fig. 2 of Uenzelmann-Neben and Gohl, 2012) could not have flown as deep as AABW does today (4000 m and deeper, Van Aken, 2007). This indicates a lower density for the water mass. The formation of a bottom/deep water with a lower density may not require full glacial conditions but only a significant sea ice cover in winter as suggested by Uenzelmann-Neben and Gohl (2012). We rule out halothermal bottom/deep water formation, since this appears to be restricted to very warm and confined basins (Van Aken, 2007). Furthermore, a cold westward flowing Antarctic Counter Current has been reported to have initiated mid Eocene cooling in Wilkes Land and downward convection after the opening of the Tasmanian Gateway ~49–50 Ma (Expedition 318 Scientists, 2011; Bijl et al., 2013) thus supporting this hypothesis.

In their reconstruction of the Antarctic topography at 34 Ma, Wilson et al. (2012) infer an increased ice volume for West Antarctica at the Eocene/Oligocene boundary. They suggest a terrestrial ice sheet for the Early Oligocene, which would have been less affected by sea level changes and ocean temperature variations. The detritus eroded by this early ice sheet was deposited mainly in the West Antarctic Rift and little material was transported towards the Amundsen Sea (Wilson et al., 2012). Combining this information with the discussion presented by Uenzelmann-Neben and Gohl (2012), who suggest a cool climate with a significant sea-ice cover to allow bottom/deep water formation

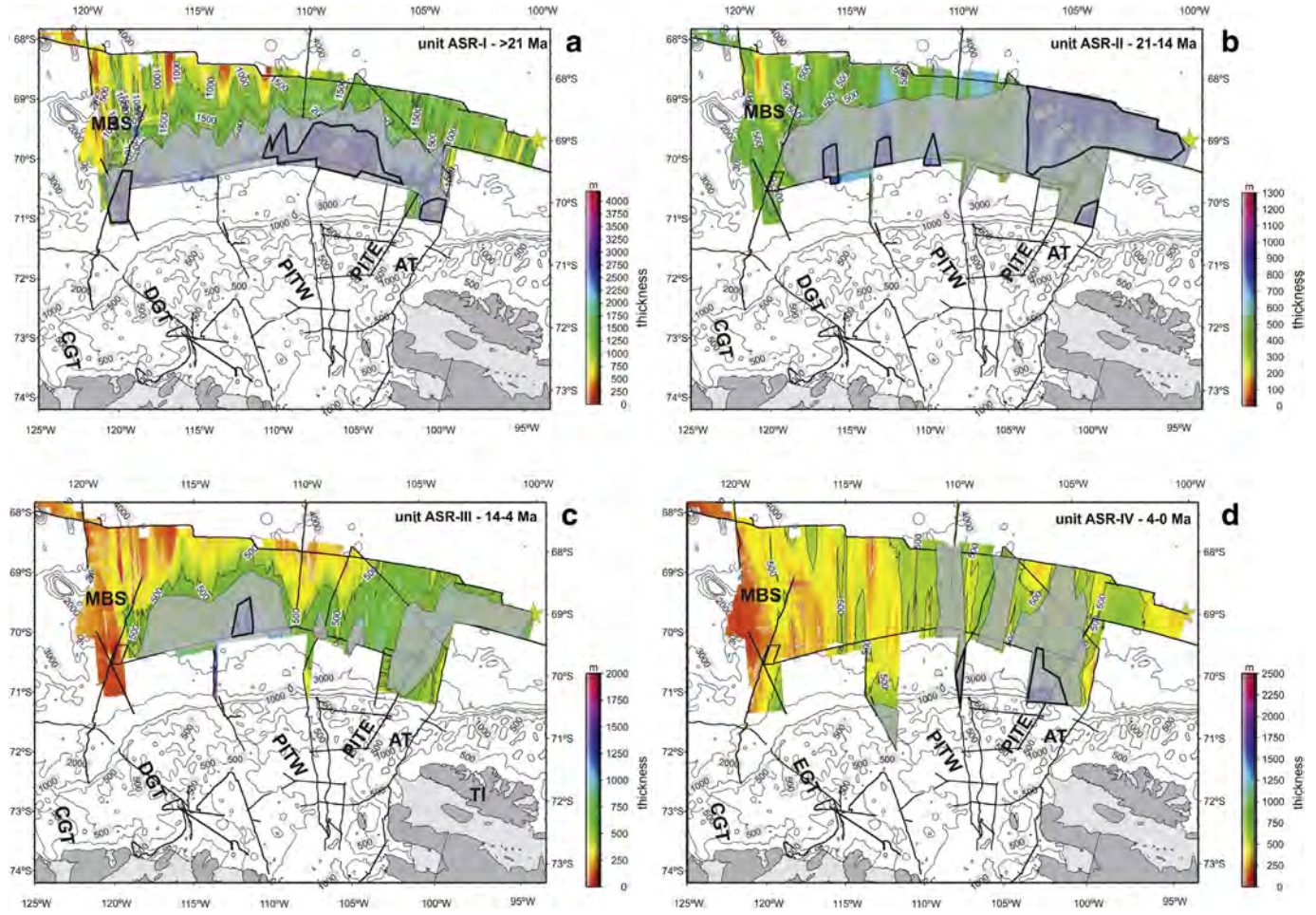

Fig. 4. Thickness maps for the sedimentary units a) ASR-I, b) ASR-II, c) ASR-III, and d) ASR-IV. Note the different thickness scales for the different maps. The shaded areas show the depocentres of the units. There, the units are thicker than the rms-value of the unit thickness. The heavily outlined areas show foci within the depocentres. AT = Abbot Trough, DGT = Dotson Getz Trough, MBS = Marie Byrd seamount area, PITE = Pine Island Trough East, PITW = Pine Island Trough West, TI = Thurston Island.

already in Eocene/Oligocene times, and the lack of channels and mass transport deposits observed in our seismic profiles for unit ASR-I (Figs. 2c and 6), we argue for a continuous, low-energy sediment input from the continent with depositional foci offshore from the DGT, the AT and the outer shelf between PITE and PITW (Fig. 5a). Graham et al. (2010) discuss a broad ice stream outflow spanning from PITE to PITW for the late Quaternary covering an accumulation area of ~500,000 km^2 at the last glacial maximum (LGM). Taking this into account we interpret the foci of the ASR-1 depocentres as palaeo-deltas and suggest that at least on the outer shelf the modern palaeo-ice stream troughs reflect the locations of river beds, which have been located there before 21 Ma. The rivers delivered the main sediment load to the palaeo-shelf break in a low energy environment (Fig. 5a).

The MBS area influences the depth of the base of unit ASR-II, with the palaeo-seafloor high having slightly shifted towards the continental slope (Fig. 3b). We interpret this shift as the consequence of the formation of the western ASR-I depocentre. The ASR-II depocentre is still broad and parallel to the continental slope but extends much farther northwards than that of unit ASR-I (Fig. 4b). It covers roughly 53,225 km^2, which is almost twice the size of unit ASR-I's depocentre (Table 2). A possible interpretation would be simply a build-out of the shelf break, which during deposition of unit ASR-I may have lain further south. Studying seismic lines on the Amundsen Sea shelf, Gohl et al. (2013) did not see any indications for progradation and a northward shift of the shelf break for the period 21–14.1 Ma, which is supported by our lines crossing the continental slope and rise (Figs. 2c, 6b, and c). Sedimentation rates also have nearly doubled within unit ASR-II (Table 2). This points towards increased sediment input along this part of the Amundsen Sea embayment (Fig. 5b), which we attribute to intensified glacial erosion in the hinterland due to a growth of mountain glaciers that may have coalesced to ice caps and not just a build-out of the shelf. Consequently, we conclude glacial conditions in this part of West Antarctica already during the Early Miocene.

This hypothesis is supported by the findings of Rocchi et al. (2006), who could demonstrate that ice caps had affected the Amundsen Sea hinterland possibly as early as 29–27 Ma and certainly by ca. 15 Ma. According to our age model unit ASR-II covers the period from Mi 1a (21.2 Ma, Miller et al., 1991) to the mid-Miocene Climatic Optimum (MMCO) (17–15 Ma, Miller et al., 1987; Zachos et al., 2001). Deep-sea oxygen isotope data on benthic foraminifera show that the Antarctic ice sheet underwent periods of instability during this time (e.g. Zachos et al., 2001). The ice sheet was polythermal, which resulted in high rates of glacial erosion and production of melt water delivering large volumes of suspended material to the continental margin (Haywood et al., 2009). The uplift of coastal Marie Byrd Land since about 29–25 Ma due to a mantle plume appears to have aided increased sediment input via the formation of mountain glaciers (LeMasurier, 2008). West of the Antarctic Peninsula, down-slope sediment transport increased from 15 to 9.5 Ma (Uenzelmann-Neben, 2006). We suggest that ice in the hinterland of the Amundsen Sea Embayment was more sensitive to warming trends towards the MMCO. This may indicate not only the existence of mountain glaciers for this period but a marine-based low-altitude ice sheet as well, which is more sensitive to variations in air temperature (e.g. Pritchard et al., 2012).

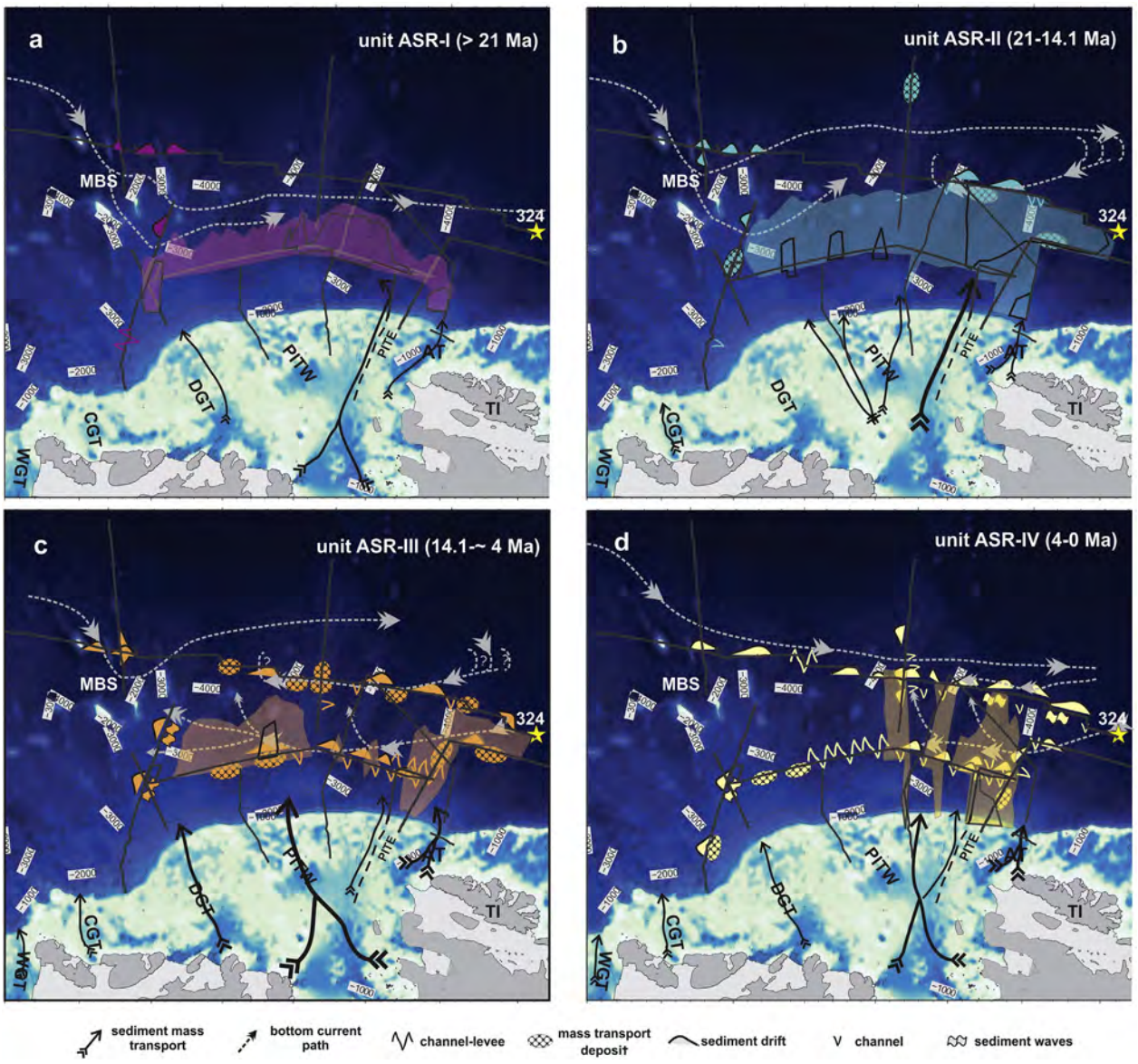

Fig. 5. Depositional and oceanographic model showing the observed sedimentary structures (Uenzelmann-Neben and Gohl, 2012), the depocentres (shaded areas) and the inferred sediment input and bottom current paths for the four distinguished sedimentary units. AT = Abbot Trough, CGT = central Getz Trough, DGT = Dotson Getz Trough, MBS = Marie Byrd seamount area, PITE = Pine Island Trough East, PITW = Pine Island Trough West, WGT = western Getz Trough.

The thickest part of unit ASR-II's depocentre is found in the NE and has a slope parallel shape (Fig. 4b). A narrower thick part of the depocentre lies directly seaward of AT. Obviously the sedimentary material was channelized through AT and PITE in a higher energy environment (please note the increased number of channels and mtds in this unit, Figs. 2b, 6a and b, and 7b), partly deposited seaward of AT and PITE (Fig. 5b), but most of the material was transported farther seawards. There, the sediment was shaped into levee-drifts by a re-circulated bottom-current (Figs. 2c and e and 5b). Three smaller foci of unit ASR-II's depocentre north of PITW are probably the result of continued input via the proposed palaeo-delta.

The MBS region still forms a palaeo-seafloor high at the base of unit ASR-III but is less elevated above the surrounding seabed (Fig. 3c). Material input from the shelf apparently was much reduced during deposition of unit ASR-III. Instead of one large depocentre, we now observe two with a size reduced to about 60% of the size of the unit ASR-II depocentre (Fig. 4c) and a sedimentation rate reduced to 70% compared to that of unit ASR-II (Table 2). The eastern unit ASR-III depocentre lies seaward of the AT, but it is smaller than the thickest part of the unit ASR-II depocentre. This depocentre is aligned perpendicular to the continental slope in its southern part and parallel to the continental slope farther in the north (Fig. 4c). We interpret this as indications for continued strong down-slope transport of glaciogenic debris sourced from the AT (Fig. 5c), which is also supported by the occurrence of mass transport deposits in this unit (Fig. 7). Farther seaward the material was then picked up by a re-circulating bottom current and shaped into levee-drifts (Figs. 2c and e and 5c).

The second depocentre lies between PITW and DGT. Its shape points towards material input along a broader front and not only via the shelf troughs (Fig. 4c). Supply of glaciogenic debris through PITW may have played a more important role than that through PITE during glacial intervals in this period (Fig. 5c). Patch drifts observed on the continental slope indicate a re-shaping of the material by bottom currents (Figs. 2b and d, 6b, and 6c). We also suggest that during

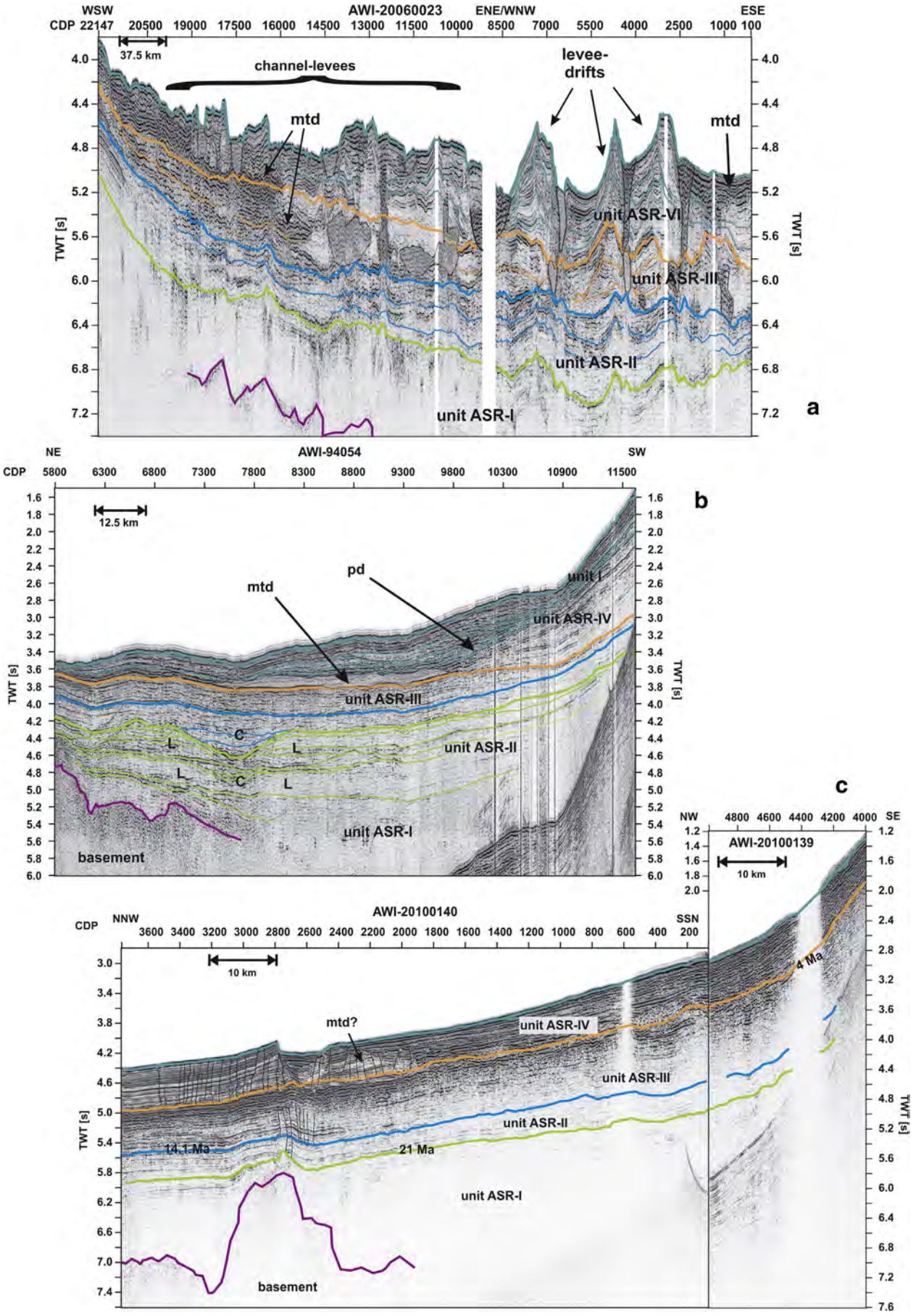
WSW
AWI-20060023
ENE/WNW
ESE
CDP 22147 20500 19000 17500 16000 14500 13000 11500 10000 8500 7000 5500 4000 2500 1000 100
37.5 km
channel-levees
levee-drifts
mtd
mtd
unit ASR-VI
unit ASR-III
unit ASR-II
unit ASR-I
TWT [s]
a
NE
AWI-94054
SW
CDP 5800 6300 6800 7300 7800 8300 8800 9300 9800 10300 10900 11500
12.5 km
b
mtd
pd
unit I
unit ASR-IV
unit ASR-III
unit ASR-II
unit ASR-I
basement
C
L
NW
AWI-20100139
SE
4800 4600 4400 4200 4000
10 km
c
CDP
NNW
AWI-20100140
SSN
3600 3400 3200 3000 2800 2600 2400 2200 2000 1800 1600 1400 1200 1000 800 600 400 200
10 km
mtd?
unit ASR-IV
unit ASR-III
unit ASR-II
unit ASR-I
4 Ma
14.1 Ma
21 Ma
basement

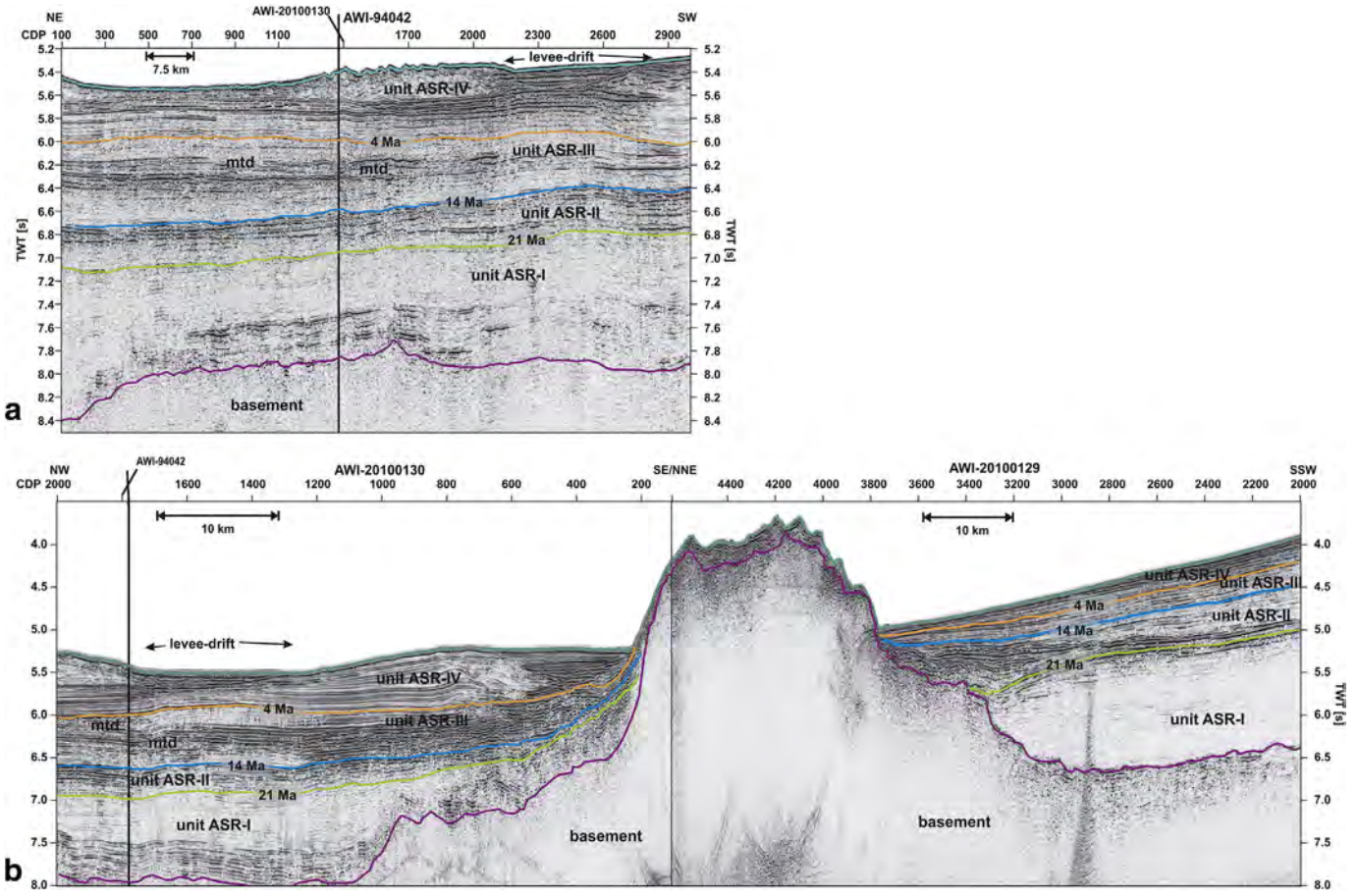

Fig. 7. a) Profile AWI-94042 from the eastern Amundsen Sea. b) Part of profiles AWI-20100130/20100129 from the eastern Amundsen Sea. mtd = mass transport deposit. The thin black lines represent small-scale faults and the shaded areas filled channels. For location see Fig. 1.

intervals between 14 and 4 Ma ice streams advanced more frequently between PITW and DGT across the shelf and supplied the material to the depocentre observed on the adjacent slope and rise (Fig. 5c).

Less detrital input from the shelf may be a result of a cooler ice sheet following the major cooling event at the mid-Miocene Climate Transition (MMCT, ~14 Ma, 1–2 my duration), which occurred at the Middle–Late Miocene boundary (Flower and Kennett, 1994). This reduced rates of glacial erosion and melt water production (Haywood et al., 2009). Gohl et al. (2013) infer a warm period for the latest Miocene/earliest Pliocene with a retreating ice sheet. According to them polythermal glacial activity resulted in high material input to the shelf, but appears to not have reached the continental slope.

For unit ASR-IV we observe three depocentres in the eastern Amundsen Sea, which are aligned perpendicular to the continental slope (Fig. 4d). The sedimentation rate has almost tripled compared to that of unit ASR-III, while the accumulation rate computed for the depocentres increased by a factor of 2.3 (Table 2). The size of the depocentres in unit ASR-IV is about the same as for unit ASR-III. Material input via AT and PITE appears to have been dominant.

Uenzelmann-Neben and Gohl (2012) report fewer mass transport deposits and sediment drifts that now are mainly observed in the central Amundsen Sea. They attributed this to less material input due to a change in ice-regime from wet- to dry based as proposed for other parts of the West Antarctic margin by Böhm et al. (2009) and Rebesco and Camerlenghi (2008), and consistent with WAIS advances across the Ross Sea shelf only during a few short glacial periods between 4 Ma and today (De Santis et al., 1999). Sedimentation rates and accumulation rates observed by us have strongly increased from unit ASR-III to unit ASR-IV (Table 2), which contradicts the formerly proposed reduced sediment input.

Unit thickness and sedimentation rates suggest a change from polythermal to dry-based ice already at 14.1 Ma with the onset of renewed cooling after the MMCT, which is consistent with the conclusion of Rocchi et al. (2006) for the glacial history of Marie Byrd Land. We propose that AT and PITE have been the primary outlets for the ice draining into the Amundsen Sea since 4 Ma (Fig. 5d). Less material was provided via the DGT. This indicates that palaeo-ice streams emanating from today's Pine Island Glacier, Thwaites Glacier and Abbot Ice Shelf as well as Cosgrove Ice Shelf were quite dynamic and were frequently waxing and waning during glacial/interglacial stages of the past 4 Ma. Hochmuth and Gohl (2013) have observed a build-out of the outermost shelf of the AT by 75 km since the onset of glacial conditions. Gohl et al. (2013) suggested repeated advances of grounded ice to the outer shelf as the reason for progradation of the continental shelf since 3.7 Ma supporting our interpretation.

6. Conclusions

We analysed seismic reflection data from the continental slope and rise aiming at reconstructing sediment input (pathways and hence source areas on the shelf, amount) and sediment transport processes and to infer climatic and oceanographic changes. Thicknesses and

Fig. 6. a) Profile AWI-20060023 parallel to the shelf break. b) Profile AWI-94054 from the western Amundsen Sea. c) Part of profiles AWI-20100140/20100139 from the eastern Amundsen Sea. C = channel, L = levee, mtd = mass transport deposit, pd = patched drift. The thin black lines represent small-scale faults and the shaded areas filled channels. For location see Fig. 1.

depocentres of four sedimentary units were studied, which varied significantly through time, similar to the inferred sedimentation rates. The depocentres show distinct differences in location and shape. The oldest unit ASR-I (>21 Ma) shows a narrow depocentre parallel to the continental slope interpreted to represent low energy input (Fig. 5a). We have observed a focus in deposition near 106°W and attribute this to sediment supply through a palaeo-delta, which later became PITE. Sediment drifts observed in the elevated MBS area indicate an active water mass with a density between that of today's AABW and LCDW. This points towards a significant sea ice cover but not full glacial conditions for the period before 21 Ma.

For unit ASR-II (21–14.1 Ma) we observe a strong increase in sediment input documented by a larger depocentre and much higher sedimentation rates. We interpret this as evidence for glacial conditions in West Antarctica already during the Early Miocene. Warming as the result of the MMCO resulted in a wet-based ice sheet and led to a higher sediment supply. Glaciogenic debris was supplied from the shelf along a broad front but with a main pathway through PITE and AT (Fig. 5b). Most of the material was transported onto the eastern Amundsen Sea rise where it was shaped into levee-drifts by a re-circulating bottom current (Fig. 5b).

Unit ASR-III (14.1–4 Ma) is characterised by two smaller depocentres seaward of AT and PITW and reduced sedimentation rates (Fig. 5c). The onset of stronger cooling after 14 Ma resulted in a cooler and dryer based ice sheet leading to less glacial erosion and less material input.

A dynamic ice sheet since 4 Ma characterised by growth and decay during cold and warm phases, respectively, is documented by a strong increase in sedimentation rates. Material was dominantly supplied to the rise via AT and PITW and much less sediment was provided from the western Amundsen Sea shelf (Fig. 5d). The pulsed glaciogenic debris input from the shelf interacted with a west-setting bottom current on the rise resulting in the continued formation of levee-drifts in the eastern and central Amundsen Sea (Fig. 5d).

The presented model is still tentative and suffers from the lack of age–depth and lithological information. Drill sites in the Amundsen Sea are desperately needed to gain high resolution insights into the evolution of climate and oceanography of West Antarctica. This study presents a basis for the identification of suitable drill locations.

Acknowledgements

We are grateful to the captains, crews and scientists for their support during the RV Polarstern cruises ANT-XI/3 (1994), ANT-XXIII/4 (2006) and ANT-XXVI-3 (2010) during which the data used in this paper were collected. Thanks go to C.-D. Hillenbrand, whose comments much improved this manuscript. We are further grateful for the helpful comments of two anonymous reviewers and the editor H. Oberhänsli.

References

Anderson, J.B., 1999. Antarctic Marine Geology. Cambridge University Press, Cambridge.
Anderson, J.B., et al., 2011. Progressive Cenozoic cooling and the demise of Antarctica's last refugium. PNAS 108, 11356–11360.
Arneborg, L., Wahlin, A.K., Bjork, G., Liljebladh, B., Orsi, A.H., 2012. Persistent inflow of warm water onto the central Amundsen shelf. Nat. Geosci. 5 (12), 876–880.
Assmann, K.M., et al., 2013. Variability of circumpolar deep water transport onto the Amundsen Sea Continental shelf through a shelf break trough. J. Geophys. Res. Oceans 118 (12), 6603–6620.
Bamber, J.L., Riva, R.E.M., Vermeersen, B.L.A., LeBrocq, A.M., 2009. Reassessment of the potential sea-level rise from a collapse of the West Antarctic Ice Sheet. Science 324 (5929), 901–903.
Bart, P.J., 2003. Were West Antarctic Ice Sheet grounding events in the Ross Sea a consequence of East Antarctic Ice Sheet expansion during the middle Miocene? Earth Planet. Sci. Lett. 216 (1–2), 93–107.
Bart, P.J., Sjunneskog, C., Chow, J.M., 2011. Piston-core based biostratigraphic constraints on Pleistocene oscillations of the West Antarctic Ice Sheet in western Ross Sea between North Basin and AND-1B drill site. Mar. Geol. 289 (1–4), 86–99.
Bentley, M.J., et al., 2010. Deglacial history of the West Antarctic Ice Sheet in the Weddell Sea embayment: constraints on past ice volume change. Geology 38 (5), 411–414.
Bijl, P.K., et al., 2013. Eocene cooling linked to early flow across the Tasmanian Gateway. Proc. Natl. Acad. Sci. 110 (24), 9645–9650.
Böhm, G., Ocakoglu, N., Picotti, S., De Santis, L., 2009. West Antarctic Ice Sheet evolution: new insights from a seismic tomographic 3D depth model in the Eastern Ross Sea (Antarctica). Mar. Geol. 266 (1–4), 109–128.
Bradley, S.L., Siddall, M., Milne, G.A., Masson-Delmotte, V., Wolff, E., 2012. Where might we find evidence of a Last Interglacial West Antarctic Ice Sheet collapse in Antarctic ice core records? Glob. Planet. Chang. 88â€“89 (0), 64–75.
Cooper, A.K., et al., 2009. Cenozoic climate history from seismic reflection and drilling studies on the Antarctic Continental Margin. In: Florindo, F., Siegert, M. (Eds.), Antarctic Climate Evolution. Developments in Earth and Environmental Sciences. Elsevier, pp. 115–228.
De Santis, L., Anderson, J.B., Brancolini, G., Zayatz, I., 1995. Seismic record of late Oligocene through Miocene glaciation on the central and eastern continental shelf of the Ross Sea. In: Cooper, A.F., Barker, P.F., Brancolini, G. (Eds.), Geology and Seismic Stratigraphy of the Antarctic Margin. American Geophysical Union, Washington, pp. 235–260.
De Santis, L., Prato, S., Brancolini, G., Lovo, M., Torelli, L., 1999. The Eastern Ross Sea continental shelf during the Cenozoic: implications for the West Antarctic Ice Sheet development. Glob. Planet. Chang. 23 (1–4), 173–196.
DeConto, R.M., Pollard, D., Kowalewski, D., 2012. Modeling Antarctic Ice Sheet and climate variations during Marine Isotope Stage 31. Glob. Planet. Chang. 88â€“89 (0), 45–52.
Domack, E.W., Jacobson, E.A., Shipp, S., Anderson, J.B., 1999. Late Pleistocene/Holocene retreat of the West Antarctic Ice-Sheet system in the Ross Sea: part 2 — sedimentologic and stratigraphic signature. Geol. Soc. Am. Bull. 111 (10), 1517–1536.
Dowdeswell, J.A., Evans, J., O Cofaigh, C., Anderson, J.B., 2006. Morphology and sedimentary processes on the continental slope off Pine Island Bay, Amundsen Sea, West Antarctica. Geol. Soc. Am. Bull. 118, 606–619.
Eagles, G., Gohl, K., Larter, R.D., 2004. High-resolution animated tectonic reconstruction of the South Pacific and West Antarctic Margin. Geochem. Geophys. Geosyst. 5.
Escutia, C., et al., 2009. Circum-Antarctic warming events between 4 and 3.5 Ma recorded in marine sediments from the Prydz Bay (ODP Leg 188) and the Antarctic Peninsula (ODP Leg 178) margins. Glob. Planet. Chang. 69 (3), 170–184.
Evans, J., Dowdeswell, J.A., O Cofaigh, C., Benham, T.J., Anderson, J.B., 2006. Extent and dynamics of the West Antarctic Ice Sheet on the outer continental shelf of Pine Island Bay during the last glaciation. Mar. Geol. 230, 53–72.
Expedition 318 Scientists, 2011. Expedition 318 summary. In: Escutia, C., Brinkhuis, H., Klaus, A., Expedition 318 Scientists (Eds.), Proceedings of the Integrated Ocean Drilling Program. IODP.
Flower, B.P., Kennett, J.P., 1994. The middle Miocene climatic transition: East Antarctic Ice Sheet development, deep ocean circulation and global carbon cycling. Palaeogeogr. Palaeoclimatol. Palaeoecol. 108 (3–4), 537–555.
Francis, J.E., et al., 2009. From greenhouse to icehouse — the Eocene/Oligocene in Antarctica. In: Florindo, F., Siegert, M. (Eds.), Antarctic Climate Evolution. Developments in Earth and Environmental Sciences. Elsevier, pp. 309–368.
Gohl, K., et al., 1997. Tectonic and sedimentary architecture of the Bellingshausen and Amundsen Sea Basins, SE Pacific, by seismic profiling. In: Ricci, C.A. (Ed.), The Antarctic Region: Geological Evolution and Processes. Terra Antartica Publication, Siena, pp. 719–723.
Gohl, K., et al., 2007. Geophysical survey reveals tectonic structures in the Amundsen Sea embayment, West Antarctica. In: Cooper, A.K., Raymond, C.R., al, e. (Eds.), Antarctica: A Keystone in a Changing World. USGS Open-File Report 2007–1047, Sta Barbara, USA.
Gohl, K., et al., 2013. Seismic stratigraphic record of the Amundsen Sea Embayment shelf from pre-glacial to recent times: evidence for a dynamic West Antarctic Ice Sheet. Mar. Geol. 344, 115–131.
Gomez, N., Mitrovica, J.X., Tamisiea, M.E., Clark, P.U., 2010. A new projection of sea level change in response to collapse of marine sectors of the Antarctic Ice Sheet. Geophys. J. Int. 180 (2), 623–634.
Gordon, A.L., et al., 2009. Western Ross Sea continental slope gravity currents. Deep-Sea Res. II Top. Stud. Oceanogr. 56 (13–14), 796–817.
Graham, A.G.C., et al., 2009. Bedform signature of a West Antarctic palaeo-ice stream reveals a multi-temporal record of flow and substrate control. Quat. Sci. Rev. 28 (25–26), 2774–2793.
Graham, A.G.C., et al., 2010. Flow and retreat of the Late Quaternary Pine Island-Thwaites palaeo-ice stream, West Antarctica. J. Geophys. Res. Earth Surf. 115, 12.
Haywood, A.M., et al., 2009. Middle Miocene to Pliocene History of Antarctica and the Southern Ocean. In: Florindo, F., Siegert, M. (Eds.), Antarctic Climate Evolution. Developments in Earth and Environmental Sciences. Elsevier, pp. 401–463.
Hernandez-Molina, F.J., Larter, R.D., Rebesco, M., Maldonado, A., 2004. Miocene changes in bottom current regime recorded in continental rise sediments on the Pacific margin of the Antarctic Peninsula. Geophys. Res. Lett. 31.
Hillenbrand, C.-D., Ehrmann, W., 2005. Late Neogene to Quaternary environmental changes in the Antarctic Peninsula region: evidence from drift sediments. Glob. Planet. Chang. 45, 165–191.
Hillenbrand, C.-D., et al., 2008. The present and past bottom-current flow regime around the sediment drifts on the continental rise west of the Antarctic Peninsula. Mar. Geol. 255.
Hillenbrand, C.-D., et al., 2013. Grounding-line retreat of the West Antarctic Ice Sheet from inner Pine Island Bay. Geology 41 (1), 35–38.
Hochmuth, K., Gohl, K., 2013. Glaciomarine sedimentation dynamics of the Abbot glacial trough of the Amundsen Sea Embayment shelf, West Antarctica. Geol. Soc. Lond., Spec. Publ. 381 (1), 233–244.
Hu, A., Meehl, G.A., Han, W., Yin, J., 2011. Effect of the potential melting of the Greenland Ice Sheet on the Meridional Overturning Circulation and global climate in the future. Deep-Sea Res. II Top. Stud. Oceanogr. 58 (17–18), 1914–1926.
Huber, M., et al., 2004. Eocene circulation of the Southern Ocean: was Antarctica kept warm by subtropical waters? Paleoceanography 19.

Ivany, L.C., Van Simaeys, S., Domack, E.W., Samson, S.D., 2006. Evidence for an earliest Oligocene ice sheet on the Antarctic Peninsula. Geology 34 (5), 377–380.
Iwai, M., Acton, G., Lazarus, D., Osterman, L.E., Williams, T., 2002. Magnetobiochronologic synthesis of ODP Leg 178 rise sediments from the Pacific Sector of the Southern Ocean: Sites 1095, 1096, and 1101. In: Barker, P.F., Camerlenghi, A., Acton, G.D., Ramsay, A.T.S. (Eds.), Proceedings of the Ocean Drilling Program, Scientific Results, volume 178. Ocean Drilling Program, College Station.
Jacobs, S.S., Hellmer, H.H., Jenkins, A., 1996. Antarctic Ice Sheet melting in the southeast Pacific. Geophys. Res. Lett. 23 (9), 957–960.
Jacobs, S.S., Jenkins, A., Giulivi, C.F., Dutrieux, P., 2011. Stronger ocean circulation and increased melting under Pine Island Glacier ice shelf. Nat. Geosci. 4 (8), 519–523.
Jacobs, S., et al., 2013. Getz Ice Shelf melting response to changes in ocean forcing. J. Geophys. Res. Oceans 118 (9), 4152–4168.
Jakobsson, M., Anderson, J.B., OSO0910, 2010. Multibeam mapping reveal past collapse of the Pine Island Bay ice shelf, West Antarctica. GEBCO 5th Science Day, Lima, Peru.
Jakobsson, M., et al., 2012. Ice sheet retreat dynamics inferred from glacial morphology of the central Pine Island Bay Trough, West Antarctica. Quat. Sci. Rev. 38, 1–10.
Kipf, A., et al., 2013. Seamounts off the West Antarctic margin: A case for non-hotspot driven intraplate volcanism. Gondwana Research 25, 1660–1667.
Kirshner, A.E., et al., 2012. Post-LGM deglaciation in Pine Island Bay, West Antarctica. Quat. Sci. Rev. 38, 11–26.
Klages, J.P., et al., 2013. First geomorphological record and glacial history of an inter-ice stream ridge on the West Antarctic continental shelf. Quat. Sci. Rev. 61, 47–61.
Konfirst, M.A., Scherer, R.P., Hillenbrand, C.-D., Kuhn, G., 2012. A marine diatom record from the Amundsen Sea: insights into oceanographic and climatic response to the Mid-Pleistocene Transition in the West Antarctic sector of the Southern Ocean. Mar. Micropaleontol. 92/93 (0), 40–51.
LeMasurier, W.E., 2008. Neogene extension and basin deepening in the West Antarctic rift inferred from comparisons with the East African rift and other analogues. Geology 36, 247–250.
Livingstone, S.J., et al., 2012. Antarctic palaeo-ice streams. Earth Sci. Rev. 111 (1/2), 90–128.
Lowe, A.J., Anderson, J.B., 2002. Reconstruction of the West Antarctic ice sheet in Pine Island Bay during the last glacial maximum and its subsequent retreat history. Quat. Sci. Rev. 21, 1879–1897.
Miller, K.G., Fairbanks, R.G., Mountain, G.S., 1987. Tertiary oxygen isotope synthesis, sea level history, and continental margin erosion. Paleoceanography 2 (1), 1–19.
Miller, K.G., Wright, J.D., Fairbanks, R.G., 1991. Unlocking the ice house: Oligocene–Miocene oxygen isotopes, eustasy, and margin erosion. J. Geophys. Res. 96, 6829–6848.
Miller, K.G., et al., 2008. A view of Antarctic ice sheet evolution from sea-level and deep-sea isotope changes during the Late Cretaceous–Cenozoic. In: Cooper, A.F., et al. (Eds.), Antarctica: A keystone in a changing world. National Academic Press, Washington, D.C., pp. 55–70.
Naish, T., et al., 2007. A record of Antarctic climate and ice sheet history recovered. Eos 88 (50), 557–558.
Naish, T., et al., 2009b. Chapter 11 Late Pliocene–Pleistocene Antarctic climate variability at orbital and suborbital scale: ice sheet, ocean and atmospheric interactions. Developments in Earth and Environmental SciencesElsevier, pp. 465–529.
Naish, T., et al., 2009a. Obliquity-paced Pliocene West Antarctic ice sheet oscillations. Nature 458 (7236), 322–328.
Nitsche, F.O., Gohl, K., Vanneste, K., Miller, H., 1997. Seismic expression of glacially deposited sequences in the Bellingshausen and Amundsen Sea, West Antarctica. In: Barker, P.F., Cooper, A.F. (Eds.), Geology and Seismic Stratigraphy of the Antarctic Margin, 2. American Geophysical Union, Washington, pp. 95–108.
Nitsche, F.O., Cunningham, A.P., Larter, R.D., Gohl, K., 2000. Geometry and development of glacial continental margin depositional systems in the Bellingshausen Sea. Mar. Geol. 162 (2–4), 277–302.
Nitsche, F.O., Jacobs, S.S., Larter, R.D., Gohl, K., 2007. Bathymetry of the Amundsen Sea continental shelf: implications for geology, oceanography, and glaciology. Geochem. Geophys. Geosyst. 8.
ÓCofaigh, C., et al., 2005. Flow of the West Antarctic Ice Sheet on the continental margin of the Bellingshausen Sea at the last glacial maximum. J. Geophys. Res. 110.
Orsi, A.H., 2010. Oceanography: recycling bottom waters. Nat. Geosci. 3 (5), 307–309.
Orsi, A.H., Wiederwohl, C.L., 2009. A recount of Ross Sea waters. Deep-Sea Res. II Top. Stud. Oceanogr. 56 (13–14), 778–795.
Orsi, A.H., Johnson, G.C., Bullister, J.L., 1999. Circulation, mixing, and production of Antarctic Bottom Water. Prog. Oceanogr. 43, 55–109.
Pollard, D., DeConto, R.M., 2009. Modelling West Antarctic ice sheet growth and collapse through the past five million years. Nature 458 (7236), 329–332.
Pritchard, H.D., et al., 2012. Antarctic ice-sheet loss driven by basal melting of ice shelves. Nature 484 (7395), 502–505.
Pross, J., et al., 2012. Persistent near-tropical warmth on the Antarctic continent during the early Eocene epoch. Nature 488.
Rebesco, M., Camerlenghi, A., 2008. Late Pliocene margin development and mega-debris flow deposits on the Antarctic continental margins: evidence of the onset of the modern Antarctic ice-sheet? Palaeogeogr. Palaeoclimatol. Palaeoecol. 260, 149–167.
Rebesco, M., Larter, R.D., Camerlenghi, A., Barker, P.F., 1996. Giant sediment drifts on the continental rise west of the Antarctic Peninsula. Geo-Mar. Lett. 16 (2), 65–75.
Rebesco, M., et al., 2002. Sediment drifts and deep-sea channel systems, Antarctic Peninsula Pacific Margin. In: Stow, D.A.V., Pudsey, C.J., Howe, J.A., Faugeres, J.-C., Viana, A.R. (Eds.), Deep-water Contourite Systems: Modern Drifts and Ancient Series, Seismic and Sedimentary Characteristics. Geological Society London, pp. 353–372.
Rocchi, S., LeMasurier, W.E., Di Vincenzo, G., 2006. Oligocene to Holocene erosion and glacial history in Marie Byrd Land, West Antarctica, inferred from exhumation of the Dorrel Rock intrusive complex and from volcano morphologies. Geological Society of America Bulletin 118 (7–8), 991–1005.
Scheuer, C., Gohl, K., Larter, R.D., Rebesco, M., Udintsev, G., 2006a. Variability in Cenozoic sedimentation along the continental rise of the Bellingshausen Sea, West Antarctica. Mar. Geol. 227 (3–4), 279–298.
Scheuer, C., Gohl, K., Udintsev, G., 2006b. Bottom-current control on sedimentation in the western Bellingshausen Sea, West Antarctica. Geo-Mar. Lett. 26 (2), 90–101.
Shipboard Scientific Party, 1975a. Site 274. In: Hayes, D.E., Frakes, L.A. (Eds.), Deep Sea Drilling Project, Initial Reports. US Government, Washington, pp. 369–433.
Shipboard Scientific Party, 1975b. Sites 270, 271, 272. In: Hayes, D.E., Frakes, L.A. (Eds.), Deep Sea Drilling Project, Initial Reports. US Government, Washington, pp. 211–334.
Shipboard Scientific Party, 1976. Site 324. In: Hollister, C.D., Craddock, C. (Eds.), Initial Reports. Deep Sea Drilling Project, Washington, D.C. , pp. 127–156.
Smellie, J.L., Haywood, A.M., Hillenbrand, C.-D., Lunt, D.J., Valdes, P.J., 2009. Nature of the Antarctic Peninsula Ice Sheet during the Pliocene: geological evidence and modelling results compared. Earth Sci. Rev. 94 (1–4), 79–94.
Thoma, M., Jenkins, A., Holland, D.M., Jacobs, S., 2008. Modelling circumpolar deep water intrusions on the Amundsen Sea continental shelf, Antarctica. Geophys. Res. Lett. 35 (18) L18602.
Tucholke, B.E., Houtz, R.E., 1976. Sedimentary framework of the Bellinghausen Basin from seismic profiler data. In: Hollister, C.D., Craddock, C. (Eds.), Initial Reports. Deep Sea Drilling Project, Washington, D.C. , pp. 197–227.
Tucholke, B.E., Edgar, N.T., Boyce, R.E., 1976a. Physical properties of sediments and correlations with acoustic stratigraphy: Leg 35, Deep Sea Drilling Project. In: Hollister, C.D., Craddock, C. (Eds.), Initial Reports. Deep Sea Drilling Project, Washington, D.C. , pp. 229–249.
Tucholke, B.E., Hollister, C.D., Weaver, F.M., Vennum, W.R., 1976b. Continental rise and abyssal plain sedimentation in the southeast Pacific Basin: Leg 35 Deep Sea Drilling Project. In: Hollister, C.D., Craddock, C. (Eds.), Initial Reports. Deep Sea Drilling Project, Washington, D.C. , pp. 359–400.
Uenzelmann-Neben, G., 2006. Depositional patterns at Drift 7, Antarctic Peninsula: along-slope versus down-slope sediment transport as indicators for oceanic currents and climatic conditions. Mar. Geol. 233, 49–62.
Uenzelmann-Neben, G., Gohl, K., 2012. Amundsen Sea sediment drifts: archives of modifications in oceanographic and climatic conditions. Mar. Geol. 299–302, 51–62.
Uenzelmann-Neben, G., Gohl, K., Larter, R.D., Schlüter, P., 2007. Differences in ice retreat across Pine Island Bay, West Antarctica, since the last glacial maximum: indications from multichannel seismic reflection data. In: Cooper, A.K., Raymond, C.R.e.a. (Eds.), Antarctica — A keystone in a changing world. USGS Open File Report.
Van Aken, H.M., 2007. The Oceanic Thermohaline circulation. Atmospheric and Oceanographic Sciences Library. , 39. Springer, New York.
Weigelt, E., Gohl, K., Uenzelmann-Neben, G., Larter, R.D., 2009. Late Cenozoic ice sheet cyclicity in the western Amundsen Sea Embayment — evidence from seismic records. Glob. Planet. Chang. 69 (3), 162–169.
Weigelt, E., Uenzelmann-Neben, G., Gohl, K., Larter, R.D., 2012. Did massive glacial dewatering modify sedimentary structures on the Amundsen Sea Embayment shelf, West Antarctica? Glob. Planet. Chang. 92–93, 8–16.
Wellner, J.S., Lowe, A.J., Shipp, S.S., Anderson, J.B., 2001. Distribution of glacial geomorphic features on the Antarctic continental shelf and correlation with substrate: implications for ice behavior. J. Glaciol. 47, 391–411.
Wilson, G.S., Pekar, S.F., Naish, T.R., Passchier, S., DeConto, R., 2009. Chapter 9 The Oligocene–Miocene Boundary — Antarctic Climate Response to Orbital Forcing. In: Florindo, F., Siegert, M. (Eds.), Developments in Earth and Environmental Sciences. Elsevier, pp. 369–400.
Wilson, D.S., et al., 2012. Antarctic topography at the Eocene–Oligocene boundary. Palaeogeogr. Palaeoclimatol. Palaeoecol. 335–336, 24–34.
Yamaguchi, K., Tamura, Y., Mizukosho, I., Tsuru, I., 1988. Preliminary report of geophysical and geological surveys in the Amundsen Sea, West Antarctica. Proc. NIPR Symp. Antarct. Geosci. 2, 55–67.
Yilmaz, Ö., 2001. Seismic Data Analysis. Investigations in Geophysics, 10. Society of Exploration Geophysicists, Tulsa (2027 pp.).
Zachos, J.C., Pagani, M., Sloan, L., Thomas, E., Billups, K., 2001. Trends, rhythms, and aberrations in global climate 65 Ma to present. Science 292, 686–693.

6.4 Glaciomarine processes on the shelf of the Amundsen Sea Embayment and their relationship to past ice sheet dynamics

Publication 6.4.1:

Nitsche, F.O., Jacobs, S., Larter, R.D., **Gohl, K.** (2007). Bathymetry of the Amundsen Sea continental shelf: implications for geology, oceanography, and glaciology. *Geochemistry Geophysics Geosystems* (G3), v. 8, Q10009, doi:10.1029/2007GC001694.

Author contributions: Nitsche compiled the bathymetric data and wrote most of the paper. Jacobs, Larter and Gohl contributed with data from expeditions they led or were project leaders. All three co-authors contributed to the paper in the discussion of the grids and implications for glaciomorphological formations.

Geochemistry Geophysics Geosystems G3
AN ELECTRONIC JOURNAL OF THE EARTH SCIENCES
Published by AGU and the Geochemical Society

Data Brief
Volume 8, Number 10
18 October 2007
Q10009, doi:10.1029/2007GC001694
ISSN: 1525-2027

Bathymetry of the Amundsen Sea continental shelf: Implications for geology, oceanography, and glaciology

F. O. Nitsche and S. S. Jacobs
Lamont-Doherty Earth Observatory of Columbia University, Route 9 W, Palisades, New York 10964, USA (fnitsche@ldeo.columbia.edu)

R. D. Larter
Geological Sciences Division, British Antarctic Survey, High Cross/Madingley Road, Cambridge CB3 0ET, UK

K. Gohl
Alfred Wegener Institute for Marine and Polar Research, P.O. Box 120161, D-27515 Bremerhaven, Germany

[1] The Amundsen Sea continental shelf is one of the most remote areas of coastal Antarctica and was relatively unexplored until the late 1980s. Over the last two decades, increased oceanographic and geological interest has led to several cruises that resulted in sufficient bathymetric data to compile a fairly detailed regional map of the Amundsen continental shelf. We have combined available multibeam and single-beam bathymetry data from various sources and created a new regional bathymetry of the Amundsen Sea continental shelf and margin. Deep trough systems that dominate the inner shelf are aligned with present glaciers and separated by shallower ridges. Shaped by paleo-ice streams, these features merge into a small number of broader troughs on the middle shelf and shoal seaward. They now serve as conduits and reservoirs for relatively warm Circumpolar Deep Water. This new compilation is a major improvement over previously available regional maps and should aid the numerical modeling of ocean circulation, the reconstructions of paleo-ice streams, and the refinement of ice sheet models.

Components: 5032 words, 5 figures, 1 table.

Keywords: West Antarctica; continental shelf; bathymetry; seafloor morphology.

Index Terms: 3002 Marine Geology and Geophysics: Continental shelf and slope processes (4219); 3045 Marine Geology and Geophysics: Seafloor morphology, geology, and geophysics; 4207 Oceanography: General: Arctic and Antarctic oceanography (9310, 9315).

Received 18 May 2007; **Revised** 6 August 2007; **Accepted** 15 August 2007; **Published** 18 October 2007.

Nitsche, F. O., S. S. Jacobs, R. D. Larter, and K. Gohl (2007), Bathymetry of the Amundsen Sea continental shelf: Implications for geology, oceanography, and glaciology, *Geochem. Geophys. Geosyst.*, *8*, Q10009, doi:10.1029/2007GC001694.

1. Introduction

[2] The Amundsen Sea continental shelf is located between 100° and 135°W, south of 71°S, along the margin of the Marie Byrd Land sector of the West Antarctic Ice Sheet (WAIS) (Figures 1 and 4). As one of the more remote Antarctic coastlines, with a nearly perennial sea ice cover and little if any bottom water formation, it remained largely unexplored until the mid 1980s. Interest in the region

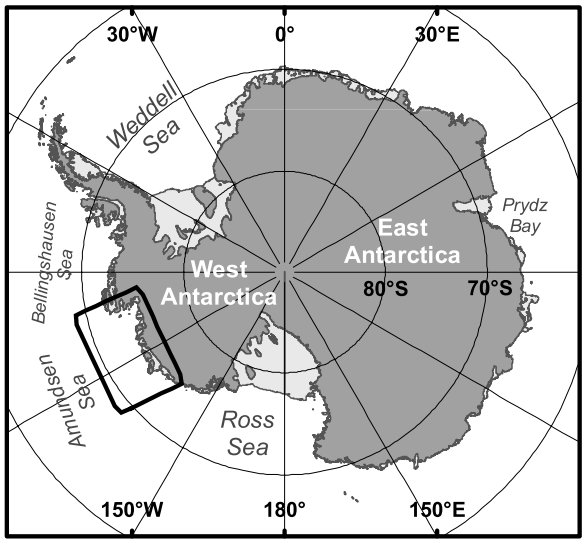

Figure 1. Antarctica with the location of the Amundsen Sea. Outline is based on Antarctic Digital Database 4.1 [*Thomson and Cooper*, 1993] (http://www.add.scar.org/).

increased with the 1994 discovery that the ice shelf at the terminus of the Pine Island Glacier was melting orders of magnitude faster than the Ross and Filchner-Ronne Ice Shelves [*Jacobs et al.*, 1996; *Jenkins et al.*, 1997; *Hellmer et al.*, 1998], accompanied by increased velocity, thinning and grounding line retreat [*Rignot*, 1998; *Rignot and Jacobs*, 2002]. A melt rate exceeding 40 m/yr near its grounding line [*Rignot and Jacobs*, 2002] appears to be driven by "warm" Circumpolar Deep Water (CDW) that floods deeper areas of the Amundsen Sea continental shelf. Subsequent investigations have revealed high melt rates for other Amundsen Sea ice shelves, thinning and increased velocities of tributary glaciers, and decreasing ice surface elevations of the adjacent WAIS drainage basins [*Wingham et al.*, 1998; *Rignot and Thomas*, 2002; *Shepherd et al.*, 2004; *Thomas et al.*, 2004; *Davis et al.*, 2005]. Such findings have revived longstanding concerns about ice sheet stability in this sector [*Hughes*, 1973], particularly as the WAIS is mostly grounded below sea level [*Drewry et al.*, 1982] and the global ocean is warming [*Levitus et al.*, 2005].

[3] Much of the rapid melting occurs within deep troughs on the inner shelf, presumably cut when the ice streams of larger ice sheets were grounded on the present seafloor [*Lowe and Anderson*, 2002; *Evans et al.*, 2006]. As these features now extend beneath the small Amundsen Sea ice shelves, it is important to understand how the troughs facilitate CDW access to the ice, along with their characteristics and connections to the shelf break. A better description of the continental shelf bathymetry could become a key element in improved models of ocean circulation, ocean-ice interactions and ice sheet behavior [*Philippon et al.*, 2006], and in reconstructions of paleo-ice flow [*Kellogg and Kellogg*, 1987; *Lowe and Anderson*, 2002; *Evans et al.*, 2006; *Larter et al.*, 2007].

[4] While several previous studies of Amundsen Sea bathymetry provided significant new insights, most have been restricted to local areas covered by single cruises. The aggregated tracks of several expeditions, including recent cruises on the RRS *James Clark Ross* and R/V *Polarstern* in 2006 and the *Nathaniel B. Palmer* in 2007, have now been compiled into a chart that provides an overview of the regional bathymetric setting and its geological, oceanographic and glaciological implications.

2. Setting of the Amundsen Sea Continental Shelf

[5] The tectonic structure of the Amundsen Sea continental shelf results mainly from the Late Cretaceous rifting and breakup between New Zealand and the Marie Byrd Land and Thurston Island blocks, and may also have been affected by the existence of an independent Bellingshausen Plate until the early Tertiary [*Stock and Molnar*, 1987; *Mayes et al.*, 1990; *Larter et al.*, 2002; *Eagles et al.*, 2004; *Gohl et al.*, 2007]. It has been suggested that the southern boundary of the Bellingshausen Plate crossed the continental shelf of the Amundsen Sea embayment [*Larter et al.*, 2002; *Eagles et al.*, 2004; *Gohl et al.*, 2007].

[6] The present continental shelf was sculpted during past glaciations, displaying surface and subsurface features that indicate grounded ice has reached the outer shelf several times [*Kellogg and Kellogg*, 1987; *Nitsche et al.*, 1997; *Lowe and Anderson*, 2002; *Evans et al.*, 2006]. Earlier cruises discovered several deep troughs on the inner shelf [*SPRITE Group*, 1992; T. B. Kellogg et al., Former rock-floored ice-streams on the Amundsen Sea continental shelf, unpublished manuscript, 2000], and subsequent investigations of the trough originating in Pine Island Bay reported exposed crystalline bedrock on the inner shelf, changing to dipping strata with overlying recent sediment cover toward the mid-shelf [*Lowe and Anderson*, 2002; *Uenzelmann-Neben et al.*, 2007]. Mega-scale glacial lineations in this trough indicate that it was occupied by paleo-ice streams. The shallower outer

shelf areas (~500 m) show widespread iceberg furrows on the seafloor, and broad shelf break depressions that may be related to inner shelf troughs [*Lowe and Anderson*, 2002; *Evans et al.*, 2006; *Walker et al.*, 2007].

3. Data Compilation

[7] Multibeam swath-mapping on several recent expeditions has significantly improved our knowledge of bathymetric features on and along the Amundsen Sea continental shelf. Here we integrate those data and add other available bathymetric and geophysical measurements to create a new regional map of this sector of the continental margin. Our sources include single-beam and multibeam bathymetry available through the NSF-funded Antarctic Multibeam synthesis database [*Carbotte et al.*, 2007], soundings from earlier cruises in the GEODAS database [*National Geophysical Data Center*, 1996], and measurements from James Clark Ross cruises JR84 and JR141, Polarstern cruises ANT-XI/3, ANT-XII/4, ANT-XVIII/5a, and ANT-XXIII/4, and NB Palmer cruise 07-02 (Table 1 and Figure 2).

[8] Usually the shoreline boundary of bathymetry compilations is simply set to 0 m, whereas bathymetric features in West Antarctica often continue below the ice shelves and ice sheet. To accommodate these sub-ice features we integrated ice sheet basement data from the US Airborne Geophysical Survey of the Amundsen Sea Embayment, Antarctica (AGASEA) and the UK Basal Balance And Synthesis (BBAS) projects [*Holt et al.*, 2006; *Vaughan et al.*, 2006] and less detailed topography from the BEDMAP project [*Lythe et al.*, 2000] for areas west and north of the AGASEA/BBAS data sets. Our compilation extends from ~100°W to 135°W and 68°S to 76°S, reaching from the Abbot, Cosgrove and Pine Island ice fronts in the eastern Amundsen Sea to the western end of the Getz Ice Shelf, and covering the entire continental slope and most of the continental rise.

[9] Data processing and integration followed the scheme in Figure 3. All single-beam soundings were converted into a common format and then imported into ArcGIS software (ESRI). Most of the swath-bathymetry data sets were initially ping edited and processed aboard ship. We reduced the swath-bathymetry data to manageable size by creating grids of 200–250 m resolution using MB-system [*Caress and Chayes*, 1996] or Fledermaus IVS [*Mayer et al.*, 2000], depending on the original format, and imported those grids into ArcGIS, reconverting raster to point data. These point data were the basis for generating new grids. Positional accuracy of the data sets varies, but most data used for this compilation (1988 and younger) were obtained with GPS systems that reached an accuracy of <100 m. Navigation data from earlier cruises, which represent a small fraction of the whole compilation and were used to fill gaps in sparsely covered parts of the continental rise, were collected using the older US Navy TRANSIT satellite navigation system, accurate to ~2 km or better, or celestial navigation. To accommodate positional inaccuracies and the varying density of available data we chose a 2 km grid resolution. After testing several interpolation schemes we settled on a "natural neighbor" algorithm [*Sibson*, 1981] as implemented by ArcGIS for grid formation. This algorithm exactly recovers reference points and can handle highly irregular data distributions [*Sambridge et al.*, 1995], suitable for the present Amundsen Sea where areas covered by high-density swath-bathymetry data are typically separated by large gaps (Figure 2). As data quality varies between individual surveys, several iterations were required to identify and remove disparate measurements. This included single or small groups of measurements that created obvious artifacts in the grid including local, unrealistically deep holes and edge effects resulting from less reliable outer beams of multibeam swaths.

4. New Amundsen Sea Bathymetric Map

[10] The resulting compilation outlines for the first time the full extent and shape of the Amundsen Sea continental shelf, defining its shelf break along most of its length (Figure 4). Seaward of the coastline, the continental shelf narrows westward from >400 km north of Pine Island Bay to 100–200 km west of Siple Island. The outstanding features on the continental shelf are its deep and rugged inner shelf troughs that typically merge and shoal seaward of the ice shelf fronts. Individual troughs often merge into single features by mid-shelf, with the eastern shelf dominated by two trough systems. The one in Pine Island Bay combines troughs that originate from the Pine Island, Thwaites, and Smith Glaciers. A second system includes troughs from the Dotson and eastern Getz ice shelves. Maximum depths in both systems exceed 1600 m, but are not always near the present-day ice fronts. These dendritic trough sys-

Table 1. Survey ID, Data Type, Navigation Equipment, Date, and Sources Used for Compilation, With Selected References Describing or Utilizing These Data

Survey ID	Data Type	Navigation	Year	Source	Reference
ELT11	single-beam PDR 12 kHz	sextant	1964	GEODAS[a]	
ELT17	single-beam PDR 12 kHz	sextant	1965	GEODAS[a]	
ELT33	single-beam PDR 12 kHz	TRANSIT/sextant	1968	GEODAS[a]	
DSDP35GC	single-beam 12 kHz/GIFFT	TRANSIT	1974	GEODAS[a]	*Tucholke and Houtz* [1976]
THB80	single-beam unknown	unknown	1981	GEODAS[a]	*Yamaguchi et al.* [1988]
DF85	single-beam SeaBeam 12 kHz	TRANSIT	1985	GEODAS[a]	*Kellogg and Kellogg* [1987]
PD190L02	single-beam EDO depth tracker	GPS	1990	GEODAS[a]	
NBP92-08	single-beam Simrad:EK500	GPS	1992	GEODAS[a]	
PS92	single-beam	GPS	1992	GEODAS[a]	*SPRITE Group* [1992]
RITS94B	multibeam SeaBeam	GPS	1993	NGDC[b]	
NBP94-02	single-beam Simrad:EK500	GPS	1994	GEODAS[a]	*Jacobs et al.* [1996]
ANT-XI/3	multibeam Hydrosweep DS-1	GPS	1994	AWI[c]	*Nitsche et al.* [2000]
ANT-XII/4	multibeam Hydrosweep DS-1	GPS	1995	AWI[c]	*Nitsche et al.* [2000]
NBP96-02	multibeam SeaBeam:2112	GPS	1996	AMBS[d]	
NBP99-02	multibeam SeaBeam:2112	GPS	1999	AMBS[d]	*Lowe and Anderson* [2002]
NBP99-09	multibeam SeaBeam:2112	GPS	1999	AMBS[d]	
NBP00-01	multibeam SeaBeam:2112	GPS	2000	AMBS[d]	
BEDMAP	various	various/GPS	2000	BEDMAP	*Lythe et al.* [2000]
ANT-XVIII/5a	multibeam Hydrosweep DS-2	GPS	2001	AWI[c]	*Scheuer et al.* [2006]
JR84	multibeam Simrad EM120	GPS	2003	SPRI[e]	*Dowdeswell et al.* [2006a]; *Evans et al.* [2006]
ANT-XXIII/4	multibeam Hydrosweep DS-2	GPS	2006	AWI[c]	*Larter et al.* [2007]; *Gohl et al.* [2007]; *Uenzelmann-Neben et al.* [2007]
JR141	multibeam Simrad EM120	GPS	2006	BAS[f]	*Larter et al.* [2007]
AGASEA/BBAS	radar	GPS	2006	AGASEA/BBAS	*Vaughan et al.* [2006]; *Holt et al.* [2006]
NBP07-02	multibeam Simrad EM120	GPS	2007	AMBS[d]	

[a] GEODAS Web site: http://www.ngdc.noaa.gov/mgg/geodas/geodas.html.
[b] National Geophysical Data Center http://www.ngdc.noaa.gov/.
[c] Alfred Wegener Institute for Polar and Marine Research.
[d] Antarctic Multibeam Bathymetry and Geophysical Data Synthesis Web site: http://www.marine-geo.org/antarctic/.
[e] Scott Polar Research Institute.
[f] British Antarctic Survey.

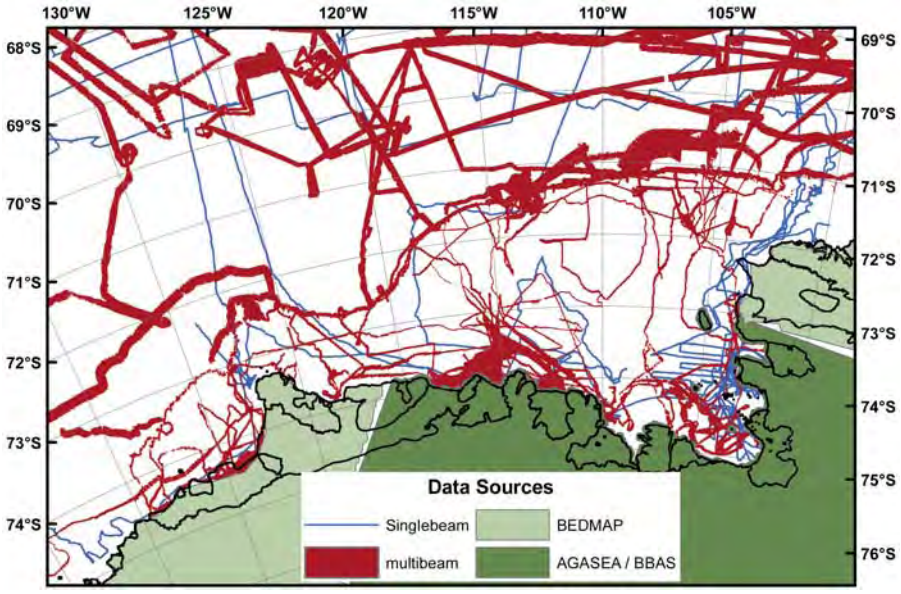

Figure 2. Distribution of the various data sources that form the basis for the new bathymetric grid. Red areas show the coverage of the multibeam bathymetry data, blue lines represent tracks of individual soundings, and green areas represent additional data sets that we used for areas covered by continental ice. Table 1 provides details.

tems are separated by a bank extending northward from the Bear Peninsula, with water depths of ~250–400 m, where deep-draft icebergs go aground. Recently collected swath bathymetry data that have been included in the new bathymetric compilation show that geomorphic features interpreted as subglacial meltwater features [*Lowe and Anderson*, 2003] are widespread throughout the inner shelf troughs.

[11] Several smaller troughs and trough systems are found near Cosgrove Ice Shelf, and off Carney Island and the central and western Getz Ice Shelf fronts. These inner shelf troughs commonly display rugged relief, to >200 m in Pine Island Bay, and a host of smaller features including striations, grooves, drumlins, and mega-scale lineations indicative of glacial erosion [*Wellner et al.*, 2001; *Lowe and Anderson*, 2002]. Similar troughs also appear along other parts of the Antarctic continental margin [*Pudsey et al.*, 1994; *Canals et al.*, 2000, 2002; *O Cofaigh et al.*, 2002, 2005] and previously glaciated margins in the northern hemisphere [e.g., *Stokes and Clark*, 2001; *Ottesen et al.*, 2005; *Dowdeswell et al.*, 2006b; *Shaw et al.*, 2006].

[12] Depths along the continental shelf break average ~500 m, but vary from ~400 to >600 m (auxiliary material[1] Figure S2). An outer shelf depression near 114°W has been charted in some detail [*Dowdeswell et al.*, 2006a; *Walker et al.*, 2007], but persistent sea ice has limited mapping of other shelf break depressions NW of Thurston and Siple Islands. Connections between these depressions and inner-shelf troughs remain to be confirmed by more detailed mapping of mid-shelf areas usually covered by perennial ice. West of Siple Island a trough near ~128°W can more clearly be followed from the ice edge to the shelf break.

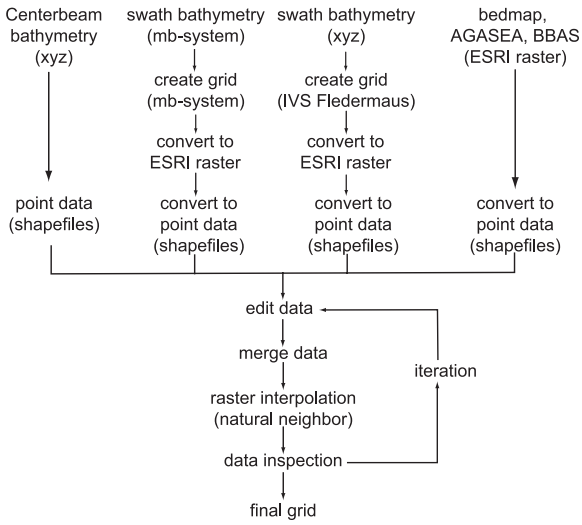

Figure 3. Processing scheme used to integrate the different data sets and create the final grid.

[1]Auxiliary materials are available in the HTML. doi:10.1029/2007GC001694.

Geochemistry Geophysics Geosystems G3 NITSCHE ET AL.: AMUNDSEN SEA CONTINENTAL SHELF 10.1029/2007GC001694

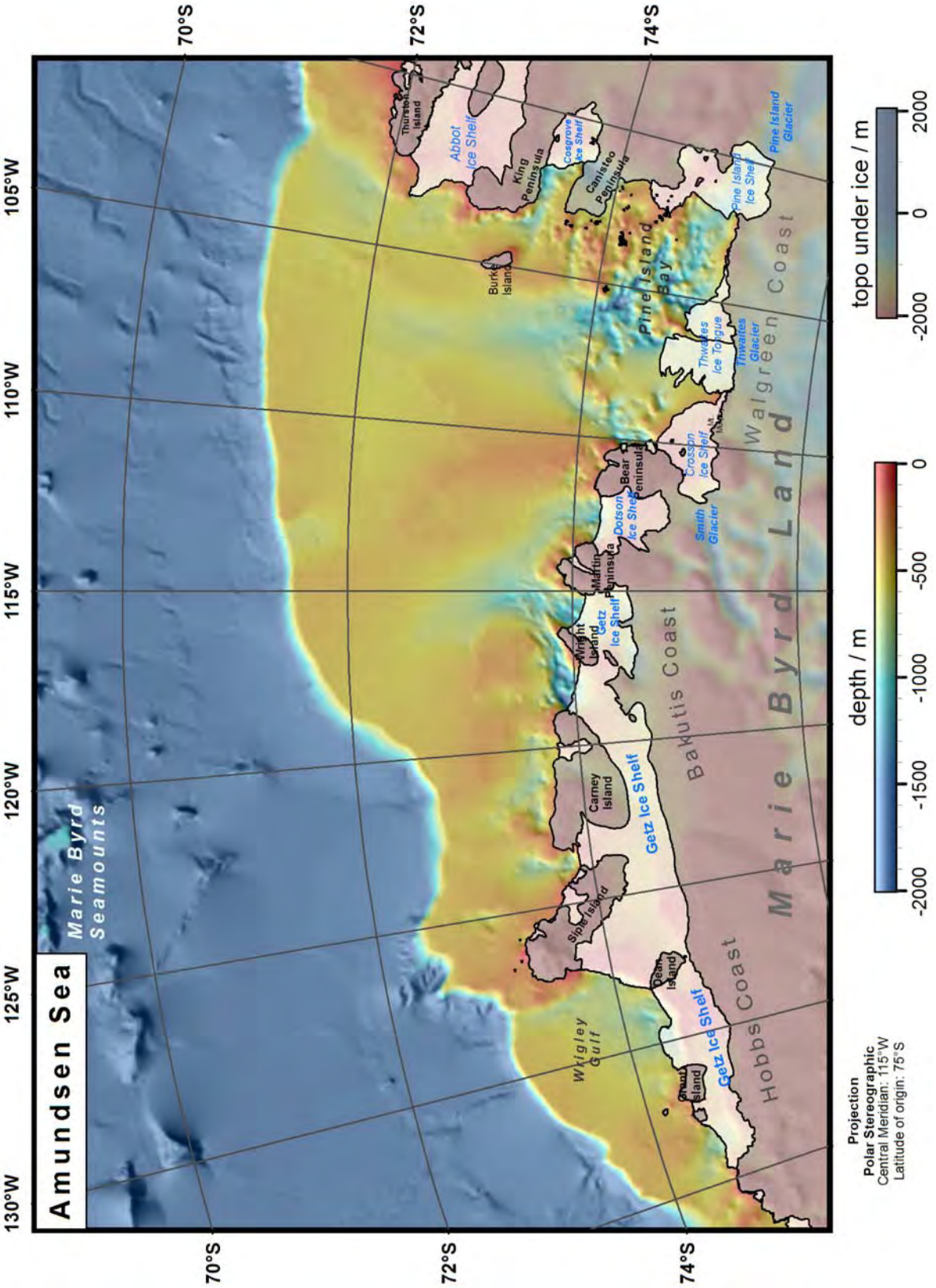

Figure 4. Bathymetry of the Amundsen Sea based on data available through March 2007 (Table 1). Grid control is based on the ship tracks shown in Figure 2. The coastline, ice shelves, and grounding lines are based on the Antarctic Digital Database 4.1 but have been modified to fit more accurate MODIS satellite image [see also *Swithinbank et al.*, 2003, 2004]. The sub-ice topography is based on AGASEA/BBAS and BEDMAP data sets.

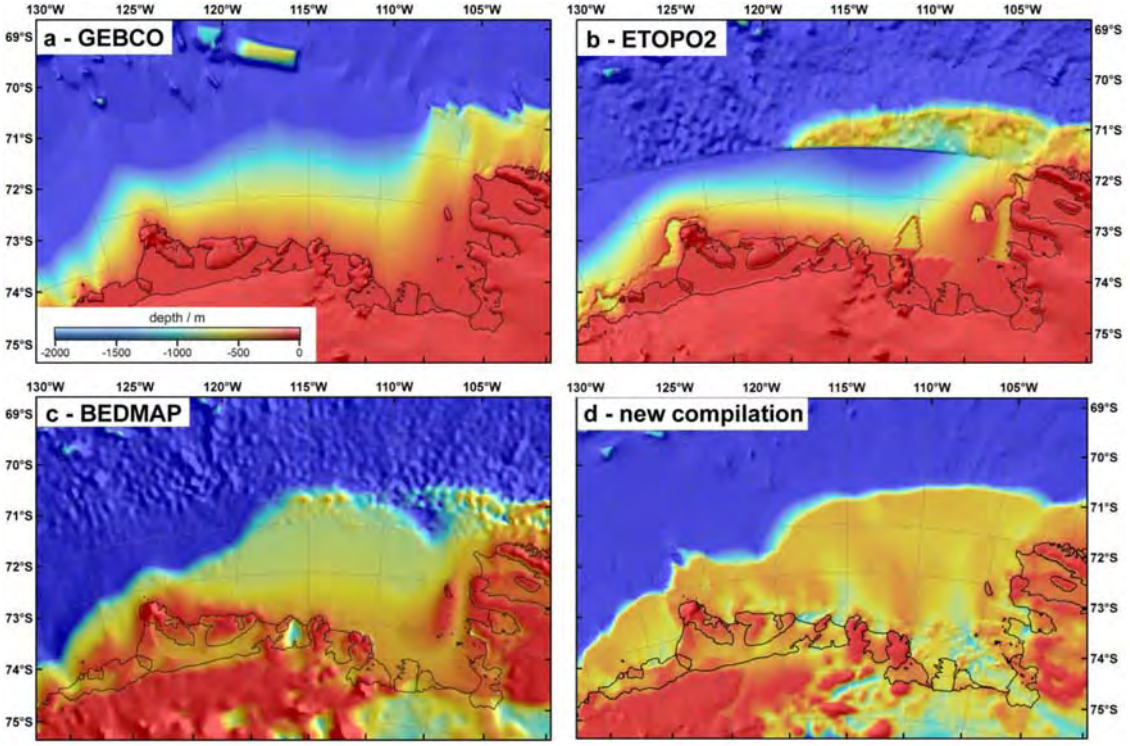

Figure 5. Other representations of Amundsen Sea bathymetry: (a) GEBCO [*Mammerix and Cande*, 1982], (b) ETOPO-2 [*Smith and Sandwell*, 1994, 1997], and (c) BEDMAP [*Lythe et al.*, 2000], compared to (d) the new bathymetry grid. The largest differences appear in the outline of the shelf break and in the trough and ridge structures.

[13] The general morphology of the continental slope and rise is comparable to other parts of the Antarctic continental margins. The slope ranges from 2°–5° with parts of the upper slope being dissected by gullies that in some areas converge downslope and feed into large channels that cross the continental rise [*Dowdeswell et al.*, 2006a; *Lowe and Anderson*, 2002]. More detailed multibeam coverage of both the slope and shelf is needed to definitively relate gullies, depressions, lineations, troughs and paleo-ice streams. In addition to sedimentary features previously reported on the continental slope [*Dowdeswell et al.*, 2006a] a series of mounds radiate away from the slope between 105°W and 110°W. These mounds connect to known features on the lower continental rise [*Yamaguchi et al.*, 1988; *Nitsche et al.*, 2000; *Scheuer et al.*, 2006]. North of Siple Island (125°W–127°W) the slope is interrupted by a large SE-NW oriented ridge at depths of 1–3 km, incised by steep canyons. Its shape and water depth preclude glacial links, but its proximity to the Mt. Siple volcano and Marie Byrd Seamounts suggests a tectonic origin.

[14] Earlier depictions of the Amundsen Sea region (BEDMAP/ETOPO/GEBCO in Figure 5) predated the marine multibeam data utilized here, and so are deficient in several important respects. However, control for the current bathymetry is still uneven, with many large gaps between ship tracks (Figure 2), some resulting from the typical distribution of perennial sea ice. The depth accuracy varies accordingly, being highest in areas with modern multibeam cover, but containing significant uncertainties in the large interpolated areas. Seams between detailed multibeam bathymetry and interpolated areas can cause artifacts such as sudden changes in seafloor roughness and the outward bulge of the lower continental slope between 121°W and 125°W. The seafloor bathymetry is still unknown beneath the ice shelves, although recent airborne radar missions suggest the continuation of some troughs below the Smith, Thwaites and Pine Island Glaciers [*Holt et al.*, 2006; *Vaughan et al.*, 2006].

5. Implications

[15] Concerns about ice sheet mass balance and sea level change have recently focused on the Amundsen Sea because high basal melt rates of its small ice shelves are positively correlated with acceler-

ating ice streams and apparent draw-down of the adjacent ice sheet [*Shepherd and Wingham*, 2007]. The shelf bathymetry is thought to play a substantial role in this process, both as a gateway facilitating CDW intrusions near the shelf break and a link to deep ice shelf grounding lines. There are indications from observations and models that warm deep water may preferentially move onto continental shelves via shelf break curvatures and depressions [*Dinniman et al.*, 2003; *Walker et al.*, 2007]. However, CDW rises well above the Amundsen shelf break across a wide area [*Jacobs et al.*, 2002], and as yet little is known about the temporal variability of its penetration onto the shelf. Once in the troughs, the saltiest and therefore densest deep water sinks and flows into the ice shelf cavities, its melting potential enhanced by the seawater freezing point depression with increasing pressure [*Jacobs et al.*, 1996].

[16] One consequence of recent work in the Amundsen Sea is that models of ice sheet behavior must now be updated to include the effects of an evolving ocean and its ice shelves. Similarly, models of the ocean circulation must properly account for this remarkable continental shelf, its fringing ice shelves and persistent sea ice cover. Quite different results may be obtained from models based on the bathymetry reported here, compared to that shown on prior maps (Figure 5). The new bathymetry could impact estimates of ice shelf melting, WAIS mass balance, and ocean freshening. The locations and depths of the trough systems are also important for reconstructions of paleo-ice flow and deglaciation. This compilation of Amundsen Sea bathymetry represents a major improvement over previously available regional data sets, which involved far more interpolation between sparser, less accurate observations. A larger-scale version of the map is available in the auxiliary material (Figure S1), and the grid may be obtained from http://www.marine-geo.org/link/entry.php?id=Amundsen_Sea_Nitsche.

Acknowledgments

[17] We thank the personnel aboard the several ships, especially the *NB Palmer*, R/V *Polarstern*, and RRS *James Clark Ross*, who have been responsible for obtaining bathymetric data in the Amundsen Sea, often under difficult conditions. Multibeam data on cruises ANT-XXIII/4 and JR141 were collected and processed by S. Gauger and T. Deen, respectively. T. Kellogg digitized bathymetry from DF85, J. Dowdeswell made data available from JR84, H.-W. Schenke provided access to *Polarstern* data, and J. Anderson, S. Cande, and others contributed observations through the Antarctic Multibeam Bathymetry Synthesis database. S. Carbotte, S. O'Hara, and the database team at Lamont provided key assistance. The manuscript benefited from the comments by two anonymous reviewers. This work was supported in part by U.S. National Science Foundation through a supplement to U.S. National Science Foundation ANT 04-40655 and by ANT 02-33303 and ANT 04-40775. It also forms part of the BAS Glacial Retreat in Antarctica and Deglaciation of the Earth System (GRADES) Program as well as the MARCOPOLI Work Packages MAR2 and POL6 of AWI. This is Lamont contribution 7068.

References

Canals, M., R. Urgeles, and A. M. Calafat (2000), Deep seafloor evidence of past ice streams off the Antarctic Peninsula, *Geology*, *28*, 31–34.

Canals, M., J. L. Casamor, R. Urgeles, A. M. Calafat, E. W. Domack, J. Baraza, M. Farran, and M. De Batist (2002), Seafloor evidence of a subglacial sedimentary system off the northern Antarctic Peninsula, *Geology*, *30*, 603–606.

Carbotte, S. M., W. B. F. Ryan, S. O'Hara, R. Arko, A. Goodwillie, A. Melkonian, R. A. Weissel, and V. L. Ferrini (2007), Antarctic multibeam bathymetry and geophysical data synthesis: An on-line digital data resource for marine geoscience research in the Southern Ocean, in *Antarctica: A Keystone in a Changing World—Proceedings for the Tenth International Symposium on Antarctic Earth Sciences*, edited by A. K. Cooper, C. R. Raymond, and the ISAES Editorial Team, *U.S. Geol. Surv. Open File Rep.*, *2007-1047*, *Short Res. Pap. 002*, doi:10.3133/of2007-1047.srp002, 4 pp.

Caress, D. W., D. N. Chayes (1996), Improved processing of Hydrosweep DS multibeam data on the R/V Maurice Ewing, *Mar. Geophys. Res.*, *18*(6), 631–650.

Davis, C. H., Y. Li, J. R. McConnell, M. M. Frey, and E. Hanna (2005), Snowfall-driven growth in East Antarctic ice sheet mitigates recent sea-level rise, *Science*, *308*, 1898–1901.

Dinniman, M. S., J. M. Klinck, and W. O. Smith (2003), Cross-shelf exchange in a model of the Ross Sea circulation and biogeochemistry, *Deep Sea Res., Part II*, *50*, 3103–3120.

Dowdeswell, J. A., J. Evans, C. Ó Cofaigh, and J. B. Anderson (2006a), Morphology and sedimentary processes on the continental slope off Pine Island Bay, Amundsen Sea, West Antarctica, *Geol. Soc. Am. Bull.*, *118*, 606–619.

Dowdeswell, J. A., D. Ottesen, and L. Rise (2006b), Flow switching and large-scale deposition by ice streams draining former ice sheets, *Geology*, *34*, 313–316.

Drewry, D. J., S. R. Jordan, and E. Jankowski (1982), Measured properties of the Antarctic ice sheet: Surface configuration, ice thickness, volume and bedrock characteristics, *Ann. Glaciol.*, *3*, 83–91.

Eagles, G., K. Gohl, and R. D. Larter (2004), High-resolution animated tectonic reconstruction of the South Pacific and West Antarctic Margin, *Geochem. Geophys. Geosyst.*, *5*, Q07002, doi:10.1029/2003GC000657.

Evans, J., J. A. Dowdeswell, C. O'Cofaigh, T. J. Benham, and J. B. Anderson (2006), Extent and dynamics of the West Antarctic Ice Sheet on the outer continental shelf of Pine Island Bay during the last glaciation, *Mar. Geol.*, *230*, 53–72.

Gohl, K., et al. (2007) Geophysical survey reveals tectonic structures in the Amundsen Sea embayment, West Antarctica, in *Antarctica: A Keystone in a Changing World—Proceedings for the Tenth International Symposium on Antarctic Earth Sciences*, edited by A. K. Cooper, C. R. Raymond, and the

ISAES Editorial Team, *U.S. Geol. Surv. Open File Rep.*, *2007-1047*, *Short Res. Pap. 047*, doi:10.3133/of2007-1047.srp047, 4 pp.

Hellmer, H. H., S. S. Jacobs, and A. Jenkins (1998), Oceanic erosion of a floating Antarctic glacier in the Amundsen Sea, *Antarct. Res. Ser.*, *75*, 83–99.

Holt, J. W., D. D. Blankenship, D. L. Morse, D. A. Young, M. E. Peters, S. D. Kempf, T. G. Richter, D. G. Vaughan, and H. F. J. Corr (2006), New boundary conditions for the West Antarctic Ice Sheet: Subglacial topography of the Thwaites and Smith glacier catchments, *Geophys. Res. Lett.*, *33*, L09502, doi:10.1029/2005GL025561.

Hughes, T. (1973), Is West Antarctic Ice-Sheet disintegrating?, *J. Geophys. Res.*, *78*, 7884–7910.

Jacobs, S. S., H. H. Hellmer, and A. Jenkins (1996), Antarctic ice sheet melting in the southeast Pacific, *Geophys. Res. Lett.*, *23*, 957–960.

Jacobs, S. S., P. A. Mele, G. Krahmann, and W. M. Smethie (2002), Coastal ocean measurements in the Amundsen and Ross Seas, 366 pp., NB Palmer Cruise 00-01, Feb–Mar 2000, *LDEO-2002–2a*, Lamont-Doherty Earth Observ., Palisades, N. Y.

Jenkins, A., D. G. Vaughan, S. S. Jacobs, H. H. Hellmer, and J. R. Keys (1997), Glaciological and oceanographic evidence of high melt rates beneath Pine island glacier, west Antarctica, *J. Glaciol.*, *43*, 114–121.

Kellogg, T. B., and D. E. Kellogg (1987), Recent glacial history and rapid ice stream retreat in the Amundsen Sea, *J. Geophys. Res.*, *92*(B9), 8859–8864.

Larter, R. D., A. P. Cunningham, P. F. Barker, K. Gohl, and F. O. Nitsche (2002), Tectonic evolution of the Pacific margin of Antarctica: 1. Late Cretaceous tectonic reconstructions, *J. Geophys. Res.*, *107*(B12), 2345, doi:10.1029/2000JB000052.

Larter, R. D., et al. (2007), West Antarctic Ice Sheet change since the Last Glacial Period, *Eos Trans. AGU*, *88*, 189–196.

Levitus, S., J. Antonov, and T. Boyer (2005), Warming of the world ocean, 1955–2003, *Geophys. Res. Lett.*, *32*, L02604, doi:10.1029/2004GL021592.

Lowe, A. L., and J. B. Anderson (2002), Reconstruction of the West Antarctic Ice Sheet in Pine Island Bay during the Last Glacial Maximum and its subsequent retreat history, *Quat. Sci. Rev.*, *21*, 1879–1897.

Lowe, A. L., and J. B. Anderson (2003), Evidence for abundant subglacial meltwater beneath the paleo-ice sheet in Pine Island Bay, Antarctica, *J. Glaciol.*, *49*, 125–138.

Lythe, M. B., D. G. Vaughan, and the BEDMAP Consortium (2000), BEDMAP—Bed topography of the Antarctic, 1:10,000,000 scale map, *Br. Antarct. Surv.*, Cambridge, U. K.

Mammerix, J., and S. Cande (1982), *General Bathymetric Charts of the Oceans (GEBCO)*, Can. Hydrogr. Surv., Ottawa, Canada.

Mayer, L. A., M. Paton, L. Gee, J. Gardner, and V. C. Ware (2000), Interactive 3D Visualization: A tool for seafloor navigation, exploration and engineering, paper presented at OCEANS 2000 MTS/IEEE Conference and Exhibition, Inst. of Electr. and Electron. Eng., Providence, 11 –14 Sept.

Mayes, C. L., L. A. Lawver, and D. T. Sandwell (1990), Tectonic history and new isochron chart of the South Pacific, *J. Geophys. Res.*, *95*(B6), 8543–8567.

National Geophysical Data Center (1996), Marine Geophysical trackline data (GEODAS/TRACKDAS), Boulder, Colo.

Nitsche, F. O., K. Gohl, K. Vanneste, and H. Miller (1997), Seismic expression of glacially deposited sequences in the Bellingshausen and Amundsen seas, West Antarctica, in *Geology and Seismic Stratigraphy of the Antarctic Margin*, *Part 2*, *Antarct. Res. Ser.*, vol. 71, edited by P. F. Barker and A. K. Cooper, pp. 95–108, AGU, Washington, D. C.

Nitsche, F. O., A. P. Cunningham, R. D. Larter, and K. Gohl (2000), Geometry and development of glacial continental margin depositional systems in the Bellingshausen Sea, *Mar. Geol.*, *162*, 277–302.

Ó Cofaigh, C., C. J. Pudsey, J. A. Dowdeswell, and P. Morris (2002), Evolution of subglacial bedforms along a paleo-ice stream, Antarctic Peninsula continental shelf, *Geophys. Res. Lett.*, *29*(8), 1199, doi:10.1029/2001GL014488.

Ó Cofaigh, C., R. D. Larter, J. A. Dowdeswell, C.-D. Hillenbrand, C. J. Pudsey, J. Evans, and P. Morris (2005), Flow of the West Antarctic Ice Sheet on the continental margin of the Bellingshausen Sea at the Last Glacial Maximum, *J. Geophys. Res.*, *110*, B11103, doi:10.1029/2005JB003619.

Ottesen, D., L. Rise, J. Knies, L. Olsen, and S. Henriksen (2005), The Vestfjorden-Trænadjupet palaeo-ice stream drainage system, mid-Norwegian continental shelf, *Mar. Geol.*, *218*, 175–189.

Philippon, G., G. Ramstein, S. Charbit, M. Kageyama, C. Ritz, and C. Dumas (2006), Evolution of the Antarctic ice sheet throughout the last deglaciation: A study with a new coupled climate-north and south hemisphere ice sheet model, *Earth Planet. Sci. Lett.*, *248*, 750–758.

Pudsey, C. J., P. F. Barker, and R. D. Larter (1994), Ice sheet retreat from the Antarctic Peninsula shelf, *Cont. Shelf Res.*, *14*, 1647–1675.

Rignot, E., and S. S. Jacobs (2002), Rapid bottom melting widespread near Antarctic Ice Sheet grounding lines, *Science*, *296*, 2020–2023.

Rignot, E., and R. H. Thomas (2002), Mass balance of polar ice sheets, *Science*, *297*, 1502–1506.

Rignot, E. J. (1998), Fast recession of a West Antarctic glacier, *Science*, *281*, 549–551.

Sambridge, M., J. Braun, and H. McQueen (1995), Geophysical parameterization and interpolation of irregular data using natural neighbors, *Geophys. J. Int.*, *122*, 837–857.

Scheuer, C., K. Gohl, and G. Eagles (2006), Gridded isopach maps from the South Pacific and their use in interpreting the sedimentation history of the West Antarctic continental margin, *Geochem. Geophys. Geosyst.*, *7*, Q11015, doi:10.1029/2006GC001315.

Shaw, J., D. J. W. Piper, G. B. J. Fader, E. L. King, B. J. Todd, T. Bell, M. J. Batterson, and D. G. E. Liverman (2006), A conceptual model of the deglaciation of Atlantic Canada, *Quat. Sci. Rev.*, *25*, 2059–2081.

Shepherd, A., and D. Wingham (2007), Recent Sea-Level Contributions of the Antarctic and Greenland Ice Sheets, *Science*, *315*, 1529–1532.

Shepherd, A., D. Wingham, and E. Rignot (2004), Warm ocean is eroding West Antarctic Ice Sheet, *Geophys. Res. Lett.*, *31*, L23402, doi:10.1029/2004GL021106.

Sibson, R. (1981), A brief description of natural neighbor interpolation, in *Interpreting Multivariate Data*, edited by V. Barnett, pp. 21–36, John Wiley, New York.

Smith, W. H. F., and D. T. Sandwell (1994), Bathymetric prediction from dense satellite altimetry and sparse shipboard bathymetry, *J. Geophys. Res.*, *99*(B11), 21,803–21,824.

Smith, W. H. F., and D. T. Sandwell (1997), Global seafloor topography from satellite altimetry and ship depth soundings, *Science*, *277*, 1956–1961.

SPRITE Group (1992), The Southern rim of the Pacific Ocean: Preliminary report of the Amundsen Sea-Bellingshausen Sea cruise of the Polar Sea, *Antarct. J. U.S.*, *27*(1), 11–14.

Stock, J., and P. Molnar (1987), Revised history of early Tertiary plate motion in the south-west Pacific, *Nature*, *325*, 495–499.

Stokes, C. R., and C. D. Clark (2001), Palaeo-ice streams, *Quat. Sci. Rev.*, *20*, 1437–1457.

Swithinbank, C., R. S. Williams Jr., J. G. Ferrigno, K. M. Foley, C. A. Hallam, and C. E. Rosanova (2003), Coastal-change and glaciological map of the Bakutis coast area, Antarctica: 1972–2002, in *Coastal-Change and Glaciological Maps of Antarctica*, 1 sheet, 1:1,000,000, *U.S. Geol. Surv. Geol. Invest. Ser.*, *Map I-2600–F*.

Swithinbank, C., R. S. Williams Jr., J. G. Ferrigno, K. M. Foley, C. E. Rosanova, and L. M. Dallide (2004), Coastal-change and glaciological map of the Eights coast area, Antarctica: 1972–2001, in *Coastal-Change and Glaciological Maps of Antarctica*, 1 sheet, 1:1,000000, *U.S. Geol. Surv. Geol. Invest. Ser.*, *Map I-2600–E*.

Thomas, R., et al. (2004), Accelerated sea-level rise from West Antarctica, *Science*, *306*, 255–258.

Thomson, J. W., and A. P. R. Cooper (1993), The Scar Antarctic Digital Topographic Database—Review, *Antarct. Sci.*, *5*(3), 239–244.

Tucholke, B. E., and R. E. Houtz (1976), Sedimentary framework of the Bellingshausen basin from seismic profiler data, *Initial Rep. Deep Sea Drill. Proj.*, *35*, 197–227.

Uenzelmann-Neben, G., K. Gohl, R. D. Larter, and P. Schlüter (2007), Differences in ice retreat across Pine Island Bay, West Antarctica, since the Last Glacial Maximum: Indications from multichannel seismic reflection data, in *Antarctica: A Keystone in a Changing World—Proceedings for the Tenth International Symposium on Antarctic Earth Sciences*, edited by A. K. Cooper, C. R. Raymond, and the ISAES Editorial Team, *U.S. Geol. Surv. Open File Rep., 2007-1047*, *Short Res. Pap. 084*, doi:10.3133/of2007-1047.srp084, 4 pp.

Vaughan, D. G., H. F. J. Corr, F. Ferraccioli, N. Frearson, A. O'Hare, D. Mach, J. W. Holt, D. D. Blankenship, D. L. Morse, and D. A. Young (2006), New boundary conditions for the West Antarctic ice sheet: Subglacial topography beneath Pine Island Glacier, *Geophys. Res. Lett.*, *33*, L09501, doi:10.1029/2005GL025588.

Walker, D. P., M. A. Brandon, A. Jenkins, J. T. Allen, J. A. Dowdeswell, and J. Evans (2007), Oceanic heat transport onto the Amundsen Sea shelf through a submarine glacial trough, *Geophys. Res. Lett.*, *34*, L02602, doi:10.1029/2006GL028154.

Wellner, J. S., A. L. Lowe, S. S. Shipp, and J. B. Anderson (2001), Distribution of glacial geomorphic features on the Antarctic continental shelf and correlation with substrate: Implications for ice behavior, *J. Glaciol.*, *47*, 397–411.

Wingham, D. J., A. J. Ridout, R. Scharroo, R. J. Arthern, and C. K. Shum (1998), Antarctic elevation change from 1992 to 1996, *Science*, *282*, 456–458.

Yamaguchi, K., Y. Tamura, I. Mizukosho, and T. Tsuru (1988), Preliminary report of geophysical and geological surveys in the Amundsen Sea, West Antarctica, *Proc. NIRP Symp. Antarct. Geosci.*, *2*, 55–67.

Publication 6.4.2:

Weigelt, E., **Gohl, K.**, Uenzelmann-Neben, G., Larter, R.D. (2009). Late Cenozoic ice sheet cyclicity in the western Amundsen Sea Embayment – Evidence from seismic records. *Global and Planetary Change*, v. 69, pp. 162-169, doi:10.1016/j.gloplacha.2009.07.004.

Author contributions: Weigelt wrote most of the paper as part of her postdoc project which was developed and applied for by Gohl and funded by the Deutsche Forschungsgemeinschaft. The data were collected during Polarstern expedition ANT-XXIII/4 (2006) under leadership of Gohl. Gohl, Uenzelmann-Neben and Larter provided ideas for the interpretation and added to the discussion.

Global and Planetary Change 69 (2009) 162–169

Contents lists available at ScienceDirect

Global and Planetary Change

journal homepage: www.elsevier.com/locate/gloplacha

Late Cenozoic ice sheet cyclicity in the western Amundsen Sea Embayment — Evidence from seismic records

Estella Weigelt [a,*], Karsten Gohl [a], Gabriele Uenzelmann-Neben [a], Robert D. Larter [b]

[a] Alfred Wegener Institute for Polar and Marine Research, Postfach 120161, 27515 Bremerhaven, Germany
[b] British Antarctic Survey, High Cross, Madingley Road, Cambridge CB3 OET, UK

ARTICLE INFO

Article history:
Received 19 December 2008
Accepted 23 July 2009
Available online 4 August 2009

Keywords:
West Antarctic Ice Sheet
Amundsen Sea
ice sheet cyclicity
Neogene
seismic reflection

ABSTRACT

Multichannel seismic reflection profiles provide a record of the glacial development in the western Amundsen Sea Embayment during the Neogene. We identified a northwest-dipping reflector series of more than 1 s TWT thickness (>800 m) on the middle continental shelf indicating well-layered sedimentary units. The dipping strata reveal a striking alternation of reflection-poor, almost transparent units and sequences of closely spaced, continuous reflectors. We suggest that the distinct changes in reflection character represent episodes of ice sheet advance and retreat forced by climate changes. Boundaries between acoustic units are sharp, but without chronological data we cannot constrain the rapidity of glacial advances and retreats. Due to the similarity between the seismic stratigraphy and the lithology in bore-hole records from the Amundsen Sea and Ross Sea, we infer that dipping strata have accumulated since an intensification of glaciation in the Miocene. On the inner and middle shelf we can identify at least four episodes of ice sheet expansion. We conclude that the West Antarctic Ice Sheet has responded sensitively to climate variations since the Miocene.

1. Introduction

There have been dramatic changes in West Antarctic Ice Sheet (WAIS) volume within short time periods since the Last Glacial Maximum (LGM). Over recent decades, the two largest ice-streams that drain into Pine Island Bay, Pine Island Glacier and Thwaites Glacier (Fig. 1), have shown rapid flow acceleration, thinning and grounding line retreat (e.g., Vaughan et al., 2001; Rignot and Jacobs, 2002; Rignot, 2008). It has been suggested that this area may be the most likely site for the initiation of a collapse of the two million km^2 WAIS which would result in a global sea-level rise of 3.3 to 6 m (Hughes, 1981; Oppenheimer, 1998; Mitrovica et al., 2009; Bamber et al., 2009). In order to predict the further development of the WAIS and its impact on sea level rise it is important to put the recent changes into context with the dynamics and development of the ice sheet in the geological past.

Reconstructions of the glacial history on the shelf of the Amundsen Sea have concentrated on the late Quaternary (e.g. Lowe and Anderson, 2002; Evans et al., 2006; Uenzelmann-Neben et al., 2007; Smith et al., 2009; Larter et al., 2009). Studies on older ice sheet dynamics in the region are restricted to the continental slope and deep sea (e.g., Nitsche et al., 1997, 2000; Scheuer et al., 2006).

In this study we present the first multichannel seismic reflection data from the western Amundsen Sea Embayment (Fig. 1) to improve understanding of older glacial development and processes on the inner and middle shelf. A record of repeated expansion of the WAIS onto the continental shelf is preserved in the local sedimentary composition and depositional style. These, in turn, are manifested in the reflection characteristics and reflector configuration on seismic reflection profiles. In this paper, we present an interpretation of seismic data in order to reconstruct climate-related late Cenozoic ice sheet variations on the shelf in the western Amundsen Sea Embayment.

2. Regional setting

The Amundsen Sea is located along the southern Pacific margin of West Antactica (Fig. 1). In common with other shelf areas of Antarctica the shelf of the Amundsen Sea Embayment deepens inshore, mainly due to cumulative glacial erosion, and also to lithospheric flexure caused by the load of the modern WAIS (e.g. ten Brink et al., 1995; Anderson, 1999). Pronounced glacial troughs incise the inner continental shelf down to 1000–1600 m water depths in their deepest parts (Nitsche et al., 2007; Larter et al., 2009). These troughs converge towards the middle shelf and extend across the outer shelf, which has a mean water depth of 500–600 m, with greatly reduced relief (Lowe and Anderson, 2002; Nitsche et al., 2007). At the present day the main ice streams flowing from the WAIS into Pine Island Bay are the Pine Island and Thwaites Glacier systems (e.g. Ferrigno et al., 1993; Vaughan et al., 2001). During glacial periods these ice streams and others carried glacial sediments onto the shelf in the Amundsen Sea Embayment, and gravity-flow processes carried sediment further down the continental slope into the deep sea.

* Corresponding author. Tel.: +49 471 48311885; fax: +49 471 48313560.
E-mail address: estella.weigelt@awi.de (E. Weigelt).

0921-8181/$ – see front matter © 2009 Elsevier B.V. All rights reserved.
doi:10.1016/j.gloplacha.2009.07.004

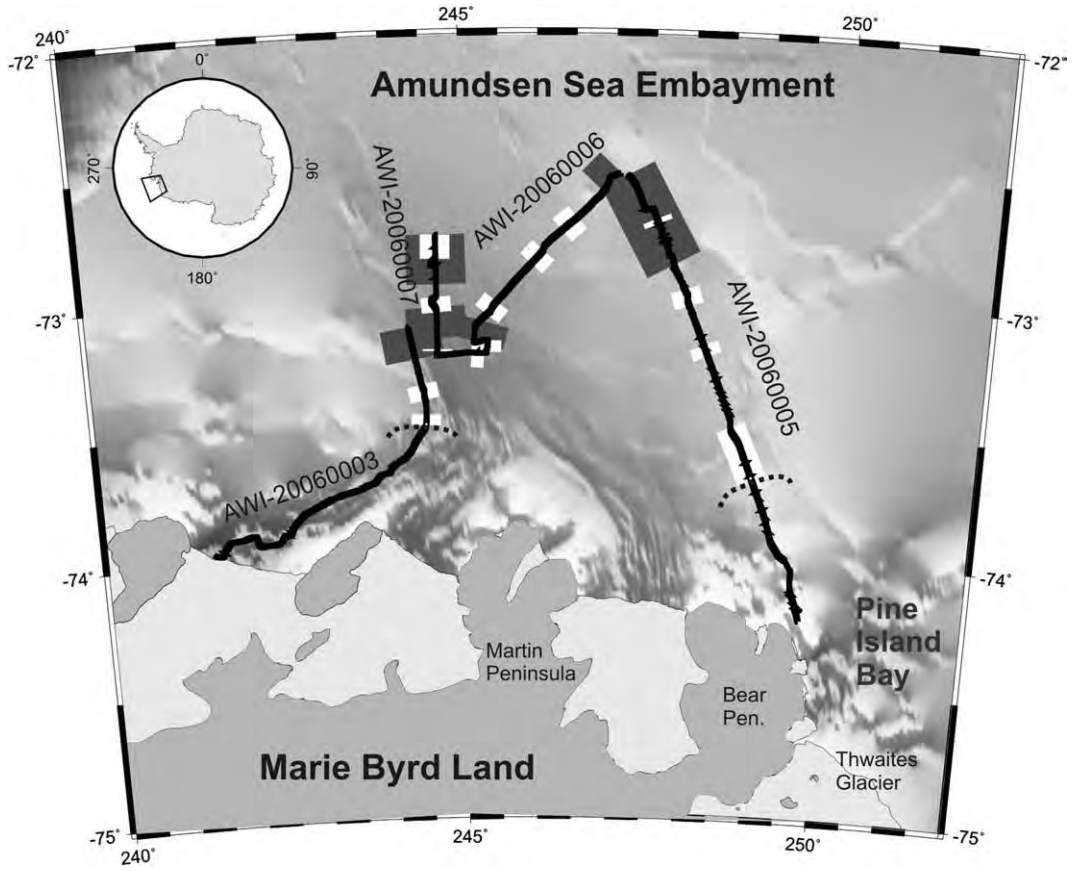

Fig. 1. Bathymetric map of the western Amundsen Sea Embayment (Nitsche et al., 2007) with the locations of the seismic reflection lines AWI-20060003 to AWI-20060007 (black lines). Dashed black lines mark the change of chaotic seismic facies to seaward dipping strata. White boxes show the locations where reflection poor sequences outcrop at the surface or toplap against grounding zone wedges. The dark grey boxes mark the location of grounding zone wedges.

The timing of the onset of glaciation in the Amundsen Sea Embayment is poorly constrained, but seismic profiles and drilling data along the Antarctic Peninsula reveal an extensive prograding and aggrading of the continental shelf during the late Cenozoic, which is associated with glacial processes (Cooper et al., 2008). Larter (2008) summarized that a regular supply of both glacially derived terrigenous sediments and interglacial biogenic sediments has reached the continental rise of the Antarctic Peninsula since at least the Middle Miocene. For late Quaternary times the development of an extended ice sheet in the Amundsen Sea Embayment is better constrained. Evans et al. (2006) proposed that the WAIS reached the shelf edge and was drained by at least one palaeo-ice stream during the LGM. Afterwards, the ice sheet retreated in phases, with the most rapid recession occurring between 16 and 12 kyr to near its present limits (Lowe and Anderson, 2002).

3. Material and methods

Multichannel seismic data were acquired from the western Amundsen Sea Embayment during RV *Polarstern* cruise ANT-XXIII/4 as part of a collaboration between the Alfred Wegener Institute for Polar and Marine Research (AWI) and the British Antarctic Survey (BAS) (Fig. 1) (Gohl et al., 2007; Larter et al., 2007). Seismic sources consisted of three GI-guns™ with a total generator volume of 2.2 l generating frequencies up to 250 Hz. Seismic reflections can be identified at frequencies up to 100 Hz which implies a vertical resolution in soft sediments of about 8 m. Shots were fired every 12 s corresponding to a distance of 31 m. The data were recorded with a 96-channel streamer (600 m active length) at a sample rate of 1 ms. The seismic data processing comprised sorting (25 m CDP interval), and a detailed velocity analysis (every 50 CDP, ~1.2 km), which enabled a successful suppression of seabed multiples in areas where the sea floor is relatively smooth and underlain by unconsolidated sediments. Noise was successfully suppressed via a Karhunen–Loeve filter (Yilmaz, 2001). Finally, the traces were stacked and migrated with a finite-difference time migration. Together with the seismic lines, sub-bottom profiler data (Parasound parametric system, with 18 kHz primary frequency and secondary frequencies 2.5–5.5 kHz) were recorded, which we incorporated in this study to provide supplementary information about the uppermost sedimentary layers on a scale of metres.

4. Results

More than 620 km of multichannel seismic reflection profiles were recorded in the western Amundsen Sea Embayment. The signal energy was sufficient to image the sedimentary column down to a sub-bottom depth of more than 800 m with a vertical resolution of about 8 m. Seismic units were classified on the base of reflection character, reflection strength and termination structures. Reflector horizon dips and the thicknesses of sedimentary units were calculated according to the velocity model used for the normal move-out correction.

The sea-floor morphology of the observed area is highly variable. Close to the present day coastline the topography is very rough (Larter et al., 2009). Several troughs with relief differences of more than 600 m cut through the shelf, and the water depth reaches almost 1600 m in some areas (Figs. 2 and 3). Here, the seismic lines show an opaque, scattered reflection pattern without any internal reflectors. Strong peg-leg multiples indicate a hard sea-floor. Only some thin

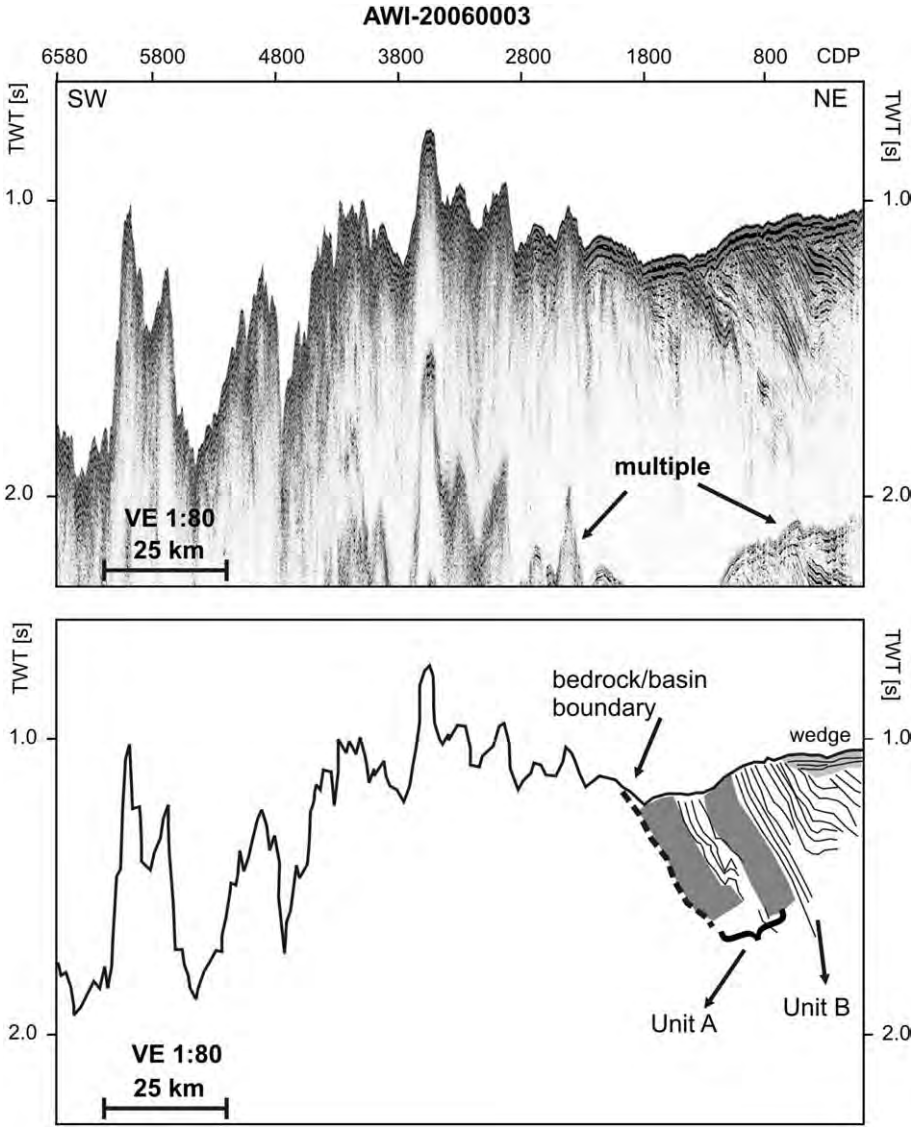

Fig. 2. Seismic line AWI-20060003 and interpretation. Dark grey parts mark reflection-poor units in between the dipping strata. Light grey colored sequences show wedges of agradational reflections which in some locations cover the seawards dipping strata. The dashed line locates the transition from bedrock on the inner shelf to seaward dipping strata on the middle shelf.

sediment pockets (<80 ms TWT (two-way traveltime) corresponding to ~60 m) in steep-sided depression can be identified (e.g. AWI-20060005, CDPs 400–500, Fig. 3).

On the middle shelf and outside the troughs, the topography is generally smooth with a water depth of 500 m on average. Only small surface undulations of few metres amplitude and width characterize the sea floor. Here, reflector series of more than 1 s TWT thickness (>800 m) were recorded indicating sedimentary sequences which cover the northward-dipping surface of acoustic basement (Fig. 3). These strata show a seaward dip with a distinct flattening from the inner to the outer shelf (Fig. 3).The changes of flattening ranges from 1.7° to 0.9° considering an interval velocity of 2300 m/s in average for the sedimentary layers.

The dipping strata show striking changes in reflection pattern. Reflection-poor, almost transparent seismic units alternate with sequences of closely spaced, continuous reflectors (Fig. 4). The P-wave velocities for all dipping strata vary between 2000 and 2500 m/s. The limited offset range of our data means we cannot constrain interval velocities precisely enough to determine whether or not there is a systematic difference between P-wave velocities in the reflection-poor and reflection-rich units.

In the inner shelf region the seawards dipping strata outcrop at the sea floor (Figs. 3, 4b, and 5). On the seismic lines, we identified no reflections between the sea floor and the truncated surface of the dipping strata, which constrains any sedimentary cover layer to be thinner than 8 m. Also, the incorporated sub-bottom profiler (Parasound) data only show one strong sea floor reflection and no coherent sub-bottom reflection signals (Fig. 6). The sea floor is furrowed by incisions of 10–15 m depth and 100–200 m width. As a consequence of numerous out-of-plane reflections due to this small-scale roughness, we could not resolve any further layering in the uppermost part of the seismic sections.

On a relatively shallow part of the middle shelf the dipping strata are covered by a wedge like sequence of horizontal reflections (Fig. 3). This wedge thickens seawards to almost 150 m at the northernmost end of our lines.

Numerous reflection-poor vertical pipes with sharp vertical boundaries were identified (Fig. 5). Those features are on average 500 m wide, and vary in length from a few metres up to 500 m. On our seismic lines we located most of those features in the middle region of shelf. We cannot observe a correlation of their locations with reflection-poor or reflection-rich strata. The pipes have their origin

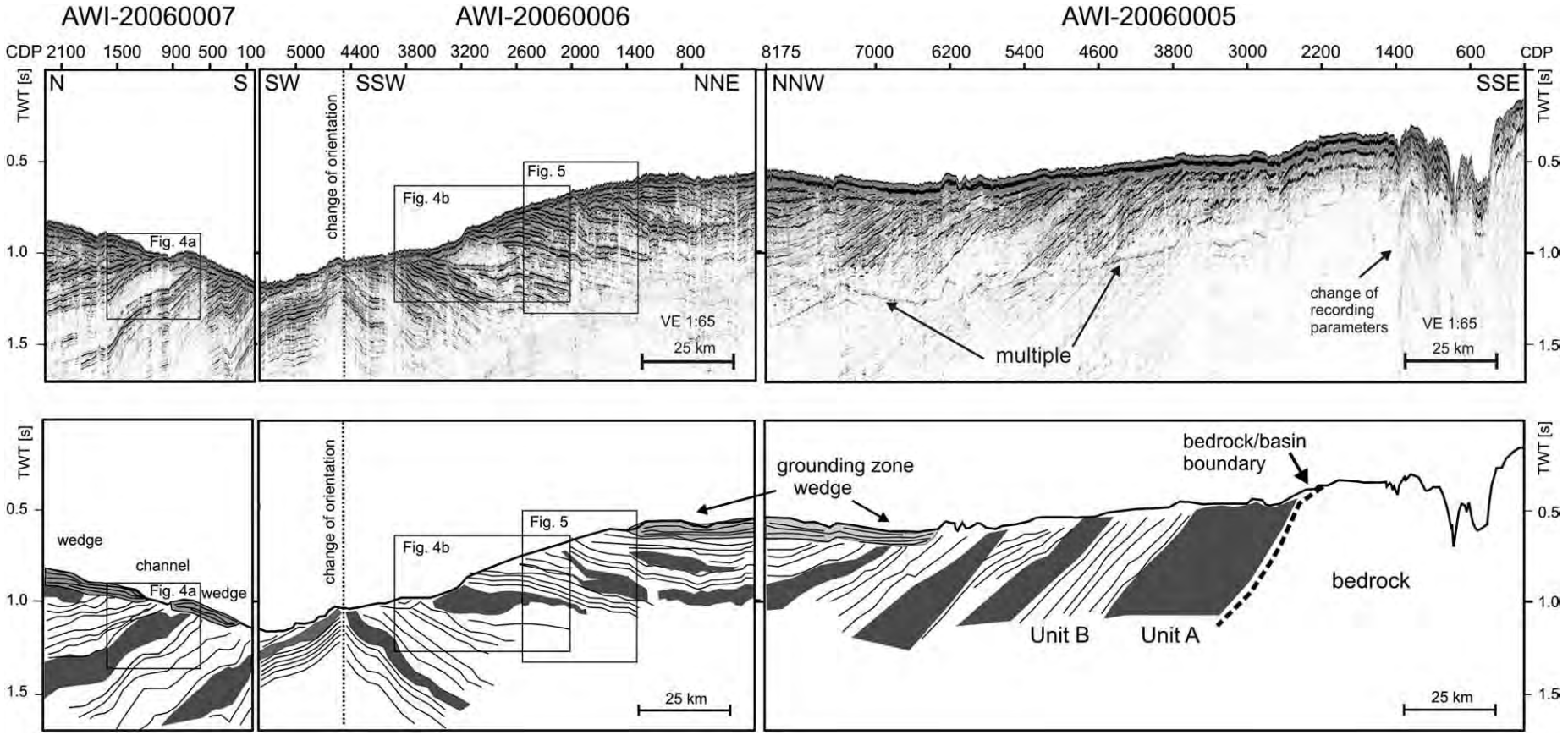

Fig. 3. Compilation and interpretation of seismic lines AWI-20060005, AWI-20060006 and AWI-20060007. Dark grey parts mark reflection- poor units in between the dipping strata. Light grey colored sequences show wedges of agradational reflections which in some locations cover the seawards dipping strata. The dashed line locates the transition from bedrock on the inner shelf to seaward dipping strata on the middle shelf.

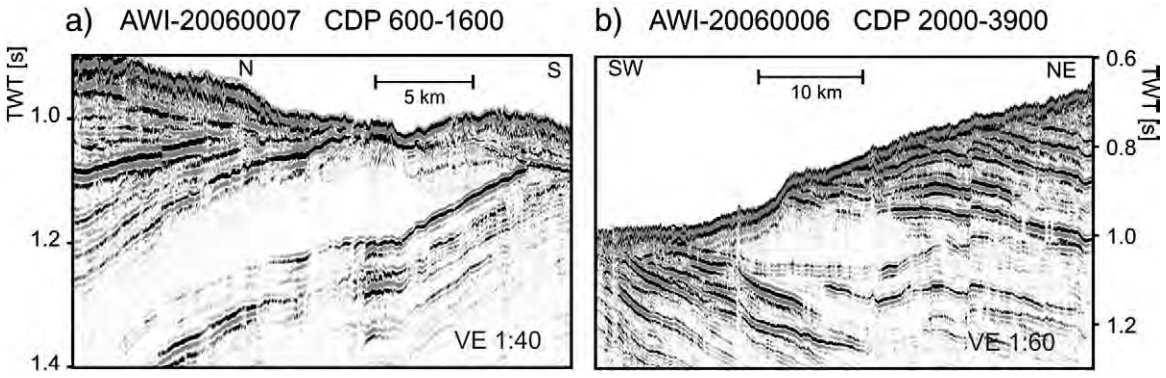

Fig. 4. Two examples of the two main acoustic facies (for location see Fig. 3). Reflection-poor units alternate with sequences of closely spaced, continuous reflectors.

and terminate at a variety of different depths and stratigraphic levels. Often, continuous reflection signals are visible below them. A lot of these vertical structures are covered by overlying reflectors, and the pipes seem not to continue to the seafloor. The Parasound data do not show evidence for leakage of fluids at the sea floor (Fig. 6).

5. Discussion

In this contribution we focus on the seaward-dipping strata displayed in our seismic records on the inner and middle shelf. Similar sequences dipping seaward at a low angle have been recorded

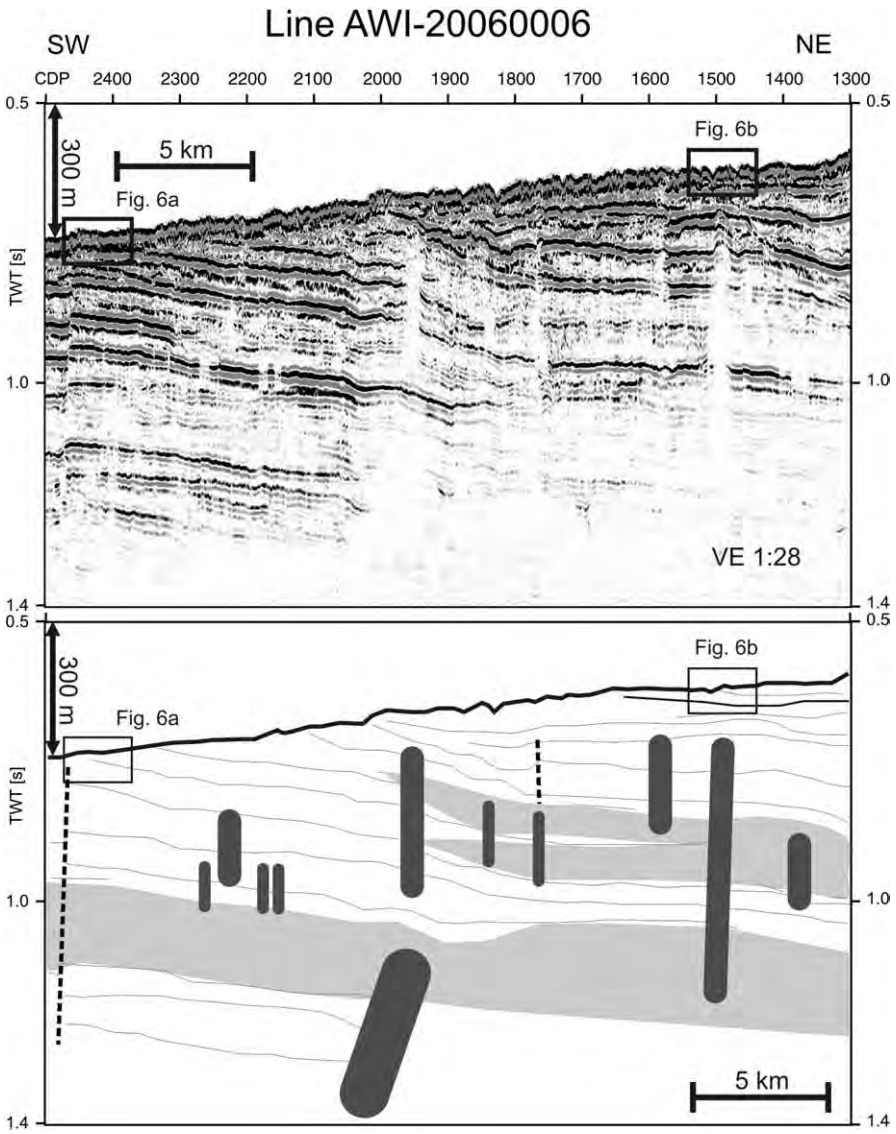

Fig. 5. Part of seismic reflection line AWI-20060006 (for location see Fig. 3). The black boxes mark the location and penetration depth of the two Parasound sections (Fig. 6). Examples for pipes are marked in dark grey, and reflection-poor sequences are displayed in light grey. Dashed black lines show the location of vertical faults.

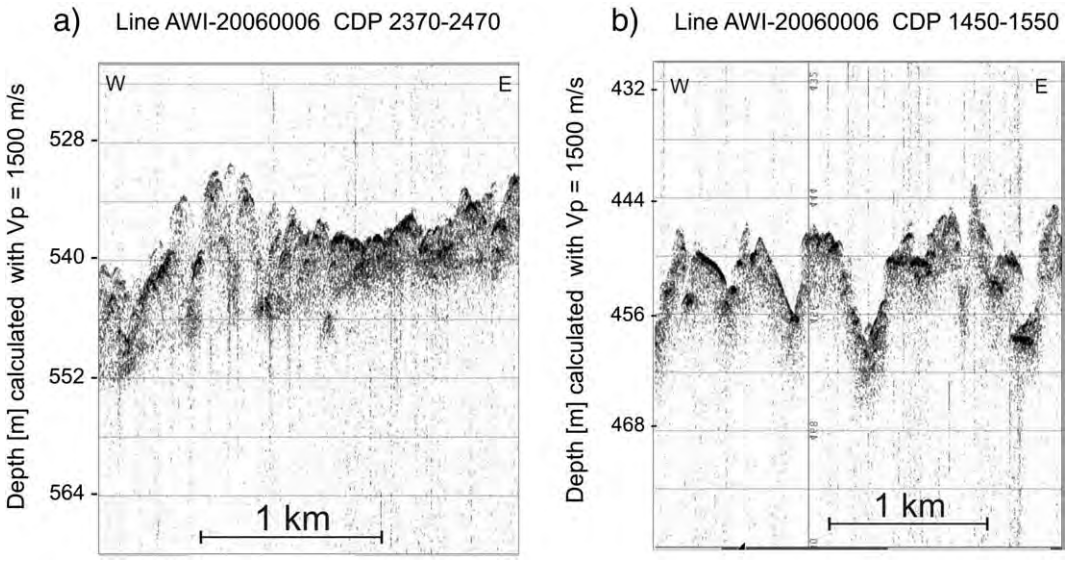

Fig. 6. Examples of Parasound recordings (for location see Fig. 3) The data show just strong surface reflections and no internal reflection signals indicating the presence of hard surface matter.

on many parts of the Antarctic shelf and are believed to result from repeated episodes of glacial erosion on the inner shelf and deposition on the outer shelf (e.g., Larter and Barker, 1989; Cooper et al., 1991; Anderson, 1999).

We identified a prominent alternation of reflection-poor units and sequences of closely spaced, continuous reflectors in the dipping strata (Figs. 2 and 3), which we suggest document strong changes in the depositional environment. Reflection-poor units indicate homogeneous or poorly-stratified deposits and/or a strong scattering of acoustic energy by point sources (large clasts). Glacially-deposited sediments typically include diamictites (tills etc.), which are poorly or non-sorted sediments with a wide range of clast sizes. Studies on other glacially modified continental shelves have shown that the acoustic signature of diamicton lithofacies ranges from chaotic to transparent (Vorren et al., 1989, King et al., 1991). Also, high-resolution acoustic data (less than 0.3 m) on the Antarctic Pensinsula Pacific Margin showed that diamictons drilled at ODP Sites 1100, 1102 and 1103 lack internal stratification (Vanneste and Larter, 1995). Comparison of seismic records from the continental shelf of the Ross Sea with cores from DSDP Sites 270 and 272 indicate that acoustically transparent facies represent subglacial strata which have a diamictite-like grain size distribution (De Santis et al., 1995, De Santis et al., 1997). A cycle of ice sheet advance and retreat across the shelf usually leaves a layer of diamictite covering the sea floor (e.g., Stoker et al., 1997; Sloan and Lawver, 1997). Moving grounded ice additionally reworks the deposits, and may mix underlying sediments or bedrock into tills through local erosion (e.g., Cooper et al., 1997). We thus propose that reflection-poor units indicate an extended and sometimes grounded ice sheet during a cold, polar climate interval.

In contrast, high-amplitude, closely-spaced reflectors result from marked changes of sedimentary physical properties. These are indications for strong variations in the composition and diagenesis of the deposited material and for changes in depositional style. Bartek et al. (1997) recorded similarly layered seismic facies in the Ross Sea and hypothesized that such strata are related to distal glacial-marine deposition. Correlations of DSDP Sites 270–272 with seismic lines imply that regularly stratified acoustic units correspond to sequences of fine grain size distribution, indicating deposition in a more ice-distal environment (De Santis et al., 1995, De Santis et al., 1997). Glacial-marine and/or open water conditions allow a stronger diversification and stratification of deposits, leading to continuous reflections. We suggest that seismic facies showing more continuous internal reflections are of glacial-marine origin, and thus indicate warmer periods. We regard the reflection pattern to be a result of climate conditions, and suggest that the alternation of reflection-poor and reflection-rich strata represents changes in depositional conditions due to ice sheet advances and retreats. Our interpretation is in good agreement with the 'glacial sequence stratigraphic model' developed by Powell and Cooper (2002). Their model depicts that glacial advances develop morainal banks consisting of unstratified gravel, sand, diamict and till, leading to chaotic or transparent seismic reflection pattern. In contrast, during glacial retreats, stratified deposition of mud prevailed, and is expressed in seismic reflection profiles as a succession of continuous reflectors.

We interpret an alternation between cold climate periods with an extended ice-sheet and more temperate periods. Sequence boundaries between reflection-poor and reflection-rich seismic units are quite distinct, but the lack of any chronostratigraphic constraints prevents an estimate of the duration of the cold and warm periods or the transitions between them.

The vertical reflection pipes we observe in our data show sharp vertical boundaries (Fig. 5). We can identify reflection signals below them and, hence, we exclude gas bearing chimneys. They can be interpreted as dewatering structures (e.g. Syvitski, 1997). We take the occurrence of dewatering pipes as further evidence for a glacial origin and overprinting of the reflection-free seismic units.

A major problem is to define the age of the dipping strata and with it the episodes of ice sheet extension because drill sites do not yet exist within the Amundsen Sea Embayment. Therefore, we tried to find constraints to estimate at least a minimum and maximum age for the strata.

The wedge-like succession on the middle shelf provides evidence for the latest grounding line retreat (Figs. 1 and 3). The dipping strata described earlier toplap beneath that wedge, suggesting a period of erosion followed by later aggradation. Lowe and Anderson (2002) described a similar sedimentary wedge in the trough extending north from Pine Island Bay and interpreted it as a grounding zone wedge, a remnant of an ice sheet retreat ~16 kyr ago. Because of the similar structure and close location of the grounding zone wedge described by Lowe and Anderson (2002) and the wedge-like succession we observe, we consider both structures to have the same origin. Therefore, we tentatively suggest that the dipping strata were formed prior to the LGM.

A maximum age is given by the strata which cover the bedrock. As bedrock we define the chaotic seismic facies present on the inner part

of the shelf, and we suggest Unit-A to be the first sequence composed of lithified sediments as indicated by weak internal reflections (Figs. 2 and 3). However, we doubt that this oldest unit consists of glacial deposits. The low reflection strength in Unit-A may be a consequence of a reduction in acoustic impedance contrasts as a result of compaction and cementation. Also, some reflections in Unit-A indicate folding, whereas the reflectors in the younger strata (from Unit-B further seawards) indicate undeformed layering (Figs. 2 and 3). A similar change of deformed to undeformed strata is recorded in the trough that extends north from Pine Island Bay (Lowe and Anderson, 2002), as well as along the Antarctic-Pacific margin (Bart and Anderson, 1995; Larter et al., 1997). Lowe and Anderson (2002) suggest that the whole sequence of seaward dipping strata in the Pine Island Bay region has accumulated since Late Cretaceous/Paleocene times. Because our data show no traces of an ancient shelf break it remains unclear if units A and B might have been deposited as prograding sequences along a palaeo-continental slope or already under subglacially conditions on the shelf. However, regular advances of grounded ice onto the continental shelf around West Antarctica started much later, in Miocene times (summarized by Anderson, 1999; Larter, 2008) with grounded ice first reaching the shelf edge during the Middle or Late Miocene (Larter et al., 1997, Barker, Camerlenghi, Acton et al., 1999). Although these time constraints are weak we suggest that only Unit B, which displays continuous strong reflectors (Figs. 2 and 3), has been deposited since the onset of glacial advances onto the shelf in the western Amundsen Sea Embayment. The high amplitude reflections indicate major changes in depositional environment probably related to changes in ice cover. With these constraints we suggest that beginning with the deposition of Unit B the succession of dipping strata records ice sheet variations between sometime in the Miocene and the LGM. We re-emphasize that this is just an assumption and drilling or coring is needed to gain an age for the formation of those strata.

Additionally, we compared our analysed stratal pattern to that observed in other regions with a better age control given by drilling records. A seismic stratigraphy, tied into ODP Leg 178 sites, indicates a steep increase of sediment deposition on the continental rise along the Bellingshausen and Amundsen Sea margin between 10 and 5 Ma which is interpreted as the beginning of ice sheet advances across the shelf (Scheuer et al., 2006). On seismic profiles across the outer shelf of the southern Amundsen Sea prograding and aggrading sequences were observed and interpreted as the result of several advances of the ice sheet across the shelf (Nitsche et al., 1997, 2000). A sedimentary succession similar to the reflection pattern identified by us is observed in the western Ross Sea. Eleven lithofacies, ranging from ice-proximal diamictites to open-marine diatomites were identified and related to frequent advances and retreats of the ice-shelf since the Middle Miocene in borehole records of the ANDRILL project (Naish et al., 2008; McKay et al., 2008). Although those drilling sites are distant from the Amundsen Sea shelf, on another part of the Antarctic margin, the data provide a clue to the age of dipping strata, and support our interpretation that the alternation in reflection pattern results from ice sheet variations due to alternation between cooler and more temperate climate conditions in West Antarctica.

Restrictions by heavy sea-ice conditions prevented seismic profiling across the outer shelf. We therefore did not record all possible cycles of ice sheet advance and retreat. On seismic line AWI-20060005, which is oriented nearly perpendicular to the coast, we observed at least five changes between layered and chaotic strata, and on section AWI-20060006, running oblique to the coast, about eight changes during the Neogene and Quaternary periods (Fig. 3).

In summary, we have evidence for at least four episodes of ice sheet expansion, but due to our seismic resolution, the fact that our seismic lines only cover the inner and middle shelf, and extensive erosional phases we cannot resolve all periods of ice sheet advance that occurred on the Amundsen Sea shelf since the Miocene. We infer that large ice sheet fluctuations occurred already in Miocene times in the Amundsen Sea, and that the WAIS has responded quite sensitively to climate changes.

6. Conclusion

New high-resolution multichannel seismic reflection data of provide a record of the glacial development and processes on the shelf of the western Amundesen Sea Embayment through late Cenozoic time.

The sea-floor morphology of the observed area is highly variable. Close to the present coast, several hundred meter-deep troughs indicate that palaeo-ice streams in a thick, grounded ice sheet caused massive erosion. On the middle shelf and outside the troughs, the topography is generally smooth and shows only small surface undulations.

The most interesting features on the seismic profiles are observed on the middle part of the shelf. Pronounced seaward-dipping reflector series indicate well layered sedimentary units of more than 1 s TWT thickness (>800 m). The units outcrop at the sea floor, which is evidence for intensive erosion during at least the last glacial cycle. On a relatively shallow part of the middle shelf the strata toplap beneath a grounding zone wedge, which resembles a grounding zone wedge reported by Lowe and Anderson (2002) and is hence considered to be related to a stillstand in grounding line retreat. The strata reveal a striking alternation of reflection-poor, almost transparent, units and sequences of closely spaced, continuous reflectors. We suggest that this alternation represents changes in depositional conditions due to repeated episodes of ice sheet extension that are related to climate variations. Reflection-poor units are regarded as indicating a cold climate period, whereas reflection-rich units developed during warmer times.

We further suggest that strata from Unit B and younger developed since the onset of glacial advances onto the continental shelf around West Antarctica in Miocene times. On the basis of the marked changes in reflection character we suggest a repeated waxing and waning of ice sheets during the Neogene and Quaternary. Beneath the inner and middle shelf we can identify at least four episodes of ice sheet expansion, but most likely more such episodes occurred. We emphasize that the ice sheet in the Amundsen Sea Embayment responded sensitively in its expansion to climate changes throughout the late Cenozoic.

Acknowledgement

We are grateful for the excellent support of Captain Pahl and his crew of RV *Polarstern* during data collection. The Deutsche Forschungsgemeinschaft provided funds for this research under contract number Go724/9. This is a contribution to the AWI programs MARCOPOLI and PACES, and a contribution to the BAS IceSheets programme.

References

Anderson, J.B., 1999. Antarctic marine Geology. Cambridge University Press, Cambridge.
Bamber, J.L., Riva, R.E.M., Vermeersen, B.L.A., LeBrocq, A.M., 2009. Reassessment of the potential sea-level rise from a collapse of the West Antarctic Ice Sheet. Science 324, 901–903. doi: 10.1126/science.1169335.
Barker, P.F., Camerlenghi, A., Acton, G.D., 1999. Proceedings of the Ocean Drilling Program, Initial Reports. [CD-ROM] Available from: Ocean Drilling Program, vol. 178. Texas A&M University, College Station, TX, pp. 77845–79547.
Bart, P.J., Anderson, J.B., 1995. Seismic record of glacial events affecting the Pacific margin of the northwestern Antarctic Peninsula. In: Cooper, A.K., Barker, P.F., Brancolini, G. (Eds.), Geology and Seismic Stratigraphy of the Antarctic Margin. Antarctic Research Series. American Geophysical Union, Washington, DC, pp. 75–95.
Bartek, L.R., Anderson, J., Oneacre, T., 1997. Ice stream troughs and variety of seismic stratigraphic architecture from a high southern latitude section: Ross Sea, Antarctica. In: Davies, T.A., et al. (Ed.), Glaciated continental margins — an atlas of acoustic images. Chapman & Hall, London, pp. 250–254.

Cooper, A.K., Barrett, P.J., Hinz, K., Traube, V., Leitchenkov, G., Stagg, H.M.J., 1991. Cenozoic prograding sequences of the Antarctic continental margin: a record of glacio-eustatic and tectonic events. Marine Geology 102, 175–213.
Cooper, A.K., Carlson, P.R., Reimnitz, E., 1997. Subglacial features. In: Davies, T.A. (Ed.), Glaciated continental margins — an atlas of acoustic images. Chapman & Hall, London, pp. 34–35.
Cooper, A.K., Brancolini, G., Escutia, C., Kristoffersen, Y., Larter, R., Leitchenkov, G., O'Brien, P., Jokat, W., 2008. Cenozoic climate history from seismic-reflection and drilling studies on the Antarctic continental margin. In: Florindo, F., Siegert, M. (Eds.), Antarctic Climate Evolution, Developments in Earth and Environmental Sciences, Vol. 8. Elsevier, p. 537.
De Santis, L., Anderson, J.B., Brancolini, G., Zayatz, I., 1995. Seismic record of late Oligocene through Miocene glaciation on the central and eastern continental shelf on the Ross Sea. In: Cooper, A.K., Barker, P.F., Brancolini, G. (Eds.), Geology and Seismic Stratigraphy of the Antarctic Margin. Antarctic Research Series. American Geophysical Union, Washington, DC, pp. 235–260.
De Santis, L., Anderson, J.B., Brancolini, G., Zayatz, I., 1997. Glaciomarine deposits on the continental shelf of Ross Sea, Antarctica. In: Davies, T.A., et al. (Ed.), Glaciated continental margins — an atlas of acoustic images. Chapman & Hall, London, pp. 110–113.
Evans, J., Dowdeswell, J.A., Ò Cofaigh, C., Benham, T.J., Anderson, J.B., 2006. Extent and dynamics of the West Antarctic Ice Sheet on the outer continental shelf of Pine Island Bay during the last glaciation. Marine Geology 230, 53–72.
Ferrigno, J.G., Lucchitta, B.K., Mullins, K.F., Allison, A.L., Allen, R.J., Gould, W.G., 1993. Velocity measurements and changes in position of Thwaites Glacier/iceberg tongue from aerial photography, Landsat images and NOAA AVHRR data. Annals of Glaciology 17, 239–242.
Gohl, K., Teterin, D., Eagles, G., Netzeband, G., Grobys, J., Parsiegla, N., Schlüter, P., Leinweber, V., Larter, R.D., Uenzelmann-Neben, G., Udintsev, G.B., 2007. Geophysical survey reveals tectonic structures in the Amundsen Sea Embayment, West Antarctica. In: Cooper, A.K., Raymond, C.R., et al. (Eds.), Proceedings of the 10th Int. Symposium of Antarctic Earth Sciences, USGS Open-File Report 2007-1047. doi: 10.3133/of2007-1047.srp047.
Hughes, T.J., 1981. The weak underbelly of the West Antarctic ice sheet. Journal of Glaciology 27, 518–525.
King, L.H., Rokoengen, K., Fader, G.B.J., Gunleiksrund, T., 1991. Till-tongue stratigraphy. Geological Society of America Bulletin 103, 637–659 1991.
Larter, R., 2008. Antarctic Peninsula. In: Cooper, A.K., Brancolini, G., Escutia, C., Kristoffersen, Y., Larter, R., Leitchenkov, G., O'Brien, P., Jokat, W., Cenozoic climate history from seismic-reflection and drilling studies on the Antarctic continental margin. In: Florindo, F., Siegert, M. (Eds), Antarctic Climate Evolution, Developments in Earth and Environmental Sciences, Vol. 8, Elsevier, 537 pp.
Larter, R.D., Barker, P.F., 1989. Seismic stratigraphy of the Antarctic Peninsula Pacific Margin: a record of Pliocene–Pleistocene ice volume and paleoclimate. Geology 17, 731–734.
Larter, R.D., Rebesco, M., Vanneste, L.E., Barker, P.F., 1997. Cenozoic Tectonic, sedimentary and glacial history on the continental shelf west of Graham Land, Antarctic Peninsula. In: Barker, P.F., Cooper, A.D. (Eds.), Geology and seismic stratigraphy of the Antarctic Margin. Antarctic Research Series, 71. American Geophysical Union, Washington, D.C., pp. 1–27.
Larter, R., Gohl, K., Hillenbrand, C.D., Kuhn, G., Deen, T.J., Dietrich, R., Eagles, G., Johnson, J.S., Livermore, R.A., Nitsche, F.O., Pudsey, C.J., Schenke, H.W., Smith, J.A., Udintsev, G., Uenzelmann-Neben, G., 2007. West Antarctic Ice Sheet change since the last glacial period. Eos Transactions American Geophysical Union 88, 189–196.
Larter, R.D., Graham, A.G.C., Gohl, K., Kuhn, G., Hillenbrand, C.D., Smith, J.A., Deen, T.J., Livermore, R., Schenke, H.W., 2009. Subglacial bedforms reveal complex basal regime in a zone of paleo-ice stream convergence, Amundsen Sea Embayment, West Antarctica. Geology 37, 411–414. doi: 10.1130/G25505A.
Lowe, A.L., Anderson, J.B., 2002. Reconstruction of the West Antarctic ice sheet in Pine Island Bay during the Last Glacial Maximum and its subsequent retreat history. Quaternary Science Reviews 21, 1879–1897.
McKay, R., Carter, L., Browne, G., Cowan, E., Dunbar, G., Krissek, L., Naish, T., Powell, R., Wilch, T., 2008. A 13 million year history of ice advance and retreat in the Western Ross Embayment — stratigraphic evidence from ANDRILL Site 1B. Geophysical Research Abstracts: EGU2008-A-05723, EGU General Assembly 2008, vol. 10.
Mitrovica, J.X., Gomez, N., Clark, P.U., 2009. The sea-level fingerprint of West Antarctic collapse. Science 323, 753. doi: 10.1126/science.1166510.
Naish, T.R., Powell, R.D., Barrett, P.J., Levy, R.H., Henrys, S., Wilson, G.S., Krisek, L.A., Niessen, F., Pompilio, M., Ross, J., Scherer, R., Talarico, F., Pyne, A., 2008. Late Cenozoic climate history of the Ross Embayment from the AND-1B drill hole: culmination of three decades of Antarctic margin drilling. In: Cooper, A.K. (Ed.), Antarctica: A Keystone in a Changing World: Proceedings of the 10th International Symposium on Antarctic Earth Sciences, Santa Barbara, California, August 26 to September 1, 2007; National Research Council (U.S.). Polar Research Board; Geological Survey (U.S.). The National Academic Press, Washington, DC, pp. 71–82. doi: 10.3133/of2007-1047.
Nitsche, F.O., Gohl, K., Vanneste, K., Miller, H., 1997. Seismic expression of glacially deposited sequences in the Bellingshausen and Amundsen Seas, West Antarctica. In: Barker, P.F., Cooper, A.K. (Eds.), Geology and Seismic Stratigraphy of the Antarctic Margin 2, Antarctic Research Series, vol. 71. American Geophysical Union, Washington, D.C., pp. 95–108. 71.
Nitsche, F.O., Cunningham, A.P., Larter, R.D., Gohl, K., 2000. Geometry and development of glacial continental margin depositional systems in the Bellingshausen Sea. Marine Geology 162, 277–302.
Nitsche, F.O., Jacobs, S.S., Larter, R.D., Gohl, K., 2007. Bathymetry of the Amundsen Sea continental shelf: implications for geology, oceanography, and glaciology. Geochemistry, Geophysics, Geosystems 8 (10), Q10009. doi: 10.1029/2007GC001694.
Oppenheimer, M., 1998. Global warming and the stability of the West Antarctic Ice Sheet. Nature 393, 325–332.
Powell, R.D., Cooper, J.M., 2002. A glacial sequence stratigraphic model for temperate, glaciated continental shelves. In: Dowdeswell, J.A., Cofaigh, Ó (Eds.), Glacier-influenced sedimentation on high-latitude continental margins, 203. Geological Society, London, pp. 215–244. Special Publications.
Rignot, E., 2008. Changes in West Antarctic ice stream dynamics observed with ALOS PALSAR data. Geophysical Research Letters 35, L12505. doi: 10.1029/2008GL033365.
Rignot, E., Jacobs, S.S., 2002. Rapid bottom melting widespread near Antarctic ice sheet grounding lines. Science 296, 2020–2023.
Scheuer, C., Gohl, K., Larter, R.D., Rebesco, M., Udintsev, G., 2006. Variability in Cenozoic sedimentation along the continental rise of the Bellingshausen Sea, West Antarctica. Marine Geology 277, 279–298. doi: 10.1016/j.margeo.2005.12.007.
Sloan, B.J., Lawver, L.A., 1997. Larsen Shelf, Eastern Antarctica Pensinsula continental margin. In: Davies, T.A., et al. (Ed.), Glaciated continental margins — an atlas of acoustic images. Chapman & Hall, London, pp. 224–227.
Smith, J.A., Hillenbrand, C.D., Larter, R.D., Graham, A.G.C., Kuhn, G., 2009. The sediment infill of subglacial meltwater channels on the West Antarctic continental shelf. Quaternary Research 71, 190–200. doi: 10.1016/j.yqres.2008.11.005.
Stoker, M.S., Pheasant, J.B., Josenhans, H., 1997. Seismic methods and interpretation. In: Davies, T.A., et al. (Ed.), Glaciated continental margins — an atlas of acoustic images. Chapman & Hall, London, pp. 9–26.
Syvitski, J.P., 1997. Water-escape sea floor depressions. In: Davies, T.A., et al. (Ed.), Glaciated continental margins — an atlas of acoustic images. Chapman & Hall, London, pp. 160–162.
ten Brink, U.S., Schneider, C., Johnson, A.H., 1995. Morphology and stratal geometry of the Antarctic continental shelf: insights from models. In: Cooper, A.K., Barker, P.F., Brancolini, G. (Eds.), Geology and Seismic Stratigraphy of the Antarctic Margin, Antarctic Research Series, 68. AGU, Washington, D.C., pp. 1–24.
Uenzelmann-Neben, G., Gohl, K., Larter, R.D., Schlüter, P., 2007. Differences in ice retreat across Pine Island Bay, West Antarctica, since the Last Glacial Maximum: indications from multichannel seismic reflection data. In: Cooper, A.K., Raymond, C.R., et al. (Eds.), A Keystone in a changing World-Online Proceedings of the 10th ISAES, USGS Open-File Report 2007-1047, Short Research Paper, 084. doi: 10.3133/of2007-1047.srp084.
Vanneste, L.E., Larter, R.D., 1995. Deep-tow boomer survey on the Antarctic Peninsula Pacific Margin: an investigation of the morphology and acoustic characteristcs of late Quaternary sedimentary deposits on the outer continental shelf and upper slope. In: Cooper, A.K., Barker, P.F., Brancolini, G. (Eds.), Geology and Seismic Stratigraphy of the Antarctic Margin, Antarctic Research Series, 68. AGU, Washington, D.C., pp. 97–121.
Vorren, T.O., Lebesbye, E., Andreassen, K., Larsen, K.B., 1989. Glacigenic sediments on a passive continental margin as exemplified by the Barents Sea. Marine Geology 85, 251–272.
Vaughan, D.G., Corr, H.F.J., Smith, A.M., Jenkings, A., Bentley, C.R., Stenoien, M.D., Jacobs, S.S., Kellogg, T.B., Rignot, E., Lucchitta, B.K., 2001. A review of ice sheet dynamics in the Pine Island Glacier basin, West Antarctica: hypotheses of instability vs. observations of change. In: Alley, R.B., Bindschadler, R.A. (Eds.), The West Antarctic Ice Sheet: Behavior and Environment. American Geophysical Union, Washington, DC, pp. 237–256.
Yilmaz, Ö., 2001. Seismic data analysis. Investigations in Geophysics, vol. 10. Society of Exploration Geophysicists, Tulsa. 2027.

Publication 6.4.3:

Larter, R.D., Graham, A.G.C., **Gohl, K.**, Kuhn, G., Hillenbrand, C.-D., Smith, J.A., Deen, T.J., Livermore, R., Schenke, H.-W. (2009). Subglacial bedforms reveal complex basal regime in a zone of paleo-ice stream convergence, Amundsen Sea Embayment, West Antarctica. *Geology*, v. 37, pp. 411-414, doi:10.1130/G25505A.

Author contributions: Larter wrote most of this paper, and Graham drafted most of the figures. Gohl, Kuhn and Schenke provided a large processed bathymetric dataset to this paper and added – with the other co-authors – to the discussion of the interpreted bedforms.

Subglacial bedforms reveal complex basal regime in a zone of paleo–ice stream convergence, Amundsen Sea embayment, West Antarctica

Robert D. Larter[1], Alastair G.C. Graham[1], Karsten Gohl[2], Gerhard Kuhn[2], Claus-Dieter Hillenbrand[1], James A. Smith[1], Tara J. Deen[1], Roy A. Livermore[1], and Hans-Werner Schenke[2]
[1]British Antarctic Survey, High Cross, Madingley Road, Cambridge CB3 0ET, UK
[2]Alfred Wegener Institut für Polar und Meeresforschung, Postfach 120161, D-27515 Bremerhaven, Germany

ABSTRACT

The flow of ice streams, which account for most discharge from large ice sheets, is controlled by processes operating at the ice stream bed. Data from modern ice stream beds are difficult to obtain, but where ice advanced onto continental shelves during glacial periods, extensive areas of the former bed can be imaged using modern swath sonar tools. We present new multibeam swath bathymetry data analyzed alongside sparse preexisting data from the Amundsen Sea embayment. The compilation is the most extensive, continuous area of multibeam data coverage yet obtained on the inner continental shelf of Antarctica. The data reveal streamlined subglacial bedforms that define a zone of paleo–ice stream convergence, but, in contrast to previous models, do not show a simple downflow progression of bedform types along paleo–ice stream troughs. We interpret high spatial variability of bedforms as indicating a complex mechanical and hydrodynamic regime at the former ice stream beds, consistent with observations from some modern ice streams. We conclude that care must be taken when using bedforms to infer paleo–ice stream velocities.

INTRODUCTION

The Intergovernmental Panel on Climate Change (IPCC, 2007) has highlighted future changes in the dynamics of large ice sheets as the largest uncertainty in sea level–rise projections. Understanding processes that control ice discharge is therefore of societal and economic importance. Ice discharge from the Antarctic and Greenland ice sheets occurs mainly through fast-flowing ice streams (Bamber et al., 2007). Geophysical and drilling investigations of mechanisms at ice-stream beds that enable streaming flow have been conducted over more than two decades (e.g., Alley et al., 1986; Engelhardt and Kamb, 1998; Smith et al., 2007), but have been limited by inaccessibility of field sites and the difficulty of investigating an interface buried beneath hundreds of meters of ice.

Although investigating modern ice sheet beds is difficult, pristine subglacial bedforms from a formerly more extensive ice sheet are preserved in many deep troughs on the Antarctic continental shelf, and large areas of the former ice base can be imaged using modern swath sonar tools (Pudsey et al., 1994; Canals et al., 2000; Wellner et al., 2001, 2006; Ó Cofaigh et al., 2002).

Wellner et al. (2001) described a typical progression of bedform types along paleo–ice flow paths, from grooves, roches moutonnées, and subglacial meltwater channels on the inner shelf, through a zone of drumlins associated with a transition from crystalline to sedimentary substrates, to mega-scale glacial lineations on the outer shelf. Furthermore, Wellner et al. (2001, 2006) interpreted this progression of bedform types as being associated with accelerating ice flow rates, with the zone of drumlins marking the onset of streaming flow. Ó Cofaigh et al. (2002) showed that extensive multibeam swath bathymetry data collected along Marguerite trough, Antarctic Peninsula, was generally consistent with this model.

Here we present new multibeam swath bathymetry data collected from the Amundsen Sea embayment, compiled with sparse preexisting data, covering the most extensive, continuous area (9950 km^2) yet imaged on the inner continental shelf around Antarctica. We describe subglacial bedforms that indicate a zone of paleo–ice stream convergence, and interpret the high spatial variability in seafloor morphology as indicating a complex regime at the former ice base.

PREVIOUS WORK IN THE AMUNDSEN SEA EMBAYMENT

Approximately 25% of the area of the West Antarctic Ice Sheet (WAIS) drains into the Amundsen Sea embayment (Fig. 1). Hughes (1981) suggested that the Amundsen Sea embayment sector is the most likely site for initiation of WAIS collapse. This remains a concern today (Vaughan, 2008), but relatively little is known about the history of the major glacial systems in the Amundsen Sea embayment sector.

Wellner et al. (2001) published the first multibeam bathymetry and seismic reflection data from the Amundsen Sea embayment, and recognized that there was a change in subglacial morphology associated with a substrate transition from acoustic basement on the inner shelf to sedimentary strata further offshore. Additional geophysical data and sediment cores from a large cross-shelf trough that extends offshore from Pine Island Bay (Fig. 1) were interpreted by Lowe and Anderson (2002, 2003) as showing that grounded ice had extended onto the outer shelf during the last glacial cycle. From radiocarbon dates on calcareous microfossils in sediment cores, Lowe and Anderson (2002) concluded that ice retreated from the outer shelf prior to ca. 16 ka (^{14}C yr) and had retreated to the inner shelf by 12 ka. Evans et al. (2006) presented multibeam data showing streamlined bedforms that extend to the shelf edge in a trough at 114°W, and argued that their characteristics suggested that the WAIS was grounded to the shelf edge during the Last Glacial Maximum (LGM).

DATA ACQUISITION

Multibeam echo-sounding data were collected on RRS *James Clark Ross* and RV *Polarstern* in early 2006. On *James Clark Ross* a Kongsberg EM120 system with 191 beams in the range 11.25–12.75 kHz was used, and on *Polarstern*, an Atlas Hydrosweep DS-2 system with 59 beams at 15.5 kHz was used. Beam raypaths and seafloor depths were calculated in near real time using sound velocity profiles derived from conductivity-temperature-depth casts on the same cruises. Processing consisted of rejecting outlying values and gridding using a near-neighbor algorithm. Sparse, preexisting multibeam data were included in the grid (GSA Data Repository item DR1[1]). Subbottom echo sounder profiles were collected along all survey lines. Navigation data were acquired using the global positioning system.

GENERAL PHYSIOGRAPHY

In the western Amundsen Sea embayment, three 17–39-km-wide troughs extend seaward from modern ice shelf fronts (Figs. 1, 2, and Fig. DR2). Within 70 km of the ice fronts these troughs merge northward into a single trough that is 65 km wide at 600 m depth (Larter et al., 2007; Nitsche et al., 2007). This trough becomes shallower with increasing distance offshore, but

[1]GSA Data Repository item 2009104, multibeam bathymetry grid, large map display of multibeam batyhmetry grid, examples of subbottom echo sounder profiles, subbottom echo-sounder profile data, is available online at www.geosociety.org/pubs/ft2009.htm, or on request from editing@geosociety.org or Documents Secretary, GSA, P.O. Box 9140, Boulder, CO 80301, USA.

continues northwest to the shelf edge where its axis, between 118° and 119°W, is still deeper than 500 m (Figs. 1 and 3).

The easternmost tributary trough extends from the Dotson Ice Shelf and the other two extend from parts of the Getz Ice Shelf either side of Wright Island. We refer to them as, from east to west, the Dotson, Getz A, and Getz B troughs. These troughs are all more than 1000 m deep at the modern ice fronts.

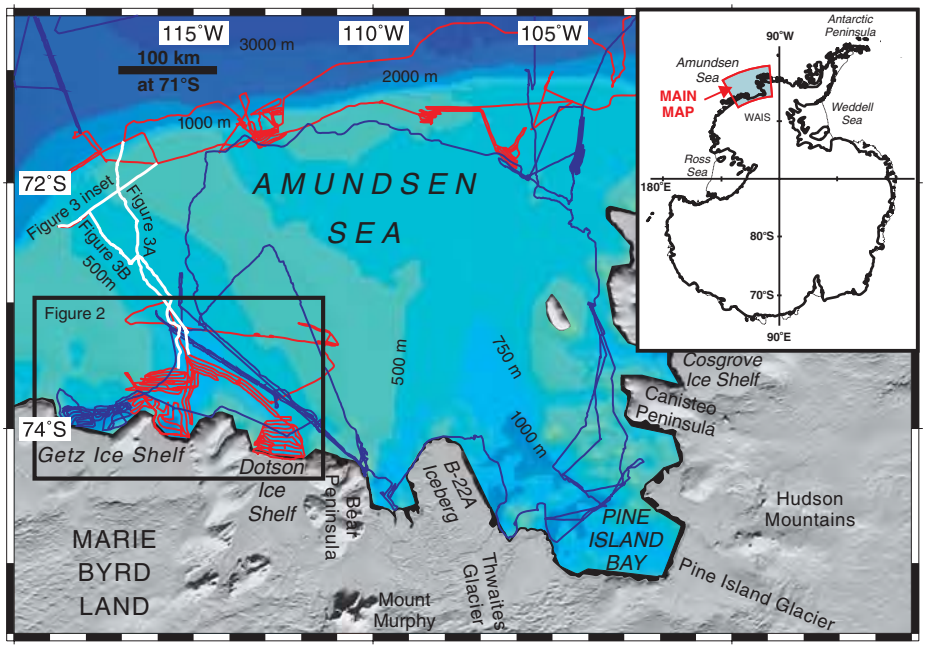

Figure 1. Amundsen Sea embayment map showing tracks of 2006 cruises on RRS *James Clark Ross* (red) and RV *Polarstern* (blue). Regional bathymetry from Nitsche et al. (2007). Moderate resolution imaging spectroradiometer (MODIS) mosaic of Antarctica is shown in onshore areas. Box indicates location of Figure 2. White lines indicate locations of profiles in Figure 3. Inset shows location of main map.

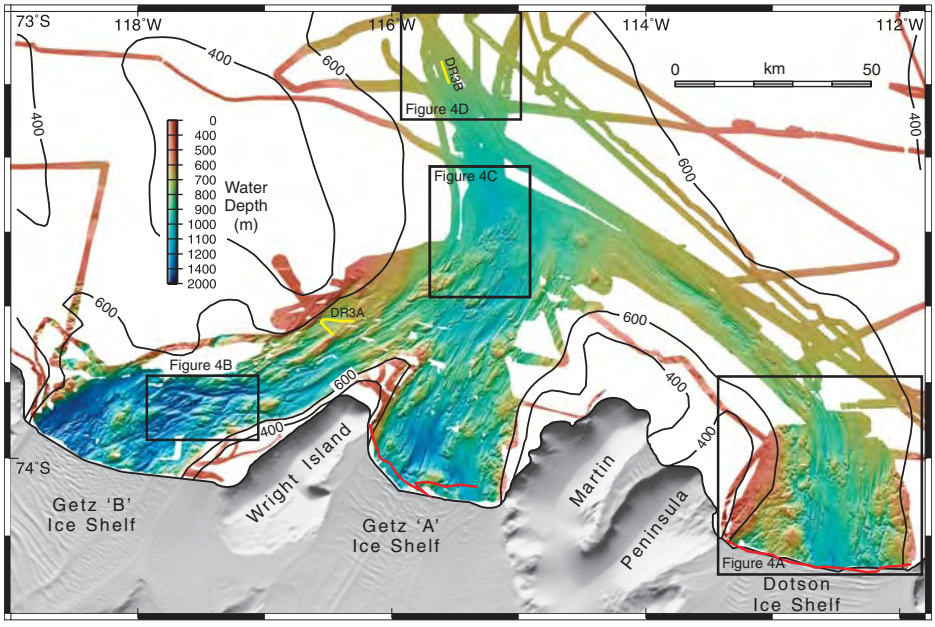

Figure 2. Multibeam swath bathymetry data in western Amundsen Sea embayment, illuminated from northwest. Grid cell size is 50 m. Boxes indicate locations of data panels in Figure 4. Yellow lines indicate locations of profiles in Figure DR3 (see footnote 1). Regional 400 m and 600 m bathymetry contours from Nitsche et al. (2007) show general form of seafloor beyond multibeam data limits. Moderate resolution imaging spectroradiometer (MODIS) mosaic of Antarctica is shown in onshore areas (cropped along ice shelf fronts to avoid obscuring multibeam data). Red lines indicate January 2006 positions of Dotson and Getz A ice fronts.

SUBGLACIAL BEDFORMS

Elongated bedforms revealed by the multibeam data are aligned parallel to the axes of the tributary troughs and show overall convergence with increasing distance from the ice margin (Fig. 2). The data show a large amount of variability in seafloor morphology across, along, and between the troughs. The morphology in the southern part of the Getz B trough is markedly different from that in the other two.

In the southernmost Dotson trough, within 30 km of the 2006 ice front, the range of bedforms observed includes irregular scours, linear grooves, drumlins, mega-scale glacial lineations, and channels with variable orientations and undulating thalwegs (Fig. 4A). The streamlined bedforms have elongation ratios ranging from 3.5:1 to 40:1. Clusters of drumlins are spread across the trough axis 20–25 km north of the ice front, and ~20 km farther north, where both the trough axis and the elongation direction of bedforms have rotated to a northwest trend. Farther northwest, mega-scale glacial lineations are the dominant bedforms along the axis of the Dotson trough, but continue to be interspersed with drumlins (Fig. 2).

The Getz A trough within 30 km of the 2006 ice front exhibits a range of bedforms similar to that observed in the Dotson trough. Streamlined bedforms with a range of elongation ratios similar to those in the Dotson trough are the dominant bedforms in the central 25 km of the Getz A trough, although isolated, scoured highs, some with amplitudes exceeding 300 m, also occur within this zone (Fig. 2). Approximately 30 km north of the ice front, a zone of drumlins and grooves occurs on a sill that extends across the trough and rises to <900 m (Fig. 2).

In addition to bedforms indicative of glacial overriding, the southern part of the Getz B trough also exhibits a range of bedforms suggestive of erosion by flowing water. Anastomosing channels are the dominant bedforms in the central part of the trough within 25 km of the ice front. Many of the channels have undulating thalwegs, and the network of channels extends over highs within the trough that rise more than 300 m above its floor (Fig. 2). The largest channels (as wide as 4500 m, incised to 450 m) merge eastward in a dendritic pattern, and some contain meanders (Fig. 4B). There is a transition to northeast-trending, elongated drumlins and mega-scale glacial lineations as the dominant bedforms in the trough 35–40 km northeast of the ice front (Fig. 2). Some of the mega-scale glacial lineations continue across a broad sill at the mouth of the Getz B trough, parts of which rise to <700 m (Fig. 2). This sill is colinear with the one at the mouth of the Getz A trough.

In the 35 km to the north of the sills, mega-scale glacial lineations are interrupted by further bands of scoured highs and drumlins. There is an abrupt northern limit to this zone of varied bed-

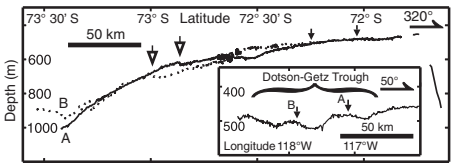

Figure 3. Bathymetric profiles along Dotson-Getz trough. Open arrows mark short seaward-inclined ramps. Inset shows profile across outer shelf part of trough, with vertical scale expanded compared to main figure. Small filled arrows mark intersections of profiles A and B with the cross-trough profile. Profile locations are shown in Figure 1. Scale bars represent distances along and across trough when profiles are projected in true geographic directions indicated in top right of figure and inset.

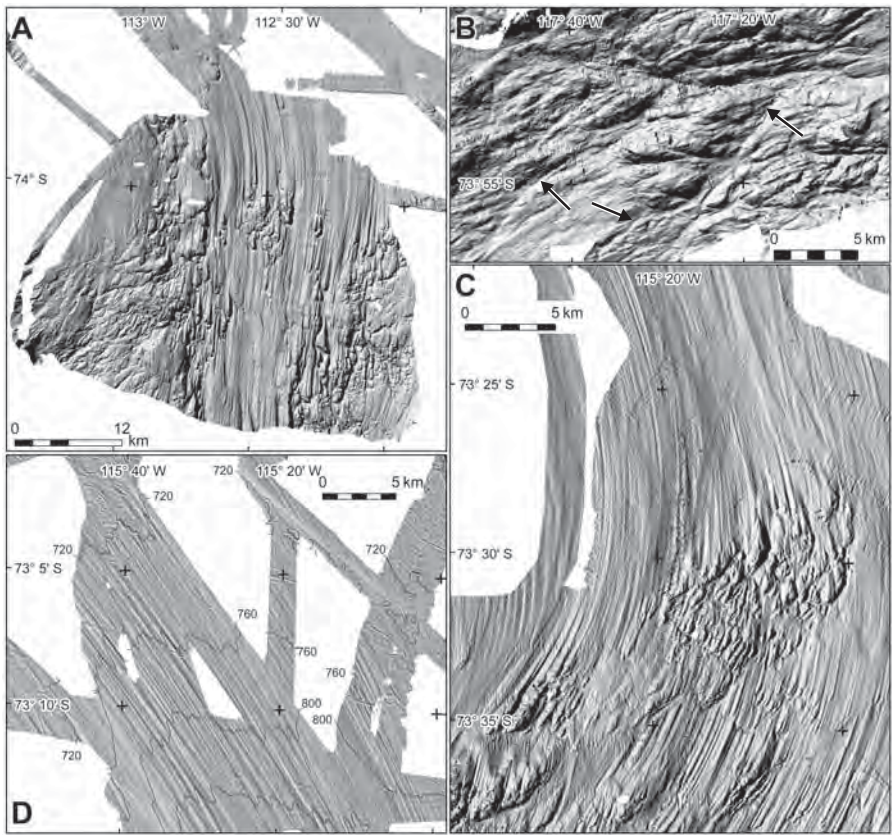

Figure 4. Shaded relief images of selected multibeam bathymetry data areas. Grid cell size is 30 m, projected in Universal Transverse Mercator zone 11S. Locations are shown in Figure 2. A and B are illuminated from northwest, C from west, D from northeast; all with 45° elevation. A: Varied bedforms in Dotson trough. B: Channels in Getz B trough; arrows mark meanders. C: Boundary between zone of varied bedforms and zone containing only mega-scale glacial lineations (MSGL), which coincides with substrate boundary in seismic profiles. D: Transition from MSGL to iceberg furrows in Dotson-Getz trough, with bathymetric contours at 40 m intervals.

forms at ~73°30′S, beyond which mega-scale glacial lineations are the only bedforms in the next 40 km along the trough (Figs. 2 and 4C). Seismic profiles show that this boundary coincides with a change in substrate from acoustic basement to the south to northward-dipping sedimentary strata to the north (Wellner et al., 2001; Larter et al., 2007). Subbottom profiler data show either no seafloor penetration or very thin sediment cover everywhere to the south of this boundary (Fig. DR3A), suggesting that the observed bedforms are eroded into or directly overlie bedrock.

As the main Dotson-Getz trough shallows northward, randomly oriented furrows cutting across mega-scale glacial lineations are encountered at 760 m depth (Fig. 4D). Such furrows are characteristic of ploughing by iceberg keels (Barnes and Lien, 1988; Pudsey et al., 1994). Shallower than 700 m, only 20 km farther north along the trough axis, mega-scale glacial lineations are completely obliterated by iceberg furrows.

The Dotson-Getz trough continues to shallow northward all the way to the shelf break (Fig. 1; Nitsche et al., 2007), with an average gradient of 0.08° (Fig. 3). On each profile shown in Figure 3, the only interruption to this northward shoaling is one <30-m-high, seaward-inclined ramp near 73°S. These profiles preclude the existence of any large grounding zone wedges or moraine banks farther seaward on the shelf that could plausibly be interpreted as marking the limit of LGM grounding line advance (cf. Shipp et al., 1999; O'Brien et al., 1999). This is consistent with the interpretation that the grounding line in the Amundsen Sea embayment advanced to the shelf edge (Evans et al., 2006). The cross-trough profile in the inset in Figure 3 demonstrates that the trough continues across the outer shelf, albeit with a relief of only ~70 m.

DISCUSSION AND CONCLUSIONS

Bedform elongation ratios of as much as 40:1 close to the modern ice fronts in the Dotson and Getz A tributary troughs indicate that paleo–ice streams flowed along them during the last glacial period (cf. Canals et al., 2000; Ó Cofaigh et al., 2002; Stokes and Clark, 2002). Similarly elongated bedforms, within 40 km of the Getz B ice front, indicate that streaming flow also occurred at least in the northeast part of that tributary trough. The pattern of bedforms indicates flow convergence northward, which necessarily also implies flow acceleration.

Using sparser multibeam bathymetry data, Wellner et al. (2001) suggested that initiation of streaming flow was coincident with the change in substrate at ~73°30′S. This boundary coincides with downflow change to very uniform bedforms, which suggest a uniform basal dynamic regime, probably involving an extensive basal till layer (Fig DR3B; cf. Alley et al., 1986; Dowdeswell et al., 2004). However, the new data presented here leave little doubt there was streaming flow much farther south that continued until a late stage during the last glacial cycle.

Many channels observed in the inner part of the Getz B trough and near the flanks of the Getz A and Dotson troughs have undulating thalwegs and run into shallower water depths with increasing distance offshore. These characteristics indicate that they were formed by subglacial water flow, like similar features in Pine Island Bay (Lowe and Anderson 2002, 2003), Marguerite trough (Ó Cofaigh et al., 2002), Palmer Deep (Domack et al., 2006), and Wright Valley in the Transantarctic Mountains (Lewis et al., 2006). The extent and size of the channels indicate that there have been times of abundant subglacial meltwater supply in this area, but over what period and how frequently flows occurred, how water flowed farther offshore where obvious channels are lacking, and what happened to the meltwater bedload, are all unresolved questions (Smith et al., 2009).

Within the tributary troughs, mega-scale glacial lineations are interspersed with drumlins, scoured bedrock highs, and channeled areas, and mega-scale glacial lineations are disrupted by bands of drumlins several times along some paleo–flow lines. The close spatial association and alternation of these different types of bedforms makes it implausible that they could result from substantial spatial variations in paleo–ice

flow velocity. The high spatial variability suggests a complex ice stream basal regime, probably involving patches of dilated, deforming till interspersed with basal sliding over so-called "sticky spots" (Stokes et al., 2007) and areas of channelized subglacial meltwater flow. This interpretation is consistent with results of geophysical investigations of conditions at the base of several modern ice streams, including Rutford Ice Stream (Smith, 1997; Smith et al., 2007; King et al., 2007), Talutis Inlet (Vaughan et al., 2003), and Pine Island Glacier (Smith and Scott, 2007). The extensive area covered by the data presented here suggests that such complex basal regimes cannot be dismissed as exceptions, and therefore reliable prediction of the future behavior of modern ice streams may require collection of extensive geophysical data to map their bed conditions. Furthermore, although there are few data on geological structure beneath the WAIS, what little information exists suggests the substrate is likely to be variable (e.g., Bentley and Clough, 1972), and therefore more similar to the inner shelf area studied here than areas further offshore that are underlain by extensive sedimentary strata.

The extensive new data presented here from a zone of paleo–ice stream convergence and acceleration show that downflow progression of bedform types is not necessarily as simple as proposed by Wellner et al. (2001, 2006). High local variability suggests that the main controls on bed morphology in this largely bedrock-floored, inner shelf area are spatial variations in basal processes and resistance of the bedrock to erosion, rather than flow velocity. This in turn implies that caution must be exercised in inferring paleo-flow rates from relict bedforms alone. While mega-scale glacial lineations are a reliable indication of intermediate to fast flow, the absence of elongated bedforms does not necessarily indicate slow flow, and there is a substantially increased risk of past flow regimes being misinterpreted if data coverage is only partial.

ACKNOWLEDGMENTS

This work was supported by the Alfred Wegener Institute for Polar and Marine Research (AWI) Marine, Coastal and Polar Systems (MARCOPOLI) programs MAR2 and POL6, and the British Antarctic Survey Glacial Retreat in Antarctica and Deglaciation of the Earth System program. We thank the captains, officers, crew, technical support staff, and other scientists who participated in the two research cruises. We particularly thank Steffen Gauger for processing the Hydrosweep data collected on RV *Polarstern*. RVIB *Nathaniel B. Palmer* multibeam echo-sounding data were obtained from the Lamont multibeam synthesis. We are grateful to Eugene Domack, Phil O'Brien, and an anonymous reviewer for constructive reviews.

REFERENCES CITED

Alley, R.B., Blankenship, D.D., Bentley, C.R., and Rooney, S.T., 1986, Deformation of till beneath ice stream B: West Antarctica: Nature, v. 322, p. 57–59, doi: 10.1038/322057a0.

Bamber, J.L., Alley, R.B., and Joughin, I., 2007, Rapid response of modern day ice sheets to external forcing: Earth and Planetary Science Letters, v. 257, p. 1–13, doi: 10.1016/j.epsl.2007.03.005.

Barnes, P.W., and Lien, R., 1988, Icebergs rework shelf sediments to 500 m off Antarctica: Geology, v. 16, p. 1130–1133, doi: 10.1130/0091-7613(1988)016<1130:IRSSTM>2.3.CO;2.

Bentley, C.R., and Clough, J.W., 1972, Antarctic subglacial structure from seismic refraction measurements, *in* Adie, R.J., ed., Antarctic geology and geophysics: Oslo, Universitetsforlaget, p. 683–691.

Canals, M., Urgeles, R., and Calafat, A.M., 2000, Deep sea-floor evidence of past ice streams off the Antarctic Peninsula: Geology, v. 28, p. 31–34, doi: 10.1130/0091-7613(2000)028<0031:DSEOPI>2.0.CO;2.

Domack, E., Amblàs, D., Gilbert, R., Brachfeld, S., Camerlenghi, A., Rebesco, M., Canals, M., and Urgeles, R., 2006, Subglacial morphology and glacial evolution of the Palmer deep outlet system, Antarctic Peninsula: Geomorphology, v. 75, p. 125–142.

Dowdeswell, J.A., Ó Cofaigh, C., and Pudsey, C.J., 2004, Thickness and extent of the subglacial till layer beneath an Antarctic paleo–ice stream: Geology, v. 32, p. 13–16.

Engelhardt, H., and Kamb, B., 1998, Basal sliding of Ice Stream B, West Antarctica: Journal of Glaciology, v. 44, p. 223–230.

Evans, J., Dowdeswell, J.A., Ó Cofaigh, C., Benham, T.J., and Anderson, J.B., 2006, Extent and dynamics of the West Antarctic Ice Sheet on the outer continental shelf of Pine Island Bay during the last glaciation: Marine Geology, v. 230, p. 53–72, doi: 10.1016/j.margeo.2006.04.001.

Hughes, T.J., 1981, The weak underbelly of the West Antarctic ice sheet: Journal of Glaciology, v. 27, p. 518–525.

Intergovernmental Panel on Climate Change, 2007, Climate change 2007: The physical science basis—Summary for policy makers: IPCC Secretariat, Geneva, Switzerland, http://www.ipcc.ch/pdf/assessment-report/ar4/syr/ar4_syr_spm.pdf (January 2009).

King, E.C., Woodward, J., and Smith, A.M., 2007, Seismic and radar observations of subglacial bed forms beneath the onset zone of Rutford Ice Stream, Antarctica: Journal of Glaciology, v. 53, p. 665–672, doi: 10.3189/002214307784409216.

Larter, R.D., and 14 others, 2007, West Antarctic Ice Sheet change since the Last Glacial Period: Eos (Transactions, American Geophysical Union), v. 88, p. 189–190, doi: 10.1029/2007EO170001.

Lewis, A.R., Marchant, D.R., Kowalewski, D.E., Baldwin, S.L., and Webb, L.E., 2006, The age and origin of the Labyrinth, western Dry Valleys, Antarctica: Evidence for extensive middle Miocene subglacial floods and freshwater discharge to the Southern Ocean: Geology, v. 34, p. 513–516, doi: 10.1130/G22145.1.

Lowe, A.L., and Anderson, J.B., 2002, Reconstruction of the West Antarctic ice sheet in Pine Island Bay during the Last Glacial Maximum and its subsequent retreat history: Quaternary Science Reviews, v. 21, p. 1879–1897, doi: 10.1016/S0277-3791(02)00006-9.

Lowe, A.L., and Anderson, J.B., 2003, Evidence for abundant subglacial meltwater beneath the paleo-ice sheet in Pine Island Bay, Antarctica: Journal of Glaciology, v. 49, p. 125–138, doi: 10.3189/172756503781830971.

Nitsche, F.O., Jacobs, S.S., Larter, R.D., and Gohl, K., 2007, Bathymetry of the Amundsen Sea continental shelf: Implications for, geology, oceanography and glaciology: Geochemistry, Geophysics, Geosystems, v. 8, Q10009, doi: 10.1029/2007GC001694.

O'Brien, P.E., De Santis, L., Harris, P.T., Domack, E., and Quilty, P.G., 1999, Ice shelf grounding zone features of western Prydz Bay, Antarctica: Sedimentary processes from seismic and sidescan images: Antarctic Science, v. 11, p. 78–91, doi: 10.1017/S0954102099000115.

Ó Cofaigh, C., Pudsey, C.J., Dowdeswell, J.A., and Morris, P., 2002, Evolution of subglacial bedforms along a paleo-ice stream, Antarctic Peninsula continental shelf: Geophysical Research Letters, v. 29, p. 41-1–41-4, doi: 10.1029/2001GL014488.

Pudsey, C.J., Barker, P.F., and Larter, R.D., 1994, Ice sheet retreat from the Antarctic Peninsula shelf: Continental Shelf Research, v. 14, p. 1647–1675, doi: 10.1016/0278-4343(94)90041-8.

Shipp, S., Anderson, J., and Domack, E., 1999, Late Pleistocene–Holocene retreat of the West Antarctic Ice Sheet system in the Ross Sea: Part 1—Geophysical results: Geological Society of America Bulletin, v. 111, p. 1486–1516, doi: 10.1130/0016-7606(1999)111<1486:LPHROT>2.3.CO;2.

Smith, A.M., 1997, Variations in basal conditions on Rutford Ice Stream, West Antarctica: Journal of Glaciology, v. 43, p. 245–255.

Smith, A., and Scott, J., 2007, Basal conditions on Pine Island Glacier: 2007 WAIS/FRISP Workshop (14th Annual WAIS) Agenda and Abstracts: http://neptune.gsfc.nasa.gov/wais/pastmeetings/abstracts07/SmithA.pdf (January 2009).

Smith, A.M., Murray, T., Nicholls, K.W., Makinson, K., Aðalgeirsdottir, G., Behar, A.E., and Vaughan, D.G., 2007, Rapid erosion, drumlin formation, and changing hydrology beneath an Antarctic ice stream: Geology, v. 35, p. 127–130, doi: 10.1130/G23036A.1.

Smith, J.A., Hillenbrand, C.-D., Larter, R.D., Graham, A.G.C., and Kuhn, G, 2009, The sediment infill of subglacial meltwater channels on the West Antarctic continental shelf: Quaternary Research, v. 71, p. 190–200 , doi: 10.1016/j.yqres.2008.11.005.

Stokes, C.R., and Clark, C.D., 2002, Are long subglacial bedforms indicative of fast ice flow?: Boreas, v. 31, p. 239–249, doi: 10.1080/030094802760260355.

Stokes, C.R., Clark, C.D., Lian, O.B., and Tulaczyk, S., 2007, Ice stream sticky spots: A review of their identification and influence beneath contemporary and palaeo-ice streams: Earth-Science Reviews, v. 81, p. 217–249.

Vaughan, D.G., 2008, West Antarctic Ice Sheet collapse—The fall and rise of a paradigm: Climatic Change, v. 91, p. 65–79, doi: 10.1007/s10584-008-9448-3.

Vaughan, D.G., Smith, A.M., Nath, P.C., and LeMeur, E., 2003, Acoustic impedance and basal shear stress beneath four Antarctic ice streams: Annals of Glaciology, v. 36, p. 225–232, doi: 10.3189/172756403781816437.

Wellner, J.S., Lowe, A.L., Shipp, S.S., and Anderson, J.B., 2001, Distribution of glacial geomorphic features on the Antarctic continental shelf and correlation with substrate: Implications for ice behaviour: Journal of Glaciology, v. 47, p. 397–411, doi: 10.3189/172756501781832043.

Wellner, J.S., Heroy, D.C., and Anderson, J.B., 2006, The death mask of the Antarctic ice sheet: Comparison of glacial geomorphic features across the continental shelf: Geomorphology, v. 75, p. 157–171, doi: 10.1016/j.geomorph.2005.05.015.

Manuscript received 22 September 2008
Revised manuscript received 9 December 2008
Manuscript accepted 14 December 2008

Printed in USA

Publication 6.4.4:

Gohl, K. (2012). Basement control on past ice sheet dynamics in the Amundsen Sea Embayment, West Antarctica. *Palaeogeography, Palaeoclimatology, Palaeoecology*, v. 335-336, pp. 35-41, doi:10.1016/j.palaeo.2011.02.022.

Author contribution: This paper was solely written by Gohl who developed the concept of glacial basement control in the Amundsen Sea Embayment, analysed the data and produced the figures.

Palaeogeography, Palaeoclimatology, Palaeoecology 335-336 (2012) 35–41

Contents lists available at ScienceDirect

Palaeogeography, Palaeoclimatology, Palaeoecology

journal homepage: www.elsevier.com/locate/palaeo

Basement control on past ice sheet dynamics in the Amundsen Sea Embayment, West Antarctica

Karsten Gohl *

Alfred Wegener Institute for Polar and Marine Research, Dept. of Geosciences, Am Alten Hafen 26, 27568 Bremerhaven, Germany

ARTICLE INFO

Article history:
Received 4 September 2010
Received in revised form 10 February 2011
Accepted 19 February 2011
Available online 26 February 2011

Keywords:
Geophysics
Bathymetry
Tectonics
Rifting
Plate boundaries
Erosion
Paleo-ice streams

ABSTRACT

The development of landscapes and morphologies follows initially the tectonic displacement structures of the basement and sediments. Such fault zones or lineaments are often exploited by surface erosional processes and play, therefore, an important role in reconstructing past ice sheet dynamics. Observations of bathymetric features of the continental shelf of the Amundsen Sea Embayment and identification of tectonic lineaments from geophysical mapping indicate that the erosional processes of paleo-ice stream flows across the continental shelf followed primarily such lineaments inherited from the tectonic history since the Cretaceous break-up between New Zealand and West Antarctica. Three major ice flow trends correspond to different tectonic phases in east–west, northwest–southeast and north–south directions. East–west oriented basement trends correlate with coastline trends and overlay tectonic lineaments caused by former rift activities. Directional trends with northwest–southeast orientation are observed for the glacial troughs of the western embayment outer shelf, the western Pine Island Bay coastal zones, and the inner Pine Island glacial trough and are associated with a distributed southern plate boundary zone of the former Bellingshausen Plate. The north–south trend of the main Pine Island glacial trough and the north–northeast trend of the Abbot Ice Shelf trough on the outer shelf follow the predicted lineation trend of an eastern branch of the West Antarctic Rift System extending from the Thwaites drainage basin northward into Pine Island Bay. An understanding of this context helps better constrain the geometries and sea-bed substrate conditions for regional paleo-ice sheet models.

1. Introduction

Tectonically induced displacements of crust, basement and sediments are the underlining process controlling the development of landscapes and morphologies which are exploited by surface erosional activities. This context becomes in particular important for reconstructing continental ice sheets at various stages since the beginning of glacial cyclicity. Reconstructing past West Antarctic ice sheet dynamics in the area of the Amundsen Sea Embayment plays an important role as the Pine Island, Thwaites, Smith and Kohler glacier systems of the Amundsen Sea Embayment have thinned at an alarming rate, while flow speed of some of them has dramatically increased (e.g. Rignot et al., 2008; Pritchard et al., 2009). Their catchment area alone has an ice-mass potential for about 1.5 m of sea-level rise (Vaughan, 2008). Modeling results by Pollard and DeConto (2009) suggest that the ice sheet in the Amundsen Sea Embayment has behaved with similar retreat dynamics in earlier epochs, at least since the Pliocene. This paper demonstrates that there is a relationship between the tectonic lineaments inherited from the complex tectonic history of this area since the Cretaceous rifting between New Zealand and West Antarctica, and the flow paths taken by major ice streams. This helps better constrain the geometries and sea-bed substrate conditions for regional paleo-ice sheet models.

2. Tectonic background

The geological history of the Amundsen Sea Embayment and its present geographical outline was controlled by several distinct tectonic phases.

The processes during rifting and break-up of New Zealand from West Antarctica dominate most of the present tectonic nature of the continental margin of the Amundsen Sea (Fig. 1). Eagles et al. (2004a) illustrate that early Pacific–Antarctic separation evolved first as rifting and crustal extension between Chatham Rise and western Thurston Island block and along the present-day Bounty Trough between Chatham Rise and Campbell Plateau (Grobys et al., 2007) as early as 90 Ma. Rifting possibly continued along the present Great South Basin between the Campbell Plateau and the South Island of New Zealand until the rift was abandoned in favor of a new extensional locus to the south, forming the earliest oceanic crust between Campbell Plateau and Marie Byrd Land at 84–83 Ma. The eastern boundary between Chatham Rise and Campbell Plateau at 90 Ma – before the formation of Bounty Trough – was situated off the western Amundsen Sea Embayment at about 120°–125° W.

* Tel.: +49 471 48311361.
E-mail address: karsten.gohl@awi.de.

0031-0182/$ – see front matter © 2011 Elsevier B.V. All rights reserved.
doi:10.1016/j.palaeo.2011.02.022

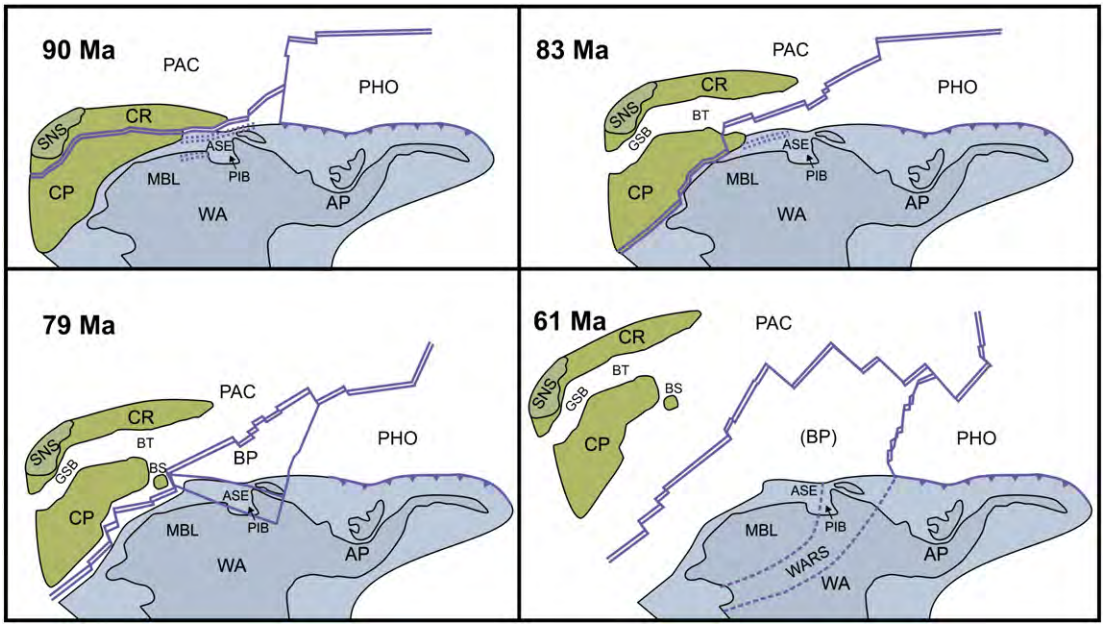

Fig. 1. Plate-kinematic reconstruction of the tectonic development in the Amundsen Sea area from 90 to 61 Ma. The plates are rotated according to rotation parameters compiled and derived by Eagles et al. (2004a). Abbreviations are: PAC Pacific plate, PHO Phoenix Plate, CR Chatham Rise, CP Campbell Plateau, SNS South Island New Zealand, GSB Great South Basin, BT Bounty Trough, BS Bollons Seamount, WA West Antarctica, MBL Marie Byrd Land, AP Antarctic Peninsula, ASE Amundsen Sea Embayment, PIB Pine Island Bay, BP Bellingshausen Plate, and WARS West Antarctic Rift System faults. The development is explained in the main text.

From about 79 Ma or earlier, the Bellingshausen Plate (Fig. 1) moved as a micro-plate independently on the southern flank of the mid-Pacific spreading ridge until about 61 Ma when a major plate reorganization occurred in the South Pacific (e.g. Larter et al., 2002; Eagles et al., 2004a,b). The small plate's western boundary was situated in the area of the Marie Byrd Seamounts; its eastern transpressional boundary lies along the Bellingshausen Gravity Anomaly lineament in the western Bellingshausen Sea (Gohl et al., 1997; Eagles et al., 2004a). Although its southern plate boundary has been projected to extend from the Marie Byrd Seamount area onto the shelf and mainland for reasons of completeness (Eagles et al., 2004a,b), it is not clearly identified and it may be of a distributed boundary type.

The plan shape of Pine Island Bay has stimulated several researchers to suggest that the bay is the location of a major crustal boundary between the Marie Byrd Land block to the west and the Thurston Island/Ellsworth Land blocks to the east (e.g. Dalziel and Elliot, 1982; Grunow et al., 1991; Storey, 1991) which may have been active during the Late Cretaceous New Zealand–Antarctic break-up or even before in the early Mesozoic or Paleozoic. However, direct evidence is still missing. Conceptual models suggest that Pine Island Bay was affected by the West Antarctic Rift System, which may have played a deformational role in the onshore and offshore eastern Amundsen Sea Embayment at some stage (Fig. 1). Jordan et al. (2010) invert airborne gravity data for crustal thickness revealing extremely thin crust and low lithospheric rigidity for the onshore Pine Island Rift and interpret this as a result of West Antarctic Rift activity. Müller et al. (2007) suggest that from chron 21 (48 Ma) to chron 8 (26 Ma) the West Antarctic Rift System was characterized by the extension in the Ross Sea embayment and dextral strike-slip in the east, where it was connected to the Pacific–Phoenix–East Antarctic triple junction (Fig. 1) via the Byrd Subglacial Basin and the Bentley Subglacial Trench, interpreted as pull-apart basins. Müller et al. (2007) infer that transtensional tectonic reactivation may have occurred along a zone from the Thurston Island/Ellsworth Land block into the western Bellingshausen Sea in the Eocene/Oligocene as part of the eastern tectonic activity of the West Antarctic Rift System. It is also possible that such transtensional activity also occurred earlier farther west in Pine Island Bay along a north–south striking zone (Dalziel, 2006; Ferraccioli et al., 2007; Gohl et al., 2007; Jordan et al., 2010), either as a reactivation of a former crustal block boundary or an initial deformation forming the paleogeographic outline of Pine Island Bay.

A further aspect of the tectonically induced geomorphological development of the Amundsen Sea Embayment is the as yet little-quantified effect of the Marie Byrd Land dome uplift. The erosion surface across the dome is uplifted to elevations of 400–600 m along the coast and rises to 2700 m inland at the crest (LeMasurier, 2008). Crustal thickness estimates are derived from receiver function analysis and show that the crust beneath the central dome is about 25 km thick and that it is supported by a low-density mantle, which may indicate a hot spot (Winberry and Anandakrishnan, 2004). This thickness is consistent with the measured crustal thickness of 22–24 km at the adjacent western Amundsen Sea Embayment shelf (Gohl et al., 2007). The Marie Byrd Land dome is not considered a northern flank of the West Antarctic Rift System, as earlier studies suggested, but it is an integrated feature within the rift system and has risen since about 29–25 Ma (LeMasurier, 2008).

3. Geophysically observed lineaments

Grids of geophysical potential field data of the Amundsen Sea Embayment reveal distinct trends of lineaments, which can be linked to tectonic phases. Linear trends in the satellite-derived gravity anomaly grid of McAdoo and Laxon (1997) (Fig. 2) as well as magnetic anomalies (Gohl et al., 2007) of the western Amundsen Sea embayment, running sub-parallel to each other, are interpreted as indicating an intrusive crustal origin. Their NE–SW trend parallels the initial spreading center's azimuth between Chatham Rise and West Antarctica and can thus be related to rift processes occurring during breakup or just beforehand. The only 22–24 km thick crust beneath the inner shelf, as derived from seismic refraction data (Gohl et al., 2007), suggests a crustal thinning process. These observations infer tectonic and magmatic processes leading to a failed initial rift or distributed crustal extension in the Amundsen Sea Embayment. Such rifting must have been active before 90 Ma or accompanied the rifting in Bounty Trough and its northward translation of Chatham Rise at

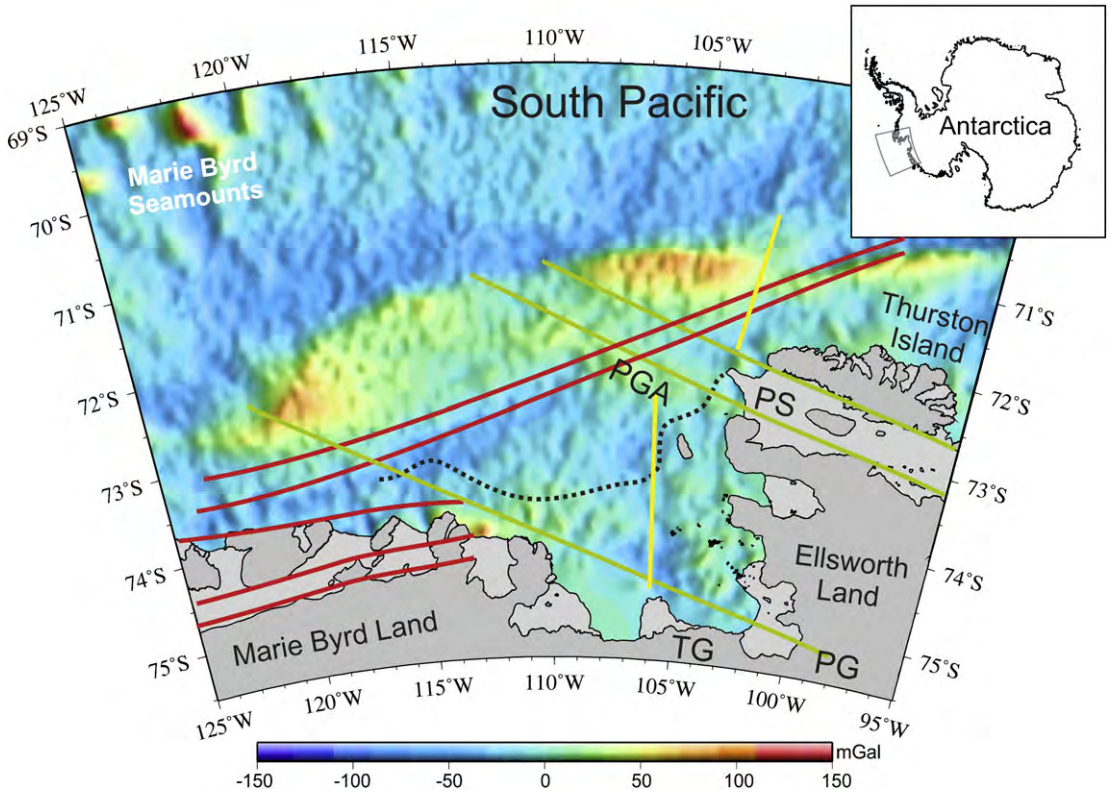

Fig. 2. Satellite-derived gravity anomaly map of the Amundsen Sea Embayment (McAdoo and Laxon, 1997) with interpreted tectonic lineaments. Red lines mark lineaments generated during pre-breakup rifting between New Zealand and West Antarctica; green lines represent lineaments caused by a distributed system of a shifting southern Bellingshausen Plate boundary; yellow lines indicate possible traces of a northward trending branch of the eastern West Antarctic Rift System. The black dotted line shows the boundary between outcropping basement to the south and the sediment basin on the shelf as identified by seismics (Graham et al., 2009; Weigelt et al., 2009). Abbreviations are: PS Peacock Sound, PGA Peacock Gravity Anomaly, PG Pine Island Glacier, and TG Thwaites Glacier.

this time. Although earlier reconstructions demonstrate a reasonable break-up fit of the shelf-break lines of the conjugate New Zealand eastern plateau and West Antarctic margins (e.g. Larter et al., 2002), recent geophysical data indicate that the crust of the outer Amundsen Sea Embayment thinned or fragmented extremely before break-up, leaving the continent–ocean boundary several tens of kilometers oceanward of the shelf-break (Gohl, 2008, 2010).

The gravity anomaly grid (Fig. 2) also shows a distinct linear, WNW–ESE striking positive anomaly across the outer continental shelf of the Amundsen Sea Embayment in northwestward extension from Peacock Sound between Thurston Island and the mainland (Larter et al., 2002; Eagles et al., 2004a,b). This so-called Peacock Gravity Anomaly is modeled with an underlying high-density body (Gohl et al., 2007) and is interpreted as a magmatic zone, which overprinted the NE–SW trending rift structure. Magnetic data show that magmatic intrusions were emplaced in some places along this boundary (Gohl et al., 2007). Consistent with the plate-kinematic process described for the Bellingshausen Plate (Eagles et al., 2004a), one can infer that this feature acted as an active southern Bellingshausen Plate boundary of relatively minor extensional and translational movements.

A geophysical signature of a major crustal block boundary in Pine Island Bay, separating the Marie Byrd Land and Thurston Island blocks, is not obvious from potential field data (Gohl et al., 2007; Gohl, 2010). If such a crustal boundary exists, its signature is possibly overprinted by the effects of Cenozoic magmatic intrusions and recent volcanism (e.g. LeMasurier, 1990; Corr and Vaughan, 2008). The deeply incised inner and middle shelf of Pine Island Bay with glacial troughs and channels reaching 1000–1500 m depth (Lowe and Anderson, 2002; Larter et al., 2007; Graham et al., 2010) may in addition obscure interpretations of the magnetic anomaly field. It seems likely that the surface-erosional processes exploited such a crustal boundary zone, as originally suggested by the SPRITE Group (1992), and/or further eroded a major fault system generated by West Antarctic Rift System activity. This may have laid the base for the formation of the main Pine Island Trough, stretching from the mouth of the Pine Island Glacier to the middle shelf in NW and NNW orientations.

4. Basement relief and sediments

The compiled bathymetry of the Amundsen Sea Embayment by Nitsche et al. (2007) illustrates a continental shelf, which is divided into two bathymetric provinces, the eastern and western Amundsen Sea Embayment, each heavily incised by a deeply eroded glacial trough system (Fig. 3). The provinces are separated by a northwest trending ridge of less than 500 m water-depth. The deepest troughs reach 1600 to 1200 m water-depth near the glacier mouths from where they converge onto the middle shelf (Larter et al., 2007; Graham et al., 2009). The glacial troughs shallow to about 700–500 m depth on the middle to outer shelf. Multi-beam data from both provinces reveal streamlined subglacial bedforms which change spatially in substrate characteristics (Graham et al., 2009, 2010; Larter et al., 2009). On the inner shelf, some troughs are incised by narrow channels which, in the case of the Getz B Ice Shelf trough, strike in east–west direction parallel to the main trough, before a transition to a northeast-trend occurs farther offshore (Larter et al., 2009). This divergence of the erosional path from the direct outflow to the outer shelf can best be explained by the blockage of the flow path by highly resistive basement rock units such as high-grade magmatic dikes, striking in an east–west direction.

Geophysical surveys in the last decade have revealed some insight into the structure of the basement and sediments of the Amundsen

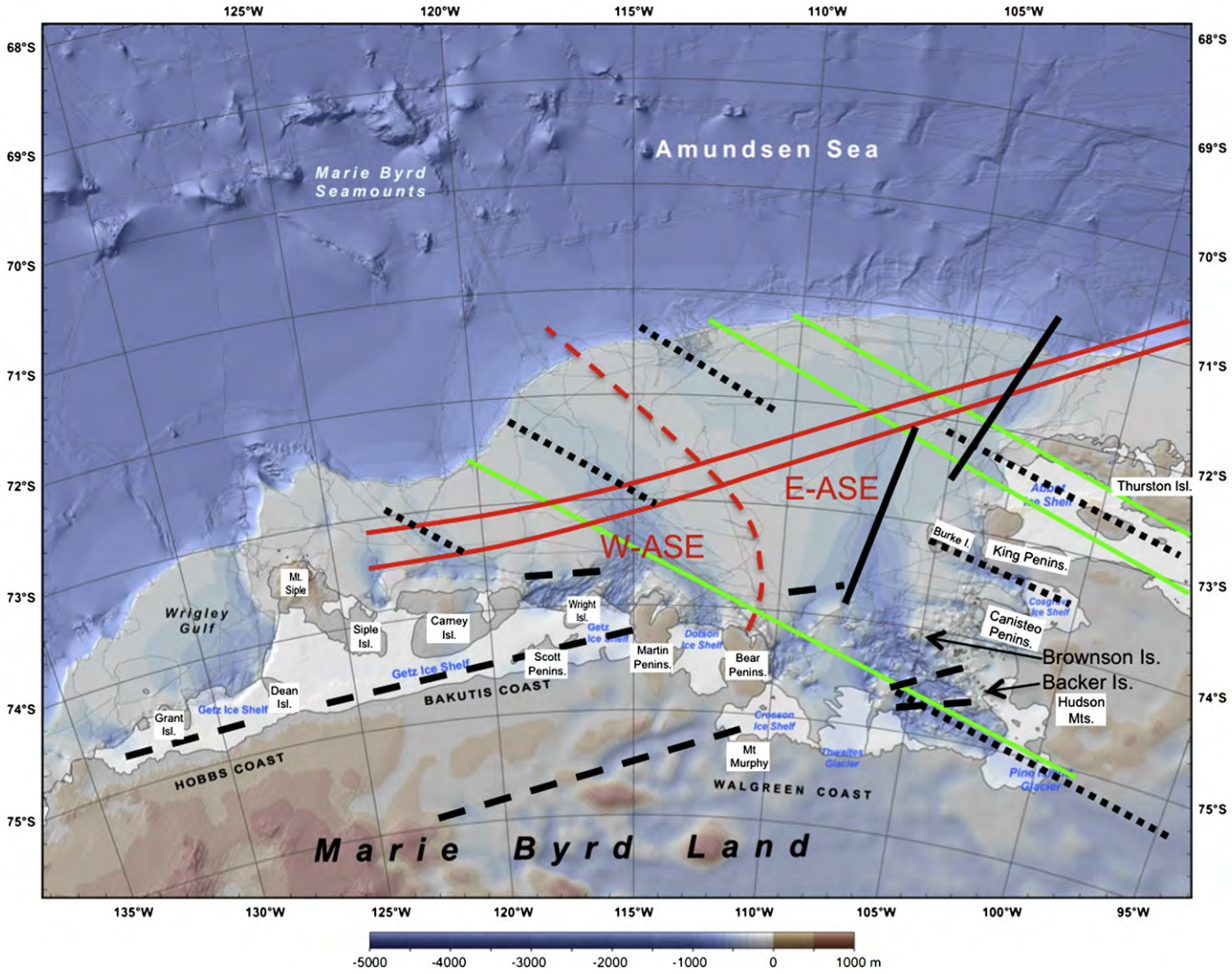

Fig. 3. Bathymetric pattern of the Amundsen Sea Embayment, compiled by Nitsche et al. (2007) from single and multibeam data along indicated ship-tracks until 2006, and with the following interpreted underlying tectonic lineaments: black hashed lines are lineaments from distributed parallel rift axes before the New Zealand–West Antarctic breakup, black dotted lines represent a shifting southern Bellingshausen Plate boundary, black solid lines indicate a projected West Antarctic Rift System lineament. Solid red and green lines are tectonic lineaments interpreted from the gravity anomaly field of Fig. 2 for comparison. The red hashed line indicates the topographic and basement ridge which acts as boundary between western (W–ASE) and eastern embayment (E–ASE).

Sea Embayment shelf. A distinct boundary between outcropping crystalline basement of relatively rough morphology to the south and the sedimentary shelf basin of oceanward dipping strata to the north is clearly imaged in seismic profiles (Lowe and Anderson, 2002; Larter et al., 2007; Graham et al., 2009; Weigelt et al., 2009; Gohl, 2010) and can be mapped across the embayment (Fig. 2). The sediments north of the boundary increase in thickness to at least 800 m, possibly much thicker.

Seismic data from RV *Polarstern* cruise ANT-XXIII/4 and RRS *James Clark Ross* cruise JR141 in 2006 indicate that the bathymetric ridge, separating the eastern from the western embayment (Fig. 3), is underlain by elevated older sediments which dip westward towards the main glacial trough (Graham et al., 2009; Weigelt et al., 2009). New, as yet unprocessed seismic data from the RV *Polarstern* cruise ANT-XXVI/3 in early 2010 (Gohl, 2010) also indicate a similar declining pattern to the east of the ridge crest towards the eastern embayment trough. It can therefore be assumed that this ridge is underlain by elevated crystalline basement extending north of Bear Peninsula.

Basement crops out or is scarcely covered by sediments with a few narrow pockets and troughs of thicker sediments along the eastern side of Pine Island Bay between the Pine Island Glacier Trough, Canisteo Peninsula, Burke Island and northward to the Abbot Ice Shelf mouth (Uenzelmann-Neben et al., 2007). This also includes a narrow trough south of King Peninsula connecting to the Cosgrove Ice Shelf. Groups of tiny granitoid and gneissic islands, some cut by mafic dikes, line up mostly in northwest trending clusters, such as the Brownson Islands and Backer Islands southwest and south of Canisteo Peninsula (Fig. 3). This directional trend coincides with the general strike directions of the bathymetric ridge between the eastern and western embayments and the main glacial troughs of the middle to outer shelf of the western embayment (Fig. 3). The bathymetry and seismic records of inner Pine Island Bay show numerous distributed basement ridges and domes within the main glacial Pine Island Trough. Some are aligned in an east–west orientation, others do not show any preferred aligned orientation. Lacking samples from the submarine basement, it can only be assumed that they consist of rock material similar to that of the adjacent small islands. These edifices have

probably served as pinning points at times when the ice shelf covered the inner shelf and, therefore, affected its retreat mechanism and rates.

5. Glacial pathways

Seismic reflection data in the Pine Island Bay region show that the outer shelf and slope have undergone both progradational and aggradational deposition of sediments since the mid-Miocene. Erosional unconformities are present on the outer shelf, implying the former presence of a grounded ice sheet (e.g. Nitsche et al., 2000; Lowe and Anderson, 2002). The presence of mega-scale glacial lineations and grounding zone wedges on the outer shelf indicates that the ice sheet extended to, or near, the shelf edge during the last glacial maximum (Lowe and Anderson, 2002; Evans et al., 2006; Graham et al., 2010) and possibly during glacial periods prior to the last one. Ice stream advances would have followed low-lying morphologies such as pre-existing troughs. Three main groups of directional trends can be observed in the compiled bathymetric and topographic grid of the Amundsen Sea Embayment (Fig. 3). In superposing the bathymetric impression of the main glacial troughs and intra-trough channels onto an interpreted map of tectonic features in the embayment, it can be inferred that past ice streams followed primarily tectonically inherited lineaments.

(1) The east–west oriented basement features and deviated glacial trough morphology of the inner shelf of the western embayment align with general trends in the Bakutis Coast coastline and the elongated inner Getz Ice Shelf. This east–west trend also correlates with the dominant trends in basement ridges crossing the main Pine Island Trough of inner Pine Island Bay and with the ESE-trending onshore subglacial topography of the Crosson Ice Shelf drainage basin. This trend field coincides with the distributed series of rift axes during the New Zealand–Marie Byrd Land separation process before break-up in the Late Cretaceous, as derived from plate-kinematic reconstructions (Figs. 1 and 2).

(2) A remarkable coinciding NW–SE to WNW–ESE directed trend can be observed for the glacial troughs of the western embayment outer shelf, the Peacock Sound (Abbott Ice Shelf), the Cosgrove Ice Shelf and glacial trough, and the Pine Island glacial trough of the inner Pine Island Bay shelf and onshore. Plate-kinematic models predict that the southern boundary of the Bellingshausen Plate existed in the same directional trend. This observation of parallel trending morphological expressions suggests that this plate boundary must have acted as a distributed plate boundary system crossing oceanic and continental crust with a shifting boundary axis.

(3) The north–south trend of the main Pine Island glacial trough on the middle shelf and the NNE-trend of the outer Abbot Ice Shelf trough on the outer shelf follow the predicted lineation trend of an eastern branch of the West Antarctic Rift System extending from the Thwaites drainage basin northward into Pine Island Bay (Dalziel, 2006; Ferraccioli et al., 2007; Gohl et al., 2007; Jordan et al., 2010). Graham et al. (2010) describe that the extended Pine Island–Thwaites paleo-ice stream possibly took the westerly path on the outer shelf and switched to the northerly path at a later time. The timing of such a switch cannot be established at this stage, but it cannot be excluded that younger tectonic processes changed the bathymetry on the shelf.

Much of the shelf and the near-shelf continental basins of the Amundsen Sea Embayment would have been below sea-level (Holt et al., 2006; Vaughan et al., 2006), making significant pre-glacial erosion less likely. By the time major glacial cycles occurred in the coastal and shelf areas in the early to middle Miocene, almost all tectonic basement features and faults had already existed and were exploited by glacial erosional processes of periodically advancing grounded ice streams. It seems obvious that erosional and ice-flow processes are largely controlled by outcropping basement lineaments. It is less obvious how tectonic lineaments under a thick sediment cover, as observed for the middle and outer shelf (Weigelt et al., 2009), control ice stream flows. An explanation is that the sediment morphologies along these major tectonic lineaments became never entirely leveled before glacial onset and during interglacial times due to continuous oceanward flowing bottom currents.

Regarding the uncertainty of the timing of any West Antarctic Rift activity in this region, it is not impossible that continued tectonic movements occurred in Pine Island Bay and altered the early flow paths of the Pine Island and Thwaites ice stream systems. However, a better understanding of the processes, extent and timing of the West Antarctic Rift System tectonics is urgently needed.

As the retreat history of glacial cycles before the last glacial period cannot be reconstructed for the Amundsen Sea Embayment at this stage, due to an yet uncompleted stratigraphic model and missing age constraints for the shelf, an attempt is made to illustrate the retreat of grounded ice sheet since the last glacial maximum in a schematic sketch (Fig. 4). The Holocene age constraints come from cosmogenic exposure dating results from rock samples on the mainland and islands (Johnson et al., 2008), from carbon isotope dates of foraminifera samples in shelf

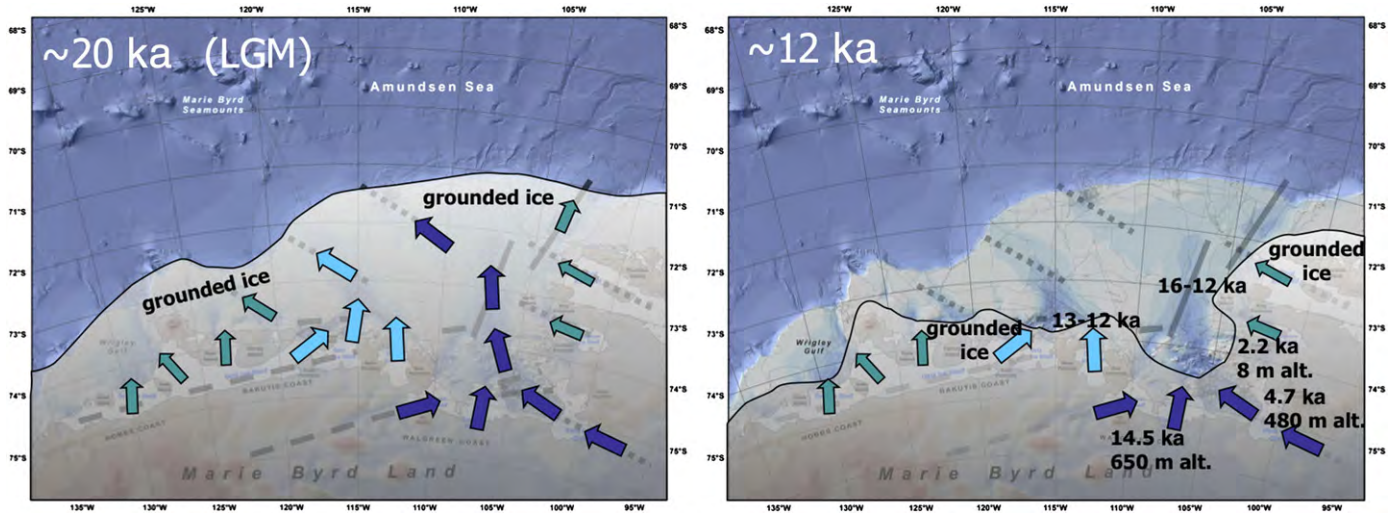

Fig. 4. Models of ice sheet extent and retreat paths in the Amundsen Sea Embayment at the last glacial maximum (LGM) at about 20 ka and at 12 ka. Retreat ages are from cosmogenic exposure dates by Johnson et al. (2008) and microfossil analyses by Lowe and Anderson (2002) and Hillenbrand et al. (2009). Arrows indicate major ice stream flow directions and are colored according to drainage basin groups. Tectonic lineaments in the background (gray solid, dotted and hashed lines) are according to Fig. 3. The bathymetric/topographic compilation is from Nitsche et al. (2007).

sediments of Pine Island Bay (Lowe and Anderson, 2002), and from diatomaceous ooze and mud cored at the inner shelf of the western embayment (Hillenbrand et al., 2009). It must be noted that the individual retreat ages suffer from large uncertainties. However, the fact that the different methods of different areas converge to similar ages for retreat to the inner shelf in the early Holocene places some degree of confidence in the general retreat trend. The retreating ice limits along the shelf are estimated by interpolating between the benchmark locations of age control. Independent of the processes causing ice sheet retreats (e.g. warm Circum-Polar Deep Water incursions), it is valid to assume that the retreat paths of the main ice streams follow the present glacial troughs due to the loss of ground control in their deeper bathymetry (Fig. 4), while pinning points of shallow banks and ridges continued to hold back the retreat for a little longer until continued melting thinned the grounded ice enough for farther retreat.

6. Conclusions

Observations of the bathymetric pattern of the Amundsen Sea Embayment shelf and identification of tectonic structures from geophysical mapping indicate that the erosional processes of paleo-ice stream flow across the continental shelf followed primarily tectonic lineaments inherited from the complex tectonic history since the Cretaceous break-up between New Zealand and West Antarctica. East–west oriented basement features of the embayment and glacial trough morphology of the inner shelf of the western embayment correlate with coastline trends and overlay tectonic lineaments interpreted as rifting axis active at pre-breakup times. Directional trends in NW–SE to WNW–ESE orientation are observed for the glacial troughs of the western embayment outer shelf, the Peacock Sound, the Cosgrove Ice Shelf and trough, and the inner Pine Island glacial trough and are superposed on lineaments of a distributed southern plate boundary zone of the former Bellingshausen Plate. The dominant north–south trend of the main Pine Island glacial trough on the middle shelf and the NNE-trend of the outer Abbot Ice Shelf trough on the outer shelf follow the predicted lineation trend of an eastern branch of the West Antarctic Rift System extending from the Thwaites drainage basin northward into Pine Island Bay.

These results help better constrain the geometries and sea-bed substrate conditions for regional paleo-ice sheet models.

Acknowledgments

The author thanks innumerable persons for fruitful discussions on this topic, two anonymous reviewers for their helpful comments, and in particular Rob DeConto for suggesting to submit this paper to this volume.

References

Corr, H.F.J., Vaughan, D.G., 2008. A recent volcanic eruption beneath the West Antarctic ice sheet. Nature Geoscience 1. doi:10.1038/ngeo106.

Dalziel, I.W.D., 2006. On the extent of the active West Antarctic rift system. In: Siddoway, C.S., Ricci, C.A. (Eds.), Proceedings of Workshop on Frontiers and Opportunities in Antarctic Geosciences. Terra Antartica Reports, 12. Terra Antartica Publications, Siena, Italy, pp. 193–202.

Dalziel, I.W.D., Elliot, D.H., 1982. West Antarctica: problem child of Gondwanaland. Tectonics 1, 3–19.

Eagles, G., Gohl, K., Larter, R.D., 2004a. High resolution animated tectonic reconstruction of the South Pacific and West Antarctic margin. Geochemistry, Geophysics, Geosystems 5. doi:10.1029/2003GC000657.

Eagles, G., Gohl, K., Larter, R.D., 2004b. Life of the Bellingshausen plate. Geophysical Research Letters 31, L07603. doi:10.1029/2003GL019127.

Evans, J., Dowdeswell, J.A., Ó Cofaigh, C., Benham, T.J., Anderson, J.B., 2006. Extent and dynamics of the West Antarctic Ice Sheet on the outer continental shelf of Pine Island Bay during the last glaciation. Marine Geology 230, 53–72. doi:10.1016/j.margeo.2006.04.001.

Ferraccioli, F., Jordan, T.A., Vaughan, D.G., Holt, J., James, M., Corr, H., Blankenship, D.D., Fairhead, J.D., Diehl, T.M., 2007. New aerogeophysical survey targets the extent of the West Antarctic Rift System over Ellsworth Land. In: Cooper, A.K., Raymond, C.R. (Eds.), Proceedings of the 10th Int. Symposium of Antarctic Earth Sciences, USGS Open-File Report 2007-1047, Extended Abstract 113.

Gohl, K., 2008. Antarctica's continent–ocean transitions: consequences for tectonic reconstructions. In: Cooper, A.K., Barrett, P.J., Stagg, H., Storey, B., Stump, E., Wise, W. (Eds.), Antarctica: A Keystone in a Changing World. Proceedings of the 10th International Symposium on Antarctic Earth Sciences. The National Academies Press, Washington, DC, pp. 29–38. doi:10.3133/of2007-1047.kp04.

Gohl, K., 2010. The expedition of the research vessel "Polarstern" to the Amundsen Sea, Antarctica, in 2010 (ANT-XXVI/3). Berichte zur Polar- und Meeresforschung / Reports on Polar and Marine Research, 617. http://epic.awi.de/epic/Main?static=yes&page=abstract&entry_dn=Goh2010f.

Gohl, K., Nitsche, F., Miller, H., 1997. Seismic and gravity data reveal Tertiary interplate subduction in the Bellingshausen Sea, southeast Pacific. Geology 25, 371–374.

Gohl, K., Teterin, D., Eagles, G., Netzeband, G., Grobys, J., Parsiegla, N., Schlüter, P., Leinweber, V., Larter, R.D., Uenzelmann-Neben, G., Udintsev, G.B., 2007. Geophysical survey reveals tectonic structures in the Amundsen Sea embayment, West Antarctica. In: Cooper, A.K., Raymond, C.R. (Eds.), Proceedings of the 10th Int. Symposium of Antarctic Earth Sciences, USGS Open-File Report 2007-1047. doi:10.3133/of2007-1047.srp047.

Graham, A.G.C., Larter, R.D., Gohl, K., Hillenbrand, C.D., Smith, J.A., Kuhn, G., 2009. Bedform signature of a West Antarctic palaeo-ice stream reveals a multi-temporal record of flow and substrate control. Quaternary Science Reviews 28, 2774–2793. doi:10.1016/j.quascirev.2009.07.003.

Graham, A.G.C., Larter, R.D., Gohl, K., Dowdeswell, J.A., Hillenbrand, C.D., Smith, J.A., Evans, J., Kuhn, G., 2010. Flow and retreat of the Late Quaternary Pine Island–Thwaites palaeo-ice stream, West Antarctica. Journal of Geophysical Research — Earth Surfaces 115, F03025. doi:10.1029/2009JF001482.

Grobys, J.W.G., Gohl, K., Davy, B., Uenzelmann-Neben, G., Deen, T., Barker, D., 2007. Is the Bounty Trough, off eastern New Zealand, an aborted rift? Journal of Geophysical Research 112, B03103. doi:10.1029/2005JB004229.

Grunow, A.M., Kent, D.V., Dalziel, I.W.D., 1991. New paleomagnetic data from Thurston Island: implications for the tectonics of West Antarctica and Weddell Sea opening. Journal of Geophysical Research 96 (B11), 17935–17954.

Hillenbrand, C.-D., Smith, J.A., Kuhn, G., Esper, O., Gersonde, R., Larter, R.D., Maher, B., Moreton, S.G., Shimmield, T.M., Korte, M., 2009. Age assignment of a diatomaceous ooze deposited in the western Amundsen Sea Embayment after the Last Glacial Maximum. Journal of Quaternary Sciences. doi:10.1002/jqs.1308.

Holt, J.W., Blankenship, D.D., Morse, D.L., Young, D.A., Peters, M.E., Kempf, S.D., Richter, T.G., Vaughan, D.G., Corr, H.F.J., 2006. New boundary conditions for the West Antarctic ice sheet: subglacial topography beneath Thwaites and Smith glaciers. Geophysical Research Letters 33, L09502.

Johnson, J.S., Bentley, M.J., Gohl, K., 2008. First exposure ages from the Amundsen Sea embayment, West Antarctica: the late Quaternary context for recent thinning of Pine Island, Smith and Pope Glaciers. Geology 36, 223–226. doi:10.1130/G24207A.1.

Jordan, T.A., Ferraccioli, F., Vaughan, D.G., Holt, J.W., Corr, H., Blankenship, D.D., Diehl, T.M., 2010. Aerogravity evidence for major crustal thinning under the Pine Island Glacier region (West Antarctica). Geological Society of America Bulletin 122, 714–726. doi:10.1130/B26417.1.

Larter, R.D., Cunningham, A.P., Barker, P.F., Gohl, K., Nitsche, F.O., 2002. Tectonic evolution of the Pacific margin of Antarctica — 1. Late Cretaceous tectonic reconstructions. Journal of Geophysical Research 107, 2345. doi:10.1029/2000JB000052.

Larter, R.D., Gohl, K., Hillenbrand, C.D., Kuhn, G., Deen, T.J., Dietrich, R., Eagles, G., Johnson, J.S., Livermore, R.A., Nitsche, F.O., Pudsey, C.J., Schenke, H.-W., Smith, J.A., Udintsev, G., Uenzelmann-Neben, G., 2007. West Antarctic Ice Sheet change since the last glacial period. Eos Transactions, American Geophysical Union 88, 189–196.

Larter, R.D., Graham, A.G.C., Gohl, K., Kuhn, G., Hillenbrand, C.-D., Smith, J.A., Deen, T.J., Livermore, R., Schenke, H.-W., 2009. Subglacial bedforms reveal complex basal regime in a zone of paleo-ice stream convergence, Amundsen Sea Embayment, West Antarctica. Geology 37, 411–414. doi:10.1130/G25505A.

LeMasurier, W.E., 2008. Neogene extension and basin deepening in the West Antarctic rift inferred from comparisons with the East African rift and other analogs. Geology 36, 247–250.

LeMasurier, W.E., 1990. Late Cenozoic volcanism on the Antarctic plate: an overview. In: LeMasurier, W.E., Thomson, J.W. (Eds.), Volcanoes of the Antarctic Plate and Southern Oceans, American Geophysical Union Antarctic Research Series, 48, pp. 1–17.

Lowe, A.L., Anderson, J.B., 2002. Reconstruction of the West Antarctic ice sheet in Pine Island Bay during the Last Glacial Maximum and its subsequent retreat history. Quaternary Science Reviews 21, 1879–1897.

McAdoo, D.C., Laxon, S., 1997. Antarctic tectonics: constraints from an ERS-1 satellite marine gravity field. Science 276, 556–560.

Müller, R.D., Gohl, K., Cande, S.C., Goncharov, A., Golynsky, A.V., 2007. Eocene to Miocene geometry of the West Antarctic rift system. Australian Journal of Earth Sciences 54, 1033–1045. doi:10.1080/08120090701615691.

Nitsche, F.O., Cunningham, A.P., Larter, R.D., Gohl, K., 2000. Geometry and development of glacial continental margin depositional systems in the Bellingshausen Sea. Marine Geology 162, 277–302.

Nitsche, F.O., Jacobs, S., Larter, R.D., Gohl, K., 2007. Bathymetry of the Amundsen Sea continental shelf: implications for geology, oceanography, and glaciology. Geochemistry Geophysics Geosystems 8, Q10009. doi:10.1029/2007GC001694.

Pollard, D., DeConto, R.M., 2009. Modelling West Antarctic ice sheet growth and collapse through the past five million years. Nature 458. doi:10.1038/nature07809.

Pritchard, H.D., Arthern, R.J., Vaughan, D.G., Edwards, L.A., 2009. Extensive dynamic thinning on the margins of the Greenland and Antarctic ice sheets. Nature 461. doi:10.1038/nature08471.

Rignot, E.J., Bamber, J.L., van den Broeke, M.R., Davis, C., Li, Y., van de Berg, W., van Meijgaard, 2008. Recent Antarctic ice mass loss from radar interferometry and regional climate modelling. Nature Geoscience 1. doi:10.1038/ngeo102.

SPRITE Group, 1992. The southern rim of the Pacific Ocean: preliminary geologic report of the Amundsen Sea–Bellingshausen Sea cruise of the *Polar Sea*, 12 February–21 March 1992. Antarctic Journal of the United States of America 27, 11–14.

Storey, B.C., 1991. The crustal blocks of West Antarctica within Gondwana: reconstruction and break-up model. In: Thomson, M.R.A., Crane, J.A., Thomson, J.W. (Eds.), Geological Evolution of Antarctica. Cambridge University Press, Cambridge.

Uenzelmann-Neben, G., Gohl, K., Larter, R.D., Schlüter, P., 2007. Differences in ice retreat across Pine Island Bay, West Antarctica, since the Last Glacial Maximum: indications from multichannel seismic reflection data. In: Cooper, A.K., Raymond, C.R. (Eds.), Proceedings of the 10th Int. Symposium of Antarctic Earth Sciences, USGS Open-File Report 2007-1047. doi:10.3133/of2007-1047.srp084.

Vaughan, D.G., 2008. West Antarctic Ice Sheet collapse — the fall and rise of a paradigm. Climate Change 91, 65–71.

Vaughan, D.G., Corr, H.F.J., Ferraccioli, F., Frearson, N., O'Hare, A., Mach, D., Holt, J.W., Blankenship, D.D., Morse, D., Young, D.A., 2006. New boundary conditions for the West Antarctic ice sheet: subglacial topography beneath Pine Island Glacier. Geophysical Research Letters 33, L09501.

Weigelt, E., Gohl, K., Uenzelmann-Neben, G., Larter, R.D., 2009. Late Cenozoic ice sheet cyclicity in the western Amundsen Sea Embayment — evidence from seismic records. Global and Planetary Change 69, 162–169. doi:10.1016/j.gloplacha.2009.07.004.

Winberry, P., Anandakrishnan, S., 2004. Crustal structure of the West Antarctic rift system and Marie Byrd Land hotspot. Geology 32, 977–980.

Publication 6.4.5:

Nitsche, F.O., **Gohl, K.**, Larter, R., Hillenbrand, C.-D., Kuhn, G., Smith, J., Jacobs, S., Anderson, J., Jakobsson, M. (2013). Paleo ice flow and subglacial meltwater dynamics in Pine Island Bay, West Antarctica. *The Cryosphere*, v. 7, pp. 249-262, doi:10.5194/tc-7-249-2013.

Author contributions: This paper was primarily written by Nitsche who complied the bathymetric data and analysed most of the glaciomorphological features. Gohl contributed with data and analysis of an inner shelf sedimentary basin and added to the discussion. The other co-authors also contributed to the text with valuable additions and comments. Data were provided by several expeditions led by Gohl, Jakobsson, and Larter.

The Cryosphere, 7, 249–262, 2013
www.the-cryosphere.net/7/249/2013/
doi:10.5194/tc-7-249-2013

The Cryosphere Open Access

Paleo ice flow and subglacial meltwater dynamics in Pine Island Bay, West Antarctica

F. O. Nitsche[1], K. Gohl[2], R. D. Larter[3], C.-D. Hillenbrand[3], G. Kuhn[2], J. A. Smith[3], S. Jacobs[1], J. B. Anderson[4], and M. Jakobsson[5]

[1]Lamont-Doherty Earth Observatory of Columbia University, Palisades, New York, USA
[2]Alfred Wegener Institute for Polar and Marine Research, Bremerhaven, Germany
[3]British Antarctic Survey, Cambridge, UK
[4]Department of Earth Sciences, Rice University, Houston, Texas, USA
[5]Department of Geological Sciences, Stockholm University, Stockholm, Sweden

Correspondence to: F. O. Nitsche (fnitsche@ldeo.columbia.edu)

Received: 9 August 2012 – Published in The Cryosphere Discuss.: 4 October 2012
Revised: 7 January 2013 – Accepted: 11 January 2013 – Published: 8 February 2013

Abstract. Increasing evidence for an elaborate subglacial drainage network underneath modern Antarctic ice sheets suggests that basal meltwater has an important influence on ice stream flow. Swath bathymetry surveys from previously glaciated continental margins display morphological features indicative of subglacial meltwater flow in inner shelf areas of some paleo ice stream troughs. Over the last few years several expeditions to the eastern Amundsen Sea embayment (West Antarctica) have investigated the paleo ice streams that extended from the Pine Island and Thwaites glaciers. A compilation of high-resolution swath bathymetry data from inner Pine Island Bay reveals details of a rough seabed topography including several deep channels that connect a series of basins. This complex basin and channel network is indicative of meltwater flow beneath the paleo-Pine Island and Thwaites ice streams, along with substantial subglacial water inflow from the east. This meltwater could have enhanced ice flow over the rough bedrock topography. Meltwater features diminish with the onset of linear features north of the basins. Similar features have previously been observed in several other areas, including the Dotson-Getz Trough (western Amundsen Sea embayment) and Marguerite Bay (SW Antarctic Peninsula), suggesting that these features may be widespread around the Antarctic margin and that subglacial meltwater drainage played a major role in past ice-sheet dynamics.

1 Introduction

Response of the Antarctic ice sheets to changing climate conditions is one of the largest uncertainties in the prediction of future sea-level (IPCC, 2007). Much of that response will depend on the behaviour of large ice streams, the main conduits of ice flux from the inner portions of the ice sheets to the coast (Bentley, 1987; Bennett, 2003). Understanding how ice streams behaved in the past can improve predictions of future changes (e.g., Stokes and Clark, 2001; Anderson et al., 2002; Vaughan and Arthern, 2007; Livingstone et al., 2012).

The West Antarctic Ice Sheet (WAIS) is considered especially vulnerable, because the WAIS is mainly grounded below sea level (Hughes, 1973), with ice shelf margins exposed to "warm" Southern Ocean water masses (Joughin and Alley, 2011). About 25–35 % of the WAIS is currently draining into the Amundsen Sea, mostly through the Pine Island and Thwaites glaciers (Drewry et al., 1982; Rignot et al., 2008). These ice streams are potential weak points in the ice sheet because they occupy troughs that become steadily deeper towards the WAIS interior and are buttressed by relatively small ice shelves (Hughes, 1973; Vaughan et al., 2006). Theoretical studies have concluded that ice grounding lines are unstable on such reverse gradients and, therefore, once retreat starts it may proceed rapidly (Weertman, 1974; Schoof, 2007), as recently observed under the Pine Island Ice Shelf (Jenkins et al., 2010).

Interest in the Amundsen Sea sector has increased since studies showed that Pine Island and Thwaites Glaciers are presently thinning significantly (Wingham et al., 1998; Shepherd et al., 2001) and that their flow velocity has increased up to 4000 m yr^{-1} (Rignot and Thomas, 2002; Joughin et al., 2010). These changes appear to be caused by strong melting under their floating extensions, driven by the intrusion of relatively warm Circumpolar Deep Water (CDW) onto the continental shelf (Jacobs et al., 1996; Jenkins et al., 1997; Hellmer et al., 1998; Rignot and Jacobs, 2002; Shepherd et al., 2004; Jacobs et al., 2011; Pritchard et al., 2012). As a consequence, these ice streams now account for an ice loss of $\sim$ 50–85 Gt yr^{-1} (Rignot et al., 2008; Pritchard et al., 2009) and already contribute to current sea-level rise (Shepherd and Wingham, 2007; Rignot et al., 2011).

While those observations document ice stream change over the last few decades, detailed marine geological studies of the previously glaciated seafloor have established a framework of past ice sheet extent, flow pattern, and grounding line retreat in the Amundsen Sea sector since the Last Glacial Maximum (LGM), defined as the time interval $\sim$ 23–19 kyr before present (BP) in the Southern Hemisphere (Livingstone et al., 2012). The regional bathymetry shows a large cross-shelf trough system that extends from the present Thwaites and Pine Island ice shelves to the outer continental shelf (Fig. 1; Nitsche et al., 2007). Detailed studies of this trough system revealed that it was occupied by a paleo ice stream and documented an episodic retreat soon after the LGM on the outer and middle continental shelf (Graham et al., 2010; Jakobsson et al., 2011, 2012).

The grounding line of the paleo-Pine Island Ice Stream shifted from the outer shelf to the central shelf by $\sim$ 16 400 cal yr^{-1} BP, followed by another landward shift that left the central shelf covered by an ice shelf from $\sim$ 12 300 to $\sim$ 10 600 cal yr^{-1} BP (Lowe and Anderson, 2002; Kirshner et al., 2012). An episode of ice shelf collapse believed to have been triggered by warm deep water incursion onto the shelf prompted rapid grounding line retreat towards the inner shelf (Kirshner et al., 2012).

The retreat history and dynamics of the paleo ice stream in inner Pine Island Bay is less well understood. New radiocarbon dates from sediment cores located $\sim$ 93 km from the modern grounding line of Thwaites Glacier and $\sim$ 112 km from that of Pine Island Glacier suggest minimum ages for grounded ice retreat of $\sim$ 10 350 and $\sim$ 11 660 cal yr^{-1} BP, respectively (Hillenbrand et al., 2013). Cosmogenic surface exposure ages on erratics from the flanks of Pine Island Glacier in the Hudson Mountains yielded a record of progressive ice thinning for the last $\sim$ 14.5 ka BP that is consistent with the marine record, although the few available dates do not provide much detail about variations in thinning rates or different episodes of retreat of the Pine Island-Thwaites drainage basin (Johnson et al., 2008).

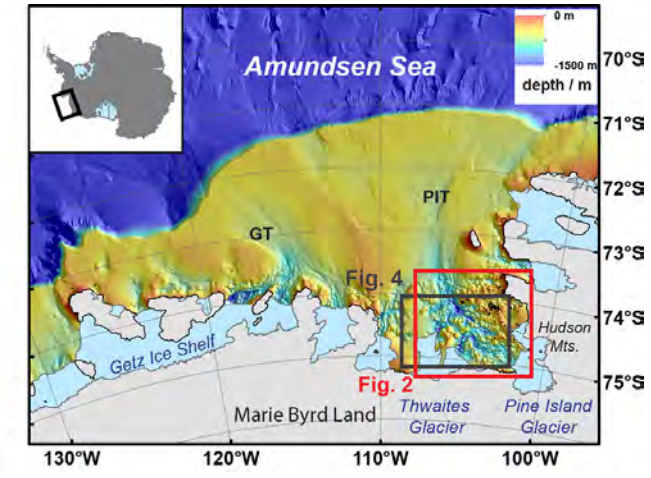

Fig. 1. Bathymetry map of the Amundsen Sea shelf with the red rectangle marking the location of the Pine Island Bay study area in Figs. 2 and 4 (based on Nitsche et al., 2007). PIT marks the Pine Island Trough system and GT the Dotson-Getz Trough System.

Published bathymetry data from Pine Island Bay revealed a complex seafloor dominated by deep bedrock basins with local patches of a generally thin sedimentary cover (Fig. 2b) (Kellogg and Kellogg, 1987b; Lowe and Anderson, 2002). Lowe and Anderson (2002) identified a series of detailed morphological features, which they interpreted as gouges, p-forms and drumlins formed by glacial erosion (their zones 1, 2; see Fig. 2b) and mega-scale glacial lineations formed by ice streams overriding sediment deposits (zone 3). The change in seafloor morphology was linked to changes in subglacial substrate from crystalline bedrock to sediment near the inner to middle shelf transition (Wellner et al., 2001; Lowe and Anderson, 2002). These data also led to the first identification of subglacial meltwater channels on the Antarctic continental shelf (Lowe and Anderson, 2003). Both the presence of subglacial meltwater and the variability of subglacial substrate could have significantly influenced ice stream behaviour, as lubricated beds and sedimentary substrate tend to allow faster ice flow, whereas dryer beds and exposed bedrock may result in higher bed friction (Bennett, 2003). A detailed understanding of the origin of the subglacial features, configurations and substrates could, thus, provide critical information on the dynamics of these ice streams.

Here we present extensive new high-resolution swath bathymetry with almost complete coverage of inner Pine Island Bay (Figs. 1, 2). These data reveal networks of channels eroded by subglacial meltwater, with possible implications for ice flow mechanisms and subglacial water sources of the Pine Island and Thwaites Ice Streams.

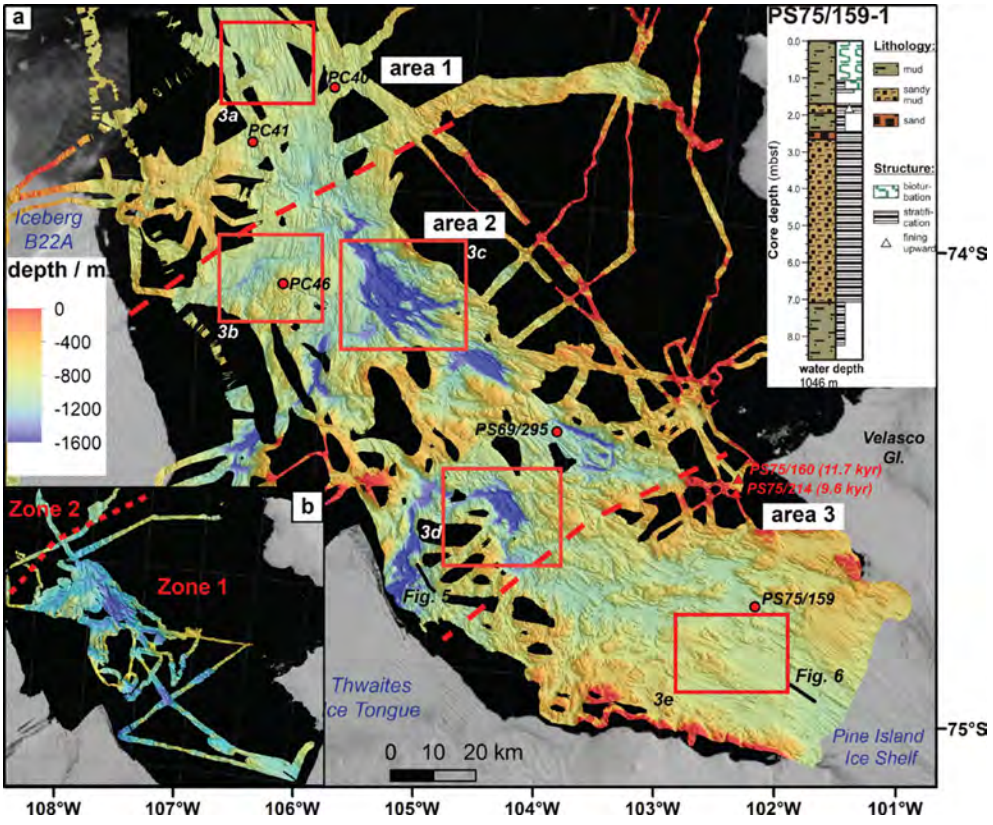

Fig. 2. (a) High-resolution bathymetry map of Pine Island Bay with artificial sun-illumination from the NE. Many of the larger gaps in the data set are due to icebergs at the time of data collection. Dashed red lines mark boundaries between morphological distinct areas 1 to 3. Red boxes mark detailed views shown in Fig. 3. Red dots mark sediment core locations. The inset in the upper right corner shows lithology of sediment core PS75/159. Background image is from the Landsat Image Mosaic of Antarctica (LIMA). **(b)** Multibeam bathymetry data from the same area published previously by Lowe and Anderson (2002, 2003). Red dotted line marks the boundary between the geomorphic zones 1 and 2 defined by Lowe and Anderson (2002).

2 Data and methods

Since 1999, several expeditions have obtained swath bathymetry data in the Pine Island Bay area (Table 1). In particular, unusually favourable sea ice and weather conditions in early 2009 and 2010 permitted the acquisition of high-quality data for most of Pine Island Bay directly seaward of the Pine Island Ice Shelf. Operating equipment included various Seabeam, Kongsberg, and Atlas Hydrosweep swath sonar systems (Table 1). Data were corrected for sound velocity based on numerous CTD and XBT casts. The raw soundings were processed and edited on-board using MB-system (Caress and Chayes, 1996) on R/V *Nathaniel B. Palmer* and RRS *James Clark Ross*, and CARIS/HIPS (Hydrographic Information Processing System) on R/V *Polarstern* and IB *Oden*.

We combined the different swath bathymetry data and generated a new bathymetry grid of Pine Island Bay at 35 m resolution using mbgrid from MB-system. The final grid was imported into ESRI's ArcGIS geographic information system for further analysis.

Simultaneously with its multibeam bathymetry survey, R/V *Polarstern* acquired PARASOUND sub-bottom profiler data. The PARASOUND system is a hull-mounted sub-bottom profiler that transmits two primary frequencies at around 18 kHz to produce a parametric secondary pulse with frequencies selectable between 2.5–5.5 kHz (Grant and Schreiber, 1990). We used a 4 kHz signal and processed it including signal correlation, basic filtering (2–6 kHz band-pass), amplitude normalisation and noise reduction. Maximum penetration depths were digitised by hand and georeferenced using the ship GPS navigation (Rackebrandt, 2006). Sub-bottom data collected on other cruises listed in Table 1 were not available for this study or were of poor quality caused by the rough terrain.

Multichannel seismic profiling in proximity to the ice shelf edge of the Pine Island Glacier was conducted from R/V *Polarstern* in 2010 with a source array consisting of two generator-injector (GI) air guns shot every 6 s, and recorded with a 600 m long analogue hydrophone streamer of 96 channels. We applied standard seismic data processing including a predictive deconvolution filter for the removal of the

Table 1. Expeditions with multibeam data used for this compilation.

Cruise	Ship	Year	System	PI
NBP9902[a]	NB Palmer	1999	SeaBeam 2112	J. Anderson (Rice U.)
NBP0001[a]	NB Palmer	2000	SeaBeam 2112	S. Jacobs (LDEO)
ANT-XXIII/4	Polarstern	2006	HydroSweep DS2	K. Gohl (AWI)
NBP0702[a]	NB Palmer	2007	EM 120	S. Jacobs (LDEO)
JR179	James C. Ross	2008	EM 120	R. Larter (BAS)
OSO0708[b]	Oden	2008	EM 120	M. Jakobsson (U. Stockholm)
NBP0901[a]	NB Palmer	2009	EM 120	S. Jacobs (LDEO)
ANT-XXVI/3	Polarstern	2010	HS DS2	K.Gohl (AWI)

[a] From Antarctic and Southern Ocean Data Portal (http://www.marine-geo.org/).
[b] From Oden Mapping Data Repository (http://oden.geo.su.se/)

receiver and source ghost signal and a bandpass filter of 15–100 Hz.

3 Results

The compilation of swath bathymetry data resulted in a comprehensive 35 m-grid that covers large parts of Pine Island Bay (Fig. 2). The grid includes most of the main paleo-ice stream trough while data gaps remain in shallow areas northeast of the trough and around Iceberg B22A, which was formerly an ice tongue extending from Thwaites Glacier.

The overall seafloor morphology varies significantly over the mapped region, but three areas with different seabed characteristics can be distinguished. The seafloor morphology of the northernmost study area 1 (north of $\sim 74°$ S) is characterised by moderate relief with water depths in the range 500–1100 m, gradually shoaling seaward and dominated by linear features (Fig. 2). This pattern continues northward towards the mid-shelf, where it changes into megascale glacial lineations (MSGL) interrupted by grounding zone wedges as described by Graham et al. (2010) and Jakobsson et al. (2012). Area 2 adjacent to the southeast, between 74.8° S and 74° S, is characterised by a very rugged terrain with shallow ridges and deep (1400–1650 m) basins. The innermost section (area 3) directly in front of the Pine Island Ice Shelf has a moderate relief with water depths between 500 and 1000 m, clearly defined parallel, linear features orientated along the trough axis, and a few ridges and mounds orientated oblique to the trough axis.

3.1 Linear features

Pine Island Bay is characterised by various types of linear subglacial features (Fig. 3). The central part of area 1 is dominated by drumlin-shaped ridges, which are elongated and tear-shaped, with some "whaleback" ridges and crag-and-tail features (Fig. 3a). These mostly parallel or sub-parallel features are 25–80 m high, 300–1500 m wide and between 1500 and 8000 m long. They taper from south to north, thus, indicating paleo-ice flow in that direction (Bennett and Glasser, 1996). Crossing acoustic sub-bottom profiles demonstrate that the sedimentary cover of these bedforms is very thin or absent (Figs. 4, 5) and suggests formation of the crag-and-tail and drumlin shapes in a hard substrate such as stiff till or rock. The absence of a thick sediment cover is consistent with evidence from seismic profiles showing that the seafloor south of $\sim 73.5°$ S is mainly underlain by acoustic basement interpreted as crystalline bedrock (Lowe and Anderson, 2002, 2003; Uenzelmann-Neben et al., 2007). This has also been observed in inner sections of several other Antarctic paleo-ice stream troughs (e.g., Wellner et al., 2001; Ó Cofaigh et al., 2002; Larter et al., 2009). Sediment cores from area 1 recovered thin layers (< 2.2 m) of mud intercalated with diamicton (site PC40; Lowe and Anderson, 2003) and silty diamicton (site PC41; Lowe and Anderson, 2002), respectively (see Fig. 2 for locations). The occurrence of diamicton in such shallow depths also indicates that these features were probably formed subglacially.

The central area 2 contains fewer drumlin-shaped features. Instead the data show widespread grooves, mainly on ridges and bedrock highs (e.g., Fig. 3b, c, d). Most of the grooves are 2–10 m deep, 50–150 m wide and incised into the underlying substrate. They generally follow the orientation of the main trough and are likely to have been created by ice flowing across topographic highs (Bennett and Glasser, 1996).

The smoother, innermost area 3 is also dominated by linear features, here 10–20 m high, 200–400 m wide and 2–8 km long (Fig. 3e). In contrast to the other regions, many of these lineations appear to be depositional, with elongation ratios $> 10:1$ comparable to that of MSGLs (Stokes and Clark, 2001). Several other features are drumlin-shaped, but the lack of good-quality acoustic sub-bottom data from this area precludes attribution of their formation in a sedimentary substrate. However, multichannel seismic data from the southern part of area 3 show that part of this section consists of > 100 m of sedimentary strata (Fig. 6). Following examples from other Antarctic shelf areas we interpret these features as glacial lineations and drumlins that are more typical for sedimentary substrate (e.g., Wellner et al., 2001; Ó Cofaigh et al., 2002).

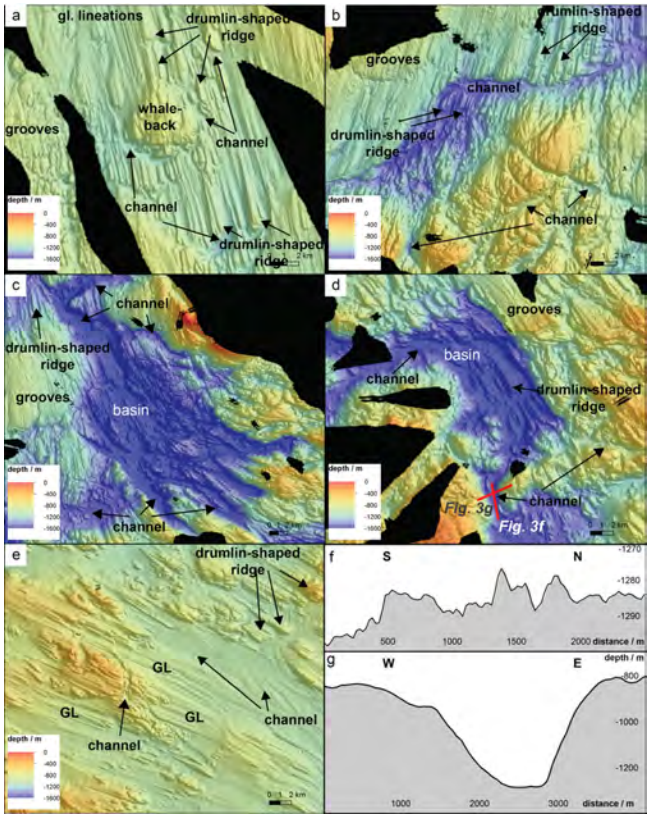

Fig. 3. (a–e) Detailed examples of morphological features including glacial lineations (GL), basins, channels, drumlin-shaped ridges and grooves. **(f)** Undulating thalweg and **(g)** cross-section of large channel marked in **(d)**.

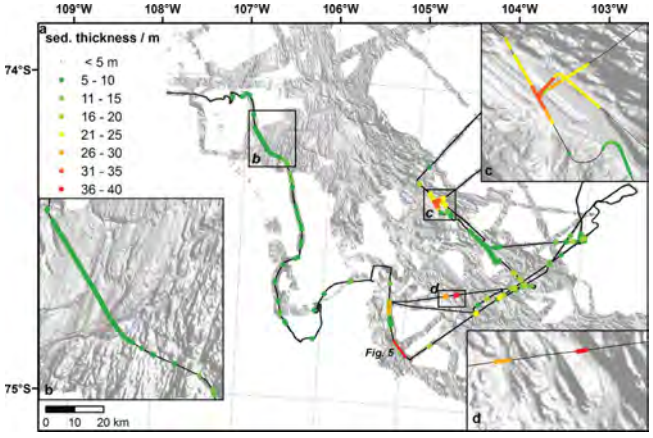

Fig. 4. (a) Sediment thickness (coloured dots) derived from PARASOUND data, modified from Rackebrandt (2006). Black line indicates segments of R/V *Polarstern* ANT-XXIII/4 ship track where no significant sediment thickness was identified. Multibeam bathymetry data with artificial sun-illumination are shown as background. Details in insets **(b)**, **(c)**, and **(d)** show that thicker sediment deposits occur mainly in channels, but not in every channel. Location of Fig. 5 is marked by red line.

The comprehensive data coverage allows us to map the orientation of these linear features in detail (Fig. 7). The parallel and sub-parallel features are oriented from 285–290° in the inner part of area 3 (Fig. 2) and progressively change in orientation through area 2 (330–340°) to 350–360° in outer area 1. These directions correspond to the general orientation of the paleo-ice stream trough system.

3.2 Basins

The dominant morphological features of area 2 are slightly elongated, deep (up to 1650 m), and several kilometre wide seafloor depressions more than 300 m below the surrounding seafloor (800–1100 m). Often the edges of these basins are marked by steep slopes, which are intersected by numerous channels (Fig. 3c, d). Maximum water depths are several hundred meters greater than near the present ice shelf front (1000–1100 m; Fig. 2a). Lowe and Anderson (2003) have interpreted some of the basins as features initially eroded into bedrock by ice and later modified by meltwater flow. Similar basins have been observed in several other inner shelf locations around Antarctica (Wellner et al., 2006) including the Dotson-Getz Trough (Larter et al., 2009), and Marguerite Bay (Anderson and Fretwell, 2008).

The deepest parts of some basins show linear or drumlin-shaped features (Fig. 3d), indicating they were filled with grounded ice during previous glaciations. Acoustic sub-bottom profiles from the inner shelf generally show sediment cover < 5 m thick, but with localised, 10–40 m thick sediment pockets in some of the deepest basins (Fig. 4; Rackebrandt, 2006). Seismic lines crossing the northern basins have revealed over 75 m (> 50 m) of sediment fill in some places (Uenzelmann-Neben et al., 2007), and at least 300 m of sediment near the Pine Island Ice Shelf edge (Fig. 6). Sediment cores from the basins of area 2 have typically recovered long (up to 10 m) sequences of unconsolidated mud and sandy mud, occasionally with a diamicton at the core base (e.g., site PS69/295-1; Ehrmann et al., 2011). These pockets of unconsolidated sediment have likely been deposited since the last retreat of grounded ice from these basins (Smith et al., 2009b).

3.3 Channels

The detailed bathymetry shows two types of channels in Pine Island Bay. The first type connects the deep basins and is 200–400 m deep, 1–2 km wide, and 10–15 km long (Figs. 2, 3c, d, f, g). The second type is smaller and more variable in size and geometry, 10–200 m deep, 150–1500 m wide and 2–25 km long (Fig. 3a–e). Most channels of both types are anastomosing with undulating and meandering thalwegs. Channel orientation varies, with some connecting to the main channels and others almost perpendicular

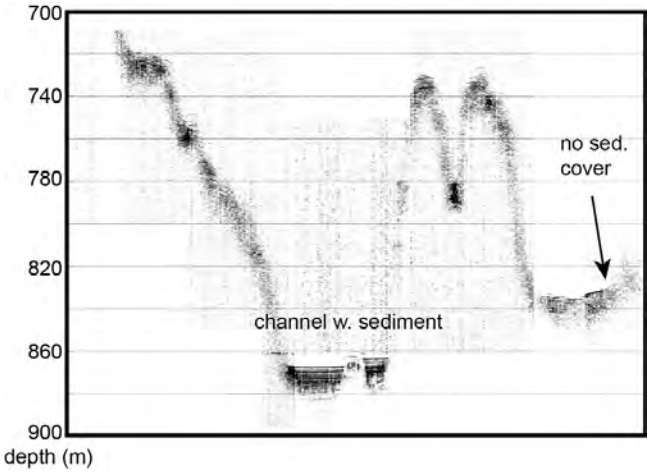

Fig. 5. PARASOUND example showing ∼ 20 m of sediment fill in the channels and no sediments on slopes and ridges. See Fig. 4 for location.

to the paleo-ice flow defined by glacial lineations (Fig. 7, blue lines). The undulating and meandering geometry of the channels (Fig. 3f) and their oblique orientation with regard to the general trough direction indicate that they were not formed by grounded ice flow. A sediment core from a channel in area 2 (PC 46) recovered a ∼ 0.5 m thick section of mostly sand and gravel at the top that may have originated from the bed-load of former meltwater flows (Lowe and Anderson, 2003). Similar channels have been observed in inner shelf regions of other paleo-ice stream troughs around Antarctica (e.g., Wellner et al., 2006; Anderson and Fretwell, 2008; Smith et al., 2009b), on previously glaciated margins in the Northern Hemisphere (e.g., Booth and Hallet, 1993; Jorgensen and Sandersen, 2006), and onshore in the Dry Valleys in the Transantarctic Mountains (Lewis et al., 2006).

3.4 Thickness of unconsolidated sediments

The maximum sub-bottom penetration depth of the PARASOUND signal in areas 2 and 3 indicates the presence or minimum thickness of unconsolidated sediments (Fig. 4). Most of the track does not show any sedimentary cover, confirming earlier interpretations that the inner Pine Island Bay seafloor consists mostly of a hard substrate, presumably bedrock. However, some channels and basins are characterised by significant sediment infill (> 5 m) (Figs. 4c, 5), while other channels are barren of unconsolidated sediments. Since the PARASOUND signal is unlikely to penetrate consolidated stiff till, most sediment layers visible in the PARASOUND data probably correspond to sands, silts and muds that have not been consolidated by overriding ice and, therefore, are likely to be of post-glacial origin. Turbidity currents or other mass transport mechanisms may have concentrated sediment in the deeper basins by scouring and redepositing material from shallower shelf areas or other channels, but the available acoustic sub-bottom data are still too sparse to clearly verify such a pattern.

4 Discussion

This new compilation of high-resolution bathymetry from Pine Island Bay allows a more detailed analysis and interpretation of ice flow and subglacial meltwater drainage than in previous studies (Kellogg and Kellogg, 1987b; Lowe and Anderson, 2002, 2003).

4.1 Paleo-ice flow

Linear morphological features observed in Pine Island Bay are typical of Antarctic paleo-ice stream troughs (e.g., Canals et al., 2000; Ó Cofaigh et al., 2002; Wellner et al., 2006; Dowdeswell et al., 2007). Their orientation can be interpreted as the direction of past ice flow (Boulton and Clark, 1990; Clark, 1993). In area 3, i.e., in front of the present Pine Island Ice Shelf, the past ice flow was in the same direction as the present flow of Pine Island Glacier. The flow direction turned slightly northward in area 2 at the confluence with the paleo-ice stream extending offshore from Thwaites Glacier, and then followed the outline of the main trough (Fig. 7, black lines).

A few lineations at the southern edge of the data between 104° W and 106° W indicate that streaming ice flow also occurred in the area between Pine Island and Thwaites glaciers, which indicates that during the LGM the ice streams were wider than today or, less likely, their trunks shifted their locations.

The flow lines joining the main flow north of ∼ 74.5° S document the confluence of Pine Island and Thwaites glaciers, and farther north the convergence with Smith Glacier (Nitsche et al., 2007; Graham et al., 2010). This flow convergence would have resulted in an increase in flow speed, which is suggested by the higher elongation ratios of lineations and other subglacial bedforms at this point, compared to those of features further south.

Previous studies of paleo-ice stream troughs on the Antarctic continental shelf have shown that the innermost shelf usually consists of rugged terrain similar to the central part of Pine Island Bay, i.e., area 2, and that this morphology often changes in the mid-shelf region towards a smoother topography and well-defined, more elongated subglacial lineations (MSGL) (see review in Livingstone et al., 2012). This change usually coincides with the transition from exposed bedrock on the inner shelf towards sedimentary substrate on the middle-outer shelf, the rugged terrain resulting from subglacial bedrock erosion of the sediment cover (Wellner et al., 2006). Based on these differences in seafloor morphology and underlying seismic character, Lowe and Anderson (2002) distinguished two zones in Pine Island Bay. They describe their innermost zone 1 as being dominated by

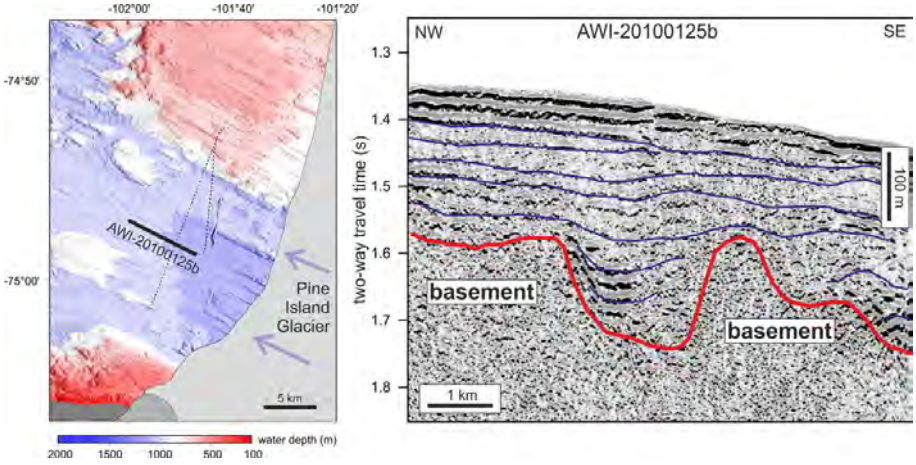

Fig. 6. Seismic profile (bold solid line) recording a sedimentary basin of at least 300 m thickness off the ice shelf edge of Pine Island Glacier. Dotted lines mark other seismic profiles. Blue lines in seismic section mark a set of horizons within the sedimentary strata. The vertical scale bar is based on an estimated seismic velocity of 2000 m s^{-1} in the sediments. See Fig. 2 for location.

crystalline bedrock and observed that the onset of ice streaming coincided with the transition to sedimentary substrate which dominates in zone 2.

Area 1 of this paper basically coincides with zone 2 of Lowe and Anderson (2002), while the new bathymetry compilation reveals a distinct change in seafloor morphology near the present ice shelf, allowing us to subdivide their zone 1 into areas 2 and 3. Area 3 is less rugged and the shape of several features indicates a depositional origin rather than bedrock erosion (Figs. 2, 3). The absence of deep basins in this area suggests that they were either not excavated, e.g., due to different substrate properties or, if such basins were formed in the past, they have been filled with sediment as indicated by seismic data (Fig. 6), e.g., while the grounding line of the ice stream was located farther north. Smooth bottom morphology of some other deep basins in area 2 suggests they might be partly filled with sediment as well.

Lowe and Anderson (2002, 2003) argued that sedimentary substrate is largely absent south of the transition from sedimentary strata on the middle shelf to acoustic basement on the inner shelf at $\sim 73.5°$ S. The only exception is a small patch of ~ 100 m thick, layered sediments overlying acoustic basement on the up-stream flank of a crystalline bedrock outcrop that was recorded directly west of the Pine Island Glacier front by Kellogg and Kellogg (1987a). Lowe and Anderson (2003) assumed that these sediments are related to subglacial meltwater flow and form a seaward thinning wedge. Seismic profiling from R/V *Polarstern* in area 3 (Fig. 6) reveals > 300 m thick layered sedimentary strata extending over at least 10 km, however. The near-horizontal strata indicate basin-wide regular vertical deposition more indicative of basin fill than a wedge. Moreover, our multibeam data from this region clearly show subglacial lineations, which closely resemble sedimentary features of the mid- and outer shelf areas (Fig. 3e). This observation may imply that either the near-surface sediments are subglacial till or, if the assumption of Lowe and Anderson (2003) is correct, Pine Island Glacier overrode the subglacial meltwater sediments after their deposition. The lithology of core PS75/159-1 (Fig. 2) does not confirm the presence of till or meltwater deposits, but it does document the presence of unconsolidated sediments near the seabed (Gohl, 2010).

Based on observations of present ice flow and models of shear stress, Joughin et al. (2009) concluded that the main trunk of the modern Pine Island Glacier is resting on a mixed bed of soft sedimentary strata alternating with a hard substrate, possibly consisting of crystalline bedrock. This conclusion was recently supported by analyses of bed roughness under Pine Island Glacier and its tributaries (Rippin et al., 2011). The presence of crystalline bedrock and sedimentary beds in inner Pine Island Bay demonstrates that such a mixed bed also existed there. The sedimentary substrate possibly enabled or facilitated fast ice flow (e.g., Studinger et al., 2001). This finding implies that bed conditions and resulting flow of the paleo-Pine Island Ice Stream varied much more spatially than previously thought.

The general scarcity of sediment cover in areas 1 and 2 also suggests rapid post-LGM grounding-line retreat from the middle to inner shelf, assuming that subglacial sediment transport rates were as high as envisaged (e.g., Alley et al., 1989; Nygård et al., 2007). Although several shoals cross these areas, there is no geomorphological indication of a prolonged still stand of the grounding line, which would have resulted in the formation of a sedimentary ridge or grounding zone wedge as observed farther north in the Pine Island Trough (e.g., Lowe and Anderson, 2002; Graham et al., 2010; Jenkins et al., 2010; Jakobsson et al., 2011, 2012). Rapid deglaciation is also consistent with the radiocarbon chronology of sediment cores that indicates fast grounding-line retreat from a grounding zone wedge north of the study

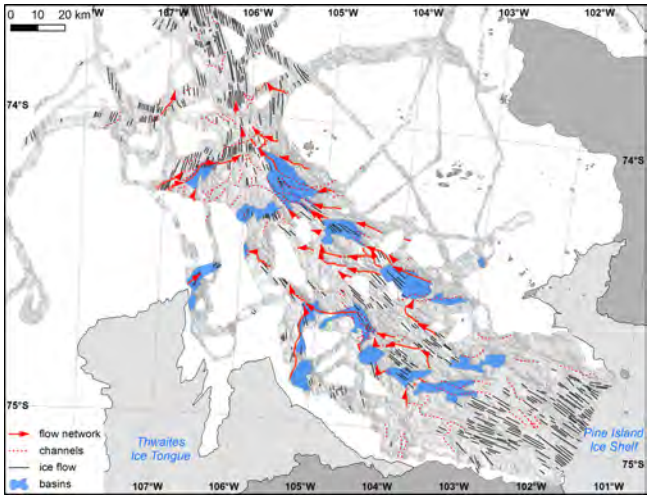

Fig. 7. Digitised lineations indicating ice flow (black), minor (dotted red) and major meltwater channels (red with arrows). The extent of swath bathymetry data is shown as grey shaded area. Light and dark grey shaded areas represent ice shelves and land, respectively, from the Antarctic Digital Database v6 (http://www.add.scar.org/). Note that smaller channels are cutting into the bottom of some larger basins.

area at ∼12 cal kyr (Kirshner et al., 2012) and from inner Pine Island Bay before ∼10.3–11.7 cal kyr (Hillenbrand et al., 2013).

While there is evidence that grounded ice retreated rapidly from the mid-shelf to the inner shelf and probably reached within 93 km of its current position as early as ∼11 kyr ago (Hillenbrand et al., 2013), retreat might have been slower across area 3, allowing sediments to be deposited in inner Pine Island Bay. This could have been a result of ice-shelf buttressing caused by local pinning of grounded ice on islands and peninsulas surrounding inner Pine Island Bay. Modern observations indicate that the grounding line of Pine Island Glacier has retreated by ∼30 km since 1973 (Jenkins et al., 2010), with ∼20 km of this retreat occurring rapidly from 1992 to 2007 (Rignot, 1998; Shepherd et al., 2001; Jenkins et al., 2010). A stable grounding line deep within inner Pine Island Bay, caused by buttressing from the surrounding land (Fig. 1) or pinning on the shallower ridges in this area for much of the Holocene, could have provided a source for the observed sediments in this area. In addition, some of the sediments of 300 m thick sequence could have been deposited during previous glaciations and escaped excavation during the last glacial period. Determining the origin and age of these sediments will require longer sediment cores than can be recovered with standard gravity and piston coring.

4.2 Meltwater flow

Studies that first reported some of the seafloor basins and channels in Pine Island Bay interpreted them as meltwater features (Lowe and Anderson, 2002, 2003). The more detailed mapping of these basins and channels allows reconstruction of the associated flow network (Fig. 7). The undulating character of many channels and their deep incision into bedrock strongly suggests subglacial formation, and the extensive network of channels and basins indicates the former presence of abundant subglacial meltwater. In general, low basal shear stress over sedimentary substrate facilitates fast ice flow, whereas high basal shear stress over hard, rugged bedrock results in slow flow (Bell et al., 1998; Wellner et al., 2001). However, abundant subglacial meltwater in innermost Pine Island Bay could have lubricated the paleo-ice stream bed, allowing fast ice flow across stretches of rugged bedrock topography if the volume of meltwater was sufficient to flow both within major channels and across non-channelised areas (cf. Kamb, 2001; Bell, 2008). If meltwater flow was restricted to a channel system, then basal shear stresses are likely to have been higher, with the possibility that rugged bedrock perturbations acted as localised sticky spots.

Basins and channels are most abundant in area 2. No large channels are present in area 3 and north of area 1, although there are a few smaller ones (Fig. 3e). Subglacial meltwater channels with dimensions greater than the spatial resolution of multibeam swath bathymetry systems have been observed in sedimentary substrate underlying modern Antarctic ice streams (e.g., King et al., 2004). Large channels have also been reported near the mouth of the Belgica Trough (Noormets et al., 2009) and on the mid-shelf in the Ross Sea (Wellner et al., 2006), but overall there is a lack of such features in sediments covering the mid- and outer shelf sections of all known Antarctic paleo-ice stream troughs (Ó Cofaigh et al., 2005). One mechanism to explain their absence is that water could be transported through the sediment, i.e., by Darcian flow within the subglacial till, which has a higher permeability than the acoustic basement (Kamb, 2001). Although low till permeability might not be sufficient to transport large amounts of water quickly, microscopic studies on tills from Antarctic paleo-ice stream troughs have revealed ductile deformation structures in soft till overlying dewatered stiff till (Reinardy et al., 2011). This observation suggests significant basal meltwater transfer within the subglacial sediment bed. The water could also be distributed and transported in a broad, thin layer at the ice-sediment interface (Walder and Fowler, 1994; Noormets et al., 2009), which is apparently occurring at the bed of some modern ice streams (e.g., Peters et al., 2007). In these cases, constant reworking of sediment could prevent the establishment of a permanent channel system. Since overriding grounded ice probably overprinted previously formed sedimentary features on the Antarctic continental shelf throughout the last glacial period, the subglacial sedimentary bedforms observed today in soft substrate areas

are likely to be only the last snapshot of basal conditions just before the grounded ice retreated (e.g., Smith et al., 2007; King et al., 2009). For smaller meltwater volumes, transport in the sediment layer is the most likely scenario, while we would expect larger, episodic floods to create meltwater channels in sediments underneath grounded ice. If such floods happened earlier during the last glacial period or during previous glaciations, their deposits could have been reworked by grounded ice during the last ice stream advance.

4.3 Potential sources of meltwater

Although we can measure the size of the basins and channels, it is unclear when, to what extent and how long they contained meltwater. It is unlikely that all large basins were completely filled with meltwater. Instead, the basins were probably partially filled with meltwater at the bottom and ice above. And even if different basins harboured meltwater at different times, a significant amount of sub-glacial meltwater would have been required to form such an extensive channel network.

The most common source of subglacial water is melting at the bottom of the ice sheet due to a combination of ice thickness, geothermal heat flux at the bed, and frictional heating due to rapid ice flow (Joughin et al., 2004; Llubes et al., 2006). Meltwater production could be enhanced by a higher geothermal gradient underneath parts of the WAIS (Shapiro and Ritzwoller, 2004). Joughin et al. (2009) modelled a basal melt rate of $1.7\,km^3\,yr^{-1}$ for the present day Pine Island Glacier system, which is significantly higher than previous, conservative estimates of 0.24–$0.5\,km^3\,yr^{-1}$ by Lowe and Anderson (2003). If the water flowed continuously through the $0.49\,km^2$ cross-section of one of the major channels (Fig. 3g), it would trickle along at $0.1\,mm\,s^{-1}$, and increase only to a few $mm\,s^{-1}$ if the channel was mostly filled by ice. Although sufficient to transport the meltwater generated by pressure melting, it seems unlikely that such low flow rates could erode the observed channel network.

Joughin et al. (2009) calculated a higher melt rate of $3.5\,km^3\,yr^{-1}$ for the current Thwaites Glacier. If the potential meltwater production of the Thwaites Glacier was also larger than that of Pine Island Glacier in the past, we would expect a major contribution from the Thwaites system to the meltwater network in Pine Island Bay. Indeed, the bathymetry shows several large channels originating from the grounding line of Thwaites Glacier, indicating meltwater contribution from this system. The channel network also indicates that meltwater entered the paleo-ice stream trough from the Velasco Glacier and northern Hudson Mountains northeast of the main trough (Figs. 2, 7), where no large ice stream is currently located. There, thicker ice and a modified ice flow pattern during periods of maximum glaciation could have created basal conditions that also favoured subglacial melting.

An alternative or additional source of meltwater could be related to subglacial volcanic activity. The hinterland of the Amundsen Sea contains numerous volcanoes including the Hudson Mountains just east of Pine Island Bay (LeMasurier, 1990). Studies have shown that volcanoes, in the Marie Byrd Land volcanic province were active during the Pleistocene when this area was covered with an ice sheet (Blankenship et al., 1993; Wilch et al., 1999). An unusual reflector in radar data suggests a volcanic eruption in the Hudson Mountains as recently as 2200 yr ago (Corr and Vaughan, 2008). A volcanic eruption has the potential to produce large amounts of meltwater and, thus, could trigger a large flood event (Roberts, 2005; Bennett et al., 2009). If it covered a large area with volcanic ash that reduced albedo and facilitated surface melting, water might penetrate through the glacier to its bed and form highly erosive moulins as in Greenland today (Eyles, 2006; Sundal et al., 2011).

Overall, it seems likely that meltwater erosion of these large basins and channels occurred episodically over many glacial cycles. The question remains as to when these basins and channels formed and when they were last subject to subglacial water storage and drainage.

4.4 Timing of meltwater flow and channel development

The deep ($> 300\,m$) incisions of the large channels and the formation of the deep bedrock basins suggest that these features formed as a result of many flow events over the period of many glacial cycles, possibly since the Mid-Miocene (Lowe and Anderson, 2003). Although we do not know the precise nature of the bedrock, the lack of visible reflections in available seismic data suggests that these are not sedimentary, but rather igneous or metamorphic rocks, which are less erodible and were reported from several outcrops in the Pine Island Bay region (e.g., Debese et al., 2012; Sheen et al., 2012).

The development of similar channels and basins over many glacial cycles has also been suggested for the neighbouring Getz and Dotson areas (Graham et al., 2009; Smith et al., 2009b) and Marguerite Bay (Anderson and Fretwell, 2008). A larger number of smaller channels and basins may have been active during early glaciations, with some capturing more of the ice and meltwater flow over time and, as a result, have become larger, capturing more and more of the subglacial meltwater flow. In addition to meltwater flow, formation of the larger basins could have been initiated by overdeepening processes that are often observed under glaciers (Cook and Swift, 2012).

So far no dates have been reported that would directly allow the identification and timing of different flow events. Based on thick coarse-grained layers found in a sediment core from a smaller channel (PC46; Fig. 2) Lowe and Anderson (2003) suggested that a major outburst flood occurred at the end of the last glaciation, since these units are not overlain by post LGM sediments. However, Smith et al. (2009b) concluded that similar layers recovered from subglacial meltwater channels in front of the Dotson-Getz ice shelves might

have been re-deposited from the steep sides of the channels by gravitational down-slope processes. One of their studied cores recovered LGM till, but no sediments of possibly fluvial origin, giving evidence for channel formation before the last grounded ice advance.

As sediment core PC46 was taken from a smaller side channel (Fig. 2), that core may not be representative of the entire flow network. No sediment cores have been recovered from the main channels despite several attempts, but numerous cores successfully targeted the basin infills of area 2. Some of these basins contain several 10 s of metres of sediment and the up to 10 m-long cores recovered unconsolidated fine-grained glacimarine sediments of probable Holocene age (Ehrmann et al., 2011), but no thick units of coarse-grained fluvial sediments similar to those in core PC46 were found as would have been expected from meltwater flow deposits at the LGM or during the last deglaciation. We cannot rule out the possibility that LGM meltwater flow deposits are present within the basins at larger sub-bottom depth, i.e., beyond the reach of standard gravity and piston coring. However, the recovery of a basal diamicton possibly representing a subglacial till at site PS69/295-1 (Ehrmann et al., 2011), combined with the lack of sediment indicating recently active channel-basin networks (Figs. 4, 5), suggests that such flows were mainly active during pre-LGM times and that grounded ice-sheet advance during more recent glacial periods eroded the coarse material and transported it offshore.

Kirshner et al. (2012) argued that a widespread draping silt unit within Pine Island Bay (Unit 1) may have been sourced by plumes of sediment-laden water flowing from beneath the Pine Island ice stream based on its unique character (well sorted silt with virtually no ice-rafted debris [IRD] or microfossils) and the rapid and dramatic change from more proximal glacimarine sedimentation to this style of sedimentation at $\sim$ 7000 cal yr BP.

4.5 Comparison with other Antarctic meltwater networks

The subglacial meltwater features in Pine Island Bay are not unique. Similar features have been observed in other parts of the inner Antarctic continental shelf (Wellner et al., 2006) including Marguerite Bay (Ó Cofaigh et al., 2002, 2005; Anderson and Fretwell, 2008), the Dotson-Getz Trough (Larter et al., 2009; Smith et al., 2009b), and the western Antarctic Peninsula (Evans et al., 2004; Domack et al., 2006). In addition, similar terrestrial meltwater features discovered in the Transantarctic Mountains have been interpreted to have formed between 12.2 and 14.4 Myr ago through erosion by fast-flowing subglacial meltwater during multiple flow events (Sugden and Denton, 2004; Lewis et al., 2006).

There is increasing evidence for active subglacial lakes below the Antarctic ice sheets (Bell et al., 2007; Fricker et al., 2007; Smith et al., 2009a). Satellite altimetry data show changes in surface elevations that indicate draining of some lakes and refilling of others (Wingham et al., 2006; Fricker et al., 2007). Fricker and Scambos (2009) identified a series of 20–30 km-wide subglacial lakes close to the grounding line of Mercer and Whillans ice streams (Siple Coast, West Antarctica). These dimensions are of the same order as the large basins described in this paper, although the bedrock geology might be different. Similar to the proposed mechanisms described by Fricker and Scambos (2009), subglacial meltwater draining into inner Pine Island Bay could have collected in one basin until a water pressure threshold was reached. When water pressure lifted the ice barrier in the connecting channels, the water drained into the next basin downstream. More generally, the observed bedrock structures in Pine Island Bay seem likely to channelise meltwater flow between basins at the expense of sheet flow at the ice-bed interface.

Details on scales up to a few hundred metres are usually not resolved in radar data. High-resolution swath bathymetry data capable of resolving such features on the continental shelves of formerly glaciated margins can, thus, provide valuable information about subglacial meltwater flow and help to understand drainage processes at the base of contemporary ice sheets.

5 Conclusions

This compilation of old and new swath bathymetry data from Pine Island Bay provides a coherent and detailed picture of a formerly glaciated inner continental shelf allowing more complete mapping and analysis of bedforms than previously available from discrete swath tracks. The resulting map reveals details that are critical for the understanding of past ice flow behaviour, subglacial processes and their spatial variability.

Our compilation confirms and extends the general zonation of erosional subglacial bedforms in crystalline bedrock on the inner shelf and subglacial depositional features on sedimentary substrate on the mid-shelf as previously identified by Lowe and Anderson (2002). Added here is a zone nearest the Pine Island Ice Shelf front characterised by smooth topography and showing up to 300 m of sediments. This finding documents that sedimentary substrate on the inner shelf of Pine Island Bay is more widespread than previously thought. The complex pattern of rugged crystalline basement alternating with smooth sedimentary substrate in inner Pine Island Bay is consistent with observations under the modern Pine Island Glacier. The seafloor topography and sediment presence of inner Pine Island Bay indicate that post-LGM floating and partially grounded ice may have persisted in the area directly in front of the modern ice front for a longer time than in other parts of the Pine Island Trough system.

The orientation and location of the complex subglacial meltwater channel network suggest significant meltwater supply not only from Pine Island Glacier, but also from the

Thwaites Glacier and from the Hudson Mountains. Meltwater volumes currently generated underneath the Pine Island and Thwaites glaciers would probably not be sufficient to generate the observed channel-basin network if discharged continuously. More likely this network was generated over several glacial cycles by episodic flow events caused by storage and release of meltwater through subglacial lakes, with possible additional contributions from subglacial volcanic eruptions.

Comparison of basin dimensions with those of modern subglacial lakes suggests that the active systems might be connected by channel networks resembling those in Pine Island Bay. The increasing number of paleo-meltwater features discovered by high-resolution swath bathymetry on different parts of the Antarctic continental margin provides a detailed, view of subglacial flow systems that should allow further consideration of related hydrodynamic processes and ice dynamics. A better understanding of the timing and nature of subglacial meltwater flow in Pine Island Bay will require more targeted sediment sampling from the large basins and channels, some beyond the range of standard piston coring, and improved sub-bottom or high-resolution seismic coverage of these features.

Acknowledgements. We thank the masters and crews of the research vessels, R/V *Nathaniel B. Palmer*, RRS *James Clark Ross*, IB *Oden* and R/V *Polarstern* for their support during the data acquisition. Numerous people were directly involved in processing and editing the data. Nick Rackebrandt (University of Bremen) provided the map with estimated sediment thickness in Pine Island Bay. F. Nitsche was supported by NSF grants ANT 08-38735 and ANT 06-32282, S. Jacobs by NSF grant ANT 06-32282 and J. Anderson by NSF/ARRA grant ANT-0837925. The IB Oden expedition OSO0708 was carried out as collaboration between Swedish Polar Research Secretariat, the Swedish Research Council and the US National Science Foundation (NSF).

Edited by: C. R. Stokes

References

Alley, R. B., Blankenship, D., Rooney, S. T., and Bentley, C. R.: Sedimentation beneath ice shelves – the view from Ice Stream B, Mar. Geol., 85, 101–120, 1989.

Anderson, J. B. and Fretwell, L. O.: Geomorphology of the onset area of a paleo-ice stream, Marguerite Bay, Antarctic Peninsula, Earth Surf. Processes, 33, 503–512, 2008.

Anderson, J. B., Shipp, S. S., Lowe, A. L., Wellner, J. S., and Mosola, A. B.: The Antarctic Ice Sheet during the Last Glacial Maximum and its subsequent retreat history: a review, Quaternary Sci. Rev., 21, 49–70, 2002.

Bell, R. E., Blankenship, D. D., Finn, C. A., Morse, D. L., Scambos, T. A., Brozena, J. M., and Hodge, S. M.: Influence of subglacial geology on the onset of a West Antarctic ice stream from aerogeophysical observations, Nature, 394, 58–62, 1998.

Bell, R. E., Studinger, M., Shuman, C. A., Fahnestock, M. A., and Joughin, I.: Large subglacial lakes in East Antarctica at the onset of fast-flowing ice streams, Nature, 445, 904–907, 2007.

Bell, R. E.: The role of subglacial water in ice-sheet mass balance, Nature Geosci., 1, 297–304, 2008.

Bennett, M. R.: Ice streams as the arteries of an ice sheet: their mechanics, stability and significance, Earth-Sci. Rev., 61, 309–339, 2003.

Bennett, M. R. and Glasser, N. F.: Glacial geology: ice sheets and landforms, John Wiley and Sons Ltd, Chichester, UK, 364 pp., 1996.

Bennett, M. R., Huddart, D., and Gonzalez, S.: Glaciovolcanic landsystems and large-scale glaciotectonic deformation along the Brekknafjöll-Jarlhettur, Iceland, Quaternary Sci. Rev., 28, 647–676, 2009.

Bentley, C. R.: Antarctic ice streams: A review, J. Geophys. Res., 92, 8843–8858, 1987.

Blankenship, D. D., Bell, R. E., Hodge, S. M., Brozena, J. M., Behrendt, J. C., and Finn, C. A.: Active volcanism beneath the West Antarctic ice sheet and implications for ice-sheet stability, Nature, 361, 526–529, 1993.

Booth, D. B. and Hallet, B.: Channel networks carved by subglacial water: Observations and reconstruction in the eastern Puget Lowland of Washington, Geol. Soc. Am. Bull., 105, 671–683, 1993.

Boulton, G. S. and Clark, C. D.: A highly mobile Laurentide ice sheet revealed by satellite images of glacial lineations, Nature, 346, 813–817, 1990.

Canals, M., Urgeles, R., and Calafat, A. M.: Deep sea-floor evidence of past ice streams off the Antarctic Peninsula, Geology, 28, 31–34, 2000.

Caress, D. W. and Chayes, D. N.: Improved processing of Hydrosweep DS multibeam data on the R/V *Maurice Ewing*, Mar. Geophys. Res., 18, 631–650, 1996.

Clark, C. D.: Mega-scale glacial lineations and cross-cutting ice-flow landforms, Earth Surf. Processes, 18, 1–29, 1993.

Cook, S. J. and Swift, D. A.: Subglacial basins: Their origin and importance in glacial systems and landscapes, Earth-Sci. Rev., 115, 332–372, doi:10.1016/j.earscirev.2012.09.009, 2012.

Corr, H. F. J. and Vaughan, D. G.: A recent volcanic eruption beneath the West Antarctic ice sheet, Nature Geosci., 1, 122–125, 2008.

Debese, N., Moitié, R., and Seube, N.: Multibeam echosounder data cleaning through a hierarchic adaptive and robust local surfacing, Comp. Geosci., 46, 330–339, doi:10.1016/j.cageo.2012.01.012, 2012.

Domack, E., Amblàs, D., Gilbert, R., Brachfeld, S., Camerlenghi, A., Rebesco, M., Canals, M., and Urgeles, R.: Subglacial morphology and glacial evolution of the Palmer deep outlet system, Antarctic Peninsula, Geomorphology, 75, 125–142, 2006.

Dowdeswell, J. A., Ottesen, D., Rise, L., and Craig, J.: Identification and preservation of landforms diagnostic of past ice-sheet activity on continental shelves from three-dimensional seismic evidence, Geology, 35, 359–362, 2007.

Drewry, D. J., Jordan, S. R., and Jankowski, E.: Measured properties of the Antarctic ice sheet: surface configuration, ice thickness, volume and bedrock characteristics, Ann. Glaciol., 3, 83–91, 1982.

Ehrmann, W., Hillenbrand, C. D., Smith, J. A., Graham, A. G. C., Kuhn, G., and Larter, R. D.: Provenance changes between

recent and glacial-time sediments in the Amundsen Sea embayment, West Antarctica: clay mineral assemblage evidence, Antarct. Sci., 1, 1–16, 2011.

Evans, J., Dowdeswell, J. A., and Ó Cofaigh, C.: Late Quaternary submarine bedforms and ice-sheet flow in Gerlache Strait and on the adjacent continental shelf, Antarctic Peninsula, J. Quaternary Sci., 19, 397–407, 2004.

Eyles, N.: The role of meltwater in glacial processes, Sediment. Geol., 190, 257–268, 2006.

Fricker, H. A. and Scambos, T. A.: Connected subglacial lake activity on lower Mercer and Whillans Ice Streams, West Antarctica, 20032008, J. Glaciol., 55, 303–315, doi:10.3189/002214309788608813, 2009.

Fricker, H. A., Scambos, T., Bindschadler, R., and Padman, L.: An Active Subglacial Water System in West Antarctica Mapped from Space, Science, 315, 1544–1548, doi:10.1126/science.1136897, 2007.

Gohl, K.: The Expedition of the Research Vessel "Polarstern" to the Amundsen Sea, Antarctica, in 2010 (ANT-XXVI/3), Berichte zur Polar- und Meeresforschung, Alfred Wegener Institute for Polar and Marine Research, Bremerhaven, Germany, 168 pp., 2010.

Graham, A. G. C., Larter, R. D., Gohl, K., Hillenbrand, C.-D., Smith, J. A., and Kuhn, G.: Bedform signature of a West Antarctic palaeo-ice stream reveals a multi-temporal record of flow and substrate control, Quaternary Sci. Rev., 28, 2774–2793, 2009.

Graham, A. G. C., Larter, R. D., Gohl, K., Dowdeswell, J. A., Hillenbrand, C.-D., Smith, J. A., Evans, J., Kuhn, G., and Deen, T.: Flow and retreat of the Late Quaternary Pine Island-Thwaites palaeo-ice stream, West Antarctica, J. Geophys. Res., 115, F03025, doi:10.1029/2009jf001482, 2010.

Grant, J. A. and Schreiber, R.: Modern swath sounding and subbottom profiling technology for research applications: The Atlas Hydrosweep and Parasound Systems, Mar. Geophys. Res., 12, 9–19, doi:10.1007/bf00310559, 1990.

Hellmer, H. H., Jacobs, S. S., and Jenkins, A.: Oceanic Erosion of a Floating Antarctic Glacier in the Amundsen Sea, Antarct. Res. Ser., 75, 83–99, 1998.

Hillenbrand, C.-D., Kuhn, G., Smith, J. A., Gohl, K., Graham, A. G. C., Larter, R. D., Klages, J. P., Downey, R., Moreton, S. G., Forwick, M., and Vaughan, D. G.: Grounding-line retreat of the West Antarctic Ice Sheet from inner Pine Island Bay, Geology, 41, 35–38, doi:10.1130/G33469.1, 2013.

Hughes, T.: Is West Antarctic Ice-Sheet Disintegrating?, J. Geophys. Res., 78, 7884–7910, 1973.

IPCC: Climate Change 2007: The Physical Science Basis, Contribution of Working Group I to the Fourth Assessment Report of the Intergovernmental Panel on Climate Change, edited by: Solomon, S., Qin, D., Manning, M., Chen, Z., Marquis, M., Averyt, K. B., Tignor, M., and Miller, H. L., Cambridge University Press, Cambridge, UK, and New York, NY, USA, 996 pp., 2007.

Jacobs, S. S., Hellmer, H. H., and Jenkins, A.: Antarctic ice sheet melting in the Southeast Pacific, Geophys. Res. Lett., 23, 957–960, 1996.

Jacobs, S. S., Jenkins, A., Giulivi, C. F., and Dutrieux, P.: Stronger ocean circulation and increased melting under Pine Island Glacier ice shelf, Nature Geosci., 4, 519–523, doi:10.1038/ngeo1188, 2011.

Jakobsson, M., Anderson, J. B., Nitsche, F. O., Dowdeswell, J. A., Gyllencreutz, R., Kirchner, N., Mohammad, R., O'Regan, M., Alley, R. B., Anandakrishnan, S., Eriksson, B., Kirshner, A., Fernandez, R., Stolldorf, T., Minzoni, R., and Majewski, W.: Geological record of ice shelf break-up and grounding line retreat, Pine Island Bay, West Antarctica, Geology, 39, 691–694, doi:10.1130/g32153.1, 2011.

Jakobsson, M., Anderson, J. B., Nitsche, F. O., Gyllencreutz, R., Kirshner, A. E., Kirchner, N., O'Regan, M., Mohammad, R., and Eriksson, B.: Ice sheet retreat dynamics inferred from glacial morphology of the central Pine Island Bay Trough, West Antarctica, Quaternary Sci. Rev., 38, 1–10, doi:10.1016/j.quascirev.2011.12.017, 2012.

Jenkins, A., Vaughan, D. G., Jacobs, S. S., Hellmer, H. H., and Keys, J. R.: Glaciological and oceanographic evidence of high melt rates beneath Pine island glacier, west Antarctica, J. Glaciol., 43, 114–121, 1997.

Jenkins, A., Dutrieux, P., Jacobs, S. S., McPhail, S. D., Perrett, J. R., Webb, A. T., and White, D.: Observations beneath Pine Island Glacier in West Antarctica and implications for its retreat, Nature Geosci., 3, 468–472, 2010.

Johnson, J. S., Bentley, M. J., and Gohl, K.: First exposure ages from the Amundsen Sea Embayment, West Antarctica: The Late Quaternary context for recent thinning of Pine Island, Smith, and Pope Glaciers, Geology, 36, 223–226, 2008.

Jorgensen, F. and Sandersen, P. B. E.: Buried and open tunnel valleys in Denmark–erosion beneath multiple ice sheets, Quaternary Sci. Rev., 25, 1339–1363, 2006.

Joughin, I. and Alley, R. B.: Stability of the West Antarctic ice sheet in a warming world, Nature Geosci., 4, 506–513, 2011.

Joughin, I., Tulaczyk, S., MacAyeal, D. R., and Engelhardt, H.: Melting and freezing beneath the Ross ice streams, Antarctica, J. Glaciol., 50, 96–108, doi:10.3189/172756504781830295, 2004.

Joughin, I., Tulaczyk, S., Bamber, J. L., Blankenship, D., Holt, J. W., Scambos, T., and Vaughan, D. G.: Basal conditions for Pine Island and Thwaites Glaciers, West Antarctica, determined using satellite and airborne data, J. Glaciol., 55, 245–257, 2009.

Joughin, I., Smith, B. E., and Holland, D. M.: Sensitivity of 21st century sea level to ocean-induced thinning of Pine Island Glacier, Antarctica, Geophys. Res. Lett, 37, L20502, doi:10.1029/2010GL044819, 2010.

Kamb, B.: Basal zone of the West Antarctic ice streams and its role in lubrication of their rapid motion, in: The West Antarctic Ice Sheet: Behavior and Environment, Antarct. Res. Ser., 77, edited by: Alley, R. B. and Bindschadler, R. A., 0066-4634, American Geophysical Union, Washington, DC, USA, 157–199, 2001.

Kellogg, T. B. and Kellogg, D. E.: Late Quaternary deglaciation of the Amundsen Sea: implications for ice sheet modelling, in: The Physical Basis of Ice Sheet Modelling, Proceedings of the Vancouver Symposium, edited by: Waddington, E. D. and Walder, J. S., IAHS Publication, Vancouver, Canada, 349–357, 1987a.

Kellogg, T. B. and Kellogg, D. E.: Recent glacial history and rapid ice stream retreat in the Amundsen Sea, J. Geophys. Res., 92, 8859–8864 1987b.

King, E. C., Woodward, J., and Smith, A. M.: Seismic evidence for a water-filled canal in deforming till beneath Rutford Ice Stream, West Antarctica, Geophys. Res. Lett., 31, L20401, doi:10.1029/2004GL020379, 2004.

King, E. C., Hindmarsh, R. C. A., and Stokes, C. R.: Formation of mega-scale glacial lineations observed beneath a West Antarctic ice stream, Nature Geosci., 2, 585–588, 2009.

Kirshner, A. E., Anderson, J. B., Jakobsson, M., O'Regan, M., Majewski, W., and Nitsche, F. O.: Post-LGM deglaciation in Pine Island Bay, West Antarctica, Quaternary Sci. Rev., 38, 11–26, doi:10.1016/j.quascirev.2012.01.017, 2012.

Larter, R. D., Graham, A. G. C., Gohl, K., Kuhn, G., Hillenbrand, C.-D., Smith, J. A., Deen, T. J., Livermore, R. A., and Schenke, H.-W.: Subglacial bedforms reveal complex basal regime in a zone of paleo-ice stream convergence, Amundsen Sea embayment, West Antarctica, Geology, 37, 411–414, doi:10.1130/g25505a.1, 2009.

LeMasurier, W. E.: Late Cenozoic Volcanism on the Antarctic Plate: An Overview, in: Volcanoes of the Antarctic Plate and Southern Oceans, edited by: LeMasurier, W. E. and Thomson, J. W., Antarctic Research Series, Vol. 48, American Geophysical Union, Washington, DC, USA, 1–17, 1990.

Lewis, A. R., Marchant, D. R., Kowalewski, D. E., Baldwin, S. L., and Webb, L. E.: The age and origin of the Labyrinth, western Dry Valleys, Antarctica: Evidence for extensive middle Miocene subglacial floods and freshwater discharge to the Southern Ocean, Geology, 34, 513–516, doi:10.1130/g22145.1, 2006.

Livingstone, S. J., Ó Cofaigh, C., Stokes, C. R., Hillenbrand, C. D., Vieli, A., and Jamieson, S. S. R.: Antarctic palaeo-ice streams, Earth-Sci. Rev., 111, 90–128, 2012.

Llubes, M., Lanseau, C., and Rémy, F.: Relations between basal condition, subglacial hydrological networks and geothermal flux in Antarctica, Earth Planet. Sci. Lett., 241, 655–662, doi:10.1016/j.epsl.2005.10.040, 2006.

Lowe, A. L. and Anderson, J. B.: Reconstruction of the West Antarctic Ice Sheet in Pine Island Bay during the Last Glacial Maximum and its subsequent retreat history, Quaternary Sci. Rev., 21, 1879–1897, 2002.

Lowe, A. L. and Anderson, J. B.: Evidence for abundant subglacial meltwater beneath the paleo-ice sheet in Pine Island Bay, Antarctica, J. Glaciol., 49, 125–138, 2003.

Nitsche, F. O., Jacobs, S., Larter, R. D., and Gohl, K.: Bathymetry of the Amundsen Sea Continental Shelf: Implications for Geology, Oceanography, and Glaciology, Geochem. Geophys. Geosyst., 8, Q10009, doi:10.1029/2007GC001694, 2007.

Noormets, R., Dowdeswell, J. A., Larter, R. D., Ó Cofaigh, C., and Evans, J.: Morphology of the upper continental slope in the Bellingshausen and Amundsen Seas – Implications for sedimentary processes at the shelf edge of West Antarctica, Mar. Geol., 258, 100–114, 2009.

Nygård, A., Sejrup, H. P., Haflidason, H., Lekens, W. A. H., Clark, C. D., and Bigg, G. R.: Extreme sediment and ice discharge from marine-based ice streams: New evidence from the North Sea, Geology, 35, 395–398, doi:10.1130/g23364a.1, 2007.

Ó Cofaigh, C., Pudsey, C. J., Dowdeswell, J., and Morris, P.: Evolution of subglacial bedforms along a paleo-ice stream, Antarctic Peninsula continental shelf, Geophys. Res. Lett., 29, 1199, doi:10.1029/2001GL014488, 2002.

Ó Cofaigh, C., Dowdeswell, J. A., Allen, C. S., Hiemstra, J. F., Pudsey, C. J., Evans, J., and J.A. Evans, D.: Flow dynamics and till genesis associated with a marine-based Antarctic palaeo-ice stream, Quaternary Sci. Rev., 24, 709–740, 2005.

Peters, L. E., Anandakrishnan, S., Alley, R. B., and Smith, A. M.: Extensive storage of basal meltwater in the onset region of a major West Antarctic ice stream, Geology, 35, 251–254, doi:10.1130/g23222a.1, 2007.

Pritchard, H. D., Arthern, R. J., Vaughan, D. G., and Edwards, L. A.: Extensive dynamic thinning on the margins of the Greenland and Antarctic ice sheets, Nature, 461, 971–975, 2009.

Pritchard, H. D., Ligtenberg, S. R. M., Fricker, H. A., Vaughan, D. G., van den Broeke, M. R., and Padman, L.: Antarctic ice-sheet loss driven by basal melting of ice shelves, Nature, 484, 502–505, doi:10.1038/nature10968, 2012.

Rackebrandt, N.: Mapping of the PARASOUND penetration depth in the Pine Island Bay, West Antarctica, Term Paper, Master of Science Marine Geosciences, Department of Geosciences, University of Bremen, Germany, 22 pp., 2006.

Reinardy, B. T. I., Hiemstra, J. F., Murray, T., Hillenbrand, C.-D., and Larter, R. D.: Till genesis at the bed of an Antarctic Peninsula palaeo-ice stream as indicated by micromorphological analysis, Boreas, 40, 498–517, doi:10.1111/j.1502-3885.2010.00199, 2011.

Rignot, E. and Jacobs, S. S.: Rapid Bottom Melting Widespread near Antarctic Ice Sheet Grounding Lines, Science, 296, 2020–2023, doi:10.1126/science.1070942, 2002.

Rignot, E. and Thomas, R. H.: Mass balance of polar ice sheets, Science, 297, 1502–1506, 2002.

Rignot, E. J.: Fast recession of a West Antarctic glacier, Science, 281, 549–551, 1998.

Rignot, E., Bamber, J. L., van den Broeke, M. R., Davis, C., Li, Y., van de Berg, W. J., and van Meijgaard, E.: Recent Antarctic ice mass loss from radar interferometry and regional climate modelling, Nature Geosci., 1, 106–110, 2008.

Rignot, E., Velicogna, I., van den Broeke, M. R., Monaghan, A., and Lenaerts, J.: Acceleration of the contribution of the Greenland and Antarctic ice sheets to sea level rise, Geophys. Res. Lett., 38, L05503, doi:10.1029/2011gl046583, 2011.

Rippin, D. M., Vaughan, D. G., and Corr, H. F. J.: The basal roughness of Pine Island Glacier, West Antarctica, J. Glaciol., 57, 67–76, doi:10.3189/002214311795306574, 2011.

Roberts, M. J.: Jökulhlaups: A reassessment of floodwater flow through glaciers, Rev. Geophys., 43, RG1002, doi:10.1029/2003rg000147, 2005.

Schoof, C.: Ice sheet grounding line dynamics: Steady states, stability, and hysteresis, J. Geophys. Res., 112, F03S28, doi:10.1029/2006JF000664, 2007.

Shapiro, N. M. and Ritzwoller, M. H.: Inferring surface heat flux distributions guided by a global seismic model: particular application to Antarctica, Earth Planet. Sci. Lett., 223, 213–224, doi:10.1016/j.epsl.2004.04.011, 2004.

Sheen, K. L., White, N. J., Caulfield, C. P., and Hobbs, R. W.: Seismic imaging of a large horizontal vortex at abyssal depths beneath the Sub-Antarctic Front, Nature Geosci., 5, 542–546, doi:10.1038/ngeo1502, 2012.

Shepherd, A. and Wingham, D.: Recent Sea-Level Contributions of the Antarctic and Greenland Ice Sheets, Science, 315, 1529–1532, doi:10.1126/science.1136776, 2007.

Shepherd, A., Wingham, D. J., Mansley, J. A. D., and Corr, H. F. J.: Inland thinning of Pine Island Glacier, West Antarctica, Science, 291 862–864, 2001.

Shepherd, A., Wingham, D., and Rignot, E.: Warm ocean is eroding West Antarctic Ice Sheet, Geophys. Res. Lett., 31, L23402, doi:10.1029/2004GL021106, 2004.

Smith, A. M., Murray, T., Nicholls, K. W., Makinson, K., Adjalgeirsdóttir, G., Behar, A. E., and Vaughan, D. G.: Rapid erosion,

drumlin formation, and changing hydrology beneath an Antarctic ice stream, Geology, 35, 127–130, doi:10.1130/g23036a.1, 2007.

Smith, B. E., Fricker, H. A., Joughin, I. R., and Tulaczyk, S.: An inventory of active subglacial lakes in Antarctica detected by ICESat (2003–2008), J. Glaciol., 55, 573–595, 2009a.

Smith, J. A., Hillenbrand, C.-D., Larter, R. D., Graham, A. G. C., and Kuhn, G.: The sediment infill of subglacial meltwater channels on the West Antarctic continental shelf, Quaternary Res., 71, 190–200, 2009b.

Stokes, C. R. and Clark, C. D.: Palaeo-ice streams, Quaternary Sci. Rev., 20, 1437–1457, 2001.

Studinger, M., Bell, R. E., Blankenship, D. D., Finn, C. A., Morse, D. L., and Joughin, I.: Subglacial sediments: a regional geological template for ice flow in West Antarctica, Geophys. Res. Lett., 28, 3493–3496, 2001.

Sugden, D. and Denton, G.: Cenozoic landscape evolution of the Convoy Range to Mackay Glacier area, Transantarctic Mountains: Onshore to offshore synthesis, Geol. Soc. Am. Bull., 116, 840–857, doi:10.1130/b25356.1, 2004.

Sundal, A. V., Shepherd, A., Nienow, P., Hanna, E., Palmer, S., and Huybrechts, P.: Melt-induced speed-up of Greenland ice sheet offset by efficient subglacial drainage, Nature, 469, 521–524, doi:10.1038/nature09740, 2011.

Uenzelmann-Neben, G., Gohl, K., Larter, R. D., and Schlüter, P.: Differences in ice retreat across Pine Island Bay, West Antarctica, since the Last Glacial Maximum: indications from multichannel seismic reflection data, in: Antarctica: A Keystone in a Changing World – Proceedings for the Tenth International Symposium on Antarctic Earth Sciences, edited by: Cooper, A. K., Raymond, C. R., and the ISAES Editorial Team, US Geological Survey and The National Acadamies; USGS OF-2007-1047, Short Research Paper 084, 4 pp., 2007.

Vaughan, D. G., Corr, H. F. J., Ferraccioli, F., Frearson, N., O'Hare, A., Mach, D., Holt, J. W., Blankenship, D. D., Morse, D. L., and Young, D. A.: New boundary conditions for the West Antarctic Ice Sheet: Subglacial topography beneath Pine Island Glacier, Geophys. Res. Lett., 33, L09501, doi:10.1029/2005GL025588 2006.

Vaughan, D. G. and Arthern, R.: CLIMATE CHANGE: Why Is It Hard to Predict the Future of Ice Sheets?, Science, 315, 1503–1504, doi:10.1126/science.1141111, 2007.

Walder, J. and Fowler, A.: Channelized subglacial drainage over a deformable bed, J. Glaciol., 40, 3–15, 1994.

Weertman, J.: Stability of the junction of an ice sheet and an ice shelf, J. Glaciol., 13, 3–11, 1974.

Wellner, J. S., Lowe, A. L., Shipp, S. S., and Anderson, J. B.: Distribution of glacial geomorphic features on the Antarctic continental shelf and correlation with substrate: implications for ice behavior, J. Glaciol., 47, 397–411, 2001.

Wellner, J. S., Heroy, D. C., and Anderson, J. B.: The death mask of the antarctic ice sheet: Comparison of glacial geomorphic features across the continental shelf, Geomorphol., 75, 157–171, 2006.

Wilch, T. I., McIntosh, W. C., and Dunbar, N. W.: Late Quaternary volcanic activity in Marie Byrd Land: Potential 40Ar/39Ar-dated time horizons in West Antarctic ice and marine cores, Geol. Soc. Am. Bull., 111, 1563–1580, doi:10.1130/0016-7606, 1999.

Wingham, D. J., Ridout, A. J., Scharroo, R., Arthern, R. J., and Shum, C. K.: Antarctic elevation change from 1992 to 1996, Science, 282, 456–458, 1998.

Wingham, D. J., Siegert, M. J., Shepherd, A., and Muir, A. S.: Rapid discharge connects Antarctic subglacial lakes, Nature, 440, 1033–1036, 2006.

Publication 6.4.6:

Hochmuth, K., **Gohl, K.** (2013). Glaciomarine sedimentation dynamics of the Abbot glacial trough of the Amundsen Sea Embayment shelf, West Antarctica. In: Hambrey, M.J., Barker, P.F., Barrett, P.J., Bowman, V., Davies, B., Smellie, J.L., Tranter, M. (Eds.), *Antarctic Palaeoenvironments and Earth-Surface Processes*. Geological Society, London, Special Publications, v. 381, pp. 233-244, The Geological Society of London, doi:10.1144/SP381.21.

Author contributions: Hochmuth and Gohl wrote this paper in equal parts. Most of the data analysis and interpretation were results of Hochmuth's MSc thesis project supervised by Gohl. The data were collected during Polarstern expedition ANT-XXVI/3 (2010) with Gohl as chief-scientist.

Glaciomarine sedimentation dynamics of the Abbot glacial trough of the Amundsen Sea Embayment shelf, West Antarctica

KATHARINA HOCHMUTH* & KARSTEN GOHL

Department of Geosciences, Alfred Wegener Institute for Polar and Marine Research, Am Alten Hafen 26, 27568 Bremerhaven, Germany

**Corresponding author (e-mail: Katharina.Hochmuth@awi.de)*

Abstract: Sedimentary sequences of the continental shelf of the eastern Amundsen Sea Embayment in West Antarctica represent records of past outlet glaciers and ice streams. The former flow of ice streams was channelled through glacial troughs, which now form large bathymetric depressions. We therefore selected one of the largest troughs, the Abbot glacial trough in the outer shelf, to analyse its glacial depositional and erosional history, based on horizon-stratigraphy derived from seismic data. Several basement highs channellized the delivery of sediment and controlled the grounded ice sheet in early glacial periods. Both pre-glacial and full glacial seismic facies were identified. Glacially transported and deposited sediments extended the shelf break by 75 km from the pre-glacial shelf-edge. The main Abbot glacial trough contains sediment from confluent ice flows of the Pine Island/Thwaites, Cosgrove and Abbot Glacier systems, as well as smaller contributions from local ice streams emanating from Thurston Island. Sherman Island of Peacock Sound played an important role in the dynamics of the Abbot Glacier by dividing the ice flow into two ice streams, which interfered with the main glacial sediment transport paths from the south. This study contributes to an understanding of the formation of the Amundsen Sea shelf and the extent of past ice sheet advances.

The continental shelf of the Amundsen Sea Embayment holds a sedimentary archive that, if deciphered, has the potential to help reconstruct the major glacial periods of the West Antarctic Ice Sheet from early glacial advances to the grounded ice sheet retreat since the Last Glacial Maximum. Unlike the continental shelves of the Ross Sea and Filchne–Ronne embayments, the Amundsen Sea Embayment was fed entirely by the West Antarctic Ice Sheet, since it was unaffected by flow dynamics of the East Antarctic and Antarctic Peninsula ice sheets. Despite this significance for understanding past advance and retreat cycles of West Antarctic Ice Sheet, the shelf of the embayment has rarely been investigated. Most of its sea-floor stratigraphy remains unknown owing to unfavourable sea ice conditions that have prevented systematic seismic survey and drilling programmes. The first seismic profiles and analyses of an improving grid of multibeam bathymetric data (Nitsche *et al.* 1997, 2007; Lowe & Anderson 2002, 2003; Evans *et al.* 2006; Graham *et al.* 2010; Jakobsson *et al.* 2011, 2012) have shown that the ice sheet was grounded on the middle continental shelf, with excursions onto the outer shelf in some glacial periods.

This study focuses on the herein-named Abbot glacial trough, which represents the easternmost glacier outlet of the Amundsen Sea Embayment, incised into the outer continental shelf west and NW of Thurston Island (Fig. 1). Newly acquired seismic-reflection profiles crossing the outer continental shelf allow, in combination with gravimetric measurements, an analysis of the sedimentary strata and their underlying crystalline basement. By introducing a first horizon-stratigraphic model of the area, the glacial and pre-glacial sedimentary history of the Abbot glacial trough can partly be deciphered. In addition, the influence of the crystalline basement on the behaviour of the local ice streams will be discussed. Furthermore, sedimentation in this area, as well as additional sedimentation provided by medium-sized ice streams coming from Peacock Sound (Abbot Ice Shelf) and smaller glaciers originating on Thurston Island, are evaluated.

Geological background

The Amundsen Sea Embayment (Fig. 1) formed as a consequence of the Cretaceous breakup between the former Gondwanian blocks of greater New Zealand (Zealandia) and West Antarctica (Eagles *et al.* 2004; Gohl *et al.* 2007). Later, internal rifting related to the West Antarctic Rift System was active in this region during the Cenozoic Era (Dalziel 2006; Gohl *et al.* 2007; Jordan *et al.* 2009). Therefore, the Amundsen Sea Embayment

From: Hambrey, M. J., Barker, P. F., Barrett, P. J., Bowman, V., Davies, B., Smellie, J. L. & Tranter, M. (eds) 2013. *Antarctic Palaeoenvironments and Earth-Surface Processes*. Geological Society, London, Special Publications, **381**, 233–244. First published online July 24, 2013, http://dx.doi.org/10.1144/SP381.21

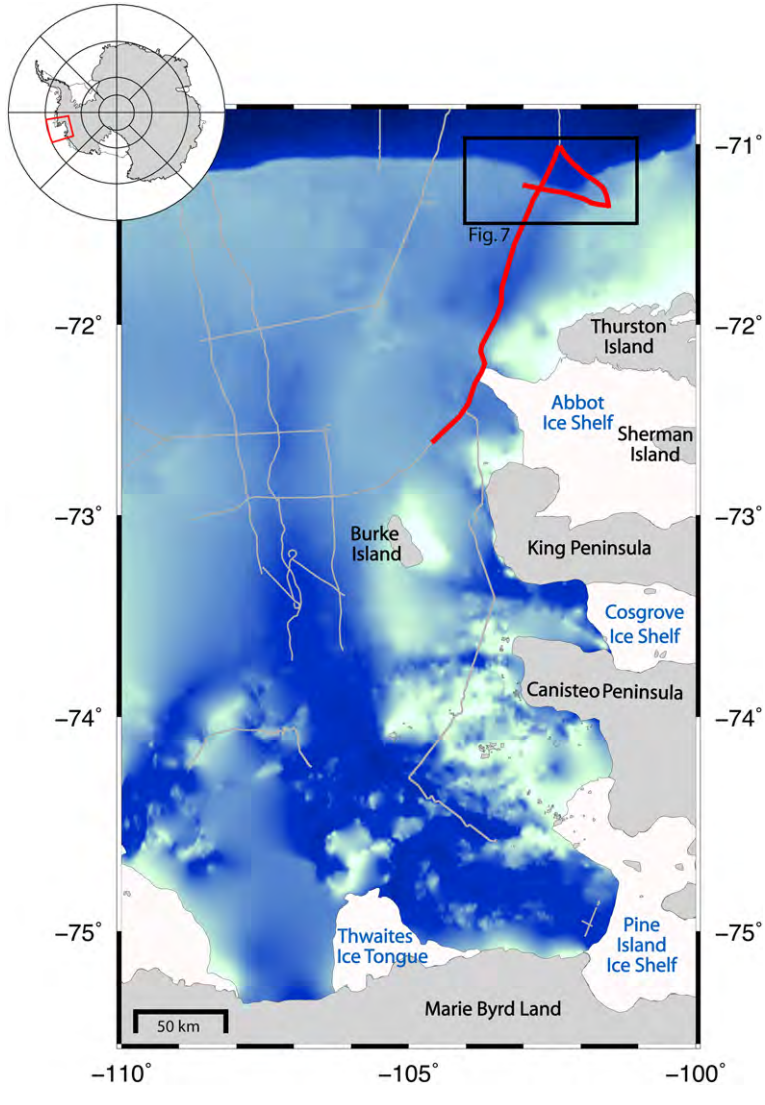

Fig. 1. Overview of the bathymetry of the eastern Amundsen Sea Embayment and Pine Island Bay after *Nitsche et al.* (2007). Red lines mark multichannel seismic profiles discussed in this study. Grey lines mark other existing seismic lines, including single-channel profile NBP-9902 (Lowe & Anderson 2002). Mean water-depths on the continental shelf reach 400–600 m (white to light blue zones) and extend to more than 1200 m (middle to dark blue zones).

was subject to extensional and rifting forces acting in both east–west and north–south directions, which thereby shaped the current structure of the crust and basement (Gohl *et al.* 2013).

Repeated advance and retreat of the West Antarctic Ice Sheet sculpted the present day bathymetry of the continental shelf (Lowe & Anderson 2002; Evans *et al.* 2006; Nitsche *et al.* 2007; Larter *et al.* 2009; Jakobsson *et al.* 2011, 2012). Similar to other continental polar shelves, the Amundsen Sea Embayment shelf deepens inshore and shows a reduced relief on the middle and outer shelf, where the water depth is between 400 and 600 m (Nitsche *et al.* 2007). On the middle shelf, south of Burke Island, the boundary between the outcropping crystalline basement and the oceanward-dipping sedimentary sequences is clearly observed (Lowe & Anderson 2002; 2003; Uenzelmann-Neben *et al.* 2007; Gohl *et al.* 2013).

The large Pine Island/Thwaites glacial trough dominates the bathymetry of the inner and middle continental shelf of the eastern embayment

(Fig. 1). It was carved by the Pine Island and Thwaites ice streams, which converged in the mid-shelf area (Nitsche *et al.* 2007). On the outer shelf, the trough branches into a system of shallow and wide depressions with multiple glacial outlets incising the shelf break (Nitsche *et al.* 2007). Whether these outlets acted simultaneously during an advanced ice sheet or resulted from a change in flow direction of the major ice stream is still being debated. Graham *et al.* (2010) argued that an eastern outlet was established later than the western outlet and therefore the main outlet during later expansions of the West Antarctic Ice Sheet. This concept of flow-switching is supported by a different degree of overprinting of mega-scale glacial lineations in both outlets. Possibly, younger mega-scale glacial lineations are present at the eastern outlet. Little is known about the Abbot glacial trough in the easternmost outer shelf, or its relationship with the ice streams of the main Pine Island/Thwaites trough, the outlet of Cosgrove glacier (Cosgrove Ice Shelf) between Canisteo Peninsula and King Peninsula, and the Abbot glacier (Abbot Ice Shelf) in Peacock Sound. Most of the outer shelf remained outside the range of detailed ship-borne geophysical surveys because of severe sea-ice conditions, until an unusual open-water situation occurred in early 2010, allowing the acquisition of such data.

Data acquisition and processing

As part of the geophysical data-acquisition programme during the R/V *Polarstern* expedition ANT-XXVI/3 in 2010 (Gohl 2010), multichannel seismic reflection profiles were also collected on the outer continental shelf and the Abbot trough in the eastern Amundsen Sea Embayment (Fig. 1). The seismic data discussed here were recorded with a 3000 m-long digital solid streamer, of the type Sercel Sentinel^{TM}, with 240 channels towed at a constant water-depth of 10 m. A cluster of three GI-Guns^{TM}, each with a volume of 0.72 l for the generator and 1.72 l for the injector, was towed at 5 m water-depth. The shot interval was 12 s, and records with 1 ms interval were sampled. Gravimetric measurements were carried out simultaneously with an on-board Bodenseewerke KSS31 gravimeter.

All seismic lines were treated with the same general processing flow. The shot-gathers were

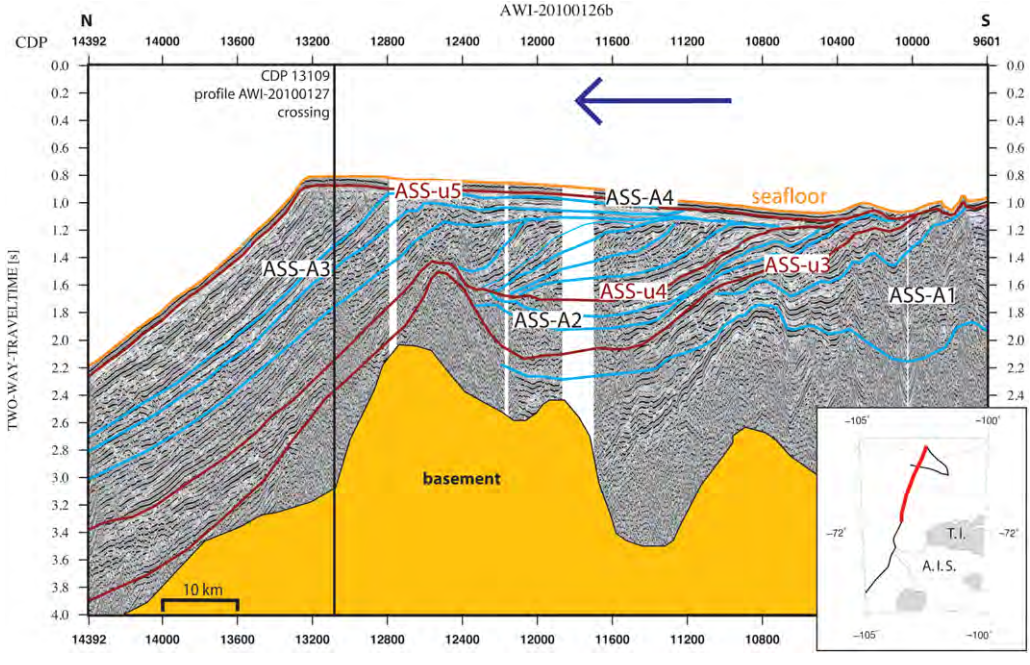

Fig. 2. Northern segment of seismic-reflection profile AWI-20100126b (marked by red line in the inset map; dotted black line shows the shelf edge) with basement depths derived from gravity-anomaly modelling. Unconformities ASS-u3, ASS-u4 and ASS-u5 are marked in red; internal structures of sedimentary units ASS-A1, ASS-A2, ASS-A3 and ASS-A4 are marked in blue. The ice-flow direction is indicated by the dark blue arrow.

sorted into CDP (common depth point) bins of 25 m. General band-pass filtering of 10–120 Hz was applied to the data. A detailed velocity analysis was followed by a parabolic radon transformation to reduce the strong multiple reflections that are typically observed on glaciated continental shelves, as well as to enhance the visibility of underlying reflectors. After stacking, an omega-x finite-difference migration was applied to image the position of dipping reflectors. For further enhancement of the resolution of particular profile sections, multiple filters were applied before final editing.

Even after careful multiple suppression, deeper-lying basement reflections are not visible or remain uncertain in large parts of the profiles, possibly because of the relatively small airgun source and attenuating effect of the multiples. Therefore gravimetric recordings were used and forward density-depth modelling was applied to the free-air anomaly data in order to aid outlining of the sediment-to-basement boundary. A constant crust-mantle depth of 22 km, derived by Gohl *et al.* (2007) for this region of the shelf, was used to constrain the lower model boundaries.

Seismic horizon stratigraphy

Based on the seismic reflection profiles (Figs 2–4 & 6), we derived a basic horizon stratigraphy for the area of the Abbot glacial trough (Fig. 5). Datable sediment samples only exist from shallow gravity-cores and box-samplers that were used to reconstruct the timing of grounding zone retreat since the Last Glacial Maximum (Lowe & Anderson 2002, 2003; Hillenbrand *et al.* 2009; Kirshner *et al.* 2012). Deeply penetrating drill cores from the Amundsen Sea shelf do not exist. Therefore, the seismic horizon stratigraphy that is presented here relies entirely on the observation of seismic reflection characteristics and its comparison with other glaciated continental shelves, such as on dated sequences from the Ross Sea shelf (Anderson & Bartek 1992; Bart & Anderson 2000; Chow & Bart 2003).

Where acoustic basement is relatively shallow, it can be identified mainly in the seismic sections as a reflective band, setting the lower limit of layered sequences. Deeper lying basement of uncertain seismic identification, or lack of it, had to be verified by gravity modelling. Four large sedimentary units

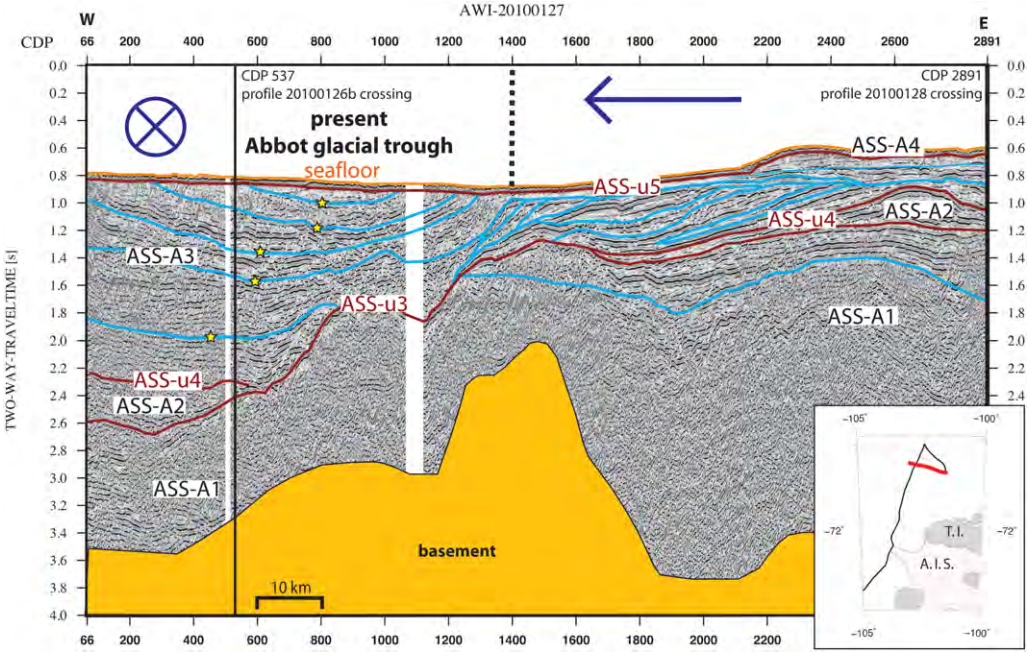

Fig. 3. Seismic-reflection profile AWI-20100127 (marked red line in inset map, dotted black line shows the shelf edge) with basement depths derived from gravity-anomaly modelling. The profile crosses the Abbot glacial trough. Major unconformities and layer boundaries are marked as in Figure 2. The flow-direction of smaller ice streams from Thurston Island is indicated by the dark blue arrow, and the crossed circle annotates the northward flow direction of the main Pine Island ice stream. Yellow stars indicate the location of the different depocentres within the unit ASS-A3.

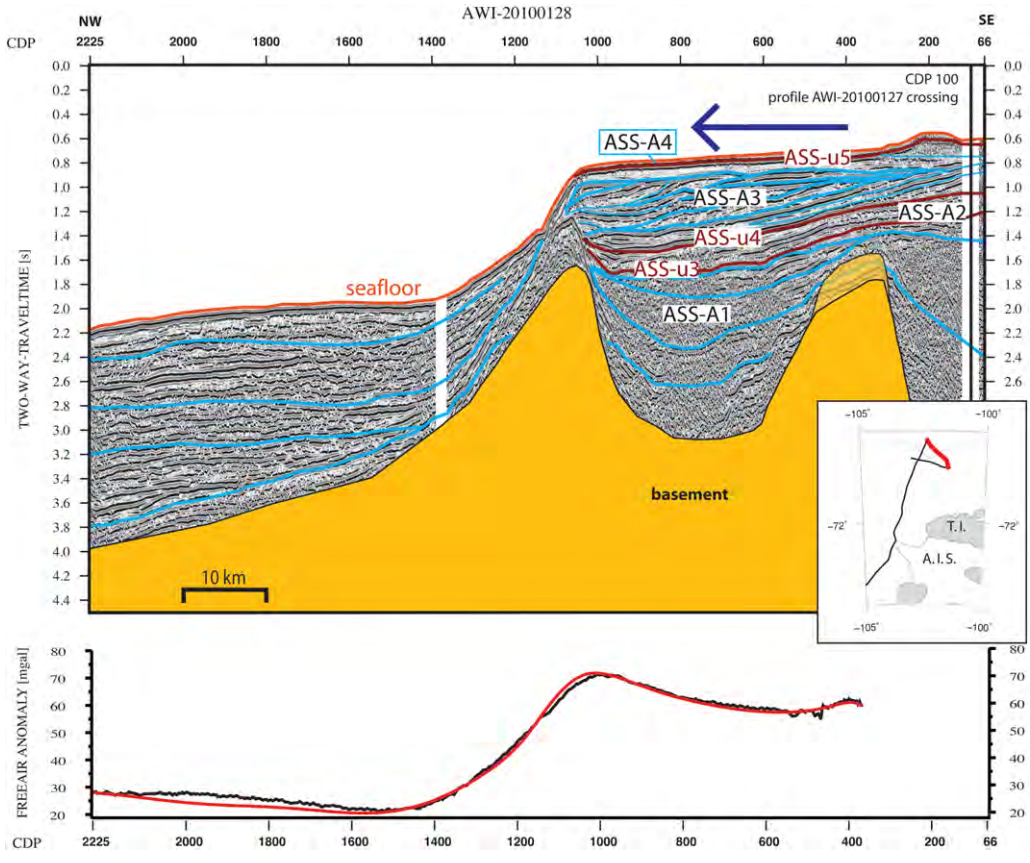

Fig. 4. Seismic-reflection profile AWI-20100128 (marked red line in inset map, dotted black line shows the shelf edge) with basement depths derived from gravity-anomaly modelling. The profile crosses the outer shelf and slope east of the main Abbot glacial trough. Major unconformities and layer boundaries are marked as in Figure 2. The dark blue arrow indicates the flow-direction of smaller ice streams from Thurston Island. The corresponding ship-borne free-air gravity-anomaly profile is shown in the bottom graph, with the black line being the measured data, and the red line being the calculated model response (see text for explanation).

can be distinguished from their seismic facies and from observations of erosional discontinuities. The discontinuities are labelled, from the oldest to the youngest, as ASS-u3 to ASS-u5 (Amundsen Sea Shelf unconformity). The sedimentary units are named ASS-A1 to ASS-A4 (Amundsen Sea Shelf Abbot glacial trough) from oldest to youngest (Fig. 5).

Sedimentary unit ASS-A1 consists of short reflectors, which have mainly low amplitudes and are discontinuously layered (Figs 2–4). This homogeneous unit is interlayered with occasional bands of closely spaced reflectors of high amplitude, which are traceable across the shelf. ASS-A1 is present in all seismic lines as a massive sedimentary package with a thickness of between 3 and 6.5 km that crops out at the sea floor on parts of the middle shelf. On the outer shelf, ASS-A1 thins and is mainly overlain by an erosional unconformity ASS-u3. ASS-u3 is also present on the mid-shelf, cutting into ASS-A1 as a trough-like structure.

Sedimentary unit ASS-A2 occurs on top of unconformity ASS-u3 on the outer shelf (Figs 2–4). This unit shows continuous, strong, slightly inclined reflectors. It varies little in thickness throughout the outer shelf, but could not be identified in the Peacock Sound area.

Above discontinuity ASS-u4, the sedimentary strata of unit ASS-A3 consist of prograding clinoforms and sequences, showing continuous layering between high-and low-amplitude reflections (Figs 2–4). This unit is present mainly on the outer shelf, but also in the trough-like structure on the outer middle shelf.

In all profiles, a third major erosional discontinuity ASS-u5 cuts into the older strata (Figs 2–4).

sedimentary unit	erosional discontinuity	Age (approximated)	description of sedimentary unit	sedimentary processes & environment
ASS-A4		Pleistocene	continuous strong reflectors, mimicing the seafloor	retreat of the WAIS after the LGM, glaciomarine deposition
	ASS-u5			
ASS-A3		Pliocene - Pleistocene	prograding clinoforms, continous layering between high and low amplitudes	full glacial environment, glacial-interglacial cyclicity, shelf progadation and aggradation
	ASS-u4			
ASS-A2		late Miocene - early Pliocene	continous, slightly inclined reflectors (not identified in Peacock Sound)	establishment of the WAIS in the Amundsen Sea, partly grounded ice
	ASS-u3			
ASS-A1		Cretaceous (?) - middle/late Miocene (?)	short reflectors, low amplitude, occasional bands of closely spaced reflectors	ice-free shelf with occasional advances of smaller ice streams, aggrational sedimentation on the middle shelf
basement				

Fig. 5. Overview of sedimentary units and erosional discontinuities from the Abbot glacial trough, including description of the unit and sedimentary processes and depositional environment.

Above ASS-u5, a small sedimentary unit, ASS-A4, is present throughout the continental shelf. It mimics the sea floor with continuous and strong reflectors. This sedimentary package varies only slightly in thickness. The sea floor is represented by a very strong reflector, which shows diffraction hyperbolae, as a result of the abundant iceberg-scouring and the resulting roughness of the sea floor.

In order to outline the depth of the crystalline basement more accurately, 2-D forward modelling on ship-borne free-air gravity-anomaly data was performed along all seismic profiles (example in Fig. 4). The depth of the crust-mantle boundary was kept constant at 22 km after Gohl *et al.* (2007), and the crystalline crust subdivided into three layers of typical continental crustal densities of between 2.70 and 2.90 g cm^{-3} from top to bottom. The combination of the gravimetric models and the depth-converted seismic profiles helped identify the weak reflectors that represent the top of the crystalline basement. The resulting basement topography varies strongly towards the continental slope. Here, several areas with elevated basement reach a depth of up to 500 m below the sea floor (Figs 2–4), whereas adjacent basins have a depth of between 3.4 and 4.5 km. Two deeper basins with depths of over 6 km, located north of Thurston Island and at Peacock Sound, were also modelled.

Comparison with horizon stratigraphy of outer Ross Sea shelf

The major sedimentary units and unconformities identified (Figs 2–4) can be related to the drilled (DSDP Leg 28; Hayes *et al.* 1975) and dated strata of the Ross Sea continental shelf by similarities in the seismic facies and erosional pattern. ASS-u3 is a strong erosional discontinuity, representing the change of the depositional environment from aggradational to progradational. On the Ross Sea shelf, this corresponds to RSU-4, marking the interface of the first advance of the West Antarctic Ice Sheet across the continental shelf (Anderson & Bartek 1992). Therefore, the underlying unit ASS-A1 is likely to represent the strata deposited in a pre-glacial environment (possibly Cretaceous to middle/late Miocene; Anderson & Bartek 1992; Chow & Bart 2003). ASS-A2 represents the transition towards a full glacial environment in Antarctica when ice sheets were present on the continent and advanced occasionally onto the shelf (Anderson & Bartek 1992). The discontinuity ASS-u4 marks the changeover between a transitional to a full glacial environment. The prograding sequences of ASS-A3 are comparable with unit RSS-7 of the Ross Sea, which was deposited during the Pliocene and Pleistocene epochs (Anderson & Bartek 1992).

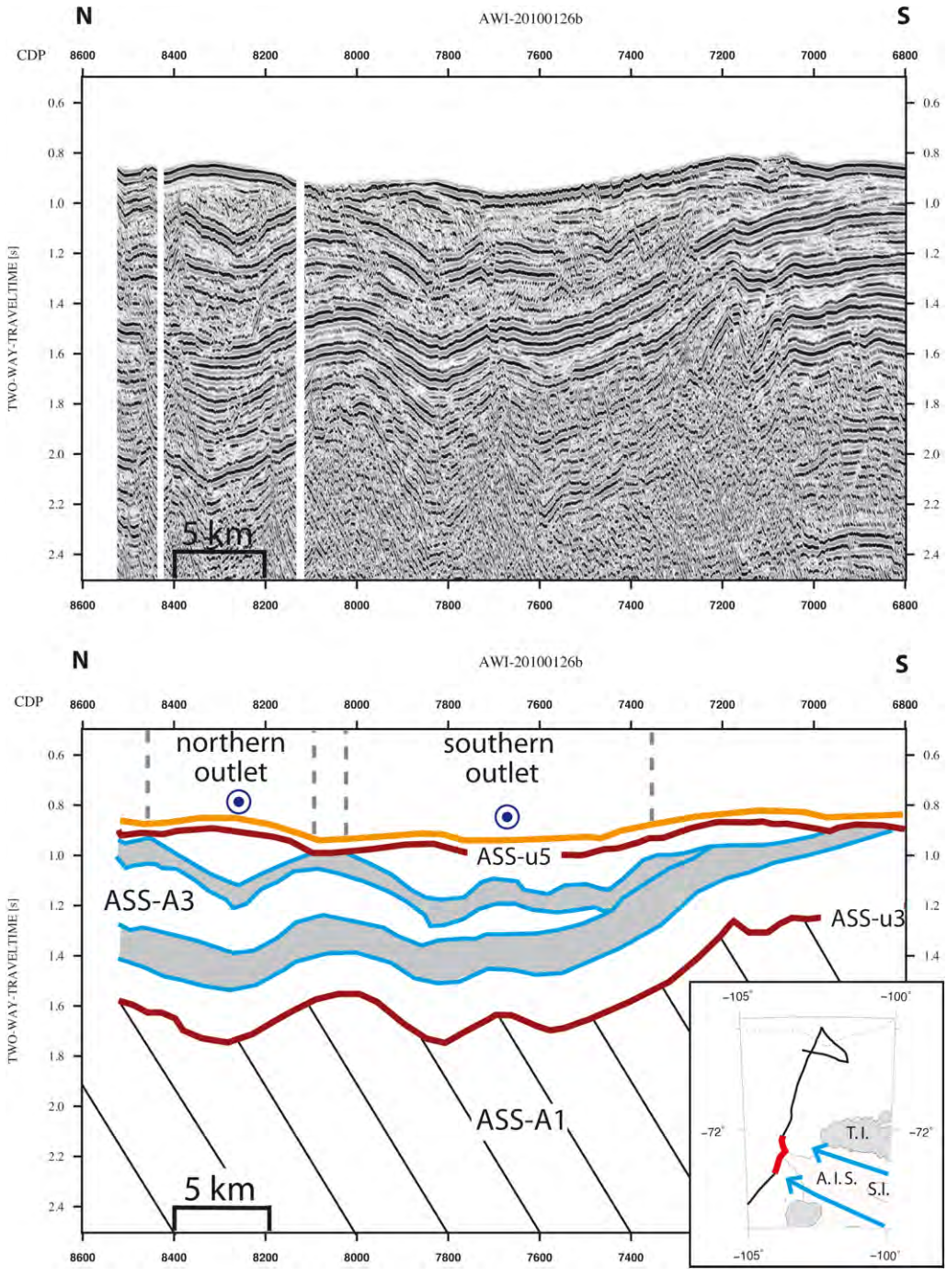

Fig. 6. Southern part of seismic profile AWI-20100126b, which bypasses the Abbot Ice Shelf of Peacock Sound (red line of inset map with ice-flow indicated by blue arrows; dotted black line shows the shelf edge). The interpretation of the bottom profile shows alternating zones of strong (grey) and weak (white) reflectivities in transitional and glacially dominated periods. The pre-glacial strata (ASS-A1) lie beneath unconformity ASSu-1.

ASS-A4 consists of the sediments deposited after the last glacial maximum, and ASS-u5 represents the erosional surface of this last advance of the ice sheet to the outer shelf.

Discussion

Pre-glacial setting of the outer shelf

The outer continental shelf of the eastern Amundsen Sea Embayment is crossed by tectonic lineaments, striking mainly NE–SW as interpreted from gravity and magnetic anomaly data (Gohl 2012; Gohl *et al.* 2013). Our observed and modelled basement highs and lows appear as horst-and-graben structures that correlate with one of the tectonic lineaments, which has been associated with Cretaceous rifting between New Zealand and West Antarctica (Fig. 7; Gohl 2012; Gohl *et al.* 2013).

Despite the lack of any drilling and outcropping sediment samples from the Amundsen Sea Embayment, the observation of seismic-reflection characteristics leads to the inference that sequence unit ASS-A1 represents the building-up of sediments on the continental shelf before the glaciation of West Antarctica took place. Multiple basement highs with adjacent small basins are present on the outer shelf (Fig. 7), channellizing the pre-glacial deposition. At the location where ASS-A1 crops out at the sea floor at its northernmost position (CDP 9700 of Fig. 2), the sediments are highly reworked and show only little lamination. This location represents the pre-glacial shelf break. Therefore, the pre-glacial shelf break in the area of the Abbot trough is 75 km further inshore than the present-day shelf break (Figs 2 & 8). The undulating basement topography of the present outer shelf and slope is covered by a few hundred metres of sediment of pre-glacial origin within the glacial trough (Figs 2 & 3), whereas few to no pre-glacial strata cover the basement ridges outside of the glacial trough off Thurston Island (Fig. 4). A distinct basement-high limits the pre-glacial and glacial shelf extent at this location, highlighting the role of basement tectonics on the outer shelf.

Glacial sedimentation

The Cretaceous tectonic lineaments and basement ridges of the outer shelf appear to have also constrained deposition of glacially eroded and

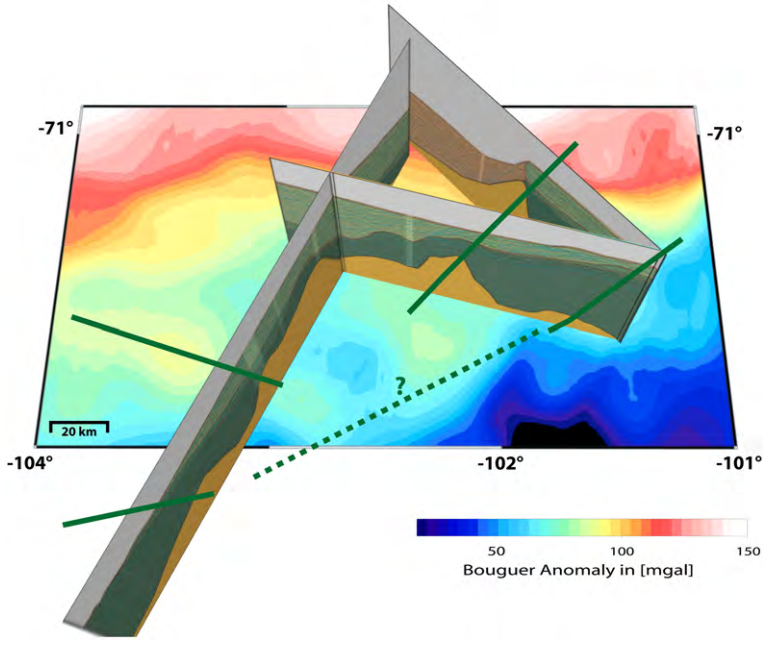

Fig. 7. Bird's-eye view of the three interpreted seismic profiles of the outer Abbot glacial trough, on top of a Bouguer gravity-anomaly map calculated from satellite-derived gravity data of Andersen *et al.* (2010). Solid dark green lines illustrate the locations and directional trends of basement ridges observed from seismic data and gravity modelling, and which correspond to positive Bouguer-anomaly lineaments. The dotted green line symbolizes a possible connecting basement ridge or escarpment between observed ridge segments.

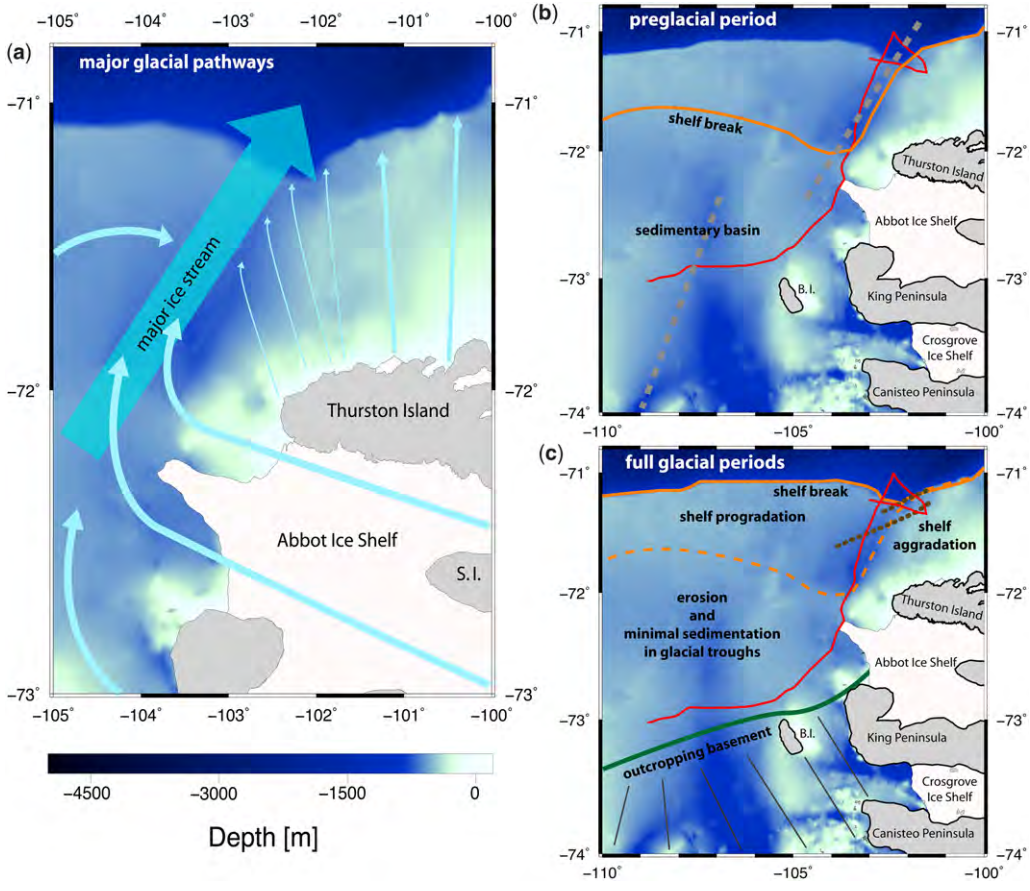

Fig. 8. Bathymetric maps illustrating the ice flow pattern during glacial maxima as interpreted from the seismic data (**a**) and the growth of the outer shelf and outward migration of the shelf break (orange solid and hashed lines) from pre-glacial times (**b**) to full glacial periods (**c**). The solid red line marks the seismic profiles in this paper. The dark green line illustrates the boundary between outcropping inner shelf basement and the shelf sedimentary basin. Basement-highs on the outer shelf are indicated by the brown dotted lines and the grey hashed lines of (b) are projected tectonic lineaments from Gohl (2012). Bathymetry is from Nitsche *et al.* (2007). B.I. is Burke Island. S.I. is Sherman Island.

transported sediment (Figs 2–4). Inside the Abbot trough, the glacial strata (ASS-A3) consists of multiple prograding sequences leading to growth of the outer shelf from the pre-glacial shelf break into the position of the present-day continental slope (Fig. 2). ASS-A3 consists of smaller clinoforms in the south and larger sequences after depositing over the top of the northern basement ridge. Thus, younger strata extend into the former basin, creating a till delta (Anderson & Bartek 1992; Larter & Vanneste 1995; Bart & Anderson 2000; Smith *et al.* 2011). A cross-section of this till delta can be observed in a section across the Abbot trough between CDP 66 and 500 (Fig. 3). Following further examination of the internal structure, the position of the former depositional centre of the glacial trough can be identified (Fig. 3). In the younger strata, an eastward shift of the depocentre is visible. Graham *et al.* (2010) proposed an eastwards trend of the main Pine Island/Thwaites ice stream in younger glacial periods. In earlier glacial cycles, the sedimentation in the Abbot glacial trough was channellized into the basin between the two basement-highs north of the pre-glacial shelf break (Figs 3 & 7). Only after sedimentation had become level with the northern basement-high did progradation proceed northwards down the slope during later glacial cycles, leading to relocation of the depocentre of the till delta to the east. Dowdeswell *et al.* (2006*a*) showed in 3D seismic data from the Norwegian continental margin that the change in ice-stream flow can occur between

glacial advances because of the accessibility of new sedimentary basins. Therefore, the Abbot trough may have experienced a higher discharge of ice and sediment during later glacial cycles, since formerly inaccessible accommodation space had become available. This led to continental shelf progradation by the build-up of a till delta.

East of the main Abbot trough, the configuration of the slope differs strongly (Fig. 4). Only thin sediments cover the northern basement-high, and the glacial sedimentary sequences are limited by the basement, resulting in shelf aggradation (Dowdeswell *et al.* 2006*b*). We also observe that the orientation of the clinoforms of ASS-A3 creates a radial pattern (Figs 4 & 7). Therefore, multiple small ice streams originating from Thurston Island seem to have been the source of these sequences (Fig. 8). Such small ice streams had insufficient capacity to overcome the basement-high, and thus enabled significant deposition on the shelf break and slope.

Through the limited supply of sediment to the outer shelf, deposition was restricted to the pre-existing basins between the basement ridges. Thus sedimentation was limited to the outer shelf, leading to aggradation, with minimal to no change in the position of the shelf break between pre-glacial and glacial periods.

In the section crossing the Abbot trough from west to east, a distinct boundary between the glacial infill structure of the till delta and small prograding sequences from the east is exposed (Fig. 3). At this location, the larger, fast-flowing ice stream following the main Abbot trough absorbed the smaller ice streams from the east, merging their ice masses and deflecting sediment transport from a westwards to northwards flow direction towards the shelf slope.

Abbot Ice Shelf

The seismic profile AWI-20100126b bypasses the outlet of the west-flowing Abbot Ice Shelf in Peacock Sound (Fig. 6). The record shows distinct bands of strong reflectors enclosing zones of weak and partially chaotic reflections within the sedimentary unit ASS-A3. A similar record has been interpreted, for the western Amundsen Sea Embayment, as depositional sequences alternating between full glacial and less glacially dominated periods in Miocene times (Weigelt *et al.* 2009). Although the age is speculative, the depositional processes appear to have been similar to those in the eastern embayment. Two small troughs, with a small sedimentary high in between, form a W-shaped reflection pattern between CDPs 7500 and 8500, partly representing local erosional unconformities. It can be inferred from this observation that the ice streams from Peacock Sound carved two individual glacier outlet troughs, a southern and a northern outlet, orthogonally or obliquely into the main Pine Island/Thwaites and Cosgrove glacial trough deposits of the shelf. The dividing sedimentary high lies along the ice flow-direction and inline with the location of Sherman Island, an island in Peacock Sound which divides the Abbot Ice Shelf (Figs 1 & 6). In the pre-glacial sequence ASS-A1, the two-outlet pattern is also visible but less pronounced compared with the glacial strata. This island seems to have played an important role in the ice-sheet dynamics of the Abbot Ice Sheet, channellizing the flow of ice into a southern and northern stream.

Conclusions

Seismic-reflection data, supplemented by gravity modelling results for basement depths, reveal the pre-glacial and glacial sedimentary dynamics of the outer shelf of the eastern Amundsen Sea Embayment, which is dominated by the Abbot glacial trough as a major bathymetric depression. Several basement-highs, inherited from Cretaceous breakup and Cenozoic rifting processes, have constrained sedimentation. These basement ridges played a key role in the development of the Abbot glacial trough. They channellized sediment deposition, and may have controlled the ice-sheet dynamics by acting as pinning points or barriers in early glacial periods.

By establishing a first basic horizon stratigraphy, we identify pre-glacial (ASS-A1), transitional (ASS-A2) and glacial (ASS-A3) seismic facies. The pre-glacial continental shelf-break was located approximately 75 km further inshore than the present-day Abbot glacial trough. When the first ice sheet advances onto the outer shelf took place, the depocentre moved towards the outer shelf and the continental slope. The NE–SW-striking basement-highs restricted deposition to NW of Thurston Island throughout early glacial advances, leading to aggradation of glaciomarine sediment on the continental shelf. Later, this basement barrier was partly overcome, allowing progradational deposition over the shelf break in younger glacial periods.

The main Abbot glacial trough contained merged flows from the Pine Island/Thwaites, Cosgrove and Abbot glacier systems, in addition to small contributions from local ice streams on Thurston Island. Sherman Island of Peacock Sound played an important role in the ice-dynamics of the Abbot glacier, by dividing the northwestwards ice-flow into two ice streams, which interfered with the main glacial sediment transport from the south.

The support of the master and crew of RV *Polarstern* during expedition ANT-XXVI/3 (2010) is gratefully acknowledged. Parts of this paper have resulted from the M.Sc. thesis of K.H., who was co-supervised by H. Keil of University of Bremen. We would also like to thank the joint Volume Editor/Corresponding Editor, M. Hambrey, J. B. Anderson and one anonymous reviewer for their comments and suggestions. Seismic data-processing was performed using the *Paradigm Focus*™ software package. This study has been funded through Work Package 3.2 of the AWI research programme PACES.

References

Anderson, J. & Bartek, L. R. 1992. Cenozoic glacial history of the Ross Sea revealed by intermediate resolution seismic reflection data combined with drill site information. *Antarctic Research Series*, **56**, 231–263.

Andersen, O. B., Knudsen, P. & Berry, P. 2010. The DNSC08GRA global marine gravity field from double retracked satellite altimetry. *Journal of Geodesy*, **84**, 191–199.

Bart, P. J. & Anderson, J. B. 2000. Relative temporal stability of the Antarctic ice sheets during the late Neogene based on the minimum frequency of outer shelf grounding events. *Earth and Planetary Science Letters*, **182**, 259–272.

Chow, J. M. & Bart, P. J. 2003. West Antarctic Ice Sheet grounding events on the Ross Sea outer continental shelf during the middle Miocene. *Palaeogeography, Palaeoclimatology, Palaeoecology*, **198**, 169–186.

Dalziel, I. W. D. 2006. On the extent of the active West Antarctic rift system. *In*: Siddoway, C. S. & Ricci, C. A. (eds) *Proceedings of Workshop on Frontiers and Opportunities in Antarctic Geosciences*. Terra Antartica Reports **12**. Terra Antartica, Siena, 193–202.

Dowdeswell, J. A., Ottensen, D. & Reise, L. 2006*a*. Flow switching and large-scale deposition by ice streams draining former ice sheet. *Geology*, **34**, 313–316.

Dowdeswell, J. A., Cofaigh, C. Ó. & Anderson, J. B. 2006*b*. Morphology and sedimentary processes on the continental slope off Pine Island Bay, Amundsen Sea, West Antarctica. *Bulletin of the Geological Society of America*, **118**, 606–619.

Eagles, G., Gohl, K. & Larter, R. D. 2004. High-resolution animated tectonic reconstruction of the South Pacific and West Antarctic Margin. *Geochemistry Geophysics Geosystems*, **5**, 1–21, doi: 10.1029/2003GC000657.

Evans, J., Dowdeswell, J. A., Cofaigh, C. Ó., Benham, T. J. & Anderson, J. B. 2006. Extent and dynamics of the West Antarctic Ice Sheet on the outer continental shelf of Pine Island Bay during the last glaciation. *Marine Geology*, **230**, 53–70.

Gohl, K. 2010. *The expedition of the research vessel 'Polarstern' to the Amundsen Sea, Antarctica, in 2010*. Berichte zur Polar- und Meeresforschung/Reports on Polar and Marine Research, **617**, http://epic.awi.de/epic/Main?static=yes&page=abstract&entry_dn=Goh2010f

Gohl, K. 2012. Basement control on past ice sheet dynamics in the Amundsen Sea Embayment, West Antarctica. *Palaeogeography Palaeoclimatology, Palaeoecology*, **335–336**, 35–41, doi: 10.1016/j.palaeo.2011.02.022.

Gohl, K., Teterin, D. *et al.* 2007. Geophysical survey reveals tectonic structures in the Amundsen Sea embayment, West Antarctica. *In*: Cooper, A. K. & Raymond, C. R. (eds) *Proceedings of the 10th Int. Symposium of Antarctic Earth Sciences*. USGS Open-File Report 2007–1047. US Geological Survey, Reston, VA, doi: 10.3133/of2007-1047.srp047.

Gohl, K., Denk, A., Eagles, G. & Wobbe, F. 2012. Deciphering tectonic phases of the Amundsen Sea Embayment shelf, West Antarctica, from a magnetic anomaly grid. *Tectonophysics*, **585**, 113–123, doi: 10.1016/j.tecto.2012.06.036.

Graham, A. G. C., Larter, R. D. *et al.* 2010. Flow and retreat of the Late Quaternary Pine Island-Thwaites paleo-ice stream, West Antarctica. *Journal of Geophysical Research–Earth Surfaces*, **115**, 1–12, doi: 10.1029/2009JF001482.

Hayes, D. E. & Frakes, L. A. 1975. General synthesis. *Initial Reports of the Deep Sea Drilling Project*, **28**, 919–942.

Hillenbrand, C.-D., Smith, J. A. *et al.* 2009. Age assignment of a diatomaceous ooze deposited in the western Amundsen Sea Embayment after the Last Glacial Maximum. *Journal of Quaternary Science*, **25**, 280–295, doi: 10.1002/jqs.1308.

Jakobsson, M., Anderson, J. B. *et al.* 2011. Geological record of ice shelf break-up and grounding line retreat, Pine Island Bay, West Antarctica. *Geology*, **39**, 691–694, doi: 10.1130/G32153.1.

Jakobsson, M., Anderson, J. B. *et al.* 2012. Ice sheet retreat dynamics inferred from glacial morphology of the central Pine Island Bay Trough, West Antarctica. *Quaternary Science Reviews*, **38**, 1–10, doi: 10.1016/j.quascirev.2011.12.017.

Jordan, T. A., Ferraccioli, F., Vaughan, D. G., Holt, J. W., Corr, H., Blankenship, D. D. & Diehl, T. M. 2009. Aerogravity evidence of a major crustal thinning under the Pine Island Glacier region (West Antarctica). *Bulletin of the Geological Society of America*, **122**, 714–726, doi: 10.1130/B26417.1.

Kirshner, A. E., Anderson, J. B., Jakobsson, M., O'Regan, M., Majewski, W. & Nitsche, F. O. 2012. Post-LGM deglacation in Pine-Island Bay, West Antarctica. *Quaternary Science Reviews*, **38**, 1–16, doi: 10.1016/j.quascirev.2012.01.017.

Larter, R. D. & Vanneste, L. E. 1995. Relict subglacial deltas on the Antarctic Peninsula outer shelf. *Geology*, **23**, 33–36.

Larter, R. D., Graham, A. G. C. *et al.* 2009. Subglacial bedforms reveal complex basal regime in a zone of paleo-ice stream convergence, Amundsen Sea Embayment, West Antarctica. *Geology*, **37**, 411–414.

Lowe, A. L. & Anderson, J. B. 2002. Reconstruction of the West Antarctic ice sheet in Pine Island Bay during the Last Glacial Maximum and its subsequent retreat history. *Quaternary Science Reviews*, **21**, 1879–1897.

Lowe, A. L. & Anderson, J. B. 2003. Evidence for abundant subglacial meltwater beneath the paleo-ice sheet in Pine Island Bay, Antarctica. *Journal of Glaciology*, **46**, 125–138.

Nitsche, F. O., Gohl, K., Vanneste, K. & Miller, H. 1997. Seismic expression of glacially deposited sequences in the Bellinghausen and Amundsen Sea, West Antarctica. *Antarctic Research Series*, **71**, 95–108.

Nitsche, F. O., Jacobs, S. S., Larter, R. D. & Gohl, K. 2007. Bathymetry of the Amundsen Sea continental shelf: implications for geology, oceanography, and glaciology. *Geochemistry Geophysics Geosystems*, **8**, 1–10, doi: 10.1029/2007GC001694.

Smith, J. A., Hillenbrand, C.-D. *et al.* 2011. Deglacial history of the West Antarctic Ice Sheet in the western Amundsen Sea Embayment. *Quaternary Science Reviews*, **30**, 488–505.

Uenzelmann-Neben, G., Gohl, K., Larter, R. D. & Schlüter, P. 2007. Differences in ice retreat across Pine Island Bay, West Antarctica, since the Last Glacial Maximum: indications from multichannel seismic reflection data. *In*: Cooper, A. K. & Raymond, C. R. (eds) *Proceedings of the 10th Int. Symposium of Antarctic Earth Sciences*. USGS Open-File Report **2007-1047**. US Geological Survey, Reston, VA, doi: 10.3133/of2007-1047.srp084.

Weigelt, E., Gohl, K., Uenzelmann-Neben, G. & Larter, R. D. 2009. Late Cenozoic ice sheet cyclicity in the western Amundsen Sea Embayment – evidence from seismic records. *Global and Planetary Change*, **69**, 162–169.

Publication 6.4.7:

Gohl, K., Uenzelmann-Neben, G., Hillenbrand, C.-D., Larter, R.D., Hochmuth, K., Kalberg, T., Weigelt, E., Davy, B., Kuhn, G., Nitsche, F.-O., (2013b). Seismic stratigraphic record of the Amundsen Sea Embayment shelf from pre-glacial to recent times: Evidence for a dynamic West Antarctic ice sheet. *Marine Geology*, 344, 115-131, doi:10.1016/j.margeo.2013.06.011.

Author contributions: Gohl processed and analysed most of the data, developed the seismostratigraphic model and interpretation and wrote most of this paper. Uenzelmann-Neben, Hochmuth, Kalberg and Weigelt processed and modelled some of the data. Larter and Hillenbrand contributed with some seismic data. All co-authors added to the interpretation and discussion. Most of the data were collected during Polarstern expeditions ANT-XXIII/4 (2006) and ANT-XXVI/3 (2010) with Gohl as chief-scientist.

Marine Geology 344 (2013) 115–131

Contents lists available at ScienceDirect

Marine Geology

journal homepage: www.elsevier.com/locate/margeo

Seismic stratigraphic record of the Amundsen Sea Embayment shelf from pre-glacial to recent times: Evidence for a dynamic West Antarctic ice sheet

Karsten Gohl [a,*], Gabriele Uenzelmann-Neben [a], Robert D. Larter [b], Claus-Dieter Hillenbrand [b], Katharina Hochmuth [a], Thomas Kalberg [a], Estella Weigelt [a], Bryan Davy [c], Gerhard Kuhn [a], Frank O. Nitsche [d]

[a] Alfred Wegener Institute,Helmholtz-Centre for Polar and Marine Research, Bremerhaven, Germany
[b] British Antarctic Survey, Cambridge, UK
[c] GNS Science, Avalon, Lower Hutt, New Zealand
[d] Lamont-Doherty Earth Observatory, Palisades, NY, USA

ARTICLE INFO

Article history:
Received 27 February 2013
Received in revised form 12 June 2013
Accepted 18 June 2013
Available online 26 June 2013

Communicated by J.T. Wells

Keywords:
West Antarctic margin
seismic stratigraphy
ice sheet dynamics
Pine Island Bay

ABSTRACT

Studies of the sedimentary architecture and characteristics of the Antarctic continental margin provide clues about past ice sheet advance–retreat cycles and help improve constraints for paleo-ice dynamic models since early glacial periods. A first seismostratigraphic analysis of the Amundsen Sea Embayment shelf and slope of West Antarctica reveals insights into the structural architecture of the continental margin and shows stages of sediment deposition, erosion and transport reflecting the history from pre-glacial times to early glaciation and to the late Pleistocene glacial–interglacial cycles. The shelf geometry consists of a large pre- and syn-rift basin in the middle shelf region between basement cropping out on the inner shelf and buried basement ridge and highs on the outer shelf. A subordinate basin within the large basin on the mid-shelf may be associated with motion along an early West Antarctic Rift System branch. At least 4 km of pre-glacial strata have been eroded from the present inner shelf and coastal hinterland by glacial processes. Six major sedimentary units (ASS-1 to ASS-6) separated by five major erosional unconformities (ASS-u1 to ASS-u5) are distinguished from bottom to top. Unconformity ASS-u4 results from a major truncational event by glacial advance to the middle and outer shelf, which was followed by several episodes of glacial advance and retreat as observed from smaller-scale truncational unconformities within the units above ASS-u4. Some of the eroded sediments were deposited as a progradional wedge that extends the outer shelf by 25 to 65 km oceanward of the pre-glacial shelf-break. We compare the observed seismic characteristics with those of other Antarctic shelf sequences and assign an Early Cretaceous age to bottom sedimentary unit ASS-1, a Late Cretaceous to Oligocene age to unit ASS-2, an Early to Mid-Miocene age to unit ASS-3, a Mid-Miocene age to unit ASS-4, a Late Miocene to Early Pliocene age to unit ASS-5, and a Pliocene to Pleistocene age to the top unit ASS-6. Buried grounding zone wedges in the upper part of unit ASS-5 on the outer shelf suggest pronounced warming phases and ice sheet retreats during the early Pliocene as observed for the Ross Sea shelf and predicted by paleo-ice sheet models. Our data also reveal that on the middle and outer shelf the flow-path of the Pine Island-Thwaites paleo-ice stream system has remained stationary in the central Pine Island Trough since the earliest glacial advances, which is different from the Ross Sea shelf where glacial troughs shifted more dynamically. This study and its stratigraphic constraints will serve as a basis for future drilling operations required for an improved understanding of processes and mechanisms leading to change in the West Antarctic Ice Sheet, such as the contemporary thinning and grounding line retreat in the Amundsen Sea drainage sector.

1. Introduction

The reconstruction of the dynamic history of Antarctic Ice Sheet (inlay map of Fig. 1) expansion and retreat since the onset of Southern Hemisphere glaciation improves our understanding of ice sheet growth and melting processes and thus predictions of future ice-sheet behavior. Because the West Antarctic Ice Sheet (WAIS) has a lower elevation than the East Antarctic Ice Sheet (EAIS) and most of its base is grounded below sea level, the WAIS is likely to have been more sensitive to changes in atmospheric and oceanographic conditions. Results from deep drilling on the Ross Sea shelf have shown that open-water conditions prevailed in that region for long periods of the Early Pliocene (5–3 m.y. ago) (McKay et al., 2009; Naish et al., 2009), suggesting a

* Corresponding author at: Alfred Wegener Institute,Helmholtz-Centre for Polar and Marine Research, Dept. of Geosciences, Section of Geophysics, Am Alten Hafen 26, 27568 Bremerhaven, Germany. Tel.: +49 471 48311361.
E-mail address: karsten.gohl@awi.de (K. Gohl).

0025-3227/$ – see front matter © 2013 Elsevier B.V. All rights reserved.
http://dx.doi.org/10.1016/j.margeo.2013.06.011

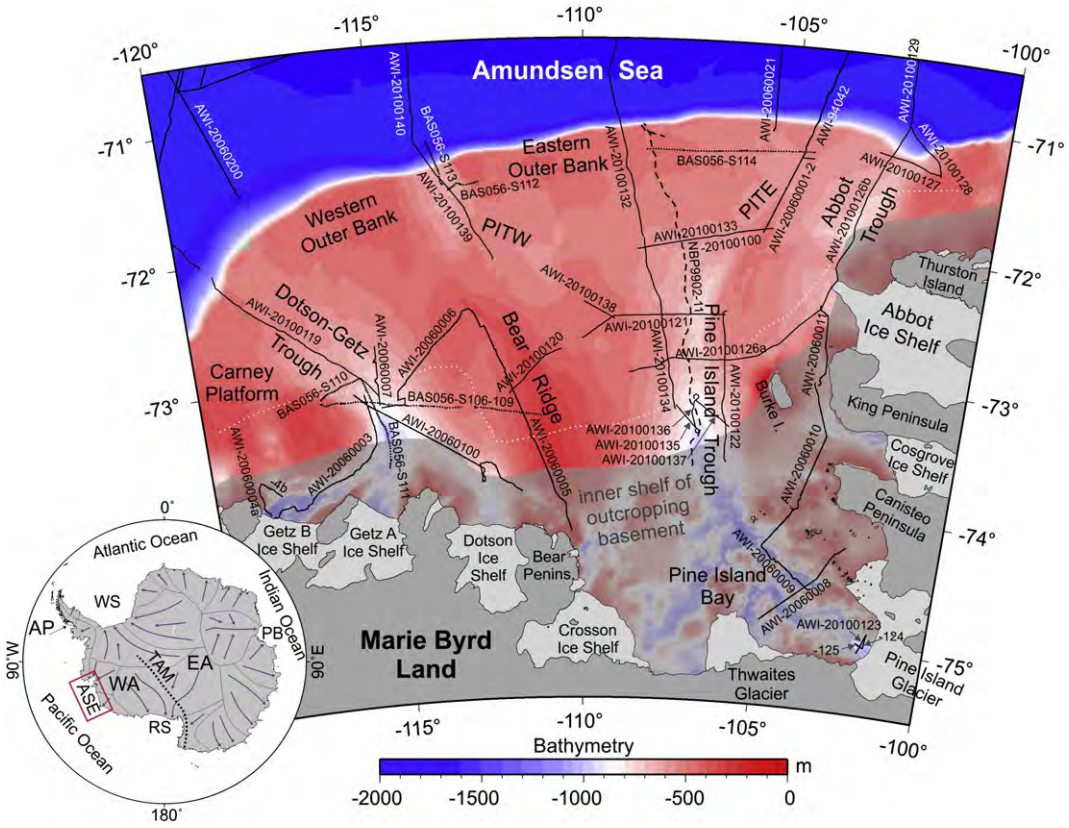

Fig. 1. Bathymetric map of Amundsen Sea Embayment (ASE) (updated version from Nitsche et al., 2007, 2013) illustrating main glacial troughs which are deeply incised into the outcropping basement (gray semi-transparent area) of the inner shelf. Black lines mark all existing multi-channel (solid lines) and single-channel seismic profiles (hashed and dotted lines) annotated with their profiles names. Carney Platform, Bear Ridge, Western Outer Bank, Eastern Outer Bank, Abbot Trough, Pine Island Trough, Pine Island Trough West (PITW) and Pine Island Trough East (PITE) are yet unofficial geographical names used in this paper for better orientation. In the text we refer to the "western ASE shelf" being the Amundsen Sea shelf west of Bear Ridge, Western Outer Bank, Dotson-Getz Trough and Carney Platform, the "central ASE shelf" being the area between Eastern Outer Bank, PITW and the eastern flank of Bear Ridge, and the "eastern ASE shelf" being the area of Pine Island Trough, PITE, Abbot Trough and Pine Island Bay. The inlay map of Antarctica shows the ice divides (black lines), main ice flow directions (dark blue arrows) (both simplified after Drewry (1983)), the outline of the Transantarctic Mountains (dotted bold black line; TAM), and the study area of the ASE (red box). Other abbreviations in the inlay map are: WA West Antarctica, EA East Antarctica, AP Antarctic Peninsula, RS Ross Sea, PB Prydz Bay, WS Weddell Sea.

partial or full collapse of the WAIS at times when atmospheric carbon dioxide concentrations were as high as 400 ppm (which will be reached again within the next 5 years on current trends: http://www.esrl.noaa.gov/gmd/ccgg/trends/) and planetary temperatures were up to 3 °C higher than today. However, the data used for interpreting past WAIS behavior are extremely scarce and may be spatially biased to some degree. The continental shelf and slope drill sites of the Antarctic Drilling Program ANDRILL (Harwood et al., 2009; Levy et al., 2012), the Deep Sea Drilling Project DSDP Leg 28 (Hayes and Frakes, 1975) and the Cape Roberts Project CRP (Cape Roberts Science Team, 1999, 2000) are all located in the western and central regions of the Ross Sea Embayment where the signals interpreted for WAIS dynamics cannot be clearly separated from the influence of ice draining the EAIS through the Transantarctic Mountains (Kerr and Huybrechts, 1999; Bart, 2005).

Ice sheet discharge into the Amundsen Sea Embayment (ASE) (Fig. 1) is entirely sourced from the WAIS (inlay map Fig. 1). The WAIS volume corresponds to an equivalent of 3–5 m eustatic sea level change (Bamber et al., 2009; Fretwell et al., 2013), and about one third of it is stored in drainage basins that discharge through outlet glaciers onto the ASE shelf. The largest drainage systems are those of the Pine Island and Thwaites glaciers, which are known for their current flow acceleration, fast retreat, rapid thinning and high basal melt rates of floating ice at their termini that exceed those of any other Antarctic outlet glacier outside the Antarctic Peninsula (Rignot, 2008; Rignot et al., 2011; Pritchard et al., 2012). Past expansion and retreat of grounded and floating ice across the continental shelf of the ASE must have left signals and traces of glacial sediment accumulation, transport and erosion. Thus, a study of the sedimentary architecture and characteristics of the ASE margin will provide clues of past ice sheet advance–retreat cycles and help improve constraints for paleo-ice dynamic models of the WAIS since early glacial periods.

Seismic profiles acquired over recent years enabled us for the first time to characterize and map seismostratigraphic sequences from a large part of the ASE shelf and slope (Fig. 1). The dataset reveals the architecture of the continental margin, with patterns of sediment deposition, erosion and transport allowing the reconstruction of its history from pre-glacial times to early glaciation and to late Pleistocene glacial–interglacial cycles. We infer ages for the seismostratigraphic units and present a depositional model that serves as a basis for understanding processes of glacial advance and retreat of the WAIS.

2. Tectonic and depositional setting

The ASE comprises one of the broadest continental shelves along the Pacific margin of West Antarctica (Fig. 1). Pine Island Bay in the eastern ASE has long been suggested to delineate a Paleozoic/Mesozoic crustal boundary between the Thurston Island block and the Marie Byrd Land block, because its eastern border offsets the coastlines of Marie Byrd Land and the Thurston Island region (Dalziel and Elliot, 1982; Storey, 1991; DiVenere et al., 1994). Plate-tectonic reconstructions infer that this region was a key area for continental rifting and breakup between the Chatham Rise east of New Zealand and Marie Byrd Land starting at 90 Ma (Larter et al., 2002; Eagles et al., 2004; Wobbe et al., 2012), about 10–15 m.y. after the collision of the Hikurangi Plateau with

Chatham Rise and the cessation of the Gondwana margin subduction (e.g., Davy et al., 2008; Kipf et al., 2012). Airborne magnetic and satellite-derived gravity data grids revealed a series of quasi-linear southwest-northeast directed anomalies on the ASE shelf, interpreted as traces of magmatism along distributed rift axes before breakup (Gohl et al., 2007, 2013). The relatively small crustal thickness of 22–24 km measured on the inner to middle shelf (Gohl et al., 2007) supports the hypothesis of a rifted and thinned continental crust in the ASE. Plate-kinematic reconstructions also suggest that the ASE crust has been subject to deformation along the southern boundary of the Bellingshausen Plate which was active between about 79 and 61 Ma (Eagles et al., 2004; Wobbe et al., 2012). This deformation is supported by observations of northwest–southeast trending lineaments in the potential field grids (Gohl et al., 2007, 2013). A third set of lineaments, striking north–northeast, suggests a third phase of deformation and intrusion, which has been associated with a possible branch of the West Antarctic Rift System (Gohl et al., 2007, 2013). The existence of such a rift branch in the ASE was also postulated by Dalziel (2006) and Jordan et al. (2010). A north–south oriented strike–slip motion with transtensional deformation can be derived for the Amundsen–Bellingshausen Sea sector of West Antarctica by applying rotation parameters for East–west Antarctic relative motion, as a study by Müller et al. (2007) demonstrated for the Eocene to Miocene. Gohl (2012) and Gohl et al. (2013) suggested that the tectonic–magmatic architecture inherited from the three main crustal deformation phases has placed some degree of control on sedimentation and glacial flow directions at later times as observed by correlation to the directional bathymetric trends of paleo-ice stream troughs (Nitsche et al., 2007).

The earliest recorded multi-channel seismic (MCS) reflection data from the ASE show that at 104° W (Fig. 1) the outer shelf and slope sediments have undergone both progradational and aggradational deposition probably since the Middle Miocene (Nitsche et al., 1997, 2000). Aggradation dominated the strata geometry in younger stages. A long single-channel seismic (SCS) profile (Lowe and Anderson, 2002, 2003) follows the main glacial Pine Island Trough and reveals oceanward inclined sediment sequences on the middle shelf north of bedrock cropping out on the inner shelf. The dipping strata typical for Antarctic shelves (e.g., Cooper et al., 1991, 2008; Anderson, 1999) are possibly of Cretaceous to Miocene age and buried by aggradational, less consolidated strata of supposedly Pliocene–Pleistocene age (Lowe and Anderson, 2002). Several unconformities separate the dipping strata and may represent phases of subglacial erosion. Dowdeswell et al. (2006) describe these SCS data from the outer shelf and upper slope close to 108º W (Fig. 1) as showing mainly aggradation on the shelf and minor progradation on the shelf edge and slope. While most of the inner shelf of Pine Island Bay is void of major sedimentary cover, as observed in seismic and acoustic subbottom profiles (Lowe and Anderson, 2003; Nitsche et al., 2013) and inferred from magnetic data (Gohl et al., 2013), a few small and shallow basins are observed close to its eastern shore (Uenzelmann-Neben et al., 2007) and close to the front of Pine Island Glacier (Kellogg and Kellogg, 1987; Nitsche et al., 2013). The western ASE shelf is separated from the eastern shelf by a bathymetric high (Nitsche et al., 2007), here named 'Bear Ridge' as it extends north from Bear Peninsula (Fig. 1). Oceanward dipping mid-shelf strata north of outcropping basement are observed in seismic data from the Dotson–Getz Trough collected in 1999 and 2006 (Wellner et al., 2001; Graham et al., 2009; Weigelt et al., 2009, 2012) and exhibit alternating sequences of low and high reflectivity, which Weigelt et al. (2009) interpret as episodes of major glacial advances and retreat in the Miocene.

Observations of sub- and proglacial bedforms in multi-beam swath bathymetry surveys, such as mega-scale lineations and grounding zone wedges, indicate that grounded ice expanded onto the middle to outer shelf during the last glacial maximum (LGM) (Lowe and Anderson, 2003; Dowdeswell et al., 2006; Evans et al., 2006; Graham et al., 2009, 2010; Larter et al., 2009; Jakobsson et al., 2012; Klages et al., 2013). The retreat of the ice sheet from the ASE shelf since the LGM is documented in both these swath-bathymetric records and sedimentary facies sequences recovered in cores (Lowe and Anderson, 2002; Smith et al., 2009, 2011; Hillenbrand et al., 2010, 2013; Ehrmann et al., 2011; Jakobsson et al., 2011; Kirshner et al., 2012; Nitsche et al., 2013). According to these studies, most of the grounded ice had retreated to the inner shelf already by the early Holocene.

To date, no core records of the stratigraphic composition and chronology of the major depositional sequences on the ASE continental shelf and slope exist. Onshore outcrops on islands, coastal cliffs and nunataks above the ice sheet in the ASE consist entirely of Mesozoic and Permian granitoids, gneisses and volcanics as well as Cenozoic volcanic rocks (e.g., Pankhurst et al., 1993, 1998; Mukasa and Dalziel, 2000; Rocchi et al., 2006; LeMasurier, 2008; Kipf et al., 2012). Although predominantly unconsolidated subglacial and glacimarine sediments on the shelf have been sampled by shallow sediment coring and grab sampling, drilling of more consolidated strata has not been attempted yet.

3. Data acquisition and processing

The database of SCS and MCS records from the shelf and slope of the ASE (Fig. 1) used for this study was acquired during five ship expeditions from 1994 to 2010. The first MCS data were collected from the outer shelf, slope and rise during RV *Polarstern* expedition ANT-XI/3 in 1994 and described in Nitsche et al. (1997, 2000). Wellner et al. (2001), Lowe and Anderson (2002, 2003) and Dowdeswell et al. (2006) described SCS datasets collected along Pine Island Trough and the Dotson-Getz Trough during RV *Nathaniel B. Palmer* cruise NBP9902 in 1999. More SCS data were collected on the outer shelf and the middle shelf of the western ASE during RRS *James Clark Ross* cruise JR141 in early 2006 (Larter et al., 2007; Graham et al., 2009), followed by MCS data recorded on RV *Polarstern* cruise ANT-XXIII/4 in the same season of 2006 (Gohl, 2007; Uenzelmann-Neben et al., 2007; Weigelt et al., 2009, 2012). Due to unusually favorable sea-ice conditions in the season of early 2010, we were able to acquire more than 3500 km of MCS data from the middle to outer shelf, the slope and the continental rise of the Amundsen Sea during RV *Polarstern* expedition ANT-XXVI/3 (Gohl, 2010). The shelf profiles targeted the strata along the main axes of the Dotson–Getz Trough, the Pine Island Trough and the Abbot Trough, which is a glacial trough extending NNE-wards offshore from the western end of the Abbot Ice Shelf (Fig. 1), with some profiles crossing the troughs, inter-ice stream ridges between the troughs and tributaries feeding into the main troughs on the inner shelf or branching off them on the outer shelf.

Most MCS data of the 2010 expedition were collected using a 3000 m long digital solid streamer (Sercel Sentinel) with 240 channels. Only in areas with sea-ice coverage, we changed to an older 600 m long analogue streamer (Prakla) with 96 channels. Both streamers were towed at a nominal water depth of 10 m. We recorded the data of both systems with a 1 ms sampling interval and did not apply a filter during recording with the exception of an anti-alias filter. As airgun source, we used a cluster of up to three GI-Guns (Sercel) of 150 in.^{3} volume (sum of 45 in.^{3} generator and 105 in.^{3} injector volumes) each, assembled underneath a steel frame to prevent ice damage, set to 'True GI-Mode' for minimizing the bubble effect, and fired at 3 m water depth with 195 bar operational pressure at intervals between 6 and 12 s. Due to an unsolved permitting issue with the German Federal Environment Agency, we had to refrain from using airguns of larger volumes that would have been necessary in order to obtain reflections from the basement in large parts of the middle to outer shelf and slope. In order to obtain better P-wave velocities from the shelf sedimentary rocks, we deployed six ocean-bottom seismometers (OBS) along the east–west aligned profile AWI-20100100/AWI-20100133 (Fig. 1) over the middle to outer shelf of the eastern ASE. The OBS systems recorded the GI-Gun shots fired every full minute. A summary of the acquisition instruments as well as the recording and data processing

parameters of all seismic surveys of the ASE shelf and slope is given in Tab. S1 of the electronic supplement.

Standard data processing was initially applied to all seismic reflection records of the 2010 expedition (Tab. S1). The presence of over-compacted sediments (glacial tills) close to the seafloor is typical for polar continental shelves and, consequently, seafloor multiples of particularly large amplitudes are present throughout all seismic profiles. We applied various processing strategies to suppress seafloor multiples as much as possible, which included filtering in the frequency–wave number (f–k) domain or through a Radon transform (τ–p domain). In case of good signal-to-noise ratios of the data in regular time–distance (t–x) domain, multiples were suppressed to a large degree, improving the appearance of primary reflections. In areas of low signal-to-noise ratios, and for data recorded with the short streamer, the suppression results are rather meager. A particular problem affects profiles that cross shallow parts of the outer shelf, e.g. profile AWI-20100132. Here, numerous icebergs plowed deeply into the seafloor (Evans et al., 2006; Graham et al., 2010). Such furrows generate large amplitude diffractions in the seismic wave-field and attenuate the deeply penetrating energy, in particular at the higher frequency band emitted by GI-Guns. They also aggravate attempts to remove seafloor multiples because the diffractive energy also reverberates as part of the multiple reflection signal. A configuration of airguns with larger volumes and, thus, a lower mean frequency, probably would have enabled a penetration of primary energy down to basement depths even in shelf areas where sedimentary strata are thickest. Numerous seismic profiles have data gaps due to shut-downs of the airgun sources when marine mammals were observed.

4. Seismic characterization and horizon stratigraphy

Given the absence of physical properties data for ASE shelf sediments measured on long drill cores or determined by borehole logging, our interpretation of seismic facies has to rely exclusively on the observation of seismic horizon analysis and reflection characteristics. A comparison to interpreted seismic sections and drill-hole controlled seismostratigraphy from other Antarctic continental shelves – mainly the Ross Sea shelf – is used to aid in our seismic profile characterization and our assignment of ages to the seismostratigraphic units observed on the ASE shelf. The main observational parameters in our analysis include (1) continuity of seismic reflectors, (2) distribution of relative reflection amplitudes, (3) stratigraphic and structural seismic layer boundaries (discontinuities, faults, downlapping, onlapping), (4) geometry of reflectors (horizontal, disturbed, undisturbed, folded, faulted, inclined/dipping), and (5) internal acoustic structure of seismic units (transparent, stratified).

We conduct our analysis beginning in the western ASE and progressively move eastward to the eastern embayment, thereby proceeding from the inner to outer shelf and slope in each region (Fig. 1). Emphasis is placed on profiles parallel and perpendicular to the main paleo-ice stream troughs in order to obtain an indication for structural trends and true dips. Up to six major sedimentary units (ASS-1 to ASS-6) and five dominant erosional unconformities (ASS-u1 to ASS-u5) can be identified for most of the ASE shelf from bottom to top.

4.1. Western ASE shelf

A transect of combined MCS and SCS profiles AWI-20100119 and BAS056-S111 (Fig. 2) follows the Dotson–Getz Trough from the inner to outer shelf and slope. It shows reflection characteristics representing the main depositional sequences along this trough, although the outer shelf profile had to deviate from the trough axis due to thick sea-ice cover. Oceanward dipping strata overlying acoustic basement that were previously recorded in profiles at the inner-to-middle shelf transition (Graham et al., 2009; Weigelt et al., 2009) continue seaward across the middle shelf. In the section extending from outcropping basement to about 73° S (shot-points 6700 to 4000 of BAS056-S111), the reflector sequences are continuous, highly stratified, of medium to high amplitudes, and dip between 4.2° and 2.0° at the inner to mid-shelf transition (Fig. 2). ASS-u1 marks an unconformity between 70 and 200 ms two-way travel-time (TWT) above the northward dipping basement. Deformation from faulting and folding appears locally deeper than 1.1 s TWT at shot-points 4200 and 5400 of BAS056-S111 (Fig. 2). The inclination of the strata decreases to 1.0–0.5° on the middle shelf within sequence ASS-3. ASS-3 and younger sequences exhibit more variable, less laminated seismic facies than the underlying strata and display alternating zones of strong and poor reflectivity, which Weigelt et al. (2009) also observed in other profiles from the ASE mid-shelf (Figs. S1–S3 in supplementary material). A series of short unconformities and erosional truncations affects ASS-3 and all younger sequences. The major unconformities are annotated with ASS-u3 and ASS-u4 (Fig. 2). The outer shelf northwest of about 72° 40′ S (CDP 3000 of AWI-20100119) is dominated by strong progradation towards the shelf break. The lowermost prograding sequences downlap onto the older strata, and downlapping also characterizes the younger prograding units. A major erosional unconformity, ASS-u5, truncates most of the dipping sequences beneath horizontally stratified, undisturbed deposits thinning from the topmost 0.2 s TWT on the outer shelf to less than 0.05 s TWT on the middle shelf. Two large grounding zone wedges (GZW) observed in the topmost sequence on the middle shelf correlate with seaward-inclined ramps observed on parallel bathymetric profiles (Larter et al., 2009) and document temporary stillstands of grounding line retreat since the LGM (e.g. Alley et al., 1989; Larter and Vanneste, 1995; Howat and Domack, 2003; Graham et al., 2009, 2010).

4.2. Central ASE shelf

Profile AWI-20100139 (Fig. 3) follows the outer Pine Island Trough West (PITW), which branches off westward from the main Pine Island Trough (Evans et al., 2006). The lowermost sequence overlying the acoustic basement consists of semi-continuous reflectors between 3.2 and 4.4 s TWT that rise northward from the middle shelf to the shelf edge. We interpret this thin unit as partially stratified sedimentary sequence (ASS-1) lying on top of the upward tilted basement surface with regionally concordant dip and, thus, being of pre-breakup age. Basement reflections are rather subtle in terms of amplitude and continuity, possibly due to minor acoustic impedance contrasts between crystalline bedrock and the highly compacted and indurated sedimentary rocks of units ASS-1. A thick sequence of sedimentary strata (ASS-2) downlaps onto unconformity ASSu-1, which truncates these oldest sedimentary rocks. The top of unit ASS-2 is locally truncated by unconformity ASSu-2 onto which another stratified set of oceanward inclined reflectors (ASS-3) downlaps. ASS-3 is erosionally truncated by unconformity ASSu-3 that is overlain by unit ASS-4. This sequence of sedimentary strata dips oceanward from the mid-shelf. Unconformity ASSu-4 truncates unit ASS-4 and is overlain by an up to 1.5 km (1.3 s TWT) thick sequence of horizontal strata of varying reflection characteristics. We distinguish various zones of strong reflections alternating with reflection-poor zones within this unit, separated by continuous horizons of relatively large amplitude. These high-amplitude horizons exhibit locally restricted unconformities, but it remains unclear from the data, whether these unconformities indicate any significant shift in deposition and/or age. The uppermost sequence ASS-6 on top of unconformity ASSu-5 can be clearly distinguished from the sequences below by its almost transparent reflection character in the MCS data. Northward of CDP 3000 (Fig. 3), the sediment strata of units ASS-5 and ASS-6 form a progradational wedge building the outermost 25 km of the modern top shelf. However, it is interesting to note that these prograding strata directly downlap onto unconformity ASSu-4.

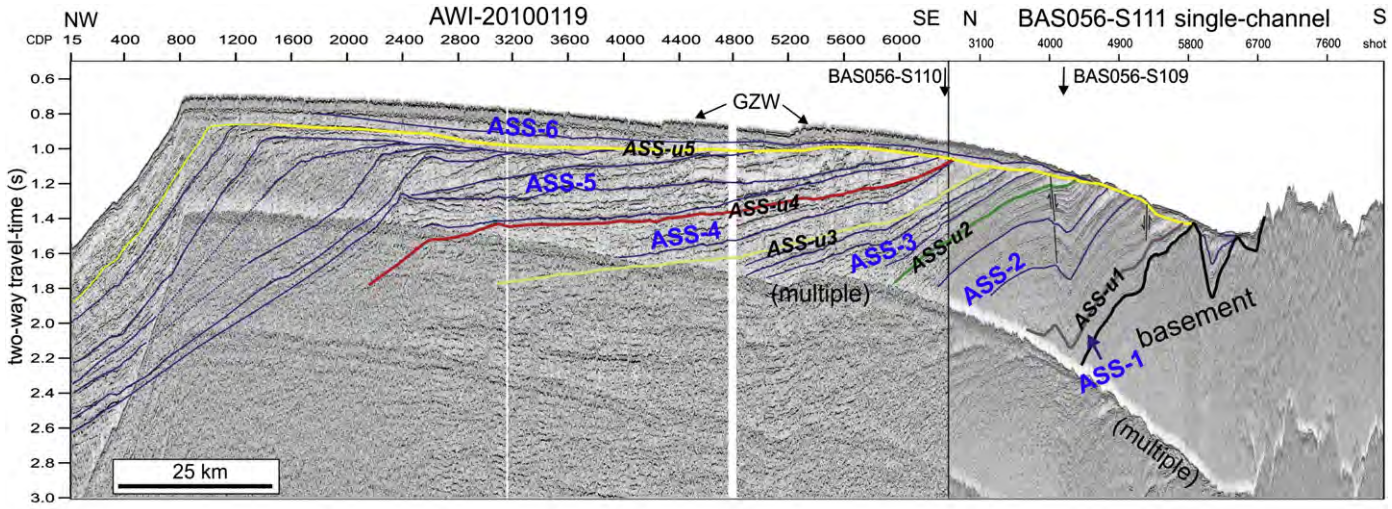

Fig. 2. Composite of seismic profiles BAS056-S111 and AWI-20100119 following the Dotson-Getz Trough of the western ASE shelf and across the upper slope. Main unconformities ASS-u1 to ASS-u5 separating the major seismostratigraphic units ASS-1 to ASS-6 are marked and annotated. Other dominant reflectors within these units are highlighted by the dark blue lines. Note normal faults within folded strata on the inner shelf. Black arrows indicate crossing seismic lines. GZW stands for grounding zone wedge. Description of seismic horizons and reflection characteristics is in the text. See profile locations in Fig. 1. (For interpretation of the references to color in this figure legend, the reader is referred to the web version of this article.)

Within the upper sequences of unit ASS-5 (Fig. 3), two lens-shaped features are observed that have a geometry typical for GZWs with a steeper ice-distal (lee) side and a more attenuated ice-proximal (stoss) side. We interpret these features as buried grounding zone wedges (bGZW) (Dowdeswell and Fugelli, 2012). bGZWs were formed on the shelf by retreating grounded ice sheets when the retreat of the grounding zone came to a temporary halt (e.g. Larter and Vanneste, 1995; Dowdeswell and Fugelli, 2012). bGZW 1 shows at 1.25 s TWT near CDP 500, and the stratigraphically higher bGZW 2 can be observed at 1.20 s TWT near CDP 2300. The surfical GZW at CDP 1400 is identified as an exposed bedform feature of uppermost unit ASS-6. The two crossing SCS lines BAS056-S112 and BAS056-S113 (R. Larter, unpublished data) show buried and exposed grounding-zone wedges of similar shape and lack of internal stratification within the upper part of units ASS-5 and ASS-6.

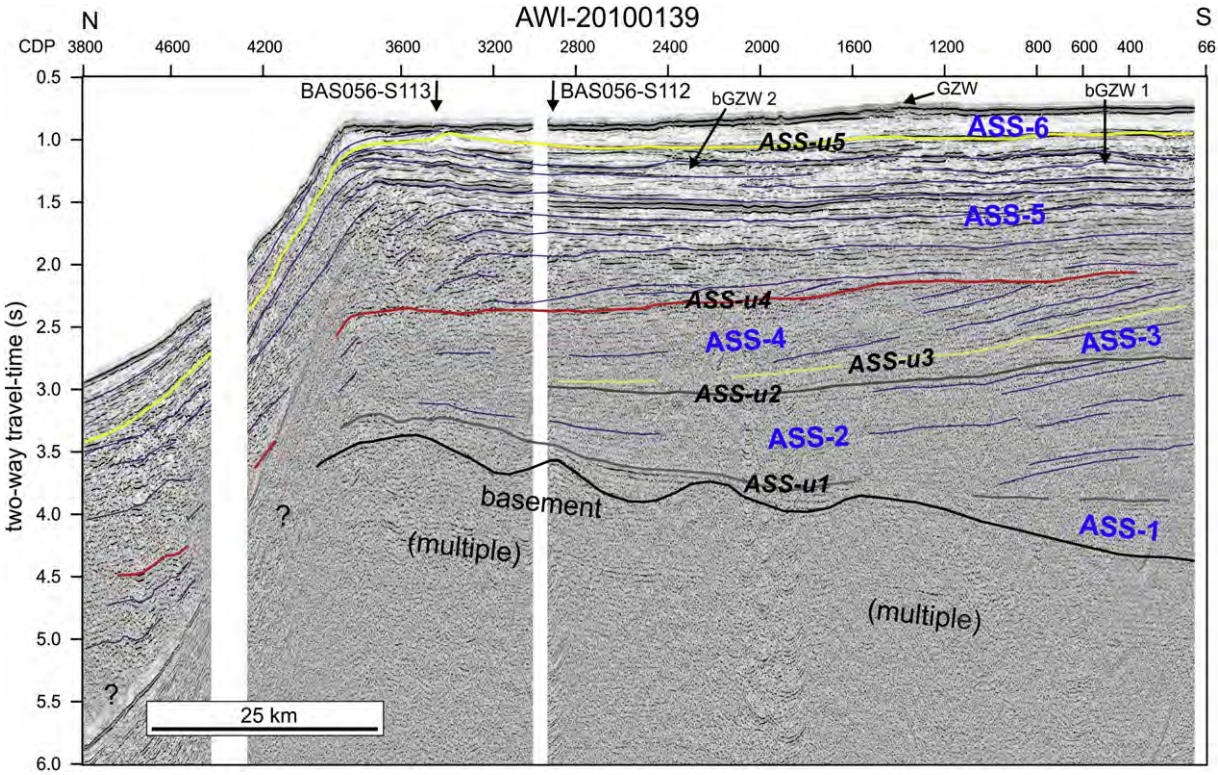

Fig. 3. Seismic profile AWI-20100139 following the outer Pine Island Trough West of the central ASE shelf and across the upper slope. Main unconformities ASS-u1 to ASS-u5 separating the main sedimentary units ASS-1 to ASS-6 are marked and annotated. Other dominant seismic horizons within the sediment units are line-drawn. Black arrows indicate seismic cross-lines. GZW stands for grounding zone wedge; bGZW stands for buried GZW. Description of seismic horizons and reflection characteristics is in the text. See profile location in Fig. 1.

4.3. Eastern ASE shelf and Pine Island Bay

A set of north–south trending seismic profiles and several crossing profiles cover a large part of the central Pine Island Trough from the inner shelf to its outer shelf branches. The composite MCS transect consisting of profiles AWI-20100132, AWI-20100134 and AWI-20100135 (Fig. 4a) follows the western trough flank and images sequences of sedimentary strata down to maximum basement depths of about 7 km below seafloor on the middle shelf (using an average P-wave velocity of 3.5 km/s for the sedimentary column). However, the relatively small airgun source and strong seafloor multiple reflections prevent unambiguous identification of a deep continuous reflector as the top of the acoustic basement. Our interpretation is derived from the observation that the lowermost northward dipping sedimentary strata downlap onto a deep-lying, discontinuous and weak reflector rising from the middle to outer shelf. We cannot entirely exclude the possibility, however, that the apparent top of the acoustic basement represents the top of compact, highly consolidated or even lithified sedimentary strata.

We observe five main unconformities in this composite profile (Fig. 4a). Lowermost unconformity ASS-u1 separates units that exhibit minor deformation but dip slightly in opposite directions underneath the inner shelf. The unit between unconformities ASS-u1 and ASS-u2 is partially deformed and disrupted by faults on the inner shelf. The strongest erosional signature characterizes unconformity ASS-u4 in the mid-shelf section of the profile, where it truncates the strata of unit ASS-4. ASS-u4 can be traced seaward to the outer shelf. There, a wedge of progradational foreset beds downlaps onto it, as observed in profile AWI-20100139 from the outer PITW (Fig. 3). The lack of progradation beneath ASS-u4 on the outer shelf indicates that it may represent the paleo-shelf seabed before grounded ice reached the outer shelf. Despite the remnants of seafloor multiple reflections at the shelf break, it is possible to trace ASS-u4 to the base of the continental slope and farther onto the continental rise where it can be correlated with the top of seismostratigraphic Unit 2 of Uenzelmann-Neben and Gohl (2012). They estimated an age of 21–14 Ma for their Unit 2 from an indirect correlation to a pre-glacial to glacial transitional stage with ice caps expanding onto the eastern Ross Sea shelf as observed by De Santis et al. (1999). The uppermost unconformity ASS-u5 truncates middle shelf strata down to about 400 m depth below seafloor and can also be traced onto the continental rise, where it corresponds to the top reflector of Unit 3 with an age of 4 Ma (Uenzelmann-Neben and Gohl, 2012) derived from long-distance horizon correlation to DSDP Site 324 in the western Bellingshausen Sea (Tucholke et al., 1976).

The SCS profile NBP9902-11 of Lowe and Anderson (2002, 2003) (Fig. S4) follows the deepest section of the central Pine Island Trough and then crosses the outer shelf. The strata and unconformity sequence above the seafloor multiple resembles that of our composite MCS profile (Fig. 4), except that on NBP9902-11 we identify ASS-u2 with a rather large uncertainty. The strata beneath this unconformity are moderately folded and faulted, while strata above it and further seaward exhibit little evidence of deformation. ASS-u4 is the dominant unconformity and separates oceanward dipping strata from more horizontally layered sequences. The “amalgamated glacial unconformity” of Lowe and Anderson (2002) is named ASS-u5 in our analysis. Graham et al. (2010) and Jakobsson et al. (2012) identified a large GZW on the seafloor above ASS-u5 at the transition from the inner to middle shelf (Fig. S4).

MCS line AWI-20100122 (Fig. S5) follows the eastern flank of the central Pine Island Trough. Although the top of the acoustic basement north of CDP 3600 is poorly imaged, it appears that between CDP 3600 and CDP 1800 the configuration of the overlying strata (below ASSu-5) largely conforms with the undulating basement relief. Folding and faulting of the oldest sedimentary strata is clearer than in the two parallel profiles further to the west. The reflection character changes from deformed reflectors to steadily northward dipping strata in the northern part of this profile. The youngest unconformity ASS-u5 with up to 250 m of overlying horizontally layered strata can be traced along most of the profile.

Progradational deposits characterize the outer shelf along the eastern flank of the central Pine Island Trough as the composite of profiles AWI-20060001, -0002 and AWI-94042 (Fig. 5) reveal. The progradational wedge of the outermost shelf is overlain by an aggradational unit that is up to 460 m thick, as previously described by Nitsche et al. (1997). However, the new seismic profiles presented here extend further landward and reveal that the onset of oldest progradation was located at least 60 km south of the present shelf break above unconformity ASS-u4. The crossing, east–west striking SCS profile BAS056-S114 (Fig. S6) shows eastward prograding sequences overlain by aggradational, slightly wavy strata. The aggradational units in profiles AWI-20060001, -0002 and BAS056-S114 are up to 700 m thick (conversion of 0.6 s TWT by using a P-wave velocity of 2300 m/s for highly consolidated sedimentary strata). Unfortunately, the use of the short streamer for the 2006 MCS surveys and numerous diffractions from iceberg scours compromised attempts to suppress seafloor multiple reflections and, thus, deeper horizons could not be imaged.

Uenzelmann-Neben et al. (2007) analyzed seismic profiles AWI-20060010 and -0011 along the easternmost Pine Island Bay close to the shores of Canisteo Peninsula and King Peninsula (Fig. 1a,b). They identified up to 300 m thick sedimentary strata in a glacial trough extending WNW-wards from the Cosgrove Ice Shelf (‘Cosgrove Trough’ in Klages et al., 2013) and northward dipping and thickening strata in the NNE-ward striking Abbot paleo-ice stream trough, which is wider and deeper than the western and eastern branches of outer Pine Island Trough (Fig. 1). The new seismic profiles AWI-20100126b, -0127 and -0128 (Fig. 1) have recently revealed that the seabed underlying Abbot Trough is characterized by strong progradation and that its sedimentary architecture is controlled by various basement highs and ridges (Hochmuth and Gohl, in press).

The seismic profiles AWI-20100126a, AWI-20100121, AWI-20100133 and BAS056-S114 cross the central Pine Island Trough and its eastern outer shelf branch (PITE) in an east–west direction, link the trough-parallel lines (Fig. 1) and enable a detailed spatial analysis of the seismostratigraphic units and unconformities. Profile AWI-20100126a (Fig. 6) and composite profiles AWI-20100120 and -0121 (Fig. 7) reveal a sedimentary sub-basin within the mid-shelf part of central Pine Island Trough with up to 4–4.5 km thick infill at about 108° 30′ W. To the east, this sub-basin is bound by a steeply rising basement, which further ascends towards a basement high northwest of Burke Island (Fig. 6). In the central Pine Island Trough we correlated major unconformities with those observed in the trough-parallel profiles. Unconformity ASS-u1 terminates at the basement flank, while unconformity ASS-u2 can be traced along the entire profile AWI-20100126a. The major glacial unconformity ASS-u5, whose subbottom depth roughly conforms with the bathymetric incision of the central Pine Island Trough, truncates the unit ASS-3 on AWI-20100126a (Fig. 6) while ASS-u4 truncates the reflectors in unit ASS-4 farther north (Fig. 7). In general, the seismic reflectors in profile AWI-20100126a appear more irregular and chaotic within the sub-basin than outside of it. This situation contrasts with the parallel profile AWI-20100121 farther north, where the reflectors both within and outside the sub-basin are rather smooth. In profile AWI-20100133 (Fig. S7) on the outer shelf the bathymetric expression of the central Pine Island Trough is rather subdued (the total bathymetric difference along the 120 km long profile is just 150 m) and both the seismostratographic sequences and correlated unconformities are mostly horizontal. Only ASS-u3 truncates northwest-dipping older strata, and ASS-u5 truncates slightly eastward dipping reflectors. We assume that the sequences of sedimentary strata in profile AWI-20100133 rise eastwards, because near the eastern flank of PITE

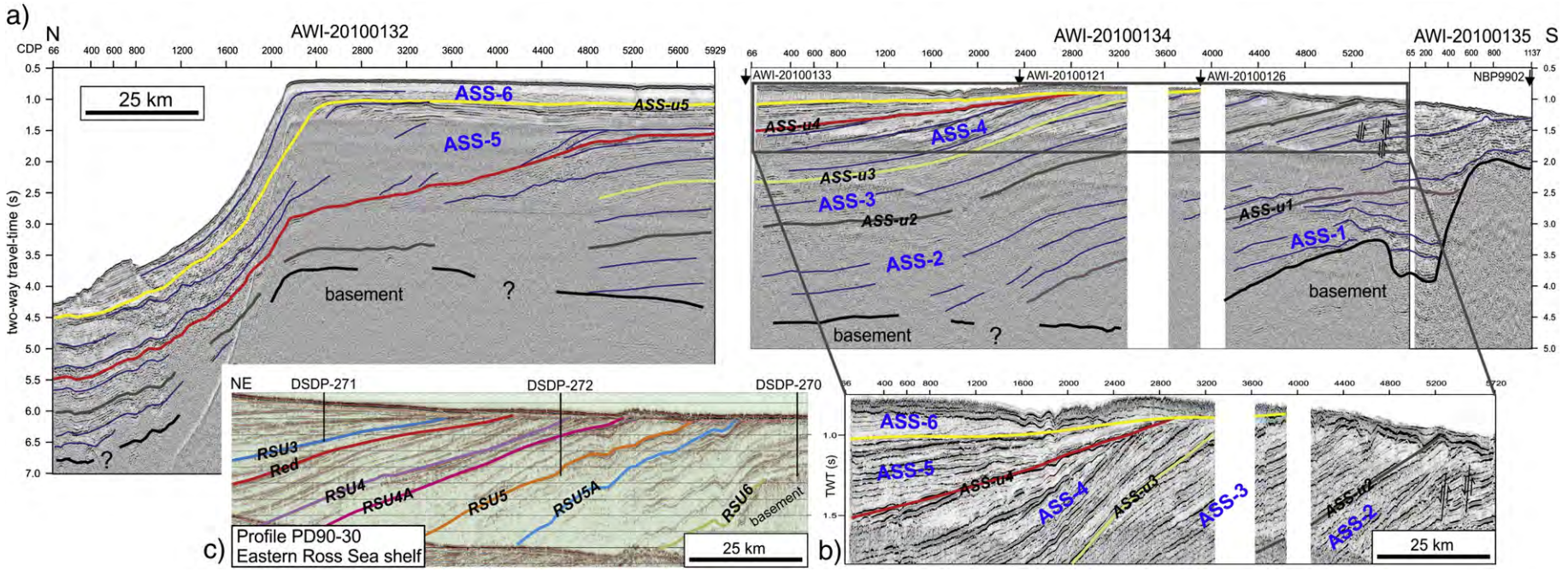

Fig. 4. (a) Composite of seismic profiles AWI-20100135, AWI-20100134 and AWI-20100132 from the central Pine Island Trough across the outer shelf and slope of the eastern ASE shelf. Main unconformities ASS-u1 to ASS-u5 separating the main sedimentary units ASS-1 to ASS-6 are marked and annotated. Other dominant seismic horizons within the sediment units are line-drawn. Note some normal faults within folded strata in the South. Black arrows indicate seismic cross-lines. Description of seismic horizons and reflection characteristics is in the text. See profile locations in Fig. 1. (b) The seismic reflection pattern of the top segment of profile AWI-20100134 has a large degree of similarity with that of (c) seismic profile PD90-30 collected across the Eastern Basin of the Ross Sea shelf (Anderson and Bartek, 1992). This profile crosses the DSDP Leg 28 Sites 270, 271 and 272 (Hayes and Frakes, 1975). The drawn and named unconformities are from Decesari et al. (2007) and Sorlien et al. (2007).

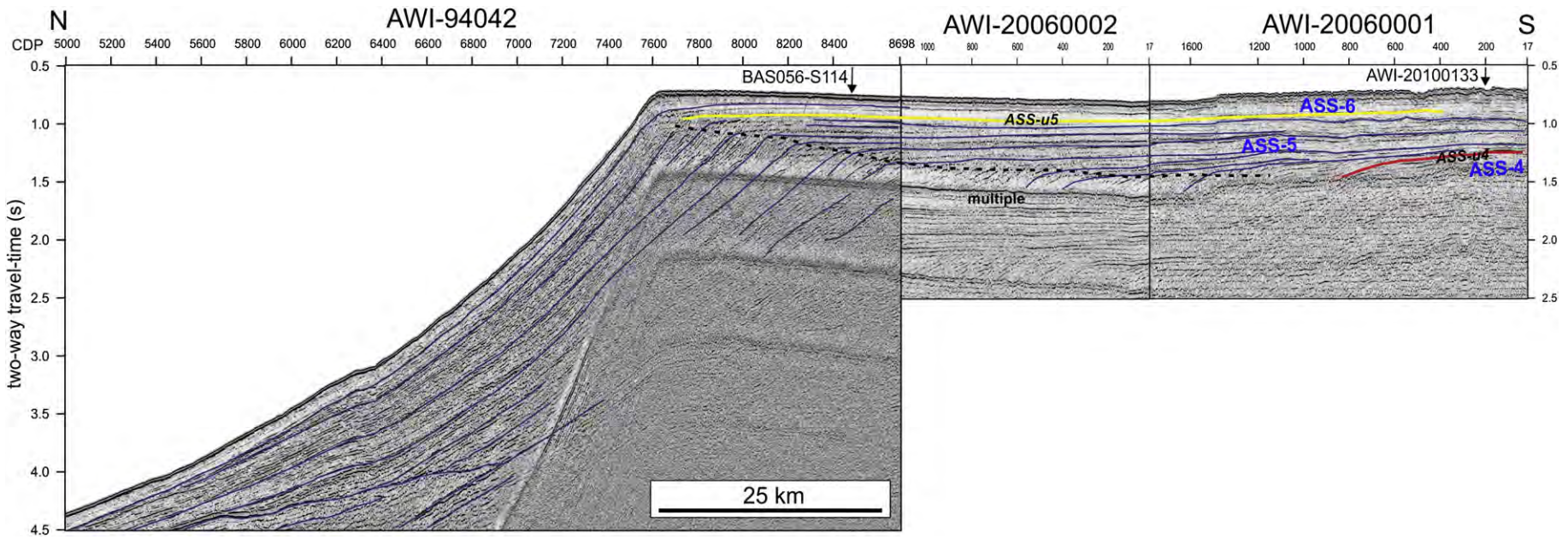

Fig. 5. Composite of seismic profiles AWI-20060001, AWI-20060002 and AWI-94042 from the central Pine Island Trough across the outer shelf and slope of the eastern ASE shelf. Main unconformities ASS-u4 and ASS-u5 separating the main sedimentary units ASS-4 to ASS-6 are marked and annotated. Other dominant seismic horizons within the sediment units are line-drawn. Black arrows indicate seismic cross-lines. Description of seismic horizons and reflection characteristics is in the text. See profile locations in Fig. 1.

they overlie a basement high, which possibly extends seaward from the basement ridge north of Burke Island identified in profile AWI-20100126a (Fig. 6). However, the low-fold quality of seismic profile AWI-20100133 does not reveal the top of the basement and neither does that of the crossing line AWI-20060001 (Fig. 5).

5. Sedimentation patterns and chronological constraints

We used the composite profiles AWI-20100132 to 20100135 (Fig. 4a) and the southernmost part of the SCS profile NBP9902-11 (Fig. S4) for a depth-converted transect from the inner to outer shelf of the eastern ASE, primarily using seismic velocities we derived from a velocity-depth model from seismic refraction phases recorded by the OBS systems along profile AWI-20100100/AWI-20100133 (Fig. 8). Our P-wave velocities in this seismic refraction model range from 2.0 km/s for sediments near the seafloor to 4.2 km/s for sedimentary rocks at 3.7 km depth below seafloor (b.sf.). The velocity–depth distribution is almost uniform along the east–west oriented profile. Compared to sedimentary rock velocities of other glaciated shelves (e.g., Cochrane et al., 1995; Larter et al., 1997), the relatively high velocities of the upper sediments are characteristic for overcompaction resulting from the pressure exercised by the repeated overriding by an ice sheet. A P-wave velocity of ca. 1750 m/s measured on a subglacial till recovered within 1 m b.sf. in the eastern ASE (Klages et al., 2013) is consistent with these high sediment velocities near the seafloor. As refraction arrivals from deeper seated sedimentary sequences were not recorded due to the small airgun configuration, we used a velocity of 4.5 km/s for sedimentary rocks deeper than 4 km b.sf.

The depth-converted transect (Fig. 9) follows along the western flank of the central Pine Island Trough. It clearly illustrates a large basin infill between the basement high underneath the Eastern Outer Bank and the basement cropping out on the inner shelf, with sub-horizontal sedimentary strata lapping onto the basement flanks. We assume that pre- and syn-rift sediments filled the deeper part of the basin, which likely developed as part of the rifting process before and during the breakup between the Chatham Rise and West Antarctica. Post-rift sediments were deposited on top of the Eastern Outer Bank basement block. The outer shelf is characterized by considerable progradation of sedimentary strata that downlap onto an at least 1300 m thick sequence of aggraded sedimentary strata deposited over the basement high. Similar to observations on other Antarctic shelves (e.g., Cooper et al., 1991; Anderson et al., 1992; Eittreim et al., 1995; De Santis et al., 1999), the onset of progradation may be interpreted as the beginning of major subglacial sediment transport across the entire ASE shelf by an advanced grounded ice sheet. Although ASS-u4 is observed as a major glacial erosional unconformity, ASS-u3 is likely to mark the beginning of the pre-glacial to glacial transition with first glacier advances onto the inner to middle shelf. Taking into account the depth difference between ASS-u3 and ASS-u1, we conclude that at least 4 km of pre-glacial strata must have been eroded from the present inner shelf and coastal hinterland since the onset of grounded ice-sheet advance across the entire ASE shelf.

We attempt to constrain a chronology for the seismostratigraphic units on the ASE shelf by comparing their reflection characteristics with those of other Antarctic shelves, for which chrono-stratigraphic models were derived from drill cores and borehole records. The best analogue for the ASE shelf appears to be the Eastern Basin of the Ross Sea shelf, because both regions share a similar continental breakup history and glacial sedimentation processes by the same ice sheet. Seismic profiles BGR80-07 and PD90-30 (Cooper et al., 1991; Anderson and Bartek, 1992; De Santis et al., 1995, 1999; Brancolini et al., 1997; Anderson, 1999; Chow and Bart, 2003) cross DSDP Sites 270, 272 and 271 and show a striking similarity in the pattern and sequence of seismic units and unconformities with those of our transect AWI-20100132 to -0135 (Fig. 4b,c). In particular, the major glacial unconformity ASS-u4 cuts strata with a high truncation angle similar to unconformity RSU3 in the Ross Sea. By assuming that this unconformity represents the same major glacial advance period, our ASE shelf unconformities (from bottom to top) ASS-u2, ASS-u3, ASS-u4 and ASS-u5 consequently may correspond to the Ross Sea unconformities (from bottom to top) RSU5, RSU4/RSU4A, RSU3 and RSU2 (Cooper et al., 1991; De Santis et al., 1995, 1999; Anderson, 1999; Decesari et al., 2007; Sorlien et al., 2007; C. Sorlien, pers. comm.), respectively. The unconformity RSU2 correlates to the Ri unconformity in the Victoria Land Basin and was drilled in the ANDRILL cores (Fielding et al., 2008; Wilson et al., 2012). Only the oldest unconformity ASS-u1 does not correlate well with RSU6. By adopting the ages of the correlation chart for the Ross Sea shelf by De Santis et al. (1999), we estimate a preliminary age model for the ASE shelf sediments (Fig. 10).

6. Discussion of a sedimentation model and implications for ice sheet dynamics

As demonstrated by geophysical and petrological/geochemical data, the continental margin of the Amundsen Sea and the Marie Byrd Land/Thurston Island blocks was formed by rifting prior to and during the breakup of New Zealand's Chatham Rise and Campbell Plateau (Larter et al., 2002; Eagles et al., 2004; Kipf et al., 2012; Wobbe et al., 2012; Gohl et al., 2013) (Fig. 9). Gravity and magnetic anomalies (Gohl et al., 2007, 2013) coincide with the location of a basement ridge underneath the Eastern and Western Outer Bank (Figs. 1, 4, 9), indicating that this ridge may represent the remnant of a crustal block that rifted a distance apart from Marie Byrd Land before breakup occurred north of it at 90–85 Ma. Although the onlapping of the sedimentary sequences of unit ASS-1 onto the Outer Bank basement ridge indicates that syn-rift sediments had filled most of the basin south of it, possibly in a back-arc setting, the southernmost strata show the most pronounced deformation. They may represent pre-rift sediments that were folded during the convergent plate boundary phase before or during the collision of Hikurangi Plateau with Chatham Rise at about 105–100 Ma (Davy et al., 2008). The sparse observation of horizons below ASS-u1 does not allow the identification of any faulting in the sediments and basement that would further support this interpretation. However, it is possible that ASS-u1 (~105–90 Ma?) marks the transition from a convergent to a divergent margin when the basin subsided at a different rate (Fig. 9). Unit ASS-2, which has an estimated Late Cretaceous age, was deposited unconformably on sediments of the convergent plate boundary phase. Passive margin shelf deposition was dominated by sedimentation of horizontal strata, continued without any clear hiatus into Oligocene times and buried the Outer Bank basement ridge. Folding and faulting observed in the southernmost sections of unit ASS-2, in particular on the inner shelf of the western ASE transect, indicate that convergent or transpressional tectonic processes were active at least until the latest Cretaceous or into the Oligocene. This deformation may have been caused by transpressional and translateral motion of the southern Bellingshausen Plate boundary (Eagles et al., 2004; Gohl et al., 2013) and/or the West Antarctic Rift System (Müller et al., 2007; Jordan et al., 2010) (Fig. 9).

Unconformity ASS-u2 (~21–19 Ma?) marks a very subtle and gradual change in depositional processes towards those dominating the formation of unit ASS-3 (Fig. 9). Decesari et al. (2007) correlated RSU5, which we compare with ASS-u2, from the eastern Ross Sea to the Victoria Land Basin where it was dated with ~21 Ma from the chronostratigraphy of CRP-1 and CRP-2/2A drill cores (Fielding et al., 2008, and references therein). ASS-3 is characterized by increasingly distinct alternations between seismically transparent and more reflective horizons. The first subglacially transported sediments reached the inner Ross Sea shelf in the Oligocene and were supplied by outlet glaciers draining local ice caps rather than an ice sheet (e.g., De Santis et al., 1999). This is also possible for the ASE, because

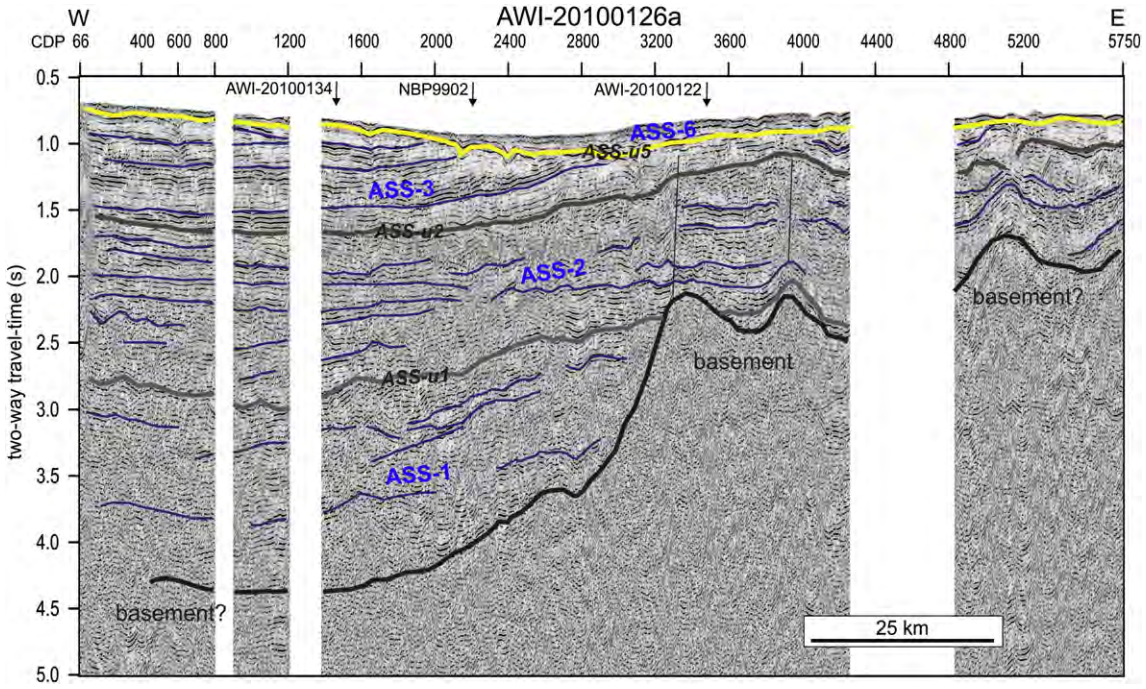

Fig. 6. Seismic profile AWI-20100126 crossing the central Pine Island Trough of the eastern ASE shelf from West to East. Main unconformities ASS-u1, ASS-u2 and ASS-u5 separating the main sedimentary units ASS-1 to ASS-3 and ASS-6 are marked and annotated. Note that unconformities ASS-u3 and ASS-u4 as well as sedimentary units ASS-4 and ASS-5 are missing. Other dominant seismic horizons within the sediment units are line-drawn. Black arrows indicate seismic cross-lines. Description of seismic horizons and reflection characteristics is in the text. See profile location in Fig. 1.

an elevated hinterland, in particular an uplifted central Marie Byrd Land block (LeMasurier, 2008) and the mountain ranges of Ellsworth Land, could have already in the Late Oligocene or Early Miocene provided nucleation points for such regional ice caps that modified the character of the inner to middle shelf deposition with additional supply of glacial debris. At this time, the outer shelf and continental slope were probably not yet affected by deposition of glacigenic debris. We name this period the 'pre-glacial to glacial transitional phase'. The landscape evolution of Marie Byrd Land, together with volcanic products of ice-contact eruptions and the composition of lake sediments, indicate that ice caps had affected the ASE hinterland possibly as early as in Oligocene times (Rocchi et al., 2006).

First advance of grounded ice onto the middle ASE shelf is evident from erosional unconformity ASS-u3 (Fig. 9) and seems to have occurred as early as 14 Ma, if the analogue to the similar Ross Sea event is applicable. Progradation within unit ASS-4 is not observed suggesting that grounded ice did not advance to the outer shelf.

The largest erosional event by grounded ice advancing to the outer shelf is marked by the dominant unconformity ASS-u4 (~12–10 Ma) (Fig. 9). Similar to unconformity RSU3 on the Ross Sea shelf, it truncates older middle shelf strata obliquely and forms the basal surface on which major progradational sequences build the upper 40–70% of the outer shelf. The numerous subordinate and shorter unconformities within units ASS-5 to ASS-6 (e.g., Figs. 2 and S4) indicate frequent advance and retreat episodes of grounded ice beginning in the Late Miocene and continuing to the Pliocene and Pleistocene according to our age model. Buried grounding zone wedges in the upper sequences of unit ASS-5 (Fig. 3) suggest ice sheet advance to the outer shelf in the early Pliocene. These bGZWs could only survive later overriding by grounded ice, if thick (glaci-)marine sediments were deposited on top of them during times when the grounding line was located farther landward (i.e. during long interglacial periods). The prolonged accumulation of pelagic sediment resulted in the observed burial of the grounding zone wedges, which prevented them from being eroded by subsequent grounding line advances during later glacial periods. Their preservation on the ASE shelf may, therefore, indicate an extended warm period with a retreated ice sheet and polythermal glacial activity resulting in high subglacial erosion and high offshore sedimentation rates. With the existing sparse data, it remains speculative whether this period was characterized by an entirely ice-free ASE shelf and a WAIS significantly smaller than today, which would be consistent with the results of ice sheet modeling (Pollard and DeConto, 2009) and evidence for prolonged (seasonal) open-marine conditions during the early Pliocene (~5–3 Ma) at core site ANDRILL AND-1B from the Ross Sea shelf (Naish et al., 2009). However, we argue that a sub-ice shelf situation proximal to a grounding line cannot be sustained over long periods, because this would make occasional advances of the grounding zone with erosion of the GZWs very likely. More importantly, a sub-ice shelf environment distal from the grounding line or a setting under perennial sea-ice coverage would imply low sedimentation rates that range in modern Antarctica usually in the order of just 1–10 cm/kyr (e.g., Domack et al., 2005; Hemer et al., 2007; McKay et al., 2008). Given the fact that the crest-base height difference of the bGZWs is approximately 50–60 m and assuming that they were buried under sustained coverage with floating ice at sedimentation rates of 25–100 cm/kyr, i.e. the highest sub-ice shelf sedimentation rates reported for Antarctica (Pudsey and Evans, 2001), the observed GZW burial must have taken at least 55–225 kyr. We consider this scenario to be very unlikely and, therefore, suggest GZW burial in a seasonal to permanently open-marine setting with high plankton productivity far away from the grounding line, which must have retreated at least onto the middle or inner shelf.

Cooling in the Late Pliocene, as documented for the Ross Sea sector (McKay et al., 2012), allowed grounded ice to advance across the middle and outer shelf of the ASE again, which is evident from the truncation of strata in unit ASS-5 and younger units on the inner to middle shelf (unconformity ASS-u5) (Fig. 9). Progradation of unit ASS-6 continued the oceanward growth of the outer shelf. Numerous unconformities and surficial GZWs within ASS-6 indicate that grounded ice repeatedly advanced to the outer shelf during late Pleistocene glacial periods and that subsequent retreat often was episodic.

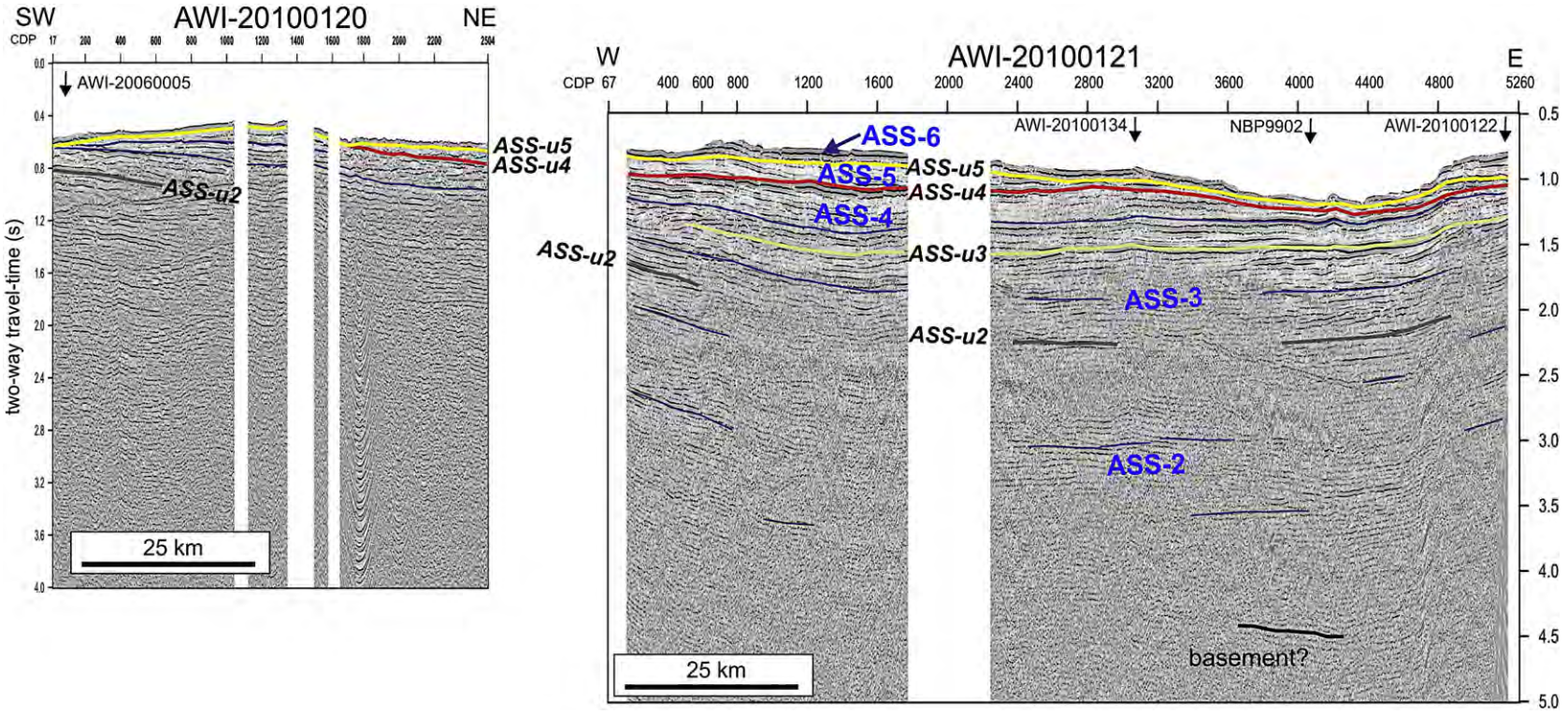

Fig. 7. Composite of seismic profiles AWI-20100120 and AWI-20100121 crossing Bear Ridge of the central ASE shelf and the central Pine Island Trough from West to East. Main unconformities ASS-u2 to ASS-u5 separating the main sedimentary units ASS-2 to ASS-6 are marked and annotated. Other dominant seismic horizons within the sediment units are line-drawn. Black arrows indicate seismic cross-lines. Description of seismic horizons and reflection characteristics is in the text. See profile location in Fig. 1.

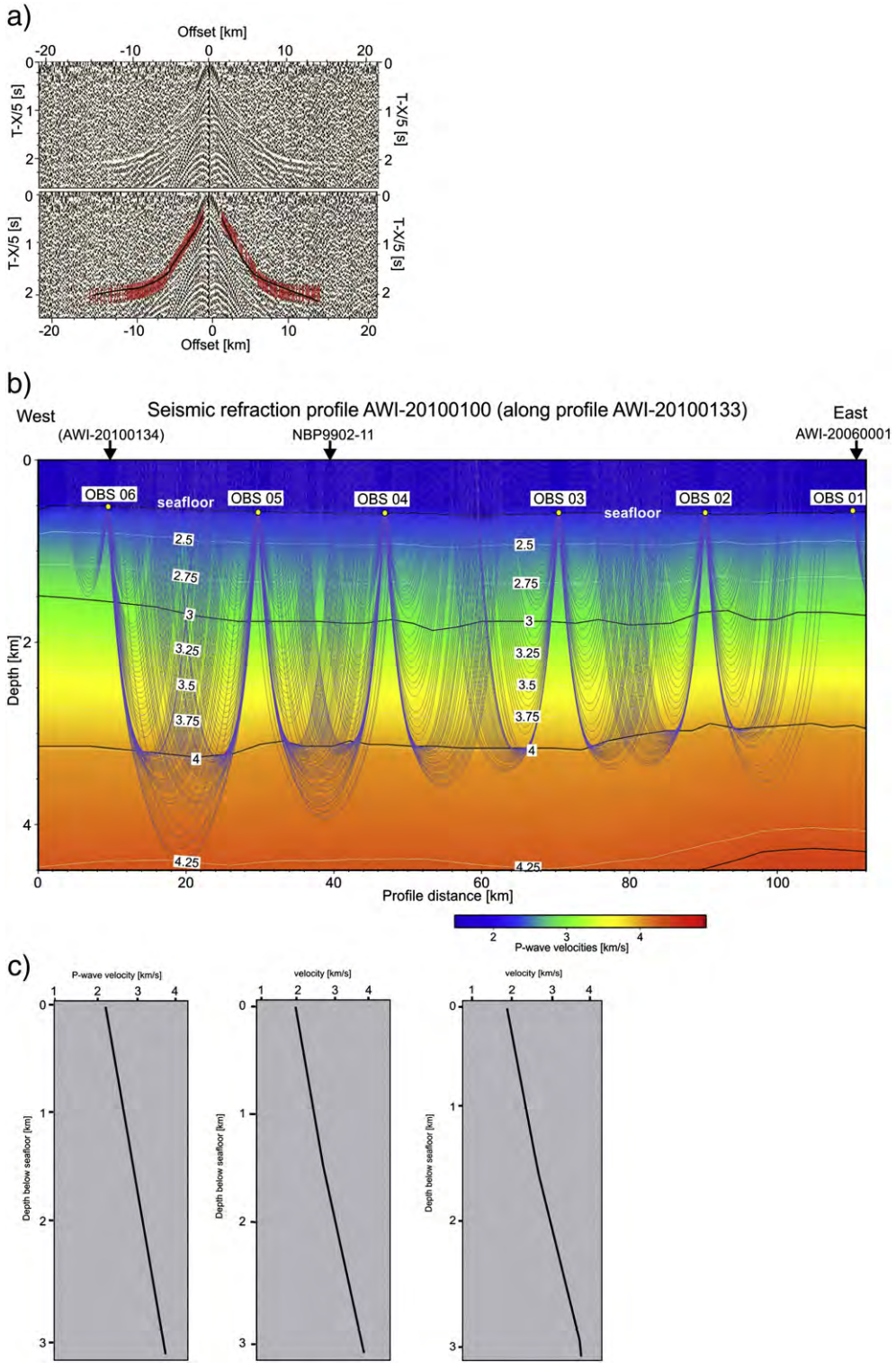

Fig. 8. (a) Top: example of ocean-bottom seismograph (OBS) recording (OBS station 04) of seismic refraction profile AWI-20100100 on eastern ASE shelf. Shown is the hydrophone channel having the best quality of the four channels. Travel-time is reduced with a reduction velocity of 5 km/s. Offset is distance from OBS position. Bottom: Same OBS record with picked refracted P-wave phases (red vertical bars indicate picking uncertainty range) and travel-time response (black lines) calculated from ray-tracing model. (b) Velocity-depth model along profile AWI-20100100 with ray paths. The profile follows the MCS profile AWI-20100133 (Fig. S7) in east–west direction. The OBS stations are marked in yellow; crossing seismic lines are marked with black arrows. The profile was acquired in order to better resolve velocities of the sedimentary sequences of the shelf. (c) One-dimensional velocity–depth functions at the three seismic crossing points indicated in (b). (For interpretation of the references to color in this figure legend, the reader is referred to the web version of this article.)

The east–west orientated seismic profiles on the middle shelf of the eastern ASE clearly illustrate a sub-basin with its long axis striking NNE–SSW (Fig. 11). While its gentle western flank peters out towards Bear Ridge, its sickle-shaped, steeper eastern flank is bordered by a basement high that underlies most of the easternmost shelf, i.e. from the islands in eastern Pine Island Bay to a ridge underlying Burke Island and extending further north. The seismic expression of this sub-basin coincides with a large area of smooth magnetic anomaly lows (Gohl et

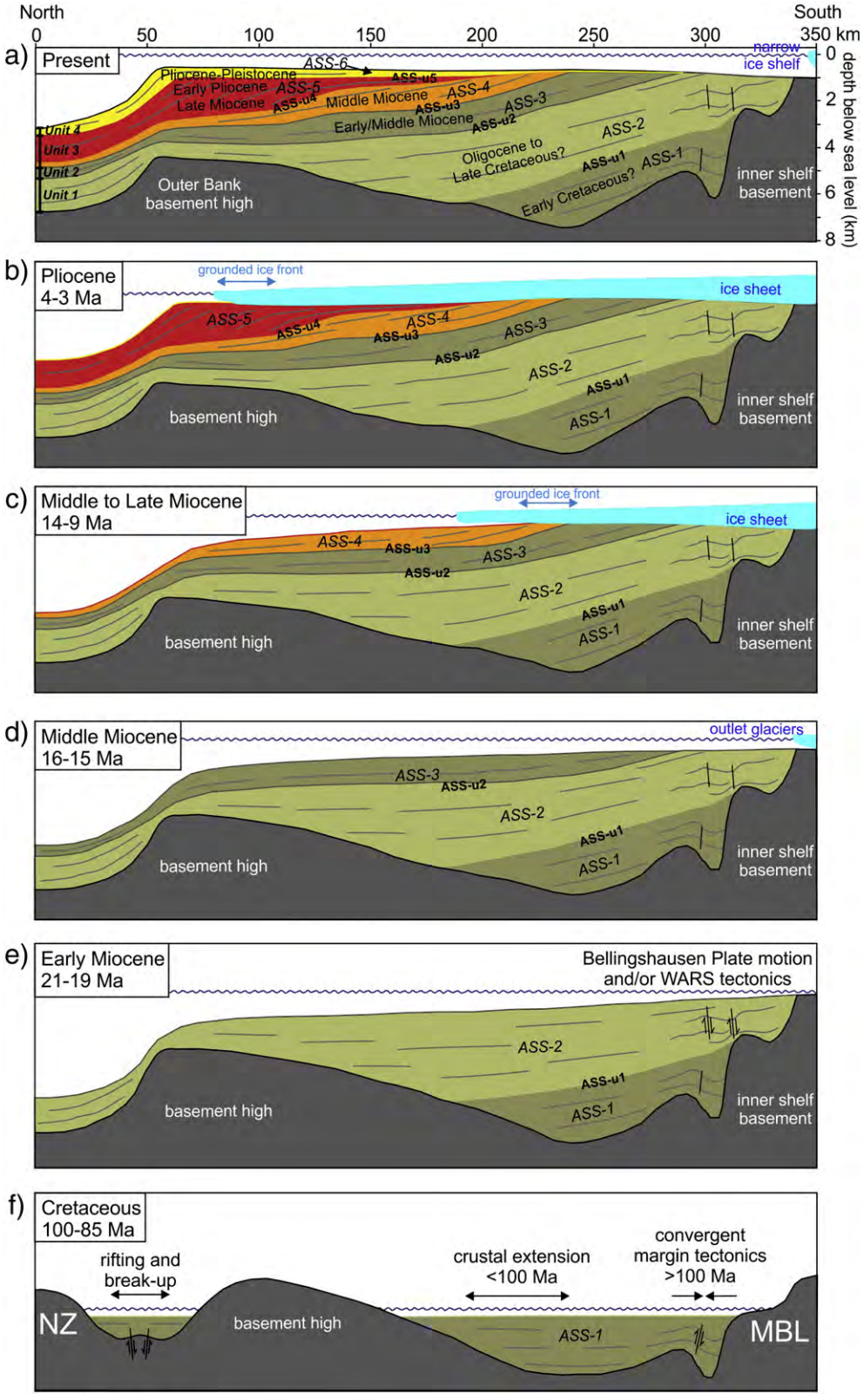

Fig. 9. (a) Interpreted depth-converted seismic transect consisting of profiles NBP9902-11 (southernmost part only), AWI-20100135, AWI-20100134 and AWI-20100132 of the eastern ASE, following the central Pine Island Trough from the inner and middle shelf and continuing across the outer shelf and slope. Sedimentary units ASS-1 to ASS-6 are colored and contain schematic line drawings of main reflection horizons. The main observed unconformities of the ASE shelf are marked and annotated with ASS-u1 to ASS-u5. Units 1–4 correspond to sedimentary units of the ASE continental rise according to Uenzelmann-Neben and Gohl (2012). The units ASS-6 to ASS-1 are schematically backstripped to (b) the Pliocene, (c) the Mid-Late Miocene, (d) the Middle Miocene, (e) the Early Miocene and (f) the Cretaceous when the main unconformities were generated. Other abbreviations are NZ for New Zealand, MBL for Marie Byrd Land and WARS for West Antarctic Rift System. This basin development model is explained in the text.

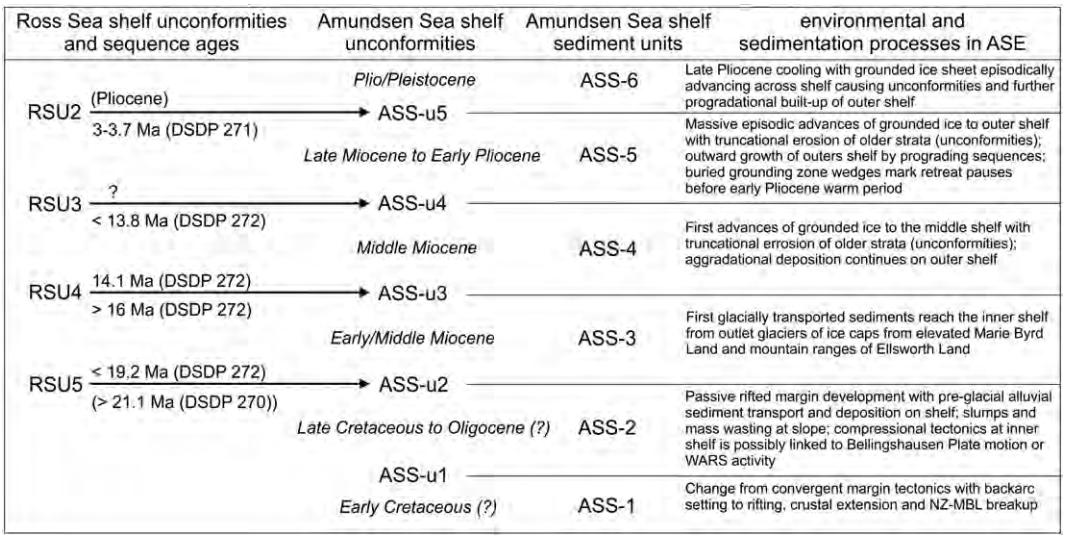

Fig. 10. Stratigraphic model and sedimentation processes of ASE shelf based on suggested correlation of unconformities of the Eastern Basin of the Ross Sea shelf, drilled during DSDP Leg 28, with observed unconformities of the ASE shelf. Unconformities RSU2 to RSU5 and sequence ages from DSDP Sites 270, 272 and 271 are from De Santis et al. (1995, 1999) and Anderson (1999) and references therein. Age epochs suggested for the ASE shelf units are proposed tentatively due to the lack of drill and outcrop records.

al., 2013). We interpret this sub-basin as part of a transtensional or strike-slip/pull-apart West Antarctic Rift System (WARS) branch that accommodated the Byrd Subglacial Basin and Bentley Subglacial Trench of central West Antarctica and extended to the north through the ASE before its rift axis migrated east of the Thurston Island block at about 60 Ma (Müller et al., 2007). Dalziel (2006) postulated the extent of the WARS into the ASE shelf, and our geophysical data confirm the existence of such a basin.

The relatively good coverage of seismic profiles in the eastern ASE allows us to describe the development of the main flow-paths of Pine Island Glacier and Thwaites Glacier across the shelf. We consider the deepest parts of unconformity ASS-u4 in profiles AWI-20100121 (Fig. 7) and AWI-20100133 (Fig. S7) as the base of the initial central Pine Island Trough, which developed when the first grounded ice streams advanced across the middle shelf in the Middle to Late Miocene. Compared to its present bathymetric configuration, the paleo-position of the trough has not changed on the middle shelf segment. Unconformity ASS-u5, marking the onset of enhanced late Pliocene glaciation, also parallels the present seafloor from the middle to outer shelf (Figs. 7, S6, S7). We infer that the central Pine Island Trough, whose location is constrained by the eastern WARS subbasin flank and shallow basement structures along tectonic lineaments (Gohl, 2012; Gohl et al., 2013), remained at the same position on the shelf since early glacial advances. With the growth of the progradational wedge, which moved the shelf break between 25 and 65 km oceanwards (Fig. 11), the paleo-positions of the PITE and PITW also did not change much on the newly extended outer shelf. A gap in seismic data coverage south of the Eastern Outer Bank (Fig. 1) does not allow us to specify the paleo-position of the glacial trough system between the outer PITW and the central Pine Island Trough. This uncertainty applies also to the western ASE shelf where the seismic data coverage on the outer shelf is relatively sparse. However, our observation of relatively stable paleo-positions of the three branches of Pine Island Trough suggests a glacial history in the ASE that is different from that on the Ross Sea shelf. There, paleo-ice stream troughs shifted more frequently during the early phase of grounded ice-sheet advance, resulting in a greater along-strike stratigraphic complexity (Alonso et al., 1992; Anderson and Bartek, 1992). The long post-rift, pre-glacial interval in the ASE resulted in a more deeply buried basement before the first ice sheets advanced across the shelf. In contrast, basement control on paleo-drainage of ice streams persisted much longer on the Ross Sea and Antarctic Peninsula shelves (Alonso et al., 1992; Smith and Anderson, 2010; Anderson and Bartek, 1992).

Our seismostratigraphic model of the ASE shelf (Fig. 9) provides the prerequisite for an improved understanding of the West Antarctic paleoenvironment from Cretaceous to Quaternary times and helps to decipher WAIS dynamic history. Unlike the shelves of the Ross Sea and Filchner-Ronne/Weddell Sea embayments, the ASE shelf consists of glacimarine and subglacial sedimentary strata that were entirely supplied from a West Antarctic source and thus from ice drainage basins unaffected by the East Antarctic Ice Sheet. Even for pre-glacial times, the reconstructed Antarctic paleotopography at 34 Ma of Wilson et al. (2012) indicates that an alluvial system draining into the Amundsen Sea had its catchment in the West Antarctic hinterland. Shallow and deep drilling at selected sites on the shelf, slope and rise, identified from the seismic records, would provide records urgently needed for an improved understanding of processes and mechanisms leading to West Antarctic Ice Sheet deglaciation as presently observed in the Amundsen Sea drainage sector.

7. Conclusions

This study presents a first seismostratigraphic analysis of the Amundsen Sea Embayment shelf and slope using the extensive seismic profile network acquired in this region during the last decade. The main results are:

- The seismic data outline the geometry of a large pre- and syn-rift basin on the middle shelf between the basement cropping out on the inner shelf and an east–west striking basement ridge and other basement highs on the outer shelf.
- A sub-basin with a NNE–SSW-striking axis underlies the mid-shelf in the eastern ASE. We attribute its formation to transtensional or strike–slip/pull-apart motion along an early WARS branch.
- We identify five major erosional unconformities (from bottom to top: ASS-u1 to ASS-u5) and interpret ASS-u3 as the result of minor erosion caused by early advances of grounded ice onto the middle shelf, and ASS-u4 as the result of major subglacial erosion caused by grounded ice sheet advances onto the middle and outer shelf.
- The reflection characteristics of the seismostratigraphic units identified on the ASE shelf are remarkably similar to those on the Ross Sea shelf for which age models exist from drill records. The unconformities ASS-u2, ASS-u3, ASS-u4 and ASS-u5 correspond, from bottom

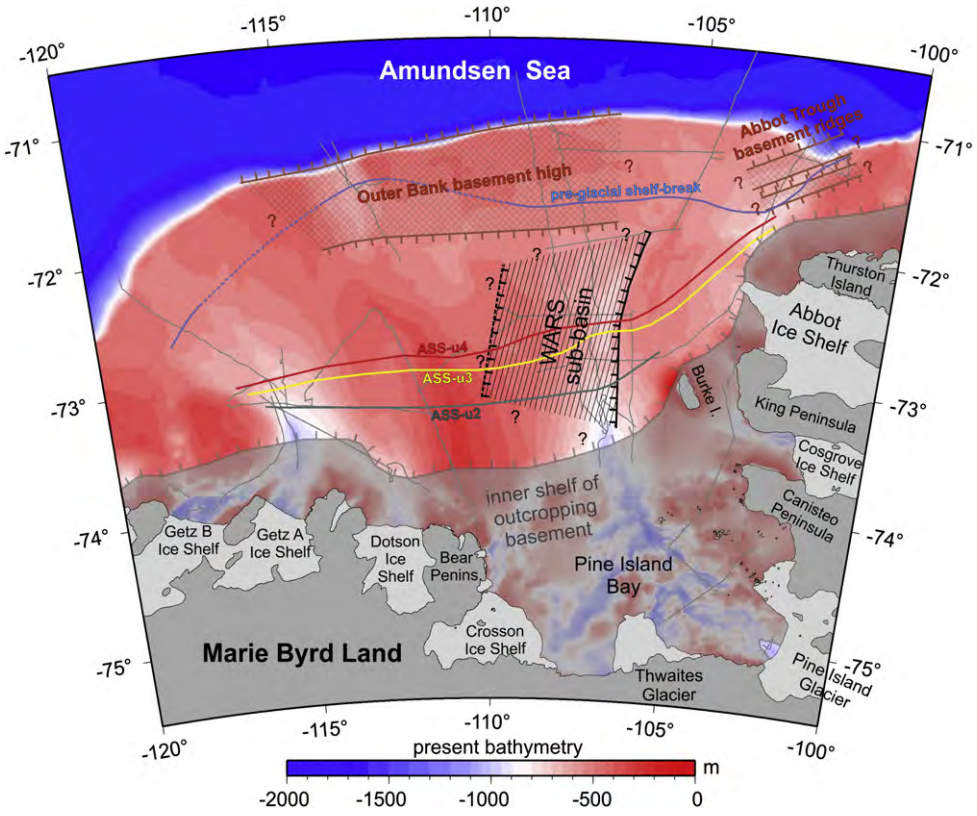

Fig. 11. Outline map with main structural units of ASE shelf observed from seismic profiles. The solid colored lines annotated with ASS-u2, ASS-u3 and ASS-u4 mark the southernmost observed limit of these erosional unconformities. The pre-glacial shelf-break is interpreted from the onset of major progradational deposition of the outer shelf. The western limit of the WARS sub-basin cannot be clearly determined but extends probably farther to the West. The gray transparent area of the inner shelf marks outcropping basement. Thin solid gray lines mark seismic profiles.

to top, to the Ross Sea shelf unconformities RSU5, RSU4A (or RSU4), RSU3 and RSU2, respectively. In a chronostratigraphic model for the seismostratigraphic units on the ASE shelf, we assign an Early Cretaceous age to the oldest sedimentary unit ASS-1, a Late Cretaceous to Oligocene age to unit ASS-2, an Early to Mid-Miocene age to unit ASS-3, a Mid-Miocene age to unit ASS-4, a Late Miocene to Early Pliocene age to unit ASS-5, and a Pliocene to Pleistocene age to the top unit ASS-6.

- Numerous minor truncational unconformities within units ASS-u5 and ASS-u6 indicate frequent advance and retreat episodes of grounded ice across the middle and outer shelf in the Late Miocene and Plio/Pleistocene.
- At least 4 km of pre-glacial strata were eroded from the present inner shelf and coastal hinterland since the onset of major ice sheet advance across the ASE shelf. Parts of the eroded sediments were deposited as a progradional wedge that extends the outer shelf by 25 to 65 km oceanward of the pre-glacial shelf break.
- The preservation of buried grounding zone wedges in the upper part of unit ASS-5 on the outer shelf is consistent with prolonged continuous accumulation of (glaci-)marine sediments, probably during a long interglacial period with a significantly reduced WAIS in the early Pliocene as observed on the Ross Sea shelf. A seasonal to permanently open-marine setting, similar as observed for the Ross Sea shelf for the same time, was likely the case.
- The paleo-position of central Pine Island Trough has been constrained by the eastern WARS sub-basin flank and shallow basement structures along tectonic lineaments. Consequently, central Pine Island Trough has remained in the same position on the shelf since early glacial advances. The paleo-positions of the PITE and PITW on the outer shelf also remained unchanged. We explain this difference to the Ross Sea shelf, where paleo-positions of the glacial troughs have shifted more dynamically, by a long post-rift, pre-glacial deposition history and deeper-seated basement on the ASE shelf.

The seismostratigraphic model of the ASE shelf opens the door to an improved understanding of the West Antarctic paleoenvironment from Cretaceous to Quaternary times. Shallow and deep drilling at selected sites on the shelf would provide stratigraphic control, and analyses of paleoclimate proxies on the recovered sediments would help to reconstruct past WAIS dynamics, which would improve the understanding of the processes and mechanisms leading to West Antarctic Ice Sheet deglaciation as presently observed in the Amundsen Sea drainage sector.

Supplementary data to this article can be found online at http://dx.doi.org/10.1016/j.margeo.2013.06.011.

Acknowledgments

The authors are grateful for the support of the masters and crews of RV *Polarstern* during expeditions ANT-XXIII/4 (2006) and ANT-XXVI/3 (2010), and of RRS *James Clark Ross* during expedition JR141 (2006). We extend our gratitude to the seismic teams on board of both vessels, including staff of the British Geological Survey Marine Operations Group on JR141, for successful data acquisition. Geoff Shipton (Triton Imaging) and David Mucciarone (Stanford University) are gratefully acknowledged for their SEG-Y conversion of the native SCS data from the RV *Nathaniel B. Palmer* cruise NBP9902 (1999). We thank the *German Instrument Pool for Amphibian Seismology* (DEPAS), hosted by the Alfred Wegener Institute, for providing the ocean-bottom seismometers. We thank John B. Anderson of Rice University for giving permission to use the seismic line NBP9902-11 as well as the seismic image of the PD90-30 line from the Ross Sea shelf for Fig. 4c, and we thank Christopher Sorlien and the ROSSMAP group for providing a section of PD90-30 with interpreted horizons. A large part of this paper was drafted during a research visit of K.G. to GNS Science, New Zealand, funded by the International

Bureau of the German Federal Ministry of Education and Research (IB-BMBF) through contract no. 01DR12043. The paper improved from the helpful review comments and suggestions by Julia Wellner and John B. Anderson. R.D.L and C.D.H. were supported through the BAS *IceSheets Programme* which is funded by the UK Natural Environment Research Council. This study has primarily been funded through Work Package 3.2 of the AWI research program PACES.

References

Alley, R.B., Blankenship, D.D., Rooney, S.T., Bentley, C.R., 1989. Sedimentation beneath ice shelves: the view from ice stream B. Marine Geology 85, 101–120.
Alonso, B., Anderson, J.B., Diaz, J.T., Bartek, L.R., 1992. Pliocene–Pleistocene seismic stratigraphy of the Ross Sea: evidence for multiple ice sheet grounding episodes. In: Elliot, D.H. (Ed.), Contributions to Antarctic Research III. Antarctic Research Series, vol. 57. American Geophysical Union, Washington, D.C, pp. 93–103.
Anderson, J.B., 1999. Antarctic Marine Geology. Cambridge University Press, New York (289 pp.).
Anderson, J.B., Bartek, L.R., 1992. Cenozoic glacial history of the Ross Sea revealed by intermediate resolution seismic reflection data combined with drill site information. In: Kennett, J.P., Warnke, D.A. (Eds.), The Antarctic Paleoenvironment: A Perspective on Global Change, Part One. Antarctic Research Series, vol. 56. American Geophysical Union, Washington, DC, pp. 231–263.
Anderson, J.B., Shipp, S.S., Siringan, F.P., 1992. Preliminary seismic stratigraphy of the northwestern Weddell Sea continental shelf. In: Yoshida, Y., Kaminuma, K., Shiraishi, K. (Eds.), Recent Progress in Antarctic Earth Science. Terra Scientific Publishing, Tokyo, pp. 603–612.
Bamber, J.L., Riva, R.E.M., Vermeersen, B.L.A., LeBrocq, A.M., 2009. Reassessment of the potential sea-level rise from a collapse of the West Antarctic Ice Sheet. Science 324, 901–903. http://dx.doi.org/10.1126/science.1169335.
Bart, P.J., 2005. West-directed flow of the West Antarctic Ice Sheet across Eastern Basin, Ross Sea during the Quaternary. Earth and Planetary Science Letters 228, 425–438. http://dx.doi.org/10.1016/j.epsl.2004.10.014.
Brancolini, G., De Santis, L., Lovo, M., Prato, S., 1997. Cenozoic glacial history in the Ross Sea (Antarctica): constraints from seismic reflection data. Terra Antartica 4 (1), 57–60.
Cape Roberts Science Team, 1999. Studies from the Cape Roberts Project, Ross Sea, Antarctica, Initial report on CRP-2/2A. Terra Antartica 6, 1–173.
Cape Roberts Science Team, 2000. Studies from the Cape Roberts Project, Ross Sea, Antarctica, Initial report on CRP-3. Terra Antartica 7, 1–209.
Chow, J.M., Bart, P.J., 2003. West Antarctic Ice Sheet grounding events on the Ross Sea outer continental shelf during the middle Miocene. Palaeogeography, Palaeoclimatology, Palaeoecology 198, 169–186.
Cochrane, G.R., De Santis, L., Cooper, A.K., 1995. Seismic velocity expression of glacial sedimentary rocks beneath the Ross Sea from sonobuoy seismic-refraction data. In: Cooper, A.K., Barker, P.F., Brancolini, G. (Eds.), Geology and Seismic Stratigraphy of the Antarctic Margin. Antarctic Research Series, 68. American Geophysical Union, Washington, DC, pp. 261–270.
Cooper, A.K., Barrett, P.J., Hinz, K., Traube, V., Leitchenkov, G., Stagg, H.M.J., 1991. Cenozoic prograding sequences of the Antarctic continental margins: a record of glacio-eustatic and tectonic events. Marine Geology 102, 175–213.
Cooper, A.K., Brancolini, G., Escutia, C., Kristoffersen, Y., Larter, R., Leitchenkov, G., O'Brien, P., Jokat, W., 2008. Cenozoic climate history from seismic-reflection and drilling studies on the Antarctic continental margin. In: Florindo, F., Siegert, M. (Eds.), Antarctic Climate Evolution. Developments in Earth and Environmental Sciences, vol. 8. Elsevier, pp. 115–228.
Dalziel, I.W.D., 2006. On the extent of the active West Antarctic rift system. In: Siddoway, C.S., Ricci, C.A. (Eds.), Proceedings of Workshop on Frontiers and Opportunities in Antarctic Geosciences. Terra Antartica Reports, 12. Terra Antartica Publications, Siena, Italy, pp. 193–202.
Dalziel, I.W.D., Elliot, D.H., 1982. West Antarctica: problem child of Gondwanaland. Tectonics 1, 3–19.
Davy, B., Hoernle, K., Werner, R., 2008. Hikurangi Plateau: crustal structure, rifted formation, and Gondwana subduction history. Geochemistry, Geophysics, Geosystems 9. http://dx.doi.org/10.1029/2007GC001855.
De Santis, L., Anderson, J.B., Brancolini, G., Zayatz, I., 1995. Seismic record of late Oligocene through Miocene glaciation on the Central Eastern continental shelf of Ross Sea. In: Cooper, A.K., Barker, P.F., Brancolini, G. (Eds.), Geology and Seismic Stratigraphy of the Antarctic Margin. Antarctic Research Series, vol. 68. American Geophysical Union, Washington, D.C., pp. 235–260.
De Santis, L., Prato, S., Brancolini, G., Lovo, M., Torelli, L., 1999. The Eastern Ross Sea continental shelf during the Cenozoic: implications for the West Antarctic ice sheet development. Global and Planetary Change 23, 173–196.
Decesari, R.C., Sorlien, C.C., Luyendyk, B.P., Wilson, D.S., Bartek, L., Diebold, J., Hopkins, S.E., 2007. Regional seismic stratigraphic correlations of the Ross Sea: implications for the tectonic history of the West Antarctic Rift System. In: Cooper, A.K., Raymond, C.R. (Eds.), Proceedings of the 10th Int. Symposium of Antarctic Earth Sciences. USGS Open-File Report 2007–1047. http://dx.doi.org/10.3133/of2007-1047.srp052.
DiVenere, V., Kent, D.V., Dalziel, I.W.D., 1994. Mid-Cretaceous paleomagnetic results from Marie Byrd Land, West Antarctica: A test of post-100 Ma relative motion between East and West Antarctica. Journal of Geophysical Research 99, 15115–15139.
Domack, E., Duran, D., Leventer, A., Ishman, S., Doane, S., McCallum, S., Amblas, D., Ring, J., Gilbert, R., Prentice, M., 2005. Stability of the Larsen B ice shelf on the Antarctic Peninsula during the Holocene epoch. Nature 436, 681–685.
Dowdeswell, J.A., Fugelli, E.M.G., 2012. The seismic architecture and geometry of grounding-zone wedges formed at the marine margins of past ice sheets. Geological Society of America Bulletin 124, 1750–1761. http://dx.doi.org/10.1130/B30628.1.
Dowdeswell, J.A., Cofaigh, C.Ó., Anderson, J.B., 2006. Morphology and sedimentary processes on the continental slope off Pine Island Bay, Amundsen Sea, West Antarctica. Geological Society of America Bulletin 118, 606–619.
Drewry, D.J., 1983. Antarctica: Glaciological and Geophysical Folio. Scott Polar Research Institute, Cambridge, UK (9 sheets).
Eagles, G., Gohl, K., Larter, R.D., 2004. High-resolution animated tectonic reconstruction of the South Pacific and West Antarctic Margin. Geochemistry, Geophysics, Geosystems 5 (7). http://dx.doi.org/10.1029/2003GC000657.
Ehrmann, W., Hillenbrand, C.-D., Smith, J.A., Graham, A.G.C., Kuhn, G., Larter, R.D., 2011. Provenance changes between recent and glacial-time sediments in the Amundsen Sea embayment, West Antarctica: clay mineral assemblage evidence. Antarctic Science 23, 471–486.
Eittreim, S.L., Cooper, A.K., Wannesson, J., 1995. Seismic stratigraphic evidence of ice-sheet advances on the Wilkes Land margin of Antarctica. Sedimentary Geology 96, 131–156.
Evans, J., Dowdeswell, J.A., Cofaigh, C.Ó., Benham, T.J., Anderson, J.B., 2006. Extent and dynamics of the West Antarctic Ice Sheet on the outer continental shelf of Pine Island Bay during the last glaciation. Marine Geology 230, 53–70.
Fielding, C.R., Whittaker, J., Henrys, S.A., Wilson, T.J., Naish, T.R., 2008. Seismic facies and stratigraphy of the Cenozoic succession in McMurdo Sound, Antarctica: implications for tectonic, climatic and glacial history. Palaeogeography, Palaeoclimatology, Palaeoecology 260, 8–29. http://dx.doi.org/10.1016/j.palaeo.2007.08.016.
Fretwell, P., et al., 2013. Bedmap2: improved ice bed, surface and thickness datasets for Antarctica. The Cryosphere 7, 375–393. http://dx.doi.org/10.5194/tc-7-375-2013.
Gohl, K., 2007. The Expedition ANTARKTIS-XXIII/4 of the Research Vessel "Polarstern" in 2006. Berichte zur Polar- und Meeresforschung (Reports on Polar and Marine Research) 557 (166 pp., http://epic.awi.de/26756/).
Gohl, K., 2010. The Expedition of the Research Vessel "Polarstern" to the Amundsen Sea, Antarctica, in 2010 (ANT-XXVI/3). Berichte zur Polar- und Meeresforschung (Reports on Polar and Marine Research) 617 (173 pp., http://epic.awi.de/29635/).
Gohl, K., 2012. Basement control on past ice sheet dynamics in the Amundsen Sea Embayment, West Antarctica. Palaeogeography, Palaeoclimatology, Palaeoecology 335–336, 35–41. http://dx.doi.org/10.1016/j.palaeo.2011.02.022.
Gohl, K., Teterin, D., Eagles, G., Netzeband, G., Grobys, J., Parsiegla, N., Schlüter, P., Leinweber, V., Larter, R.D., Uenzelmann-Neben, G., Udintsev, G.B., 2007. Geophysical survey reveals tectonic structures in the Amundsen Sea embayment, West Antarctica. In: Cooper, A.K., Raymond, C.R. (Eds.), Proceedings of the 10th Int. Symposium of Antarctic Earth Sciences. USGS Open-File Report 2007–1047. http://dx.doi.org/10.3133/of2007-1047.srp047.
Gohl, K., Denk, A., Eagles, G., Wobbe, F., 2013. Deciphering tectonic phases of the Amundsen Sea Embayment shelf, West Antarctica, from a magnetic anomaly grid. Tectonophysics 585, 113–123. http://dx.doi.org/10.1016/j.tecto.2012.06.036.
Graham, A.G.C., Larter, R.D., Gohl, K., Hillenbrand, C.-D., Smith, J.A., Kuhn, G., 2009. Bedform signature of a West Antarctic palaeo-ice stream reveals a multi-temporal record of flow and substrate control. Quaternary Science Reviews 28, 2774–2793. http://dx.doi.org/10.1016/j.quascirev.2009.07.003.
Graham, A.G.C., Larter, R.D., Gohl, K., Dowdeswell, J.A., Hillenbrand, C.-D., Smith, J.A., Evans, J., Kuhn, G., Deen, T.J., 2010. Flow and retreat of the Late Quaternary Pine Island-Thwaites paleo-ice stream, West Antarctica. Journal of Geophysical Research - Earth Surfaces 115. http://dx.doi.org/10.1029/2009JF001482.
Harwood, D., Florindo, F., Talarico, F., Levy, R., Kuhn, G., Naish, T., Niessen, F., Powell, R., Pyne, A., Wilson, G., 2009. Antarctic drilling recovers stratigraphic records from the continental margin. EOS Transactions 90, 90–91.
Hayes, D.E., Frakes, L.A., 1975. General synthesis. Initial Report of the Deep Sea Drilling Project 28. 919–942.
Hemer, M., Post, A.L., O'Brien, P.E., Craven, M., Truswell, E.M., Roberts, D., Harris, P.T., 2007. Sedimentological signatures of the sub-Amery Ice Shelf circulation. Antarctic Science 19, 497–506.
Hillenbrand, C.-D., Smith, J.A., Kuhn, G., Esper, O., Gersonde, R., Larter, R.D., Maher, B., Moreton, S.G., Shimmield, T.M., Korte, M., 2010. Age assignment of a diatomaceous ooze deposited in the western Amundsen Sea Embayment after the Last Glacial Maximum. Journal of Quaternary Science 25, 280–295. http://dx.doi.org/10.1002/jqs.1308.
Hillenbrand, C.-D., Kuhn, G., Smith, J.A., Gohl, K., Graham, A.G.C., Larter, R.D., Klages, J.P., Downey, R., Moreton, S.G., Forwick, M., Vaughan, D.G., 2013. Grounding-line retreat of the West Antarctic Ice Sheet from inner Pine Island Bay. Geology 41, 35–38. http://dx.doi.org/10.1130/G33469.1.
Hochmuth, K., Gohl, K., 2013. Glaciomarine sedimentation dynamics of the Abbot glacial trough of the Amundsen Sea Embayment shelf, West Antarctica. In: Hambrey, M.J., et al. (Ed.), Antarctic Palaeoenvironments and Earth-Surface Processes. Geological Society Special Publications. The Geological Society of London (in press), http://dx.doi.org/10.1144/SP381.21.
Howat, I.M., Domack, E.W., 2003. Reconstructions of western Ross Sea palaeo-ice-stream grounding zones from high-resolution acoustic stratigraphy. Boreas 32, 56–75.
Jakobsson, M., Anderson, J.B., Nitsche, F.O., Dowdeswell, J.A., Gyllencreutz, R., Kirchner, N., Mohammad, R., O'Regan, M., Alley, R.B., Anandakrishnan, S., Eriksson, B., Kirshner, A., Fernandez, R., Stolldorf, T., Minzoni, R., Majewski, W., 2011. Geological record of ice shelf break-up and grounding line retreat, Pine Island Bay, West Antarctica. Geology 39, 691–694. http://dx.doi.org/10.1130/G32153.1.
Jakobsson, M., Anderson, J.B., Nitsche, F.O., Gyllencreutz, R., Kirshner, A.E., Kirchner, N., O'Regan, M., Mohammad, R., Eriksson, B., 2012. Ice sheet retreat dynamics inferred

from glacial morphology of the central Pine Island Bay Trough, West Antarctica. Quaternary Science Reviews 38, 1–10. http://dx.doi.org/10.1016/j.quascirev.2011.12.017.
Jordan, T.A., Ferraccioli, F., Vaughan, D.G., Holt, J.W., Corr, H., Blankenship, D.D., Diehl, T.M., 2010. Aerogravity evidence of a major crustal thinning under the Pine Island Glacier region (West Antarctica). Bulletin of the Geological Society of America 122, 714–726. http://dx.doi.org/10.1130/B26417.1.
Kellogg, T.B., Kellogg, D.E., 1987. Late Quaternary deglaciation of the Amundsen Sea: implications for ice sheet modelling. In: Waddington, E.D., Walder, J.S. (Eds.), The Physical Basis of Ice Sheet Modelling, 170. IAHS Publ., pp. 349–357.
Kerr, A., Huybrechts, P., 1999. The response of the East Antarctic ice-sheet to the evolving tectonic configuration of the Transantarctic Mountains. Global and Planetary Change 23, 213–229.
Kipf, A., Mortimer, N., Werner, R., Gohl, K., van den Bogaard, P., Hauff, F., Hoernle, K., 2012. Granitoids and dykes of the Pine Island Bay region, West Antarctica. Antarctic Science 24 (5), 473–484. http://dx.doi.org/10.1017/S0954102012000259.
Kirshner, A.E., Anderson, J.B., Jakobsson, M., O'Regan, M., Majewski, W., Nitsche, F.O., 2012. Post-LGM deglaciation in Pine Island Bay, West Antarctica. Quaternary Science Reviews 38, 11–26. http://dx.doi.org/10.1016/j.quascirev.2012.01.017.
Klages, J.P., Kuhn, G., Hillenbrand, C.-D., Graham, A.G.C., Smith, J.A., Larter, R.D., Gohl, K., 2013. First geomorphological record and glacial history of an inter-ice stream ridge on the West Antarctic continental shelf. Quaternary Science Reviews 61, 47–61. http://dx.doi.org/10.1016/j.quascirev.2012.11.007.
Larter, R.D., Vanneste, L.E., 1995. Relict subglacial deltas on the Antarctic Peninsula outer shelf. Geology 23, 33–36.
Larter, R.D., Rebesco, M., Vanneste, L.E., Gambôa, L.A.P., Barker, P.F., 1997. Cenozoic tectonic, sedimentary and glacial history of the continental shelf west of Graham Land, Antarctic Peninsula. In: Barker, P.F., Cooper, A.K. (Eds.), Geology and Seismic Stratigraphy of the Antarctic Margin 2. Antarctic Research Series, v. 71. American Geophysical Union, pp. 1–27.
Larter, R.D., Cunningham, A.P., Barker, P.F., Gohl, K., Nitsche, F.O., 2002. Tectonic evolution of the Pacific margin of Antarctica — 1. Late Cretaceous tectonic reconstructions. Journal of Geophysical Research 107 (B12), 2345. http://dx.doi.org/10.1029/2000JB000052.
Larter, R., Gohl, K., Hillenbrand, C.-D., Kuhn, G., Deen, T.J., Dietrich, R., Eagles, G., Johnson, J.S., Livermore, R.A., Nitsche, F.O., Pudsey, C.J., Schenke, H.-W., Smith, J.A., Udintsev, G., Uenzelmann-Neben, G., 2007. West Antarctic Ice Sheet change since the last glacial period. Eos, Transactions of the American Geophysical Union 88, 189–196.
Larter, R.D., Graham, A.G.C., Gohl, K., Kuhn, G., Hillenbrand, C.-D., Smith, J.A., Deen, T.J., Livermore, R.A., Schenke, H.-W., 2009. Subglacial bedforms reveal complex basal regime in a zone of paleo-ice stream convergence, Amundsen Sea Embayment, West Antarctica. Geology 37 (5), 411–414. http://dx.doi.org/10.1130/G25505A.
LeMasurier, W.E., 2008. Neogene extension and basin deepening in the West Antarctic rift inferred from comparisons with the East African rift and other analogs. Geology 36, 247–250. http://dx.doi.org/10.1130/G24363A.
Levy, R., Cody, R., Crampton, J., Fielding, C., Golledge, N., Harwood, D., Henrys, S., McKay, R., Naish, T., Ohneiser, C., Wilson, G., Wilson, T., Winter, D., 2012. Late Neogene climate and glacial history of the Southern Victoria Land coast from integrated drill core, seismic and outcrop data. Global and Planetary Change 96–97, 157–180. http://dx.doi.org/10.1016/j.gloplacha.2012.02.005.
Lowe, A.L., Anderson, J.B., 2002. Reconstruction of the West Antarctic ice sheet in Pine Island Bay during the Last Glacial Maximum and its subsequent retreat history. Quaternary Science Reviews 21, 1879–1897.
Lowe, A.L., Anderson, J.B., 2003. Evidence for abundant subglacial meltwater beneath the paleo-ice sheet in Pine Island Bay, Antarctica. Journal of Glaciology 46 (164), 125–138.
McKay, R.M., Dunbar, G.B., Naish, T.R., Barrett, P.J., Carter, L., Harper, M., 2008. Retreat history of the Ross Ice Sheet (Shelf) since the Last Glacial Maximum from deep-basin sediment cores around Ross Island. Palaeogeography, Palaeoclimatology, Palaeoecology 260, 245–261. http://dx.doi.org/10.1016/j.palaeo.2007.08.015.
McKay, R., Browne, G., Carter, L., Cowan, E., Dunbar, G., Krissek, L., Naish, T., Powell, R., Reed, J., Talarico, F., Wilch, T., 2009. The stratigraphic signature of the late Cenozoic Antarctic Ice Sheets in the Ross Embayment. Geological Society of America Bulletin 121, 1537–1561. http://dx.doi.org/10.1130/B26540.1.
McKay, R., Naish, T., Carter, L., Riesselman, C., Dunbar, R., Sjunneskog, C., Winter, D., Sangiorgi, F., Warren, C., Pagani, M., Schouten, S., Willmott, V., Levy, R., DeConto, R., Powell, R.D., 2012. Antarctic and Southern Ocean influences on Late Pliocene global cooling. Proceedings of the National Academy of Sciences of the United States of America (PNAS) 109, 6423–6428. http://dx.doi.org/10.1073/pnas.1112248109.
Mukasa, S.B., Dalziel, I.W.D., 2000. Marie Byrd Land, West Antarctica: evolution of the Gondwana's Pacific margin constrained by zircon U–Pb geochronology and feldspar common-Pb isotopic compositions. Geological Society of America Bulletin 112, 611–627.
Müller, R.D., Gohl, K., Cande, S.C., Goncharov, A., Golynsky, A.V., 2007. Eocene to Miocene geometry of the West Antarctic rift system. Australian Journal of Earth Sciences 54, 1033–1045. http://dx.doi.org/10.1080/08120090701615691.
Naish, T., Powell, R., Levy, R., Wilson, G., Scherer, R., Talarico, F., Krissek, L., Niessen, F., Pompilio, M., Wilson, T., Carter, L., DeConto, R., Huybers, P., McKay, R., Pollard, D., Ross, J., Winter, D., Barrett, P., Browne, G., Cody, R., Cowan, E., Crampton, J., Dunbar, G., Dunbar, N., Florindo, F., Gebhardt, C., Graham, I., Hannah, M., Hansaraj, D., Harwood, D., Helling, D., Henrys, S., Hinnov, L., Kuhn, G., Kyle, P., Läufer, A., Maffioli, P., Magens, D., Mandernack, K., McIntosh, W., Millan, C., Morin, R., Ohneiser, C., Paulsen, T., Persico, D., Raine, I., Reed, J., Riesselman, C., Sagnotti, L., Schmitt, D., Sjunneskog, C., Strong, P., Taviani, M., Vogel, S., Wilch, T., Williams, T., 2009. Obliquity-paced Pliocene West Antarctic ice sheet oscillations. Nature 458, 322–328. http://dx.doi.org/10.1038/nature07867.
Nitsche, F.O., Gohl, K., Vanneste, K., Miller, H., 1997. Seismic expression of glacially deposited sequences in the Bellingshausen and Amundsen Seas, West Antarctica. In: Barker, P.F., Cooper, A.K. (Eds.), Geology and Seismic Stratigraphy of the Antarctic Margin 2. Antarctic Research Series, Vol. 71. American Geophysical Union, Washington, D.C., pp. 95–108.
Nitsche, F.O., Cunningham, A.P., Larter, R.D., Gohl, K., 2000. Geometry and development of glacial continental margin depositional systems in the Bellingshausen Sea. Marine Geology 162, 277–302.
Nitsche, F.O., Jacobs, S.S., Larter, R.D., Gohl, K., 2007. Bathymetry of the Amundsen Sea continental shelf: implications for geology, oceanography, and glaciology. Geochemistry, Geophysics, Geosystems 8 (10). http://dx.doi.org/10.1029/2007GC001694.
Nitsche, F.O., Gohl, K., Larter, R., Hillenbrand, C.-D., Kuhn, G., Smith, J., Jacobs, S., Anderson, J., Jakobsson, M., 2013. Paleo ice flow and subglacial meltwater dynamics in Pine Island Bay, West Antarctica. The Cryosphere 7, 249–262. http://dx.doi.org/10.5194/tc-7-249-2013.
Pankhurst, R.J., Millar, I.L., Grunow, A.M., Storey, B.C., 1993. The pre-Cenozoic magmatic history of the Thurston Island crustal block, West Antarctica. Journal of Geophysical Research 98, 11835–11849.
Pankhurst, R.J., Weaver, S.D., Bradshaw, J.D., Storey, B.C., Ireland, T.R., 1998. Geochronology and geochemistry of pre-Jurassic superterranes in Marie Byrd Land, Antarctica. Journal of Geophysical Research 103, 2529–2547.
Pollard, D., DeConto, R.M., 2009. Modelling West Antarctic ice sheet growth and collapse through the past five million years. Nature 458. http://dx.doi.org/10.1038/nature07809.
Pritchard, H.D., Ligtenberg, S.R.M., Fricker, H.A., Vaughan, D.G., van den Broeke, M.R., Padman, L., 2012. Antarctic ice-sheet loss driven by basal melting of ice shelves. Nature 484, 502–505. http://dx.doi.org/10.1038/nature10968.
Pudsey, C.J., Evans, J., 2001. First survey of Antarctic sub-ice shelf sediments reveals mid-Holocene ice shelf retreat. Geology 29, 787–790.
Rignot, E., 2008. Changes in West Antarctic ice stream dynamics observed with ALOS PALSAR data. Geophysical Research Letters 35. http://dx.doi.org/10.1029/2008GL033365.
Rignot, E., Mouginot, J., Scheuchl, B., 2011. Ice flow of the Antarctic ice sheet. Science 333. http://dx.doi.org/10.1126/science.1208336.
Rocchi, S., LeMasurier, W.E., Di Vincenzo, G., 2006. Oligocene to Holocene erosion and glacial history in Marie Byrd Land, West Antarctica, inferred from exhumation of the Dorrel rock intrusive complex and from volcano morphologies. Geological Society of America Bulletin 118, 991–1005. http://dx.doi.org/10.1130/B25675.1.
Smith, R.T., Anderson, J.B., 2010. Ice-sheet evolution in James Ross Basin, Weddell Sea margin of the Antarctic Peninsula: The seismic stratigraphic record. Geological Society of America Bulletin 122, 830–842. http://dx.doi.org/10.1130/B26486.1.
Smith, J.A., Hillenbrand, C.-D., Larter, R.D., Graham, A.G.C., Kuhn, G., 2009. The sediment infill of subglacial meltwater channels on the West Antarctic continental shelf. Quaternary Research 71, 190–200.
Smith, J.A., Hillenbrand, C.-D., Kuhn, G., Larter, R.D., Graham, A.G.C., Ehrmann, W., Moreton, S.G., Forwick, M., 2011. Deglacial history of the West Antarctic Ice Sheet in the western Amundsen Sea Embayment. Quaternary Science Reviews 30, 488–505.
Sorlien, C.C., Luyendyk, B.P., Wilson, D.S., Decesari, R.C., Bartek, L., Diebold, J.B., 2007. Oligocene development of the West Antarctic Ice Sheet recorded in eastern Ross Sea strata. Geology 35, 467–470. http://dx.doi.org/10.1130/G23387A.
Storey, B.C., 1991. The crustal blocks of West Antarctica within Gondwana: reconstruction and break-up model. In: Thomson, M.R.A., Crane, J.A., Thomson, J.W. (Eds.), Geological Evolution of Antarctica. Cambridge University Press, Cambridge.
Tucholke, B.E., Edgar, N.T., Boyce, R.E., 1976. Physical properties of sediments and correlations with acoustic stratigraphy: Leg 35, deep sea drilling project. In: Hollister, C.D., Craddock, C. (Eds.), Initial Reports. Deep Sea Drilling Project, Washington, D.C., pp. 229–249.
Uenzelmann-Neben, G., Gohl, K., 2012. Amundsen Sea sediment drifts: archives of modifications in oceanographic and climatic conditions. Marine Geology 299–302, 51–62. http://dx.doi.org/10.1016/j.margeo.2011.12.007.
Uenzelmann-Neben, G., Gohl, K., Larter, R.D., Schlüter, P., 2007. Differences in ice retreat across Pine Island Bay, West Antarctica, since the Last Glacial Maximum: indications from multichannel seismic reflection data. In: Cooper, A.K., Raymond, C.R. (Eds.), Proceedings of the 10th Int. Symposium of Antarctic Earth Sciences. USGS Open-File Report 2007–1047. http://dx.doi.org/10.3133/of2007-1047.srp084.
Weigelt, E., Gohl, K., Uenzelmann-Neben, G., Larter, R.D., 2009. Late Cenozoic ice sheet cyclicity in the western Amundsen Sea Embayment—evidence from seismic records. Global and Planetary Change 69, 162–169.
Weigelt, E., Uenzelmann-Neben, G., Gohl, K., Larter, R.D., 2012. Did massive glacial dewatering modify the sedimentary structures of the Amundsen Sea Embayment shelf, West Antarctica? Global and Planetary Change 92–93, 8–16. http://dx.doi.org/10.1016/j.gloplacha.2012.04.006.
Wellner, J.S., Lowe, A.L., Shipp, S.S., Anderson, J.B., 2001. Distribution of glacial geomorphic features on the Antarctic continental shelf and correlation with substrate: implications for ice behavior. Journal of Glaciology 48, 397–411.
Wilson, D.S., Jamieson, S.S., Barrett, P.J., Leitchenkov, G., Gohl, K., Larter, R.D., 2012. Antarctic topography at the Eocene–Oligocene boundary. Palaeogeography, Palaeoclimatology, Palaeoecology 335–336, 24–34. http://dx.doi.org/10.1016/j.palaeo.2011.05.028.
Wobbe, F., Gohl, K., Chambord, A., Sutherland, R., 2012. Structure and breakup history of the rifted margin of West Antarctica in relation to Cretaceous separation from Zealandia and Bellingshausen plate motion. Geochemistry, Geophysics, Geosystems 13, Q04W12. http://dx.doi.org/10.1029/2011GC003742.